University habilitation to direct research

Heather Etchevers

HABILITATION A DIRIGER LES RECHERCHES

UNIVERSITE DE LA MEDITERRANEE AIX-MARSEILLE II

Présentée par

Heather Corbett Etchevers

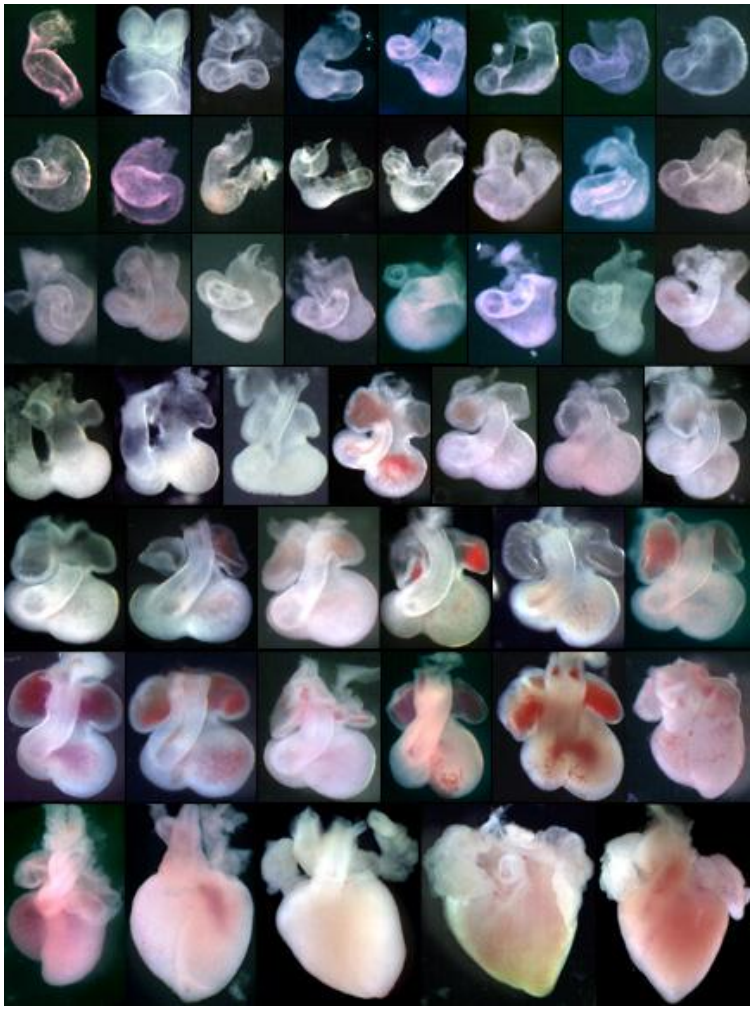

Année 2012

INSERM unité mixte de recherche S910
Faculté de Médecine
27 boulevard Jean Moulin
13005 Marseille

COVER IMAGE LEGEND

Composite image of embryonic hearts at stages ranging from the beginning of the fourth to the ninth week of human gestation (upper left to lower right, Carnegie stages 10-23). Congenital heart and great vessel malformations arise during this time window when molecular signaling between cardiac progenitors and their environment is impaired.

TABLE OF CONTENTS

ACKNOWLEDGEMENTS

It is both a source of pride and humility, to think back on the diverse influences that have shaped the scientist I am today. When I omit to mention names, it is a reflection of the limitations of my memory rather than a measure of my gratitude. I am irrevocably indebted for the one-sided gifts of confidence that my mentors have had in my ability to conceive of and to conduct valuable scientific projects, for the kindness of these mentors and innumerable colleagues to impart both technical and intellectual training, and for the trust invested in me by collaborators, sometimes sight unseen.

The only way I can hope to repay their generosity is by becoming a valuable mentor myself for those who look to me for instruction. This document is the means by which I intend to demonstrate to a committee of peers that I have the wherewithal and merit to continue in this tradition and to try to inspire the scientific community in my turn, over time. For a developmental biologist, there is no more attractive analogy than that of maintaining the long-term potential to be a progenitor, to maintain both plasticity and to make definitive contributions to an organism that will continue to evolve and that is so much greater than the sum of its individual parts. I am one cell in a complex and changing body of knowledge, a cell with its autonomous heritage, but always receptive to instructive signals from its environment. Through both its inductive nature and the production of intellectual descendents, perhaps someday it shall exert systemic effects of its own.

In this light, I would like to warmly thank the following non-exhaustive list of people for being an integral part of my developmental environment over the years, in particular many others from the now-defunct Institut d'Embryologie Moléculaire et Cellulaire du CNRS et du Collège de France, the Departments of Genetics at the Purpan and Timone Hospitals, and particularly from the Department of Genetics at the Necker Children's Hospital: Jeanne Amiel, Tania Attie-Bitach, Patrick Calvas, Nicolas Chassaing, Gérard Couly, Elisabeth Dupin, Delphine Duprez, Ferechté Encha-Razavi, John Gilbert, Pierre Lasjaunias, Nicole Le Douarin, Nicolas Levy, Susan Lindsay, Stanislas Lyonnet, François Malecaze, Arnold Munnich, Asma Smahi, Marcy Speer, Marie-Aimée Teillet, Michel Vekemans and Stéphane Zaffran.

I would also like to thank my trainees to date, who have taught me consciously or unconsciously in counterpart to what I have taught them, which exchange I hope will benefit future generations of scientists.

Finally, I must also thank my two wonderful children and their father for their steady support and encouragement over the years.

PREFACE

Born and educated for the most part in the United States, I have enjoyed the luxury of excellent mentorship during my career thus far as an independent scientist in France. All these mentors have taken it on trust that my training for a Ph.D. also included the necessary tools for directing original research responsibly, at all levels. However, the habilitation is an obligate rite of passage for researchers in France, Germany, Sweden and a number of other European countries. It ensures both that I am competent to not only continue to conduct original research, and that I have a directive seam in my research interests over time that is sufficiently rich to support myself and those trainees who will learn from my experience and contribute their efforts by my side to advancing science. To demonstrate that the faith of these esteemed colleagues has been well-placed since my Ph.D., I hereby present, to the best of my ability, my acquired credentials and my near- to mid-term projects.

CURRICULUM VITAE

Heather Corbett Etchevers

née Heather Mirth Corbett in the United States
Married, two children

EDUCATION

INSTITUTION AND LOCATION	DIPLOMA	DATES	FIELD OF STUDY
Wellesley College, Wellesley, MA, USA	B.A.	09/88-06/92	Biology, Music
Somerville College, Oxford Univ., UK		10/90-06/91	Biology
University of California at Berkeley, CA, USA (joint enrollment)	Ph.D.	09/92-12/98	Neurobiology
Université de Paris 6, France (joint enrollment)	Doctorat	08/94-06/99	Dev. Biology
Institut d‟Embryologie - CNRS UMR 7218	Postdoc	06/99-09/01	Dev. Biology
INSERM U393, France	Postdoc	09/01-03/03	Human genetics/embryology

OTHER TRAINING

Animal experimentation, level I. Training at CNRS center Joseph Aiguier, Marseille, from 21 June to 2 July 2011.

Radiation safety officer training for qualification as “personne compétente en radioprotection”, Hôpital Pitié-La Salpêtrière, Paris, December 2003.

Course in Scientific Management for the. Beginning Academic Investigator by the Howard Hughes Medical Institute and Burroughs-Wellcome Fund, Bethesda, MD (USA), July, 2002.

Summer student program at the Jackson Laboratory, Bar Harbor, Maine (USA), June-Aug,1990.

POSITIONS AND EMPLOYMENT

2002-2005 “Avenir” startup group leader INSERM U393 (U781 after 2004), Hôpital Necker – Enfants Malades, Paris

2004-2008 Chargé de recherche class 2 (tenured research scientist), INSERM U781

2008-2010 Chargé de recherche class 1, INSERM U781

2010- Chargé de recherche class 1, INSERM UMR_S910, Université de la Méditerranée Aix-Marseille II, Marseilles

PROFESSIONAL MEMBERSHIPS

1992- Member, Sigma Xi and Phi Beta Kappa honors societies (USA)

1993-2003 Member, Society for Neuroscience (USA)

1995- Member, Société Française de la Biologie du Développement (France)

1999- Senior scientific advisor, Naevus 2000 France-Europe

2006-2010 Member, International Society for Stem Cell Research

2007- Scientific advisor, Nevus Outreach, Inc.

2010 Strategic planning committee, Nevus Outreach, Inc.

AWARDS

2002-2005 "Avenir" program, INSERM (150K euros consumables, 126K euros salaries)

2001-2002 Sturge-Weber Foundation Postdoctoral Fellow

2001 Travel award from the Société Française de la Biologie du Développement to attend the 14th International Congress of Developmental Biology, Kyoto, Japan

1993-1998 Predoctoral Fellow in the Biological Sciences, Howard Hughes Medical Institute

RESEARCH FUNDING

Nevus Outreach, Inc Etchevers (PI) 2010-11
Time course of normal melanocytic differentiation in the avian model, $3K
Study of four markers of different stages of pigment cell commitment during embryonic development.

Nevus Outreach, Inc. Etchevers (PI) 2010
Biological resource constitution, $3.1K
Collection of a cohort of patient DNAs derived from blood to conduct prospective genetic studies into the constitutional bases of the congenital giant naevus.

"Equipe FRM" Fondation pour la Recherche Médicale Amiel (PI) 2008-10
Normal and pathological development of the neural crest in humans. 240K€.
This large study was devoted to finding new genes and better dissecting the pathophysiology of those that are known to lead to abnormal neural crest development and thereby to certain congenital malformations and oncogenic predispositions. In a team composed of my group and that of Jeanne Amiel, we received this award and label on the basis of the quality and interoperability of our research programs and their applicability to human health. *Role*: Co-PI

Fondation pour la Recherche Médicale Etchevers (PI) 2008-9
Role of the FGF10-FGFR2b pathway in cardiac morphogenesis. 15K€.

This support for a Ph.D. student was devoted to dissecting the molecular control and role of the growth factor FGF10 in heart development and to finding candidate genes for cardiopathies within its signalling pathway.

Programme National de Recherche en Dermatologie Etchevers (PI) 2006-7
Physiopathology of giant congenital melanocytic naevi. 20K€.
This pilot study defined conditions necessary for differentiation of cultured human embryonic neural crest cells into melanocytes and began to explore molecular differences between these and cells of the congenital giant nevus.

Association Française contre les Myopathies 2004-1287 Etchevers (PI) 2004-5
Transcriptome and differentiation analysis of multipotent human neural crest cells. 40K€.
The aim of this study was to corroborate a quantitative analysis of the neural crest transcriptome using a custom DNA microarray and to compare this to that of neural crest derivatives such as the enteric ganglia.

Genoscope d'Evry AP2004-5 Etchevers (PI) 2005
Capillary resequencing of **SAGE banks of human embryonic primordia and cells**.
Approximate commercial value of up to 100K€.

TRAINEES

Technicians under my supervision: Géraldine Goudefroye, Nora Brahimi, Geneviève Guédu, Candice Babarit, Céline Gomez

M2-level technical internships: Abee Boyles 2004 (Duke University); Sadaf Sanii 2009 (U Paris 7)

M.D./Ph.D. technical internship : Jean-Claude Quintyn, 2006-2007 (Toulouse). Currently ophthalmologist at CHU Toulouse.

Four students in week-long science career shadowing programs in 9th grade (collège 3^{e})

« Magistère » internship: Fabrice Chatonnet, 1998 (ENS Lyon). Currently postdoctoral fellow at the Institute for Functional Genomics, Lyon.

L3 internship : Floriane Faure, 2010 (Rennes)

L3 internship : Stéphanie Da Silva, 2007 (Toulouse). Currently Ph.D. student, INSA, Toulouse.

M1 internship : Jessica Guirchoun, 2005 (U Paris 12; paper : Golzio et al., 2006)

M1 internship: Sarah Lechat, 2011 (Marseille). Currently in M2 internship with Isabelle André-Schmutz, Necker Children‟s Hospital, Paris.

Post-M1 equivalent internship (3 months): Min Kim, 2005 (Wellesley College). Currently MBA candidate at the Kellogg School of Management, Chicago.

M2 (DEA): Soraya Gritli, 1999 (U Paris 6). Currently dental surgeon in private practice, Villepreux.

M2: Laurence Benouaiche, 2001 (U Paris 5). Currently “chef de Clinique” in pediatric reconstructive surgery, Necker Children‟s Hospital, Paris.

M2: Alexis Arnaud 2008-2009 (U Paris 11). Currently pediatric surgeon at CHU Rennes.

M2: Adeline Vigouroux 2007-2008 (Toulouse). Currently medical geneticist at CHU Toulouse.

M2 rotation (one of two in “Development and Immunology”): Najla El Fissi, 2011-2012 (Marseille)

M2 then Ph.D.: Christelle Golzio 2004-2009 (U Paris 5&7; 7 papers under my direction, of which two first-author ; an additional first-author paper in revision). Currently postdoctoral fellow at Duke University with Nicolas Katsanis.

Ph.D.: Nicolas El Robrini, 2011-2014 (Marseille)

Postdoctoral fellows :

Eric Detrait, 2003-2004 (3 papers under my direction, of which two reviews as first author). Currently group leader of *in vivo* pharmacology at UCB Pharma, Belgium.

Lekbir Baala, 2005-2007 (1 first-author paper under my direction). HDR, engineer at U Orléans.

Sophie Thomas, 2005-2010 (7 papers under my direction, of which three first-author).

TEACHING ACTIVITIES

November 2010 European Course of Neuroradiology 11 Tarragona
2 hours on "Development of the branchial arches" and "Maxillofacial Embryology and Development" with multiple choice exam. CME accreditation by the UEMS and AMA.

October 2008 European Course of Neuroradiology 10 Tarragona
2 hours on "Development of the branchial arches" and "Maxillofacial Embryology and Development" with multiple choice exam. CME accreditation by the UEMS and AMA. Courses available at http://www.slideshare.net/Alethea/development-of-the-branchial-arches-presentation (8173 views) and http://www.slideshare.net/Alethea/maxillofacial-embryology-and-development-presentation (4558 views)

May 2007 Master 1 Santé Paris
3 hour on normal and pathological development of the neural crest, Paris V/VII

May 2007 DU d‟ophtalmologie pédiatrique Paris
1 hour on embryological development of the eyes, Paris V

January 2007 ABC-WIN Val d‟Isère

1 hour on the molecular identity of the endothelial cell
(CME-accredited training for neuroradiologists)

Mai 2006 Master 1 Santé Paris
3 hour on normal and pathological development of the neural crest, Paris V/VII

March 2006 DU d"ophtalmologie pédiatrique Paris
1 hour on embryological development of the eyes, Paris V

January 2006 ABC-WIN Val d"Isère
1 hour on neural crest influence on cephalic angiogenesis
(CME-accredited training for neuroradiologists)

Novembre 2005 Master 2 des Sciences et Techniques – Mention Européenne Paris
1 hour on neural crest formation ; 1 hour on human embryonic stem cells : ethical considerations Normal and pathological mammalian development module, Paris V & VII

Octobre 2005 DIU Imagerie ORL et cervico-faciale Le Kremlin-Bicêtre
1 hour on the development of the base of the skull, Paris IX, CHU Bicêtre

May 2005 Master 1 Santé Paris
3 hours on normal and pathological neural crest development, Paris V/VII

May 2005 DU pathologie hypothalamo-hypophysaire Le Kremlin-Bicêtre
1 hour on embryological development of the pituitary, Paris IX, CHU Bicêtre

April 2005 International Master in Neurovascular Diseases Chiang Mai
5 hours on neurovascular development (Mahidol University et Paris XI)

February 2005 DU d"ophtalmologie pédiatrique Paris
1 hour on embryological development of the eyes, Paris V

November 2004 Master des Sciences et Techniques Mention Européenne Paris
1 hours on neural crest formation (Paris V/VII)

October 2004 International Master in Neurovascular Diseases Phuket
4 hours on neurovascular development (Mahidol University et Paris XI)

October 2004 European Course in Neuroradiology Basel
1.5 hours on brain development (European Masters qualification)

Octobre 2004 DIU Imagerie ORL et cervico-faciale Le Kremlin-Bicêtre
1 hour on the development of the base of the skull, Paris IX, CHU Bicêtre

January 2004 ABC-WIN Val d"Isère
1 hour on vascular anatomy, CME-accredited training for neuroradiologists

December 2003 DU d"ophtalmologie pédiatrique Paris
1 hour on embryological development of the eyes, Paris V

November 2003 DEA de génétique Paris
1.5 hours on normal and pathological neural crest development, Paris V

June 2003 DU pathologie hypothalamo-hypophysaire Le Kremlin-Bicêtre
1 hour on embryological development of the pituitary, Paris IX, CHU Bicêtre

February 2002 DU d'ophtalmologie pédiatrique Paris
1 hour on embryological development of the eyes, Paris V

February 2001 DU d'ophtalmologie pédiatrique Paris
1 hour on embryological development of the eyes, Paris V

Before teaching in France, I had hands-on training in teaching as a graduate student at the University of California at Berkeley. I led a general biology study and lab section for pre-medical students at the L2 level (for France) in the second semester of 1993, for an estimated 20 hours. In the first semester of 1996, I undertook both study section and main lectures for the human physiology course for an equivalent number of hours. Finally, on invitation, I designed a teaching module in applied embryology for 6 hours the same semester for undergraduates at Mills College, Oakland, California.

INVITED ORAL COMMUNICATIONS

Session chair and invited lecturer, International Pigment Cell Conference, Bordeaux. 23/9/2011

2011 International Expert Meeting on Large Congenital Melanocytic Nevi and Neurocutaneous Melanocytosis, Tübingen. 7/5/2011

2010 International Nevus Outreach Conference, Westlake, TX. 10/7/2010

Institut IMAGINE, Hôpital Necker, Paris. 25/3/2010

Institut Albert Bonniot, Grenoble, 1/12/2009

6th International Neural Tube Defects Conference, Burlington, Vermont. 12/9/2009

Société de Biologie, Institut Curie, Paris, France. 21/1/2009

Session moderator and invited lecturer, Science Blogging 2008, Royal Institution of Great Britain, London. 30/8/2008 (talk on online laboratory notebooks available at http://www.slideshare.net/Alethea/sciblog2008-etchevers-presentation [3223 views])

Groupe de Génétique de l'Ouest, Ile de Berder, France. 4/7/2008 (talk on vertebral development available at http://www.slideshare.net/Alethea/vertebral-development-presentation [3184 views])

4e Assises de Génétique Humaine et Médicale, Lille, 17 - 19/1/2008

Duke University Center for Human Genetics, Durham, USA. 11/5/2007

SOFFOET (Société Française de Foetopathologie) – Paris, 15/6/2007

Institut de Biologie du Development, University of Toulouse – Rangueil; 15/3/2007

Symposium on Developing Governance by PEALS (Policy, Ethics and Life Sciences) and DGEMap (Developmental Gene Expression Map), in Newcastle, England: 27/2/2007

(talk available at http://www.slideshare.net/Alethea/necker-human-embryo-resource-presentation [1003 views])

Third Melanoma Meeting by Institut Curie, Institut Gustave Roussy and Hôpital St. Louis, Paris, 3/2/2006

Séminaires de l'Institut Fédéré de Recherche 30, Hôpital Purpan, Toulouse, 18/5/2006

Séminaires de l'Institut Fédéré de Recherche 94, Hôpital Necker, Paris, 3/1/2006

Necker Children‟s Hospital "3rd Thursdays in Genetics" national lecture series, Paris, 17/2/2005

Society for Pediatric Pathology/Paediatric Pathology Society Joint Meeting, Tours. 2005

Société Européenne de Neurologie Pédiatrique, Paris. 1/12/2002

XVIIth Symposium Neuroradiologicum (two oral presentations), Paris. 18-24/8/2002

CONFERENCE ORGANIZATION

2011	Co-organizer, International Expert Meeting on Large Congenital Melanocytic Nevi and Neurocutaneous Melanocytosis, Tübingen, Germany
2010-2011	Member, national committee for the International Pigment Cell Conference 2011
2009	Moderator of national conference on congenital giant nevus, Vichy
2008	Selection committee, "Journées scientifiques" of the IFR30 and IFR31, Toulouse
2005-2008	Selection committee, Congrès Jeunes Chercheurs (Université Paris Descartes)
2005	Co-organizer of national conference on congenital giant nevus, Marne-la-Vallée
2002	Organizer and moderator of symposium on congenital giant nevus, satellite to the International Pigment Cell Conference, Egmond-aan-See, Holland

COMMUNITY RESPONSIBILITIES AND PEER REVIEW

2010	Grant Reviewer, Association Française contre les Myopathies
2008-	Reviewer, Human Molecular Genetics, Human Genetics, Anatomical Record and Human Reproduction journals
2008	Invited scientific advisory committee representative for Naevus 2000 France-Europe by Drug Information Association Euromeeting, Barcelona, 2-5 March 2008
2006-2008	Grant Reviewer, Agence Nationale de la Recherche (France), National Science Foundation (Georgia), Rappaport Institute (Israel)

2005 Report for the scientific directions workgroup "Stem cells and therapy" of the future IMAGINE Institute of Genetic Disease, Paris, France

2004-2009 Radiation safety officer, INSERM U781. Designed training presentation available at http://www.slideshare.net/Alethea/comment-travailler-en-scurit-avec-de-la-radioactivit (3729 views; used beyond our research unit.)

M.D. thesis committees: A. Vigouroux (2008), L. Benouaiche (2009), M. Chaabouni (2009)

Ph.D. thesis committees: C. Bonnart (2007); C. Golzio (as co-director, 2009)

INTERNET-BASED COMMUNICATIONS

2010 An abstract on the **Large congenital melanocytic nevus** for the Orphanet medical encyclopaedia is now available on-line at the following address:
http://www.orpha.net/consor/cgi-bin/OC_Exp.php?lng=EN&Expert=626

I am currently writing, on invitation, a similar abstract on the subject of **Neurocutaneous melanocytosis** for Orphanet, and a summary information sheet on both topics for the (United States-based) National Organisation for Rare Diseases (http://www.rarediseases.org/).

2010- Guest blogger, The Node (Development journal‟s website at http://thenode.biologists.com/).

Gordon C, Etchevers H (2010) Meeting report from the 2nd joint meeting of the SFBD AND JSDB 2010 – “From Cells to Organs” http://thenode.biologists.com/meeting-report-from-the-2nd-joint-meeting-of-the-sfbd-and-jsdb-2010-from-cells-to-organs/

2006-2010 My research group webpage, accessed >18,500 times, at http://openwetware.org/wiki/Etchevers:Main (not current after 2010).

2004-2010 Two successive English-language blogs about conducting science: "Humans in Science" (http://humans.scienceboard.net) on the *Science Advisory Board*, then "A Developing Passion" (http://blogs.nature.com/etchevers) on *Nature Network*. 652 posts, 1881 comments.

PEER-REVIEWED PUBLICATIONS

My participation in **boldface** (**red** for first/last authorships since Ph.D.), and those of my students, postdocs and technical assistants in blue.

Submitted or in revision as of June, 2011:

1. Golzio C, Havis E, Daubas P, Nuel G, Babarit C, Munnich A, Vekemans M, Zaffran S, Lyonnet S, **Etchevers HC**. ISL1 is a major orchestrator of morphogenetic signaling pathways in the embryonic human heart (preparation).
2. Cluzeau C, Mou C, Bal E, Benko S, Babarit C, Overbeek P, Perret C, Memet S, Courtois G, Lyonnet S, **Etchevers H**, Mikkola M, Munnich A, Headon D, Smahi A. Down-regulation of Wnt/β-catenin signalling by Edar involves Hipk2, a new NF-κB target gene (revision).
3. van der Werf C, Wabbersen T, Hsiao NH, Parades J, **Etchevers H**, Kroise P, Tibboel D, Babarit C, Schreiber R, Hoffenberg E, Vekemans M, Zeder S, Ceccherini I, Lyonnet S, Ribeiro A, Seruca R, te Meerman G, Ijzendoorn S, Shepherd I, Verheij J, Hofstra RMW. Mutations in *CLMP* cause Congenital Short Bowel Syndrome, pointing to the major role of CLMP in intestinal development. Gastroenterology (minor revision).

Accepted articles in press:

4. **Etchevers HC**. Primary culture of chick, mouse or human neural crest cells. Nat Protoc. Accepted 14 June 2011.
5. Krengel S, Breuninger H, Beckwith M, **Etchevers HC**. (2011) Meeting report from the 2011 International Expert Meeting on Large Congenital Melanocytic Nevi and Neurocutaneous Melanocytosis, Tübingen. Pigment Cell Melanoma Res. Accepted manuscript online: 15 Jun 2011, doi: 10.1111/j.1755-148X.2011.00875.x
6. Macé M, Galiacy S, Erraud A, Mejía JE, **Etchevers H**, Allouche M, Desjardins L, Calvas P, Malecaze F. (2011) Comparative transcriptome and network biology analyses demonstrate antiproliferative and hyperapoptotic phenotypes in human keratoconus corneas. Invest Ophthalmol Vis Sci. Accepted manuscript online: 15 Jun 2011, doi:10.1167/iovs.10-70981
7. Reyes-Mùgica M, Beckwith M, **Etchevers HC**. (2011) Etiology of congenital melanocytic nevi and related conditions. In: Nevogenesis (Practical Clinical Medicine series) eds. A. Marghoob, J. Grinchik, A. Scope and S. Dusza. Springer, New York.

Published (since doctorate):

8. de Pontual L, Kettaneh D, Gordon CT, Oufadem M, Boddaert N, Lees M, Balu L, Lachassinne E, Petros A, Mollet J, Wilson LC, Munnich A, Brugière L, Delattre O, Vekemans M, **Etchevers H**, Lyonnet S, Janoueix-Lerosey I, Amiel J. (2011) Germline gain-of-function mutations of *ALK* disrupt central nervous system development. Human Mutation, 32: 272–276. doi: 10.1002/humu.21442

9. Cognet M, Nougayrede A, Malan V, Callier P, Cretolle C, Faivre L, Genevieve D, Goldenberg A, Heron D, Mercier S, Philip N, Sigaudy S, Verloes A, Sarnacki S, Munnich A, Vekemans M, Lyonnet S, **Etchevers H**, Amiel J, de Pontual L. (2011) Dissection of the *MYCN* locus in Feingold syndrome and isolated oesophageal atresia. Eur J Hum Genet. 19:602–606 doi:10.1038/ejhg.2010.225

10. Thomas S, Encha-Razavi F, Devisme L, **Etchevers H**, Bessières-Grattagliano B, Goudefroye G, Elkhartoufi N, Pateau E, Ichkou A, Bonnière M, Marcorelle P, Parent P, Manouvrier S, Holder M, Laquerrière A, Loeuillet L, Roume J, Martinovic J, Mougou-Zerelli S, Gonzales M, Meyer V, Wessner M, Bole-Feysot C, Nitschke P, Leticee N, Munnich A, Lyonnet S, Wookey P, Gyapay G, Foliguet B, Vekemans M, Attié-Bitach T. (2010) High-Throughput Sequencing of a 4.1 Mb Linkage Interval Reveals *FLVCR2* Deletions and Mutations in Lethal Cerebral Vasculopathy. Hum Mut 31(10):1134-41.

11. Chaabouni M, **Etchevers H**, De Blois MC, Calvas P, Waill-Perrier MC, Vekemans M, Romana SP. (2010) Identification of the *IRX B* genes cluster as candidate genes in severe dysgenesis of the ocular anterior segment. Invest Ophthalmol Vis Sci 51(9):4380-6.

12. de Pontual L*, Zaghloul NA*, Thomas S*, Davis EE, McGaughey DM, Dollfus H, Baumann C, Bessling SL, Babarit C, Pelet A, Gascue C, Beales P, Munnich A, Lyonnet S, **Etchevers H**, Attie-Bitach T, Badano JL, McCallion AS, Katsanis N, Amiel J. (2009). Epistasis between *RET* and *BBS* mutations modulates enteric innervation and causes syndromic Hirschsprung disease. Proc Natl Acad Sci U S A 2009 Aug 18;106(33):13921-6. doi: 10.1073/pnas.0901219106

13. Bessières-Grattagliano B, Foliguet B, Devisme L, Loeuillet L, Marcorelles P, Bonnière M, Laquerrière A, Fallet-Bianco C, Martinovic J, Zrelli S, Leticee N, Cayol V, **Etchevers HC**, Vekemans M, Attie-Bitach T, Encha-Razavi F. (2009). Refining the clinicopathological pattern of cerebral proliferative glomeruloid vasculopathy (Fowler syndrome): Report of 16 fetal cases. Eur J Med Genet 52(6):386-92. Epub 2009 Jul 25.

14. Boissel S, Reish O, Proulx K, Kawagoe-Takaki H, Sedgwick B, Yeo GS, Meyre D, Golzio C, Molinari F, Kadhom N, **Etchevers HC**, Saudek V, Farooqi IS, Froguel P, Lindahl T, O'Rahilly S, Munnich A, Colleaux L. (2009). Loss-of-function mutation in the dioxygenase-encoding *FTO* gene causes severe growth retardation and multiple malformations. Am J Hum Genet 85:106-11.

15. Chassaing N, Golzio C, Odent S, Lequeux L, Vigouroux A, Martinovic-Bouriel J, Tiziano FD, Masini L, Piro F, Maragliano G, Delezoide AL, Attié-Bitach T, Manouvrier-Hanu S, **Etchevers HC**, Calvas P. (2009). Phenotypic spectrum of *STRA6* mutations: from Matthew-Wood syndrome to non-lethal anophthalmia. Hum Mutat 30(5):E673-81.

16. de Pontual L, Mathieu Y, Golzio C, Rio M, Malan V, Boddaert N, Soufflet C, Picard C, Durandy A, Dobbie A, Heron D, Isidor B, Motte J, Newburry-Ecob R, Pasquier L, Tardieu M, Viot G, Jaubert F, Munnich A, Colleaux L, Vekemans M, **Etchevers H**, Lyonnet S, Amiel J. (2009). Mutational, functional, and expression studies of the *TCF4* gene in Pitt-Hopkins syndrome. Hum Mutat 30(4):669-76.

17. Benko S, Fantes JA, Amiel J, Kleinjan D-J, Thomas S, Ramsay J, Jamshidi N, Essafi A, Heaney S, Gordon CT, McBride D, Golzio C, Fisher M, Perry P, Abadie V, Ayuso C, Holder-Espinasse M, Kilpatrick N, Lees MM, Picard A, Temple IK,

Thomas P, Vazquez M-P, Vekemans M, Crollius HR, Hastie ND, Munnich A, **Etchevers HC**, Pelet A, Farlie PG, FitzPatrick DR, Lyonnet S. (2009). Highly conserved non-coding elements on either side of *SOX9* associated with Pierre Robin sequence. Nat Genet 41(3):359-64. doi:10.1038/ng.329.

18. Lequeux L, Rio M, Vigouroux A, Titeux M, **Etchevers H**, Malecaze F, Chassaing N, Calvas P. (2008). Confirmation of *RAX* gene involvement in human anophthalmia. Clin Genet 74:392-5.
19. Thomas S, Thomas M, Wincker P, Xu P-T, Speer MC, Munnich A, Lyonnet S, Vekemans M, **Etchevers HC**. (2008). Human neural crest cells share a complex molecular signature with embryonic stem cells. Hum Mol Genet 17(21):3411-25. doi:10.1093/hmg/ddn235.
20. Sajedi E, Gaston-Massuet C, Signore M, Andoniadou CL, Kelberman D, Castro S, **Etchevers HC**, Gerrelli D, Dattani MT, Martinez-Barbera J.-P. (2008). Analysis of mouse mutants carrying the I26T and R160C substitutions in the transcriptional repressor *HESX1* as models for septo-optic dysplasia and hypopituitarism. Dis Model Mech 2: in press. doi: 10.1242/dmm.000711.
21. de Pontual L, Trochet D, Bourdeaut F, Thomas S, **Etchevers H**, Chompret A, Minard V, Valteau D, Brugières L, Munnich A, Delattre O, Lyonnet S, Janouiex-Lerosey I, Amiel J. (2007). Methylation-associated *PHOX2B* gene silencing is a rare event in human neuroblastoma. Eur J Cancer. 2007 Aug 30; [Epub ahead of print]. doi:10.1016/j.ejca.2007.07.016.
22. Golzio C, Martinovic-Bouriel J, Thomas S, Mougou-Zrelli S, Grattagliano-Bessières B, Bonnière M, Delahaye S, Munnich A, Encha-Razavi F, Lyonnet S, Vekemans M, Attié-Bitach T, **Etchevers HC**. (2007). Matthew-Wood syndrome is caused by truncating mutations in the retinol binding protein receptor gene *STRA6*. Am J Hum Genet. 80(6): 1179-87.
23. **Etchevers HC**, Amiel J, Lyonnet S. (2007). Bases génétiques et moléculaires des neurocristopathies. Arch Pédiatr. 14(6): 668-672. doi:10.1016/j.arcped.2007.02.072.
24. Baala L, Briault S, **Etchevers HC**, Laumonnier F, Natiq A, Amiel J, Boddaert N, Picard C, Sbiti A, Asermouh A, Attie-Bitach T, Encha-Razavi F, Munnich A, Sefiani A, Lyonnet S. (2007). Homozygous silencing of T-box transcription factor *EOMES* leads to microcephaly with polymicrogyria and corpus callosum agenesis. Nat Genet. 39(4):454-6.
25. Martinovic-Bouriel J, Bernabe-Dupont C, Golzio C, Grattagliano-Bessieres B, Malan V, Bonniere M, Esculpavit C, Fallet-Bianco C, Mirlesse V, Le Bidois J, Aubry MC, Vekemans M, Morichon N, **Etchevers H**, Attie-Bitach T, Encha-Razavi F, Benachi A. (2007). Matthew-Wood syndrome: report of two new cases supporting autosomal recessive inheritance and exclusion of *FGF10* and *FGFR2*. Am J Med Genet A. 143(3):219-28.
26. Golzio C, Guirchoun J, Ozilou C, Thomas S, Goudefroye G, Morichon-Delvallez N, Vekemans M, Attie-Bitach T, **Etchevers HC**. (2006). Cytogenetic and histological features of a human embryo with homogeneous chromosome 8 trisomy. Prenat Diagn 26(13):1201-1205.
27. **Etchevers HC**, Amiel J, Lyonnet S (2006). Molecular bases of human neurocristopathies. In: Neural Crest Induction and Differentiation, ed. J.-P. Saint-

Jeannet. Landes Biosciences, Georgetown, TX. ISBN: 1-58706-070-1 (also ISBN : 978-0-387-35136-0 as Adv Exp Med Biol. 2006 589:213-34.)

28. Sanlaville D,* **Etchevers HC**,* Gonzales M,* Martinovic J, Clément-Ziza M, Delezoide A-L, Aubry M-C, Pelet A, Chemouny S, Cruau C, Audollent S, Esculpavit C, Goudefroye G, Ozilou C, Fredouille C, Joye N, Morichon-Delvallez N, Dumez Y, Weissenbach J, Munnich A, Amiel J, Encha-Razavi F, Lyonnet S, Vekemans M, Attié-Bitach T (2006). Phenotypic spectrum of CHARGE syndrome in fetuses with *CHD7* truncating mutations correlates with expression during human development. J Med Genet (doi:10.1136/jmg.2005.036160) 43(3):211-317.

29. Detrait ER, **Etchevers H** (2005). Vascularisation of the head and the neck during embryogenesis. J Neurorad 32(3), 147-56.

30. Deak KL, Boyles AL, **Etchevers HC**, Melvin EC, Siegel DG, Graham FL, Slifer SH, Enterline DS, George TM, Vekemans M, McClay D, Bassuk AG, Kessler JA, Linney E, Gilbert JR, Speer MC; NTD Collaborative Group. (2005) SNPs in the neural cell adhesion molecule 1 gene (*NCAM1*) may be associated with human neural tube defects. Human Genetics. 117(2-3):133-42.

31. Detrait E, George T, **Etchevers H**, Gilbert J, Vekemans M, Speer M (2005). Human neural tube defects: Developmental biology, epidemiology, and genetics. Neurotoxicol Teratol. 27(3):515-24.

32. **Etchevers HC** (2005). Cap „n‟collar family member NF-E2-related factor 3 (*Nrf3*) is expressed in mesodermal derivatives of the developing avian embryo. Int J Dev Biol. 49(2-3):363-67.

33. Cai J, Ash D, Kotch LE, Jabs EW, Attie-Bitach T, Auge J, Mattei G, **Etchevers H**, Vekemans M, Korshunova Y, Tidwell R, Messina DN, Winston JB, Lovett M. (2005). Gene expression in pharyngeal arch 1 during human embryonic development. Hum Mol Genet. 14(7):903-12.

34. Karmous-Benailly H, Martinovic J, Gubler MC, Sirot Y, Clech L, Ozilou C, Auge J, Brahimi N, **Etchevers H**, Detrait E, Esculpavit C, Audollent S, Goudefroye G, Gonzales M, Tantau J, Loget P, Joubert M, Gaillard D, Jeanne-Pasquier C, Delezoide AL, Peter MO, Plessis G, Simon-Bouy B, Dollfus H, Le Merrer M, Munnich A, Encha-Razavi F, Vekemans M, Attie-Bitach T. (2005). Antenatal presentation of Bardet-Biedl syndrome may mimic Meckel syndrome. Am J Hum Genet. Mar;76(3):493-504.

35. Trueba SS, Auge J, Mattei G, **Etchevers H**, Martinovic J, Czernichow P, Vekemans M, Polak M, Attie-Bitach T. (2005). *PAX8*, *TITF1*, and *FOXE1* gene expression patterns during human development: new insights into human thyroid development and thyroid dysgenesis-associated malformations. J Clin Endocrinol Metab. 90:455-62.

36. Pinson, L., Augé, J., Audollent, S., Mattei, G., **Etchevers, H.**, Gigarel, N., Razavi, F., Lacombe, D., Odent, S., Le Merrer, M., Amiel, J., Munnich, A., Meroni, G., Lyonnet, S., Vekemans, M., Attié-Bitach, T. (2004) Embryonic expression of the human MID1 gene and its mutations in Opitz syndrome. Journal of Medical Genetics 41(5):381-6.

37. **Etchevers HC** (2003) Vasculo- and angiogenesis in the head and neck. Rivista di Neuroradiologia 16 : 735-8.

38. Amiel, J., Laudier, B., Attié-Bitach, T., Trang, H., De Pontual, L., Gener, B., Trochet, D., **Etchevers, H**., Ray, P., Simonneau, M., Vekemans, M., Munnich, A., Gaultier, C., Lyonnet, S. (2003). Polyalanine expansion and frameshift mutations of the paired-like homeobox gene *PHOX2B* in congenital central hypoventilation syndrome. Nat Genet 33: 459-61.

39. **Etchevers HC** (2003) Early expression of hypoxia-inducible factor 1a in the chicken embryo. Gene Expression Patterns 3:49-52.

Published (pre-doctoral work):

40. **Etchevers HC**, Couly G, Le Douarin NM (2002) Morphogenesis of the branchial vascular sector. Trends in Cardiovascular Medicine 12: 299-304.

41. **Etchevers HC**, Vincent C, Couly GF (2001) Neural crest and pituitary development. Dans Hypothalamic-Pituitary Development: Genetic and Clinical Aspects. R. Rappaport, ed. S. Karger AG, Bâle, Suisse, 13-29.

42. **Etchevers HC**, Vincent C, Le Douarin NM, Couly GF (2001) The cephalic neural crest provides pericytes and smooth muscle cells to all blood vessels of the face and forebrain. Development 128: 1059-1068.

43. Duprez D, Leyns L, Bonnin M-A, Lapointe F, **Etchevers H**, De Robertis EM, Le Douarin N (1999) Expression of *Frzb-1* during chick development. Mechanisms of Development 89: 179-183.

44. **Etchevers HC**, Couly G, Vincent C, Le Douarin NM (1999) Anterior cephalic neural crest is required for forebrain viability. Development 126: 3533-3543.

OTHER COMMUNICATIONS

Oral presentations at conferences based on work in which I participated (asterisk = presenter):

60th annual meeting of the American Society for Human Genetics, 2-6 November 2010, Washington, D.C.

- N Chassaing, S Sorrentino*, A Iacovelli, D Martin-Coignard, P McGuire, O Faye-Petersen, F Encha-Razavi, L Lequeux, A Vigouroux, P Calvas, P Loget, G Santiago, PJ Taub, A Greenberg, HC Etchevers, E Rose, CL Mercer, EW Jabs. Mutations in the OTX2 gene are involved in Otocephaly-Dysgnathia.

- S. Thomas, F.Encha-Razavi, L. Devisme, H. Etchevers, B. Bessière, G. Goudefroye, N. Elkhartoufi, A. Ichkou, M. Bonnière, P. Marcorelle, P. Parent, S. Manouvrier, M. Holder, A. Laquerrière, L. Loeuillet, J. Roume, J. Martinovic, S. Mougou-Zerelli, M. Gonzales, P. Wookey, V. Meyer, C. Boyle Feysot, P. Nitschke, N.Leticee, A. Munnich, S. Lyonnet, G. Guapay, B. Folliguet, M. Vekemans, T. Attié-Bitach*. Next-Generation Sequencing of a 4.1 Mb Linkage Interval Reveals FLVCR2 Deletions and Mutations in Lethal Cerebral Vasculopathy (Fowler Syndrome).

5èmes Assises de Génétique Humaine et Médicale, 28-30 Janvier 2010, Strasbourg, France

- S. Benko*, J.A. Fantes, J. Amiel, D.J. Kleinjan, J. Ramsay, N. Jamshidi, A. Essafi, V. Abadie, M. Holder-Espinasse, H. Roest Crollius, H. Etchevers, A. Munnich, A.

Pelet , P.G. Farlie, D.R. FitzPatrick, S. Lyonnet. Altérations génomiques à grande distance (>1,4 Mb) et dérégulation tissu-spécifique au locus SOX9.

- S. Thomas, C. Thauvin-Robinet, C. Gomes , E. Escudier, B. Aral, J. Amiel, H. Etchevers, N. Boddaert, L. Faivre, L. Burglen, S. Lyonnet, M. Vekemans, T. Attié-Bitach*. Mutations du gène OFD1 dans les ciliopathies chez le garçon : syndrome de Joubert avec obésité, polydactylie et anomalies respiratoires.

- S. Thomas, L. De Pontual, N.A. Zaghloul, E.E. Davis, D.M. McGaughey, H. Dollfus, C. Baumann, S.L. Bessling, C. Babarit , A. Pelet , C. Gascue, P. Beales, A. Munnich, S. Lyonnet, H.C. Etchevers, T. Attie-Bitach, J.L. Badano, A.S. McCallion, N. Katsanis, J. Amiel*. La maladie de Hirschsprung dans les ciliopathies a révélé le rôle du cil primaire dans le développement normal du système nerveux entérique.

European Human Genetics Conference, 23-26 May 2009, Vienna, Austria.

- J. Amiel*, L. De Pontual, S. Thomas, N. A. Zaghloul, D. M. McGaughey, E. E. Davis, H. Dollfus, C. Baumann, S. L. Bessling, S. Audollent, A. Pelet, P. Beales, A. Munnich, S. Lyonnet, H. C. Etchevers, M. Vekemans,T. Attié-Bitach, A. S. McCallion, N. Katsanis. The association of Bardet-Biedl syndrome and Hirschsprung disease highlights the role of the primary cilium in ENS development.

American Society for Human Genetics 58th annual meeting, 11-15 November 2008, Philadelphia, PA, USA

- S. Boissel*, O. Reish, F. Molinari, N. Kadhom, C. Golzio, H. Etchevers, A. Munnich, L. Colleaux. Homozygous R316Q mutation in the obesity-associated FTO gene causes a severe polymalformative syndrome.

4èmes Assises de Génétique Humaine et Médicale 17-19 janvier 2008 Lille, France

- S. Benko*, J. A. Fantes , J. Amiel , S. Heaney , S. Thomas, J. Ramsay , N. Jamshidi, D.-J. Kleinjan, C. T. Gordon, D. McBride , C. Golzio , N. McGill , P. Perry , V. Abadie, C. Ayuso, M. Holder-Espinasse, N. Kilpatrick, M. M. Lees, I. K. Temple, P. Thomas, M.-P. Vazquez, M. Vekemans , H. Roest-Crollius, A. Munnich, A. Pelet , P. Farlie, H. Etchevers, D. R. FitzPatrick, S. Lyonnet. Mutations de sequences non codantes hautement conserves à grande distance (> 1,2 Mb) de part et d"autre du locus SOX9 dans la sequence de Pierre-Robin.

- C. Golzio*, N. Chassaing, J. Martinovic-Bouriel, S. Thomas, S. Zrelli, B. Grattagliano-Bessières, S. Odent, M. Bonnière, S. Delahaye, A. Munnich, F. Encha-Razavi, S. Lyonnet, M. Vekemans, T. Attié-Bitach, P. Calvas, H. Etchevers. Spectre clinique des mutations du gène STRA6 : du syndrome de Matthew-Wood à une microphtalmie syndromique non létale.

3e Assises de Génétique Humaine – Montpellier 26-28 janvier 2006.

- D. Sanlaville*, H. Etchevers, D. Genevieve, V. Abadie, C. Baumann, D. Bonnet, H. Dollfus, L. Faivre, P. Hubert,M. Gonzales, D. Lacombe, J. Martinovic, S. Marlin, J. Roume, A. Toutain, Y. Dumez, A. Munnich, F. Encha-Razavi , M. Vekemans, J. Amiel, T. Attié-Bitach, S. Lyonnet Spectre des mutations du gène CHD7 dans le syndrome CHARGE et profil d"expression au cours du développement.

37 poster presentations at international conferences since 2001.

RESEARCH THEMES

Neural crest fate determination

The over-arching theme of my work has been to identify molecular hallmarks and improve the physiopathological understanding of congenital and progressive conditions implicating a highly plastic embryological cell population known as the neural crest. These neural crest cells (NCC) participate directly or indirectly in the formation of a stunning array of tissues organs during embryogenesis. When the genes regulating the differentiation, proliferation, or migratory and appropriately invasive behavior of NCC are muted, this can lead to associations of pediatric congenital malformations or tumorigenesis. I make use of avian and, more recently, murine models, as well as careful observations effected on tissues derived from normal human embryos, to tease apart those mechanisms.

My Ph.D. thesis concerned the contributions of transitory progenitor cell subpopulations to the developing vertebrate embryo. The first part, which was never published, demonstrated that limited deletions of the neural folds along the dorso-ventral axis only appeared to lead to regeneration of NCC at points where non-neural ectoderm contacts the remaining neuroectoderm, as the published dogma was at the time and remains, to a large extent, today. Indeed, the story is more nuanced than we understood at the time, and gradients of either morphogenetic signals or, more likely, the capacity of neuroepithelial cells to respond and initiate transdifferentiation into neural crest make the assignment of a positional and temporal limit to the *de novo* induction of NCC difficult if not impossible to resolve.

Nonetheless, I established that there were points along the dorsoventral axis at which the neuroepithelium would not respond to the contact of non-neural ectoderm by expressing markers of NCC specification, and that the resultant central nervous system, at least with respect to the hindbrain, clearly did not regenerate at all. Thus, the dominant hypothesis in the field, that the entire dorsoventral gradient was respecified in the residual tissue and led thereby to the regeneration of neural crest cells, was incorrect. In addition, it showed me the limitations of the use of a small palette of molecular markers to define a cell population.

The more fruitful part of my Ph.D. work concerned, first, ablation of more rostral neural folds in the chicken embryo. The resultant embryos not only had brain malformations as expected from the earlier work at the level of the rhombencephalon, but also a striking craniofacial phenotype ranging from maxillary hypoplasia, hypotelorism and synophthalmia to cyclopia and aprosencephaly. This last was surprising, since the neural folds corresponding to the prosencephalon, future territory of the diencephalon and telencephalon, had been left intact by the intervention. These observations have laid the groundwork for other researchers to continue to explore the trophic molecular cross-talk between NCC and the tissues into which these cells integrate during development, and is a theme to which I return repeatedly in my ongoing and future projects.

At this point, I returned to an interesting observation on the replacement of these ablated neural folds in the chicken by the equivalent tissue from a stage-matched quail donor. Making use of the powerful chimera fate-mapping tool that had been developed and exploited by my advisor, Nicole Le Douarin, and her many collaborators, I took a closer look at the cephalic and particularly vascular derivatives of NCC. I demonstrated the existence of a discrete vascular sector in which all non-endothelial components of blood vessel walls were constituted by NCC precursors. In addition, the original anterioposterior position of the NCC predicted its distoproximal location within the arboresence of that sector. In this way, I identified a cryptic axis in the highly dynamic cardiovascular system that had implications for capillary and arteriovenous malformations. I continue to be interested in this cellular interaction over the years, and in particular, in the role of the NCC derivative in most intimate juxtaposition to the vascular endothelium within this rostral sector, known as the pericyte. These cells, of NCC origin in the head, but of mesodermal origin elsewhere in the body, retain multipotency late in life. This property perhaps renders them uniquely susceptible to the effects of somatic mutations occurring during mid- to late gestation, especially if they take place on a predisposing genetic heritage. Recent research on Parkes-Weber and Sturge-Weber syndromes and other capillary malformations tend to support this hypothesis (Limaye, Boon, and Vikkula 2009).

The concept of pathogenesis of localized, apparently sporadic congenital malformations through a two-step mutation mechanism is one I continue to actively explore in the context of a pure and indiscutable neurocristopathy, the giant congenital melanocytic nevus (see Future Projects).

Through a desire to apply my knowledge about NCC differentiation to understanding the etiologies of human pathologies, I joined an INSERM research group in the Department of Genetics at the Necker Children‟s Hospital in Paris. Here, I had the opportunity to develop an original project in which I wished to study the transcriptome and alterations therein of human NCC. This ambitious approach attracted the approval of the new Avenir startup program that had been established by the INSERM, which supported the creation of my own research group over a three-year period. By these means, I was able to attract and provide research subjects to students and postdocs in an extraordinarily collaborative and fecund intellectual environment. This was enriched by the reference center aspect of our department, which brought me into contact with doctors discussing a rich and inspiring variety of rare pediatric genetic diseases, as well as with the patients themselves. In this way, I contributed my perspective and skills to studies concerning congenital malformations that had only a tangential neurocristopathic component, such as the cerebral proliferative vasculopathy known as Fowler syndrome; or cardiopathies not only involving the NCC-invested outflow tract but also *situs inversus*; or the Matthew-Wood syndrome.

Developmental biology being a parsimonious field, and co-option of gene function being the rule rather than the exception (Meulemans and Bronner-Fraser 2005), the molecular pathways I have studied in these apparently disparate conditions have invariably been of

interest in the study of normal and pathological NCC fate determination. Thus I have found that the diversity of projects in which I have been involved has permitted unexpected synergies, and my research group will never lack for subjects as a result.

RELATED PAPERS:

Etchevers HC. Primary culture of chick, mouse or human neural crest cells. Nat Protoc. Accepted 14 June 2011.

de Pontual L*, Zaghloul NA*, Thomas S*, Davis EE, McGaughey DM, Dollfus H, Baumann C, Bessling SL, Babarit C, Pelet A, Gascue C, Beales P, Munnich A, Lyonnet S, **Etchevers H**, Attie-Bitach T, Badano JL, McCallion AS, Katsanis N, Amiel J. (2009). Epistasis between *RET* and *BBS* mutations modulates enteric innervation and causes syndromic Hirschsprung disease. Proc Natl Acad Sci U S A 2009 Aug 18;106(33):13921-6. doi: 10.1073/pnas.0901219106

Thomas S, Thomas M, Wincker P, Xu P-T, Speer MC, Munnich A, Lyonnet S, Vekemans M, **Etchevers HC**. (2008). Human neural crest cells share a complex molecular signature with embryonic stem cells. Hum Mol Genet 17(21):3411-25. doi:10.1093/hmg/ddn235.

de Pontual L, Trochet D, Bourdeaut F, Thomas S, **Etchevers H**, Chompret A, Minard V, Valteau D, Brugières L, Munnich A, Delattre O, Lyonnet S, Janouiex-Lerosey I, Amiel J. (2007). Methylation-associated *PHOX2B* gene silencing is a rare event in human neuroblastoma. Eur J Cancer. 2007 Aug 30; [Epub ahead of print]. doi:10.1016/j.ejca.2007.07.016.

Etchevers HC, Amiel J, Lyonnet S. (2007). Bases génétiques et moléculaires des neurocristopathies. Arch Pédiatr. 14(6): 668-672. doi:10.1016/j.arcped.2007.02.072.

Etchevers HC, Amiel J, Lyonnet S (2006). Molecular bases of human neurocristopathies. In: Neural Crest Induction and Differentiation, ed. J.-P. Saint-Jeannet. Landes Biosciences, Georgetown, TX. ISBN: 1-58706-070-1 (also ISBN : 978-0-387-35136-0 as Adv Exp Med Biol. 2006 589:213-34.)

Etchevers HC, Amiel J, Lyonnet S. (2007). Bases génétiques et moléculaires des neurocristopathies. Arch Pédiatr. 14(6): 668-672. doi:10.1016/j.arcped.2007.02.072.

Etchevers HC (2003) Vasculo- and angiogenesis in the head and neck. Rivista di Neuroradiologia 16 : 735-8.

Etchevers HC, Couly G, Le Douarin NM (2002) Morphogenesis of the branchial vascular sector. Trends in Cardiovascular Medicine 12: 299-304.

Etchevers HC, Vincent C, Couly GF (2001) Neural crest and pituitary development. Dans Hypothalamic-Pituitary Development: Genetic and Clinical Aspects. R. Rappaport, ed. S. Karger AG, Bâle, Suisse, 13-29.

Etchevers HC, Vincent C, Le Douarin NM, Couly GF (2001) The cephalic neural crest provides pericytes and smooth muscle cells to all blood vessels of the face and forebrain. Development 128: 1059-1068.

Etchevers HC, Couly G, Vincent C, Le Douarin NM (1999) Anterior cephalic neural crest is required for forebrain viability. Development 126: 3533-3543.

GENE EXPRESSION IN THE AVIAN EMBRYO

During the early years of my postdoc, I published a few gene expression papers designed to offer insight as to the function of certain proteins over the course of development. These are the building blocks for embryologists through which they can elaborate hypotheses as to the sequence of events leading to differentiation and morphogenesis. I remain interested in the role of hypoxia in the remodeling of the pharyngeal arch arteries as they branch off the great vessels of the outflow tract, and intrigued by the genomic localization and perhaps concomitant transcriptional regulation of *Nrf3* with the nearby *Hox* gene cluster, in particular in the heart.

RELATED PAPERS:

Etchevers HC (2005). Cap „n‟collar family member NF-E2-related factor 3 (*Nrf3*) is expressed in mesodermal derivatives of the developing avian embryo. Int J Dev Biol. 49(2-3):363-67.

Etchevers HC (2003) Early expression of hypoxia-inducible factor 1α in the chicken embryo. Gene Expression Patterns 3:49-52.

Duprez D, Leyns L, Bonnin M-A, Lapointe F, **Etchevers H**, De Robertis EM, Le Douarin N (1999) Expression of *Frzb-1* during chick development. Mechanisms of Development 89: 179-183.

GENE EXPRESSION IN THE HUMAN EMBRYO AND FETUS

I have applied the expertise gained in embryos of amniotes to intimately study the anatomy of the human embryo during the third to twelfth weeks of gestation, within the legal window for the termination of pregnancy and the donation of embryonic tissues to research. This has also acquainted me with French, American and European bioethical legislation governing the oversight of acquiring such delicate material.

Just before I arrived for my postdoc, the group directed by Michel Vekemans, with years of experience in fetal pathology, cytogenetics and the study of normal gene expression in human embryos, and the group directed by Stanislas Lyonnet, studying the molecular genetics of neurocristopathies, had recently combined. The project I designed, to derive

human NCC and study their molecular characteristics before and after differentiation, was integrally dependent on both poles.

Over the years, I slowly helped and then assumed much of the responsibility from Tania Attié-Bitach, in managing the human embryo collection so critical for our research. The rare and precious nature of these materials meant that every tissue was conserved and exploited, even if not immediately useful in the frame of the research projects underway. Conservation took the form of freezing microdissected primordia or fixing and processing whole embryos for the sparing use of sections for *in situ* hybridization and immunohistochemistry. Exploitation took the form of participating in numerous collaborations, in particular with members of our research unit, in which the spatiotemporal localization of a given gene transcript could provide clues as to its function during human development. Our ability to demonstrate and interpret expression results was highly sought after by collaborators who had identified genes for congenital malformations both locally and from around the world.

For organizational reasons, the supply of embryos tapered off in Paris. They had been supplied by the Orthogenics Service of the Broussais Hospital, one of the rare clinics in which they encouraged women who had undergone the RU486 abortion protocol to remain through the period of expulsion, to accompany them and intervene in the rare cases of complications. The expelled material could then be donated to research. In 2001 a law was voted and applied in 2004, whereby women could undergo the protocol accompanied by their general physician and no longer through specialized clinics. Since we were not routinely managing materials obtained by the aspiration technique, due to their often being older first-trimester abortions not eligible for the RU486 protocol, we continued to make use of earlier banked tissues for our studies.

During the period 2006-2009, I continued to manage my research subgroup in Paris, but also worked part-time with a team studying the genetic bases of diseases affecting the anterior chamber of the eye, run by the ophthalmologist François Malecaze and the geneticist Patrick Calvas in Toulouse. The immediate justification was related to the work we had recently conducted on candidate genes involved in the polymalformative Matthew-Wood syndrome (discussed further below).

In order to carry out work identifying new candidate genes for severe micro-/anopthalmia (MAO), Nicolas Chassaing and I undertook the identification of genomic targets of four transcription factors already known to be implicated in human isolated or syndromic MAO. This work is still ongoing in Toulouse, but entailed the establishment of a new source of human embryonic tissues and a distinct request to the French Agency for Biomedicine, which was approved in 2008.

RELATED PAPERS:

Golzio C, Havis E, Daubas P, Nuel G, Babarit C, Munnich A, Vekemans M, Zaffran S, Lyonnet S, **Etchevers HC**. ISL1 is a major orchestrator of morphogenetic signaling pathways in the embryonic human heart.

Cluzeau C, Mou C, Bal E, Benko S, Babarit C, Overbeek P, Perret C, Memet S, Courtois G, Lyonnet S, **Etchevers H**, Mikkola M, Munnich A, Headon D, Smahi A. Down-regulation of Wnt/β-catenin signalling by Edar involves Hipk2, a new NF-κB target gene.

van der Werf C, Wabbersen T, Hsiao NH, Parades J, **Etchevers H**, Kroise P, Tibboel D, Babarit C, Schreiber R, Hoffenberg E, Vekemans M, Zeder S, Ceccherini I, Lyonnet S, Ribeiro A, Seruca R, te Meerman G, Ijzendoorn S, Shepherd I, Verheij J, Hofstra RMW. Mutations in *CLMP* cause Congenital Short Bowel Syndrome, pointing to the major role of CLMP in intestinal development. Gastroenterology.

de Pontual L, Kettaneh D, Gordon CT, Oufadem M, Boddaert N, Lees M, Balu L, Lachassinne E, Petros A, Mollet J, Wilson LC, Munnich A, Brugière L, Delattre O, Vekemans M, **Etchevers H**, Lyonnet S, Janoueix-Lerosey I, Amiel J. (2011) Germline gain-of-function mutations of *ALK* disrupt central nervous system development. Human Mutation, 32: 272–276. doi: 10.1002/humu.21442

Cognet M, Nougayrede A, Malan V, Callier P, Cretolle C, Faivre L, Genevieve D, Goldenberg A, Heron D, Mercier S, Philip N, Sigaudy S, Verloes A, Sarnacki S, Munnich A, Vekemans M, Lyonnet S, **Etchevers H**, Amiel J, de Pontual L. (2011) Dissection of the *MYCN* locus in Feingold syndrome and isolated oesophageal atresia. Eur J Hum Genet. 2011 Jan 12 doi:10.1038/ejhg.2010.225

Thomas S, Encha-Razavi F, Devisme L, **Etchevers H**, Bessières-Grattagliano B, Goudefroye G, Elkhartoufi N, Pateau E, Ichkou A, Bonnière M, Marcorelle P, Parent P, Manouvrier S, Holder M, Laquerrière A, Loeuillet L, Roume J, Martinovic J, Mougou-Zerelli S, Gonzales M, Meyer V, Wessner M, Bole-Feysot C, Nitschke P, Leticee N, Munnich A, Lyonnet S, Wookey P, Gyapay G, Foliguet B, Vekemans M, Attié-Bitach T. (2010) High-Throughput Sequencing of a 4.1 Mb Linkage Interval Reveals *FLVCR2* Deletions and Mutations in Lethal Cerebral Vasculopathy. Hum Mut Hum Mut 31(10):1134-41.

Chaabouni M, **Etchevers H**, De Blois MC, Calvas P, Waill-Perrier MC, Vekemans M, Romana SP. (2010) Identification of the *IRX B* genes cluster as candidate genes in severe dysgenesis of the ocular anterior segment. Invest Ophthalmol Vis Sci 51(9):4380-6..

de Pontual L*, Zaghloul NA*, Thomas S*, Davis EE, McGaughey DM, Dollfus H, Baumann C, Bessling SL, Babarit C, Pelet A, Gascue C, Beales P, Munnich A, Lyonnet S, **Etchevers H**, Attie-Bitach T, Badano JL, McCallion AS, Katsanis N, Amiel J. (2009). Epistasis between *RET* and *BBS* mutations modulates enteric innervation and causes syndromic Hirschsprung disease. Proc Natl Acad Sci U S A 2009 Aug 18;106(33):13921-6. doi: 10.1073/pnas.0901219106

Bessières-Grattagliano B, Foliguet B, Devisme L, Loeuillet L, Marcorelles P, Bonnière M, Laquerrière A, Fallet-Bianco C, Martinovic J, Zrelli S, Leticee N, Cayol V, **Etchevers HC**, Vekemans M, Attie-Bitach T, Encha-Razavi F. (2009). Refining the

clinicopathological pattern of cerebral proliferative glomeruloid vasculopathy (Fowler syndrome): Report of 16 fetal cases. Eur J Med Genet 52(6):386-92. Epub 2009 Jul 25.

Boissel S, Reish O, Proulx K, Kawagoe-Takaki H, Sedgwick B, Yeo GS, Meyre D, Golzio C, Molinari F, Kadhom N, **Etchevers HC**, Saudek V, Farooqi IS, Froguel P, Lindahl T, O'Rahilly S, Munnich A, Colleaux L. (2009). Loss-of-function mutation in the dioxygenase-encoding *FTO* gene causes severe growth retardation and multiple malformations. Am J Hum Genet 85:106-11.

de Pontual L, Mathieu Y, Golzio C, Rio M, Malan V, Boddaert N, Soufflet C, Picard C, Durandy A, Dobbie A, Heron D, Isidor B, Motte J, Newburry-Ecob R, Pasquier L, Tardieu M, Viot G, Jaubert F, Munnich A, Colleaux L, Vekemans M, **Etchevers H**, Lyonnet S, Amiel J. (2009). Mutational, functional, and expression studies of the *TCF4* gene in Pitt-Hopkins syndrome. Hum Mutat 30(4):669-76.

Benko S, Fantes JA, Amiel J, Kleinjan D-J, Thomas S, Ramsay J, Jamshidi N, Essafi A, Heaney S, Gordon CT, McBride D, Golzio C, Fisher M, Perry P, Abadie V, Ayuso C, Holder-Espinasse M, Kilpatrick N, Lees MM, Picard A, Temple IK, Thomas P, Vazquez M-P, Vekemans M, Crollius HR, Hastie ND, Munnich A, **Etchevers HC**, Pelet A, Farlie PG, FitzPatrick DR, Lyonnet S. (2009). Highly conserved non-coding elements on either side of *SOX9* associated with Pierre Robin sequence. Nat Genet 41(3):359-64. doi:10.1038/ng.329.

Sajedi E, Gaston-Massuet C, Signore M, Andoniadou CL, Kelberman D, Castro S, **Etchevers HC**, Gerrelli D, Dattani MT, Martinez-Barbera J.-P. (2008). Analysis of mouse mutants carrying the I26T and R160C substitutions in the transcriptional repressor *HESX1* as models for septo-optic dysplasia and hypopituitarism. Dis Model Mech 2: in press. doi: 10.1242/dmm.000711.

Baala L, Briault S, **Etchevers HC**, Laumonnier F, Natiq A, Amiel J, Boddaert N, Picard C, Sbiti A, Asermouh A, Attie-Bitach T, Encha-Razavi F, Munnich A, Sefiani A, Lyonnet S. (2007). Homozygous silencing of T-box transcription factor *EOMES* leads to microcephaly with polymicrogyria and corpus callosum agenesis. Nat Genet. 39(4):454-6.

Karmous-Benailly H, Martinovic J, Gubler MC, Sirot Y, Clech L, Ozilou C, Auge J, Brahimi N, **Etchevers H**, Detrait E, Esculpavit C, Audollent S, Goudefroye G, Gonzales M, Tantau J, Loget P, Joubert M, Gaillard D, Jeanne-Pasquier C, Delezoide AL, Peter MO, Plessis G, Simon-Bouy B, Dollfus H, Le Merrer M, Munnich A, Encha-Razavi F, Vekemans M, Attie-Bitach T. (2005). Antenatal presentation of Bardet-Biedl syndrome may mimic Meckel syndrome. Am J Hum Genet. Mar;76(3):493-504.

Trueba SS, Auge J, Mattei G, **Etchevers H**, Martinovic J, Czernichow P, Vekemans M, Polak M, Attie-Bitach T. (2005). *PAX8*, *TITF1*, and *FOXE1* gene expression patterns during human development: new insights into human thyroid development and thyroid dysgenesis-associated malformations. J Clin Endocrinol Metab. 90:455-62.

Pinson, L., Augé, J., Audollent, S., Mattei, G., **Etchevers, H.**, Gigarel, N., Razavi, F., Lacombe, D., Odent, S., Le Merrer, M., Amiel, J., Munnich, A., Meroni, G., Lyonnet, S., Vekemans, M., Attié-Bitach, T. (2004) Embryonic expression of the human MID1 gene and its mutations in Opitz syndrome. Journal of Medical Genetics 41(5):381-6.

Amiel, J., Laudier, B., Attié-Bitach, T., Trang, H., De Pontual, L., Gener, B., Trochet, D., **Etchevers, H**., Ray, P., Simonneau, M., Vekemans, M., Munnich, A., Gaultier, C., Lyonnet, S. (2003). Polyalanine expansion and frameshift mutations of the paired-like homeobox gene *PHOX2B* in congenital central hypoventilation syndrome. Nat Genet 33: 459-61.

HUMAN ORGANOGENESIS

EYE

As mentioned above, I have had some interest in the anterior chamber of the eye and its relationship to the appropriate formation of the cartilaginous sclera and its underlying choroid plexus, all of which are cephalic NCC derivatives, ever since my Ph.D. This area is a rich source of NCC-derived pericytes, and is affected by the absence of NCC by the two ocular primordial and their surrounding tissues fusing. Incidentally, my work in isolating vascular pericytes from this capillary plexus was hampered by the presence of numerous melanocytes I had also given annual courses in eye development to resident ophthalmologists since 2001.

When a fetal pathology staff meeting at Necker in 2006 discussed a case with diaphragmatic hernia and absence of lungs, associated with bilateral clinical anophthalmia and a family history, and this was shortly followed by the discussion of a second similar case from the Institut de Puériculture, the embryologist in me had enough confidence to suggest examining a candidate gene coding the morphogen FGF10, based on what I knew of some overlapping features in the mouse knockout phenotype. We did this first by establishing the normal expression pattern of *FGF10* and its cognate receptor *FGFR2* in the human embryo during embryogenesis of the affected organ systems (both cases had atresic or absent pulmonary arteries and the second, a ventricular septal defect). We then sequenced both genes (and excluded coding mutations) in these patients.

At that time, multiple French research groups were interested in this clinical association, from the perspective of different affected organ systems. This interest led our group to discussions with Fanny Bajolle, Stéphane Zaffran, and Margaret Buckingham from the Institut Pasteur and Fanny‟s chief of service in pediatric cardiology at Necker hospital, Damien Bonnet, because of the heart implications and their ongoing work on the role of Fgf10 in outflow tract development; with Patrick Calvas and Nicolas Chassaing for their interest in transcription factors responsible for micro-/anophthalmia and the idea that in their cohort, they may have postnatal examples of the same broad spectrum; and with the interests one of the local fetal pathologists (Jelena Martinovic) in congenital

diaphragmatic hernia. My Ph.D. student, Christelle Golzio, was particularly interested in the cardiac side of the story as well, leading to the development of collaborative projects concerning cardiovascular development in the human embryo and implications for congenital heart defect patients treated at Necker (discussed below).

In the end, we and others (Pasutto et al. 2007) identified mutations in the *STRA6* gene in Matthew-Wood patients , a protein necessary for the normal transfer of fat-soluble vitamin A into the cytoplasm (Kawaguchi et al. 2007) and to an intracellular carrier for further metabolism to the nuclear transcriptional signal, retinoic acid. Many organ systems are exquisitely sensitive to dosage fluctuations in the pool of retinoic acid during susceptible windows in development, including the major ones most often affected in this syndromic microphthalmia: eyes, heart, lungs, diaphragm and gut (Niederreither and Dolle 2008) . This paved the way for reflection on how retinoic acid might interact with genes implicated in human anophthalmia such as *PAX6*, *RAX*, *SOX2* or *OTX2* (work continues on retinoic acid-induced Rax-expressing embryonic stem cells in Toulouse) (Danno et al. 2008); or other ocular defects such as *CHD7* (involved in a syndromic coloboma also affecting heart development) (Bajpai et al. 2010) given their spatiotemporal overlap in these sites, and more generally on the transcriptional regulation of *FGF10* (Desai et al. 2004).

RELATED PAPERS:

Chaabouni M, **Etchevers H**, De Blois MC, Calvas P, Waill-Perrier MC, Vekemans M, Romana SP. (2010) Identification of the *IRX B* genes cluster as candidate genes in severe dysgenesis of the ocular anterior segment. Invest Ophthalmol Vis Sci 51(9):4380-6.

Chassaing N, Golzio C, Odent S, Lequeux L, Vigouroux A, Martinovic-Bouriel J, Tiziano FD, Masini L, Piro F, Maragliano G, Delezoide AL, Attié-Bitach T, Manouvrier-Hanu S, **Etchevers HC**, Calvas P. (2009). Phenotypic spectrum of *STRA6* mutations: from Matthew-Wood syndrome to non-lethal anophthalmia. Hum Mutat 30(5):E673-81.

Lequeux L, Rio M, Vigouroux A, Titeux M, **Etchevers H**, Malecaze F, Chassaing N, Calvas P. (2008). Confirmation of *RAX* gene involvement in human anophthalmia. Clin Genet 74:392-5.

Golzio C, Martinovic-Bouriel J, Thomas S, Mougou-Zrelli S, Grattagliano-Bessières B, Bonnière M, Delahaye S, Munnich A, Encha-Razavi F, Lyonnet S, Vekemans M, Attié-Bitach T, **Etchevers HC**. (2007). Matthew-Wood syndrome is caused by truncating mutations in the retinol binding protein receptor gene *STRA6*. Am J Hum Genet. 80(6): 1179-87.

Martinovic-Bouriel J, Bernabe-Dupont C, Golzio C, Grattagliano-Bessieres B, Malan V, Bonniere M, Esculpavit C, Fallet-Bianco C, Mirlesse V, Le Bidois J, Aubry MC, Vekemans M, Morichon N, **Etchevers H**, Attie-Bitach T, Encha-Razavi F, Benachi A. (2007). Matthew-Wood syndrome: report of two new cases supporting autosomal

recessive inheritance and exclusion of *FGF10* and *FGFR2*. Am J Med Genet A. 143(3):219-28.

Sanlaville, D.*, **Etchevers, HC.***, Gonzales, M.*, Martinovic, J., Clément-Ziza, M., Delezoide, A.-L., Aubry, M.-C., Pelet, A., Chemouny, S., Cruau, C., Audollent, S., Esculpavit, C., Goudefroye, G., Ozilou, C., Fredouille, C., Joye, N., Morichon-Delvallez, N., Dumez, Y., Weissenbach, J., Munnich, A., Amiel, J., Encha-Razavi, F., Lyonnet, S., Vekemans, M., Attié-Bitach, T. (2006) Phenotypic spectrum of CHARGE syndrome in fetuses with *CHD7* truncating mutations correlates with expression during human development. J Med Genet 43(3):211-317.

NEURAL TUBE

Interestingly, one of the postnatal cases we identified with *STRA6* mutations in Matthew-Wood syndrome presented a spinal bifida occulta, which has in animal models been one of the many signs associated with vitamin A deficiency.

I return on occasion to an ongoing interest in neural tube closure and brain and spinal cord anatomical morphogenesis developed in the early years of my Ph.D. By combining that interest with new expertise in human embryology and a highly fruitful collaboration cut short by the untimely death of the geneticist Marcy Speer (Duke University Medical Center), I was able to make limited contributions to understanding the process and one of the molecular players involved in the less extreme but far more common forms of human neural tube closure defects. Collaboration continues slowly but surely with the group of John Gilbert, now at the Hussman Institute for Human Genomics at the Miami University School of Medicine. One paper, being written up, involves the differential transcriptome established by use of the sensitive Serial Analysis of Gene Expression (SAGE) technique, of human neural tubes at four spatiotemporal points immediately following neural tube closure. Another topic, in continued three-way collaboration with the group of Stanislas Lyonnet at the Necker Children‟s Hospital, makes use of high-throughput genomics technologies to pinpoint the genetic bases of an unrelated congenital malformation syndrome.

Chassaing N, Golzio C, Odent S, Lequeux L, Vigouroux A, Martinovic-Bouriel J, Tiziano FD, Masini L, Piro F, Maragliano G, Delezoide AL, Attié-Bitach T, Manouvrier-Hanu S, **Etchevers HC**, Calvas P. (2009). Phenotypic spectrum of *STRA6* mutations: from Matthew-Wood syndrome to non-lethal anophthalmia. Hum Mutat 30(5):E673-81.

Deak KL, Boyles AL, **Etchevers HC**, Melvin EC, Siegel DG, Graham FL, Slifer SH, Enterline DS, George TM, Vekemans M, McClay D, Bassuk AG, Kessler JA, Linney E, Gilbert JR, Speer MC; NTD Collaborative Group. (2005) SNPs in the neural cell adhesion molecule 1 gene (*NCAM1*) may be associated with human neural tube defects. Human Genetics. 117(2-3):133-42.

Detrait E, George T, **Etchevers H**, Gilbert J, Vekemans M, Speer M (2005). Human neural tube defects: Developmental biology, epidemiology, and genetics. Neurotoxicol Teratol. 27(3):515-24.

BLOOD VESSELS AND HEART

The outflow tract of the heart starts as a two-dimensional sheet, which remodels to form a tube, like so many other embryonic primordia. I have been interested in its continuous distal aspect, the branchial vascular sector, since my Ph.D. This interest has brought me into contact with the dynamic discipline of interventional neuroradiology, in which a fascinating variety of natural anatomical variations in the blood vessels irrigating the central nervous system, particularly complex in the head, are present in the pool of patients seeking treatment (Krings et al. 2007). It is around the major arteries that over time form a remodeling and dynamic cage around the pharynx, that all lower facial tissues are organized, and this has formed a leitmotif during my career to date.

Etchevers HC, Vincent C, Le Douarin NM, Couly GF (2001) The cephalic neural crest provides pericytes and smooth muscle cells to all blood vessels of the face and forebrain. Development 128: 1059-1068.

Detrait ER, **Etchevers H** (2005) Vascularisation of the head and the neck during embryogenesis. J Neurorad 32(3), 147-56.

Cai J, Ash D, Kotch LE, Jabs EW, Attie-Bitach T, Auge J, Mattei G, **Etchevers H**, Vekemans M, Korshunova Y, Tidwell R, Messina DN, Winston JB, Lovett M. (2005). Gene expression in pharyngeal arch 1 during human embryonic development. Hum Mol Genet. 14(7):903-12.

Golzio C, Guirchoun J, Ozilou C, Thomas S, Goudefroye G, Morichon-Delvallez N, Vekemans M, Attie-Bitach T, **Etchevers HC**. (2006). Cytogenetic and histological features of a human embryo with homogeneous chromosome 8 trisomy. Prenat Diagn 26(13):1201-1205.

Martinovic-Bouriel J, Bernabe-Dupont C, Golzio C, Grattagliano-Bessieres B, Malan V, Bonniere M, Esculpavit C, Fallet-Bianco C, Mirlesse V, Le Bidois J, Aubry MC, Vekemans M, Morichon N, **Etchevers H**, Attie-Bitach T, Encha-Razavi F, Benachi A. (2007). Matthew-Wood syndrome: report of two new cases supporting autosomal recessive inheritance and exclusion of *FGF10* and *FGFR2*. Am J Med Genet A. 143(3):219-28.

Golzio C, Martinovic-Bouriel J, Thomas S, Mougou-Zrelli S, Grattagliano-Bessières B, Bonnière M, Delahaye S, Munnich A, Encha-Razavi F, Lyonnet S, Vekemans M, Attié-Bitach T, **Etchevers HC**. (2007). Matthew-Wood syndrome is caused by truncating mutations in the retinol binding protein receptor gene *STRA6*. Am J Hum Genet. 80(6): 1179-87.

Chassaing N, Golzio C, Odent S, Lequeux L, Vigouroux A, Martinovic-Bouriel J, Tiziano FD, Masini L, Piro F, Maragliano G, Delezoide AL, Attié-Bitach T, Manouvrier-Hanu S, **Etchevers HC**, Calvas P. (2009). Phenotypic spectrum of *STRA6* mutations: from Matthew-Wood syndrome to non-lethal anophthalmia. Hum Mutat 30(5):E673-81.

One major area of curiosity has been the definition of the role of Fgf10 on one hand, and signaling through the Fgfr2 receptor on the other, in the morphogenesis of the cardiac outflow tract and/or the pulmonary vessels. We had identified expression of the isoform of *Fgfr2* to which Fgf10 preferentially binds in both human and chicken embryonic NCC, Fgf10 being strongly produced by the second heart field preceding and during its septation. The second heart field is that part of the splanchnic mesoderm that will be incorporated into the right ventricle, *conus cordis* and *truncus arteriosus* (or conotruncus). Recent work by other groups having invalidated that necessity of direct Fgf10 signaling to Fgfr2-expressing NCC by performing genetic ablations of the receptor only in the NCC (Park et al. 2008), but maintaining a yet-important role for Fgf10 in cardiac morphogenesis (Watanabe et al. 2010; Urness, Wright, and Mansour 2010), we have examined the upstream regulation of this gene. A clearly indispensable transcription factor for development of the conotruncus is Islet-1(Cai et al. 2003). My group has been examining a combinatorial role of ISL1 in the direct transcriptional regulation of *FGF10*, supporting the importance of these proteins in human cardiogenesis. Below is a paper in progress that describes that work in more detail, an ideal transition to the new group in which I work and will train students with an eye toward developing complementary and synergistic research themes.

New data at the end, and items that will be taken into consideration for the rewrite underway.

ISL1 is a Major Orchestrator of Morphogenetic Signalling Pathways in the Embryonic Human Heart

Christelle Golzio[1,2], Emmanuelle Havis[3], Gregory Nuel[4], Candice Babarit[1], Arnold Munnich[1,2], Michel Vekemans[1,2], Stanislas Lyonnet[1,2], Heather C. Etchevers[1,*]

1. INSERM U781, Université Paris Descartes, Faculté de Médecine, 75015 Paris, France
2. Service de Génétique Médicale, Hôpital Necker-Enfants Malades, 75015 Paris, France
3. UPMC Univ Paris 06, CNRS UMR 7622, 9 Quai Saint Bernard, Boîte 24 75005 Paris, France
4. CNRS 8145, Mathématiques appliquées, Université Paris Descartes, 75005 Paris, France

Running title: ISL1 regulates human cardiac genes

Abstract

The LIM homeodomain-containing transcription factor Islet-1 (Isl1) is critical for cardiogenesis in animal models. We demonstrate that ISL1 is instrumental in human heart development. It demarcates an anatomical region that supports the conserved existence of a second heart field and that co-expresses *GATA4* during the same period *in situ*. ISL1 directly activates human cardiac *FGF10* transcription in a spatiotemporally specific manner by occupying a novel intronic regulatory element containing ISL1- and GATA-binding sites. ISL1 also binds regulatory elements of additional cardiac genes transcribed at the beginning of the second month of human gestation, as observed after ChIP-sequencing. Some of these elements are predicted to contain GATA-binding motifs, arranged similarly to the ISL1-GATA element identified in the *FGF10* gene. ISL1 is thus positioned to directly coordinate FGF, BMP and cell polarity signalling pathways in cells of the prospective outflow tract of the human heart.

Introduction

Congenital heart malformations occur in approximately 3 per 1000 births, more than half of which are potentially lethal malformations of the outflow tract (OFT) (Hoffman and Kaplan, 2002). Extensive studies have been undertaken to identify factors driving the differentiation of cell populations that participate in OFT formation.

Two spatially distinct groups of myocardiac progenitors, the first and the second heart fields, contribute to the definitive amniote heart. The chambers proper are derived from the former, while the outflow segment of the right ventricle and great arteries, and the inflow portion of the atrial sac, come from the latter. Coordination between these separate but adjacent mesodermal primordia is orchestrated by signaling events that converge on a common palette of transcription factors necessary for the site-appropriate differentiation of the multiple cell types present in a mature heart (Rochais et al., 2009).

The LIM homeodomain transcription factor Islet-1 (Isl1) is one of these. *Isl1* is necessary for multipotent cardiovascular progenitors within the second heart field to proliferate, survive, and migrate into the forming heart. *Isl1*-null mice die at embryonic day (ED) 10 from gross cardiac malformations, notably the lack of the OFT and right ventricle. The residual hearts no longer express bone morphogenetic protein (Bmp) family members 2 and 7, or fibroblast growth factor (Fgf) ligands 8 and 10 (Cai et al., 2003). *Fgf10* expression also characterizes splanchnic mesoderm of the murine second heart field (Kelly et al., 2001). Its genetic ablation leads to malposition of the heart apex and absence of pulmonary arteries and veins; the absence of the cognate specific receptor isoform for Fgf10, Fgfr2-IIIb, leads to pulmonary vessel aplasia and to OFT malformations such as double outlet right ventricle or ventricular septal defects with overriding aorta (Marguerie et al., 2006). These effects are similar to combinatorial reduction of both *Fgf8* and *Fgf10* in the future myocardium (Watanabe et al., 2010).

To date, the spatiotemporal conservation of *ISL1* expression in the developing human heart or the identity of cardiac genes putatively regulated by human ISL1, were unknown. Based on murine studies, human malformations of the inflow or outflow tracts could result from mutations in coding or non-coding regions of ISL1 transcriptional gene targets, although some highly conserved developmental genes are known to have species-

specific domains of action (Fougerousse et al., 2000). We identified a novel intronic element in *FGF10* that is not only regulated directly by ISL1 but also by the transcription factor GATA4 when they are expressed in the presumptive OFT of the human heart. As demonstrated by chromatin immunoprecipitation from embryonic human cardiac primordia, ISL1 occupied this as well as other binding sites across the genome *in vivo*. Such elements corresponded to regulatory regions of genes also expressed in the developing human heart. Some of the newly identified ISL1-bound sites were organized in similar ISL1-GATA modules to that observed in *FGF10*; such modules potentially represent a novel developmental cardiac enhancer motif.

Materials and Methods

Expression studies

ISL1 and *GATA4 in situ* hybridizations were performed with transverse sections of normal human embryos from Carnegie stages (CS) 12 to 15 (O'Rahilly and Müller, 1987). Embryos were obtained from electively terminated pregnancies in concordance with French legislation (94-654 and 08-400) with approval from the Necker ethical review committee. Tissue fixation, sectioning, *in situ* hybridization were carried out as previously described (Delous et al., 2007). Total RNA was extracted from hearts at CS13 to CS16 and RT-PCR was carried out using the GeneAmp kit (Roche) with 500 ng total RNA input for first strand synthesis. Primers are listed in Table S1.

Plasmid constructs

Human TBX20 and ISL1 expression vectors were generated. Full-length *TBX20* cDNA and a fragment of *ISL1* cDNA with the N-terminal 142 amino acids removed (Sanchez-Garcia and Rabbitts, 1993) were inserted into the multiple cloning site of pcDNA3.1C (Invitrogen). Human *GATA4* was purchased from GenScript (GN026113).

Electrophoretic Mobility Shift Assays

HeLa cells were transfected with either ISL1 or GATA4 expression constructs. Nuclear protein extracts were made using standard protocols. EMSA was performed using the LightShift Chemiluminescent EMSA Kit (Pierce) as specified. Primers are listed in Table S1.

Transactivation assays and reporter constructs

For the *FGF10* reporter construct (LUC-*FGF10*-Int1), 1047 bp of the *FGF10* first intron (chromosome 5:44421556-44422602) were subcloned into the BamHI site 3' to luc+ in pGL3 (Promega). Mouse 10T1/2 cells in DMEM/10% fetal calf serum were transfected with FuGeneHD (Roche). Cells were harvested and lysed 24h after transfection. Firefly and Renilla luciferase activities were measured on a Berthold Centro LB960 using the Dual-Luciferase Reporter assay system (Promega). Firefly luciferase activity was normalized to the Renilla luciferase internal control, pRL-CMV (Promega). Experiments were repeated in triplicate in three independent assays.

Chromatin immunoprecipitation

ChIP was carried out as described, starting from nuclear isolation (Havis et al., 2006), using 11 microdissected and flash-frozen human cardiac tubes from CS14-15. An anti-ISL1 (10 µL, Santa Cruz Sc-23590X) or an anti-GFP antibody as negative control (10 µL, Abcam ab1218), were used per 10 µg of sonicated chromatin. Immunoprecipitated DNA was analysed by end-point PCR (primers, Table S1).

High throughput sequencing

ISL1-bound DNA resulting from ChIP described above, was purified and sequenced on an Illumina Genome Analyzer II station, according to manufacturer‟s instructions provided by Fasteris SA (http://www.fasteris.com).

Bioinformatics

Sequence reads were mapped to the human genome, allowing up to two mismatches, using the Efficient Alignment of Nucleotide Databases module within the Illumina Genome Analyzer Pipeline software. Genome-wide distribution of identified binding peaks was considered to correlate with a gene when they fell within the 10 kilobases 5‟ to predicted transcriptional start sites or 3‟ to the last exon of RefSeq genes positioned in the UCSC genome browser (http://genome.ucsc.edu, hg18). Identification of putative consensus sites was performed with rVista 2.0 (http://rvista.dcode.org). A bioperl script, available on request, was written to screen sequences for the ISL1-GATA4 binding motif.

Results and Discussion

Expression of conserved human genes essential for cardiac development

Isl1, normally expressed by second heart field cells and subsequently in the OFT, affects the expression of murine *Fgf10* (Cai et al., 2003). Three of the six GATA transcription factors, Gata4, -5 and -6, are also expressed in the early cardiac primordium (Molkentin, 2000), and Isl1 cooperates with Gata4 to directly co-regulate additional transcription factors needed for early mouse heart development (Dodou et al., 2004; Takeuchi et al., 2005). We first examined the expression of *ISL1*, *GATA4, GATA5, GATA6,* and *FGF10* during human cardiac development to assess possible functional conservation.

To obtain spatial information about the expression patterns of *ISL1* and *GATA4* in the human embryonic heart, we performed *in situ* hybridizations at each Carnegie stage (CS) between CS12 and CS15. This period covers morphogenetic changes from directional S-shaped looping of the primitive cardiac tube to the appearance of four distinct chambers (Moorman et al., 2003). At CS12, unlike the equivalent stage in the mouse (Rojas et al., 2005), no *GATA4* expression was observed in this vicinity; *ISL1* was expressed in ventral foregut (Fig. 1A). However, between CS13 and 15, *ISL1* and *GATA4* were both transcribed within the cardiac mesenchyme surrounding the aorticopulmonary canal (see magnifications Fig. 1F, G, H and I, J, K respectively). *ISL1* was also expressed at CS15 in continuity with mesenchyme between the trachea and the heart, as reported for the mouse [cf. Fig. 1G of (Snarr et al., 2007)].

Next, RT-PCR of mRNAs extracted from microdissected, staged heart primordia pooled by stage confirmed that *ISL1*, *GATA4, GATA5, GATA6,* and *FGF10* were all transcribed by the embryonic human heart from CS13 to CS15 included. In contrast, although beta-actin expression continued unabated, these genes were abruptly no longer transcribed at CS16 (37-40 days of gestation) (Fig. 1 inset).

During OFT maturation, *ISL1*- and *GATA4*-expressing cardiac mesenchyme is colonized by neural crest cells. Neural crest cells are probably not present in this vicinity at CS13, but may be at CS14-CS15 (Thomas et al., 2008). Murine *Isl1* is not expressed in migrating neural crest cells (Cai et al., 2003), and *Gata4* is rapidly downregulated in the mesectodermal and cardiac subpopulations (Tomita et al., 2005). Human cardiac cells expressing *ISL1* at CS14-15 (equivalent to ED10.5-11) are likely to be mesodermal in origin, supporting the novel assertion that a SHF also exists and contributes to heart development in humans.

In order to find cardiac transcriptional targets of ISL1 in this time window, we adapted ChIP to staged and prospectively frozen embryonic human hearts. DNA obtained after immunoprecipitation was analyzed using both end-point PCR and, for the first time using such starting material, high-throughput sequencing.

ISL1 binds a novel intronic element of the FGF10 *gene in heart but not hindlimb*

A bioinformatics analysis of the *FGF10* locus to search for putative ISL1 consensus binding sites yielded two candidates. The first was previously predicted within the *FGF10* promoter (Ohuchi et al., 2005) and termed *FGF10*-Pr2 (Fig. 2A); the latter within the intron 1 of *FGF10*, was termed *FGF10*-Int1 (Fig. 2A-2B). Using ChIP, we demonstrated that in the developing human heart at CS14-15, ISL1 bound to only the *FGF10*-Int1 fragment. In contrast, it did not occupy *FGF10*-Pr2 or a different promoter fragment without an ISL1 consensus site, termed *FGF10*-Pr1 (Fig. 2C). In parallel, we observed that acetylated histone H4 bound the *ISL1* and *FGF10* promoters. As expected, the chromatin around these two promoters was thus transcriptionally active in the human heart at CS14-15, consistent with the expression studies above (Fig. S1 in supplementary material).

Both Isl1 and Fgf10 play early and interdependent roles in the specification and outgrowth of vertebrate limb buds (Sekine et al., 1999). We therefore tested whether ISL1 occupied the *FGF10*-Int1 element in human limb buds. *FGF10* and *ISL1* are indeed co-expressed at foot plate stages in the human hindlimb, as shown by RT-PCR. However, by contrast with ChIP using CS14-15 hearts, ChIP using CS16-17 hindlimbs demonstrated no interaction between ISL1 and the *FGF10*-Int1 element (Fig. S2).

ISL1 *and* GATA4 *bound the* FGF10-*Int1 element* in vitro

To investigate the ability of ISL1 to bind to its conserved consensus site (*FGF10*-ISL1) within *FGF10*-Int1, we performed EMSA assays (Fig. 2D). ISL1 bound robustly to *FGF10*-ISL1 as well as to a known positive control site, termed *Insulin I*-ISL1 (Dodou et al., 2004) (Fig. 2D, lanes 2 and 7 respectively). Binding of ISL1 to its *FGF10*-ISL1 cognate site was specific, since it could be partially competed off by excess unlabeled probe (Fig. 2D, lane 3) but not by a hundredfold excess of unlabeled mutated probe (Fig. 2D, lane 4). In addition, ISL1 did not bind to a labeled, mutated version of *FGF10*-ISL1 (Fig. 2D, lane 5).

ISL1, similar to other LIM domain-containing transcription factors, may not act alone in binding the *FGF10* intron 1 region. Concordantly, we identified a potential binding site for GATA4/5/6-type transcription factors in *FGF10*-Int1 (Merika and Orkin, 1993) (Fig. 2B). This non-canonical GATA binding site (i.e. 5‟-TGATTA-3‟) is 52 nucleotides distant from the ISL1-binding site we demonstrated by ChIP.

Similarly, GATA4 bound specifically to this non-canonical GATA4 site within *FGF10*-Int1 (Fig. 2D, lane 12), and binding to this site was completely abrogated by the addition of unlabeled *FGF10*-GATA4 probe (Fig. 2D, lane 13).

ISL1 and GATA4 activate FGF10 via *its intronic enhancer in cooperation with TBX20*

Murine Isl1 and Gata4 directly co-activate transcription of downstream cardiac transcription factors *Nkx2.5* and *Mef2c* (Dodou et al., 2004; Takeuchi et al., 2005). We thus tested the potential of the *FGF10*-Int1 element to direct the transcription of a luciferase reporter gene in the presence of ISL1 and/or GATA4. Co-transfection in 10T1/2 cells of a GATA4 or ISL1 expression construct together with the LUC-*FGF10*-Int1 reporter resulted in strong activation of luciferase activity (Fig. 3).

The transcriptional response of murine *Nkx2.5* to Isl1 and Gata4 *in vitro* can be potentiated by Tbx20, a member of a large family of genes related to the *T* (brachyury) transcription factor (Takeuchi et al., 2005). We therefore examined the potential for human TBX20 to activate the LUC-*FGF10*-Int1 reporter transfected into 10T1/2 cells. Co-transfection of a TBX20 expression construct, as for GATA4 and ISL1, indeed activated the reporter alone. Additional transfection of GATA4 and ISL1 expression constructs along with TBX20 resulted in the most efficient activation of LUC-*FGF10*-Int1 (Fig. 3). Curiously, there is no T-box within the response element of *FGF10*. However, the response of murine *Nkx2.5* to Tbx20 also occurs without a cognate T-box element.

At CS14-15, cardiac neural crest cells, expressing *FGFR2* (Thomas et al., 2008), may thus sense the *FGF10* secreted by SHF-derived cells in the human OFT, under the control of mesodermal transcription factors such as ISL1 and GATA4/5/6. This cell-cell communication between cardiac neural crest cells, secondary and primary heart field cells is critical for the growth, maturation and septation of the OFT.

ChIP-sequencing identifies in vivo *ISL1-binding sites throughout the genome*

In order to find additional cardiac targets of ISL1 at CS14-15, we turned to high-throughput sequencing (ChIP-sequencing). Sequences were mapped to the human genome and putative ISL1-bound regions represented by the enrichment of overlapping, mapped sequences, or peaks. A total of 4.98 million initial sequences were generated, of which 39% were mapped and retained for peak generation. We chose to focus on the 124 peaks defined by coverage of at least 20 hits within a gap interval of 100 bp between first position matches. Peaks mapped to simple repeat regions were excluded.

Of the twenty sites within ten kilobases (kb) of a predicted gene, thirteen were localized in intronic regions, four were located 5‟ to the nearest first exon and three were located 3‟ to the nearest last exon of a gene. A canonical 5‟-(C/T)TAATG(A/G)-3‟ ISL1-binding motif was found in thirteen loci, of which eight were expressed in the embryonic heart (Fig. S3). We also scanned a window of 100bp flanking these eight ISL1 sites in

light of the presence of a GATA4/5/6-binding site in the *FGF10*-Int1 element. Consensus GATA sequences were present in the loci corresponding to *BMP2*, *DOK5*, *JAKMIP3* and *NUP54*. Including *FGF10*, the GATA site was located between 55 and 80bp of the ISL1 site in all five genes, defining a novel ISL-GATA regulatory motif.

Many of the 124 original peaks did not have canonical ISL1 recognition sequences, indicating that the rather short consensus sequence may not account for all ISL1 binding to DNA. ISL1 may target these regions through protein-protein interactions (Takeuchi et al., 2005) or degenerate binding sites (Johnson et al., 2007). We re-scanned all 124 peaks for canonical GATA sites. In addition to those sites near canonical ISL1 consensus sequences identified above, we found two additional peaks with only a GATA consensus binding site. These were within an intron of *PDE3A* and 3‟ to the last exon of *BARX1*. We confirmed that *PDE3A* was transcribed at the same time as *ISL1* in the heart by RT-PCR (Fig. S3).

In addition to *FGF10*, the genes transcribed in the human cardiac primordium at CS14-15 whose loci are occupied by ISL1 were: *NUP54*, *JAKMIP3*, *BMP2*, *DOK5*, *MAP4K4*, *MYO1D*, *UNC45B*, *ROCK1*, and *PDE3A*. Many of these are signals or effectors that may poise SHF-derived cells to respond to their environment.

NUP54 encodes a nucleoporin, part of a complex involved in nuclear protein transport, about which little else is known to date, although it may be involved in maintaining the tone of arterial smooth muscle (Sabri et al., 2007). ISL1 may also directly regulate two intracellular effectors involved in signalling associated with cell shape changes, *JAKMIP3* and *ROCK1*. Wnt11, a ligand used to establish planar cell polarity and required for proper invasion of the OFT by cardiac neural crest cells, transduces *via* both Jakmip3 and Rock1 (Zhou et al., 2007).

Bmp2 is required for the recruitment of SHF cells during murine OFT formation (Waldo et al., 2001). Its cardiac expression profile (Fig. S3) and the presence of an ISL1-bound site located 6 kb after the last exon of *BMP2* confirmed this potential role in humans. It was independently found that the 3‟ region of human *BMP2* is responsible for its transcriptional regulation (Dathe et al., 2009).

MAP4K4 and DOK5 are intermediates between extracellular signals like FGF10, and a transcriptional response. The Dok family of proteins comprises common adaptor substrates for growth factor receptor tyrosine kinases. MAP4K4 activates c-Jun N-terminal kinase (Machida et al., 2004). Possible effects are activation of the transcription factors JUN or ERK.

MYO1D and UNC45B are required for muscle myosin and sarcomere organization. *Myo1D* is expressed in the developing *Xenopus* embryo in cephalic and cardiac neural crest cells as they infiltrate the branchial arches (LeBlanc-Straceski et al., 2009). Its *Drosophila* homologue, *Dm*Myo31DF, leads to *situs inversus* upon mutation and co-localizes with beta-catenin, implying a potential role for MYO1D in cytoskeletal changes and human heart looping (Speder et al., 2006). The myosin chaperone protein Unc-45 is expressed in cardiac and striated muscles of the developing zebrafish. Morpholinos against *Unc-45* lead to major cardiac malformations including *situs inversus*, as well as branchial arch cartilage dysmorphy (Wohlgemuth et al., 2007).

Phosphodiesterase 3A, present in murine cardiomyocytes, regulates sensitivity to cAMP-inducing prostaglandins by directly hydrolyzing cAMP (Sun et al., 2007). During

gestation, *PDE3A* expression increases in the muscle wall of the *ductus arteriosus*, a transient vessel derived from the sixth pharyngeal arch that shunts before birth between the aorta and the pulmonary trunk of the OFT (Liu and Maurice, 1998). The role of PDE3A is to increase its tension and permit postnatal remodelling of this region. An earlier, embryonic role in cardiac formation has been hitherto unsuspected.

The ISL1-GATA4 motif

A total of 5/10 novel ISL1 binding sites were within 80bp of a GATA binding site. Similarly, 52 nucleotides separate a functionally validated Isl1 site from a Gata site in the murine *Nkx2.5* promoter and this motif is highly conserved in human *NKX2.5*. Therefore, we tested the hypothesis that the close association of ISL1 to GATA binding sites represents an indissociable module rather than a fortuitous observation.

An ISL1-GATA motif was defined as (C/T)TAATG(A/G) with 55-80 intervening base pairs from (A/T/C)GATA(A/G). Then, the entire sequence of human chromosome 5 was scanned for it in both directions, with 2,279 occurrences. Using parameters generated by a Markov chain 1 model, we simulated 1000 same-sized virtual chromosomes and scanned these for the defined motif. There was a mean of 3,306 occurrences, which is significantly more than observed in the biological dataset (Z_M-score of -17.95 with an associated p-value $2.5e^{-72}$). The fewer incidences found *in vivo* mean that the ISL1-GATA motif underwent evolutionary selection pressure. Moreover, similar analyses conducted for ISL1 or GATA sites individually showed observed versus simulated incidences of 58,498 versus 83,258 for ISL1 (Z_I-score of -90.27) and 242,329 versus 281,028 for GATA (Z_G-score of -74.67).

As for the whole motif, each binding site is found less frequently *in vivo* than would be expected by chance alone. The discrepancy between observed versus simulated incidences of the ISL1-GATA motif (Z_M-score) is greater than for either site alone (Z_I-score and Z_G-score), further suggesting that this regulatory module is a *bona fide* functional unit.

The relatively short length of the spacer sequence led us to align the sequences separating the ISL1 and GATA-binding sites in the *FGF10, NUP54, JAKMIP3, BMP2,* and *DOK5* genes, as well as the equivalent spacer sequence conserved in human *NKX2.5*. We found 29 nucleotides aligned among at least four of the six spacers. However, we observed an average of the same number of alignments in five groups of six randomly chosen intervals within ISL1-GATA motifs taken from one of the simulated chromosomes above, and the difference between the number of aligned residues in the biological versus simulated spacer sequences was not statistically significant.

Overall, the data presented here support the idea that ISL1 confers a spatially restricted potential on human SHF progenitors to respond in a sensitive manner to morphogens in the cellular environment. ISL1 regulates the expression of several downstream effectors of signalling pathways involving FGFs, BMPs or cytoskeletal changes by means of non-promoter, primarily intronic, elements.

A conserved mechanism may exist between humans and mice for the regulation of cardiac gene transcription by the convergence of several transcription factors during development. This hypothesis was supported by transactivation assays that confirmed the

ability of the human forms of ISL1 and GATA4 to act in cooperation to activate a reporter gene under the control of a *FGF10* intronic element (i.e. Luc-*FGF10*-Int1). In addition, our statistical analyses support the conclusion that the proximity of ISL1 and GATA binding sites confers an evolutionary advantage.

Knock-out models of many ISL1 targets, including *Fgf10* and *Bmp2*, give rise to murine cardiac malformations of the OFT and have served as candidate genes for mutation screening in patients affected by congenital heart malformations (Martinovic-Bouriel et al., 2007; Posch et al., 2008). Mutations in either the coding sequences of ISL1 targets or in non-coding regulatory sequences recognized by ISL1 now become equally compelling candidates in human conotruncal heart defects.

Acknowledgements

The authors wish to thank Dr. M. Téboul and the Service d"Orthogénie of the Broussais Hospital in Paris for the human tissues and Dr. D. Montarras for the 10T1/2 cells used in this work. Drs. D. Bonnet, M. Buckingham, C. Fournier-Thibault, R. Kelly, and S. Zaffran provided invaluable discussion. The Fondation pour la Recherche Médicale (DEQ20071210511 and a fellowship to C.G.), the Agence Nationale pour la Recherche (ANR2007-CRANIRARE) and the Institut **Pasteur-Necker** Transverse Research Program supported this work.

References

Cai, C. L., Liang, X., Shi, Y., Chu, P. H., Pfaff, S. L., Chen, J. and Evans, S. (2003). Isl1 identifies a cardiac progenitor population that proliferates prior to differentiation and contributes a majority of cells to the heart. *Dev Cell* **5**, 877-889.

Dathe, K., Kjaer, K. W., Brehm, A., Meinecke, P., Nurnberg, P., Neto, J. C., Brunoni, D., Tommerup, N., Ott, C. E., Klopocki, E. et al. (2009). Duplications involving a conserved regulatory element downstream of BMP2 are associated with brachydactyly type A2. *Am J Hum Genet* **84**, 483-492.

Delous, M., Baala, L., Salomon, R., Laclef, C., Vierkotten, J., Tory, K., Golzio, C., Lacoste, T., Besse, L., Ozilou, C. et al. (2007). The ciliary gene RPGRIP1L is mutated in cerebello-oculo-renal syndrome (Joubert syndrome type B) and Meckel syndrome. *Nat Genet* **39**, 875-881.

Dodou, E., Verzi, M. P., Anderson, J. P., Xu, S. M. and Black, B. L. (2004). Mef2c is a direct transcriptional target of ISL1 and GATA factors in the anterior heart field during mouse embryonic development. *Development* **131**, 3931-3942.

Fougerousse, F., Bullen, P., Herasse, M., Lindsay, S., Richard, I., Wilson, D., Suel, L., Durand, M., Robson, S., Abitbol, M. et al. (2000). Human-mouse differences in the embryonic expression patterns of developmental control genes and disease genes. *Hum Mol Genet* **9**, 165-173.

Havis, E., Anselme, I. and Schneider-Maunoury, S. (2006). Whole embryo chromatin immunoprecipitation protocol for the in vivo study of zebrafish development. *Biotechniques* **40**, 34, 36, 38 passim.

Hoffman, J. I. and Kaplan, S. (2002). The incidence of congenital heart disease. *J Am Coll Cardiol* **39**, 1890-1900.

Johnson, D. S., Mortazavi, A., Myers, R. M. and Wold, B. (2007). Genome-wide mapping of in vivo protein-DNA interactions. *Science* **316**, 1497-1502.

Kelly, R. G., Brown, N. A. and Buckingham, M. E. (2001). The arterial pole of the mouse heart forms from Fgf10-expressing cells in pharyngeal mesoderm. *Dev Cell* **1**, 435-440.

LeBlanc-Straceski, J. M., Sokac, A., Bement, W., Sobrado, P. and Lemoine, L. (2009). Developmental expression of Xenopus myosin 1d and identification of a myo1d tail homology that overlaps TH1. *Dev Growth Differ* **51**, 443-451.

Liu, H. and Maurice, D. H. (1998). Expression of cyclic GMP-inhibited phosphodiesterases 3A and 3B (PDE3A and PDE3B) in rat tissues: differential subcellular localization and regulated expression by cyclic AMP. *Br J Pharmacol* **125**, 1501-1510.

Machida, N., Umikawa, M., Takei, K., Sakima, N., Myagmar, B. E., Taira, K., Uezato, H., Ogawa, Y. and Kariya, K. (2004). Mitogen-activated protein kinase kinase kinase kinase 4 as a putative effector of Rap2 to activate the c-Jun N-terminal kinase. *J Biol Chem* **279**, 15711-15714.

Marguerie, A., Bajolle, F., Zaffran, S., Brown, N. A., Dickson, C., Buckingham, M. E. and Kelly, R. G. (2006). Congenital heart defects in Fgfr2-IIIb and Fgf10 mutant mice. *Cardiovasc Res* **71**, 50-60.

Martinovic-Bouriel, J., Bernabe-Dupont, C., Golzio, C., Grattagliano-Bessieres, B., Malan, V., Bonniere, M., Esculpavit, C., Fallet-Bianco, C., Mirlesse, V., Le Bidois, J. et al. (2007). Matthew-Wood syndrome: report of two new cases supporting autosomal recessive inheritance and exclusion of FGF10 and FGFR2. *Am J Med Genet A* **143**, 219-228.

Merika, M. and Orkin, S. H. (1993). DNA-binding specificity of GATA family transcription factors. *Mol Cell Biol* **13**, 3999-4010.

Molkentin, J. D. (2000). The zinc finger-containing transcription factors GATA-4, -5, and -6. Ubiquitously expressed regulators of tissue-specific gene expression. *J Biol Chem* **275**, 38949-38952.

Moorman, A., Webb, S., Brown, N. A., Lamers, W. and Anderson, R. H. (2003). Development of the heart: (1) formation of the cardiac chambers and arterial trunks. *Heart* **89**, 806-814.

O'Rahilly, R. and Müller, F. (1987). Developmental Stages in Humans: including a revision of Streeter's "Horizons" and a survey of the Carnegie collection. Washington, D.C.: Carnegie Institution of Washington.

Ohuchi, H., Yasue, A., Ono, K., Sasaoka, S., Tomonari, S., Takagi, A., Itakura, M., Moriyama, K., Noji, S. and Nohno, T. (2005). Identification of cis-element regulating expression of the mouse Fgf10 gene during inner ear development. *Dev Dyn* **233**, 177-187.

Posch, M. G., Perrot, A., Schmitt, K., Mittelhaus, S., Esenwein, E. M., Stiller, B., Geier, C., Dietz, R., Gessner, R., Ozcelik, C. et al. (2008). Mutations in GATA4, NKX2.5, CRELD1, and BMP4 are infrequently found in patients with congenital cardiac septal defects. *Am J Med Genet A* **146A**, 251-253.

Rochais, F., Mesbah, K. and Kelly, R. G. (2009). Signaling pathways controlling second heart field development. *Circ Res* **104**, 933-942.

Rojas, A., De Val, S., Heidt, A. B., Xu, S. M., Bristow, J. and Black, B. L. (2005). Gata4 expression in lateral mesoderm is downstream of BMP4 and is activated directly by Forkhead and GATA transcription factors through a distal enhancer element. *Development* **132**, 3405-3417.

Sabri, N., Roth, P., Xylourgidis, N., Sadeghifar, F., Adler, J. and Samakovlis, C. (2007). Distinct functions of the Drosophila Nup153 and Nup214 FG domains in nuclear protein transport. *J Cell Biol* **178**, 557-565.

Sanchez-Garcia, I. and Rabbitts, T. H. (1993). Redox regulation of in vitro DNA-binding activity by the homeodomain of the Isl-1 protein. *J Mol Biol* **231**, 945-949.

Sekine, K., Ohuchi, H., Fujiwara, M., Yamasaki, M., Yoshizawa, T., Sato, T., Yagishita, N., Matsui, D., Koga, Y., Itoh, N. et al. (1999). Fgf10 is essential for limb and lung formation. *Nat Genet* **21**, 138-141.

Snarr, B. S., O'Neal, J. L., Chintalapudi, M. R., Wirrig, E. E., Phelps, A. L., Kubalak, S. W. and Wessels, A. (2007). Isl1 expression at the venous pole identifies a novel role for the second heart field in cardiac development. *Circ Res* **101**, 971-974.

Speder, P., Adam, G. and Noselli, S. (2006). Type ID unconventional myosin controls left-right asymmetry in Drosophila. *Nature* **440**, 803-807.

Sun, B., Li, H., Shakur, Y., Hensley, J., Hockman, S., Kambayashi, J., Manganiello, V. C. and Liu, Y. (2007). Role of phosphodiesterase type 3A and 3B in regulating platelet and cardiac function using subtype-selective knockout mice. *Cell Signal* **19**, 1765-1771.

Takeuchi, J. K., Mileikovskaia, M., Koshiba-Takeuchi, K., Heidt, A. B., Mori, A. D., Arruda, E. P., Gertsenstein, M., Georges, R., Davidson, L., Mo, R. et al. (2005).

Tbx20 dose-dependently regulates transcription factor networks required for mouse heart and motoneuron development. *Development* **132**, 2463-2474.

Thomas, S., Thomas, M., Wincker, P., Babarit, C., Xu, P., Speer, M. C., Munnich, A., Lyonnet, S., Vekemans, M. and Etchevers, H. C. (2008). Human neural crest cells display molecular and phenotypic hallmarks of stem cells. *Hum Mol Genet* **17**, 3411-3425.

Tomita, Y., Matsumura, K., Wakamatsu, Y., Matsuzaki, Y., Shibuya, I., Kawaguchi, H., Ieda, M., Kanakubo, S., Shimazaki, T., Ogawa, S. et al. (2005). Cardiac neural crest cells contribute to the dormant multipotent stem cell in the mammalian heart. *J Cell Biol* **170**, 1135-1146.

Waldo, K. L., Kumiski, D. H., Wallis, K. T., Stadt, H. A., Hutson, M. R., Platt, D. H. and Kirby, M. L. (2001). Conotruncal myocardium arises from a secondary heart field. *Development* **128**, 3179-3188.

Watanabe, Y., Miyagawa-Tomita, S., Vincent, S. D., Kelly, R. G., Moon, A. M. and Buckingham, M. E. (2010). Role of mesodermal FGF8 and FGF10 overlaps in the development of the arterial pole of the heart and pharyngeal arch arteries. *Circ Res* **106**, 495-503.

Wohlgemuth, S. L., Crawford, B. D. and Pilgrim, D. B. (2007). The myosin co-chaperone UNC-45 is required for skeletal and cardiac muscle function in zebrafish. *Dev Biol* **303**, 483-492.

Zhou, W., Lin, L., Majumdar, A., Li, X., Zhang, X., Liu, W., Etheridge, L., Shi, Y., Martin, J., Van de Ven, W. et al. (2007). Modulation of morphogenesis by noncanonical Wnt signaling requires ATF/CREB family-mediated transcriptional activation of TGFbeta2. *Nat Genet* **39**, 1225-1234.

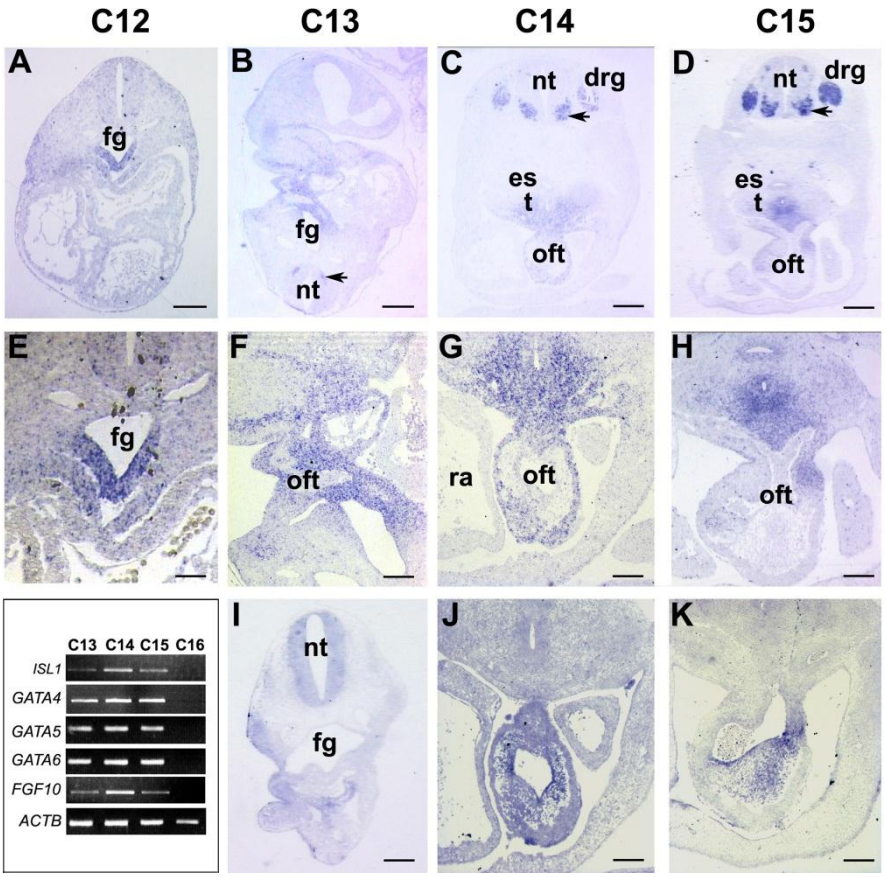

Fig. 1: Expression of *ISL1* and *GATA4* transcripts in the human heart between 26 and 38 days of gestation.

A-G *ISL1 in situ* at Carnegie stages (CS)12 (26-30 days post fertilization [dpf]), CS13 (28-32 dpf), CS14 (31-35 dpf) and CS15 (35-38 dpf) respectively. **E-G** are magnifications of **B-D** respectively. **H-J** show *GATA4* expression in adjacent sections to **B-D**. (**A)**: *ISL1* is expressed at CS12 in foregut endoderm, splanchnic mesoderm, and early motoneurons. (**B, E)**: At CS13, *ISL1* is transcribed by mesenchyme around the cardiac OFT and pharyngeal arches. *ISL1* expression continues in the splanchnic mesoderm between the trachea and OFT, and is visible in dorsal root ganglia, at CS14 (**C, F**) and CS15 (**D, G**). (**H-J)**: *GATA4* is expressed in the endocardium and myocardium of the arterial pole CS13, CS14 and CS15 (**H, I, J** respectively). **Inset**: RT-PCR of *ISL1, GATA4, GATA5, GATA6, FGF10* and positive control *ACTB* mRNAs in embryonic human hearts at stages CS13-16. Abbreviations: drg, dorsal root ganglia; es, esophagus; fb, forebrain; fg, foregut; ph, pharynx; nt, neural tube; oft, OFT; ra, right atrium; t, trachea. Arrows, motoneurons. Bar: 110 µm (A,B,C,D,I) and 55 µm (E,F,G,H,J,K).

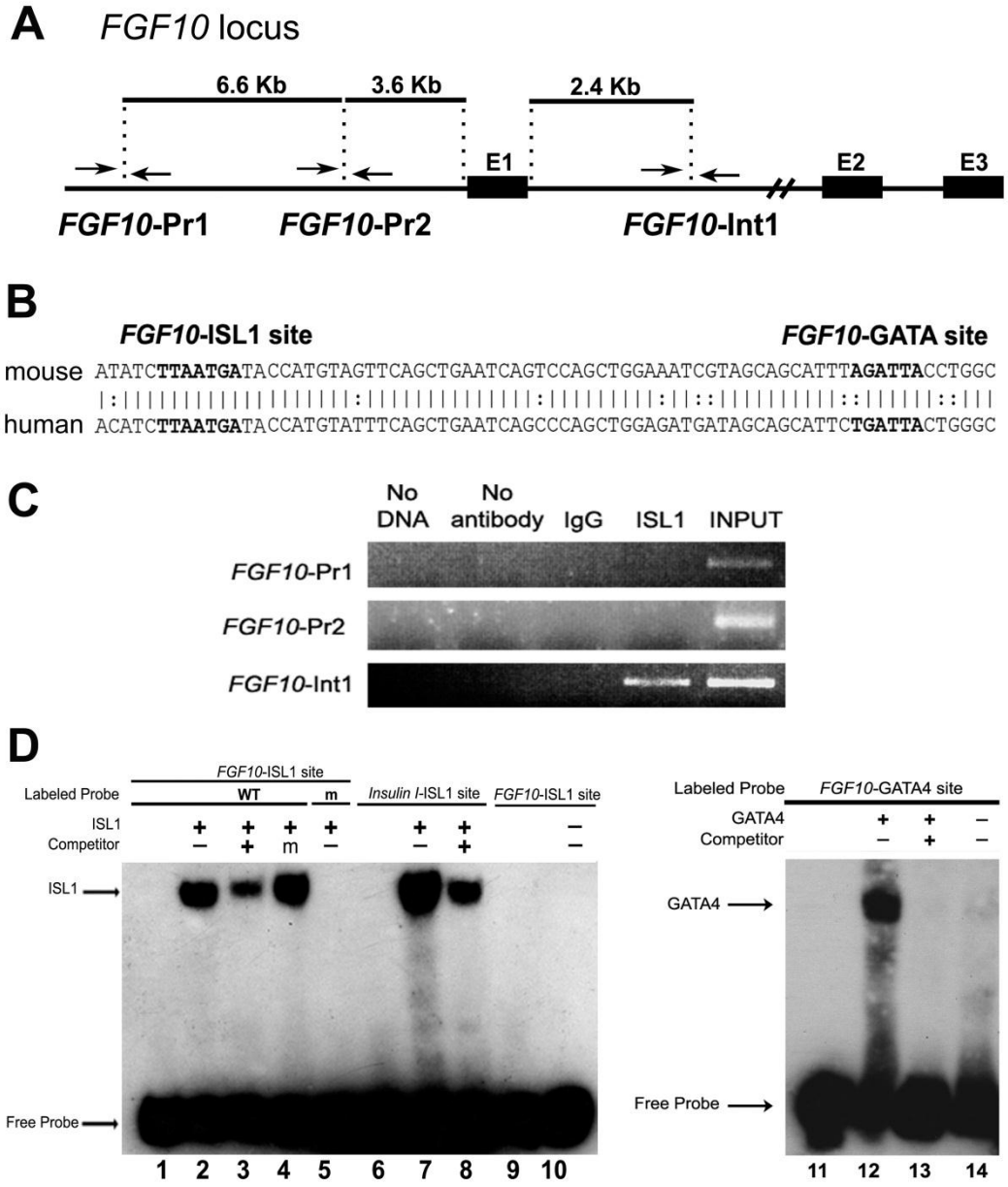

Fig. 2: *In vivo* and *in vitro* binding of ISL1 and GATA4 within the first intron of *FGF10*.

A: The FGF10-Pr1, FGF0-Pr2 and FGF10-Int1 fragments are positioned relative to the human *FGF10* locus. FGF10-Int1 fragment contains two consensus binding sites for ISL1 and GATA factors (Fig. 2B). **B**: The sequence of the FGF10-Int1 fragment and position of conserved putative ISL1 and GATA binding sites. **C**: Results of PCR after ChIP from human embryonic hearts at CS14-15. **D**: Results of EMSA assays demonstrate specific binding of ISL1 and GATA4 to the *FGF10* intronic element (*FGF10*-Int1).

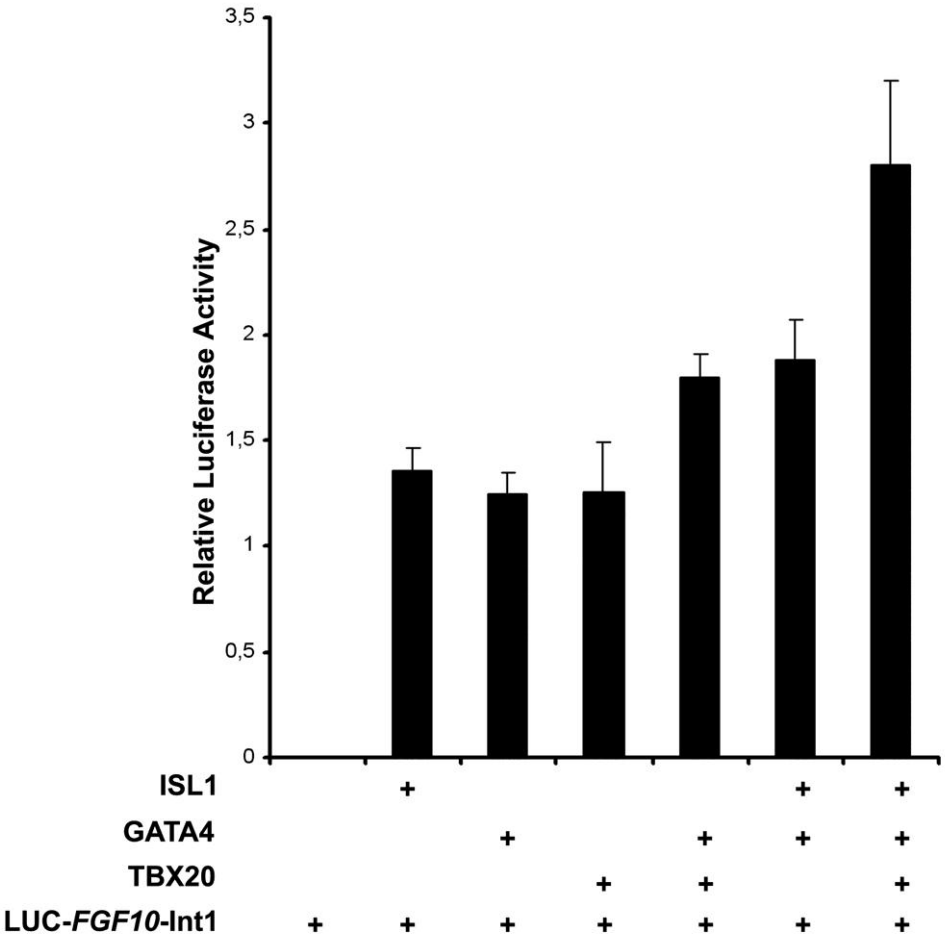

Fig. 3: *In vitro* transcriptional activation assays.

LUC-*FGF10*-Int1, which placed the luciferase gene under the control of the FGF10-Int1 element, was transfected alone or together with *ISL1*, *GATA4* and *TBX20* expression vectors into 10T1/2 cells. Each factor alone potentiated luciferase expression and these effects were additive.

Gene	RefSeq	Chromo-some	Position	Genomic Coordinates ISL1	ISL1 CBS	Spacer length (bp)	Genomic Coordinates GATA	GATA CBS
NUP54	NM_017426	4	intron	77,266,265	ACATTAA	70	77,266,195	ATATCT
JAKMIP3	NM_001105521	10	intron	133,836,145	TTAATGT	65	133,836,080	GTATCG
BMP2	NM_001200	20	3'	6,770,105	TCATTAT	65	6,770,180	CTATCA
DOK5	NM_018431	20	intron	52,663,020	TCATTAG	80	52,663,100	TTATCT
MAP4K4	NM_145687	2	intron	101,816,800	TTTATGA			
MYO1D	NM_015194	17	intron	28,174,005	CTAATGT			
UNC45B	NM_173167	17	intron	30,502,300	CCATTAC			
ROCK1	NM_005406	18	3'	16,770,325	TTAATGA			
PDE3A	NM_000921	12	intron				20,595,645	TGATAG

Table 1: Transcriptional targets of ISL1 identified by ChIP-sequencing. Abbreviation: CBS, consensus binding site.

Supplementary Information

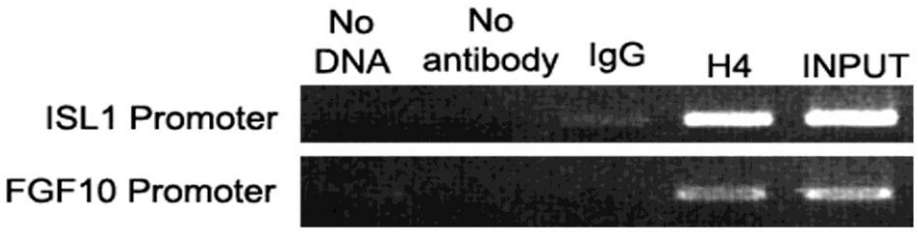

Fig. S1. ChIP assay on human embryonic heart chromatin using anti-acetylated histone H4.

Using chromatin preparations from hearts at Carnegie stages 14-15, we observed that acetylated histone H4 bound the *ISL1* and *FGF10* promoters. The chromatin around the *ISL1* and *FGF10* promoters was therefore transcriptionally **active** at these stages in the heart (1).

Reference: 1. Vettese-Dadey M, *et al.* (1996) Acetylation of histone H4 plays a primary role in enhancing transcription factor binding to nucleosomal DNA in vitro. *Embo J* 15(10):2508-2518.

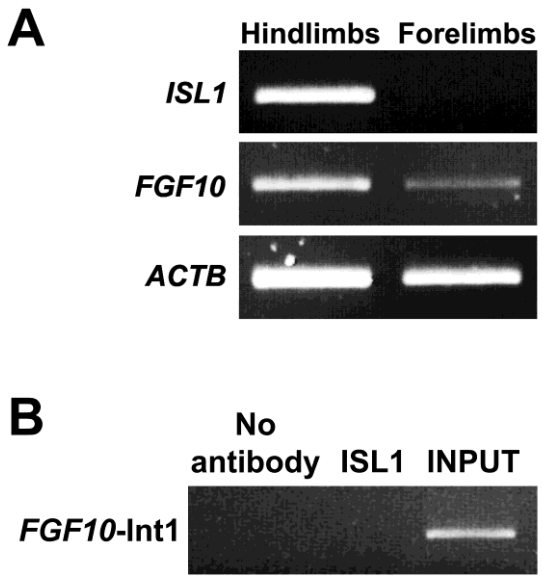

Fig. S2. RT-PCR of *ISL1* and *FGF10* transcripts in the human forelimb and hindlimb buds and ChIP of human hindlimb bud chromatin using an anti-ISL1 antibody.

A: *FGF10* and *ISL1* were co-expressed at foot plate stages (Carnegie stages [CS]16-17, i.e. 37-44 days of gestation) in human hindlimbs as seen by RT-PCR. **B:** However, chromatin immunoprecipitation from this tissue demonstrated no interaction between ISL1 and the *FGF10* first intron element we identified as bound in DNA derived from the CS14-15 heart.

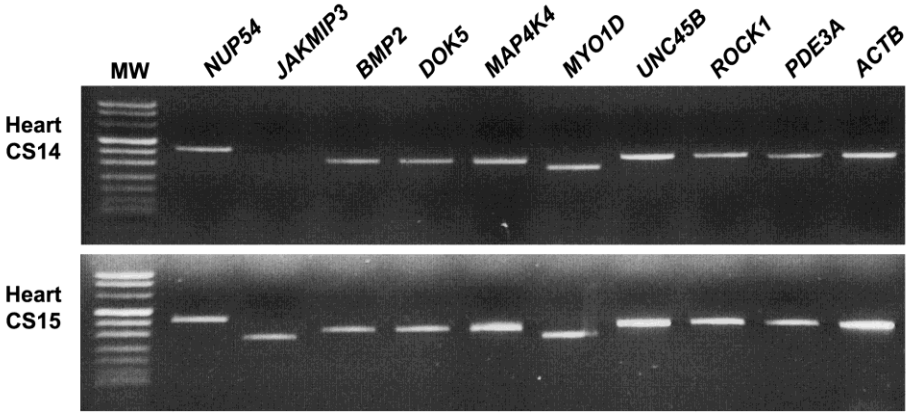

Fig. S3. RT-PCR of ISL1 identified targets in the human heart from CS14 and CS15.

All targets reported in this study (Table 1) were expressed at both Carnegie stages (CS)14 and CS15 in the human heart except for *JAKMIP3*, only expressed at CS15.

For *in situ* hybridization

hISL1-T7-F	TAATACGACTCACTATAGGGAGA GGTTGTACGGGATCAAATGC
hISL1-R	GCCCGTCATCTCTACCAGTT
hISL1-T7-R	TAATACGACTCACTATAGGGAGA GCCCGTCATCTCTACCAGTT
hISL1-F	GGTTGTACGGGATCAAATGC
hGATA4-T7-F	TAATACGACTCACTATAGGGAGA TCTTGCAATGCGGAAAGAG
hGATA4-R	CAGTGATTATGTCCCCGTGA
hGATA4-T7-R	TAATACGACTCACTATAGGGAGA CAGTGATTATGTCCCCGTGA
hGATA4-F	TCTTGCAATGCGGAAAGAG

For RT-PCR

hISL1-F	GGTTGTACGGGATCAAATGC
hISL1-R	GCCCGTCATCTCTACCAGTT
hGATA4-F	TCTTGCAATGCGGAAAGAG
hGATA4-R	CAGTGATTATGTCCCCGTGA
hGATA5-F	CCTGCGGCCTCTACATGA
hGATA5-R	AGGCTCGAACTTGAACTCCA
hGATA6-F	GTGCCCAGACCACTTGCTAT
hGATA6-R	GCGAGACTGACGCCTATGTA
hFGF10-F	TGCTGCTTTTTGTTGCTGTT
hFGF10-R	CATTTGCCTCCCATTATGCT
hACTB-F	ATTGGCAATGAGCGGTTCCGC
hACTB-R	TCCTGCTTGCTGATCCACATC
hNUP54-F	ACGCTGTTGGGAGATGAGAG
hNUP54-R	GCTTGTTCAAAATGGGCATA
hJAKMIP3-F	AGCTGCTGTCAGAGGAGGAG
hJAKMIP3-R	AAAGGGTCCGATTCAATGTG
hBMP2-F	GTTCGGCCTGAAACAGAGAC
hBMP2-R	AATTCGGTGATGGAAACTGC
hDOK5-F	TCAATGACATCAGCCTTGGA
hDOK5-R	AGGCAGCAGAGTGGACTTTC
hMAP4K4-F	AGGCCAGAGGTTGAAAGTGA
hMAP4K4-R	TGACCAGTTTCCACAGATCG
hMYO1D-F	CCCTTCTTTACCGGACTGTG
hMYO1D-R	GCTGCTGCAGTTTCTCATTG
hUNC45B-F	GCCATTCATGACAACTCACG
hUNC45B-R	TAGTGCCACCATCATCTCCA
hROCK1-F	CAACAACGGTTAGAACAAGAGG
hROCK1-R	TTGTCTGCCTCAAATGCTTG
hPDE3A-F	TCATCCAGGAAGGACTAATGC
hPDE3A-R	GGACCATTGATATCAGCCAAC

For ChIP

hISL1-Prom-F	CCTCCCACCCAACGTTTTTA
hISL1-Prom-R	CGAGTGGCTGGTGGGTAG
hFGF10-Prom-F	TTTGTTCACCGTGCTGTCAT
hFGF10-Prom-R	GATGCAAGGCAAGGAGAGAG
FGF10-Pr1-F	GGGAGCCAATTTCATTTTCA
FGF10-Pr1-R	GGAGCACTGTGACAAAA
FGF10-Pr2-F	TTCTTTTCTGTGCAGCCTTTC
FGF10-Pr2-R	TGTCCTTTTCAATCCTAGCAAA
FGF10-Int1-F	GGAAAAGGAATTGACACTCTTCA
FGF10-Int1-R	GGAGGGGTTCACTCTGCTAA

For EMSA

InsulinS (+ control)	GCCCTTGTTAATAATCTAATTAC CCTAG
InsulinAS	CTAGGGTAATTAGATTATTAACA AGGGC
FGF10-int1-S	TAGACAATATCTTAATGATACCA TGTAG
FGF10-int1-AS	CTACATGGTATCATTAAGATATT GTCTA
FGF10-int1mut-S	TAGACAATATCTTAGCTATACCA TGTAG
FGF10-int1mut-AS	CTACATGGTATAGCTAAGATATT GTCTA
GATA4-S	GTAGCAGCATTTAGATTACCTGG CCACATG
GATA4-AS	CATGTGGCCAGGTAATCTAAATG CTGCTAC
GATA4mut-S	GTAGCAGCATTTACCATACCTGG CCACATG
GATA4mut-AS	CATGTGGCCAGGTGGTATAAATG CTGCTAC

Since the last submission of this text, we have carried out additional work and reflection with the assistance of two scientists whom we have included as authors. Some of this work and the new perspectives it has opened on studies of outflow tract development will be described hereafter.

The authors and acknowledgement lists will therefore be revised to reflect their contributions (and my affiliation updated):

Christelle Golzio[1], Emmanuelle Havis[2], Philippe Daubas[3], Gregory Nuel[4], Candice Babarit[5], Arnold Munnich[5,6], Michel Vekemans[5,6], Stéphane Zaffran[7], Stanislas Lyonnet[5,6], Heather C. Etchevers[7,*]

1. Duke University Medical Center, Box 3709, Durham, NC, 27710, USA
2. UPMC Univ Paris 06, CNRS UMR 7622, 9 Quai Saint Bernard, Boîte 24 75005 Paris, France
3. CNRS URA 2578, Institut Pasteur, 75724 Paris Cedex 15, France
4. CNRS 8145, Mathématiques appliquées, Université Paris Descartes, 75005 Paris, France
5. INSERM U781, Université Paris Descartes, Faculté de Médecine, 75743 Paris Cedex, France
6. Service de Génétique Médicale, Hôpital Necker-Enfants Malades, 75015 Paris, France
7. INSERM UMR_S910, Université de la Méditerranée Aix-Marseille II, Faculté de Médecine, 13385 Marseille Cedex, France

* Corresponding author:

Heather Etchevers, INSERM UMR_S910, Université de la Méditerranée Aix-Marseille II, Faculté de Médecine, 13385 Marseille Cedex, France

Tel: (+33) 491 324 937; fax: (33) 491 797 227. heather.etchevers@inserm.fr

Acknowledgements *will include the following*:

Dr F. Langa Vives provided indispensible expertise to the generation of transgenic mice at the Centre d'Ingénierie Génétique Murine, Institut Pasteur, Paris. Drs. D. Bonnet, M. Buckingham, C. Fournier-Thibault, and R. Kelly provided invaluable discussion.

Materials and Methods *will include the following*:

All mice were maintained at the Animal **Facility** of the **Pasteur** Institute. The same 1047 bp FGF10-Int1 fragment (chr 5:44421556-44422602) was subcloned into the BamHI site in the pSKT-TK-nLacZ plasmid and orientation verified by capillary sequencing with a standard T3 primer. The plasmid was linearized with SalI for injection at 2 ng/mL into mouse blastocysts. β-galactosidase-containing cells that had transcribed the reporter plasmid were stained in whole mount by the catalysis of the X-gal (5-bromo-4-chloro-3-indolyl β-D-galactopyranoside) substrate.

Results *will include the following*:

Of 249 construct-injected blastocysts, 148 embryos were recovered at four different stages: E8.5 (n=43), E9.5 (n=22), E10.5 (n=46) and E11.5 (n=37). Of these, only a fraction had integrated the transgene at E11.5 (n=3), E10.5 (n=1), E9.5 (n=3), E8.5 (n=2), as confirmed by both X-gal staining and by genotyping for the presence of plasmid in a piece of tail.

LacZ+ cells were observed in the sites shown in Table [1 – *if we remove the current Table 1*]. Most of these sites are normal expression domains for Islet-1. Curiously, although many cells were observed in the walls of the common carotid arteries in one E11.5 embryo, only a few superficial cells were observed in the third aortic arch in the E10.5 embryo. Both E8.5 embryos had expression in cells of the presomitic mesoderm, one exclusively.

Age	forebrain	lens	MNs	DRGs	pancreas	PA1	PA2	PA3	OFT
E8.5	.	n/a	.	n/a	n/a	.	n/a	n/a	.
E8.5	+	n/a	.	n/a	n/a	.	n/a	n/a	.
E9.5	.	n/a	.	.	.	+	+	.	.
E9.5	.	n/a	.	.	.	.	+	.	+
E9.5	.	n/a	.	.	+	+	+	.	.
E10.5	+	+	.	+	.	+	+	+	+
E11.5	+	+	+	+	+	.	.	+	.
E11.5	+	+	+	+	.	.	.	.	.
E11.5	+		+	+	.	.	.	.	.

Table 1 Sites of β-galactosidase activity in transgenic embryos. MN = motoneurons, DRGs = dorsal root ganglia

We will not be able to obtain more human embryonic tissues with which to repeat or carry out qPCR experiments to validate our ChIP experiments with the Islet-1 antibody, or indeed with a Gata-4 antibody. We may therefore remove the ChIP-sequencing results, for which coverage was not as deep as today's standards would require, because it will be difficult to validate the data more than we had done. The existence of a repeated ISL1-GATA motif throughout the genome whereby cardiac transcription factors might poise the chromatin to respond transcriptionally would need further evidence to support.

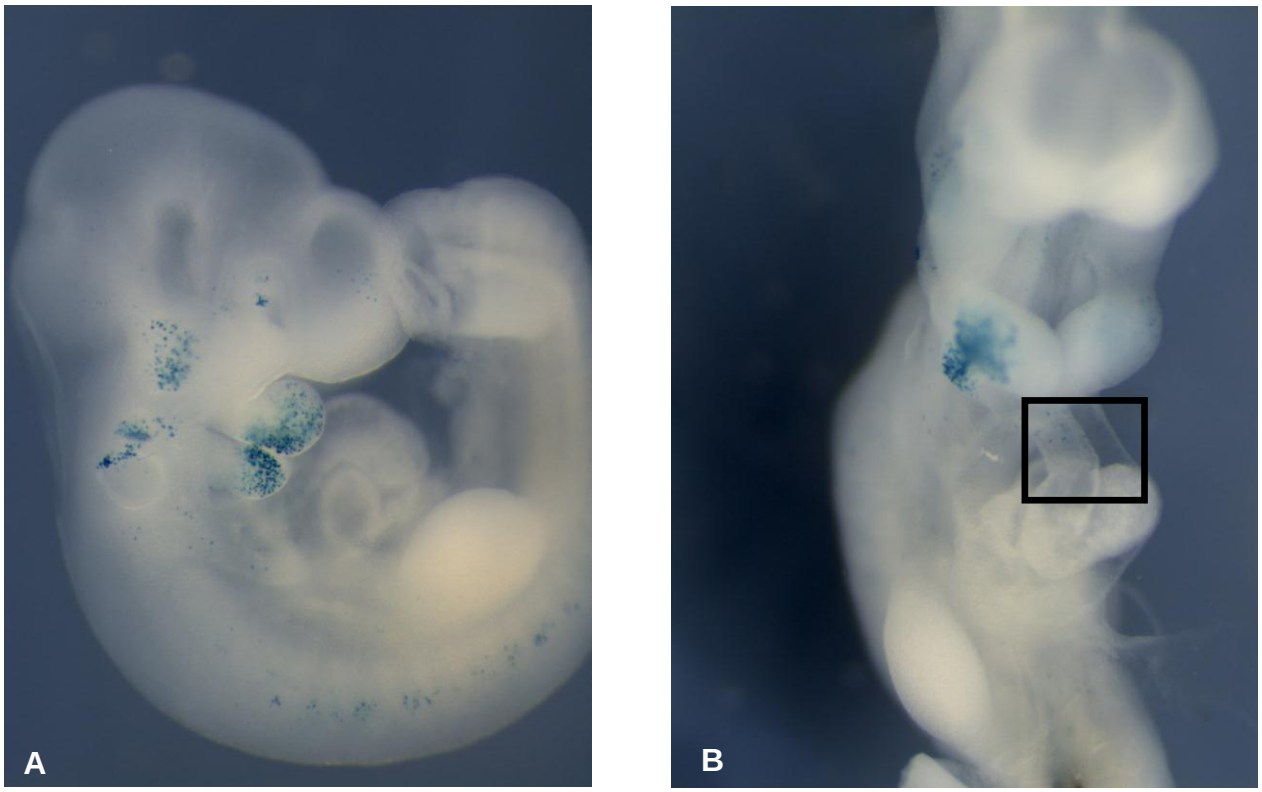

Figure 4. A 1014 bp enhancer region within the first intron of human *FGF10*, containing ISL1 and GATA-binding sites, was placed ahead of a *lacZ* reporter gene under a thymidine kinase-driven promoter. This transgene, introduced by injection into mouse blastocysts, yielded animals in which the reporter enzymatic activity demonstrated the responsiveness of the intronic enhancer to endogenous signals, and in which tissues. In this example at embryonic day 10.5, the transgene was activated in some cells of the posterior outflow tract, in a subdomain of the first two pharyngeal arches, in the trigeminal and acoustic ganglia, and in the lens. No expression was ever observed in the limb buds.

FUTURE PROJECTS

ETIOLOGY OF CONGENITAL HEART MALFORMATIONS OF THE OUTFLOW TRACT

Slowly but surely, like the NCC themselves over time, I am becoming involved in studying progressively more proximal segments of the cardiovascular tree from my originally more distal interest, such as the pulmonary trunk, the semilunar valves, the aortic arch and the coronary vessels.

After having studied a number of rare congenital malformations, the knowledge and approaches I can bring to the study of the most common group of congenital malformations, those of the heart, may benefit more people. Fully a third of these malformations concern the outflow tract and closely associated blood vessels, such as the coronary arteries. Since the early observations in the 1980s that ablation of the neural crest in chicks leads to conotruncal heart defects resembling those often seen in humans (double outlet right ventricle, tetralogy of Fallot), demonstrating an important inductive role for these in the septation of the outflow tract into aorta and pulmonary trunk, the precise nature of that role still remains to be elucidated (Kirby, Gale, and Stewart 1983; Kirby, Turnage, and Hays 1985).

The prospective and carefully annotated collection of constitutive DNA from patients seen in the pediatric cardiology unit by Damien Bonnet at the Necker Children‟s Hospital, instigated by my student in order to investigate a potential role of mutations in non-coding genomic binding sites for ISL1 in outflow tract anomalies, has become a rich resource for all the collaborators working on heart development, including my group. Specific sub-phenotypes can be examined in greater detail and with this cohort of many hundreds of patients, increasing clinical homogeneity can be obtained, which will help the identification of the genetic bases of such malformations. Classical homozygosity mapping is possible for the many families also represented in this collection.

The other means by which such genetic bases can be discovered is by the proposal of candidate genes, based on their functions having been elucidated in animal model cardiogenesis. To continue with my group‟s work on genes involved in the second heart field, I plan to undertake collaborative and complementary experiments with other members of Stephan Zaffran‟s group.

Currently I am trying to define the involvement and cross-species conservation of homeobox genes in addition to *Hoxa1*, *Hoxa3* and *Hoxb1*, which this group has recently shown to molecularly define a subdomain of the pulmonary trunk myocardium in the conus (Bertrand et al. 2011). (*Hoxa3* for example has recently been shown to not have exactly the same expression domains between chick and mouse).This region is anatomically interesting because it not only elongates but rotates over time, and cryptic domains in an otherwise homogeneous-appearing tube define the entry points of coronary

arteries into the aorta and the positions of the interventricular septum and valve leaflets (Bajolle et al. 2006; Bajolle et al. 2008).

Because of the above-described interest in retinoic acid signaling and its known effects on both neural crest differentiation and on *Hox* gene expression, we will see if removing an enzyme essential for retinoic acid metabolism, Raldh2, specifically from the NCC lineage has an effect on cardiac development. Raldh2-/- mutants for whom the maternal diet is supplemented in retinoic acid can survive to a stage where their patent heart defects can be examined, and among these are deficient outflow tract septation (Ryckebusch et al. 2008), a process known to be dependent on NCC. We will first examine the cardiac NCC lineage in such diet-supplemented Raldh2-/- embryos by making crosses with a Wnt1-Cre;Rosa26R –lacZ line (Echelard, Vassileva, and McMahon 1994). We will then use mouse-chick neural tube chimeras (Fontaine-Pérus and Chéraud 2005) to determine whether retinoic acid is playing more than one cell-autonomous role in different cardiac cell lineages, and if the migratory NCC population does not also vehicle a secreted signal into the outflow tract that is necessary for its development.

MOLECULAR ETIOLOGY OF LARGE AND GIANT CONGENITAL MELANOCYTIC NEVI

A new research theme I have finally been able to launch this last academic year aims to understand the molecular causes of proliferative diseases of pigment cells by using the extreme and rare case of the large congenital melanocytic nevus (LCMN) as an exemplary pathology to elucidate others, such as neurocutaneous melanocytosis, malignant melanoma, and the lentigines and cafe-au-lait spots characteristic of a number of other syndromes. Localized excess skin pigmentation is the visible sign of both the common and rare congenital nevus as well as the relatively common adult-onset melanoma and the rarer, often lethal, pediatric forms. Our working hypothesis is that studying the rare disease will also shed mechanistic light on the more common presentations.

My group is currently addressing the following questions: Which sequence variations of the human genome are associated with a predisposition to, or the onset of, LCMN? Can more indirect effects on genomic function or organization cause a LCMN to develop?

Over the near term, I aim to study how some of these direct changes in genomic organization, first identified in preliminary genomic screens, may lead to abnormal melanocyte development during prenatal life. With the knowledge gained about the control of melanocyte proliferation, it should be possible to model and test treatments for human disease. Ultimately, I wish to examine the functional effects of physiological molecular modifications on melanocytes and their NCC precursors, using *in vitro* and *in vivo* models to recapitulate aspects of CMN development.

RATIONALE

Description of LCMN

Congenital melanocytic naevi (CMN) can arise in all areas of the skin. Their frequency decreases from 1 in every 100 births for the smallest lesions to an estimated 1 in 50,000 births or more, for surfaces extending over 100 cm^2. All CMN have an abnormally high concentration of melanocytes, the pigment cells of the skin and iris, in sharply defined regions. Large and giant CMN (OMIM 137550) are variable in presentation, often comprising increased hair density and growth along with disparate levels of pigmentation, proliferative nodules and deficient skin annexes. Like other CMN, they can be located anywhere in the body, but are often localized along the midline of the head and trunk, including the face, most frequently over the shoulders or buttocks.

Treatment protocols for CMN are highly variable, tethered to reconstructive surgery and based on anecdotal reports of risk management. The disfiguring aspect of the disease is coupled with a currently unmeasurable risk of severe neurological associations and oncological transformation – among which, pediatric malignant melanoma, with very poor prognosis. There appears to be increased incidence of degenerative complications in patients with the giant forms of CMN (Marghoob et al. 2004; Kinsler, Birley, and Atherton 2009). Aside from incomplete epidemiological observations, such as more frequent onset during early childhood, no environmental or genetic risk factors for these life-threatening additional conditions are currently known.

LCMN are part of a family of developmental diseases known as neurocristopathies: disorders in the migration, proliferation or differentiation of a population of pluripotent embryonic cells called the neural crest (NC) (Etchevers, Amiel, and Lyonnet 2006). LCMN can be associated with malformations in other neural crest-derived tissues, and other forms of NC-derived tumors such as neurofibroma, schwannoma, or certain forms of head/neck rhabdomyosarcoma. The fact that associated conditions are regularly reported but not systematic implies that a second molecular event may have occurred among a subset of cells predisposed to it by the first, and that identification of both would be beneficial for patients. Initial studies have suggested that benign pigmented proliferations can be distinguished from malignant ones on the basis of the high frequency of large structural chromosomal aberrations in the latter (Broekaert et al. 2010).

Embryological bases of congenital pigment cell proliferation disorders

Human skin is made up of two distinct compartments, the epidermis and dermis, which are normally separated by a basal lamina. The epidermis, derived from the ectoderm, ensures a semi-permeable barrier function with the extracorporeal environment. It

contains annexes that develop from placodes into hair follicles, sebaceous and sudoripal glands. These are embedded into the dermis and the underlying adipose hypodermis, in such a way that the continuous epidermis folds and buckles. The dermis is an innervated and vascularized connective tissue, made up of fibroblasts, which secrete the collagen and elastin fibers that confer local mechanical properties on the organ as a whole. This layer also plays an important role in the homeostasis of the overlying epidermis (Cario-André et al. 2006). NC cells form in the human embryo during the first few weeks of pregnancy from the tissue that will give rise to the central nervous system. They migrate away from it throughout the body, integrating into nearly every tissue. All skin melanocytes, like all components of the peripheral nervous system, are derived from NC, which also gives rise to dermis, cartilage, adipocytes and vascular smooth muscle of the head and neck, among other tissues (Le Douarin and Kalcheim 1999).

Over the course of development, after their precursors settle evenly within the basal layer of the stratified human epidermis, melanocytes normally begin to produce specialized organelles that contain the pigments eumelanin or pheomelanin. At a proportion of about one melanocyte to 30 neighboring epidermal keratinocytes, the former distribute these melanosomes to the latter by means of dendritic prolongations, and do not themselves retain pigment. Once incorporated, eumelanin protects the genetic material of the otherwise exposed keratinocytes from the effects of UV and superoxide damage. Melanocytes also distribute melanin to the cells lining the hair follicles and thereby tint hairs from the inside for as long as a resident melanoblast population in the cycling follicle is able to self-renew. NC-like stem cells persist in hair follicles (Fernandes et al. 2004) and the dermis (Li et al. 2010) after birth.

The structure of CMN skin is quite different. Massive and circumscribed aggregates of sometimes heavily self-pigmented melanocytes accumulate at the basal surface of the epidermis, while nests of these cells can extend throughout the thickness of the structurally disrupted dermis into subcutaneous tissues, often along nerves. Thick and abnormally dense hair is often observed, and other skin annexes can be disrupted. Even the subcutaneous tissues can be malformed, with nevus development occurring at the expense of hypodermic adipocytes, or on the contrary presenting large lipoma-like proliferations. Some remodeling of LCMN architecture occurs over the first years of life.

“Tardive" congenital lesions are present as precursor conditions at birth but only manifest thereafter; the emergence of so-called "satellite" naevi throughout the first few years of life is indicative of the postnatal maturation of these precursors. In a long prospective study of an American cohort, the presence of >20 satellite nevi was found to be a significant risk marker for neurocutaneous melanocytosis (NCM), that is, a CMN, sometimes proliferative, that is tangled into the leptomeninges of the brain or spinal cord(Marghoob et al. 2004). A recent retrospective study of a large English cohort placed the presence of congenital satellite naevi as the primary prognostic factor for potential complications (Kinsler et al. 2008). Like the cutaneous LCMN with which it is associated, NCM is considered to be a kind of hamartoma (Fu et al. 2010). Most publications describe the often life-threatening epilepsy and/or hydrocephalus that NCM

can cause, but the long-term prognosis of non-symptomatic NCM remains unknown. Symptomatic NCM occurs in approximately 7% of patients with large CMN (≥ 20 cm diameter projected adult size [PAS]) (Slutsky et al. 2010). The incidence of malignant transformation remains controversial. A meta-study finds malignancy in around 1% of large CMN patients, with a range in reports to up to nearly 10% in patients with the giant forms of >40 cm PAS (Krengel, Hauschild, and Schafer 2006; Kinsler, Birley, and Atherton 2009). This incidence is thousands of times greater than the general European population (Holterhues 2010), although malignant melanoma is one of the more common cancers.

Pathways common to normal neural crest development, nevogenesis and transformation

Melanocyte proliferation can be stimulated by a number of ligand-tyrosine kinase receptor binomes, through intracellular effectors of the RAS family that activate the mitogen-activated protein (MAP) kinase pathway. Two important molecules in this transduction are NRAS and the next effector in the MAP kinase pathway, BRAF. Reproducible somatic mutations in *BRAF*, leading to abnormally high enzymatic activity, are involved in many cancers, malignant melanoma in particular (Brose et al. 2002), and, surprisingly, are also found in a number of clinically benign acquired naevi (Pollock et al. 2003).

Human neural crest-derived tissue lineages appear to be particularly sensitive to hyperactive RAS signaling overall, as exemplified by the Noonan, cardio-facio-cutaneous, Costello and LEOPARD syndromes, in which autosomal dominant germline mutations of different MAPK effectors have been identified. In addition to malformations of other craniofactial or cardiac neural crest derivatives, these present pigment anomalies, including dark skin, woolly or curly hair, multiple lentigines or café-au-lait spots. Neurofibromatosis 1, also distinguished by multiple café-au-lait spots, can occur in conjunction with Noonan syndrome; the causative gene, *NF1*, normally also represses RAS activity. Interestingly, two patients in our initial cohort, collected with the collaboration of the American patient association Nevus Outreach, Inc., have tested positive for constitutional *NF1* mutations after biopsy of neurofibromas, in addition to their LCMN.

Patients with large or giant CMN on the whole, though not always, are exempt from other symptoms, pointing toward sporadic somatic mutations that occur early during embryonic life and present in a mosaic fashion n(Happle 1999). In a Belgian LCMN cohort of 24 cases, 18 presented activating germline mutations in NRAS and only 3 in BRAF, in contrast to acquired naevi as mentioned above (Dessars et al. 2007; Dessars et al. 2009). The examination of the corresponding LCMN melanocyte transcriptome showed a non-intuitive, significant downregulation of the transcription of a few dozen eumelanogenesis-related genes, relative to a pool of melanocytes cultured from normal neonatal foreskin (Dessars et al. 2009). These findings imply a complex balance between surface receptor stimulation, in particular that of the melanocortin 1 receptor (MC1R), intracellular signal

transduction, and the activity of such developmentally important transcription factors as MITF over the course of embryonic and perinatal skin development (**see Figure 2 of Reyes-Mugica et al. 2011, in Appendix**).

Animal models of LCMN

Transgenic over-expression of stem cell factor (KITL) in the basal layer of mouse epidermis results in a hyperpigmented phenotype, with increased densities of melanocytes localized at the basal keratinocyte layer (Kunisada et al. 1998). However, this was not an ideal model for CMN, since the phenotype was uniform. Nevertheless, injection of soluble KITL into human skin grafts increased the number of melanocytes, while inhibition of its action through its receptor, KIT, resulted in the loss of melanocytes (Grichnik et al. 1998). These data demonstrate that this signaling pathway may be active even in postnatal skin and critical for the survival and persistence of melanocytes in the epidermis.

We have already directly examined the *BRAF* gene sequence for known hotspot mutations in exon 15 in twelve tissue samples derived from LCMN in a preliminary collaborative study with Sylvie Fraitag in the pathology department of the Necker Children‟s Hospital, without finding any mutations. Dr. Kinsler in London (Great Ormond Street Hospital) has conducted a similar examination on blood samples from LCMN patients, with the same result (personal communication). The activating mutation of *BRAF* found most frequently in humans has been expressed in zebrafish pigment cells, under the control of the MITF promoter. While wild-type *Braf* did not change the pigmentation of the zebrafish, the activated form of the gene led to the appearance of nevus-like clusters of pigment covering large areas, up to 40% of the body surface (Patton et al. 2005). Interestingly, crossing these fish to those *deficient* in the tumor suppressor transcription factor p53 (product of the *CDKN2A* gene) led to the development of aggressively invasive melanoma, in which the MAP kinase pathway was unduly active.

p53 protein is increased in the keratinocytes and melanocytes of acquired pigmented nevi in conjunction with keratinocyte KITL, while inhibition leads to a decrease in transcription of *MC1R* and the KITL receptor *KIT* and *EDNRB* in the melanocytes of organotypic cultures of the same lesions (Murase et al. 2009). It was demonstrated recently that NC progenitors from the *mitfa:BRAF(V600E);p53*$^{-/-}$ zebrafish do not terminally differentiate, but retain many embryonic molecular characteristics that make the melanomas developing therefrom, more aggressive (Ceol et al. 2011). Blocking transcriptional elongation specifically inhibits both normal neural crest development and melanoma progression in this model(White et al. 2011). A complex and networked signaling cascade makes the immediate effects of loss- or gain-of-function of any of the components rather difficult to predict (Reyes-Mùgica et al., in press [Appendix]).

APPROACHES FORESEEN

I have undertaken a strategy in collaboration with the group of Greg Barsh at the HudsonAlpha Institute, Alabama (USA) to identify the nature of both constitutive and "second hit" molecular events by using both germline and lesional DNAs, and study their effects *in vitro*. For constitutive (germline) DNA, we are using blood and saliva donations from patients and their parents, and have already subjected a number of samples to hybridization to Illumina Omni 1M single nucleotide polymorphism arrays. This has given us provocative information about unusual copy number variations, which in a few of the patients has implicated the availability of molecules we already know can be involved in melanocyte development.

A masters student last year began to study the role of Mc1r and its natural agonist and antagonist in the embryonic chicken model, whose cutaneous melanocyte development is more similar to humans than the mouse. With a second-year masters student in 2011, we plan to examine the spatiotemporal distribution of some of these newly implicated molecules in the melanocytes and their precursors, in comparison to the pattern of *Sox10* expression in undifferentiated melanocyte precursors, that we have recently established.

LCMN skin may maintain higher levels of KITL in the dermis, or more KIT receptor in the pigmented cells. To test this hypothesis, and to constitute the critical resource for further high-throughput sequencing strategy, I have established agreements with local surgeons and pathologists to collect donations of ten nevus samples from children being operated at the Timone Hospital, which will serve to prepare a formal request to the ethics committee. These samples will be subdivided. They will be subjected to immunohistochemical observation of the distribution of KITL and KIT, but also of other receptors including MET and two common intracellular effectors of these pathways that are indicated by our initial CNV results. More importantly, we will constitute the resource necessary to compare germline and somatic mutations in the same patients, subject to institutional approval that is currently being sought. Finally, we will also derive the pigment cells from a portion of these nevi for cell culture (Cario-André et al. 2006).

Having recently published a protocol by which it is possible to derive undifferentiated human neural crest cell lines, already characterized by my group previously, I would like to have the possibility to establish new cell lines (see below). These could be infected with a lentiviral vector that will vehicle the over-expression of activated BRAF or NRAS, to test if potentiation of the RAS pathway is sufficient to drive phenotypic transformation of these cells, or to alter their response to the defined factors that drive melanocytic differentiation *in vitro*. BrdU incorporation could allow the comparison of proliferation rates between experimental and mock-transfected cultures.

In collaboration with Alain Taieb‟s group in Bordeaux, we have long hoped to make three-dimensional epidermal reconstructs in order to examine the histology of the distribution of these constitutively active BRAF/NRAS-expressing melanocytes derived from our cultures as compared to normally induced melanocytes or naturally occurring

nevomelanocytes. Their proliferative response to MC1R binding or inactivation will also be tested, as polymorphisms in this modifier gene may be involved in the severity of LCMN phenotype (Kinsler et al., personal communication and (Krengel et al. 2011)). Finally, we would like to transplant the four different cell types (NC cells induced to become melanocytes, the same with activated BRAF or NRAS, and nevocytes) into chicken embryos to characterize and compare their migratory and proliferative behaviour *in vivo*.

Meanwhile, electroporation of activated KIT receptor, upstream of the MAPK signalling pathway among other options, can be carried out directly into prospective neural crest cells in the chicken embryo. This may render them more sensitive to stochastic events that favor melanocytosis, similar to the *mitfa:BRAF(V600E)* zebrafish. In order to provoke such events artificially, we will locally transfect the surface ectoderm or the forebrain with either the secreted or membrane-bound isoforms of KITL, which may have different biological activity (Paulhe et al. 2009). In these ways we shall try to develop an animal model of LCMN and/or NCM in which to better characterize the process of nevogenesis and assess eventual therapies.

RELATED ARTICLES:

Krengel S, Breuninger H, Beckwith M, **Etchevers HC**. (2011) Meeting report from the 2011 International Expert Meeting on Large Congenital Melanocytic Nevi and Neurocutaneous Melanocytosis, Tübingen. Pigment Cell Melanoma Res. Accepted manuscript online: 15 Jun 2011, doi: 10.1111/j.1755-148X.2011.00875.x

Reyes-Mùgica M, Beckwith M, **Etchevers HC**. (2011) Etiology of congenital melanocytic nevi and related conditions. In: Nevogenesis (Practical Clinical Medicine series) eds. A. Marghoob, J. Grinchik, A. Scope and S. Dusza. Springer, New York.

CONSTITUTION OF HUMAN TISSUE BIOLOGICAL RESOURCES

In the near future, I will begin the process of building two distinct biobanks. The first is underway with respect to DNA derived from the blood of CMN patients and their parents, but it is under an authorization dependent on my collaborators at the Necker Children‟s Hospital and its ISO9001-approved DNA bank. Given that we have similarly excellent facilities in Marseille, that this city is a major regional center for pediatric surgery of large/giant CMN, and I have the agreement of Nathalie Dugardin to participate in this tissue banking, it will be ideal to simultaneously collect and then compare constitutional DNA from the blood of affected children and their parents, and the somatic DNA derived from the surgical samples.

The second biobank will be a new human embryo collection, once the logistical details have been examined, to mirror that of Toulouse and perhaps complement the dwindling resources at the Necker Hospital. Ultimately, I would like to see the establishment of a permanent service platform from which it is possible to provide an informed, functional characterization of developmental genes in human tissues that is so often needed to

understand the phenotypes of certain gene mutations (Ostrer, Wilson, and Hanley 2006). Histological sections appropriate for spatiotemporal localization, but also frozen, cleanly microdissected tissues appropriate for chromatin immunoprecipitation or the isolation of nucleic acids and proteins for comparative analyses, will all constitute a precious commodity for my research group and collaborators, but I also aspire to have this become a self-sustaining resource over the long term.

APPENDIX

BIBLIOGRAPHY

Bajolle, Fanny, Stephane Zaffran, Sigolene Meilhac, Mathieu Dandonneau, T Chang, Robert G Kelly, and ME Buckingham. 2008. Myocardium at the base of the aorta and pulmonary trunk is prefigured in the outflow tract of the heart and in subdomains of the second heart field. *Developmental Biology* 313: 25 - 34.

Bajolle, Fanny, Stéphane Zaffran, Robert G Kelly, Juliette Hadchouel, Damien Bonnet, Nigel A Brown, and ME Buckingham. 2006. Rotation of the myocardial wall of the outflow tract is implicated in the normal positioning of the great arteries. *Circulation Research* 98, no. 3 (February 17): 421-8.

Bajpai, Ruchi, D A Chen, Alvaro Rada-Iglesias, Junmei Zhang, Yiqin Xiong, Jill Helms, C-P Chang, Yingming Zhao, Tomek Swigut, and Joanna Wysocka. 2010. CHD7 cooperates with PBAF to control multipotent neural crest formation. *Nature* 463, no. 7283: 958-62. doi:10.1038/nature08733.

Bertrand, Nicolas, Marine Roux, Lucile Ryckebüsch, Karen Niederreither, Pascal Dollé, A Moon, Mario Capecchi, and Stéphane Zaffran. 2011. Hox genes define distinct progenitor sub-domains within the second heart field. *Developmental Biology* 353, no. 2 (March 6): 266-74. doi:10.1016/j.ydbio.2011.02.029.

Broekaert, Sigrid M C, Ritu Roy, Ichiro Okamoto, Joost van den Oord, Jürgen Bauer, Claus Garbe, Raymond L Barnhill, et al. 2010. Genetic and morphologic features for melanoma classification. *Pigment Cell & Melanoma Research* 23, no. 6 (December): 763-70.

Brose, Marcia S, Patricia Volpe, Michael Feldman, Madhu Kumar, Irum Rishi, Renee Gerrero, Eugene Einhorn, et al. 2002. BRAF and RAS mutations in human lung cancer and melanoma. *Cancer Research* 62, no. 23 (December): 6997-7000.

Cai, C L, X Liang, Y Shi, P H Chu, S L Pfaff, J Chen, and S Evans. 2003. Isl1 identifies a cardiac progenitor population that proliferates prior to differentiation and contributes a majority of cells to the heart *Developmental Cell* 5, no. 6: 877-889.

Cario-André, Muriel, Catherine Pain, Yvon Gauthier, Vincent Casoli, and Alain Taieb. 2006. In vivo and in vitro evidence of dermal fibroblasts influence on human epidermal pigmentation. *Pigment Cell Research* 19, no. 5 (October): 434-42.

Ceol, Craig J., Yariv Houvras, Judit Jane-Valbuena, Steve Bilodeau, David a. Orlando, Valentine Battisti, Lauriane Fritsch, et al. 2011. The histone methyltransferase SETDB1 is recurrently amplified in melanoma and accelerates its onset. *Nature* 471, no. 7339: 513-517.

Danno, Hiroki, Tatsuo Michiue, Keisuke Hitachi, Akira Yukita, Shoichi Ishiura, and Makoto Asashima. 2008. Molecular links among the causative genes for ocular malformation: Otx2 and Sox2 coregulate Rax expression. *Proceedings of the National Academy of Sciences of the United States of America* 105, no. 14: 5408-13.

Desai, Tushar J, Sarah Malpel, George R Flentke, SM Smith, and Wellington V Cardoso. 2004. Retinoic acid selectively regulates Fgf10 expression and maintains cell identity in the prospective lung field of the developing foregut. *Developmental Biology* 273, no. 2: 402-15.

Dessars, Barbara, Linda E De Raeve, Hakim El Housni, Catherine J Debouck, Pierre J Sidon, Renato Morandini, Diane Roseeuw, Ghanem E Ghanem, Gilbert Vassart, and Pierre Heimann. 2007. Chromosomal translocations as a mechanism of BRAF activation in two cases of large congenital melanocytic nevi. *The Journal of Investigative Dermatology* 127, no. 6: 1468-70.

Dessars, Barbara, Linda E De Raeve, Renato Morandini, Anne Lefort, Hakim El Housni, Ghanem E Ghanem, Benoît J Van den Eynde, et al. 2009. Genotypic and gene expression studies in congenital melanocytic nevi: insight into initial steps of melanotumorigenesis. *The Journal of Investigative Dermatology* 129, no. 1: 139-47.

Echelard, Y, G Vassileva, and A P McMahon. 1994. Cis-acting regulatory sequences governing Wnt-1 expression in the developing mouse CNS. *Development* 120, no. 8: 2213-24.

Etchevers, Heather C, Jeanne Amiel, and Stanislas Lyonnet. 2006. Molecular Bases of Human Neurocristopathies. In *Neural Crest Induction and Differentiation*. Texas: Eurekah.

Fernandes, Karl J L, Ian a McKenzie, Pleasantine Mill, KM Smith, Mahnaz Akhavan, Fanie Barnabé-Heider, Jeff Biernaskie, et al. 2004. A dermal niche for multipotent adult skin-derived precursor cells. *Nature Cell Biology* 6, no. 11: 1082-93.

Fontaine-Pérus, Josiane, and Yvonnick Chéraud. 2005. Mouse-chick neural chimeras. *The International Journal of Developmental Biology* 49, no. 2-3 (January): 349-53.

Fu, Yong-Juan, Nobuhito Morota, Atsuko Nakagawa, Hitoshi Takahashi, and Akiyoshi Kakita. 2010. Neurocutaneous melanosis: surgical pathological features of an apparently hamartomatous lesion in the amygdala. *Journal of Neurosurgery. Pediatrics* 6, no. 1: 82-6.

Grichnik, J M, J A Burch, J Burchette, and C R Shea. 1998. The SCF/KIT pathway plays a critical role in the control of normal human melanocyte homeostasis. *The Journal of Investigative Dermatology* 111, no. 2 :233-8.

Happle, R. 1999. Loss of heterozygosity in human skin. *Journal of the American Academy of Dermatology* 41, no. 2 Pt 1: 143-64.

Holterhues, C. 2010. Trends in incidence of cutaneous malignant melanoma in Europe: analysis of population based cancer registry data. *Melanoma Research* 20: e3. doi:10.1097/01.cmr.0000382744.23097.a8.

Kawaguchi, R, J Yu, J Honda, J Hu, J Whitelegge, P Ping, P Wiita, D Bok, and H Sun. 2007. A Membrane Receptor for Retinol Binding Protein Mediates Cellular Uptake of Vitamin A. *Science* 315, no. 5813: 820-825.

Kinsler, V A, J Birley, and D J Atherton. 2009. Great Ormond Street Hospital for Children Registry for congenital melanocytic naevi: prospective study 1988-2007. Part 1-epidemiology, phenotype and outcomes. *The British Journal of Dermatology* 160, no. 1: 143-50.

Kinsler, V A, W K Chong, S E Aylett, and D J Atherton. 2008. Complications of congenital melanocytic naevi in children: analysis of 16 years' experience and clinical practice. *The British Journal of Dermatology* 159, no. 4:907-14.

Kirby, M L, T F Gale, and D E Stewart. 1983. Neural crest cells contribute to normal aorticopulmonary septation. *Science* 220, no. 4601: 1059-1061.

Kirby, M L, K L Turnage, and B M Hays. 1985. Characterization of conotruncal malformations following ablation of "cardiac" neural crest. *The Anatomical Record* 213, no. 1: 87-93.

Krengel, S, Helmut Breuninger, Mark Beckwith, and Heather C Etchevers. 2011. Meeting report from the 2011 International Expert Meeting on Large Congenital Melanocytic Nevi and Neurocutaneous Melanocytosis, Tübingen. *Pigment Cell & Melanoma Research* (June 15). doi:10.1111/j.1755-148X.2011.00875.x.

Krengel, S., A. Hauschild, and T. Schafer. 2006. Melanoma risk in congenital melanocytic naevi: a systematic review. *British Journal of Dermatology* 155, no. 1: 1-8.

Krings, T, S Geibprasert, C B Luo, J J Bhattacharya, H Alvarez, and Pierre Lasjaunias. 2007. Segmental neurovascular syndromes in children. *Neuroimaging clinics of North America* 17, no. 2: 245-58. doi:10.1016/j.nic.2007.02.006.

Kunisada, T, S Z Lu, H Yoshida, S Nishikawa, M Mizoguchi, S Hayashi, L Tyrrell, D a Williams, X Wang, and B J Longley. 1998. Murine cutaneous mastocytosis and epidermal melanocytosis induced by keratinocyte expression of transgenic stem cell factor. *The Journal of Experimental Medicine* 187, no. 10: 1565-73.

Le Douarin, N, and C Kalcheim. 1999. *The Neural Crest*. 2nd ed. Cambridge, U.K. Cambridge University Press.

Li, Ling, Mizuho Fukunaga-Kalabis, H Yu, Xiaowei Xu, Jun Kong, JT Lee, and Meenhard Herlyn. 2010. Human dermal stem cells differentiate into functional epidermal melanocytes. *Journal of Cell Science* 123, no. Pt 6: 853-60. doi:10.1242/jcs.061598.

Limaye, Nisha, Laurence M Boon, and Miikka Vikkula. 2009. From germline towards somatic mutations in the pathophysiology of vascular anomalies. *Human Molecular Genetics* 18, no. R1: R65-74.

Marghoob, Ashfaq A, Stephen Dusza, Susan Oliveria, and Allan C Halpern. 2004. Number of satellite nevi as a correlate for neurocutaneous melanocytosis in patients with large congenital melanocytic nevi. *Archives of dermatology* 140, no. 2: 171-5.

Meulemans, D, and M Bronner-Fraser. 2005. Central role of gene cooption in neural crest evolution. *J Exp Zoolog B Mol Dev Evol* 304B, no. 4: 298-303.

Murase, Daiki, Akira Hachiya, Yasuko Amano, Atsushi Ohuchi, Takashi Kitahara, and Yoshinori Takema. 2009. The essential role of p53 in hyperpigmentation of the skin via regulation of paracrine melanogenic cytokine receptor signaling. *The Journal of Biological Chemistry* 284, no. 7: 4343-53.

Niederreither, Karen, and Pascal Dolle. 2008. Retinoic acid in development: towards an integrated view. *Nature Reviews Genetics* 9, no. 7: 541-53.

Ostrer, H, D I Wilson, and N a Hanley. 2006. Human embryo and early fetus research. *Clinical Genetics* 70, no. 2 (August): 98-107.

Park, E J, Y Watanabe, G Smyth, S Miyagawa-Tomita, E Meyers, J Klingensmith, T Camenisch, M Buckingham, and A M Moon. 2008. An FGF autocrine loop initiated in second heart field mesoderm regulates morphogenesis at the arterial pole of the heart. *Development* 135, no. 21: 3599-3610.

Pasutto, Francesca, Heinrich Sticht, Gerhard Hammersen, Gabriele Gillessen-Kaesbach, David R Fitzpatrick, G Nürnberg, Frank Brasch, et al. 2007. Mutations in STRA6 cause a broad spectrum of malformations including anophthalmia, congenital heart defects, diaphragmatic hernia, alveolar capillary dysplasia, lung hypoplasia, and mental retardation. *American Journal of Human Genetics* 80, no. 3: 550-60.

Patton, E Elizabeth, Hans R Widlund, Jeffery L Kutok, Kamden R Kopani, James F Amatruda, Ryan D Murphey, Stephane Berghmans, et al. 2005. BRAF Mutations Are Sufficient to Promote Nevi Formation and Cooperate with p53 in the Genesis of Melanoma. *Current Biology* 15: 249-254.

Paulhe, Frédérique, M Wehrle-Haller, Marie-Claude Jacquier, Beat a Imhof, Séverine Tabone-Eglinger, and B Wehrle-Haller. 2009. Dimerization of Kit-ligand and efficient cell-surface presentation requires a conserved Ser-Gly-Gly-Tyr motif in its transmembrane domain. *The FASEB Journal* 23, no. 9: 3037-48.

Pollock, P M, U L Harper, K S Hansen, L M Yudt, M Stark, C M Robbins, T Y Moses, et al. 2003. High frequency of BRAF mutations in nevi. *Nature Genetics* 33, no.1:19-20.

Ryckebusch, Lucile, Z Wang, Nicolas Bertrand, S-C Lin, Xuan Chi, Robert Schwartz, Stéphane Zaffran, and Karen Niederreither. 2008. Retinoic acid deficiency alters second heart field formation. *Proceedings of the National Academy of Sciences of the United States of America* 105, no. 8 (February): 2913-8.

Slutsky, Jordan B, Jeffrey M Barr, Alisa N Femia, and Ashfaq A Marghoob. 2010. Large congenital melanocytic nevi: associated risks and management considerations. *Seminars in cutaneous medicine and surgery* 29, no. 2 (June): 79-84.

Urness, Lisa D., Tracy J. Wright, and Suzanne L. Mansour. 2010. Fgf3 and Fgf10 are required redundantly for neural crest migration and cardiovascular development. *Developmental Biology* 344, no. 1: 481-481.

Watanabe, Y, Sachiko Miyagawa-Tomita, Stéphane D Vincent, Robert G Kelly, Anne M Moon, and ME Buckingham. 2010. Role of mesodermal FGF8 and FGF10 overlaps in the development of the arterial pole of the heart and pharyngeal arch arteries. *Circulation research* 106, no. 3:495-503.

White, Richard Mark, Jennifer Cech, Sutheera Ratanasirintrawoot, CY Lin, Peter B. Rahl, Christopher J. Burke, Erin Langdon, et al. 2011. DHODH modulates transcriptional elongation in the neural crest and melanoma. *Nature* 471, no. 7339: 518-22.

Development 126, 3533-3543 (1999)
Printed in Great Britain © The Company of Biologists Limited 1999
DEV2431

Anterior cephalic neural crest is required for forebrain viability

Heather C. Etchevers, Gérard Couly, Christine Vincent and Nicole M. Le Douarin*

Institut d'Embryologie Cellulaire et Moléculaire du CNRS et du Collège de France, 49 bis avenue de la Belle Gabrielle, 94736 Nogent-sur-Marne Cedex, France

*Author for correspondence (e-mail: etchever@infobiogen.fr; ledouari@infobiogen.fr)

Accepted 25 May; published on WWW 19 July 1999

SUMMARY

The prosencephalon, or embryonic forebrain, grows within a mesenchymal matrix of local paraxial mesoderm and of neural crest cells (NCC) derived from the posterior diencephalon and mesencephalon. Part of this NCC population forms the outer wall of capillaries within the prosencephalic leptomeninges and neuroepithelium itself. The surgical removal of NCC from the anterior head of chick embryos leads to massive cell death within the forebrain neuroepithelium during an interval that precedes its vascularization by at least 36 hours. During this critical period, a mesenchymal layer made up of intermingled mesodermal cells and NCC surround the neuroepithelium. This layer is not formed after anterior cephalic NCC ablation. The neuroepithelium then undergoes massive apoptosis. Cyclopia ensues after forebrain deterioration and absence of intervening frontonasal bud derivatives. The deleterious effect of ablation of the anterior NC cannot be interpreted as a deficit in vascularization because it takes place well before the time when blood vessels start to invade the neuroepithelium. Thus the mesenchymal layer itself exerts a trophic effect on the prosencephalic neuroepithelium. In an assay to rescue the operated phenotype, we found that the rhombencephalic but not the truncal NC can successfully replace the diencephalic and mesencephalic NC. Moreover, any region of the paraxial cephalic mesoderm can replace NCC in their dual function: in their early trophic effect and in providing pericytes to the forebrain meningeal blood vessels. The assumption of these roles by the cephalic neural crest may have been instrumental in the rostral expansion of the vertebrate forebrain over the course of evolution.

Key words: Pericyte, Telencephalon, Vascularization, Neural crest, Meninges, Forebrain, Chimera, Chick, Quail

INTRODUCTION

After neurulation, the cells of the vertebrate central nervous system proliferate extensively as they organize into functionally and morphologically distinct regions. The forebrain, derived from the embryonic prosencephalic vesicle, is structurally subdivided into (1) the diencephalon, yielding the eyes, optic nerves and chiasm, thalamus, hypothalamus and neurohypophysis, and (2) the telencephalon, essentially composed of the olfactory bulbs and cerebral hemispheres. Among chordates, the paired cerebral hemispheres are a vertebrate-specific evolutionary development. A fate map of the early anterior neural plate, constructed by the quail-chick chimera technique (Couly and Le Douarin, 1985, 1987), shows that, in birds, the presumptive territories of the cerebral hemispheres are located in two anterolateral areas adjacent to the neural folds. In contrast, the ventral diencephalic areas destined to yield the unique hypothalamus, posthypophysis and optic chiasm are found medially, separating the anlagen of the eyes; the territory of the adenohypophysis is located in the rostral transverse neural fold. The dorsal diencephalon, including the epiphysis, arises from the caudally adjacent region. Cephalic neural crest cells (NCC) emigrate from the fused neural folds caudal to the epiphysis, from neural plate levels corresponding to the presumptive regions of the posterior diencephalon, mesencephalon and rhombencephalon (Fig. 1A; c.f. Couly and Le Douarin, 1987). Similar organization of the anterior neural plate appears to be conserved, with minor variations, in other vertebrate classes (reviewed in Rubenstein et al., 1998).

Following the mediodorsal closure of the neural tube, the eyes and telencephalon are sites of particularly intense growth. This cell proliferation leads to the rostral protrusion of first the eyes and then the cerebral hemispheres beyond the anterior end of the notochord and prechordal plate (e.g. Couly and Le Douarin, 1988; Shimamura et al., 1995).

Forebrain growth is accompanied by the concomitant development of the meninges, membranes surrounding the central nervous system, which comprise an outer dura mater and an inner leptomeninx (*lepto-*, thin). The leptomeningeal matrix is initially composed of mesenchymal NCC and a primitive vascular net of endothelial cells. Johnston (1966) first observed a potential contribution of NCC to the forebrain meninges, using a short-lived radioactive tracer. Subsequently, systematic labeling of defined regions of the cephalic neural folds, using the quail-chick chimera system, demonstrated that not only each layer of the forebrain meninges (Fig. 1B) but also the facial skeleton, frontal and parietal bones, and overlying

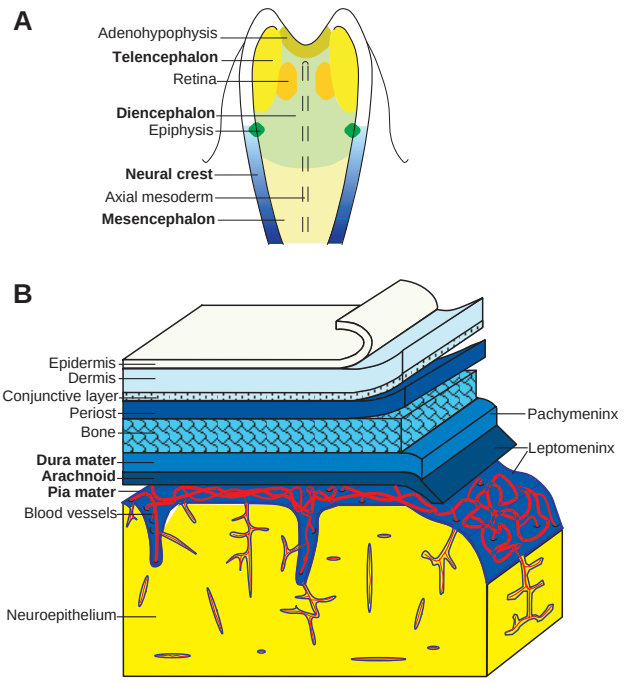

Fig. 1. (A) Fate map of the anterior neural plate. Adapted from Couly et al. (1987, 1988). The paired territories of the presumptive telencephalon lie in the lateral neural plate, dorsal to the future anterior diencephalon and rostral to neural crest-producing neural folds (blue). (B) Anatomy of the layers of the late embryonic head. Blue layers correspond to derivatives of the neural crest surrounding the anterior brain. The meninges (dura mater, arachnoid and pia mater) enclose the entire central nervous system (CNS). The pia mater continuously surrounds all of the circumconvolutions of the CNS and isolates ingressing arachnoidal blood vessels from the neuroepithelium. It is a constituent of the blood-brain barrier. The subarachnoid space, well-defined in humans, is obscured in the chicken. The term 'leptomeninx', employed in the text, thus refers to both the arachnoid and pial layers of the meninges.

dermis originate from the cephalic neural crest (Le Lièvre and Le Douarin, 1975; Couly and Le Douarin, 1987; Couly et al., 1993). The NC contribution to the leptomeninx includes pericytes and connective tissue cells (H. C. E., G. C. and N. M. Le D., unpublished data), but excludes the endothelial cells, which arise from a small territory of the anterior paraxial mesoderm within the head fold, adjacent to the prosencephalon (Couly et al., 1995).

Thus, the cephalic NCC penetrate the forebrain neuroepithelium together with vascular buds made up of endothelial cells. This double origin of the leptomeninx from the NC and paraxial mesoderm is exclusively found in the forebrain; in the rest of the central nervous system (CNS), the meninges are entirely of mesodermal origin (Le Lièvre, 1976; Couly et al., 1992).

Unlike pericytes, which can be either of neural crest or mesodermal origin, blood vessel endothelial cells of both the head and body are strictly mesodermal in origin (reviewed in Le Douarin, 1982). The blood vessel endothelium segregates from other cephalic mesodermal derivatives as early as the head-fold stage, as seen by the precocious expression of a tyrosine kinase receptor to the vascular endothelium growth factor (VEGF), designated as VEGFR2 (Eichmann et al., 1993). VEGFR2-expressing cells give rise to the endothelial walls of blood vessels, which form the perineural vascular plexus of the developing leptomeninges in the head (Eichmann et al., 1993).

The coincidence of meningeal construction with the initial phase of forebrain growth led to the present investigation, aimed at exploring how the anterior cephalic NCC might participate in the development of the forebrain. Strikingly, after removal of the posterior diencephalic and mesencephalic neural folds, the neuroepithelium of the entire future forebrain underwent apoptosis within 1 day following closure of the anterior neural tube, although the telencephalic neural folds had been left intact. Cell death occurred well before the onset of budding of the bulbs destined to form the telencephalic cerebral hemispheres. The ventral diencephalon and retinae were not included in this degenerative process because ectopic migration and proliferation of NCC populations caudal to the excised territory partially compensated for the rostral deficiency. Embryos subjected to neural fold ablation became cyclopic, while the mesencephalon and a variable extent of the caudal and ventral diencephalon became in turn the rostralmost portion of the brain.

The timing of forebrain apoptosis led to the conclusion that the presence of NC-derived mesenchyme is necessary for the survival and growth of the prosencephalic neuroepithelium during a phase preceding the onset of its vascularization by at least 36 hours. NCC transplanted heterotopically from the level of the rhombencephalon, but not the trunk, can compensate for the effects of anterior neural fold ablations. The grafted compensatory cells later differentiate into rostral head-specific derivatives such as meningeal and intraencephalic pericytes. The entire cephalic NC is therefore capable of participating together with endothelial cells to build the meninges. In normal development, however, only the rostral population does so. This emphasizes that the paraxial mesodermal population near the prosencephalon behaves differently from that of the rest of the head, since on its own it is not capable of constructing forebrain meninges.

In all other parts of the CNS, the paraxial mesoderm ensures the construction of the leptomeninx. The reason for which it is not so for the anterior brain may be because the amount of paraprosencephalic mesoderm is scanty during forebrain expansion. To compensate this deficit of mesodermal cells, NCC take over the production of pericytes and other connective tissue in this area. In fact, NCC have already been shown to play this role in the construction of the skull around the forebrain and in forming the dermis in the facial and forehead areas.

We have thus tested the capacity of various types of mesoderm to replace the anterior NC and to form a complete leptomeninx, which permits the survival and development of the cerebral hemispheres. When added to neural fold-ablated embryos, any level of the paraxial mesoderm (but not trunk lateral plate mesoderm) can replace the NCC to partially or fully maintain viability in the forebrain neuroepithelium. Grafted paraxial mesoderm differentiates into both endothelial cells and pericytes under these circumstances. Our results thus indicate that it is the presence of a primitive leptomeninx that is needed for the survival and subsequent growth of the developing prosencephalon.

MATERIALS AND METHODS

Operations

Chimeras were constructed between quail and chick embryos by grafting either mesoderm or neural folds from the rhombencephalic or truncal levels of stage-matched quail donors to the prosencephalic area of chick hosts. These are described below and schematized in Fig. 2. *Gallus gallus* (JA57 line, Institut de Sélection Animale, Lyon, France) and *Coturnix coturnix japonica* eggs were incubated for approximately 30 hours to obtain embryos from between the 2- and 5-somite stage, stage 7 to 8 of Hamburger and Hamilton (1951, HH7-8), or between the 7- and 10-somite stage, HH9-10 for late controls.

The fate maps of the neural folds constructed by Couly et al. (1993) and Grapin-Botton et al. (1995) were used to define the regions corresponding respectively to the telencephalon, diencephalon, mesencephalon and first rhombomere (r1) at the stage of the operation. The length of each presumptive area was then determined in a case-specific manner by using an ocular micrometer; the anterior extremity of the embryo and the anterior limit of the first somite pair were chosen as fixed reference points. Host embryos were visualized by injection under the blastoderm of 5% India ink in PBS, or in Tyrode's solution, supplemented with antibiotics (Gibco). Embryos were subsequently fixed at a range of times from 6 hours after the operation to embryonic day 9 (E9).

Experiment 1: neural fold ablations

The cephalic neural folds release NCC from the mid-diencephalic level caudally (Couly and Le Douarin, 1987). Anterior to this level, which corresponds to the site of the prospective epiphysis, the neural folds remain epithelial. The effects of the removal of the entire pool of NCC that invest the anterior head were examined in this group of experiments. The neural folds of the posterior diencephalon, mesencephalon and rhombomere 1 (r1) (Experiment 1a, 1d), or the posterior diencephalic and mesencephalic neural folds alone (Experiment 1b, 1c), were ablated by extirpation with tungsten scalpels. Neural folds were removed either bilaterally (Experiments 1a, 1b, 1d) or unilaterally (Experiment 1c). To confirm that none of these ablations included the presumptive territory of the telencephalon, a length of neural folds including the levels of posterior diencephalon, mesencephalon and r1 was replaced bilaterally with the equivalent tissue from stage-matched quail donors (Experiment 1d). In Experiment 1e, similar bilateral neural fold ablations to Experiment 1a were made at HH9-10, after NCC emigration had begun.

Experiment 2: capacity of r1 and posterior neural folds to compensate for removal of the anterior source of NCC

This experimental series was aimed at testing the capacity of NCC from posterior axial levels to replace the rostral cephalic NCC. Three types of experiments were performed, in all of which the neural folds from the posterior diencephalon, mesencephalon and r1 were removed bilaterally. For Experiment 2a, the r1 segment was replaced bilaterally by its quail counterpart, leaving the posterior diencephalon and mesencephalon without neural folds. In Experiment 2b, the entire length of the ablation was replaced by unilateral or bilateral grafts of neural folds corresponding to r4 through r8 (limit between somite pairs 4 and 5). The same length of neural folds from the unsegmented trunk level of quail donors, at stages ranging from 10 to 17 somites, was grafted bilaterally in Experiment 2c.

Experiment 3: cephalic mesoderm grafts

The paraxial mesoderm adjacent to the presumptive ventrolateral diencephalon (area C of Couly et al., 1995; area 5 of Couly et al., 1992) was exposed by surgical removal of the ectoderm from quail donors at 2- to 5-somite stages. In order to test its endogenous capacity to give rise to pericytes, this 'paraprosencephalic' mesodermal population was removed by means of a Pasteur pipette pulled to a diameter of approximately 80 μm, and transferred to stage-matched chick hosts in which the homotopic mesenchyme had been disrupted (Experiment 3a). In another experiment, the same graft was placed heterotopically at the level of the mesencephalon (Experiment 3b).

Experiment 4: mesodermal grafts after neural fold ablations

Bilateral neural fold ablations were performed as described in Experiment 1a on chick hosts. Next, paraxial mesoderm from adjacent to the ventrolateral diencephalon (Experiment 4a, 'paraprosencephalic' mesoderm) or lateral mesencephalon (Experiment 4b, 'paramesencephalic' mesoderm) was surgically removed from quail donors and grafted into the chick host dorsally, and secured under adjacent rostral ectoderm. Paraprosencephalic and paramesencephalic mesoderm correspond respectively to areas 5 and 3 of Couly et al. (1992) or areas C and D of Couly et al. (1995). In Experiments 4c and 4d, large pieces of trunk mesoderm were isolated from 10- to 17-somite-stage quail donors in the non-segmented region and cleaned of surrounding tissues (including ectoderm) by means of 1× pancreatin (Gibco) in PBS. Then grafts of approximately 150×300 μm were cut from paraxial (Experiment 4c) or lateral plate (Experiment 4d) mesoderm for transfer to hosts as above.

Immunohistochemistry

Three monoclonal antibodies (mAb) were used: QCPN (anti-quail, Developmental Studies Hybridoma Bank; undiluted hybridoma supernatant of IgG1 isotype), MB1/QH1 (anti-quail endothelium and white blood cells, Péault et al., 1983, and Pardanaud et al., 1987; 1:1500 dilution of ascites fluid of IgM isotype), and 1A4 (anti-smooth muscle actin, Sigma; 1:400 dilution of ascites fluid of IgG2a isotype). Embryos were processed as described by Catala et al. (1996), using appropriate goat secondary antibodies conjugated to alkaline phosphatase (AP) or horseradish peroxidase (HRP). The chromogenic reaction for AP was performed using the Vector AP substrate kit III according to manufacturer's instructions; for HRP, 0.1 mg/ml diaminobenzidine (Sigma) and 0.005% H_2O_2 in PBS were used. In triple-stained sections, slides were bathed in 0.1 M glycine, pH 2.2 after the first AP reaction, before applying the next primary antibody and another AP-conjugated secondary antibody. Under these circumstances, the second AP-conjugated immunocomplex was revealed with Fast Red substrate tablets (Sigma). Sections were generally counterstained in Gill's hematoxylin solution and observed under a Leica light microscope.

Cell death and proliferation

29 embryos from Experiment 3a were harvested at HH19. All were soaked in Nile blue-containing Pannett and Compton's solution (Jeffs and Osmond, 1992) to examine cell death in toto, and photographed while the embryos were still alive. After paraffin sections were cut at 5 μm and rehydrated, the TUNEL reaction was carried out on 23 embryos according to the instructions in the kit by Boehringer Mannheim, using 0.1 mg/ml diaminobenzidine, 0.005% H_2O_2 in PBS as the chromogenic substrate for localization of cell death.

In situ hybridization

Probes were synthesized from linearized template plasmid for chicken *Hoxa3* (a kind gift of Dr R. Krumlauf). *Hoxa3* riboprobe incorporating ^{35}S-UTP (Amersham) were applied to sections of embryos fixed in Carnoy's solution, pretreated as described by Eichmann et al. (1993). Rinses were performed according to Wilkinson and Nieto (1993). Slides were dipped in 1:1 water/Kodak NTB-2 photographic emulsion, developed 10 days later in Kodak D-19 and counterstained with Gill's hematoxylin.

RESULTS

Gross anatomy of the head following the partial ablation of cephalic neural folds

We first examined the effects of ablation of the neural folds from which NCC emigrate to participate in the telencephalic

and diencephalic meninges (Experiment 1). These correspond to the neural folds of the future diencephalon, caudal to the level of the epiphysis, and the mesencephalon (Couly et al., 1987).

In Experiment 1a (Fig. 2), a length of neural folds including those of the posterior diencephalon, mesencephalon and the first rhombomere (r1) was removed bilaterally (Fig. 3A-C). As a result, the telencephalon and dorsal diencephalon of operated embryos were strikingly absent in 37/37 cases observed from embryonic day (E)3 on (E3, *n*=26; E4, *n*=1; E5, *n*=2; E6, *n*=1; E7, *n*=3; E8, *n*=4). The interocular distance was visibly reduced in 14/24 embryos at E2 (HH15-HH18). This phenotype was always accompanied by the severe reduction or absence of the frontonasal bud, resulting in various degrees of fusion of the optic cups going from synophthalmia with associated hypotelorism (Fig. 3H-J) to complete cyclopia (Fig. 3D-G). In operated embryos, the two independent retinal domains had converged after formation, but the eyes shared a medial lens and orbit (Fig. 3F). Oculomotor muscles of the rectus medialis were equally absent in cyclopic embryos. While the cerebral hemispheres were never present, the size of the ventral prosencephalon varied. In many animals, the optic chiasm, hypothalamus and neurohypophysis were present. In extreme cases (*n*=6 out of 37 embryos at E3-E8), the diencephalon was reduced to a stub with a recognizable neurohypophysis (Fig. 3F). The adenohypophysis was always formed as well. The volume of the mesencephalic ventricle varied, but the morphology and neuronal lamination of the optic tecta appeared essentially normal (Fig. 3F).

Experiment 1b consisted of a similar ablation that did not include the neural folds of r1. In 4 out of 7 cases, we saw the same severe deficiencies as when the ablation included the neural folds of r1. However, normal external head morphology was observed in 3 out of 7 embryos between E4 and E7 (not

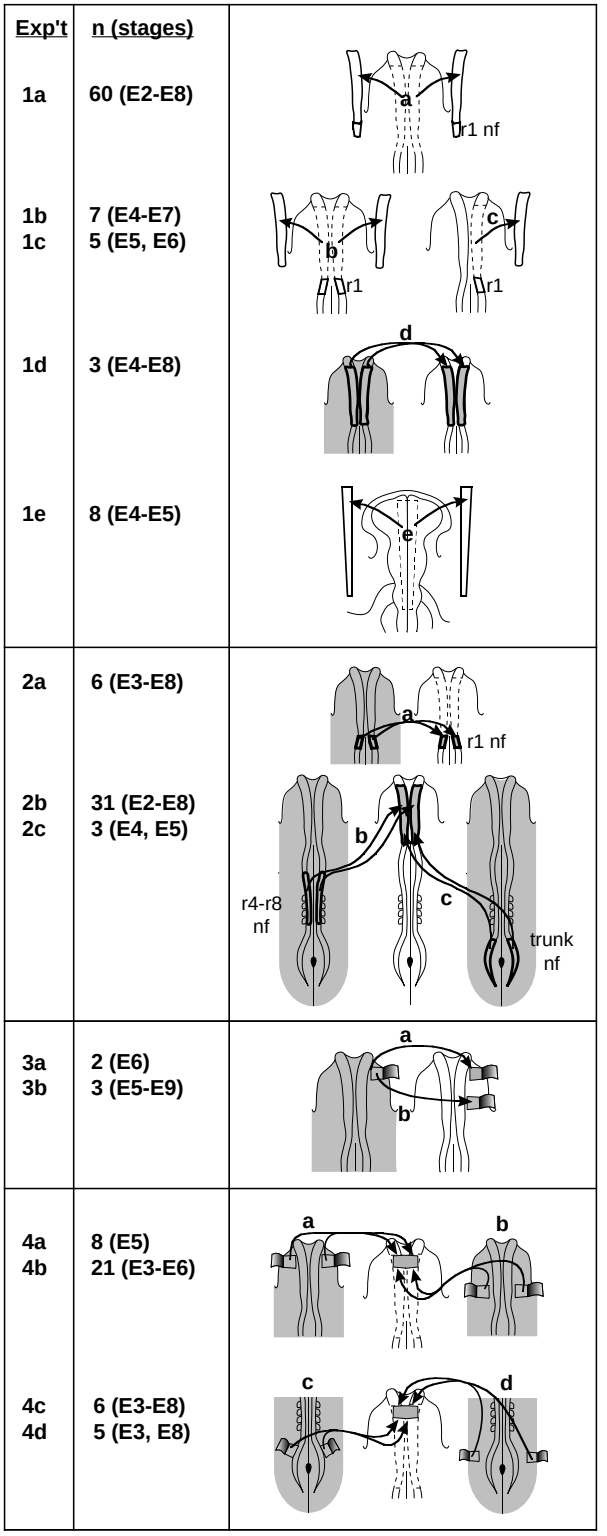

Fig. 2. Schematic representation of the experimental strategy. The number of cases for each type of experiment, and their ages at harvest, are indicated next to a diagram illustrating the manipulation or graft. Host embryos were operated at HH7-8 unless otherwise indicated. Experiment 1a: ablation of posterior diencephalic, mesencephalic and first rhombomeric (r1) neural folds (nf). Experiment 1b: ablation of posterior di- and mesencephalic neural folds alone. Experiment 1c: unilateral ablation of posterior di- and mesencephalic neural fold. Experiment 1d: homotopic, bilateral replacement of posterior di- and mesencephalic neural folds of chick with quail equivalent. Experiment 1e: ablation of posterior di-, mesencephalic and r1 neural folds in HH9-10 embryos, after NCC migration had begun. Experiment 2a: homotopic, bilateral replacement of r1 neural folds of chick with quail equivalent, after ablation of posterior diencephalic, mesencephalic and r1 neural folds in host. Experiment 2b: heterotopic, bilateral replacement of posterior di-, mesencephalic and r1 neural folds of chick with a length of quail neural folds corresponding to r4-r8. Experiment 2c: heterotopic, bilateral replacement of posterior di-, mesencephalic and r1 neural folds of chick with a length of quail neural folds corresponding to unsegmented somitic levels of donors at HH10-12. Experiment 3a: homotopic graft of paraprosencephalic mesoderm from quail to chick. Experiment 3b: heterotopic graft of paraprosencephalic mesoderm from quail to chick at level of mesencephalon. Experiment 4a: addition of paraprosencephalic mesoderm from quail to chick in which posterior diencephalic, mesencephalic and r1 neural folds had been previously ablated. Experiment 4b: addition of paramesencephalic mesoderm from quail to chick in which posterior di-, mesencephalic and r1 neural folds had been previously ablated. Experiment 4c: addition of trunk-level paraxial mesoderm from HH10-12 quail to chick in which posterior di-, mesencephalic and r1 neural folds had been previously ablated. Experiment 4d: addition of trunk-level lateral plate mesoderm from HH10-12 quail to chick in which posterior di-, mesencephalic and r1 neural folds had been previously ablated.

shown). In these cases, the telencephalon, though present, was reduced in size compared to stage-matched control embryos.

In order to see that the effects of neural fold ablation were indeed due to the NCC, three control experiments were performed (not shown). First, unilateral neural fold ablations (Experiment 1c, Fig. 2) did not lead to significant morphological consequences in any of 5 operated embryos, through contralateral NC compensation. Second, bilateral replacement of the ablated tissue in 3 embryos (Experiment 1d, Fig. 2) with similarly excised neural folds from stage-matched quails, confirmed that the normally formed telencephalon and anterior diencephalon were of host origin when examined at E4 and E8, although the meninges were graft-derived. Third, bilateral ablation of the dorsal neural tube, including the neural folds, from embryos in which NCC migration had previously begun (Experiment 1e, Fig. 2) led to the maintenance of telencephalic cerebral hemispheres in all 8 embryos examined at E4 and E5.

Removal of the anterior neural folds prior to NCC emigration thus severely hampers the development of the telencephalon, the dorsal diencephalon, the frontonasal bud and the anterior part of the ventral diencephalon, while not affecting that of the eyes. As a consequence of the defect in telencephalic and frontonasal development, the two eye fields tend to fuse at the midline, generating various degrees of cyclopia.

Defective forebrain development is a result of massive cell death in the telencephalic and diencephalic neuroepithelium

Cell death was examined in toto, in control embryos and after bilateral neural fold ablations (Experiment 1a), prior to fixation at HH15 (E2), HH18 (late E2) and HH19 (early E3). Control embryos (*n*=8) took up Nile blue sulfate, showing cell death concentrated in the ventral optic lens (Fig. 4A,G, arrows) and nasal epithelium (Fig. 4G, arrowhead). However, a prominent blue zone of cell death was apparent in the prosencephalon at HH15 (Fig. 4D, arrow) or localized in its protuberant remnant below the eyes at HH18-19 (Fig. 4J, arrow). The TUNEL technique confirmed numerous apoptotic figures in sections through the same areas (HH15, *n*=6/6; HH18-19, *n*=15/17). In unoperated embryos, apoptosis within the prosencephalon was sparse at all ages with the exception of a dense, localized region of the future olfactory neuroepithelium (Fig. 4C at HH15; Fig. 4I at HH18). Stage-matched operated embryos had a zone of apoptosis which included and extended beyond these areas to comprise most of the prosencephalic vesicle (Fig. 4F). The telencephalon is substantially reduced by the third embryonic day (Fig. 4J,K), and what is left is undergoing apoptosis (Fig. 4L). In unoperated embryos, NCC and mesodermal cells finish surrounding the anterior encephalic vesicle and form the leptomeninges at HH15, while vascular invasion of the telencephalic neuroepithelium by NC-supported capillaries normally begins at HH24 (H. C. E., G. C. and N. M. Le D., unpublished data). In the absence of the anterior NC population, prosencephalic cell death is underway on HH15 (Fig. 4E) and the prospective telencephalon already eliminated

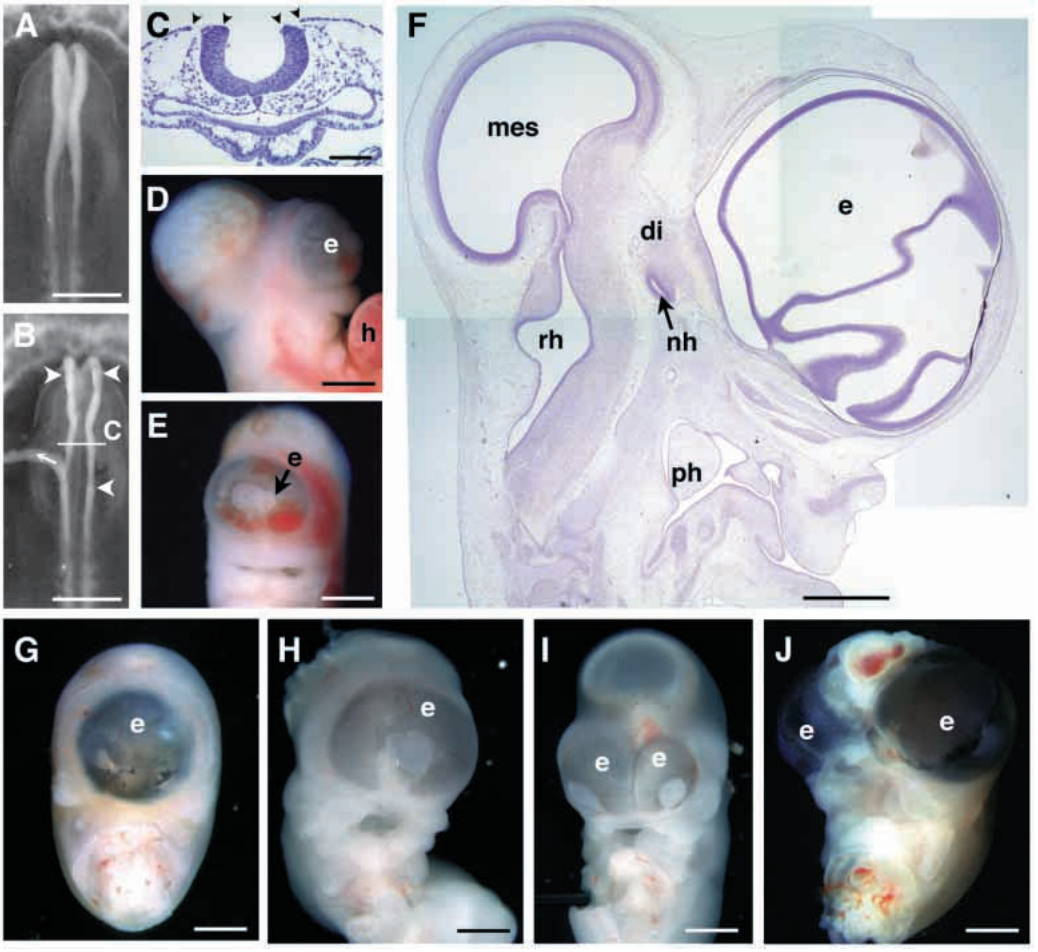

Fig. 3. Ablation of cephalic NC causes the subsequent absence of forebrain territories (Experiment 1). Embryo before (A) and after operation (B, between arrowheads) at 5-somite stage. The right neural fold has been ablated but is still being detached on the left (arrow). (C) Transverse section taken through the level of operation of same embryo, fixed 2 hours after neural fold ablation (arrowheads). (D,E) A synophthalmic embryo at E8 in side and frontal view (h, heart). (F) In a parasagittal section from the same embryo, the fused eyes (e) are directly apposed to the remnant of the diencephalon (di), and the entire telencephalon is missing. The retinal fusion interface is apparent; part of the neurohypophysis (nh) is visible (mes, mesencephalon, rh, rhombencephalon, ph, pharynx). (G-J) Examples of facial malformations range from complete cyclopia and reduction of naso-fronto-maxillary structures (G) to synophthalmia (H, I) to hypotelorism (J). Bars: A,B,F, 0.5 mm; C, 100 μm; D,E,G-J, 1 mm.

by HH19. Apoptosis thus begins up to 58 hours before normal vascularization of the forebrain and is complete 22 hours later.

Because the presumptive telencephalic territory itself is not included in the neural fold ablations of Experiment 1, damage to it cannot be responsible for the telencephalic deficiency and cell death observed. One hypothesis to explain the elimination of the forebrain in absence of NCC is that their proximity is critical for survival and further development of the forebrain. We then explored whether other cell populations also had the capacity to restore telencephalic growth in place of the endogenous NC.

NCC from r1 can migrate rostrally and partly rescue the survival of the telencephalon

When only the diencephalic and mesencephalic neural folds were removed in Experiment 1b, nearly half of the embryos retained diencephalic and some telencephalic tissue. One would expect that these regions would be absent, since the diencephalic and mesencephalic neural crest give rise to meninges that cover the entire diencephalon and telencephalon. Based on previous results (see Fig. 7 of Couly et al., 1996), we postulated that the host NC could be responsible for a partial compensatory effect through rostral migration. Experiment 2a was designed to see whether NCC from r1, which does not normally make meningeal pericytes, would be able to migrate rostrally in the absence of anterior NCC. A length of neural folds including those of the posterior diencephalon, mesencephalon and r1 was ablated as in Experiment 1a, and the neural folds of r1 were replaced bilaterally by their quail equivalent (Figs 2, 5A). Out of the 6 embryos observed, 3 embryos retained some telencephalic neuroepithelium (E3, *n*=1; E6, *n*=1; E8, *n*=1; Fig. 5D), while 3 embryos lacked the entire telencephalon (E3, *n*=1; E6, *n*=2; Fig. 5B). In the embryos examined at E3, quail cells were found to have migrated into the mesenchyme ventral and anterior to the eyes (not shown). At E6 and E8, grafted cells from r1 became pericytes within either the residual diencephalon (Fig. 5C) or the diencephalon and telencephalon (Fig. 5E,F). These cells did not express the antigen for MB1/QH1, a mAb recognizing quail endothelial and blood cells (Fig. 5C), but did contain

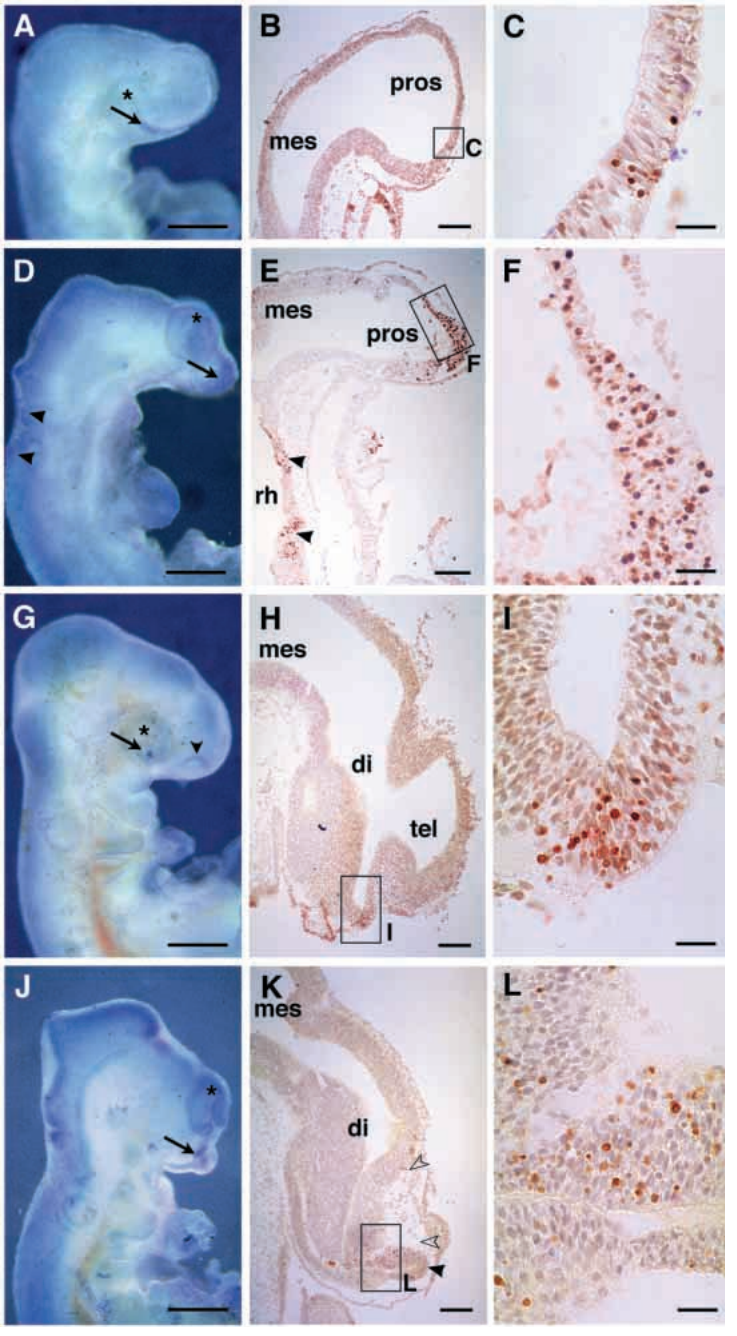

Fig. 4. The prosencephalon undergoes progressive apoptosis after removal of the diencephalic and mesencephalic NC (Experiment 1). (A) Unoperated embryo stained with Nile blue, HH15. A stripe of normal cell death is indicated in the ventral eye and prosencephalon (arrow). (B) Parasagittal section through the embryo in A, after the TUNEL reaction. The region magnified in C is indicated. (C) Natural apoptosis occurs in a restricted part of the ventral prosencephalon. (D) Operated embryo at HH15, Nile blue. The eyes are closer together and a large zone of apoptosis is visible (arrow). Two normal domains of cell death in the rhombencephalon are indicated with arrowheads. (E) Parasagittal section through the embryo in D, after the TUNEL reaction. The region magnified in F is indicated, and the two zones of normal hindbrain apoptosis shown with arrowheads. (F) Most of the prosencephalon is undergoing vigorous apoptosis at this stage, although dying cells have not yet been cleared (compare brain profiles in B and E). (G) Unoperated embryo stained with Nile blue, HH18. Normal cell death is present in the optic lens (arrow) and nasal epithelium (arrowhead), as well as in scattered ectodermal cells. (H) Parasagittal section through the embryo in G, after the TUNEL reaction. The region magnified in I is indicated. (I) A restricted zone of the prospective olfactory neuroepithelium is undergoing apoptosis, but cell death is sparse elsewhere in the forebrain. (J) Operated embryo at HH18, Nile blue. The eyes are nearly synophthalmic in this case, and a dying remnant of the forebrain is indicated with an arrow. (K) Parasagittal section through the embryo in J, after the TUNEL reaction. The region magnified in L is indicated. Note that the caudal diencephalon is mostly intact in this embryo, but the telencephalon is severely reduced (arrowhead). Many cells have already been cleared dorsally (between open arrowheads; compare profiles in H and K). (L) The remnant of telencephalon is undergoing widespread cell death. Pros, prosencephalon; tel, telencephalon; di, diencephalon; mes, mesencephalon; rh, rhombencephalon; asterisk, eye. Bars: A,D,G,J, 0.5 mm; B,E,H,K, 100 μm; C,F,I,L, 20 μm.

alpha smooth muscle actin, characteristic of pericytes (Fig. 5E,F). The majority of NCC from r1 remained ventrolateral to the eyes, participating in the first branchial arch, mesenchymal cells of the adenohypophysis and some ventrolateral periocular mesenchyme.

NCC from r1 normally migrate into the first branchial arch and give rise to mandibular and hyoid components (Couly et al., 1996; Köntges and Lumsden, 1996). We show here that when the neural folds anterior to r1 are removed, NCC from r1 are capable of a significant rostral migratory diversion, into areas normally colonized by NCC from diencephalic and mesencephalic neural folds, where they partially compensate for the ablation and rescue forebrain tissue. Such compensation attenuates to varying degrees the phenotype observed after removal of the anterior cephalic neural crest.

NCC from the posterior rhombencephalon can substitute for anterior populations and rescue telencephalic survival

In a second step, we tested the capacity of posterior rhombencephalic NCC to prevent forebrain cell death. NCC from rhombomeres 4 to 8, like the neuroepithelium from which they derive, express *Hox* genes of the first four paralogue groups when migrating in situ. They normally do not participate in the meninges of the hindbrain or any other region, but do migrate into all branchial arches except for the first arch (Couly et al., 1996). In Experiment 2b (Fig. 2), the neural fold corresponding to r4 to r8 included (i.e. from the r3/r4 limit to the level of the fourth somite), was transplanted unilaterally (E2, *n*=9; E3, *n*=2; E5, *n*=2; E6, *n*=8; E8, *n*=1) or bilaterally (E2, *n*=3; E3, *n*=1; E5, *n*=2; E6, *n*=2; E7, *n*=1) from quail donors into chick hosts after an ablation including the neural folds of the posterior diencephalon, mesencephalon and r1 (Fig. 6A). The grafted neural fold integrated seamlessly into the host, and embryos formed normally (Fig. 6B). The heterotopic NCC contributed to each of the derivative cell types described for the homotopic anterior NCC population: meningeal pericytes (Fig. 6C), frontonasal bud cartilage, dermis, periocular structures and connective tissue of the oculomotor muscles and adenohypophysis. Pericytes derived from the grafted NCC were found uniquely within the prosencephalon and its meninges. Nonetheless, some of the posterior rhombomeric crest population retained the expression of *Hoxa3* in ectopic locations such as the mesenchyme surrounding Rathke's pouch and the ventral diencephalon as well as the first branchial arch (Fig. 6D,E). Interestingly, *Hoxa3* was not visible in the meninges or pericytes that colonized the forebrain region (not shown). These grafted cells apparently downregulated *Hoxa3* expression after having reached the anterior neuroepithelium.

In Experiment 2c, a length of approximately 450 μm of neural folds from the unsegmented trunk level of 10- to 17-somite-stage quail donors was grafted bilaterally into the di-/mesencephalic region (E4, *n*=1; E5, *n*=2). Embryos presented defects identical to those in which the ablation of the endogenous neural folds was not followed by any graft (c.f. Le Douarin et al., 1977). The few migratory cells observed were sometimes associated with cranial nerve IV (data not shown).

Restoration of prosencephalic development by mesoderm addition

After bilateral ablation of a length of neural folds

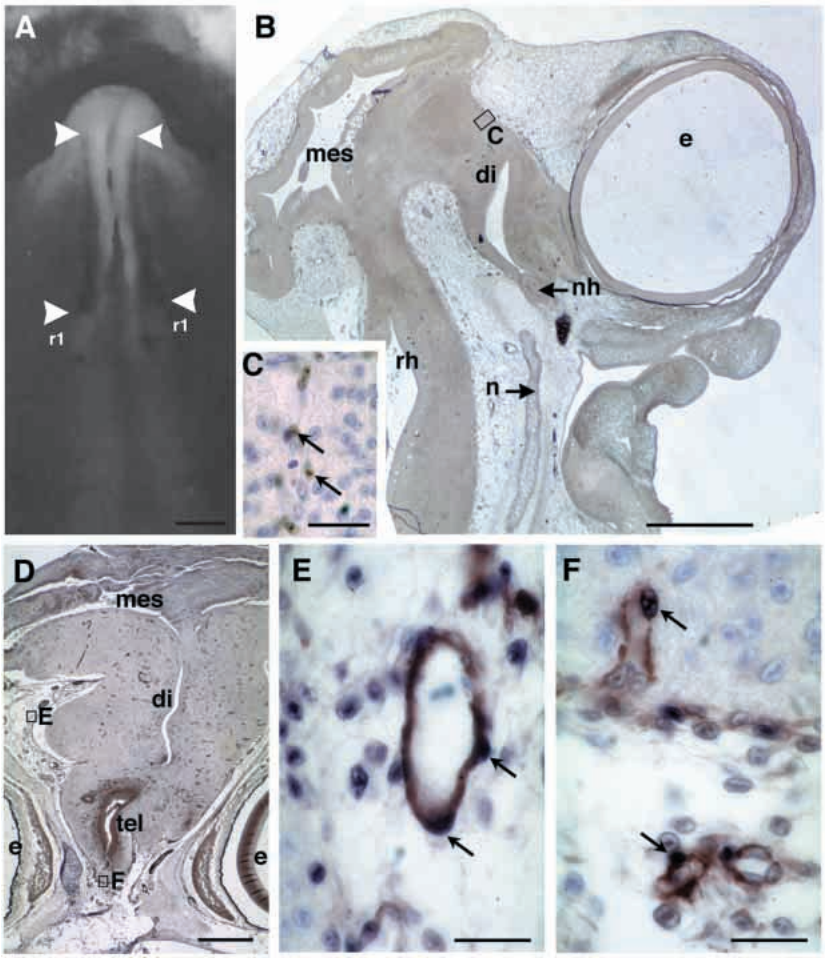

Fig. 5. Partial compensation for the NC deficiency after ablation of diencephalic and mesencephalic neural folds comes from NCC of the first rhombomere (Experiment 2a). (A) Immediately after operation, at 4-somite stage. The length of the neural fold ablation is indicated between the arrowheads and bilaterally grafted r1 neural folds are visible below the ablation. (B) The range of external defects in the 6 embryos examined resembled that observed after Experiment 1b. This case, shown in slightly parasagittal section at E6, lacked a telencephalon and was synophthalmic (di, diencephalon; mes, mesencephalon; rh, rhombencephalon; n, notochord; nh, neurohypophysis). (C) Grafted cells are found within the diencephalic meninges and penetrating the neuroepithelium (arrows), in association with blood vessels. (D) Another case, shown in transverse section at E6, had some telencephalic tissue (tel) and normally spaced eyes (e). Areas enlarged in E and F are indicated. (E) r1 NCC (blue), when associated with blood vessels, colocalize with alpha-smooth muscle actin (brown), confirming that they are pericytes. (F) Graft-derived pericytes are found in the telencephalic meninges and neuroepithelium, although r1 NCC do not normally participate in meninges. Bars: A, 200 μm, B,D, 0.5 mm; C,E,F, 20 μm.

corresponding to the posterior diencephalon, mesencephalon and r1, the endogenous paraxial mesoderm, adjacent to the ventrolateral prosencephalon at HH7-8 (termed 'paraprosencephalic'), is not sufficient to support prosencephalic viability and growth. This might be due either to the incapacity of this mesodermal area to yield pericytes in the brain, or to the fact that the number and placement of mesodermal cells in the paraprosencephalic area do not allow the production of both endothelial and pericytic cell populations for the dorsal prosencephalon.

First, to establish if the paraprosencephalic mesoderm normally differentiates into pericytes as well as endothelial cells (Couly et al., 1995), we grafted it from quail donors into chicken hosts at the prosencephalic level near the neural tube

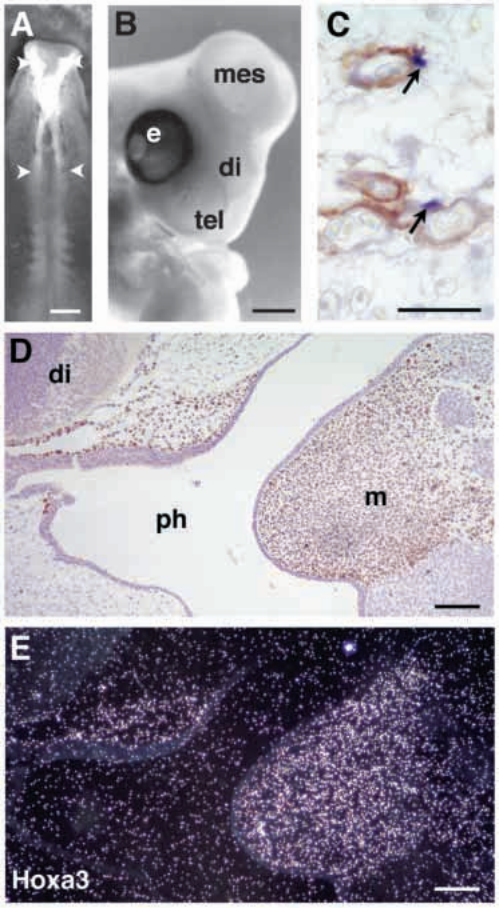

Fig. 6. Heterotopic substitution of the diencephalic and mesencephalic neural folds by those of the posterior rhombencephalon leads to respecification of the fate of the grafted NCC (Experiment 2b). (A) Operated embryo, with neural folds from the level of r4 to r8 grafted between the arrowheads (corresponding to the level of the posterior diencephalon, mesencephalon and r1). (B) The same embryo at E6, with normal forebrain vesicles. (C) Grafted NCC within the forebrain meninges (blue, arrows) also make alpha-smooth muscle actin (brown). (D) The ectopic NCC (brown, QCPN; parasagittal section of embryo in B) retain expression of the anteroposterior position gene *Hoxa3* in inappropriate locations. (E) In an adjacent section, *Hoxa3* expression in the first branchial arch and around the ventral diencephalon. Di, diencephalon; m, maxillary arch; ph, pharynx. Bars: A, 200 μm; B, 1 mm; C-E, 50 μm.

in addition to the endogenous paraprosencephalic mesoderm (Experiment 3a, Fig. 2). At HH29 (E6, not shown), grafted cells participated in the endothelial wall of blood vessels both in and around the forebrain (n=2). While most quail cells were MB1/QH1 positive, a few were identified by the mAb 1A4 as pericytes in blood vessels near the eyes (not shown), although grafted pericytes were not observed in the brain. When placed lateral to the mesencephalon (Experiment 3b, Fig. 2), the same population of cells differentiated only into endothelium, but not into pericytes, in blood vessels external to the brain (E5, n=1; E6, n=1; E9, n=1). In conclusion, the paraprosencephalic mesoderm yields mostly endothelial cells of blood vessels within and outside of the brain, and virtually no pericytes, although it does possess the capacity to differentiate into this cell type. However, it never contributes to the pericytes of the prosencephalic meningeal or intraencephalic vessels, nor to pericytes of the mesencephalon when grafted ectopically (also see Couly et al., 1995). Endogenous pericyte-forming populations in either location contribute to the blood vessels of the brain and its meninges, at the expense of the grafted paraprosencephalic mesoderm.

To remove this competition, in Experiment 4a (Fig. 2), quail paraprosencephalic mesoderm was grafted above the dorsal prosencephalon after bilateral ablation of posterior diencephalic, mesencephalic and r1 neural folds (Fig. 7A). In 5 out of 8 embryos observed at E5, the telencephalon was restored (Fig. 7B,C). The grafted tissue, localized by QCPN mAb immunoreactivity, was found adjacent to the neuroepithelium, and quail cells were visible within the forebrain tissue and meninges (Fig. 7D) as 1A4 mAb-positive pericytes and MB1/QH1-positive endothelial cells. In the 3 other embryos, the forebrain had not developed; while the grafted cells were present within the head mesenchyme, they were not adjacent to the neuroepithelium. The capacity of the paraprosencephalic mesoderm to yield pericytes within the forebrain meninges or parenchyme is thus restricted to experimental situations where the normal source of forebrain pericytes (the NC) is lacking and where this mesodermal population is grafted in a dorsal position over the neuroepithelium to support its host counterpart.

Paramesencephalic mesoderm was similarly grafted above the dorsal prosencephalon (Experiment 4b, Fig. 2). During normal development, this mesodermal population yields all components of the midbrain leptomeninx, including blood vessel endothelial cells and pericytes (Couly et al., 1995). It was therefore interesting to test the capacity of the paramesencephalic mesoderm to rescue neuroepithelial survival in the forebrain region and to examine the subsequent differentation of the grafted cells. In 14/21 embryos, both telencephalon and diencephalon developed (Fig. 7E). Localized in the host by the QCPN mAb, the grafted paramesencephalic mesoderm gave rise to both intraencephalic endothelial cells and pericytes (Fig. 7F-H). Vessels were generally chimeric, with host pericytes and donor endothelial cells (Fig. 7F), donor pericytes and host endothelial cells, or combinations of both (Fig. 7G,H). Here too, in successful rescues, the grafted cells were located dorsally and in contact with the telencephalon. NC-derived mesenchyme is therefore not the only tissue able to promote forebrain development.

Lastly, embryos received grafts of the paraxial mesoderm of

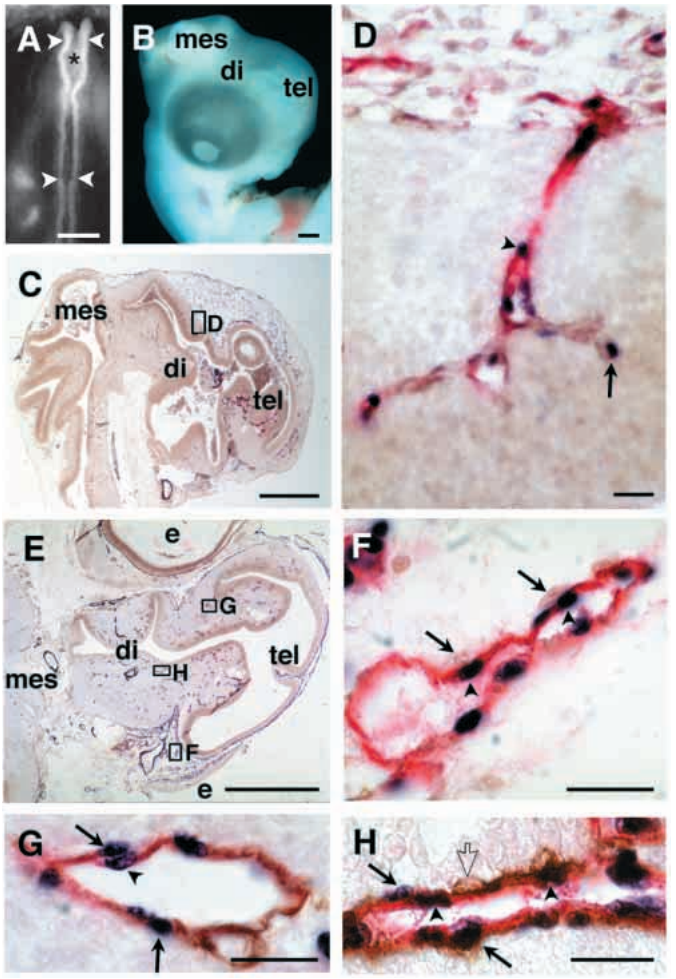

Fig. 7. The addition of paraxial mesoderm from lateral to the prosencephalon or mesencephalon to anterior NC-ablated embryos rescues the forebrain (Experiment 4). (A) Operated embryo from Experiment 4a, from which posterior diencephalic, mesencephalic and r1 neural folds were removed (between arrowheads) and a graft of paraprosencephalic mesoderm placed over the prosencephalon (asterisk). (B) The same embryo at E5, with normal forebrain vesicles. (C) Parasagittal section of the same embryo, with region enlarged in D indicated. (D) Triple stain of grafted mesoderm (QCPN, blue nuclei), pericytes (1A4, brown) and grafted endothelial cells (MB1/QH1, red) shows that chimeric blood vessels penetrate the forebrain neuroepithelium, and that grafted cells may become both endothelial cells and pericytes. (E) Parasagittal section of an E5 embryo from Experiment 4b, grafted with paramesencephalic mesoderm as above. Vessels magnified in F-H are indicated. (F) Meningeal blood vessel, with endothelial cells of graft origin (arrowheads) and pericytes of host origin (arrows). (G) Telencephalic blood vessel, with endothelial cells of host origin (arrowhead) and pericytes of graft origin (arrows). (H) Diencephalic blood vessel, with graft-derived pericytes (arrows) and endothelial cells (arrowhead) but also host-derived pericytes (open arrow). Tel, telencephalon; di, diencephalon; mes, mesencephalon; e, eye. Bars: A, 200 μm; B,C,E, 1 mm; D,F-H, 20 μm.

the trunk after NC ablation (Experiment 4c). We observed a delay in the degeneration of the forebrain neuroepithelium with respect to embryos having undergone NC ablation without an additional graft. Both of the 2 cases examined at E3 had normal prosencephalic morphology (not shown). In contrast, in 4 other embryos at E5 to E8, the same experiment led to the absence of telencephalon and dorsal diencephalon, despite the presence of quail endothelial cells in the head.

The lateral plate mesoderm of the trunk (Experiment 4d) was unable to rescue telencephalic growth at all at E3 (n=2), E6 (n=1) or E8 (n=1), nor did it differentiate into endothelial cells or pericytes in this context. Among mesodermal populations, the mesenchymal paraxial mesoderm of the head is best capable of replacing the anterior cephalic NCC in order to maintain viability in the forebrain.

DISCUSSION

The major finding of this work is that after formation of the primitive encephalic vesicles, in order to survive and grow, the prosencephalon needs to be surrounded by mesenchymal cells that are normally derived from the neural folds of the prospective diencephalon and mesencephalon. These cells yield the leptomeninges, in cooperation with the anteriormost region of the cephalic paraxial mesoderm (paraprosencephalic mesoderm).

The mesodermal component of the forebrain leptomeninx normally provides the endothelial walls of blood vessels that penetrate the neuroepithelium (Couly et al., 1995), while the neural crest component yields accompanying pericytes plus connective tissue cells. We have shown here that, when the anterior neural folds are removed from the presumptive level of the epiphysis down to r2, most of the forebrain undergoes cell death during a period that precedes the onset of vascularization by 36 to 58 hours, but which coincides with the assembly of the perineural vascular network of the forebrain during normal development. Progressive cell death in the prospective telencephalon and dorsal diencephalon takes place during the late second and early third embryonic days (HH15-19); vascularization would begin within the neuroepithelium of these areas only on the fourth embryonic day (HH24; unpublished results). The deleterious effect of ablation of the anterior NC cannot be interpreted as a deficit in vascularization because it takes place well before the time when blood vessels start to invade the neuroepithelium.

The outcome of this early cell death is the elimination of neuroepithelial territory destined to become the cerebral hemispheres and rhinencephalon, as well as a variable amount of the diencephalon, resulting in fusion of the two eyes over the area normally occupied by the telencephalon. This phenotype is reminiscent of the organization of the rostral head of *Amphioxus*, an invertebrate chordate considered to be the nearest evolutionary relative to vertebrates. Like the residual forebrain of the chicken embryo without anterior NCC, the cerebral vesicle of larval *Amphioxus* terminates in a number of unpaired, median structures associated with the vertebrate diencephalon: an infundibular organ, an epiphysis and a frontal 'eye' (Lacalli et al., 1994). Confirming its similarity to the diencephalon, the anterior end of the *Amphioxus* cerebral vesicle expresses a unique *Distal-less* gene homologue, reminiscent of the forebrain-restricted neuroepithelial expression of related vertebrate *Dlx* genes (Holland et al., 1996). A homologue to the *Drosophila Orthodenticle* gene is also expressed in the cerebral vesicle and frontal eye (Williams

and Holland, 1996). In both agnathan and gnathostome vertebrates, NCC that express the related *Otx* gene(s), derived from *Otx*-expressing diencephalon and mesencephalon, fill a head region that contains the forebrain as well as the first pharyngeal arch (Tomsa and Langeland, 1999). The removal of these NCC from the anterior head of the chicken embryo phenocopies some aspects of a putative ancestral brain organization. The expansion of the prosencephalic vesicle in vertebrates is likely to be a direct consequence of the appearance of the NC cell type and its extension of the vascular system of the brain, as has been proposed for the skeletogenic components of the head (Gans and Northcutt, 1983; reviewed in Kuratani et al., 1997).

When the anterior neural folds have not been replaced, the ventral and caudal diencephalon nonetheless survives and develops to a variable extent. The anterior rhombencephalic NC (r1) can partially compensate for the ablation of the diencephalic and mesencephalic NC by extending its migration cranially. We attempted to rescue the cyclopic phenotype induced by NC ablation by grafting either rhombencephalic or truncal NC heterotopically to the site of ablation, or by adding mesoderm of cephalic and trunk origin to the presumptive forebrain level. When the rhombencephalic NC is substituted for the diencephalic and mesencephalic NC, at least one *Hox* gene continues to be expressed in some NCC derivatives. Nonetheless, posterior cephalic NCC have the developmental potential to maintain forebrain viability like anterior cephalic NCC, although only the anterior population normally contributes pericytes to brain meninges and intraencephalic blood vessels. In contrast to cephalic NCC, the trunk NCC cannot participate in the formation of the anterior meninges, nor does it prevent cell death in the developing forebrain. This population, unlike the cephalic NC, does not normally participate in the smooth muscle walls of blood vessels or spinal cord meninges in the body. Its incapacity for alternative differentiation in the environment of the head (Le Douarin et al., 1977) extends to its lack of a trophic effect for the forebrain neuroepithelium.

When cephalic or somitic paraxial mesoderm is grafted over the dorsal prosencephalon of neural fold-deprived embryos, cell death is prevented in the forebrain. This demonstrates that the environment of the anterior head does not in itself prevent mesodermal differentiation into pericytes. Under experimental circumstances, even the paraprosencephalic mesoderm can provide the meningeal and parenchymal blood vessels with pericytes, although it does not do so during normal development. It should be noted that the paraprosencephalic mesoderm also does not participate in the construction of meninges when the NC is simply eliminated. Its incapacity might therefore lie either in cell quantity or in localization. Endogenous paraprosencephalic mesoderm is located adjacent to the ventral part of the neuroepithelium (Couly et al., 1993); in the absence of NCC it fails to spread dorsally to cover the developing forebrain (H. C. E., G. C. and N. M. Le D., unpublished data). A perineural capillary plexus forms only once endothelial cells derived from the paraprosencephalic mesoderm surround the prosencephalon after migration in normal development, or through substitution of the endogenous anterior NC by dorsal grafts of extra paraxial mesoderm or any other cephalic NC. In contrast, the local paramesencephalic mesoderm ensures all meningeal and blood vessel formation of the midbrain (Couly et al., 1992). During normal development, diencephalic and mesencephalic NCC might act as a scaffold to promote the dorsal migration of paraprosencephalic mesodermal cells so that the expanding neuroepithelium becomes fully surrounded by the meningeal anlage.

Our work identifies an important step in neurogenesis: it follows neural induction and precedes vascularization, and requires the presence of ‘paraneural’ mesenchymal cells for growth to proceed. Are the NCC-derived pericytes and connective cells, or the mesodermally derived endothelial cells, the necessary component of the forming meninges for the forebrain? In the absence of NCC, the prosencephalon perishes, despite the presence of endothelial cells near its ventral aspect. Pericytes are not necessary for the construction of vascular plexi from endothelial precursors in vitro (reviewed in Pepper and Montesano, 1990) or in vivo (Benjamin et al., 1998). If a proximate vascular plexus was sufficient to maintain forebrain viability, one would predict that, after anterior NCC ablations, the ventral telencephalon would persist. It does not. However, cephalic NCC can be replaced in their trophic capacity by mesodermal cells. The mixture of mesenchymal cells, of both mesodermal and NCC origin, of the future leptomeninges may thus secrete trophic factor(s) necessary for neuroepithelial viability before the blood supply has been ensured. Such factor(s) remain to be identified.

The authors gratefully acknowledge the technical assistance of Louis Addade and Fabrice Chatonnet, the aid of Françoise Viala, Francis Beaujean and Sophie Gournet in preparing the figures, and extensive and helpful commentary from Dr Anne Eichmann and Dr Marie-Aimée Teillet. We would also like to thank Dr Robb Krumlauf for the chicken *Hoxa3* probe. The QCPN hybridoma was obtained from the Developmental Studies Hybridoma Bank, Iowa City, IA, under contract NO1-HD-6-2915 from the National Institute of Child Health and Human Development. This work was supported by the Centre National de la Recherche Scientifique and the Collège de France. H. C. E. was a Predoctoral Fellow in the Biological Sciences of the Howard Hughes Medical Institute.

REFERENCES

Benjamin, L. E., Hemo, I. and Keshet, E. (1998) A plasticity window for blood vessel remodelling is defined by pericyte coverage of the preformed endothelial network and is regulated by PDGF-B and VEGF. *Development* **125**, 1591-1598.

Catala, M., Teillet, M.-A., De Robertis, E. M. and Le Douarin, N. M. (1996). A spinal cord fate map in the avian embryo: while regressing, Hensen’s node lays down the notochord and floor plate thus joining the spinal cord lateral walls. *Development* **122**, 2599-2610.

Couly, G., Coltey, P., Eichmann, A. and Le Douarin, N. M. (1995). The angiogenic potentials of the cephalic mesoderm and the origin of brain and head blood vessels. *Mech. Dev.* **53**, 97-112.

Couly, G., Grapin-Botton, A., Coltey, P., Ruhin, B. and Le Douarin, N. M. (1998). Determination of the identity of the derivatives of the cephalic neural crest: incompatibility between *Hox* gene expression and lower jaw development. *Development* **125**, 3445-3459.

Couly, G., Grapin-Botton, A., Coltey, P. and Le Douarin, N. M. (1996). The regeneration of the cephalic neural crest, a problem revisited: the regenerating cells originate from the contralateral or from the anterior and posterior neural fold. *Development* **122**, 3393-3407.

Couly, G. and Le Douarin, N. M. (1988). The fate map of the cephalic neural primordium at the presomitic to the 3-somite stage in the avian embryo. *Development* **103 Supplement**, 101-113.

Couly, G. F., Coltey, P. M. and Le Douarin, N. M. (1992). The

developmental fate of the cephalic mesoderm in quail-chick chimeras. *Development* **114**, 1-15.

Couly, G. F., Coltey, P. M. and Le Douarin, N. M. (1993). The triple origin of skull in higher vertebrates: a study in quail-chick chimeras. *Development* **117**, 409-429.

Couly, G. F. and Le Douarin, N. M. (1985). Mapping of the early neural primordium in quail-chick chimeras. I. Developmental relationships between placodes, facial ectoderm, and prosencephalon. *Dev. Biol.* **110**, 422-439.

Couly, G. F. and Le Douarin, N. M. (1987). Mapping of the early neural primordium in quail-chick chimeras. II. The prosencephalic neural plate and neural folds: implications for the genesis of cephalic human congenital abnormalities. *Dev. Biol.* **120**, 198-214.

Eichmann, A., Corbel, C., Nataf, V., Vaigot, P., Breant, C. and Le Douarin, N. M. (1997). Ligand-dependent development of the endothelial and hemopoietic lineages from embryonic mesodermal cells expressing vascular endothelial growth factor receptor 2. *Proc. Natl Acad. Sci. USA* **94**, 5141-5146.

Eichmann, A., Marcelle, C., Bréant, C. and Le Douarin, N. M. (1993). Two molecules related to the VEGF receptor are expressed in early endothelial cells during avian embryonic development. *Mech. Dev.* **42**, 33-48.

Gans, C. and Northcutt, R. G. (1983). Neural crest and the origin of vertebrates: a new head. *Science* **220**, 268-274.

Grapin-Botton, A., Bonnin, M. A., McNaughton, L. A., Krumlauf, R. and Le Douarin, N. M. (1995). Plasticity of transposed rhombomeres: *Hox* gene induction is correlated with phenotypic modifications. *Development* **121**, 2707-2721.

Hamburger, V. and Hamilton, H. L. (1951). A series of normal stages in the development of the chick embryo. *J. Morph.* **88**, 49-67.

Henrique, D., Adam, J., Myat, A., Chitnis, A., Lewis, J. and Ish-Horowicz, D. (1995). Expression of a Delta homologue in prospective neurons in the chick. *Nature* **375**, 787-790.

Holland, N. D., Panganiban, G., Henyey, E. L. and Holland, L. Z. (1996). Sequence and developmental expression of *AmphiDll*, an amphioxus *Distal-less* gene transcribed in the ectoderm, epidermis and nervous system: insights into evolution of craniate forebrain and neural crest. *Development* **122**, 2911-2920.

Jeffs, P. and Osmond, M. (1992). A segmented pattern of cell death during development of the chick embryo. *Anat. Embryol. (Berl)* **185**, 589-598.

Johnston, M. C. (1966). A radioautographic study of the migration and fate of cranial neural crest cells in the chick embryo. *Anat. Rec.* **156**, 143-155.

Köntges, G. and Lumsden, A. (1996). Rhombencephalic neural crest segmentation is preserved throughout craniofacial ontogeny. *Development* **122**, 3229-3242.

Kuratani, S., Matsuo, I. and Aizawa, S. (1997). Developmental patterning and evolution of the mammalian viscerocranium: genetic insights into comparative morphology. *Dev. Dyn.* **209**, 139-155.

Lacalli, T. C., Holland, N. D. and West, J. E. (1994). Landmarks in the anterior central nervous system of amphioxus larvae. *Phil. Trans. R. Soc. Lond. B* **344**, 165-185.

Le Douarin, N. M. (1982). *The Neural Crest.* Cambridge, UK: Cambridge University Press.

Le Douarin, N. M., Teillet, M. A. and Le Lièvre, C. (1977). Influence of the tissue environment on the differentiation of neural crest cells. In *Cell and Tissue Interactions* (ed. J. W. Lash and M. M. Burger), pp. 11-27. New York: Raven Press.

Le Lièvre, C. (1976). Contribution des crêtes neurales à la genèse des structures céphaliques et cervicales chez les Oiseaux. Doctoral thesis, Université de Nantes, France.

Le Lièvre, C. S. and Le Douarin, N. M. (1975). Mesenchymal derivatives of the neural crest: analysis of chimaeric quail and chick embryos. *J. Embryol. Exp. Morph.* **34**, 125-154.

Pardanaud, L., Altmann, C., Kitos, P., Dieterlen-Lièvre, F. and Buck, C. A. (1987). Vasculogenesis in the early quail blastodisc as studied with a monoclonal antibody recognizing endothelial cells. *Development* **100**, 339-349.

Péault, B. M., Thiery, J. P. and Le Douarin, N. M. (1983). Surface marker for hemopoietic and endothelial cell lineages in quail that is defined by a monoclonal antibody. *Proc. Natl. Acad. Sci. USA* **80**, 2976-2980.

Pepper, M. S. and Montesano, R. (1990). Proteolytic balance and capillary morphogenesis. *Cell Diff. Devel.* **32**, 319-328.

Rubenstein, J. L., Shimamura, K., Martinez, S., and Puelles, L. (1998). Regionalization of the prosencephalic neural plate. *Ann. Rev. Neurosci.* **21**, 445-477.

Shimamura, K., Hartigan, D. J., Martinez, S., Puelles, L. and Rubenstein, J. L. (1995). Longitudinal organization of the anterior neural plate and neural tube. *Development* **121**, 3923-3933.

Tomsa, J. M. and Langeland, J. A. (1999). *Otx* expression during lamprey embryogenesis provides insights into the evolution of the vertebrate head and jaw. *Dev. Biol.* **207**, 26-37.

Wilkinson, D. G. and Nieto, M. A. (1993). Detection of messenger RNA by in situ hybridization to tissue sections and whole mounts. *Methods Enzymol.* **225**, 361-373.

Williams, N. A. and Holland, P. W. H. (1996). Old head on young shoulders. *Nature* **383**, 490.

ELSEVIER

Mechanisms of Development 89 (1999) 179–183

www.elsevier.com/locate/modo

Gene expression pattern

Expression of Frzb-1 during chick development

Delphine Duprez[a,*], Luc Leyns[b,1], Marie-Ange Bonnin[a], Françoise Lapointe[a], Heather Etchevers[a], Eddy M. De Robertis[b], Nicole Le Douarin[a]

[a]*Institut D'Embryologie Cellulaire et Moleculaire du CNRS (UPR 9024) et du College de France, 49 bis avenue de Ia Belle Gabrielle, 94736 Nogent-sur-Marne Cedex, France*

[b]*Howard Hughes Medical Institute and Department of Biological Chemistry, University of California, Los Angeles, CA 90095-1662, USA*

Received 6 July 1999; received in revised form 13 August 1999; accepted 13 August 1999

Abstract

We cloned the chick homolog of *Xenopus* and mouse *Frzb-1*, a secreted Wnt antagonist and performed in situ hybridisations to determine the pattern of *cFrzb-1* expression in the developing chick embryo. At early stages, *cFrzb-1* transcripts are located exclusively in the ectodermal layer corresponding to the neural plate. The labelling continues in the neural tube, but is always excluded from the floor plate. *cFrzb-1* mRNA is expressed by migrating cephalic and truncal neural crest cells. Later, *cFrzb-1* transcripts are found in a subset of neural crest derivatives such as cephalic cartilage, nerves and spinal ganglia. In addition to ectodermal derivatives, *cFrzb-1* transcripts were also observed in mesodermal derivatives such as vertebral and limb cartilage, the adrenal cortex, the gonads, and a subpopulation of blood cells.

Keywords: Frzb-1; Wnt antagonist; Chick embryo; Neurulation; Neural crest; Cartilage

1. Results and discussion

Frzb Frizzled Bone proteins were first identified by a biochemical approach, as peptides from bovine cartilage extracts that contained bone inducing activity (Hoang et al., 1996) and have been now isolated from *Xenopus* (Leyns et al., 1997; Wang et al., 1997) and mouse (Leyns et al., 1997; Mayr et al., 1997). Frzbs are secreted soluble proteins of approximately 300 amino acids containing a cysteine-rich domain (CRD) similar to the Wnt-binding region of the Frizzled transmembrane receptor family (Moon et al., 1997; Wodarz and Nusse, 1998). *Xenopus* Frzb-1 binds Wnt proteins and blocks their signalling, suggesting a competition for Wnt binding between a receptor and a structurally related soluble antagonist (Leyns et al., 1997).

We have cloned by PCR a chick homologue of *Frzb-1*. The cloned fragment of 138 amino acids comprises most of the CRD region and is considered to be the *Frzb-1* ortholo-gue because of its high amino acid identity to *Xenopus* and mouse *Frzb-1* (see Section 2). Chick *Frzb-1* shows important differences in expression patterns with both its *Xenopus* and mouse counterparts.

1.1. cFrzb-1 expression maps to the neural plate

During early neurulation, there is no detection of *cFrzb-1* transcripts until the stage Hamburger Hamilton (HH) 4−, when *cFrzb-1* transcripts show a restricted expression pattern in the neural plate (Fig. 1A–F). In contrast, *xFrzb-1* is excluded from the neuroectodermal layer (Leyns et al., 1997) or *mFrzb-1* (Mayr et al., 1997; Leyns et al., 1997; Hoang et al., 1998) can be found in all three germ layers, including anterior central nervous system, during development. The caudal extension of the neural plate (Fig. 1A,B,F,G,H) is marked by *cFrzb-1* expression. Strong expression at 14 somite-stage marks the medullary cord (Fig. 1J), which gives rise to the neural tube during secondary neurulation (Catala et al., 1995). Strikingly, there is never any expression in Hensen's node (HN) or in the HN-derived notochord (No) and floor plate (FP) (Fig. 1A,B,E–G,I,M). In *Xenopus* the dorsal blastopore lip (Spemann Organizer) expresses *xFrzb-1* at early stages, becoming gradually restricted to anterior endomesoderm and prechordal plate, lacking expression in the notochord

* Corresponding author. Tel. +33-1-4514-15365/4514-1515; fax: +33-1-4873-4377.

E-mail address: duprez@infobiogen.fr (D. Duprez)

[1] Present address: Department of Biology, Free University of Brussels (VUB) – Pleinlaan, 2-1050 Brussels, Belgium.

0925-4773/99/$ - see front matter
PII: S0925-4773(99)00206-3

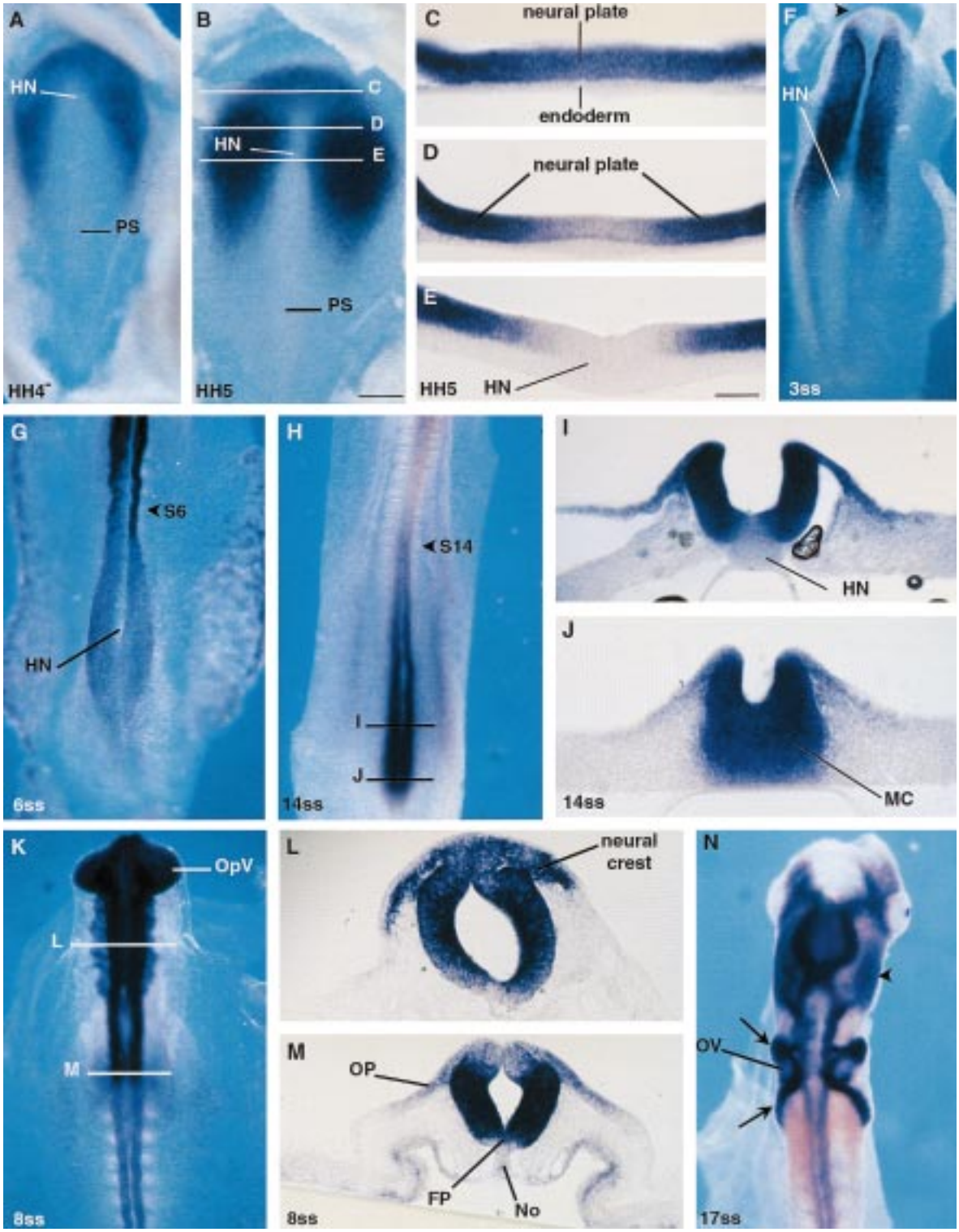

Fig. 1. Expression pattern of *cFrzb-1* during neurulation and neural crest cell migration. Wholemount in situ hybridisation and subsequent histological analysis. Dorsal views of embryos at HH4- (A), HHS (B), 3 somite stage (ss) (F), 6ss (G), 8ss (K), l4ss (H) and l7ss (N). Vibratome sections of embryos at stage HH5 (C–E), 8ss (L,M) and l4ss (I,J). HN, Hensen's Node; No, notochord; MC, medullary cord; OpV, optic vesicle; OP, otic placode; OV, otic vesicle. PS, Primitive streak. Scale bars (A,B,F–H,K,N), 355 μm; (C–E,I,J,L,M), 68 μm.

(Leyns et al., 1997). Quail/chick grafting experiments demonstrated that FP and No share the same embryological origin in HN (Catala et al., 1996; Teillet et al., 1998). The expression of *cFrzb-1* in the spinal cord but not in the HN (Fig. 1I) provides molecular confirmation that the FP and No arise from the same group of cells (Teillet et al., 1998).

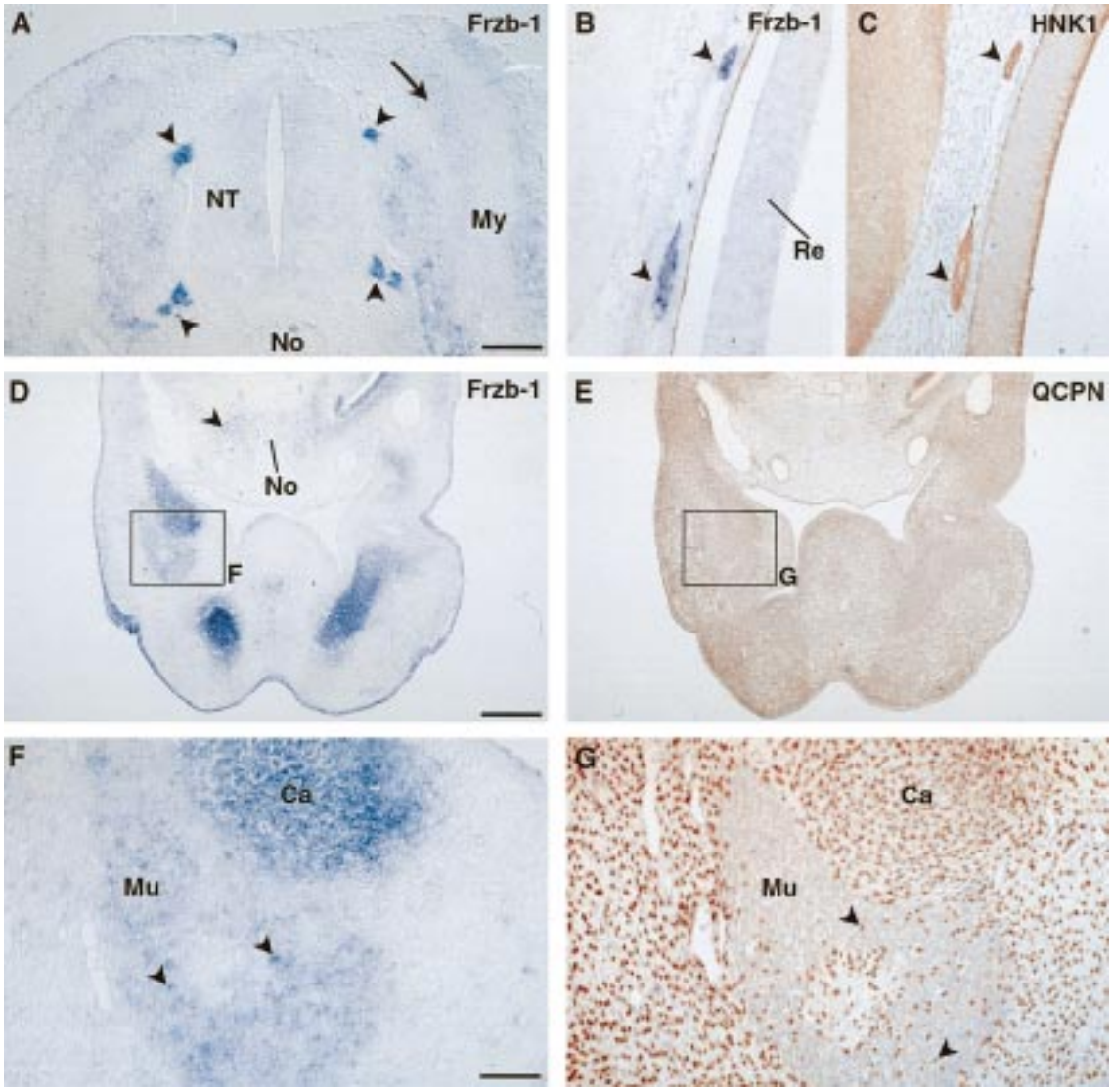

Fig. 2. Location of cFrzb-1 transcripts in neural crest derivatives. (A) Transverse section of an E6 embryo hybridised with *cFrzb-1* probe. (B) Adjacent frontal head sections at E6 were hybridised with *cFrzb-1* probe or (C) incubated with HNK1 antibody. Consecutive frontal sections of HH26 (E5) quail-chick chimera at the mandibular level (D–G), hybridised with cFrzb-1 probe (D,F). Quail cells, which correspond strictly to NC cells, are revealed using QCPN mAb (E,G). My, Myotome; NT, neural tube; No, notochord; Re, retina; Ca, cartilage; Mu, muscle. Scales bars (A), 136 μm; (D,E), 340 μm; (B,C,F,G), 68 μm.

In addition, the optic vesicles (Fig. 1K) and the otic placodes (Fig. 1M) express *cFrzb-1*.

1.2. Neural crest cells express cFrzb-1

cFrzb-1 transcripts are not detected in the most anterior domain of the neural folds (Fig. 1F, arrowhead), a region that does not give rise to any neural crest (NC) cells (Couly and Le Douarin, 1987). At 8 somite-stage, cephalic NC cell progenitors and NC cells migrating from the midbrain strongly express *cFrzb-1* (Fig. 1K,L). At 17ss-stage, two streams of rhombencephalic NC cells migrating rostrally and caudally to the otic vesicle are strongly labelled (Fig. 1N, arrows), like the NC-containing mesenchyme of the head (Fig. 1N, arrowhead).

1.3. cFrzb-1 transcripts are located in a subset of NC-derived cell

Within the peripheral nervous system, *cFrzb-1* is expressed in a subpopulation of cells in the spinal ganglia (Fig. 2A). Since the most intense expression was found in the dorsal and ventral roots of the spinal nerves (arrowheads), which contain many glial cells, we concluded that *cFrzb-1* probe in the ganglia labels essentially glial cells rather than the neural component. Comparative analysis of *cFrzb-1* transcripts location and HNK1 immunohistochemistry (which recognises most of the NC-derivatives) shows that NC cells of the oculomotor nerves strongly express the *cFrzb-1* gene (Fig. 2B,C). In order to follow the NC cells in the branchial arches, we replaced cephalic neural folds from

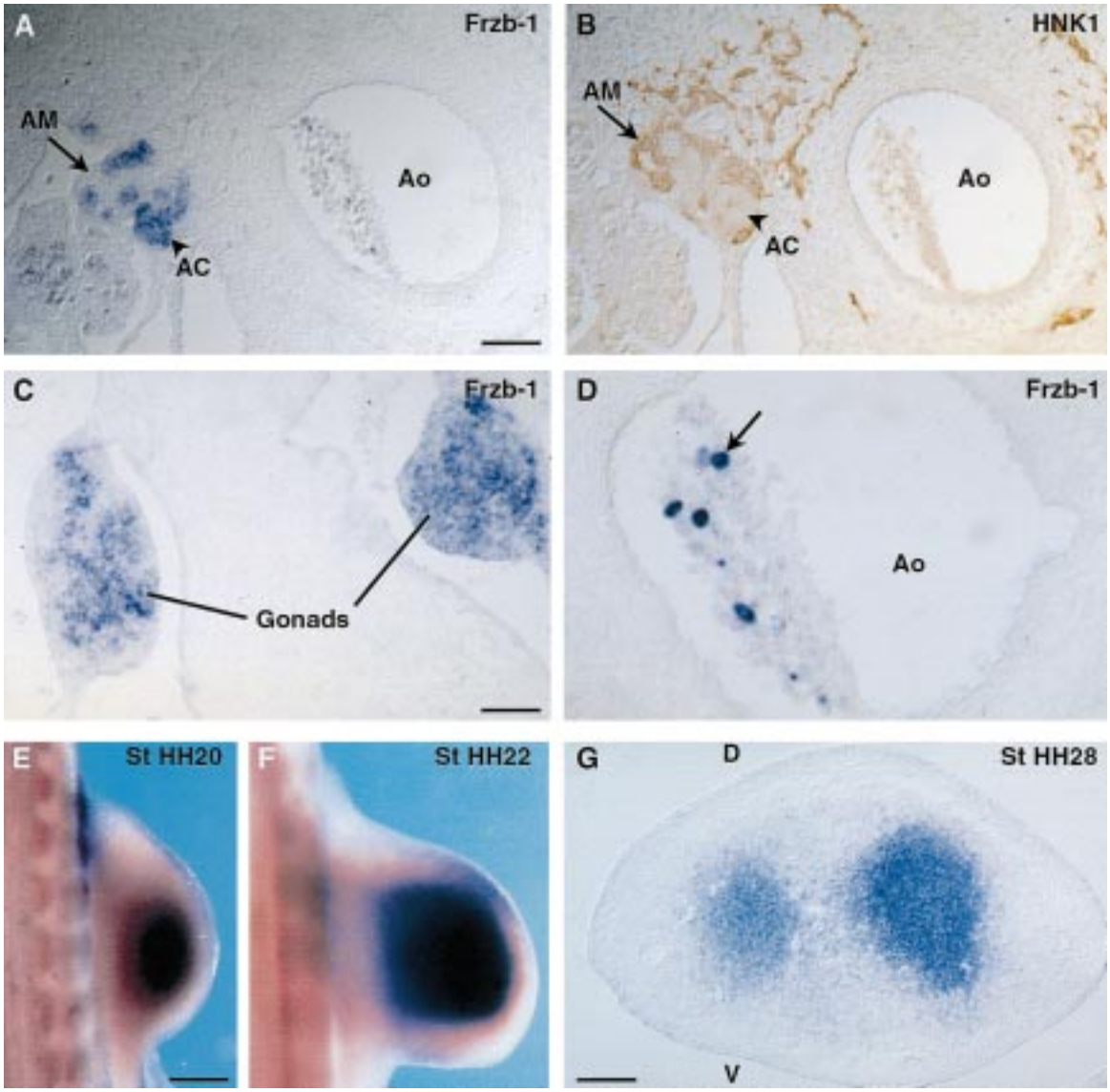

Fig. 3. Expression of cFrzb-1 in mesodermal derivatives. Consecutive transverse sections from HH28 (E6) embryo at the level of the adrenal gland, incubated with *cFrzb-1* probe (A) or HNK1 antibody (B). The gonads (C) and a subpopulation of blood cells (D) are positive for *cFrzb-1*. Distribution of *cFrzb-1* transcripts in wings of HH2O (E) and 22 (F) embryos. (G) Wing of stage HH28 embryo (E6) was cut transversally and sections were hybridised with *cFrzb-1* probe. AM, adrenal medulla; AC, adrenal cortex; Ao, Aorta. D, dorsal; V, ventral. Scale bars (A,B), 68 μm; (C,D), 34 μm; (E,F), 355 μm; G,136 μm.

4-somites chick embryos with the quail equivalent, using the QCPN antibody as a quail-specific marker. The chick *Frzb-1* probe reacts both with chick and quail tissues. In situ hybridisation on such chimeras at embryonic day 5 showed a restricted expression of *cFrzb-1* (Fig. 2D) among the QCPN-positive NC cells invading the branchial arches (Fig. 2E). The differentiating cartilage (Fig. 2E, high magnification, 2G) is *cFrzb-1* positive (Fig. 2D, high magnification 2F). Muscle cells, which are QCPN-negative because not derived from the NC (Fig. 2G), do not express *cFrzb-1* (Fig. 2F). However, isolated cells in muscle areas are positive for *cFrzb-1* (Fig. 2F, arrowheads). These cells correspond to connective tissue within the muscles which are of NC origin and are labelled with QCPN (Fig. 2G, arrowheads). We concluded that *cFrzb-1* is expressed in a wide range of NC-derivatives.

1.4. cFrzb-1 is also expressed in mesoderm derivatives

cFrzb-1 gene is expressed in the adrenal gland (Fig. 3A). Precise comparison with HNK1 shows that *cFrzb-1* transcripts are located in the adrenal cortex (Fig.3A, arrowheads) and not in the adrenal medulla, which is NC-derived and HNK1-positive (Fig. 3B). In addition, *cFrzb-1* transcripts are also detected in the gonads (Fig. 3C) and in a subpopulation of circulating blood cells (Fig. 3D). Moreover, sclerotomal cells (future vertebral cartilage) surrounding myotomes (Fig. 2A, arrow) and notochord (Fig. 2D) are

positive for *cFrz-1*. *cFrzb-1* mRNA is found from HH19 (E3) in the limb mesenchyme (Fig. 3E,F). In situ hybridisation on transverse sections along the proximo-distal axis of a HH28 (E6) wing limb reveals that *cFrzb-1* transcripts localised to the cartilage region (Fig. 3G).

In conclusion, we cloned the chick homolog of the secreted Wnt-antagonist *Frzb-1* gene. Despite the high sequence conservation, the expression pattern of *cFrzb-1* shows differences with its mouse and frog homologues, in particular during early development.

2. Methods

2.1. Cloning

A partial clone of chick *Frzb-1* was isolated by PCR, using degenerated oligonucleotides located in conserved regions of *xFrzb-1* and *mFrzb-1*. The *cFrzb-1* clone encodes a 138 aminoacid fragment comprising most of the CRD region (also known as *sFRP-3*, Wodarz and Nusse, 1998), with 86 and 88% homology to *Xenopus* and mouse proteins, respectively. The next closest related protein is mouse sFRP-4 (66% identity). The Genbank accession number is AF153476.

2.2. In situ hybridisation and immunohistochemistry

Embryos were processed for in situ hybridisation to wholemounts and sections as previously described by Duprez et al. (1998). NC and quail cells were detected using HNK-1 and QCPN mAbs, respectively (Developmental Hybridoma Bank, University of Iowa, Iowa City).

2.3. Quail/chick chimeras

Microsurgery was performed on embryos at stage HH7. Bilateral cephalic neural folds from chick embryos were replaced by their quail counterparts. Embryos were fixed 3 days after grafting, embedded in paraffin and sectioned onto alternating slides.

Acknowledgements

We are grateful to Francis Beaujean, Sophie Gournet, Helene San Clemente and Françoise Viala for help with the illustrations. This work was supported by the Association Française contre les myopathies (AFM) and the Centre National de Ia Recherche Scientifique (CNRS). E.M.D.R. is an Investigator of the Howard Hughes Medical Institute, which partially funded this work.

References

Catala, M., Teillet, M.A., Le Douarin, N., 1995. Organization and development of the tail bud analysed with the quail-chick chimaera system. Mech. Dev. 51, 51–65.

Catala, M., Teillet, M.A., De Robertis, E.M., Le Douarin, N., 1996. A spinal cord fate map in the avian embryo: while regressing. Hensen's node lays down the notochord and floor plate thus joining the spinal cord lateral walls. Development 122, 2599–2610.

Couly, G., Le Douarin, N.M., 1987. Mapping of the early neural primordium in quail-chick chimeras. Dev. Biol. 120, 198–214.

Duprez, D., Fournier-Thibault, C., Le Douarin, N., 1998. SHH induces proliferation of committed skeletal muscle cells in the chick limb. Development 125, 495–505.

Hoang, B., Moos, M., Vukicevic, S., Luyten, F.P., 1996. Primary structure and tissue distribution of FRZB, a novel protein related to Drosophila Frizzled, suggests a role in skeletal morphogenesis. J. Biol. Biochem. 42, 26131–26137.

Hoang, B., Thomas, J.T., Abdul-Karim, F.W., Correla, K.M., Colon, R.A., Luyten, F.P., Ballock, T., 1998. Expression pattern of two Frizzled-related genes. Frzb-1 and Sfrp1, during mouse embryogenesis suggests a role for modulating action of Wnt family members. Dev. Dyn. 212, 364–372.

Leyns, L., Bouwmeester, T., Kim, S.H., Piccolo, S., De Robertis, E.M., 1997. Frzb-1 is a secreted antagonist of Wnt signaling expressed in the Spemann organizer. Cell 88, 747–756.

Mayr, T., Deutsh, U., Kühl, M., Drexler, H.C.A., Lottspeich, F., Deutzmann, R., Wedlich, D., Risau, W., 1997. Fritz: a secreted frizzled protein that inhibits Wnt activity. Mech of Dev. 63, 109–125.

Moon, R.T., Brown, J.D., Yang-Snyder, J.A., Miller, J.R., 1997. Structurally related receptors and antagonists compete for secreted Wnt ligands. Cell 88, 725–728.

Teillet, M.A., Lapointe, F., Le Douarin, N.M., 1998. The relationship between notochord and floor plate in vertabrate development revisited. Proc. Natl. Acad. Sci. USA 95, 11733–11738.

Wang, S., Krinks, M., Lin, K., Luyten, F.P., Moos, M., 1997. Frzb, a secreted protein expressed in the Spemann organizer, binds and inhibits Wnt-8. Cell 88, 757–766.

Wodarz, A., Nusse, R., 1998. Mechanisms of Wnt signaling in development. Ann. Rev. Cell Dev. Biol. 14, 59–88.

Development 128, 1059-1068 (2001)
Printed in Great Britain © The Company of Biologists Limited 2001
DEV2684

The cephalic neural crest provides pericytes and smooth muscle cells to all blood vessels of the face and forebrain

Heather C. Etchevers*, Christine Vincent, Nicole M. Le Douarin and Gérard F. Couly

Institut d'Embryologie Cellulaire et Moléculaire du CNRS et du Collège de France, 49 bis avenue de la Belle Gabrielle, 94736 Nogent-sur-Marne Cedex, France
*Author for correspondence (e-mail: etchever@infobiogen.fr)

Accepted 4 January 2001

SUMMARY

Most connective tissues in the head develop from neural crest cells (NCCs), an embryonic cell population present only in vertebrates. We show that NCC-derived pericytes and smooth muscle cells are distributed in a sharply circumscribed sector of the vasculature of the avian embryo. As NCCs detach from the neural folds that correspond to the future posterior diencephalon, mesencephalon and rhombencephalon, they migrate between the ectoderm and the neuroepithelium into the anterior/ventral head, encountering mesoderm-derived endothelial precursors. Together, these two cell populations build a vascular tree rooted at the departure of the aorta from the heart and ramified into the capillary plexi that irrigate the forebrain meninges, retinal choroids and all facial structures, before returning to the heart. NCCs ensheath each aortic arch-derived vessel, providing every component except the endothelial cells. Within the meninges, capillaries with pericytes of diencephalic and mesencephalic neural fold origin supply the forebrain, while capillaries with pericytes of mesodermal origin supply the rest of the central nervous system, in a mutually exclusive manner. The two types of head vasculature contact at a few defined points, including the anastomotic vessels of the circle of Willis, immediately ventral to the forebrain/midbrain boundary. Over the course of evolution, the vertebrate subphylum may have exploited the exceptionally broad range of developmental potentialities and the plasticity of NCCs in head remodelling that resulted in the growth of the forebrain.

Key words: Pericyte, Vascular, Carotid, Branchial, Quail-chick chimera, Evolution, Neural crest, Meninges, Forebrain, Head

INTRODUCTION

Over chordate evolution, the anterior brain and its surrounding head expanded spectacularly in vertebrates. This development coincided with the appearance within the subphylum of a pluripotent embryonic cell population called the neural crest.

Evidence that the neural crest was instrumental in shaping the head began to accrue from fate-mapping experiments that showed the distribution of neural crest cells (NCCs) in the avian embryo (Johnston, 1966). The use of a stable selective cell-marking technique, based on the construction of quail-chick chimeras allowed the definitive demonstration that NCCs give rise to most connective components of the head, including dermis, tendons and intercalating membranes of cephalic muscles (Le Lièvre and Le Douarin, 1975; Noden, 1983; Couly et al., 1993; Couly et al., 1996; Köntges and Lumsden, 1996). Such soft tissues are associated with the NCC-derived bones that make up most of the skull, notably the jawed facial skeleton and the brain case (Couly et al., 1993; Couly et al., 1996; Köntges and Lumsden, 1996).

In addition to their role in forming the head, NCCs may have participated in the enlargement of the brain itself within members of the vertebrate subphylum. Initial support for this hypothesis comes from the demonstration that, in the chicken embryo, neural crest-derived mesenchyme is necessary for the early survival of the forebrain neuroepithelium, upon which it exerts a trophic influence (Etchevers et al., 1999). Many of these NCCs participate in the forebrain meninges (Johnston, 1966; Le Lièvre and Le Douarin, 1975), which enclose the capillary network necessary for later neuroepithelial growth via its blood supply.

All blood vessels are composed of an inner layer of endothelial cells and an immediately adjacent layer of pericytes. Pericytes are indispensable for the formation of mature blood vessels (reviewed in Doherty and Canfield, 1999). They also mediate capillary vasoconstriction and secrete specialised extracellular matrices for microvessels within the neuroepithelium (Balabanov and Dore-Duffy, 1998), kidney (Schlondorff, 1987), liver (Kawada, 1997) and bone (Doherty and Canfield, 1999). In addition to endothelial and pericytic components, larger blood vessels also possess one or more concentric layers of connective and smooth muscle cells, constituting the elastic tunica media and the fibrous tunica externa.

Endothelial cells are derived from mesodermal precursors able to yield both the angiogenic and haematopoietic lineages, the most primitive of which are characterised by the expression of the vascular endothelial growth factor receptor 2 (Vegfr2) (Eichmann et al., 1993; Couly et al., 1995).

In contrast, the outer wall layers, while originating from the mesoderm in the body, can be made by NCCs in the head (reviewed in Le Douarin and Kalcheim, 1999). Cephalic NCC contribute to the muscular and connective wall of large arteries derived from the branchial arches (Le Lièvre and Le Douarin, 1975), including the cardiac septum that separates the aorta from the pulmonary artery trunk (Waldo et al., 1998). Continued ramifications of the branchial arteries define a distinct anatomical sector of the ventral and anterior head. A second vascular sector of non-branchial arteries irrigates the dorsal, posterior head (Fig. 1). These two domains meet behind the optic chiasm in an anastomotic structure known as the circle of Willis. Strikingly, the branchial sector overlaps that part of the head to which the NCC mesenchyme makes major structural contributions.

In the present work we have analysed the precise contribution of NCCs that originate from successive anteroposterior levels of the neural folds to cephalic blood vessels. We find that the dorsal/posterior vascular compartment depends upon the cephalic paraxial mesoderm for all components of the blood vessel wall, while the ventral/anterior compartment derives its pericytes and musculo-connective wall entirely from NCCs. The two domains are delimited distally within the meninges by a sharp boundary between the forebrain and the midbrain.

The forebrain and the retinae are thus irrigated by capillaries of composite mesoderm and neural crest origin, consistent with their support by other neural crest-derived connective tissues. In addition to the trophic role we have previously demonstrated for cephalic NCCs in early forebrain development, it appears plausible that there was a causal relationship between the construction of a NCC-dependent vascular domain and the continued expansion of the anterior brain and head over the course of evolution.

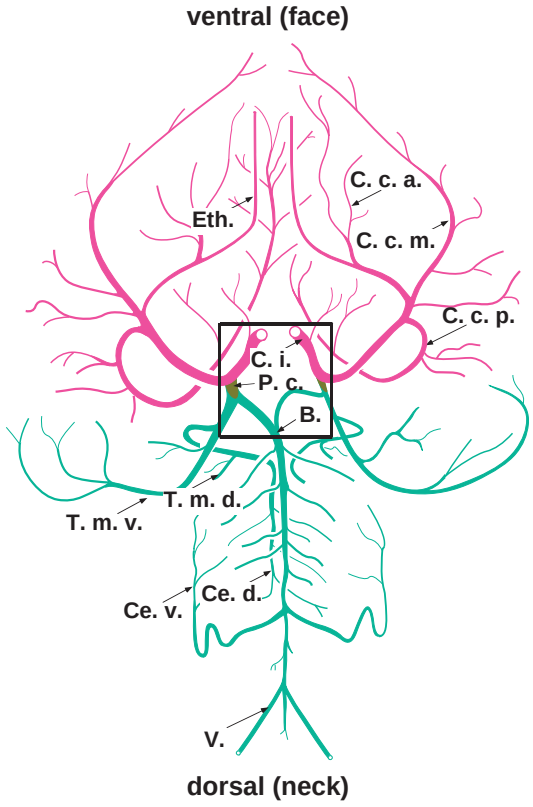

Fig. 1. The dorsal cephalic vascular tree, excluding the jaws, ventral view. Six pairs of aortic arch arteries form during amniote embryogenesis, looping from the ventral to the dorsal aorta. Three of them persist in the adult: the third pair, as a segment of the common carotid arteries; one of the fourth pair, as the aorta; and the sixth, as a segment of the pulmonary arteries. The common carotid arteries give rise to a ventral arterial pathway, of which the internal carotid (C. i.) and derived arteries (pink) target the upper face, eyes, and forebrain. The distal part of this route is made of vascular elements derived from the first three aortic arches. The other arterial pathway in the head (green) targets the midbrain and hindbrain, and arises from the vertebral arteries (V.). Both trees start from the brachiocephalic artery trunks, which diverge from the ventral (ascending) aorta. The common carotid arteries immediately course into the neck and face. The vertebral arteries project into the head along the underside of the hindbrain after fusing to form the basilar artery. The two systems contact at the circle of Willis (box), which surrounds the optic chiasm ventral to the diencephalon. The posterior sides of this famous vascular polygon are made by the bifurcation of the basilar artery, while derivative branches of the internal carotid arteries constitute the anterior sides. An anastomotic artery, the posterior communicante (P. c.), connects them; in humans, a median fusion between the anterior cerebral arteries completes the 'circle'. The circle of Willis represents the anatomical interface between the ventral and dorsal vascular trees. B., basilaris; C. c. a., carotis cerebralis anterior; C. c. m., carotis cerebralis medialis; C. c. p., carotis cerebralis posterior; Ce. d., cerebellaris dorsalis; Ce. v., cerebellaris ventralis; C. i., carotis interna; Eth., ethmoidalis; T. m. d., tecti mesencephalis dorsalis; T. m. v., tecti mesencephalis ventralis; V, vertebralis. Adapted, with permission, from Baumel (Baumel, 1979).

MATERIALS AND METHODS

Isotopic grafts of the right neural fold were performed from quail donors into stage-matched chick hosts at the three to five somite stage (ss), on embryonic day (E) 2. The length of the neural fold taken corresponded to the posterior half of the diencephalon (PD), the anterior half of the mesencephalon (AM) or the posterior half of the mesencephalon (PM) regions, approximately 100 μm each, or the AM and PM together. Stage- and position-specific micrometry was performed as outlined previously (Grapin-Botton et al., 1995).

Additional chicken embryos were examined in which an individual rhombomeric neural fold had been replaced by its isotopic, isochronic quail counterpart, as described previously (Couly et al., 1996). Neural folds from given rhombomeric levels are referred to as r1-r8. The neural folds of r8 were mapped over the length of each of the first three somites, but the results, being similar, were grouped. All chimeras were incubated at 38°C in humidified chambers and cleaned in PBS before fixation for immunohistochemistry (IHC) or in situ hybridisation (ISH). Numbers and stages at harvest for IHC are summarised in Table 1.

Ink injections into the left ventricle of the heart of E8 chicken embryos were followed by fixation in Carnoy's solution, dehydration in ethanol and clearing in 100% methyl salicylate (Fig. 4B).

IHC using the monoclonal antibodies QCPN (anti-quail, DSHB), QH-1/MB-1 (anti-quail vascular endothelium and white blood cells) and 1A4 (anti-alpha smooth muscle actin, Sigma) on sections was performed as previously described (Etchevers et al., 1999). Tissues were counterstained with Gill's Haematoxylin. Some of the rhombencephalic-grafted embryos were fixed in Zenker's solution and treated with the Feulgen-Rossenbeck stain procedure, described previously (Le Douarin, 1969), as an alternative method to localise quail cells in older embryos.

ISH of Vegfr2 (Eichmann et al., 1993), and the premigratory and

Table 1. Chimeric embryos used to construct fate map of cephalic vascular walls

Graft NF	Di	Ant mes	Post mes	Mes	R1	R2	R4	R5	R6	R7	R8 (s1-3)
HH stage at harvest	16 (6)	10 (2)	26 (1)	10 (1)	29 (2)	35 (2)	33 (2)	18 (1)	28 (1)	26 (1)	29 (2)
(number of samples)	33 (1)	14 (1)		12 (1)	33 (1)		35 (1)	27 (1)	35 (2)	29 (1)	33 (1)
	38 (1)	27 (1)		16 (3)				28 (1)		32 (1)	
		32 (1)		20 (1)				32 (1)		33 (2)	
		35 (1)		24 (2)				35 (2)		34 (1)	
		38 (2)		27 (2)						35 (1)	
				28 (1)							
				29 (3)							
				33 (1)							
Total (59)	8	8	1	15	3	2	3	6	3	7	3

Ant mes, anterior mesencephalic; Di, diencephalic; Mes, mesencephalic; NF, neural folds; Post mes, posterior mesencephalic; R, rhombomere; s1-3, at the level of somites 1 to 3.

early migratory neural crest marker Sox10 (Cheng et al., 2000) was performed directly on 5 μm paraffin sections of embryos fixed in 11% formaldehyde, 60% ethanol, 10% acetic acid. Digoxigenin-UTP-labelled Vegfr2 probe and fluorescein-labelled Sox10 probe were diluted in hybridisation mix to approximately 1 ng/μl each. The probes were applied to sections, which had been deparaffinated, rehydrated, digested with 10 μg/ml proteinase K for 7 minutes, postfixed in 4% paraformaldehyde and rinsed. After hybridisation overnight at 60°C, slides were washed twice in 50% formamide, 2×SSC at 65°C, then in MABT (0.1 M maleic acid, 150 mM NaCl, 0.1% Tween-20, pH 7.5). Nonspecific antibody binding was blocked by incubation in MABT with 20% goat serum, 2% blocking reagent (Roche) for 60 minutes. AP-conjugated anti-digoxigenin antibody (Roche) was diluted in this solution to 1/2000 and applied. The following day, slides were rinsed in MABT before equilibration in 100 mM NaCl, 50 mM $MgCl_2$, 100 mM Tris (pH 9.5) and 0.1% Tween-20 (NTMT). For a blue precipitate, 33.8 μg/ml nitro blue, tetrazolium chloride (NBT) with 175 μg/ml 5-bromo-4-chloro-3-indolyl phosphate, toluidinium salt (BCIP) were used in NTMT. The slides were then treated with 0.1 M glycine, pH 2.2 for 15 minutes, equilibrated in MABT and AP-conjugated anti-fluorescein antibody (Roche) applied at 1:8000 for IHC. For a red precipitate, 2-(4-iodophenyl)-3-(4-nitrophyenyl)-5-phenyl tetrazolium chloride (INT) and BCIP were used at 248 μg/ml each in NTMT.

RESULTS

The prosencephalic vascular plexus forms concomitantly with the arrival of NCCs

Cephalic mesenchyme may come from either NCCs or cephalic mesoderm. In order to recognise the distinct origins of the cells that give rise to the early vascular system of the anterior head, the relative positions of its neural crest and endothelial components over time were examined by in situ hybridisation. Vegfr2 is expressed in endothelial cells and their precursors (Eichmann et al., 1993). *Sox10* is a homeobox-containing gene that is specifically expressed in all early migrating cephalic NCC, later functioning in both central and peripheral nervous system glial lineages (Cheng et al., 2000).

Preceding NCC emigration, the bilateral telencephalic primordia occupy dorsolateral domains within the anterior neural plate (Couly and Le Douarin, 1987). At HH8 (4-6ss, early E2), endothelial cell precursors, marked by *Vegfr2* expression, are found close to the ventral neuroepithelium and the foregut (Fig. 2A). As the neural folds of the anterior neural plate approach during HH8, the presumptive telencephalic domains come to directly underlie the ectoderm.

These epithelia are subsequently separated by NCCs between HH9 and HH15. At HH9 (7-9ss, E2), NCCs emigrate from the diencephalic and mesencephalic neural folds, spreading both toward the pharynx and rostrally toward the anterior neural fold (Fig. 2B), but they do not encounter endothelial cells before HH10.

At HH14 (Fig. 2C,D), mesoderm-derived endothelial precursors have mixed with the NCCs. Together, they intervene between the ectoderm and the caudal telencephalon, but have not yet spread over the rostral telencephalon. Chimeric embryos made with unilateral neural fold grafts at the mesencephalic level show that anterior NCCs fan out bilaterally, whereas those that migrate towards the pharynx remain essentially unilateral (Fig. 2E). The rostral-moving NCCs continue to lead the invasive front, closely followed by capillaries that are organising adjacent to the neuroepithelium (Fig. 2D,F).

Two bilateral eminences evaginate from the prosencephalon during this period. The first, the optic vesicles, appear in the ventrolateral prosencephalon at HH9. The second, the telencephalic vesicles, only emerge from the dorsolateral prosencephalon at HH19 (E3). Capillaries begin to penetrate the chicken ventral rhombencephalic and mesencephalic neuroepithelium on HH18 (late E2), but the telencephalon is invaded by blood vessels ventrally at HH24 (E4) and dorsally after HH26 (E5; not shown). In chimeras, quail NCCs are first seen within the host telencephalon associated with the first capillaries on HH24 (Fig. 2G).

Anterior cephalic NCCs participate in all forebrain vasculature

After isotopic grafts of neural folds at the levels of the posterior diencephalon or the mesencephalon, quail NCCs are abundant within the meninges of the forebrain, to the exclusion of the rest of the central nervous system (Fig. 3A). The greatest contribution to the telencephalic meninges is from mesencephalic NCCs, while posterior diencephalic NCCs favour the ventral diencephalic meninges, although both regions of the neural folds give rise to cells in all parts of the forebrain meninges. There is no apparent difference in distribution within the meninges between NCCs from the anterior or posterior mesencephalon.

Avian meninges are made of two layers. The outer dura mater is continuous with the condensing periosteum of the overlying NCC-derived skull (Couly et al., 1993), and is also NCC-derived (data not shown). The inner arachnoid, rich in

blood vessels, is inseparable from the pia mater, which constitutes a component of the blood-brain barrier; pial pericytes are closely associated with the outer aspect of the vascular endothelium that penetrates the neuroepithelium. The arachnoid/pia mater, known collectively as the leptomeninges, include numerous NCC located in the walls of parenchymal blood vessels (Fig. 3B, HH32).

Grafted cells found in the forebrain are not labelled after IHC with the QH-1/MB-1 antibody, and hence are not endothelial (data not shown). Quail NCC reside on the outside of the capillaries and co-localise with alpha smooth muscle actin, seen via 1A4 IHC (Fig. 3B,D). These observations are consistent with pericytic identity. In larger arteries, such as the internal carotid, NCCs are located within the 1A4-immunolabelled smooth muscular tunica media (Fig. 3C).

Caudal NCCs map to proximal vessels, rostral NCCs map to distal vessels

Given a number of shared characteristics between pericytes and smooth muscle cells (Alliot et al., 1999), we examined other blood vessels derived from the aortic arches for the presence of NCC. All arteries of the face and jaw that we examined, which branch off from the common carotid arteries, have tunica media of NCC origin.

The more distal an artery from the heart, the further rostral the origin of the NCCs that give rise to the pericytes and/or smooth muscle cells of that part of the vessel (Fig. 4A). Examples of distalmost blood vessels include the meningeal capillaries of the prosencephalon (Fig. 3B), and the pituitary and ophthalmic arteries. The non-endothelial components of these vessels come from posterior diencephalic and mesencephalic NCCs. As shown in Fig. 4, cells from the posterior diencephaloin also contribute to part of the wall of the internal carotid artery (Fig. 4C), r2 NCCs to the proximal maxillary artery (Fig. 4D), r4 NCCs to the stapedian artery (Fig. 4E) and r5 NCCs to the common carotid artery (Fig. 4F). Grafts from adjacent levels of the neural folds gave rise to cells in overlapping domains of the same complement of blood vessels, indicating a gradual transition within the vascular wall from NCCs of one origin to NCCs of a neighbouring origin. The tunica media of long arteries such as the internal carotids spans multiple subdivisions of the neural folds (in this example, from PD to r4 included). The same holds true for the ventral and anterior cephalic veins, such as the jugulars, to which NCC from r4 to r6 contribute (not shown).

Likewise, the more proximal an artery to the heart, the further caudal the origin of the NCC along the neuraxis. The distribution of NCCs derived from r6, r7 and r8 within the musculo-connective wall of the large arteries overlapped greatly (Fig. 5A). All three contributed to the ventral aorta as

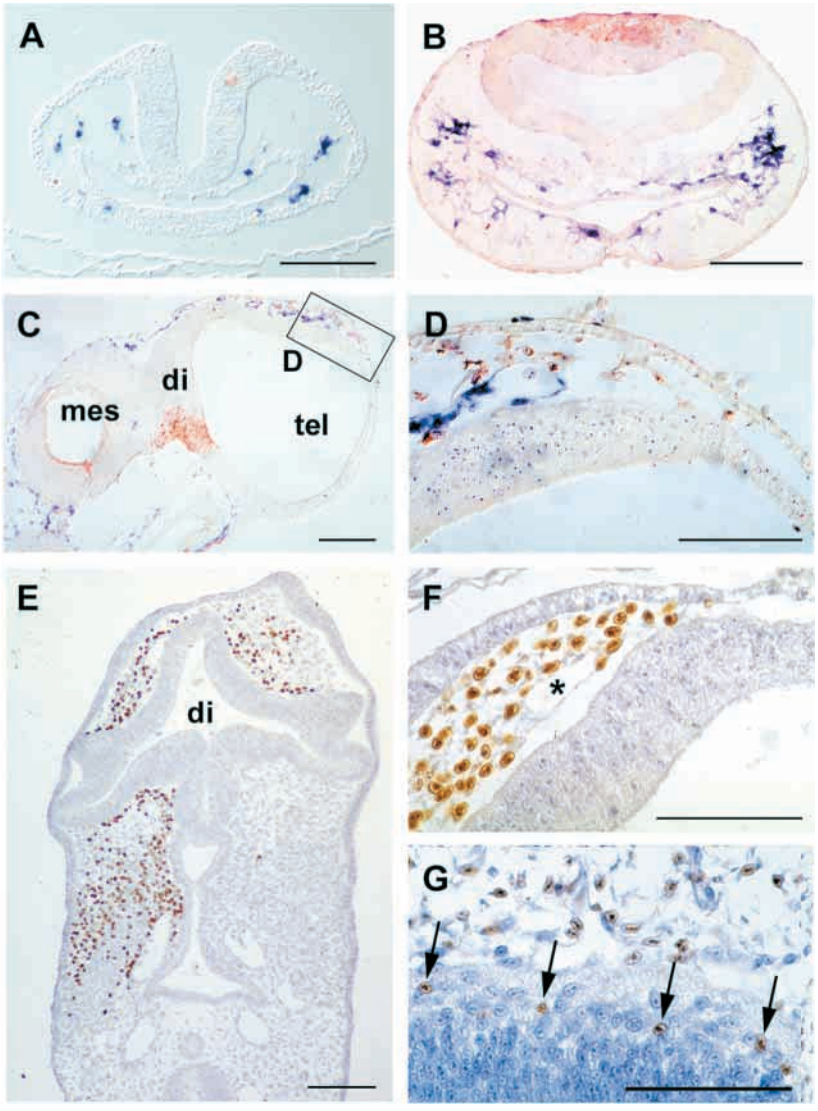

Fig. 2. Cephalic NCCs and mesodermal cells intermingle by way of opposing dispersion patterns. (A) Section through a HH7 (4ss, early E2) embryo at level of the presumptive diencephalon. No mesodermal cells, in particular endothelial precursors (blue, *Vegfr2* expression), intervene between the ectoderm and the prosencephalic alar plate. (B) Distribution of rostral-spreading NCC (red, *Sox10* expression) and endothelial cells (blue, *Vegfr2* expression) at early HH10 (10ss, E2) in a transverse section at the level of the anterior prosencephalon. (C) Parasagittal section of HH14 (E2) embryo, anterior right. Endothelial cells (blue, *Vegfr2* expression) and NCCs (red, *Sox10* expression) occupy the mesenchyme intervening between the neuroepithelium and ectoderm except around the rostral telencephalon. *Sox10* is also expressed in the ventral diencephalon (see Cheng et al., 2000). Boxed region is magnified in D. (D) NCCs precede endothelial tubes as they insinuate together between the ectoderm and neuroepithelium of the telencephalon. (E) Distribution of NCCs (brown, QCPN IHC) at HH14 after a unilateral graft of an anterior mesencephalic neural fold, in transverse section at the level of the ventral diencephalon. NCCs disperse bilaterally rostral to the graft but remain unilateral near the pharynx. (F) On a slightly more anterior section of the same embryo, grafted NCCs can be seen to separate neuroepithelium from ectoderm and to be accompanied by capillaries (asterisk) as in D. (G) NCCs (arrows) from a grafted mesencephalic neural fold begin to penetrate the telencephalic neuroepithelium from the surrounding mesenchyme at HH24 (E4). Scale bars: 100 μm in A-C,E,G: 50 μm in D,F.

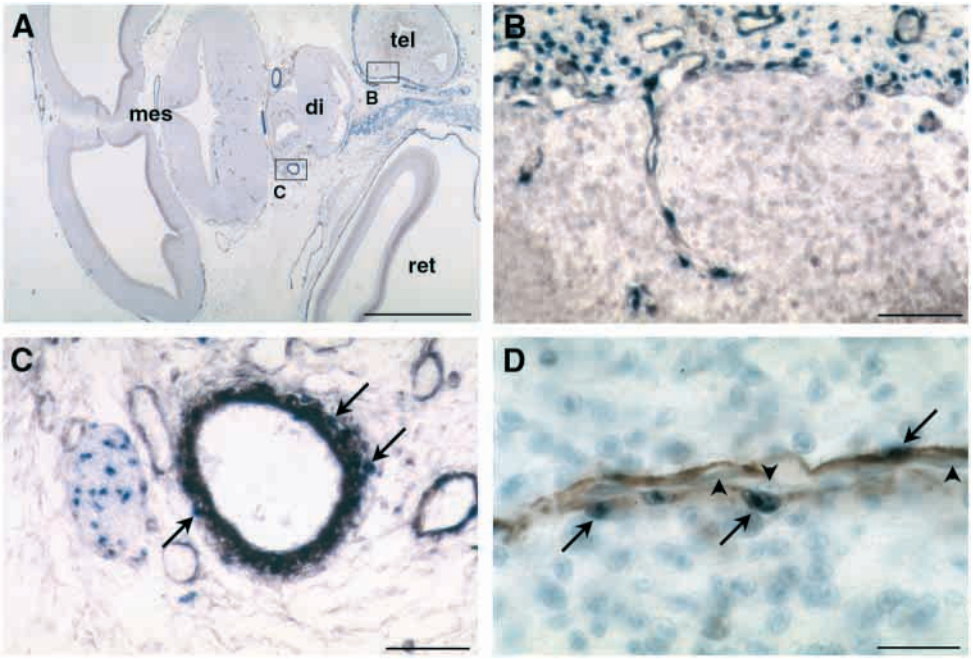

Fig. 3. NCCs associated with blood vessels in the head are pericytes or smooth muscle cells. (A) Slightly oblique transverse section of an embryo grafted with an anterior mesencephalic neural fold at HH32 (E8). Quail cells are visualised with QCPN IHC in blue; α smooth muscle actin IHC is in brown. Note that blue NCCs are concentrated around the forebrain, in contrast to the rest of the central nervous system. Regions magnified in B and C are indicated. (B) Telencephalic meninges are full of quail cells, some of which penetrate the neuroepithelium and co-localise with α smooth muscle actin. (C) The double labelling of grafted cells with α smooth muscle actin within the internal carotid artery tunica media indicates that these NCCs have become smooth muscle cells (arrows). (D) Similar double-labelling within the neuroepithelial capillaries shows NCC-derived pericytes (arrows); unlabelled endothelial cells are indicated with arrowheads. Scale bars: 1 mm in A; 50 μm in B,C; 100 μm in D.

seen by E5 and later (Fig. 5B,C,F,H,J), as well as to the thin tunica media of the cardinal veins and the sinus venosus (Fig. 5I). NCCs from r6 were found in the wall of the proximal common carotid arteries, relaying the r5 NCCs. NCCs from r7 and r8 participated in the brachiocephalic arteries (Fig. 5D-G,J-K), sigmoid valves of both the aorta (Fig. 5J,L) and pulmonary artery trunk (Fig. 5F,G,J), and the distal conotruncus. The deeper part of the conotruncus contained NCC of solely r8 origin at HH29 (E6.5) and HH33 (E8.5) (not shown).

No NCCs from any level of the cephalic neural folds were found in the media of the cerebellar or occipital arteries at the ages examined (not shown). These vessels are directly connected to the vertebral arteries. The head is thus divided into two vascular domains that meet at the forebrain/midbrain boundary both within the meninges and in the larger vessels, at the circle of Willis (Figs 1, 4). They occupy distinct ventral and dorsal domains from the heart to the brain.

Anterior cephalic NCCs occupy overlapping but distinct niches in connective tissues

We examined the distribution of cephalic NCC in other soft connective tissues in further detail. In these derivatives as well, a similar logic was maintained in the fate map.

Grafted NCC from PD are apparent in the ventrolateral periocular structures (sclera, choroid and interstitial cells of the ventral oculomotor muscles and lachrymal glands) (Fig. 6A-C). PD quail cells also surround and infiltrate the developing pituitary and salivary glands.

NCCs from the AM region incorporate largely into dorsomedial periocular structures, the scleral papillae and dermis, the nasal septum and the telencephalic choroid plexus. Examples of their presence as pericytes within oculomotor muscles, the optic chiasm, the neurohypophysis and the adenohypophysis are shown in Fig. 6E-H, respectively. Most or all NCCs in these locations can be double-labelled with α smooth muscle actin (not shown). However, many NCC in the adenohypophysis did not, representing interstitial cells.

NCCs from the PM region migrate largely into the first branchial arch maxillary processes. They also participate in the ciliary ganglia, optic nerves and coalescing ventromedial periocular structures (choroid pericytes, sclera, oculomotor muscle interstitial cells) as observed at HH26 (E5).

DISCUSSION

NCCs are distributed along the proximal-distal axis of cephalic vascular media

The frontier of the NC- and mesoderm-derived meninges surrounding the brain coincides with a classically described anatomical interface in the head between two distinct vasculatures. We have shown here that the forebrain (telencephalon and diencephalon) is the only part of the central nervous system into which NCCs penetrate. Arteries with walls composed of NCC derivatives also supply the entire ventral (facial) and anterior head, the connective tissues of which are likewise of NCC origin. In contrast, the fully mesodermal vertebral arteries supply the dorsal/posterior part of the head and neck, caudal to the diencephalon (Couly et al., 1992; Couly et al., 1993). The two vascular trees join and re-diverge at the level of the optic chiasm, within the circle of Willis (Fig. 1).

This striking demarcation of vascular domains reveals the point from which a new part of the head expanded in vertebrates with respect to the chordate phylum as a whole. Gans and Northcutt proposed that the neural crest played a key role in the evolution of the face, in particular for the skeletal and muscular elements of the jaws (Gans and Northcutt, 1983). The essence of their theory is that these novel NCC-derived

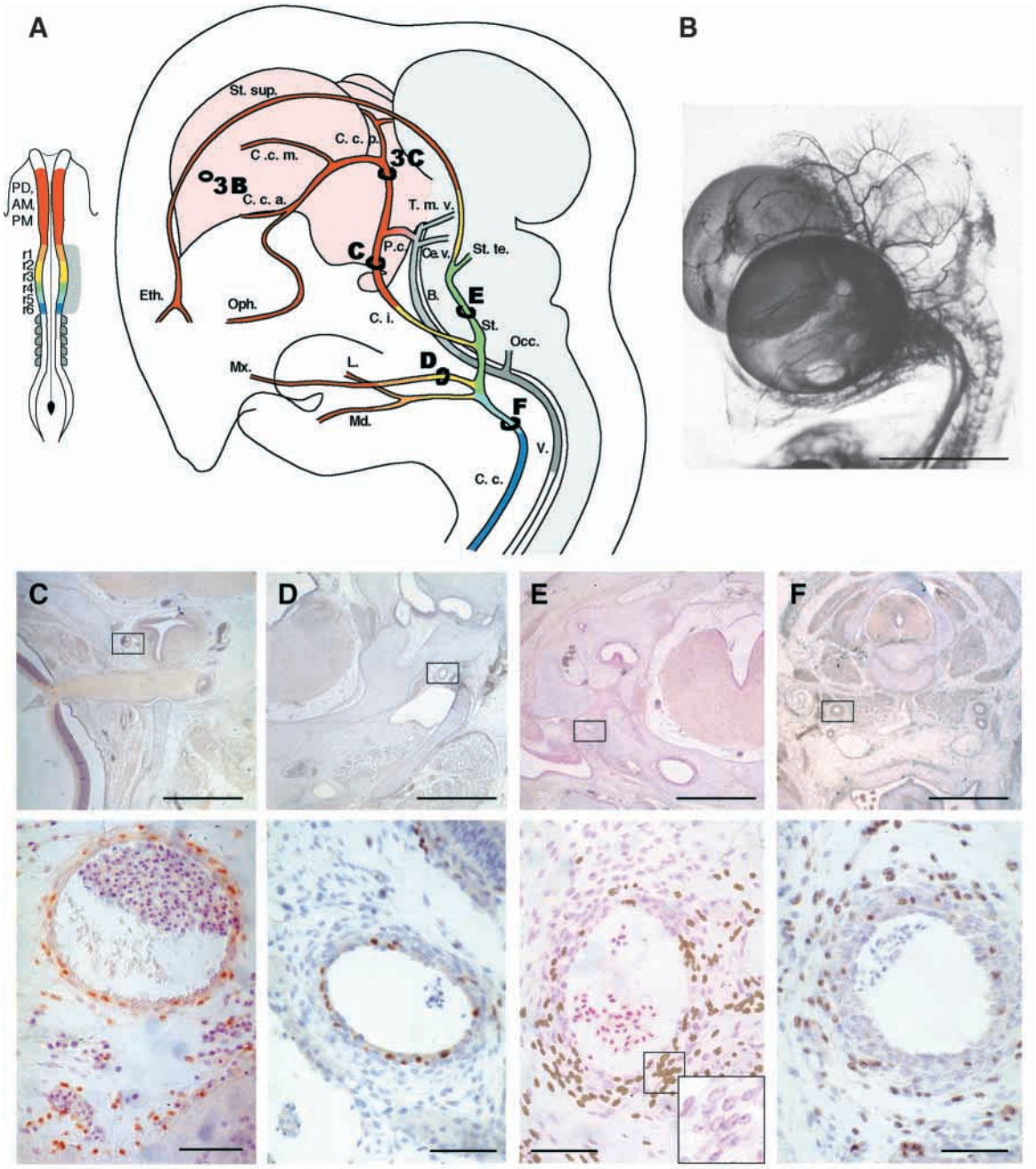

Fig. 4. Sequential distribution of NCC from successive neural fold origins in the walls of cephalic arteries. (A) Cephalic NCCs (colours, this study) and mesoderm (greys; Le Lièvre, 1976; Couly et al., 1987) contribute to the musculo-connective wall of separate arterial trees in the head. Red corresponds to cells derived from posterior diencephalic (PD), anterior and posterior mesencephalic (AM, PM) neural folds; orange corresponds to rhombomere (r)1; yellow to r2; green to r4; turquoise to r5; and blue to r6 (in the vascular media of a schematic E7.5 chicken head). Boundaries overlap between domains ensured by NCCs of given origins in vessel walls. Within the meninges of the central nervous system, pink denotes those derived from PD, AM and PM NCCs; grey denotes those of mesodermal origin, with a sharp boundary between the two at the diencephalon/mesencephalon junction. Levels of sections shown in C-F are indicated, where lower panel is a magnification of the artery indicated in the upper panel. Levels of Fig. 3B and 3C are also shown. (B) Ink-injected E8 quail, showing both branchial and vertebral artery ramifications. (C-F) The lower panels show the enlargement of the areas boxed in the upper panels. (C) E8 chimera after graft of PD neural fold, in transverse section – internal carotid artery. (D) E8 chimera after graft of r2 neural fold, in transverse section – maxillary artery. (E) E8 chimera after graft of r4 neural fold, in transverse section – stapedian artery. Quail cells revealed by Feulgen-Rossenbeck stain (lower panel inset) are false-coloured in brown in the lower panel. (F) E8 chimera after graft of r5 neural fold, in transverse section – common carotid artery. B., basilaris; C. c. a., carotis cerebralis anterior; C. c. m., carotis cerebralis medialis; C. c. p., carotis cerebralis posterior; Ce. v., cerebellaris ventralis; C. i., carotis interna; Eth., ethmoidalis; L., lingualis; Md., mandibularis; Mx., maxillaris; Occ., occipitalis; Oph., ophthalmica interna; P. c., posterior communicante (circle of Willis); St., stapedia; St. te., stapedia temporalis; St. sup., stapedia supraorbitalis; T. m. v., tecti mesencephalis ventralis; V, vertebralis. Adapted, with permission, from Hughes (Hughes, 1934) and Baumel (Baumel, 1979). Scale bars: 0.5 cm in B; 250 μm in C-F (top); 50 μm in C-F (bottom).

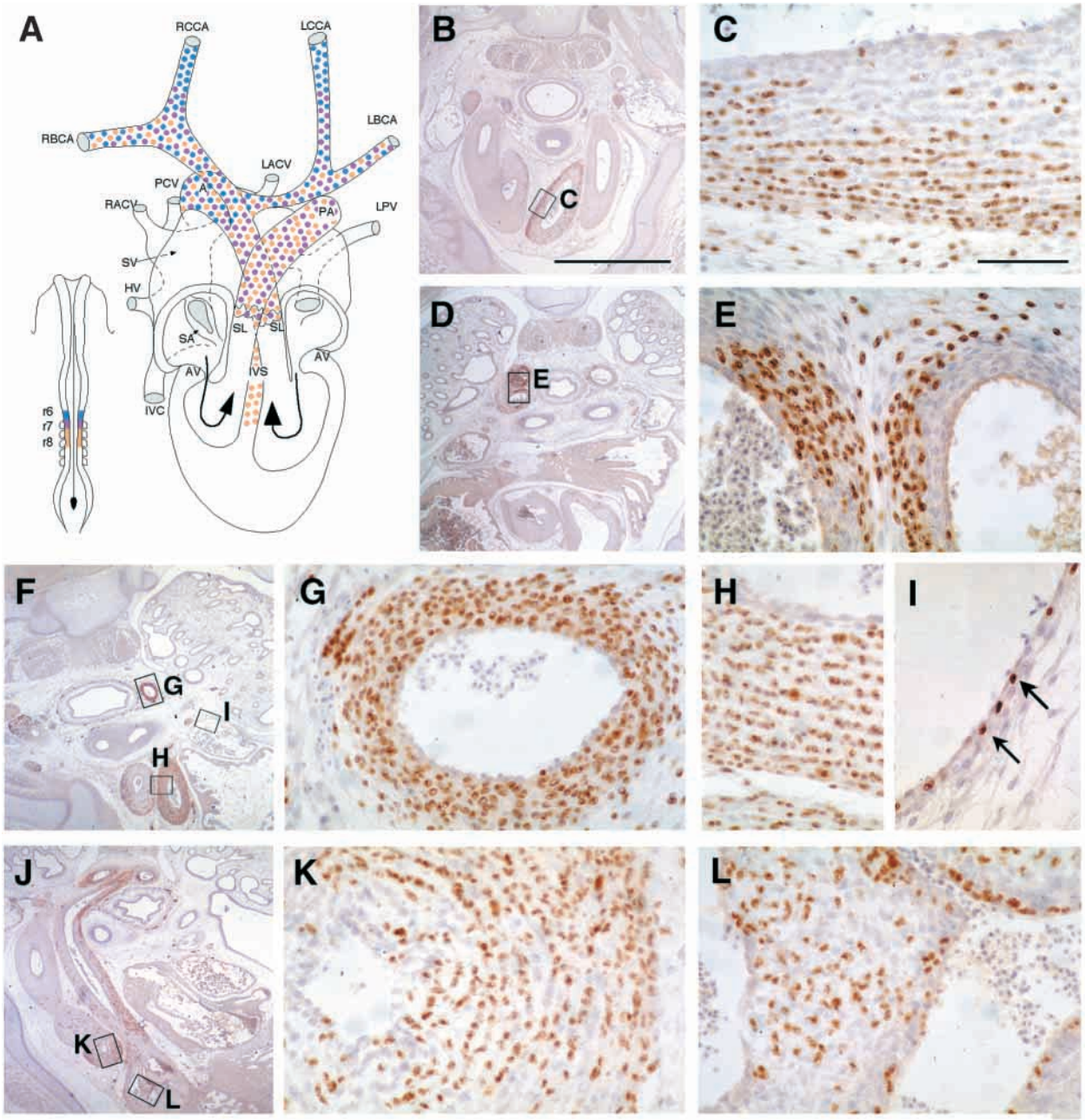

Fig. 5. Overlapping contributions of NCC from the last three rhombomeres to proximal cardiac arteries. (A) The E12 chicken heart, with NCC from r6 (blue), r7 (purple) and r8 (pink) in its major arteries. (B) Graft of r6 neural folds, at HH35 (E9). Abundant quail cells (QCPN IHC, brown) are present in the aorta, magnified in C. (D) After graft of r7 neural folds, at HH35 (E9). Quail cells are visible in the outer vessel walls at the divergence of the right brachiocephalic and common carotid arteries, magnified in E. (F) After graft of r8 neural folds, at HH33 (E8.5). Left common carotid artery magnified in G. Aorta and pulmonary trunk walls magnified in H, and pericytes in the wall of the sinus venosus are indicated by arrows in I. (J) Caudal section of same embryo, showing quail NCC abundant in the aorta, in the pulmonary trunk and arteries, in the right brachiocephalic artery (magnified in K) and aortic semilunar valve (magnified in L). A, aorta; AV, atrioventricular valve; HV, hepatic vein; IVC, inferior vena cava; IVS, interventricular septum; LACV, RACV, left and right anterior cardinal veins; LBCA, RBCA, left and right brachiocephalic arteries; LCCA, RCCA, left and right common carotid arteries; LPV, left pulmonary vein (right hidden); PA, common pulmonary artery trunk; PCV, posterior cardinal vein; SA, sinoatrial valve; SL, semilunar valve; SV, sinus venosus. Scale bars: in B, 250 μm for B,D,F,I; in C, 50 μm for E,G-I,K,L.

cephalic structures may have permitted vertebrates to adopt an advantageously active feeding lifestyle. Supporting evidence comes from demonstrations that the face, jaws and skull are derived from the neural crest in modern-day vertebrates (see, for example, Couly et al., 1993; Imai et al., 1996).

The forebrain, in particular the telencephalon, embodies an evolutionarily recent morphological change in the central nervous system, not a novel structure altogether. The faceless and jawless cephalochordate *Amphioxus* presents sensory and endocrine functions in the anterior end of its nerve cord (Lacalli et al., 1994; Lacalli and Kelly, 2000). Gene expression patterns in this region recall those present in the vertebrate

forebrain (reviewed by Zimmer, 2000). The common chordate ancestor to vertebrates and cephalochordates probably had a similarly rudimentary forebrain, whose functions were amplified and developed in the vertebrate diencephalon (photosensation via the eyes and pineal gland, hormone secretion from the ventral diencephalon and pituitary) and telencephalon (chemosensation).

Within vertebrates, the telencephalon assumed integrative functions and importance over time, possibly owing to the presence of a blood supply consecrated directly to its growing needs for oxygen and nutrition. Our current observations demonstrate that a NCC-supported vasculature developed to irrigate both the NCC-derived jaws, already present in lower vertebrates, and the forebrain, greatly expanded in higher vertebrates. We have previously shown that NCC mesenchyme has a trophic effect on the early forebrain, namely on the cerebral hemispheres. In the absence of this mesenchyme, achieved by ablation of the posterior diencephalic and mesencephalic neural folds, the forebrain neuroepithelium undergoes massive cell death preceding its normal period of vascularisation (Etchevers et al., 1999). Thus, the neural crest has three distinct roles in the development of the forebrain: an antiapoptotic effect at an early stage of neurogenesis, a second trophic role via its contribution to the leptomeninges and cephalic vasculature, and a third role, in the protection of the forebrain by means of the dura mater and the skull.

Initial dispersion of anterior cephalic NCCs accounts for their final distribution

The lack of cell emigration from the neural folds of the prosencephalon, anterior to the burgeoning eyes (Couly and Le Douarin, 1988), creates a rostral niche that is filled by NCCs spreading forward, fan-like, from the posterior diencephalic neural folds. In the posterior head, NCCs from any given rhombomere colonise more than one branchial arch to surround its aortic artery (Birgbauer et al., 1995; Köntges and Lumsden, 1996; Couly et al., 1996). When part of the cephalic neural folds are removed by surgical ablation, NCC from regions rostral and/or caudal to the excision disperse to ectopic compensatory locations in the head (Couly et al., 1996; Salvidar et al., 1997; Etchevers et al., 1999; Kulesa et al., 2000). In this way, cephalic NCCs radiate from their dorsal points of origin into wider ventral swathes, with some limited mixing among cells of neighbouring origins.

The patterns of dispersion that establish the anterior mesenchyme early on presage the final distribution of NCCs in the head mesectoderm. Fate-mapping small domains of the anterior neural folds shows that NCC from the posterior

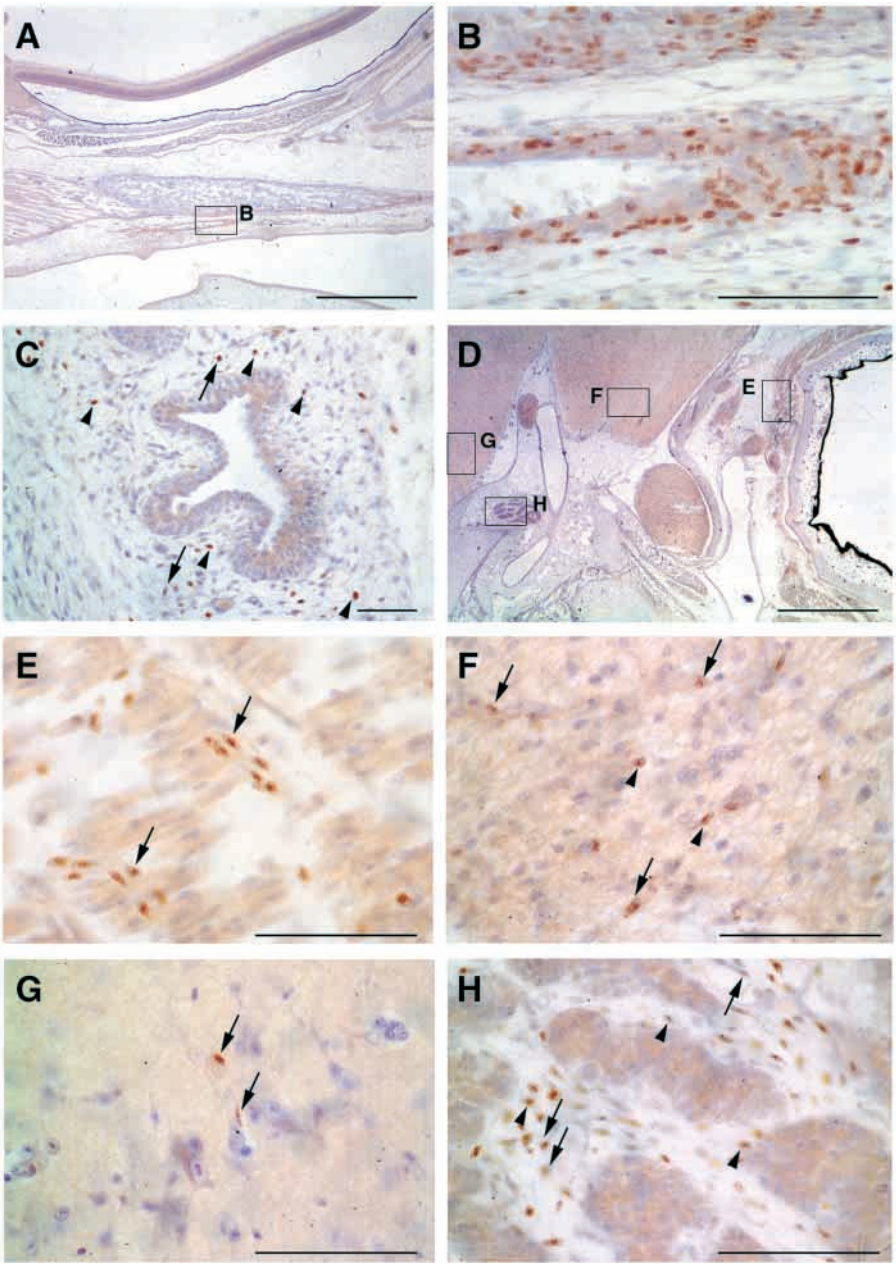

Fig. 6. NCCs integrate into periocular and secretory tissues. (A) Parasagittal section of E12 embryo grafted with posterior diencephalic neural folds, in area of ventral eye. (B) Area enlarged shows the palatine artery with NCC-derived smooth muscle cells and a portion of the palatine membrane bone. (C) Part of a lachrymal gland, showing interstitial (arrowheads) and pericytic (arrows) participation of NCCs. (D) Lateral parasagittal section of E12 embryo grafted with anterior mesencephalic neural folds, indicating regions magnified in E-H. (E) NCC-derived pericytes (arrows) accompany the capillaries of the dorsal rectus oculomotor muscle. (F) Both glia (arrowheads) and capillary pericytes (arrows) within the optic chiasm are derived from NCCs. (G) Pericytes (arrows) are the only cells of graft origin within the neurohypophysis. (H) Both interstitial cells (arrowheads) and pericytes (arrows) in the adenohypophysis come from NCCs. Scale bars: 250 μm in A; 100 μm in B,C,E-H; 1 mm in D.

diencephalic or anterior mesencephalic neural folds occupy the ventral and dorsal anterior heads respectively, the posterior mesencephalic NCCs remaining essentially lateral to their original rostrocaudal level in the jaws.

In particular, we have observed that posterior diencephalic NCCs are found within the walls of the pituitary vascular plexus (Fig. 6G,H and Etchevers et al., 2001), adjacent to the first branchial arch with its complement of anterior rhombencephalic NCC. This surprising distribution reflects the topological deformation of the longitudinal axis of the head around the end of the notochord, which brings the anterior transverse neural fold ventral and caudal to the future hypothalamus (Couly et al., 1987). The mesencephalic NCC participate in the meninges of the forebrain (this study) as well as its overlying dermis and skull (Couly et al., 1993). Mesencephalic NCCs actually constitute the most anterior mesectoderm, by occupying a rostrally expanding area dorsal to that populated by diencephalic NCC.

There are two conclusions to be drawn from these results. First, adjacent points in the neural folds map to contiguous areas of the head along its original rostrocaudal axis, reflecting the dispersion of cephalic NCC during migration. Second, cooperation between the cephalic mesoderm and the neural crest is necessary to build a vascular tree in that part of the head that is constructed predominantly by NCCs. Mesodermal cells initially located in a ventral position migrate dorsally and mix with the ectomesenchyme of neural fold origin. Cephalic mesodermal mesenchyme is the site of two successive waves of cell determination and differentiation. Cells expressing Vegfr2 (Eichmann et al., 1993) become endothelial cells of the developing blood vessels. From this stage onwards, they become associated with NCCs that differentiate into the pericytes and musculo-connective tissue of the outer blood vessel walls. The second wave of commitment affecting mesodermal cells concerns the head muscles, for which ectomesenchymal cells form connective components such as membranes and tendons (Noden, 1983; Couly et al., 1996; Köntges and Lumsden, 1996).

NCC may be involved in human vascular pathologies

Recent fate maps of NCC in the mouse (Imai et al., 1996; Jiang et al., 2000) confirm the importance of avian studies to interpreting mammalian vascular remodelling. Although we have observed NCC from r8 in the proximal portion of the pulmonary arteries, the posterior limit of r8 was not mapped in this study. Waldo and Kirby have also found that the NCCs of rostral r8 do not participate in the distal pulmonary arteries but rather continue in the media of the transient ductus arteriosus (sixth aortic arch), connecting their proximal portion to the dorsal aorta (Waldo and Kirby, 1993). At this intersection, vascular media no longer contain NCCs. According to the logic of the vascular fate map we establish in this paper, it appears likely that caudal r8 cells temporarily contribute to the distal ductus arteriosus, rather than the distal pulmonary arteries. These latter vessels are probably the product of remodelling between two initially distinct parts of the vascular tree. The pulmonary arteries thus would recombine a proximal, NCC-ensheathed portion with a distal, mesoderm-ensheathed segment. This situation resembles the late anastomosis that occurs to establish the circle of Willis. Waldo and Kirby also proved the necessity for NCCs in the septation of the aorta from the pulmonary artery trunk within the mesodermal context of the heart (Waldo and Kirby, 1993). Septation is compromised in a number of congenital conditions that affect other derivatives of the neural crest (reviewed in Le Douarin and Kalcheim, 1999). As is the case for forebrain vessels, cephalic NCCs make the musculo-connective wall of large vessels near the heart, suggesting that vascular remodelling in the head, neck and heart is dependent on NCC participation.

The fact that the branchial arteries give rise to a distinct vascular domain is pertinent to phakomatoses such as Sturge-Weber syndrome (reviewed by Masson, 1970) or meningioangiomatosis (reviewed by Chakrabarty and Franks, 1999). These diseases involve calcification of forebrain capillary pericytes in the cerebral hemispheres; Sturge-Weber syndrome is also associated with ipsilateral facial angiomas. It is striking that NCCs from the same source as the forebrain meninges and pericytes normally differentiate into membrane bones when they are located in a subectodermal position (Couly et al., 1993).

Pericytes and smooth muscle cells share a common lineage

Pericytes, immediately adjacent to the vascular endothelium of both arteries and veins, are not in themselves smooth muscle cells. They do, however, share some properties and markers, of which one interesting representative is nestin (Alliot et al., 1999). Like other nestin-expressing cell types, vascular pericytes seem to retain a certain context-dependent flexibility in their differentiation, acquiring characteristics suggestive of smooth muscle, fibroblasts, osteoblasts, adipocytes or chondrocytes in vitro (reviewed in Doherty and Canfield, 1999). Our results demonstrate unequivocally and for the first time that in an entire vascular circuit, from the heart to capillaries and back, there can be one common source of precursor cells for both the smooth muscle walls and the pericytes.

The authors thank Louis Addade, Pierre Coltey, Sophie Gournet, Michel Fromaget and Francis Beaujean for their technical and graphical assistance. This work was underwritten by the Centre National de la Recherche Scientifique. H. C. E. was a predoctoral fellow of the Howard Hughes Medical Institute and was additionally supported by the Société de Secours des Amis des Sciences.

REFERENCES

Alliot, F., Rutin, J., Leenen, P. J. and Pessac, B. (1999). Pericytes and periendothelial cells of brain parenchyma vessels co-express aminopeptidase N, aminopeptidase A, and nestin. *J. Neurosci. Res* **58**, 367-378.

Balabanov, R. and Dore-Duffy, P. (1998). Role of the CNS microvascular pericyte in the blood-brain barrier. *J. Neurosci. Res.* **53**, 637-644.

Baumel, J. J. (1979). Systema cardiovasculare. In *Nomina Anatomica Avium* (ed. J. J. Baumel, A. S. King, A. M. Lucas, J. E. Breazile and H. E. Evans), pp. 354-79. London: Academic Press.

Birgbauer, E., Sechrist, J., Bronner-Fraser, M. and Fraser, S. (1995). Rhombomeric origin and rostrocaudal reassortment of neural crest cells revealed by intravital microscopy. *Development* **121**, 935-945.

Bockman, D. E. and Kirby, M. L. (1984). Dependence of thymus development on derivatives of the neural crest. *Science* **223**, 498-500.

Chakrabarty, A. and Franks, A. J. (1999) Meningioangiomatosis: a case report and review of the literature. *Br. J. Neurosurg.* **13**, 167-173.

Cheng, Y., Cheung, M., Abu-Elmagd, M. M., Orme, A. and Scotting, P. J. (2000). Chick sox10, a transcription factor expressed in both early neural crest cells and central nervous system. *Dev. Brain Res.* **121**, 233-241.

Couly, G. F. and Le Douarin, N. M. (1987). Mapping of the early neural primordium in quail-chick chimeras. II. The prosencephalic neural plate and neural folds: implications for the genesis of cephalic human congenital abnormalities. *Dev. Biol.* **120**, 198-214.

Couly, G. and Le Douarin, N. M. (1988). The fate map of the cephalic neural primordium at the presomitic to the 3-somite stage in the avian embryo. *Development* **103**, Suppl., 101-113.

Couly, G. F., Coltey, P. M. and Le Douarin, N. M. (1992). The developmental fate of the cephalic mesoderm in quail-chick chimeras. *Development* **114**, 1-15.

Couly, G. F., Coltey, P. M. and Le Douarin, N. M. (1993). The triple origin of skull in higher vertebrates: a study in quail-chick chimeras. *Development* **117**, 409-429.

Couly, G., Coltey, P., Eichmann, A., Le Douarin, N. M. (1995). The angiogenic potentials of the cephalic mesoderm and the origin of brain and head blood vessels. *Mech Dev* **53**, 97-112.

Couly, G., Grapin-Botton, A., Coltey, P. and Le Douarin, N. M. (1996). The regeneration of the cephalic neural crest, a problem revisited: the regenerating cells originate from the contralateral or from the anterior and posterior neural fold. *Development* **122**, 3393-3407.

Doherty, M. J. and Canfield, A. E. (1999). Gene expression during vascular pericyte differentiation. *Crit. Rev. Eukaryotic Gene Expr.* **9**, 1-17.

Eichmann, A., Marcelle, C., Breant, C. and Le Douarin, N. M. (1993). Two molecules related to the VEGF receptor are expressed in early endothelial cells during avian embryonic development. *Mech. Dev.* **42**, 33-48.

Etchevers, H. C., Couly, G., Vincent, C. and Le Douarin, N. M. (1999). Anterior cephalic neural crest is required for forebrain viability. *Development* **126**, 3533-3543.

Etchevers, H. C., Vincent, C. and Couly, G. (2001). Neural crest and pituitary development. In *Hypothalamic-Pituitary Development: Genetic and Clinical Aspects* (ed. R. Rappaport). Basel, Switzerland: S. Karger AG (in press).

Gans, C. and Northcutt, R. G. (1983). Neural crest and the origin of vertebrates: a new head. *Science* **220**, 268-274.

Grapin-Botton, A., Bonnin, M. A., McNaughton, L. A., Krumlauf, R. and Le Douarin, N. M. (1995). Plasticity of transposed rhombomeres: Hox gene induction is correlated with phenotypic modifications. *Development* **121**, 2707-2721.

Hughes, A. F. V. (1934). On the development of the blood vessels in the head of the chick. *Philos. Trans. R. Soc. London Ser. B* **224**, 75-129.

Imai H., Osumi-Yamashita, N., Ninomiya, Y. and Eto, K. (1996). Contribution of early-emigrating midbrain crest cells to the dental mesenchyme of mandibular molar teeth in rat embryos. *Dev. Biol.* **176**, 151-165.

Jiang, X., Rowitch, D. H., Soriano, P., McMahon, A. P. and Sucov, H. M. (2000). Fate of the mammalian cardiac neural crest. *Development* **127**, 1607-1616.

Johnston, M. C. (1966). A radioautographic study of the migration and fate of cranial neural crest cells in the chick embryo. *Anat. Rec.* **156**, 143-55.

Kawada, N. (1997). The hepatic perisinusoidal stellate cell. *Histol. Histopathol.* **12,** 1069-1080.

Köntges, G. and Lumsden, A. (1996). Rhombencephalic neural crest segmentation is preserved throughout craniofacial ontogeny. *Development* **122**, 3229-3242.

Kulesa, P., Bronner-Fraser, M. and Fraser, S. (2000). In ovo time-lapse analysis after dorsal neural tube ablation shows rerouting of chick hindbrain neural crest. *Development* **127**, 2843-2852.

Lacalli, T. C., Holland, N. D. and West, J. E. (1994). Landmarks in the anterior central nervous system of *amphioxus* larvae. *Philos. Trans. R. Soc. Lond. Ser. B* **344**, 165-185.

Lacalli, T. C. and Kelly, S. J. (2000). The infundibular organ in Amphioxus larvae and related aspects of cerebral vesicle organization. *Acta Zoologica* **81**, 37-48.

Le Douarin, N. (1969). Particularités du noyau interphasique chez la caille japonaise (Coturnix coturnix japonica). Utilisation de ces particularités comme ‘marquage biologique’ dans les recherches sur les interactions tissulaires et les migrations cellulaires au cours de l'ontogenèse. *Bull Biol. Fr. Belg.* **103**, 435-452.

Le Douarin, N. M. and Kalcheim, C. (1999). *The Neural Crest*. Cambridge: Cambridge University Press.

Le Lièvre, C. S. and Le Douarin, N. M. (1975). Mesenchymal derivatives of the neural crest: analysis of chimaeric quail and chick embryos. *J. Embryol. Exp. Morphol.* **34**, 125-154.

Masson, M. (1970). La maladie de Sturge-Weber. *La Revue du Practicien* **20**, 4455-4461.

Noden, D. M. (1983). The role of the neural crest in patterning of avian cranial skeletal, connective, and muscle tissues. *Dev. Biol.* **96**, 144-165.

Saldivar, J. R., Sechrist, J. W., Krull, C. E., Ruffins, S. and Bronner-Fraser, M. (1997). Dorsal hindbrain ablation results in rerouting of neural crest migration and changes in gene expression, but normal hyoid development. *Development* **124**, 2729-2739.

Schlondorff, D. (1987)**.** The glomerular mesangial cell: an expanding role for a specialized pericyte. *FASEB J.* **1**, 272-281.

Waldo, K., Miyagawa-Tomita, S., Kumiski, D. and Kirby, M. L. (1998). Cardiac neural crest cells provide new insight into septation of the cardiac outflow tract: aortic sac to ventricular septal closure. *Dev. Biol.* **196**, 129-144.

Waldo, K. L. and Kirby, M. L. (1993). Cardiac neural crest contribution to the pulmonary artery and sixth aortic arch artery complex in chick embryos aged 6 to 18 days. *Anat. Rec.* **237**, 385-99.

Zimmer, C. (2000). In search of vertebrate origins: beyond brain and bone. *Science* **287**, 1576-1579.

Rappaport R, Amselem S (eds): Hypothalamic-Pituitary Development. Genetic and Clinical Aspects.
Endocr Dev. Basel, Karger, 2001, vol 4, pp 13–29

Neural Crest and Pituitary Development

Heather C. Etchevers[a], *Christine Vincent*[a], *Gérard Couly*[b]

[a] Institut d'Embryologie Cellulaire et Moléculaire du CNRS et du Collège de France, Nogent-sur-Marne et
[b] Service de Stomatologie, Hôpital Necker – Enfants Malades, Paris, France

Introduction

The pituitary gland is composed of three functionally and histologically distinct regions, the anterior, intermediate and posterior lobes. These arise from two distinct embryonic primordia. The anterior (adeno)hypophysis becomes visible in humans at the end of the first month of development. It develops from an invagination of the ectoderm of the stomodeal roof, called Rathke's pouch. The intermediate lobe arises from the dorsal part of Rathke's pouch closest to the diencephalon, as has been shown in the fetal rabbit by Schimchowitsch et al. [1]. In contrast, the posterior (neuro)hypophysis pinches off of the ventral diencephalon, remaining attached by a bridge which will develop into the hypophyseal stalk.

Towards the end of the second month, the developing pituitary establishes its links to the hypothalamus by the progressive elaboration of the hypophyseal stalk, the median eminence and the venous portal circulations. The architecture of the human hypothalamo-hypophyseal system is schematized in figure 1. At the end of embryonic development, the diverse elements of the pituitary gland are grouped together within the sella turcica of the sphenoid bone complex. This chapter discusses the origins of the anlagen of the pituitary gland and their relationship to the embryological cell population, the neural crest.

Fish, amphibian, avian and mammalian animal model systems have all made contributions to understanding the multiple origins of pituitary components and inductive influences acting during embryogenesis. Our work has employed the technique of creating quail-chick chimeras, developed by Le Doua-

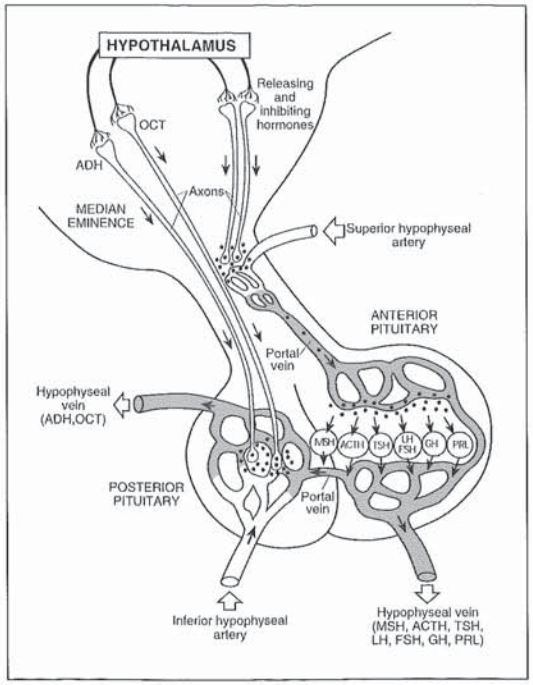

Fig. 1. Schematic diagram of the mature human hypothalamo-hypophyseal complex and its vasculature [adapted from 39]. MSH = Melanocyte-stimulating hormone; ACTH = adrenocorticotropic hormone; TSH = thyroid-stimulating hormone; LH = luteinizing hormone; FSH = follicle-stimulating hormone; GH = growth hormone; PRL = prolactin.

rin [2; reviewed in 3]. Cells from the donor species can be distinguished from those of the host by a choice of histological or immunocytochemical techniques. As there is perfect integration of the donor cells within the host, it is possible to follow their differentiation in any given location and from various time points in embryogenesis. This technique has been particularly useful in the study of the embryonic cell population known as the neural crest. Neural crest cells (NCC) delaminate from the boundary between ectoderm and the neuroepithelial plate as the latter forms a tube which will create the axis of the central nervous system. They then disperse throughout the body and participate in the development of a plethora of tissues and organs (table 1).

Using such quail-chick chimeras, we constructed a map of the presumptive territories corresponding to the adenohypophysis and neurohypophysis in the

Table 1. Derivatives of NCC in the vertebrate body

Mesectoderm	Peripheral nervous system	Endocrine cells	Pigment cells
Connective tissue of glands	*Sensory neurons of:*	*Adrenal medulla*	*All, excepting retinal pigment cells*
Pituitary	Spinal ganglia		
Lacrimal	Trigeminal (nerve V) ganglion in par	*Carotid body:*	
Salivary	Facial (nerve VII) ganglion	Type I satellite-type cells	
Thyroid	Glossopharyngeal (nerve IX) superior ganglion	Type II satellite-type cells	
Parathyroid	Vagal (nerve X) jugular ganglion	*Calcitonin-producing 'C' cells*	
Thymus	Rohon-Beard cells (amphibians)		
Head:			
Skull (details in table 3)	*Satellite/glial cells of:*		
Odontoblasts and tooth papillae	All sensory ganglia		
Dermis	Includes geniculate (nerve VII), otic (nerve VIII), petrosal (nerve IX) and nodose (nerve X) ganglia		
Smooth muscle and pericytes of vascular walls	All autonomic ganglia and plexi		
Connective tissue of ocular and masticatory muscles	Schwann cells of all peripheral nerves		
Adipose tissue in calvarium, face and ventral neck	*Autonomic neurons of:*		
Heart:	Sympathetic ganglia and plexi		
Conotruncus	Parasympathetic ganglia and plexi		
Sigmoid valves	Enteric plexi		
Smooth muscle walls of ventral aorta, aortic arches			
Trunk:			
Dorsal fins of lower vertebrates			

open neural plate [4, 5]. We also observed that cephalic NCC penetrate into the tissue of the pituitary gland. There they give rise to interstitial cells and vascular pericytes [4, 6]. Surrounding the gland, NCC also participate in the smooth muscle walls of the hypophyseal arteries and veins, and compose the bones of the anterior part of the sella turcica [7].

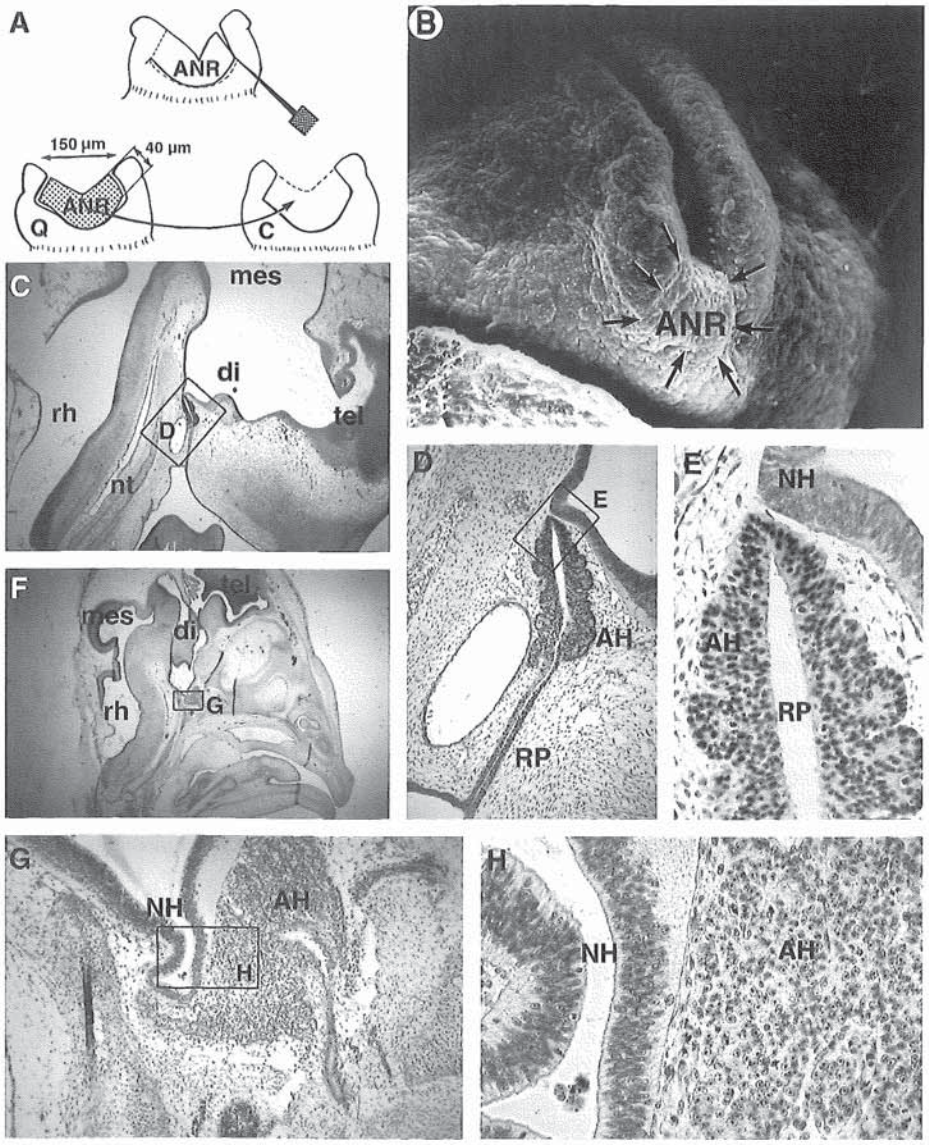

Fig. 2. Graft of quail anterior neural ridge into chicken host at 3ss leads to an adenohypophysis of donor origin [4]. ***A*** At the 3 somite stage, the anterior neural ridge (ANR) of a quail (Q) embryo is excised and substituted for the same region in a chicken (C) embryo

The Presumptive Adenohypophysis Is Located in the Anterior Transverse Neural Fold

When determining the location of the presumptive anterior pituitary in the avian neurula, we examined the derivatives of the anterior neural plate and its surrounding neural folds using small grafts. The sum of this data is known as a fate map, and the chimeras were constructed at a stage when the embryos had 3 somite pairs (3ss). Pieces of quail embryos on the order of 0.006 mm^2 were grafted into isochronic chicken embryos, after removing the equivalent regions of the host. Chimeric embryos were sacrificed on embryonic days (E)3, E5, E7 and E12, and the grafted cells traced.

At E3, after grafting a median piece of the anterior transverse neural fold (fig. 2A, B) one can already see that Rathke's pouch, the precursor to the adenohypophysis, is of donor origin. At E5 (fig. 2C–E) and E12 (fig. 2F–H), using the same types of grafts, the glandular cords may be seen to come from the quail graft, while the neurohypophysis and adenohypophyseal interstitial mesenchyme is contributed by the chicken host. Using similar methods, we were also able to observe that the territory corresponding to the future hypothalamus is located immediately posterior to that of the adenohypophysis. Located within the neural plate, it contains the presumptive neurohypophysis in its posterior portion [5].

In figure 3, parts of the avian fate map [8] are projected onto a neural plate seen in perspective, in order to demonstrate the morphological changes that take place over a few hours' time at the neurula stage. Similar fate maps have been constructed for zebrafish, the African clawed toad *Xenopus*, and mouse neurulas, leading to the conclusion that the underlying regional organization of the anterior neural plate is the same across all vertebrate species, including humans [reviewed in 9].

host. ***B*** The graft is seen 4 h later by scanning electron microscopy, and is delimited by arrows. ***C*** Similarly operated embryo on the 5th day of incubation, in sagittal section. Area enlarged in ***D*** indicated. Tel = Telencephalon; Di = diencephalon; Mes = mesencephalon; Rh = rhombencephalon; NT = notochord. ***D*** Rathke's pouch (RP) and the developing adenohypophysis (AH) contain quail cells, as revealed by immunohistochemistry with the quail-specific monoclonal antibody, QCPN [40]. Area enlarged in ***E*** indicated. ***E*** Close apposition of the AH with the future neurohypophysis (NH) of host origin. ***F*** Chimera on the 12th day of incubation in sagittal section. Area enlarged in ***G*** indicated. ***G*** Both AH and NH regions have developed. Area enlarged in ***H*** indicated. ***H*** Localization of quail cells by the Feulgen-Rossenbeck technique [2] shows the condensed heterochromatin of the graft present in the mature AH but not within the immediately adjacent NH.

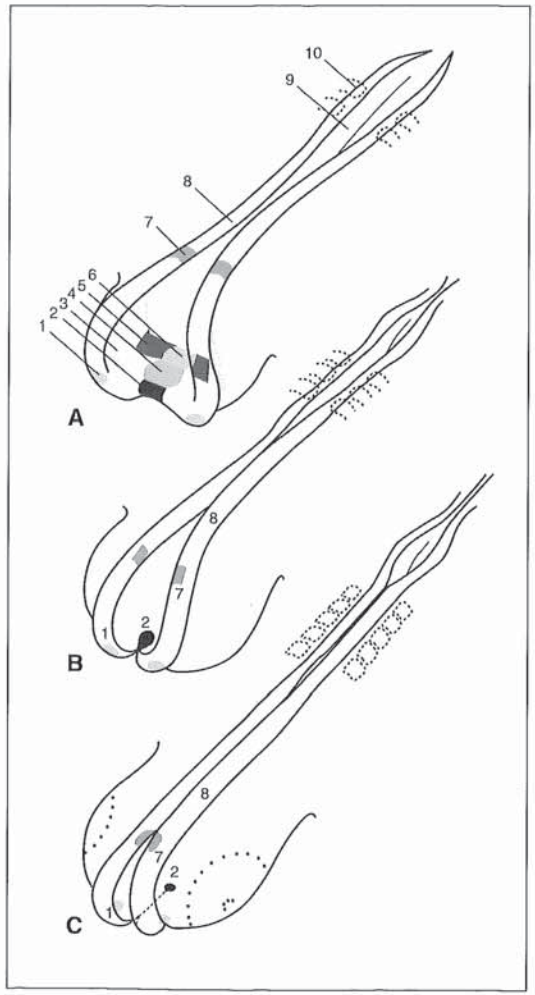

Fig. 3. Depiction of the avian neurula fate map [adapted from 8], at three different stages. ***A*** At the 2 somite stage (ss), the neural plate is relatively flat, though the neural folds are beginning to rise and approach each other dorsally. The shaded territories correspond by number to the following structures: 1 = olfactory placodes (future nasal epithelium); 2 = anterior neural ridge (future adenohypophysis); 3 = telencephalon; 4 = diencephalon (future hypothalamus); 5 = retinae; 6 = diencephalon (future neurohypophysis); 7 = epiphysis or pineal gland; 8 = neural crest; 9 = notochord; 10 = somite. ***B*** At 3ss, the fate map of the olfactory placodes, the adenohypophysis, the epiphyseal placodes and the neural crest has undergone morphological transformation as the neural folds contact each other and the newly formed neural tube flexes forward and rolls beyond the anterior neural ridge. ***C*** At 5ss, the olfactory placodes now reside in an area of ectoderm which directly overlies the rhinencephalon; the adenohypophysis directly overlies the neurohypophysis, the bilaterally paired epiphyseal placodes join at the dorsal midline, and the neural folds caudal to that point will give rise to migratory NCC within a few hours. The future retinal outpocketings are depicted with dotted arcs, whereas the relative caudal regression of the adenohypophysis and joining of the immediately contiguous neural folds at the ventral midline is shown by a dashed line.

The Presumptive Adenohypophysis Is Subject to the Topological Deformations of the Anterior Neural Plate

Between 3ss and 10ss, the vertebrate neural plate undergoes some major morphological transformations. The anterior neural plate extends, widens, its edges rise dorsally to meet one another, and the transverse anterior edge is forced to bend ventrally (fig. 3). We examined this complex morphogenesis more closely after grafting the transverse anterior neural fold [4]. The adenohypophyseal placode territory may be seen to be transported ventral to the plane of the neuroepithelium. In the E5 chicken host, a graft of the median anterior neural fold becomes Rathke's pouch (fig. 2D). It lies underneath the diencephalon, within the posterior roof of the stomodeum. The flanking presumptive olfactory placodes roll down to lie ventral to the prosencephalic neural plate (fig. 3C). The future adenohypophysis thus comes into contact with that part of the floor of the prosencephalon from which the neurohypophysis will arise. At the same time, the hypothalamic territory, which had lain immediately adjacent inside the neural plate, slides forward to finish anterior to both of them.

Recent work in rodent models has demonstrated that separate inductive steps from the diencephalon are necessary for Rathke's pouch formation and for its differentiation [10]. The molecular signals and relays involved in these steps are beyond the scope of this chapter but are reviewed by Watkins-Chow and Camper [11], and the list continues to grow.

Colonization of the Anterior Pituitary by NCC

NCC derived from the posterior diencephalic and anterior mesencephalic neural folds begin to surround the ventral diencephalon on E3 [6]. They subsequently colonize the spaces between the glandular cords between E4 and E5 in the avian embryo (fig. 4A, B) [4, 12].

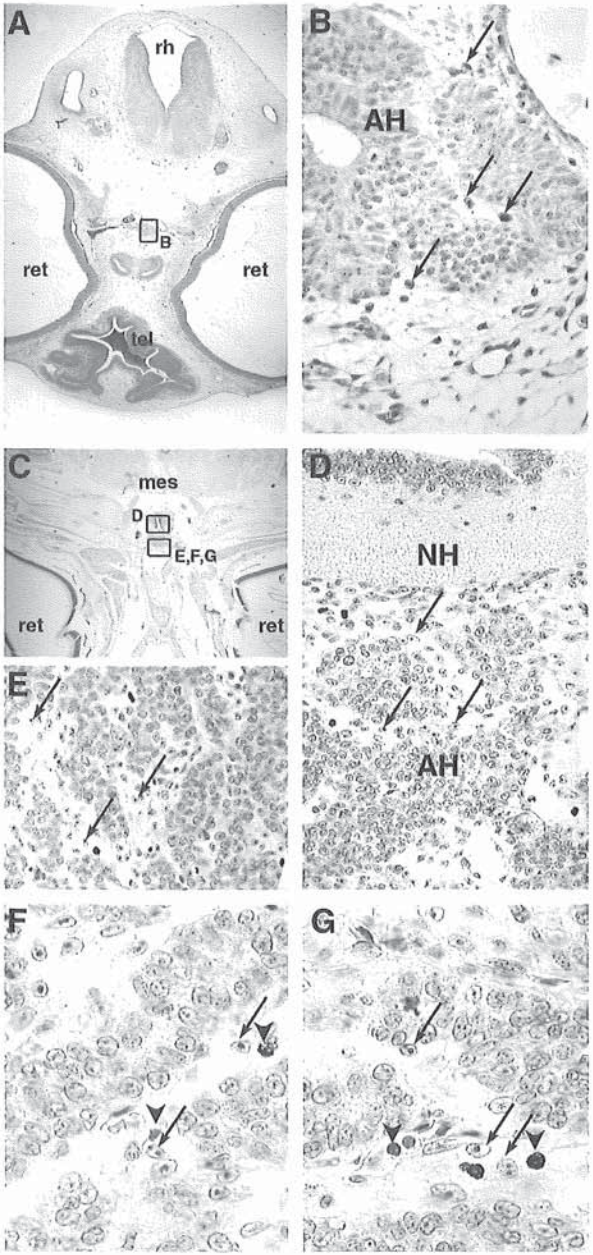

NCC Constitute Nonendothelial Components of the Pituitary Vascular Network

NCC which migrate into the adenohypophysis will give rise to both interstitial cells and pericytes of its capillary plexus (fig. 4C–G, 5A, B). Pericytes are smooth muscle-like cells which constitute a sheath around the capillary endothelium and regulate its local vasoconstriction or vasodilation. They express a smooth muscle-specific actin isoform, other properties reviewed by Diaz-Flores et al. [13]. Some, but not all, of the grafted NCC from the diencephalic and mesencephalic neural folds are immunoreactive for α smooth muscle actin within the adenohypophysis [14]. NCC-derived pericytes colonize the hypophyseal arteries, portal and exit veins (fig. 1). NCC are also found, less numerous, within the neurohypophysis at E12 (fig. 5B), where they appear to become exclusively pericytes since they all express α smooth muscle actin [unpubl. data].

The Adenohypophysis Does Not Develop in the Absence of the Neural Crest

We have recently shown the effects of an ablation of the neural folds of the posterior diencephalon, mesencephalon and first rhombomere, preceding the emergence of NCC [14]. Over the next day, the forebrain undergoes widespread cell death to such an extent that the retinal fields approach and cyclopia may result from their fusion (fig. 5C). Telencephalic and diencephalic tissues die from the lack of a trophic effect mediated directly or indirectly by the anteriormost NCC by way of the forming meninges.

Most of the diencephalon is eliminated after such operations (fig. 5D). Since all of the diencephalic meninges, the choroid of the eyes, and the capillary plexus of the pituitary contain NCC of anterior origin, these tissues should be affected by the absence of NCC. However, the posterior and ventral diencephalon, as well as the retinae and anterior/posterior pituitary, persist after neural fold ablations as

Fig. 4. Neural crest cells (NCC) which migrate into the adenohypophysis will give rise to both interstitial cells and pericytes of its capillary plexus. ***A*** Chimera on E7, after an isotopic graft of quail anterior mesencephalic NCC to chicken, in transverse section. Region enlarged in ***B*** indicated; ret = retina; tel = telencephalon; rh = rhombencephalon. ***B*** QCPN immunohistochemistry reveals labeled quail interstitial cells (arrows) surrounding and penetrating the adenohypophysis (AH). ***C*** Chimera on E9, after a similar graft, in transverse section and treated with the Feulgen-Rossenbeck technique. Regions enlarged in ***D***–G indicated; mes = mesencephalon. ***D***, ***E*** The interstitial tissue of the AH glandular cords is composed of the distinctive quail nuclei (arrows), indicating that it comes from the graft of mesencephalic NCC. ***F***, ***G*** Some quail NCC-derived pericytes (arrows) are located in close association with capillaries containing erythrocytes (arrowheads).

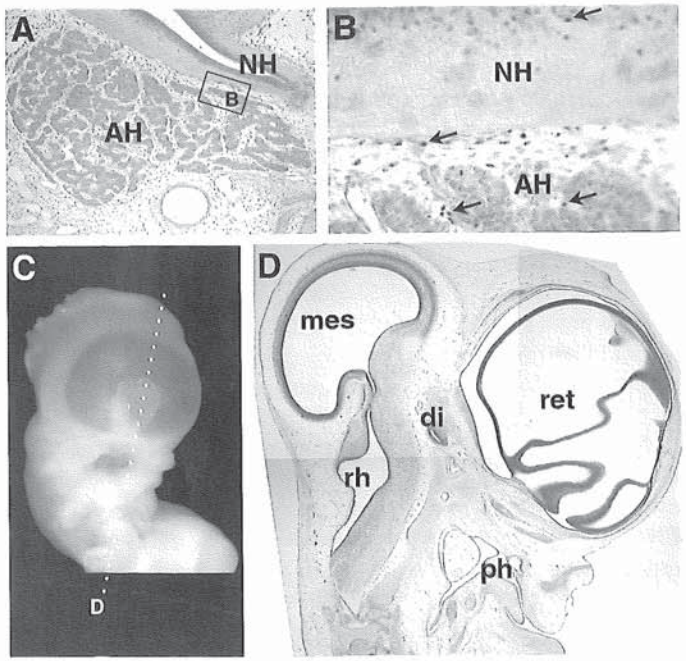

Fig. 5. NCC-derived mesenchyme which participates in pituitary gland construction is also necessary for the survival of the entire forebrain and associated structures. **A** Chick-quail chimera on 12th day of incubation, in parasagittal section with QCPN immunohistochemistry. Rectangle indicates area enlarged in **B**. **B** Grafted posterior diencephalic NCC are found to be numerous among the glandular cords and surrounding the adenohypophysis, but are fewer within the neurohypophysis, where they only contribute to the pericytic lineage. **C** Embryo in which posterior diencephalic, mesencephalic and first rhombomeric neural folds have been ablated at 5ss, preceding NCC migration. The two retinal fields have fused, yielding this E8 cyclops. Plane of section in **D** is depicted with dotted line. **D** Parasagittal section shows that the telencephalon and most of the diencephalon are absent, while only a small vestige of the posterior diencephalon and the retinae persist. The midbrain and the caudal central nervous system are unaffected by the operation. AH = adenohypophysis; di = diencephalon; mes = mesencephalon; NH = neurohypophysis; ph = pharynx; ret = retinae; rh = rhombencephalon.

described above. Isotopic grafts of the neural folds of the first rhombomere from quail, after the same long ablations in chick hosts, demonstrate that NCC of graft origin migrate rostrally. In ectopic locations, they proliferate to surround the remaining vestiges of the diencephalon, the retinae and infiltrate the adenohypophysis [14].

Nonetheless, in the most severely affected cyclops, the entire pituitary is absent, although its disappearance occurs subsequent to Rathke's pouch invagination. It takes an additional ablation of the neural folds down to the sixth rhombomere to sufficiently deprive the mesenchyme of NCC for the retinae as well as the ventral diencephalon to undergo cell death by E4 [unpubl. data]. These results suggest that the mesenchyme supplies a trophic factor, not only to the telencephalon, but also to the diencephalon and its associated outpocketings of retinae, pineal and pituitary glands, during a critical period of development which precedes vascularization.

In vitro, combinations of Rathke's pouch or head ectoderm not usually involved in pituitary development, with the ventral diencephalon, lead to induction of anterior pituitary-specific cell types in the former [15, 16]. The concomitant presence of NCC-containing mesenchyme in these avian, mammalian or mixed culture systems is necessary for Rathke's pouch survival and subsequent differentiation, in agreement with our in vivo observations.

Cephalic NCC Deficiencies May Underlie Both Congenital Hypopituitarism and Associated Human Prosencephalic and Nasofrontal Malformations

At birth, congenital hypopituitarism is evoked by symptoms such as hypoglycemia, micropenis and cryptorchidism in boys, diabetes insipidus, and/or a decrease in postnatal growth rate. A later evaluation of somatotropic, corticotropic, thyrotropic and prolactin secretions as well as neuroradiology confirm the diagnosis.

Throughout the medical literature, human pituitary deficiencies are frequently reported in association with numerous other defects of the forebrain and with premaxillary nasofrontal malformations. The associations are summarized in a nonexhaustive manner in table 2. These engendered a hypothesis that facial dysmorphologies are predictive of cephalic dysfunction [17]. The experimental data we describe above support that classic observation by showing that rostral cephalic NCC are primordial for nasofrontal and maxillary skull formation as well as prosencephalic, ocular and adenohypophyseal development in animal models. The defects and syndromes presented in table 2 are hence either themselves or are associated with cephalic neurocristopathies.

Table 2. Craniofacial and forebrain defects associated with human pituitary dysfunction

Prosencephalic malformations	Ref.	Nasofrontal, premaxillary, facial malformations	Ref.
Holoprosencephaly	17–19	Hypoplasia with hypotelorism and median cleft lip	17
Anosmia (Kallmann syndrome)	20	Iris-dental dysplasia (Rieger's syndrome	21
Optic hypoplasia; Leber disease	22, 23	Strabism	23
Septo-optic dysplasia	24, 25	Silver-Russell syndrome	26
Agenesis of the corpus callosum	22, 23, 27	Agenesis or solitary upper central and lateral incisors	19, 27, 28
		Facial clefts: lip, maxillary, palatal – isolated or in syndromes such as EEC or CHARGE association	27, 29, 30
		Maxillonasal hypoplasia (Binder syndrome)	18, 27
		Nasal alar hypoplasia (Johanson-Blizzard syndrome)	31
		Oculoauriculovertebral dysplasia (Goldenhar syndrome)	27, 32
		Congenital facial dysplasia (Möbius syndrome)	32
		Oral-facial-digital syndrome type VI (Varadi syndrome)	33, 34

Table 3. Origins of the bones of the vertebrate skull (membrane bones in italics)

Prechordal skull		Chordal skull	
Neural crest-derived		Cephalic mesoderm-derived	Somitic mesoderm-derived
Viscerocranium (face)	**Neurocranium (brain case)**		
Angular	Columella	Supraoccipital	Occipital
Dentary	Ethmoid	Sphenoid (basipost-, orbito-)	Otic capsule (pars ampullaris)
Epibranchial	*Frontal*	Otic capsule (pars canalicularis, pars cochlearis in part)	
Hyoid	*Interorbital septum*		
Jugal, quadratojugal	Otic capsule (pars cochlearis in part, parotic process)		
Meckel's cartilage	*Parietal*		
Maxilla	Sphenoid (basipre-)		
Nasal	*Squamosal*		
(Odontoblasts, tooth papillae)			
Opercular			
Palatine			
Pterygoid			
Scleral ossicles			
Superangular			
Vomer			

The Rostral Half of the Sella turcica Derives from Mesencephalic NCC

The sphenoid bone complex consists of numerous bones. These can be segregated into two parts based on their embryological origin, demonstrated using quail-chick chimeras. The posterior region, the basipostsphenoid, is derived from the cephalic mesoderm [35]. The anterior portion, the basipresphenoid, derives from the neural crest of the mesencephalic neural folds [7]. Both portions contain cartilaginous bones. The sphenoid bone complex represents an interface between the mesodermally-derived 'chordal' skull, located in proximity to the notochord, and the 'prechordal' skull, which grows in front of the anterior end of the notochord and differentiates from NCC (table 3).

A theory presented by Gans and Northcutt [36] proposed that a 'new head' was added over the course of evolution to the 'old head' of jawless ancestors to the vertebrates. Structural adaptations afforded by NCC conferred a selective advantage on animals which were able to assume a more aggressive feeding lifestyle. The enormous contribution of the 'new head' to the vertebrate skull may be seen in the derivative bones of the NCC (fig. 6). They constitute the major part of the vertebrate head, in particular the jaws and face. We recently proposed that the telencephalon also expanded over the course of evolution due to NCC plasticity in head morphogenesis [14].

The pituitary gland lies within the boundary between the NCC-dependent and NCC-independent head, within the composite sella turcica. On the one hand, predating the development of the 'new head', pituitary development genes and some of its endocrine functions may be found in jawless chordates such as *Amphioxus* [37, 38]. On the other hand, dependence on mesenchyme for survival and differentiation of the pituitary gland argues that the organization and range of hypophyseal activity was extended in concert with the development of the cephalic NCC population in vertebrates. Like the bone by which it is encased, the pituitary gland has multiple embryonic origins, doubtless reflecting the continuous evolution of its many physiological roles over time.

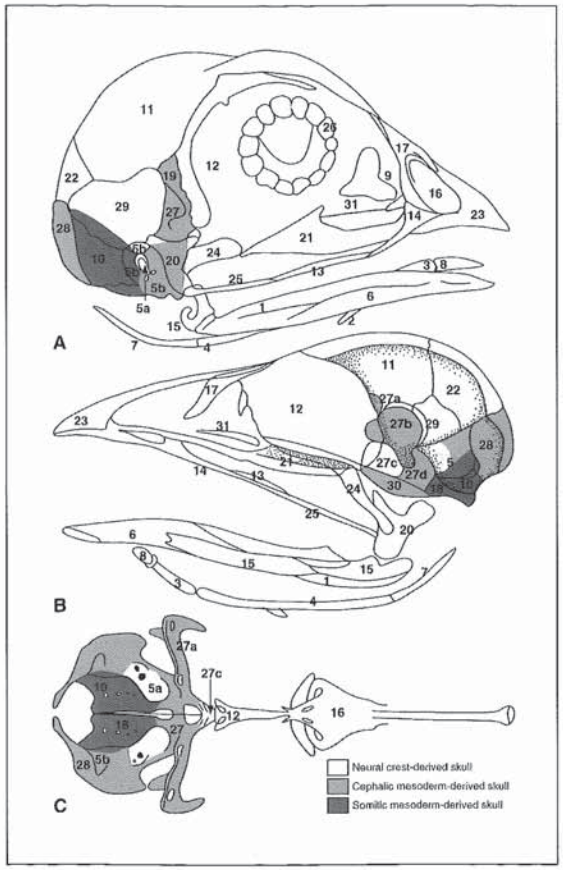

Fig. 6. Drawing of the multiple origins of the bones in the avian skull [7]. ***A*** View of the right exterior. ***B*** View of the right interior. ***C*** View from underneath. Note that the sella turcica is composed of bones of both neural crest (27c) and mesodermal (27d) origin. 1 = Angular; 2 = basibranchial; 3 = basihyal; 4 = ceratobranchial; 5 = columellar (a) and otic capsule (b); 6 = dentary; 7 = epibranchial; 8 = entoglossal; 9 = ethmoid; 10 = exoccipital; 11 = frontal; 12 = interorbital septum; 13 = jugal; 14 = maxillary; 15 = Meckel's cartilage; 16 = nasal capsule; 17 = nasal; 18 = basioccipital; 19 = postorbital; 20 = square; 21 = palatine; 22 = parietal; 23 = premaxillary; 24 = pterygoid; 25 = quadratojugal; 26 = sclerotic; 27 = sphenoid (a, orbitosphenoid; b, pleurosphenoid; c, basipresphenoid; d, basipostsphenoid); 28 = supraoccipital; 29 = squamosal; 30 = temporal; 31 = vomer.

Conclusions

The pituitary gland is made of two functional areas which occupy distinct regions within the rostral neural plate of the early vertebrate embryo. The adenohypophyseal placode is located in the medial portion of the anterior neural fold. The presumptive neurohypophysis lies within the neural plate, immediately caudal to an intervening region of the ventral hypothalamus which neighbors the neural fold. These distinct areas come together due to the topological deformations of the anterior neural plate and the surrounding head. During early development, the pituitary is ensconced in a matrix of cephalic mesoderm and NCC. These mesenchymal cells associate to create both arterial and venous aspects of the specialized vascular system of the pituitary, and in their absence, glandular survival and differentiation do not occur. Simultaneously, the sella turcica develops, of which the anterior and dorsal bones are derived from NCC while the posterior, ventral bones come from cephalic mesoderm. The neural crest population thus intervenes in an indispensable manner at multiple stages of pituitary development.

Acknowledgements

The authors warmly thank Professor Nicole Le Douarin for her long-term collaboration over the course of the work described herein as well as for her constructive criticism. They also acknowledge the technical assistance of Louis Addade, Pierre Coltey and Monique Le Thierry, and the graphical expertise of Michel Fromaget and Sophie Gournet.

References

1 Schimchowitsch S, Plant M, Klein MJ, Stoeckel ME: Ontogeny of the rabbit pituitary intermediate lobe. An ultrastructural and immunocytochemical study. Anat Embryol (Berl) 1993;187:87–97.
2 Le Douarin N: Particularités du noyau interphasique chez la caille japonaise *(Coturnix coturnix japonica)*. Utilisation de ces particularités comme 'marquage biologique' dans les recherches sur les interactions tissulaires et les migrations cellulaires au cours de l'ontogenèse. Bull Biol Fr Belg 1969; 103:435–452.
3 Le Douarin NM, Kalcheim C: The Neural Crest, ed 2. Cambridge, Cambridge University Press, 1999.
4 Couly GF, Le Douarin NM: Mapping of the early neural primordium in quail-chick chimeras. I. Developmental relationships between placodes, facial ectoderm, and prosencephalon. Dev Biol 1985;110:422–439.
5 Couly GF, Le Douarin NM: Mapping of the early neural primordium in quail-chick chimeras. II. The prosencephalic neural plate and neural folds: Implications for the genesis of cephalic human congenital abnormalities. Dev Biol 1987;120:198–214.
6 Etchevers HC, Vincent C, Le Douarin NM, Couly GF: The cephalic neural crest provides pericytes and smooth muscle cells to all blood vessels of the face and forebrain. Development 2001;128: 1059–1068.

7 Couly GF, Coltey PM, Le Douarin NM: The triple origin of skull in higher vertebrates: A study in quail-chick chimeras. Development 1993;117:409–429.
8 Couly G, Le Douarin NM: The fate map of the cephalic neural primordium at the presomitic to the 3-somite stage in the avian embryo. Development 1988;103(suppl):101–113.
9 Rubenstein JL, Shimamura K, Martinez S, Puelles L: Regionalization of the prosencephalic neural plate. Annu Rev Neurosci 1998;21:445–477.
10 Takuma N et al: Formation of Rathke's pouch requires dual induction from the diencephalon. Development 1998;125:4835–4840.
11 Watkins-Chow DE, Camper SA: How many homeobox genes does it take to make a pituitary gland? Trends Genet 1998;14:284–290.
12 Le Lièvre CS, Le Douarin NM: Mesenchymal derivatives of the neural crest: Analysis of chimaeric quail and chick embryos. J Embryol Exp Morphol 1975;34:125–154.
13 Diaz-Flores L, Gutierrez R, Varela H, Rancel N, Valladares F: Microvascular pericytes: A review of their morphological and functional characteristics. Histol Histopathol 1991;6:269–286.
14 Etchevers HC, Couly G, Vincent C, Le Douarin NM: Anterior neural crest is required for forebrain viability. Development 1999;126:3533–3543.
15 Treier M, Gleiberman AS, O'Connell SM, Szeto DP, McMahon JA, McMahon AP, Rosenfeld MG: Multistep signaling requirements for pituitary organogenesis in vivo. Genes Dev 1998;12:1691–1704.
16 Gleiberman AS, Fedtsova NG, Rosenfeld MG: Tissue interactions in the induction of anterior pituitary: Role of the ventral diencephalon, mesenchyme, and notochord. Dev Biol 1999;213:340–353.
17 De Myer W, Zeman W, Palmer CG: The face predicts the brain: Diagnostic significance of median facial anomalies for holoprosencephaly (arhinencephaly). Pediatrics 1964;34:256.
18 Binder KH: Dystostosis maxillo-nasalis, ein arhinencephaler Missbildungskomplex. Dtsch Zahnärztl Z 1962;17:438.
19 Fleming P, Nelson J, Gorlin RJ: Single maxillary central incisor in association with mid-line anomalies. Br Dent J 1990;168:476–479.
20 Bardin CW, Ross GT, Rifkind AB, Cargille CM, Lipsett MB: Studies of the pituitary Leydig cell axis in young men with hypogonadotropic hypogonadism and hyposmia: Comparison with normal men, prepubertal boys, and hypo-pituitary patients. J Clin Invest 1969;48:2046–2056.
21 Sadeghi-Nejad A, Senior B: Autosomal dominant transmission of isolated growth hormone deficiency in iris-dental dysplasia (Rieger's syndrome). J Pediatr 1974;85:644.
22 Gendrel D, Chaussin JL, Job JC: Les hypopituitarismes congénitaux par anomalie de la ligne médiane. Arch Fr Pediatr 1981;38:227–232.
23 Liapi C, Ginisty D, Chaussain JL, Job JC: Les malformations dentaire et faciales associées à l'insuffisance hypophysaire en hormone de croissance. Arch Fr Pediatr 1985;42:829–833.
24 De Morsier G: Etudes sur les dysraphies craniocéphaliques. III. Agénésie du septum lucidum avec malformation du tractus optique: La dysplasie septo-optique. Schweiz Arch Neurol Neurochir Psychiatr 1956;77:267–292.
25 Hoyt WT, Kaplan SL, Grumbach MM: Septo-optic dysplasia with hypopituitary dwarfism. Lancet 1970;i:893.
26 Kotilainen J, Holtta P, Mikkonen T, Arte S, Sipila I, Pirinen S: Craniofacial and dental characteristics of Silver-Russell syndrome. Am J Med Genet 1995;56:229–236.
27 Ajacques JC, David M, Disant F, Sann L, Bey-Omar F: Malformations de l'étage moyen de la face et déficit hypothalamo-hypophysaire. Pédiatrie 1982;37:417–432.
28 Rappaport EB, Ulstrom RA, Gorlin RJ, Lucky AW, Colle E, Miser J: Solitary maxillary central incisor and short stature. J Pediatr 1977;91:924–928.
29 Rudman D, Davis T, Priest JH, Patterson JH, Kutner MH, Heymsfield SB, Bethel RA: Prevalence of GH deficiency in children with cleft lip and palate. J Pediatr 1978;93:378–382.
30 Goumy P, Dalens B, Malpuech G: Association d'une dysraphie de la ligne médiane et d'une insuffisance hypophysaire congénitale avec micropenis et hypoglycémie néonatale. J Pediatr 1978;93:551–559.
31 Johanson AJ, Blizzard RM: A syndrome of congenital aplasia of the alae nasi, deafness, hypothyroidism, dwarfism, absent permanent teeth, and malabsorption. J Pediatr 1971;79:982–987.
32 Couly G, Rappaport R, Brauner R et al: Association of facial malformations with primary hypopituitarism as possible incidence for a common developmental defect of prosencephalic neural crest derivatives. Pediatr Res 1982;16:886–907.
33 Varadi V, Szabo L, Papp Z: Syndrome of polydactyly, cleft lip/palate or lingual lump, and psychomotor retardation in endogamic gypsies. J Med Genet 1980;17:119–122.
34 Munke M, McDonald DM, Cronister A, Stewart JM, Gorlin RJ, Zackai EH: Oral-facial-digital syndrome type VI (Varadi syndrome): Further clinical delineation. Am J Med Genet 1990;35:360–369.
35 Couly GF, Coltey PM, Le Douarin NM: The developmental fate of the cephalic mesoderm in quail-chick chimeras. Development 1992;114:1–15.
36 Gans C, Northcutt RG: Neural crest and the origin of vertebrates: A new head. Science 1983;220:268–274.
37 Candiani S, Pestarino M: Expression of the tissue-specific transcription factor Pit-1 in the lancelet, *Branchiostoma lanceolatum*. J Comp Neurol 1998;392:343–351.
38 Glardon S, Holland LZ, Gehring WJ, Holland ND: Isolation and developmental expression of the amphioxus Pax-6 gene (AmphiPax-6): Insights into eye and photoreceptor evolution. Development 1998;125:2701–2710.
39 Berne RM, Levy MN: Principles of Physiology, ed 2. St Louis, Mosby-Year Book, 1996.
40 Lance-Jones CC, Lagenaur CF: A new marker for identifying quail cells in embryonic avian chimeras: A quail-specific antiserum. J Histochem Cytochem 1987;35:771–780.

Dr. Heather C. Etchevers, Institut d'Embryologie Cellulaire et Moléculaire du CNRS et du Collège de France, 49bis avenue de la Belle Gabrielle, F–94736 Nogent-sur-Marne Cedex (France)
Tel. +33 1 45 14 15 15, Fax +33 1 48 73 43 77, E-Mail etchever@infobiogen.fr

Morphogenesis of the Branchial Vascular Sector

Heather C. Etchevers, Gérard Couly, and Nicole M. Le Douarin*

The branchial and dorsal cephalic vascular sectors correspond to the blood vessels contained within evolutionarily recent and ancestral parts of the head, respectively. Recent work demonstrates that neural crest cells (NCCs) provide the pericytes, and connective and smooth muscle cells to the entire branchial sector in an ordered fashion. Initial NCC position is transposed to the vascular distal-to-proximal axis, explaining why circumscribed cephalic vascular anomalies are often associated with reproducible malformations in head tissues derived from the neural crest. Unlike the rest of the central nervous system, the forebrain requires mesenchyme-containing vascular-competent NCCs to survive during embryogenesis and beyond. (Trends Cardiovasc Med 2002;12:299–304). *© 2002, Elsevier Science Inc.*

Vascular anatomy is determined by topology. The adult head presents a particularly complex three-dimensional structure, with heavy localized demands for oxygenation and nutrition within the brain. Despite this complexity, underlying structural principles of cephalic blood vessel circuitry become apparent after examining the developing embryo.

• Cephalic Blood Vessels Have Different Origins According to Their Position

The vertebrate head starts out as a superposition of three cellular sheets: the endoderm, mesoderm, and ectoderm. Deformation of these germ layers around the anterior end of the notochord provides a cul-de-sac—the head fold—in which the brain, skull, mouth, cephalic muscles, and their blood vessels will later develop. Experimental embryology has discovered many of the mechanisms by which developing cephalic tissues contact each other and differentiate appropriately to their local environment.

One major technique, the construction of quail-chick chimeras, exploits species differences in nuclear structure to permanently mark cells grafted from a donor to a host embryo (Le Douarin 1969). By following the fate of grafted cells at later time points, it was shown that the mesoderm lateral to the neural plate of the future brain gives rise to both striated muscles and the endothelium of all cephalic blood vessels. According to the anteroposterior level at which a given graft was performed, a corresponding segment of the cephalic and encephalic vasculature contained endothelial cells of graft origin, whereas the nearby muscles also contained grafted cells (Couly et al. 1992 and 1995). The endothelial cell lineage becomes distinct from other future mesodermal progeny at a very early time point, when the future head is barely distinguished by an anterior transverse buckling in the germ layers. A tyrosine kinase receptor to the vascular endothelium growth factor, known as VEGFR2, is already expressed at this time point in a subset of cephalic mesodermal cells that subsequently acquire characteristics of endothelial cells (Eichmann et al. 1993).

Neural crest cells (NCCs) also contribute to much of the cephalic vasculature, but never to blood vessels in the body. NCCs delaminate from the boundaries between the ectoderm and the median neural plate as the latter forms the tube that will give rise to the central nervous system. They remain mesenchymal during their ventral migration toward the gut and their dorsolateral migration under the ectoderm. After colonizing the appropriate location, NCCs differentiate into the peripheral nervous system, certain types of endocrine cells, and all pigment cells aside from the retinal pigmented epithelium (reviewed in Le Douarin and Kalcheim 1999). Specifically in the head, NCCs also give rise to the "mesectoderm," tissues that, in the body, are mesodermally derived. These include the intercalating connective components of the cephalic glands, muscles, and tendons. The dermis and adipose tissue overlying the jawed facial skeleton and brain case, the bones of that part of the skull, and certain regions of the meninges underlying it are also mesectodermal (Couly et al. 1993 and 1996, Köntges and Lumsden 1996, Le Lièvre 1974, Le Lièvre and Le Douarin 1975, Noden 1983).

Early indications of the role of NCCs in cephalic blood vessels came from fate-mapping experiments that showed their constitution of the branchial arch mesenchyme and subsequent incorporation into the smooth muscle walls of the corresponding large arteries (Johnston 1966, Le Lièvre and Le Douarin 1975). In particular, NCCs derived from the posterior rhombencephalon contribute all components of the proximal large arteries to the heart, with the exception of the endothelium (Le Lièvre and Le Douarin 1975). NCCs of this origin also play an important role in the septation of the pulmonary trunk from the aorta (Nishibatake et al. 1987, Waldo and Kirby 1993, Waldo et al. 1998). Although many of these experiments have been performed in the avian embryo, data from rodents confirm that NCCs are equally important to cephalic and outflow tract formation in mammals (Imai et al. 1996, Jiang et al. 2000).

Heather C. Etchevers, Gérard Couly, and Nicole M. Le Douarin are at the Institute of Cellular and Molecular Embryology, College of France, Nogent-sur-Marne, France.

*Address correspondence to: Nicole M. Le Douarin, Institut d'Embryologie Cellulaire et Moléculaire du CNRS et du Collège de France, 49 bis avenue de la Belle Gabrielle, 94736 Nogent-sur-Marne Cedex, France. Tel.: (+33) 1-45-14-15-15; fax: (+33) 1-48-73-43-77; e-mail: nicole.le-douarin@college-de-france.fr.

 1050-1738/02/$-see front matter

- **Blood Vessels are Constructed from Locally Available Cellular Materials**

The extent of NCC incorporation into cephalic blood vessels was recently demonstrated experimentally (Etchevers et al. 2001b). A series of quail-chick chimeras were made by successively transplanting small fragments of the brain neural folds from donors to the equivalent anteroposterior level of hosts preceding cephalic NCC migration. Embryos were then examined at different stages during the first half of gestation to see where the NCCs had integrated in the blood vessels.

Grafts from anterior brain levels corresponding to the diencephalon and mesencephalon resulted in abundant cells within the forebrain meninges, with a sharp border at the forebrain–midbrain boundary (Etchevers et al. 2001b). These cells, adjacent to endothelial capillary walls within the parenchyma, were identified with the marker α-smooth muscle actin as being pericytes. All blood vessels are composed of endothelial cells, an immediately adjacent layer of pericytes, and a basal lamina (reviewed in Doherty and Canfield 1999). Signaling between endothelial cells and pericytes is necessary for the formation of mature blood vessels, as has been demonstrated in transgenic mice for the platelet-derived growth factor-B/platelet-derived growth factor receptor β (Lindahl et al. 1997 and 1998) and angiopoietin/tie-2 (Suri et al. 1996) ligand/receptor systems. In contrast, outer wall structures (the tunicae media and externa) vary according to vessel type as to the presence and number of concentric layers of smooth muscle and connective cells.

In addition to the pericytes, smooth muscle and connective tissue cells of graft origin were observed in the distal portions of the major cephalic arteries. Grafts of neural folds at the level of the anterior rhombencephalon, in contrast, gave rise to the nonendothelial cells of the proximal (closer to the heart) segments of the same arteries as well as the distal internal carotid arteries. Median rhombencephalic neural folds contributed cells to the carotid arteries and cardinal veins, whereas posterior rhombencephalic NCCs tended to incorporate into proximal segments of the carotid arteries, as well as into the aortic and pulmonary trunks and the conotruncus and semilunar valves of the heart itself. As seen in Figure 1, the original anteroposterior origin of a cell within the neural folds corresponds to its final distoproximal distribution in a defined subset of cephalic blood vessels. This subset, designated the "branchial vascular sector," is a distinct circuit of blood vessels originating in the ventral aorta and branchial arches, ramifying into circumscribed capillary plexuses, and terminating in their venous return to the heart. These vessels correspond to the forebrain, face, and jaws.

A second vascular division can be distinguished in the head by virtue of its vessels not belonging to the branchial sector. Its component arteries and veins share the property of being entirely constructed from the embryonic cephalic and somitic mesoderm (Figure 1A). In mature vertebrates, vessels derived from the vertebral arteries, which converge into the basilar artery as they enter the occipital region, irrigate the dorsal head, including the midbrain, cerebellum, and hindbrain. The two vascular domains contact at the circle of Willis, a large anastomosis between the bifurcation of the basilar artery and the cerebral arteries, which are branches of the internal carotids. This polygon surrounds the optic nerves and ventral diencephalon, reflecting the transition within the meninges from an entirely mesoderm-derived region, the midbrain, to a composite mesoderm/NCC-derived region, the forebrain.

- **The Vertebrate Head is Sculpted in NCCs**

NCCs constitute a somewhat, but not strictly, stratified mesenchyme in the head, according to their neural-fold origin. Grafts from adjacent levels of the neural folds give rise to cells in overlapping domains of the branchial sector, indicating a gradual succession from NCCs of one origin to NCCs of a neighboring origin. There is a similar composite distribution of NCCs from neighboring neural-fold origins in the bones of the jaw (Couly et al. 1996) and in the interstitial cells of the various cephalic muscles (Köntges and Lumsden 1996). The morphology of head elements is imposed secondarily, immobilizing the initial NCC distributions. Recent data show that the endoderm exerts a major instructive influence on facial skeletal patterning (Couly et al. 2002). Definitive vascular architecture is shaped concomitant or

Figure 1. (A) Depiction of the origin of the pericytes, smooth muscle, and connective tissue of cephalic and proximal cardiac blood vessels. Embryonic day 8 (E8) head and E12 heart of chicken. *Colors* correspond to cell origins from the cephalic neural folds; *grays* correspond to cephalic and somitic mesoderm from the indicated regions in the neurula. Within the meninges of the central nervous system, *pink* denotes meninges derived from anterior cephalic neural crest cells; *grey* denotes meninges of mesodermal origin, with a sharp boundary between the two at the forebrain–midbrain junction. A major anastomosis (P.c.) between the two vascular sectors corresponds to the posterior communicating artery in the circle of Willis. Levels of transverse sections shown in **(B–F)** are indicated; the *lower panel* is a magnification of the artery within rectangles in the *upper panel*. *Brown cells* correspond to those of quail (graft) origin. **(B)** E8 chimera after graft of posterior diencephalon neural fold—arteria carotis interna. **(C)** E8 chimera after graft of r5 neural fold—arteria carotis communis. **(D)** E9 chimera after graft of r6 neural fold—aorta. **(E)** E9 chimera after graft of r7 neural folds—divergence of the arteriae brachiocephalica dextra et carotis communalis. **(F)** E8.5 chimera after graft of r8 neural folds—aorta et truncus pulmonaris *above*, pericytes in the wall of the sinus venosus indicated by *arrows*, *below*. Cephalic arteriae: B., basilaris; C. c., carotis communis; C. c. a., carotis cerebralis anterior; C. c. m, media; C. c. p., posterior; Ce. v., cerebellaris ventralis; C. i., carotis interna; Eth., ethmoidalis; L., lingualis; Md., mandibularis; Mx., maxillaris; Occ., occipitalis; Oph., ophthalmica externa; P.c., communicans posterior; St., stapedia; St. te., temporalis; St. sup., supraorbitalis, T. m. v., tecti mesencephalis ventralis; V., vertebralis. Neurula: PD, posterior diencephalon; AM, PM, anterior/posterior mesencephalon; r1–8, rhombomeres 1–8. Heart: A, aorta; AV, valva atrioventricularis; HV, vena hepatica; IVC, vena cava inferior; IVS, septum interventriculare; LACV, RACV, vena cardinalis rostralis (sinistra, dextra); LBCA, RBCA, arteria brachiocephalica (sinistra, dextra); LCCA, RCCA, arteria carotis communis (sinistra, dextra); LPV, vena pulmonalis sinistra (dextra hidden); PA, truncus pulmonalis; PCV, vena cardinalis caudalis; SA, valva sinoatrialis; SL, valva semilunaris; SV, sinus venosus. Terminology for vascular system from Baumel (1979). Reprinted with permission from Etchevers et al. 2001b, p. 1064. Copyright 2001, The Company of Biologists Limited.

subsequent to the morphogenesis of these structures, from the same pool of mesenchyme.

The lack of sharp boundaries in the neural crest-derived sector of the head contrasts with its strictly observed segregation from the posterior part of the head, where the mesoderm furnishes the same connective tissue types as in the body—for example, bone, cartilage, and dermis. Nearly 20 years ago, a theory was announced in which the development of the anterior and ventral head was attributed to the phylogenetic emergence of the NCC population (Gans and Northcutt 1983). The "new head" evolutionary theory was based on data demonstrating the unique NCC composition of the jaw bones and cartilage, as well as the facial and neck dermis (Le Lièvre 1974, Le Lièvre and Le Douarin 1975). This theory was later supported by the discovery that in addition to the jaws, nearly all of the skull brain case is NCC

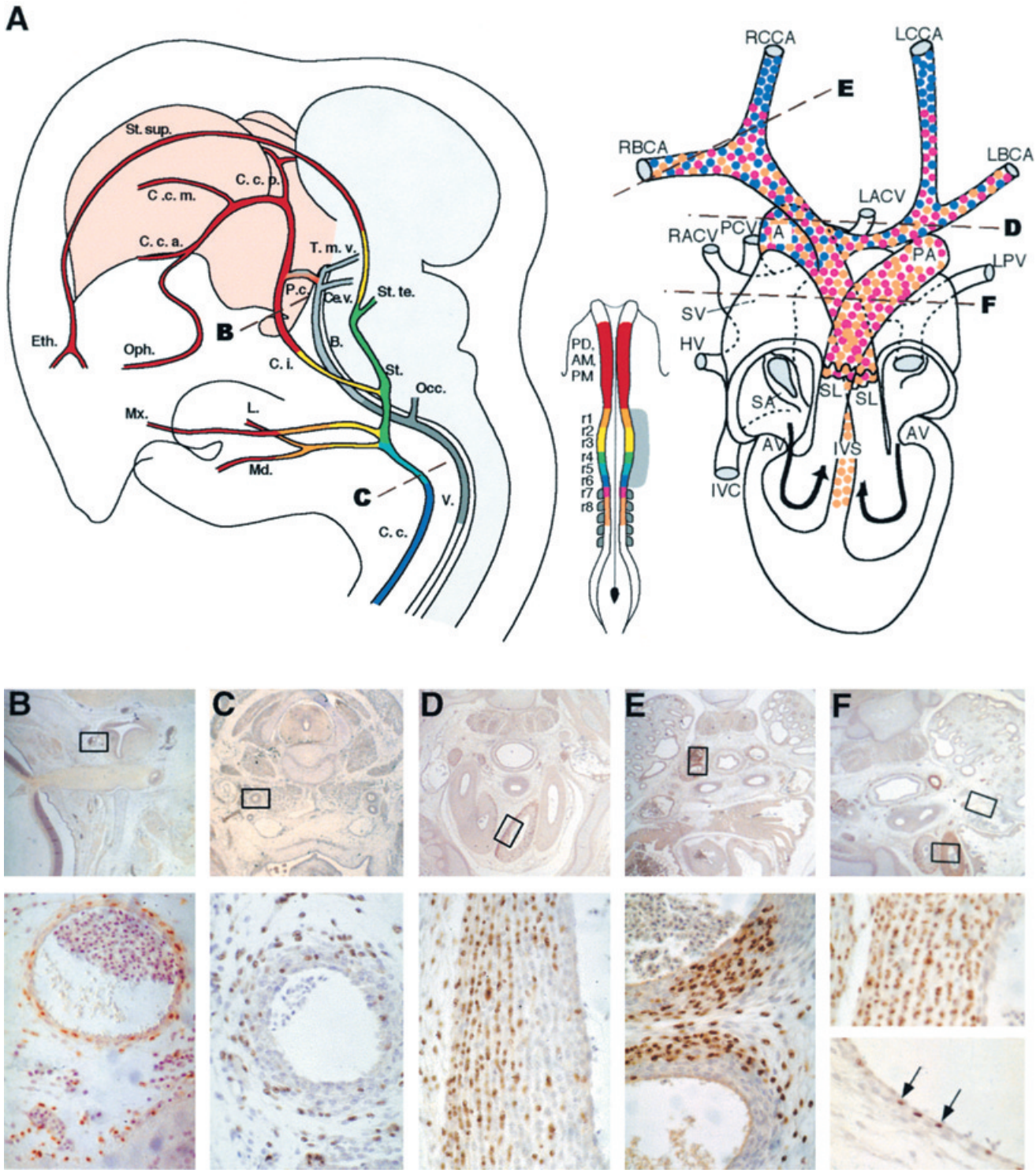

Figure 1

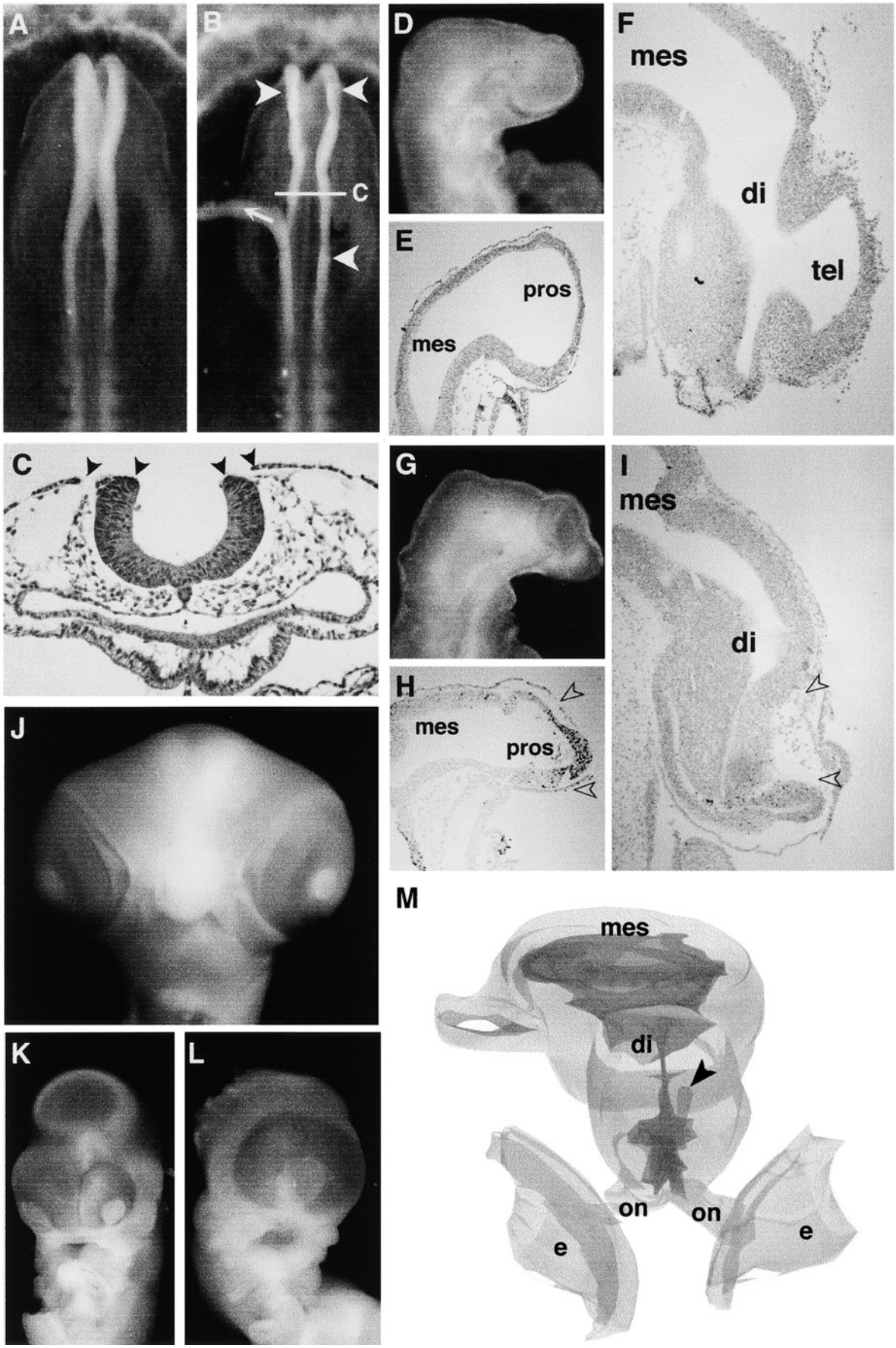
A
B
C
D
E
pros
mes
F
mes
di
tel
G
H
mes
pros
I
mes
di
J
K
L
M
mes
di
on
on
e
e

Figure 2

Figure 2. Ablation of cephalic neural crest cell causes the subsequent absence of forebrain territories. Head of a neurula before **(A)** and after bilateral neural-fold ablation, which prevents neural crest cell genesis (**B**, between *arrowheads*). The right neural fold is nearly detached (*arrow*). **(C)** Transverse section taken through the level of operation of the same embryo, fixed 2 h after neural-fold ablation (*arrowheads*). **(D)** 24 h after sham operation, lateral view. **(E)** Sagittal section through the same embryo, TUNEL (terminal deoxynucleotidyl transferase biotin d-UTP nick end labeling) reaction to reveal apoptosis (limited to pharyngeal endoderm). **(F)** Embryo day 3 (E3) sham-operated embryo, sagittal section, TUNEL. **(G)** Neural crest-ablated embryo, 24 h after operation, lateral view. The eyes converge over the prosencephalon, which is undergoing apoptosis (**H**, between *arrowheads*). **(I)** Apoptosis in the prosencephalon is nearly complete at E3. Missing tissues are indicated between *arrowheads* (compare with **F**). **(J)** Face of unoperated embryo, E8. Cyclopic **(K)** and synophthalmic **(L)** embryos at E8 after cephalic neural-crest ablation. Naso-fronto-maxillary structures are severely reduced or altogether absent. **A–I, K,** and **L** reprinted from Etchevers et al. 1999, p 3537–3538. Copyright 1999, The Company of Biologists Limited. (**M**) Reconstruction from serial sections of an operated embryonic brain at E8 with synophthalmia, frontal view. The telencephalon and rostral diencephalon have disappeared, but the mesencephalon and caudal diencephalon, from which the neural folds were removed, remain present. Darker areas represent the ventricle. *Arrowhead*, epiphysis. Hindbrain not shown. di, diencephalon; e, eye; mes, mesencephalon; on, optic nerve; pros, prosencephalon; tel, telencephalon.

derived (Couly et al. 1993). The development of NCCs in vertebrates may thus be fundamental to the origin of the face and the expansion of an anterior head cavity, as well as the sustained enlargement of the forebrain over time. These regions correspond precisely to that of the branchial vascular sector.

More recently, ablation experiments in the chick contributed evidence that the morphology of the upper head depends directly on the presence of NCCs (Figure 2). Removal of the neural folds along the length of the prospective diencephalon, mesencephalon, and anterior rhombencephalon deprives the rostral head of NCCs. Under these experimental conditions, the tissues directly derived from these cells are missing: the nasal septum and capsule, the upper beak and jaw, the frontal and ethmoid bones, the dermis over these regions, and the forebrain meninges. Surprisingly, other tissues, not themselves NCC derivatives, are also missing: the forebrain itself, the anterior pituitary, the median oculomotor muscles, and the superior salivary glands (Etchevers et al. 1999 and 2001b). Over time, holoprosencephaly and hypotelorism or outright cyclopia develop in operated embryos.

Normally, NCCs and mesodermal cells surround the forebrain from the dorsal and ventral sides, respectively. They combine to form a leptomeningeal plexus by the second day of incubation in the chick. Vascular invasion of the forebrain parenchyma occurs during the fifth day. In embryos lacking rostral NCCs, forebrain apoptosis occurs on the second and third days of incubation, such that prospective forebrain tissue is no longer present on the fifth day (Etchevers et al. 1999). Therefore, the phenotype of operated chicks is due to a trophic effect of NCC-containing mesenchyme on the early forebrain neuroepithelium. An alternative hypothesis would be that the lack of characteristically differentiated pericytes causes a deficit in brain vascularization. This, however, is belied by the timing of the apoptosis, which precedes the appearance of any pericytic markers known to date, as well as the entry of capillaries into brain tissue.

A number of syndromes affect NC derivatives in the head as well as vessels of the branchial sector; in particular, those near the heart. These include, but are not restricted to, the syndromes of Von Hippel-Lindau, Dubowitz, DiGeorge, and hemifacial microsomia. In most cases, the defects in cranial NC tissues are probably downstream from a more general pathogenic cause. Nonetheless, it is important to formulate the hypothesis that a cascade of malformations is responsible for the multifactorial nature of these syndromes and that, for instance, a problem induced in NCCs could give rise to the pituitary malfunctions present in Harrod or Dubowitz syndrome. In Sturge-Weber syndrome, the colocalization of angiomas in the telencephalic meninges, the ocular choroid, and the facial dermis (port-wine stain) leads us to propose that the rostral cephalic NC is directly at cause, because its distribution in the branchial vascular sector corresponds to the affected regions in Sturge-Weber patients. Moyamoya disease is a bilateral stenosis of the internal carotid arteries, which is circumvented by a profusion of telangiectatic blood vessels. The fact that moyamoya is restricted to this region of the cephalic arteries, and that it has been associated with Sturge-Weber syndrome, neurofibromatosis type II, or incontinentia pigmenti (Echenne et al., 1995) implies a primary or secondary deficit in NC-derived pericytes and, in particular, those derived from the mid-rhombencephalon (rhombomeres 4-5).

In summary, there exist two vascular sectors in the head, a branchial sector and a dorsal sector. Their localizations correspond to evolutionarily novel and ancestral parts of the head, respectively. Cephalic NCCs give rise to all the components of the branchial vascular sector, with the exception of the endothelium, of mesodermal origin. Cephalic NCCs also differentiate into the meninges of the forebrain, containing capillary beds derived from the branchial blood vessels, in contrast to all other regions of the central nervous system.

Muscles and glands that disappear after NCC ablation may also undergo apoptosis, or may never form at all in the absence of the connective tissue framework supplied by the mesectoderm. The initial formation of Rathke's pouch, but lack of subsequent pituitary differentiation, would support the former hypothesis (Etchevers et al. 2001a). Such questions, as well as the nature of the trophic activity of prevascular cephalic NCCs, are still under investigation.

• Acknowledgments

The authors thank Sophie Gournet, Michel Fromaget, Hélène San Clemente, and Francis Beaujean for their assistance with the figures. This work was supported by the Centre National de la Recherche Scientifique and the Collège de France. H.C.E. is a postdoctoral fellow of the Sturge-Weber Foundation.

References

Baumel JJ: 1979. Systema cardiovasculare. *In* Baumel JJ, King AS, Lucas AM, et al., eds. Nomina Anatomica Avium. London, U.K., Academic Press, pp 346–407.

Couly G, Coltey P, Eichmann A, Le Douarin NM: 1995. The angiogenic potentials of the

cephalic mesoderm and the origin of brain and head blood vessels. Mech Dev 53:97–112.

Couly GF, Coltey PM, Le Douarin NM: 1992. The developmental fate of the cephalic mesoderm in quail-chick chimeras. Development 114:1–15.

Couly GF, Coltey PM, Le Douarin NM: 1993. The triple origin of skull in higher vertebrates: a study in quail-chick chimeras. Development 117:409–429.

Couly G, Creuzet S, Bennaceur S, et al.: 2002. Foregut endoderm patterns the facial skeleton. Development 129:1061–1073.

Couly G, Grapin-Botton A, Coltey P, Le Douarin NM: 1996. The regeneration of the cephalic neural crest, a problem revisited: the regenerating cells originate from the contralateral or from the anterior and posterior neural fold. Development 122:3393–3407.

Doherty MJ, Canfield AE: 1999. Gene expression during vascular pericyte differentiation. Crit Rev Eukaryot Gene Expr 9:1–17.

Echenne BP, Leboucq N, Humbertclaude V: 1995. Ito hypomelanosis and moyamoya disease. Pediat Neurol 13:169–171.

Eichmann A, Marcelle C, Breant C, Le Douarin NM: 1993. Two molecules related to the VEGF receptor are expressed in early endothelial cells during avian embryonic development. Mech Dev 42:33–48.

Etchevers HC, Couly G, Vincent C, Le Douarin NM: 1999. Anterior cephalic neural crest is required for forebrain viability. Development 126:3533–3543.

Etchevers HC, Vincent C, Couly G: 2001a. Neural crest and pituitary development. *In* Rappaport R, ed. Hypothalamic–Pituitary Development: Genetic and Clinical Aspects. Basel, Switzerland, S. Karger AG, pp 13–29.

Etchevers HC, Vincent C, Le Douarin NM, Couly GF: 2001b. The cephalic neural crest provides pericytes and smooth muscle cells to all blood vessels of the face and forebrain. Development 128:1059–1068.

Gans C, Northcutt RG: 1983. Neural crest and the origin of vertebrates: a new head. Science 220:268–274.

Imai H, Osumi-Yamashita N, Ninomiya Y, Eto K: 1996. Contribution of early-emigrating midbrain crest cells to the dental mesenchyme of mandibular molar teeth in rat embryos. Dev Biol 176:151–165.

Jiang X, Rowitch DH, Soriano P, et al.: 2000. Fate of the mammalian cardiac neural crest. Development 127:1607–1616.

Johnston MC: 1966. A radioautographic study of the migration and fate of cranial neural crest cells in the chick embryo. Anat Rec 156:143–155.

Köntges G, Lumsden A: 1996. Rhombencephalic neural crest segmentation is preserved throughout craniofacial ontogeny. Development 122:3229–3242.

Le Douarin N: 1969. Particularités du noyau interphasique chez la caille japonaise (Coturnix coturnix japonica). Utilisation de ces particularités comme "marquage biologique" dans les recherches sur les interactions tissulaires et les migrations cellulaires au cours de l'ontogenèse. Bull Biol Fr Belg 103:435–452.

Le Douarin N, Kalcheim C: 1999. The Neural Crest, 2nd ed. Cambridge, U.K., Cambridge University Press.

Le Lièvre C: 1974. Rôle des cellules mésectodermiques issues des crêtes neurales céphaliques dans la formation des arcs branchiaux et du squelette viscéral. J Embryol Exp Morph 31:453–477.

Le Lièvre CS, Le Douarin NM: 1975. Mesenchymal derivatives of the neural crest: analysis of chimaeric quail and chick embryos. J Embryol Exp Morphol 34:125–154.

Lindahl P, Hellstrom M, Kalen M, et al.: 1998. Paracrine PDGF-B/PDGF-Rbeta signaling controls mesangial cell development in kidney glomeruli. Development 125:3313–3322.

Lindahl P, Johansson BR, Leveen P, Betsholtz C: 1997. Pericyte loss and microaneurysm formation in PDGF-B-deficient mice. Science 277:242–245.

Nishibatake M, Kirby ML, Van Mierop LH: 1987. Pathogenesis of persistent truncus arteriosus and dextroposed aorta in the chick embryo after neural crest ablation. Circulation 75:255–264.

Noden DM: 1983. The role of the neural crest in patterning of avian cranial skeletal, connective, and muscle tissues. Dev Biol 96: 144–165.

Suri C, Jones PF, Patan S, et al.: 1996. Requisite role of angiopoietin-1, a ligand for the TIE2 receptor, during embryonic angiogenesis. Cell 87:1171–1180.

Waldo KL, Kirby ML: 1993. Cardiac neural crest contribution to the pulmonary artery and sixth aortic arch artery complex in chick embryos aged 6 to 18 days. Anat Rec 237:385–399.

Waldo K, Miyagawa-Tomita S, Kumiski D, Kirby ML: 1998. Cardiac neural crest cells provide new insight into septation of the cardiac outflow tract: aortic sac to ventricular septal closure. Dev Biol 196:129–144.

PII S1050-1738(02)00178-0 **TCM**

Gene Expression Patterns 3 (2003) 49–52

www.elsevier.com/locate/modgep

Early expression of hypoxia-inducible factor 1α in the chicken embryo

Heather C. Etchevers*

Institut d'Embryologie Cellulaire et Moléculaire du CNRS et du Collège de France, 49 bis avenue de la Belle Gabrielle, 94736 Nogent-sur-Marne Cedex, France

Received 29 October 2002; received in revised form 21 November 2002; accepted 27 November 2002

Abstract

Hypoxia is known to regulate angiogenesis and tissue growth by the induction of the alpha subunit of the heterodimeric transcription factor, hypoxia-inducible factor 1. The expression pattern of HIF1α in both epithelial and mesenchymal structures of the chicken embryo through the first 7 days of development is reported here. HIF1α transcript is expressed diffusely throughout the neuroepithelium, limb, mesonephritic and cephalic mesenchyme, progressively becoming restricted to known proliferative zones of the central nervous system. Specific, strong expression is unexpectedly found in the endoderm of Sessel's pouch and in the ectoderm of both Rathke's pouch and the first branchial arch before the disappearance of the buccopharyngeal membrane.

Keywords: Aortic arch; bHLH-PAS; Branchial arch; Ectoderm; Embryo; Endoderm; Heart; Hypothalamus; Hypoxia; Neuroepithelium; Neural tube; Pharynx; Transcription factor; Rathke's pouch

1. Results and discussion

Hypoxia-inducible factor 1 is a heterodimeric basic helix-loop-helix transcription factor of the PAS (Per-ARNT-Sim domain) family. The promoters of genes involved in vascular development, such as vascular endothelial growth factor, erythropoietin A and endothelin-1, contain HIF1 binding sites (Hu et al., 1998; Semenza et al., 1999). HIF1 acts specifically through its α subunit, which is transcribed in an inversely proportional manner to cellular O_2 concentration (Jiang et al., 1996). It is subject to non-hypoxic regulation as well. The aryl hydrocarbon receptor nuclear translocator (ARNT/HIF1β) dimerizes with HIF1α (Semenza et al., 1997) but also with other bHLH-PAS proteins including HIF2α (EPAS-1; Favier et al., 1999) and single-minded-2 (Moffett et al., 1997). Thus, the activities of different bHLH-PAS family members are probably modulated according to their spatiotemporal domains of expression (Jain et al., 1998). Homozygous HIF1α knockout mice show VEGF-independent, abnormal vascular remodeling and widespread apoptosis of the cephalic mesenchyme before embryonic death at E10.5 (Kotch et al., 1999).

In the chicken embryo at the 10 somite stage (ss), HIF1α transcripts appear within the pharyngeal endoderm (Fig. 1A). Pharyngeal expression of HIF1α increases over time to its most intense at 22ss, in endoderm underlying the ventral diencephalon and Rathke's pouch (Fig. 1B). During this time window, HIF1α message distribution changes. At a transverse level corresponding to the posterior diencephalon and the most rostral tip of Sessel's pouch, the endoderm expresses HIF1α equally around its circumference at both 13ss (Fig. 1C) and 16ss (Fig. 1F). Underneath the mesencephalon, HIF1α expression diminishes in the ventral midline of Sessel's pouch at 13ss (Fig. 1D). The zone of diminished expression extends laterally to encompass the ventral half of the pouch by 16ss, while expression remains strong in the thin dorsal epithelium (Fig. 1G). The ectoderm around the buccopharyngeal membrane (the point of nearest contact with the endoderm) and the distal ectoderm of the first branchial arch (BA1) also express HIF1α (Fig. 1C,D,F,G). Between the rhombencephalon and developing heart at both 13ss (Fig. 1E) and 16ss (Fig. 1H), expression of HIF1α is restricted to the dorsal face of the endoderm, where it is thinnest, and is excluded from the thicker ventral region near the heart. Notably, HIF1α transcripts are found in areas of the endoderm not overlapping the expression domain of

* Present address: INSERM U393, Hôpital Necker – Enfants Malades, 149 rue de Sèvres, 75743 Paris Cedex 15, France. Tel.: +33-1-4449-5136; fax: +33-1-4449-5150.

E-mail address: etchever@infobiogen.fr (H.C. Etchevers).

1567-133X/03/$ - see front matter © 2003 Elsevier Science B.V. All rights reserved.
doi:10.1016/S1567-133X(02)00076-5

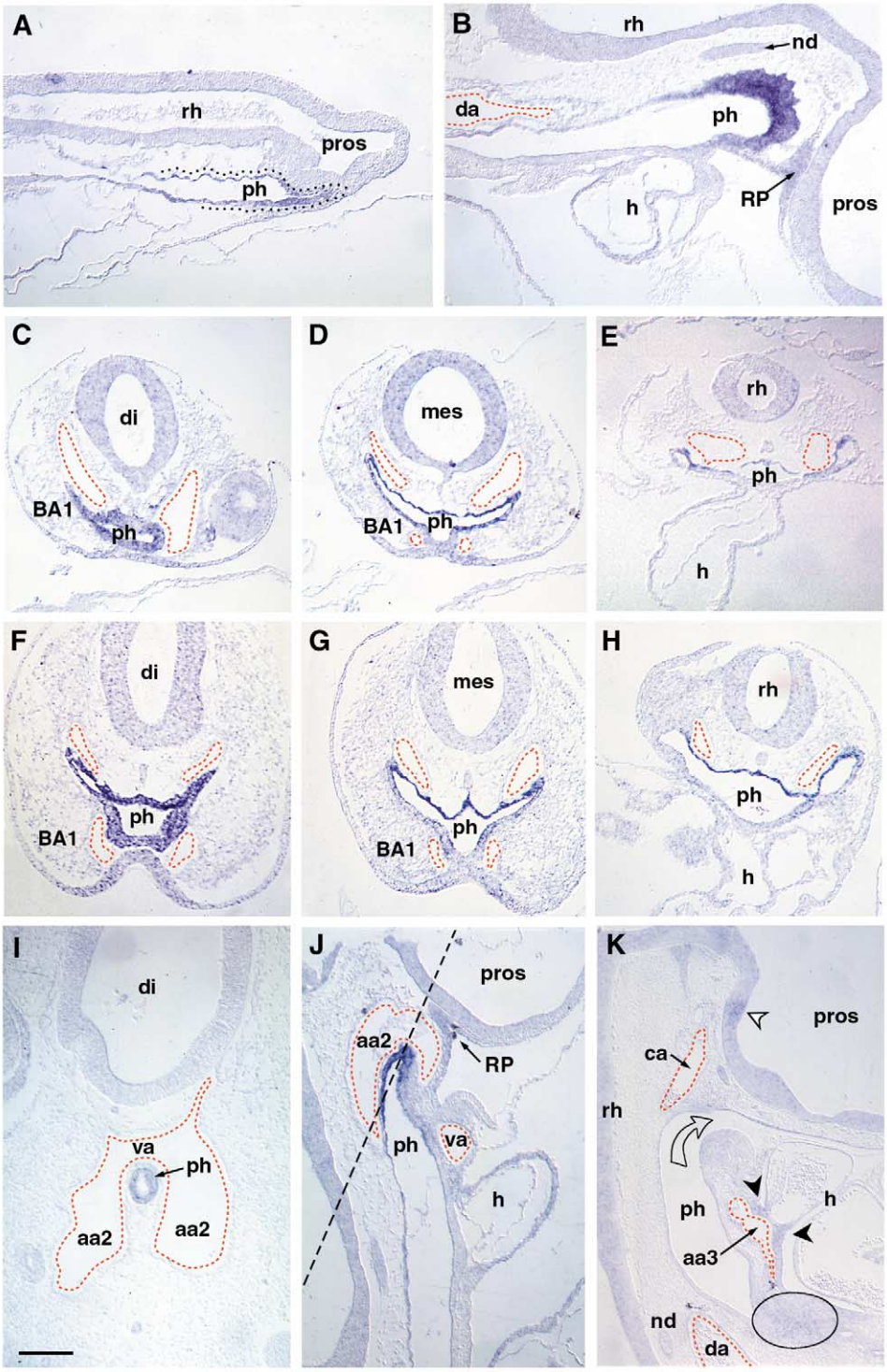

Fig. 1. HIF1α expression is strongest in the rostral pharyngeal endoderm. (A) Sagittal sections of 10ss and (B) 22ss embryos, rostral to right, dorsal to top. The pharynx is outlined by black dots in (A); the aorta and aortic arch arteries are lined by red dashes in (B–K). At 13ss, transverse sections at the level of the diencephalon (C), mesencephalon (D) and rhombencephalon (E) show diffuse HIF1α expression in the neuroepithelium and cephalic mesenchyme, stronger expression in the ectoderm of the 1st branchial arch (C,D), and strongest expression in the pharynx. At 16ss, transverse sections at the level of diencephalon (F), mesencephalon (G) and rhombencephalon (H) confirm the downregulation of HIF1α expression in the ventral pharyngeal endoderm at caudal cephalic levels. (I) An oblique coronal section at 23ss shows the 2nd aortic arch that has formed at this time around the rostral tip of the HIF1α-expressing endoderm, under the diencephalon. Their adjoined portion corresponds to the ventral aorta. The approximate level of section is indicated by a dashed line in a parasagittal section at 23ss (J), where some HIF1α expression is observed in Rathke's pouch. (K) By 36ss (Hamburger–Hamilton 18), the buccopharyngeal membrane has disappeared (open arrow) along with endodermal HIF1α transcripts. Some expression is seen in the hypothalamus (open arrowhead), outflow tract into the 3rd aortic arch (arrowheads) and lung mesenchyme (oval). aa#, aortic arch #; BA1, 1st branchial arch; ca, carotid artery; da, dorsal aorta; di, diencephalon; h, heart; mes, mesencephalon; nd, notochord; rh, rhombencephalon; ph, pharynx; pros, prosencephalon; RP, Rathke's pouch; va, ventral aorta. Bar, 120 μm.

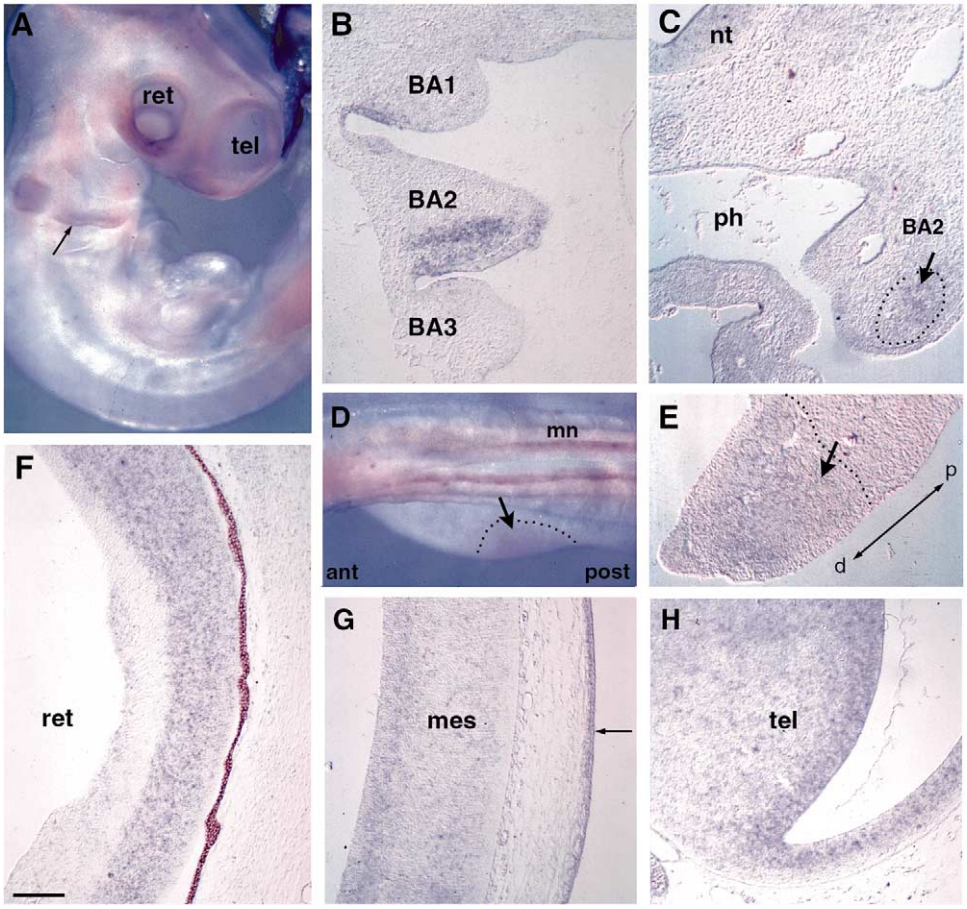

Fig. 2. (A) HIF1α transcripts are visible in whole-mount embryo at HH17 in the retina, in dorsal and rostral cephalic ectoderm, and in ventral BA2. The signal in the otic vesicle is non-specific. (B) In parasagittal section, expression is present in lateral ectoderm between BA1 and BA2 and restricted to BA2 ventral mesenchyme. (C) At HH19, BA2 mesenchymal expression (dotted) is seen in transverse section to be ventral and diffuse (dorsal to top). Weak expression is also present in the neural tube (nt). (D,E) At HH20, HIF1α transcripts are also faintly expressed in a distal/caudal quadrant of wing bud mesenchyme (dotted) and the mesonephros (mn, parallel stripes). Whole-mount in (D) in dorsal view, ant(erior) and post(erior) indicated; distoproximal axis (d-p) indicated in section (E). (F–H) Central nervous system expression is strongest within proliferative neuronal layers as seen in the retina (F), the mesencephalon (G) and the telencephalon (H) at HH30. BA#, branchial arch #; mes, mesencephalon; mn, mesonephros; nt, neural tube; ph, pharynx; ret, retina; tel, telencephalon. Bar, 525 μm in (A), 400 μm in (D) and 120 μm in all others.

endothelin-1 in ventral foregut of BA2 at the same stages (Nataf et al., 1998; data not shown).

During a limited time window, BA2 arteries issue directly from the outflow tract of the developing heart and curve dorsally to feed into the paired dorsal aortae, temporarily constituting the ventral aorta at the point of bifurcation. Between 18ss and 25ss, BA2 arteries have formed in apposition to HIF1α-expressing pharyngeal endoderm (Fig. 1I,J). By 25ss, when the buccopharyngeal membrane has opened to create the oral cavity, HIF1α message rapidly begins to disappear from the pharyngeal endoderm. While transcripts are no longer visible in the endoderm, low levels of expression continue in the heart outflow tract and appear in the future lung mesenchyme at 36ss (Fig. 1K).

After 30ss, equivalent to Hamburger–Hamilton (HH) stage 17 (Hamburger and Hamilton, 1951), novel expression of HIF1α appears specifically in the ectodermal fold between BA1 and BA2, and in the caudal mesenchyme of BA2 (Fig. 2A,B). Seen transversally at HH19 (Fig. 2C), the diffuse BA2 expression is reminiscent of that found in the distal/caudal mesenchyme of the forelimb bud at HH20 (Fig. 2D,E). The mesonephros also contains low levels of transcript (Fig. 2D).

Baseline HIF1α expression is visible in the neuroepithelium at HH8 (5ss, data not shown) and continues throughout the first 3 days of incubation (Fig. 1). A small region of the posterior hypothalamus accumulates HIF1α transcripts from HH18 on (Fig. 1K, arrow). Expression intensifies by HH30 in proliferative cell layers of the retina (Fig. 2F), mesencephalon (Fig. 2G), telencephalon (Fig. 2H) and the ventricular zone of the spinal cord (data not shown), while transcript remains present at low levels throughout the parenchyme. HIF1α message is also observed in portions of the middle ear epithelium at HH30 (data not shown) and the epidermis of the head (Fig. 2G).

HIF1α is transcribed at baseline levels in many dense, proliferating tissues of the chicken embryo, consistent with observations of tissue hypoxia in these areas of murine

embryos (Lee et al., 2001). However, strong HIF1α expression is shown here to be restricted to the rostral endoderm down to the level of the hindbrain. This pharyngeal endoderm is essential for patterning of the cephalic neural crest-derived branchial arch skeleton (Couly et al., 2002), perhaps explaining the early, dramatic head phenotype of HIF1α knockout mice (Kotch et al., 1999). HIF1α is also expressed in the future oral ectoderm but disappears from the buccal orifice shortly after ectoderm and pharyngeal endoderm have joined.

2. Experimental procedures

Plasmid pCHIF-1α-F2 was kindly provided by Dr Toshiyuki Takahashi (Takahashi et al., 2001) and corresponds to nucleotides 1623–2384 of chicken HIF1α (GenBank Accession number: AB013746). In situ hybridization was performed using digoxygenin-labeled RNA probes transcribed by SP6 on 7 μm paraffin sections of chicken embryos as described (Etchevers et al., 2001), or on embryos in toto as described (Henrique et al., 1995).

Acknowledgements

I am grateful to Professor Nicole Le Douarin and Dr Marie-Aimée Teillet for their comments. Anne Lehmann provided excellent technical assistance, and Michel Fromaget, Sophie Gournet and Francis Beaujean helped with the figures. This work was supported by the Collège de France, the Centre National de la Recherche Scientifique and the Sturge-Weber Foundation of America.

References

Couly, G., Creuzet, S., Bennaceur, S., Vincent, C., Le Douarin, N.M., 2002. Interactions between Hox-negative cephalic neural crest cells and the foregut endoderm in patterning the facial skeleton in the vertebrate head. Development 129, 1061–1073.

Etchevers, H.C., Vincent, C., Le Douarin, N.M., Couly, G.F., 2001. The cephalic neural crest provides pericytes and smooth muscle cells to all blood vessels of the face and forebrain. Development 128, 1059–1068.

Favier, J., Kempf, H., Corvol, P., Gasc, J.M., 1999. Cloning and expression pattern of EPAS1 in the chicken embryo. Colocalization with tyrosine hydroxylase. FEBS Lett. 462, 19–24.

Hamburger, V., Hamilton, H.L., 1951. A series of normal stages in the development of the chick embryo. J. Morphol. 88, 49–92.

Henrique, D., Adam, J., Myat, A., Chitnis, A., Lewis, J., Ish-Horowicz, D., 1995. Expression of a Delta homologue in prospective neurons in the chick. Nature 375, 787–790.

Hu, J., Discher, D.J., Bishopric, N.H., Webster, K.A., 1998. Hypoxia regulates expression of the endothelin-1 gene through a proximal hypoxia-inducible factor-1 binding site on the antisense strand. Biochem. Biophys. Res. Commun. 245, 894–899.

Jain, S., Maltepe, E., Lu, M.M., Simon, C., Bradfield, C.A., 1998. Expression of ARNT, ARNT2, HIF1 alpha, HIF2 alpha and Ah receptor mRNAs in the developing mouse. Mech. Dev. 73, 117–123.

Jiang, B.H., Semenza, G.L., Bauer, C., Marti, H.H., 1996. Hypoxia-inducible factor 1 levels vary exponentially over a physiologically relevant range of O_2 tension. Am. J. Physiol. 271, C1172–C1180.

Kotch, L.E., Iyer, N.V., Laughner, E., Semenza, G.L., 1999. Defective vascularization of HIF-1alpha-null embryos is not associated with VEGF deficiency but with mesenchymal cell death. Dev. Biol. 209, 254–267.

Lee, Y.M., Jeong, C.H., Koo, S.Y., Son, M.J., Song, H.S., Bae, S.K., Raleigh, J.A., Chung, H.Y., Yoo, M.A., Kim, K.W., 2001. Determination of hypoxic region by hypoxia marker in developing mouse embryos in vivo: a possible signal for vessel development. Dev. Dyn. 220, 175–186.

Moffett, P., Reece, M., Pelletier, J., 1997. The murine Sim-2 gene product inhibits transcription by active repression and functional interference. Mol. Cell. Biol. 17, 4933–4947.

Nataf, V., Grapin-Botton, A., Champeval, D., Amemiya, A., Yanagisawa, M., Le Douarin, N.M., 1998. The expression patterns of endothelin-A receptor and endothelin 1 in the avian embryo. Mech. Dev. 75, 145–149.

Semenza, G.L., Agani, F., Booth, G., Forsythe, J., Iyer, N., Jiang, B.H., Leung, S., Roe, R., Wiener, C., Yu, A., 1997. Structural and functional analysis of hypoxia-inducible factor 1. Kidney Int. 51, 553–555.

Semenza, G.L., Agani, F., Iyer, N., Kotch, L., Laughner, E., Leung, S., Yu, A., 1999. Regulation of cardiovascular development and physiology by hypoxia-inducible factor 1. Ann. N. Y. Acad. Sci. 874, 262–268.

Takahashi, T., Sugishita, Y., Nojiri, T., Shimizu, T., Yao, A., Kinugawa, K., Harada, K., Nagai, R., 2001. Cloning of hypoxia-inducible factor 1alpha cDNA from chick embryonic ventricular myocytes. Biochem. Biophys. Res. Commun. 281, 1057–1062.

Polyalanine expansion and frameshift mutations of the paired-like homeobox gene *PHOX2B* in congenital central hypoventilation syndrome

Published online 17 March 2003, doi:10.1038/ng1130

Congenital central hypoventilation syndrome (CCHS or Ondine's curse; OMIM 209880) is a life-threatening disorder involving an impaired ventilatory response to hypercarbia and hypoxemia. This core phenotype is associated with lower-penetrance anomalies of the autonomic nervous system (ANS) including Hirschsprung disease and tumors of neural-crest derivatives such as ganglioneuromas and neuroblastomas. In mice, the development of ANS reflex circuits is dependent on the paired-like homeobox gene *Phox2b*. Thus, we regarded its human ortholog, *PHOX2B*, as a candidate gene in CCHS. We found heterozygous *de novo* mutations in *PHOX2B* in 18 of 29 individuals with CCHS. Most mutations consisted of 5–9 alanine expansions within a 20-residue polyalanine tract probably resulting from non-homologous recombination. We show that *PHOX2B* is expressed in both the central and the peripheral ANS during human embryonic development. Our data support an essential role of PHOX2B in the normal patterning of the autonomous ventilation system and, more generally, of the ANS in humans.

A genetic origin of CCHS[1] has long been suspected based on concordance in monozygotic twins[2], rare familial cases (siblings, half-siblings, and mother-to-child transmission)[3] and segregation analysis suggesting an autosmal dominant locus with low penetrance or a multigenic model[4]. So far, only low-penetrant predisposing mutations of the RET-Glial cell line-derived neurotrophic factor (GDNF), endothelin 3 (EDN3) and brain-derived neurotrophic factor (BDNF) pathways have been reported in a few individuals with CCHS[5–7]. Considering the broad range of defects in the ANS in CCHS on the one hand and the key role of Phox2b in the ontogeny of the ANS reflex circuits in mice[8,9] on the other hand, we regarded *PHOX2B* (also called *PMX2B* and *NBPHOX*) as a candidate gene in the disease.

PHOX2B maps to chromosome 4p12 and encodes a highly conserved homeobox transcription factor of 314 amino acids with two short and stable polyalanine

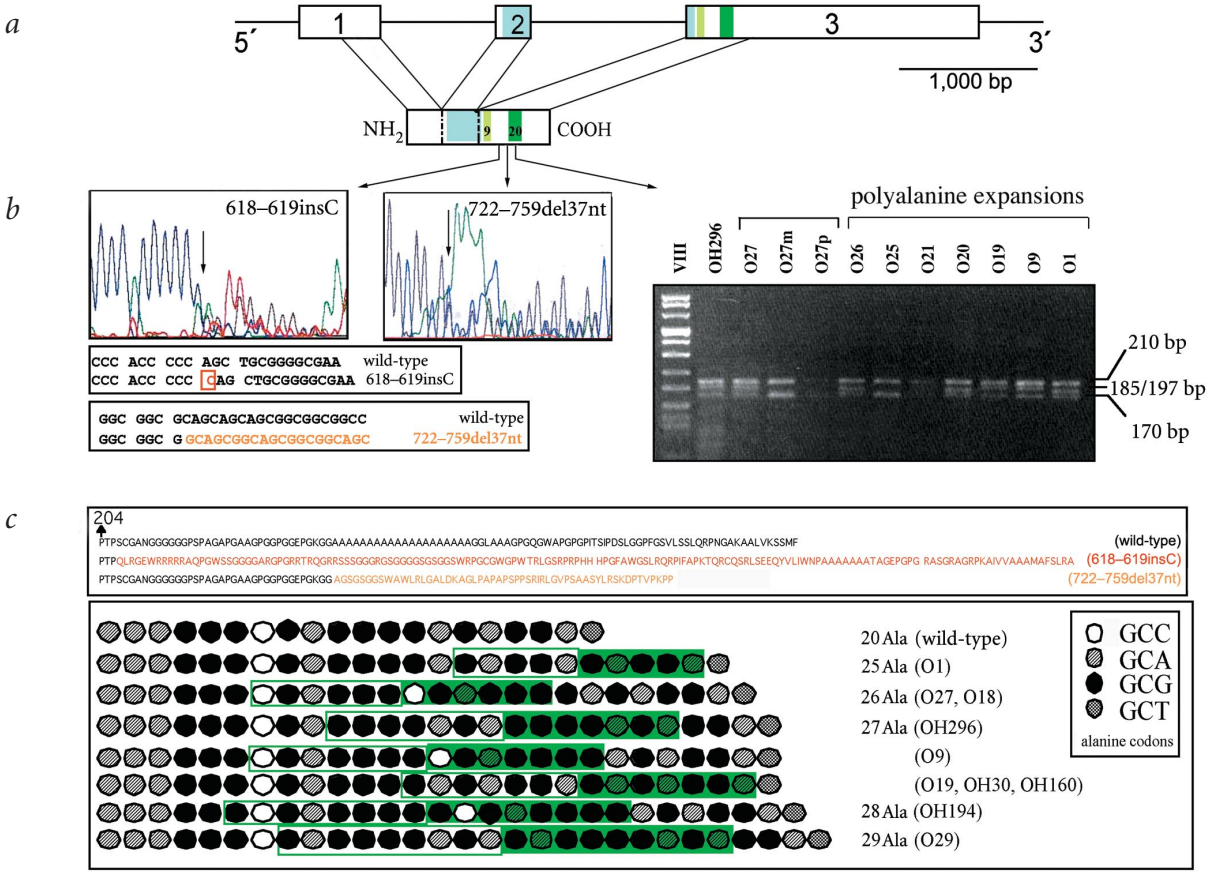

Fig. 1 Mutations of *PHOX2B* in CCHS. ***a***, Genomic organization of *PHOX2B* and schematic representation of the PHOX2B protein. The homeobox domain and the 9- and 20-residue polyalanine tracts are indicated (blue and green boxes, respectively). ***b***, DNA sequence electropherogram and PCR digestion showing the identified mutations in *PHOX2B*. Left, Heterozygous frameshift mutations. Right, Heterozygous alanine triplet expansions. Mutated alleles are seen as extra bands of variable size between the 170- and 210-bp bands after enzymatic digestion with *Stu*I of the 380-bp PCR product of *PHOX2B* exon 3 and migration on a 3% agarose gel (see Supplementary Note 1 online). ***c***, Mutant PHOX2B proteins. Top, 618–619insC and 722–759del37nt frameshift mutations. Bottom, various polyalanine expansions observed. The duplicated codons are shown in green boxes.

repeats of 9 and 20 residues, respectively (Fig. 1*a*). The length of the polyalanine tracts is conserved in mice and humans. We screened the coding sequence of *PHOX2B* in a series of 29 unrelated individuals with CCHS (see Supplementary Note 1 online). Direct DNA sequencing showed heterozygosity with respect to *PHOX2B* variations in 18 of 29 cases. In 16 of 18 cases, the nucleotide variation was a triplet expansion of 15–27 nucleotides (nt 721–780; Fig. 1*b* and Supplementary Table 1 online) adding 5–9 alanines to the 20-residue polyalanine tract (Fig. 1*c*). Most mutant genotypes were different, suggesting that they derived from independent mutational events (Fig. 1*c*). In addition, whenever parents were available, we found that the polyalanine triplet expansion occurred *de novo*, supporting its role in the disease phenotype (see Supplementary Table 1 online). In two other CCHS cases, a *de novo* cytosine insertion in a stretch of four cytosines (618–619insC) and a deletion of 37 nucleotides (722–759del37nt) resulted in a frame shift downstream of the homeobox, predicting a mutant protein with no known function or homology (Fig. 1*b*,*c*). The 722–759del37nt mutation could be regarded as an out-of-frame contraction of the polyalanine tract. We found neither alanine triplet expansions nor frameshift mutations in 250 control chromosomes from various ethnic backgrounds. Notably, 2 of 250 control alleles had a small polyalanine contraction (5 and 6 triplets, data not shown), suggesting an unequal crossing-over during meiosis rather than a polymerase slippage during replication. In the former case, polyalanine expansions and contractions are equally likely to occur; *PHOX2B* contractions were found as a rare variant in controls.

We found that 2 of 29 individuals with CCHS carried heterozygous variants in genes involved in the same developmental pathway, namely *RET* and *GDNF* (amino-acid substitutions P1039L and R93W, respectively; see Supplementary Table 1 online; ref. 5), in addition to polyalanine expansions in *PHOX2B*. Notably, *Phox2* genes control *Ret* expression in both sympathetic and enteric neurons in mice[8]. Unlike the polyalanine expansions, however, these variants are neither necessary (most individuals with CCHS do not have any *RET* or *GDNF* gene variant) nor sufficient for the disease to occur (carrier parents have no phenotypic expression). These data suggest that *PHOX2B* is the primary disease locus in CCHS. Moreover, we found mutations in *PHOX2B* not only in isolated cases of CCHS but also in individuals with a more complex neural-crest involvement including CCHS and Hirschsprung disease (Haddad syndrome) as well as early-onset neuroblastoma. We did not find any correlation between the size of the polyalanine tract and the complexity of the disease in our analyses.

To confirm the involvement of mutations in *PHOX2B* in the disease phenotype, we studied the expression pattern of *PHOX2B* in early human development (see Supplementary Note 1 online). In accordance with the wide spectrum of ANS dysfunction observed in individuals with CCHS, the expression pattern of *PHOX2B* involved both central autonomic circuits and peripheral neural-crest derivatives. From day 32 of development, *PHOX2B* was expressed in the seventh ganglion and the ninth/tenth ganglionic complex (Fig. 2*a*–*d*). From day 33 of development, we observed strong expression of *PHOX2B* in terminal rhombomeres 4–8, in the presumptive enteric ganglia and in the sympathetic chain ganglia (Fig. 2*g*–*l*). Finally, we detected expression of *PHOX2B* in the presumptive carotid body at the carotid bifurcation, ventral to the superior cervical ganglion, which also expressed *PHOX2B* (Fig. 2*e*,*f*). We did not detect any *PHOX2B* expression in adrenal medulla at the stages investigated.

Polyalanine expansion mutations involving homeodomain or non-homeodomain transcription factors (*HOXA13*, *HOXD13*, *ARX*, *RUNX2*, *ZIC2*, *FOXL2*) have been described in several human malformations[10,11]. In each of these cases, both the normal and expanded alanine tracts range in a similar size, suggesting a common underlying mechanism. In the case of *HOXD13* and *ZIC2*, the expansions are not just loss-of-function mutations but are responsible for a dominant negative effect[12,13]. In the case of *PHOX2B*, a loss-of-function mutation with lower penetrance for the enteric nervous system anomalies is a possibility, as we found frameshift mutations in two individuals. Assuming that the protein is stable, however, the homeodomain is preserved in

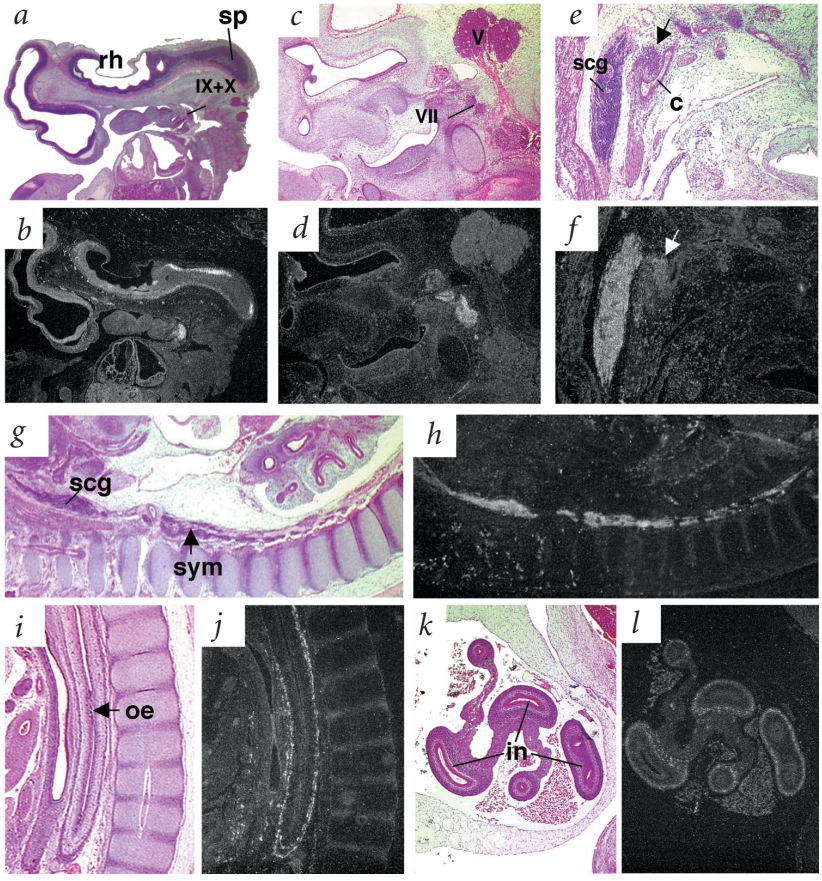

Fig. 2 *PHOX2B* gene expression in developing human brainstem and enteric nervous system. Slides stained with hematoxylin and eosin (***a***,***c***,***e***,***g***,***i***,***k***) and dark-field illumination of the hybridized adjacent sections (***b***,***d***,***f***,***h***,***j***,***l***) at day 33 (*a*,*b*), day 54 (*c*–*f*) and day 47 of development (*g*–*l*). Parasagittal sections showing expression of *PHOX2B* in rhombencephalon (rh; *a*,*b*), cervical spinal cord (sp; *a*,*b*), seventh (VII) ganglia and ninth/tenth (IX+X) ganglionic complex (*a*–*d*), presumptive enteric ganglia of oesophagus (oe) and intestine (in; *i*–*l*) and paravertebral sympathetic ganglia (sym), including the superior cervical ganglion (scg; *g*,*h*). *PHOX2B* expression was also detected in the presumptive carotid body (arrow) at the carotid (c) bifurcation, ventral to the superior cervical ganglion (e,*f*). Magnifications: *a*,*b*,*g*,*h*, ×15; *c*,*d*, ×25; *i*–*l*, ×30; *e*,*f*, ×40.

both cases. As far as the ocular phenotype is concerned, one can speculate that PHOX2B mutant protein products exert a dominant negative effect on PHOX2A, considering the overlapping features observed in CCHS and congenital fibrosis of the extra ocular muscle type 2 (CFEOM2) resulting from homozygous mutations of the gene *PHOX2A* (ref. 14). Indeed, it has been shown that the third and fourth motor nuclei express both Phox2A and Phox2b in mice and are Phox2a-dependent[8]. The mechanism for a putative involvement of *PHOX2B* in isolated neural-crest tumors is undefined at present, but it is worth mentioning that Phox2b has been shown to regulate neuronal cell cycle[15].

Little is known regarding the bases of ventilatory control anomalies in CCHS. It has been speculated that the disease involves a defect in the integration by the nucleus of the solitary tract and interneurons of the inputs from the central CO_2/pH-sensitive chemoreceptors (medulla oblongata) and the peripheral O_2, CO_2 and pH-sensitive chemoreceptors in the carotid bodies[1]. Notably, several of these structures express Phox2b in mice[8,9] and humans (this study) and fail to form or degenerate in Phox2b$^{-/-}$ mouse mutants (refs. 8,9 and J.-F. Brunet, pers. comm.). So far, no phenotype has been reported in Phox2b$^{+/-}$ mice. Our mutation and expression studies strongly support the view that *PHOX2B* is a master gene for the formation and/or function of the neuronal network for autonomous control of ventilation and further suggests that *PHOX2B* mutations trigger a wide spectrum of ANS disorders ranging from dysgenetic malformations to tumor predisposition.

Note: Supplementary information is available on the Nature Genetics website.

Acknowledgments

We thank the individuals with CCHS, their families and the Association Française du Syndrome d'Ondine who participated in this study, J.-F. Brunet and C. Goridis for helpful comments and discussions and G. Mattéi for technical help. This study was supported by grants from the European Community, Association Française contre les Myopathies-INSERM (Maladies Rares) and Hoechst-Marion-Roussel. B.L. is a recipient of a Sanofi-Synthelabo grant.

Competing interests statement

The authors declare that they have no competing financial interests.

Jeanne Amiel[1], Béatrice Laudier[1], Tania Attié-Bitach[1], Ha Trang[2], Loïc de Pontual[1], Blanca Gener[3], Delphine Trochet[1], Heather Etchevers[1], Pierre Ray[1], Michel Simonneau[2], Michel Vekemans[1], Arnold Munnich[1], Claude Gaultier[2] & Stanislas Lyonnet[1]

[1]Unité de Recherches sur les Handicaps Génétiques de l'Enfant INSERM U-393, et Département de Génétique, Hôpital Necker-Enfants Malades, 149, rue de Sèvres, 75743 Paris Cedex 15, France. [2]Service de Physiologie CIC INSERM 9202, et Equipe INSERM E9935, Hôpital Robert Debré, Paris, France. [3]Clinica Materno-Infantil, Hospital de Cruces, 48903 Barakaldo, Spain. Correspondence should be addressed to J.A. (e-mail: amiel@necker.fr).

Received 31 October 2002; accepted 20 February 2003.

1 Gozal, D. *Pediatr. Pulmonol.* **26**, 273–282 (1998).
2. Khalifa, M.M., Flavin, M.A. & Wherrett, B.A. *J. Pediatr.* **113**, 853–855 (1988).
3. Sritippayawan, S. *et al. Am. J. Respir. Crit. Care Med.* **166**, 367–369 (2002).
4. Weese-Mayer, D.E., Silvestri, J.M., Marazita, M.L. & Hoo, J.J. *Am. J. Med. Genet.* **47**, 360–367 (1993).
5. Amiel, J. *et al. Am. J. Hum. Genet.* **62**, 715–717 (1998).
6. Bolk, S. *et al. Nat. Genet.* **13**, 395–396 (1996).
7. Weese-Mayer, D.E., Bolk, S., Silvestri, J.M. & Chakravarti, A. *Am. J. Med. Genet.* **107**, 306–310 (2002).
8. Brunet, J.F. & Pattyn, A. *Curr. Opin. Genet. Dev.* **12**, 435–440 (2002).
9. Pattyn, A., Morin, X., Cremer, H., Goridis, C. & Brunet, J.F. *Nature* **399**, 366–370 (1999).
10. Goodman, F.R. & Scambler, P.J. *Clin. Genet.* **59**, 1–11 (2001).
11. Stromme, P. *et al. Nat. Genet.* **30**, 441–445 (2002).
12. Bruneau, S., Johnson, K.R., Yamamoto, M., Kuroiwa, A. & Duboule, D. *Dev. Biol.* **237**, 345–353 (2001).
13. Brown, S.A., Abigani, M. & Brown, L.Y. *Am. J. Hum. Genet.* **71** Supp. 166 (2002).
14. Nakano, M. *et al. Nat. Genet.* **29**, 315–320 (2001).
15. Dubreuil, V., Hirsch, M.R., Pattyn, A., Brunet, J.F. & Goridis, C. *Development* **127**, 5191–5201 (2000).

Supplementary Note 1

Methods

Patients

A total of 29 patients fulfilled the criteria for inclusion in the study[1], namely: *i)* persistent central alveolar hypoventilation (PaCO2 > 60 mmHg) during sleep detected by polysomnography while the patient spontaneously breathed room air, *ii)* lack of ventilatory responses to inhaled CO_2, and *iii)* absence of primary lung, neuromuscular, or cardiac disease. Twenty patients were evaluated in the department of physiology of Hôpital Robert Debré, and the other 9 had their medical histories and sleep recordings reviewed. We evaluated ANS dysfunction based on: i) esophageal dysmotility[2], ii) decreased heart rate variability[3], and iii) ocular anomalies including miotic pupils with decreased pupillary reaction to light[4]. We also noted oculomotor dysfunction (exotropia, esotropia, convergence insufficiency, supplementary Table)[4,5], and one patient (OH22) has congenital ptosis in addition to exotropia and miotic pupils. Histopathological criteria for Hirschsprung disease (HSCR)[6] were: i) absence of enteric plexuses at histological examination and ii) increased acetylcholinesterase histochemical staining in nerve fibers. HSCR was diagnosed in 12/29 CCHS cases (40%, 6 long-segment HSCR, 2 short-segment HSCR, 4 cases of unknown length). Finally, two patients presented with tumours of neural crest origin (ganglioblastoma for patient OH22 and multiple neuroblastoma for patient OH253, supplementary Table)[7]. We obtained blood samples with informed consent of the parents, and we extracted DNA according to standard protocols.

Molecular studies

We screened the entire coding sequence of the *PHOX2B* gene by single strand conformation polymorphism (SSCP) analysis and direct DNA sequencing (Fig. 1*a*). Primers are available from authors upon request. The PCR reaction mixture (25µl) contained 100 ng of leukocyte DNA, 20 pmol of each primers, 0.1 µM dNTP, 0.07µl of ^{33P}dCTP, and 1 U Taq DNA polymerase (Invitrogen, Expand). We heated the PCR products for 10 min at 95°C, loaded them onto a Hydrolink MDE gel (Bioprobe) and electrophoresed them at 6-8 W. We then dried the gel and autoradiographed it for 48 h. We performed DNA sequencing by the fluorometric method on both strands (Big DyeTerminator Cycle Sequencing kit, Applied Biosystems, Warrington, UK). We typed poly (CA) microsatellite markers flanking the *PHOX2B* locus on both leukocyte and tumour DNA for patient S253 (D4S1536 and D4S2974, primer sequences available through the Genome Database). We performed screening for and sizing of polyalanine expansions using a StuI enzymatic digestion of the 378 bp PCR product of *PHOX2B* exon 3B, followed by migration on an 8% acrylamide gel (wild type bands of 168 and 210 bp). When parents' DNA were available, we assessed the probability of false paternity to be less than 10^{-3} using unlinked poly(CA) microsatellite markers with heterozygosity of 80% or more (not shown). Finally, we had studied the coding sequence of the *RET*, *EDN3* (7/29 patients), *GDNF* and *BDNF* genes by SSCP and/or direct sequencing in the series of CCHS patients (data not shown).

***In situ* hybridisation**

We collected human embryos and foetal tissues from legally terminated pregnancies in agreement with the French law and Ethics Committee recommendations. We prepared issues as previously described[8]. We amplified a 351bp PCR fragment encoding *PHOX2B* exon 1 from human genomic DNA with a T7 extension (TAATACGACTCACTAGGGAGA) added to both primers to generate the antisense and the control sense probes. We labelled probes P-[^{35}S]UTP labelled and purified as described[8]. We dehydrated slides, exposed them to BIOMAX MR X-ray films (Amersham) for 3 days, and dipped them in Kodak NTB2 emulsion for 3 weeks at + 4°C.Wwe analyzed developed- and toluidine blue counterstained slides with dark and bright field illumination. We did not detect any hybridisation signal with the sense probe (data not shown).

References to Supplementary Note 1 and Supplementary Table 1

1. Weese-Mayer, D.E., Shannon, D.C., Keens, T.G. & Silvestri, J.M. Idiopathic congenital central hypoventilation syndrome: diagosis and management. *Am. J. Respir. Crit. Care Med.* **160**, 368-373 (1999).

2. Faure, C. *et al.* Abnormal esophageal motility in children with congenital central hypoventilation syndrome. *Gastroenterology* **122**, 1258-1263 (2002).

3. Woo, M.S. *et al.* Heart rate variability in congenital central hypoventilation syndrome. *Pediatr. Res.* **31**, 291-296 (1992).

4. Goldberg, D.S. & Ludwig, I.H. Congenital central hypoventilation syndrome: ocular findings in 37 children. *J. Pediatr. Ophthalmol. Strabismus* **33**, 175-180 (1996).

5. Wang, S.M. *et al.* Congenital fibrosis of the extraoclar muscles type2, an inherited exotropic strabismus fixus, map to distal 11q13. *Am. J. Hum. Genet.* **63**, 517-525 (1998).

6. Croaker, G.D., Shi, E., Simpson, E., Cartmill, T. & Cass, D.T. Congenital central hypoventilation syndrome and Hirschsprung's disease. *Arch. Dis. Child.* **78**, 316-322 (1998).

7. Rohrer, T., Trachsel, D., Engelcke, G. & Hammer, J. Congenital central hypoventilation syndrome associated with Hirschsprung's disease and neuroblastoma: case of multiple neurocristopathies. *Pediatr Pulmonol* **33**, 71-76 (2002).

8. Odent, S. *et al.* Expression of the Sonic hedgehog (SHH) gene during early human development and phenotypic expression of new mutations causing holoprosencephaly. *Hum. Mol. Genet.* **8**, 1683-1689 (1999).

Supplementary Table 1

Clinical data and *PHOX2B* gene mutations in congenital central hypoventilation syndrome (CCHS)

	CLINICAL DATA				MOLECULAR ANALYSIS		
Patients	**CCHS**	**ANSD**	**HSCR**	**Tumour**	***PHOX2B* Mutation**	**Alanine tract expansion**	**Transmission**
O1	+	E	-	-	dup15nt	A20>A25	?
O2	+	H, O	-	-	dup15nt	A20>A25	*de novo*
O3	+	H, O	constipation	-	-		
O5	+	E, H, O	-	-	-		
O6	+	E, H, O	-	-	-		
O7	+	H, O	-	-	-		
O9	+	H	constipation	-	dup21nt	A20>A27	?
O10	+	E, H, O	+ (?)	-	dup15nt	A20>A25	?
O11	+	H, O	-	-	dup18nt	A20>A26	*de novo*
O12	+	nd	-	-	dup18nt	A20>A26	?
O15	+	H, O	-	-	dup18nt	A20>A26	
O17	+	H, O	-	-	dup18nt	A20>A26	*de novo*
O18	+	H, O	-	-	dup18nt	A20>A26	?
O19	+	H, O	-		dup21nt	A20>A27	?
O21	+	H, O	-	-	dup15nt	A20>A25	
OH22	+	E, H, O	+ (LS)	+	-		
O27	+	E, H, O	-	-	dup18nt	A20>A26	*de novo*
O29	+	E, H, O	-	-	dup27nt	A20>A29	?
OH30		H, O	+ (SS)	-	dup21nt	A20>A27	?
O33	+	nd	constipation	-	dup15nt	A20>A25	*de novo*
OH123	+	nd	+ (?)	-	-		
OH160	+	H, O	+ (LS)	-	dup21nt	A20>A27	*de novo*
OH194	+	H	+ (LS)	-	dup24nt	A20>A28	?
OH198	+	H, O	+ (SS)	-	-		
OH225	+	nd*	+ (LS)	-	-		
OH245	+	H, O	+ (LS)	-	-		
OH247	+	nd	+ (?)	-	722-759del38nt		?
OH253	+	O	+ (?)	+	618-619insC		*de novo*
OH296	+	nd	+ (LS)	-	dup21nt	A20>A27	*de novo*

ANSD: autonomic nervous system dysfunction; ?: unknown; nd: not determined (*died in the neonatal period); E: esophageal dysmotility[2]; H: decreased heart rate variability[3]; O: abnormal pupillary reaction to light[4]; HSCR: Hirschsprung disease[6]. Tumour in patients OH22 and OH253 were ganglioneuroblastoma and neuroblastoma respectively[7]. OH160 and O2 were previously shown to carry a heterozygous *RET* and *GDNF* gene mutation respectively (P1039L and R93W).

Vasculo- and Angio-Genesis in the Head and Neck

H. ETCHEVERS

Collège de France, Nogent sur Marne; France

Key words: vasculogenesis, angiogenesis, head & neck

The adult head of vertebrates presents a particularly complex three-dimensional volume, with heavy localized demands for oxygenation and nutrition within the dense parenchyma of the brain. Despite the structural complexity of the head, underlying principles of its organization become apparent after examining the developing embryo.

The head starts out as a superposition of three cellular sheets: the endoderm, mesoderm and ectoderm. Deformation of these apparently uniform sheets around the anterior end of the notochord, providing the longitudinal axis of the organism, creates a cul-de-sac in which the structures of the head will later develop.

Blood vessels are constructed from endothelial cells, in direct contact with the circulating blood and in tight contact with each other; from pericytes, multipotent contractile cells on the abluminal surface of the endothelial cells that are responsible for the secretion of a tissue-specific basal lamina [6]; from concentric layers of smooth muscle cells (one or more depending on vessel type), and from connective cells which maintain the position of the blood vessel within the tissue or cavity.

In order to discover the origins of the components of blood vessels, one major technique used in experimental embryology has been the construction of quail-chick chimeras, which exploits species differences in nuclear structure to permanently mark cells ("fate map") grafted from a donor to a host embryo [16]. The endothelial cell lineage becomes distinct from other future mesodermal progeny at a very early time point, when the future head is barely distinguished by an anterior transverse buckling in the germ layers. A tyrosine kinase receptor to the vascular endothelium growth factor, known as VEGFR2, is already expressed at this time point in a subset of cephalic mesodermal cells that subsequently acquire characteristics of endothelial cells [8].

Vasculogenesis, the *de novo* creation of vascular tubes from endothelial and pericytic precursors, takes place in the early embryonic yolk sac and allantois, as well as in intraembryonic sites such as the bilaterally paired dorsal aortae. VEGFR2-expressing precursors coalesce and cavitate to create a primary capillary network. Thereafter, new vessels are created by sprouting from pre-existing vessels, even primitive ones. This process is known as angiogenesis and occurs throughout life.

By following the fate of grafted cells in early chick-quail chimeras, it has been shown, for example, that the loose mesoderm lateral to the future brain gives rise to both striated muscles and the endothelium of all cephalic blood vessels. According to the anteroposterior level at which grafts were performed at one developmental stage, corresponding segments of the ensuing cephalic blood vessels contained endothelial cells of graft origin (nearby muscles also contained grafted cells) [1,4].

Neural crest cells (NCC) delaminate from the left and right boundaries between the ectoderm and the median neural plate as the latter forms the tube which will give rise to the central nervous system. NCC remain mesenchymal until they colonize the appropriate locations, where they differentiate into the peripheral nervous system, certain types of endocrine cells, and all pigment cells aside from the retinal pigmented epithelium [17].

Specifically in the head, NCC also give rise to many tissues which in the body are mesodermally derived. These include the intercalating connective compo-

nents of the cephalic glands, muscles and tendons. The dermis and adipose tissue overlying the jawed facial skeleton and brain case, the bones of that part of the skull, and certain regions of the meninges underlying it are also of neural crest origin [3,5,15,18,19,21].

Early indications of the role of NCC in cephalic blood vessels came from fate-mapping experiments that showed their constitution of the branchial arch mesenchyme and subsequent incorporation into the smooth muscle walls of the corresponding large arteries [14,19]. In particular, NCC derived from the posterior rhombencephalon contribute all components of the proximal large arteries to the heart, with the exception of the endothelium [19]. NCC of this origin also play an important role in the septation of the pulmonary trunk from the aorta [20,22,23]. NCC are equally important to aortic arch vessel formation in mammals [12,13].

We have recently demonstrated the extent of NCC incorporation into cephalic blood vessels [10]. A series of quail-chick chimeras were made by successively transplanting small fragments of the brain neural folds from donors to the equivalent anteroposterior level of hosts preceding cephalic NCC migration. Embryos were then examined at different stages during the first half of gestation to see where the NCC had integrated in the blood vessels. Grafts from anterior brain levels corresponding to the diencephalon and mesencephalon resulted in abundant cells within the forebrain meninges, with a sharp border at the forebrain-midbrain boundary [10]. These cells, adjacent to endothelial capillary walls within the parenchyma, were identified with the marker α-smooth muscle actin as being pericytes. Smooth muscle and connective tissue cells of graft origin were observed in the distal portions of the major cephalic arteries. Grafts of neural folds at the level of the anterior rhombencephalon, in contrast, gave rise to the non-endothelial cells of the proximal (closer to the heart) segments of the same arteries as well as the distal internal carotid arteries. Median rhombencephalic neural folds contributed cells to the carotid arteries and cardinal veins, while posterior rhombencephalic NCC tended to incorporate into proximal segments of the carotid arteries, as well as into the aortic and pulmonary trunks and the conotruncus and semilunar valves of the heart itself. Thus, the original anteroposterior origin of a cell within the neural folds corresponds to its final distoproximal distribution in a defined subset of cephalic blood vessels. This subset, designated the "branchial vascular sector", is a distinct circuit of blood vessels originating in the ventral aorta and aortic arches, ramifying into circumscribed capillary plexuses, and terminating in their venous return to the heart. These vessels irrigate the forebrain, face and jaws.

A second vascular division can be distinguished in the head by virtue of its vessels not belonging to the branchial sector. Its component arteries and veins share the property of being entirely constructed from the embryonic mesoderm. In mature vertebrates, vessels branching rostrally from the dorsal aorta irrigate the dorsal head, including the midbrain, cerebellum and hindbrain. The two vascular domains contact at the circle of Willis, a large anastomosis between the bifurcation of the basilar artery and the cerebral arteries, branches of the internal carotids. This polygon surrounds the optic nerves and ventral diencephalon, reflecting the transition within the meninges from an entirely mesoderm-derived region, the midbrain, to a composite mesoderm/NCC-derived region, the forebrain. NCC constitute a somewhat, but not strictly, stratified or "segmental" mesenchyme in the head, according to their neural fold origin.

Grafts from adjacent levels of the neural folds give rise to cells in overlapping domains of the branchial sector, indicating a gradual succession from NCC of one origin to NCC of a neighboring origin. There is a similar composite distribution of NCC from neighboring neural fold origins in the bones of the jaw [3] and in the interstitial cells of the various cephalic muscles [15]. The morphology of head elements is imposed secondarily, immobilizing the initial NCC distributions. Recent data shows that the endoderm exerts a major instructive influence on facial skeletal morphogenesis [2]. Definitive vascular architecture in the head is certainly subject to the same sculpting influences as these other cephalic structures, since they are organized from the same original pool of mesenchyme. Ablation experiments in the chick have contributed evidence that the morphology of the upper head depends directly on the presence of NCC. Removal of the neural folds along the length of the prospective diencephalon, mesencephalon and anterior rhombencephalon deprives the rostral head of NCC. Under these experimental conditions, the tissues directly derived from these cells are missing: the nasal septum and capsule, the upper beak and jaw, the frontal and ethmoid bones, the dermis over these regions, the forebrain meninges.

Surprisingly, other tissues, not themselves NCC derivatives, are also missing: the forebrain itself, the anterior pituitary, the median oculomotor muscles, the superior salivary glands [10]. Over time, holoprosencephaly and hypotelorism or outright cyclopia develop in operated embryos, if they have been operated early enough.

Normally, NCC and VEGFRexpressing mesodermal cells surround the forebrain from the dorsal and ventral sides, respectively. They combine to form a leptomeningeal plexus by the second day of incubation in the chick, although vascular penetration of the forebrain only occurs during the fifth day. In embryos lacking rostral NCC, forebrain cell death occurs on the second and third days of incubation, such that the prospective forebrain tissue is not even present on the fifth day [9]. Therefore, the phenotype of operated chicks is due to a survival effect of NCC-containing mesenchyme on the early forebrain neuroepithelium.

Factors responsible for this trophic effect are currently being investigated.

A number of syndromes affect NCC derivatives in the head as well as vessels of the branchial sector, in particular those near the heart. These include, but are not at all restricted to, the syndromes of Von Hippel-Lindau, Dubowitz, DiGeorge, and hemifacial microsomia. In most cases, the defects in cranial NC tissues are probably downstream from a more general pathogenic cause. Nonetheless, it is important to realize that a causal cascade of malformations could be responsible for the multifactorial nature of these syndromes and that, for instance, a problem induced in NCC could give rise to the pituitary malfunctions present in Harrod or Dubowitz syndrome. In Sturge-Weber disease, the co-localization of angiomas in the telencephalic meninges, the ocular choroid and the facial dermis (port-wine stain) leads us to hypothesize that clonal progeny of the rostral cephalic NCC are directly deficient, since NCC distribution in the branchial vascular sector corresponds to the affected regions in Sturge-Weber patients. Moya-moya disease is a bilateral stenosis of the internal carotid arteries, which is circumvented by a profusion of telangiectatic blood vessels.

The fact that moya-moya is restricted to this particular region of the cephalic arteries, and that it has been associated with neurocristopathies [7] implies the involvement of deficient NC-derived pericytes and in particular, those derived from the mid-rhombencephalon (rhombomeres 4-5).

Acknowledgements

This work was supported by the Centre National de la Recher-che Scientifique and the Collège de France. H.C.E. is a postdoctoral fellow of the Sturge-Weber Foundation.

References

1 Couly G, Coltey P et Al: The angiogenic potentials of the cephalic mesoderm and the origin of brain and head blood vessels. Mech Dev 53: 97-112, 1995.
2 Couly G, Creuzet S et Al: Foregut endoderm patterns the facial skeleton. Development 129: 1061-1073, 2002.
3 Couly G, Grapin-Botton A et Al: The regeneration of the cephalic neural crest, a problem revisited: the regenerating cells originate from the contralateral or from the anterior and posterior neural fold. Development 122: 3393-3407, 1996.
4 Couly GF, Coltey PM, Le Douarin NM: The developmental fate of the cephalic mesoderm in quail-chick chimeras. Development 114: 1-15, 1992.
5 Couly GF, Coltey PM, Le Douarin NM: The triple origin of skull in higher vertebrates: a study in quail-chick chimeras. Development 117: 409-429, 1993.
6 Doherty MJ, Canfield AE: Gene expression during vascular pericyte differentiation. Crit Rev Eukaryot Gene Expr 9: 1-17, 1999.
7 Echenne BP, Leboucq N, Humbert-claude V: Ito hypomelanosis and moyamoya disease. Pediat Neurol 13: 169-171, 1995.
8 Eichmann A, Marcelle C et Al: Two molecules related to the VEGF receptor are expressed in early endothelial cells during avian embryonic development. Mech Dev 42: 33-48, 1993.
9 Etchevers HC, Couly G et Al: Anterior cephalic neural crest is required for forebrain viability. Development 126: 3533-3543, 1999.
10 Etchevers HC, Vincent C et Al: The cephalic neural crest provides pericytes and smooth muscle cells to all blood vessels of the face and forebrain. Development 128: 1059-1068, 2001.
11 Etchevers HC, Vincent C, Couly G: Neural crest and pituitary development. In: Rappaport R (ed). Hypothalamic-Pituitary Development: Genetic and Clinical Aspects. Basel, Switzerland, S Karger AG: 13-29, 2001.
12 Imai H, Osumi-Yamashita N et Al: Contribution of early-emigrating midbrain crest cells to the dental mesenchyme of mandibular molar teeth in rat embryos. Dev Biol 176: 151-165, 1996.
13 Jiang X, Rowitch DH et Al: Fate of the mammalian cardiac neural crest. Development 127: 1607-1616, 2000.
14 Johnston MC: A radioautographic study of the migration and fate of cranial neural crest cells in the chick embryo. Anat Rec 156: 143-155, 1996.
15 Köntges G, Lumsden A: Rhombencephalic neural crest segmentation is preserved throughout craniofacial ontogeny. Development 122: 3229-3242, 1996.
16 Le Douarin N: Particularités du noyau interphasique chez la caille japonaise (Coturnix coturnix japonica). Utilisation de ces particularités comme "marquage biologique" dans les recherches sur les interactions tissulaires et les migrations cellulaires au cours de l'ontogénèse. Bull Biol Fr Belg 103: 435-452, 1969.
17 Le Douarin N, Kalcheim C: The Neural Crest (2nd ed) Cambridge, Cambridge University Press, 1999.
18 Le Lièvre C: Rôle des cellules mésectodermiques issues des crêtes neurales céphaliques dans la formation des arcs branchiaux et du squelette viscéral. J Embryol Exp Morph 31: 453-477, 1974.
19 Le Lièvre CS, Le Douarin NM: Mesenchymal derivatives of the neural crest: analysis of chimaeric quail and chick embryos. J Embryol Exp Morphol 34: 125-154, 1975.
20 Nishibatake M, Kirby ML, Van Mierop LH: Pathogenesis of persistent truncus arteriosus and dextroposed aorta in the chick embryo after neural crest ablation. Circulation 75: 255-264, 1987.
21 Noden DM: The role of the neural crest in patterning of avian cranial skeletal, connective, and muscle tissues. Dev Biol 96: 144-165, 1983.
22 Waldo K, Miyagawa-Tomita S et Al: Cardiac neural crest cells provide new insight into septation of the cardiac outflow tract: aortic sac to ventricular septal closure. Dev Biol 196: 129-144, 1998.
23 Waldo KL, Kirby ML: Cardiac neural crest contribution to the pulmonary artery and sixth aortic arch artery complex in chick embryos aged 6 to 18 days. Anat Rec 237: 385-399, 1993.

Heater Etchevers, M.D.
Collège de France
49 bis, Avenue de la Belle Gabrielle
49736 Nogent sur Marne
France

Embryonic expression of the human MID1 gene and its mutations in Opitz syndrome

L Pinson, J Augé, S Audollent, G Mattéi, H Etchevers, N Gigarel, F Razavi, D Lacombe, S Odent, M Le Merrer, J Amiel, A Munnich, G Meroni, S Lyonnet, M Vekemans and T Attié-Bitach

J. Med. Genet. 2004;41;381-386
doi:10.1136/jmg.2003.014829

LETTER TO JMG

Embryonic expression of the human *MID1* gene and its mutations in Opitz syndrome

L Pinson, J Augé, S Audollent, G Mattéi, H Etchevers, N Gigarel, F Razavi, D Lacombe, S Odent, M Le Merrer, J Amiel, A Munnich, G Meroni, S Lyonnet, M Vekemans, T Attié-Bitach

J Med Genet 2004;**41**:381–386. doi: 10.1136/jmg.2003.014829

Opitz syndrome (G/BBB syndrome, MIM145410 and MIM300000) is a midline congenital malformation characterised by hypertelorism, hypospadias and oesophagolaryngotracheal defects leading to swallowing difficulties and a hoarse cry.[1] Additional defects include cleft lip with or without cleft palate, imperforate anus, anomalies of the central nervous system (including corpus callosum agenesis or vermis agenesis and hypoplasia),[2] congenital heart defects (atrial and ventricular septal defects, patent ductus arteriosus and coarctation of the aorta),[3] and developmental delay in two thirds of patients. This condition is genetically heterogeneous with an X-linked recessive form mapped to Xp22.3 and at least one autosomal dominant form mapped to chromosome 22q11.2.[4] Also, several patients with an autosomal Opitz syndrome have been reported with a 22q11 deletion.[5 6] Recently, mutations in *MID1*, a member of the B-box protein family have been identified in the X-linked form of the disease[7] but the gene for the autosomal dominant form on 22q11 remains unknown.

MID1 encodes a protein belonging to a novel subclass of RING, B-box, Coiled-Coil proteins characterised by a fibronectin type III motif and a C-terminal domain. Although the function of MID1 remains unknown, recent experiments have demonstrated that MID1 is a microtubule associated protein, belonging to a large multiprotein complex[8 9] involved in ubiquitination through microtubules.[10] MID1 association with microtubules is regulated by dynamic phosphorylation involving MAP kinase and protein phosphatase 2A that is targeted specifically to MID1 by a regulatory α4 subunit.

Here, we report on six *MID1* mutations in a cohort of 14 patients with Opitz syndrome and on heart and hindbrain expression of *MID1* during early human development using mRNA in situ hybridisation. In addition, we investigate the contribution of chromosome X-inactivation studies to identify the X-linked form of the disease.

Key points

- Opitz syndrome (G/BBB syndrome, MIM145410, and MIM300000) is a midline congenital malformation characterised by hypertelorism, hypospadias and oesophagolaryngotracheal defects leading to swallowing difficulties and hoarse voice. This condition is genetically heterogeneous with an X-linked recessive form mapped to Xp22.3 and at least one autosomal dominant form mapped to chromosome 22q11.2. Recently, mutations in *MID1* have been identified in the X-linked form of the disease but the gene for the autosomal dominant form on 22q11 remains unknown.
- Here we report on *MID1* mutations screening in a series of 14 patients with Opitz syndrome and the *MID1* expression pattern in human embryos using hybridisation in situ. Finally, we investigated the contribution of chromosome X-inactivation studies to identify the X-linked form of the disease.
- Six *MID1* mutations were identified in our series. All mutations were novel except the R495X mutation previously reported in three unrelated patients. We report heart and hindbrain expression of *MID1* during early human development. Obligate carrier mothers showed a random pattern of X-inactivation.
- Vermis hypoplasia or agenesis was frequently present (4/9) in patients with *MID1* mutation. The heart and hindbrain expression of *MID1* during early human development further supports the view that heart defects and vermis hypoplasia or agenesis are features to be included in the malformative spectrum of the syndrome. Finally, the study of X-inactivation pattern in women does not help discrimination between X-linked and autosomal forms of the disease.

METHODS

Patients

A total of 14 cases were included in the study, namely six familial forms consistent with X-linked inheritance and eight isolated cases (11 males and 3 severely affected females). Minimal inclusion criteria were: three major signs (hypertelorism, hypospadias in males or genital abnormalities in females, oesophagolaryngotracheal defects) or two major and at least two minor signs (cleft lip with or without cleft palate, anal malformation, congenital heart defects, central nervous system malformation, and limb or skeletal abnormalities). Patients were tested for 22q11 deletion using fluorescent in situ hybridisation. Magnetic resonance imaging of the brain was performed in most cases. Table 1 summarises the clinical findings and molecular data of patients with a known *MID1* mutation.

Patient 1 belongs to a large family (fig 1, family 1) with several affected individuals. The proband had hypertelorism, a broad nasal bridge, swallowing difficulties, laryngeal cleft, and hypospadias (fig 1A). He was not developmentally delayed. His mother only had hypertelorism and his brother had hypertelorism, swallowing difficulties, and posterior urethral valves.

Patient 2a (fig 1, family 2) had hypertelorism, anteverted nostrils, laryngeal diastema, bilateral cleft lip, hypospadias and developmental delay. Magnetic resonance imaging showed vermis hypoplasia. His half brother (2b) had hypertelorism, severe pharyngotracheal fistula, and hypospadias. In addition, he had a unilateral cleft lip with a broad nasal bridge and a widow's peak, a flat philtrum, and

Abbreviation: DHPLC, denaturing high performance liquid chromatography

Table 1 Clinical and molecular data of Opitz syndrome patients with a known *MID1* mutation

	Our series familial (F) and sporadic (S) cases												
	Family 1		Family 2				Family 6						Total
	(F)		(F)		Patient 3	Patient 4	(F)		Patient 9	Total	Previous studies[11]		%
Main features	proband	brother	proband	brother	(F)	(F)	proband	brother	(S)	/9	/28	%	/37
Hypertelorism or telecantus	+	+	+	+	+	+	+	+	+	9	28	100	100
Hypospadias	+	−	+	+	+	+	+	+	+	8	25	89	89
Urogenital abnormalities		+				+			+				
Oesophagolaryngotracheal anomalies	+	+*	+	+	+	+	+*	+*	+*	9	21	75	78
Cleft lip or palate	−	−	+	+	−	−	+	−	−	3	15	54	49
Ear abnormalities	+	+	+	+	−	+	+	?	+	7	11	39	48
Anteverted nostrils	−	−	+	−	+	+	+	+	−	5	11	39	43
Heart defects	−	−	−	−	+	−	−	+	−	2	9	32	30
Anal abnormalities	−	−	−	−	−	+	+	−	−	2	8	28	27
Brain anomalies	−	−	+†	?	−	+‡	+†	+§	?	4	6	21	27
Developmental delay	−	−	+	+	+	−	+	+	−	5	14	50	51
MID1 mutation	G452S		R277X		a.1285+2 delGAGT	1447–1448 insAACA	R495X		403–411 del				

*patients presenting with swallowing difficulties but no anatomical defects
†vermis hypoplasia
‡inferior vermis agenesis
§vermis and posterior corpus callosum hypoplasia

low set ears. He required special education. Their mother had a normal phenotype.

Patient 3 had a prominent forehead, hypertelorism, anteverted nostrils, and a widow's peak (fig 1, family 3). He also had swallowing difficulties with laryngeal cleft and severe hypospadias with micropenis, umbilical and inguinal hernia, and mild mental retardation. No brain investigation was available. His mother had hypertelorism and required surgery for a short nose and a broad nasal bridge.

Patient 4 (fig 1, family 4) was the first child of healthy parents. He had hypertelorism, papillar coloboma, anteverted nostrils, low set ears, swallowing difficulties with laryngeal diastema, and nasal voice, hypospadias, imperforate anus, and bilateral ureteral reflux (fig 1B). Magnetic resonance imaging showed inferior vermis agenesis but no developmental delay was noted. His family history was suggestive of Opitz syndrome segregating over three generations. Indeed, his maternal grandmother, his mother (fig 1B), his maternal

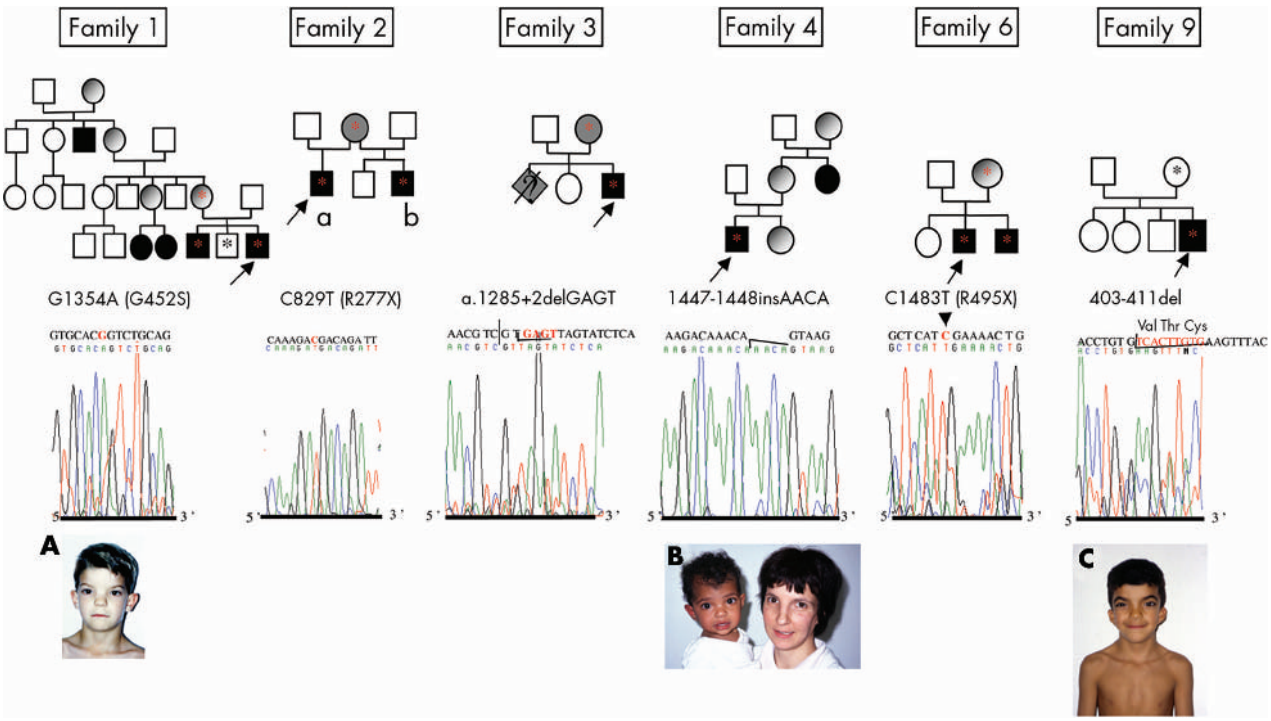

Figure 1 Pedigree and sequence of probands with a *MID1* mutation. Photographs of three probands (A, B, C) (*Reproduced with parents' permission*) and a mother (B) (*Reproduced with mother's permission*). Pedigree and mutations in the X-linked locus. In family 3, the proband brother died during pregnancy and had bilateral cleft lip and palate. The DNA sequence chromatograms are shown below the normal nucleotide sequence. * Patients for whom molecular analysis was performed, carrying the mutation (red) or not (black).

aunt, and his sister had hypertelorism. His sister also had an anal malformation.

Patient 6 and his young affected brother had microcephaly, vermis hypoplasia, hypertelorism, swallowing difficulties in early childhood, and hypospadias (fig 1, family 6). He also had a broad nasal bridge, a single central incisor, a cleft lip and palate, and growth retardation. Psychomotor delay with severe speech delay was present at 4½ years of age. The proband's brother had a ventricular septal defect, a recto-urethral fistula, a wide anterior fontanelle and hypoplasia of the posterior part of the corpus callosum. His sister had hypertelorism and anal anteposition.

Patient 9 had hypertelorism, low set posteriorly rotated ears, swallowing difficulties in childhood, hypospadias, and bilateral ureteral reflux (fig 1C). He had normal intelligence at 10 years of age and no brain investigation was performed.

MID1 mutation screening

Genomic DNA was extracted from peripheral blood leucocytes using standard procedures. The nine exons of the *MID1* gene were PCR amplified using 12 *MID1*-specific primer pairs as reported by Gaudenz et al[12] except for exon 5 which was amplified using another reverse primer (5′-aagacaatacctg-taaggtaatc). Denaturing high performance liquid chromatography (DHPLC) was used to detect nucleotide variants. We determined the optimal analysis conditions, as previously reported[13] (mobile phase temperatures and acetonitrile gradients are available on request). PCR products demonstrating DHPLC variants were sequenced on both strands using the big dye terminator cycle sequencing kit (Applied Biosystems) and analysed on an ABI 377A automated sequencer. For X-inactivation studies, we analysed the methylation pattern at the human androgen receptor locus as previously described by Hickey et al.[14]

MID1 in situ hybridisation

Human embryos were collected from terminated pregnancies in agreement with French law (94–654 of July 29, 1994) and the National Ethics Committee recommendations (No 1 of May 22, 1984).

Tissues were fixed in 4% paraformaldehyde, embedded in paraffin blocks and sectioned at 5 µm. Exon 9 primers were selected for PCR amplification (F: ggcttctatcgccttttatga, R: cacaggcttcatgagtgtaa). A T7 promoter sequence extension (taatacgactcactatagggaga) was added at the 5′ end of each primer. T7F/R and F/T7R primers allowed the amplification of sense and antisense templates. Riboprobes were labelled using T7 polymerase in the presence of α[^{35}S]UTP (1200 Ci/mmol; NEN). Riboprobes were then purified on Sephadex G50 columns. Hybridisation and posthybridisation washes were carried out according to standard protocols.[15] Slides were dehydrated, exposed to BIOMAX MR X-ray films (Amersham) for 3 days, dipped in Kodak NTB2 emulsion for 3 weeks at +4°C, then developed and counterstained with toluidine blue, coverslipped with Eukitt, and analysed under dark and bright field illumination. No hybridisation signal was detected with the α[^{35}S]-labelled sense probe (fig 3Y and not shown), confirming that the expression pattern obtained with the α[^{35}S]-labelled antisense probe was specific.

RESULTS

Denaturing high performance liquid chromatography and direct sequencing analysis of the nine exons of the *MID1* gene detected six mutant genotypes among our 14 unrelated Opitz syndrome patients (figs 1 and 2). In patient 1, a G1354A missense mutation in exon 7 changed a glycine into a serine (G452S) in the FNIII domain of the protein, the function of which remains unknown (fig 2). The mutation was also detected in the mildly symptomatic mother and her two affected sons but not in the unaffected brother. In patient 2, a C829T nonsense mutation (R277X) in exon 3 truncated the C-terminal domain, the FNIII and the coiled-coil domains of the protein, the latter domain mediating homodimerisation.[16 17] The mutation was also observed in his mother and his affected half brother but not in his unaffected brother. In patient 3 and his mildly affected mother, we identified a 4 bp deletion in the splice donor site of intron 6 (a.1285+2delGAGT), which was expected to result in either an unstable transcript or a significant alteration at the C terminal end of the protein because of aberrant splicing. Unfortunately, no cell line from patient 3 was available to test this hypothesis by reverse transcription experiments. Patient 4 carried a 4 bp insertion in exon 7 (1447–1448 insAACA), predicting a premature stop codon five amino acids downstream, truncating the MID1 protein and lacking the C terminal domain. No DNA was available for other family members. In patient 6, a C1483T nonsense mutation (R495X) truncated the C-terminal domain of the MID1 protein

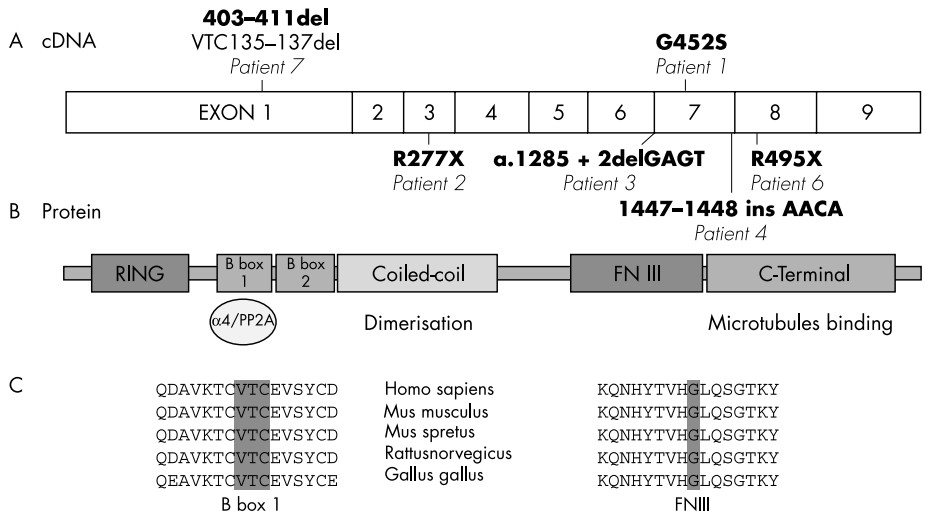

Figure 2 *MID1* mutations identified in our series. Schematic representation of *MID1* cDNA (A) and protein with respect to the different functional domains (B). Mutations identified in our series are indicated. C: MID1 alignment by CLUSTAL W* in five species is shown for the two domains where the three amino acid deletion (B-Box 1) and the missense mutation are located (FNIII). The concerned amino acids are conserved in all species.

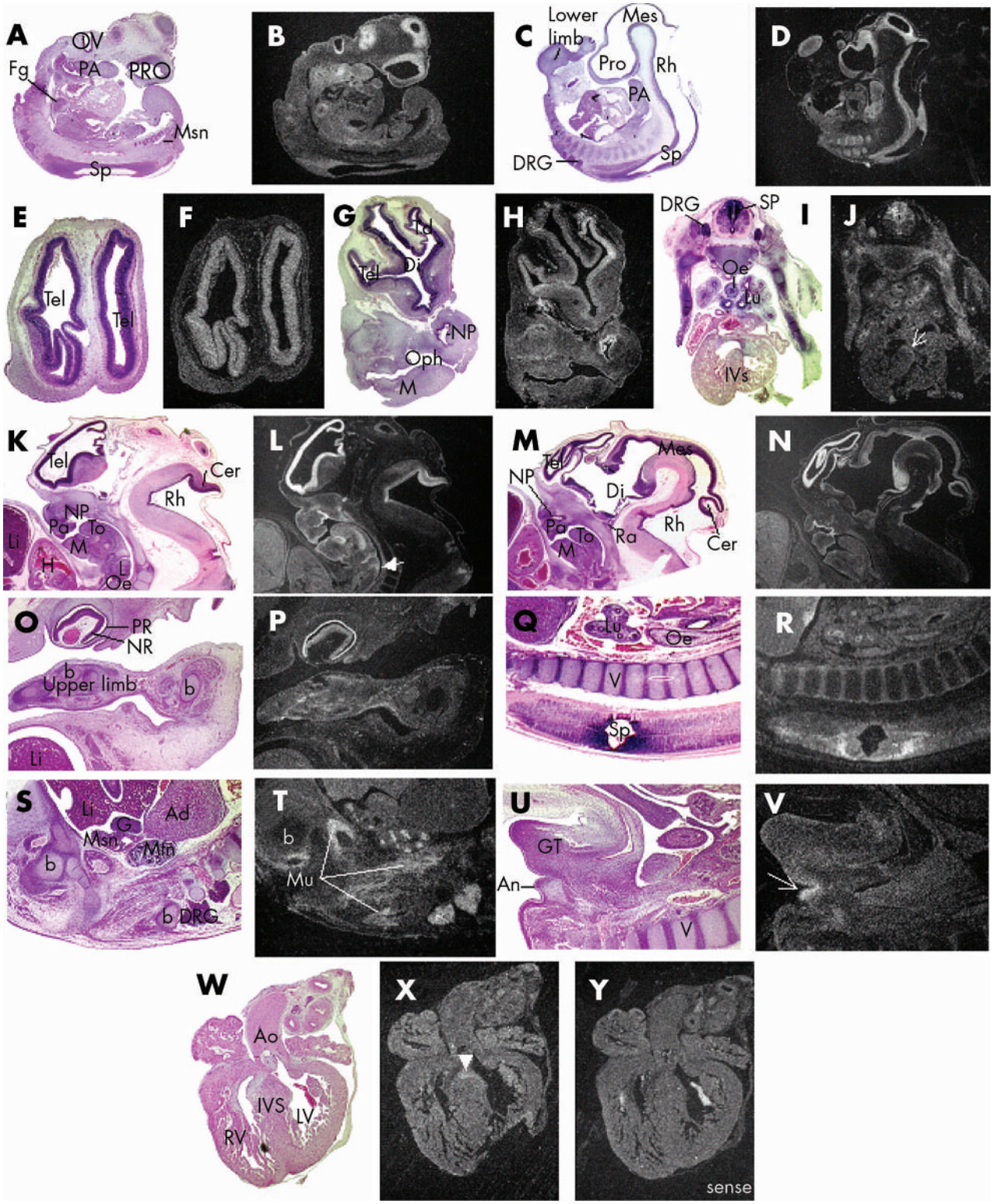

Figure 3 *MID1* expression in human embryos. *MID1* expression by in situ hybridisation on human embryos (A–V) and fetal tissues (W–Y). A, C, E, G, I, K, M, O, Q, S, U, and W are bright field illuminations of slides stained with haematoxylin, eosin, and safran adjacent to the ones presented for in situ hybridisation studies in dark field illumination (B, D, F, H, J, L, N, P, R, T, V, X, Y). (A–D) Sagittal and parasagittal sections of 5 week old human embryos showing *MID1* expression in prosencephalon (Pro), mesencephalon (Mes), rhombencephalon (Rh), spinal cord (Sp), dorsal root ganglia (DRG), otic vesicle (OV), pharyngeal arches (PA), foregut (Fg), mesonephros (Msn), and limb buds. (E–J) Transverse sections of 6 week old human embryo through the head (E–H) showing the expression in telencephalic vesicle (Tel), and in nasal (NP) and oropharynx epithelia (Oph). I and J are sections through the body at the thoracic level, showing the *MID1* transcripts in spinal cord, dorsal root ganglia, epithelium of lung (Lu), and oesophagus (Oe). Very localised *MID1* expression is observed at the top of the interventricular septum (IVS, arrow). (K–V): sagittal and parasagittal sections of 7 week old human embryo. In the head, (K-N), *MID1* is strongly expressed in telencephalon, cerebellum bud (Cer), nasopharyngeal (NP) epithelia, and at the oesophagolaryngeal junction (arrow). O and P show *MID1* expression in limb mesenchyme but not in developing bones (b) and in neural retina (NR). Note the false positive signal given by the pigmented retina (PR). Q and R show the *MID1* expression in the spinal cord and the respiratory and digestive tract epithelia. S, T: strong *MID1* expression is observed in epithelia derivatives of developing kidney (Mtn) and in muscular cells of proximal limbs (Mu). No expression is observed in adrenal glands (Ad), gonads (G), or liver (Li). U, V: *MID1* is expressed in the anal folds (arrow, An) and in the genital tubercle (GT). (W–Y) *MID1* expression at the tip of the interventricular septum is clearly observed (arrowhead) in an 8.5 week old heart as compared to the control hybridised adjacent section (Y). Ao, aorta; H, Heart; L, larynx; LV, left ventricle; M, mandible; Oe, oesophagus; Pa, palate; Ra, Rathke pouch; RV, right ventricle; To, tongue.

involved in microtubule binding. Previous immunohistochemical experiments have shown that a MID1 protein carrying a mutation in the C-terminal domain does not associate with microtubules but rather forms cytoplasmic clots.[18] Restriction analysis using the *Taq 1* restriction enzyme detected the same mutation in his mother and his young brother. Finally, a 9 bp in frame deletion in patient 9 (403-411del) abolished three conserved amino acids (valine, threonine, and cysteine) in the B-box1 domain (fig 2a) which interacts specifically with phosphatase 2A through its α4 subunit.[10] These findings suggest an important role of these three amino acids for binding the α4 subunit to the MID1 protein. The asymptomatic mother did not carry the mutation, which therefore occurred de novo.

These nucleotide changes were not observed in 100 control chromosomes. Sequencing of two additional abnormal DHPLC patterns revealed conservative polymorphisms in exon 3 and 8 (G287G and S410S) in patients 4 and 12 respectively.

X-inactivation studies revealed a skewed inactivation pattern (91%:9%) in a severely affected female with Opitz syndrome, who had hypertelorism, laryngeal diastema, oesophageal atresia, anterior placement of the anus, and developmental delay. However, we failed to detect any *MID1* mutation in this patient. The other two affected females with Opitz syndrome and the three obligate carrier mothers showed a random X-inactivation pattern.

MID1 expression pattern was studied during early human development using in situ hybridisation on human embryo sections at Carnegie stages 14 (that is, day 32), 15 (day 33), 18 (day 44), and 19 (day 47) and at 8.5 weeks of development (fig 3). At day 32, *MID1* was strongly expressed in the central nervous system, from the prosencephalon (except its most anterior part) to the spinal cord. *MID1* expression was also observed in the ventral part of the otic vesicle, the pharyngeal arches, the gastrointestinal tract, and the mesonephros (fig 3A, B). The same expression pattern was observed at day 34 in the central nervous system. In addition, a signal was observed in dorsal root ganglia, sclerotomes and limb buds (fig 3C, D). At day 44, *MID1* expression was observed in telencephalic vesicles (fig 3E, F) but not in the medial diencephalon (fig 3G, H). Also, it was expressed in the respiratory and digestive tract epithelium (fig 3I, J) and in the vertebra, where the expression was restricted to the undifferentiated mesenchyme (data not shown). Interestingly, a weak signal was detected in a restricted area of the heart, at the apex of the interventricular septum (fig 3I, J). By day 47, *MID1* expression increased in telencephalic vesicles and was also observed in the lateral part of the ventral diencephalon (fig 3O, P), the rhombencephalon (mainly in the cerebellar bud, fig 3K, N), the neurosensorial retina (fig 3K, L), the spinal cord (fig 3Q, R), and the dorsal root ganglia (fig 3S, T). Meanwhile, signal intensity decreased in the mesencephalon (fig 3M, N). A strong expression was observed in the epithelia of nasal (fig 3K–N), oral and oesophago-laryngeal cavities (fig 3K, L), the medial part of the tongue (fig 3K, L) but not laterally (fig 3M, N), in the respiratory and digestive tract epithelium (fig 3Q, R), the metanephros (fig 3Q, R), and in the anal folds (fig 3U, V). *MID1* expression was also detected in myoblasts but not in forming bones or nerves (fig 3S, T). Finally, at 8.5 weeks of development, expression of the *MID1* gene in the heart was still restricted to a small area of the interventricular septum (fig 3W–Y).

DISCUSSION

Here we report on six *MID1* mutations in a series of 14 Opitz syndrome patients including five familial forms and one sporadic case. All mutations identified in our series were novel mutations except the R495X mutation, which was previously reported in three unrelated patients.[11 18] The mutations were truncating mutations (4), an in frame 9 bp deletion and a missense mutation. They were scattered along the coding sequence, but most of them were located at the C-terminal end of the protein, either in the FNIII or the C-terminal domain. Our data support the prevalence of truncating mutations, as most cases resulted in frameshift mutations. Our study also supports the high mutation detection rate in familial forms of the disease.[12 18]

As far as genotype/phenotype correlations are concerned, it is striking to note that 4/5 patients carrying the R495X mutation had a cerebellar anomaly (family 6, two cases in the present report, one patient reported by Cox et al[18] and two by De Falco et al[11]). Vermis hypoplasia or agenesis was also present in two other patients of our series, who carried a R277X and a 1047–1448insAACA mutation, respectively. Interestingly, no developmental delay was noted in the patient carrying the 1047–1448insAACA mutation. Finally, two other cerebral anomalies were described in two patients: a corpus callosum agenesis (1312delATG[7]), and a Dandy-Walker malformation (Q347X[11]). It appears therefore that vermis hypoplasia or agenesis was the most common brain anomaly in Opitz syndrome patients with *MID1* mutations, particularly in association with the R495X mutation ($p<<0.0001$). Therefore, systematic brain exploration should be performed in patients with Opitz syndrome even in the absence of mental retardation. On the other hand, no other phenotype/genotype correlation could be established in patients carrying a *MID1* mutation. In particular, no relationship was observed between the location of the mutation and the severity of the disease.[7 11 12 18]

The role of *MID1* during embryonic development has been investigated through expression studies conducted in mouse[19] and chicken.[20] The murine *Mid1* gene is nearly ubiquitously expressed but mostly in undifferentiated cells of the central nervous system, the developing branchial arches, and the gastrointestinal and urogenital systems. The developmental expression of chicken and mouse is very similar, a feature consistent with the strong homology observed between *MID1* orthologues. However, at variance with chick, no heart expression of *Mid1* was observed in the mouse.[20] The present study shows that *MID1* expression during human development correlates with organ involvement in Opitz syndrome, namely a defect in closure of the facial and pharyngeal processes (oronasal clefts and tracheo-oesophagal fistulas) and fusion defect of urethral folds (hypospadias). Moreover, the restriction of *MID1* expression to heart interventricular septum correlates with conotruncal lesions commonly seen in Opitz syndrome. Consistently, 30% of the 39 *MID1* mutated patients reported so far presented a congenital heart defect.[7 11 12 18 21 22] *MID1* is also expressed in the cerebellum bud, correlating with cerebellar involvement in Opitz syndrome (vermis hypoplasia or agenesis). Based on this study, we suggest that cardiac defects and cerebellar anomalies belong to the Opitz syndrome spectrum.

Despite the skewed pattern of X-inactivation found in a female patient with Opitz syndrome, strongly suggesting an X-linked disease, no *MID1* mutation was identified in this patient by sequencing the whole *MID1* coding sequence. We may have failed to find a *MID1* genomic duplication[7 11 12 18 21 22] or non-coding sequence alterations. On the other hand, this could suggest another X-linked Opitz gene. Finally, considering that three obligate carrier mothers showed a random pattern of X-inactivation, it appears that X-inactivation studies in females do not help when discriminating the X-linked form of the disease.

In conclusion, the present study contributes to further delineate the molecular spectrum underlying the Opitz syndrome phenotype. Furthermore, expression studies during

early human development strongly suggest that *MID1* is involved in human heart development, and also support the view that vermis hypoplasia or agenesis should be regarded as an important clinical feature of Opitz syndrome.

ACKNOWLEDGEMENTS

We thank all the clinicians for sending us patient material: Y Alembick, V Cormier-Daire, L Faivre, B Gilbert, A Goldenberg, P Jonveau, and J Martinovic.

Authors' affiliations

L Pinson, J Augé, S Audollent, G Mattéi, H Etchevers, N Gigarel, F Razavi, M Le Merrer, J Amiel, A Munnich, S Lyonnet, M Vekemans, T Attié-Bitach, Département de Génétique et Unité INSERM U-393, Hôpital Necker-Enfants Malades, Paris, France
D Lacombe, Service de Génétique Médicale, Hôpital Pellegrin Enfants, Bordeaux, France
S Odent, Service de Génétique Médicale, Hôpital Pontchaillou, Rennes, France
G Meroni, Telethon Institute of Genetics and Medicine, Naples, Italy

LP was granted a fellowship from la Fondation pour la Recherche Médicale (FRM). This work was supported by EURExpress and HMR (*Hoechst-Marion-Roussel*) grants.

Conflicts of interest: none declared.

Correspondence to: T Attié-Bitach, Département de Génétique et Unité INSERM U-393, Hôpital Necker-Enfants Malades, Paris, France; tania.attie@necker.fr

Received 23 September 2003
Accepted for publication 4 December 2003

REFERENCES

1 **Opitz J**, Frias J, Gutenberg J, *et al*. The G syndrome of multiple congenital anomalies. *Birth Defects* 1969;**2**:95–101.
2 **MacDonald MR**, Schaefer GB, Olney AH, Tamayo M, Frias JL. Brain magnetic resonance imaging findings in the Opitz G/BBB syndrome: extension of the spectrum of midline brain anomalies. *Am J Med Genet* 1993;**46**:706–11.
3 **Gorlin R**, Cohen M, Hennekam R. Opitz oculo-genito-laryngeal syndrome (Opitz BBB/G compound syndrome). In: *Syndromes of the head and neck*. Vol 19. Oxford: Oxford University Press, 2001:988–91.
4 **Robin NH**, Feldman GJ, Aronson AL, Mitchell HF, Weksberg R, Leonard CO, Burton BK, Josephson KD, Laxova R, Aleck KA. Opitz syndrome is genetically heterogeneous, with one locus on Xp22, and a second locus on 22q11.2. *Nat Genet* 1995;**11**:459–61.
5 **Fryburg JS**, Lin KY, Golden WL. Chromosome 22q11.2 deletion in a boy with Opitz (G/BBB) syndrome. *Am J Med Genet* 1996;**62**:274–5.
6 **McDonald-McGinn DM**, Emanuel BS, Zackai EH. Autosomal dominant ''Opitz'' GBBB syndrome due to a 22q11.2 deletion. *Am J Med Genet* 1996;**64**:525–6.
7 **Quaderi NA**, Schweiger S, Gaudenz K, Franco B, Rugarli EI, Berger W, Feldman GJ, Volta M, Andolfi G, Gilgenkrantz S, Marion RW, Hennekam RC, Opitz JM, Muenke M, Ropers HH, Ballabio A. Opitz G/BBB syndrome, a defect of midline development, is due to mutations in a new RING finger gene on Xp22. *Nat Genet* 1997;**17**:285–91.
8 **Schweiger S**, Foerster J, Lehmann T, Suckow V, Muller YA, Walter G, Davies T, Porter H, van Bokhoven H, Lunt PW, Traub P, Ropers HH. The Opitz syndrome gene product, MID1, associates with microtubules. *Proc Natl Acad Sci U S A* 1999;**96**:2794–9.
9 **Cainarca S**, Messali S, Ballabio A, Meroni G. Functional characterization of the Opitz syndrome gene product (midin): evidence for homodimerization and association with microtubules throughout the cell cycle. *Hum Mol Genet* 1999;**8**:1387–96.
10 **Trockenbacher A**, Suckow V, Foerster J, Winter J, Krauss S, Ropers HH, Schneider R, Schweiger S. MID1, mutated in Opitz syndrome, encodes an ubiquitin ligase that targets phosphatase 2A for degradation. *Nat Genet* 2001;**29**:287–94.
11 **De Falco F**, Cainarca S, Andolfi G, Ferrentino R, Berti C, Rodriguez Criado G, Rittinger O, Dennis N, Odent S, Rastogi A, Liebelt J, Chitayat D, Winter R, Jawanda H, Ballabio A, Franco B, Meroni G. X-linked Opitz syndrome: novel mutations in the MID1 gene and redefinition of the clinical spectrum. *Am J Med Genet* 2003;**120A**:222–8.
12 **Gaudenz K**, Roessler E, Quaderi N, Franco B, Feldman G, Gasser DL, Wittwer B, Horst J, Montini E, Opitz JM, Ballabio A, Muenke M. Opitz G/BBB syndrome in Xp22: mutations in the MID1 gene cluster in the carboxy-terminal domain. *Am J Hum Genet* 1998;**63**:703–10.
13 **Benit P**, Kara-Mostefa A, Berthelon M, Sengmany K, Munnich A, Bonnefont JP. Mutation analysis of the hamartin gene using denaturing high performance liquid chromatography. *Hum Mutat* 2000;**16**:417–21.
14 **Hickey T**, Chandy A, Norman RJ. The androgen receptor CAG repeat polymorphism and X-chromosome inactivation in Australian Caucasian women with infertility related to polycystic ovary syndrome. *J Clin Endocrinol Metab* 2002;**87**:161–5.
15 **Wilkinson DG**. *In situ hibridization: a practical approach,* 2nd ed. Oxford: Oxford University Press, 1999.
16 **Liu J**, Prickett TD, Elliott E, Meroni G, Brautigan DL. Phosphorylation and microtubule association of the Opitz syndrome protein mid-1 is regulated by protein phosphatase 2A via binding to the regulatory subunit alpha 4. *Proc Natl Acad Sci U S A* 2001;**98**:6650–5.
17 **Short KM**, Hopwood B, Yi Z, Cox Tc. MID1 and MID2 homo- and heterodimerise to tether the rapamycin- sensitive PP2A regulatory subunit, α4, to microtubules: implications for the clinical variability of X-linked Opitz GBBB syndrome and other developmental disorders. *BMC Cell Biol* 2002;**3**:1.
18 **Cox TC**, Allen LR, Cox LL, Hopwood B, Goodwin B, Haan E, Suthers GK. New mutations in MID1 provide support for loss of function as the cause of X-linked Opitz syndrome. *Hum Mol Genet* 2000;**9**:2553–62.
19 **Dal Zotto L**, Quaderi NA, Elliott R, Lingerfelter PA, Carrel L, Valsecchi V, Montini E, Yen CH, Chapman V, Kalcheva I, Arrigo G, Zuffardi O, Thomas S, Willard HF, Ballabio A, Disteche CM, Rugarli EI. The mouse Mid1 gene: implications for the pathogenesis of Opitz syndrome and the evolution of the mammalian pseudoautosomal region. *Hum Mol Genet* 1998;**7**:489–99.
20 **Richman JM**, Fu KK, Cox LL, Sibbons JP, Cox TC. Isolation and characterisation of the chick orthologue of the Opitz syndrome gene, Mid1, supports a conserved role in vertebrate development. *Int J Dev Biol* 2002;**46**:441–8.
21 **Winter J**, Lehmann T, Suckow V, Kijas Z, Kulozik A, Kalscheuer V, Hamel B, Devriendt K, Opitz J, Lenzner S, Ropers HH, Schweiger S. Duplication of the MID1 first exon in a patient with Opitz G/BBB syndrome. *Hum Genet* 2003;**112**:249–54.
22 **Schweiger S**, Schneider R. The MID1/PP2A complex: a key to the pathogenesis of Opitz BBB/G syndrome. *Bioessays* 2003;**25**:356–66.

0021-972X/05/$15.00/0
Printed in U.S.A.

The Journal of Clinical Endocrinology & Metabolism 90(1):455–462

doi: 10.1210/jc.2004-1358

PAX8, *TITF1*, and *FOXE1* Gene Expression Patterns during Human Development: New Insights into Human Thyroid Development and Thyroid Dysgenesis-Associated Malformations

Sylvia Sura Trueba, Joëlle Augé, Géraldine Mattei, Heather Etchevers, Jélééna Martinovic, Paul Czernichow, Michel Vekemans, Michel Polak, and Tania Attié-Bitach

Institut National de la Santé et de la Recherche Médicale, Unité 457 (S.S.T., P.C., M.P.), and Service d'Endocrinologie Pédiatrique (P.C.), Hôpital Robert Debré; Institut National de la Santé et de la Recherche Médicale E0363 (S.S.T., M.P.), Faculté de Médecine Necker-Enfants Malades; and Département de Génétique/Institut National de la Santé et de la Recherche Médicale, Unité 393 (J.A., G.M., H.E., J.M., M.V., T.A.-B.), and Service d'Endocrinologie Pédiatrique (M.P.), Hôpital Necker-Enfants Malades, Paris, France

Thyroid dysgenesis (TD) is responsible for most cases of congenital hypothyroidism, a condition that affects about one in 4000 newborns. Mutations in *PAX8*, *TITF1*, or *FOXE1* may account for congenital hypothyroidism in patients with either isolated TD or TD with associated malformations involving kidney, lung, forebrain, and palate. *Pax8*, *titf1*, and *foxe1* are expressed in the mouse thyroid bud as soon as it differentiates on the pharyngeal floor. Because the spatio-temporal expression of these genes is unknown in humans, we decided to study them at different stages of human embryonic and fetal development. *PAX8* and *TITF1* were first expressed in the median thyroid primordium. Interestingly, *PAX8* was also expressed in the thyroglossal duct and the ultimobranchial bodies. Human *FOXE1* expression was detected later than in the mouse. *PAX8* was also expressed in the developing central nervous system and kidney, including the ureteric bud and the main collecting ducts. *TITF1* was expressed in the ventral forebrain and lung. *FOXE1* expression was detected in the oropharyngeal epithelium and thymus. In conclusion, the expression patterns described here show some differences from those reported in the mouse. They explain the malformations associated with TD in patients carrying *PAX8*, *TITF1*, and *FOXE1* gene mutations. (*J Clin Endocrinol Metab* 90: 455–462, 2005)

NORMAL THYROID FUNCTION is essential for development, growth, and metabolic homeostasis. Defects in any step of thyroid development (such as specification, proliferation, migration, growth, organization, differentiation, and survival) may result in a congenital anomaly and/or impaired hormonogenesis, leading to variable degrees of hypothyroidism. Congenital hypothyroidism (CH) affects one in 4000 newborns, and thyroid dysgenesis (TD) accounts for about 85% of the cases; the other 10–15% result from functional disorders in hormone synthesis. TD includes absence of thyroid tissue (athyreosis), presence of ectopic tissue, as well as hypoplasia of an orthotopic gland. Ectopic thyroid is by far the most common cause of CH, followed by athyreosis. In contrast, thyroid hypoplasia is very rare (1). TD is usually sporadic, although some cases of familial forms support Mendelian inheritance (2–4).

In the human embryo, the thyroid gland is the first endocrine gland to develop. In its mature form, it is composed of two different hormone-producing cells, namely, thyroid follicular cells and parafollicular cells, also called C cells. These two cell types have distinct embryonic origins. The former derives from the floor of the foregut (median primordium), whereas the latter arises from cells within the ultimobranchial body (lateral primordia) (5). A morphological and anatomical description of thyroid development is summarized in Table 1.

A number of thyroid follicular cell-specific transcriptional regulators have been identified in various animal models. Three of these genes, namely, the paired domain factor *Pax8*, *Titf1* (also known as *Nkx2a*, *Ttf-1*, or *T/ebp*), and *Foxe1* (also called *Titf2* or *Ttf-2*), are expressed in the thyroid gland during mouse development until adult life (6–9) and are required for normal thyroid development. Indeed, in all three knockout models, a thyroid primordium forms, but fails to produce a definitive thyroid gland. In the $pax8^{-/-}$ knockout mouse, the primary thyroid primordium disappears, leading to a complete absence of follicular cells (10). In the $titf1^{-/-}$ knockout mouse, the thyroid primordium is lost by apoptosis, and neither thyroid follicular cells nor C cells can be found (11). Finally, in the $titf2^{-/-}$ knockout mouse, the thyroid primordium fails to migrate, and in half of the fetuses on embryonic d 15.5 (E15.5) it is still detectable, but by birth it has completely disappeared (12). In addition, mutations of these genes have been identified in humans providing a molecular basis for some cases of CH, frequently with associated anomalies (13–15). In the present study we describe the expression patterns of *PAX8*, *TITF1*, and *FOXE1* genes and thyroglobulin protein during human develop-

First Published Online October 19, 2004

Abbreviations: CH, Congenital hypothyroidism; CS, Carnegie staging; E15.5, embryonic d 15.5; TD, thyroid dysgenesis.

TABLE 1. Timing of events during human thyroid development

Developmental stage[a]	Anatomical or morphological events in thyroid development
CS10 (22 d)	Thickening of the floor of the primitive pharynx between the diverging aorta
CS12 (26 d)	Outgrowth and budding of the median thyroid primordium from the floor of the primitive pharynx. The inferior part of the fourth pharyngeal pouch forms the ultimobranchial body.
CS13 (28 d)	The median primordium grows caudally and appears bilobed. It is connected to the primitive pharynx by the thyroglossal duct.
CS14 (32 d)	Migration of the median primordium, still connected to the epithelium of the primitive pharynx
CS15 (33 d)	The thyroglossal duct starts to break down.
CS16 (37 d)	The median primordium consists of two lobes, an isthmus and a pedicle remnant. The continuity with the primitive pharynx is lost.
CS18 (44 d)	Median primordium fuses with the lateral components derived from the ultimobranchial bodies.
CS19 (48 d)	The thyroid reaches its final position in front of the trachea just inferior to the cricoid cartilage. It begins to form follicles.
10–12 wk	Follicles containing colloid become visible. The thyroid is able to incorporate iodine into thyroid hormones.

[a] Embryos specifically assigned to one of the recognized CS. The estimated age to the CS is given in *parentheses* (5, 45, 46).

ment. Comparison of these expression patterns with those observed in animal models provides new insights into human thyroid development and delineates a conceptual framework to better assess the phenotypes of patients bearing mutations in these genes.

Materials and Methods

Tissues

Human embryos and fetal tissues were obtained from legally terminated pregnancies in agreement with French legislation, following national ethics committee recommendations, and with approval from the Necker Hospital ethics committee. Embryonic stages were determined according to morphological criteria of the Carnegie staging (CS) classification (16). Five different developmental stages were studied: two embryos at CS14 (d 33), two embryos at CS15 (d 34), two embryos at CS19 (d 47–48), and two fetuses of 9 and 11 wk of development, respectively. Tissues were fixed in 4% phosphatase-buffered paraformaldehyde, dehydrated, and embedded in paraffin blocks, and 5-μm-thick serial sections were cut.

Hybridization probes

Coding sequences of *PAX8* (a 174-bp fragment in exon 6 corresponding to positions 603–776), *TITF1* (a 204-bp fragment in exon 2 between positions 159 and 362), and *FOXE1* (a 203-bp fragment between positions 583 and 785) were amplified by PCR from human genomic DNA using the following forward and reverse primers: *PAX8* forward, 5′-GATCAGGATAGCTGCCGACT-3′; *PAX8* reverse, 5′-GTTGTACCTGCTCGCCTTTG-3′; *TITF1* forward, 5′-TACAAGAAAGTGGGCATGGA-3′; *TITF1* reverse, 5′-CAGGTTGCCGTTGCAGTAG-3′; *FOXE1* forward, 5′-CCGTCTATGCAGGCTACGC-3′; and *FOXE1* reverse, 5′-CTGGTAGCCGGTGGTGGTAG-3′. The amplified sequences were specific for each gene respectively (not shared by other family members). A T7 (TAATACGACTCACTATAGGGAGA) extension was added to primers in the 5′ position to produce experimental (antisense) and control (sense) DNA template to generate probes. The antisense DNA template was generated after amplification using a forward primer and a T7 added reverse primer. The sense DNA template was produced from a fragment amplified with a reverse primer and a T7 added forward primer. Probes were transcribed from the corresponding sense and antisense DNA templates in the presence of [α-^{35}S]UTP (1200 Ci/mmol; NEN Life Science Products, Boston, MA) and were purified on Sephadex G-50 columns.

In situ hybridization

In situ hybridizations were performed as previously described (17, 18) with 15 μl 50% formamide, 300 mM NaCl, 20 mM Tris-HCl (pH 7.4), 5 mM EDTA, 10% dextran sulfate, 1% Denhardt's solution, 10 mM NaH_2PO_4, 0,5 mg/ml yeast total RNA, and the [α-^{35}S]UTP-labeled sense or antisense probes to a final concentration of 5×10^4 cpm/μl. Slides were incubated overnight at 50 C in a humidified chamber. After hybridization, slides were washed, dipped in Kodak NTB2 photographic emulsion (Eastman Kodak, Rochester, NY) for 3 wk at 4 C, developed, fixed, counterstained with toluidine blue, dehydrated, and coverslipped. They were analyzed under dark- and brightfield illumination. Adjacent slides were hematoxylin/eosin-stained for morphological studies.

Immunohistochemistry

Sections were heated in a microwave oven at 750 watts twice for 4 min each time to retrieve the antigen sites. The sections were additionally permeabilized with PBS- 0.1%Triton and incubated for 1 h at room temperature with universal blocking reagent (BioGenex, San Ramon, CA) and then overnight at 4 C with a commercial polyclonal antihuman thyroglobulin antibody (DakoCytomation, Carpinteria, CA) diluted 1:5000. Staining procedures and chromogenic reactions were carried out according to the protocols of the Super Sensitive Concentrated Detection System for alkaline phosphatase labeling (BioGenex) and Fast Red (Sigma Fast, Sigma-Aldrich Corp., St. Louis, MO). Sections were counterstained with hemalum. Control experiments were performed using a commercial mixture of mouse IgG1, IgG2a, IgG2b, IgG3, and IgM (DakoCytomation) instead of the primary antibody.

Results

PAX8

At CS14, the *PAX8* gene was strongly expressed in the median thyroid anlage (Fig. 1, A and B, *arrows*) and laterally in the ectodermic region of the fourth pharyngeal arch (Fig. 1, Q and R, *arrow*). At CS15, *PAX8* expression was observed in the median thyroid anlage (Fig. 1, E and F), the thyroglossal duct cells (Fig. 1F, *arrowhead*), and laterally in a deeper cell population that is consistent with the ultimobranchial body (Fig. 1, S and T, *arrow*). At CS19, after fusion of median and lateral components, the developing thyroid continued to strongly express *PAX8* (Fig. 1, I and J). This signal persisted in follicular cells at fetal stages (Fig. 1, M and N).

Outside the thyroid, expression of the *PAX8* gene was also observed in the otic vesicle, the central nervous system, and the developing kidney. At CS14, *PAX8* transcripts were found in the ventral part of the otic vesicle and in the midbrain-hindbrain boundary (Fig. 2, A and B, *arrowhead* and *arrow*, respectively). At CS15, in addition to the midbrain-hindbrain boundary (Fig. 2, E and F, *arrowhead*), *PAX8* was expressed in the lateral part of the spinal cord along the

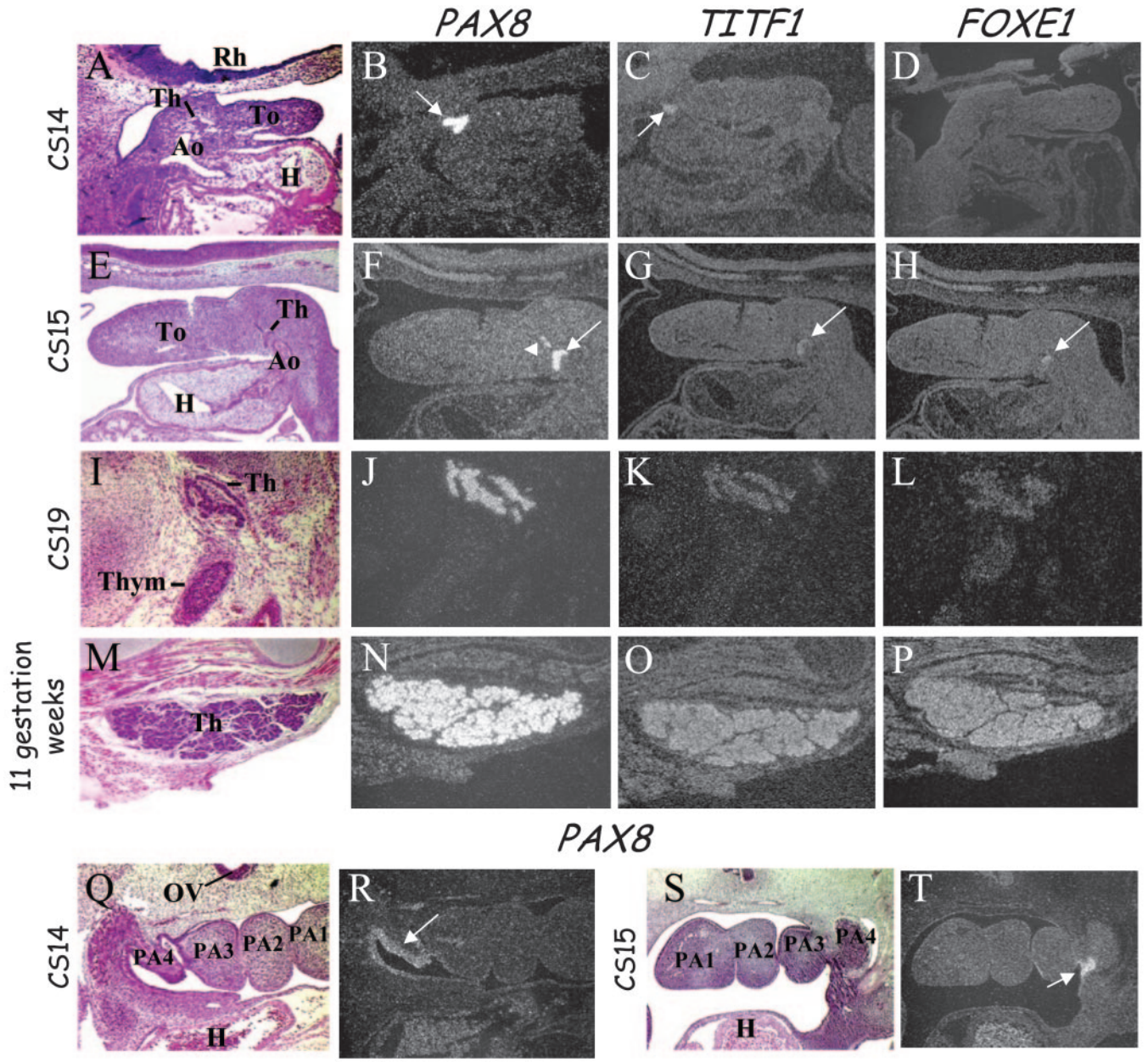

FIG. 1. Expression of the *PAX8*, *TITF1*, and *FOXE1* genes during human thyroid gland development. Hematoxylin/eosin-stained sections under brightfield illumination (A, E, I, M, Q, and S) and adjacent hybridized sections under darkfield illumination (B–D, F–H, J–L, N–P, R, and T). A–D, CS14; sagittal sections through the median thyroid primordium (Th) showing strong *PAX8* (*arrow*, B) and weak *TITF1* (*arrow*, C) expression. *FOXE1* expression is not detected. E–H, CS15; sagittal sections through median thyroid primordium. *PAX8* is strongly expressed in the thyroid primordium (*arrow*, F) and in the thyroglossal duct cells (*arrowhead*, F). *TITF1* (*arrow*, G) and *FOXE1* (*arrow*, H) are weakly detected in the thyroid anlage. I–L, CS19; sagittal sections through developing thyroid. The three genes are expressed, strongly for *PAX8*. *FOXE1* is also detected in thymus (Thym; L). M–P, Eleven weeks of development; transverse sections through fetal thyroid gland showing similar expression levels of the three genes as in thyroid at CS19. Parasagittal sections at CS14 (Q and R) and CS15 (S and T) show *PAX8* expression in the fourth pharyngeal arch ectoderm (PA4; *arrow*, R) and in the ultimobranchial body (*arrow*, T). Ao, Aorta; H, heart; OV, otic vesicle; Rh, rhombencephalon; To, tongue.

rostro-caudal axis (Fig. 2, E and F, *arrow*). At CS19, *PAX8* expression was observed in the ventral part of the myelencephalon (Fig. 2, I and J, *arrow*) and the isthmus, as well as in the dorsal part of the cerebellum anlage (Fig. 2, I–L, * and *arrow* in L, respectively). In the spinal cord, *PAX8* mRNAs were located laterally in the mantle layer of both the alar and the basal plates, next to the neuroepithelial layer (Fig. 2, M and N, *arrows*). In the developing kidney, *PAX8* transcripts were found in the mesonephros at CS14 (Fig. 2, C and D), in the metanephric blastema, and weakly in the ureteric bud at CS15 (Fig. 2, G and H). At CS19, *PAX8* was strongly expressed in the condensed mesenchyme (Fig. 2, O and P, *white arrows*) and in the ureteric bud giving rise to the collecting duct system (Fig. 2, O and P, *arrowhead*), but not at its terminal

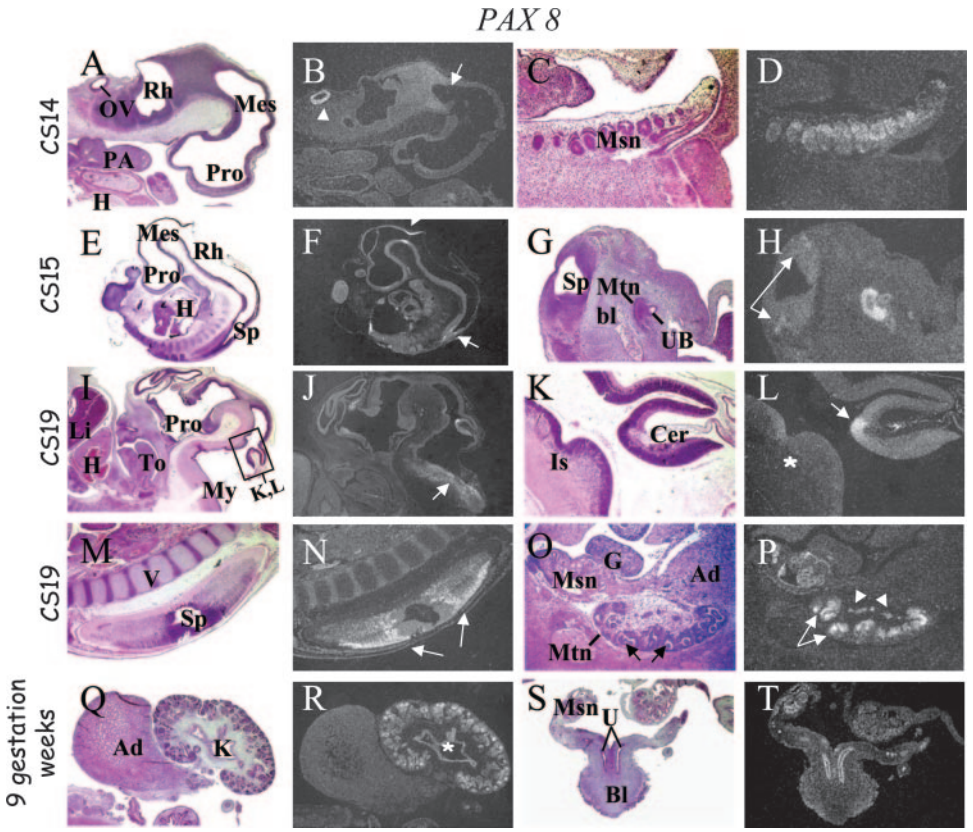

FIG. 2. *PAX8* expression during human development. Hematoxylin/eosin-stained sections under brightfield illumination (A, C, E, G, I, K, M, O, Q, and S) and adjacent hybridized sections under darkfield illumination (B, D, F, H, J, L, N, P, R, and T). At CS14 (A–D), *PAX8* expression is observed in the otic vesicle (OV; *arrowhead*, B), the midbrain-hindbrain boundary (*arrow*, B), and the mesonephros (Msn; C and D). At CS15 (E–H), *PAX8* expression is observed in midbrain-hindbrain boundary (*arrowhead*, F) and the spinal cord (Sp; *arrows*, F and H). In the developing kidney, *PAX8* is strongly expressed in the metanephric blastema (Mtn bl; G and H) and is weakly expressed in the ureteric bud (UB; G and H). At CS19 (I and J), *PAX8* expression is observed in the myelencephalon (My; *arrow*, J). K and L, Magnifications of the region boxed in I where *PAX8* is detected in the ventral region of the isthmus (Is; *, *L*) and cerebellum (Cer; *arrow*, L). It is also expressed in the lateral borders of the neuroepithelial layer of the spinal cord (M; *arrows*, N). At CS19 (O and P), *PAX8* is highly expressed in the condensed mesenchyme of the metanephros (Mtn; *white arrows*, P). It is weakly expressed in the ureteric bud (*arrowheads*, P), but is absent at its terminal tips (*black arrows*, O). *PAX8* expression is maintained in the mesonephros. In fetal kidney (K) at 9 wk of development (Q–T), *PAX8* is highly expressed in developing nephrons (mesenchyme undergoing epithelialization), in S-shaped bodies, and also in the collecting system (*, R), but not at the terminal tips. The ureter (U) arriving at the bladder (Bl) expresses *PAX8*. Ad, Adrenal; G, gonad; H, heart; Li, liver; Mes, mesencephalon; PA, pharyngeal arches; Pro, prosencephalon; Rh, rhombencephalon; To, tongue; V, vertebral column.

tips (Fig. 2, O and P, *black arrows*). Finally, at 9 wk of development, the highest *PAX8* expression was observed in the immature nephrons and in the condensed metanephric blastema, but also in the main collecting ducts (Fig. 2, Q and R, *). *PAX8* transcripts were also observed in the mesonephric ducts and the ureters reaching the bladder (Fig. 2, S and T).

TITF1

At CS14 and CS15, the *TITF1* gene was weakly expressed in the median thyroid primordium (Fig. 1, C and G, *arrows*). This expression was also observed when the thyroid gland had reached its final position at CS19 (Fig. 1K) as well as in the fetal gland (Fig. 1O).

In addition to thyroid expression, *TITF1* was detected in the forebrain and the lung. At CS15, *TITF1* was strongly expressed in the ventral forebrain, the diencephalon, and the nearby telencephalon (Fig. 3, A and B, *arrows*). At CS19, *TITF1* expression in the ventral diencephalon was located in the hypothalamic floor and the infundibulum (Fig. 3, C and D, *arrowhead*), whereas the expression in the telencephalon corresponded to the developing basal ganglia territory (Fig. 3, C and D, *arrow*). During lung development, *TITF1* was detected in the lung bud at CS14 (Fig. 3, E and F, *arrowhead*). At CS19, when the primary bronchi undergo dichotomous divisions as they grow into the surrounding splanchnic mesenchyme, *TITF1* was expressed in the primary bronchi epithelia (Fig. 3, G and H, *arrows*), whereas at 9 wk of development only the alveolar primordia epithelium retained *TITF1* expression (Fig. 3, I and J).

FOXE1

Among the three genes studied, *FOXE1* showed the weakest hybridization signal. It was first expressed at CS15 in the thyroid primordium (Fig. 1, D and H, *arrow*) and then persisted in the thyroid gland throughout development (Fig. 1, L and P).

Outside the thyroid, *FOXE1* signal, at CS19, was detected in the thymus (Fig. 1L and Fig. 3, K and L) and weakly in the

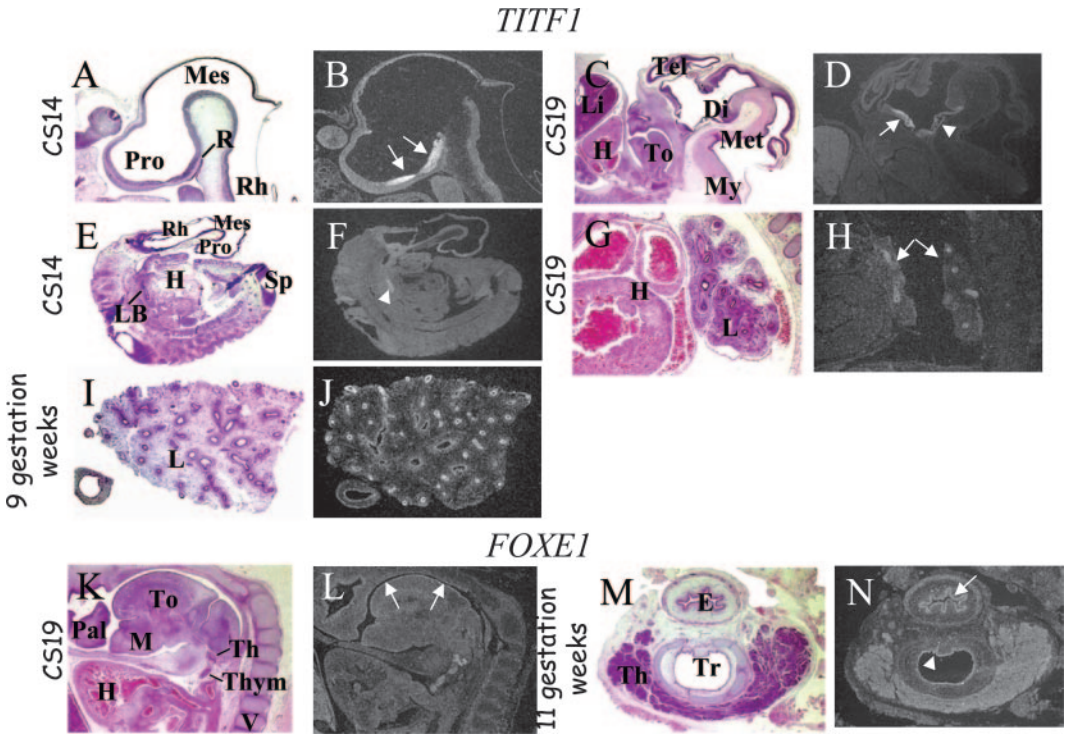

FIG. 3. *TITF1* and *FOXE1* gene expression during human development. A and B, At CS15, in sagittal sections *TITF1* transcripts are clearly found in the ventral part of the prosencephalon (Pro). At CS19 (C and D), *TITF1* hybridization signal is detected in the ventral diencephalon (Di; *arrowhead*, D), and in the nearby telencephalon (Tel; *arrow*, D). E–L, *TITF1* expression is observed in the lung bud at CS14 (LB; *arrowhead*, F) and in the lung epithelium at CS19 (*arrows*, H). At 9 wk of development, sections through the lung show that *TITF1* is expressed only in the epithelium of the most recently formed branches. *FOXE1* expression is detected in thyroid (Th) and thymus (Thym) at CS19 (K and L). A faint signal is present in the thin layer of the oropharyngeal epithelium (*arrows*, L). At 11 wk of development (M and N), *FOXE1* is detected in the tracheal (Tr; *arrowhead*, N) and esophageal (E; *arrow*, N) epithelia. H, Heart; Li, liver; M, mandible; Mes, mesencephalon; Met, metencephalon; My, myelencephalon; Pal, palate; R, Rathke's pouch; Rh, rhomboencephalon; Sp, spinal cord; To, tongue; V, vertebral column.

oropharyngeal epithelium (Fig. 3L, *arrows*). At 11 wk of development, a weak *FOXE1* signal was observed in the tracheal and esophageal epithelium (Fig. 3, M and N, *arrowhead* and *arrow*, respectively).

For all three genes, comparison of sense (data not shown) and antisense hybridization signals allowed specific signal detection from background.

Thyroglobulin

The thyroglobulin protein was not detected during early thyroid organogenesis and migration at CS15 (Fig. 4, A and B). It was first detected when the thyroid had reached its final position in front of the trachea at CS19 (Fig. 4, C and D). Thyroglobulin was still found at 11 wk of development in the thyroid gland (Fig. 4, E and F).

Discussion

Thyroid expression of *PAX8*, *TITF1*, and *FOXE1* during development supports their direct implication in TD when mutated and accounts for the associated malformations. Comparison of the expression patterns of the three genes during murine and human development highlights some differences that are summarized in Table 2.

The first difference observed between human and murine thyroid development concerns the time course of *FOXE1* gene expression. In mice, *titf1* and *titf2* are expressed as early as E8.5 in the floor of the foregut before budding of the median thyroid anlage, whereas *pax8* is expressed in the area of thyroid evagination on E10.5 (8, 9). At the earliest stages of human development studied (CS14), the median thyroid primordium starts to migrate caudally, analogous to E10.5 in mouse development. Both the *PAX8* and *TITF1* genes were expressed in the migrating primordium, whereas *FOXE1* transcripts were detected only at the CS15 stage and not as early as expected from mouse data. The human thyroglobulin promoter contains three binding sites for TITF1, one for PAX8, and one for FOXE1 (19). Nevertheless, thyroglobulin is produced only once the thyroid gland has reached its final position, as described for the mouse, suggesting that additional mechanisms exist to regulate the expression of thyroid-specific genes. The second difference concerns the expression domains of *TITF1* and *PAX8*. In the mouse, *titf1* is expressed in the fourth pharyngeal pouch, giving rise to parafollicular cells. C Cells still express *titf1* in the mature thyroid gland (7, 10). In the human, no *TITF1* expression, but *PAX8* expression, was observed at the surface ectoderm of the fourth pharyngeal pouch, followed shortly thereafter by expression in an inner structure consistent with the ultimobranchial body.

Experimental data in the chick and mouse have demonstrated that neural crest cells colonize the ultimobranchial body during development, giving rise to C cells, and it has

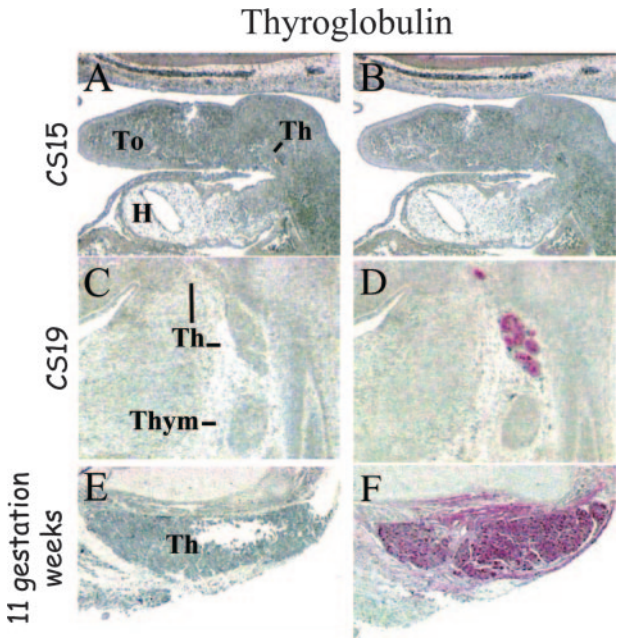

FIG. 4. Thyroglobulin production during human thyroid gland development. Hemalum-stained sections under brightfield illumination with the control of mouse Igs (A, C, and E) and adjacent sections with polyclonal antihuman thyroglobulin antibody (B, D, and F). A and B, CS15; sagittal sections through the median thyroid primordium (Th) showing no thyroglobulin production. C and D, CS19; sagittal sections through developing thyroid. The thyroglobulin protein is detected in the thyroid gland as well as in the remnant located in the migration track. E and F, Eleven weeks of development; transverse sections through the fetal thyroid gland producing thyroglobulin. H, Heart; Thym, thymus; To, tongue.

been assumed that the same would be true in all mammals (20–22). Merida-Velasco *et al.* (23) suggested that in human embryos, the ultimobranchial body is colonized at CS15 by cells of ectodermic origin, arising from the posterior margin of the fourth pharyngeal cleft. Indeed, at CS14 we observed *PAX8* expression in the surface ectoderm of the fourth pharyngeal arch and at CS15 in a deeper cell population, corresponding presumably to the ultimobranchial body. These results add additional evidence to the possible contribution of ectodermic cells to the ultimobranchial body.

TABLE 2. Human and murine *PAX8*, *TITF1*, and *FOXE1* gene expression patterns

Features shared between human and mouse	Features observed in human or mouse only
PAX8	
Thyroid	4th pharyngeal pouch in human
Brain and spinal cord	Ureteric bud and derivatives in human
Otic vesicle	
Metanephric blastema and derivatives	
TITF1	
Thyroid	4th pharyngeal pouch in mouse
Lung	
Ventral part of forebrain	
FOXE1	
Thyroid	Later onset in the median thyroid primordium in human
Foregut	Thymus in human

The *PAX8* gene has been implicated in the development and maintenance of the follicular cell phenotype by activating *thyroperoxidase*, *sodium/iodide symporter*, and *thyroglobulin* genes without apparent effect on C cell development (10, 24). Whether follicular cells also originate from the ultimobranchial body is still debated. Thyroglobulin-containing follicles have been identified in the ultimobranchial body-derived structures of the dog (25, 26). In addition, cases of lateral ectopic thyroid or lateral thyroidal cysts with follicles support the premise that some thyroid follicular cells may derive from the ultimobranchial body in humans (27, 28). *PAX8* expression in the ultimobranchial body observed in our study adds to the view that the lateral primordia may produce thyroid follicular cells in humans.

During normal development, the thyroglossal duct disappears, but remnants may persist and form cysts anywhere along the course of thyroid migration. Histological studies of these remnants show that follicles and colloid are often present (29–31). The *PAX8* gene expression observed in the thyroglossal duct cells suggests that this structure represents a cellular track left by the migrating thyroid anlage rather than a preestablished pathway for thyroid migration, and its expression may explain the capacity of these cells to differentiate into follicular cells.

The expression pattern of the *PAX8* gene in the central nervous system is similar to that observed in the mouse, *i.e.* restricted to the midbrain-hindbrain boundary, then to the myelencephalon and the spinal cord (8). However, neither homozygous $pax8^{-/-}$ mice nor humans with heterozygous *PAX8* mutations have been reported to show a central nervous system defect. This could be due to the redundancy of another gene of the same family, *PAX2*, which is similarly expressed in the central nervous system during both mouse and human development (32–35). In addition to being expressed in the condensed mesenchyme of the developing kidney, human *PAX8* is expressed in the mesonephric duct, the ureteric bud, and the collecting ducts (but not at their tips). This is different from what has been described in the mouse, where *pax8* expression has never been observed in the Wolffian duct or in the ureteric bud or its derivatives (8). Kidney malformations are not classically associated with *PAX8* mutations. Yet, two TD patients with either unilateral renal agenesis or left-sided uretero-pelvic obstruction, respectively, were found to carry a heterozygous *PAX8* mutation (36). It is worth noting that this pattern of malformations is consistent with the human-specific pattern of *PAX8* expression in the ureter and pelvis. It is likely, therefore, that renal malformations associated with TD could be underestimated, because no systematic renal studies have been performed in patients with TD. If confirmed, the presence of renal anomalies would be highly suggestive of *PAX8* involvement in TD. Finally, no *PAX8* homozygous mutations have been reported in humans. Such homozygous mutations could lead to a severe or lethal phenotype (*e.g.* bilateral renal agenesis), as described for other *PAX* genes (37, 38) (Ayme, S., and N. Philip, unpublished observations).

In humans and rats, *TITF1* transcripts are detected during lung development. *TITF1* is first expressed in epithelial cells and becomes progressively restricted to distal branches. No *TITF1* expression is detected in main bronchial epithelial cells

or in the proximal respiratory compartments of the fetal lung. This expression pattern is consistent with that described during rat development and in human fetal stages (7, 39). The expression of *TITF1* in the distal part of the lung is also consistent with its role in surfactant production and regulation and explains the postnatal respiratory distress syndrome in patients bearing a *TITF1* mutation (14, 40). *TITF1* gene expression is also observed in the ventral part of the forebrain. In the diencephalon, its expression is restricted to the hypothalamic area and then to the infundibulum. In the telencephalic floor, the signal is observed in an area corresponding to the developing striatum and the paleostriatum, as previously described (7, 9, 41). Hypotonia and dyskinesia associated with changes in the basal ganglia and pituitary in patients with *TITF1* mutations are consistent with the expression pattern of *TITF1* in the central nervous system (14, 39, 42).

During human development, a barely detectable *FOXE1* signal was observed in the pharyngeal epithelium and later in the tracheal and esophageal epithelium. In the mouse, *titf2* is also weakly expressed in the foregut endoderm and the visceral epithelium of pharyngeal arches (6, 9). However, the *FOXE1* expression pattern is consistent with the malformations associated with *FOXE1* mutations (6, 12). Indeed, both knockout mice and four reported patients with a *FOXE1* mutation displayed TD and cleft palate (13, 43). In addition, *FOXE1* mRNAs were detected in the human thymus, as previously described (44), but no abnormal thymus or immunodeficiency has been reported in the rare patients carrying a *FOXE1* mutation. An immunological analysis of these patients should allow evaluation of the biological significance of *FOXE1* expression in the thymus.

In conclusion, the present study of *PAX8*, *TITF1*, and *FOXE1* gene expression during human development sheds new light on thyroid development and on the impact of mutations in these genes. This study also highlights the differences in gene expression between species. Indeed, *PAX8* is expressed in all territories that may give rise to thyroid follicular cells and in the ultimobranchial bodies, adding support to the contribution of this structure to the follicular cell population. At variance with the mouse gene, *PAX8* was expressed in the ureteric bud and some derivatives, suggesting that patients with a *PAX8* mutation should be screened for kidney malformations. Also at variance with the mouse gene, *TITF1* expression was not detected in the pharyngeal arches, and human *FOXE1* expression in the thyroid anlage was observed later than that in the mouse and was present in the thymus. Finally, the expression patterns of the three genes correlate well with the phenotypes observed in patients carrying mutations of the corresponding gene.

Acknowledgments

We thank Marie-Claire Gubler and Féréchté Encha-Razavi for helpful discussions. We are grateful to Guy Van Vliet and Arnold Munnich for comments and suggestions about the manuscript.

Received July 13, 2004. Accepted October 11, 2004.

Address all correspondence and requests for reprints to: Dr. Michel Polak, Service d'Endocrinologie Pédiatrique, Hôpital Necker-Enfants Malades, 149 rue de Sèvres, 75743 Paris Cedex 15, France. E-mail: michel.polak@nck.ap-hop-paris.fr.

This work was supported by Association Française pour le Dépistage et la Prévention des Handicaps de l'Enfant, Hoechst-Marion-Roussel, and EURExpress. S.S.T. is supported by a Convention Industrielle de Formation par la Recherche grant in collaboration with HRA Pharma directed by Dr. André Ulmann and the Ministère de l'Education Nationale de la Recherche et de la Technologie.

References

1. **Toublanc JE** 1992 Comparaison of epidemiological data on congenital hypothyroidism in Europe with those of other parts in the world. Horm Res 38:230–235
2. **Castanet M, Lyonnet S, Bonaïti-Pellié C, Polak M, Czernichow P, Léger J** 2000 Familial forms of thyroid dysgenesis among infants with congenital hypothyroidism. N Engl J Med 343:441–442
3. **Castanet M, Polak M, Bonaïti-Pellié C, Lyonnet S, Czernichow P, Léger J** 2001 Nineteen years of national screening for congenital hypothyroidism: familial cases with thyroid dysgenesis suggest the involvement of genetic factors. J Clin Endocrinol Metab 86:2009–2014
4. **Léger J, Marinovic D, Garel C, Bonaïti-Pellié C, Polak M, Czernichow P** 2002 Thyroid developmental anomalies in first degree relatives of children with congenital hypothyroidism. J Clin Endocrinol Metab 87:575–580
5. **Hoyes AD, Kershaw DR** 1985 Anatomy and development of the thyroid gland. Ear Nose Throat J 64:318–333
6. **Dathan N, Parlato R, Rosica A, De Felice M, Di Lauro R** 2002 Distribution of the titf2/foxe1 gene product is consistent with an important role in the development of foregut endoderm, palate, and hair. Dev Dyn 224:450–456
7. **Lazzaro D, Price M, De Felice M, Di Lauro R** 1991 The transcription factor TTF-1 is expressed at the onset of thyroid and lung morphogenesis and in restricted regions of the foetal brain. Development 113:1093–1104
8. **Plachov D, Chowdhury K, Walther C, Simon D, Guenet JL, Gruss P** 1990 Pax8, a murine paired box gene expressed in the developing excretory system and thyroid gland. Development 110:643–651
9. **Zannini M, Avantaggiato V, Biffali E, Arnone MI, Sato K, Pischetola M, Taylor BA, Phillips SJ, Simeone A, Di Lauro R** 1997 TTF-2, a new Forkhead protein, shows a temporal expression in the developing thyroid which is consistent with a role in controlling the onset of the differentiation. EMBO J 16:3185–3197
10. **Mansouri A, Chowdhury K, Gruss P** 1998 Follicular cells of the thyroid gland require Pax8 gene function. Nat Genet 19:87–90
11. **Kimura S, Hara Y, Pineau T, Fernandez-Salguero P, Fox CH, Ward JM, Gonzalez FJ** 1996 The T/ebp null mouse: thyroid-specific enhancer-binding protein is essential for the organogenesis of the thyroid, lung, and ventral forebrain. Genes Dev 10:60–69
12. **De Felice M, Ovitt C, Biffali E, Rodriguez-Mallon A, Arra C, Anastassiadis K, Macchia PE, Mattei MG, Mariano A, Schöler H, Macchia V, Di Lauro R** 1998 A mouse model for hereditary thyroid dysgenesis and cleft palate. Nat Genet 19:395–398
13. **Clifton-Bligh R, Wentworth JM, Heinz P, Crisp MS, John R, Lazarus JH, Ludgate M, Chatterjee K** 1998 Mutation of the gene encoding human TTF-2 associated with thyroid agenesis, cleft palate and choanal atresia. Nat Genet 19:399–401
14. **Krude H, Schuetz B, Biebermann H, von Moers A, Schnabel D, Neitzel H, Tönnies H, Weise D, Lafferty A, Schwarz S, De Felice M, von Deimling A, van Landeghem F, Di Lauro R, Grüters A** 2002 Choreoathetosis, Hypothyroidism, and pulmonary alterations due to human NKX2.1 haploinsufficiency. J Clin Invest 109:475–480
15. **Macchia PE, Lapi P, Krude H, Pirro MT, Missero C, Chiovato L, Souabni A, Baserga M, Tassi V, Pinchera A, Fenzi G, Grüters A, Busslinger M, Di Lauro R** 1998 Pax8 mutations associated with congenital hypothyroidism caused by thyroid dysgenesis. Nat Genet 19:83–86
16. **O'Rahilly R, Müller F** 1987 Developmental stages in human embryos. Washington DC: Carnegie Institution of Washington
17. **Crosnier C, Attie-Bitach T, Encha-Razavi F, Audollent S, Soudy F, Hadchouel M, Meunier-Rotival M, Vekemans M** 2000 JAGGED1 gene expression during human embryogenesis elucidates the wide phenotypic spectrum of Alagille syndrome. Hepatology 32:574–581
18. **Wilkinson DG** 1992 In situ hybridization: a practical approach. Oxford, UK: IRL Press
19. **Kambe F, Seo H** 1997 Thyroid-specific transcription factors. Endocr J 44: 775–784
20. **Le Douarin N, Le Lievre C** 1970 Embryologie experimentale: demonstration de l'origine neurale des cellules a calcitonine du corps ultimobranchial chez l'embryon de poulet. C R Hebd Seances Acad Sci D 270:2857–2860
21. **Pearse AG, Polak JM** 1971 Cytochemical evidence for the neural crest origin of mammalian ultimobranchial C cells. Histochemie 27:96–102
22. **Polak JM, Pearse AG, Le Lievre C, Fontaine J, Le Douarin NM** 1974 Immunocytochemical confirmation of the neural crest origin of avian calcitonin-producing cells. Histochemistry 40:209–214
23. **Merida-Velasco JA, Garcia-Garcia JD, Espin-Ferra J, Linares J** 1989 Origin of

the ultimobranchial body and its colonizing cells in human embryos. Acta Anat 136:325–330
24. **Pasca di Magliano M, Di Lauro R, Zannini M** 2000 Pax8 has a key role in thyroid cell differentiation. Proc Natl Acad Sci USA 97:13144–13149
25. **Kameda Y, Ikeda A** 1980 Immunohistochemical study of the C-cell complex of dog thyroid glands with reference to the reactions of calcitonin, C-thyroglobulin and 19S thyroglobulin. Cell Tissue Res 208:405–415
26. **Kameda Y, Shigemoto H, Ikeda A** 1980 Development and cytodifferentiation of C cell complexes in dog fetal thyroids. An immunohistochemical study using anti-calcitonin, anti-C-thyroglobulin and anti-19S thyroglobulin antisera. Cell Tissue Res 206:403–415
27. **Kumar R, Gupta R, Bal CS, Khullar S, Malhotra A** 2000 Thyrotoxicosis in a patient with submandibular thyroid. Thyroid 10:363–365
28. **Williams ED, Toyn CE, Harach HR** 1989 The ultimobranchial gland and congenital thyroid abnormalities in man. J Pathol 159:135–141
29. **Chandra RK, Maddalozzo J, Kovarik P** 2001 Histological characterization of the thyroglossal tract: implications for surgical management. Laryngoscope 111:1002–1005
30. **Johnson IJ, Smith I, Akintunde MO, Robson AK, Stafford FW** 1996 Assessment of pre-operative investigations of thyroglossal cysts. J R Coll Surg Edinb 41:48–49
31. **Sprinzl GM, Koebke J, Wimmers-Klick J, Eckel HE, Thumfart WF** 2000 Morphology of the human thyroglossal tract: a histologic and macroscopic study in infants and children. Ann Otol Rhinol Laryngol 109:1135–1139
32. **Dressler GR, Deutsch U, Chowdhury K, Nornes HO, Gruss P** 1990 Pax2, a new murine paired-box-containing gene and its expression in the developing excretory system. Development 109:787–795
33. **Nornes HO, Dressler GR, Knapik EW, Deutsch U, Gruss P** 1990 Spatially and temporally restricted expression of Pax2 during murine neurogenesis. Development 109:797–809
34. **Tellier AL, Amiel J, Delezoide AL, Audollent S, Auge J, Esnault D, Encha-Razavi F, Munnich A, Lyonnet S, Vekemans M, Attie-Bitach T** 2000 Expression of the PAX2 gene in human embryos and exclusion in the CHARGE syndrome. Am J Med Genet 93:85–88
35. **Terzic J, Muller C, Gajovic S, Saraga-Babic M** 1998 Expression of PAX2 gene during human development. Int J Dev Biol 42:701–707
36. **Krude H, Macchia PE, Di Lauro R, Grüters A,** Familial hypothyroidism due to thyroid dysgenesis caused by dominant mutations of the PAX8 gene. Proc of the 37th Annual Meeting of the European Society for Paediatric Endocrinology, Florence, Italy, 1998, p 043
37. **Ayme S, Philip N** 1995 Possible homozygous Waardenburg syndrome in a fetus with exencephaly. Am J Med Genet 59:263–265
38. **Glaser T, Jepeal L, Edwards JG, Young SR, Favor J, Maas RL** 1994 PAX6 gene dosage effect in a family with congenital cataracts, aniridia, anophthalmia and central nervous system defects. Nat Genet 7:463–471
39. **Ikeda K, Clark JC, Shaw-White JR, Stahlman MT, Boutell CJ, Whitsett JA** 1995 Gene structure and expression of human thyroid transcription factor-1 in respiratory epithelial cells. J Biol Chem 270:8108–8114
40. **Pohlenz J, Dumitrescu A, Zundel D, Martiné U, Schönberger W, Koo E, Weiss RE, Cohen RN, Kimura S, Refetoff S** 2002 Partial deficiency of thyroid transcription factor 1 produces predominantly neurological defects in humans and mice. J Clin Invest 109:469–473
41. **Sussel L, Marin O, Kimura S, Rubenstein JL** 1999 Loss of Nkx2.1 homeobox gene function results in a ventral to dorsal molecular respecification within the basal telencephalon: evidence for a transformation of the pallidum into the striatum. Development 126:3359–3370
42. **Breedveld GJ, van Dongen JW, Danesino C, Guala A, Percy AK, Dure LS, Harper P, Lazarou LP, van der Linde H, Joosse M, Gruters A, MacDonald ME, de Vries BB, Arts WF, Oostra BA, Krude H, Heutink P** 2002 Mutations in TITF-1 are associated with benign hereditary chorea. Hum Mol Genet 11: 971–979
43. **Castanet M, Park SM, Smith A, Bost M, Léger J, Lyonnet S, Pelet A, Czernichow P, Chatterjee K, Polak M** 2002 A novel loss-of-function mutation in TTF-2 is associated with congenital hypothyroidism, thyroid agenesis, and cleft palate. Hum Mol Genet 11:2051–2059
44. **Chadwick BP, Obermayr F, Frischauf AM** 1997 FKHL15: a new human member of the forkhead gene family located on chromosome 9q22. Genomics 41:390–396
45. **Larsen WJ** 1997 Human embryology: development of the head, the neck, and the eyes and ears, 2nd Ed. New York: Churchill Livingston; 335–339
46. **O'Rahilly R** 1983 The timing and sequence of events in the development of the human endocrine system during the embryonic period proper. Anat Embryol 166:439–451

JCEM is published monthly by The Endocrine Society (http://www.endo-society.org), the foremost professional society serving the endocrine community.

Antenatal Presentation of Bardet-Biedl Syndrome May Mimic Meckel Syndrome

Houda Karmous-Benailly,[1] Jelena Martinovic,[1] Marie-Claire Gubler,[2] Yoann Sirot,[1] Laure Clech,[1] Catherine Ozilou,[1] Joëlle Augé,[1] Nora Brahimi,[1] Heather Etchevers,[1] Eric Detrait,[1] Chantal Esculpavit,[1] Sophie Audollent,[1] Géraldine Goudefroye,[1] Marie Gonzales,[3] Julia Tantau,[1] Philippe Loget,[5] Madeleine Joubert,[6] Dominique Gaillard,[7] Corinne Jeanne-Pasquier,[8] Anne-Lise Delezoide,[4] Marie-Odile Peter,[10] Ghislaine Plessis,[9] Brigitte Simon-Bouy,[11] Hélène Dollfus,[12] Martine Le Merrer,[1] Arnold Munnich,[1] Férechté Encha-Razavi,[1] Michel Vekemans,[1] and Tania Attié-Bitach[1]

[1]Département de Génétique et Unité INSERM U-393 and [2]Unité INSERM U-574, Hôpital Necker-Enfants Malades, Assistance Publique–Hôpitaux de Paris (AP-HP), [3]Laboratoire d'Embryologie Pathologique, Hôpital Saint Antoine, AP-HP, and [4]Service de Biologie du Développement, Hôpital Robert Debré, AP-HP, Paris; [5]Cabinet d'Anatomie et Cytologie Pathologiques Richier, Rennes, France; [6]Anatomie Pathologique, Centre Hospitalier Universitaire (CHU) de Nantes, Nantes, France; [7]Laboratoire Pol Bouin, Hôpital de la Maison Blanche, Reims, France; [8]Service d'Anatomie Pathologique, CHU Côte de Nacre, and [9]Service de Génétique, CHU de Caen, Caen, France; [10]Service de Pédiatrie, Centre Hospitalier de Mulhouse, Mulhouse, France; [11]Centre d'Étude de Biologie Prénatale, Laboratoire de Cytogénétique, Université de Versailles, Versailles; and [12]Fédération de Génétique Médicale, Hôpitaux Universitaires de Strasbourg, Strasbourg, France

Bardet-Biedl syndrome (BBS) is a multisystemic disorder characterized by postaxial polydactyly, progressive retinal dystrophy, obesity, hypogonadism, renal dysfunction, and learning difficulty. Other manifestations include diabetes mellitus, heart disease, hepatic fibrosis, and neurological features. The condition is genetically heterogeneous, and eight genes (*BBS1–BBS8*) have been identified to date. A mutation of the *BBS1* gene on chromosome 11q13 is observed in 30%–40% of BBS cases. In addition, a complex triallelic inheritance has been established in this disorder—that is, in some families, three mutations at two *BBS* loci are necessary for the disease to be expressed. The clinical features of BBS that can be observed at birth are polydactyly, kidney anomaly, hepatic fibrosis, and genital and heart malformations. Interestingly, polydactyly, cystic kidneys, and liver anomalies (hepatic fibrosis with bile-duct proliferation) are also observed in Meckel syndrome, along with occipital encephalocele. Therefore, we decided to sequence the eight *BBS* genes in a series of 13 antenatal cases presenting with cystic kidneys and polydactyly and/or hepatic fibrosis but no encephalocele. These fetuses were mostly diagnosed as having Meckel or "Meckel-like" syndrome. In six cases, we identified a recessive mutation in a *BBS* gene (three in *BBS2*, two in *BBS4*, and one in *BBS6*). We found a heterozygous *BBS6* mutation in three additional cases. No *BBS1*, *BBS3*, *BBS5*, *BBS7*, or *BBS8* mutations were identified in our series. These results suggest that the antenatal presentation of BBS may mimic Meckel syndrome.

Introduction

Bardet-Biedl syndrome (BBS [MIM 209900]) is a multisystemic genetic disorder characterized by postaxial polydactyly, progressive retinal dystrophy, obesity, hypogonadism, learning difficulty, and renal dysfunction. Other manifestations include diabetes mellitus, neurological impairments (mainly ataxia), heart disease, dental malformations, and hepatic fibrosis. This condition is genetically heterogeneous, and six genes (*BBS1–BBS6*) were identified by genetic linkage studies (Katsanis et al. 2000; Slavotinek et al. 2000; Mykytyn et al. 2001, 2002; Nishimura et al. 2001; Chiang et al. 2004; Fan et al. 2004; Li et al. 2004). Two more genes (*BBS7* [Badano et al. 2003*a*] and *BBS8* [Ansley et al. 2003]) have been identified on the basis of their homology to previously identified *BBS* genes. The major locus, *BBS1*, is on chromosome 11q13. It is responsible for 30%–40% of BBS cases (Beales et al. 2001). In addition to genetic heterogeneity, a complex mode of inheritance called "triallelism" has been established for this disorder, since, at least in some families, three mutations at two *BBS* loci are necessary for the condition to be expressed (Katsanis et al. 2001, 2002).

Because of the late onset of symptoms, the diagnosis of BBS is usually made during childhood. For example, obesity appears around age 2–3 years, and retinal de-

Received October 13, 2004; accepted for publication January 7, 2005; electronically published January 21, 2005.

Address for correspondence and reprints: Dr. Tania Attié-Bitach, Département de Génétique et Unité INSERM U-393, Hôpital Necker-Enfants Malades, Paris, France. E-mail: tania.attie@necker.fr

0002-9297/2005/7603-00XX$15.00

generation becomes clinically apparent only at age 8 years (Beales et al. 1999). The only features that may be present at birth are polydactyly, kidney anomaly, hepatic fibrosis, and genital or heart malformations. Interestingly, polydactyly and cystic kidneys are two malformations—along with occipital encephalocele—that characterize Meckel syndrome (MKS) (Mecke and Passarge 1971), a fetal-lethal autosomic recessive condition. Liver anomalies (hepatic fibrosis and bile-duct proliferation) are constant in MKS (Salonen 1984). On the basis of this phenotypic overlap between the two syndromes and the absence of major signs of BBS in the perinatal period, we hypothesized that fetuses presenting with cystic kidneys, polydactyly, and/or hepatic fibrosis but without encephalocele could be either misdiagnosed as MKS or referred to as "Meckel-like." Therefore, we decided to sequence the eight known *BBS* genes (*BBS1–BBS8*) in a series of 13 antenatal cases presenting with kidney anomaly, polydactyly, and/or hepatic fibrosis but not encephalocele. We identified a recessive mutation in a *BBS* gene in six cases and observed a heterozygous mutation in *BBS6* in three additional cases (fig. 1). In the present study, we describe the antenatal phenotype of patients with BBS and discuss the overlap with the clinical spectrum of MKS.

Material and Methods

Patients

A total of 13 patients, presenting with the association of kidney anomaly, polydactyly, and/or hepatic fibrosis, diagnosed prenatally, were included in the study. In 11 cases, pregnancy was terminated because of either severe renal dysfunction (oligohydramnios) or brain anomaly (corpus callosum agenesis/hypoplasia or Dandy-Walker malformation [DWM]), in accordance with French legislation. In the two postnatal cases (1 and 13b), the parents declined pregnancy termination, after genetic counseling. Chromosome analyses and clinicopathological examinations were performed in 11 cases after parental consent was obtained. Clinical and histological features are summarized in table 1.

Mutation Screening of BBS *Genes*

Genomic DNA was extracted from frozen fetal tissue in 11 cases and from peripheral blood samples in 2 postnatal cases, by use of standard procedures. Primers were designed using introns flanking the coding exons of the eight *BBS* genes and are available on request. Direct sequencing of both strands was performed using the Big Dye Terminator Cycle Sequencing kit (Applied Biosystems) and was analyzed on an ABI 3100 automated sequencer (Applied Biosystems).

Results

BBS2

Mutations were identified in three fetuses. Case 1 (in family FRA) was a 28-wk-old fetus presenting with enlarged hyperechogenic kidneys and unilateral foot polydactyly. After pregnancy termination, neuropathological study disclosed moderate cerebral ventricular dilatation with neuronal ectopias. Histological study of the kidneys showed preserved corticomedullar differentiation but the presence of multiple medullary cysts (fig. 2*E* and 2*F*). The liver was normal (fig. 2*G* and 2*H*). We identified two heterozygous truncating *BBS2* mutations: a 2-bp deletion in exon 15 (1909–1910delAT), resulting in a frameshift mutation (M637fsX648), which was inherited from the father, and a C→T transversion in exon 6, resulting in a nonsense mutation at codon 234 (R234X) (fig. 1*A*), which was inherited from the mother. In this fetus, a heterozygous 4-bp deletion was also detected in *BBS4* intron 7, potentially removing the lariat branch site. This mutation was inherited from the asymptomatic father. RNA was extracted from a blood sample, but RT-PCR failed to find an abnormal supernumerary transcript. This case is the only one of our series in which three *BBS* mutated alleles have been identified.

Case 2b (in family LER) was a *BBS2* compound heterozygote, 22-wk-old fetus (fig. 1*B*). He carried a paternally inherited nonsense mutation in exon 6 (R216X) and a 2-bp deletion in exon 15 (1808delAT), resulting in a frameshift mutation (Y603fsX612), which he inherited from his mother (fig. 1*B*). The pregnancy was terminated because of the presence, on ultrasound examination, of cystic kidneys associated with unilateral upper-limb and bilateral feet postaxial polydactyly. This case was first diagnosed as MKS, on the basis of kidney macroscopic and histological features showing severe disorganization of the renal parenchymal architecture, involving cortical and medullary layers (fig. 2*U* and 2*V*). However, the liver showed mild portal fibrosis but no bile-duct proliferation (fig. 2*W* and 2*X*). In this family, a previous child (case 2a) had died with hydrops at age 2 d (fig. 1*B*), and no autopsy was performed. She did not have polydactyly or brain anomaly, and the left kidney was slightly larger than normal on ultrasound examination. DNA analysis showed that she was heterozygous for the paternal R216X mutation.

Case 3 (in family KAY) was a 26-wk-old fetus of Turkish consanguineous descent. The pregnancy was terminated because the fetus presented with enlarged cystic kidneys, oligoamnios, and bilateral foot polydactyly. Histological examination of the liver showed mild portal fibrosis with no bile-duct proliferation (fig. 2*O* and 2*P*). The corticomedullary architecture of the enlarged kidneys was severely affected by numerous irregular cysts,

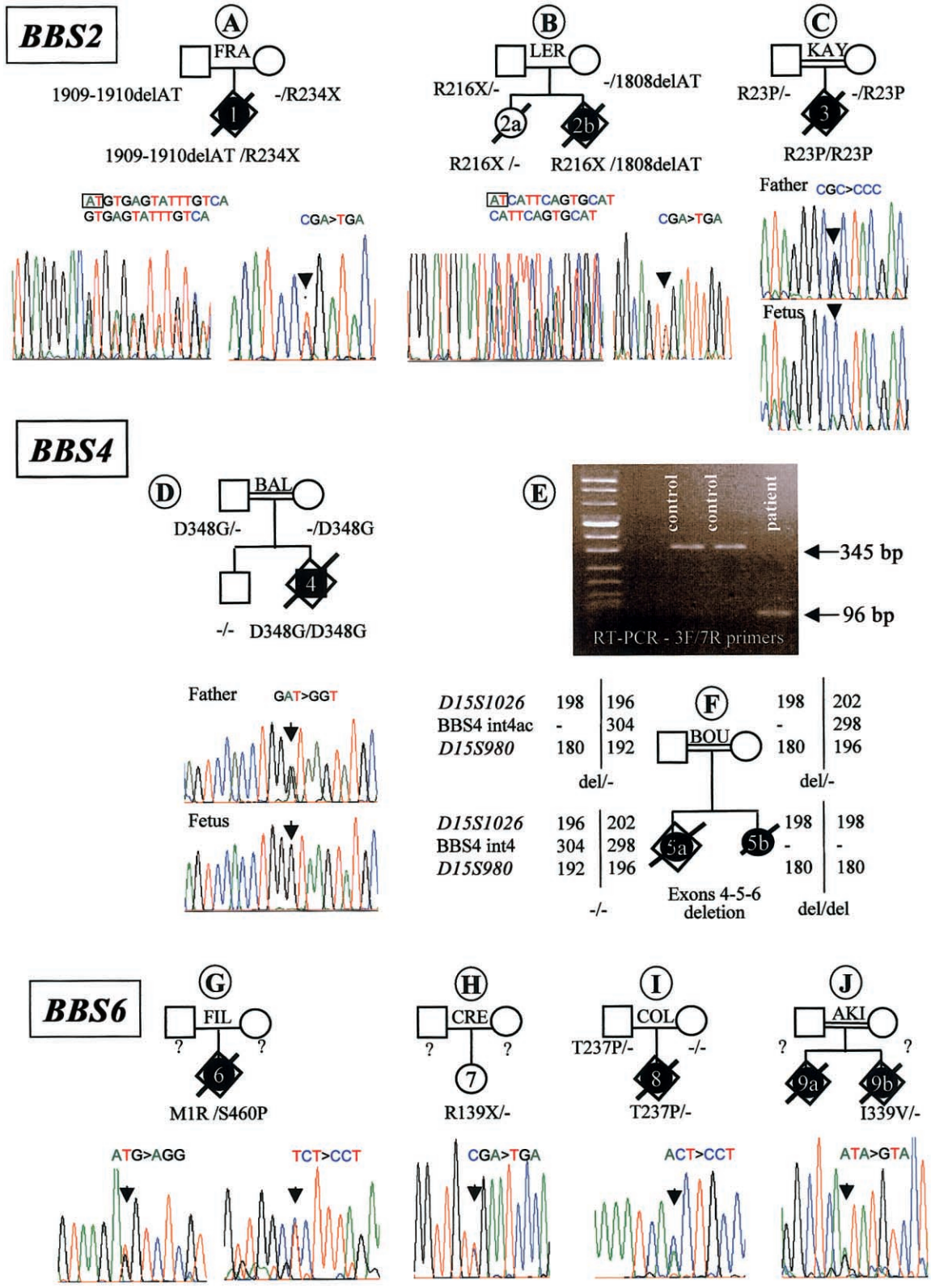

Figure 1 Results of the *BBS2*, *BBS4*, and *BBS6* mutation screening. The pedigrees and mutations are indicated. The black symbols indicate the affected cases. Below each pedigree, sequence chromatographs are shown. In family BOU, the results of the RT-PCR study confirming the deletion of three *BBS4* exons in proband 5b (*E*) and the results of haplotype analysis at the *BBS4* locus (*F*) are shown.

Table 1

Clinical and Pathological Findings Observed in Patients

Trait	Finding in Patient (Family)[a]																
	1 (FRA)	2a (LER)	2b (LER)	3 (KAY)	4 (BAL)	5a (BOU)	5b (BOU)	6 (FIL)	7 (CRE)	8 (COL)	9a (AKI)	9b (AKI)	10 (STA)	11 (AND)	12 (KAL)	13a (MOU)	13b (MOU)
Consanguinity	−	−	−	+	+	+	+	−	−	−	+	+	−	−	+	−	−
National origin	France	France	France	Turkey	Turkey	Tunisia	Tunisia	France	France	France	Turkey	Turkey	France	France	Algeria	France	France
Age[b]	28 wk	2 d	22 wk	26 wk	26 wk	26 wk	12 d	24 wk	12 years	32 wk	32 wk	?	27 wk	37 wk	25 wk	29 wk	18 wk
Brain:																	
Anomaly[c]	−	−	+	−	+	+	?	−	−	−	+	?	−	+	+	+	+
Supratentorial	VD				CCA						CCH, Arh						
Infratentorial	Nect		DWM			ME								DWM	DWM	ME, DWM	OD,DWM
Hand polydactyly	−/−	−/−	+/−	−/−	+/+	−/−	−/−	+/+	+/+	−/−	−/−	−/−	+/+	−/−	+/+	+/+	−/−
Foot polydactyly	+/−	−/−	+/+	+/+	+/+	−/−	+/−	+/+	+/−	+/+	−/−	−/−	+/−	−/−	+/+	−/−	−/−
Kidney anomaly[c]	+	Enlarged[d]	+	+	+	+	+	+	+	Enlarged	+	+	+	+	+	+	+
Pathology	MC	NA	MKL	MKL	MC	MKL	NA	MKS	Failure	Normal	MC	NA	MC	MC	MKL	MC	MC
Portal fibrosis	−	NA	+	+	−	+	NA	−	NA	−	+	NA	−	+	−	−	−
BDP	−	NA	−	−	−	+	NA	−	NA	−	+	NA	−	−	−	−	+/−
Heart defect	−	−	−	−	−	−	+	−	−	−	+	NA	−	−			
Other defects	−	−	+	−	−	+	NA	−	+	+	−	NA	−	−			
Initial diagnosis	BBS	?	MKS	MKL	MKL	MKS	MKS	MKL	BBS	BBS	MKS var	MKS var	BBS	Ago/Gold	MKS	Ago, MKS var	Ago, MKS var
BBS mutation(s)	2 Htz *BBS2* + 1 *BBS4*	1 Htz *BBS2*	2 Htz *BBS2*	1 Hmz *BBS2*	1 Hmz BBS4	None *BBS4*	1 Hmz *BBS4*	2 Htz *BBS6*	1 Htz *BBS6*	1 Htz *BBS6*	None *BBS6*	1 Htz *BBS6*					

[a] + = present; − = absent; ? = unknown; NA = not available; Ago = Agostino syndrome; Arh = arhinencephaly; BDP = bile-duct proliferation; CCA = corpus callosum agenesis; CCH = corpus callosum hypoplasia; Gold = Goldston syndrome; Htz = heterozygous mutation; Hmz = homozygous mutation; ME = meningocele; MC = medullary cysts; MKL = Meckel-like; Nect = neuronal ectopias; OD = occipital defect; var = variant; VD = ventricular dilatation.

[b] Wk indicates weeks of gestation.

[c] Detected on ultrasound examination.

[d] Enlarged left kidney.

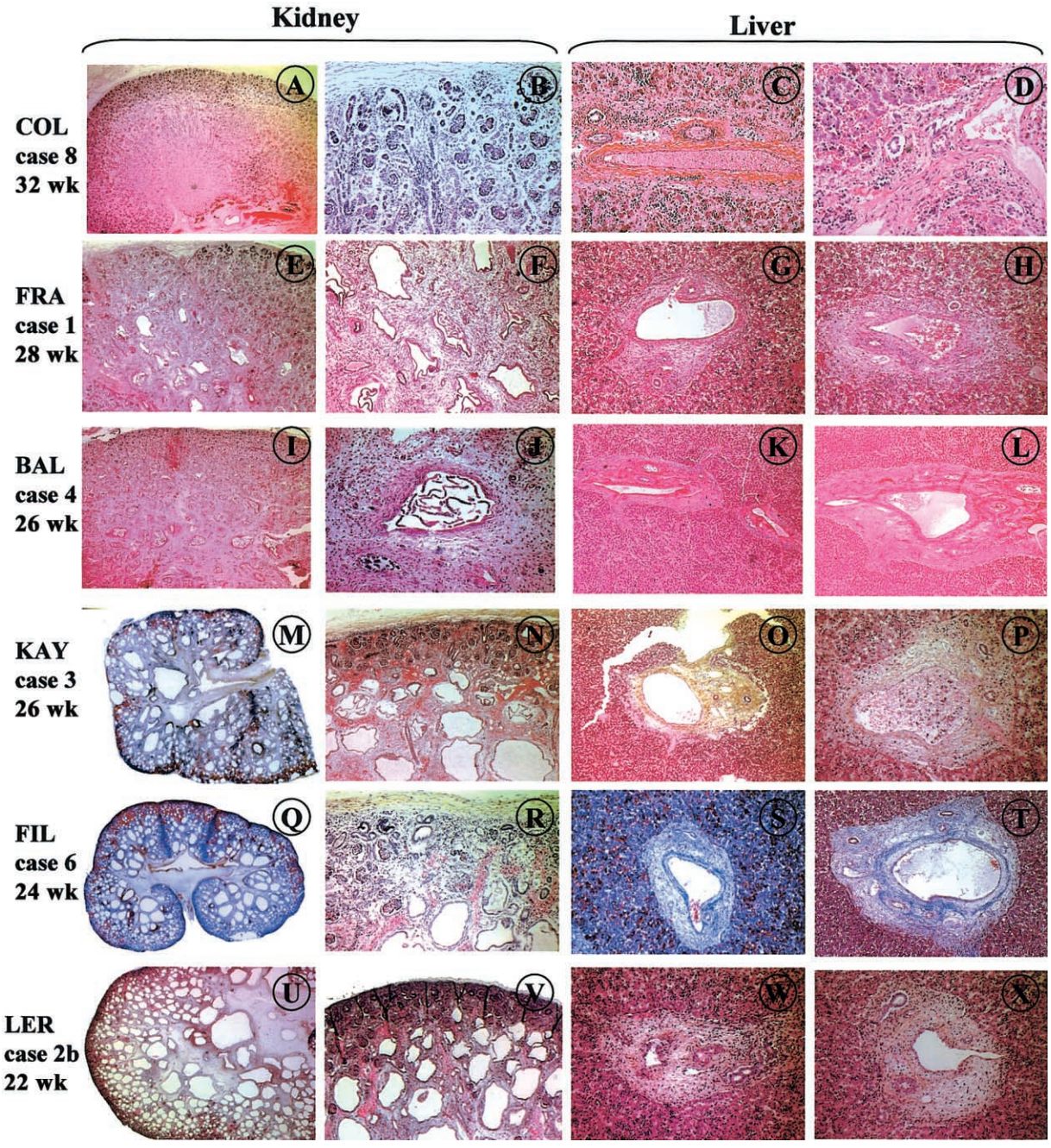

Figure 2 Histological sections (hematoxylin/eosin) of kidneys and livers of fetuses carrying *BBS* mutations. Case 8 shows normal kidney histology. Cases 1 and 4 show medullary cysts, whereas cases 3, 6, and 2b show kidneys "Meckel-like" lesions. The liver shows moderate portal fibrosis in cases 3 and 2b.

lined with a single cell layer. These cysts involved the entire renal parenchyma, with volume enlargement toward the medulla. Only one to two ranges of immature glomeruli were observed in the cortical nephrogenic zone (fig. 2*M* and 2*N*). There were no other visceral malformations, and examination of the CNS was unremarkable. In this case, a homozygous G→C transversion in exon 1 of the *BBS2* gene, leading to the substitution of an arginine with a proline at codon 23 (R23P), was identified. Both parents were heterozygous for this mutation (fig. 1*C*). This missense mutation concerned a conserved amino acid and was not detected in 100 control chromosomes.

BBS4

Mutations were identified in two fetuses. Case 4 (in family BAL) was a 26-wk-old fetus presenting with quadrilateral postaxial polydactyly and bilateral enlarged kidneys with cysts located in the deep cortex and the renal medulla (fig. 2*I* and 2*J*). The liver was normal (fig. 2*K* and 2*L*). Corpus callosum agenesis was observed on ultrasound examination and was confirmed at autopsy. No other malformation was observed. Sequence analysis of *BBS4* revealed a homozygous A→G transition in exon 13, resulting in a missense mutation (D348G) (fig. 1*D*). This mutation was inherited from consanguineous Turkish parents who were heterozygous for this mutation. A healthy brother did not carry this mutation and had inherited both wild-type alleles. This missense mutation involved a conserved amino acid and was not detected in 100 control chromosomes.

Case 5b (the proband in family BOU) was a girl who died at age 12 d. She had unilateral foot polydactyly, cystic kidneys, and endocardial cushion defects. No brain anomaly was apparent. Autopsy was refused. The absence of amplification of *BBS4* exons 4, 5, and 6 led to the suspicion of a homozygous deletion of these exons. The deletion was confirmed by RT-PCR analysis of RNA extracted from lymphoblastoid cells, by use of primers located in exons 3 and 7. The expected wild-type fragment was 345 bp in length, whereas the 96-bp amplification product (fig. 1*E*) observed in proband 5b corresponded to a lack of three exons, as confirmed by sequencing (data not shown). Haplotyping was performed using two flanking markers and one intragenic marker located in intron 4 of the *BBS4* gene. The absence of amplification of the intragenic marker in proband 5b and the hemizygosity observed in the parents are in accordance with both of the consanguineous parents being heterozygous for this deletion (fig. 1*F*). Interestingly, in this family, an earlier fetus (5a) presented with occipital meningocele, cystic kidneys, hepatic portal fibrosis, and bile-duct proliferation, a presentation considered characteristic of MKS. DNA was extracted from paraffin blocks, and haplotyping at the *BBS4* locus showed that sib 5a had a different haplotype from the proband and did not carry the *BBS4* deletion (fig. 1*F*).

BBS6

Mutations were identified in four fetuses. Case 6 (in family FIL) was a 24-wk-old fetus. The pregnancy was terminated after detection, on ultrasound examination, of enlarged and cystic kidneys, anamnios, and quadrilateral postaxial hexadactyly. Autopsy confirmed the absence of other malformations. Microscopic examination of the liver was normal (fig. 2*S* and 2*T*), but the kidneys showed histopathological changes reminiscent of MKS, with both cortical and medullar cystic formations. These cysts were larger in the medulla than in the cortex and were lined with a thin cuboidal epithelium. A thin cortical glomerular layer was present (fig. 2*Q* and 2*R*). Sequencing of the *BBS* genes revealed that this fetus was a *BBS6* compound heterozygote—the first missense mutation resulted in the substitution of the methionine initiator codon with an arginine (M1R), and the second change was a missense mutation in exon 6, resulting in the substitution of a serine with a proline at codon 460 (S460P) (fig. 1*G*). Unfortunately, DNA of the parents was not available to establish the inheritance of these mutations.

Case 7 (in family CRE) was a 12-year-old girl presenting with BBS. Enlarged kidneys, bilateral hand polydactyly, and left-foot polydactyly were detected antenatally. After a genetic-counseling discussion about the risk of MKS, the parents declined pregnancy termination. After birth, the size of the kidneys decreased to normal, whereas progressive renal failure appeared. Obesity started at age 3 years, and an electroretinogram examination established the diagnosis of BBS. At age 12 years, vision was normal. We found one heterozygous *BBS6* C→G transversion in exon 3 of the *BBS6* gene, resulting in a nonsense mutation (R139X) (fig. 1*H*). No other *BBS* mutations were identified in this patient.

In case 8 (in family COL), pregnancy was terminated at 32 wk of gestation because of enlarged kidneys and bilateral foot polydactyly detected on ultrasound examination. Autopsy and histological examination showed no other malformations. The CNS, liver, and kidneys were unremarkable (fig. 2*A*–2*D*). The diagnosis of BBS was suggested. We identified one heterozygous missense mutation in exon 3 of *BBS6,* resulting in the substitution of a threonine with a proline at codon 237 (T237P). This mutation was inherited from the father (fig. 1*I*) and was not observed in >100 control chromosomes. We failed to find any other change in the coding sequence of *BBS6* or the other *BBS* genes in this fetus.

In family 9 (AKI), a fetus (case 9a) presented with cystic kidneys and heart defect. Corpus callosum hypoplasia was detected on ultrasound examination, and

the parents elected to terminate the pregnancy at 32 wk of gestation. Brain examination showed absence of olfactory bulbs. Microscopical examination of the liver showed portal fibrosis and focal bile-duct proliferation and dilatation in some large portal areas. In the kidneys, medullary microcysts were noted. During the pregnancy that followed (proband 9b), abnormal kidneys were detected on ultrasound examination, and the pregnancy was terminated. The parents declined autopsy but agreed to molecular analysis of a blood sample. A heterozygous *BBS6* A→G transition was identified, resulting in the substitution of an isoleucine with a valine at codon 339 (I339V) (fig. 1*J*). This change was not observed in 100 control chromosomes and involved a conserved amino acid. No other *BBS6* coding-sequence mutations could be found in the fetus. Paraffin blocks were obtained from sib 9a, and DNA was extracted for molecular analysis, but we failed to find the same mutation.

No mutation was identified in the coding sequences of the *BBS1, BBS3, BBS5, BBS7,* and *BBS8* genes. Polymorphic changes observed in the *BBS* genes are summarized in table 2.

Table 2

Polymorphisms and Variants Observed in *BBS* Genes

Gene and Nucleotide Variation	Protein Change
BBS1:	
G379A	L126L
IVS6+55 C→T	
C684T	L228L
IVS8−8 G→C	
C1413T	L471L
IVS17+7 G→A	
BBS2:	
A367G	I123V
IVS5−54 G→C	
IVS6−34 C→T	
A1413C	V471V
BBS3:	
IVS4−18 T→C	
IVS5−49 A→G	
IVS8+75 A→G	
IVS8+80 A→G	
IVS8+82–86 del5	
BBS4:	
IVS1−17 C→T	
IVS1−38 C→A	
IVS2+19 G→T	
IVS2−6 A→G	
A137G	K46R
A180G	Q60Q
IVS6+7 C→T	
IVS7+23 G→C	
IVS10−17 G→C	
C1061T	T354I
BBS5:	
IVS1−40 G→C	
BBS6:	
C117T	P39P
C534T	I178I
IVS3+17 A→C	
IVS3+34 C→G	
G1595T	G532V
C1549T	R517C
BBS7:	
−133 C→G	
IVS3−45 C→T	
IVS9+32 A→G	
IVS9+32–34del4	
IVS14+24 C→A	
IVS17+16 G→A	
IVS17−12 C→A	
BBS8:	
IVS3+18 A→G	
IVS3+48 T→C	
IVS6+67 A→G	
IVS14−12 C→G	

Discussion

We sequenced the eight known *BBS* genes in 13 patients presenting prenatally with a kidney anomaly associated with polydactyly and/or hepatic fibrosis but with no encephalocele. Most of these cases were considered to be MKS or "Meckel-like" syndromes, on the basis of the presence of a CNS anomaly (cases 2b, 4, 9, 11, 12, and 13), kidney histology (cases 3 and 6), or MKS in the same family (case 5). We identified recessive mutations in *BBS* genes in six cases—*BBS2* in cases 1, 2b, and 3; *BBS4* in cases 4 and 5b; and *BBS6* in case 6—and identified a *BBS6* heterozygous mutation in cases 7, 8, and 9b. Since mutations in one of the eight known *BBS* genes are found in only 40% of BBS cases (Katsanis 2004), the diagnosis of BBS is not excluded in the remaining cases of our series.

Two mutations identified in our series have been reported elsewhere in patients with BBS. As in case 9b, the I339V *BBS6* mutation was reported in the heterozygous state in a patient with BBS in whom no other *BBS* gene mutations were identified (Slavotinek et al. 2002). Although this change may be a rare variant, neither Slavotinek et al. (2002) nor we found it in 100 controls, and it is not listed as a polymorphism in human SNP databases (see dbSNP and Ensembl Web sites). The R216X *BBS2* mutation identified in case 2b was reported in a BBS case carrying, in addition, a *BBS2* frameshift mutation and a *BBS6* missense mutation (Katsanis et al. 2001). This case presented a typical BBS phenotype with renal involvement.

No mutation in the *BBS1* gene, the major gene responsible for 30%–40% of postnatal BBS cases, was identified in our series. However, a single M390R mutation with a founder effect from Northern Europe accounts for 80% of cases with *BBS1* mutations (Beales et al. 2003; Mykytyn et al. 2003), and none of our cases was of North European extraction. In agreement with previous studies, a high rate of heterozygous *BBS6* mu-

Table 3

Syndromes Associated with or Occasionally Reported with Polydactyly, Cystic Kidney Dysplasia, and/or Brain Anomalies

		Clinical Findings[a]									
				Brain							
Syndrome	MIM	PD	CKD	DWM/VA	CCA/CCH	Other	Liver	Heart	Genital	Cleft	Other
MKS	249000	+	+	DWM	+	Occipital encephalocele	HF+BDP	+	+	+	Pancreas cysts
BBS	209900	+	+	DWM		Normal	HF+BDP	+	+		Obesity, diabetes, retinal dysplasia
Pallister-Hall	146510	+	+	−	+	Hamartoma		+		+	Imperforate anus, short limbs
Joubert	213300	+	+	DWM/VA		Occipital meningocele	HF				Coloboma,[b] retinal dystrophy, abnormal eye movements, tachypnea
Jeune	208500	+	+	−	−	−	HF+BDP				Short stature and ribs, retinal degeneration, pancreas
SLO	270400	+	+	DWM	−	Hydrocephaly, heterotopia		+	+	+	IUGR, microcephaly
CVA[c]	213010	+	+	VA	−	Occipital encephalocele	HF+BDP				Coloboma
OFDI	311200	+	+	−	+	Hamartoma, hydrocephaly, porencephaly				+	Syn-clino-brachy-dactyly, tongue anomalies, alopecia
Simpson-Golabi	312870	+	+	VA	+	Hydrocephaly		+	+	+	Pancreas and somatic overgrowth, macrocephaly, macroglossia
Miller-Diecker	247200	+	+	−	+	Lissencephaly, microcephaly		+		+	IUGR
DWM	220200	−	−	DWM			−				−
DWM with PD	220220	+	−	DWM							−
Goldston (1963)[d]		−	+	DWM			−				−
Goldston	267010	−	+	DWM			+				Pancreas
Scalp defects and PD	181250	+	+/−	DWM		Occiptial defect					Autosomic dominant
Mohr/OFDII	252100	+	+/−	DWM		Cerebellar defect				+	Lingual malformation, supernumerary sutures in skull, hearing loss, tachypnea
EVC	225500	+	+/−	DWM		Normal		+			Short limbs, ribs, nails, teeth
CDG	212065	−	+	DWM		Cerebellar defect	+				−
3C	220210	−		DWM				+		+	Coloboma
COACH	216360	−	+	VA		Occipital encephalocele					Coloboma, congenital ataxia
Hydrolethalus	236680	+	−	DWM	+	Hydrocephaly	−	+		+	−

[a] + = present; +/− = occasionally present; − = absent; PD = polydactyly; CKD = cystic kidney dysplasia; VA = vermis agenesis; CCA/CCH = corpus callosum agenesis or hypoplasia; HF = hepatic fibrosis; BDP = bile-duct proliferation.

[b] See MIM 243910.

[c] Cerebellar vermis aplasia with associated features suggesting SLO and MKS.

[d] See Goldston et al. (1963). Also reported by D'Agostino et al. (1963).

tations was observed (cases 7, 8, and 9b), and we failed to find any other *BBS* gene mutations in the three cases with a heterozygous *BBS6* mutation. These alleles might correspond to a "third allele," and further molecular analysis will be necessary to establish whether these cases carry a recessive mutation at another as-yet-unidentified *BBS* gene. In case 1, two *BBS2* mutations were identified, and, in addition, a 4-bp deletion was identified in *BBS4* intron 7, potentially located in the lariat branch site. As mentioned above, this is the only case in our series in which three *BBS* mutations were identified.

In the present study, polydactyly and cystic kidneys were the only features observed in seven fetuses on prenatal ultrasound examination (cases 1, 3, 5b, 6, 7, 8, and 10). In one of them (case 3), mild liver portal fibrosis without bile-duct proliferation was found on histological examination. A *BBS* mutation was identified in 6/7 of these cases. In two of them (cases 3 and 6), the kidney histopathological changes were reminiscent of MKS, and, interestingly, the occurrence of such severe cystic kidneys in a sib with BBS has been reported elsewhere (Gershoni-Baruch et al. 1992). The association of polydactyly and cystic kidneys is not reported as a single entity in OMIM but is observed in numerous syndromes, such as BBS, MKS, and Pallister-Hall syndrome (table 3). In addition, these features have been reported in patients with Joubert, Jeune, Smith-Lemli-Opitz, oro-facio-digital I (OFDI), and Simpson-Golabi syndromes. However, in all these syndromes, other clinical features can be detected antenatally. Cassart et al. (2004) already suggested that BBS was a possible diagnosis for cases in which polydactyly and enlarged kidneys were observed antenatally. We demonstrate that 6/7 of cases presenting this association, with or without liver portal fibrosis but with no other findings, are cases of BBS. In the absence of polydactyly, other congenital hepatorenal fibrocystic syndromes can be discussed (Johnson et al. 2003).

To our knowledge, corpus callosum agenesis has never been reported in patients with BBS. In the present study, a homozygous *BBS4* mutation was found in one patient (case 4) with corpus callosum agenesis associated with polydactyly and cystic kidneys. These data suggest that corpus callosum agenesis might be associated with the antenatal presentation of BBS. Interestingly, hypoplasia of the corpus callosum was also present in patient 9a, in addition to cystic kidneys and a heart defect. Portal fibrosis and focal bile-duct proliferation and dilatation in some large portal areas were noted on histological examination. The pregnancy that followed (case 9b) was terminated for cystic kidneys, and the fetus was found to carry a heterozygous I339V *BBS6* mutation, previously identified in a patient with BBS (Slavotinek et al. 2002). However, analysis of DNA from paraffin blocks of fetus 9a failed to find the same *BBS6* mutation. Either this change is a rare variant or this "third" *BBS* mutated allele not shared by the sibs—who may still share another homozygous *BBS* gene mutation—acts as a modifier and modulates the phenotype, as reported elsewhere in some families with BBS and a third mutation present in the more severely affected sib but not the other (Badano et al. 2003*b*).

The association of DWM with either polydactyly (Hart et al. 1972; Tal et al. 1980) or cystic kidney dysplasia (D'Agostino et al. 1963; Goldston et al. 1963) has been reported. In addition, DWM, cystic kidneys, and hepatic fibrosis have been documented in several cases (Kudo et al. 1985; Gloeb et al. 1989; Pierquin et al. 1989; Hunter et al. 1991; Walpole et al. 1991; Gulcan et al. 2001) and have been recorded as Goldston syndrome. Despite the lack of bile-duct proliferation, Goldston syndrome has been suggested to be a variant of MKS (Walpole et al. 1991; Gulcan et al. 2001). Furthermore, the association of DWM, cystic kidneys, and hepatic fibrosis with polydactyly (as observed in case 2b) has been reported several times; most authors considered these patients as having MKS (Summers and Donnenfeld 1995; Cincinnati et al. 2000), suggesting that DWM belongs to the spectrum of MKS brain malformations. By other authors, these cases were classified as "Meckel-like," in the context of the cerebro-reno-digital syndrome (Lurie et al. 1991; Genuardi et al. 1993). In these reports, however, hepatic fibrosis but no bile-duct proliferation was present (Genuardi et al. 1993; Summers and Donnenfeld 1995; Cincinnati et al. 2000). Although a molecular study is necessary to establish whether these patients had BBS, these findings suggest that they did not have MKS. Finally, the present study shows that infratentorial malformations should be added to the spectrum of malformations observed in BBS. Along this line, vermis agenesis and mega cisterna magna have been reported once in BBS (Baskin et al. 2002).

Other syndromes constantly or occasionally associating DWM with cystic kidneys and/or polydactyly—namely, MKS, Goldston, Joubert, hydrolethalus (Morava et al. 1996), Ellis-Van Creveld (EVC), SLO, congenital disorder of glycosylation (CDG), OFDII, and scalp defects with polydactyly—are summarized in table 3. In all these syndromes (except Joubert and CDG), other clinical signs, such as intrauterine growth retardation (IUGR) (in SLO), short ribs (in EVC), and tongue anomalies (in OFDII), are observed antenatally. In the present report, three cases presented with this association, but no *BBS* mutation was detected. Although other *BBS* genes could be mutated, some cases could also correspond to prenatal cases of Joubert syndrome.

Several patients with Goldston syndrome, MKS, or Joubert syndrome have been reported to have both

DWM and an occipital meningocele (Miranda et al. 1972; Malpuech et al. 1979; Walpole et al. 1991; Moerman et al. 1993; Piantanida et al. 1993; Al-Gazali et al. 1996; Yapar et al. 1996). This raised the possibility of a common mechanism for both malformations, even though discordant sibs with either encephalocele or DWM have been reported (Blankenberg et al. 1987; Moerman et al. 1993). In most cases, however, the so-called DWM was diagnosed on the basis of brain-imaging criteria alone, and one can postulate that the occipital meningo encephalocele may interfere with brainstem and cerebellum development, leading to an infratentorial dysplasia mimicking DWM. Only a neuropathological examination could help distinguish these two entities.

In view of the results of the present study, the question of whether MKS and BBS are allelic disorders arose. First, MKS is a genetically heterogeneous condition. Three loci have been mapped on 17q23 (*MKS1* [Paavola et al. 1995]), 11q14 (*MKS2* [Roume et al. 1998]), and 8q24 (*MKS3* [Morgan et al. 2002]), but no gene has been identified yet. One locus is common to both MKS and BBS, since both *BBS1* and *MKS2* map on chromosome 11q13-q14. Although the *BBS1* gene is located almost 10 cM centromeric to the *MKS2* locus, we sequenced the *BBS1* gene in 17 MKS cases, including the familial cases linked to 11q13 (Roume et al. 1998), and identified a heterozygous *BBS1* mutation in two cases: the recurrent M390R mutation and a new G559D mutation. No other *BBS* gene mutation could be identified in these two cases. These results may suggest genetic interactions between BBS and MKS. However, although renal histological features in some cases are very similar to those observed in MKS (fig. 2*M,* 2*N,* and 2*Q*), the typical liver ductal plate anomaly, considered a constant in MKS, was absent from cases in the present study. Finally, other malformations frequently found in MKS, such as cleft lip/palate and pancreatic and epidydymal cysts, are not observed in patients with BBS (Fraser and Lytwyn 1981). These observations argue against the hypothesis that the two disorders are allelic. Also, in the family in which a homozygous *BBS4* deletion was found in one sib presenting with severe BBS (case 5b), the sib born earlier (case 5a) with an MKS phenotype did not carry this deletion. Therefore, it is likely that, in this consanguineous family, two different recessive disorders—both characterized by the association of polydactyly and cystic kidneys—were segregating. Indeed, both BBS and MKS are frequently found in consanguineous populations (Teebi 1994; Zlotogora 1997). Here, also, one can hypothesize that an as-yet-unidentified MKS allele may be shared between sibs and may add to the severity of the BBS phenotype in case 5b. Interestingly, family 5 illustrates how the clinical spectrum of a genetic disorder might be extended wrongly when two different disorders segregate in consanguineous families.

In conclusion, our study shows that the association of DWM, cystic kidneys, and hepatic fibrosis without bile-duct proliferation, reported as Goldston syndrome or as "Meckel-like," belongs to the clinical spectrum of BBS. Although BBS and MKS kidney histopathological findings may be similar, the present study suggests that, although genetic interaction may exist between BBS and MKS genes, the two disorders are not caused by the same gene mutations. This hypothesis can be definitively established when MKS genes are identified. The recent demonstration of the role of BBS proteins in ciliary function and the clinical overlap between BBS and MKS will hopefully open the way to discovery of the MKS disease-causing genes.

Acknowledgments

We are thankful to the Société Française de Foetopathologie and to all the clinicians, for sending us patient data and material, in particular Sophie Chemouni, Albert David, Gérard Dray, Yvette Hillion, Nathalie Leporrier, Françoise Menez, Marie-France Nombalais, Joelle Roume, Jaqueline Vigneron, and Dominique Zachar. We thank Corinne Stoetzel for technical assistance. H.K.-B. was granted a fellowship from the Fondation pour la Recherche Médicale.

Electronic-Database Information

The URLs for data presented herein are as follows:

dbSNP, http://www.ncbi.nlm.nih.gov/SNP/
Ensembl, http://www.ensembl.org/
Online Mendelian Inheritance in Man (OMIM), http://www.ncbi.nlm.nih.gov/Omim/

References

Al-Gazali LI, Abdel Raziq A, Al-Shather W, Shahzadi R, Azhar N (1996) Meckel syndrome and Dandy Walker malformation. Clin Dysmorphol 5:73–76

Ansley SJ, Badano JL, Blacque OE, Hill J, Hoskins BE, Leitch CC, Kim JC, Ross AJ, Eichers ER, Teslovich TM, Mah AK, Johnsen RC, Cavender JC, Lewis RA, Leroux MR, Beales PL, Katsanis N (2003) Basal body dysfunction is a likely cause of pleiotropic Bardet-Biedl syndrome. Nature 425: 628–633

Badano JL, Ansley SJ, Leitch CC, Lewis RA, Lupski JR, Katsanis N (2003*a*) Identification of a novel Bardet-Biedl syndrome protein, BBS7, that shares structural features with BBS1 and BBS2. Am J Hum Genet 72:650–658

Badano JL, Kim JC, Hoskins BE, Lewis RA, Ansley SJ, Cutler DJ, Castellan C, Beales PL, Leroux MR, Katsanis N (2003*b*) Heterozygous mutations in *BBS1, BBS2* and *BBS6* have a potential epistatic effect on Bardet-Biedl patients with two mutations at a second BBS locus. Hum Mol Genet 12:1651–1659

Baskin E, Kayiran SM, Oto S, Alehan F, Agildere AM, Saatci U (2002) Cerebellar vermis hypoplasia in a patient with Bardet-Biedl syndrome. J Child Neurol 17:385–387

Beales PL, Badano JL, Ross AJ, Ansley SJ, Hoskins BE, Kirsten B, Mein CA, Froguel P, Scambler PJ, Lewis RA, Lupski JR, Katsanis N (2003) Genetic interaction of *BBS1* mutations with alleles at other *BBS* loci can result in non-Mendelian Bardet-Biedl syndrome. Am J Hum Genet 72:1187–1199

Beales PL, Elcioglu N, Woolf AS, Parker D, Flinter FA (1999) New criteria for improved diagnosis of Bardet-Biedl syndrome: results of a population survey. J Med Genet 36:437–446

Beales PL, Katsanis N, Lewis RA, Ansley SJ, Elcioglu N, Raza J, Woods MO, Green JS, Parfrey PS, Davidson WS, Lupski JR (2001) Genetic and mutational analyses of a large multiethnic Bardet-Biedl cohort reveal a minor involvement of *BBS6* and delineate the critical intervals of other loci. Am J Hum Genet 68:606–616

Blankenberg TA, Ruebner BH, Ellis WG, Bernstein J, Dimmick JE (1987) Pathology of renal and hepatic anomalies in Meckel syndrome. Am J Med Genet Suppl 3:395–410

Cassart M, Eurin D, Didier F, Guibaud L, Avni EF (2004) Antenatal renal sonographic anomalies and postnatal follow-up of renal involvement in Bardet-Biedl syndrome. Ultrasound Obstet Gynecol 24:51–54

Chiang AP, Nishimura D, Searby C, Elbedour K, Carmi R, Ferguson AL, Secrist J, Braun T, Casavant T, Stone EM, Sheffield VC (2004) Comparative genomic analysis identifies an ADP-ribosylation factor–like gene as the cause of Bardet-Biedl syndrome (BBS3). Am J Hum Genet 75:475–484

Cincinnati P, Neri ME, Valentini A (2000) Dandy-Walker anomaly in Meckel-Gruber syndrome. Clin Dysmorphol 9: 35–38

D'Agostino AN, Kernohan JW, Brown JR (1963) The Dandy-Walker syndrome. J Neuropathol Exp Neurol 22:450–470

Fan Y, Esmail MA, Ansley SJ, Blacque OE, Boroevich K, Ross AJ, Moore SJ, Badano JL, May-Simera H, Compton DS, Green JS, Lewis RA, Van Haelst MM, Parfrey PS, Baillie DL, Beales PL, Katsanis N, Davidson WS, Leroux MR (2004) Mutations in a member of the Ras superfamily of small GTP-binding proteins causes Bardet-Biedl syndrome. Nat Genet 36:989–993

Fraser FC, Lytwyn A (1981) Spectrum of anomalies in the Meckel syndrome, or: "maybe there is a malformation syndrome with at least one constant anomaly." Am J Med Genet 9:67–73

Genuardi M, Dionisi-Vici C, Sabetta G, Mignozzi M, Rizzoni G, Cotugno G, Martini Neri ME (1993) Cerebro-reno-digital (Meckel-like) syndrome with Dandy-Walker malformation, cystic kidneys, hepatic fibrosis, and polydactyly. Am J Med Genet 47:50–53

Gershoni-Baruch R, Nachlieli T, Leibo R, Degani S, Weissman I (1992) Cystic kidney dysplasia and polydactyly in 3 sibs with Bardet-Biedl syndrome. Am J Med Genet 44:269–273

Gloeb DJ, Valdes-Dapena M, Salman F, O'Sullivan MJ, Quetel TA (1989) The Goldston syndrome: report of a case. Pediatr Pathol 9:337–343

Goldston AS, Burke EC, D'Agostino A, McCaughey WT, Maccaughey WT (1963) Neonatal polycystic kidney with brain defect. Am J Dis Child 106:484–488

Gulcan YH, Duman N, Kumral A, Sagol, Lebe B, Kavukcu S, Ercal D, Celiloglu M, Ozkan H (2001) Goldston syndrome: report of a case. Genet Couns 12:263–267

Hart MN, Malamud N, Ellis WG (1972) The Dandy-Walker syndrome: a clinicopathological study based on 28 cases. Neurology 22:771–780

Hunter AG, Jimenez C, Tawagi FG (1991) Familial renal-hepatic-pancreatic dysplasia and Dandy-Walker cyst: a distinct syndrome? Am J Med Genet 41:201–207

Johnson CA, Gissen P, Sergi C (2003) Molecular pathology and genetics of congenital hepatorenal fibrocystic syndromes. J Med Genet 40:311–319

Katsanis N (2004) The oligogenic properties of Bardet-Biedl syndrome. Hum Mol Genet Suppl 13:R65–R71

Katsanis N, Ansley SJ, Badano JL, Eichers ER, Lewis RA, Hoskins BE, Scambler PJ, Davidson WS, Beales PL, Lupski JR (2001) Triallelic inheritance in Bardet-Biedl syndrome, a Mendelian recessive disorder. Science 293:2256–2259

Katsanis N, Beales PL, Woods MO, Lewis RA, Green JS, Parfrey PS, Ansley SJ, Davidson WS, Lupski JR (2000) Mutations in *MKKS* cause obesity, retinal dystrophy and renal malformations associated with Bardet-Biedl syndrome. Nat Genet 26:67–70

Katsanis N, Eichers ER, Ansley SJ, Lewis RA, Kayserili H, Hoskins BE, Scambler PJ, Beales PL, Lupski JR (2002) *BBS4* is a minor contributor to Bardet-Biedl syndrome and may also participate in triallelic inheritance. Am J Hum Genet 71:22–29

Kudo M, Tamura K, Fuse Y (1985) Cystic dysplastic kidneys associated with Dandy-Walker malformation and congenital hepatic fibrosis: report of two cases. Am J Clin Pathol 84: 459–463

Li JB, Gerdes JM, Haycraft CJ, Fan Y, Teslovich TM, May-Simera H, Li H, Blacque OE, Li L, Leitch CC, Lewis RA, Green JS, Parfrey PS, Leroux MR, Davidson WS, Beales PL, Guay-Woodford LM, Yoder BK, Stormo GD, Katsanis N, Dutcher SK (2004) Comparative genomics identifies a flagellar and basal body proteome that includes the *BBS5* human disease gene. Cell 117:541–552

Lurie IW, Lazjuk GI, Korotkova IA, Cherstvoy ED (1991) The cerebro-reno-digital syndromes: a new community. Clin Genet 39:104–113

Malpuech G, Palcoux JB, Desbordes AM, Dalens B (1979) Meckel's syndrome: an unusual pedigree. J Genet Hum 27: 167–174

Mecke S, Passarge E (1971) Encephalocele, polycystic kidneys, and polydactyly as an autosomal recessive trait simulating certain other disorders: the Meckel syndrome. Ann Genet 14:97–103

Miranda D, Schinella RA, Finegold MJ (1972) Familial renal dysplasia: microdissection studies in siblings with associated central nervous system and hepatic malformations. Arch Pathol 93:483–491

Moerman P, Pauwels P, Vandenberghe K, Lauweryns JM, Fryns JP (1993) Goldston syndrome reconsidered. Genet Couns 4: 97–102

Morava E, Adamovich K, Czeizel AE (1996) Dandy-Walker malformation and polydactyly: a possible expression of hydrolethalus syndrome. Clin Genet 49:211–215

Morgan NV, Gissen P, Sharif SM, Baumber L, Sutherland J,

Kelly DA, Aminu K, Bennett CP, Woods CG, Mueller RF, Trembath RC, Maher ER, Johnson CA (2002) A novel locus for Meckel-Gruber syndrome, *MKS3*, maps to chromosome 8q24. Hum Genet 111:456–461

Mykytyn K, Braun T, Carmi R, Haider NB, Searby CC, Shastri M, Beck G, Wright AF, Iannaccone A, Elbedour K, Riise R, Baldi A, Raas-Rothschild A, Gorman SW, Duhl DM, Jacobson SG, Casavant T, Stone EM, Sheffield VC (2001) Identification of the gene that, when mutated, causes the human obesity syndrome BBS4. Nat Genet 28:188–191

Mykytyn K, Nishimura DY, Searby CC, Beck G, Bugge K, Haines HL, Cornier AS, Cox GF, Fulton AB, Carmi R, Iannaccone A, Jacobson SG, Weleber RG, Wright AF, Riise R, Hennekam RCM, Lüleci G, Berker-Karauzum S, Biesecker LG, Stone EM, Sheffield VC (2003) Evaluation of complex inheritance involving the most common Bardet-Biedl syndrome locus (*BBS1*). Am J Hum Genet 72:429–437

Mykytyn K, Nishimura DY, Searby CC, Shastri M, Yen HJ, Beck JS, Braun T, Streb LM, Cornier AS, Cox GF, Fulton AB, Carmi R, Luleci G, Chandrasekharappa SC, Collins FS, Jacobson SG, Heckenlively JR, Weleber RG, Stone EM, Sheffield VC (2002) Identification of the gene (*BBS1*) most commonly involved in Bardet-Biedl syndrome, a complex human obesity syndrome. Nat Genet 31:435–438

Nishimura DY, Searby CC, Carmi R, Elbedour K, Van Maldergem L, Fulton AB, Lam BL, Powell BR, Swiderski RE, Bugge KE, Haider NB, Kwitek-Black AE, Ying L, Duhl DM, Gorman SW, Heon E, Iannaccone A, Bonneau D, Biesecker LG, Jacobson SG, Stone EM, Sheffield VC (2001) Positional cloning of a novel gene on chromosome 16q causing Bardet-Biedl syndrome (BBS2). Hum Mol Genet 10:865–874

Paavola P, Salonen R, Weissenbach J, Peltonen L (1995) The locus for Meckel syndrome with multiple congenital anomalies maps to chromosome 17q21-q24. Nat Genet 11:213–215

Piantanida M, Tiberti A, Plebani A, Martelli P, Danesino C (1993) Cerebro-reno-digital syndrome in two sibs. Am J Med Genet 47:420–422

Pierquin G, Deroover J, Levi S, Masson T, Hayez-Delatte F, Van Regemorter N (1989) Dandy-Walker malformation with postaxial polydactyly: a new syndrome? Am J Med Genet 33:483–484

Roume J, Genin E, Cormier-Daire V, Ma HW, Mehaye B, Attie T, Razavi-Encha F, Fallet-Bianco C, Buenerd A, Clerget-Darpoux F, Munnich A, Le Merrer M (1998) A gene for Meckel syndrome maps to chromosome 11q13. Am J Hum Genet 63:1095–1101

Salonen R (1984) The Meckel syndrome: clinicopathological findings in 67 patients. Am J Med Genet 18:671–689

Slavotinek AM, Searby C, Al-Gazali L, Hennekam RC, Schrander-Stumpel C, Orcana-Losa M, Pardo-Reoyo S, Cantani A, Kumar D, Capellini Q, Neri G, Zackai E, Biesecker LG (2002) Mutation analysis of the *MKKS* gene in McKusick-Kaufman syndrome and selected Bardet-Biedl syndrome patients. Hum Genet 110:561–567

Slavotinek AM, Stone EM, Mykytyn K, Heckenlively JR, Green JS, Heon E, Musarella MA, Parfrey PS, Sheffield VC, Biesecker LG (2000) Mutations in *MKKS* cause Bardet-Biedl syndrome. Nat Genet 26:15–16

Summers MC, Donnenfeld AE (1995) Dandy-Walker malformation in the Meckel syndrome. Am J Med Genet 55:57–61

Tal Y, Freigang B, Dunn HG, Durity FA, Moyes PD (1980) Dandy-Walker syndrome: analysis of 21 cases. Dev Med Child Neurol 22:189–201

Teebi AS (1994) Autosomal recessive disorders among Arabs: an overview from Kuwait. J Med Genet 31:224–233

Walpole IR, Goldblatt J, Hockey A, Knowles S (1991) Dandy-Walker malformation (variant), cystic dysplastic kidneys, and hepatic fibrosis: a distinct entity or Meckel syndrome? Am J Med Genet 39:294–298

Yapar EG, Ekici E, Dogan M, Gokmen O (1996) Meckel-Gruber syndrome concomitant with Dandy-Walker malformation: prenatal sonographic diagnosis in two cases. Clin Dysmorphol 5:357–362

Zlotogora J (1997) Autosomal recessive diseases among Palestinian Arabs. J Med Genet 34:765–766

Human Molecular Genetics, 2005, Vol. 14, No. 7 ***903–912***
doi:10.1093/hmg/ddi083
Advance Access published on February 9, 2005

Gene expression in pharyngeal arch 1 during human embryonic development

Juanliang Cai[1], David Ash[1], Lori E. Kotch[1], Ethylin Wang Jabs[1,*], Tania Attie-Bitach[2], Joelle Auge[2], Geraldine Mattei[2], Heather Etchevers[2], Michel Vekemans[2], Yulia Korshunova[3], Rose Tidwell[3], David N. Messina[3], Julia B. Winston[3] and Michael Lovett[3]

[1]Institute of Genetic Medicine, Johns Hopkins University, Baltimore, MD 21205, USA, [2]Department of Genetics and INSERM U-393, Hopital Necker Enfants Malades, 75743 Paris, France and [3]Department of Genetics, Washington University School of Medicine, St Louis, MO 63110, USA

Received December 3, 2004; Revised and Accepted February 1, 2005

Craniofacial abnormalities are one of the most common birth defects in humans, but little is known about the human genes that control these important developmental processes. To identify relevant genes, we analyzed transcription profiles of human pharyngeal arch 1 (PA1), a conserved embryonic structure that develops into the palate and jaw. Using microdissected, normal human craniofacial structures, we constructed 12 SAGE (serial analysis of gene expression) libraries and sequenced 606 532 tags. We also performed Affymetrix microarray analysis on 25 craniofacial targets. Our data revealed not only genes 'enriched' or differentially expressed in PA1 during fourth and fifth week of human development, but also 6927 genes newly identified to be expressed in human PA1. Many of these genes are involved in biosynthetic processes and have binding function and catalytic activity. We compared expression profiles of human genes with those of mouse homologs to look for genes more specific to human craniofacial development and found 766 genes expressed in human PA1, but not in mouse PA1. We also identified 1408 genes that were expressed in mouse as well as human PA1 and could be useful in creating mouse models for human conditions. We confirmed conservation of some human PA1 expression patterns in mouse embryonic samples with whole mount *in situ* hybridization and real-time RT–PCR. This comprehensive approach to expression profiling gives insights into the early development of the craniofacial region and provides markers for developmental structures and candidate genes, including *SET* and *CCT3*, for diseases such as orofacial clefting and micrognathia.

INTRODUCTION

Craniofacial abnormalities, such as orofacial clefting, micrognathia, hemifacial microsomia, mandibulofacial dysostosis and craniosynostosis, are among the most common malformations in humans with frequencies as high as approximately one per 1000 live births (1). More than 700 craniofacial disorders have been reported (www.ncbi.nlm.nih.gov/omim). Many affected structures, including the palate and jaw, are derived from pharyngeal arches. Therefore, these malformations may be due to abnormalities or perturbations of pharyngeal arches during the first 2 months of human embryonic development. Elucidation of the etiology of these malformations depends upon knowledge of normal patterns of gene expression during the development of pharyngeal arches.

Pharyngeal arches are a prominent feature at the cephalic end of all vertebrate embryos (2). These arches appear as pairs of mesenchymal structures during fourth and fifth week of human development. Cells from all three germ layers and neural crest contribute to pharyngeal arch development. Ectoderm is the origin of arch-associated epidermis and sensory neurons and induces odontogenesis (3), whereas mesoderm develops into striated musculature and endothelial cells of the arch arteries. Endoderm gives rise to the epithelial lining of the pharynx and provides signaling molecules necessary

*To whom correspondence should be addressed at: McKusick-Nathans Institute of Genetic Medicine, The Johns Hopkins University, 733 N Broadway, Room 419, Baltimore, MD 21205, USA. Tel: +1 4109554160; Fax: +1 4105025677; Email: ejabsl@jhem.jhmi.edu

for the development of the thymus, parathyroid and thyroid. Neural crest cells migrate from the edges of the neural folds at the levels of the lower midbrain and rhombomeric subdivisions of the hindbrain to populate pharyngeal arches (4,5). Subsequently, the first arch subdivides into maxillary and mandibular portions, which give rise to the palate and jaw, respectively. The maxillary prominence contributes to the formation of the upper midface and palate through interactions with the frontonasal prominence.

Relatively, little is known about the details of the early molecular processes during pharyngeal arch development. *HOX* genes are critical for the development of the neural crest (6). The signaling molecule *BMP4* (7) and the class II homeobox gene *MSX2* (8) expressed in migrating neural crest cells are involved in apoptotic separation of individual arches. Neural crest independent mechanisms of pharyngeal arch development have also been suggested, on the basis of expression patterns of molecules such as *Bmp7*, *Fgf8*, *Pax1* and *Shh* (9).

To generate the first comprehensive gene expression profiles during early human craniofacial development, we utilized micro-cDNA technologies for serial analysis of gene expression (SAGE) (10) and Affymetrix microarrays. Both of these methods have been successfully used to identify differential gene expression between normal and disease states, but have rarely been used for human embryonic development (11,12). More importantly, because SAGE does not require a priori knowledge of the existence of a gene, we could identify novel genes. We focused our analysis on human pharyngeal arch 1 (PA1), because more craniofacial structures are derived from this pair of arches than the others. *In situ* hybridization and RT–PCR data were used on mouse PA1 samples to study conservation and differences between species. The data from our study also identified biological markers for pharyngeal arch development and candidate genes for cleft palate and micrognathia.

RESULTS

Characterization of human PA1 SAGE libraries and microarray data

We constructed 12 SAGE libraries from various microdissected structures of early human craniofacial development (Table 1). For each library, we used only 1 μg of total RNA in our micro-SAGE protocol (13). A total of 606 352 tags were sequenced, with an average of 50 531 tags sequenced for each library, and 101 705 (16.7%) unique tags were identified. These libraries are of high quality because 1) there was no GC content bias (14), 2) the frequency of duplicate ditags and linker contamination (both $<0.5\%$) was equivalent to or less than that of other reported SAGE libraries (15), and 3) simulation analysis using R (www.r-project.org) indicated that subpopulations of data from the same SAGE library were similar.

Comparison between libraries provided further evidence of the quality of our SAGE libraries. In replicate libraries derived from independent RNA sources of microdissected fourth week frontonasal prominences, we found that the correlation coefficient was 0.96, and only 0.39% of the tags showed changes >2-fold ($P < 0.05$). In contrast, comparison between fourth week pharyngeal arch 1 (W4PA1) and fifth week pharyngeal arch 1 (W5PA1) libraries showed that the correlation coefficient was smaller (0.86), and significantly more tags (1.6%) showed changes >2-fold ($P < 0.05$).

Tag sequences from W4PA1 and W5PA1 libraries were matched to the SAGEmap database (www.ncbi.nlm.nih.gov/sage) for gene identification. In PA1, a few genes ($<5\%$) are expressed at high levels and most are expressed at moderate to low levels (Supplementary Material, Table S1). This distribution is consistent with that observed in other tissues and cell types (16–18). Of the 19 698 and 21 881 unique SAGE tags from W4PA1 and W5PA1 libraries, respectively, ~24% were novel without matches to UniGene clusters. Of the SAGE tags that matched to UniGene clusters, ~40% matched to more than one cluster. The low specificity of a SAGE tag for a specific gene was largely because of the short length (10 bp) of the SAGE tag sequence.

We also performed microarray analysis on 25 craniofacial structures, using the Affymetrix Human Genome U95Av2 chip (Table 1). By hierarchical clustering (19), duplicates of the same PA1 targets were found to cluster together in the same subnode with a correlation coefficient of 0.97, showing reproducibility between duplicate arrays. For W4PA1 and W5PA1, we found that 29–39% of all genes tested were expressed in PA1; of the total 12 600 probe sets on a chip, 3681 and 4869 are expressed in W4PA1 and W5PA1, respectively. We consider that a gene is expressed if there is a 'present' call by the Affymetrix default algorithm, which has a sensitivity of at least 70% of detecting genes expressed at the level of one per 100 000 transcripts.

Genes identified to be expressed in PA1 by SAGE or microarray were assigned to 12 different molecular function categories, on the basis of information from the Gene Ontology Consortium (www.geneontology.org). The distribution of genes in the different categories was similar for both W4PA1 and W5PA1 (Table 2; Supplementary Material, Table S2). Genes classified into binding or catalytic activity groups accounted for 61.2–62.3%, with genes of transporter, signal transducer and transcription regulator activity groups accounting for 21.4–25.0%. The remaining genes were in structural molecule, enzyme regulator, chaperone, translation regulator, motor and antioxidant activity groups.

Comparison between W4PA1 and W5PA1 libraries

To detect human genes that are differentially expressed between fourth and fifth week of PA1 development, we analyzed both SAGE libraries [using the statistical method of Audic and Claverie (20), fold change >2 and P-value <0.01] and Affymetrix data [using the statistical method of Li and Wong (19) and lower boundary fold change >2]. We identified 97 genes differentially expressed between human W4PA1 and W5PA1 by SAGE (Supplementary Material, Table S3) and 62 genes by Affymetrix microarrays (Supplementary Material, Table S4). The distribution of differentially expressed genes assigned to different molecular functional categories was similar to all genes expressed in both W4PA1 and W5PA1 libraries (Supplementary Material, Table S2). These differentially expressed genes were also assigned to different biological process categories (21).

Table 1. SAGE libraries and microarray data generated from human embryonic craniofacial structures

Abbreviation	Carnegie stage	Structures	SAGE libraries		Affymetrix microarrays
			Total tags	Unique tags	
D26E	C12	26 day embryo	51 216	19 602	+
W4PA1	C12	Fourth week pharyngeal arch 1	59 959	19 698	+
W4PA2	C12	Fourth week pharyngeal arch 2	59 964	19 698	+
W4PA3	C12	Fourth week pharyngeal arches 3 and 4	NA	NA	+
W4FNP	C12	Fourth week frontonasal prominence	55 263	15 540	+
W4MDP	C12	Fourth week mandibular prominence	17 359	7912	NA
W4ARH	C12	Fourth week anterior rhombomere	20 876	8143	+
W4PRH	C12	Fourth week posterior rhombomere	38 717	15 143	+
W5PA1	C15	Fifth week pharyngeal arch 1	67 982	21 883	+
W5PA2	C15	Fifth week pharyngeal arch 2	60 870	23 587	+
W5PA3	C15	Fifth week pharyngeal arches 3 and 4	NA	NA	+
W5FNP	C15	Fifth week frontonasal prominence	64 171	20 503	+
W5AR	C15	Fifth week anterior rhombomere	NA	NA	+
W5PR	C15	Fifth week posterior rhombomere	NA	NA	+
W6MAN	C16/C17	Sixth week mandible	NA	NA	+
W6MAX	C16/C17	Sixth week maxilla	NA	NA	+
W6LNP	C16/C17	Sixth week lateral nasal prominence	NA	NA	+
W6MNP	C16/C17	Sixth week medial nasal prominence	NA	NA	+
W85MAN	C23	8.5th week mandible	NA	NA	+
W85SG	C23	8.5th week salivary gland	NA	NA	+
W85AT	C23	8.5th week anterior tongue	NA	NA	+
W85PT	C23	8.5th week posterior tongue	NA	NA	+
W85PL	C23	8.5th week palate	48 922	17 491	+
W85DL	C23	8.5th week dental lamina	NA	NA	+
W85UL	C23	8.5th week upper lip	61 053	21 793	+
W85LL	C23	8.5th week lower lip	NA	NA	+

+, Affymetrix HG-U95Av2 data available; NA, not available.

Several biosynthesis processes, including nucleotide, protein and lipid synthesis processes, as well as the protein transport and the cell cycle processes were overrepresented in the differentially expressed genes determined by SAGE ($P < 0.05$; Table 3), whereas no biological processes were overrepresented in the differentially expressed genes detected by microarrays.

Few genes were identified to be differentially expressed by both our SAGE and microarray analyses. Only a few published studies were available to corroborate these differentially expressed genes. In the case of human *FIGF*, we detected increased expression from fourth to fifth week human PA1 SAGE libraries (zero versus eight tags). This result was confirmed by Affymetrix analysis (6.4-fold increase). Furthermore, mouse *Figf* expression was not detected in mouse PA1 at GD8.5, but was detected in PA1 at GD10.5 by *in situ* hybridization (22).

Direct validation of the expression changes would ideally be done with human samples. However, because of the limited availability of human embryos and generally presumed conservation of gene expression in mammals, mouse embryos were used to further study expression changes in PA1. We used real-time RT–PCR to analyze RNAs from corresponding mouse stages. Mouse PA1 obtained by microdissection of GD9.5 and GD10.5 embryos was analyzed, using primers specific to mouse homologs of several human genes. We found that 93% of the RT–PCR analyses agreed with our SAGE data in the direction of change and 86% had a fold change of ≥ 2 (Supplementary Material, Table S5). Although there was good agreement between our SAGE and RT–PCR differential gene expression data, complete agreement was not expected because of differences in sensitivity and specificity of the methods, intrinsic variation in gene expression and/or species differences between human and mouse.

Genes highly expressed in human PA1

Of the highly expressed tags present more than 100 times in either W4PA1 or W5PA1 SAGE library, 24 tags were uniquely matched to UniGene clusters (Supplementary Material, Table S6). Thirteen of these were among the 200 genes (~5% of all genes called 'present') with the highest normalized intensity values assayed by Affymetrix microarray. Many of these genes code for components of the ribosomal complex, reflecting the increased translational activity in PA1 during early human development. The percentage of highly expressed genes was 4-fold increased in the structural molecule activity group when compared with that of all genes identified in PA1. No highly expressed genes were identified in the transporter, signal transducer and transcription regulator activity groups.

Genes 'enriched' in human PA1

To screen for human genes that are at least 2-fold 'enriched' in PA1, we calculated the ratio of the number of tags from either W4PA1 or W5PA1 SAGE library to the average number of tags from 10 libraries derived from other embryonic,

Table 2. Functional classification of PA1 genes

Functional category	PA1[a]	Human–mouse homologs		
		Common[b] (only in JAX[c])	Only in human[d]	Only in mouse[e]
Antioxidant activity	0.3	0.3 (0.4)	0.4	0.1
Binding	37.5	39.4 (39.0)	38.9	39.4
Catalytic activity	24.7	26.7 (14.9)	24.3	22.7
Chaperone activity	1.6	0.0 (1.0)	0.0	0.1
Enzyme regulator activity	3.1	2.7 (2.0)	3.8	3.4
Motor activity	0.6	0.9 (0.0)	0.9	0.1
Signal transducer activity	9.5	7.6 (14.7)	11.6	10.2
Structural molecule activity	3.8	5.8 (2.3)	2.8	2.6
Transcription regulator activity	7.1	7.4 (17.2)	7.3	10.7
Translation regulator activity	0.8	0.7 (0.0)	0.7	0.1
Transporter activity	8.4	6.4 (4.2)	7.4	7.4
Unknown	2.6	2.1 (4.3)	1.9	3.1

Listed are percentages of genes assigned to 12 molecular function categories, on the basis of information from the Gene Ontology Consortium (www.geneontology.org).
[a]Genes from all 5055 called 'present' in microarrays of W4PA1 and W5PA1.
The groups of human–mouse homologs analyzed by microarray include:
[b]1408 genes expressed in both human (present by both SAGE and microarray) and mouse PA1 (either present in The Jackson Laboratory Mouse Genome Informatics database or by microarray).
[c]96 genes expressed in both human (present by both SAGE and microarray) and mouse PA1 (present only in The Jackson Laboratory Mouse Genome Informatics database).
[d]766 genes expressed only in human PA1 (present by both SAGE and microarray), but not in mouse (not present in The Jackson Laboratory Mouse Genome Informatics database or by microarray).
[e]940 genes expressed only in mouse, but not in human PA1.

craniofacial structures. For a gene to be considered 'enriched', both ratios had to be greater than 2. Only moderately to highly expressed SAGE tags with a combined count of more than 20 in all libraries were analyzed. We also searched for genes at least 2-fold 'enriched' in W4PA1 and W5PA1 by analyzing our Affymetrix microarray data. We found 74 'enriched' genes by SAGE (Supplementary Material, Table S7) and 96 genes by Affymetrix microarrays (Supplementary Material, Table S8). The proportion of 'enriched' genes assigned to different functional categories was also similar to that of all genes expressed in PA1 (Supplementary Material, Table S2). No biological processes were overrepresented in the SAGE 'enriched' genes, whereas the biosynthesis and energy pathway processes were overrepresented in microarray 'enriched' genes (Table 3). Some of these 'enriched' genes are known to be involved in human disorders affecting the craniofacial region such as *GPC3* in Simpson-Golabi-Behmel syndrome type I (23,24), *NOTCH3* in cerebral autosomal dominant arteriopathy with subcortical infarcts and leukoencephalopathy (25) and *TNFRSF10B* in head and neck squamous cell carcinoma (26).

Genes common to human and mouse PA1

To compare the gene expression between human and mouse craniofacial structures, we searched The Jackson Laboratory Mouse Genome Informatics database (www.informatics.jax.org) for previously reported mouse gene expression in PA1 and its quantitation. Three hundred and fifteen genes have been shown to be expressed in PA1 by immunohistochemistry, *in situ* hybridization or RT–PCR. Of these 315 genes, 228 genes have human homologs that matched uniquely to UniGene clusters. One hundred and seventy-nine (78%) were found in our SAGE analysis of human W4PA1 and W5PA1 libraries. Thirty-two percent of these genes were classified as signal transducers and transcription regulators such as HoxA1, Msx1, Msx2, Pax8, Pax9, Bmp4, Bmp5, Bmp7, Fgfr11 and Tgfb1 (Table 2). Of the 228 human genes, 174 have probe sets on Affymetrix HG-U95Av2 chip. One hundred and six (61%) were called 'present', when human PA1 targets were analyzed. Ninety-six genes were detected by both unique SAGE tags and microarray analysis. Both multiple matched SAGE tags and Affymetrix microarray data identified additional genes, such as *TWIST* and *TCOF1*, which are known to be involved in craniofacial disorders affecting pharyngeal arch development in humans (Saethre-Chotzen and Treacher Collins syndromes, respectively) and relevant mouse models (27–30).

To discover additional PA1 genes expressed in human and mouse, we performed microarray analysis on mouse PA1 microdissected at GD9.5 and compared these results with our human data. We identified an additional 7307 genes expressed in mouse PA1. Of all the genes expressed in human PA1, 2174 have mouse homologs and 1408 (64.8%) were also expressed in mouse PA1 as determined either by microarray analysis or present in The Jackson Laboratory Mouse Genome Informatics database (Supplementary Material, Table S9). These results further suggest that the large portion of genes and molecular pathways that are relatively conserved between human and mouse PA1 development account for the basic craniofacial structures present in mammals.

Temporospatial expression of mouse homologs of human genes expressed in PA1

To screen for genes that may be involved in craniofacial disorders and to investigate the temporospatial expression pattern of PA1 genes, we identified genes that are more highly expressed in pharyngeal arches than that in other embryonic,

Table 3. Biological processes

Biological processes	Genes	*P*-value
Overrepresented in differentially expressed genes detected by SAGE[a]		
Biosynthesis	SQLE; ATP6V1E1; RPL4; NME4; RPL23; RPL32; EIF3S8; RPL9; RPL14; HSPCA; SUI1; CYP51A1; RPLP2; FADS2; FASN; RPL17; ATP5L	5.91E−05
Macromolecule biosynthesis	SQLE; RPL4; RPL9; RPL14; SUI1; CYP51A1; RPLP2; RPL23; FADS2; RPL32; FASN; RPL17; EIF3S8	0.0135
Cellular physiological process	SET; ATP6V1E1; PCNA; SLC25A6; HNRPD; POLD3; FSCN1; CCNG1; RPL23; TIMM17B; NEDD5; MAC30; TOPBP1; NGFRAP1; VP16_HUMAN; EWSR1; COPB; SUI1; HSPCA; MORF4L1; FIGF; GABARAP; MARCKS; H2AFY; LAPTM4A; SEC13L1; TM4SF6; ATP5L; HMGB2	0.0231
Cell growth and/or maintenance	SET; ATP6V1E1; PCNA; SLC25A6; HNRPD; POLD3; FSCN1; CCNG1; RPL23; TIMM17B; NEDD5; MAC30; TOPBP1; VP16_HUMAN; EWSR1; COPB; SUI1; HSPCA; MORF4L1; FIGF; GABARAP; H2AFY; LAPTM4A; SEC13L1; ATP5L; HMGB2	0.0231
Intracellular transport	SET; VP16_HUMAN; SLC25A6; HSPCA; RPL23; TIMM17B; GABARAP; SEC13L1	0.0231
DNA metabolism	SET; PCNA; POLD3; NTHL1; MORF4L1; TOPBP1; H2AFY; HMGB2	0.0231
DNA replication and chromosome cycle	SET; PCNA; TOPBP1; POLD3; HMGB2	0.0231
Chromosome organization and biogenesis (*sensu* Eukarya)	SET; MORF4L1; HNRPD; H2AFY; HMGB2	0.0231
Nuclear organization and biogenesis	SET; MORF4L1; HNRPD; H2AFY; HMGB2	0.0231
Response to DNA damage stimulus	NTHL1; PCNA; HNRPD; POLD3; HMGB2	0.0231
Response to endogenous stimulus	NTHL1; PCNA; HNRPD; POLD3; HMGB2	0.0231
Chromatin assembly or disassembly	SET; MORF4L1; H2AFY; HMGB2	0.0231
Establishment and/or maintenance of chromatin architecture	SET; MORF4L1; H2AFY; HMGB2	0.0353
DNA packaging	SET; MORF4L1; H2AFY; HMGB2	0.0363
Cell cycle	SET; PCNA; POLD3; CCNG1; FIGF; NEDD5; TOPBP1; HMGB2	0.0234
Protein biosynthesis	RPL23; RPLP2; RPL4; RPL32; RPL17; RPL9; RPL14; EIF3S8; SUI1	0.0251
DNA replication	SET; PCNA; POLD3; HMGB2	0.0252
Macromolecule metabolism	SET; SQLE; ULK1; RPL4; HNRPD; PPIA; NTHL1; PTPRA; RPL23; CCNG1; TIMM17B; RPL32; DPP7; EIF3S8; MTMR4; RPL9; RPL14; HSPCA; SUI1; CS; CYP51A1; RPLP2; FADS2; GABARAP; FASN; RPL17	0.0257
Intracellular protein transport	RPL23; TIMM17B; VP16_HUMAN; GABARAP; SEC13L1	0.0264
Lipid biosynthesis	SQLE; CYP51A1; FADS2; FASN	0.0264
Protein transport	RPL23; TIMM17B; VP16_HUMAN; COPB; GABARAP; SEC13L1	0.0294
DNA repair	NTHL1; PCNA; POLD3; HMGB2	0.0349
Cell proliferation	SET; PCNA; POLD3; FSCN1; CCNG1; FIGF; NEDD5; TOPBP1; HMGB2	0.0352
Overrepresented 'enriched' genes detected by microarray[b]		
Biosynthesis	NME1; EIF3K; RPLP1; RPL38; NOLA2; RPS5; RPS21; RPL18; RPS12; GMPS; PSPH; OAZ1; FDPS; RPL28; ATP5G3; QDPR; RPS15; WBSCR1	8.84E−05
Energy pathways	UQCRC1; COX6A1; ATP5G3; COX8A; UQCR; COX6C; IDH3B	0.00565

[a]Listed are biological process annotations statistically overrepresented in 97 differentially expressed genes, as determined by SAGE ($P < 0.05$) (Supplementary Material, Table S3).
[b]Listed are biological process annotations statistically overrepresented in 96 'enriched' genes, as determined by microarray ($P < 0.05$) (Supplementary Material, Table S8).

craniofacial structures as listed in Table 1. The mouse homologs for human genes previously not known to be expressed in PA1 were studied by whole mount *in situ* hybridization analysis using mouse embryos from GD8.5 through GD10.5, the stages corresponding to fourth and fifth week human embryonic development.

One of these is the *SET* gene, which was previously identified because it was disrupted by a translocation breakpoint in human chromosome 9 associated with a subtype of acute myeloid leukemia (31). Human *SET*, matched by multiple SAGE tags, was present in 75 of 59 959 tags and 101 of 67 982 tags sequenced in W4PA1 and W5PA1 libraries, respectively. This gene was relatively 'enriched' in PA1, because it was present on average only 47 of 50 531 tags in all other libraries. Its PA1 expression was further confirmed by both human and mouse Affymetrix microarray analysis. By whole mount *in situ* hybridization, we found that at GD8.5, mouse *Set* was highly expressed in cells of the neural crest folds and less expressed in PA1 (Fig. 1). At GD9.5, a high level of *Set* expression was in the pharyngeal

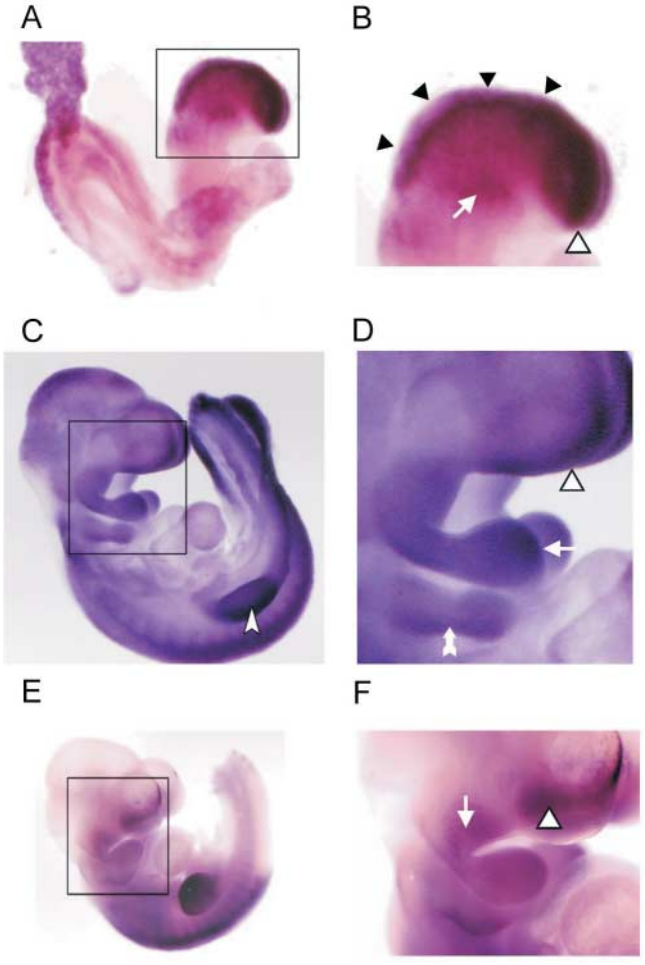

Figure 1. Mouse *in situ* hybridization of the *Set* gene. Whole embryo staining for GD8.5 (**A** and **B**), GD9.5 (**C** and **D**) and GD10.5 (**E** and **F**) shows *Set* expression throughout early craniofacial development. (B, D and F) are the higher magnifications of the boxed regions in (A, C and E), respectively. *Set* expression on GD8.5 is localized to the frontonasal prominence, crest of the neural folds and PA1. At GD9.5, expression is present throughout PA1 and also at the posterior half of PA2. By GD10.5, *Set* is expressed mostly in the maxillary portion of PA1. *Set* is expressed in the frontonasal prominence at all stages observed (B, D and F). At GD10.5, *Set* is expressed in the lateral nasal prominence (F). *Set* is expressed in the limb bud (C). ⇦, PA1; △, frontonasal prominence; ▼, neural folds; ⇧, PA2; ⍋, limb bud.

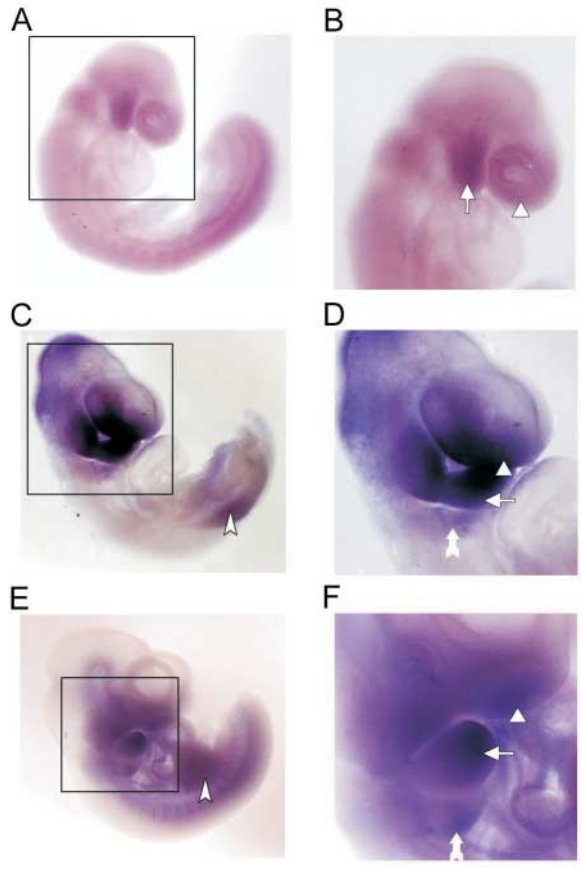

Figure 2. Mouse *in situ* hybridization of the *Cct3* gene. Whole embryo staining for GD8.5 (**A** and **B**), GD9.5 (**C** and **D**) and GD10.5 (**E** and **F**) shows *Cct3* expression throughout early craniofacial development. (B, D and F) are the higher magnifications of the boxed regions in (A, C and E), respectively. *Cct3* expression on GD8.5 is localized to PA1 and frontonasal prominence. At GD9.5, *Cct3* expression is present in the frontonasal prominence and is predominant in PA1. By GD10.5, *Cct3* expression is observed throughout PA1, but most prominently in the mandibular portion of PA1. It is also expressed in PA2 (D and F) and frontonasal prominence (B, D and F) at these stages. *Cct3* is expressed in the limb bud (C and E). ⇦, PA1; △, frontonasal prominence; ⇧, PA2; ⍋, limb bud.

arches, especially in PA1, suggesting that the *Set*-expressing neural crest cells had migrated from the hindbrain folds to the arches. Upon further development at GD10.5, *Set* expression was still strong, but restricted to the maxillary portion of PA1. During this stage, *Set* was also expressed in the frontonasal prominence, specifically in the lateral nasal prominence and, interestingly, in the limb buds.

Another gene that we studied was *CCT3*, which encodes a chaperone protein (32). Human *CCT3*, matched by multiple SAGE tags, was present in 338 of 59 959 tags and 230 of 67 982 tags sequenced in W4PA1 and W5PA1 libraries, respectively. This gene was highly expressed in PA1, being present on average only 91 of 50 531 tags in all other libraries. *CCT3* was also determined to be 'enriched' in both PA1 and PA2 using a Wilcoxon rank sum test (33), in which the normalized expression level of this gene in W4PA1, W5PA1, W4PA2 and W5PA2 was at least twice that in the other eight libraries tested with a one-sided P-value <0.05. Furthermore, Affymetrix microarray data on both human and mouse confirmed that *CCT3* was highly expressed (top 5% of genes) in PA1. In whole mount *in situ* hybridization at GD8.5, mouse *Cct3* was predominantly expressed in PA1, as well as in the frontonasal prominence (Fig. 2). Its level of expression in PA1 and the frontonasal prominence persisted, and it was also present in PA2. By GD10.5, the predominant expression of *Cct3* had moved to the mandibular portion of PA1 and the limb buds.

Genes newly identified to be expressed in human PA1

We identified 6927 genes previously not known to be expressed in human PA1. Of these genes, 4842 and 6096 were detected by SAGE and microarray, respectively. In addition, these genes had not been identified to be

expressed in mouse PA1 by The Jackson Laboratory Mouse Genome Informatics database (www.informatics.jax.org). Among these new genes are all of the highly expressed (Supplementary Material, Table S6) and most of the differentially expressed or the 'enriched' human PA1 genes (Supplementary Material, Tables S3, S4, S7 and S8). A comparison was made between our human versus mouse microarray data on PA1, using the default Affymetrix algorithm of present/absent call. We found that 35% (766 of 2174 mouse homologs) were expressed in only human PA1 (Table 4), whereas 40% (940 of 2348 human homologs) were expressed in only mouse PA1 (Supplementary Material, Table S10). The distribution of these genes that are more specific to human or mouse into molecular functional categories is similar to all genes identified in PA1 (Table 2). Therefore, species differences in gene expression levels as well as timing and localization, rather than function, may account for some of the obvious morphological differences of the craniofacial region at later stages. However, further studies will need to be performed to substantiate this hypothesis. Our data also suggest the limitation of using mouse models to study some human conditions and provide a means by which genes can be prioritized for mouse knockout studies.

Table 4. Genes newly identified to be expressed in human PA1 by SAGE and microarray

Gene	UniGene id	Gene	UniGene id
GAPD	Hs.169476	CHST3	Hs.158304
TPT1	Hs.374596	CSRP1	Hs.108080
RPS27	Hs.337307	NDUFS6	Hs.408257
RPL18A	Hs.337766	KPNB1	Hs.439683
ARL6IP	Hs.75249	RBM9	Hs.433574
RPL11	Hs.388664	ALDOB	Hs.315235
PKM2	Hs.198281	RAB22A	Hs.281117
NMB	Hs.386470	UBTF	Hs.89781
RPL38	Hs.380953	IL7R	Hs.362807
MARCKS	Hs.318603	SEC13L1	Hs.227949
HSPCB	Hs.74335	RBM12	Hs.166887
MYL6	Hs.77385	KIAA0252	Hs.83419
EPRS	Hs.171292	CENPF	Hs.77204
CLTC	Hs.187416	LSM4	Hs.76719
HNRPA0	Hs.96996	CDC10	Hs.396503
EIF3S6	Hs.405590	EIF3S10	Hs.389559
PTPN13	Hs.387553	SDCCAG1	Hs.388584
INPP4A	Hs.334575	SNRPF	Hs.105465
PDE3B	Hs.337616	SLC12A4	Hs.10094
HSPCA	Hs.446579	MCM2	Hs.57101
ACTB	Hs.426930	RAB5C	Hs.479
STMN1	Hs.209983	DKC1	Hs.4747
CRI1	Hs.381137	BSCL2	Hs.438912
MDH1	Hs.75375	GRINA	Hs.339697
BASP1	Hs.511745	MCM3	Hs.179565
CCNB1	Hs.23960	DPYSL2	Hs.173381
CRADD	Hs.155566	UQCRB	Hs.131255
KHSRP	Hs.91142	RYBP	Hs.7910
CAPZB	Hs.333417	SFRS6	Hs.6891
CYC1	Hs.289271	EIF3S5	Hs.381255
HSPA1A	Hs.75452	ZFPL1	Hs.155165
SFPQ	Hs.180610	C14orf1	Hs.15106
MSF	Hs.288094	BAIAP2	Hs.128316
ILVBL	Hs.78880	NEDD5	Hs.131736
UBE2D3	Hs.472031	COX4I1	Hs.433419
RPS10	Hs.406620	SNRPD3	Hs.356549
MDH2	Hs.405860	KRT19	Hs.309517
MCM7	Hs.438720	SLC16A3	Hs.386678
KDELR1	Hs.78040	PPOX	Hs.376314
AKAP1	Hs.78921	TNFRSF1B	Hs.256278
PLXNB1	Hs.278311	USP22	Hs.12064
TARS	Hs.84131	LSM2	Hs.103106
HSPD1	Hs.79037	NDUFA9	Hs.75227
MAFF	Hs.460889	COX7B	Hs.432170
ZNF9	Hs.2110	CREM	Hs.231975
HLA-A	Hs.181244	ZFP36L2	Hs.78909
UNC119	Hs.410455	HSPB1	Hs.76067
MYH10	Hs.280311	TUB	Hs.54468
HFE	Hs.233325	MEG3	Hs.534530
SFRS10	Hs.30035	UBXD2	Hs.350806

Listed are the 100 most highly expressed human genes in PA1 as determined by both SAGE and Affymetrix microarray. These genes are ranked by their combined tag counts in W4PA1 and W5PA1 SAGE libraries. Human genes whose mouse homologs were already known to be expressed in PA1 as noted by The Jackson Laboratory Mouse Genome Informatics database and mouse microarray analysis were excluded. For a gene to be considered 'expressed' in human PA1, the number of SAGE tags for that gene should be greater than 1, and it also should have a 'present' call by Affymetrix microarray.

DISCUSSION

This study is unique in that gene expression profiling was performed on RNAs from normal human embryos. Our analysis allowed us to identify a large number of transcripts previously not known to be expressed in the human craniofacial region. We focused on PA1, because it is essential to the development of many craniofacial structures. Although technically challenging, we were able to microdissect PA1 because of its distinct morphology and generate sufficient cDNA by adapting micromethods using very small quantities of total RNAs.

Previous studies of gene expression during normal craniofacial development have been carried out in mouse or zebrafish, using microarrays (34) and phenotype-based techniques such as ENU mutagenesis (35) or subtractive libraries (36). Microarray results were restricted to those genes present on a chip or filter and may not be as sensitive as SAGE or RT–PCR. Both mutagenesis screens and subtractive libraries were also less comprehensive.

Fowles *et al.* (36) used subtractive hybridization of a mouse PA1 cDNA library against an adult mouse liver cDNA library to identify genes 'enriched' in PA1. Their subtraction method aimed to remove ubiquitously expressed housekeeping genes and to enrich for those genes with a specific role in PA1 development. However, genes common to both liver and craniofacial development may still be important to the latter and would be missed. After sequencing 453 clones, 273 non-redundant cDNA clones were identified. One hundred and twenty-three of the latter clones had sequences homologous to unique UniGene clusters. When we compared their results with our data, we found that all were identified in our SAGE and microarray analyses. In addition, we identified thousands of more genes expressed in mouse PA1, as well as in human PA1, by SAGE and microarrays.

We identified genes that are 'enriched' in PA1 from fourth to fifth week of human development. These PA1-enriched genes are good candidates for craniofacial diseases. Some of these PA1-enriched genes when mutated could lead to significant craniofacial abnormalities or even result in embryonic lethality. As a validation, some of these genes have already

been implicated in several human craniofacial disorders. The presence of some PA1-enriched genes in our libraries that cause human diseases without craniofacial manifestations may be due to their functional redundancy and/or their functional importance in other organ systems (Supplementary Material, Tables S7 and S8).

These profiling data, in combination with *in situ* hybridization, have also identified genes that might have a role in specific craniofacial abnormalities. The high expression of the *Set* gene in PA1 and its localization in the maxillary portion by GD10.5 suggests this gene as a candidate for orofacial clefting, because the palate normally forms by the fusion of the maxillary prominences. Similarly, the localization of *Cct3* expression to the mandibular portion of the PA1 suggests this gene as a candidate for micrognathia, as well as for other jaw abnormalities. Furthermore, these genes may serve as biological markers for PA1. For example, at GD10.5, cranial derivatives for neural crest cell populations are limited to pharyngeal arches and sensory ganglia of the face (upper only). At this stage, both *Set* and *Cct3* appear to be expressed in neural crest derivatives such as both arches.

Our results show that a large portion (65%) of human genes expressed in PA1 is also expressed in mouse PA1, providing further evidence for the conservation of developmental pathways between species. Real-time RT–PCR on mouse samples confirmed several expression changes detected by human SAGE libraries. These differentially expressed genes may shed light on the pathways involved in temporal development of PA1. In addition, many of these genes are involved in biosynthetic processes of early development. To date, a significant proportion of genes studied in both human and mouse PA1 are signal transducers and transcription regulators, but our functional analysis of all genes identified by our SAGE and Affymetrix data suggest future studies should focus on the genes which have binding or catalytic activities, because they represent the majority of PA1 genes.

We also found that *Set* and *Cct3* are expressed in the limb bud, an observation that may have clinical significance. Many patients with craniofacial syndromes also manifest limb abnormalities. Classic examples include craniosynostosis syndromes such as Pfeiffer, Apert, Crouzon, Greig cephalopolysyndactyly and metabolic defects such as Smith-Lemli-Optiz syndromes (www.ncbi.nlm.nih.gov/omim). Identifying molecules and signaling pathways shared by different organ systems will reveal common factors among diverse birth defects.

We observed limited agreement between our SAGE and microarray data. Only one of the 'enriched' genes identified by SAGE was identified by Affymetrix analysis, whereas only two genes that were differentially expressed by SAGE were confirmed by Affymetrix analysis. However, when highly expressed genes were analyzed, there was better agreement. More than half of the transcripts with SAGE tag counts greater than 100 were also among the highly expressed genes by Affymetrix analysis (Supplementary Material, Table S6). These discrepancies are similar to observations reported in other comparative studies (37–39) and are highlighted by issues of sensitivity (e.g. the number of sequenced SAGE tags, Affymetrix hybridization and detection procedures), specificity (multiple and non-matched SAGE tags and Affymetrix probe sets for alternative transcripts) and analytical methodologies. These results emphasize the need to use more than one global gene expression method and gene-specific expression assays for validation.

This large-scale expression profile of normal human craniofacial development is an important initial step toward elucidating this complex process. Our data can now be used to design microarrays with genes expressed in PA1 to provide further insights into early embryonic development. Correlating gene expression patterns and abnormal craniofacial phenotypes with linkage, association and mutation analyses is a powerful integrated approach to identify the causes of malformations.

MATERIALS AND METHODS

Human RNA acquisition

Morphologically normal human embryos were obtained through legalized abortions induced by Mifepristove (RU-486), according to the recommendations of the French National Ethics Committee. The developmental stage of each embryo was estimated, according to the Carnegie classification. Common chromosomal abnormalities were excluded by fluorescent quantitative PCR on chromosomes 13, 18, 21, X and Y, which are among the most commonly occurring aneuploidies. Embryos were microdissected from the whole trophoblasts stored in Tyrode's solution. Microdissected structures were suspended in Trizol, and total RNA was isolated according to manufacturer's protocol (Invitrogen, Carlsbad, CA, USA). Structure-specific RNAs collected from three to five different embryos at the same developmental stage were pooled and subjected to gene expression analysis.

Construction and analysis of human SAGE libraries

SAGE libraries were generated using a modified micro-SAGE protocol as previously reported (13). We constructed SAGE libraries from 1 to 2 μg of total RNA isolated from pooled microdissected tissues, without any preamplification steps that would potentially compromise the quantitative nature of this method. To increase the yield of SAGE ditags, we use a single-tube procedure for all steps prior to tag release, Dynal magnetic beads (Dynal, Brown Deer, WI, USA) and PhaseLock Gel (Eppendorf AG, Hamburg, Germany). All the SAGE data are available at hg.wustl.edu/cogene. Comparisons between libraries were carried out using the SAGE2000 (www.sagenet.org) and eSAGE softwares (14).

Human Affymetrix microarray hybridization and analysis

Human cDNA was generated using the same total RNA sources for SAGE (discussed earlier) with a modified SMART oligo method (hg.wustl.edu/cogene). *In vitro* transcription was performed with 100 ng of cDNA, using a MEGAscript High Yield Transcription Kit (Ambion, Austin, TX, USA). The resulting RNA was treated with DNase I, passed through a Sephadex G50 column and ethanol precipitated. This RNA was spiked with control RNAs and used

for synthesis of cDNA primed with oligo$(T)_{18}$-T7, according to the Affymetrix GeneChip instructions (Affymetrix, Santa Clara, CA, USA). The resulting DNA was used in an *in vitro* transcription reaction with labeled ribonucleotides. These targets were used on HG-U95Av2 chips. Hybridization, washing and image scanning were performed, according to the Affymetrix protocol. Duplicate experiments were performed for each target. Estimation, normalization of gene expression values and hierarchical clustering were performed, using dChip software (19). All our Affymetrix microarray data are available at hg.wustl.edu/cogene.

Mouse Affymetrix microarray hybridization and real-time RT–PCR analysis

Mouse GD9.5 and GD10.5 embryos were collected. PA1s were microdissected from the embryos, and 10–12 PA1s (each ~200 μm in size and from the same stages) were pooled and stored in RNAlater solution (Invitrogen). Total RNA was extracted using an RNeasy Mini Kit (Qiagen, Valencia, CA, USA) and cDNA was synthesized using an Omniscript RT Kit (Qiagen), according to the manufacturer's protocol for both real-time PCR and Affymetrix microarray hybridization to MOE430A and B chip set. Analyses were performed as for the human chips (discussed earlier).

For real-time PCR, PCR primers were designed with Primer3 software (frodo.wi.mit.edu/) to amplify intron-spanning amplicons. Real-time PCR reactions were carried out with QuantiTect SYBR Master Mix (Qiagen), as described previously (40). Specific amplification from cDNA and no amplification from genomic DNA were confirmed by melting curve analysis and subsequent gel electophoresis. External standards were generated using mouse brain Poly(A) RNA (Ambion) and the OmniScript kit for reverse transcription (Qiagen). Ten-fold serial dilutions of the products were made from $1:1$ to $1:10^{-4}$ to create a standard curve. Triplicate reactions were performed for both the samples and the standards. Transcript concentrations of both GD9.5 and GD10.5 PA1s were inferred from the standard curve, and fold changes were calculated after normalizing against a reference gene. The *Tmsb4x* gene (UniGene Hs.75968) was chosen as a reference gene, because it was among the top 1% of genes with respect to constant expression level in all SAGE libraries, and a robust real-time RT–PCR assay could be developed.

Mouse whole mount *in situ* hybridization

PCR primers, designed with Primer3 software (frodo.wi.mit.edu/), were used to amplify cDNA-specific products, which were sequenced in both directions to ensure no mutations were incorporated. DIG-labeled RNA probes were generated from the PCR products using a DIG RNA transcription kit (Roche, Indianapolis, IN, USA), according to the manufacturer's protocol. Normal C57BL/6J mice were mated for 2 h. GD8.5, GD9.5 or GD10.5 mouse embryos were dissected in Ringer's solution and were fixed in 4% paraformaldehyde in PBS overnight at 4°C. Mouse whole mount *in situ* hybridization was then performed as described previously (41). Images were taken with DXM1200 digital camera (Nikon, Melville, NY, USA).

GO analysis

Functional categories for genes were assigned to top-level GO terms under the 'molecular function' hierarchy, on the basis of information from the Gene Ontology Consortium (www.geneontology.org). Gominer software (discover.nci.nih.gov/gominer) was used with data source set to 'UniProt (H. sapiens *et al.*)' and organisms set to 'H. sapiens' (42). To find statistically overrepresented biological process GO terms, GOstat program was used (gostat.wehi.edu.au) (21).

SUPPLEMENTARY MATERIAL

Supplementary Material is available at HMG Online.

ACKNOWLEDGEMENTS

We thank Drs Aravinda Chakravarti, Kenneth Kinzler and Alan F. Scott for helpful discussions on this study and Dr Barbara R. Migeon for suggestions on the manuscript. The work represents the effort of the Craniofacial and Oral Gene Expression Network (COGENE) consortium. This study was supported by National Institutes of Health grants T32 GM07814 (J.C.) and NO1DE92630.

REFERENCES

1. Gorlin, R.J., Cohen, M.M., Jr and Hennekam, R.C.M. (2001) *Syndromes of the Head and Neck.* Oxford University Press, New York.
2. Graham, A. and Smith, A. (2001) Patterning the pharyngeal arches. *Bioessays*, **23**, 54–61.
3. Neubuser, A., Peters, H., Balling, R. and Martin, G.R. (1997) Antagonistic interactions between FGF and BMP signaling pathways: a mechanism for positioning the sites of tooth formation. *Cell*, **90**, 247–255.
4. Lievre, C.L. (1974) Role of mesectodermal cells arising from the cephalic neural crest in the formation of the branchial arches and visceral skeleton. *J. Embryol. Exp. Morphol.*, **31**, 453–477.
5. Noden, D.M. (1983) The role of the neural crest in patterning of avian cranial skeletal, connective, and muscle tissues. *Dev. Biol.*, **96**, 144–165.
6. Trainor, P. and Krumlauf, R. (2000) Plasticity in mouse neural crest cells reveals a new patterning role for cranial mesoderm. *Nat. Cell Biol.*, **2**, 96–102.
7. Graham, A., Francis-West, P., Brickell, P. and Lumsden, A. (1994) The signalling molecule BMP4 mediates apoptosis in the rhombencephalic neural crest. *Nature*, **372**, 684–686.
8. Winograd, J., Reilly, M.P., Roe, R., Lutz, J., Laughner, E., Xu, X., Hu, L., Asakura, T., van der Kolk, C., Strandberg, J.D. *et al.* (1997) Perinatal lethality and multiple craniofacial malformations in MSX2 transgenic mice. *Hum. Mol. Genet.*, **6**, 369–379.
9. Veitch, E., Begbie, J., Schilling, T.F., Smith, M.M. and Graham, A. (1999) Pharyngeal arch patterning in the absence of neural crest. *Curr. Biol.*, **9**, 1481–1484.
10. Velculescu, V.E., Zhang, L., Vogelstein, B. and Kinzler, K.W. (1995) Serial analysis of gene expression. *Science*, **270**, 484–487.
11. Richards, M., Tan, S.P., Tan, J.H., Chan, W.K. and Bongso, A. (2004) The transcriptome profile of human embryonic stem cells as defined by SAGE. *Stem Cells*, **22**, 51–64.
12. Sperger, J.M., Chen, X., Draper, J.S., Antosiewicz, J.E., Chon, C.H., Jones, S.B., Brooks, J.D., Andrews, P.W., Brown, P.O. and Thomson, J.A. (2003) Gene expression patterns in human embryonic stem cells and human pluripotent germ cell tumors. *Proc. Natl Acad. Sci. USA*, **100**, 13350–13355.
13. Cai, J., Ash, D. and Jabs, E.W. (2002) SAGE analysis from 1 μg of total RNA. In Yamada, K.M. (ed.), *Current Protocols in Cell Biology.* John Wiley & Sons, Inc., Vol. 2.

14. Margulies, E.H. and Innis, J.W. (2000) eSAGE: managing and analysing data generated with serial analysis of gene expression (SAGE). *Bioinformatics*, **16**, 650–651.
15. Velculescu, V.E., Zhang, L., Zhou, W., Vogelstein, J., Basrai, M.A., Bassett, D.E., Jr, Hieter, P., Vogelstein, B. and Kinzler, K.W. (1997) Characterization of the yeast transcriptome. *Cell*, **88**, 243–251.
16. Velculescu, V.E., Madden, S.L., Zhang, L., Lash, A.E., Yu, J., Rago, C., Lal, A., Wang, C.J., Beaudry, G.A., Ciriello, K.M. *et al.* (1999) Analysis of human transcriptomes. *Nat. Genet.*, **23**, 387–388.
17. Margulies, E.H., Kardia, S.L. and Innis, J.W. (2001) A comparative molecular analysis of developing mouse forelimbs and hindlimbs using serial analysis of gene expression (SAGE). *Genome Res.*, **11**, 1686–1698.
18. Zhou, G., Chen, J., Lee, S., Clark, T., Rowley, J.D. and Wang, S.M. (2001) The pattern of gene expression in human CD34(+) stem/progenitor cells. *Proc. Natl Acad. Sci. USA*, **98**, 13966–13971.
19. Li, C. and Wong, W.H. (2001) Model-based analysis of oligonucleotide arrays: expression index computation and outlier detection. *Proc. Natl Acad. Sci. USA*, **98**, 31–36.
20. Audic, S. and Claverie, J.M. (1997) The significance of digital gene expression profiles. *Genome Res.*, **7**, 986–995.
21. Beissbarth, T. and Speed, T.P. (2004) GOstat: find statistically overrepresented gene ontologies within a group of genes. *Bioinformatics*, **20**, 1464–1465.
22. Avantaggiato, V., Orlandini, M., Acampora, D., Oliviero, S. and Simeone, A. (1998) Embryonic expression pattern of the murine *figf* gene, a growth factor belonging to platelet-derived growth factor/vascular endothelial growth factor family. *Mech. Dev.*, **73**, 221–224.
23. Pilia, G., Hughes-Benzie, R.M., MacKenzie, A., Baybayan, P., Chen, E.Y., Huber, R., Neri, G., Cao, A., Forabosco, A. and Schlessinger, D. (1996) Mutations in *GPC3*, a glypican gene, cause the Simpson-Golabi-Behmel overgrowth syndrome. *Nat. Genet.*, **12**, 241–247.
24. Veugelers, M., Cat, B.D., Muyldermans, S.Y., Reekmans, G., Delande, N., Frints, S., Legius, E., Fryns, J.P., Schrander-Stumpel, C., Weidle, B. *et al.* (2000) Mutational analysis of the GPC3/GPC4 glypican gene cluster on Xq26 in patients with Simpson-Golabi-Behmel syndrome: identification of loss-of-function mutations in the *GPC3* gene. *Hum. Mol. Genet.*, **9**, 1321–1328.
25. Joutel, A., Vahedi, K., Corpechot, C., Troesch, A., Chabriat, H., Vayssiere, C., Cruaud, C., Maciazek, J., Weissenbach, J., Bousser, M.G. *et al.* (1997) Strong clustering and stereotyped nature of Notch3 mutations in CADASIL patients. *Lancet*, **350**, 1511–1515.
26. Pai, S.I., Wu, G.S., Ozoren, N., Wu, L., Jen, J., Sidransky, D. and El-Deiry, W.S. (1998) Rare loss-of-function mutation of a death receptor gene in head and neck cancer. *Cancer Res.*, **58**, 3513–3518.
27. Howard, T.D., Paznekas, W.A., Green, E.D., Chiang, L.C., Ma, N., Ortiz de Luna, R.I., Garcia Delgado, C., Gonzalez-Ramos, M., Kline, A.D. and Jabs, E.W. (1997) Mutations in TWIST, a basic helix–loop–helix transcription factor, in Saethre-Chotzen syndrome. *Nat. Genet.*, **15**, 36–41.
28. Bourgeois, P., Bolcato-Bellemin, A.L., Danse, J.M., Bloch-Zupan, A., Yoshiba, K., Stoetzel, C. and Perrin-Schmitt, F. (1998) The variable expressivity and incomplete penetrance of the twist-null heterozygous mouse phenotype resemble those of human Saethre-Chotzen syndrome. *Hum. Mol. Genet.*, **7**, 945–957.
29. The Treacher Collins Syndrome Collaborative Group (1996) Positional cloning of a gene involved in the pathogenesis of Treacher Collins syndrome. *Nat. Genet.*, **12**, 130–136.
30. Dixon, J., Brakebusch, C., Fassler, R. and Dixon, M.J. (2000) Increased levels of apoptosis in the prefusion neural folds underlie the craniofacial disorder, Treacher Collins syndrome. *Hum. Mol. Genet.*, **9**, 1473–1480.
31. von Lindern, M., van Baal, S., Wiegant, J., Raap, A., Hagemeijer, A. and Grosveld, G. (1992) Can, a putative oncogene associated with myeloid leukemogenesis, may be activated by fusion of its 3′ half to different genes: characterization of the set gene. *Mol. Cell. Biol.*, **12**, 3346–3355.
32. Sevigny, G., Joly, E.C., Bibor-Hardy, V. and Lemieux, N. (1994) Assignment of the human homologue of the mTRiC-P5 gene (*TRIC5*) to band 1q23 by fluorescence *in situ* hybridization. *Genomics*, **22**, 634–636.
33. Wilcoxon, F. (1945) Individual comparisons by ranking methods. *Biometrics Bull.*, **1**, 80–83.
34. Li, H., Chen, Y., Jiang, Y., Bittner, M., Meltzer, P., Trent, J., Yamada, K. and Yamada, Y. (1999) Profiling expression patterns of 2214 unigenes in mouse craniofacial development by cDNA microarray analysis. *Nat. Genet.*, **23**, 57–58.
35. Neuhauss, S.C., Solnica-Krezel, L., Schier, A.F., Zwartkruis, F., Stemple, D.L., Malicki, J., Abdelilah, S., Stainier, D.Y. and Driever, W. (1996) Mutations affecting craniofacial development in zebrafish. *Development*, **123**, 357–367.
36. Fowles, L.F., Bennetts, J.S., Berkman, J.L., Williams, E., Koopman, P., Teasdale, R.D. and Wicking, C. (2003) Genomic screen for genes involved in mammalian craniofacial development. *Genesis*, **35**, 73–87.
37. Ishii, M., Hashimoto, S., Tsutsumi, S., Wada, Y., Matsushima, K., Kodama, T. and Aburatani, H. (2000) Direct comparison of GeneChip and SAGE on the quantitative accuracy in transcript profiling analysis. *Genomics*, **68**, 136–143.
38. Haverty, P.M., Hsiao, L.L., Gullans, S.R., Hansen, U. and Weng, Z. (2004) Limited agreement among three global gene expression methods highlights the requirement for non-global validation. *Bioinformatics*, **20**, 3431–3441.
39. Lu, J., Lal, A., Merriman, B., Nelson, S. and Riggins, G. (2004) A comparison of gene expression profiles produced by SAGE, long SAGE, and oligonucleotide chips. *Genomics*, **84**, 631–636.
40. Cai, J., Goodman, B.K., Patel, A.S., Mulliken, J.B., van Maldergem, L., Hoganson, G.E., Paznekas, W.A., Ben-Neriah, Z., Sheffer, R., Cunningham, M.L. *et al.* (2003) Increased risk for developmental delay in Saethre-Chotzen syndrome is associated with TWIST deletions: an improved strategy for TWIST mutation screening. *Hum. Genet.*, **114**, 68–76.
41. Henrique, D., Adam, J., Myat, A., Chitnis, A., Lewis, J. and Ish-Horowicz, D. (1995) Expression of a delta homologue in prospective neurons in the chick. *Nature*, **375**, 787–790.
42. Zeeberg, B.R., Feng, W., Wang, G., Wang, M.D., Fojo, A.T., Sunshine, M., Narasimhan, S., Kane, D.W., Reinhold, W.C., Lababidi, S. *et al.* (2003) GoMiner: a resource for biological interpretation of genomic and proteomic data. *Genome Biol.*, **4**, R28.

Table S1. Distribution of SAGE Tags in Human PA1 Libraries

W4PA1						
Tag Count	1	2 – 5	6 – 10	11 – 100	> 100	Total
Unique	13323	4839	829	651	58	19700
Novel	4299	460	39	33	3	4834
Matched	9024	4379	790	618	55	14866
Single-Matched	5650	2429	415	316	17	8827
Multiple-Matched	3374	1950	375	302	38	6039

W5PA1						
Tag Count	1	2 – 5	6 – 10	11 – 100	> 100	Total
Unique	14801	5309	955	760	60	21885
Novel	4857	451	39	43	2	5392
Matched	9944	4858	916	717	58	16493
Single-Matched	6178	2712	504	370	20	9784
Multiple-Matched	3766	2146	412	347	38	6709

Table S2. Functional Classification of PA1 Genes

	SAGE				
Functional category	W4PA1[a]	W5PA1[a]	Differential[b]	High[c]	Enriched[d]
antioxidant activity	0.2	0.3	0.0	0.0	0.0
binding	37.1	37.5	42.9	49.7	35.2
catalytic activity	25.2	23.7	19.6	10.7	26.4
chaperone activity	2.3	2.4	1.8	0.0	2.2
enzyme regulator activity	3.2	3.5	3.6	0.0	2.2
motor activity	0.6	0.8	0.0	0.0	2.2
signal transducer activity	7.0	6.7	4.5	0.0	8.8
structural molecule activity	5.5	5.1	10.7	23.7	5.5
transcription regulator activity	5.5	6.4	1.8	0.0	8.8
translation regulator activity	1.2	1.3	1.8	10.6	0.0
transporter activity	8.9	9.2	8.0	.0.0	5.5
unknown	3.4	3.2	5.4	5.3	3.3

	Affymetrix				
Functional category	W4PA1[e]	W5PA1[e]	Differential[f]	High[g]	Enriched[h]
antioxidant activity	0.3	0.3	0.0	0.4	1.0
binding	37.5	37.5	40.8	36.1	37.4
catalytic activity	24.6	24.8	21.1	15.7	26.3
chaperone activity	1.6	1.5	0.0	0.0	1.0
enzyme regulator activity	2.9	3.2	1.4	1.3	1.0
motor activity	0.6	0.7	1.4	0.4	1.0
signal transducer activity	9.3	9.6	5.6	4.3	4.0

structural molecule activity	4.0	3.6	7.0	28.7	7.1
transcription regulator activity	7.1	7.0	7.0	3.0	5.1
translation regulator activity	0.8	0.8	0.0	1.7	1.0
transporter activity	8.5	8.4	7.0	6.5	14.1
unknown	2.7	2.8	8.5	1.7	1.0

Listed are percentages of genes assigned to 12 molecular function categories based on information from the Gene Ontology Consortium (www.geneontology.org). The groups of genes analyzed by SAGE include: [a]3,177 and 3,606 unique tags with counts greater than one in W4PA1 and W5PA1, respectively; [b]97 genes differentially expressed between W4PA1 and W5PA1 (Table S3), [c]24 genes highly expressed (SAGE tag count greater than 100 in either W4PA1 or W5PA1(Table S6); [d]74 genes enriched at least two-fold in both W4PA1 and W5PA1 compared to all other SAGE libraries (Table S7). The groups of genes analyzed by Affymetrix microarray include: [e]3,681 and 4,869 genes called "present" in W4PA1 and W5PA1, respectively; [f]62 genes differentially expressed between W4PA1 and W5PA1 (Table S4); [g]200 (top 5% of all genes) most highly expressed genes; [h]96 genes enriched at least two-fold in both W4PA1 and W5PA1 compared to all other samples analyzed by microarray (Table S8).

Table S3. Genes Differentially Expressed in Human PA1 by SAGE

Gene	Tag	W4PA1[a]	W5PA1[b]	Ratio
ENT4	TCAGGGCTGA	0	36	-31.7
NME4	GGTGGTACAC	1	19	-16.7
COPB	TACCAAGACC	1	15	-13.2
CBX1	TGTTAGATTT	1	15	-13.2
TIMM17B	TACGAAGTTC	1	15	-13.2
MGC14258	TTGGAACAAT	2	29	-12.8
PCOLN3	GGCCAGGTGG	1	13	-11.5
CSPG2	TATGAATGCT	0	12	-10.6
PTPRA	GGGAGTAATA	1	12	-10.6
CLIPR-59	ACTCCTGTCC	1	11	-9.7
-	GCAACTTAAC	1	11	-9.7
PCNA	GGCGTGAACC	1	11	-9.7
MASA	TTGTGATTAA	1	11	-9.7
LSM7	GAGGCCATCC	2	20	-8.8
EGFL3	TAAACCTAGG	0	10	-8.8
TOPBP1	ATGTTTGCCA	0	10	-8.8
LOC154467	GTGCTGGTCC	0	10	-8.8
HSPCA	TACTAGTCCT	4	39	-8.6
ULK1	TGCGTGTGTC	0	9	-7.9
RPL4	GCGGAGAGAG	0	9	-7.9
ZFP91	GGAGAGACAG	0	8	-7.1
MRC2	GCCCTTTCTC	0	8	-7.1

MTMR4	CAATGTGCTG	0	8	-7.1
MARCKS	GGTGCCCAGT	0	8	-7.1
GABARAP	AAGAAGACTT	0	8	-7.1
-	TGGAACCTTG	0	8	-7.1
FIGF*	GAATGGCAGG	0	8	-7.1
NEDD5	CGGAGTCCAT	2	15	-6.6
LMNB2	CCTAATGTGT	2	15	-6.6
CS	ATGGAGACTT	2	14	-6.2
MAC30	TTGCGGAGCC	2	13	-5.7
FSCN1	CATCTCACTC	2	13	-5.7
RPLP2	GGATTTGGCC	62	365	-5.2
VPS16	GTAGCAGGGC	4	20	-4.4
H19	GGGCGAGACC	4	20	-4.4
PIG8	AGCTGGTTTC	3	15	-4.4
SET	TATCTGTCTA	10	42	-4
GHITM	AGTCTGATGT	4	18	-4
BTF3	CTGAGACGAA	4	18	-4
HNRPD	ATGTAGTAGT	16	68	-3.7
APP	ATCGCTTTCT	5	21	-3.7
RPL23	TCACCCACAC	8	33	-3.6
FADS2	TTACTTCCCC	6	23	-3.4
DPP7	GCGACAGCTC	11	39	-3.1
GSTP1	AGGTCCTAGC	7	24	-3
RPS23	CTGTTGGTGA	55	174	-2.8

MORF4L1	ATAGACGCAA	10	30	-2.6
SLC25A6	GGTGAGACAC	14	39	-2.5
GNB2L1	TTATGGGATC	16	44	-2.4
NDUFA4	TTGGAGATCT	15	41	-2.4
MATR3	TTTGGAATGT	15	40	-2.4
RPL9	ATCAAGGGTG	21	54	-2.3
ATP5L	TGTGATCAGA	18	46	-2.3
RPL17	AGCTCTCCCT	47	125	-2.3
MGC40157	AACTAATACT	17	43	-2.2
RPL32	TGCACGTTTT	131	331	-2.2
-	GTGACCACGG	39	94	-2.1
PPIA	CCTAGCTGGA	40	94	-2.1
EIF3S8	CGCCGCGGTG	41	23	2
RPL14	CAGCTCACTG	38	21	2.1
SNRPE	CTAAAAGGAG	33	17	2.2
NGFRAP1	GAAAAATTTA	98	48	2.3
TPI1	TGAGGGAATA	130	65	2.3
D1S155E	CAAATGAGGA	48	21	2.6
H2AFY	AATTTGCAAC	25	11	2.6
FASN	TGATCTCCAA	50	19	3
SUI1	TGAAGTAACA	24	9	3
LAPTM4A	TTTCTAGTTT	36	13	3.1
SEC13L1	TTACGAGGAA	19	7	3.1
-	GCACAAGAAG	113	42	3.1

ZYX	CTGCCAAGTT	24	8	3.4
HSPE1	TAAATAATTT	34	11	3.5
RPS14	TAAACTGAAA	22	7	3.6
DSS1	GTTATAAGAT	19	6	3.6
CGI-99	TTTGGAAATC	23	7	3.7
TM4SF6	TTAGATCGTT	17	5	3.9
-	TAATTTTGGA	18	5	4.1
MGC4730	GACAGACATC	15	4	4.3
SQLE	CAAATAAAAT	49	12	4.6
HMGB2	TCTGCAAAGG	26	6	4.9
LY6E	CACTTCAAGG	13	3	4.9
-	CAGTGAATGA	23	5	5.2
NTHL1	GCTCTGGCCG	14	3	5.3
RBM3	ATTATCCAGG	25	5	5.7
SF3A3	CTGGCAGATT	13	2	7.4
-	GAATAATTGT	21	3	7.9
FLJ20375	CCTCCTAAGA	7	0	7.9
POLD3	AGTTAAATAA	7	0	7.9
ATP6V1E1	AATATGCTTT	8	0	9.1
CCNG1	TTTTATGGGT	9	1	10.2
EWSR1	GACCGAGGTG	9	1	10.2
ZIM2	TCTAACTTGC	11	0	12.5
CHC1L	TAATGTAAAG	12	1	13.6
CYP51A1*	TTAAACTCTA	13	1	14.7

KIAA0111	TAAATAATAC	15	1	17
RPL4	TCTAAAGGTC	17	1	19.3
-	ATGAAACTTC	19	1	21.6

Listed are all unique SAGE tags which are differentially expressed with a ratio of < -2 or > 2, $p < 0.01$ in W4PA1 and W5PA1 libraries.

-, tags that do not match to SAGEmap database

[a]59959 tags sequenced

[b]67982 tags sequenced

*Also differentially expressed by microarray

Table S4. Genes Differentially Expressed in Human PA1 by Microarray

Gene	Probe Set ID	Ratio
ATRNL1	33743_at	-7.15
FIGF*	1958_at	-6.43
DCX	34382_at	-6.87
FHL2	38422_s_at	-6.45
ANK3	36965_at	-5.63
DDX3Y	38355_at	-5.31
WEE1	36909_at	-4.92
ZNF473	36516_at	-4.76
RPS4Y1	41214_at	-4.68
CENPF	37302_at	-4.65
XPC	1873_at	-4.51
FLRT2	34853_at	-4.38
SEPT6	38826_at	-4.24
CLASP1	39838_at	-4.09
MN1	37283_at	-4.08
C11orf8	36029_at	-4.02
ZNF278	34299_at	-3.8
TLE1	41489_at	-3.77
KIAA0157	37642_at	-3.75
MAGED2	34859_at	-3.71
CTNNA1	2085_s_at	-3.7
KIAA0711	36453_at	-3.61
MKI67	419_at	-3.61

CDC2L5	41821_at	-3.6
RNF144	37695_at	-3.57
NR2F2	39397_at	-3.48
TUBB4	471_f_at	-3.42
INPP5F	36089_at	-3.36
CXX1	33856_at	-3.26
PHF2	39117_at	-3.17
ATP6V1B2	40568_at	-3.15
PICALM	37685_at	-3.09
LASP1	36181_at	-2.99
PLSCR1	32775_r_at	-2.97
H326	39823_at	-2.97
CRABP1	543_g_at	-2.89
-	296_at	-2.88
THEM2	41058_g_at	-2.8
MSX1	40199_at	-2.8
MAEA	32832_at	-2.77
YME1L1	40988_at	-2.69
IMPA2	36496_at	-2.66
RPA1	38481_at	-2.59
USP24	35847_at	-2.55
MGC57820	40877_s_at	-2.52
MN7	40878_f_at	-2.45
ARC	36307_at	2.84
TRPC1	39124_r_at	3.03

LRRN3	35712_at	3.25
CASP9	487_g_at	3.49
SDHB	35751_at	3.53
BAX	1998_i_at	3.55
FGF18	41588_at	3.69
WWP1	40902_at	3.69
CYP51A1*	33389_at	3.7
THBS2	659_g_at	3.77
CYLN2	41396_at	3.86
JMJD3	41387_r_at	4.04
BRD1	41699_f_at	4.19
MEF2A	41747_s_at	4.39
SUPT3H	33205_at	4.47
CRYM	38285_at	4.91

Listed are all genes which are differentially expressed with a ratio of < -2 or > 2, based on Affymetrix HG-U95Av2 chip data.

*Also differentially expressed by SAGE

Table S5. Confirmation of SAGE Tag Differential Expression by RT-PCR

Human SAGE					Mouse RT-PCR
Tag	Gene	W4PA1[a]	W5PA1[b]	Fold Change[c]	Fold Change
GGAGTAAAAT	PITX2	10	2	5.7	1.9
CAAATAAAAT	SQLE	49	12	4.6	2.3
TTAGATCGTT	TM4SF6	17	5	3.9	4.7
CTGCCAAGTT	ZYX	24	8	3.4	8.0
TGAGGGAATA	TPI1	130	65	2.3	1.7
CCCTGCCTTG	MDK	23	50	-1.9	-2.4
TCTCCTGCAT	MSX1	10	26	-2.3	-10.4
TTTGGAATGT	MATR3	15	40	-2.4	-12.5
GCGACAGCTC	DPP7	11	39	-3.1	-22.9
ATGTAGTAGT	HNRPD	16	68	-3.7	2.5
CGGAGTCCAT	NEDD5	2	15	-6.6	-10.8
TACGTCTATT	PITX1	1	9	-7.9	-3.2
TACTAGTCCT	HSPCA	4	39	-8.6	-3.5
GGTGGTACAC	NME4	1	19	-16.7	-2.3

Only for the *HNRPD* gene, there was a lack of agreement in the fold change direction between SAGE and RT-PCR data.

[a]59959 tags sequenced

[b]67982 tags sequenced

[c]Fold change is significant ($p<0.05$)

Table S6. Genes Highly Expressed in Human PA1

Gene	SAGE			Affymetrix
	Tag	W4PA1[a]	W5PA1[b]	
TPT1	TAGGTTGTCT	204	369	+
RPL32	TGCACGTTTT	131	331	NA
RPLP2	GGATTTGGCC	62	365	NA
RPS25*	AATAGGTCCA	226	186	+
EEF1G*	TGGGCAAAGC	131	233	+
RPL23*	ATTCTCCAGT	174	186	+
RPL28	GCAGCCATCC	174	186	+
EEF2	AGCACCTCCA	115	218	+
HNRPA1	TGTAATCAAT	147	163	+
FLNA	GTTCGTGCCA	145	155	+
RPL13*	CCCGTCCGGA	157	141	+
CFL1*	GAAGCAGGAC	99	155	+
RPL30*	CCAGAACAGA	93	159	+
RPL39	TTACCATATC	100	149	-
RPL35*	CGCCGCCGGC	139	103	+
RPS23*	CTGTTGGTGA	55	174	+
RPS24*	GCCTGTATGA	106	106	+
RPS28*	GACGACACGA	107	105	+
GPC3	GATTTCTTTG	110	95	+
RPL5*	CTGCTATACG	125	79	+
TPI1*	TGAGGGAATA	130	65	+
C1S	GCCGAGGAAG	68	115	+

RPL17*	AGCTCTCCCT	47	125	+
EST	GCACAAGAAG	113	42	NA

Listed are all unique SAGE tags with counts greater than 100 in either W4PA1 or W5PA1 libraries.

[a]59959 tags sequenced

[b]67982 tags sequenced

+, present call

-, absent call

NA, not available on Affymetrix HG-U95Av2 chip

*Genes that are among the top 200 highly expressed as assayed by microarray.

Table S7. Genes at Least Two-fold Enriched in Human PA1 by SAGE

Gene	UniGene ID	Fold Enriched[a]	Human Disease Involved
KIAA0252	Hs.83419	8.09	
LOC128344	Hs.172510	7.55	
ERG	Hs.45514	7.30	
FLJ10439	Hs.3487	5.80	
TM6SF1	Hs.341203	5.74	
GCN1L1	Hs.75354	5.59	
NOTCH3	Hs.8546	5.41	cerebral autosomal dominant arteriopathy with subcortical infarcts and leukoencephalopathy
ERP70	Hs.93659	5.10	
CBX5	Hs.89232	5.00	
HIC2	Hs.109445	4.94	
DOK4	Hs.279832	4.87	
MTA1	Hs.101448	4.75	
ANAPC7	Hs.52763	4.64	
ZFP36L2	Hs.78909	4.47	
GEMIN4	Hs.302421	4.04	
RAB7	Hs.356386	3.99	Charcot-Marie-Tooth type 2B
CSNK2B	Hs.430522	3.79	
DDAH2	Hs.247362	3.78	
APOC1	Hs.268571	3.70	age-associated memory impairment
BAT8	Hs.75196	3.69	
BAT2	Hs.25911	3.62	

CD164	Hs.43910	3.54	
PRKCN	Hs.143460	3.49	
CIRH1A	Hs.151001	3.39	North American Indian childhood cirrhosis
PDE4D	Hs.172081	3.38	stroke
PARD3	Hs.72249	3.38	
MGC5139	Hs.127610	3.25	
MRG2	Hs.405872	3.25	
SFRS1	Hs.73737	3.22	
YWHAB	Hs.279920	3.18	
MAK3P	Hs.288932	3.18	
AMOTL1	Hs.17110	3.16	
NLI-IF	Hs.283724	3.14	
AGTPBP1	Hs.21542	3.05	
G6PD	Hs.80206	2.97	
KIF1C	Hs.139648	2.92	
LOC58486	Hs.25726	2.87	
LOC51240	Hs.7870	2.85	
SCOTIN	Hs.24220	2.83	
NFE2L1	Hs.83469	2.82	
STOML2	Hs.3439	2.78	
NR2F1	Hs.374991	2.77	
KIAA0169	Hs.374382	2.74	
TFAP2A	Hs.432765	2.73	
RPL27A	Hs.76064	2.73	

POLR2J	Hs.220255	2.72	
NMP200	Hs.173980	2.72	
INPP5E	Hs.75353	2.65	
PPIB	Hs.394389	2.64	
MYH9	Hs.146550	2.61	May-Hegglin anomaly, Fechtner syndrome and Sebastian syndrome
CENPF*	Hs.77204	2.57	
BTF	Hs.80338	2.55	
MIDN	Hs.300870	2.52	
XRN2	Hs.268555	2.51	
GPRK5	Hs.211569	2.51	
RANBP9	Hs.279886	2.51	
eIF2a	Hs.332404	2.50	
RAD21	Hs.81848	2.47	
IBA2	Hs.4944	2.45	
GPC3	Hs.119651	2.45	Simpson-Golabi-Behmel syndrome type I
USP11	Hs.171501	2.43	
RARS	Hs.180832	2.39	
PSMB6	Hs.77060	2.34	
C20orf149	Hs.79625	2.32	
TBCA	Hs.433254	2.30	
TNFRSF10B	Hs.51233	2.27	head and neck squamous cell carcinoma
GNB2	Hs.91299	2.25	
SART3	Hs.116875	2.24	

UNRIP	Hs.3727	2.22
MATR3	Hs.78825	2.21
PAI-RBP1	Hs.165998	2.17
XTP2	Hs.69559	2.07
MMP14	Hs.2399	2.03
MCM3AP	Hs.168481	2.03

[a]The ratio of the number of tags from either the W4PA1 or W5PA1 SAGE libraries to the average number of tags from the 10 other libraries was calculated. For a gene to be considered “enriched”, both the W4PA1 and W5PA1 ratios had to be greater than 2. The average ratio from these two libraries was calculated and the value listed under “Fold Enriched”. Only moderately to highly expressed SAGE tags with a combined count of more than 20 in all libraries were analyzed.

*Also two-fold enriched by microarray

Table S8. Genes at Least Two-fold Enriched in Human PA1 by Microarray

Gene	UniGene ID	Fold Enriched[a]	Human Disease Involved
RPL28	Hs.356371	3.52	
RPS21	Hs.372960	3.41	
HIST1H4I	-	3.35	
RPS12	Hs.380956	3.21	
CENPF*	Hs.77204	3.12	
GNAS	Hs.157307	2.99	McCune-Albright syndrome
COX8A	Hs.433901	2.98	
HIST1H4I	-	2.97	
RPL18	Hs.409634	2.96	
BAMBI	Hs.348802	2.96	
CKS1B	Hs.374378	2.78	
NIFIE14	Hs.9234	2.77	
GNAS	Hs.157307	2.76	McCune-Albright syndrome
HIST1H4A	Hs.248172	2.73	
GPX4	Hs.433951	2.72	
FIGF	Hs.11392	2.71	
eIF3k	Hs.143773	2.70	
POLR2I	Hs.47062	2.66	
RPS21	Hs.372960	2.65	
BTF3	Hs.446567	2.64	
C9orf36	Hs.123004	2.64	
RPS15A	Hs.370504	2.62	

MAGED2	Hs.376719	2.62	
UQCRC1	Hs.119251	2.59	
COX6B	Hs.431668	2.59	
JMJD2A	Hs.155983	2.55	
RPL37	Hs.80545	2.53	
SNRPB	Hs.83753	2.53	
SIVA	Hs.112058	2.51	
ATP5J2	Hs.235557	2.47	
HIST1H4L	-	2.42	
PDGFRA	*Hs.74615*	*2.41*	gastrointestinal stromal tumors
GPR161	Hs.271809	2.41	
S100A13	Hs.446592	2.4	
OAZ1	Hs.446427	2.39	
C14orf2	Hs.109052	2.39	
UQCR	Hs.8372	2.37	
CCT3	Hs.1708	2.37	
QDPR	Hs.75438	2.35	
ATP5G3	Hs.429	2.34	
KPNA4	Hs.288193	2.32	
SELENBP1	Hs.334841	2.32	
PIN1	-	2.32	
NAP1L1	Hs.419776	2.29	
TOE1	Hs.288198	2.28	
TMSB10	Hs.446574	2.27	

DOCK10	Hs.21126	2.27	
LSM2	Hs.103106	2.25	
RPS5	Hs.378103	2.24	
RNF144	Hs.78894	2.24	
FDPS	Hs.335918	2.23	
NME1	Hs.118638	2.22	advanced neuroblastomas
PSPH	Hs.512656	2.22	
TYRO3	Hs.381282	2.19	
PSMB4	Hs.89545	2.19	
THEM2	Hs.9676	2.19	
SSBP1	Hs.923	2.17	
NOLA2	Hs.386392	2.17	
COX6C	Hs.351875	2.16	
GNG5	Hs.436765	2.15	
RBP1	Hs.101850	2.14	
FLJ11806	Hs.323443	2.14	
RPS16	Hs.397609	2.13	
RPLP1	Hs.356502	2.12	
PTBP1	Hs.172550	2.12	
AKR1B1	Hs.75313	2.11	
TIP-1	Hs.12956	2.11	
RPS15	Hs.406683	2.10	
COX6A1	Hs.180714	2.10	
MKI67	Hs.80976	2.10	

GSTP1	Hs.411509	2.10	
SPI1	Hs.157441	2.09	
HMGB3	Hs.19114	2.09	
POLR2L	Hs.441072	2.09	
ARID1A	Hs.170333	2.08	
CFDP1	Hs.433402	2.08	
MGC5508	Hs.13662	2.08	
IDH3B	Hs.436405	2.08	
NME1	Hs.118638	2.06	advanced neuroblastomas
MYH10	Hs.280311	2.06	
TYRO3	Hs.381282	2.06	
TKT	Hs.89643	2.06	
CXX1	Hs.250708	2.05	
THEM2	Hs.9676	2.05	
GMPS	Hs.144057	2.04	
ID3	Hs.76884	2.04	
RPL38	Hs.380953	2.03	
UBE2N	Hs.458359	2.03	
WBSCR1	Hs.180900	2.03	
ANKRD12	Hs.388877	2.02	
DDX48	Hs.389649	2.02	
FABP5	Hs.408061	2.02	
PPID	Hs.143482	2.02	
AKR1A1	Hs.372170	2.01	

MRPS27	Hs.376200	2.01
ADPRT	Hs.177766	2.00

[a]The ratio of the gene expression intensity value from either W4PA1 or W5PA1 to the average expression intensity value from the 23 other libraries was calculated. For a gene to be considered "enriched", both ratios had to be greater than 2, and the average ratio was obtained and listed under "Fold Enriched".

*Also two-fold enriched by SAGE

Table S9. Genes Common to Both Human and Mouse PA1

Gene	UniGene ID
RPL21	Hs.381123
RPS18	Hs.275865
RPS29	Hs.539
RPS19	Hs.381184
EEF1A1	Hs.439552
SPAG7	Hs.90436
RPLP1	Hs.356502
HNRPA1	Hs.535072
ACTG1	Hs.14376
RPL28	Hs.356371
GNAS	Hs.157307
CCT3	Hs.1708
RPS27A	Hs.311640
TXNRD1	Hs.501739
MATR3	Hs.78825
RPL23	Hs.406300
FLNA	Hs.195464
EEF2	Hs.75309
RPS3A	Hs.356572
IGF1	Hs.308053
HDAC2	Hs.3352
CFL1	Hs.25313

RPL13	Hs.410817
H3F3A	Hs.447694
RPS20	Hs.8102
RPL35	Hs.182825
HNRPDL	Hs.372673
RPL31	Hs.523670
PPIA	Hs.356331
NPM1	Hs.411098
H3F3B	Hs.447694
GPC3	Hs.119651
RPS28	Hs.153177
RPL27	Hs.405528
HNRPA2B1	Hs.232400
RPL5	Hs.469653
IGF2	Hs.251664
RPL19	Hs.381061
RPS12	Hs.380956
ATP5A1	Hs.298280
RPS14	Hs.381126
CD164	Hs.43910
CD24	Hs.375108
DDX5	Hs.279806
PGK1	Hs.78771
RPL8	Hs.178551

RPS13	Hs.446588
GJA1	Hs.74471
PFN1	Hs.408943
RPS6	Hs.408073
EIF4A1	Hs.129673
HBE1	Hs.117848
HSPA5	Hs.310769
LDHB	Hs.234489
B2M	Hs.48516
G22P1	Hs.169744
ID2	Hs.180919
RPS17	Hs.433427
SFRS3	Hs.405144
SRP14	Hs.180394
RPS9	Hs.139876
TMSB10	Hs.446574
CCNI	Hs.369110
PCBP2	Hs.132977
RPS16	Hs.397609
RBM3	Hs.301404
RPL13A	Hs.449070
FASN	Hs.83190
CNN3	Hs.194662
PPM1G	Hs.17883

ATP5J2	Hs.235557
YWHAQ	Hs.74405
RPL22	Hs.326249
NASP	Hs.446206
RPS3	Hs.387576
NCL	Hs.79110
TRA1	Hs.390622
HNRPD	Hs.438726
ILF3	Hs.256583
GNB2L1	Hs.5662
MDK	Hs.82045
LDHA	Hs.2795
NACA	Hs.32916
UBB	Hs.356190
XRCC5	Hs.257082
TOB1	Hs.178137
HNRPL	Hs.446623
ZNF207	Hs.97128
KPNA2	Hs.252712
RANBP1	Hs.24763
RPL9	Hs.420233
EEF1D	Hs.334798
CPE	Hs.75360
OAZ1	Hs.446427

ECHS1	Hs.76394
PA2G4	Hs.374491
LMO4	Hs.3844
ERH	Hs.433413
SERPINH1	Hs.241579
PFDN5	Hs.288856

Listed are the 100 most highly expressed genes which are present in both human and mouse PA1. These genes are ranked by their combined tag counts in W4PA1 and W5PA1. For a gene to be considered "expressed" in human PA1, the number of SAGE tags for that gene should be greater than 1, and it also should have a "present" call in Affymetrix microarray. For a gene to be considered "expressed" in mouse PA1, it should have a "present" call in Affymetrix microarray, or there is experimental confirmation by *in situ* hybridization, immunohistochemistry, or RT-PCR in The Jackson Laboratory Mouse Genome Informatics database.

Table S10. Genes Expressed in Mouse but not Detected in Human PA1 by SAGE or by Microarray

Gene	UniGene ID
Copa	Mm.30041
Ppp4c	Mm.41998
Llglh	Mm.285453
Tff1	Mm.2854
Tcf4	Mm.4269
Sec23b	Mm.248492
Ctsd	Mm.231395
Pcdhga12	Mm.247203
Ivd	Mm.6635
Dlgh1	Mm.382
Eya3	Mm.227733
Lpin2	Mm.227924
Ap1s1	Mm.833
Hars	Mm.10528
Crtap	Mm.20904
Srebf1	Mm.278701
Gja7	Mm.354719
Ptpra	Mm.224246
Cul3	Mm.12665
Hexa	Mm.2284
Col9a1	Mm.154662

Fanca	Mm.6536
Acads	Mm.18759
Clk3	Mm.25720
Asb4	Mm.51340
Axin	-
Arpc1b	Mm.30010
Git2	Mm.195632
Wnt6	Mm.268282
Col5a1	Mm.7281
Krt2-19	Mm.347934
Rce1	Mm.358628
2810428C21Rik	Mm.307182
Acadl	Mm.2445
Hdh	Mm.209071
Irx5	Mm.101153
Neurod1	Mm.4636
Suclg2	Mm.359512
Fert2	Mm.280819
Pdpk1	Mm.10504
Pfkfb1	Mm.249131
Ndst2	Mm.4084
Gale	Mm.247946
Sim1	Mm.4774
Fut8	Mm.35628

Mafk	Mm.157313
Rbms2	Mm.42247
Renbp	Mm.236969
Efna2	Mm.1478
Dbh	Mm.167781
Atf1	Mm.676
Ssfa2	Mm.272881
Ptprm	Mm.311809
Spr	Mm.28393
Etv1	Mm.4866
Cdkn2c	Mm.1912
Fgd1	Mm.219461
Scap2	Mm.221479
Il1b	Mm.222830
Cdh6	Mm.57048
P2rx7	Mm.42026
Bid3	Mm.358579
Krt1-2	Mm.4161
Ptpns1	Mm.1682
Dpep1	Mm.20388
Elavl4	Mm.3970
Klrg1	Mm.20434
Prdm1	Mm.4800
Klf1	Mm.4847

Hrc	Mm.39968
Hap1	Mm.281700
Mtf1	Mm.272397
Nrf1	Mm.259258
Plcd	-
Nos3	Mm.258415
Avp	Mm.6190
Pip5k2a	Mm.313977
Pak3	Mm.40035
Tgm2	Mm.330731
hr	-
Trim10	Mm.299155
Lor	Mm.1121
Casp8	Mm.336851
Ovgp1	Mm.298812
Emr1	Mm.2254
Tmprss2	Mm.276145
Tnfsf12	Mm.344820
Slc1a3	Mm.204834
Faah	Mm.256025
Alk	Mm.311854
Tnfrsf8	Mm.12810
Tacr2	Mm.8054
Spib	Mm.8012

Gmfg	Mm.194536
Kcna6	Mm.62535
Sgcg	Mm.72173
Xdh	Mm.11223
Mapk8	Mm.21495
Cbfa2t3h	Mm.194339
Ihh	Mm.2543

Listed are the 100 most highly expressed mouse genes in PA1, excluding genes whose human homologs were shown to be expressed in PA1 by either SAGE or microarray. For a gene to be considered “expressed” in mouse PA1, it should have a “present” call in Affymetrix microarray, or be in the The Jackson Laboratory Mouse Genome Informatics database.

Int. J. Dev. Biol. 49: 000-000 NON-CORRECTED PROOF (2005)
doi: 10.1387/ijdb.041942he

The cap 'n' collar family member NF-E2-related factor 3 (Nrf3) is expressed in mesodermal derivatives of the avian embryo

HEATHER C. ETCHEVERS*

INSERM U393, Hopital Necker - Enfants Malades, Paris, France

ABSTRACT NF-E2-related factor 3 (Nrf3) is a recently identified member of a family of transcription factors homologous to the *Drosophila* «cap 'n' collar» or CNC protein. The *cnc* gene is located immediately 3' to the *Drosophila* homeobox gene cluster and has been shown to regulate at least one of those genes, *deformed*. Likewise, human and mouse CNC homologues are located immediately 3' to each of the four Hox complexes, although no genetic interactions have yet been demonstrated in vertebrates. Work presented here demonstrates that *Nrf3*, adjacent to the Hox A cluster, is expressed during early development of the chicken embryo. Expression begins in the presumptive heart myocardium from the time of cardiac tube fusion through the looping process. *Nrf3* transcripts then disappear from the heart and are next observed in the myotomal compartment of maturing somites, restricted to the medial portion along the rostrocaudal axis and fading after muscle precursors migrate. Central nervous system expression appears gradually and persists at low levels in ventricular neuroepithelial cells until at least embryonic day 6. Strong expression is observed in the early epiphysis, in the collecting ducts of the developing kidney and in individual cells of the yolk sac, underlying blood islands. This is the first description using *in situ* hybridization of the expression of a CNC family member and its dynamics through the course of early development.

KEY WORDS: *cap 'n' collar, maf, Hox, FGFR2b*

Introduction

In bilaterians, segmental identity along the rostrocaudal axis is conferred through the action of Hox transcription factors, of which the DNA-binding domains have been highly conserved over the course of evolution. Hox genes are organized in chromosomal clusters, where the order of representation in the 3' to 5' direction is reproduced in nested expression domains along the length of the body. The transcription factor cap 'n' collar is located immediately 3' to the unique *Drosophila* homeobox gene cluster (Mohler *et al.*, 1991, 1995). Four CNC homologues are found just 3' to each of the four Hox gene clusters of humans and mice: NF-E2/p45 (Andrews *et al.*, 1993) near the Hox C complex, Nrf1 (Chan *et al.*, 1996) also known as LCR-F1 (Caterina *et al.*, 1994) near the Hox B complex, Nrf2 (Moi *et al.*, 1994); also known as ECH (Itoh *et al.*, 1995) near the Hox D complex and Nrf3 (Kobayashi *et al.*, 1999; Genbank NM_004289 annotated as NFE2L3), near the Hox A complex.

The CNC factors are basic region-leucine zipper proteins and interact with structurally related factors such as c-fos, small Maf (F, G, K) or Jun proteins, for DNA binding activity. The resultant heterodimers appear to behave as transcriptional activators (reviewed in Veraksa *et al.*, 2000), with the exception of the divergent Bach proteins which show repressor activity (Muto *et al.*, 1998; Oyake *et al.*, 1996). BACH1 and BACH2 map to distinct chromosomes (6q15 and 21q22.1 in humans) and contain additional regulatory domains for protein-protein interactions (Blouin *et al.*, 1998; Ohira *et al.*, 1998; Sasaki *et al.*, 2000). In the absence of a large CNC-type subunit, the small Maf protein partners inhibit promiscuous activation of a consensus binding motif on target DNA sequences, which otherwise can be induced by AP-1-like transcription factors.

The originally identified cap 'n' collar protein exists as three isoforms through differential splicing. One of these, CncB, is expressed in the pharyngeal endoderm and has been shown to suppress the transcription of Deformed in the *Drosophila* mandible, thereby maintaining mandibular identity (McGinnis *et al.*, 1998). cncA and cncC transcripts are ubiquitously expressed. Deformed is a homeobox-containing transcription factor, located at the 3'

Abbreviations used in this paper: CNC, cap 'n' collar protein; Nrf3, NF-E2-related factor 3.

***Address correspondence to:** Dr. Heather Etchevers. INSERM U393, Hopital Necker – Enfants Malades, 149 rue de Sèvres, 75743 Paris Cedex 15, France. Fax: +33-1-4449-5150. e-mail: etchevers@necker.fr

0214-6282/2005/$25.00

Printed in Spain
www.intjdevbiol.com

end of the homeobox complex. In vertebrates, the Hoxa4, b4, c4 and d4 orthologues of Deformed are expressed within and caudal to the hindbrain in the CNS, in somites and in the esophageal and posterior gut during embryonic life (reviewed in Couly *et al.*, 1996). Expression of cnc family members in vertebrates has been restricted to Northern blot analysis. NF-E2 is only seen in hematopoietic cell lines and tissues such as mouse fetal liver and human adult spleen and bone marrow (Peters *et al.*, 1993). Nrf1 has a reportedly ubiquitous expression (Chan *et al.*, 1993). Nrf2 transcripts are found in mouse red blood cells, kidney and intestine and at lower levels in brain, liver, skeletal muscle and heart (Itoh *et al.*, 1995). Nrf3 is expressed at high levels in the placenta and lower levels in adult human heart, brain, lung, kidney and pancreas (Kobayashi *et al.*, 1999).

In the context of recent data from the Institut d'Embryologie in Nogent-sur-Marne, demonstrating the influence of pharyngeal endoderm and Hox gene expression on the morphogenesis of cephalic neural crest derivatives (Couly *et al.*, 2002; Creuzet *et al.*, 2002), I examined the developing chicken embryo for the possible presence and localization of CNC genes. One of these, the putative chicken homologue of Nrf3, showed a surprising and dynamic expression pattern in non-cephalic mesodermal derivatives during embryogenesis, notably in the heart, somites, yolk sac and kidney. This pattern was unexpected given the ubiquitous expression described for the CNC genes to date and implies an earlier, more specific role in target gene regulation by Nrf3.

Results

Nrf3 is first transcribed at detectable levels at Hamburger-Hamilton stage (HH) 10 in the wall of the fused cardiac tube (not shown). This expression becomes increasingly intense until stage 18 (Figure 1A) and disappears from the myocardium by HH20 (Figure 1G). Expression appears stronger in the inflow and outflow tracts than in the ventricular wall (Figure 1D).

Somitic expression begins at HH15 in the rostralmost somites and progresses in a caudal direction (Figure 1C). Nrf3 expression occurs in the median portion of the myotomal compartment along the rostrocaudal axis (Figure 1A, C, E). As the myotome differentiates, the strong expression levels are downregulated but not entirely abrogated; migrating hypaxial muscle precursors appear to maintain some Nrf3 expression (Figure 1A and 1F, arrows) and muscle masses in the embryonic day 5 limb continue to faintly express Nrf3 (Figure 1J, arrow). However, expression disappears from the somites by HH20, which precedes terminal muscle differentiation from the myotome; therefore, it is concluded that not all muscle precursors express Nrf3.

The pharyngeal endoderm only transcribes Nrf3 transiently and at low levels during branchial arch formation. Expression is observed within the endodermal outpocketings separating branchial arches 2-3 and 3-4 at HH18 (Figure 1A, open arrows) and is already absent from this area at HH20. Uniformly faint levels of Nrf3 mRNA are detected throughout the neuroepithelium at both HH18 and HH20, with the exception of the strongly expressing epiphyseal placode at these stages (Figure 1G, 1H, arrows). The Wolffian ducts do not express Nrf3 at any stage preceding HH18, when faint expression is observed (Figure 1A, arrowhead).

Between HH26-28, Nrf3 transcription increases dramatically in the mesonephric tubules, resembling collecting ducts (Figure 1I-K). Not all tubules are positive, but mesonephric glomeruli are essentially negative with the exception of scattered cells (Figure1L, arrow). Expression is also present in the rostral end of the regressing mesonephric duct (Figure 1M).

Concordant with studies showing the importance of CNC type genes in erythroid and platelet differentiation (Andrews *et al.*, 1993; Caterina *et al.*, 1994), Nrf3 is found in a subpopulation of cells within the yolk sac at HH26 (Figure 1N). These cells are located abutting the blood islands forming in the mesoderm on their endodermal face, a location consistent with hematopoietic precursors that have not yet matured into blood islands (Figure 1N; Manaia *et al.*, 2000).

Discussion

Nrf3 is a member of the cap 'n' collar gene family that has been largely conserved during evolution between the insect and the vertebrate subphyla. In this work, the expression pattern of Nrf3 has been examined at chosen stages of development in the avian embryo. The dynamic and specific activation of Nrf3 in tissues of mesodermal origin shown here is the first demonstration of its potential role in vertebrate embryogenesis.

Conserved Hox partners link Hox and FGF activities

Nrf2 and Nrf3 have recently been demonstrated to be upregulated through the action of FGF7, or keratinocyte growth factor (KGF), in healing skin wounds (Braun *et al.*, 2002). The embryonic expression pattern of FGF7 significantly overlaps with that of Nrf3 as shown here. Like chicken Nrf3, FGF7 is first detected in the developing heart of the mouse and at higher levels in the atrial than the ventricular end of the cardiac tube, disappearing after further differentiation (Mason *et al.*, 1994). These authors also showed that FGF7 is not detected in epithelial somites but, once the myotome differentiates, is expressed in a rostrocaudal temporal gradient within each somitic myotome and disappears from the somites with the dispersion of the myotome. While this early pattern greatly resembles that of Nrf3 (cf. Figure 1), in contrast, FGF7 continues to be strongly expressed thereafter within all skeletal muscles at levels not equivalent to the low Nrf3 expression visible in muscle masses of the chicken embryo. Other differences include strong localized expression of FGF7 within the telencephalic ventricle, foregut subepithelial mucosa, perichondral mesenchyme and the dermis (Mason *et al.*, 1994), not seen for Nrf3. Finch and colleagues (1995) extended the work of Mason *et al.* (1994) to compare the expression of FGF7 and its receptor KGFR or FGFR2b (Miki *et al.*, 1992). Examination of the mouse urogenital system revealed strong KGFR expression in the collecting duct epithelia of the kidney, analogous to Nrf3 expression. However, FGF7 itself was expressed in the surrounding mesenchyme of the collecting ducts; neither ligand nor receptor was found in the vicinity of the nephrons (Finch *et al.*, 1995). Given these expression domains, it is possible that Nrf3 is a target of FGF7 activity through FGFR2b, but that its transcription is also regulated by other factors.

Other fibroblast growth factors acting through FGFR2b include FGF3, FGF10 and FGF15. These FGFs have been shown to be modulated by the Pbx transcription factors. Like the vertebrate

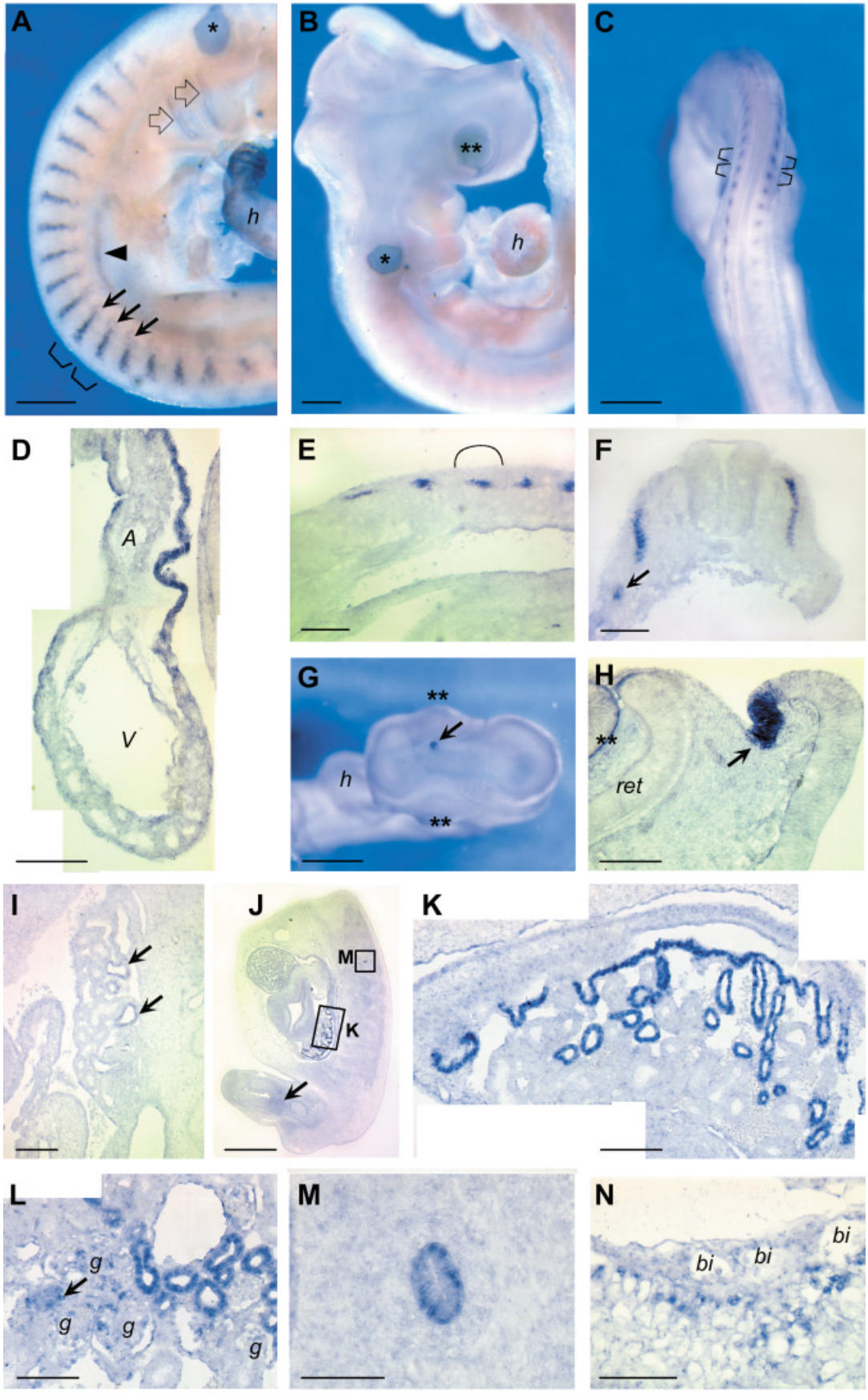

Fig. 1. Expression of *Nrf3* in the embryonic chicken. (A) In situ *hybridization with an antisense probe against* Nrf3 *mRNA in a HH18 embryo. Expression is seen in a medial stripe within each somite and in cells migrating ventrally from these stripes (arrows), in the heart (h) and faintly in the Wolffian duct (arrowhead) and the clefts between branchial arches 2/3 and 3/4 (open arrows). Brackets indicate two examples of somitic boundaries. Asterisk, non-specific signal.* **(B)** *Hybridization to a sense probe in a HH18 embryo shows non-specific signal in the optic (**) and otic (*) vesicles.* **(C)** *Somitic* Nrf3 *expression increases gradually as epithelial somites mature; at HH17, caudal somites do not yet have detectable transcripts. Brackets demonstrate somitic boundaries. Rostral to top.* **(D)** *Parasagittal section through heart of HH18 embryo showing more intense* Nrf3 *expression in the atrial (A) than the ventricular (V) portion.* **(E)** *Parasagittal section through somites showing* Nrf3 *transcripts restricted to the medial third of myotomes along the rostrocaudal axis (bracketed).* **(F)** *Myotomal* Nrf3 *expression at HH18 is evident in this transverse section at thoracic level. Note transcripts in myoblasts migrating in the hypaxial pathway (arrow).* **(G)** *HH17 epiphysis (arrow) expresses* Nrf3 *locally, seen from top. Double asterisk, eyes; h, heart.* **(H)** *Epiphyseal* Nrf3 *expression is strong at HH18 (arrow). The brain had been opened along the dorsal midline for hybridization, dorsal to right. Ret, retina.* **(I)** Nrf3 *transcripts are first seen in the developing kidney at HH26 (arrows).* **(J)** *Oblique parasagittal section of the body at HH28, rostral to top, facing left. Areas enlarged in (K,M) indicated. Note faint expression in muscle masses of proximal hindlimb, arrow.* **(K)** Nrf3+ *collecting ducts of the HH28 kidney.* **(L)** *Scattered cells, e.g. arrow, express* Nrf3 *in some glomeruli (g).* **(M)** *Rostral end of the receding pronephros also expresses* Nrf3. **(N)** *Yolk sac* Nrf3 *transcripts are seen in cells at the interface between the mesodermal blood islands (bi) and the endoderm. Bars: A,B,J, 1 mm; C,G, 2 mm; D,E,F,H,I,K,L,N, 150 μm; M,100 μm.*

CNC proteins, Pbx1 is involved in blood formation; human mutations in Pbx1 are associated with childhood leukemias (Kamps *et al.*, 1990; Nourse *et al.*, 1990). In *Drosophila* , the repressive influence of Nrf3's orthologue, cnc, on Deformed is counteracted by the action of the Pbx orthologue, extradenticle (Veraksa *et al.*, 2000). The feedback binding of Deformed to an element of its own promoter is enhanced by the addition of extradenticle to the reaction (Pinsonneault *et al.*, 1997).

Pbx1 binds DNA cooperatively with some Hox genes including those of the first four paralogue groups, targeting and modulating Hox activity (Zakany and Duboule, 1999; Selleri *et al.*, 2001; Waskiewicz *et al.*, 2002). In the zebrafish, Pbx proteins (somewhat redundant in their functions as Hox co-factors) are necessary for the early transcription of FGF3 and FGF8 in a central rhombomere, r4. The FGF signals then exert patterning effects on the flanking rhombomeres r3 and r5. For example, FGF3 from r4, acting through FGFR2b (Ornitz *et al.*, 1996), activates an indirect cascade which results in the differential transcription of Hox genes of paralogue groups 2 and 3 (Waskiewicz *et al.*, 2002).

The Pbx1 protein also directly activates FGF15 transcription, presumably in concert with a Hox protein under normal circumstances (McWhirter *et al.*, 1997). The FGF15 expression domain within the central nervous system is complementary to that of other early-expressed FGFs, including FGF3 and it is also transcribed specifically and transiently within the branchial arch endodermal pouches (McWhirter *et al.*, 1997). Recent evidence implicates FGFR2 and excludes FGFR4 as a possible transducer of the FGF15 signal in the developing mouse brain (Ishibashi and McMahon, 2002), despite an in vitro demonstration that its putative human homologue, FGF19, acts exclusively through FGFR4 (Xie *et al.*, 1999). It would be interesting to compare the FGF15 expression domain with that of members of Hox paralogue group 4, or to see if FGF15 transcription is repressed by Nrf3 in the branchial arches.

To summarize, FGF signaling through the FGFR2b isoform appears to affect Hox transcriptional activity in a feedback loop, perhaps through altering the balance between Hox repressors of the CNC family such as Nrf3 and Hox activators of the Pbx family. Given its expression pattern, Nrf3 does not appear to be a mediator of hindbrain Hox gene regulation, but it may be involved in determination of mesodermal segments, notably the somites or the embryonic mesonephric collecting ducts. Potential roles in the specification of the pineal gland and in hematopoiesis also remain to be explored.

Materials and Methods

The chick EST database maintained by the University of Delaware EST project (http://www.chickest.udel.edu/) was screened for the presence of sequences homologous to cnc. One clone, pgp1n.pk002.o10, isolated from a chicken pituitary/hypothalamic/pineal cDNA library, displayed 46% nucleotide homology to human NRF3 cDNA (Kobayashi *et al.*, 1999) using ALIGN v 2.0 (Myers and Miller, 1989) and was chosen for further analysis. The vector was linearized using Sal I; SP6 RNA polymerase was used to transcribe antisense digoxygenin-labelled RNA probes (Not I and T7 for sense) for *in situ* hybridizations. Paraffin sections at 7 μm or whole embryos were hybridized as described (Henrique *et al.*, 1995; Etchevers *et al.*, 2001); the latter were cut at 10 μm on a Leica microtome after embedding in 15% gelatin/30% sucrose/PBS that had been cross-linked with 2% gluteraldehyde. Hamburger-Hamilton stages 7-13, 15, 17, 18, 24, 26 and 28 were examined.

Acknowledgements

H.C.E. is an Avenir fellow and staff researcher of the French Institut National de la Santé et de la Recherche Médicale and was supported by the Sturge-Weber Foundation during part of this work. She expresses her warm appreciation to her mentors, Professors Nicole Le Douarin and Gérard Couly and to Dr. Tania Attié-Bitach for her constructive criticism. This paper is dedicated to the fond memory of Dr. Patrizia Cameron-Curry, a staff scientist of the Institut d'Embryologie Cellulaire et Moléculaire du CNRS et du Collège de France.

Note added in press:
Chenais *et al.* (2004) have recently demonstrated that Nrf3 and its small Maf partner, MafG, are a transcriptional activator in human placental chorionic villus cytotrophoblasts.

Bibliography

ANDREWS, N.C., ERDJUMENT-BROMAGE, H., DAVIDSON, M.B., TEMPST, P. and ORKIN, S.H. (1993). Erythroid transcription factor NF-E2 is a haematopoietic-specific basic-leucine zipper protein. *Nature* 362, 722-728.

BEL-VIALAR, S., ITASAKI, N. and KRUMLAUF, R. (2002). Initiating Hox gene expression: in the early chick neural tube differential sensitivity to FGF and RA signaling subdivides the HoxB genes in two distinct groups. *Development* 129, 5103-5115.

BLOUIN, J.L., DURIAUX SAIL, G., GUIPPONI, M., ROSSIER, C., PAPPASAVAS, M.P. and ANTONARAKIS, S.E. (1998). Isolation of the human BACH1 transcription regulator gene, which maps to chromosome 21q22.1. *Hum. Genet.* 102, 282-288.

BRAUN, S., HANSELMANN, C., GASSMANN, M.G., AUF DEM KELLER, U., BORN-BERCLAZ, C., CHAN, K., KAN, Y.W. and WERNER, S. (2002). Nrf2 transcription factor, a novel target of keratinocyte growth factor action which regulates gene expression and inflammation in the healing skin wound. *Mol. Cell. Biol.* 22, 5492-5505.

CATERINA, J.J., DONZE, D., SUN, C.W., CIAVATTA, D.J. and TOWNES, T.M. (1994). Cloning and functional characterization of LCR-F1: a bZIP transcription factor that activates erythroid-specific, human globin gene expression. *Nucleic Acids Res.* 22, 2383-2391.

CHAN, J. Y., HAN, X. L. and KAN, Y. W. (1993). Cloning of Nrf1, an NF-E2-related transcription factor, by genetic selection in yeast. *Proc. Natl. Acad. Sci. USA* 90, 11371-5.

CHAN, K., LU, R., CHANG, J.C. and KAN, Y.W. (1996). NRF2, a member of the NFE2 family of transcription factors, is not essential for murine erythropoiesis, growth and development. *Proc. Natl. Acad. Sci. USA* 96, 13943-13948.

CHENAIS, B., DERJUGA, A., MASSRIEH, W., RED-HORSE, K., BELLINGARD, V., FISHER, S.J. AND BLANK, V. (2004). Functional and placental expression analysis of the human NRF3 transcription factor. *Mol Endocrinol. doi.*10.1210/me/2003-0379.

COULY, G., GRAPIN-BOTTON, A., COLTEY, P. and LE DOUARIN, N. M. (1996). The regeneration of the cephalic neural crest, a problem revisited: the regenerating cells originate from the contralateral or from the anterior and posterior neural fold. *Development* 122, 3393-407.

COULY, G., CREUZET, S., BENNACEUR, S., VINCENT, C. and LE DOUARIN, N.M. (2002). Interactions between Hox-negative cephalic neural crest cells and the foregut endoderm in patterning the facial skeleton in the vertebrate head. *Development* 129, 1061-1073.

CREUZET, S., COULY, G., VINCENT, C. and LE DOUARIN, N.M. (2002). Negative effect of Hox gene expression on the development of the neural crest-derived facial skeleton. *Development* 129, 4301-4313.

DEBACKER, C., CATALA, M. and LABASTIE, M.C. (1999). Embryonic expression of the human GATA-3 gene. *Mech Dev.* 85, 183-7.

ETCHEVERS, H.C., VINCENT, C. and LE DOUARIN, N.M. and COULY, G.F. (2001). The cephalic neural crest provides pericytes and smooth muscle cells to all blood vessels of the face and forebrain. *Development* 128, 1059-1068.

FINCH, P.W., CUNHA, G.R., RUBIN, J.S., WONG, J. and RON, D. (1995). Pattern of keratinocyte growth factor and keratinocyte growth factor receptor expression during mouse fetal development suggests a role in mediating morphogenetic

mesenchymal-epithelial interactions. *Dev. Dyn.* 203, 223-240.

HENRIQUE, D., ADAM, J., MYAT, A., CHITNIS, A., LEWIS, J. and ISH-HOROWICZ, D. (1995). Expression of a Delta homologue in prospective neurons in the chick. *Nature* 375, 787-790.

ISHIBASHI, M. and MCMAHON, A.P. (2002). A sonic hedgehog-dependent signaling relay regulates growth of diencephalic and mesencephalic primordia in the early mouse embryo. *Development* 129, 4807-4819.

ITOH, K., IGARASHI, K., HAYASHI, N., NISHIZAWA, M. and YAMAMOTO, M. (1995). Cloning and characterization of a novel erythroid cell-derived CNC family transcription factor heterodimerizing with the small Maf family proteins. *Mol. Cell. Biol.* 15, 4184-4193.

KAMPS, M.P., MURRE, C., SUN, X.H. and BALTIMORE, D. (1990). A new homeobox gene contributes the DNA binding domain of the t(1;19) translocation protein in pre-B ALL. *Cell* 60, 547-555.

KOBAYASHI, A., ITO, E., TOKI, T., KOGAME, K., TAKAHASHI, S., IGARASHI, K., HAYASHI, N. and YAMAMOTO, M. (1999). Molecular cloning and functional characterization of a new Cap'n' collar family transcription factor Nrf3. *J. Biol. Chem.* 274, 6443-6452.

MANAIA, A., LEMARCHANDEL, V., KLAINE, M., MAX-AUDIT, I., ROMEO, P., DIETERLEN-LIEVRE, F. and GODIN, I. (2000). Lmo2 and GATA-3 associated expression in intraembryonic hemogenic sites. *Development* 127, 643-53.

MASON, I.J., FULLER-PACE, F., SMITH, R. and DICKSON, C. (1994). FGF-7 (keratinocyte growth factor) expression during mouse development suggests roles in myogenesis, forebrain regionalisation and epithelial-mesenchymal interactions. *Mech. Dev.* 45, 15-30.

MCGINNIS, N., RAGNHILDSTVEIT, E., VERAKSA, A. and MCGINNIS, W. (1998). A cap 'n' collar protein isoform contains a selective Hox repressor function. *Development* 125, 4553-4564.

MCWHIRTER, J.R., GOULDING, M., WEINER, J.A., CHUN, J. and MURRE, C. (1997). A novel fibroblast growth factor gene expressed in the developing nervous system is a downstream target of the chimeric homeodomain oncoprotein E2A-Pbx1. *Development* 124, 3221-3232.

MIKI, T., BOTTARO, D.P., FLEMING, T.P., SMITH, C.L., BURGESS, W.H., CHAN, A.M. and AARONSON, S.A. (1992). Determination of ligand-binding specificity by alternative splicing: two distinct growth factor receptors encoded by a single gene. *Proc. Natl. Acad. Sci. USA* 89, 246-250.

MOHLER, J., MAHAFFEY, J.W., DEUTSCH, E. and VANI, K. (1995). Control of *Drosophila* head segment identity by the bZIP homeotic gene cnc. *Development* 121, 237-247.

MOHLER, J., VANI, K., LEUNG, S. and EPSTEIN, A. (1991). Segmentally restricted, cephalic expression of a leucine zipper gene during *Drosophila* embryogenesis. *Mech. Dev.* 34, 3-9.

MOI, P., CHAN, K., ASUNIS, I., CAO, A. and KAN, Y.W. (1994). Isolation of NF-E2-related factor 2 (Nrf2), a NF-E2-like basic leucine zipper transcriptional activator that binds to the tandem NF-E2/AP1 repeat of the beta-globin locus control region. *Proc. Natl. Acad. Sci. USA* 91, 9926-9930.

MUTO, A., HOSHINO, H., MADISEN, L., YANAI, N., OBINATA, M., KARASUYAMA, H., HAYASHI, N., NAKAUCHI, H., YAMAMOTO, M., GROUDINE, M. and IGARASHI, K. (1998). Identification of Bach2 as a B-cell-specific partner for small maf proteins that negatively regulate the immunoglobulin heavy chain gene 3' enhancer. *EMBO J.* 17, 5734-5743.

MYERS, E. and MILLER, W. (1988) Optimal alignments in linear space. *CABIOS* 4, 11-17.

NOURSE, J., MELLENTIN, J.D., GALILI, N., WILKINSON, J., STANBRIDGE, E., SMITH, S.D. and CLEARY, M.L. (1990). Chromosomal translocation t(1;19) results in synthesis of a homeobox fusion mRNA that codes for a potential chimeric transcription factor. *Cell* 60, 535-545.

OHIRA, M., SEKI, N., NAGASE, T., ISHIKAWA, K., NOMURA, N. and OHARA, O. (1998). Characterization of a human homolog (BACH1) of the mouse Bach1 gene encoding a BTB-basic leucine zipper transcription factor and its mapping to chromosome 21q22.1. *Genomics* 47, 300-306.

ORNITZ, D.M., XU, J., COLVIN, J.S., MCEWEN, D.G., MACARTHUR, C.A., COULIER, F., GAO, G. and GOLDFARB, M. (1996). Receptor specificity of the fibroblast growth factor family. *J. Biol. Chem.* 271, 15292-15297.

OYAKE, T., ITOH, K., MOTOHASHI, H., HAYASHI, N., HOSHINO, H., NISHIZAWA, M., YAMAMOTO, M. and IGARASHI, K. (1996). Bach proteins belong to a novel family of BTB-basic leucine zipper transcription factors that interact with MafK and regulate transcription through the NF-E2 site. *Mol. Cell. Biol.* 16, 6083-6095.

PETERS, L.L. ANDREWS, N.C., EICHER, E.M., DAVIDSON, M.B., ORKIN, S.H. and'LUX, S. E. (1993). Mouse microcytic anaemia caused by a defect in the gene encoding the globin enhancer-binding protein NF-E2. *Nature* 362, 768-70.

PINSONNEAULT, J., FLORENCE, B., VAESSIN, H. and MCGINNIS, W. (1997). A model for extradenticle function as a switch that changes HOX proteins from repressors to activators. *EMBO J.* 16, 2032-2042.

SASAKI, S., ITO, E., TOKI, T., MAEKAWA, T., KANEZAKI, R., UMENAI, T., MUTO, A., NAGAI, H., KINOSHITA, T. and YAMAMOTO, M. (2000). Cloning and expression of human B cell-specific transcription factor BACH2 mapped to chromosome 6q15. *Oncogene* 19, 3739-3749.

SELLERI, L., DEPEW, M.J., JACOBS, Y., CHANDA, S.K., TSANG, K.Y., CHEAH, K.S., RUBENSTEIN, J.L., O'GORMAN, S. and CLEARY, M.L. (2001). Requirement for Pbx1 in skeletal patterning and programming chondrocyte proliferation and differentiation. *Development* 128, 3543-3557.

VERAKSA, A., MCGINNIS, N., LI, X., MOHLER, J. and MCGINNIS, W. (2000). Cap 'n' collar B cooperates with a small Maf subunit to specify pharyngeal development and suppress deformed homeotic function in the *Drosophila* head. *Development* 127, 4023-4037.

WASKIEWICZ, A.J., RIKHOF, H.A. and MOENS, C.B. (2002). Eliminating zebrafish pbx proteins reveals a hindbrain ground state. *Dev. Cell.* 3, 723-733.

XIE, M.H., HOLCOMB, I., DEUEL, B., DOWD, P., HUANG, A., VAGTS, A., FOSTER, J., LIANG, J., BRUSH, J. and GU, Q. (1999). FGF-19, a novel fibroblast growth factor with unique specificity for FGFR4. *Cytokine* 11, 729-735.

ZAKANY, J. and DUBOULE, D. (1999). Hox genes in digit development and evolution. *Cell Tissue Res.* 296, 19-25.

Available online at www.sciencedirect.com

SCIENCE DIRECT®

Neurotoxicology and Teratology 27 (2005) 515–524

NEUROTOXICOLOGY AND TERATOLOGY

www.elsevier.com/locate/neutera

Review article

Human neural tube defects: Developmental biology, epidemiology, and genetics

Eric R. Detrait[a], Timothy M. George[b], Heather C. Etchevers[a], John R. Gilbert[b], Michel Vekemans[a], Marcy C. Speer[b,*]

[a]*Hôpital Necker, Enfants Malades Unité INSERM U393, 149, rue de Sèvres, 75743 Paris Cedex 15, France*
[b]*Center for Human Genetics, Duke University Medical Center, Box 3445, Durham, NC 27710, United States*

Received 16 December 2004; accepted 17 December 2004
Available online 5 March 2005

Abstract

Birth defects (congenital anomalies) are the leading cause of death in babies under 1 year of age. Neural tube defects (NTD), with a birth incidence of approximately 1/1000 in American Caucasians, are the second most common type of birth defect after congenital heart defects. The most common presentations of NTD are spina bifida and anencephaly. The etiologies of NTDs are complex, with both genetic and environmental factors implicated. In this manuscript, we review the evidence for genetic etiology and for environmental influences, and we present current views on the developmental processes involved in human neural tube closure.

Keywords: Neural tube defect; Genetics; Teratology

Contents

Birth defects (congenital anomalies) are the leading cause of death in babies under 1 year of age. Neural tube defects (NTD), with a birth incidence of approximately 1/1000 in American Caucasians, are the second most common type of birth defect after congenital heart defects. In human, the most common NTD are anencephaly and myelomeningocele. Anencephaly results from a failed closure of the rostral end of the neural tube and is characterized by a total or partial absence of the cranial vault and cerebral hemisphere. Myelomeningocele is a defective closure of the neural tube

* Corresponding author. Tel.: +1 919 684 2063; fax: +1 919 684 0917.
E-mail address: marcy@chg.duhs.duke.edu (M.C. Speer).

0892-0362/$ - see front matter © 2004 Elsevier Inc. All rights reserved.
doi:10.1016/j.ntt.2004.12.007

in the vertebral column. Depending on the size and the location of the defect, the patient can suffer either no physical handicap or lifelong disabilities [86]. These common birth defects vary in frequency depending on the geographical localization. Anencephaly and spina bifida occur at frequencies ranging from 0.9 in Canada to 7.7 in the United Arab Emirates and 0.7 in central France to 11.7 in South America per 10,000 births [86].

The mortality rate for children with spina bifida is increased over the general population risk in the first year of life. The cost of providing for medical care for a child with myelomeningocele has been estimated to be over $70,000 (adjusted to 2001 dollars) annually for the first 20 years of life, including costs associated with an average of 5 surgeries per year [94] in the first 5 years of life (20 year lifetime cost is $1.4 million/case).

The phenotypes of the open NTDs include myelomeningocele (spina bifida cystica, open spina bifida) and anencephaly. Anencephaly, an incomplete formation of the brain and skull, is uniformly lethal. The most common form of NTD, myelomeningocele, is an open lesion in the caudal spine and contains dysplastic spinal cord, often resulting in a lack of neural function below the level of the defect. Affected patients usually have reduced ability to walk, or need the use of a wheelchair, have little or no bowel and/or bladder control, and require frequent surgical interventions to minimize the effects of hydrocephalus. The most common presentations, spina bifida and anencephaly, can occur within the same family, raising the question as to whether these phenotypes are related and due to a common underlying gene [29,31,33,38,65,77].

Defining the phenotype in affected patients is paramount to the evaluation of human neural tube defects. Phenotypic parameters include: location and level of the defect, whether the defect crosses CNS segmental boundaries, and cataloguing the variety of anomalies in a patient or family. Open defects such as anencephaly, craniorachischisis, myelomeningocele, and myeloschisis are defined based upon the location and level and are descriptive in nature. Associated anomalies, Chiari II malformation, hydrocephalus, syringomyelia, polymicrogyria, cortical heterotopias, and agenesis of the corpus callosum further add to and can confuse the phenotypic definitions.

NTDs in humans result from the combined effects of genetic and environmental influences, and as such are a classic example of a multifactorial disorder. Identifying the genetic factors is critical for characterizing the interactions between genes and the environment, and understanding these interactions will provide the basis for designing novel preventive strategies and for offering accurate reproductive risks to couples. The genetic factors will likely involve aberrant variations in genes key for the normal closure of the neural tube. Neural tube closure is a complex, early developmental process, informed not only by nascent studies in human embryos, but by the plethora of investigations in a variety of experimental systems including but not restricted to mouse, zebrafish, and chick.

1. Formation of the human neural tube

Neurulation, which is the formation of the neural tube, is an important morphogenetic event in human development.

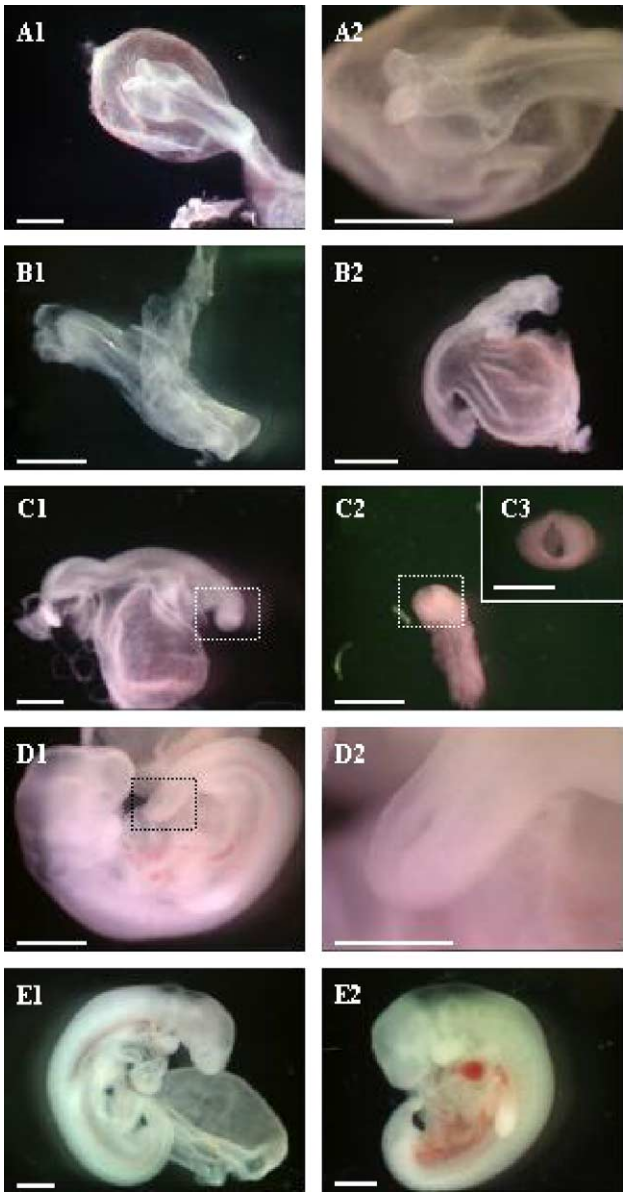

Fig. 1. Human embryonic developmental stages during which the neural tube forms. A1 and 2: Carnegie stage 9 (CS 9–20 days) the neural groove is open and anterior neural fold is visible. B1 and 2: CS 10 (22 days). The neural folds fuses centrally leaving an open tube in the rostral and caudal region. C1, 2 and 3: CS 11 (24 days). The neural tube is closed except for the rostral (C2 and 3) and caudal neuropores. D1 and 2: CS 12 (26 days) the caudal neuropore is closing (C2). E1 and 2: CS 13 (28 days). The neuropores are closed. E1 corresponds to early CS 13 and E2 to a late CS 13. The scale bars represent 1 mm in all photographs except C3 and D2 where they represent 0.5 mm.

The neural tube gives rise to the brain and the spinal cord to form the central nervous system. Neurulation in mammalian embryos occurs in two phases: primary and secondary neurulation [68]. These two phases occur in distinct areas along the rostro-caudal axis of the embryo. Secondary neurulation is limited to the tail bud, which lies beyond the caudal neuropore. In contrast to primary neurulation, described in detail below, secondary neurulation occurs by proliferation of stem cells [8], which form a rod-like condensation that subsequently cavitates. The cavitation transforms the rod into a tube, and the lumen of this tube comes into continuity with the lumen of the tube formed during primary neurulation. In tailless humans, the tail bud does not develop as in tailed animals, and secondary neurulation does not appear to be responsible for open neural tube defects. For this reason, we will focus on primary neurulation.

Primary neurulation generates the entire neural tube rostral to the caudal neuropore. During this process, occurring during the third and fourth weeks of development (Carnegie stages (CS) 8 to 13, Fig. 1), the flat layer of ectodermal cells overlying the notochord is transformed into a hollow tube.

Eighteen days after fertilization (CS 8), the midline dorsal ectoderm of the embryo thickens and forms the neural plate while cell shape changes. The neural plate first appears at the cranial end of the embryo and differentiates in the caudal direction. The edges of the plate thicken and begin to move upward forming the neural fold. The neural plate becomes narrower, longer, and is transformed from an elliptical to a key-hole shaped structure. This transformation occurs by polarized cell movements in the medial direction and cell intercalation in the midline. The mechanism of these movements, known as convergent extension, is not specific to neural tube formation. Convergent extension has been widely studied in animal models (mouse, Xenopus and Drosophila), where it depends on the highly conserved Wnt-frizzled signal transduction pathways (see Lawrence at al. 2003 [48] and Copp et al. 2003 [13] for reviews on convergent extension).

On day 19 (CS 8.5), the border of the neural plate becomes gradually more pronounced and elevated. The neural plate folds longitudinally along the midline of the plate from the head toward the tail to form the neural groove. The folds rise up dorsally, approach each other and ultimately merge together, forming a tube open at both ends by day 23 (CS 10.5) (Fig 1A and B). As the neural folds fuse, the cells adjacent to the neural plate also fuse across the midline to become the overlying epidermis. The rostral and caudal openings are called neuropores and are best distinguished around day 23 when about 17–19 somites are visible (Fig. 1C). The rostral and caudal neuropores close later, on the 26th (CS 12) and 28th (CS 13) days of gestation, respectively (Fig. 1D to E). We utilize the terminology suggested by O'Rahilly and Müller [60], who reserve the term "closure" for the closing of neuropores, while the term "fusion" is used to designate the merging of the neural folds and the formation of a tube.

Although there is general agreement on the morphogenetic movements of the first events of neural tube formation, the last event in neural tube formation, the fusion of neural folds, is subject to debate concerning the number of initiation sites of fusion and their location. Indeed, the fusion of the neural folds has originally been described in humans as a process initiated at a single site, and extending bi-directionally, rostrally and caudally, from this initiation site to the rostral and caudal neuropores [68]. However, over the past 20 years, a hypothesis of "multiple site of neural tube fusion" has been investigated in animal models and in humans. This hypothesis has been extensively studied in mice and rats [74]. According to Sakai, who wrote a comprehensive review of available data in mice and rats, rodent neural tube fusion occurs between day E8 and day

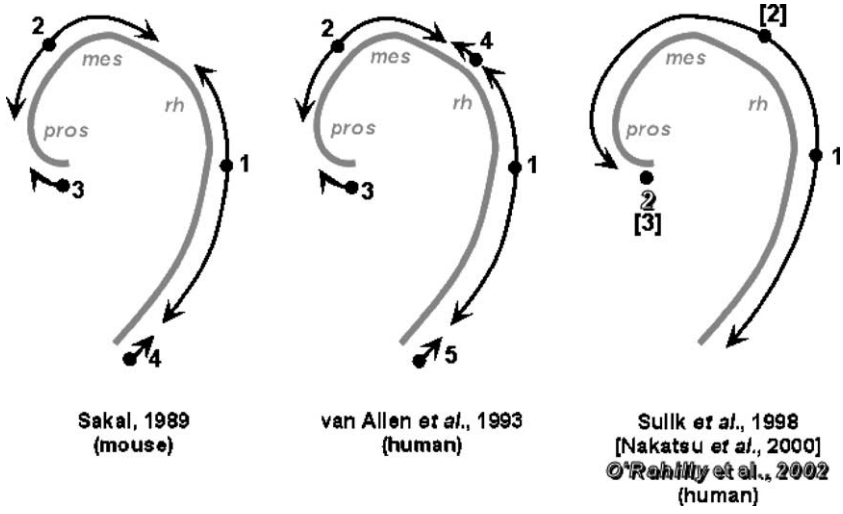

Fig. 2. Proposed mechanisms for neural tube closure in mouse and humans.

E10 of gestation [74]. Four sites of neural tube fusion were identified. Site 1 initiates in the future cervical region between the third and fourth somites at the caudal part of the hindbrain, and progresses both caudally and rostrally. Caudally, it proceeds all the way down to the end of the neural groove until the caudal neuropore. The next two sites of initiation of fusion are located rostral to site 1. A second fusion initiates at the prosencephalon–mesencephalon boundary (Site 2) and extends both rostrally and caudally. This second fusion completely closes the roof of the telencephalon and the metencephalon. A third fusion site (site 3) progresses caudally, and closes the rostral end of the neural plate. Finally, the fourth fusion site (site 4) appears at the caudal end of the neural plate and extends rostrally to meet the fusion extending back from site 1. These proposed mechanisms are summarized in Fig. 2.

2. Single site of neural fold fusion

Since the susceptibility to NTDs in human is known to vary among ethnic groups, one might hypothesize that heterogeneity of human neural tube defects could also originate from differences in fusion at site 2. This statement implies that the multiple sites of neural tube fusion occur in humans. In 1993, van Allen proposed multiple sites of fusion in human embryos, although a human site 2 had never been observed. She based her model on the observation of the type and the frequency of human tube defects. A model of a single site of fusion would predict that most human neural tube defects would be localized in the caudal and rostral ends of the tube where the neuropores close, which is not the case. Van Allen's model predicted 5 sites of fusion and four neuropores. In addition to the rostral and caudal neuropores, she postulated the existence of a prosencephalic and a mesencephalic neuropore, resulting respectively from fusion of a second and a fourth closing site [88]. In the mid 1990s, Seller [78,79] and Golden [30] arrived at similar conclusions from the study of human neural tube defects.

Although the model of multiple sites of fusion was attractive to explain such defects, experimental observation of human embryos clearly corroborates the hypothesis of a single site of fusion and a zipper-like process of neural tube closure. Using light microscopy and laser scanning electron microscopy to observe successive stages of development, Sulik and coworkers showed a zipper-like fusion of the human neural tube from a single initiation site located in the middle of the future hindbrain region [84]. This finding was later corroborated by two studies. Nakatsu and coworkers examined histological sections of human embryos at various stages of neural tube formation, and described three sites of apposition. Site 1 was the widely recognized site of true fusion located in the cervical region. From site 1, fusion extended both rostrally and caudally, reaching the caudal neuropore at the caudal end of the embryos. Site 2 was located at the boundary between mesencephalon and rhombencephalon, but was only an apposition site before being caught up by the rostralwards fusion. Site 3 corresponded to the rostral tip of the neural folds and is also an apposition, becoming fusion upon closure of the anterior neuropore [57]. Finally, a study by O'Rahilly found two regions of fusion in humans [60] as observed by Sulik and coworkers [84], extending bi-directionally from the rhombencephalic region. Caudally, the fusion extended until the caudal neuropore, while ending rostrally at the dorsal lip of the rostral neuropore, closing the neuropore rostrocaudally.

3. Relationship of human neural tube closure to mouse neural tube closure

Three initiation sites of fusion in rodent models have been confirmed by several groups [11,30,41,42], while a fourth one has not been described elsewhere (see [25] for a comparison of these studies). The locations of sites 1 and 3 were uniform between studies, but the location of site 2 showed strain differences. Genetically determined, it is considered to modify the susceptibility of each strain to neural tube defects (NTDs) [13,42].

It seems clear that in mice, the multiple sites of fusion model can be applied, even if the exact location of each site varies between mouse strains. In contrast, there seems to be a single initiation site of fusion in humans. Apposition of the neural folds may occur at several sites, but fusion itself only occurs when the extension of fusion reaches the area where the neural folds were apposed. This difference between humans and rodents does not necessarily imply that the mechanisms of fusion and closure are different; the same genes are likely to be involved in both species. Understanding the processes, both environmental and genetic, that influence neural tube closure in humans is critical so that relevant, rational interventions and preventions can be designed; but because humans are non-experimental systems, it is equally important to understand the similarities and differences between the human system and experimental systems such as mouse.

4. Clues from observational data

Attempting to define the defects based upon the underlying embryopathy may be the most appropriate method for defining NTD phenotype. Shum et al. [80] demonstrated that at least three different modes of neural tube formation might exist along the rostrocaudal axis; therefore, regional differences in modes of neural tube closure may result in different types of open defects. Mode 1 occurs in the cervicothoracic region, where a distinct medial hinge point (MHP) forms without any clear morphological evidence of

dorsolateral hinge points (DLHP) resulting in an ovoid neural tube and slit shaped central canal. Defective mode 1 has been proposed to cause craniorachischisis by interfering with MHP formation resulting in normal but widely spaced neural folds preventing proper fusion. In the midbrain/hindbrain region, mode 2 has been described as generating both MHP and DLHP prior to fusion. After fusion, the neural tube has a diamond shaped configuration, perhaps foreshadowing the shape of the adult fourth ventricle. Defects of mode 2 result in exencephaly due to defective DLHP function.

Neural tube formation in the lumbosacral region, mode 3, is different in that there is only a suggestion of DLHP formation along with a well-developed MHP. The closed tube has a more oval shape with a large patent central canal. Where the driving force of neural tube closure in mode 1 appears to be extrinsic to the neural tube, the source of the force in mode 3 is less defined.

The last embryopathic mechanism proposes that a properly neurulated (wouldn't closed be a better word here?) neural tube can be reopened. The only spontaneous mutant in which this mechanism occurs is the *curtailed* mouse in which increased cerebrospinal fluid pressure is thought to rupture a thinned roof plate and dermis in the absence of competent dorsal bony vertebrae [64]. Although the *curtailed* mutant may indeed have a reopening of a previously closed neural tube, this mechanism is not thought to be a likely cause of human NTD.

5. Evidence for a genetic factor in human neural tube defects

Several lines of evidence suggest a genetic component to NTDs. First, NTDs are associated with known genetic syndromes including Meckel syndrome, anterior sacral meningocele and anal stenosis, in addition to others. NTDs are frequently associated with trisomies 13 and 18 and various chromosome rearrangements. Secondly, in NTDs occurring without other syndromes, the recurrence risk for siblings is approximately 2–5% (giving a λ_s value [70,71] between 20 and 50), which represents up to a 50-fold increase over that observed in the general population. Khoury et al. [47] have shown that for a recurrence risk to be this high, an environmental teratogen would have to increase the risk at least 100 fold to exhibit the same degree of familial aggregation, making a genetic component essential. Such potent teratogens are extraordinarily rare; however, one example of a teratogen exerting such a high relative risk is thalidomide.

Evidence of a genetic factor is further strengthened by the presence of a family history in a number of those affected. While family history of NTDs has been reported in 8.5% of one group of families studied [66], inspection of these multiplex NTD families shows that affected parent–child pairs are rare; most affected relative pairs are related at either the second or third degree, thus suggesting oligogenic inheritance. More data on parent–child transmission will be available over the next two decades, as children born with NTDs now receive sufficiently sophisticated medical care and can live to maturity and reproduce. Segregation analysis studies demonstrating evidence of a major gene have been performed in series of NTD families, one demonstrating evidence for a major dominant gene and another for a major gene with recessive effect [16,24]. These studies are admittedly small and suffer from common problems of ascertainment. Twin studies for the NTDs are anecdotal in nature, comparing concordance in like-sex vs. unlike-sex twins instead of the more formal comparison between dizygotic and monozygotic twins. The limited available data are based on very small sample sizes, but range from 3.7% to 18% [20].

Chromosome abnormalities, specifically aneuploidy, are found in 5–17% of cases with NTDs [37,46,67]. NTDs are frequently associated with trisomies 13 and 18. A study by Kennedy et al. [46] suggests a frequency of chromosomal anomalies in 6.5% (13/212) neural tube defect patients. A gene or genes in the region of 13q33–34 associated with a 13q deletion syndrome has been shown to cause NTDs [51]. These cytogenetic rearrangements can be key positional clues to candidate genes and have been recently summarized [53].

6. If neural tube defects are genetic, how do they present in families?

One of the longest running controversies, as yet undecided, is whether NTDs at different levels represent different defects. In other words, are rostral level defects (e.g., anencephaly) different in some fundamental way than caudal defects (e.g., myelomeningocele)? Additionally, are lesions that include both rostral and caudal levels (e.g., craniorachischisis) altogether variant embryopathies? If the etiology of upper and lower lesions are different, then it would be expected that recurrences in families would breed true: affected individuals in an upper lesion family would all have upper lesions and vice versa for lower lesions. NTDs tend to breed true within families; in other words, recurrences in families in which the case is affected with spina bifida tend to be spina bifida, and recurrences in families in which the case is anencephaly tend to be anencephaly [18,26,28,33,87]. However, between 30% and 40% of recurrences involve an NTD phenotype that is different from the case phenotype. This intra-family heterogeneity may represent the pleiotropic effect of a common underlying gene or may suggest that families with different phenotypic presentations may result from different underlying genes. Alternatively, these dramatic phenotypic differences within families may suggest slight differences in timing to key environmental exposures in susceptible pregnancies, or may suggest that the underlying genes are

different. Or, these differences may represent the variable outcomes following different environmental exposures at key developmental times, or even just the result of random chance. While studies to date have provided conflicting and inconclusive results, the availability of such families will be vital to understanding the genetic and environmental influences to NTDs.

7. Clues to genes involved in human neural tube defects from mouse models

The folding of the plate results from a number of region-specific mechanisms, as suggested by the regional localization of neural tube defects observed in humans and in mutant mice. More than 80 mutations in a variety of genes have been identified and linked to a variety of rodent NTDs, implicating more than 100 genes directly or indirectly in neural tube formation. These genes have recently been comprehensively reviewed [13,34,35,95]. Unlike the majority of human cases, many of these mutants show autosomal recessive inheritance and, in addition to NTDs, these mice present other associated anomalies. Moreover, the penetrance and expression of many of these mutations are affected by the genetic background, which can increase the susceptibility to teratogen-causing NTDs, consistent with multifactorial inheritance. The mechanisms by which NTD arise in these murine models are generally unclear, even when the mutated gene has been identified. The most relevant animal model of human NTDs are the SELH mice, where the liability to exencephaly is genetic and best fits a multifactorial threshold model of inheritance involving 2 or 3 loci [43].

The best model for caudal spinal NTD, the most common presentation in humans, is the curly tail mouse, that naturally develops a lumbosacral myelomeningocele and is a phenocopy of nonsyndromic multifactorial human neural tube defects [59]. Recently, a mouse homologue of the Drosophila grainyhead transcription factor, Grhl-3, was shown to be responsible for this phenotype [85]. At the tissue level, mutant curly tail mouse embryos exhibit a cell-type-specific abnormality of cell proliferation that affects the gut endoderm and notochord but not the neuroepithelium [12]. The reduced rate of ventral embryonic cell proliferation results in a growth imbalance between ventral gut primordia and the dorsal neural elements. The result is a delay in posterior neuropore closure because of abnormal caudal flexion, resulting in spinal neural tube defects [10].

Mutations in the Macs gene in mouse lead to exencephaly and other midline NTDs; its human homologue MACS has been localized to 6q21–22.2 [4,50,83]. Most mouse models for NTD lead to exencephaly, the mouse counterpart for anencephaly, the less common but most severe NTD manifestation in humans. Murine models with hindbrain excencephaly, such as the Pax-3-splotch mutant, are noted to have defective DLHP formation in the region of the hindbrain [17,21–23]. Of relevance to the human condition, the *Pax3* gene has been reported to be defective in Waardenburg syndrome patients with a subset having spinal neural tube defects [2]. It is not known how mutant *Pax3* causes neural tube defects; increased apoptosis [5,62], faulty pyrimidine synthesis or alterations in cell migration [19,52] have been proposed. There is also good evidence that a digenic mechanism is likely.

In four mouse mutants with craniorachischisis, *dish-eveled* [3,40], *loop-tail* [45], *circletail* [56], and *crash* [14], the underlying cellular mechanism has been attributed to abnormal neural plate development as a consequence of disturbed convergent extension. Disturbing convergent extension yields a shortened and broad neural plate, thus a widened and misshapen MHP. The planar-polarity gene-Wnt signaling pathways [91] are thought to be the responsible molecular substrate.

No mutations identified in mouse have yet been shown to represent major genes for NTD in humans. Mimicking the genetic complexity seen in humans will be difficult, since it is likely to be caused by a cumulative effect of several interchangeable loci, not a major gene with modifiers. Nonetheless, since humans are a non-experimental system, understanding the relationship between humans and a model system such as mouse will be key to eventually considering interventions based on genetic and environmental risk.

8. Environmental factors associated with neural tube defects

Myriad exogenous causes for NTDs have been postulated and investigated (see [20,32] for review). Factors for which no significant association with NTDs have been found to date include maternal and paternal age effects, maternal periconceptional infections, number of prior “successful” pregnancies, recreational drug use, caffeine intake, smoking, and alcohol use. Hyperthermia (fever and/or hot tub use) has been investigated, though most of these studies are subject to extreme recall bias and have yielded inconsistent results. However, increased risk for NTDs is definitively associated with maternal diabetes and maternal obesity (both associated with glucose metabolism), and maternal use of anti-convulsant medications (for the treatment of epilepsy). For example, anti-epileptic drugs administered to pregnant mothers induce congenital malformations, the incidence rising from 3% without drug to 9% with drug administration [44]. These numbers can rise up to 28% when 3 or more antiepileptic drugs are given to the epileptic mother [36]. The well-known anti-epileptic drug, valproic acid, is teratogenic when given to pregnant women, and its administration results in 1% to 2% incidence of spina bifida [49,58]. Moreover, recent data suggests that this agent also induces mental retardation in children with no physical manifestation.

Paternal exposure to Agent Orange in Vietnam veterans has been implicated, as has water chlorination by-products [39] and maternal exposure to solvents through house cleaning occupation [7]. Exposure to fumonisins, a fungal metabolite commonly found in maize, has also been implicated and in vivo and in vitro studies have demonstrated an association of exposure with neural tube defects [73]. Prenatal exposure of mice to cadmium has shown that the metal is localized in the developing neural tube and can result in NTDs [15,92]. These known environmental associations, however, are insufficient to explain the degree of familial aggregation observed in NTDs.

Several studies have demonstrated that maternal periconceptional supplementation with folic acid reduces the recurrence risk for NTDs (e.g., [54]) by 50–70%, implicating genes involved in the metabolism of folate. Yet the recurrence risk is not entirely eliminated (e.g., above and [9], suggesting that additional, genetic factors are responsible for the development of NTDs and these non-folate responsive cases may represent highly genetic cases of NTDs [76]. The mechanism for how folic acid works to reduce the risk is unclear and likely mediated by genetic effects. Folate acts as a cofactor for an enzyme involved in DNA and RNA biosynthesis, and is also a supplier of methyl groups to the methylation cycles [75]. Folate deficiency leads to up-regulation of folate receptors, which are ubiquitous and mediate folate uptake at physiological level [1]. A recent study by Rothenberg et al. [72] showed that some mothers with a pregnancy complicated by a NTD produced autoantibodies that bind to folate receptors on the placental membrane and therefore blocked the binding of folic acid. The authors further suggest that the periconceptional administration of folate would bypass the autoantibodies that mediate a placental folate receptor blockage. Indeed, folate has a high affinity for its receptor and might displace the autoantibody when administered at high doses.

Identifying those women whose risk for NTD is minimized by folic acid supplementation would allow genotype-directed pharmacogenetic interventions. Researchers are looking at a number of different genes involved in folic acid metabolism, including those encoding folate receptors, 5,10-methylenetetrahydrofolate reductase (MTHFR), and cystathionine (beta)-synthase. Recent studies have implicated homozygosity for the C677T thermolabile variant of the MTHFR gene as a risk factor for NTDs ([27,61,93] among many others), and others have suggested that the effect may be dependent on level of lesion [90]. A recent meta-analysis [6] found a pooled odds ratio for infants homozygous at C677T of 1.7 (95% CI 1.4–2.2), with a pooled attributable fraction of 6% for homozygosity. While the paternal effect was non-significant, the odds ratios for maternal genotype, either homozygous or heterozygous for the thermolabile "T" allele, were consistent with a trend for MTHFR involvement (OR for homozygosity was 2.1 [95% CI 1.5–2.9] and for heterozygosity was 1.2 [95% CI 0.9–1.5]).

In addition, other mutations in the MTHFR gene have been investigated, including A1298C, and other genes, such as cystathionine â-synthase, that when in combination with the C677T allele may increase the risk for NTDs [82,89]. Several reports [63,69,81] have failed to demonstrate the association seen with the C677T MTHFR allele and NTDs. Additional data suggesting that MTHFR is not a major risk factor comes from a report by Molloy [55] confirming that homozygosity for the "risk" allele fails to influence maternal folate levels, which are known to predict NTD risk.

9. Synthesizing the data

Current technology for approaching complex diseases continues to be developed at a phenomenal rate. Novel approaches from the molecular, expression, and statistical realms promise enhanced ability to identify genetic influences, understand the interactions between genes, and characterize the relationship of environmental risk factors to genetic susceptibilities. Integrating these approaches will facilitate progress. Any insight into one or more genes predisposing to the development of neural tube defects will lend useful information towards more accurate genetic counseling for families and prevention of these frequent birth defects.

Acknowledgments

The authors gratefully acknowledge support from NS39818, ES11375, HD39948, NS26630, and ES011961 and the Institut National pour la Santé et la Recherche Médicale (INSERM).

References

[1] A.C. Antony, The biological chemistry of folate receptors, Blood 79 (1992) 2807–2820.
[2] C.T. Baldwin, C.F. Hoth, R.A. Macina, A. Milunsky, Mutations in PAX3 that cause Waardenburg syndrome type I: ten new mutations and review of the literature, Am. J. Med. Genet. 58 (1995) 115–122.
[3] E. Bekman, D. Henrique, Embryonic expression of three mouse genes with homology to the *Drosophila melanogaster* prickle gene, Gene Expr. Patterns 2 (2002) 73–77.
[4] P.J. Blackshear, J.S. Tuttle, R.J. Oakey, M.F. Seldin, M. Chery, C. Phillipe, D.J. Stumpo, Chromosomal mapping of the human (MACS) and mouse (Macs) genes encoding the MARCKS protein, Genomics 14 (1992) 168–174.
[5] A.G. Borycki, J. Li, F. Jin, C.P. Emerson, J.A. Epstein, Pax3 functions in cell survival and in pax7 regulation, Development 126 (1999) 1665–1674.
[6] L.D. Botto, Q. Yang, 5,10-Methylenetetrahydrofolate reductase gene variants and congenital anomalies: a HuGE review, Am. J. Epidemiol. 151 (2000) 862–877.

[7] J. Brender, L. Suarez, K. Hendricks, R.A. Baetz, R. Larsen, Parental occupation and nueral tube defect-affected pregnancies among Mexican Americans, J. Occup. Environ. Med. 44 (2002) 650–656.
[8] M. Catala, M.A. Teillet, E.M. De Robertis, M.L. LeDouarin, A spinal cord fate map in the avian embryo: while regressing, Hensen's node lays down the notochord and floor plate thus joining the spinal cord lateral walls, Development 122 (1996) 2599–2610.
[9] S. Chatkupt, J.H. Skurnick, M. Jaggi, K. Mitruka, M.R. Koenigsberger, W.G. Johnson, Study of genetics, epidemiology, and vitamin usage in familial spina bifida in the United States in the 1990s, Neurology 44 (1994) 65–69.
[10] A.J. Copp, Relationship between timing of posterior neuropore closure and development of spinal neural tube defects in mutant (curly tail) and normal mouse embryos in culture, J. Embryol. Exp. Morphol. 88 (1985) 39–54.
[11] A.J. Copp, M. Bernfield, Etiology and pathogenesis of human neural tube defects: insights from mouse models 1, Curr. Opin. Pediatr. 6 (1994) 624–631.
[12] A.J. Copp, M.J. Seller, P.E. Polani, Neural tube development in mutant (curly tail) and normal mouse embryos: the timing of posterior neuropore closure in vivo and in vitro, J. Embryol. Exp. Morphol. 69 (1982) 151–167.
[13] A.J. Copp, N.D. Greene, J.N. Murdoch, The genetic basis of mammalian neurulation, Nat. Rev., Genet. 4 (2003) 784–793.
[14] M. Dahme, U. Bartsch, R. Martini, B. Anliker, M. Schachner, N. Mantei, Disruption of the mouse L1 gene leads to malformations of the nervous system, Nat. Genet. 17 (1997) 346–349.
[15] S.K. De, S.K. Dey, G.K. Andrews, Cadmium teratogenicity and its relationship with metallothionein gene expression in midgestation mouse embryos, Toxicology 64 (1990) 89–104.
[16] F. Demenais, M. Le Merrer, M.L. Briard, R.C. Elston, Neural tube defects in France: segregation analysis, Am. J. Med. Genet. 11 (1982) 287–298.
[17] M.M. Dickie, New Splotch alleles in the mouse, J. Heredity 55 (1964) 97–101.
[18] E. Drainer, H.M. May, J.L. Tolmie, Do familial neural tube defects breed true? J. Med. Genet. 28 (1991) 605–608.
[19] G.M. Edelman, F.S. Jones, Gene regulation of cell adhesion: a key step in neural morphogenesis, Brain Res. Brain Res. Rev. 26 (1998) 337–352.
[20] J.M. Elwood, J. Little, J.H. Elwood, Epidemiology and control of neural tube defects, 1992.
[21] D.J. Epstein, D. Malo, M. Vekemans, P. Gros, Molecular characterization of a deletion encompassing the splotch mutation on mouse chromosome 1, Genomics 10 (1991) 89–93.
[22] D.J. Epstein, M. Vekemans, P. Grost, 'Splotch' (Sp2H), a mutation affecting development of the mouse neural tube, shows a deletion within the paired homeodomain of Pax-3, Cell 67 (1991) 767–774.
[23] D.J. Epstein, K.J. Vogan, D.G. Trasler, P. Gros, A mutation within intron 3 of the Pax-3 gene produces aberrantly spliced mRNA transcripts in the splotch (sp) mouse mutant, Proc. Natl. Acad. Sci. U. S. A. 90 (1993) 532–536.
[24] R.M. Fineman, L.B. Jorde, R.A. Martin, S.J. Hasstedt, S.D. Wing, M.L. Walker, Spinal dysraphia as an autosomal dominant defect in four families, Am. J. Med. Genet. 12 (1982) 457–464.
[25] R.H. Finnell, W.M. Junker, L.K. Wadman, R.M. Cabrera, Gene expression profiling within the developing neural tube, Neurochem. Res. 27 (2002) 1165–1180.
[26] M.F. Frecker, F.C. Fraser, W.D. Heneghan, Are 'upper' and 'lower' neural tube defects aetiologically different? J. Med. Genet. 25 (1988) 503–504.
[27] P. Frosst, H.J. Blom, R. Milos, P. Goyette, C.A. Sheppard, R.G. Matthews, G.J.H. Boers, M. den Heijer, L.A.J. Kluijtmans, L.P. van den Heuvel, R. Rozen, A candidate genetic risk factor for vascular disease: a common mutation in methylenetetrahydrofolate reductase, Nat. Genet. 10 (1995) 111–113.
[28] B.H. Garabedian, F.C. Fraser, Upper and lower neural tube defects: an alternate hypothesis, J. Med. Genet. 30 (1993) 849–851.
[29] T.M. George, C.M. Wolpert, G. Worley, J.F. Mackey, H.E. Fuchs, M.C. Speer, Variable presentation of neural tube defects in three families, Am. J. Hum. Genet. 59 (1996) A93.
[30] J.A. Golden, G.F. Chernoff, Intermittent pattern of neural tube closure in two strains of mice, Teratology 47 (1993) 73–80.
[31] J.G. Hall, Neural tube defects, sex ratios, and X inactivation, Lancet (1986) 1334–1335.
[32] J.G. Hall, J.M. Friedman, B.A. Kenna, J. Popkin, M. Jawanda, W. Arnold, Clinical, genetic, and epidemiological factors in neural tube defects, Am. J. Hum. Genet. 43 (1988) 827–837.
[33] J.G. Hall, B.A. Keena, Adjusting recurrence risks for neural tube defects based on B.C. data, Am. J. Hum. Genet. 39 (1986) A64.
[34] M.J. Harris, D.M. Juriloff, Genetic landmarks for defects in mouse neural tube closure, Teratology 56 (1997) 177–187.
[35] M.J. Harris, D.M. Juriloff, Mini-review: toward understanding mechanisms of genetic neural tube defects in mice, Teratology 60 (1999) 292–305.
[36] L.B. Holmes, E.A. Harvey, B.A. Coull, K.B. Huntington, S. Khoshbin, A.M. Hayes, L.M. Ryan, The teratogenicity of anticonvulsant drugs, N. Engl. J. Med. 344 (2001) 1132–1138.
[37] R.F. Hume, A. Drugan, A. Reichler, J. Lampinen, L.S. Martin, M.P. Johnson, M.I. Evans, Aneuploidy among prenatally detected neural tube defects, Am. J. Med. Genet. 61 (1996) 171–173.
[38] A.G.W. Hunter, Brain and spinal cord, in: R.E. Stevenson, J.G. Hall, R.M. Goodman (Eds.), Human Malformations and Related Anomalies, Oxford University Press, Oxford, 1993.
[39] B.F. Hwang, P. Magnus, J.J. Jaakkola, Risk of specific birth defects in relation to chlorination and the amount of natural organic matter in the water supply, Am. J. Epidemiol. 156 (2002) 374–382.
[40] M.A. Julius, B. Schelbert, W. Hsu, E. Fitzpatrick, E. Jho, F. Fagotto, F. Costantini, J. Kitajewski, Domains of axin and disheveled required for interaction and function in wnt signaling, Biochem. Biophys. Res. Commun. 276 (2000) 1162–1169.
[41] D.M. Juriloff, M.J. Harris, Mouse models for neural tube closure defects, Hum. Mol. Genet. 9 (2000) 993–1000.
[42] D.M. Juriloff, M.J. Harris, C. Tom, K.B. Macdonald, Normal mouse strains differ in the site of initiation of closure of the cranial neural tube, Teratology 44 (1991) 225–233.
[43] D.M. Juriloff, T.M. Gunn, M.J. Harris, D.G. Mah, M.K. Wu, S.L. Dewell, Multifactorial genetics of exencephaly in SELH/Bc mice, Teratology 64 (2001) 189–200.
[44] S. Kaneko, D. Battino, E. Andermann, K. Wada, R. Kan, A. Takeda, Y. Nakane, Y. Ogawa, G. Avanzini, C. Fumarola, T. Granata, F. Molteni, G. Pardi, L. Minotti, R. Canger, L. Dansky, M. Oguni, I. Lopes-Cendas, A. Sherwin, F. Andermann, M.H. Seni, M. Okada, T. Teranishi, Congenital malformations due to antiepileptic drugs, Epilepsy Res. 33 (1999) 145–158.
[45] C. Kapron, Identification of the mouse loop-tail gene: a model for human craniorachischisis? BioEssays 24 (2002) 580–583.
[46] D. Kennedy, D. Chitayat, E.J.T. Winsor, M. Silver, A. Toi, Prenatally diagnosed neural tube defects: ultrasound, chromosome, and autopsy or postnatal findings in 212 cases, Am. J. Med. Genet. 77 (1998) 317–321.
[47] M.J. Khoury, T.H. Beaty, K.Y. Liang, Can familial aggregation of disease be explained by familial aggregation of environmental risk factors? Am. J. Epidemiol. 127 (1988) 674–683.
[48] N. Lawrence, V. Morel, Dorsal closure and convergent extension: two polarised morphogenetic movements controlled by similar mechanisms? Mech. Dev. 120 (2003) 1385–1393.
[49] D. Lindhout, D. Schmidt, In-utero exposure to valproate and neural tube defects (letter), Lancet 1 (1986) 1392–1393.
[50] D.F. Lobach, J.M. Rochelle, M.L. Watson, M.F. Seldin, P.J. Blackshear, Nucleotide sequence, expression, and chromosomal mapping of Mrp and mapping of five related sequences, Genomics 17 (1993) 194–204.

[51] J. Luo, N. Balkin, J.F. Stewart, J.F. Sarwark, J. Charrow, J.S. Nye, Neural tube defects and the 13q deletion syndrome: evidence for a critical region in 13q33–34, Am. J. Med. Genet. 91 (2000) 227–230.
[52] C.S. Mayanil, D. George, B. Mania-Farnell, C.L. Bremer, D.G. McLone, E.G. Bremer, Overexpression of murine Pax3 increases NCAM polysialylation in a human medulloblastoma cell line, J. Biol. Chem. 275 (2000) 23259–23266.
[53] E.C. Melvin, T.M. George, G. Worley, A. Franklin, J. Mackey, K. Viles, N. Shah, C.R. Drake, D.S. Enterline, D. McLone, J. Nye, W.J. Oakes, C. McLaughlin, M.L. Walker, P. Peterson, T. Brei, C. Buran, J. Aben, B. Ohm, I. Bermans, M. Qumsiyeh, J. Vance, M.A. Pericak-Vance, M.C. Speer, Genetic studies in neural tube defects. NTD collaborative group, Pediatr. Neurosurg. 32 (2000) 1–9.
[54] A. Milunsky, H. Jick, S.S. Jick, C.L. Bruell, D.S. MacLaughlin, K.J. Rothman, W. Willett, Multivitamin/folic acid supplementation in early pregnancy reduces the prevalence of neural tube defects, JAMA 262 (1991) 2847–2852.
[55] A.M. Molloy, J.L. Mills, P.N. Kirke, D. Ramsbottom, J.M. McPartlin, H. Burke, M. Conley, A.S. Whitehead, D.G. Weir, J.M. Scott, Low blood folates in NTD pregnancies are only partly explained by thermolabile 5,10 methylenetetrahydrofolate reductase: low folate status alone may be the critical factor, Am. J. Med. Genet. 78 (1998) 155–159.
[56] J.N. Murdoch, R.A. Rachel, S. Shah, F. Beermann, P. Stanier, C.A. Mason, A.J. Copp, Circletail, a new mouse mutant with severe neural tube defects: chromosomal localization and interaction with the loop-tail mutation, Genomics 78 (2001) 55–63.
[57] T. Nakatsu, C. Uwabe, K. Shiota, Neural tube closure in humans initiates at multiple sites: evidence from human embryos and implications for the pathogenesis of neural tube defects, Anat. Embryol. (Berl.) 201 (2000) 455–466.
[58] H. Nau, Valproic acid-induced neural tube defects, Ciba Found. Symp. 181 (1994) 144–152.
[59] P.E. Neumann, W.N. Frankel, V.A. Letts, J.M. Coffin, A.J. Copp, M. Bernfield, Multifactorial inheritance of neural tube defects: localization of the major gene and recognition of modifiers in *ct* mutant mice, Nat. Genet. 6 (1994) 357–362.
[60] R. O'Rahilly, F. Muller, The two sites of fusion of the neural folds and the two neuropores in the human embryo, Teratology 65 (2002) 162–170.
[61] C.Y. Ou, R.E. Stevenson, V.K. Brown, C.E. Schwartz, W.P. Allen, M.J. Khoury, G.P. Oakley Jr., M.J. Adams Jr., C677T homozygosity associated with thermolabile 5, 10 methylenetetrahydrofolate reductase as a risk factor for neural tube defects, Am. J. Hum. Genet. 57 (1995) A223.
[62] L. Pani, M. Horal, M.R. Loeken, Rescue of neural tube defects in Pax-3-deficient embryos by p53 loss of function: implications for Pax-3-dependent development and tumorigenesis, Genes Dev. 16 (2002) 676–680.
[63] C. Papapetrou, S.A. Lynch, J. Burn, Y.H. Edwards, Methylenetetrahydrofolate reductase and neural tube defects, Lancet 348 (1996) 58.
[64] C.H. Park, J.H. Pruitt, D. Bennett, A mouse model for neural tube defects: the curtailed (Tc) mutation produces spina bifida occulta in Tc/+ animals and spina bifida with meningomyelocele in Tc/t, Teratology 39 (1989) 303–312.
[65] C.H. Park, W. Stewart, M.J. Khoury, J. Mulinare, Is there etiologic heterogeneity between upper and lower neural tube defects, Am. J. Epidemiol. 136 (1992) 1493–1501.
[66] M.D. Partington, D.G. McLone, Hereditary factors in the etiology of neural tube defects, Pediatr. Neurosurg. (1995) 311–316.
[67] T. Philipp, D.K. Kalousek, Neural tube defects in missed abortions: embryoscopic and cytogenetic findings, Am. J. Med. Genet. 107 (2002) 52–57.
[68] D. Purves, J.W. Lichtman, Principles of Neural Development, Sinauer Assocs, Sunderlande, 1985.
[69] E. Rampersaud, E.C. Melvin, D. Siegel, L. Mehltretter, M.E. Dickerson, T.M. George, D. Enterline, J.S. Nye, M.C. Speer, NTD Collaborative Group, Updated investigations of the role of methylenetetrahydrofolate reductase in human neural tube defects, Clin. Genet. 63 (2003) 210–214.
[70] N. Risch, Linkage strategies for genetically complex traits: II. The power of affected relative pairs, Am. J. Hum. Genet. 46 (1990) 229–241.
[71] N. Risch, Linkage strategies for genetically complex traits: III. The effect of marker polymorphism on analysis of affected relative pairs, Am. J. Hum. Genet. 46 (1990) 242–253.
[72] S.P. Rothenberg, M.P. da Costa, J.M. Sequeira, J. Cracco, J.L. Roberts, J. Weedon, E.V. Quadros, Autoantibodies against folate receptors in women with a pregnancy complicated by a neural-tube defect, N. Engl. J. Med. 350 (2004) 134–142.
[73] T.W. Sadler, A.H. Merrill, V.L. Stevens, M.C. Sullards, E. Wang, P. Wang, Prevention of fumonisin B1-induced neural tube defects by folic acid, Teratology 66 (2002) 169–176.
[74] Y. Sakai, Neurulation in the mouse: manner and timing of neural tube closure, Anat. Rec. 223 (1989) 194–203.
[75] J.M. Scott, D.G. Weir, A. Molloy, J. McPartlin, L. Daly, P. Kirke, Folic acid metabolism and mechanisms of neural tube defects, Ciba Found. Symp. 181 (1994) 180–187.
[76] C.R. Scriver, Vitamins: an evolutionary perspective, J. Inherit. Metab. Dis. 8 (Suppl. 1) (1985) 2–7.
[77] M.J. Seller, Neural tube defects: are neurulation and canalization forms causally distinct? Am. J. Med. Genet. 35 (1990) 394–396.
[78] M.J. Seller, Further evidence for an intermittent pattern of neural tube closure in humans, J. Med. Genet. 32 (1995) 205–207.
[79] M.J. Seller, Neural tube defects, chromosome abnormalities and multiple closure sites for the human neural tube, Clin. Dysmorph. 4 (1995) 202–207.
[80] A.S. Shum, A.J. Copp, Regional differences in morphogenesis of the neuroepithelium suggest multiple mechanisms of spinal neurulation in the mouse, Anat. Embryol. (Berl.) 194 (1996) 65–73.
[81] M.C. Speer, G. Worley, J.F. Mackey, E. Melvin, W.J. Oakes, T.M. George, NTD Collaborative Group, The thermolabile variant of methylenetetrahydrofolate reductase (MTHFR) is not a major risk factor for neural tube defect in American Caucasians, Neurogenetics 1 (1997) 149–150.
[82] M.C. Speer, J. Nye, D. McLone, G. Worley, E.C. Melvin, K.D. Viles, A. Franklin, C. Drake, J. Mackey, T.M. George, Possible interaction of genotypes at cystathionine beta-synthase and methylenetetrahydrofolate reductase (MTHFR) in neural tube defects. NTD Collaborative Group, Clin. Genet. 56 (1999) 142–144.
[83] D.J. Stumpo, R.L. Eddy Jr, L.L. Haley, S. Sait, T.B. Shows, W.S. Lai, W.S. Young III, M.C. Speer, A. Dehejia, M. Polymeropoulos, P.J. Blackshear, Promoter sequence, expression, and fine chromosomal mapping of the human gene (MLP) encoding the MARCKS-like protein: identification of neighboring and linked polymorphic loci for MLP and MACS and use in the evaluation of human neural tube defects, Genomics 49 (1998) 253–264.
[84] K.K. Sulik, R.M. Zucker, D.B. Dehart, et al., Normal patterns of neural tube closure differ in the human and mouse, Proc. Greenwood Genet. Cent. 18 (1998) 129–130.
[85] S.B. Ting, T. Wilanowski, A. Auden, M. Hall, A.K. Voss, T. Thomas, V. Parekh, J.M. Cunningham, S.M. Jane, Inositol- and folate-resistant neural tube defects in mice lacking the epithelial-specific factor Grhl-3, Nat. Med. 9 (2003) 1513–1519.
[86] J. Tolmie, Neural tube defects and other congenital malformations of the central nervous system, in: A.E. Emery, D.L. Rimoins (Eds.), Principles and Practice of Medical Genetics, Churchill Livingston, New York, 1996, p. 2152.
[87] H.V. Toriello, J.V. Higgins, Possible causal heterogeneity in spina bifida cystica, Am. J. Med. Genet. 21 (1985) 13–20.
[88] M.I. Van Allen, D.K. Kalousek, G.F. Chernoff, D. Juriloff, M. Harris, B.C. McGillivray, S.L. Yong, S. Langlois, P.M. Macleod, D. Chitayat,

J.M. Freidman, D. Wilson, D. McFadden, J. Pantzar, S. Ritchie, J.G. Hall, Evidence for multi-site closure of the neural tube in humans, Am. J. Med. Genet. 47 (1993) 723–743.

[89] N.M. van der Put, F. Gabreels, E.M. Stevens, J.A. Smeitink, F.J. Trijbels, T.K. Eskes, L.P. van den Heuvel, H.J. Blom, A second common mutation in the methylenetetrahydrofolate reductase gene: an additional risk factor for neural-tube defects? Am. J. Hum. Genet. 62 (1998) 1044–1051.

[90] K.A. Volcik, S.H. Blanton, M.C. Kruzel, I.T. Townsend, G.H. Tyerman, R.J. Mier, H. Northrup, Testing for genetic associations in a spina bifida population: analysis of the HOX gene family and human candidate gene regions implicated by mouse models of neural tube defects, Am. J. Med. Genet. 110 (2002) 203–207.

[91] J.B. Wallingford, R.M. Harland, Neural tube closure requires dishevelled-dependent convergent extension of the midline, Development 129 (2002) 5815–5825.

[92] W.S. Webster, K. Messerle, Changes in the mouse neuroepithelium associated with cadmium-induced neural tube defects, Teratology (1980) 79–88.

[93] A.S. Whitehead, P. Gallagher, J.L. Mills, P.N. Kirke, H. Burke, A.M. Molloy, D.G. Weir, D.C. Shields, J.M. Scott, A genetic defect in 5,10 methylenetetrahydrofolate reductase in neural tube defects, Q. J. Med. 88 (1995) 763–766.

[94] G. Worley, L.R. Rosenfeld, J. Lipscomb, Financial counseling for families of children with chronic disabilities, Dev. Med. Child Neurol. 33 (1991) 679–689.

[95] W. Wurst, L. Bally-Cuif, Neural plate patterning: upstream and downstream of the isthmic organizer, Nat. Rev., Neurosci. 2 (2001) 99–108.

Hum Genet (2005) 117: 133–142
DOI 10.1007/s00439-005-1299-7

ORIGINAL INVESTIGATION

**Kristen L. Deak · Abee L. Boyles · Heather C. Etchevers
Elizabeth C. Melvin · Deborah G. Siegel
Felicia L. Graham · Susan H. Slifer · David S. Enterline
Timothy M. George · Michel Vekemans · David McClay
Alexander G. Bassuk · John A. Kessler · Elwood Linney
John R. Gilbert · Marcy C. Speer
NTD Collaborative Group**

SNPs in the neural cell adhesion molecule 1 gene (*NCAM1*) may be associated with human neural tube defects

Received: 7 February 2005 / Accepted: 21 February 2005 / Published online: 10 May 2005

Abstract Neural tube defects (NTDs) are common birth defects, occurring in approximately 1/1,000 births; both genetic and environmental factors are implicated. To date, no major genetic risk factors have been identified. Throughout development, cell adhesion molecules are strongly implicated in cell–cell interactions, and may play a role in the formation and closure of the neural tube. To evaluate the role of neural cell adhesion molecule 1 (NCAM1) in risk of human NTDs, we screened for novel single-nucleotide polymorphisms (SNPs) within the gene. Eleven SNPs across *NCAM1* were genotyped using TaqMan. We utilized a family-based approach to evaluate evidence for association and/or linkage disequilibrium. We evaluated American Caucasian simplex lumbosacral myelomeningocele families ($n = 132$ families) using the family based association test (FBAT) and the pedigree disequilibrium test (PDT). Association analysis revealed a significant association between risk for NTDs and intronic SNP rs2298526 using both the FBAT test ($P = 0.0018$) and the PDT ($P = 0.0025$). Using the HBAT version of the FBAT to look for haplotype association, all pairwise comparisons with SNP rs2298526 were also significant. A replication study set, consisting of 72 additional families showed no significant association; however, the overall trend for overtransmission of the less common allele of SNP rs2298526 remained significant in the combined sample set. In addition, we analyzed the expression pattern of the NCAM1 protein in human embryos, and while NCAM1 is not expressed within the neural tube at the time of closure, it is expressed in the surrounding and later in differentiated neurons of the CNS. These results suggest variations in NCAM1 may influence risk for human NTDs.

Other members of NTD Collaborative Group involved in this study are listed in the appendix

K. L. Deak · A. L. Boyles · E. C. Melvin · D. G. Siegel
F. L. Graham · S. H. Slifer · J. R. Gilbert · M. C. Speer (✉)
Center for Human Genetics, Duke University Medical Center,
Box 3445, Durham, NC 27710, USA
E-mail: marcy@chg.duhs.duke.edu
Tel.: +1-919-684-2063
Fax: +1-919-684-0917

D. S. Enterline
Department of Radiology, Duke University Medical Center,
Box 3808, Durham, NC 27710, USA

T. M. George
Department of Surgery, Duke University Medical Center,
Box 3272, Durham, NC 27710, USA

E. Linney
Department of Molecular Genetics and Microbiology,
Duke University Medical Center, Box 3020,
Durham, NC 27710, USA

H. C. Etchevers · M. Vekemans
Département de Génétique Médicale and INSERM U393,
Hôpital Necker, Paris, France

D. McClay
Department of Biology, Duke University Medical Center,
Box 3445, Durham, NC 27710, USA

A. G. Bassuk · J. A. Kessler
Northwestern University's Feinberg School of Medicine,
Chicago, IL, USA

Introduction

Neural tube defects (NTDs) result from failure of neural tube closure and are one of the most common human malformations, occurring at an average rate of 1 per 1,000 human pregnancies (Campbell et al. 1986). Both genetic and environmental components have been implicated; however, no causative genes have been

identified. Formation of the neural tube is driven by several morphogenetic cell behaviors, including changes in cell–cell and cell–matrix interactions. During neural tube closure, the neural folds are brought together at the dorsal midline to form the neural tube and adhere to each other. In humans and other mammals, closure of the neural tube is thought to be initiated by sites of fusion at more than one place along the anterior–posterior axis (Van Allen et al. 1993; O'Rahilly and Muller 2002; Sulik et al. 1998). The first fusion occurs in humans when there are 4–6 somite pairs present, at Carnegie stage (C) 10, and closure continues though C12 with the closure of the caudal neuropore (O'Rahilly and Muller 2002).

The cell adhesion molecules (CAMs) are involved in defining the interaction of cell collectives and their borders during morphogenesis. Neural cell adhesion molecule 1 (NCAM1), an integral membrane protein belonging to the immunoglobulin superfamily (Edelman 1983), is involved in cell adhesion-dependent morphogenetic events, including the migration of various cells to the proper sites in neural tissues. NCAM is an important player in cell–cell and cell–matrix adhesion and is involved in many activities, including cell migration, neurite growth, axonal guidance, and synaptic plasticity (Thiery et al. 1982; Edelman 1983; Rutishauser and Jessell 1988).

A diverse group of NCAM molecules can be achieved from a single locus due to both transcriptional and posttranslational modifications. Alterative splicing, which is regulated in a cell and developmental stage-specific manner, produces three major isoforms. Two isoforms, NCAM-140 and NCAM-180, are membrane-spanning with a variable cytoplasmic domain and NCAM-120 is linked to the membrane by a glycosyl phosphatidylinositol lipid anchor (Cunningham et al. 1987). There are two alternate exons that can be included in the final *NCAM1* transcript. The VASE or variable alternative spliced exon contains an additional 30-bp insertion that results in an additional ten amino acids in the fourth immunoglobulin-like loop. Inclusion of the SEC exon results in a premature termination of translation and a secreted isoform (Small and Akeson 1990). In mouse cell lines, it has been shown that the binding of transcription factors encoded by *Hox*- and *Pax*-gene controls regulation of the *NCAM* promoter (Jones et al. 1992).

In the mouse, *Ncam* transcripts are first detected around day 8.5 in the somites and in the forming neural tube. Expression is not uniform along the rostrocaudal axis, with stronger expression in the caudal region of the neural tube and neural plate. *Ncam* expression continues until day 12.5, but is restricted to postmitotic neurons at later stages (Bally-Cuif et al. 1993). In *Ncam*-knockout mice with a targeted replacement with a *lacZ* reporter gene under control of endogenous *Ncam* regulatory sequences, β-galactosidase staining was seen throughout the spinal cord and dorsal root ganglia from E9.5 to E13.5 (Holst et al. 1998). This expression coincides with the neural tube formation in mouse embryos, around day 8 of gestation, and complete elevation and closure around day 10 (Harris and Juriloff 1999).

NCAM expression is also found in the neural tube in several other species. At the 15-somite stage of chicken embryos, NCAM is found in the neural plate and the adjacent ectoderm near Hensen's node, where the neural tube is not closed, but is exclusively expressed in the neural tube during and after closure at more rostral trunk levels (Thiery et al. 1982). By immunocytochemical analysis, both cell adhesion molecules N-cadherin and NCAM are detected on the cranial neural folds prior to neural tube closure and on migrating neural crest cells thereafter (Bronner-Fraser et al. 1992). Chicken NCAM is visible in the otic placode (Thiery et al. 1982) and later in differentiating auditory nuclei of the hindbrain, appearing progressively in differentiating neuron groups of the CNS (Hrynkow et al. 1998). The NCAM is also expressed in *Xenopus* embryos in a radial pattern within the neural tube during and for several hours after neural tube closure (Balak et al. 1987), and both zNCAM and zPCAM in zebrafish are expressed throughout the length of the closing neural tube from 11 to 30 hpf, during somitogenesis (Mizuno et al. 2001).

In the mouse, deletion of exons 3 and 4 of *Ncam1* prevents any isoform from being produced. The null mutants have few defects and are otherwise healthy and fertile (Cremer et al. 1994). However, by using homologous recombination to introduce a premature stop codon, a secreted form of NCAM can be produced in the absence of any membrane-associated protein. No heterozygous progeny were obtained from chimera crosses, suggesting dominant lethality. Chimeric embryos (E8.5) with a high ES cell contribution had poorly formed somites with kinking of the neural tube, and by E9.5, the anterior neuropore remained open in the mutant embryos (Rabinowitz et al. 1996). NCAM is a known downstream target of the *Pax*-3 transcription factor (Moase and Trasler 1991; Neale and Trasler 1994). *Pax-3* (splotch) mutant mice display multiple defects, including neural tube closure in the form of both spina bifida and exencephaly. In these mutants, altered NCAM isoform ratio and a decrease in the sialylation of the protein may alter the adhesive properties of NCAM (Epstein et al. 1991; Glogarova and Buckiova 2004). Quail embryos with spontaneous neural tube defects were shown to have disturbed matrix and cell adhesion molecule expression, including NCAM, by immunocytochemistry. The embryos expressed both N-cadherin and NCAM, not normally found at the stage examined (Newgreen et al. 1997). It was proposed that disruption of cell adhesion or extracellular matrix molecules that result in greater adhesion may impede appropriate morphogenetic movements, resulting in NTDs (Newgreen et al. 1997).

Given the importance of cell morphogenic events in neural tube closure, we hypothesized that a genetic variant that compromises the ability of a cell adhesion molecule in neural tissue may be associated with an

increased risk for human neural tube defects. For this reason, we investigated 11 SNPs across *NCAM1* for possible association with neural tube defects. We evaluated the promoter region, coding sequences, and alternative exons of *NCAM1* for polymorphisms that may play a role in NTDs. In addition, we examined the distribution of NCAM1 protein in human embryo sections of the neural tube and lateral tissues by immunohistochemistry.

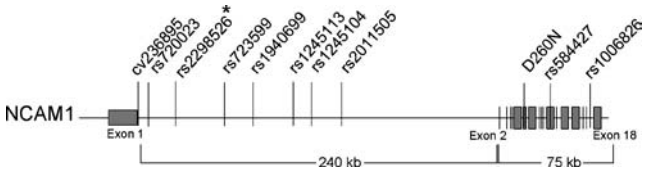

Fig. 1 Diagram of SNPs analyzed in the *NCAM1*-association study. The SNP with the *asterisk* shows the significant association

Materials and methods

Sample population

To identify novel polymorphisms within *NCAM1*, we screened 230 individuals with lumbosacral myelomeningocele by HPLC and sequencing methods, as described below. The simplex families ($n = 204$) used for frequency and association analysis consisted of a sampled affected individual with lumbosacral myelomeningocele and nuclear families, including unaffected siblings where available. In this study all individuals were American Caucasian. The complete sample set included an initial group of 132 families (Series 1), as well as a replication set of 72 additional families (Series 2) of the same phenotype and ethnicity. The Series 1 families were those first collected and included 107 complete triads and 25 families with one parent; this sample included 121 discordant sibling pairs. Series 2 families are the next set of families collected and included 49 complete triads and 23 families with one parent; this sample included 56 discordant sibling pairs. All data and samples were collected following informed consent of subjects; this study was approved by the Duke University Medical Center Institutional Review Board.

SNP selection and genotyping

Initially, a set of five SNPs (cv236895, rs2298526, rs2011505, rs584427, and rs1006826) were chosen to characterize association between *NCAM1* and human neural tube defects. The SNPs were spaced across the gene, with four being intronic and one coding. Following analysis in the Series 1 families ($n = 132$), an additional five SNPs (rs720023, rs723599, rs1940699, rs1245113, and rs1245104) were typed surrounding the marker that showed association. Where available, SNPs in conserved non-coding sequences were included in the selection. All known SNPs that were genotyped had a heterozygosity of 0.28 or greater. We also initiated dHPLC screening to identify novel SNPs, leading to the identification of one novel coding SNP (see below). SNP locations are shown in Fig.1.

The TaqMan allelic discrimination assays were used for the genotyping of these 11 SNPs across *NCAM1* (Assay-on-demand and Assay-by-Design, Applied Biosystems, Foster City, Calif., USA). The PCR amplification was performed using the GeneAmp PCR system 9700 thermocyclers (Applied Biosystems) according to the assay specifications. Fluorescence detection was performed with the ABI Prism 7900 and analyzed with SDS software (Applied Biosystems). Quality control measures consisted of 24 duplicated individuals per 384-well plate and were blinded from laboratory technicians. In addition, two samples from CEPH individuals were located across all plates for internal control. To pass quality control, data plates had to pass 100% matching for all 26 duplicated samples and 95% overall plate efficiency. The SNPs were tested in the family set for Mendelian inconsistencies.

Variation detection

To search for novel polymorphisms within *NCAM1*, the genomic sequence was divided into individual segments that included one exon each and minimal surrounding intronic sequence. In addition, the alternative exons VASE and SEC were evaluated in this study. For analysis for the promoter region, the size of the region evaluated was dependent upon regions of mouse homology and presence of predicted promoter element. Primers were designed flanking each region of interest by the use of the program Primer3 (Primer 3 website). For each fragment, a total of 30 ng of pooled DNA was amplified using standard PCR protocols (Table 1). DNA was extracted from blood samples of NTD patients and their families using the PureGene system and the Autopure LS (Gentra Systems, Minneapolis, Minn., USA) according to the manufacturer's protocol. The DNA samples were prepared and stored by the Duke Center for Human Genetics DNA bank Core. Following visualization and quantitation on a 2% agarose gel, PCR products were heteroduplexed by heating samples to 95°C for 3 min and slowly cooling to 30°C over 40 min. For polymorphism detection by denaturing high performance liquid chromatography (DHPLC), samples were injected into the Transgenomic WAVE Fragment Analysis System (version 4.1) for separation at various melting temperatures, as determined by WAVEMAKER software, version 4.1.42 (Transgenomic, San Jose, Calif., USA). When an apparent variation was noted by DHPLC, the individual samples exhibiting the variable pattern were directly sequenced. The PCR product was purified using QIAquick PCR Purification kit (Qiagen, Valencia, Calif., USA) according to the

Table 1 PCR fragments, primers, and conditions for all *NCAM1* fragments analyzed

Fragment name	Forward primer (5′-3′)	Reverse primer (5′-3′)	HPLC temp (°C)
Exon 1	ggctgggactgtcactcatt	gcaaaccagattgagaattaaaa	60
Exon 2	gggtttcattcttgaacattgg	cctgagggctcctgctctac	60
Exon 3	ggggacttattagtcttttcgactt	gcagaagaagaaggaggctct	61
Exon 4	gaagcagctgttttccctca	tgaaaaagctagggaacttgg	60.5
Exon 5	tgcagatgctctctgactga	ccaaggttgtagcaatgcag	60
Exon 6	tgtctcttctccaggccatt	gactttgtgatgccccattc	59.5
Exon 7	tggtcgaaatcatgctactttg	attgtggcagagcagtgacc	60.5
VASE	ctaaggggaaaaaaagctggaca	tcatccactcccaacacagc	56
Exon 8	tgcatgccatcatttaaacc	attccaaggccctgaaactc	56, 60.5
Exon 9	ccttgggctctgacatgc	catcctgaccctgccttg	63.5
Exon 10	aatcatggcagtcatcctga	ttggagcccacctagagtca	61
Exon 11	tgaccatcccataggacactt	attgggctggcagggttag	60
Exon 12	atggtcttgggccaaactg	caggtggggacatctgagta	61
SEC	gagggtgatgccgagaaggaa	cacacggagggaacaccaaga	57
Exon 13	gaaatagaattgctggaccaaa	aaggtgggctgggaaaag	57
Exon 14	cctgtcactccatcccattc	cagggttctggtgaagtctga	60
Exon 15	tcccgtaagttttgcctattg	caagcaagttgtcagggttg	60.5
Exon 16	gtctggaggtctcgcatctc	caaacctcagcaaggtggac	63
Exon 17	gccttgggttgagtcatagc	gggtctctacggagcaggt	63
Exon 18	agaccgtggtctcagtggtt	tggaaatgctctggtgaagc	60.5
Promoter 1	gagggtttcagtgttctaggc	aagaaaactccgatgtttggaa	54
Promoter mid	ttttcttcgggttatttctgga	ccagccttccttaatcagca	56.5
Promoter 2	ctgattaaggaaggctgggta	tttttgcagaattgtttcctg	63

manufacturer's directions. The sample was then sequenced using the BigDye Terminator version 3.1 Cycle Sequencing Ready Reaction kit (Applied Biosystems) and purified using Performa DTR Gel Filtration Cartridges (Edge Biosystems, Gaithersburg, Md., USA). In order to determine and confirm putative polymorphisms, sequence analysis was performed using ABI 3100 Data Collection Software Version 1.01 and ABI Sequencing Analysis 3.7.

Statistical analysis

All SNPs were tested for departure from Hardy-Weinberg equilibrium using a single affected and separately using an unaffected individual randomly selected from each family. These tests were conducted using the Genetic Data Analysis (GDA) software with a permutation test to estimate the *P* value (Lewis Lab Software Website). Pairwise calculations of linkage disequilibrium (LD) were computed with the Graphical Overview of Linkage Disequilibrium (GOLD) software for both the squared correlation coefficient (r^2) and Lewontin's standardized disequilibrium coefficient (D') (Abecasis and Cookson 2000). Single-locus association analysis was performed using the pedigree disequilibrium test (PDT) for allelic association and the genotype-based version, the geno-PDT (Martin et al. 2000, 2003). We used the PDTave statistic, giving equal weight to all families, for comparison of allele frequencies between affected individuals and their unaffected parents or siblings (Martin et al. 2000). In addition, the family-based association test (FBAT) was performed to test for association in both single loci and in haplotypes (Horvath et al. 2004). Haplotype analysis was performed with the HBAT function, using windows of three adjacent SNPs across *NCAM1*. Haplotypes with frequencies of $< 1\%$ were excluded from this analysis.

Bioinformatics

Genomic and protein sequences were obtained from The Human Genome Browser (assembly July 2003) University of California, Santa Cruz (UCSC web site) with additional information from Ensembl at http://www.ensembl.org/. Genomic and mRNA sequences were obtained from NCBI (accession numbers NM_000615 and NM_000615.1). All SNP references are based on NM_00615, with the ATG initiation codon being +1, and are named according to the recommendations of the Nomenclature Working Group (Antonarakis 1998). Protein references are based on NCAM140 (NP_00606). Promoter regions were chosen based on the prediction of promoter elements using Proscan and the Transfac databases (Wingender et al. 2001). Sequence alignment of human and mouse NCAM (GenBank accession numbers NM_000615 and NM_010875, respectively) was performed using PipMaker (Schwartz et al. 2000) to search for conserved non-coding sequences.

Immunohistochemistry

For NCAM expression analysis, unaffected human embryos were obtained from legally terminated pregnancies in agreement with French law 00–800 and with recommendations by the Necker Hospital ethics committee. Sections from embryos ranging from Carnegie stage 9 to

19 and spinal cords from 22 to 27sa fetuses as positive controls were chosen. When available, sections from levels of both open and closed neural tube from the same embryo underwent classical immunohistochemistry using two different primary antibodies: 1:100 dilution of a CD56/NCAM mAb (1B6, Novocastra), recognizing the 120/140-kDa forms or a rabbit pAb to NCAM (Chemicon, AB5032), recognizing all isoforms. Tissues had been fixed with 4% paraformaldehyde, embedded in paraffin blocks, and 5-μm sections were processed in 0.1% Tween-20-containing PBS. Anti-rabbit-555 (Invitrogen/Molecular Probes) was used for visualization at a dilution of 1:400 or anti-mIgG-biotin and ABC-HRP from the Vector MOM kit, PK2200 according to manufacturer's instructions. Specimens were examined on a Nikon EclipseTE300 fluorescent microscope equipped with a Roper Scientific CCD camera for image capture using Metaview (UIC) software.

Results

SNP detection

No variations were detected by DHPLC in exons 1–4, 8, and 10–18, in addition to two promoter regions and the VASE and SEC exons. However, six novel SNPs were detected and several known SNPs were verified in our population (Table 2). Only two of the SNPs occurred in exonic regions, one resulting in an amino acid change. Of the novel SNPs, one was analyzed in the entire family series via TaqMan allelic discrimination assays based on the frequency and putative correlation with disease status. All other novel SNPs were found to be in five or fewer individuals. Because the variant would have been too rare for identification of linkage disequilibrium in our family sample series ($\leq 1\%$), we pursued no further analysis.

Association studies

No SNP tested in the family-based series showed evidence for deviation from Hardy-Weinberg equilibrium in either the affected or unaffected individuals (data not shown). Pairwise LD across all 11 markers is shown in Table 3. The LD analysis based on r^2 (>0.5) revealed strong LD between all intron 1 SNPs cv236895, rs720023, rs2298526, rs723599, and rs1940699, as well as between SNPs rs1245113 and rs2011505, in both the affected and unaffected individuals. Values of D' were also large for several SNP pairs, suggesting little recombination in the region over evolutionary time. Although novel polymorphism D260N has large values of D' with several SNPs, the minor allele frequency is very small.

The results of the single-locus analysis are summarized in Table 4.The family-based association analysis using FBAT demonstrated strong evidence for association of intronic SNP rs2298526 ($P=0.0018$; C allele positively associated), and this association was also seen using the PDT test ($P=0.0025$) with the NTD phenotype in the first data series. Global tests for genotype association were approaching significance ($P=0.06$) for SNP rs2298526. Upon analysis of the initial five SNPs in the original family set ($n=132$), we attempted to replicate the findings using an additional 72 families. Single-locus association tests for the five SNPs in this family set did not reveal evidence for association in any marker. To further test for possible influence of *NCAM1* on NTDs, we typed five additional SNPs within the large first intronic region where significant SNP rs2298526 is located. In addition, one novel coding SNP found by DHPLC, resulting in the amino acid change D260N, was also followed up in the family set based on its frequency in affected and controls. This secondary screen and all additional SNPs were tested in both sample sets. Analysis of the two data sets as a combined group ($n=204$) of families, suggested no evidence for association with any of the new SNPs tested. Association with marker rs2298526 in the entire sample set was marginally significant using FBAT ($P=0.06$). None of the other SNPs tested showed significant evidence for association in any test (Table 4).

Results from the haplotype analysis, using a sliding window analysis of three markers, are shown in Table 5 for the haplotype displaying the highest Z-statistic showing association. In the original 132 family sample set, all windows that contain the SNP rs2298526 are significant with the haplotype A-C-G for SNPs rs720023, rs2298526, and rs723599 being the most highly associated ($P=0.00028$). The transmission of a haplotype window containing up to seven markers remains significant ($P=0.05$) with inclusion of the SNP rs2298526. In the combined sample set ($n=204$ families), transmission of this same haplotype remains significant ($P=0.02$).

Table 2 Novel polymorphisms in *NCAM1*

Fragment	SNP	Surrounding sequence
Exon 5	g.244569G > A	gaatggtgagG/Aagagtccgtt
Exon 6	g.245781C > T	tggctC/TataccttttatcatgG/Aactag
	g.245797G > A	See above
Exon 7	c.958G > A; D260N	agaggaagacG/Aatgagaagta
	c.1032G > A; E284E	acgaggctgaG/Atacatctgca
Exon 9	g.270021C > A	ccttccccccC/Aacccccggca

Immunohistochemistry

The NCAM1 protein expression is present in the paraxial mesoderm at C9 and later in the epithelial somites at stages C10 (data not shown). However, no expression is seen in the open or closed neural tube at these stages. At C11, the first neural tube expression appears, with NCAM1 on a few cells in the ventral

Table 3 Measures of linkage disequilibrium between *NCAM1* SNPs. The r^2 values are given above the diagonal and D' values are given below the diagonal

	cv236895	rs720023	rs2298526	rs723599	rs1940699	rs1245113	rs1245104	rs2011505	D260N	rs584427	rs1006826
cv236895	–	0.575	0.556	0.524	0.545	0.243	0.090	0.196	0.028	0.019	0.007
rs720023	0.991	–	0.957	0.959	0.960	0.390	0.052	0.313	0.014	0.005	0.011
rs2298526	0.98	0.987	–	0.994	1	0.396	0.048	0.306	0.017	0.009	0.009
rs723599	0.96	0.988	1	–	1	0.399	0.046	0.302	0.007	0.004	0.014
rs1940699	0.971	0.988	1	1	–	0.406	0.045	0.310	0.014	0.005	0.385
rs1245113	0.695	0.669	0.667	0.664	0.673	–	0.385	0.847	0.013	0.026	0.009
rs1245104	0.338	0.335	0.329	0.320	0.312	0.974	–	0.340	0.014	0.026	0.003
rs2011505	0.678	0.643	0.623	0.620	0.631	0.986	1	–	0.012	0.032	0.012
D260N	1	1	1	0.658	1	1	0.616	1	–	0.013	0.002
rs584427	0.241	0.099	0.125	0.684	0.090	0.202	0.319	0.211	1	–	0
rs1006826	0.236	0.217	0.213	0.239	0.974	0.187	0.154	0.195	0.775	0.001	–

Table 4 Results from single-locus family-based tests of association for *NCAM1* SNPs. No *P* value (n/a) is reported for D260N in the FBAT test due to the low minor allele frequency

SNP	*P* value						
	Series 1		Series 2		Combined 204 families		
	FBAT	PDT	FBAT	PDT	FBAT	PDT	GenoPDT
cv236895[a]	0.38	0.47	0.66	0.73	0.68	0.69	0.86
rs720023	0.041	0.035	0.31	0.17	0.28	0.37	0.28
rs2298526[a]	0.0018	0.0025	0.11	0.075	0.06	0.09	0.14
rs723599	0.0081	0.0059	0.12	0.077	0.22	0.37	0.20
rs1940699	0.012	0.012	0.16	0.11	0.23	0.27	0.10
rs1245113	0.64	0.57	0.78	0.81	0.59	0.77	0.60
rs1245104	0.46	0.49	0.83	0.55	0.49	0.36	0.51
rs2011505[a]	0.33	0.22	1.00	0.75	0.43	0.41	0.87
D260N	n/a	0.40	n/a	0.65	n/a	0.41	0.41
rs584427[a]	0.39	0.45	0.49	0.65	0.67	0.45	0.70
rs1006826[a]	0.18	0.24	0.24	0.25	0.06	0.11	0.66

[a]The original five SNPs

rhombencephalon and a faint, diffuse expression dorsally at the contact of the roofplate with the ectoderm (Fig.2b) that is absent at trunk levels. Similar expression is observed at stage C12, characterized by strong expression in discrete ventral areas of the hindbrain (Fig.2d) and individual ventrolateral cells of the spinal cord at all levels (Fig.2e, f). The position of these cells and fiber tracts, distant from the ventricle, is consistent with motoneuron identity. Epithelial somite expression persists (Fig.2f). At C12, human neural tube closure is complete aside from the caudal neuropore (K. Sulik, personal communication, and our observations). At C13, NCAM1 is expressed more robustly in the ventral midbrain, hindbrain, and spinal cord (Fig.2h, j, k) and becomes apparent in the ventral roots as well. As somites mature, expression becomes restricted to a dorsomedial sector in phase with but not surrounding the ventral roots (Fig.2i, j). NCAM1 is also visible in the epithelial mesonephros from C13 (Fig.2i, k). By C16, spinal cord NCAM1 expression has extended to mediolateral axon tracts and continues in the motor roots, but is absent from immature ventricular cells, commissural axons crossing the floorplate or dorsal roots/ganglia (Fig.2l). At C19, this pattern persists; strong annular expression is also seen in a cross-section of spinal nerves (Fig.2m).

Discussion

Although rs2298526 appears to be associated with increased risk for neural tube defects, the functional significance of this association remains unclear. Our sample set of American Caucasian simplex lumbosacral myelomeningocele families ($n = 132$ families), revealed a significant association between risk for NTDs and intronic SNP rs2298526 using both the FBAT test ($P = 0.0018$) and the PDT ($P = 0.0025$). Using the HBAT for haplotype association, all pairwise comparisons with SNP rs2298526 were also significant. In a replication study set of 72 additional families, no significant association was detected in this sample set, however; the overall trend for overtransmission of the less common allele of SNP rs2298526 remains significant in the combined sample set.

Our failure to replicate the significant association in the additional Series 2 families added to our screen may be the result of spurious association in the original

Table 5 Haplotype results for sliding three-marker window across *NCAM1*

Window	SNP											Series 1		Combined set	
	cv236895	rs720023	rs2298526	Rs723599	rs1940699	rs1245113	rs1245104	rs2011505	D260N	rs584427	rs1006826	Haplotype frequency	*P* value	Haplotype frequency	*P* value
1	C	A	C									0.26	0.015	0.116	0.24
2		A	C	G								0.381	0.00028	0.391	0.02
3			C	G	A							0.392	0.0011	0.398	0.05
4				G	A	C						0.333	0.059	0.329	0.28
5					A	C	G					0.191	0.102	0.177	0.012
6						C	G	G				0.531	0.045	0.185	0.096
7							G	G	G			0.223	0.096	0.221	0.10
8								G	G	G		0.333	0.28	0.332	0.31
9									G	G	T	0.467	0.48	0.456	0.58

sample set, or could simply be due to the genetic complexity NTDs in humans. It may also be that the Series 2 families differ in the risk associated with NCAM1 from the initial set of families, or that the smaller sample size (approximately 40% smaller) in Series 2 decreases the power enough so that no association is found. Differences in the family characteristics between the two series may also account for the differences. For instance, in the Series 1 families, 19% of the families had one missing parent, compared with 32% of the families in the Series 2 set. Series 1 families also had a higher proportion of discordant sibling pairs than the Series 2 families (0.92 versus 0.78 per family). Both these differences are statistically significant ($P = 0.003$ and 0.01, respectively). Future follow-up is necessary to assess any role that NCAM1 may have in other ethnic groups or NTD phenotypes.

The significant association could be explained by either some functional significance of the rs2298526 C allele itself, or by LD between this SNP and one that confers a functional role. The SNP is a potential binding site for several transcription factors, some of which are created or eliminated by the C allele, and could explain a possible function. The fact that rs2298526 is within intron 1, a large intron more than 240 kb in size, may suggest a regulatory role. Recent reports have suggested that segments of DNA that are highly conserved across vertebrates from fugu to mouse to humans may represent regions of fundamental importance to vertebrate development (Bejerano et al. 2004; Woolfe et al. 2004). Although none of these are near *NCAM1*, it is clear that non-coding DNA elements may have a significant functional role.

Alternatively, the association we have found could be due to LD between this marker and some untyped functional variant with an unknown role; several SNPs within this first intron are within a strong LD block. Furthermore, variations that are detected at the nucleotide level may contribute to the development of NTDs only in the presence of other genetic or environmental factors. Such polymorphisms may alter NCAM1 expression or adhesive properties that alone or when combined with other factors may contribute to failure of neural crest elevation and/or neural tube closure. During creation of the neural folds, there is pushing of the presumptive epidermis toward the midline and anchoring of the neural plate to the underlying mesoderm (Alvarez and Schoenwolf 1992). In this process, cells of the epidermis must slide over the mesoderm during neural fold elevation and closure. Newgreen et al. (1997) suggests that the ectopic NCAM expression in the neural tube observed in avian embryos with spontaneous neural tube defects caused a tendency toward greater adhesion, which may impede this process. However, the ectopic expression may be a secondary effect rather than causative. Ectopic expression of NCAM alone in *Xenopus* embryos does not cause abnormal neural tube closure (Kintner 1988). It is maintained that the differential adhesion between the ectoderm and neural plate plays

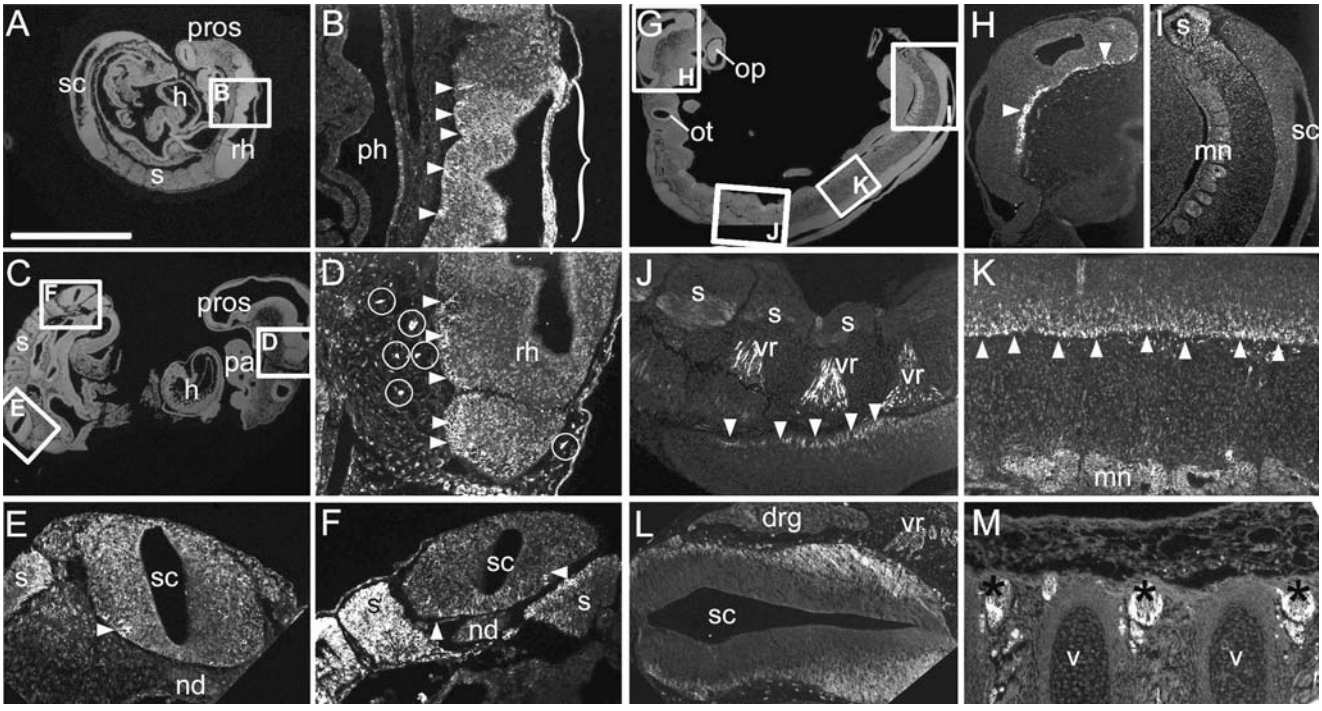

Fig. 2 **a** Parasagittal section of human embryo stained with DAPI at C11 (24 days), with enlargement in **b** indicated. **b** NCAM1 expression is visible on isolated cells of the ventral rhombencephalon (*arrowheads*). It is also specifically present in its wide, thin roofplate, a region-specific anatomical feature. **c** Parasagittal-to-transverse section of human embryo at C12 (26 days), DAPI stain, position of **d–f** indicated. NCAM expression is present in future motor areas of the rhombencephalon (*arrowheads*, **d**) and in sparse cells of head mesenchyme, possibly neural crest cells (*circled*). A few ventrolateral cells of the spinal cord at all levels are NCAM1$^+$ and epithelial somite expression persists (**e, f**, transverse section). **g** Parasagittal section of human embryo at C13 (29 days), DAPI stain and photo reconstruction. **h** Robust NCAM1 expression in the ventral midbrain and hindbrain (*arrowheads*). **i** NCAM1 is present in both a trunk-level epithelial somite and in the mesonephros (also see **k**). **j** Spinal cord ventral roots are highly immunoreactive and ventral spinal cord expression persists (*arrowheads*). As somites mature, expression is restricted to a dorsomedial sector in phase with but not in contact with the ventral roots. **k** NCAM1 is visible in the mesonephros and in ventrolateral spinal cord (*arrowheads*). **l** By C16 (37 days), mediolateral axon tracts and ventral roots of the spinal cord are immunoreactive for NCAM1, but not immature ventricular cells, commissural axons crossing the floorplate or dorsal roots or associated ganglia. Dorsal to *left*. **m** At C19 (47 days), this pattern persists; strong annular expression is also visible in the cross-section of segmental nerves (*asterisks*). Dorsal to bottom (*drg* dorsal root ganglion, *h* heart, *mn* mesonephros, *op* optic vesicle, *ot* otic vesicle, *pa* pharyngeal arch(es), *pros* prosencephalon, *s* somite, *sc* spinal cord, *v* vertebra, *vr* ventral root). *Bar*: in **a, c, h, i**, 0.5 mm; in **b, d–f, l**, 0.2 mm; in **g**, 0.71 mm; in **j**, 0.29 mm; in **k**, 0.22 mm; in **m**, 0.27 mm

an important role in neural tube closure, since injection of N-cadherin into a *Xenopus* embryo results in the failure of the neural tube tissues to separate from the presumptive epidermis (Detrick et al. 1990). Unfortunately, ectopic (in)activation of NCAM was not examined in these experiments.

It has been suggested that NCAM1 may not play an essential role in mammalian neurulation (Copp et al. 2003), based on the *Xenopus* model and the fact that mice with null mutations in *Ncam* have normal closure (Cremer et al. 1994). However, interestingly, among the brain defects in null mice is a large reduction in the size of the olfactory bulbs, into which NCAM-expressing neuronal stem cell progeny migrate throughout adult life (Pennartz et al. 2004). Producing only the extracellular domain of the NCAM molecule in mammals results in lethality and serious morphological defects (Rabinowitz et al. 1996), possibly through a dominant negative effect on heterophilic adhesion. Prag et al. (2002) suggest that this puzzling observation may be explained by the fact that both the cytoplasmic and extracellular parts of NCAM are capable of modifying the motility and migration of cells. Indeed, the intracellular domain of NCAM mobilizes integrin signaling through association with the fibroblast growth factor receptor 4 (Cavallaro et al. 2001).

In *Xenopus*, chicken, and mouse, NCAM appears to be expressed in the immature neural tube during closure, although closer examination reveals that expression in frogs and mice is essentially restricted to migrating neural crest cells or to fiber-projecting, differentiated neurons at later stages. The chicken data, most detailed, vary from our findings in human embryos with respect to expression in the closing avian neural tube, cephalic placodes and derivatives, and the cardiac mesoderm (Thiery et al. 1982). However, our results are concordant with respect to the somites, the presence of positive enteric ganglia and absence of dorsal root ganglion expression. The discordances are probably species-specific, but differences in antibody sensitivity are not to be excluded. We have found that the timing of NCAM1 expression in the dorsal neural tube does not correlate with closure in humans. Nonetheless, it is likely that

variations that cause inappropriate or increased NCAM1 expression could incur a risk for NTDs by altering the heterophilic adhesive properties of neural tube cells relative to their NCAM1-expressing somitic environment, rather than homophilic adhesion to each other at the line of closure. In addition, the transitory NCAM1 immunoreactivity we observed in the dorsal roof of the human hindbrain just after neural tube closure may correlate with the propensity of this region to develop occipital encephalocele.

In conclusion, the trend for over-transmission of the rs2298526 C allele is significant in NTD cases. Haplotype analysis in both the original and combined sample sets suggests a role for SNPs located within the first intron of *NCAM1*. In addition, the expression pattern of the NCAM1 protein in human shows no expression within the neural tube at the time of closure, but it appears to be expressed in the surrounding mesoderm and later in differentiated neurons of the CNS. Our results show a possible involvement of polymorphisms in *NCAM1* with the risk for human neural tube defects.

Acknowledgements The authors wish to thank the families who participated in this study; without their interest, this work could not be performed. We also thank Silke Schmidt for helpful comment on this manuscript and Pat Hurban and Paradigm Genetics for bioinformatics support. We gratefully acknowledge support from grants HD39948, ES11375, NS39818, ES011961, and NS26630.

Appendix

NTD Collaborative Group

Joanna Aben, Children's Rehabilitation Service, Birmingham, Alabama; Arthur Aylsworth, Cynthia Powell, University of North Carolina, Chapel Hill, North Carolina; Joanne Mackey, Gordon Worley, Duke University Medical Center; Timothy Brei, Connie Buran, Indiana University School of Medicine, Indianapolis, Indiana; Joann Bodurtha, Kathleen Sawin, Virginia Commonwealth University, Richmond, Virginia; Mark S. Dias, Children's Hospital of Buffalo, Buffalo, N.Y.; Philip Mack, Elli Meeropol, Shriner's Hospital, Springfield, Massachusetts; Nicole Lasarsky, Carolinas Medical Center, Charlotte, NC; David McLone, Joy Ito, Children's Memorial Hospital, Chicago, Illinois; W. Jerry Oakes, University of Alabama, Birmingham, Alabama; Marion Walker, University of Utah, Salt Lake City, Utah; Bermans Iskandar, University of Wisconsin Hospitals, Madison, Wisconsin.

References

Abecasis GR, Cookson WO (2000) GOLD—graphical overview of linkage disequilibrium. BioInformatics 16:182–183

Alvarez IS, Schoenwolf GC (1992) Expansion of surface epithelium provides the major extrinsic force for bending of the neural plate. J Exp Zool 261:340–348

Antonarakis SE (1998) Recommendations for a nomenclature system for human gene mutations. Nomenclature Working Group. Hum Mutat 11:1–3

Balak K, Jacobson M, Sunshine J, Rutishauser U (1987) Neural cell adhesion molecule expression in *Xenopus* embryos. Dev Biol 119:540–550

Bally-Cuif L, Goridis C, Santoni MJ (1993) The mouse NCAM gene displays a biphasic expression pattern during neural tube development. Development 117:543–552

Bejerano G, Pheasant M, Makunin I, Stephen S, Kent WJ, Mattick JS, Haussler D (2004) Ultraconserved elements in the human genome. Science 304:1321–1325

Bronner-Fraser M, Wolf JJ, Murray BA (1992) Effects of antibodies against N-cadherin and N-CAM on the cranial neural crest and neural tube. Dev Biol 153:291–301

Campbell LR, Dayton DH, Sohal GS (1986) Neural tube defects: a review of human and animal studies on the etiology of neural tube defects. Teratology 34:171–187

Cavallaro U, Niedermeyer J, Fuxa M, Christofori G (2001) N-CAM modulates tumour-cell adhesion to matrix by inducing FGF-receptor signalling. Nat Cell Biol 3:650–657

Copp AJ, Greene ND, Murdoch JN (2003) The genetic basis of mammalian neurulation. Nat Rev Genet 4:784–793

Cremer H, Lange R, Christoph A, Plomann M, Vopper G, Roes J, Brown R, Baldwin S, Kraemer P, Scheff S (1994) Inactivation of the N-CAM gene in mice results in size reduction of the olfactory bulb and deficits in spatial learning. Nature 367:455–459

Cunningham BA, Hemperly JJ, Murray BA, Prediger EA, Brackenbury R, Edelman GM (1987) Neural cell adhesion molecule: structure, immunoglobulin-like domains, cell surface modulation, alternative RNA splicing. Science 236:799–806

Detrick RJ, Dickey D, Kintner CR (1990) The effects of N-cadherin misexpression on morphogenesis in *Xenopus* embryos. Neuron 4:493–506

Edelman GM (1983) Cell adhesion molecules. Science 219:450–457

Epstein DJ, Vekemans M, Gros P (1991) Splotch (Sp2H), a mutation affecting development of the mouse neural tube, shows a deletion within the paired homeodomain of Pax-3. Cell 67:767–774

Glogarova K, Buckiova D (2004) Changes in sialylation in homozygous Sp2H mouse mutant embryos. Birth Defects Res Part A Clin Mol Teratol 70:142–152

Harris MJ, Juriloff DM (1999) Mini-review: toward understanding mechanisms of genetic neural tube defects in mice. Teratology 60:292–305

Holst BD, Vanderklish PW, Krushel LA, Zhou W, Langdon RB, McWhirter JR, Edelman GM, Crossin KL (1998) Allosteric modulation of AMPA-type glutamate receptors increases activity of the promoter for the neural cell adhesion molecule, N-CAM. Proc Natl Acad Sci USA 95:2597–2602

Horvath S, Xu X, Lake SL, Silverman EK, Weiss ST, Laird NM (2004) Family-based tests for associating haplotypes with general phenotype data: application to asthma genetics. Genet Epidemiol 26:61–69

Hrynkow SH, Morest DK, Bilak M, Rutishauser U (1998) Multiple roles of neural cell adhesion molecule, neural cell adhesion molecule-polysialic acid, and L1 adhesion molecules during sensory innervation of the otic epithelium in vitro. Neuroscience 87:423–437

Jones FS, Prediger EA, Bittner DA, De Robertis EM, Edelman GM (1992) Cell adhesion molecules as targets for *Hox* genes: neural cell adhesion molecule promoter activity is modulated by cotransfection with *Hox-2.5* and *−2.4*. Proc Natl Acad Sci USA 89:2086–2090

Kintner C (1988) Effects of altered expression of the neural cell adhesion molecule, N-CAM, on early neural development in *Xenopus* embryos. Neuron 1:545–555

Martin ER, Monks SA, Warren LL, and Kaplan NL (2000) A test for linkage and association in general pedigrees: the pedigree disequilibrium test. Am J Hum Genet 67:146–154

Martin ER, Bass MP, Gilbert JR, Pericak-Vance MA, Hauser ER (2003) Genotype-based association test for general pedigrees: the genotype-PDT. Genet Epidemiol 25:203–213

Mizuno T, Kawasaki M, Nakahira M, Kagamiyama H, Kikuchi Y, Okamoto H, Mori K, Yoshihara Y (2001) Molecular diversity in zebrafish NCAM family: three members with different VASE usage and distinct localization. Mol Cell Neurosci 18:119–130

Moase CE, Trasler DG (1991) N-CAM alterations in splotch neural tube defect mouse embryos. Development 113:1049–1058

Neale SA, Trasler DG (1994) Early sialylation on N-CAM in splotch neural tube defect mouse embryos. Teratology 50:118–124

Newgreen DF, Kerr RS, Minichiello J, Warren N (1997) Changes in cell adhesion and extracellular matrix molecules in spontaneous spinal neural tube defects in avian embryos. Teratology 55:195–207

O'Rahilly R, Muller F (2002) The two sites of fusion of the neural folds and the two neuropores in the human embryo. Teratology 65:162–170

Pennartz S, Belvindrah R, Tomiuk S, Zimmer C, Hofmann K, Conradt M, Bosio A, Cremer H (2004) Purification of neuronal precursors from the adult mouse brain: comprehensive gene expression analysis provides new insights into the control of cell migration, differentiation, and homeostasis. Mol Cell Neurosci 25:692–706

Prag S, Lepekhin EA, Kolkova K, Hartmann-Petersen R, Kawa A, Walmod PS, Belman V, Gallagher HC, Berezin V, Bock E, Pedersen N (2002) NCAM regulates cell motility. J Cell Sci 115:283–292

Rabinowitz JE, Rutishauser U, Magnuson T (1996) Targeted mutation of Ncam to produce a secreted molecule results in a dominant embryonic lethality. Proc Natl Acad Sci USA 93:6421–6424

Rutishauser U, Jessell TM (1988) Cell adhesion molecules in vertebrate neural development. Physiol Rev 68:819–857

Schwartz S, Zhang Z, Frazer KA, Smit A, Riemer C, Bouck J, Gibbs R, Hardison R, Miller W (2000) PipMaker—a web server for aligning two genomic DNA sequences. Genome Res 10:577–586

Small SJ Akeson R (1990) Expression of the unique NCAM VASE exon is independently regulated in distinct tissues during development. J Cell Biol 111:2089–2096

Sulik KK, Zucker RM, Dehart DB et al (1998) Normal patterns of neural tube closure differ in the human and mouse. Proc Greenwood Genet Ctr 18:129–130

Thiery JP, Duband JL, Rutishauser U, Edelman GM (1982) Cell adhesion molecules in early chicken embryogenesis. Proc Natl Acad Sci USA 79:6737–6741

Van Allen MI, Kalousek DK, Chernoff GF, Juriloff D, Harris M, McGillivray BC, Yong SL, Langlois S, Macleod PM, Chitayat D, Freidman JM, Wilson D, McFadden D, Pantzar J, Ritchie S, Hall JG (1993) Evidence for multi-site closure of the neural tube in humans. Am J Med Genet 47:723–743

Wingender E, Chen X, Fricke E, Geffers R, Hehl R, Liebich I, Krull M, Matys V, Michael H, Ohnhauser R, Pruss M, Schacherer F, Thiele S, Urbach S (2001) The TRANSFAC system on gene expression regulation. Nucleic Acids Res 29:281–283

Woolfe A, Goodson M, Goode DK, Snell P, McEwen GK, Vavouri T, Smith SF, North P, Callaway H, Kelly K, Walter K, Abnizova I, Gilks W, Edwards YJ, Cooke JE, Elgar G (2004) Highly conserved non-coding sequences are associated with vertebrate development. PLoS Biol 3:e7

J. Neuroradiol., 2005, *32*, 147-156

VASCULARISATION DE LA TÊTE ET DU COU AU COURS DU DÉVELOPPEMENT

E. DETRAIT, H.C. ETCHEVERS

INSERM U-393, Hôpital Necker – Enfants Malades, 149 rue de Sèvres, 75743 Paris Cedex 15.

RÉSUMÉ

Au cours de l'embryogenèse, le premier rôle de la vascularisation est d'assurer les besoins métaboliques de la tête, ceci dès les stades les plus précoces. Le présent article passe en revue quelques principes qui gouvernent la construction cellulaire des vaisseaux et leur emplacement. Pour comprendre l'organisation et la mise en place de l'arbre vasculaire céphalique, il est nécessaire de rappeler d'une part les mouvements morphogénétiques qui dirigent la formation de la tête des vertébrés et d'autre part les cellules à partir desquelles les vaisseaux se constituent. Certaines des principales molécules de signalisation impliquées dans le développement vasculaire, notamment les angiopoïétines, les endothélines, les FGFs, les Notchs, les PDGFs, Sonic hedgehog, les TGFs et les VEGFs, sont évoquées afin de souligner les similitudes entre la vascularisation embryonnaire et postnatale, même dans le contexte de morphologies de plus en plus divergentes.

Mots-clés : angiogenèse, vasculogenèse, crête neurale, mésoderme.

SUMMARY

Vascularization of the head and neck during development

One of the earliest priorities of the embryonic vascular system is to ensure the metabolic needs of the head. This review covers some of the principles that govern the cellular assembly and localization of blood vessels in the head. In order to understand the development and organization of the cephalic vascular tree, one needs to recall the morphogenetic movements underlying vertebrate head formation and giving rise to the constituent cells of the vascular system. Some of the major signaling molecules involved in vascular development are discussed, including the angiopoietins, the endothelins, the FGFs, the Notch receptors, the PDGFs, Sonic hedgehog, the TGF family and the VEGFs, in order to underline similarities between embryonic and postnatal vascular development, even in the context of increasingly divergent form.

Key words: *angiogenesis, vasculogenesis, neural crest, mesoderm.*

MORPHOGENÈSE ET SPÉCIFICATION DES COMPOSANTS VASCULAIRES DE L'EMBRYON HUMAIN

Durant les troisième et quatrième semaines après la fécondation, l'embryon, jusqu'alors bidermique, est le lieu d'importants mouvements cellulaires qui le transforment en un embryon à trois couches cellulaires. Durant ce processus dénommé gastrulation, des cellules mésodermiques mésenchymateuses générées au niveau de ligne primitive s'intercalent entre l'ectoderme et l'endoderme. Le mésoderme naît donc sur la ligne médiane et migre ensuite vers les bords latéraux de l'embryon. Simultanément, l'ectoderme de la partie rostrale de l'embryon, au devant de la ligne primitive, s'épaissit pour former le neurectoderme. Le neurectoderme s'enroule et se soude sur sa face dorsale pour donner naissance à un tube qui sera à l'origine de tout le système nerveux central. Lors de la soudure du tube, des cellules se détachent de la frontière entre le neurectoderme et l'ectoderme. Ces cellules, dénommées crêtes neurales, migreront dans tout l'embryon pour donner de multiples dérivés dont certains participeront à la vascularisation de la tête et du cou. L'excellent livre illustré de Larsen [48] en embryologie humaine retrace ces étapes en détail.

La matière première des vaisseaux sanguins est la cellule endothéliale (CE). Elle tapisse l'intérieur du vaisseau et se trouve au contact direct avec le sang. Pendant la gastrulation et la neurulation, les hémangioblastes se différencient à partir de cellules souches issues du mésoderme. Ces cellules, apparaissant dans les membranes extra-embryonnaires, ont la capacité de devenir soit des cellules hématopoïétiques, soit des angioblastes, les précurseurs des cellules endothéliales [72].

Une fois spécifiées, les angioblastes migrent, se différencient et s'assemblent en plexus vasculaire primaire en jouant notamment sur la modification des caractéristiques de l'adhésion à la matrice extracellulaire [24, 39]. Ce processus d'assemblage *in situ* de vaisseaux à partir de composants réunis sur place est dénommé vasculogenèse. L'aorte et les veines cardinales se forment de la sorte. La vasculogenèse est suivie par l'angiogenèse, c'est-à-dire la croissance, le remodelage et l'extension de ce réseau primitif pour former un réseau vasculaire mature. Ce second processus constitue le mécanisme principal de la vascularisation des tissus en croissance, tant chez l'embryon que chez l'organisme adulte.

La morphogenèse vasculogenèse au niveau du tronc comporte deux phases marquantes : a) le rassemblement des angioblastes de l'endocarde pré-

Tirés à part : H.C. ETCHEVERS, à l'adresse ci-dessus.
e-mail : etchevers@necker.fr

somptif autour de la porte intestinale antérieure en dessous de la tête [58] et, b) le rassemblement d'angioblastes en deux colonnes de part et d'autre de la notochorde pour former les aortes dorsales. Ces artères primaires de la neurula longent l'axe antéropostérieur du corps et fusionnent pour devenir l'aorte définitive, entre la notochorde et l'intestin. La première angiogenèse des artères intersomitiques segmentaires se produira à partir des aortes dorsales. Simultanément, d'autres vaisseaux se brancheront bilatéralement près de la sortie du coeur et se dirigeront ultérieurement vers la tête.

Au niveau de la tête, la vasculogenèse se produit au sein du mésoderme mésenchymateux entre l'ectoderme et le neurectoderme et genère une accumulation d'angioblastes à proximité du cerveau [14]. Le reste de ce mésoderme est consacré au précurseurs des muscles céphaliques, qui se développent grâce aux signaux secrétés par les cellules de la CN céphalique [89]. Par le biais de l'embryologie expérimentale, on a pu souligner de nombreuses différences de devenir entre les cellules de CN émigrant à partir de différents niveaux antéropostérieurs du neurectoderme. Ainsi, les cellules de CN sortant au niveau du futur cerveau ont la capacité de se différencier en cellules de muscle lisse vasculaire, en péricytes, en méninges, en derme, en os ou en cartilage de la tête, alors que leurs consoeurs sortant au niveau de la moelle épinière ont une différenciation plus restreinte en cellules du système nerveux périphérique, en mélanocytes ou en certaines cellules endocriniennes [51].

Le cœur, localisé coté ventral *(figure 1a)*, expulse du sang oxygéné dans les aortes dorsales par le biais d'une artère en forme d'épingle à cheveux dont la partie ventrale est désignée comme l'aorte ventrale *(figure 1b)*. L'épingle s'allonge en direction de la tête, et des connections symétriques, les arcs aortiques, se forment autour de l'endoderme pharyngien entre l'aorte ventrale et dorsale. L'organisation des feuillets embryonnaires autour de ces paires d'artères, et notamment la différenciation localement dirigée de la CN céphalique, donnera lieu aux éléments du visage inférieur et du cou. Au moment où se forme la troisième paire d'arcs aortiques, la première paire se détache et les artères se ramifient en direction du cerveau antérieur ; c'est le début de l'important remodelage des gros vaisseaux pendant l'embryogenèse. Ainsi, les 5 paires d'arcs aortiques (numérotés 1 à 4 et 6 pour des raisons historiques) n'existent jamais simultanément. Des éléments de la première à la troisième paire d'arcs aortiques se trouveront au sein de la paroi de la carotide interne par exemple, alors que seul l'arc gauche de la quatrième paire persistera en tant que crosse de l'aorte et les sixièmes arcs s'intégreront dans le canal artériel qui disparaîtra après la naissance chez l'homme.

Les cellules endothéliales assument des fonctions différentes suivant le tissu et le type de vaisseau dans lequel elles se trouvent [7]. L'acquisition de ces caractéristiques propre à chaque localisation est le résultat de la double influence de l'environnement et des programmes génétiques endogènes.

CASCADES GÉNÉTIQUES IMPLIQUÉS DANS LA VASCULOGENÈSE

Durant plusieurs décennies, l'hypothèse dominante expliquant la différenciation entre veine et artère postulait que la pression et la direction du flux sanguin à l'intérieur d'un vaisseau déterminaient sa destinée. Des données récentes ont remis cette hypothèse en cause. Ainsi, le Noble et ses collaborateurs ont démontré que les caractéristiques moléculaires des artères et des veines s'exprimaient avant le début du flux sanguin mais qu'elles se ségrégeaient sur les vaisseaux appropriés une fois que le flux était établi dans le sac vitellin [52]. Par contre, des données obtenues notamment chez le poisson zèbre suggèrent que cette détermination se produit au sein même de l'embryon avant l'apparition de toute circulation sanguine dans le futur vaisseau et se maintient par la suite [101].

Une structure clé de l'organisation vasculaire est la notochorde. La notochorde est un bâton mésodermique s'étendant sous le tube neural ventral, le long de l'axe antéropostérieur de l'embryon *(figure 1)*. Depuis longtemps, cette structure est connue comme le centre organisateur du développement du tube neural [28] et des somites [9, 20]. Des travaux récents ont également démontré un rôle prépondérant au cours de l'induction de l'endoderme [10] et des artères et veines axiales (discuté plus loin). Par conséquent, les facteurs de transcription régulant la mise en place de la notochorde interviennent en amont des gènes responsables de l'organisation de l'aorte et, à un moindre degré, de la veine cardinale [36, 85]. Ces facteurs de transcription sortent du cadre de cette revue.

Des lignées de poisson-zèbres issues de criblage par la mutagenèse permettent une caractérisation moléculaire des phénotypes morphologiques décrits. Ainsi, des poissons sans notochorde, normalement située au-dessus de l'aorte dorsale, ou avec des malformations de l'endoderme, sous la veine axiale (future cardinale inférieure) *(figure 1d)*, manifestent des anomalies vasculaires dont les molécules responsables ont pu être identifiées. Certaines, comme Sonic hedgehog, émanent directement de la notochorde alors que d'autres, comme Notch-1 ou VEGF, sont induites dans les tissus avoisinants.

Sonic hedgehog

Sonic hedgehog (Shh) est un facteur sécrété, très conservé au cours de l'évolution, et principal médiateur des effets induits par la notochorde. Par exemple, la sécrétion de Shh vers le somite induit sa différenciation en précurseurs des cartilages costaux et vertébraux [33].

Chez des embryons de poisson-zèbres normaux, l'application d'un excès de Shh entraîne une différenciation artérielle ectopique qui se substitue à la veine cardinale postérieure. La surexpression de Shh au sein du système nerveux central du poulet embryonnaire résulte en son hypervascularisation [76]. Comme tous les nouveaux capillaires, ceux-là expriment initialement des marqueurs spécifiques aux artères avant de les perdre du coté veineux au cours de leur maturation [37], ce qui renforce l'hypo-

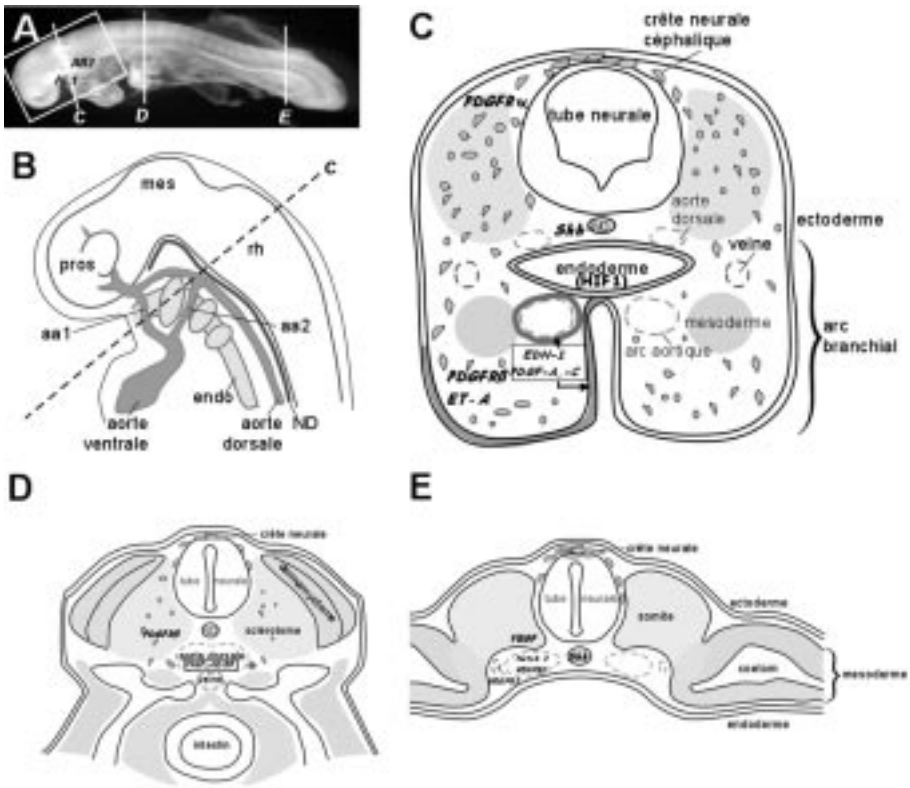

FIG. 1. – a) Embryon humain 23 jours après fécondation montrant deux arcs branchiaux (AB1 et 2) et 19 paires de somites. Les niveaux approximatifs des schémas de B (cadre) et C-E (lignes pour coupes transversales) sont indiqués. Rostral à gauche. b) Schéma de la morphologie des premiers arcs aortiques (aa1 et aa2) par rapport aux structures céphaliques : le cerveau (pros, prosencéphale ; mes, mésencéphale ; rh, rhombencéphale), la notochorde (ND) et l'endoderme pharyngien (endo). c-e) Quelques signaux et leurs récepteurs discutés dans le texte sont indiqués en italiques à l'emplacement de leur synthèse. c) Schéma d'une coupe au niveau d'un arc branchial hypothétique, dorsal vers le haut. Les artères se forment à proximité de l'endoderme ; celles de l'aorte dorsale du coté dorsal et celles des arcs aortiques du coté ventral. Les cellules de crête neurale céphalique, mésenchymateuses, traversent le mésoderme (gris) qui flanque le tube neurale pour atteindre l'arc branchial. d, e) Schémas de coupes transversales à un niveau rostral du corps (d), où la morphogenèse est plus avancée qu'au niveau caudal du corps (e). Le somite se différencie en la sclérotome mésenchymateux qui sera traversé par la crête neurale et les angioblastes, et en la dermamyotome. L'espace du cœlome isole et entoure l'intestin ; les premiers vaisseaux sanguins se différencient entre la notochorde et l'endoderme. Les aortes dorsales fusionnent ainsi que les veines cardinales postérieures pour donner des structures uniques et médianes.

FIG. 1. – *a) Human embryo at 23 days post-fertilization with two branchial arches (AB1 and 2) and 19 pairs of somites. Approximate levels of the drawings in B (frame) and C-E (lines for transverse sections) are shown. Rostral to left. b) Diagram of the morphology of the first aortic arches (aa1 and aa2) with respect to other cephalic structures: the brain (pros, prosencephalon; mes, mesencephalon; rh, rhombencephalon), the notochord (ND) and the pharyngeal endoderm (endo). c-e) Some of the ligand/receptors discussed in the text are indicated in italics at the location where they are synthesized. C) Diagram of a transverse section at the level of a hypothetical branchial arch, dorsal to top. Arteries form close to the endoderm: those of the dorsal aorta on the dorsal side and of the aortic arches on the ventral side. Migrating cephalic neural crest cells penetrate the mesoderm (gray) flanking the neural tube to fill out the branchial arch. d, e) Diagrams of transverse sections at a rostral (d) or more caudal (e) level of the body, where morphogenesis is more advanced in d than e. The somite differentiates into loose sclerotome, through which the trunk neural crest and angioblasts migrate, and the dermamyotome. The space of the coelom isolates and surrounds the intestine; the first blood vessels of the body differentiate between the notochord and the endoderm. The dorsal aortae fuse as do the posterior cardinal veins to give rise to unique midline structures.*

thèse que Shh aurait un effet positif sur la formation des artères.

Pourtant, Shh n'agit pas directement sur la prolifération ni sur la migration des cellules endothéliales, mais induit l'expression du **v**ascular **e**ndothelial **g**rowth **f**actor (VEGF) dans les somites à proximité. Le VEGF est très impliqué dans l'angiogenèse classique et sera discuté plus en détail dans la partie consacrée à ce sujet. L'application exogène de VEGF permet de préserver l'aorte dorsale chez les embryons déficients en Shh ; ces embryons sont normalement dépourvus d'artères telles qu'identifiées par des marqueurs moléculaires [50]. L'effet de Shh est une induction de vaisseaux à grande lumière, comme des fistules artériovéneuses, alors que VEGF promeut la croissance d'un plexus de petits vaisseaux homogènes possédant des marqueurs artériaux [74]. On considère que les grands vaisseaux sont assimilables à des vaisseaux matures alors que le plexus capillaire ressemble plus aux vaisseaux immatures. Cette différence est attribuée à l'activation simultanée d'autres facteurs par Shh, dans la maturation vasculaire [74]. Pour résumer, Shh joue un rôle de coordinateur moléculaire de la vasculogenèse.

Les récepteurs Notch

Les récepteurs transmembranaires de la famille Notch, hautement conservés au cours de l'évolution,

reconnaissent deux familles de ligands, les Deltas ou les Jagged/Serrates. Chez l'homme, trois molécules Delta-like et deux molécules Jagged sont reconnues par quatre récepteurs Notch, mais, différentes combinaisons de ligands et de récepteurs ont été retenues au cours de l'évolution. Les récepteurs Notchs 1, 3, 4, et certains ligands (Delta-4 et les deux Jagged) sont exprimés dans les artères embryonnaires ; par contre, aucun de ceux-ci n'est exprimé dans les veines [91].

Des mutations de *NOTCH3* chez l'homme ont été mis en évidence dans la maladie CADASIL (**C**erebral **A**utosomal **D**ominant **A**rteriopathy with **S**ubcortical **I**nfarcts and **L**eukoencephalopathy) [45]. CADASIL se manifeste par des migraines dues à une dégradation de la paroi musculaire des petits vaisseaux cérébraux. Dans le modèle murin de la maladie comme chez l'homme, des mutations stéréotypées de Notch-3 conduisent à une accumulation anormale du récepteur au sein de la membrane des cellules de soutien des vaisseaux matures [77]. L'effet cellulaire de cette accumulation est encore inconnu mais on peut supposer qu'elle est à l'origine de la désintégration de la paroi.

Le rôle de Notch-3 a aussi été étudié chez l'embryon du poisson-zèbre. Par contraste avec son rôle dans les vaisseaux matures, Notch-3 confère une identité artérielle et réprime le phénotype veineux au moment de la vasculogenèse [49]. En l'absence de Shh dans ce modèle, l'apport exogène de VEGF peut restaurer la différentiation artérielle. De même, après réduction expérimentale de VEGF, Notch-1 ectopique permet le sauvetage des artères ou même la stimulation l'artériogenèse ectopique en présence de VEGF physiologique [50]. La différentiation de l'aorte est régulée par une cascade de régulation, où Shh induit l'expression de VEGF dans les cellules mésenchymateuses du somite, ce qui provoque l'agrégation des CE. Le VEGF induit également l'expression de Notch-3 qui à son tour réprime le récepteur VEGFR3 dans l'aorte dorsale. Pour preuve, l'absence de Notch-3 dans la veine cardinale postérieure, éloignée de la source de Shh et du VEGF des somites, permet la persistance de VEGFR3 [50] *(figure 1e)*. La signalisation VEGF contribue à renforcer l'identité artérielle de l'aorte par le biais de VEGFR2 et l'identité veineuse dans la veine axiale par le biais de VEGFR3.

Lors d'expériences de surexpression de Notch chez le xénope, Notch-1 est capable de réduire l'expression de Shh dans la notochorde et de le surexprimer dans le plancher du neurectoderme [57]. Cet effet survient pendant une décision binaire de la gastrulation où les cellules pénétrantes s'intègrent dans l'une ou l'autre structure. Ainsi, le moment où survient la signalisation embryonnaire par des récepteurs Notch est déterminant ; une réduction précoce de la notochorde réduirait la taille de l'aorte dorsale en faveur de la veine cardinale postérieure alors qu'une augmentation de la signalisation Notch quand ces gènes sont exprimés dans les CE conduirait à l'effet inverse.

Fibroblast growth factors

Le facteur de croissance secrété FGF2 (*fibroblast growth factor 2*) induit une différenciation angioblastique dans les somites *in vitro* et *in vivo* chez les embryons aviaires [17]. Ce facteur est largement connu pour son rôle mitogénique et tropique pendant l'angiogenèse adulte [75]. Le rôle essentiel et conservé de la famille des FGFs dans la formation de tubes se trouve confirmé par l'utilisation de cette voie de signalisation dans la trachéogenèse chez le Drosophile [99] ainsi que dans la migration d'angioblastes pour la formation de tubes capillaires chez la souris [88] *(figure 2)*. La migration et la tubulogenèse s'arrêtent lors de la maturation vasculaire grâce à l'action de cellules de soutien qui freinent activité de FGF-2, laquelle molécule, peut donner lieu à des hémangiomes lorsqu'elle n'est pas contrôlée [54, 86, 98]. FGF-2 est aussi un facteur fortement angiogénique ; c'est-à-dire que sa présence entraîne la formation de nouveaux vaisseaux à partir de cellules endothéliales *in vitro* [64] ainsi qu'à partir de vaisseaux existants *in vivo* [69].

CASCADES GÉNÉTIQUES IMPLIQUÉS DANS L'ANGIOGENÈSE ET LA MATURATION VASCULAIRE

VEGF

Les VEGFs constituent une super-famille de cinq molécules (VEGF-A à VEGF-E) homologues et structurellement apparentés au PDGF (*platelet-derived growth factor*) et au PlGF (*placental growth factor*) [13]. Les membres de cette super-famille agissent sous forme d'homodimères et d'hétérodimères [67, 75]. VEGF-A, particulièrement étudié dans le contexte de l'angiogenèse, est exprimé d'une façon quasi-ubiquitaire chez l'embryon à l'exception des cellules endothéliales elles-mêmes [4, 5]. L'inactivation d'un seul allèle de VEGF-A diminue la capacité des îlots sanguins à effectuer l'hématopoïèse, réduit le nombre de cellules endothéliales et empêche leur organisation correcte [8, 34].

Un des trois récepteurs pour le VEGF, le VEGFR2, est exprimé par les hémangioblastes à partir d'un stade très précoce du développement et continue à être exprimé par leur descendance angioblastique et endothéliale [27, 93] *(figure 2)*. La souris knock-out de VEGFR2 n'accomplit ni l'hématopoïèse, ni la vasculogenèse [81]. Lorsqu'il se lie au VEGFR2, le VEGF-C peut aussi stimuler la différenciation d'angioblastes en cellules endothéliales [26]. Alors que le VEGF-C est particulièrement impliqué dans la lymphangiogenèse à des stades embryonnaires plus tardif [47], sa séquestration par le VEGFR3 dans les angioblastes serait critique pour la transition de la vasculogenèse vers l'angiogenèse effectuée par les CE, qui continuent à exprimer le VEGFR2 [40].

L'expression de VEGF par la zone marginale ventriculaire du système nerveux central en formation attire et dirige l'ingression des capillaires [60]. Cette expression est elle-même indirectement induite par l'hypoxie résultant des divisions cellulaires rapides dans la zone ventriculaire. Certains facteurs nucléiques, tels les HIFs (**h**ypoxia **i**nducible **f**actors), répondent directement au taux d'oxygène ambiant

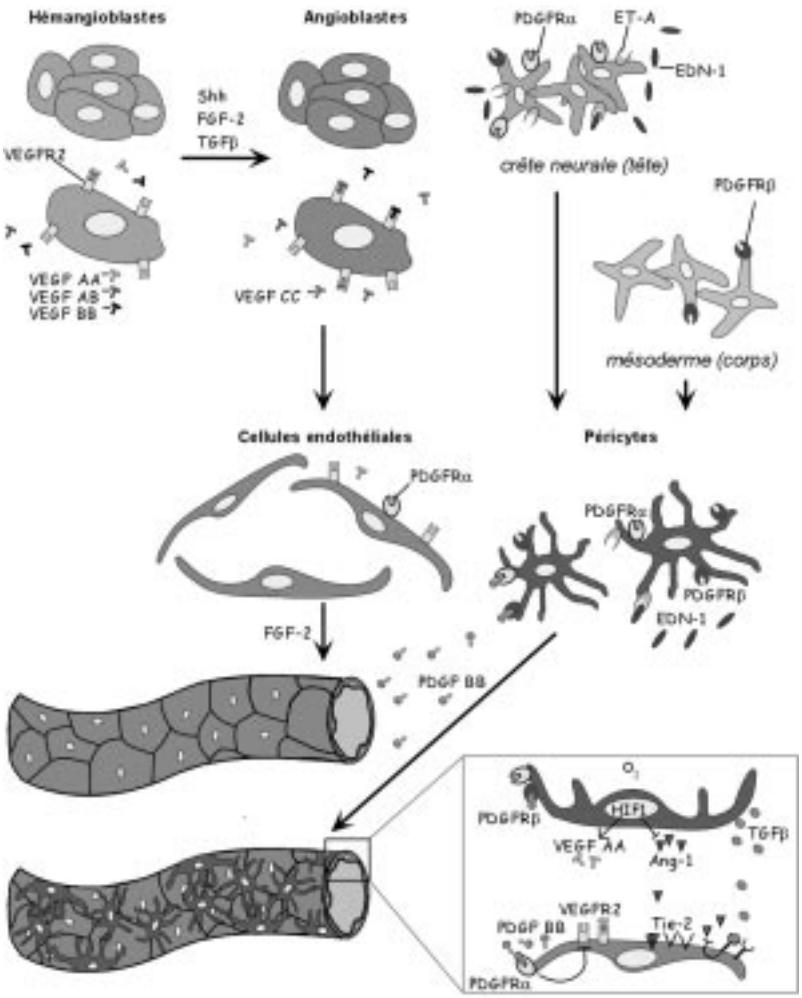

FIG. 2. – Schéma non exhaustif de la différenciation d'un capillaire lambda en insistant sur les quelques signaux mentionnés dans le texte. La différenciation progresse temporellement du haut vers le bas de la page et de la gauche vers la droite. Un agrandi du vaisseau en cours de maturation en bas de page permet de voir quelques-uns des nombreux échanges moléculaires entre péricytes et cellules endothéliales qui peuvent être modulés par les conditions environnementales.

FIG. 2. – *Diagram of some aspects of the differentiation of an idealized capillary with emphasis on those signals discussed in the text. Differentiation progresses temporally from the top to the bottom of the drawing, and from left to right. The enlargement of a maturing vessel toward the bottom of the figure allows the depiction of some of the molecular exchanges between pericytes and endothelial cells, that can be modulated by environmental conditions.*

[44]. Ces facteurs déclenchent des programmes angiogéniques en activant la transcription de gènes cibles tels VEGF ou endothéline-1, discutée plus loin [35, 42].

Au niveau de la tête, HIF1α, la sous-unité des HIF leur conférant leur spécificité, est exprimée dans l'endoderme pharyngien au moment de la formation des vaisseaux des arcs aortiques [30]. Cette expression lors de la mise en place des arcs aortiques suggère que les anastomoses entre aorte ventrale et dorsale se forment par une réponse angiogénique des cellules endothéliales VEGFR2$^+$ à un plus fort taux local de VEGF-A sous l'influence d'HIF1α. Des expériences chez le xénope et chez la caille montrent également que les CE sont bien présentes, mais incapables de s'assembler en vaisseaux, en l'absence d'endoderme [92].

Les endothélines

Les endothélines 1, 2 et 3 (EDN1-3) sont des hormones peptidiques secrétées [43] et présentes depuis l'embryogenèse précoce jusqu'à la fin de la vie. Les EDN ont été identifiées grâce à leur effet vasoconstricteur sur les vaisseaux matures [97] mais elles participent aussi à la mise en place du système nerveux entérique, de la pigmentation, de la morphogenèse des vaisseaux issus des arcs aortiques et surtout à l'angiogenèse. Comme le VEGF, l'EDN-1, la plus étudiée, est transcrite en réponse à l'hypoxie, lors de la liaison de HIF1 à son promoteur [95].

Dans les vaisseaux embryonnaires ou immatures, l'application d'EDN-1 exogène entraîne une fort angiogenèse autour de sa source, vraisemblablement par l'intermédiaire de VEGF [18]. Le signal est reçu par des CE possédant au moins le récepteur B parmi les trois récepteurs connus des endothélines : ET-A, ET-B et ET-C. À la suite de l'angiogenèse, des cellules mésenchymateuses s'accumulent autour des nouveaux vaisseaux et se différencient en constituants muraux qui s'organisent en couches concentriques. Les premières cellules au contact de l'endothélium sont les péricytes, des cellules multipotentes qui peuvent se différencier en muscle lisse vasculaire, en adipocytes, en cartilage ou en os, [23].

L'effet vasoconstricteur d'EDN-1 sur les vaisseaux matures est médié par le récepteur ET-A présent sur les péricytes. EDN-1 aurait également une activité trophique pour les péricytes exprimant ET-A *in vitro* [94]. En réponse à la stimulation d' ET-A, les péricytes inhibent la prolifération endothéliale tout en augmentant l'expression d'EDN-1 endothéliale, ce qui stabilise les vaisseaux déjà formés par une boucle de régulation [61].

Les EDNs sont particulièrement importantes pour la différenciation des cellules de CN chez l'embryon. Au niveau moléculaire, le schisme entre

la tête et le tronc est représenté par la dépendance de la CN céphalique, exprimant ET-A, de la présence d'EDN-1 dans l'environnement céphalique et cardiaque, par rapport à celle de la CN troncale, ET-C^+, de la présence d'EDN-3 dans le reste du corps [73].

Le système d'EDN-1/ET-A participe également à la constitution d'une partie de la paroi vasculaire par des cellules de CN *(figure 2)*. Chaque paire d'arcs aortiques entoure l'endoderme pharyngien exprimant HIF1α d'une manière transitoire [30]. En même temps, chaque grande artère se trouve à proximité d'un petit amas de cellules mésodermiques, source d'angioblastes et de précurseurs musculaires, entourée d'un nombre croissant de cellules mésenchymateuses de CN qui s'infiltrent entre l'ectoderme et l'endoderme. Les ensembles métamériques de ce type s'appellent les arcs branchiaux ou pharyngiens *(figure 1c)*.

La CN colonise chaque paire d'arcs branchiaux à partir des différents niveaux du cerveau en formation. Cette distribution n'est pas strictement délimitée mais les cellules voisines tendent à provenir de régions voisines au sein du neuroépithélium. Quand les structures dérivées de la crête neurale se différencient, elles maintiennent cette provenance vaguement métamérique. Ainsi, les différents os du crâne peuvent être cartographiés et attribués à de la CN issue de segments distincts du cerveau [16] ; les vaisseaux sanguins du cerveau antérieur, du visage et du cou peuvent aussi l'être en ce qui concerne leurs péricytes et leurs muscles lisses [32]. On comprend mieux le caractère segmentaire de certaines maladies vasculaires tels le Sturge-Weber ou le moya-moya, qui sont localisées dans des régions distinctes de la tête car elles ont la même origine que les cellules de CN de la paroi des vaisseaux pathologiques [31].

L'ectoderme et l'endothélium de chaque arc branchial expriment EDN-1 pendant que la CN céphalique, exprimant ET-A, emplit chaque arc branchial [66]. Des expériences d'abrogation génétique d'EDN-1 ou d'ET-A chez la souris ont montré clairement que les déficiences de remodelage des arcs aortiques et les malformations craniofaciales (mâchoires hypoplastiques, fusions osseuses, dents ectopiques) étaient toutes dues à un comportement anormal de la CN céphalique [97]. En l'absence de communication par le pôle EDN-1/ET-A, les cellules de CN céphalique colonisent incomplètement la partie la plus ventrale des arcs branchiaux et les quelques cellules colonisatrices ont une différentiation anormale ou subissent une mort cellulaire programmée [11, 12]. Ainsi, cette voie de signalisation module la migration et la différentiation des CN céphalique dans les arcs, impliquant directement l'endothélium des arcs aortiques dans la morphogenèse craniofaciale et cardiovasculaire. La mise en évidence du rôle essentiel de l'endoderme pharyngien dans ces processus conforte cette hypothèse [15].

Platelet-derived growth factors

L'un des premiers facteurs impliqués dans l'attraction des péricytes vers l'endothélium est le PDGF, apparenté structurellement au VEGF. Il existe 4 gènes, PDGF-A à -D, codant pour des unités s'assemblant en homo- ou hétérodimères [3]. Ces molécules se lient à deux types de récepteurs transmembranaires dimériques : le PDGFRα reconnaissant les isoformes PDGF-AA, -AB, -BB, et -CC, et le PDGFRß reconnaissant les isoformes PDGF-BB et -DD.

Récemment, une activité angiogénique de PDGF-AB, -BB et surtout -CC a été mise en évidence [6]. Ces chercheurs ont montré *in vivo* chez la souris que des billes recouvertes de ces isoformes de PDGF sont aussi attirantes pour la formation de nouveaux vaisseaux que le VEGF ou le FGF2. L'isoforme PDGF-CC agirait uniquement par liaison du récepteur PDGFRα [6]. PDGF-BB, en agissant sur le PDGFRα endothélial dans un modèle de vasculogenèse *in vitro,* abrogerait l'effet positif de FGF-2 sur la migration des CE et leur organisation en tubules [19]. Les études de localisation des isoformes de PDGF montrent une distribution dans de nombreux tissus chez des modèles animaux, quoique en dehors du système rénal, peu d'études au niveau cellulaire ont été effectué pour es molécules. En ce qui concerne les récepteurs, le PDGFRß est absent de la membrane des CE mais est présent sur celle des péricytes et des cellules de muscle et sur leurs précurseurs mésodermiques [82] *(figure 2)*. Le PDGFRα est plus ubiquitaire et présent sur tous les types cellulaires de la paroi vasculaire [62]. Ainsi, les PDGF-AB, -BB et -CC pourraient moduler l'angiogenèse indirectement par activation de muscle lisse des vaisseaux déjà existants, et par une déstabilisation de la structure murale qui permettrait le bourgeonnement endothélial. Un tel processus a déjà été décrit dans le cœur. La liaison de PDGFRα par le PDGF-AB endothélial y induit dans les myocytes la synthèse de VEGF et entraîne une néovascularisation après ischémie myocardiaque [25].

Le PDGF intervient également lors de la stabilisation et de la maturation des nouveaux capillaires suite à l'association avec des péricytes. Les CE secrètent PDGF-AB et -BB du coté abluminal vers le mésenchyme [25]. Les souris knock-out pour le gène de PDGF-B ont un phénotype très sévère présentant une mort fœtale avec des microanévrysmes au niveau du cerveau et une hémorragie importante, secondaire à un manque de péricytes autour des lits capillaires [56]. Chez ces souris mutantes, les microanévrysmes sont accompagnés d'une accumulation de CE, ce qui confirme le rôle anti-mitoique des péricytes pour les CE dans les vaisseaux stabilisés [41]. Les souris dont le PDGFRß a été inactivé sont également hemorragiques et oedémateuses mais survivent jusqu'à la période périnatale [83].

Ainsi, le PDGF-BB endothélial a une double fonction. Il agit d'une manière paracrine, sur le PDGFRß des péricytes afin de les attirer vers les capillaires primaires, mais aussi d'une manière autocrine par le biais de PDGFRα, afin de ralentir l'angiogenèse des tubules à stabiliser.

Le récepteur PDGFRα est présent sur des cellules multipotentes de la CN céphalique à l'exclusion des précurseurs neuronaux [65]. Les knock-outs de PDGFRα associent hémorrhagies et œdèmes, surtout au niveau du système nerveux central, à de

sévères malformations des os craniofaciaux, à des fusions costales et vertébrales et à des malformations cardiaques dues au problèmes de remaniement des arcs aortiques [84, 87]. Les ARNs messagers pour le PDGF-A et PDGF-C sont, eux, exprimés au sein des couches épithéliales des arcs branchiaux [1]. Ainsi, il existe des parallèles entre le système des endothélines et celui des PDGFs puisque les ligands EDN-1 et PDGF-AA/AB/CC sont exprimés par l'endothélium (et l'ectoderme) des arcs branchiaux et leurs récepteurs ET-A et PDGFRα par les cellules de CN qui entourent cet endothélium. Il est probable que les rôles de ces systèmes ne soient pas restreints à ces types cellulaires, car les EDNs et PDGFs sont exprimés dans de nombreux autres types cellulaires ailleurs. Les rôles décrits ci-dessus reflèteraient plutôt un exemple des interactions entre épithélium et mésenchyme nécessaires tant pour l'organogenèse du système vasculaire (construction et maturation de la paroi) que pour les poumons, le squelette, ou les reins.

Les angiopoïétines

Les angiopoïétines (1 et 2) et leur récepteur tie-2 sont impliqués dans la communication entre cellules endothéliales et péricytes. L'inactivation de tie-2 chez la souris entraîne la mort embryonnaire à la mi-gestation, sans vascularisation du cerveau et avec des gros vaisseaux dilatés [79]. Chez l'humain, une activation constitutive de la signalisation effectuée par tie-2 est responsable d'une malformation veineuse avec peu de cellules de soutien autour des gros vaisseaux dilatés [90]. Les péricytes secrètent normalement l'angiopoïétine-1, alors que tie-2 est présent sur les CE. L'angiopoïétin-1 est nécessaire pour que les péricytes quiescents restent autour des vaisseaux mais on ne sait pas encore quel système de dialogue péricyte-CE serait impliqué. L'antagoniste naturel de l'angiopoïétine-1, l'angiopoïétine-2, est exprimé dans les sites de remodelage vasculaire chez l'homme et chez la souris et induit une régression vasculaire [59]. En situation hypoxique, les deux angiopoïétines sont moins transcrites dans les cellules de soutien vasculaire alors que la synthèse du VEGF est activée, d'une manière coordonnée, ce qui permet une nouvelle angiogenèse [46] *(figure 2)*.

La superfamille TGFβ

La famille étendue de cytokines TGFβ (***t**ransforming **g**rowth **f**actor*) régule de nombreux processus cellulaires dans tout le règne animal parmi lesquels on trouve la prolifération, la migration, la différenciation et l'apoptose. Le prototype, TGFβ, est indispensable pour l'hématopoïèse et la vasculogenèse embryonnaire. L'inactivation de ce gène chez la souris entraîne la mort à mi-gestation suite à une fusion excessive des capillaires dans le sac vitellin et à l'hyperdilatation des grands vaisseaux [21].

Des voies impliquant TGFβ ont également été rapportées dans la maturation vasculaire tardive. TGFβ ligand, son récepteur TβRII et son co-récepteur endogline sont des partenaires dans une voie de signalisation qui inhibe l'activation génique effectuée par un récepteur concurrent de TGFβ, Alk5 [68]. Chez l'humain, des mutations dans les gènes d'endogline ou d'Alk1, un récepteur d'activine, sont à l'origine des malformations vasculaires des maladies HHT1 et 2 (***H**ereditary Haemorrhagic Telangiectasia*) respectivement [63]. Les embryons de souris chez lesquelles Alk1 est inactivé ont un phénotype vasculaire qui ressemble à celles des knock-out de TGFβ1, de TβRII [71] ou d'endogline [53], ce qui laisse penser que l'activine pourrait aussi jouer un rôle physiologique dans la constitution de la paroi vasculaire. On constate néanmoins que la malformation vasculaire des maladies HHT humains consiste en une prolifération excessive du muscle lisse artériel, alors que chez les souris mutantes pour Alk1 ou pour l'endogline, l'endothélium est plutôt négligé par les cellules périvasculaires. Dans les cultures de crête neurale de rat, le TGFβ1 force la différenciation en cellules de muscle lisse à l'exclusion des autres dérivés de ces cellules multipotentes [80]. Il est possible que chez les rongeurs mutants de la famille TGFβ, il manque autour des vaisseaux des péricytes à recruter, quoique des études fonctionnelles de l'activité des récepteurs Alk1 ou endogline n'ont pas été effectuées *in vitro* de la même manière. Chez l'homme, l'absence d'endogline et d'Alk1 permet une suractivation de Alk5 par le TGFβ1 ambiant et produit l'effet inverse de prolifération périvasculaire.

In vitro, l'expression de TGFβ par des péricytes inhibe la prolifération endothéliale [2, 79]. TGFβ inhibe la production de angiopoïétine-1 [29], mais on ne sait toujours pas si cette inhibition se fait par la voie d'Alk5 ou de TβRII. Il reste pourtant probable que TGFβ participe à une boucle de régulation et devient sa propre cible à différents moments de la vasculogenèse puis de la maturation des parois vasculaires.

CONCLUSION

Chronologiquement, la vasculogenèse est la première phase de formation des vaisseaux sanguins embryonnaires. Elle est rapidement suivie par le processus d'angiogenèse. La différenciation des CE à partir d'angioblastes se fait pendant et après une dissémination de ces précurseurs à travers le corps et notamment dans le mésenchyme qui entoure le cerveau et d'autres organes en cours de formation.

L'organisation des premiers tubes endothéliaux commence d'une manière indépendante d'autres types cellulaires. Rapidement, une communication s'établit entre ces tubes et le mésenchyme qui les entoure. Au niveau céphalique, cette communication est nécessaire pour la survie et la morphogenèse appropriée du mésenchyme qui a pour origine les crêtes neurales ainsi que des vaisseaux dont il construit les parois abluminales. Quand les vaisseaux commencent à rassembler leurs composants périvasculaires, une signalisation paracrine entre les CE et les péricytes induit la maturation et la permanence du vaisseau.

Alors que tous les vaisseaux ont des caractéristiques spécifiques, telles celles qui participent à la barrière hémato-encéphalique, ils passent inévitablement par des étapes de constitution de la paroi, de

sécrétion d'une matrice extracellulaire appropriée et par le remodelage dû aux variations du flux sanguin. Ainsi, les vaisseaux restent plastiques tout au long de la vie et maintiennent un certain potentiel adaptatif leur permettant de répondre aux modifications environnementales en réactivant des cascades génétiques employées pendant la vie embryonnaire et fœtale.

REMERCIEMENTS : Les auteurs sont très reconnaissants au Dr J. Steffann pour ses critiques. Ce travail est soutenu par l'Institut National de la Santé et de la Recherche Médicale (INSERM) et par l'Association Française contre les Myopathies.

RÉFÉRENCES

[1] AASE K, ABRAMSSON A, KARLSSON L, BETSHOLTZ C and ERIKSSON U. "Expression analysis of PDGF-C in adult and developing mouse tissues." *Mech Dev* 2002; *110:* 187-191.

[2] ANTONELLI-ORLIDGE A, SAUNDERS KB, SMITH SR, D'AMORE PA. "An activated form of transforming growth factor beta is produced by cocultures of endothelial cells and pericytes." *Proc Natl Acad Sci U S A* 1989; *86:* 4544-4548.

[3] BERGSTEN E, UUTELA M, LI X, PIETRAS K, OSTMAN A, HELDIN CH, ALITALO K and ERIKSSON, U. "PDGF-D is a specific, protease-activated ligand for the PDGF beta-receptor." *Nat Cell Biol* 2001; *3:* 512-516.

[4] BREIER G, ALBRECHT U, STERRER S and RISAU W. "Expression of vascular endothelial growth factor during embryonic angiogenesis and endothelial cell differentiation." *Development* 1992; *114:* 521-532.

[5] BREIER G, CLAUSS M and RISAU W. "Coordinate expression of vascular endothelial growth factor receptor-1 (flt-1) and its ligand suggests a paracrine regulation of murine vascular development." *Dev Dyn* 1995; *204*: 228-239.

[6] CAO R, BRAKENHIELM E, LI X, PIETRAS K, WIDENFALK J, OSTMAN A, ERIKSSON U and CAO Y. "Angiogenesis stimulated by PDGF-CC, a novel member in the PDGF family, involves activation of PDGFR-alphaalpha and -alphabeta receptors." *Faseb J* 2002; *16:* 1575-1583.

[7] CARMELIET P. "Mechanisms of angiogenesis and arteriogenesis." *Nat Med* 2000; *6:* 389-395.

[8] CARMELIET P, FERREIRA V, BREIER G, POLLEFEYT S, KIECKENS L, GERTSENSTEIN M, FAHRIG M, VANDENHOECK A, HARPAL K, EBERHARDT C, DECLERCQ C, PAWLING J, MOONS L, COLLEN D, RISAU W and NAGY A. "Abnormal blood vessel development and lethality in embryos lacking a single VEGF allele." *Nature* 1996; *380:* 435-439.

[9] CHRIST B, HUANG R and WILTING J. "The development of the avian vertebral column." *Anat Embryol (Berl)* 2000; *202:* 179-194.

[10] CLEAVER O and KRIEG PA. "Notochord patterning of the endoderm." *Dev Biol* 2001; *234:* 1-12.

[11] CLOUTHIER DE, HOSODA K, RICHARDSON JA, WILLIAMS SC, YANAGISAWA H, KUWAKI T, KUMADA M, HAMMER RE and YANAGISAWA M. "Cranial and cardiac neural crest defects in endothelin-A receptor-deficient mice." *Development* 1998; *125:* 813-824.

[12] CLOUTHIER DE, WILLIAMS SC, HAMMER RE, RICHARDSON JA and YANAGISAWA, M. "Cell-autonomous and nonautonomous actions of endothelin-A receptor signaling in craniofacial and cardiovascular development." *Dev Biol* 2003; *261:* 506-519.

[13] CONWAY EM, COLLEN D and CARMELIET P. "Molecular mechanisms of blood vessel growth." *Cardiovasc Res* 2001; *49:* 507-521.

[14] COULY G, COLTEY P, EICHMANN A and LE DOUARIN NM. "The angiogenic potentials of the cephalic mesoderm and the origin of brain and head blood vessels." *Mech Dev* 1995; *53:* 97-112.

[15] COULY G, CREUZET S, BENNACEUR S, VINCENT C and LE DOUARIN NM. "Interactions between Hox-negative cephalic neural crest cells and the foregut endoderm in patterning the facial skeleton in the vertebrate head." *Development* 2002; *129:* 1061-1073.

[16] COULY GF, COLTEY PM, LE DOUARIN NM. "The triple origin of skull in higher vertebrates: a study in quail-chick chimeras." *Development* 1993; *117:* 409-429.

[17] COX CM and POOLE TJ. "Angioblast differentiation is influenced by the local environment : FGF-2 induces angioblasts and patterns vessel formation in the quail embryo." *Dev Dyn* 2000; *218:* 371-382.

[18] CRUZ A, PARNOT C, RIBATTI D, CORVOL P and GASC JM. "Endothelin-1, a regulator of angiogenesis in the chick chorioallantoic membrane." *J Vasc Res* 2001; *38:* 536-545.

[19] DE MARCHIS F, RIBATTI D, GIAMPIETRI C, LENTINI A, FARAONE D, SCOCCIANTI M, CAPOGROSSI MC and FACCHIANO A. "Platelet-derived growth factor inhibits basic fibroblast growth factor angiogenic properties in vitro and in vivo through its alpha receptor." *Blood* 2002; *99:* 2045-2053.

[20] DETWILER SR and HOLTZER H. "The inductive and formative influence of the spinal cord upon the vertebral column." *Bull Hosp Joint Dis* 1954; *15:* 114-123.

[21] DICKSON MC, MARTIN JS, COUSINS FM, KULKARNI AB, KARLSSON S and AKHURST RJ. "Defective haematopoiesis and vasculogenesis in transforming growth factor-beta 1 knock out mice." *Development* 1995; *121:* 1845-1854.

[22] DING H, WU X, KIM I, TAM PP, KOH GY and NAGY A. "The mouse Pdgfc gene: dynamic expression in embryonic tissues during organogenesis." *Mech Dev* 2000; *96:* 209-213.

[23] Doherty MJ and Canfield AE. "Gene expression during vascular pericyte differentiation." *Crit Rev Eukaryot Gene Expr* 1999; *9:* 1-17.

[24] DRAKE CJ, DAVIS LA and LITTLE CD. "Antibodies to beta 1-integrins cause alterations of aortic vasculogenesis, in vivo." *Dev Dyn* 1992; *193:* 83-91.

[25] EDELBERG JM, AIRD WC, WU W, RAYBURN H, MAMUYA WS, MERCOLA M and ROSENBERG, RD. "PDGF mediates cardiac microvascular communication." *J Clin Invest* 1998; *102:* 837-843.

[26] EICHMANN A, CORBEL C, JAFFREDO T, BREANT C, JOUKOV V, KUMAR V, ALITALO K and LE DOUARIN NM. "Avian VEGF-C: cloning, embryonic expression pattern and stimulation of the differentiation of VEGFR2-expressing endothelial cell precursors." *Development* 1998; *125:* 743-752.

[27] EICHMANN A, MARCELLE C, BREANT C and LE DOUARIN NM. "Two molecules related to the VEGF receptor are expressed in early endothelial cells during avian embryonic development." *Mech Dev* 1993; *42:* 33-48.

[28] EISEN JS. "Patterning motoneurons in the vertebrate nervous system." *Trends Neurosci* 1999; *22:* 321-326.

[29] ENHOLM B, PAAVONEN K, RISTIMAKI A, KUMAR V, GUNJI Y, KLEFSTROM J, KIVINEN L, LAIHO M, OLOFSSON B, JOUKOV V, ERIKSSON U and ALITALO K. "Comparison of VEGF, VEGF-B, VEGF-C and Ang-1 mRNA regulation by serum, growth factors, oncoproteins and hypoxia." *Oncogene* 1997; *14:* 2475-2483.

[30] ETCHEVERS HC. "Early expression of hypoxia-inducible factor 1alpha in the chicken embryo." *Gene Expr Patterns* 2003; *3:* 49-52.

[31] ETCHEVERS HC, COULY G and LE DOUARIN NM. "Morphogenesis of the branchial vascular sector." *Trends Cardiovasc Med* 2002; *12:* 299-304.

[32] ETCHEVERS HC, VINCENT C, LE DOUARIN NM and COULY GF. "The cephalic neural crest provides pericytes and smooth muscle cells to all blood vessels of the face and forebrain." *Development* 2001; *128:* 1059-1068.

[33] FAN CM and TESSIER-LAVIGNE M. "Patterning of mammalian somites by surface ectoderm and notochord: evidence for sclerotome induction by a hedgehog homolog." *Cell* 1994; *79:* 1175-1186.

[34] FERRARA N, CARVER-MOORE K, CHEN H, DOWD M, LU L, O'SHEA KS, POWELL-BRAXTON L, HILLAN KJ and MOORE MW. "Heterozygous embryonic lethality induced by targeted inactivation of the VEGF gene." *Nature* 1996; *380:* 439-442.

[35] FORSYTHE JA, JIANG BH, IYER NV, AGANI F, LEUNG SW, KOOS RD and SEMENZA GL. "Activation of vascular endo-

thelial growth factor gene transcription by hypoxia-inducible factor 1." *Mol Cell Biol* 1996; *16:* 4604-4613.

[36] FOUQUET B, WEINSTEIN BM, SERLUCA FC and FISHMAN MC. "Vessel patterning in the embryo of the zebrafish: guidance by notochord." *Dev Biol* 1997; *183:* 37-48.

[37] GALE NW, BALUK P, PAN L, KWAN M, HOLASH J, DECHIARA TM, MCDONALD DM and YANCOPOULOS GD. "Ephrin-B2 selectively marks arterial vessels and neovascularization sites in the adult, with expression in both endothelial and smooth-muscle cells." *Dev Biol* 2001; *230:* 151-160.

[38] GALE NW, THURSTON G, HACKETT SF, RENARD R, WANG Q, MCCLAIN J, MARTIN C, WITTE C, WITTE MH, JACKSON D, SURI C, CAMPOCHIARO PA, WIEGAND SJ and YANCOPOULOS GD. "Angiopoietin-2 is required for postnatal angiogenesis and lymphatic patterning, and only the latter role is rescued by Angiopoietin-1." *Dev Cell* 2002; *3:* 411-423.

[39] GORY-FAURE S, PRANDINI MH, POINTU H, ROULLOT V, PIGNOT-PAINTRAND I, VERNET M and HUBER P. "Role of vascular endothelial-cadherin in vascular morphogenesis." *Development* 1999; *126:* 2093-2102.

[40] HAMADA K, OIKE Y, TAKAKURA N, ITO Y, JUSSILA L, DUMONT DJ, ALITALO K and SUDA T. "VEGF-C signaling pathways through VEGFR-2 and VEGFR-3 in vasculoangiogenesis and hematopoiesis." *Blood* 2000; *96:* 3793-3800.

[41] HELLSTROM M, KALEN M, LINDAHL P, ABRAMSSON A and BETSHOLTZ C. "Role of PDGF-B and PDGFR-beta in recruitment of vascular smooth muscle cells and pericytes during embryonic blood vessel formation in the mouse." *Development* 1999; *126:* 3047-3055.

[42] HU J, DISCHER DJ, BISHOPRIC NH and WEBSTER KA. "Hypoxia regulates expression of the endothelin-1 gene through a proximal hypoxia-inducible factor-1 binding site on the antisense strand." *Biochem Biophys Res Commun* 1998; *245:* 894-899.

[43] INOUE A, YANAGISAWA M, KIMURA S, KASUYA Y, MIYAUCHI T, GOTO K and MASAKI T. "The human endothelin family : three structurally and pharmacologically distinct isopeptides predicted by three separate genes." *Proc Natl Acad Sci U S A* 1989; *86:* 2863-2867.

[44] JIANG BH, SEMENZA GL, BAUER C and MARTI HH. "Hypoxia-inducible factor 1 levels vary exponentially over a physiologically relevant range of O2 tension." *Am J Physiol* 1996; *271:* 1172-1180.

[45] JOUTEL A, CORPECHOT C, DUCROS A, VAHEDI K, CHABRIAT H, MOUTON P, ALAMOWITCH S, DOMENGA V, CECILLION M, MARECHAL E, MACIAZEK J, VAYSSIERE C, CRUAUD C, CABANIS EA, RUCHOUX MM, WEISSENBACH J, BACH JF, BOUSSER MG and TOURNIER-LASSERVE E. "Notch3 mutations in CADASIL, a hereditary adult-onset condition causing stroke and dementia." *Nature* 1996; *383:* 707-710.

[46] KELLY BD, HACKETT SF, HIROTA K, OSHIMA Y, CAI Z, BERG-DIXON S, ROWAN A, YAN Z, CAMPOCHIARO PA and SEMENZA GL. "Cell type-specific regulation of angiogenic growth factor gene expression and induction of angiogenesis in nonischemic tissue by a constitutively active form of hypoxia-inducible factor 1." *Circ Res* 2003; *93:* 1074-1081.

[47] KUKK E, LYMBOUSSAKI A, TAIRA S, KAIPAINEN A, JELTSCH M, JOUKOV V and ALITALO K. "VEGF-C receptor binding and pattern of expression with VEGFR-3 suggests a role in lymphatic vascular development." *Development* 1996; *122:* 3829-3837.

[48] LARSEN WJ. (1993). *Human Embryology*. New York, Churchill Livingston, Inc.

[49] LAWSON ND, SCHEER N, PHAM VN, KIM CH, CHITNIS AB, CAMPOS-ORTEGA JA and WEINSTEIN BM. "Notch signaling is required for arterial-venous differentiation during embryonic vascular development." *Development* 2001; *128:* 3675-3683.

[50] LAWSON ND, VOGEL AM and WEINSTEIN BM. "Sonic hedgehog and vascular endothelial growth factor act upstream of the Notch pathway during arterial endothelial differentiation." *Dev Cell* 2002; *3:* 127-136.

[51] LE DOUARIN NM and KALCHEIM C. (1999). *The Neural Crest*. Cambridge, Cambridge University Press.

[52] LE NOBLE F, MOYON D, PARDANAUD L, YUAN L, DJONOV V, MATTHIJSEN R, BREANT C, FLEURY V and EICHMANN A. "Flow regulates arterial-venous differentiation in the chick embryo yolk sac." *Development* 2004; *131:* 361-375.

[53] LI DY, SORENSEN LK, BROOKE BS, URNESS LD, DAVIS EC, TAYLOR DG, BOAK BB and WENDEL DP. "Defective angiogenesis in mice lacking endoglin." *Science* 1999; *284:* 1534-1537.

[54] LIEKENS S, NEYTS J, DE CLERCQ E, VERBEKEN E, RIBATTI D and PRESTA M. "Inhibition of fibroblast growth factor-2-induced vascular tumor formation by the acyclic nucleoside phosphonate cidofovir." *Cancer Res* 2001; *61:* 5057-5064.

[55] LINDAHL P, HELLSTROM M, KALEN M, KARLSSON L, PEKNY M, PEKNA M, SORIANO P and BETSHOLTZ C. "Paracrine PDGF-B/PDGF-Rbeta signaling controls mesangial cell development in kidney glomeruli." *Development* 1998; *125:* 3313-3322.

[56] LINDAHL P, JOHANSSON BR, LEVEEN P and BETSHOLTZ C. "Pericyte loss and microaneurysm formation in PDGF-B-deficient mice." *Science* 1997; *277:* 242-245.

[57] LOPEZ SL, PAGANELLI AR, SIRI MV, OCANA OH, FRANCO PG and CARRASCO AE. "Notch activates sonic hedgehog and both are involved in the specification of dorsal midline cellfates in Xenopus." *Development* 2003; *130:* 2225-2238.

[58] LOUGH J and SUGI Y. "Endoderm and heart development." *Dev Dyn* 2000; *217:* 327-342.

[59] MAISONPIERRE PC, SURI C, JONES PF, BARTUNKOVA S, WIEGAND SJ, RADZIEJEWSKI C, COMPTON D, MCCLAIN J, ALDRICH TH, PAPADOPOULOS N, DALY TJ, DAVIS S, SATO TN and YANCOPOULOS GD. "Angiopoietin-2, a natural antagonist for Tie2 that disrupts in vivo angiogenesis." *Science* 1997; *277:* 55-60.

[60] MARTI HJ, BERNAUDIN M, BELLAIL A, SCHOCH H, EULER M, PETIT E and RISAU W. "Hypoxia-induced vascular endothelial growth factor expression precedes neovascularization after cerebral ischemia." *Am J Pathol* 2000; *156:* 965-976.

[61] MARTIN AR, BAILIE JR, ROBSON T, MCKEOWN SR, ALASSAR O, MCFARLAND A and HIRST DG. "Retinal pericytes control expression of nitric oxide synthase and endothelin-1 in microvascular endothelial cells." *Microvasc Res* 2000; *59:* 131-139.

[62] MARX M, PERLMUTTER RA and MADRI JA. "Modulation of platelet-derived growth factor receptor expression in microvascular endothelial cells during in vitro angiogenesis." *J Clin Invest* 1994; *93:* 131-139.

[63] MCALLISTER KA, GROGG KM, JOHNSON DW, GALLIONE CJ, BALDWIN MA, JACKSON CE, HELMBOLD EA, MARKEL DS, MCKINNON WC, MURRELL J and *et al.* "Endoglin, a TGF-beta binding protein of endothelial cells, is the gene for hereditary haemorrhagic telangiectasia type 1." *Nat Genet* 1994; *8:* 345-351.

[64] MONTESANO R, VASSALLI JD, BAIRD A, GUILLEMIN R and ORCI L. "Basic fibroblast growth factor induces angiogenesis in vitro." *Proc Natl Acad Sci U S A* 1986); *83:* 7297-7301.

[65] MORRISON-GRAHAM K, SCHATTEMAN GC, BORK T, BOWEN-POPE DF and WESTON JA. "A PDGF receptor mutation in the mouse (Patch) perturbs the development of a non-neuronal subset of neural crest-derived cells." *Development* 1992; *115:* 133-142.

[66] NATAF V, GRAPIN-BOTTON A, CHAMPEVAL D, AMEMIYA A, YANAGISAWA M and LE DOUARIN NM. "The expression patterns of endothelin-A receptor and endothelin 1 in the avian embryo." Mech Dev 1998; *75:* 145-149.

[67] NEUFELD G, TESSLER S, GITAY-GOREN H, COHEN T and LEVI BZ. "Vascular endothelial growth factor and its receptors." *Prog Growth Factor Res* 1994; *5:* 89-97.

[68] OH SP, SEKI T, GOSS KA, IMAMURA T, YI Y, DONAHOE PK, LI L, MIYAZONO K, TEN DIJKE P, KIM S and LI E. "Activin receptor-like kinase 1 modulates transforming growth factor-beta 1 signaling in the regulation of angiogenesis." *Proc Natl Acad Sci U S A* 2000; *97:* 2626-2631.

[69] OLIVO M, BHARDWAJ R, SCHULZE-OSTHOFF K, SORG C, JACOB HJ and FLAMME I. "A comparative study on the effects of tumor necrosis factor-alpha (TNF-alpha), human angiogenic factor (h-AF) and basic fibroblast growth factor (bFGF) on the chorioallantoic membrane of the chick embryo." *Anat Rec* 1992; *234:* 105-115.

[70] Orr-Urtreger A and Lonai P. "Platelet-derived growth factor-A and its receptor are expressed in separate, but adjacent cell layers of the mouse embryo." *Development* 1992; *115:* 1045-1058.

[71] Oshima M, Oshima H and Taketo MM. "TGF-beta receptor type II deficiency results in defects of yolk sac hematopoiesis and vasculogenesis." *Dev Biol* 1996; *179:* 297-302.

[72] Pardanaud L and Dieterlen-Lievre F. "Ontogeny of the endothelial system in the avian model." *Adv Exp Med Biol* 2000; *476:* 67-78.

[73] Pla P. and Larue L. "Involvement of endothelin receptors in normal and pathological development of neural crest cells." *Int J Dev Biol* 2003; *47:* 315-325.

[74] Pola R, Ling LE, Silver M, Corbley MJ, Kearney M, Blake Pepinsky R, Shapiro R, Taylor FR, Baker DP, Asahara T and Isner JM. "The morphogen Sonic hedgehog is an indirect angiogenic agent upregulating two families of angiogenic growth factors." *Nat Med* 2001; *7:* 706-711.

[75] Poole TJ, Finkelstein EB and Cox CM. "The role of FGF and VEGF in angioblast induction and migration during vascular development." *Dev Dyn* 2001; *220:* 1-17.

[76] Rowitch DH, B, SJ, Lee SM, Flax JD, Snyder EY and McMahon AP "Sonic hedgehog regulates proliferation and inhibits differentiation of CNS precursor cells." *J Neurosci* 1999; *19:* 8954-8965.

[77] Ruchoux MM, Domenga V, Brulin P, Maciazek J, Limol S, Tournier-Lasserve E and Joutel A. "Transgenic mice expressing mutant Notch3 develop vascular alterations characteristic of cerebral autosomal dominant arteriopathy with subcortical infarcts and leukoencephalopathy." *Am J Pathol* 2003;*162:* 329-342.

[78] Sato TN, Tozawa Y, Deutsch U, Wolburg-Buchholz K, Fujiwara Y, Gendron-Maguire M, Gridley T, Wolburg H, Risau, W and Qin Y. "Distinct roles of the receptor tyrosine kinases Tie-1 and Tie-2 in blood vessel formation." *Nature* 1995; *376:* 70-74.

[79] Sato Y and Rifkin DB. "Inhibition of endothelial cell movement by pericytes and smooth muscle cells : activation of a latent transforming growth factor-beta 1-like molecule by plasmin during co-culture." *J Cell Biol* 1989; *109:* 309-315.

[80] Shah NM, Groves AK and Anderson DJ. "Alternative neural crest cell fates are instructively promoted by TGFbeta superfamily members." *Cell* 1996; *85:* 331-343.

[81] Shalaby F, Rossant J, Yamaguchi TP, Gertsenstein M, Wu XF, Breitman ML and Schuh AC. "Failure of blood-island formation and vasculogenesis in Flk-1-deficient mice." *Nature* 1995; *376:* 62-66.

[82] Shinbrot E, Peters KG and Williams LT. "Expression of the platelet-derived growth factor beta receptor during organogenesis and tissue differentiation in the mouse embryo." *Dev Dyn* 1994; *199:* 169-175.

[83] Soriano P. "Abnormal kidney development and hematological disorders in PDGF beta-receptor mutant mice." *Genes Dev* 1994; *8:* 1888-1896.

[84] Soriano P. "The PDGF alpha receptor is required for neural crest cell development and for normal patterning of the somites." *Development* 1997; *124:* 2691-2700.

[85] Sumoy L, Keasey JB, Dittman TD and Kimelman D. "A role for notochord in axial vascular development revealed by analysis of phenotype and the expression of VEGR-2 in zebrafish flh and ntl mutant embryos." *Mech Dev* 1997; *63:* 15-27.

[86] Takahashi K, Mulliken JB, Kozakewich HP, Rogers RA, Folkman J and Ezekowitz RA. "Cellular markers that distinguish the phases of hemangioma during infancy and childhood." *J Clin Invest* 1994; *93:* 2357-2364.

[87] Tallquist MD and Soriano P. "Cell autonomous requirement for PDGFRalpha in populations of cranial and cardiac neural crest cells." *Development* 2003; *130:* 507-518.

[88] Tsuda S, Ohtsuru A, Yamashita S, Kanetake H, Kanda S. "Role of c-Fyn in FGF-2-mediated tube-like structure formation by murine brain capillary endothelial cells." *Biochem Biophys Res Commun* 2002; *290:* 1354-1360.

[89] Tzahor E, Kempf H, Mootoosamy RC, Poon AC, Abzhanov A, Tabin CJ, Dietrich S and Lassar AB. "Antagonists of Wnt and BMP signaling promote the formation of vertebrate head muscle." *Genes Dev* 2003; *17:* 3087-3099.

[90] Vikkula M, Boon LM, Carraway KL, 3rd Calvert JT, Diamonti AJ, Goumnerov B, Pasyk KA, Marchuk DA, Warman ML, Cantley LC, Mulliken JB and Olsen BR. "Vascular dysmorphogenesis caused by an activating mutation in the receptor tyrosine kinase TIE2." *Cell* 1996; *87:* 1181-1190.

[91] Villa N, Walker L, Lindsell CE, Gasson J, Iruela-Arispe ML and Weinmaster G. "Vascular expression of Notch pathway receptors and ligands is restricted to arterial vessels." *Mech Dev* 2001; *108:* 161-164.

[92] Vokes SA and Krieg PA. "Endoderm is required for vascular endothelial tube formation, but not for angioblast specification." *Development* 2002; *129:* 775-785.

[93] Wilting J, Eichmann A and Christ B. "Expression of the avian VEGF receptor homologues Quek1 and Quek2 in blood-vascular and lymphatic endothelial and non-endothelial cells during quail embryonic development." *Cell Tissue Res* 1997; *288:* 207-223.

[94] Yamagishi S, Hsu CC, Kobayashi K and Yamamoto H. "Endothelin 1 mediates endothelial cell-dependent proliferation of vascular pericytes." *Biochem Biophys Res Commun* 1993; *191:* 840-846.

[95] Yamashita K, Discher DJ, Hu J, Bishopric NH and Webster KA. "Molecular regulation of the endothelin-1 gene by hypoxia. Contributions of hypoxia-inducible factor-1, activator protein-1, GATA-2, AND p300/CBP." *J Biol Chem* 2001; *276:* 12645-12653.

[96] Yanagisawa H, Hammer RE, Richardson JA, Williams SC, Clouthier DE and Yanagisawa M. "Role of Endothelin-1/Endothelin-A receptor-mediated signaling pathway in the aortic arch patterning in mice." *J Clin Invest* 1998; *102:* 22-33.

[97] Yanagisawa M, Kurihara H, Kimura S, Tomobe Y, Kobayashi M, Mitsui Y, Yazaki Y, Goto K and Masaki T. "A novel potent vasoconstrictor peptide produced by vascular endothelial cells." *Nature* 1988; *332:* 411-415.

[98] Yu Y, Varughese J, Brown LF, Mulliken JB and Bischoff J. "Increased Tie2 expression, enhanced response to angiopoietin-1, and dysregulated angiopoietin-2 expression in hemangioma-derived endothelial cells." *Am J Pathol* 2001; *159:* 2271-2280.

[99] Zelzer E and Shilo BZ. "Cell fate choices in Drosophila tracheal morphogenesis." *Bioessays* 2000; *22:* 219-226.

[100] Zerwes HG and Risau W. "Polarized secretion of a platelet-derived growth factor-like chemotactic factor by endothelial cells in vitro." *J Cell Biol* 1987; *105:* 2037-2041.

[101] Zhong TP, Childs S, Leu JP and Fishman MC. "Gridlock signalling pathway fashions the first embryonic artery." *Nature* 2001; *414:* 216-220.

Phenotypic spectrum of CHARGE syndrome in fetuses with CHD7 truncating mutations correlates with expression during human development

D Sanlaville, H C Etchevers, M Gonzales, J Martinovic, M Clément-Ziza, A-L Delezoide, M-C Aubry, A Pelet, S Chemouny, C Cruaud, S Audollent, C Esculpavit, G Goudefroye, C Ozilou, C Fredouille, N Joye, N Morichon-Delvallez, Y Dumez, J Weissenbach, A Munnich, J Amiel, F Encha-Razavi, S Lyonnet, M Vekemans and T Attié-Bitach

J. Med. Genet. 2006;43;211-317; originally published online 16 Sep 2005; doi:10.1136/jmg.2005.036160

ORIGINAL ARTICLE

Phenotypic spectrum of CHARGE syndrome in fetuses with *CHD7* truncating mutations correlates with expression during human development

D Sanlaville*, H C Etchevers*, M Gonzales*, J Martinovic, M Clément-Ziza, A-L Delezoide, M-C Aubry, A Pelet, S Chemouny, C Cruaud, S Audollent, C Esculpavit, G Goudefroye, C Ozilou, C Fredouille, N Joye, N Morichon-Delvallez, Y Dumez, J Weissenbach, A Munnich, J Amiel, F Encha-Razavi, S Lyonnet, M Vekemans, T Attié-Bitach

J Med Genet 2006;**43**:211–217. doi: 10.1136/jmg.2005.036160

Supplementary data are available online at http://www.jmedgenet.com/supplemental

See end of article for authors' affiliations

Correspondence to: T Attié-Bitach, Département de Génétique et Unité INSERM U-393, Hôpital Necker-Enfants Malades, 149, rue de Sèvres, 75743 Paris Cedex 15, France; tania.attie@necker.fr

Revised version received 11 August 2005
Accepted for publication 18 August 2005
Published Online First 23 September 2005

Background: The acronym CHARGE refers to a non-random cluster of malformations including coloboma, heart malformation, choanal atresia, retardation of growth and/or development, genital anomalies, and ear anomalies. This set of multiple congenital anomalies is frequent, despite rare patients with normal intelligence, and prognosis remains poor. Recently, *CHD7* gene mutations have been identified in CHARGE patients; however, the function of CHD7 during development remains unknown.
Methods: We studied a series of 10 antenatal cases in whom the diagnosis of CHARGE syndrome was suspected, considering that a careful pathological description would shed light on the *CHD7* function during development. *CHD7* sequence analysis and in situ hybridisation were employed.
Results: The diagnosis of CHARGE syndrome was confirmed in all 10 fetuses by the identification of a *CHD7* heterozygous truncating mutation. Interestingly, arhinencephaly and semi-circular canal agenesis were two constant features which are not included in formal diagnostic criteria so far. In situ hybridisation analysis of the *CHD7* gene during early human development emphasised the role of *CHD7* in the development of the central nervous system, internal ear, and neural crest of pharyngeal arches, and more generally showed a good correlation between specific *CHD7* expression pattern and the developmental anomalies observed in CHARGE syndrome.
Conclusions: These results allowed us to further refine the phenotypic spectrum of developmental anomalies resulting from *CHD7* dysfunction.

CHARGE syndrome refers to an association of defects including ocular coloboma (C), heart disease (H), choanal atresia (A), retarded growth and/or anomalies of the central nervous system (R), genito-urinary defects and/or hypogonadism (G), and ear anomalies and/or deafness (E). The acronym was coined by Pagon *et al*,[1] but the syndrome was first reported by Hall[2] and Hittner *et al*.[3] Other diagnostic criteria were proposed based on major/minor anomalies,[4–6] however, all features have variable expression and can be inconsistent, and many are non-specific. The incidence of CHARGE syndrome has been estimated to range from 0.1 to 1.2/100 000 live births with the highest incidence (to 1/8500 live births) in Canada.[7]

Recently, Vissers *et al* reported mutations in the *CHD7* gene in two out of three CHARGE patients tested.[8] CHD7 belongs to a large family of evolutionarily conserved proteins thought to play a role in chromatin organisation. However, although more than 200 newborns and infants with CHARGE syndrome have been described, only two prenatally detected cases have been reported to date[9 10] and nothing is known about CHD7 function during fetal development. In the present study, we analysed the coding sequence of the *CHD7* gene in 10 fetuses presenting with clinical features of CHARGE syndrome, considering that a careful pathological description would shed light on the CHD7 function during development. Clinical features as well as criteria necessary to establish the diagnosis of CHARGE syndrome prenatally remained to be defined. In fetuses, coloboma, heart malformation, choanal atresia, intrauterine growth retardation, genital anomalies, and external ear anomalies can be identified, while clinical symptoms such as mental retardation and deafness have to be replaced by their equivalents: central nervous system (CNS) anomalies and semi-circular canal (SCC) hypoplasia or agenesis, respectively. In this series, four of the above major anomalies were required for the diagnosis of CHARGE syndrome because the other features, such as growth retardation, cryptorchidism, or cranial nerve dysfunction, appear only in the postnatal period. All fetuses underwent autopsy and a detailed neuropathological examination with close attention to olfactory bulbs and tracts, brainstem, and cerebellum.

We identified a truncating mutation in all cases examined, confirming the diagnosis of CHARGE syndrome in all 10 fetal cases and allowing the phenotypic spectrum of the developmental anomalies resulting from *CHD7* dysfunction to be further envisaged. In addition, in situ hybridisation analysis of the *CHD7* gene at different stages of early human development emphasised the role of *CHD7* in the development of the central nervous system, internal ear, and neural crest of pharyngeal arches, and more generally showed a good correlation between specific *CHD7* expression pattern and the developmental anomalies observed in CHARGE syndrome.

METHODS

Patients

In all cases, the presence of severe malformations was noted at ultrasound (US) examination and pregnancies were terminated in accordance with French law. Detailed clinicopathological examination was carried out after parental consent. For all cases, the diagnosis of CHARGE syndrome was established either based on US evaluation or after fetopathological examination using the diagnostic criteria described above. For all cases, karyotype and *CHD7* mutation screening was performed. Clinical and genetic data are summarised in table 1 and detailed in supplementary data available online at http://www.jmedgenet.com/supplemental.

CHD7 sequence analysis

DNA was extracted from frozen tissues according to standard protocols. We designed 42 primer pairs covering the 37 *CHD7* coding exons (exons 2–38) and the corresponding exon-intron boundaries. Primer sequences and PCR conditions are available on request. PCR products were purified and directly sequenced in both directions on an ABI PRISM 3730 DNA sequencer (Perkin Elmer-Applied Biosystems, Courtaboeuf, France) using the dye terminator method according to the manufacturer's instructions.

In situ hybridisation

Normal human embryos and fetal tissues were obtained after elective termination of pregnancy in agreement with French legislation (law no. 94-654 of July 29, 1994), Necker Hospital, and the National Ethics Committee recommendations (report no. 1 of May 22, 1984). Embryonic stages were established according to the Carnegie staging (CS) classification.[11] Seven different embryonic stages (CS9 (d20), CS10 (d22), CS11 (d24), CS12 (d26), CS14 (d33), CS15 (d34), and CS19 (d 47–48)) as well as two fetal stages (9 and 11 weeks) were studied. Tissues were fixed in 4% phosphate buffered paraformaldehyde, dehydrated, and embedded in paraffin blocks. Five micron thick serial sections were cut. Exon 35 primers were selected for PCR amplification (F: 5′-GCTGTTCCCAAACAACTAGACATTG-3′ R: 5′-GAAACATTCAAGGAAAAGGCAGAG-3′). A T7 promotor sequence extension (TAATACGACTCACTATAGGGAGA) was added at the 5′ end of each primer. T7F/R and F/T7R primers allowed the amplification of sense and antisense templates specific to the *CHD7* gene. Riboprobes labelling, tissue fixation, hybridisation, and developing were carried out according to standard protocols,[12] as previously described.[13]

RESULTS

Molecular results

Direct sequencing of the 37 *CHD7* coding exons (gene ID 55636, NM_017780, NCBI: http://www.ncbi.nlm.nih.gov/) detected ten heterozygous truncating mutations. They are summarised in fig 1. Six were nonsense mutations (cases 2, 3, 4, 7, 8, 10), and four were frameshift mutations predicting a premature stop codon (cases 1, 5, 6, 9). In seven cases, parental DNA was studied (cases 1, 3, 6, 7, 8, 9, 10). All mutations occurred de novo (table 1). None of the 10 mutations was described previously. We found two mutations in exon 2, two mutations in exon 8 (at the end of the first chromodomain), and two identical mutations in exon 12 (R987X, unrelated cases 2 and 8) located in the SNF2 domain. In patient 5, the mutation (N1371fsX1374) is located in another domain of *CHD7* encoding the putative helicase domain. None of the remaining mutations involved known functional domains of the protein.

Clinical analysis

This series of 10 fetuses (seven male and three female) ranged from 21 to 36 weeks of gestation (WG) with a mean of 27 WG. Mean paternal age was 35 years and 8 months and mean maternal age was 30 years and 6 months. Prenatal US was abnormal in all patients. It disclosed polyhydramnios in 3/8 cases. Although two fetuses (cases 7 and 9) weighed between the 3rd and the 10th percentile, intrauterine growth retardation was never observed. All fetuses presented bilateral and asymmetric external ear abnormalities, semicircular canal hypoplasia/agenesis, and arhinencephaly. As shown in fig 2A, the ears were typically low set, asymmetric with a small or absent lobe, posteriorly rotated and triangular or square shaped.

Coloboma was found in seven patients, always affecting the retina or the choroid segment (fig 2Be,f). Microphthalmia was observed in two out the 10 cases in accordance with earlier postnatal observations.[14]

A congenital heart defect was found in 9/10 patients. These defects were complex cardiopathies and five involved the conotruncal region (cases 2, 3, 4, 5, 9). They frequently included atrial and/or ventricular septal defects, in accordance with earlier postnatal observations.[15]

Choanal atresia was found in six out of 10 patients (four bilateral and two unilateral). Among the four remaining patients, three had a cleft lip and/or palate. In two cases unilateral choanal atresia was found with a controlateral cleft palate. In one patient (case 6), neither choanal atresia nor facial clefting was found.

CHD7 expression during human embryonic development

At CS9 (d20; not shown), CS10 (d22; fig 3A), and CS11 (d24; fig 3B), *CHD7* is ubiquitously expressed, with a distinct signal in the neural tube. At CS12 (d26), *CHD7* is expressed throughout the CNS and neural crest-containing mesenchyme of the pharyngeal arches. At CS14 (d33), *CHD7* transcripts continue to be expressed in the cephalic mesenchyme, pharyngeal arches, and the brain. Expression is observed in the otic vesicle (fig 3C) as well as in the limb bud mesenchyme; it is more intense in the spinal cord and dorsal root ganglia (fig 3D). By CS15 (d34; fig 3E), expression continues to be intense within the CNS but is restricted to the dorsal part of the otic vesicle. Interestingly, no expression is observed in the nasal placode, neural retina, or pharyngeal endoderm. Also no expression is detected in the heart at any age. By CS19 (d47), *CHD7* is strongly expressed in the neural retina and rhombencephalon. It is moderately expressed in the semicircular canals (fig 3F), as well as in the forebrain, pituitary gland, and olfactory bulbs and nerves (fig 3G). Expression at 9 weeks of development is localised in the nasal epithelia (fig 3H), the neural retina, the optic nerve sheath (fig 3I), and the anterior and median lobes of the pituitary gland (fig 3J).

DISCUSSION

Here we report on a series of fetuses with CHARGE syndrome using diagnostic criteria adapted to the prenatal situation. All

Table 1 Summary of the clinical features of the 10 CHARGE fetuses

Case	1 (LAS)	2 (B0S)	3 (GAL)	4 (BAR)	5 (GOD)	6 (LAN)	7 (COQ)	8 (BEL)	9 (RAB)	10 (DER)	Mean
Age/sex											
Fetal age (WG)	21	21	23	23	28	29	29	29	32	36	27.1
Sex	M	M	M	M	M	M	F	M	F	F	7M/3F†
Maternal age	35	26	32	30	24	31	37	31	28	31	30.5
Paternal age	30	35	41	30	38	39	39	46	28	31	35.7†
Genetics											
Karyotype	46,XY	46,XY	46,XY	46,XY	46,XY	46,XY	46,XX	46,XY	46,XX	46,XX	
FISH 22q11.2 (*Tuple1*)	N	N	N	N	N	N	N	N	N	N	
CHD7 nucleotide change	2550_2554del	2959C>T	763C>T	6157C>T	4112_4113insT	808delG	5458C>T	2959C>T	2260_2266dup	2584A>T	100%
CHD7 protein change	K850fsX855	R987X	Q255X	Arg2053X	N1371fsX1374	A270fsX304	P1820X	R987X	V754fsX764	K862X	100%
De novo?	Yes	?	Yes	?	?	Yes	Yes	Yes	Yes	Yes	
CHARGE acronym											
Coloboma	+	+	+	+	−	−	+	+	+	−	70%
Heart malformations	+	+	+	+	+	+	+	+	+	−	90%
Atresia choanal/cleft	AC	Cl	AC/Cl	Cl	Cl	−	AC/Cl	AC	AC	AC	90%
AC unilateral/bilateral	B		U				U	B	B	B	
Cleft palate/lip		L+P	P	L+P	P		L+P				
CNS anomalies											
Arhinencephaly	+	+	+	+	+	+	+	+	+	+	100%
Others CNS anomalies	+	+	+	+	+	+	+	+	−	−	80%
Genital anomalies	−	+*	−	+	+*	+*	+	+	−	−	60%
Ears											
Anomalies of external ears	+	+	+	+	+	+	+	+	+	+	100%
Agenesis/hypoplasia CSC	+	+	+	+	+	+	+	+	+	+	100%
Others											
Thymic hypo/agenesis	+	+	−	−	+	−	+	+	+	+	70%
Limb anomalies	+	+	−	−	−	−	+	−	+	+	50%
Renal anomalies	−	−	−	+	−	+	+	−	−	+	40%
Skeletal anomalies	+	+	?	−	−	+	−	−	+	−	40%
Polyhydramnios	−	−	−	−	−	+	−	−	+	+	30%
Oesophageal anomalies	−	−	−	−	−	−	−	−	+	+	20%
IUGR	−	−	−	−	−	−	−	−	−	−	0%

N, normal; WG, weeks of gestation.
*Leydig cell rarefaction; †the increased male population and paternal age in this study were first documented by Blake *et al*.[31]

fetuses underwent an extensive necropsy as well as molecular analysis of the *CHD7* gene. This study confirms the role of the *CHD7* gene in CHARGE syndrome and allows delineation of the antenatal clinical spectrum of *CHD7* mutations.

Molecular analysis of *CHD7*

Nine different mutations were identified in our series. One, the R987X mutation, was found in two unrelated fetuses (cases 2 and 8). Interestingly, they differed as regards the presence of distal arthrogryposis and hemivertebra (case 2), suggesting that other additional factors might be involved. However, based on our results and in agreement with Vissers *et al*, so far it is not possible to establish a genotype/phenotype correlation.[8] Large deletions and nonsense mutations in the first exon(s) of the *CHD7* gene are observed. This suggests that haploinsufficiency of the *CHD7* gene is probably the mechanism accounting for CHARGE syndrome. Because the mutations occurred de novo, genetic counselling can be reassuring, although germ-line mosaicism can never be excluded.

Clinical analysis

In our series of fetal CHARGE syndrome, our detailed clinicopathological evaluation led to the identification of three constant features: anomalies of the external ear, agenesis/hypoplasia of the semi-circular canals, and arhinencephaly. Six other features occur frequently (in at least in seven of 10 cases), namely genital anomalies, thymic hypoplasia, ocular coloboma, other CNS anomalies (other than arhinencephaly), choanal atresia/cleft palate, and heart defect.

Bilateral and asymmetric external ear malformations are found in all our cases. As shown in fig 2A, typical features are small, low set, posteriorly rotated ears, with a prominent crux helix, a small or absent lobe, and a triangular shape as described previously.[5 15 16] In the literature, internal ear anomalies, ranging from subtle modular deficiencies to Mondini malformation and semi-circular canal hypoplasia or agenesis, are classically reported in CHARGE syndrome.[7 17 18] Semi-circular hypoplasia/agenesis was reported in up to 100% of cases in the literature.[15 18] We confirm these data and emphasise the necessity of detecting temporal bone anomalies though cephalic x ray evaluation for the antenatal diagnosis of CHARGE syndrome (fig 2Ba,b).

Interestingly, among CNS anomalies, arhinencephaly was found in all our cases (fig 2Bc,d). Arhinencephaly has already been reported by Lin *et al* in some patients.[19] However, its frequency among CHARGE patients has not been evaluated in the literature, aside from the observation of Harvey *et al* who found arhinencephaly in 7/7 CHARGE postnatal cases.[20] More recently, Chalouhi *et al* assessed olfactory deficiency in 14 children with CHARGE syndrome. Half of them were anosmic and the others had olfactory residual function (hyposmic). All nine MRIs showed anomalies of the olfactory tracts and bulbs varying from moderate hypoplasia to complete aplasia, without any relationship between the radiological and functional results.[21] Our systematic neuropathological examination clearly shows that arhinencephaly is a constant sign of *CHD7* mutation. We propose it should be considered a major sign for prenatal CHARGE diagnosis. Other CNS anomalies included brainstem and cerebellum abnormalities. They were observed in eight of our 10 fetuses, but were reported also in postnatal cohorts.[19 20] They are mainly characterised by hypoplasia of the inferior cerebellar vermis and brain stem (cases 1, 5, 7) and severe cerebellar heterotopia (case 8).

The high incidence of heart defects, cleft lip/palate, and brain anomalies in our series when compared to postnatal data can probably be explained by detection by US during pregnancy. It has been shown that CHARGE individuals have increased mortality due to AVSD defects and cerebellar and or brain stem anomalies associated with ventriculomegaly.[7 15] Moreover, males have been reported to have an increased mortality compared to females.[15 22] This study presents a population of 10 fetuses with a severe phenotype of CHARGE syndrome, with an especially high number of complex cardiopathies, bilateral posterior choanal atresia, tracheo-oesophageal fistula,[22] brain anomalies, and increased representation of males (7/10).

Among other frequent features, genital anomalies deserve special attention: they were found in 7/10 cases. In three male fetuses, they were noticed only at the histological level (Leydig cell rarefaction). To our knowledge these histological anomalies have not been described previously. This may explain the delay in puberty noticed more in males than females that has been reported postnatally.[23] In a female fetus, the only genital anomaly found was a hypoplastic ovary. According to the postnatal literature, female genital hypoplasia is rare and micropenis or cryptorchidism are more frequent features observed in males.[24]

Interestingly, thymus hypoplasia or agenesis was found in seven of out 10 cases. This contrasts with postnatal cases where thymic hypoplasia is rarely reported.[5] The association of CHARGE and DiGeorge syndromes reported previously[25] suggests a neural crest defect causes the clinical overlap of both syndromes. Whether the *CHD7* gene could be responsible for a CHARGE-DiGeorge association should be tested further, particularly in postnatal patients.

Our study also confirms that growth retardation is usually observed postnatally.[26] Indeed, no intrauterine growth retardation was observed in our antenatal series. In addition to the severe feeding problems related to gastro-oesophageal reflux and brain stem anomalies, the postnatal growth retardation could be explained in part by a pituitary gland dysfunction. Interestingly, *CHD7* gene expression is observed within this tissue during the embryonic period.

It is worth stressing that case 9 presented with ectrodactyly (fig 2C), which has not been reported so far in CHARGE syndrome. Four patients presented limb anomalies although minor, such as clinodactyly. Skeletal (including costal and vertebral defects) or renal anomalies were found in four out of 10 cases. Finally, among other features, tracheo-oesophageal fistulas were noticed twice.

Based on our clinicopathological observations, we consider semicircular canal agenesis as well as arhinencephaly highly predictive diagnostic criteria of CHARGE syndrome. We suggest that they should be added to the two major diagnostic criteria described by Pagon, along with the external ears malformations. Indeed, four of six major criteria of CHARGE (coloboma, choanal atresia and/or cleft lip/palate, heart defect, arhinencephaly, semi-circular canal agenesis, and external ear anomalies) were necessary and sufficient for the diagnosis of CHARGE in our series. As previously suggested for postnatal cases, minor diagnostic criteria such as facial dysmorphism and renal, digestive, and skeletal anomalies should also be considered for fetal CHARGE syndrome in addition to thymus hypoplasia/agenesis and polyhydramnios. Interestingly, in most patients with three major features and three minor features proposed as CHARGE syndrome,[5] the presence of arhinencephaly and semi-circular canals hypoplasia/agenesis was not evaluated and we recommend brain MRI to assess the diagnosis of CHARGE syndrome in these cases.

Our study contributes to the development of a strategy for the diagnosis of CHARGE syndrome during pregnancy. Indeed, features of CHARGE syndrome detected at routine US such as hydramnios, heart defects, cleft lip/palate, CNS anomalies, and kidney or gastrointestinal anomalies are

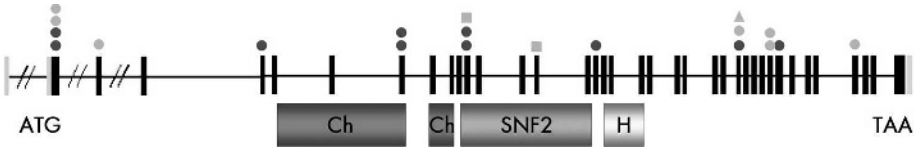

Figure 1 Schematic representation of the *CHD7* mutations identified so far. The mutations found by Vissers *et al*[8] are shown in orange; the ten nonsense mutations found in our cohort are shown in blue. Circles indicate the nonsense mutations, squares the missense mutations, and triangles the intron-exon boundary mutations. On the bottom, functional CHD7 domains are indicated: chromodomains in red, SNF2 domain in green, and helicase domain in yellow.

common. More specific features would help in the diagnosis of CHARGE syndrome. We thus propose that focussed US and/or brain MRI should be performed for the detection of external ear anomalies, choanal atresia, semi-circular canal agenesis, and arhinencephaly. This strategy will certainly lead to a higher prenatal detection rate of CHARGE syndrome.

Embryonic function of *CHD7*

The CHD7 protein encompasses several important domains. The chromatin organisation modifier (chromo) domain is a conserved region of around 50 amino acids found in a variety of chromosomal proteins that appear to play a role in the functional organisation of the eukaryotic nucleus. Experimental evidence shows that the chromodomain is involved in binding proteins to histone and possibly RNA. CHD7-like helicase domains are involved in ATP-dependent unwinding of DNA or RNA duplexes and histone deacetylation.[27 28] Certain CHD proteins have been shown to participate in nucleosome remodeling deacetylase (NuRD) protein complexes which interact with sequence-specific DNA-binding factors for targeted repression.[29] Presumably, the CHD7 protein plays an important role in chromatin remodelling during early development and allows a level of epigenetic control over target genes expressed in mesenchymal cells derived from the cephalic neural crest.

We analysed the expression pattern of the *CHD7* gene during early human development. *CHD7* is widely expressed in the undifferentiated neuroepithelium and in mesenchyme of neural crest origin. Towards the end of the first trimester it is expressed in dorsal root ganglia, cranial nerves/ganglia, and auditory, pituitary, and nasal tissues as well as in the neural retina. Absent from the myocardium, bones of mesodermal or neural crest origin, and the genital ridge, *CHD7* expression correlates with defects observed in these tissues because of its presence in neural crest cells investing the outflow tract of the heart, and in the hypothalamus and pituitary gland. Endocrine deficiency may occur centrally, in the differentiation of hypothalamic nuclei secreting somatostatin or GnRH, or more peripherally in the differentiation of somatotropic or gonadotropic cells of the anterior pituitary. It could be related to the clinical findings of delayed puberty in the adolescent and adult population with CHARGE

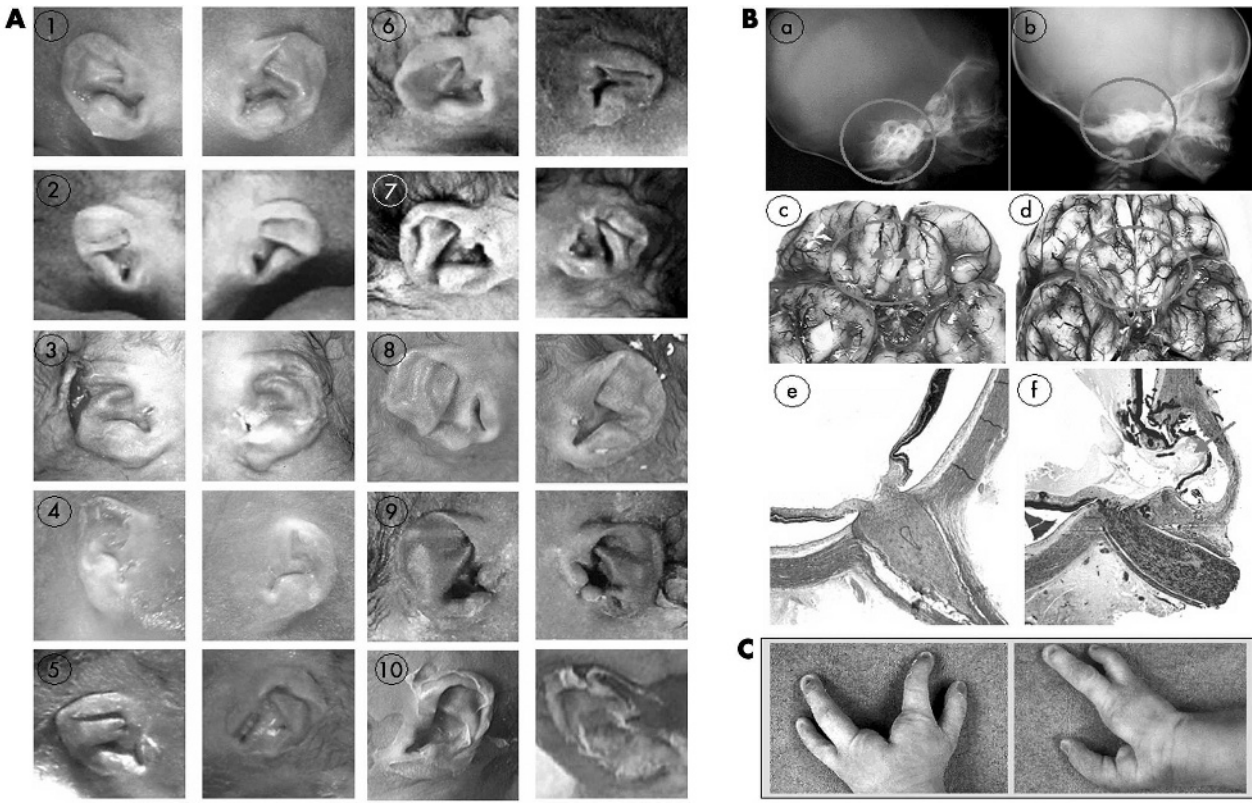

Figure 2 (A) External ear dysmorphism in the 10 fetuses. Note the characteristic triangular or square shaped and wrinkled morphology in all cases. (B) Normal (on the left) and pathological (on the right) view of three of the major clinical findings, namely severe semicircular canal hypoplasia (b: fetus 10) on profile babygram at 19 weeks (control at 19 weeks), arhinencephaly (d: fetus 10) at 34 weeks (control at 34 weeks), and retinal coloboma (f: fetus 1) at 19 weeks (control at 19 weeks). (C) Hands of fetus 9 showing the ectrodactyly. (These images are published with consent.)

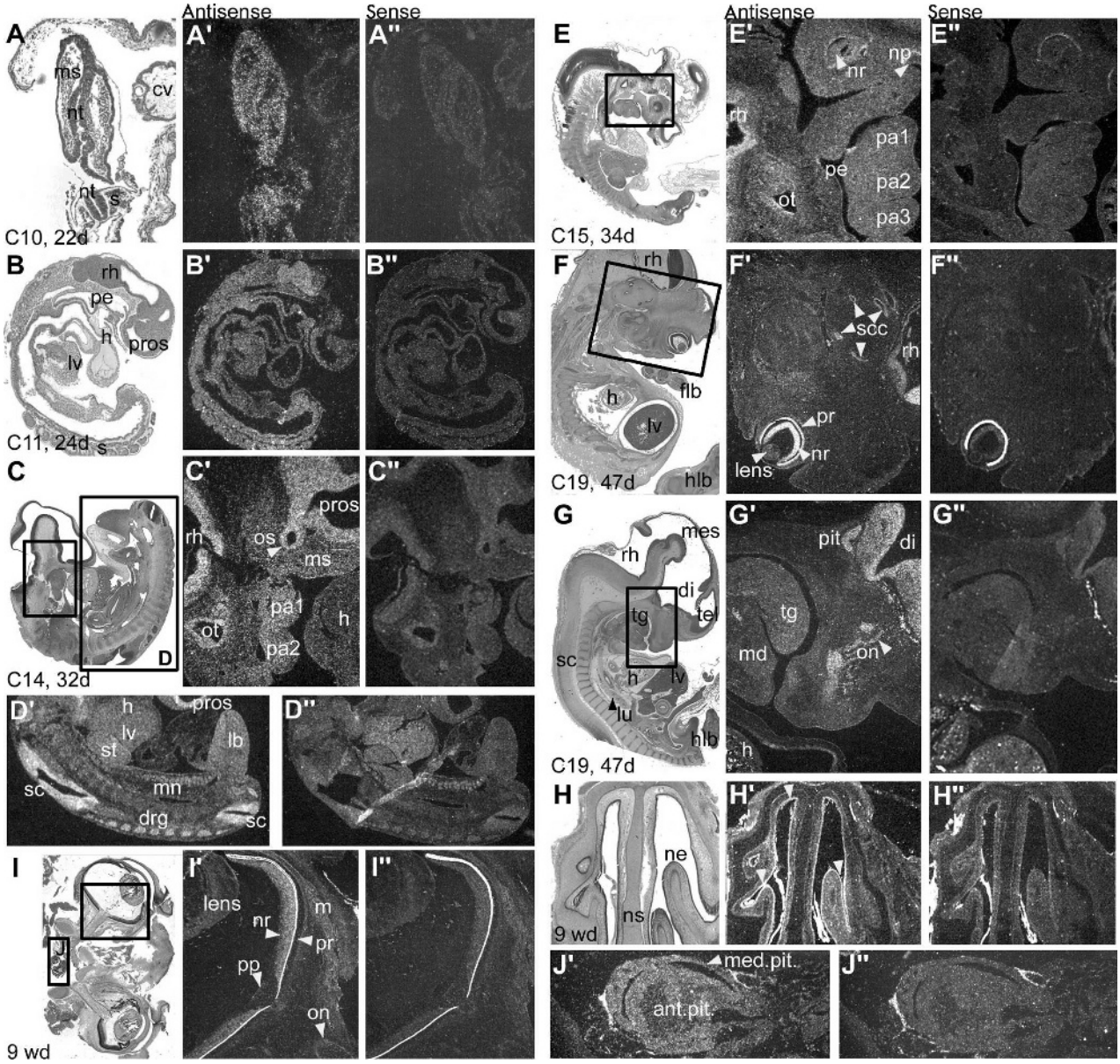

Figure 3 Expression of the *CHD7* gene during human embryonic development. Adjacent sections are coloured with haematoxylin/eosin (X), treated with antisense or sense control riboprobes (X′ and X′′, respectively). Ventral to right, rostral to top where applicable. (A) At Carnegie stage (C)10, after 22 days (d) of development, *CHD7* is expressed ubiquitously within embryonic but not extraembryonic tissues (cv) seen in transverse section. (B) By C11, expression is slightly more intense within the rhombencephalon, as observed in parasagittal section, but is not markedly present within the heart (h), liver (lv), or pharyngeal endoderm (pe). (C) A stronger signal is observed in the entire central nervous system (prosencephalon (pros) and rhombencephalon (rh)) by C14, including the diencephalic optic stalk (os), and is also seen in the cephalic mesenchyme (ms) of the frontonasal bud and pharyngeal arches (pa1, pa2). Heart expression is non-existent/not found (h). The otic vesicle, negative at C12 (not shown), expresses *CHD7* in its epithelium (ot) and associated acoustic ganglion (*) at this stage. Parasagittal section. (D) Enlargement of the body of the same C14 embryo shows a strong *CHD7* signal in the spinal cord (sc) and dorsal root ganglia (drg), and a weak signal in limb bud mesenchyme (lb). (E) At C15, *CHD7* expression is restricted to the dorsal epithelium of the otic vesicle (ot), presumptive inner ear, and the rhombencephalon (rh), spinal cord, and dorsal root ganglia (not shown); however, expression is barely above background in pharyngeal arch mesenchyme (pa1–3) and absent from the neural retina (nr), pharyngeal endoderm (pe), and nasal placode (np). (F, G) By C19, the *CHD7* signal becomes intense in the entire neural retina (nr), rhombencephalon (rh), anterior pituitary gland (pit), diencephalon (di; in particular the hypothalamus (hyp)), and olfactory nerve (on, arrowhead) and bulb and is more discrete but distinct within the semicircular canals (scc). Expression continues to be absent from any portion of the heart (h). md, mandible; tg, tongue. (H) At 9 weeks of development (wd), *CHD7* transcripts are detectable in the nasal epithelium (ne) but not within the nasal septum (ns) in coronal section. (I) Also at 9 wd, *CHD7* expression is observed in neuronal soma of the neural retina in contrast to the absence of signal in the axon fascicles at the optic papilla (pp) and nerve (on), although the outer sheath of the nerve continues to express *CHD7* (compare frame C′). (J) An enlargement of the pituitary gland in the same coronal section as (I) demonstrates continued *CHD7* expression within anterior and median lobes at 9 wd.

syndrome.[23] A major testable hypothesis in this context is that CHD7 regulates paired domain- or homeobox domain-containing transcription factor genes important for the development of the pituitary gland and other organ systems, such as *Hesx1*, *Otx1*, *Prop1*, *Krox20*, *Pitx2*, and *Titf1/Nkx2a*. Other regulatory transcription factor genes such as *Pax2* or *Tbx1*, with multiple expression sites in many affected organ systems or inductive tissues for these organ anlages, still remain attractive and non-exclusive CHD7 functional targets.[30]

CONCLUSION

In the present study we confirmed the predominant role of the *CHD7* gene during fetal development. The clinicopathological spectrum of *CHD7* mutations in a series of 10 fetuses examined at the anatomical as well as histological level allowed the phenotypic spectrum of the developmental anomalies resulting from *CHD7* dysfunction to be further envisaged and led us to propose agenesis of the semi-circular canals and arhinencephaly as major diagnostic criteria of CHARGE syndrome. Further postnatal studies are needed to confirm these data.

ACKNOWLEDGEMENTS

We are thankful to Eric Detrait, Sophie Delahaie, Boris Keren, Daniel Sidi, the French patients' group for the CHARGE association, and the SOFFOET (Société Française de FOETopathologie) for their help and collaboration. We also thank Han Brunner for sharing unpublished data.

ELECTRONIC-DATABASE INFORMATION

The NCBI website is at http://www.ncbi.nlm.nih.gov/

Authors' affiliations

D Sanlaville, H C Etchevers, J Martinovic, M Clément-Ziza, A Pelet, S Audollent, C Esculpavit, G Goudefroye, C Ozilou, N Morichon-Delvallez, A Munnich, J Amiel, F Encha-Razavi, S Lyonnet, M Vekemans, T Attié-Bitach, Département de Génétique et Unité INSERM U-393, Hôpital Necker-Enfants Malades, AP-HP, 75015 Paris, France
M Gonzales, C Fredouille, N Joye, Unité de Foetopathologie, Hôpital Saint Antoine, AP-HP, 75012 Paris, France
A-L Delezoide, Service de Biologie du Développement, Hôpital Robert Debré, AP-HP, 75019 Paris, France
M-C Aubry, S Chemouny, Y Dumez, Service d'Obstétrique, Hôpital Necker-Enfants Malades, AP-HP, 75015 Paris, France
C Cruaud, J Weissenbach, Genoscope and CNRS UMR8030, Evry, France

DS was supported by the Programme de Recherche Clinique AOM 02-122. HCE was supported by the Association Française contre les Myopathies and the INSERM Avenir program

Competing interests: none declared

*These authors contributed equally to this work

Consent has been given for the publication of the details in this report

REFERENCES

1 **Pagon RA**, Graham JM Jr, Zonana J, Yong SL. Coloboma, congenital heart disease, and choanal atresia with multiple anomalies: CHARGE association. *J Pediatr* 1981;**99**(2):223–7.
2 **Hall BD**. Choanal atresia and associated multiple anomalies. *J Pediatr* 1979;**95**(3):395–8.
3 **Hittner HM**, Hirsch NJ, Kreh GM, Rudolph AJ. Colobomatous microphthalmia, heart disease, hearing loss, and mental retardation–a syndrome. *J Pediatr Ophthalmol Strabismus* 1979;**16**(2):122–8.
4 **Oley CA**, Baraitser M, Grant DB. A reappraisal of the CHARGE association. *J Med Genet* 1988;**25**(3):147–56.
5 **Blake KD**, Davenport SL, Hall BD, Hefner MA, Pagon RA, Williams MS, Lin AE, Graham JM Jr. CHARGE association: an update and review for the primary pediatrician. *Clin Pediatr (Phila)* 1998;**37**(3):159–73.
6 **Verloes A**. Updated diagnostic criteria for CHARGE syndrome: a proposal. *Am J Med Genet A* 2005;**133**(3):306–8.
7 **Issekutz KA**, Graham JM Jr, Prasad C, Smith IM, Blake KD. An epidemiological analysis of CHARGE syndrome: preliminary results from a Canadian study. *Am J Med Genet A* 2005;**133**:309–17.
8 **Vissers LE**, van Ravenswaaij CM, Admiraal R, Hurst JA, de Vries BB, Janssen IM, van der Vliet WA, Huys EH, de Jong PJ, Hamel BC, Schoenmakers EF, Brunner HG, Veltman JA, van Kessel AG. Mutations in a new member of the chromodomain gene family cause CHARGE syndrome. *Nat Genet* 2004;**36**(9):955–7.
9 **Becker R**, Stiemer B, Neumann L, Entezami M. Mild ventriculomegaly, mild cerebellar hypoplasia and dysplastic choroid plexus as early prenatal signs of CHARGE association. *Fetal Diagn Ther* 2001;**16**(5):280–3.
10 **Hertzberg BS**, Kliewer MA, Lile RL. Antenatal ultrasonographic findings in the CHARGE association. *J Ultrasound Med* 1994;**13**(3):238–42.
11 **O'Rahilly R**, Muller F. *Developmental stages in human embryos*. Washington, DC: Carnegie Institution of Washington, 1987.
12 **Wilkinson DG**. *In situ hybridization: a practical approach*. Oxford: IRL Press, 1992.
13 **Trueba SS**, Auge J, Mattei G, Etchevers H, Martinovic J, Czernichow P, Vekemans M, Polak M, Attie-Bitach T. PAX8, TITF1, and FOXE1 gene expression patterns during human development: new insights into human thyroid development and thyroid dysgenesis-associated malformations. *J Clin Endocrinol Metab* 2005;**90**(1):455–62.
14 **Russell-Eggitt IM**, Blake KD, Taylor DS, Wyse RK. The eye in the CHARGE association. *Br J Ophthalmol* 1990;**74**(7):421–6.
15 **Tellier AL**, Cormier-Daire V, Abadie V, Amiel J, Sigaudy S, Bonnet D, de Lonlay-Debeney P, Morrisseau-Durand MP, Hubert P, Michel JL, Jan D, Dollfus H, Baumann C, Labrune P, Lacombe D, Philip N, LeMerrer M, Briard ML, Munnich A, Lyonnet S. CHARGE syndrome: report of 47 cases and review. *Am J Med Genet* 1998;**76**(5):402–9.
16 **Davenport SL**, Hefner MA, Thelin JW. CHARGE syndrome. Part I. External ear anomalies. *Int J Pediatr Otorhinolaryngol* 1986;**12**(2):137–43.
17 **Guyot JP**, Gacek RR, DiRaddo P. The temporal bone anomaly in CHARGE association. *Arch Otolaryngol Head Neck Surg* 1987;**113**(3):321–4.
18 **Morgan D**, Bailey M, Phelps P, Bellman S, Grace A, Wyse R. Ear-nose-throat abnormalities in the CHARGE association. *Arch Otolaryngol Head Neck Surg* 1993;**119**(1):49–54.
19 **Lin AE**, Siebert JR, Graham JM Jr. Central nervous system malformations in the CHARGE association. *Am J Med Genet* 1990;**37**(3):304–10.
20 **Harvey AS**, Leaper PM, Bankier A. CHARGE association: clinical manifestations and developmental outcome. *Am J Med Genet* 1991;**39**(1):48–55.
21 **Chalouhi C**, Faulcon P, Le Bihan C, Hertz-Pannier L, Bonfils P, Abadie V. Olfactory evaluation in children: application to the CHARGE syndrome. *Pediatrics* 2005;**116**(1):e81–8.
22 **Blake KD**, Russell-Eggitt IM, Morgan DW, Ratcliffe JM, Wyse RK. Who's in CHARGE? Multidisciplinary management of patients with CHARGE association. *Arch Dis Child* 1990;**65**(2):217–23.
23 **Blake KD**, Salem-Hartshorne N, Daoud MA, Gradstein J. Adolescent and adult issues in CHARGE syndrome. *Clin Pediatr (Phila)* 2005;**44**(2):151–9.
24 **Ragan DC**, Casale AJ, Rink RC, Cain MP, Weaver DD. Genitourinary anomalies in the CHARGE association. *J Urol* 1999;**161**(2):622–5.
25 **de Lonlay-Debeney P**, Cormier-Daire V, Amiel J, Abadie V, Odent S, Paupe A, Couderc S, Tellier AL, Bonnet D, Prieur M, Vekemans M, Munnich A, Lyonnet S. Features of DiGeorge syndrome and CHARGE association in five patients. *J Med Genet* 1997;**34**(12):986–9.
26 **Blake K**, Kirk JM, Ur E. Growth in CHARGE association. *Arch Dis Child* 1993;**68**(4):508–9.
27 **Woodage T**, Basrai MA, Baxevanis AD, Hieter P, Collins FS. Characterization of the CHD family of proteins. *Proc Natl Acad Sci U S A* 1997;**94**(21):11472–7.
28 **Wade PA**, Jones PL, Vermaak D, Veenstra GJ, Imhof A, Sera T, Tse C, Ge H, Shi YB, Hansen JC, Wolffe AP. Histone deacetylase directs the dominant silencing of transcription in chromatin: association with MeCP2 and the Mi-2 chromodomain SWI/SNF ATPase. *Cold Spring Harb Symp Quant Biol* 1998;**63**:435–45.
29 **Xue Y**, Wong J, Moreno GT, Cote J, Wang W. NURD, a novel complex with both ATP-dependent chromatin-remodeling and histone deacetylase activities. *Mol Cell* 1998;**2**(6):851–61.
30 **Williams MS**. Speculations on the pathogenesis of CHARGE syndrome. *Am J Med Genet A* 2005;**133**(3):318–25.
31 **Blake KD**, Brown D. CHARGE association looking at the future–the voice of a family support group. *Child Care Health Dev* 1993;**19**(6):395–409.

Case 1 (LAS):

A 35-year-old woman was referred for termination of the pregnancy due to severe congenital heart defect, namely pulmonary artery atresia with intact septum, detected by US at 20 weeks of gestation (WG). Fetal external examination revealed dysmorphic features with bilateral choanal atresia, short nose, anteverted nostrils, large mouth with "M"-shaped upper lip, retrognathia and dysplastic ears without lobe. In addition a short neck, and abnormally set toes were noted. The X-ray examination revealed semi-circular canal agenesis as well as splitting of the lumbar vertebrae. Autopsy confirmed the heart defect and disclosed thymic hypoplasia, bilateral retinal coloboma (Fig 1B,f), and CNS gross abnormalities (arhinencephaly, thick corpus callosum, ponto-cerebellar hypoplasia involving mainly the inferior vermis). Histological study revealed immature lateral geniculate body with hypoplastic cranial nerve nuclei of predominantly the VIIth and VIIIth nerve. The karyotype was normal, 46,XY. No 22q11.2 deletion was detected using Fluorescence *In Situ* Hybridization (FISH).

Case 2 (BOS):

At 22 WG during the second pregnancy of a 26 year-old mother, US examination revealed cleft lip, congenital heart defect and hydrocephaly. Pregnancy was terminated at 21 WG. Fetal examination showed an eutrophic fetus with distinctive facial features including hypertelorism, bilateral microphthalmia, right cleft lip/palate, short nose, microretrognathia, and short, asymmetric dysplastic ears without a lobe. The neck was short. In addition, distal arthrogryposis was noted. Semi-circular canal agenesis and the presence of T2 hemivertebra were depicted by X-ray. Visceral examination confirmed the heart defect with type I truncus arteriosus. In addition, it revealed complete thymic agenesis. Neuropathological examination showed the absence of olfactory bulbs (arhinencephaly), moderate ventricular enlargement and cerebellar hypoplasia. Focal retinal dysplasia with colobomatous cysts was also found.

Amniocentesis revealed a normal karyotype 46,XY. Using FISH no 22q11.2 microdeletion was detected.

Case 3 (GAL):

It is the fourth pregnancy of a 32 year-old mother an increased nuchal translucency (4 mm) was noted on first trimester (11 WG) US examination. The second trimester US evaluation disclosed multiple malformations leading to pregnancy termination at 23 WG. X-ray showed bilateral semi-circular agenesis. Fetal examination showed facial dysmorphism including left microphtalmia, asymmetric dysplastic ears, and short neck with left choanal atresia. Autopsy disclosed aortic dextroposition, ventricular septal defect (VSD), and persistent left superior caval vein. CNS examination revealed arhinencephaly with moderate hydrocephaly and retinal coloboma. The brain stem and cerebellum were unremarkable. Amniocentesis revealed a normal karyotype, 46,XY. Using FISH no 22q11.2 microdeletion was detected.

Case 4 (BAR) :

A 27-year-old woman was referred for severe malformations depicted by US examination, including heart defect, cleft palate, and short ears. Pregnancy was terminated at 23 WG. Fetal examination revealed an eutrophic male fetus presenting brachycephaly, hypertelorism, bilateral labio-palatine complete cleft, asymmetric dysplastic ears, limb malformations (quadrilateral hypoplastic nails and short halluces) with micropenis. X-ray examination revealed severe bilateral semi-circular canal hypoplasia. Autopsy disclosed a type II truncus arteriosus with ventricular septal defect (VSD), bilateral hydronephrosis and tubular stomach. Histological examination showed decreased Leydig cell population in both testicles. Neuropathological findings included left olfactory bulb agenesis and retinal coloboma. The brain stem and cerebellum were well developed. Karyotype was normal, 46,XY. No 22q11.2 deletion was detected using FISH.

Case 5 (GOD) :

A 24-year-old woman was referred at 28 WG for heart defect, dysplastic ears, hypoplastic thymus and vermis hypoplasia detected by US. Fetal X-ray disclosed agenesis of semi-circular canals. The pathological examination of this eutrophic male fetus revealed facial dysmorphism with broad nose tip, anteverted nostrils, asymmetric small dysplastic ears, retrognathia, short neck and cleft palate. Visceral malformations included conotruncal heart defect with aortic atresia and ventricular septal defect, thymic agenesis, and left pulmonary isomerism. Histological examination revealed decreased Leydig cell population. Neuropathological examination showed bilateral arhinencephaly and inferior vermis hypoplasia. Karyotype was normal, 46,XY. No 22q11.2 deletion was detected using FISH.

Case 6 (LAN):

A 31 year-old woman was referred because of multiple fetal malformations detected on US. The pregnancy was terminated at 29 WG for heart and brain malformations and abnormal ears. X-ray examination revealed the absence of semi-circular canals and a left 13th additional rib. External examination of this eutrophic male fetus revealed brachycephaly with flat occiput, hypertelorism, hypoplastic alae nasi, malar hypoplasia, microstomia, micrognathia, asymmetric and dysplastic ears, and short neck. Fetal autopsy confirmed the atrio-ventricular septal defect with a right retro-oesophageal subclavian artery, and disclosed left cryptorchidism with increased testicular connective tissue. CNS abnormalities were bilateral agenesis of olfactory bulbs, ventricular enlargement and posterior partial corpus callosum agenesis. Histology demonstrated an increase of connective tissue in the testicles. Karyotype was normal, 46,XY. No 22q11.2 deletion was detected using FISH.

Case 7 (COQ):

This was the first pregnancy of a young non-consanguineous couple (respectively 37 and 39 year-old mother and father). At 22 WG, US suspected cleft lip/palate. At 25 WG, the presence of a large facial clefting was confirmed. Additionally, bilateral renal

hypoplasia, small stomach, and a single umbilical artery were depicted. The pregnancy was terminated at 29 WG. X-ray examination showed semi-circular canal agenesis and the absence of ossification of the 12th rib pair. The female fetus showed a moderate growth retardation (10th-20th percentile), facial asymmetry with right choanal atresia, left cleft lip/palate, dysplastic ears and short neck. Visceral malformations included ectopic and hypoplastic thymus, congenital heart malformation with atrioventricular septal defect (AVSD) and hypoplastic aortic arch, single umbilical artery, bilateral renal hypoplasia, and small ovaries. Neuropathological examination revealed arhinencephaly with brain stem and vermian hypoplasia, and colobomatous retinal cysts. Karyotype was normal, 46,XX. No 22q11.2 deletion was detected using FISH.

Case 8 (BEL) :

This case is the first pregnancy of a 31 year-old mother. First trimester (11 WG) US detected fetal hygroma. At the second trimester, US as well as Magnetic Resonance Imaging (MRI) showed multiple malformations including cleft lip, thymic hypoplasia, bilateral microphthalmia and heart defect. Pregnancy was terminated at 29 WG. X-ray examination of the fetus showed severe hypoplasia of the semi-circular canals. Fetal examination showed an eutrophic male fetus presenting bilateral choanal atresia, blepharophimosis, an asymmetric microphthalmia (right > left) with right microcornea, asymmetric dysplastic ears and phimosis. Visceral malformations included right heart hypoplasia, atretic pulmonary artery with an intact septum, thymic hypoplasia and absent ossification of the 12th rib. Neuropathological examination revealed bilateral retinal coloboma and arhinencephaly with a well-developed brainstem and cerebellum but severe cerebellar heterotopias. The karyotype was normal, 46,XY. No 22q11.2 deletion was detected using FISH.

Case 9 (RAB):

This was the second pregnancy of a young non-consanguineous couple (28 year-old parents). A previous spontaneous abortion occurred at 12 WG (unknown cause). US at 24 WG revealed short nasal bones, frontal oedema, and suspected heart malformation, which was confirmed by US at 32 WG. In addition, retrognathia and polyhydramnios were observed. The pregnancy was terminated. Cranial X-ray examination revealed semi-circular canal agenesis. Fetal examination disclosed bilateral choanal atresia and craniofacial dysmorphic features including microcephaly with small anterior fontanel, frontal bossing, hypertelorism, broad nasal bridge, large mouth with "M" shaped upper lip, microretrognathia, and abnormal external ears. In addition, upper limb malformations with bilateral ectrodactyly were observed (Fig. 1C). Visceral malformations included Fallot's tetralogy with a right retro-oesophageal subclavian artery, severe thymic hypoplasia, abnormal left pulmonary segmentation, oesophageal atresia (type III), and a small supernumerary spleen. Neuropathological examination showed the absence of olfactory bulbs. Brain stem and cerebellum were unremarkable. The karyotype was normal, 46,XX. No 22q11.2 deletion was detected using FISH.

Case 10 (DER) :

In a 31-year-old woman, severe polyhydramnios, vermis hypoplasia, thin brainstem and ventricular dilatation were detected on US examination during the second trimester of the pregnancy. Brain malformations were confirmed by MRI and the pregnancy was terminated at 36 WG. Fetal examination showed a female fetus with a weight between the 3rd and the 10th percentile. Length and head circumference were around the 50th percentile. Hypoplasia of the semi-circular canals was the only significant radiologic feature (Fig 1B,b). The fetus presented bilateral choanal atresia, asymmetric dysplastic ears and retrognathia. Visceral malformations included thymic hypoplasia, ventricular disequilibrium with right retro-oesophageal subclavian artery, oesophageal type III atresia with tracheo-oesophageal fistula and left hydronephrosis.

Neuropathological examination revealed arhinencephaly (Fig 1B,d) and retinal coloboma. The brain stem and cerebellum were well developed, except for an ectopic olivary nucleus in the medulla. Karyotype was normal, 46,XX. No 22q11.2 deletion was detected using FISH.

Molecular Bases of Human Neurocristopathies

Heather C. Etchevers,* Jeanne Amiel and Stanislas Lyonnet

Introduction

Neural crest cells (NCC) form in the human embryo during the third to fifth weeks of pregnancy, within the neural folds that delineate the neural plate from the ectoderm. During the fusion of the neural folds, which ultimately yields a tube that will become the central nervous system (CNS), NCC detach and become mesenchymal. They migrate throughout the body, integrating nearly every organ.

NCC derivatives include the neurons and support cells of the entire peripheral nervous system (sensory and autonomic), adrenergic and other endocrine cells, and all pigment cells except those arising from the retina (reviewed by Le Douarin and Kalcheim[1]). In the head, in addition to the cell types mentioned above, NCC differentiate into connective and structural tissues such as dermis,[2,3] bones and cartilage of most of the skull[3,4] and muscle tendons.[5,6] They also infiltrate and are essential for the function of glandular and vascular elements such as the thymus, the thyroid and parathyroid glands, the conotruncal region of the heart and the entire branchial vascular sector,[7-9] giving rise to connective, adipose and smooth muscle cells.

The astonishing diversity of NCC derivatives has led to this population being nicknamed the "fourth embryonic germ layer." The fact that NCC were known to exist only in the embryo precluded their being perceived as a true stem cell type. Recently, however, it was demonstrated that the enteric nervous system of the adult rat contains neural crest stem cells that self-renew and remain oligopotent.[10] Avian melanocytes are able to transdifferentiate into glial cells, neurons or smooth muscle-like cells in vitro, also implying the long-term existence of multipotent progenitors.[11] It is thought that NCC derivatives are generated through progressive restriction of developmental potential.[12,13]

The ultimate choice in phenotype made at a given site of differentiation is the result of a combination of extrinsic factors in the embryonic microenvironment and cell-intrinsic properties that modify its responsiveness to these external influences. The former have been documented through observation of the disruption of neurotrophic growth factors and receptor genes that result in deficiencies of selected subsets of NCC derivatives.[14,15] Both their migration pathways and fate are imposed on NCC by surrounding tissues as they leave the neural primordium; these are not dependent on intrinsic properties regionally distributed along the neuraxis, as had initially been presumed. For instance, truncal NCC transplanted at the vagal level colonize the gut and differentiate into enteric ganglia in which neurons synthesize acetylcholine rather than catecholamines, as they would have done normally at the truncal level.[3] A notable exception, the cephalic NCC contributing to the branchial arch-derived facial skeleton has some intrinsic positional information and commitment,[16,17] apparently imparted by the rostral endoderm before and during their emigration from the neural folds.[18,19]

*Corresponding Author: Heather C. Etchevers—INSERM U393, Hôpital Necker – Enfants Malades, 149 rue de Sèvres, 75743 Paris Cedex 15, France. Email: etchevers@necker.fr

Neural Crest Induction and Differentiation, edited by Jean-Pierre Saint-Jeannet.

Definition of a Neurocristopathy

Abnormal migration, differentiation, division or survival of NCC lead to organ and tissue dysplasias with highly diverse clinical and pathological features. Referring to their proposed common embryological origin, Bolande first introduced the concept of "neurocristopathy" in order to highlight the potential for shared pathogenetic mechanisms.[20]

Nuanced definitions of a "neurocristopathy" have been made due to the great diversity in NCC derivatives and the organs in which they play an integral functional role over time. One can attempt to remain "purist," including only those clinical entities where direct derivatives of the neural crest are affected. However, in order to be useful, the term neurocristopathy over the last thirty years has also been applied to include entities where abnormal NCC affect the development of other tissues not themselves solely derived from NCC, such as the heart or the thyroid gland. Unfortunately, there have been inconsistencies in the inclusion (neurofibromatosis type II) or exclusion (craniostenoses) of many pathologies. At the time any given disease has been termed a neurocristopathy, its classification was based on a corpus of knowledge that has been subject to enormous change with the advent and renewal of experimental molecular embryology.

The situation has hardly been clarified by molecular studies. In those rare cases where truly only NCC derivatives are affected and the responsible gene is identified, it usually turns out to be an evolutionarily conserved gene with distinct known functions in separate organ systems (or "fields") in humans or animals. Early developmental genes seem to affect multiple germ layers and moments in cellular existence through an evolutionary sort of functional recycling known as "cooption" (reviewed in ref. 21). Why are NCC more vulnerable than other cell types? Like many other embryonic cell types, they undergo all the processes of epithelial-mesenchymal transition, proliferation, migration, a drawn-out period of differentiation with maintenance of plasticity, niche occupation and apoptosis. Perhaps the adaptability of the evolutionarily recent NCC,[22] useful for making wildly diverse head and body appendices,[23] is its Achilles' heel with respect to pathogenesis.

Certain disorders have not been included as neurocristopathies below. In particular, we have excluded those that arise from functional deficiencies in differentiated NCC. Thus, although oculocutanous albinism does indeed affect neural crest-derived melanocytes, it is less directly a result of their *development* but rather of their final *metabolic function* (to synthesize melanin). We have also, with more difficulty, left aside those clinical entities largely involving fields in which NCC play no part during development. These would comprise the limb, kidney, and liver, all of which can be associated with defects in NCC-derived tissues (e.g., von Hippel-Lindau syndrome with pheochromocytoma; tuberous sclerosis syndrome with hypopigmented or café-au-lait macules). The aim is to restrict the definition to those entities in which a NCC defect is causative, excluding secondary phenomena. Simple craniostenoses (craniosynostoses), for example, have not been included because they appear to represent defects in osteoblast function and are also associated, in syndromic forms, with bone problems in the limbs, ribs or vertebrae, none of which have a NCC component. One exception, craniofrontonasal syndrome, will be mentioned among the gene cascades involved in NCC migration.

Here, we attempt to describe which entities we consider to be neurocristopathies and why, based on recent advances in basic and clinical research.

Clinical Appreciation of Neurocristopathies

When considering a patient with multiple congenital birth defects, it is clearly useful to take an embryological point of view in order to find an underlying common cause. NCC colonize four compartments unequal in size: the skin, the peripheral nervous system, some of the endocrine system and a pharyngocephalic pole. Anomalies affecting any of these compartments can be considered to arise from one initial field, and warrant closer examination of the other compartments. Table 1 presents isolated versus syndromic neurocristopathies on one axis

Table 1. Examples of neurocristopathies according to compartment and type

	Skin	Peripheral Nervous System	Endocrine	Pharyngocephalic
Cancer:				
Isolated	·Melanoma ·Merkel cell carcinoma	·Neuroblastoma ·Schwannoma ·Paraganglioma	·Pheochromocytoma ·Familial or sporadic medullary thyroid carcinoma ·Chromaffin paraganglioma ·Carcinoid tumors	·Hemangiocytoma ·Non-chromaffin paraganglioma (ear)
Syndromic	·Neurofibromatosis I[#] ·Neurocutaneous melanosis	·Hirschsprung+neuroblastoma	·Multiple endocrine neoplasias 2A,B	·Congenital central hypoventilation
Malformation:				
Isolated	·Congenital giant nevus ·Piebaldism	·Hirschsprung	·	·Cerebrodural arteriovenous malformations ·Cleft palate/lip ·Moya-moya ·Isolated conotruncal cardiopathies ·Aplasia of lacrymal and salivary glands
Syndromic	·Sturge-Weber	·Waardenburg ·Familial dysautonomia type 2	·Allgrove ·Bamforth-Lazarus	·CHARGE* ·DiGeorge ·Pierre Robin ·Holoprosencephaly*[#] ·Kallmann* ·Rieger* ·Binder* ·Mœbius* ·Johanson-Blizzard* ·Treacher-Collins-Franceschetti ·Craniofrontonasal[#] ·Goldenhar*[#] ·Oro-facial-digital*[#]

The endocrine component of the syndromes marked with an asterisk (*) may be imputed to non-endocrine neural crest cells that are necessary for the formation of the pituitary gland. Conditions that combine a neurocristopathy with non-neurocristopathic malformations are indicated by a number sign (#).

and the useful distinction between cancers or malformations on the other. Naturally, the syndromic neurocristopathies may have both cancerous and malformative components. It is truly rare among these rare diseases, to see a "pure" syndromic neurocristopathy. However, the concept of "neurocristopathy" is useful to the clinician in orienting their approach to the patient by grouping apparently divergent and unrelated signs under one umbrella.

Isolated Neurocristopathic Tumors

Although the following tumors occur sporadically in many cases, all have been demonstrated to be transmitted in families to some extent. They also all occur in syndromic forms, with one another or with the neurocristopathic malformations. In particular, neuroblastoma and medullary thyroid carcinoma occur in conjunction with Hirschsprung disease, as discussed below.

Neuroblastoma (MIM 256700) is the most common extracranial childhood solid tumor, and the one with the highest rate of remission (around 90%; reviewed in ref. 24). Neuroblastomas, derived from sympathetic components, as schwannomas are from sensory components, possess phenotypic markers common to components of the peripheral nervous system. Histologically, they consist of cells that resemble undifferentiated NCC mesenchyme and, upon tumor regression, acquire nonmalignant characteristics resembling neurofibromas or ganglioneuromas.

Medullary thyroid carcinomas (MTC, MIM 155240), derived from calcitonin-producing C cells of the thyroid gland, exist in both sporadic (~75%) and familial forms (~25%). MTC cells inappropriately (over) express peptides such as serotonin, vasoactive intestinal peptide or calcitonin, leading to hypercalcemia among other effects. Histologically, they resemble carcinoid tumors, which occur usually in endodermally-derived organs such as the digestive or pulmonary tracts and are diagnosed at all ages.

Pheochromocytomas (MIM 171300) are derived from chromaffin cells of the adrenal medulla and also cause systemic effects such as sweating, tachycardia and hypertension (with subsequent effects on, for example, the retinal or cerebral vasculature), arising from an increase in epinephrine and norepinephrine production. Both sporadic and familial forms exist. Pheochromocytoma is a hallmark of a number of neurocristopathic syndromes discussed below, as well as of von Hippel-Lindau syndrome (VHL; MIM 193300), in some forms in conjunction with renal carcinomas. Paragangliomas (MIM 168000) arise in the complementary, nonchromaffin chemoreceptors of the head and neck region. Tumors of the glomus jugulare and carotid body are often seen in this heterogeneous familial neurocristopathy with complex inheritance—at least one of the genes is subject to imprinting and is only transmitted from the paternal line.[25]

The cutaneous NCC cancers, melanoma (MIM 155600) and Merkel cell (MC) carcinoma, are both locally and systemically aggressive in behavior. Malignant melanoma arises in melanocytes that are one of the latest-differentiating and most widely disseminated NCC phenotypes, and can occur in any part of the skin, even those never exposed to the sun (for instance, the nasal epithelium or the genitals). Childhood melanoma, while rare, carries one of the highest rates of distant metastasis among cancers. In contrast, around half of MC carcinomas are localized in the head and neck region, with mostly limited spread,[26] and they arise preferentially in the dermis of elderly adult patients.[27] MC carcinomas are occasionally associated with neurofibromatosis type 1[28] or breast and ovarian adenocarcinomas, and more frequently with squamous cell carcinomas.[26] Recently, the controversial hypothesis that mammalian MCs, commonly found in the basal epidermis, are in fact NCC derivatives was supported by experimental evidence.[29] MC cells, in synaptic-like contact with sensory nerve terminals in the skin, appear to have a local neuroendocrine or mechanosensory function, much as melanocytes are postulated to have had earlier in evolution.[30]

Isolated Neurocristopathic Malformations

These include many of the most frequent birth defects such as Hirschsprung disease (1 in 5000 births), cleft lip and/or palate (1 in 1000 births), conotruncal heart malformations involving (or not) the great arteries (1 in 500 births), and congenital nevi (1 in 100 births).

Indeed, such malformations overlap to some extent with neural tube closure defects (1 in 1000 births) by virtue of a segmentally defective specification or fusion of the neural folds from which NCC emigrate. Isolated defects in neural tube closure are not considered to be neurocristopathies as they are in and of themselves a very heterogeneous group of disorders that derive from an embryological event preceding that of NCC specification.[31] Nonetheless, as will be discussed in the section devoted to genetic cascades, common molecular origins can be at the root of both neural tube closure defects and various neurocristopathies.

Hirschsprung disease (HSCR), or aganglionic megacolon, is a congenital malformation characterized by the absence of enteric ganglia along a variable length of the intestine. It was first reported by Harald Hirschsprung in 1886. The enteric ganglia, components of the autonomic nervous system, are organized in two concentric rings throughout the gut wall: the outer myenteric plexus (Auerbach plexus) and the inner submucosal plexus (Meissner plexus). The neurons making up these ganglia include: sensorineurons detecting information from the gut, interneurons processing the sensory information, and motor neurons that provide innervation to smooth muscles regulating the contractility of the gut as well as the secretory activity of glands. In the late 1940's, a surgical procedure was developed in which the aganglionic segment of the bowel is resected by an abdomino-anal pull-through (reviewed in ref. 32). This previously fatal disorder became surgically treatable and enabled the survival of patients and the discovery of familial transmission of HSCR.[33]

Orofacial clefting arises from defects in the fusion of the palatal shelves, derived from the maxillary portion of the first pharyngeal arch. Mesenchymal NCC derived from the mid- and hindbrain migrate toward the endoderm and into the five bilaterally paired arches. The mesenchyme surrounds transitory pairs of aortic arch arteries that circumvent the pharynx and act as organizing centers for the structures of the lower face and neck.

The heart is essentially a mesodermal derivative. However, the NCC that enter the most caudal pharyngeal arches encase both the arteries (the left part of the fourth pair will persist as the aorta) and the cardiac tube in its conotruncal extremity.[3] Within the wall of the outflow tract, thickenings of this mesenchyme will lead to separation of the aorta from the pulmonary trunk, formation of the semilunar valves and completion of ventricular septation. Experimental removal of NCC lead to defects in all of these processes[8] as well as atrophy of the thymus and parathyroid glands.[7] Clonal expansion of a single defective NCC precursor in the cardiac region may lead to the individualized, spatially restricted phenotypes.

A similar mechanism could explain how congenital melanocytic nevi arise in any area of the skin at a frequency decreasing inversely proportionally to surface, from 1 in 100 births for the smallest lesions, to an estimated 1 in 20,000 for surfaces over 100 cm.^{2} All melanocytic nevi are characterized by an abnormally high and localized concentration of melanocytes, and are often associated with hyperpilosity and variable coloration. The giant congenital melanocytic nevi (GCMN, OMIM 137550) can also present with nodules, absent or deficient skin annexes and abnormal dermis.

Complex Tumor Predisposition Syndromes

These include neurofibromatosis I (NF1), the multiple endocrine neoplasias (MEN) type 2A and 2B, familial medullary thyroid carcinoma (FMTC), Sturge-Weber syndrome and neurocutaneous melanosis.

NF1, also known as Recklinghausen disease (MIM 162200), is one of the most common neurocristopathies with a prevalence of 1/2000 to 1/3000 live births. Both Schwann cells and melanocytes are affected, undergoing abnormal proliferations that give rise to neurofibromas and "café au lait" spots. Neurofibrosarcomas as well as leukemia, and Wilms tumors in tissues not themselves derived from NCC, can also occur in patients. NF1 is an autosomal dominant disorder with high penetrance. However, since the disease is expressed in a broadly variable manner, clinical criteria for diagnosis need to be searched for carefully. Lisch nodules, visible as spots on the iris (colored by NCC-derived melanocytes), are one of the most penetrant features after the age of 20.

Familial medullary thyroid carcinoma (FMTC, MIM 155240), MEN type 2A (MEN2A, MIM 171200) and type 2B (MEN2B, MIM 162300) are also transmitted with autosomal dominant inheritance. MEN2A is characterized by hyperplasia of the calcitonin-producing parafollicular cells of the thyroid with subsequent neoplastic progression to medullary thyroid carcinoma (MTC) as described earlier, but also pheochromocytoma and parathyroid hyperplasia. Patients affected with MEN2B can also present with oral neuromas, marfanoid habitus and hyperganglionosis of the hindgut (contrasting with HSCR), although the clinical presentation can be similar to functional intestinal obstruction syndromes. The penetrance of MEN2 is age-related; only about 70% of MEN2A gene carriers will present with MTC by the age of 70 years, but precursor C-cell hyperplasia is detectable in almost all carriers prior to 40 years of age.

Sturge-Weber syndrome (around 1 in 50000 births, MIM 185300) merits discussion as it is not usually included as an example of a neurocristopathy, yet it is the only one of the classical "phakomatoses" (a term invented by Van der Hœve in 1921, not yet fallen into complete disuse) that from an embryological viewpoint can be unequivocally attributed to a simple NCC defect. Symptoms include a facial capillary hemangioma along the trigeminal nerve, with soft tissue or skeletal hypertrophy beneath it; leptomeningeal angioma with occasional calcification in the underlying cortex and ensuing epilepsy or hemiparesis; ocular choroid angioma with ipsilateral glaucoma due to permeable blood vessels. It is now understood that one discrete segment of cephalic NCC gives rise to vascular wall components within all affected areas,[9,34] and a single event in a clonal precursor could find itself expressed in a somatically mosaic manner.[35] The same mechanism may be responsible for the association of neurocutaneous melanosis (melanocytic tumor of the meninges) with congenital giant nevus of the skin and, more infrequently, with malignant melanoma.

Complex NCC-Related Malformative Syndromes

Waardenburg syndrome (WS), a genetically heterogeneous condition, combines pigmentary anomalies and sensorineural deafness. At a frequency of 1 in 50,000 live births, WS accounts for 2-5% of all congenital deafness. The condition results from the absence or reduction of melanocytes in both the skin and the stria vascularis of the cochlea.[10] WS is clinically and genetically heterogeneous (OMIM 193500, 148820 and 193510). The combination of HSCR with WS defines the WS4 type (Shah-Waardenburg syndrome, OMIM 277580). The addition to of a Peripheral demyelinating neuropathy and a Central dysmyelinating leukodystrophy to Waardenburg and Hirschsprung disease (WS4) define the PCWH syndrome[36] (MIM 609136). The close lineage relationship between glial cells and melanocytes[11] also justifies grouping these diverse clinical entities together on a continuum, pointing at the defective specification of a single NCC precursor type.

CCHS (Ondine's curse, MIM 209880) is a life-threatening disorder primarily manifesting as sleep-associated respiratory insufficiency and markedly impaired ventilatory responses to hypercapnia and hypoxaemia.[37] The autonomic nervous system is affected: from the level of its central control in the hindbrain through the vagus nerve and out to the peripheral, NCC-derived target ganglia. In addition, HSCR or tumors such as neuroblastoma, ganglioneuroblastoma and ganglioneuroma are noted in 20-30% and 5-10% of CCHS patients respectively (e.g., see ref. 38).

Most of the other malformative syndromes markedly affect the cardio-cephalic pole (Table 1). Facial dysmorphy is a distinguishing feature, as expected from the enormous contribution of NCC to the face and brain vault. However, it has only recently been acknowledged that pituitary development, like that of the heart outflow tract, depends on the presence and participation of cephalic NCC,[39] although the final contribution of these cells to the gland is negligible. Thus, syndromes that entail growth or genital abnormalities in addition to more obvious effects on NCC derivatives should be considered as potential neurocristopathies. One example is that of Allgrove syndrome (MIM 231550), an autosomal recessive disorder also known as AAA syndrome for alacrima, achalasia of the esophagus due to neurological impairment and adreno-corticotropic hormone (ACTH)-resistant adrenal failure. Bamforth-Lazarus

syndrome (MIM 241850) associates cleft palate and choanal atresia with thyroid agenesis.[40] A NCC contribution to the connective tissue of the thyroid gland has been recognized for decades[3,7] but is not commonly evoked.

Gene Cascades Implicated in Human Neurocristopathies

Breaking down the timeline of NCC development into stages is one approach to considering the abundant molecules that are now known to be involved in or suspected in pathogenesis.

Neural Crest Induction

Specification of the neural folds is the subject of many excellent reviews[41-43] and ongoing research,[44-47] going beyond the scope of this chapter. To resume, the roles of signaling molecules such as members of the Wnt,[45,46,48,49] fibroblast growth factor (FGF), bone morphogenetic protein (BMP) or hedgehog families and their control by gradients of retinoic acid and *Hox* transcription factor expression have been underlined. Several transcription factors are also expressed during early induction of the vertebrate neural crest lineage in the neural folds or surrounding tissues such as members of the highly conserved families *Slug/Snail*, *Sox*, *Fox*, and *Pax*.

To date, germline mutations of the *PAX3*,[50] *MITF*,[51] *SNAI2*[52] and *SOX10*[53] genes have been demonstrated to be directly involved in pure syndromic neurocristopathies (WS1-4 respectively), suggesting that impairment of the other pathways may be lethal or, as yet, unrecognized. The spontaneous mouse mutation in *Pax3*,[54] known as Splotch for its heterozygous coat color defect, leads to hindbrain exencephaly in homozygous mice; it was somewhat of a surprise to find that its later role in glial/melanocyte lineage determination was predominant in human disease, rather than its earlier one in NCC specification (similar findings for *SNAI2* and *SOX10*, see below). Although no PAX3 mutations have been demonstrated in isolated neural tube closure defects to date, some WS1 patients do have spinal neural tube defects and WS3 patients, skeletal muscular abnormalities.[55] *SNAI2*, also known as *SLUG*, is mutated in WS2D[52] and piebaldism[56] but also is possibly an oncogene in an activated form.[57] Expressed in premigratory and migrating NCC throughout the vertebrate subclass, *Snail* or *Slug* homologues are also found in the gastrulating mesoderm and are generally implicated in the epitheliomesenchymal transition.[58]

NCC Migration

The term migration describes a long period in NCC existence: from the epithelio-mesenchymal transition and delamination from the neural folds, to reorganisation of the cytoskeleton, to migration along pathways constrained by anatomy and the local extracellular matrix (ECM) in order to encounter appropriate orientation and differentiation cues. The mechanism of migration has an intrinsic component, represented by the capacity of a given NCC to respond to its environment by physical changes and motility, and an extrinsic component, represented by the extracellular matrix or cellular/anatomical environment through which NCC migrate. It is the latter component that may explain the neurocristopathic contribution to other malformation syndromes (e.g., basal cell nevus syndrome), in particular those involving the cardio-cephalic pole and its abundant NCC-derived mesenchyme.

The noncanonical Wnt signaling pathway, exemplified physiologically by Wnt11 and its receptor Fz7 in mouse,[46] the EphB-ephrinB,[59] neuregulin-ErbB[60] and endothelin-endothelin receptor[61] families of ligands and their receptors, are known to be involved in initiating and maintaining migratory behavior of NCC. The transcription factors Sox9, then Slug/Snail, FoxD3 and Sox10 appear to control the cell-autonomous acquisition of a migratory phenotype.[47,62] The composition of the ECM in fibronectin[63,64] and vitronectin[65] and appropriate collagens[66,67] and laminins[68,69] is certainly relevant to the direction of integrin-bearing NCC as they distance themselves from the neural tube and enter either the dorsoventral or the dorsolateral compartment pathways. Integrins, like both Eph receptors and their ephrin ligands, effect changes in the cytoskeleton upon binding their substrates. Their specificity is

Table 2. Known genes or loci in neurocristopathies

Pathology	MIM	Transmission	Gene	Chromosomal Localization	Spontaneous Mouse Model or Transgenic (+)
Piebaldism	172800	AD	*KIT*	4q12	*White-spotting*, +
Melanoma	155600	AD		1p36	
Melanoma	155600	S	*NRAS*	1p13.1	+
Melanoma	155600	S	*BRAF*	7q34	+
Melanoma	155600	AD, S	*CDKN2A*	9p21	+
Melanoma	155600	AR, S	*MC1R*	16q24.3	*Tawny, recessive yellow, tobacco-darkening, sombre*, +
Melanoma	155600	AD, S	*CDK4*	12q14	+
WS1	193500	AD	*PAX3*	2q35	*Splotch*, +
WS3	193500	AR	*PAX3*	2q35	*Splotch*, +
WS2A	193510	AD	*MITF*	3p14	*Microphthalmia, vitiligo, white, red eyed white, brownish*, +
WS2B	600193	AD		1p	
WS2C	606662	?		8p23	
WS2D	608890	AR	*SNAI2*	8q11	+
WS4	277580	AR	*EDNRB*	13q22	*Piebald, piebald lethal*, +
WS4	277580	AR	*EDN3*	20q13	*Lethal spotting*,+
WS4	277580	AD	*SOX10*	22q13	*Dominant megacolon*, +
HSCR	142623	CI*	*RET*	10q11.2	+
HSCR	142623	CI	*GDNF*	5p13.2	+
HSCR	142623	CI	*ARAF*	Xp11.3	+
HSCR	142623	CI	*NTN*	19p13.3	+
HSCR	142623	CI	*EDNRB*	13q22	*Piebald, piebald lethal*, +
HSCR	142623	CI	*EDN3*	20q13	*Lethal spotting*,+
HSCR	142623	AD	*PHOX2B*	4p12	+
HSCR	142623			3p12	
HSCR	142623			19q13	
HSCR	142623	AD	*L1CAM*	Xq28	+

continued on next page

Table 2. Continued

Pathology	MIM	Transmission	Gene	Chromosomal Localization	Spontaneous Mouse Model or Transgenic (+)
NB	256700	AD, S	*PHOX2B*	4p12	+
Haddad	209880	AD, S	*PHOX2B*	4p12	+
CCHS	209880	AD, S	*PHOX2B*	4p12	+
Pheochromocytoma	171300	AD	*RET*	10q12	+
Pheochromocytoma	171300	AD	*SDHB*	1p36	
Paraganglioma 4	115310	AD	*SDHB*	1p36	
Paraganglioma 2	601650	AD		11q13.1	
Paraganglioma 3	605373	AD	*SDHC*	1q21	
Paraganglioma 1	168000	AD	*SDHD*	11q23	+
Pheochromocytoma	171300	AD	*SDHD*	11q23	+
MC carcinoma	602690.0019	S	*SDHD*	11q23	+
MEN2A	171400	AD	*RET*	10q12	+
MEN2B	162300	AD	*RET*	10q12	+
MTC	155240	AD	*RET*	10q12	+
Familial dysautonomia 2	256800	AR	*NTRK1*	1q21	+
NF1	162200	AD	*NF1*	17q11	+
DiGeorge	188400	AD	*TBX1*	22q11.2	+
CHARGE	214800	AD	*CHD7*	8q12	+
Goldenhar	164210	AD		14q32	
Moebius	157900	AD		13q12.2-q13	
Bamforth-Lazarus	241850	AR	*FOXE1*	9q22	+
Rieger 1	180500	AD	*PITX2*	4q25	+
Rieger 2	601499	AD	*FOXC1*	13q14	*Congenital hydrocephalus*, +
Craniofrontonasal	304110	XLD	*EFNB1*	Xq13.1	+
Allgrove	231550	AR	*ALADIN*	12q13	

AD or R, autosomal dominant/recessive; XL, X-linked; CI, complex inheritance; * major locus; S, somatic mutation.

partly conferred by the numerous alpha integrin subunits, of which alpha-1, alpha-4, alpha-5 and alpha-v appear to be widely expressed, like the beta-1 subunit, on emigrating NCC;[63-65,67,68,70] alpha-6 and alpha-7 appear on subsets of cranial[71] or trunk[72] NCC respectively. Some alterations in ECM molecules have been observed in HSCR patients,[66] although their distribution may be a secondary effect of changes in intestinal architecture rather than causative. In mouse and chick models, the alpha-4 subunit and its specific binding site to fibronectin are needed for normal NCC emigration from the neural tube to occur.[64]

If the recently identified role of ephrin signaling is a typical example, mutations in any of these adhesion molecules should affect NCC derivatives but are likely to lead to broader polymalformative syndromes. Binding of ephrinB to its receptor, EphB, leads to contact-mediated repulsion by the bilateral activation of protease activity and the rapid release of adhesion via the integrins.[73,74] Human and mouse mutations in the *EPHRB* (ephrinB) gene lead to severe clinical effects on NCC derivatives such as the skull (coronal craniosynostosis), the palate and the face, but also lead to effects on the chest and limb skeleton and fingernails; this association is known as craniofrontonasal syndrome).[75,76]

Differentiation of NCC

The restriction of the ability of NCC to develop into the various lineages begins before migration. In vivo, cranial NCC are distinct in their potential from trunk-level NCC. The cranial crest lineages include mesectoderm derivatives such as bone, cartilage, teeth, adipocytes, dermis, glandular and vascular connective tissue and smooth muscle, as well as the possibility to become all other derivatives of trunk NCC if transplanted into the appropriate location in the body.[77] Only after a long sojourn in vitro and apparent reprogramming can trunk NCC acquire some chondrogenic ability.[78]

The subsequent refinement of the different classes of NCC derivatives is done over time in different locations in the body. We have judged it convenient to address the involvement of the three major gene groups sequentially. However, it is important to keep in mind that any individual NCC is subject to interactions between these gene cascades as it differentiates and its increasingly fate-restricted progeny proliferate. Genes affecting pigmentation, neural differentiation or the establishment of cardiocephalic structures are grouped separately simply for the purpose of discussion.

The Pigmentation Gene Cascade

In vitro, embryonic NCC will give rise over successive generations to a mix of stem-like cells with varying degrees of potential to differentiate into all or only some NCC derivatives.[13] In particular, the bipotent glia-melanocyte precursor[79] as well as a tripotent melanocyte-neural-adrenergic precursor[80] have been shown to proliferate and expand preferentially in the presence of endothelin-3 (EDN3). The three known endothelins are peptides, first identified by their potent vasoconstrictive activity on vascular smooth muscle, but soon understood to be mitogens for melanocytes.[81]

Deletion of the mouse endothelin type B receptor (*Ednrb*) gene produces an autosomal recessive phenotype of white spotting and megacolon, bringing to light the critical role of endothelins in melanocytic and enteric development.[82] Mutations in human *EDNRB* lead to HSCR isolated or syndromic (WS4), according to the type and copy number of the mutation.[83-85] A patient with HSCR, heterozygous for weak hypomorphic mutations in both the *RET* receptor gene (see the "neural selector" group below) and *EDNRB*, has recently been reported.[86] Each mutation was inherited from a healthy parent. Interestingly, overexpression of EDNRB is sufficient to direct NCC-like migration in vivo and melanocytic differentiation in noncommitted embryonic stem cells.[61]

Although EDNRB can bind all three EDNs, only EDN3 is a physiologically relevant ligand in the enteric environment.[87] Homozygous EDN3 mutations have also been found in patients with WS4.[88] Mutant heterozygotes in one of these families were either unaffected or had mild

pigmentary anomalies, as did other untested family members. In addition, an EDN3 frameshift mutation has been identified in a patient with CCHS and chronic constipation.[89] Thus, distinct human tissues—melanocytes versus components of the autonomic nervous system—appear to have different sensitivities to EDN3/EDNRB dosage.

EDNRB, like many other growth factor receptors, transduces its activation to nuclear targets via the Ras signaling cascade. N-ras is a direct component of the MAPK/Erk pathway but also can activate phosphatidylinositol-3-kinase and its targets.[90] Ras molecules in general activate the mitogen-activated protein (MAP) kinase pathway to induce proliferation; EDNRB binding also counters apoptosis through the parallel activation of phosphatidylinositol-3-kinase. Two important molecules in the formation of nevi appear to be N-RAS and the next effector in the MAP kinase pathway, B-RAF. An early indication of *B-raf* function came from the initial knockout mice in which endothelial cells underwent abnormal differentiation and did not organize into mature, functional blood vessels,[91] as happens in numerous models with mutated growth factor receptors. However, it was upon the recent demonstration that reproducible mutations in *BRAF* were involved in highly diverse cancers, malignant melanoma in particular,[92,93] and, surprisingly, in a number of clinically benign nevi,[94] that a more specific role of this molecule in the development of NCC derivatives began to be explored.

The activating mutation of *BRAF* found most frequently in humans was specifically expressed in zebrafish melanophores experimentally. While wild-type *B-Raf* did not change the pigmentation of the zebrafish, the activated form of the gene led to the appearance of nevus-like clusters of pigment covering large areas, up to 40% of the body surface.[95] This was the first animal model of nevus formation. Crossing these fish to those deficient in the tumor suppressor p53 (product of the *CDKN2A* gene) led to the development of aggressively invasive melanoma in which the MAPK/Erk pathway was unduly active.

Dominant mutations of the *PAX3* transcription factor and the *MITF* (Microphthalmia-associated transcription factor) genes have been reported in WS1, WS2 or Tietz syndrome[96] (MIM 103500). In the mouse, *Pax3* is critical for skeletal muscle development as well as the development of the dorsal neural tube and the NCC that migrate from it.[97] *Mitf*, *Trp-1* (tyrosinase-related protein-1) and the tyrosine kinase receptor *c-met*, all expressed in melanocytes, appear to be transcriptional targets of Pax3.[51,98,99]

WS4 patients can also carry mutations of the Sry-type HMG box family transcription factor member, *SOX10*. This implies some interaction between endothelin signaling and Sox10 transcriptional effects. Indeed, *Sox10* is expressed in premigratory NCC, then in both melanocytes and enteric ganglia, as well as in glia of both CNS and PNS origin.[100] It is involved in cell lineage determination and is capable of transactivating *MITF* synergistically with *PAX3*.[101,102] *SOX10* mutations can cause either WS4[53] or PCWH:[36] Translated, mutant Sox10 proteins, whose mRNAs are *not* degraded by the nonsense-mediated decay pathway, lead to the more severe form associated with peripheral neuropathy. Mere haploinsufficiency through the proper degradation of mutant *SOX10* mRNAs leads to WS4.[36] Combined with the observed lack of *Ednrb* transcripts in mice with a truncating mutation of *Sox10*,[103] one might postulate that yet unidentified genes regulate the different response of melanocytes[104] or glia versus precursor NCC to *Sox10* dosage, and that *Ednrb* lies downstream of both *Sox10* and these other genes. Indeed, additional modifying loci for aganglionosis have been identified recently in mice.[105,106] Misregulated control of mRNA degradation is likely to be found with increasing frequency in human pathology and offers an additional explanation for how different mutations in the same gene can result in very distinct diseases, especially for master regulatory transcription factors of development.

The Neural Selector Gene Cascade

The *Drosophila achaete-scute* complex is a cluster of four proneural genes coding for basic helix-loop-helix domain-containing transcription factors achaete, scute, lethal of scute and asense.[107] The complex controls early development of both the central and peripheral nervous

system in the insect by instructing the differentiation of neuroblasts from ectodermal precursors. In the mouse, two homologues of the *achaete-scute* complex (ash) are known as *Mash-1* and *Mash-2*.[108] *Mash-2* is an imprinted gene expressed only in the trophoblast lineage.[109] In contrast, *Mash-1* expression is restricted to the CNS and PNS within a restricted spatiotemporal window.[110] The entire ventricular zone of the CNS expresses *Mash-1* at one point or another during the proliferation of neurectodermal precursors. The enteric and sympathetic neurons of the PNS also express *Mash-1*.[111] Homozygous *Mash-1* knockout mice die within the day following birth due to respiratory failure and inability to suckle.[112] The PNS is dramatically affected with an absence of the sympathetic and parasympathetic ganglia as well as the esophageal enteric neurons. Mash-1, like its evolutionary forerunner, has proneural properties.[113,114]

The human homologue to Mash1, *HASH1*, is a small, two-exon gene localized at 12q24. It is involved in a feedback loop with the PHOX2 (paired homeobox 2) homeodomain-containing transcription factors. *PHOX2A* and *PHOX2B* are very similar in their homeodomains but divergent in their promoters. Both are expressed in all CNS or PNS neurons that embark upon the noradrenergic synthesis pathway, be it temporarily or permanently.[115] They are both found in the branchiomotor and visceromotor neurons and the motor tracts of cranial nerves VII, IX and X. Only *PHOX2A* is expressed in the nuclei corresponding to cranial nerves III and IV. In the autonomic nervous system, *Phox2b* has been shown to act upstream of *Mash1*[116] and *Phox2a*,[115,117] but the feedback control of *Phox* genes by *Mash1* is not direct.[118]

Mutations in *PHOX2B* have recently been shown to be responsible for CCHS[37] but, according to the type of mutation, also can predispose to neuroblastoma or HSCR.[38,119] Phox2b promotes cell cycle exit and neuronal differentiation in the sympatho-adrenal lineage (ref). Downstream, *Phox2b* directly binds the promoter of the dopamine beta-hydroxylase (*DBH*) gene (the key enzyme of noradrenaline synthesis)[120] and, indirectly, activates *TH* (tyrosine hydroxylase)[121] and the *Ret* receptor tyrosine kinase, which is the major gene involved in HSCR, MEN2 syndromes and isolated pheochromocytoma (see below). *Phox2b*+/- mice present a dysfunction of their respiratory system that is similar to the one observed in CCHS patients, although it remains mild and transient.[122,123] They do display a temporarily altered response to hypoxia and hypercapnia[122] as well as sleep-disordered breathing (apnea and hypoventilation).[123] Ventilatory changes induced by hypoxia are mediated by afferents from carotid body glomus cells to the nucleus of the solitary tract (nTS) via the IXth cranial ganglion, where tyrosine hydroxylase (TH) expression is significantly decreased during the same period. All of these structures express *Phox2b* in mice[115,121] and humans[37] and fail to form or degenerate in *Phox2b*-/- mouse mutants.[116]

Most patients with *RET* mutations have HSCR only, but some develop pheochromocytoma or MEN2. A multiplicative oligogenic model with three loci has been proposed for isolated, nonsyndromic HSCR, with *RET* being the major susceptibility gene and the two other genes remaining to be identified.[124] The RET mutations identified in HSCR are unique and occur throughout the gene. This is in contrast to MEN2A, for which RET mutations occur in a cluster of six cysteines,[125-127] and MEN2B, which is uniquely associated with an M918T mutation.[128,129] Remarkably, some HSCR mutations occur at the same cysteines as the ones involved in MEN2A. *RET* mutations in MEN2 are activating mutations which constitutively dimerize the receptor, leading to transformation,[130] while those in HSCR are generally inactivating mutations which lead to misfolding or failure to transport the protein to the cell surface. The identification of HSCR patients with *RET* deletions[131] argues in favor of haploinsufficiency as a mechanism for pathogenesis. Consequently, although a MEN2A/MTC-type activating mutation has been observed in HSCR, haploinsufficiency may have occurred due to inefficient transport to the cell surface[132] at a key period in enteric development.

In mice, the Ret signaling pathway is implicated in the development of all noradrenergic derivatives[133,134] as well as the kidney, an organ rarely affected in human mutations of *RET*.[135] Likewise, a major ligand for RET, GDNF (glial-derived neurotrophic factor), is exceptionally responsible for HSCR,[136] but in mice it is essential for both enteric nervous system and renal

development.[134] GDNF, being a TGF-β related protein, is unusual in activating RET only in the presence of a glycosylphosphatidylinositol (GPI)-linked coreceptor, GFRA1. No mutations in GFRA1 have been discovered despite a careful search for variants in HSCR patients with similar phenotypes to Gfra1$^{-/-}$ mice.[137-139] Four structurally related GPI-linked coreceptors, GFRA1-4, and four related soluble growth factors, GDNF, neurturin (NTN), persephin (PSPN) and artemin, have been identified to date (reviewed in ref. 140). Of these, one family with a putative *NTN* mutation, in conjunction with a *RET* mutation, has been identified.[141] Like GDNF, NTN does not appear to have a major effect on HSCR and probably can only exert its mutational effect in conjunction with other disruptions of RET signaling.

Genetic interactions between *RET* and *EDNRB*/*EDN3* have been demonstrated in both humans and mice for the HSCR phenotype.[142,143] Indeed, similar interactions of many of the molecules in the pigmentation group with those of the neural selector group lead to the conclusion that a wide and complex cascade of events fine-tunes NCC differentiation. For instance, while human *BRAF* and *NRAS* mutations are causal in nevogenesis and formation of melanoma as mentioned above, *A-Raf* null mice have megacolon.[144] However, *A-raf*-deficient fibroblasts are able to maintain normal signalling through the MAPK/Erk pathway via increased activity in *B-raf* and *Raf-1*,[145] implicating target genes in the appropriate differentiation of neurons, glia and melanocytes from their common progenitor.

The Cardio-Cephalic Gene Cascade

In the 1980's and 1990's, experimental embryologists demonstrated that ablation of most or all posterior cephalic NCC phenocopies many of the aspects of the 22q11.2 deletion syndromes (DiGeorge; MIM 188400).[7,8,146] For many years, these results were interpreted to mean that NCC deficiency was directly responsible for outflow tract and caudal pharyngeal arch anomalies, especially since the affected structures had long been known to have a significant NCC component (although transient in the heart[3]). However, it was recently discovered that the pharyngeal endoderm is responsible for the survival and patterning of cephalic NCC.[19] This nonautonomous effect may initially be due to early mesendodermal production of retinoic acid[147,148] and subsequent activation of transcription factors regulating rostrocaudal identity, the *Hox* genes, in nested domains within surrounding tissues (reviewed in ref. 149), and finally the production of secreted signaling molecules such as Sonic hedgehog (Shh) or FGFs.[150,151]

FGF8 (one of >23 different FGFs), on chromosome 10q24, is transcribed during neurulation by the paraxial mesoderm and, later, by defined regions of the forebrain and cerebellar primordia, facial ectoderm and pharyngeal endoderm.[151] In animal models, a second wave of retinoic acid synthesis in these latter epithelia is responsible for the spatiotemporal coordination of Fgf8 localization with Shh.[150] Mutations in *Shh*, in genes coding for enzymes responsible for its biosynthesis, or in components of its intracellular signaling cascade lead to holoprosencephaly and fusion of the retinal fields (from hypotelorism to cyclopia, reviewed in ref. 152). Absence of cephalic NCC, exposure to high levels of maternal ethanol or maternal diabetes can also lead to a holoprosencephalic phenotype.[153-155]

Among its many roles, Fgf8 both induces and maintains proliferation of cephalic NCC.[45,156] *Fgf8* haploinsufficiency in mice gives rise to an intriguing spectrum of malformations also recalling that of 22q11.2 chromosomal deletions in humans.[151,157] All mutants, with *Fgf8* levels intermediate between a half and full dose, have micrognathia, many have cleft palate, otic ossicle and external ear anomalies and all mutants have central nervous system malformations, including hypoplasia or aplasia of the cerebellum and olfactory bulbs. Nearly all have outflow tract defects of the heart, including persistent truncus arteriosus, and hypoplasic or aplasic thymus and parathyroid glands.

Fgf10, another member of this large family of growth factors, signals through a different splice isoform of the same receptor as Fgf8, and is present in many organs where epithelia bud into *Fgf10*-expressing mesenchyme: lung, spleen, teeth, pituitary, salivary and lachrymal glands. Interestingly, in the developing limb bud, pharyngeal arches and heart, and pituitary gland, *Fgf10* and *Fgf8* lie within an autoregulatory loop controlling each other's expression.[157,158]

Tbx1, a T-box and homeodomain-containing transcription factor directly produced by the pharyngeal endoderm, is also expressed in the mesenchyme of the branchial arches and rostral head, in discrete areas of the outflow tract of the heart, in the ventral otocyst and sclerotome in both mouse[159-161] and human embryos (HCE, unpublished observations). *Tbx1* is a target of Shh signaling in the pharyngeal endoderm.[162]

Given that it is physically located in the 22q11.2 critical interval for DiGeorge syndrome, it had long been thought to be the best candidate gene. Recent efforts have identified *TBX1* mutations in DiGeorge patients.[163,164] *Tbx1* haploinsufficiency in mice affects the remodeling of the definitive aorta at the level of the fourth aortic arch and conotruncal septation in the heart.[165] These mice also have malformed, tiny external ears as in DiGeorge syndrome.[159]

Recently, it was demonstrated that *Tbx1* affects morphogenesis of the great vessels of the heart in a non cell-autonomous manner, meaning that its normal transcription affects the function of another, secreted mediator of its activity.[166] Tbx1 directly upregulates the transcription of *Fgf10*, and *Tbx1*$^{-/-}$ mice lack *Fgf10* expression specifically in the mesoderm of the secondary heart field.[165,166] Fgf10 normally maintains the proliferation and incorporation of myocytes from the splanchnic mesoderm into the outflow tract region of the growing cardiac tube.[167] Likewise, *Tbx1*$^{-/-}$ mice lack pharyngeal endodermal expression of *Fgf8*, probably similarly responsible for the proliferation of the rhombencephalic neural crest cells necessary for colonization of the outflow tract and subsequent mediation of correct septation.

Neurocristopathies affecting the cardiocephalic pole often leave their most visible mark on the face, since most facial tissues (bone, cartilage, teeth, vascular walls, and dermis) are direct NCC derivatives. In addition, when cephalic NCC are reduced in number or completely ablated in the embryonic chicken, other non NCC elements such as the forebrain, the pituitary gland, the thymus or facial muscles are themselves severely hypoplasic or absent.[7,153] Compromised pituitary function or holoprosencephaly can therefore be considered to be part of the spectrum of cephalic neurocristopathies, in the way that malformations of the heart outflow tract have long been admitted to be. Indeed, numerous forebrain and premaxillary nasofrontal malformations are frequently reported in association with human pituitary deficiencies (reviewed in ref. 39). The NCC surrounding the forebrain are supported in their proliferation and survival by a localized source of Fgf8 at the anterior neural ridge and, in return, maintain that source for forebrain outgrowth to take place (ref. 156 and S. Creuzet, personal communication).

Part of the patterning activity of cephalic NCC on non NCC head elements can be accounted for by the secretion of proteins belonging to other well-known signaling cascades as well. Cephalic NCC synthesize the BMP antagonists Gremlin and Noggin[168] and the Wnt antagonist Frzb.[49] Frzb acts by inhibiting the canonical Wnt signaling pathway via beta-catenin, which is normally activated by the local expression of *Wnt-3a* by the dorsal neural tube and/or *Wnt-2b/Wnt-13* by the facial ectoderm.[168] Recently, it has been demonstrated that induction of migratory behavior only takes place upon the reception of a noncanonical Wnt11 signal, again synthesized by the ectoderm, by Frizzled-7 receptors on NCC.[46]

The phenotypic spectrum of the murine *Fgf8* hypomorphs resembles CHARGE syndrome (MIM 214800) as much, if not more, than DiGeorge syndrome.[151] The acronym CHARGE refers to an association of congenital malformations first described by Hall et al[169] including ocular Coloboma, Heart outflow tract malformations, choanal Atresia, Retarded growth and mental development, Genital hypoplasia, Ear abnormalities and/or deafness. The *CHD7* gene has recently been shown to be mutated in 60% of CHARGE postnatal patients[170] and 100% of prenatally diagnosed patients.[171] *CHD7* belongs to a family of proteins thought to play a role in chromatin organization through their conserved chromodomain (reviewed in refs. 172,173). Chromodomain-containing proteins maintain a silencing, heterochromatin-like structure around such embryologically important genes as the *HOX* transcription factor clusters or tumor suppressors like *CDKN2A*.[174] In addition, CHD subfamily members also contain a helicase-ATPase domain that is directly involved in histone deacetylation.[175] Indirect targets of CHD7 activity in the cardiocephalic pole, given their phenotypes in mouse inactivation

models, are likely to include some of the genes previously investigated as candidates for CHARGE or DiGeorge syndrome such as *TBX1*, among others.

Discussion

Cooption of Developmental Gene Cascades during Evolution and Teratogens

Many syndromic neurocristopathies also affect tissues that are not directly derived from the neural crest. Nearly all genes identified as involved in seemingly isolated neurocristopathies are well known in the development of other, non NCC derivatives. The primary reason for these observations is that molecular cascades are conserved and coopted for new purposes during embryonic development of diverging species over the course of evolution. (The secondary reason has involved the historical inclusion or exclusion of given clinical entities in the definition of a neurocristopathy, as discussed earlier). Indeed, molecular inroads into the mechanisms of development are blurring the distinction between what is or is not a neurocristopathy so that it is probably a more useful term for clinicians than for embryologists or molecular biologists.

In various instances, neurocristopathies arise from embryonic exposure to teratogens such as vitamin A derivatives, high maternal blood glucose, cyclopamine or ethanol. Retinoic embryopathy MIM 243430, is a distinct clinical entity associating conotruncal heart or great artery defects, micrognathia and malformed external ears, and posterior fossa malformations. Known effects on the hedgehog signaling pathway by retinoic acid[147,148,150] or cyclopamine[176] contrast in their specificity with more general possible effects on mitochondrial respiration and oxygen management,[177-179] to which migrating, undifferentiated cells such as the NCC could be more vulnerable. Thus, environmental teratogens particularly affect NCC by coopting those genetic programs used to maintain plasticity and adaptation in NCC during the course of vertebrate evolution.

Neurocristopathy Genetics in Mouse and Man

Many mouse models for HSCR, carrying mutations in known HSCR or WS genes, do not transmit the phenotype in the same way as in humans. Full phenotypic penetrance is usually observed in the mouse models and generally not in humans, as there is enormous intra- and inter-familial variation in presentation. This observation can be explained by the fact that mouse models are made on homogeneous backgrounds, which is not the case within even a given human family. Thus, the expression of phenotype is subject to variations in genetic background. In addition, many of the mouse models are made with homozygous null mutations, whereas most HSCR patients have heterozygous mutations that range in potency from weak hypomorphic changes to complete loss of function. The conclusion that HSCR is a genetically heterogeneous, oligogenic disease is now uncontested. HSCR is the best studied neurocristopathy from a genetic point of view, but its complex inheritance is likely to apply to other neurocristopathies affecting the same subset of NCC derivatives.

Malformations and Carcinogenesis

It has long been suspected that, depending on the nature of gene mutations or on the gene series involved, mutations of developmental pathways in humans may result in either malformative syndromes or cancer predispositions. The field of neurocristopathies has already been been rewarding for that hypothesis, with the following examples: (i) RET mutations in HSCR and in MEN2 syndromes; (ii) PHOX2B gene mutation in CCHS and neuroblastoma; (iii) BRAF and NRAS mutations in congenital naevi, lung and prostate cancers and melanoma; (iv) FOXC1 mutations in Rieger syndrome and rhabdomyosarcoma;[180] (v) *PAX3* mutations in WS and its fusion to *FOXO1*, also in rhabdomyosarcoma;[99,181] (vi) SNAI2 mutations in WS and a likely role in leukemia (reviewed in ref. 182). Clearly, the identification of new genes involved in rare congenital malformations will ultimately continue to bear fruit in the wide field of cancer research.

Acknowledgements

The authors are supported by the Institut National de la Santé et de la Recherche Médicale (and its *Avenir* program), the Association pour la Recherche sur le Cancer, the Association Française contre les Myopathies and Assistance Publique – Hôpitaux de Paris. We especially thank Drs. Michel Vekemans, Linda Gibbs, Sophie Thomas, Tania Attié-Bitach, Gérard Couly and Arnold Munnich for their insight and assistance. HCE dedicates this work to the memory of Christiane Ayer-Le Lièvre, a dedicated and much regretted researcher who performed seminal experimental studies on the plasticity of the neural crest.

References

1. Le Douarin N, Kalcheim C. The Neural Crest. 2nd ed. Cambridge: Cambridge University Press, 1999.
2. Johnston MC. A radioautographic study of the migration and fate of cranial neural crest cells in the chick embryo. Anat Rec 1966; 156(2):143-155.
3. Le Lievre CS, Le Douarin NM. Mesenchymal derivatives of the neural crest: Analysis of chimaeric quail and chick embryos. J Embryol Exp Morphol 1975; 34(1):125-154.
4. Couly GF, Coltey PM, Le Douarin NM. The triple origin of skull in higher vertebrates: A study in quail-chick chimeras. Development 1993; 117(2):409-429.
5. Köntges G, Lumsden A. Rhombencephalic neural crest segmentation is preserved throughout craniofacial ontogeny. Development 1996; 122(10):3229-3242.
6. Noden DM. The role of the neural crest in patterning of avian cranial skeletal, connective, and muscle tissues. Dev Biol 1983; 96(1):144-165.
7. Bockman DE, Kirby ML. Dependence of thymus development on derivatives of the neural crest. Science 1984; 223(4635):498-500.
8. Bockman DE, Redmond ME, Waldo K et al. Effect of neural crest ablation on development of the heart and arch arteries in the chick. Am J Anat 1987; 180(4):332-341.
9. Etchevers HC, Vincent C, Le Douarin NM et al. The cephalic neural crest provides pericytes and smooth muscle cells to all blood vessels of the face and forebrain. Development 2001; 128(7):1059-1068.
10. Kruger GM, Morrison S. Neural crest stem cells persist in the adult gut but undergo changes in self-renewal, neuronal subtype potential, and factor responsiveness. Neuron 2002; 35(4):657-669.
11. Dupin E, Real C, Glavieux-Pardanaud C et al. Reversal of developmental restrictions in neural crest lineages: Transition from Schwann cells to glial-melanocytic precursors in vitro. Proc Natl Acad Sci USA 2003; 100(9):5229-5233.
12. Real C, Glavieux-Pardanaud C, Vaigot P et al. The instability of the neural crest phenotypes: Schwann cells can differentiate into myofibroblasts. Int J Dev Biol 2005; 49(2-3):151-159.
13. Trentin A, Glavieux-Pardanaud C, Le Douarin NM et al. Self-renewal capacity is a widespread property of various types of neural crest precursor cells. Proc Natl Acad Sci USA 2004; 101(13):4495-4500.
14. Liebl DJ, Tessarollo L, Palko ME et al. Absence of sensory neurons before target innervation in brain-derived neurotrophic factor-, neurotrophin 3-, and TrkC-deficient embryonic mice. J Neurosci 1997; 17(23):9113-9121.
15. Chalazonitis A. Neurotrophin-3 in the development of the enteric nervous system. Prog Brain Res 2004; 146:243-263.
16. Creuzet S, Couly G, Vincent C et al. Negative effect of Hox gene expression on the development of the neural crest-derived facial skeleton. Development 2002; 129(18):4301-4313.
17. Schneider RA, Helms JA. The cellular and molecular origins of beak morphology. Science 2003; 299(5606):565-568.
18. Ruhin B, Creuzet S, Vincent C et al. Patterning of the hyoid cartilage depends upon signals arising from the ventral foregut endoderm. Dev Dyn 2003; 228(2):239-246.
19. Couly G, Creuzet S, Bennaceur S et al. Interactions between Hox-negative cephalic neural crest cells and the foregut endoderm in patterning the facial skeleton in the vertebrate head. Development 2002; 129(4):1061-1073.
20. Bolande RP. The neurocristopathies: A unifying concept of disease arising in neural crest maldevelopment. Hum Pathol 1974; 5:409-429.
21. Meulemans D, Bronner-Fraser M. Central role of gene cooption in neural crest evolution. J Exp Zoolog B Mol Dev Evol 2005; 304B(4):298-303.
22. Jeffery WR, Strickler AG, Yamamoto Y. Migratory neural crest-like cells form body pigmentation in a urochordate embryo. Nature 2004; 431(7009):696-699.

23. Cebra-Thomas J, Tan F, Sistla S et al. How the turtle forms its shell: A paracrine hypothesis of carapace formation. J Exp Zoolog B Mol Dev Evol 2005.
24. Weinstein JL, Katzenstein HM, Cohn SL. Advances in the diagnosis and treatment of neuroblastoma. Oncologist 2003; 8(3):278-292.
25. Heutink P, van der Mey AG, Sandkuijl LA et al. A gene subject to genomic imprinting and responsible for hereditary paragangliomas maps to chromosome 11q23-qter. Hum Mol Genet 1992; 1(1):7-10.
26. Akhtar S, Oza KK, Wright J. Merkel cell carcinoma: Report of 10 cases and review of the literature. J Am Acad Dermatol 2000; 43(5 Pt 1):755-767.
27. Goessling W, McKee PH, Mayer RJ. Merkel cell carcinoma. J Clin Oncol 2002; 20(2):588-598.
28. Antoniades K, Giannouli T, Kaisaridou D. Merkel cell carcinoma in a patient with Recklinghausen neurofibromatosis. Int J Oral Maxillofac Surg 1998; 27(3):213-214.
29. Szeder V, Grim M, Halata Z et al. Neural crest origin of mammalian Merkel cells. Dev Biol 2003; 253(2):258-263.
30. Baker CV, Bronner-Fraser M. The origins of the neural crest. Part II: An evolutionary perspective. Mech Dev 1997; 69(1-2):13-29.
31. Detrait ER, George TM, Etchevers HC et al. Human neural tube defects: Developmental biology, epidemiology, and genetics. Neurotoxicol Teratol 2005; 27(3):515-524.
32. Swenson O, Sherman JO, Fisher JH et al. The treatment and postoperative complications of congenital megacolon: A 25 year followup. Ann Surg 1975; 182(3):266-273.
33. Passarge E. The genetics of Hirschsprung's disease: Evidence for heterogeneous etiology and a study of sixty-three families. Eng J Med 1967; 276:138-143.
34. Etchevers HC, Couly G, Le Douarin NM. Morphogenesis of the branchial vascular sector. Trends Cardiovasc Med 2002; 12(7):299-304.
35. Danarti R, Konig A, Happle R. Large congenital melanocytic nevi may reflect paradominant inheritance implying allelic loss. Eur J Dermatol 2003; 13(5):430-432.
36. Inoue K, Khajavi M, Ohyama T et al. Molecular mechanism for distinct neurological phenotypes conveyed by allelic truncating mutations. Nat Genet 2004; 36(4):361-369.
37. Amiel J, Laudier B, Attie-Bitach T et al. Polyalanine expansion and frameshift mutations of the paired-like homeobox gene PHOX2B in congenital central hypoventilation syndrome. Nat Genet 2003; 33(4):459-461.
38. Trochet D, Bourdeaut F, Janoueix-Lerosey I et al. Germline mutations of the paired-like homeobox 2B (PHOX2B) gene in neuroblastoma. Am J Hum Genet 2004; 74(4):761-764.
39. Etchevers HC, Vincent C, Couly GF. Neural crest and pituitary development. In: Rappaport R, ed. Hypothalamic-Pituitary Development: Genetic and Clinical Aspects. Basel: Karger, 2001:13-29.
40. Clifton-Bligh RJ, Wentworth JM, Heinz P et al. Mutation of the gene encoding human TTF-2 associated with thyroid agenesis, cleft palate and choanal atresia. Nat Genet 1998; 19(4):399-401.
41. Baker CV, Bronner-Fraser M. The origins of the neural crest. Part I: Embryonic induction. Mech Dev 1997; 69(1-2):3-11.
42. Huang X, Saint-Jeannet JP. Induction of the neural crest and the opportunities of life on the edge. Dev Biol 2004; 275(1):1-11.
43. Aybar MJ, Mayor R. Early induction of neural crest cells: Lessons learned from frog, fish and chick. Curr Opin Genet Dev 2002; 12(4):452-458.
44. Sato T, Sasai N, Sasai Y. Neural crest determination by coactivation of Pax3 and Zic1 genes in Xenopus ectoderm. Development 2005; 132(10):2355-2363.
45. Monsoro-Burq AH, Wang E, Harland R. Msx1 and Pax3 cooperate to mediate FGF8 and WNT signals during Xenopus neural crest induction. Dev Cell 2005; 8(2):167-178.
46. De Calisto J, Araya C, Marchant L et al. Essential role of noncanonical Wnt signalling in neural crest migration. Development 2005; 132(11):2587-2597.
47. Cheung M, Chaboissier MC, Mynett A et al. The transcriptional control of trunk neural crest induction, survival, and delamination. Dev Cell 2005; 8(2):179-192.
48. Lewis JL, Bonner J, Modrell M et al. Reiterated Wnt signaling during zebrafish neural crest development. Development 2004; 131(6):1299-1308.
49. Duprez D, Leyns L, Bonnin MA et al. Expression of Frzb-1 during chick development. Mech Dev 1999; 89(1-2):179-183.
50. Dow E, Cross S, Wolgemuth DJ et al. Second locus for Hirschsprung disease/Waardenburg syndrome in a large Mennonite kindred. Am J Med Genet 1994; 53(1):75-80.
51. Watanabe A, Takeda K, Ploplis B et al. Epistatic relationship between Waardenburg syndrome genes MITF and PAX3. Nat Genet 1998; 18(3):283-286.
52. Sanchez-Martin M, Rodriguez-Garcia A, Perez-Losada J et al. SLUG (SNAI2) deletions in patients with Waardenburg disease. Hum Mol Genet 2002; 11(25):3231-3236.

53. Pingault V, Bondurand N, Kuhlbrodt K et al. SOX10 mutations in patients with Waardenburg-Hirschsprung disease. Nat Genet 1998; 18(2):171-173.
54. Epstein DJ, Malo D, Vekemans M et al. Molecular characterization of a deletion encompassing the splotch mutation on mouse chromosome 1. Genomics 1991; 10(1):89-93.
55. Baldwin CT, Hoth CF, Macina RA et al. Mutations in PAX3 that cause Waardenburg syndrome type I: Ten new mutations and review of the literature. Am J Med Genet 1995; 58(2):115-122.
56. Sanchez-Martin M, Perez-Losada J, Rodriguez-Garcia A et al. Deletion of the SLUG (SNAI2) gene results in human piebaldism. Am J Med Genet A 2003; 122(2):125-132.
57. Perez-Mancera PA, Gonzalez-Herrero I, Perez-Caro M et al. SLUG in cancer development. Oncogene 2005; 24(19):3073-3082.
58. Locascio A, Manzanares M, Blanco MJ et al. Modularity and reshuffling of Snail and Slug expression during vertebrate evolution. Proc Natl Acad Sci USA 2002; 99(26):16841-16846.
59. Davy A, Aubin J, Soriano P. Ephrin-B1 forward and reverse signaling are required during mouse development. Genes Dev 2004; 18(5):572-583.
60. Britsch S, Li L, Kirchhoff S et al. The ErbB2 and ErbB3 receptors and their ligand, neuregulin-1, are essential for development of the sympathetic nervous system. Genes Dev 1998; 12(12):1825-1836.
61. Pla P, Alberti C, Solov'eva O et al. Ednrb2 orients cell migration towards the dorsolateral neural crest pathway and promotes melanocyte differentiation. Pigment Cell Res 2005; 18(3):181-187.
62. Zhu L, Lee HO, Jordan CS et al. Spatiotemporal regulation of endothelin receptor-B by SOX10 in neural crest-derived enteric neuron precursors. Nat Genet 2004; 36(7):732-737.
63. Duband JL, Rocher S, Chen WT et al. Cell adhesion and migration in the early vertebrate embryo: Location and possible role of the putative fibronectin receptor complex. J Cell Biol 1986; 102(1):160-178.
64. Kil SH, Krull CE, Cann G et al. The alpha4 subunit of integrin is important for neural crest cell migration. Dev Biol 1998; 202(1):29-42.
65. Delannet M, Martin F, Bossy B et al. Specific roles of the alpha V beta 1, alpha V beta 3 and alpha V beta 5 integrins in avian neural crest cell adhesion and migration on vitronectin. Development 1994; 120(9):2687-2702.
66. Parikh D, Tam P, Van Velzen D et al. Abnormalities in the distribution of laminin and collagen type IV in Hirschsprung's disease. Gastroenterology 1992; 102:1236.
67. Perris R, Syfrig J, Paulsson M et al. Molecular mechanisms of neural crest cell attachment and migration on types I and IV collagen. J Cell Sci 1993; 106(Pt 4):1357-1368.
68. Lallier T, Bronner-Fraser M. Alpha 1 beta 1 integrin on neural crest cells recognizes some laminin substrata in a Ca(2+)-independent manner. J Cell Biol 1992; 119(5):1335-1345.
69. Desban N, Duband JL. Avian neural crest cell migration on laminin: Interaction of the alpha1beta1 integrin with distinct laminin-1 domains mediates different adhesive responses. J Cell Sci 1997; 110(Pt 21):2729-2744.
70. Bednarczyk JL, McIntyre BW. Expression and ligand-binding function of the integrin alpha 4 beta 1 (VLA-4) on neural-crest-derived tumor cell lines. Clin Exp Metastasis 1992; 10(4):281-290.
71. Lallier TE, Whittaker CA, DeSimone DW. Integrin alpha 6 expression is required for early nervous system development in Xenopus laevis. Development 1996; 122(8):2539-2554.
72. Kil SH, Bronner-Fraser M. Expression of the avian alpha 7-integrin in developing nervous system and myotome. Int J Dev Neurosci 1996; 14(3):181-190.
73. Zimmer M, Palmer A, Kohler J et al. EphB-ephrinB bi-directional endocytosis terminates adhesion allowing contact mediated repulsion. Nat Cell Biol 2003; 5(10):869-878.
74. Huynh-Do U, Vindis C, Liu H et al. Ephrin-B1 transduces signals to activate integrin-mediated migration, attachment and angiogenesis. J Cell Sci 2002; 115(Pt 15):3073-3081.
75. Wieland I, Reardon W, Jakubiczka S et al. Twenty-six novel EFNB1 mutations in familial and sporadic craniofrontonasal syndrome (CFNS). Hum Mutat 2005; 26(2):113-118.
76. Twigg SR, Kan R, Babbs C et al. Mutations of ephrin-B1 (EFNB1), a marker of tissue boundary formation, cause craniofrontonasal syndrome. Proc Natl Acad Sci USA 2004; 101(23):8652-8657.
77. Le Lievre CS, Schweizer GG, Ziller CM et al. Restrictions of developmental capabilities in neural crest cell derivatives as tested by in vivo transplantation experiments. Dev Biol 1980; 77(2):362-378.
78. Abzhanov A, Tzahor E, Lassar AB et al. Dissimilar regulation of cell differentiation in mesencephalic (cranial) and sacral (trunk) neural crest cells in vitro. Development 2003; 130(19):4567-4579.
79. Dupin E, Glavieux C, Vaigot P et al. Endothelin 3 induces the reversion of melanocytes to glia through a neural crest-derived glial-melanocytic progenitor. Proc Natl Acad Sci USA 2000; 97(14):7882-7887.
80. Stone JG, Spirling LI, Richardson MK. The neural crest population responding to endothelin-3 in vitro includes multipotent cells. J Cell Sci 1997; 110(Pt 14):1673-1682.

81. Imokawa G, Yada Y, Miyagishi M. Endothelins secreted from human keratinocytes are intrinsic mitogens for human melanocytes. J Biol Chem 1992; 267(34):24675-24680.
82. Hosoda K, Hammer RE, Richardson JA et al. Targeted and natural (piebald-lethal) mutations of endothelin-B receptor gene produce megacolon associated with spotted coat color in mice. Cell 1994; 79:1267.
83. Puffenberger EG, Hosoda K, Washington SS et al. A missense mutation of the endothelin-B receptor gene in multigenic Hirschsprung's disease. Cell 1994; 79:1257-1266.
84. Attie T, Till M, Pelet A et al. Mutation of the endothelin-receptor B gene in Waardenburg-Hirschsprung disease. Hum Mol Genet 1995; 4(12):2407-2409.
85. Amiel J, Attie T, Jan D et al. Heterozygous endothelin receptor B (EDNRB) mutations in isolated Hirschsprung disease. Hum Mol Genet 1996; 5(3):355-357.
86. Auricchio A, Griseri P, Carpentieri ML et al. Double heterozygosity for a RET substitution interfering with splicing and an EDNRB missense mutation in Hirschsprung disease. Am J Hum Genet 1999; 64:1216.
87. Bidaud C, Salomon R, Edery P et al. Mutations of the endothelin-3 gene in isolated and syndromic forms of Hirschsprung disease. Gastroenterol Clin Biol 1997; 21(8-9):548-554.
88. Edery P, Attie T, Amiel J et al. Mutation of the endothelin-3 gene in the Waardenburg-Hirschsprung disease (Shah-Waardenburg syndrome). Nat Genet 1996; 12(4):442-444.
89. Bolk S, Angrist M, Schwartz S et al. Congenital central hypoventilation syndrome: Mutation analysis of the receptor tyrosine kinase RET. Am J Med Genet 1996; 63:603-610.
90. Hu L, Shi Y, Hsu JH et al. Downstream effectors of oncogenic ras in multiple myeloma cells. Blood 2003; 101(8):3126-3135.
91. Wojnowski L, Zimmer AM, Beck TW et al. Endothelial apoptosis in Braf-deficient mice. Nat Genet 1997; 16(3):293-297.
92. Davies H, Bignell GR, Cox C et al. Mutations of the BRAF gene in human cancer. Nature 2002; 417(6892):949-954.
93. Brose MS, Volpe P, Feldman M et al. BRAF and RAS mutations in human lung cancer and melanoma. Cancer Res 2002; 62(23):6997-7000.
94. Pollock PM, Harper UL, Hansen KS et al. High frequency of BRAF mutations in nevi. Nat Genet 2003; 33(1):19-20.
95. Patton EE, Widlund HR, Kutok JL et al. BRAF mutations are sufficient to promote nevi formation and cooperate with p53 in the genesis of melanoma. Curr Biol 2005; 15(3):249-254.
96. Tassabehji M, Newton VE, Read AP. Waardenburg syndrome type 2 caused by mutations in the human microphthalmia (MITF) gene. Nat Genet 1994; 8(3):251-255.
97. Maroto M, Reshef R, Munsterberg AE et al. Ectopic Pax-3 activates MyoD and Myf-5 expression in embryonic mesoderm and neural tissue. Cell 1997; 89(1):139-148.
98. Galibert MD, Yavuzer U, Dexter TJ et al. Pax3 and regulation of the melanocyte-specific tyrosinase-related protein-1 promoter. J Biol Chem 1999; 274(38):26894-26900.
99. Relaix F, Polimeni M, Rocancourt D et al. The transcriptional activator PAX3-FKHR rescues the defects of Pax3 mutant mice but induces a myogenic gain-of-function phenotype with ligand-independent activation of Met signaling in vivo. Genes Dev 2003; 17(23):2950-2965.
100. Cheng Y, Cheung M, Abu-Elmagd MM et al. Chick sox10, a transcription factor expressed in both early neural crest cells and central nervous system. Brain Res Dev Brain Res 2000; 121(2):233-241.
101. Potterf SB, Furumura M, Dunn KJ et al. Transcription factor hierarchy in Waardenburg syndrome: Regulation of MITF expression by SOX10 and PAX3. Hum Genet 2000; 107(1):1-6.
102. Bondurand N, Pingault V, Goerich DE et al. Interaction among SOX10, PAX3 and MITF, three genes altered in Waardenburg syndrome. Hum Mol Genet 2000; 9(13):1907-1917.
103. Southard-Smith EM, Kos L, Pavan WJ. Sox10 mutation disrupts neural crest development in Dom Hirschsprung mouse model. Nat Genet 1998; 18(1):60-64.
104. Potterf SB, Mollaaghababa R, Hou L et al. Analysis of SOX10 function in neural crest-derived melanocyte development: SOX10-dependent transcriptional control of dopachrome tautomerase. Dev Biol 2001; 237(2):245-257.
105. Cantrell VA, Owens SE, Chandler RL et al. Interactions between Sox10 and EdnrB modulate penetrance and severity of aganglionosis in the Sox10Dom mouse model of Hirschsprung disease. Hum Mol Genet 2004; 13(19):2289-2301.
106. Owens SE, Broman KW, Wiltshire T et al. Genome-wide linkage identifies novel modifier loci of aganglionosis in the Sox10Dom model of Hirschsprung disease. Hum Mol Genet 2005; 14(11):1549-1558.
107. Campuzano S, Modolell J. Patterning of the Drosophila nervous system: The achaete-scute gene complex. Trends Genet 1992; 8(6):202-208.

108. Johnson JE, Birren SJ, Anderson DJ. Two rat homologues of Drosophila achaete-scute specifically expressed in neuronal precursors. Nature 1990; 346(6287):858-861.
109. Guillemot F, Caspary T, Tilghman SM et al. Genomic imprinting of Mash2, a mouse gene required for trophoblast development. Nat Genet 1995; 9(3):235-242.
110. Guillemot F, Joyner AL. Dynamic expression of the murine Achaete-Scute homologue Mash-1 in the developing nervous system. Mech Dev 1993; 42(3):171-185.
111. Lo LC, Johnson JE, Wuenschell CW et al. Mammalian achaete-scute homolog 1 is transiently expressed by spatially restricted subsets of early neuroepithelial and neural crest cells. Genes Dev 1991; 5(9):1524-1537.
112. Guillemot F, Lo LC, Johnson JE et al. Mammalian achaete-scute homolog 1 is required for the early development of olfactory and autonomic neurons. Cell 1993; 75(3):463-476.
113. Parras CM, Galli R, Britz O et al. Mash1 specifies neurons and oligodendrocytes in the postnatal brain. Embo J 2004; 23(22):4495-4505.
114. Pattyn A, Simplicio N, van Doorninck JH et al. Ascl1/Mash1 is required for the development of central serotonergic neurons. Nat Neurosci 2004; 7(6):589-595.
115. Pattyn A, Morin X, Cremer H et al. Expression and interactions of the two closely related homeobox genes Phox2a and Phox2b during neurogenesis. Development 1997; 124(20):4065-4075.
116. Pattyn A, Morin X, Cremer H et al. The homeobox gene Phox2b is essential for the development of autonomic neural crest derivatives. Nature 1999; 399(6734):366-370.
117. Hong SJ, Kim CH, Kim KS. Structural and functional characterization of the 5' upstream promoter of the human Phox2a gene: Possible direct transactivation by transcription factor Phox2b. J Neurochem 2001; 79(6):1225-1236.
118. Hirsch MR, Tiveron MC, Guillemot F et al. Control of noradrenergic differentiation and Phox2a expression by MASH1 in the central and peripheral nervous system. Development 1998; 125(4):599-608.
119. Trochet D, O'Brien LM, Gozal D et al. PHOX2B genotype allows for prediction of tumor risk in congenital central hypoventilation syndrome. Am J Hum Genet 2005; 76(3):421-426.
120. Yang C, Kim HS, Seo H et al. Paired-like homeodomain proteins, Phox2a and Phox2b, are responsible for noradrenergic cell-specific transcription of the dopamine beta-hydroxylase gene. J Neurochem 1998; 71(5):1813-1826.
121. Brosenitsch TA, Katz DM. Expression of Phox2 transcription factors and induction of the dopaminergic phenotype in primary sensory neurons. Mol Cell Neurosci 2002; 20(3):447-457.
122. Dauger S, Pattyn A, Lofaso F et al. Phox2b controls the development of peripheral chemoreceptors and afferent visceral pathways. Development 2003; 130(26):6635-6642.
123. Durand E, Dauger S, Pattyn A et al. Sleep-disordered breathing in newborn mice heterozygous for the transcription factor Phox2b. Am J Respir Crit Care Med 2005; 172(2):238-243.
124. Gabriel SB, Salomon R, Pelet A et al. Segregation at three loci explains familial and population risk in Hirschsprung disease. Nat Genet 2002; 31(1):89-93.
125. Edery P, Lyonnet S, Mulligan LM et al. Mutations of the RET proto-oncogene in Hirschsprung's disease. Nature 1994; 367:378-380.
126. Mulligan L, Kwok JB, Healey CS et al. Germ-line mutations of the RET proto-oncogene in multiple endocrine neoplasia type 2A. Nature 1993; 363(6428):458-460.
127. Mulligan LM, Eng C, Attie T et al. Diverse phenotypes associated with exon 10 mutations of the RET proto-oncogene. Hum Mol Genet 1994; 3(12):2163-2167.
128. Hofstra R, Landsvater RM, Ceccherini I et al. A mutation in the RET proto-oncogene associated with multiple endocrine neoplasia type 2B and sporadic medullary thyroid carcinoma. Nature 1994; 367:375.
129. Carlson K, Dou S, Chi D et al. Single missense mutation in the tyrosine kinase catalytic domain of the RET protooncogene is associated with multiple endocrine neoplasia type 2B. Proc Natl Acad Sci USA 1994; 15:1579.
130. Edery P, Eng C, Munnich A et al. RET in human development and oncogenesis. Bioessays 1997; 19(5):389-395.
131. Luo Y, Ceccherini I, Pasini B et al. Close linkage with the RET protooncogene and boundaries of deletion mutations in autosomal dominant Hirschsprung disease. Hum Mol Genet 1993; 2:1803.
132. Takahashi M, Iwashita T, Santoro M et al. Cosegregation of MEN2 and Hirschsprung's disease: The same mutation of RET with both gain and loss-of-function? Hum Mutat 1999; 13(4):331-336.
133. Durbec PL, Larsson-Blomberg LB, Schuchardt A et al. Common origin and developmental dependence on c-ret of subsets of enteric and sympathetic neuroblasts. Development 1996; 122(1):349-358.
134. Durbec P, Marcos-Gutierrez CV, Kilkenny C et al. GDNF signalling through the Ret receptor tyrosine kinase. Nature 1996; 381(6585):789-793.

135. Attie-Bitach T, Abitbol M, Gerard M et al. Expression of the RET proto-oncogene in human embryos. Am J Med Genet 1998; 80(5):481-486.
136. Ivanchuk SM, Myers SM, Eng C et al. De novo mutation of GDNF, ligand for the RET/GDNFR-alpha receptor complex, in Hirschsprung disease. Hum Mol Genet 1996; 5(12):2023-2026.
137. Angrist M, Jing S, Bolk S et al. Human GFRA1: Cloning, mapping, genomic structure, and evaluation as a candidate gene for Hirschsprung disease susceptibility. Genomics 1998; 48(3):354-362.
138. Myers SM, Salomon R, Goessling A et al. Investigation of germline GFR alpha-1 mutations in Hirschsprung disease. J Med Genet 1999; 36(3):217-220.
139. Borrego S, Fernandez RM, Dziema H et al. Investigation of germline GFRA4 mutations and evaluation of the involvement of GFRA1, GFRA2, GFRA3, and GFRA4 sequence variants in Hirschsprung disease. J Med Genet 2003; 40(3):e18.
140. Sariola H, Saarma M. Novel functions and signalling pathways for GDNF. J Cell Sci 2003; 116(Pt 19):3855-3862.
141. Doray B, Salomon R, Amiel J et al. Mutation of the RET ligand, neurturin, supports multigenic inheritance in Hirschsprung disease. Hum Mol Genet 1998; 7(9):1449-1452.
142. Carrasquillo MM, McCallion AS, Puffenberger EG et al. Genome-wide association study and mouse model identify interaction between RET and EDNRB pathways in Hirschsprung disease. Nat Genet 2002; 32(2):237-244.
143. McCallion AS, Stames E, Conlon RA et al. Phenotype variation in two-locus mouse models of Hirschsprung disease: Tissue-specific interaction between Ret and Ednrb. Proc Natl Acad Sci USA 2003; 100(4):1826-1831.
144. Pritchard CA, Bolin L, Slattery R et al. Post-natal lethality and neurological and gastrointestinal defects in mice with targeted disruption of the A-Raf protein kinase gene. Curr Biol 1996; 6(5):614-617.
145. Mercer K, Chiloeches A, Huser M et al. ERK signalling and oncogene transformation are not impaired in cells lacking A-Raf. Oncogene 2002; 21(3):347-355.
146. Kirby ML, Gale TF, Stewart DE. Neural crest cells contribute to normal aorticopulmonary septation. Science 1983; 220(4601):1059-1061.
147. Halilagic A, Zile MH, Studer M. A novel role for retinoids in patterning the avian forebrain during presomite stages. Development 2003; 130(10):2039-2050.
148. Bohnsack BL, Lai L, Dolle P et al. Signaling hierarchy downstream of retinoic acid that independently regulates vascular remodeling and endothelial cell proliferation. Genes Dev 2004; 18(11):1345-1358.
149. Santagati F, Rijli FM. Cranial neural crest and the building of the vertebrate head. Nat Rev Neurosci 2003; 4(10):806-818.
150. Schneider RA, Hu D, Rubenstein JL et al. Local retinoid signaling coordinates forebrain and facial morphogenesis by maintaining FGF8 and SHH. Development 2001; 128(14):2755-2767.
151. Abu-Issa R, Smyth G, Smoak I et al. Fgf8 is required for pharyngeal arch and cardiovascular development in the mouse. Development 2002; 129(19):4613-4625.
152. Lazaro L, Dubourg C, Pasquier L et al. Phenotypic and molecular variability of the holoprosencephalic spectrum. Am J Med Genet A 2004; 129(1):21-24.
153. Etchevers HC, Couly G, Vincent C et al. Anterior cephalic neural crest is required for forebrain viability. Development 1999; 126(16):3533-3543.
154. Blader P, Strahle U. Ethanol impairs migration of the prechordal plate in the zebrafish embryo. Dev Biol 1998; 201(2):185-201.
155. Barr Jr M, Hanson JW, Currey K et al. Holoprosencephaly in infants of diabetic mothers. J Pediatr 1983; 102(4):565-568.
156. Creuzet S, Schuler B, Couly G et al. Reciprocal relationships between Fgf8 and neural crest cells in facial and forebrain development. Proc Natl Acad Sci USA 2004; 101(14):4843-4847.
157. Frank DU, Fotheringham LK, Brewer JA et al. An Fgf8 mouse mutant phenocopies human 22q11 deletion syndrome. Development 2002; 129(19):4591-4603.
158. Boulet AM, Moon AM, Arenkiel BR et al. The roles of Fgf4 and Fgf8 in limb bud initiation and outgrowth. Dev Biol 2004; 273(2):361-372.
159. Jerome LA, Papaioannou VE. DiGeorge syndrome phenotype in mice mutant for the T-box gene, Tbx1. Nat Genet 2001; 27(3):286-291.
160. Lindsay EA, Vitelli F, Su H et al. Tbx1 haploinsufficieny in the DiGeorge syndrome region causes aortic arch defects in mice. Nature 2001; 410(6824):97-101.
161. Merscher S, Funke B, Epstein JA et al. TBX1 is responsible for cardiovascular defects in velo-cardio-facial/DiGeorge syndrome. Cell 2001; 104(4):619-629.

162. Yamagishi H, Maeda J, Hu T et al. Tbx1 is regulated by tissue-specific forkhead proteins through a common Sonic hedgehog-responsive enhancer. Genes Dev 2003; 17(2):269-281.
163. Yagi H, Furutani Y, Hamada H et al. Role of TBX1 in human del22q11.2 syndrome. Lancet 2003; 362(9393):1366-1373.
164. Baldini A. Dissecting contiguous gene defects: TBX1. Curr Opin Genet Dev 2005; 15(3):279-284.
165. Vitelli F, Taddei I, Morishima M et al. A genetic link between Tbx1 and fibroblast growth factor signaling. Development 2002; 129(19):4605-4611.
166. Xu H, Morishima M, Wylie JN et al. Tbx1 has a dual role in the morphogenesis of the cardiac outflow tract. Development 2004; 131(13):3217-3227.
167. Kelly RG, Brown NA, Buckingham ME. The arterial pole of the mouse heart forms from Fgf10-expressing cells in pharyngeal mesoderm. Dev Cell 2001; 1(3):435-440.
168. Tzahor E, Kempf H, Mootoosamy RC et al. Antagonists of Wnt and BMP signaling promote the formation of vertebrate head muscle. Genes Dev 2003; 17(24):3087-3099.
169. Hall BD. Choanal atresia and associated multiple anomalies. J Pediatr 1979; 95(3):395-398.
170. Vissers LE, van Ravenswaaij CM, Admiraal R et al. Mutations in a new member of the chromodomain gene family cause CHARGE syndrome. Nat Genet 2004; 36(9):955-957.
171. Sanlaville D, Etchevers HC, Gonzales M et al. Phenotypic spectrum of CHARGE syndrome in fetuses with CHD7 truncating mutations correlates with expression during human development. J Med Genet 2005; doi:10.1136/jmg.2005.036160.
172. Jones DO, Cowell IG, Singh PB. Mammalian chromodomain proteins: Their role in genome organisation and expression. Bioessays 2000; 22(2):124-137.
173. Brehm A, Tufteland KR, Aasland R et al. The many colours of chromodomains. Bioessays 2004; 26(2):133-140.
174. Isono K, Fujimura Y, Shinga J et al. Mammalian polyhomeotic homologues phc2 and phc1 act in synergy to mediate polycomb repression of hox genes. Mol Cell Biol 2005; 25(15):6694-6706.
175. Wade PA, Jones PL, Vermaak D et al. Histone deacetylase directs the dominant silencing of transcription in chromatin: Association with MeCP2 and the Mi-2 chromodomain SWI/SNF ATPase. Cold Spring Harb Symp Quant Biol 1998; 63:435-445.
176. Dunn MK, Mercola M, Moore DD. Cyclopamine, a steroidal alkaloid, disrupts development of cranial neural crest cells in Xenopus. Dev Dyn 1995; 202(3):255-270.
177. Etchevers HC. Early expression of hypoxia-inducible factor 1alpha in the chicken embryo. Gene Expr Patterns 2003; 3(1):49-52.
178. Bruyere Jr HJ, Stith CE, Thorn TA. Cardioteratogenic dose of ethanol reduces both lactic dehydrogenase and succinic dehydrogenase activity in the bulbar ridges of the embryonic chick heart. J Appl Toxicol 1994; 14(1):27-31.
179. Maher ER, Eng C. The pressure rises: Update on the genetics of phaeochromocytoma. Hum Mol Genet 2002; 11(20):2347-2354.
180. Phillips JC, del Bono EA, Haines JL et al. A second locus for Rieger syndrome maps to chromosome 13q14. Am J Hum Genet 1996; 59(3):613-619.
181. Barr FG, Galili N, Holick J et al. Rearrangement of the PAX3 paired box gene in the paediatric solid tumour alveolar rhabdomyosarcoma. Nat Genet 1993; 3(2):113-117.
182. De Craene B, van Roy F, Berx G. Unraveling signalling cascades for the Snail family of transcription factors. Cell Signal 2005; 17(5):535-547.

PRENATAL DIAGNOSIS
Prenat Diagn 2006; **26**: 1201–1205.
Published online 30 October 2006 in Wiley InterScience
(www.interscience.wiley.com) **DOI:** 10.1002/pd.1588

SHORT COMMUNICATION

Cytogenetic and histological features of a human embryo with homogeneous chromosome 8 trisomy

Christelle Golzio[2], Jessica Guirchoun[1], Catherine Ozilou[1], Sophie Thomas[2], Géraldine Goudefroye[2], Nicole Morichon-Delvallez[1], Michel Vekemans,[1,2] Tania Attié-Bitach[1,2] and Heather C. Etchevers[2]*

[1]*AP-HP, Hôpital Necker—Enfants Malades, Service de Cytogénétique et d'Embryologie, 149 rue de Sèvres, 75743 Paris Cedex 15, France*
[2]*INSERM U781, Hôpital Necker—Enfants Malades, 149 rue de Sèvres, 75743 Paris Cedex 15, France*

Background Homogeneous and complete trisomy 8 is extremely rare. With one recent neonatal exception, all reported cases have been mosaic, due to mitotic non-disjunction during early zygotic development. We report a case of chromosome 8 trisomy in a human embryo examined at Carnegie stage 11 (25 days post-fertilization). It presented severe cardiovascular and central nervous system malformations.

Methods The unusual bifid heart in this embryo spurred a detailed histological examination, karyotyping of a chorionic villus sample and subsequent FISH on inter-phase nuclei of intra-embryonic sections.

Results Trophoblast cells had a karyotype of 47,XX, +8. Within the embryo proper, FISH demonstrated that the trisomy 8 was homogeneous in embryonic as well as extra-embryonic tissues. FQ-PCR supports a meiosis I origin of non-disjunction. In sections, the pharyngeal arches (including cardiac outflow tract), forebrain, mesonephros and liver were absent. Somites and yolk sac blood vessels were irregularly shaped.

Conclusion We show that homogeneous, intra-embryonic trisomy 8 is compatible with implantation and early human development. Molecular pathways that may be compromised and their impact on organogenesis are discussed. Copyright © 2006 John Wiley & Sons, Ltd.

KEY WORDS: trisomy 8; cardia bifida; liver; forebrain; FOG2; SOX7

INTRODUCTION

Mosaic trisomy 8 or Warkany syndrome has been reported in over a hundred still or live births (Chen *et al*., 1998a; Henderson and Crawford, 1996a; Jay *et al*., 1999a) and may be more frequent than these figures would indicate (Wang *et al*., 1993). Clinical signs are highly variable but include mental retardation, agenesis of the corpus callosum, renal and hepatic malformations or polycystosis (Jay *et al*., 1999a), cardiomegaly or perforate inter-ventricular septal defect, skeletal anomalies of the limbs (Alvi *et al*., 2004) and facial dysmorphism including cleft palate and micrognathia (Chen *et al*., 1998a; Henderson and Crawford, 1996a; Jay *et al*., 1999a).

Physical anomalies associated with trisomy 8 can be detected prenatally by ultrasound (Henderson and Crawford, 1996a) although the fetus may appear normal if it has a low proportion of aneuploid cells. Amniocentesis is used to confirm trisomy 8 (Hsu *et al*., 1997). It has been demonstrated, however, that karyotypes from both amniocentesis and direct chorionic villi sampling (CVS) of cytotrophoblasts can yield apparently normal results, while only the cultured CVS mesodermal core allowed the detection of trisomy 8 in a mosaic case presenting with multiple malformations (Hahnemann and Vejerslev, 1997).

When trisomy 8 mosaicism is confined to the placenta, extra-embryonic tissues have a variable proportion of trisomic cells while fetal tissues can be normal (Karadima *et al*., 1998a). At least one case of confined placental mosaicism for trisomy 8 has been reported with intra-uterine growth retardation, although after birth the child grew normally with no subsequent problems (Saks *et al*., 1998). However, apparently confined placental mosaicism and a normal karyotype from a fetal blood sample still require strict surveillance of the pregnancy (de Pater *et al*., 2000; Wolstenholme, 1996); the proportion of aneuploid cells can be homogenous within the placenta but may vary according to the fetal tissue studied (blood, skin or muscle) (Jay *et al*., 1999a).

Acquired or constitutional chromosome 8 trisomy is often associated with myelodyplasia and acute monoblastic leukaemia (Batanian *et al*., 2001; Haferlach *et al*., 2002; Le Beau *et al*., 2002; Secker-Walker and Fitchett, 1995). It is not currently known at what level the trisomy induces carcinogenesis, but mosaicism within the granulocytic lineage is sufficient. In murine models for leukaemia resulting from the human PML-RARA fusion product, gain of a chromosome syntenic to human chromosome 8 is often observed secondarily

*Correspondence to: Heather C. Etchevers, INSERM U781, Hôpital Necker—Enfants Malades, 149 rue de Sèvres, 75743 Paris Cedex 15, France. E-mail: etchevers@necker.fr

Received: 27 June 2006
Revised: 21 September 2006
Accepted: 27 September 2006
Published online: 30 October 2006

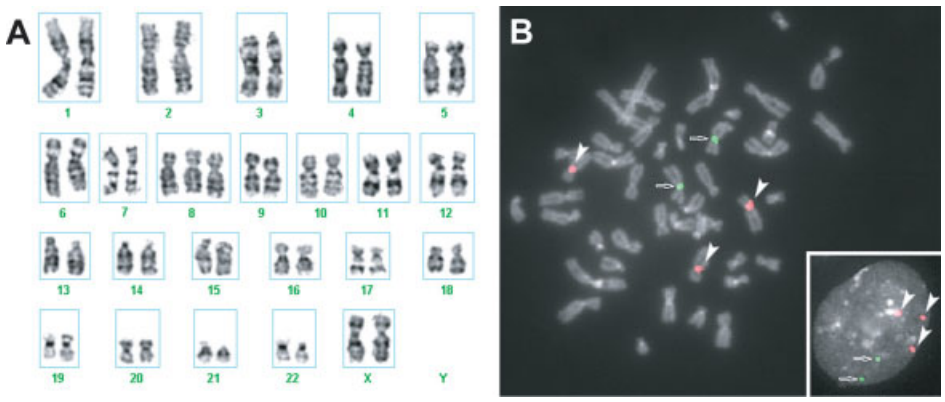

Figure 1—(A) Representative karyotype from chorionic villus sample of embryo R900 showing complete trisomy of chromosome 8. (B) FISH using centromeric markers for chromosome 8 (red, arrowheads) and chromosome 12 (green, arrows) on trophoblastic nuclei in metaphase and on intra-embryonic nuclei in inter-phase (inset). Three chromosome 8 signals were observed in 198/200 nuclei with two chromosome 12 signals present

and is necessary for the progression of leukemogenesis (Le Beau *et al*., 2002).

Homogeneous trisomy 8 occurs in an estimated 0.1% of recognized pregnancies and is responsible for 0.7% of spontaneous abortions (Hassold *et al*., 1980). Only one post-natal case has ever been reported to date, and the child died in its second month from cardiac failure (Hendson *et al*., 2003). It remains plausible that this patient was a severely affected mosaic, having lost a third copy of chromosome 8 in tissues that had not been sampled and supporting its brief survival. Here, we report an unusually malformed human embryo after elective abortion with homogeneous trisomy 8 in both embryonic and extra-embryonic tissues.

METHODS

Anonymous human conceptuses were collected from elective pregnancy terminations using the mefiprestone protocol, in agreement with French law 2004–800 and hospital ethics committee recommendations. Embryos are staged using the Carnegie system according to criteria of gestational age, size and morphological features. When destined for histology, they are fixed in 4% paraformaldehyde in PBS, pH 7.5 overnight before rinsing in PBS, dehydrating and embedding in Paraplast, using standard techniques. Sections were cut at 5 μm and collected individually on Superfrost Plus™ slides (Fisher-Bioblock) and coloured using standard hematoxylin–eosin staining.

Direct karyotyping of the chorionic villi was carried out in parallel using the standard colchemid protocol.

Centromeric alphoid sequence probes were derived from pBR12 for chromosome 12 (Baldini *et al*., 1990) and BAC pZ8.4 for chromosome 8 (Archidiacono *et al*., 1995). Double FISH on inter-phase nuclei of embryonic sections at 5 μm was performed as per protocols available from Resources for Molecular Cytogenetics in Bari, Italy (http://www.biologia.uniba.it/rmc/index.html) and as described elsewhere (Archidiacono *et al*., 1995; Aubele *et al*., 1997), with the exception of using proteinase K rather than pronase E. Two hundred nuclei with two signals for chromosome 12 were scored for the number and presence of chromosome 8 hybridization signals.

PCR products using fluorochrome-tagged primers for the following polymorphic markers were evaluated by standard Genescan™ analysis: D8S1706, D8S1839, D8S1820, D8S538, D8S285, D8S260, D8S279 and D8S1793.

RESULTS

Embryo R900 presented with externally normal chorionic villi on its placental sac. The embryo itself (Figure 2(A)) had an abnormally small head with blebbed anterior and dorsal vesicles, a flexed trunk region with small, irregularly spaced somites and a dorsally oriented caudal extremity. The 16 somite pairs present were not aligned symmetrically. The number of somites and the size of the yolk sac were consistent with the assignation of Carnegie stage 11 (13–20 somites, 22 days after fertilization). The heart was bifid (Figure 2(C)) and abnormally dilated vessels were observed in the yolk sac (asterisk), in which some blood islands were present.

Histological examination (Figure 2(E)) showed absence of the forebrain and otic vesicles, with a closed rostral neuropore. A structure resembling a severely hypoplastic first pharyngeal arch could be distinguished. Identifiable cardiac tissue was continuous with the atrial end of the cardiac tube, implying lack of development of the secondary cardiac field giving rise to the conotruncal pole. Cardiac jelly and endocardium were present but the dorsal aortae were not apparent caudally. No liver bud or mesonephros was distinguishable, although embryonic endoderm had formed. The absence of other internal organs and limb buds is normal for this stage of development (*cf* Figure 2(F)).

CVS was made for direct karyotyping and, in parallel, DNA was extracted for fluorescent quantitative PCR (FQ-PCR). The karyotype of R900 was 47,XX,+8, as counted on five trophoblast metaphases (Figure 1(A)).

DOI: 10.1002/pd

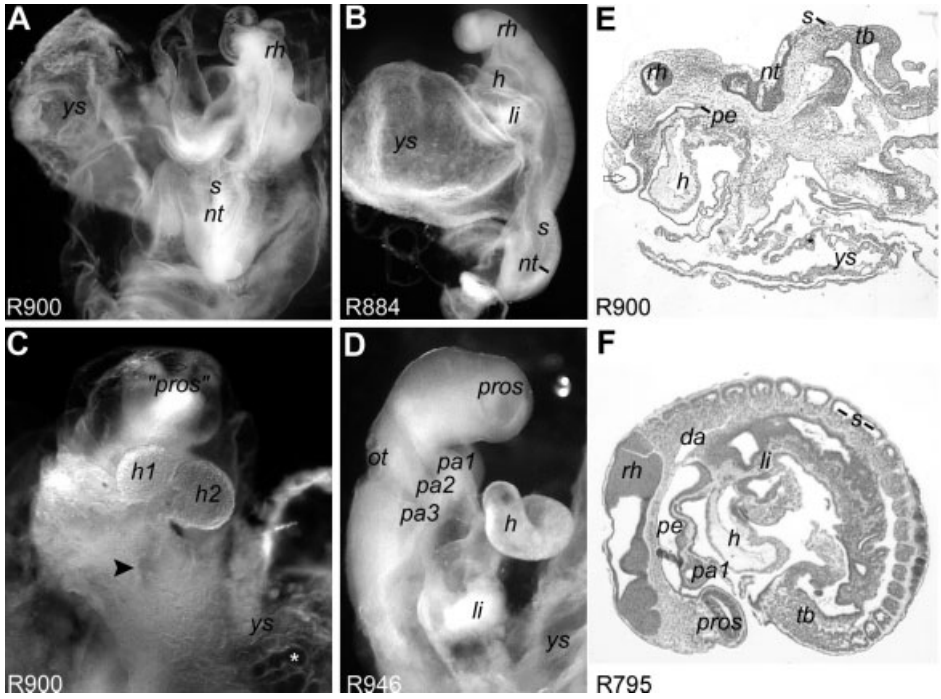

Figure 2—(A–D) Rostral to top. (A) Dorsal view of embryo R900, to compare with dorsolateral-left view of stage-matched normal embryo R884 ((B), early Carnegie stage 11–24 days post-fertilization). (C) Ventral view of embryo R900, to compare with ventrolateral-right view of stage-matched normal embryo R946 ((D), late Carnegie stage 11–25 days post-fertilization). (E–F) Rostral to left, dorsal to top. (E) Parasagittal section of embryo R900. The embryo was small for its stage based on the number of somites visible and its tissues disorganized. (F) Stage-matched normal embryo R795 (late Carnegie stage 11). The anterior intestinal portal in R900 was located directly caudal to the bifid heart primordia (arrowhead, C) without an intervening liver bud, and dilated blood vessels were visible in the yolk sac (asterisks, C, E). da, dorsal aorta; h, heart; li, liver bud; nt, neural tube; ot, otic vesicle; pa#, pharyngeal arch #; pe, pharyngeal endoderm; pros, prosencephalon; rh, rhombencephalon; s, somite; tb, tail bud; ys, yolk sac

FISH, tested first on trophoblastic metaphase nuclei (Figure 1(B)), was performed on inter-phase nuclei derived from histological sections of the embryo itself. Two hundred of these nuclei were counted, with 198/200 showing three hybridization signals for pZ8.4, demonstrating that the trisomy 8 was homogeneous and intra-embryonic (Figure 1(B) inset).

FQ-PCR performed for markers on chromosome 8 supported the conclusion of non-disjunction during the first division of meiosis: markers D8S1706, D8S1839, D8S1820 and D8S279 were triallelic, as were centromeric markers D8S538 and D8S260; only markers D8S285 and marker D8S1793 gave trisomic, biallelic profiles (Figure 3). Parental DNA was not available for further analyses.

DISCUSSION

Embryo R900, a product of elective abortion, was diagnosed fortuitously with homogeneous trisomy of chromosome 8. Until this case, FQ-PCR of polymorphic markers on chromosomes 13, 18, 21, X and Y was routinely performed in multiplex to determine if morphologically normal embryos recruited for ongoing gene expression studies were exempt from common aneuploidies (Megarbane *et al*., 2001; Germanaud *et al*., 2003). Our laboratory now performs initial screening by karyotyping of cytotrophoblasts from CVS in both externally normal and abnormal embryos.

On the basis of the polymorphic markers of chromosome 8 that were used, it was possible to distinguish between non-disjunction occurring in the first or second meiotic division by the use of pericentromeric markers D8S538 and D8S260. These, like most of the markers examined, gave triallelic profiles, because of heterozygosity in the parent of origin. The non-reduction of heterozygosity infers failure of the homologous chromosomes to separate during meiosis I. However, the parental origin of the meiotic non-disjunction was not ascertainable in R900, as the embryo was an anonymous donation to research. Errors in maternal meiosis are more common in spontaneous first-trimester abortions due to trisomy 8 (James and Jacobs, 1996; Karadima *et al*., 1998b; Nicolaidis *et al*., 1998), although pericentromeric markers were not available in these initial studies to pinpoint the stage of non-disjunction (James and Jacobs, 1996). Mitotic errors and mosaicism appear to be more compatible with full-term pregnancies (Karadima *et al*., 1998b). It is easier to prove mosaicism than non-mosaicism as fetuses grow and the possibility of sampling all tissues decreases. The small size of the case presented here allowed sampling of nuclei across its whole-body sections and represent intra-embryonic as well as extra-embryonic tissues. The paucity of reports of non-mosaic trisomy 8 supports our contention that

DOI: 10.1002/pd

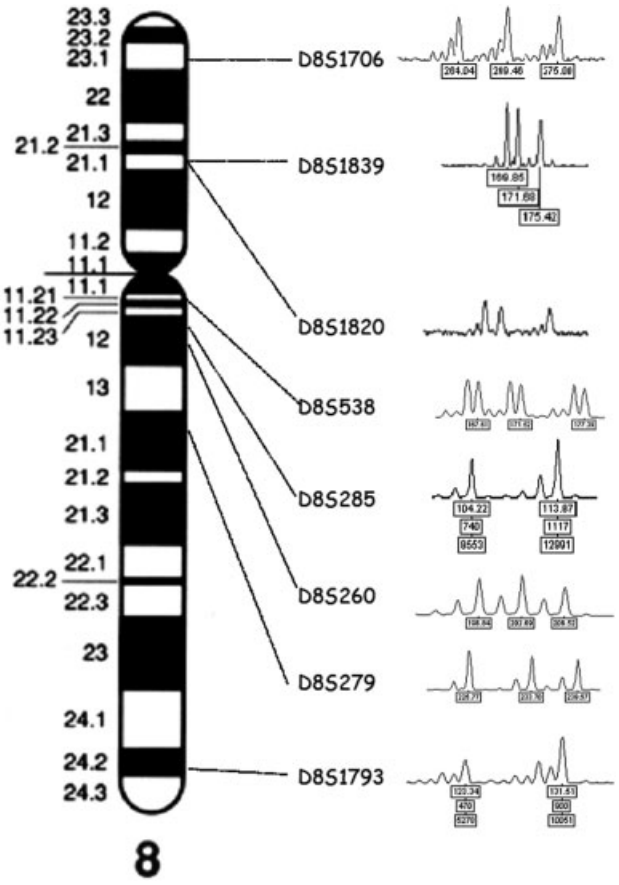

Figure 3—Diagram of the localization on human chromosome 8 of eight markers examined by FQ-PCR in embryo R900. On the long arm, markers D8S285 and D8S1793 were trisomic and biallelic; however, both markers on the short arm (D8S1706, D8S1839 and D8S1820) and long arm (D8S538, D8S260, D8S279) were triallelic. We conclude that the origin of non-disjunction was during meiosis I because of the non-reduction of heterozygosity in pericentromeric markers

meiotic non-disjunction leading to trisomy 8 is lethal early in the first trimester.

The malformations observed were consistent with, but far more severe than, the wide range of anomalies associated with mosaic or partial trisomy 8. In R900, the forebrain, mesonephros, pharyngeal arches and liver were absent. Mental retardation is common in mosaic trisomy 8 (Fineman *et al*., 1975) and frontal meningocoele has been reported in a partial trisomy 8q (Schinzel, 1977). Pharyngeal arch development is frequently impaired in all forms of trisomy 8, as seen in facial dysmorphology and clefting (Fan and Siu, 2001; Henderson and Crawford, 1996b) and diverse cardiac defects (Pezzolo *et al*., 1990; Winters *et al*., 1995; Jay *et al*., 1999b; Hendson *et al*., 2003). Hepatic malformations and hepatoblastoma are also associated with abnormal chromosome 8 copy numbers (Winters *et al*., 1995; Jay *et al*., 1999b; Parada *et al*., 2000). The absence of embryonic kidney primordia (mesonephros) in our case may be analogous to the hydronephrosis and abnormal kidney morphogenesis seen in mosaic or partial trisomy 8, although the definitive kidney primordia are not normally present at stage C11 (Chen *et al*., 1998b; Fan and Siu, 2001; Fineman *et al*., 1975; Schofield *et al*., 1992). Appendage and skeletal abnormalities are reported in post-natal cases; R900 was too young to have developed limb buds but its abnormally formed somites would probably have led to hypoplastic sclerotome compartments, from which the body cartilage is derived.

Candidate genes on chromosome 8 for the severe malformations observed in embryo R900 include those coding the transcription factors *SOX7* and *ZFPM2/FOG2* and the Wnt morphogen receptors *FRIZZLED3* and *FRIZZLED6*. Large-scale genetic screens of zebrafish have identified at least eight distinct loci associated with cardia bifida, including homologues of fibronectin, the sphingosine 1-phosphate receptor, and a number of transcription factors important for endoderm and cardiac formation such as the colourfully named *casanova* and *faust* (Chen *et al*., 1996; Stainier *et al*., 1996). The *casanova* locus corresponds to an atypical 'F-type' Sox-family factor similar to Sox7, shown recently to be essential for cardiac formation in Xenopus (Zhang *et al*., 2005). Human ZFPM2, also known as FOG2 (friend of GATA 2), interacts physically and functionally with the GATA5 transcription factor at the *faust* locus (Stainier, 2001). Interestingly, human missense mutations in *FOG2* have been found in isolated tetralogy of Fallot (Pizzuti *et al*., 2003), implying dose sensitivity to these transcription factors in cardiac morphogenesis.

The fact that embryo R900 lacked a liver bud, in addition to its cardia bifida and defective somitogenesis, implies misregulation of earlier endodermal specification needed for all three processes through a balance of transcription factors such as *SOX7* or *FOG2*. Among the zebrafish loci associated with cardia bifida, a cascade of transcriptional activation including sox and gata factors has been established in normal heart development that converges on the highly conserved, 'master' cardiac transcription factor, nkx2.5. Indeed, human *NKX2.5* is also mutated, infrequently, in a wide phenotypic range of isolated congenital heart defects (Akazawa and Komuro, 2005). Finally, essential to the convergence of the bilaterally paired cardiac fields and numerous endodermal primordia, as well as somite maturation, is the establishment of planar cell polarity mediated by the Frizzled receptor family (Eisenberg and Eisenberg, 2006; Matsui *et al*., 2005). Haploinsufficiency of *Frizzled3* and *Frizzled6* have been shown in mice to cause neural tube closure defects through perturbation of the vectorial organization of cells within the early ectodermal and endodermal epithelia (Wang *et al*., 2006). Clearly, additional work in both experimental embryology and in cytogenetics will be necessary to shed light on the lethal effects of homogeneous trisomy 8 on early human development.

ACKNOWLEDGEMENTS

The authors wish to thank S. Lyonnet and A. Munnich for providing a conducive research environment, M. Teboul and the staff of the Centre d'Orthogénie at the Broussais hospital in Paris for their contributions,

DOI: 10.1002/pd

S. Zrelli and D. Sanlaville for troubleshooting the FISH inter-phase technique, and partial funding from the Institut National pour la Santé et la Recherche Médicale, the Association Française contre les Myopathies and Assistance Publique—Hôpitaux de Paris.

REFERENCES

Akazawa H, Komuro I. 2005. Cardiac transcription factor csx/nkx2-5: Its role in cardiac development and diseases. *Pharmacol Ther* **107**: 252–268.

Alvi F, Alonso A, Brewood AF. 2004. Upper limb abnormalities in mosaic trisomy 8 syndrome. *Arch Orthop Trauma Surg* **124**: 718–719.

Archidiacono N, Antonacci R, Marzella R, *et al*. 1995. Comparative mapping of human alphoid sequences in great apes using fluorescence in situ hybridization. *Genomics* **25**: 477–484.

Aubele M, Zitzelsberger H, Szucs S, *et al*. 1997. Comparative fish analysis of numerical chromosome 7 abnormalities in 5-micron and 15-micron paraffin-embedded tissue sections from prostatic carcinoma. *Histochem Cell Biol* **107**: 121–126.

Baldini A, Rocchi M, Archidiacono N, Miller OJ, Miller DA. 1990. A human alpha satellite DNA subset specific for chromosome 12. *Am J Hum Genet* **46**: 784–788.

Batanian JR, Ma E, Huang Y, Gadre B. 2001. Co-existence of alternative forms of 8q gain in cytogenetic clones of three patients with acute myeloid leukemia, pointing to 8q22 approximately 8qter as a region of biologic significance. *Cancer Genet Cytogenet* **126**: 20–25.

Chen C, Lee C, Pan C, Kir T, Chen B. 1998a. Partial trisomy 8q and partial monosomy 15q associated with congenital hydrocephalus, diaphragmatic hernia, urinary tract anomalies, congenital heart defect and kyphoscoliosis. *Prenat Diagn* **18**: 1289–1293.

Chen CP, Lee CC, Pan CW, Kir TY, Chen BF. 1998b. Partial trisomy 8q and partial monosomy 15q associated with congenital hydrocephalus, diaphragmatic hernia, urinary tract anomalies, congenital heart defect and kyphoscoliosis. *Prenat Diagn* **18**: 1289–1293.

Chen JN, Haffter P, Odenthal J, *et al*. 1996. Mutations affecting the cardiovascular system and other internal organs in zebrafish. *Development* **123**: 293–302.

de Pater JM, Schuring-Blom GH, Nieste-Otter MA, *et al*. 2000. Trisomy 8 in chorionic villi-unpredictable results in follow-up. *Prenat Diagn* **20**: 435–437.

Eisenberg LM, Eisenberg CA. 2006. Wnt signal transduction and the formation of the myocardium. *Dev Biol* **293**: 305–315.

Fan YS, Siu VM. 2001. Molecular cytogenetic characterization of a derivative chromosome 8 with an inverted duplication of 8p21.3–>p23.3 and a rearranged duplication of 8q24.13–>qter. *Am J Med Genet* **102**: 266–271.

Fineman RM, Ablow RC, Howard RO, Albright J, Breg WR. 1975. Trisomy 8 mosaicism syndrome. *Pediatrics* **56**: 762–767.

Germanaud D, Audollent S, Auge J, Vekemans M, Attie-Bitach T. 2003. Molecular diagnosis for the most frequent aneuploidies with quantitative fluorescent pcr. *Arch Pediatr* **10**: 347–349.

Haferlach T, Schoch C, Schnittger S, *et al*. 2002. Distinct genetic patterns can be identified in acute monoblastic and acute monocytic leukaemia (fab aml m5a and m5b): a study of 124 patients. *Br J Haematol* **118**: 426–431.

Hahnemann J, Vejerslev L. 1997. Accuracy of cytogenetic findings on chorionic villus sampling (cvs)-diagnostic consequences of cvs mosaicism and non-mosaic discrepancy in centres contributing to eucromic 1986–1992. *Prenat Diagn* **17**: 801–820.

Hassold T, Chen N, Funkhouser J, *et al*. 1980. A cytogenetic study of 1000 spontaneous abortions. *Ann Hum Genet* **44**: 151–178.

Henderson N, Crawford P. 1996a. The oro-facial manifestations of trisomy 8 mosaicism: a case report. *Int J Paediatr Dent* **6**: 129–132.

Henderson NJ, Crawford PJ. 1996b. The oro-facial manifestations of trisomy 8 mosaicism: a case report. *Int J Paediatr Dent* **6**: 129–132.

Hendson W, Levin SE, Govendrageloo K, Hunter V. 2003. Multiple cardiac abnormalities in a case of non-mosaic trisomy 8. *Cardiovasc J S Afr* **14**: 138–140.

Hsu L, Yu M, Neu R, *et al*. 1997. Rare trisomy mosaicism diagnosed in amniocytes, involving an autosome other than chromosomes 13, 18, 20, and 21: Karyotype/phenotype correlations. *Prenat Diagn* **17**: 201–242.

James RS, Jacobs PA. 1996. Molecular studies of the aetiology of trisomy 8 in spontaneous abortions and the liveborn population. *Hum Genet* **97**: 283–286.

Jay A, Kilby M, Roberts E, *et al*. 1999a. Prenatal diagnosis of mosaicism for partial trisomy 8: a case report including fetal pathology. *Prenat Diagn* **19**: 976–979.

Jay A, Kilby MD, Roberts E, *et al*. 1999b. Prenatal diagnosis of mosaicism for partial trisomy 8: a case report including fetal pathology. *Prenat Diagn* **19**: 976–979.

Karadima G, Bugge M, Nicolaidis P. 1998a. Origin of nondisjunction in trisomy 8 and trisomy 8 mosaicism. *Eur J Hum Genet* **6**: 432–438.

Karadima G, Bugge M, Nicolaidis P, *et al*. 1998b. Origin of nondisjunction in trisomy 8 and trisomy 8 mosaicism. *Eur J Hum Genet* **6**: 432–438.

Le Beau MM, Bitts S, Davis EM, Kogan SC. 2002. Recurring chromosomal abnormalities in leukemia in pml-rara transgenic mice parallel human acute promyelocytic leukemia. *Blood* **99**: 2985–2991.

Matsui T, Raya A, Kawakami Y, *et al*. 2005. Noncanonical wnt signaling regulates midline convergence of organ primordia during zebrafish development. *Genes Dev* **19**: 164–175.

Megarbane A, Le Lorc HM, Elghezal H, *et al*. 2001. Pure partial 7p trisomy including the twist, hoxa, and gli3 genes. *J Med Genet* **38**: 178–182.

Nicolaidis P, von Beust G, Bugge M, *et al*. 1998. Analysis of the origin of the extra chromosome in trisomy 8 in 4 cases of spontaneous abortions. *Fetal Diagn Ther* **13**: 42–45.

Parada LA, Limon J, Iliszko M, *et al*. 2000. Cytogenetics of hepatoblastoma: further characterization of 1q rearrangements by fluorescence in situ hybridization: an international collaborative study. *Med Pediatr Oncol* **34**: 165–170.

Pezzolo A, Bicocchi MP, Zampatti C, Cuoco C, Gimelli G. 1990. Prenatal diagnosis of a partial 8p trisomy. *Prenat Diagn* **10**: 533–538.

Pizzuti A, Sarkozy A, Newton AL, *et al*. 2003. Mutations of zfpm2/fog2 gene in sporadic cases of tetralogy of fallot. *Hum Mutat* **22**: 372–377.

Saks E, McCoy M, Damron J, Kelly T. 1998. Confined placental mosaicism for trisomy 8 and intra-uterine growth retardation. *Prenat Diagn* **18**: 1202–1204.

Schinzel A. 1977. Partial trisomy 8q in half-sisters with distinct dysmorphic patterns not similar to the trisomy 8 mosaicism syndrome. *Hum Genet* **37**: 17–26.

Schofield B, Babu A, Punales-Morejon D, *et al*. 1992. Double mosaic aneuploidy: 45,x/47,xy,+8 in a male infant. *Am J Med Genet* **44**: 7–10.

Secker-Walker LM, Fitchett M. 1995. Constitutional and acquired trisomy 8. *Leuk Res* **19**: 737–740.

Stainier DY. 2001. Zebrafish genetics and vertebrate heart formation. *Nat Rev Genet* **2**: 39–48.

Stainier DY, Fouquet B, Chen JN, *et al*. 1996. Mutations affecting the formation and function of the cardiovascular system in the zebrafish embryo. *Development* **123**: 285–292.

Wang BB, Rubin CH, Williams J 3rd. 1993. Mosaicism in chorionic villus sampling: an analysis of incidence and chromosomes involved in 2612 consecutive cases. *Prenat Diagn* **13**: 179–190.

Wang Y, Guo N, Nathans J. 2006. The role of frizzled3 and frizzled6 in neural tube closure and in the planar polarity of inner-ear sensory hair cells. *J Neurosci* **26**: 2147–2156.

Winters J, Markello T, Nance W, Jackson-Cook C. 1995. Mosaic "tetrasomy" 8p: case report and review of the literature. *Clin Genet* **48**: 195–198.

Wolstenholme J. 1996. Confined placental mosaicism for trisomies 2, 3, 7, 8, 9, 16, and 22: Their incidence, likely origins, and mechanisms for cell lineage compartmentalization. *Prenat Diagn* **16**: 511–524.

Zhang C, Basta T, Klymkowsky MW. 2005. Sox7 and sox18 are essential for cardiogenesis in xenopus. *Dev Dyn* **234**: 878–891.

Rapid Publication

Matthew-Wood Syndrome: Report of Two New Cases Supporting Autosomal Recessive Inheritance and Exclusion of *FGF10* and *FGFR2*

Jelena Martinovic-Bouriel,[1]* Céline Bernabé-Dupont,[2] Christelle Golzio,[4,5] Bettina Grattagliano-Bessières,[3] Valérie Malan,[1,4] Maryse Bonnière,[1] Chantal Esculpavit,[4] Catherine Fallet-Bianco,[3] Véronique Mirlesse,[3] Jerôme Le Bidois,[3] Marie-Cécile Aubry,[2] Michel Vekemans,[1,4,5] Nicole Morichon,[1,4] Heather Etchevers,[4,5] Tania Attié-Bitach,[1,4,5] Féréchté Encha-Razavi,[1,4] and Alexandra Benachi[2,4]

[1]Assistance Publique—Hôpitaux de Paris; Hôpital Necker—Enfants Malades, Department of Genetics, Embryo-Fetal Pathology Unit, Paris, France
[2]Assistance Publique—Hôpitaux de Paris; Hôpital Necker—Enfants Malades, Department of Obstetrics, Paris, France
[3]Institut de Puériculture, Department of Fetal Pathology, Paris, France
[4]Université Paris-Descartes; Hôpital Necker—Enfants Malades, Paris, France
[5]INSERM U781, Hôpital Necker—Enfants Malades, Paris, France

Received 28 July 2006; Accepted 27 October 2006

We describe two fetal cases of microphthalmia/anophthalmia, pulmonary agenesis, and diaphragmatic defect. This rare association is known as Matthew-Wood syndrome (MWS; MIM 601186) or by the acronym "PMD" (Pulmonary agenesis, Microphthalmia, Diaphragmatic defect). Fewer than ten pre- and perinatal diagnoses of Matthew-Wood syndrome have been described to date. The cause is unknown, and the mode of transmission remains unclear. Most cases have been reported as isolated and sporadic, although recurrence among sibs has been observed once. Our two cases both occurred in consanguineous families, further supporting autosomal recessive transmission. In addition, in one family at least one of the elder sibs presented an evocatively similar phenotype. The spatiotemporal expression pattern of the *FGF10* and *FGFR2* genes in human embryos and the reported phenotypes of knockout mice for these genes spurred us to examine their coding sequences in our two cases of MWS. While in our patients, no causative sequence variations were identified in *FGF10* or *FGFR2*, this cognate ligand-receptor pair and its downstream effectors remain functional candidates for MWS and similar associations of congenital ocular, diaphragmatic and pulmonary malformations. © 2007 Wiley-Liss, Inc.

Key words: microphthalmia; pulmonary hypoplasia; congenital diaphragmatic defect; polymalformative syndrome; association; growth retardation; facial dysmorphy; prenatal diagnosis; fibroblast growth factor; embryo

How to cite this article: Martinovic-Bouriel J, Bernabé-Dupont C, Golzio C, Grattagliano-Bessières B, Malan V, Bonnière M, Esculpavit C, Fallet-Bianco C, Mirlesse V, Le Bidois J, Aubry M-C, Vekemans M, Morichon N, Etchevers H, Attié-Bitach T, Encha-Razavi F, Benachi A. 2007. Matthew-Wood syndrome: Report of two new cases supporting autosomal recessive inheritance and exclusion of *FGF10* and *FGFR2*. Am J Med Genet Part A 143A:219–228.

INTRODUCTION

A distinct association of pulmonary, ocular, and diaphragmatic congenital malformations has been reported occasionally over the last 25 years. Spear et al. [1987] examined a patient with bilateral pulmonary agenesis, eventration of the left diaphragm, bilateral microphthalmia, and a complex cardiac defect with a ventricular septal defect and absent pulmonary vessels. Engellenner et al. [1989]

Jelena Martinovic-Bouriel, Céline Bernabé-Dupont, and Christelle Golzio have contributed equally to this work.

Grant sponsor: Association Française contre les Myopathies; Grant sponsor: Institut National pour la Santé et la Recherche Médicale (INSERM).

*Correspondence to: Dr. Jelena Martinovic-Bouriel, Embryo-Fetal Pathology Unit, Department of Genetics, Hopital Necker-Enfants Malades, 149 rue de Sevres, 75015 Paris, France.
E-mail: jelena.martinovic@nck.aphp.fr

DOI 10.1002/ajmg.a.31599

described another patient with bilateral pulmonary agenesis, an inverted right diaphragm, right microphthalmia and a small heart with absent pulmonary veins. Seller et al. [1996] coined the term Matthew-Wood syndrome (MWS) in reference to an association of microphthalmia and pulmonary hypoplasia, after the name of a firstborn sib. Berkenstadt et al. [1999] reported the coincidence of unilateral *p*ulmonary agenesis, *m*icrophthalmia, *d*iaphragmatic hernia, and intrauterine growth retardation under the acronym "PMD." The authors proposed that PMD might be a new entity, and that MWS, reported as anophthalmia and pulmonary hypoplasia, might represent an incomplete form of PMD.

A few cases have been observed in the peri- and postnatal period [Spear et al., 1987; Enns et al., 1998; Priolo et al., 2004; Li and Wei, 2006; Robert Lee et al., 2006] as well as three cases of prenatal diagnosis of the syndrome at the respective ages of 18, 22, and 36 weeks' gestation [Engellenner et al., 1989; Seller et al., 1996; Berkenstadt et al., 1999]. While most cases were apparently sporadic and isolated, MWS seems to have a genetic basis because of one report of familial recurrence [Seller et al., 1996]. A similar phenotype, presenting in addition with tetralogy of Fallot, was observed in a patient with a balanced reciprocal translocation de novo 46,XY,t(1;15) (q41; 21.2) [Smith et al., 1994]. No one animal model recapitulates this particular human association. However, knock-outs of the murine *Fgf10* (fibroblast growth factor 10) [Min et al., 1998; Sekine et al., 1999] or its binding-specific receptor isoform, *Fgfr2(IIIb)* [De Moerlooze et al., 2000], have multiple congenital defects including pulmonary agenesis. Other organ systems are affected including ablepharon for *Fgfr2b*, atretic or stenotic colon [Fairbanks et al., 2005] or imperforate anus, hypoplasic pituitary, lacrimal and salivary glands, pancreas and spleen, abnormal limbs and, inconsistently, kidneys [Ohuchi et al., 1997; Min et al., 1998]. Cardiac outflow tract malformations have also been noted.

Given a certain number of similarities between these animal models and the clinical signs of Matthew-Wood cases described here and elsewhere in the literature, we therefore undertook a molecular analysis of the *FGF10* and *FGFR2* genes in our two patients and were able to exclude both genes as pathogenic candidates in these individuals.

METHODS

Standard Karyotype and FISH (Fluorescence In Situ Hybridization) Analysis on Chromosomes

Standard karyotyping using GTG and RHG banding analysis was carried out on cultured amniotic fluid cells according to standard procedures. FISH was performed using BACs, RP11-297K5, RP11-1149B18, RP11-239E10 spanning the *GATA4* (8p23.1) and *CHD2* (15q26.1) genes and the 1q41 region, respectively, to rule out any possible deletions. BACs were selected from several databases accessible through the Internet (UCSC, University of California, Santa Cruz http://www.genome.ucsc.edu/ and NCBI, National centre for Biotechnology Information http://www.ncbi.nlm.nih.gov/). FISH experiments were performed on chromosome preparations as described previously [Romana et al., 1993].

In Situ Hybridization

Human embryos were collected from pregnancies legally terminated using the mefiprestone protocol, in concordance with French law 00-800 and hospital ethics committee recommendations. Primers were selected for PCR amplification (*FGF10*: [F] 5′-CTGGATGGCTTGTATCAAATG-3′ [R] 5′-TTGGCAAAAGAGCCATTGGT-3′ corresponding to exon 3; *FGFR2(IIIb)*: [F] 5′-CTTTAATGCCGCTGTTTAG-3′ [R] 5′-TCTTTTCAGCTTCTATATCCAG-3′ corresponding to alternatively spliced exon 9, included as the 8th exon in the IIIb RNA isoform). A T7 promotor sequence extension (TAATACGACTCACTATAGGGAGA) was added at the 5′ end of each primer. T7F/R and F/T7R primer pairs allowed the amplification of sense and antisense templates respectively, specific to the *FGF10* or the *FGFR2(IIIb)* transcripts. Riboprobe labeling, tissue fixation, hybridization, and developing were carried out according to standard protocols, as previously described [Wilkinson, 1992; Trueba et al., 2005].

DNA Analysis

Both cases had normal chromosomes according to karyotype. DNA was extracted from thymus samples after informed consent and autopsy using standard protocols. PCRs were carried out using intronic primers for the 3 exons of the *FGF10* gene and the 18 coding exons (including the alternatively included exons 8 and 9) for the *FGFR2* gene; sequences and conditions presented in Table II.

CLINICAL REPORT

Patient 1

A consanguineous healthy couple of Romanian origin presented with a history of neonatal demise in their two first-born children. The first child, a boy delivered vaginally at 33 weeks' gestation (birthweight: 800 g, <3rd centile), died on the first day postpartum with no autopsy. The second child, a girl delivered at 43 weeks' gestation (birthweight: 2,800 g, 3rd centile), died within the first hour of life. The parents brought to our attention her respiratory

problems associated with a bilateral absence of ocular globes. However, the parents had no medical records and autopsy was not performed. Over the following years, the mother had four healthy children. Her seventh pregnancy ended in a voluntary interruption.

Their eighth child is a boy who developed ocular troubles but he has had neither medical follow-up nor an obvious diagnosis.

In the ninth pregnancy, at a maternal age of 34 years, the first sonogram, performed at 12 weeks' gestation showed normal nuchal translucency and no anomalies. A second sonogram at 23 weeks' gestation showed bilateral anophthalmia (Fig. 1) and gastro-duodenal dilatation in a male fetus. The control ultrasound at 29 weeks' gestation confirmed the absence of ocular globes and jejunal distension. In addition, polyhydramnios, a left diaphragmatic defect (Fig. 2), and a short femoral length, measured at the 3rd centile, were noted. A TORCH study was negative. Amniocentesis showed a normal male karyotype (46,XY). After genetic counseling, the parents opted for termination of pregnancy at 31 weeks, in the light of a poor prognosis.

The fetus (birth weight: 1,250 g, <3rd centile; length: 38 cm, 3rd centile; head circumference: 28 cm, 10th–25th centile) presented with bilateral microphthalmia with recessed orbits, hypotelorism, narrow palpebral fissures, short nose, large ears, and retrognathia (Fig. 3A,B). Autopsy showed the bilateral absence of bronchial and pulmonary *anlage* below blind-ended tracheae. The heart was normal, except for the absence of pulmonary artery branches and pulmonary veins. Bilateral diaphragmatic eventration, as well as stomach and duodenal dilatation upstream of stenosis at the duodeno-jejunal junction were confirmed (Fig. 4). In addition, a common mesentery was noted. Microscopic ocular examination showed bilateral cataracts and the presence of retinal tissue in severely hypoplastic globes. The

Fig. 1. Ultrasonography at 29 SA in Patient 1 showing a left diaphragmatic defect with an ascended stomach. [Color figure can be viewed in the online issue, which is available at www.interscience.wiley.com.]

Fig. 2. 3D ultrasonography at 29 SA in Patient 1 showing bilateral microphthalmia. [Color figure can be viewed in the online issue, which is available at www.interscience.wiley.com.]

cerebral examination was normal, except for a slightly hypoplastic lateral geniculate body. The vermis displayed a few heterotopic Purkinje cells (not shown).

Patient 2

A 32-year-old G2P2 (Tanner scale) woman presented on her second pregnancy with no particular medical history and a previous, healthy

Fig. 3. Facial gestalt in Patient 1 (**A**: front, **B**: profile) and Patient 2 (**C**: front, **D**: profile) showing common features: narrow palpebral fissures with microphthalmia, high forehead, short nose with anteverted nostrils. [Color figure can be viewed in the online issue, which is available at www.interscience.wiley.com.]

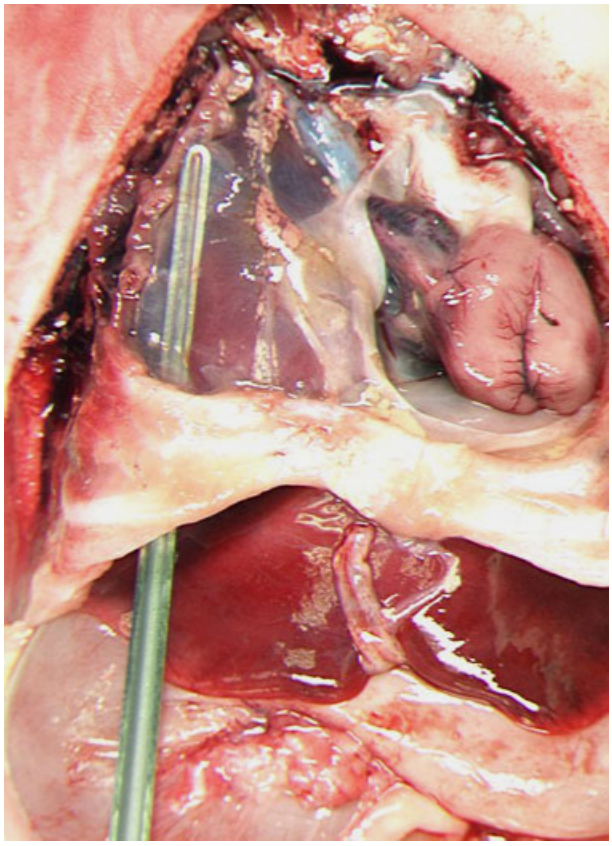

FIG. 4. Diaphragmatic eventration and pulmonary agenesis in Patient 1. [Color figure can be viewed in the online issue, which is available at www.interscience.wiley.com.]

son. The couple is consanguineous, of Portuguese origin.

The second sonogram, performed at 23 weeks' gestation, showed a left diaphragmatic defect with mediastinal shift, hypoechogenic digestive tract, bilateral anophthalmia, long philtrum, abnormal ears, and moderate renal dysplasia. Amniocentesis yielded a normal female karyotype (46,XX). Echocardiography showed atresia of the pulmonary artery with ventricular septal defect. Given a very poor prognosis, the parents opted for termination of the pregnancy at 29 weeks.

The fetus (birthweight: 1,160 g, 10th centile; length: 37 cm, 10th centile; HC: 27.5 cm, 25th–50th centile) presented bilateral microphthalmia, a high forehead, a flat nose with anteverted nares, a bifid uvula, a large neck, and camptodactyly (Fig. 3C,D). The autopsy showed bilateral pulmonary agenesis with no main bronchi, bilateral diaphragmatic eventration, a horizontalized heart with pulmonary artery agenesis and perimembraneous septal defect (Fig. 5). In addition, duodenal stenosis (Fig. 6), pancreatic agenesis, and a multilobulated spleen were noted. Microscopic ocular examination confirmed bilateral microphthalmia with retinal dysplasia and cataracts (Fig. 7). No

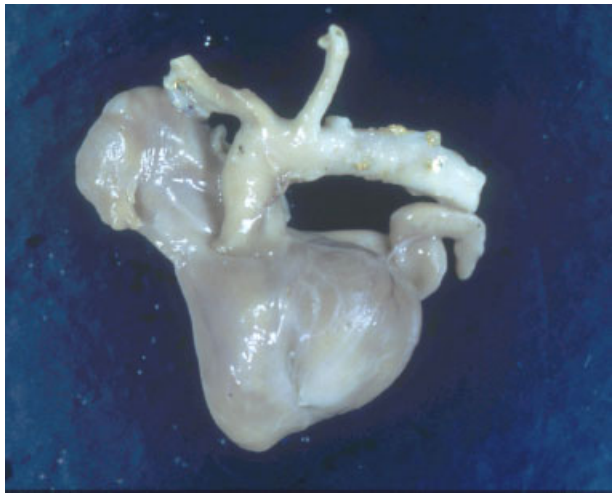

FIG. 5. Pulmonary artery agenesis in Patient 2. [Color figure can be viewed in the online issue, which is available at www.interscience.wiley.com.]

anomalies were found on neuropathologic examination.

MOLECULAR STUDIES

Standard Karyotype and FISH Analysis

In all 20 metaphases analyzed, chromosomal analysis of the fetus 1 and 2 were normal. FISH analysis with BAC clones RP11-297K5, RP11-1149B18, RP11-239E10 showed two hybridization signals on chromosomes 8, 15, and 1, respectively. According to these results, a submicroscopic deletion was excluded.

In Situ Hybridization

The expression patterns of *FGF10* and the *FGFR2(IIIb)* isoform, corresponding to the only receptor form to which FGF10 specifically binds,

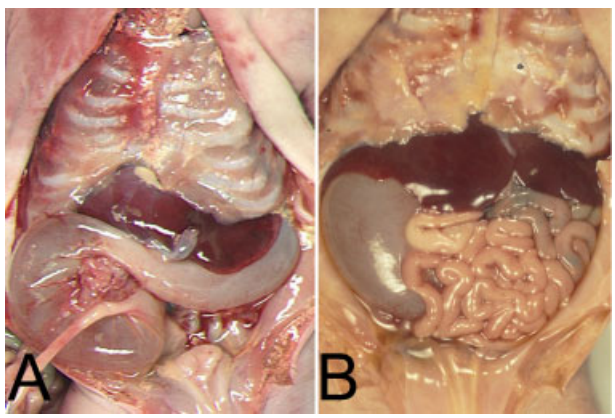

FIG. 6. Duodenal dilatation in Patient 1 (**A**) and Patient 2 (**B**). [Color figure can be viewed in the online issue, which is available at www.interscience.wiley.com.]

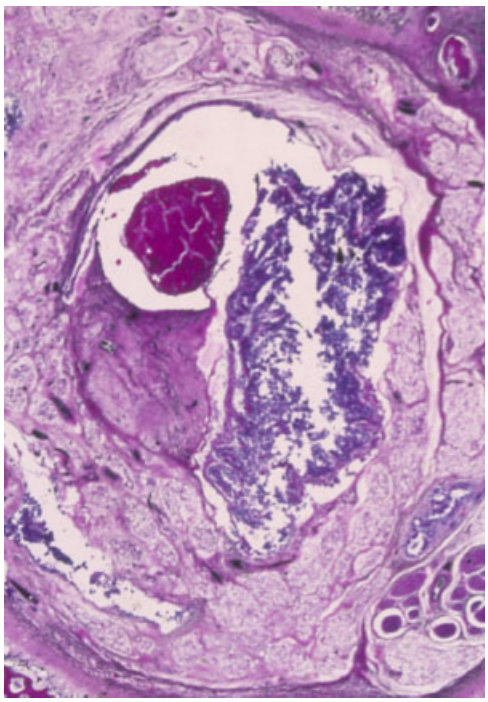

FIG. 7. Ocular histology (hematoxylin/eosin) in Patient 2 showing retinal dysplasia and cataract. [Color figure can be viewed in the online issue, which is available at www.interscience.wiley.com.]

were analyzed at multiple stages of development of normal human embryos.

At Carnegie stage (C) 11 (24 days' development, not shown) *FGF10* was restricted to the mesenchyme of the secondary heart field (future outflow tract) andweak expression began in the *anlage* of the adenohypophysis; diffuse central nervous system (CNS) expression was seen at C12 (26 days). *FGFR2(IIIb)* was transcribed in both cardiac inflow and outflow segments, throughout the CNS, and strongly expressed in the pharyngeal endoderm and lateral plate mesoderm. *FGF10* transcripts were observed at C13–C14 (28–32 days) in restricted portions of the otic vesicle and pharyngeal arch mesenchyme, as well as uniformly in fore- and hindlimb bud mesenchyme in similar domains to those already noted in vertebrate animal models. *FGFR2(IIIb)* began to be expressed at higher levels in both dorsal and ventral posterior diencephalon, in the ventral CNS elsewhere, in the ectodermal/endodermal epithelia of the pharyngeal arches, in the gut endoderm, and in the otic vesicle. At C15 (34 days, not shown) and C19 (47 days), *FGF10* expression was present in the nasal pit ectoderm as well as in the neural retina (Fig. 8A, inset). An equivalent retinal expression domain had not hitherto been noted in the reports of spatiotemporal transcript distribution in the mouse or chick.

Expression was maintained in the germinal layers of the CNS for both *FGF10* and *FGFR2(IIIb)* at C19. Particularly intense *FGF10* signal was observed in the future hypothalamus (mirroring the strong receptor expression visible between C12 and C15), while both *FGF10* and its receptor were expressed in the developing adenohypophysis (ah; Fig. 8A–C). Complementary patterns were observed in the facial primordia, with strong *FGF10* expression in the tooth mesenchyme and tongue muscle (tb, to; Fig. 8C), and more discretely in the nasal and palatial mesenchyme (fm), while *FGFR2(IIIb)* was transcribed within the buccal ectoderm (be) and pharyngeal endodermal epithelia, within the thymic and thyroid primordia (thry, tm), and around the condensing mesenchyme of Meckel's cartilage (MC; Fig. 8D). Intense *FGF10* expression was found in the muscular layer of the stomach (not shown), intestine and rectum (int; Fig. 8A), and lower levels were observed in the mesenchyme of the urogenital folds (uf); *FGFR2(IIIb)* transcripts were localized to the urogenital fold epithelium (Fig. 8B) and their signal was only above background within the intestinal mucosal epithelium. However, both ligand and receptor were expressed in the muscular layer of the physiological (at this stage) intestinal hernia into the umbilical cord (Fig. 8A,B). Lung (lu) expression patterns were also complementary, with *FGF10* transcripts observed in the interstitial mesenchyme between the developing lobes (Fig. 8E), and *FGFR2(IIIb)* highly expressed in the tracheal and bronchial epithelia (Fig. 8F). Both genes were expressed in the pericartilaginous condensations of the developing digits at this stage (Fig. 8A,B).

FGF10 and *FGFR2* Gene Analyses

Direct sequencing of both cases was carried out for the *FGF10* and *FGFR2* genes. Case 1 had a heterozygous, conservative substitution in *FGFR2* at V534V, inherited from his non-affected mother. *FGF10* had no sequence variations from the published sequence (RefSeq NM_004465). Genescan analysis showed that unaffected parents and affected fetus shared one common allele encompassing the entire gene and flanking regions (data not shown), rendering an interstitial chromosomal deletion unlikely in the face of probable familial recurrence.

Case 2 had no coding variations in *FGF10* but demonstrated heterozygosity at IVS2-15g > c, thereby excluding a heterozygous deletion of the entire gene. For *FGFR2*, while no coding variations were seen, a known SNP was identified at V232V (dbSNP: rs17859273), allowing the same conclusion to be drawn.

DISCUSSION

The principal clinical signs of hitherto reported cases of MWS or PMD syndrome in comparison to our two cases, are presented in Table I. In both our cases, bilateral pulmonary agenesis is associated

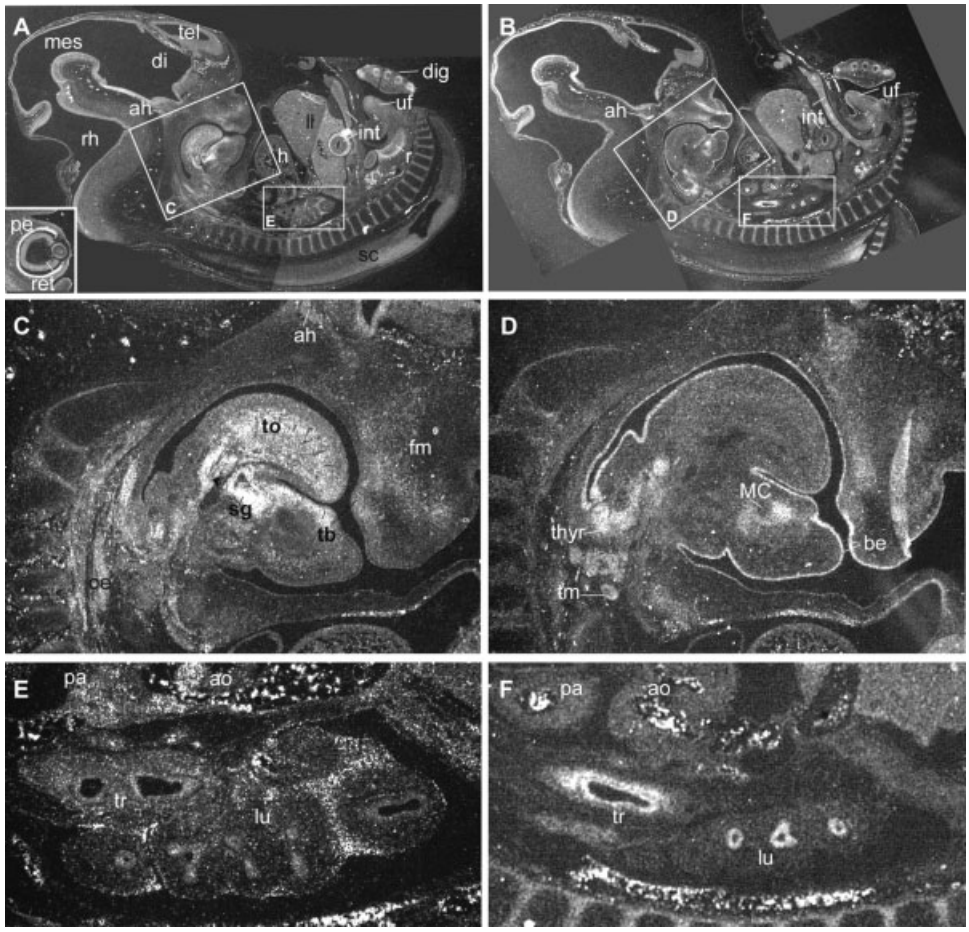

FIG. 8. In situ hybridization on human parasagittal embryo sections at Carnegie stage 19 (47 days) using ribosondes against *FGF10* (**A**,**C**,**E**) or *FGFR2(IIIb)* (**B**,**D**,**F**). Signal in white, aside from refringent red blood cells. Rostral left, ventral top. A: *FGF10* transcripts are observed in this near-sagittal section in the germinal zone of the CNS, in particular in the ventral diencephalon; in the muscle of the tongue, esophagus and intestine, with strong expression in the rectum, and in the mesenchyme of the urogenital folds. Inset: distinct expression is observed in the neural retina. B: An adjacent section hybridized with the *FGFR2(IIIb)* antisense probe. Transcripts are observed in the endodermal and ectodermal epithelia, in the adenohypophysis, the urogenital fold and hindlimb ectoderm. C: A close-up of the craniofacial region shows low *FGF10* expression in the adenohypophysis, more intense signal in the tooth buds and forming salivary glands, and in the facial mesenchyme and oesophageal muscles. D: *FGFR2(IIIb)* is expressed complementarily in the buccal ectoderm and pharyngeal endodermal epithelium; in the thyroid and thymic primordia, and around but not within Meckel's cartilage. E: FGF10 transcripts are seen at low levels in the muscular walls of the pulmonary artery and aorta, and in the interlobar mesenchyme of the lung. F: Its receptor is transcribed within the tracheal and bronchial epithelia, but not in the great vessels. Non-specific, flocular signal is seen at the sites of red blood cell accumulation.

with diaphragmatic eventration. In one case, the pulmonary artery was absent, in the other pulmonary artery branches were missing. Two other cases described previously had bilateral pulmonary agenesis associated with unilateral diaphragmatic eventration [Spear et al., 1987; Engellenner et al., 1989]. Similar facial gestalt exists in our cases, and included a high forehead, short palpebral fissures and microphthalmia, short nose with anteverted nostrils and a small chin. Similar features such as flat face, long philtrum, narrow palpebral fissures, prominent nose have been observed by other groups [Seller et al., 1996; Steiner et al., 2002].

It is noteworthy that duodenal stenosis was present in both of our cases, though not previously reported. Moreover, we have observed pancreatic agenesis and a multilobulated spleen in the second case. Seller et al. [1996] had observed a case with a hypoplastic spleen. Two other cases presented with renal dysplasia and malrotation [Engellenner et al., 1989; Priolo et al., 2004]. In our second case, the sonogram noted a moderate renal dysplasia which was not confirmed at the autopsy.

Microphthalmia/anophthalmia in association with diaphragmatic defect and pulmonary hypoplasia has been reported in multiple syndromes, including Fryns syndrome [Lubinsky et al., 1983], Fraser syndrome, Goldenhar syndrome, and Goltz–Gorlin syndrome [Kunze et al., 1979; Warburg et al., 1997]. Fryns syndrome is the best-characterized syndrome of diaphragmatic defects with eye abnormalities [reviewed in Fryns, 1987; Cunniff et al., 1998]. The combination of features in Fryns syndrome was described as follows: hydramnios, coarse face, cleft palate, distal limb hypoplasia, diaphragmatic defect, lung hypoplasia, cloudy cornea,

TABLE I. Comparison of Clinical Findings in Matthew-Wood Syndrome Reported in the Literature

Finding	Patient 1	Patient 2	Berkenstadt et al.	Spear et al.	Engellener et al.	Seller et al. (two sibs)	Steiner et al. (two sporadic cases)	Priolo et al.
Microphthalmia/ anophthalmia	Bilateral	Bilateral	Bilateral	Bilateral	Unilateral	Bilateral (2/2)	Bilateral (2/2)	Bilateral
Pulmonary malformation	Bilateral agenesis of pulmonary artery branches	Bilateral agenesis	Unilateral agenesis	Bilateral agenesis	Bilateral agenesis	Bilateral agenesis of upper lobes (1/2), bilateral hypoplasia (1/2)	No lung anomaly (1/2), bilateral broncho-pulmonary dysplasia (1/2)	Bilateral hypoplasia
Diaphragmatic defect	Bilateral (eventration)	Bilateral (eventration)	Unilateral (hernia)	Unilateral (eventration)	Unilateral (inverted)	No (2/2)	Bilateral (eventration) (2/2)	Unilateral (hernia)
Cardiac malformation	No	Pulmonary artery agenesis, ventricular septal defect	No	Pulmonary artery agenesis, ventricular septal defect	Moderate dilatation of right atrium, closed narrow ductus	Single ventricle, hypoplastic left atrium, enlarged pulmonary trunk	Ostium primum ASD, right ventricular hypertrophy (1/2)	No
Facial anomalies	Short palpebral fissures, short nose, retrognathia, large ears	Short palpebral fissures, long philtrum, large ears	Not documented	Not documented	Not documented	Prominent nose, short upper lip, micrognathia with cleft palate, low-set ears (1/2)	Short palpebral fissures, prominent nose with anteverted nares	
Other	Duodenal stenosis, hypoplastic pancreatic structures	Duodenal stenosis, poly-lobed spleen, agenesis of pancreas	−	−	Renal dysplasia	Hypoplastic spleen and uterus	Cryptorchidism (1/2)	Malrotation of the left kidney
Growth retardation	+	+	+	+	+	+	+ (1/2)	+
Polyhydramnios	+	+	+	−	+	−	+ (1/2)	+
Karyotype	Normal	Normal	Normal	Normal	Normal	Normal	Normal (2/2)	Normal
Consanguinity	Yes, three sibs	Yes	No	No	No	No, two sibs	No (2/2)	No

American Journal of Medical Genetics Part A: DOI 10.1002/ajmg.a

TABLE II. PCR Primers for Direct Sequencing of Human FGF10 and FGFR2

	Name	Temperature	Amplicon size
TCCAGTATGTTCCTTCTGATG	FGF10-1F	54.5°C	424 bp
TGGGGGTGGATAATTGGAA	FGF10-1R	54.5°C	
TTGCCGGGTTTTAAGACACA	FGF10-2F	55°C	332 bp
GGTAATGGTTTACTGGAGTGG	FGF10-2R	55°C	
CTGGATGGCTTGTATCAAATG	FGF10-3F	54.5°C	319 bp
TTGGCAAAAGAGCCATTGGT	FGF10-3R	54.5°C	
TCCCTGACTCGCCAATCTCTTTC	FGFR2-EX2-F	55°C	343 bp
TGCCCCCAGACAAATCCCAAAAC	FGFR2-EX2-R	55°C	
CACTGACCTTTGTTGGACGTTC	FGFR2-EX3-F	55°C	380 bp
GAGAAGAGAGAGCATAGTGCTGG	FGFR2-EX3-R	55°C	
TGGAGAAGGTCTCAGTTGTAGAT	FGFR2-EX4-F	55°C	232 bp
AGACAGGTGACAGGCAGAACT	FGFR2-EX4-R	55°C	
CAAAGCGAAATGATCTTACCTG	FGFR2-EX5-F	55°C	291 bp
AGAAATGTGATGTTCTGAAAGC	FGFR2-EX5-R	55°C	
GCTAGGATTGTTAAATAACCGCC	FGFR2-EX6-F	55°C	226 bp
AAACGAGTCAAGCAAGAATGGG	FGFR2-EX6-R	55°C	
ACAGCCCTCTGGACAACACA	FGFR2-EX7-F	55°C	393 bp
CTGGCTAGTCAAAAAAGAGAA	FGFR2-EX7-R	55°C	
CTTTAATGCCGCTGTTTAG	FGFR2-EXIIIB-F	54°C	333 bp
TCTTTTCAGCTTCTATATCCAG	FGFR2-EXIIIB-R	54°C	
ATCATTCCTGTGTCGTCTAG	FGFR2-EXIIIC-F	54°C	224 bp
AAAAACCCAGAGAGAAAGAACAGTATA	FGFR2-EXIIIC-R	54°C	
TGCGTCAGTCTGGTGTGCTAAC	FGFR2-EX9-F	55°C	341 bp
AGGACAAGATCCACAAGCTGGC	FGFR2-EX9-R	55°C	
TGACTTCCAGCCTTCTCAGATG	FGFR2-EX10-F	55°C	252 bp
AGTCTCCATCCTGGGACATGG	FGFR2-EX10-R	55°C	
CCCCATCACCAGATGCTATGTG	FGFR2-EX11-F	55°C	221 bp
TTGATAAGACTCTCCACCCAGCC	FGFR2-EX11-R	55°C	
GAGGAAATGAACTGATTTGTG	FGFR2-EX12-F	55°C	192 bp
GCAGAGTATTTGGGCGAATG	FGFR2-EX12-R	55°C	
CTGGATTCTCTCTTTAGGGAG	FGFR2-EX13-F	55°C	263 bp
CACCCAGCCAAGTAGAATG	FGFR2-EX13-R	55°C	
ACATATTTCCTTTTTGTTCTGG	FGFR2-EX14-F	55°C	256 bp
TCTTCCTGGAACATTCTGAG	FGFR2-EX14-R	55°C	
GAGCCTGCTAAGATAAATTCTT	FGFR2-EX15-F	55°C	180 bp
AGCTCAAGCCCAGGAAAAAG	FGFR2-EX15-R	55°C	
GGTTTTGGCAACGTGGATGGG	FGFR2-EX16-F	55°C	254 bp
GAGAGGTATTACTGGTGTGGCAAG	FGFR2-EX16-R	55°C	
ACACCACGTCCCCATATTGCC	FGFR2-EX17-F	55°C	243 bp
CTCACAAGACAACCAAGGACAAG	FGFR2-EX17-R	55°C	
TCCCACGTCCAATACCCACAT	FGFR2-EX18-F	55°C	368 bp
TTCCCAGTGCTGTCCTGTTTGG	FGFR2-EX18-R	55°C	

microphthalmia, renal dysplasia, and cerebral malformations. It is interesting that primary pulmonary hypoplasia without a diaphragmatic defect has also been described in Fryns syndrome [Willems et al., 1991; Wilgenbus et al., 1994]. Furthermore, chromosomal abnormalities, such as deletions of 15q26.2, 8p23.1, and 1q41-q42.12, have been associated with the congenital diaphragmatic herniaof Fryns syndrome [Slavotinek et al., 2005; Kantarci et al., 2006]. We excluded submicroscopic deletions in these regions of both present patients using FISH.

The hallmarks of Fraser syndrome are cryptophtalmos or anophthalmia (93%), laryngeal atresia with enlarged lungs, cutaneous syndactyly of digits (54%), genital or renal anomalies with frequent renal agenesis (90%), abnormal ears and an anomaly of cord implantation on the abdominal wall [Tibboel and Gaag, 1996]. Almost half of the affected infants are stillborn or die in infancy, and mental retardation is common. In humans, this autosomal recessive disorder is genetically heterogeneous. The *FRAS1* gene maps to 4q21 and encodes a large extracellular matrix protein highly homologous to the murine equivalent [McGregor et al., 2003]. In two families with Fraser syndrome unlinked to the *FRAS1* gene, Jadeja et al. [2005] found a missense mutation in the *FREM2* gene. Both proteins are involved in ectodermal adhesion to underlying basal mesenchyme during development [reviewed in Smyth and Scambler, 2005]. The absence of characteristic signs of Fraser syndrome, in particular, digital and renal anomalies, support a different condition in our cases, although they may be functionally related through impaired epithelial-mesenchymal signaling during fetal life.

The mode of transmission of the Matthew-Wood syndrome has been a subject of debate. Most cases reported in the literature appear to be isolated. However, Seller et al. [1996] reported two sibs of

a non-consanguineous Caucasian couple who presented MWS. Both children had pulmonary hypoplasia and anophthalmia. One also had a number of other malformations, as micrognathia, a cleft palate reminiscent of the bifid uvula in our second case, a short upper lip and low-set ears. The autopsy showed a single ventricle, an hypoplastic left atrium, an hypoplastic spleen and a bicornuate uterus.

Both our cases occurred in consanguineous couples, as may have been the case for one of the original reports comprising bilateral colobomatous microphthalmia and diaphragmatic eventration [Radhakrishnan, 1981], highly supporting a recessive autosomal inheritance. Moreover, in our first case an additional sibling presented with similar features (respiratory anomalies and anophthalmia).

Our cases, together with previously published cases with similar features, strongly support the hypothesis that this combination of defects is non-random [Steiner et al., 2002]. The spectrum of malformations seems to correspond to organs developing simultaneously from the fourth week of gestation on [Priolo et al., 2004]. The expression patterns in both animal models and humans of *FGF10* and *FGFR2(IIIb)* were evocative of the organ systems affected in MWS, although coding anomalies in these genes were excluded in our cases. The presence of *FGF10* transcripts in the human neural, non-pigmented retina was novel relative to reports made in animal models to date, demonstrating the relevance of performing expression analysis in human embryos. Further studies will be needed to rule out mutations in the promoter regions of these genes spread over large genomic territories, as well as modified functional interactions with heparin sulfate or intracellular effector gene candidates.

In summary, rare cases of microphthalmia/anophthalmia associated with pulmonary hypoplasia/agenesis have been hitherto reported in the literature. We report on two patients presenting microphthalmia and pulmonary agenesis associated with bilateral diaphragmatic eventration. In addition, not previously reported, both cases presented duodenal stenosis. Facial gestalt is rather similar to hitherto reported cases. Most cases of Matthew-Wood syndrome are described as sporadic. Our cases occurred in consanguineous families with recurrence among sibs in the first family. As in a similar, published case [Seller et al., 1996], these observations strongly support autosomal recessive inheritance of the syndrome. However, additional cases will be necessary to further delineate this syndrome, as well as to provide some information on its natural history. Further molecular studies may help us understand these pleiotropic field defects. Meanwhile, careful sonogram examination in further pregnancies should be offered to the families.

ACKNOWLEDGMENTS

We thank the medical staff of the Centre d'Orthogénie at the Hôpital Broussais for their collaboration and G. Goudefroye, C. Ozilou, and M. Alcaraz for their excellent technical assistance. We offer our appreciation to the families for participating in this study. The support of A. Munnich is also gratefully acknowledged. This work was supported by the Association Française contre les Myopathies, the Institut National pour la Santé et la Recherche Médicale (INSERM) "Avenir" program and the Assistance Publique—Hôpitaux de Paris (AP-HP).

REFERENCES

Berkenstadt M, Lev D, Achiron R, Rosner M, Barkai G. 1999. Pulmonary agenesis, microphthalmia, and diaphragmatic defect: New syndrome or association? Am J Med Genet 86:6–8.

Cunniff C, Curtis M, Hassed SJ, Hoyme HE. 1998. Blepharophimosis: A causally heterogeneous malformation frequently associated with developmental disabilities. Am J Med Genet 75:52–54.

De Moerlooze L, Spencer-Dene B, Revest J, Hajihosseini M, Rosewell I, Dickson C. 2000. An important role for the IIIb isoform of fibroblast growth factor receptor 2 (FGFR2) in mesenchymal-epithelial signalling during mouse organogenesis. Development 127:483–492.

Engellenner W, Kaplan C, Van de Vegte GL. 1989. Pulmonary agenesis association with nonimmune hydrops. Pediat Path 9:725–730.

Enns GM, Cox VA, Goldstein RB, Gibbs DL, Harrison ML, Golabi M. 1998. Congenital diaphragmatic defects and associated syndromes, malformations, and chromosome anomalies: A retrospective study of 60 patients and literature review. Am J Med Genet 79:215–225.

Fairbanks TJ, Kanard RC, Del Moral PM, Sala FG, De Langhe SP, Lopez CA, Veltmaat JM, Warburton D, Anderson KD, Bellusci S, Burns RC. 2005. Colonic atresia without mesenteric vascular occlusion. The role of the fibroblast growth factor 10 signaling pathway. J Pediatr Surg 40:390–396.

Fryns JP. 1987. Fryns syndrome: A variable MCA syndrome with diaphragmatic defects, coarse face, and distal limb hypoplasia. J Med Gen 24:271–274.

Jadeja S, Smyth I, Pitera JE, Taylor MS, van Haelst M, Bentley E, McGregor L, Hopkins J, Chalepakis G, Philip N, Perez Aytes A, Watt FM, Darling SM, Jackson I, Woolf A, Scambler PJ. 2005. Identification of a new gene mutated in Fraser syndrome and mouse myelencephalic blebs. Nat Genet 37:520–525.

Kantarci S, Casavant D, Prada C, Russell M, Byrne J, Haug LW, Jennings R, Manning S, Blaise F, Boyd TK, Fryns JP, Holmes LB, Donahoe PK, Lee C, Kimonis V, Pober BR. 2006. Findings from aCGH in patients with congenital diaphragmatic hernia (CDH): A possible locus for Fryns syndrome. Am J Med Genet Part A 140A:17–23.

Kunze J, Heyne K, Wiedemann HR. 1979. Diaphragmatic hernia in a female newborn with focal dermal hypoplasia and marked asymmetric malformations (Goltz-Gorlin syndrome). Eur J Pediatr 28:213–218.

Li L, Wei J. 2006. A newborn with anophthalmia and pulmonary hypoplasia (the Matthew-Wood syndrome). Clin Dysmorphol 15:43–44.

Lubinsky M, Severn C, Rapoport JM. 1983. Fryns syndrome: A new variable multiple congenital anomaly (MCA) syndrome. Am J Med Genet 14:461–466.

McGregor L, Makela V, Darling SM, Vrontou S, Chalepakis G, Roberts C, Smart N, Rutland P, Prescott N, Hopkins J, Bentley E, Shaw A, Roberts E, Mueller R, Jadeja S, Philip N, Nelson

J, Francannet C, Perez-Aytes A, Megarbane A, Kerr B, Wainwright B, Woolf AS, Winter RM, Scambler PJ. 2003. Fraser syndrome and mouse blebbed phenotype caused by mutations in *FRAS1/Fras1* encoding a putative extracellular matrix protein. Nat Genet 34:203–208.

Min H, Danilenko DM, Scully SA, Bolon B, Ring BD, Tarpley JE, DeRose M, Simonet WS. 1998. Fgf-10 is required for both limb and lung development and exhibits striking functional similarity to Drosophila brancheless. Genes Dev 12:3156–3161.

Ohuchi H, Nakagawa T, Yamamoto A, Araga A, Ohata T, Ishimaru Y, Yoshioka H, Kuwana T, Nohno T, Yamasaki M, Itoh N, Nijo S. 1997. The mesenchymal factor, FGF10, initiates and maintains the outgrowth of the chick limb bud through interaction with FGF8, an apical ectodermal factor. Development 124:2235–2244.

Priolo M, Casile G, Lagana C. 2004. Pulmonary agenesis/hypoplasia, microphthalmia, and diaphragmatic defects: Report of an additional case. Clin Dysmorphol 13:45–46.

Radhakrishnan N. 1981. Colobomatous microphthalmia with diaphragmatic eventration (a case report). Indian J Ophthalmol 28:221–222.

Robert Lee SYR, Shiu YK, Ng WF, Chow CB. 2006. Another patient with pulmonary hypoplasia, microphthalmia and diaphragmatic hernia. Clin Dysmorphol 15:43–44.

Romana SP, Cherif D, Le Coniat M, Derre J, Flexor MA, Berger R. 1993. *In situ* hybridization to interphase nuclei in acute leukemia. Genes Chromosomes Cancer 8:98–103.

Sekine K, Ohuchi H, Fujiwara M, Yamasaki M, Yoshizawa T, Sato T, Yagishita N, Matsui D, Koga Y, Itoh N, Kato S. 1999. Fgf10 is essential for limb and lung formation. Nat Genet 21:138–141.

Seller MJ, Davis TB, Fear CN, Flinter FA, Ellis I, Gibson AG. 1996. Two sibs with anophthalmia and pulmonary hypoplasia (the Matthew-Wood syndrome). Am J Med Genet 62:227–229.

Slavotinek A, Lee SS, Davis R, Shrit A, Leppig KA, Rhim J, Jasnosz K, Albertson D, Pinkel D. 2005. Fryns syndrome phenotype caused by chromosome microdeletions at 15q26.2 and 8p23.1. J Med Genet 42:730–736.

Smith SA, Martin KE, Dodd KL, Young ID. 1994. Severe microphthalmia, diaphragmatic hernia and Fallot's tetralogy associated with a chromosome 1;15 translocation. Clin Dysmorphol 3:287–291.

Smyth I, Scambler P. 2005. The genetics of Fraser syndrome and the blebs mouse mutants. Hum Mol Genet 14:R269–R274.

Spear GS, Yetur P, Beyerlein RA. 1987. Bilateral pulmonary agenesis and microphthalmia. Am J Med Genet 3:379–382.

Steiner RD, Dignan PSJ, Hopkin RJ, Kozielski R, Bove KE. 2002. Combination of diaphragmatic eventration and microphthalmia/anophthalmia is probably non-random. Am J Med Genet 108:45–50.

Tibboel D, Gaag AV. 1996. Etiologic and genetic factors in congenital diaphragmatic hernia. Clin Perinatol 23:689–699.

Trueba SS, Auge J, Mattei G, Etchevers H, Martinovic J, Czernichow P, Vekemans M, Polak M, Attie-Bitach T. 2005. PAX8, TITF1, and FOXE1 gene expression patterns during human development: New insights into human thyroid development and thyroid dysgenesis-associated malformations. J Clin Endocrinol Metab 90:455–462.

Warburg M, Jensen H, Prause JU, Bolund S, Skovby F, Miranda MJ. 1997. Anophthalmia-microphthalmia-oblique clefting syndrome: Confirmation of the Fryns anophthalmia syndrome. Am J Med Genet 73:36–40.

Wilgenbus KK, Engers R, Crombach G, Majewski F. 1994. Two fetuses with Fryns syndrome without diaphragmatic defect. J Med Genet 31:962–964.

Wilkinson DG. 1992. *In situ* hybridization: A practical approach. UK: IRL Press.

Willems PJ, Keersmaekers GHA, Dom KE, Colpaert C, Schatteman E, Vergote IBP, Dumon JE. 1991. Fryns syndrome without diaphragmatic hernia? Am J Med Genet 41:255–257.

nature genetics

Homozygous silencing of T-box transcription factor *EOMES* leads to microcephaly with polymicrogyria and corpus callosum agenesis

Lekbir Baala[1,2], Sylvain Briault[3,8], Heather C Etchevers[2], Frédéric Laumonnier[3], Abdelhafid Natiq[1], Jeanne Amiel[2], Nathalie Boddaert[4], Capucine Picard[5], Aziza Sbiti[1], Abdellah Asermouh[6], Tania Attié-Bitach[2,7], Féréchté Encha-Razavi[2,7], Arnold Munnich[2,7], Abdelaziz Sefiani[1] & Stanislas Lyonnet[2,7]

Neural progenitor proliferation and migration influence brain size during neurogenesis. We report an autosomal recessive microcephaly syndrome cosegregating with a homozygous balanced translocation between chromosomes 3p and 10q, and we show that a position effect at the breakpoint on chromosome 3 silences the eomesodermin transcript (*EOMES*), also known as T-box-brain2 (*TBR2*). Together with the expression pattern of *EOMES* in the developing human brain, our data suggest that *EOMES* is involved in neuronal division and/or migration. Thus, mutations in genes encoding not only mitotic and apoptotic proteins but also transcription factors may be responsible for malformative microcephaly syndromes.

Microcephaly syndromes are a heterogeneous group of genetic disorders in which affected individuals have a head circumference below 3 s.d., a small and malformed brain and cognitive deficiency. A large consanguineous Moroccan family was referred to us with a marked prenatal-onset microcephaly (mean occipitofrontal circumference at birth = –4 s.d.) and severe motor delay with hypotonia in four affected children. Early lethality was observed in three children (death at 15–18 months of age) due to respiratory distress after chronic infections. The surviving child (patient V.6) has had a persistent fever since birth and recurrent infections (**Supplementary Note** online).

Notably, in addition to congenital microcephaly, these individuals consistently showed corpus callosum agenesis, bilateral polymicrogyria, ventricular dilatation and a small cerebellum, as demonstrated by brain CT and MRI scans (**Supplementary Fig. 1** online). This defines a congenital microcephaly with extensive polymicrogyria[1], the mechanisms of which are not known and are presumably ascribed to abnormal neuronal and/or glial proliferation or apoptosis. This condition is clearly different from primary microcephaly syndromes.

Despite a pattern of affected individuals in the pedigree suggestive of an autosomal mode of inheritance, chromosomal analysis on leukocytes showed a reciprocal balanced translocation between chromosomes 3p and 10q segregating in the family (**Fig. 1a**). We found that the translocation was homozygous in each of the four affected individuals studied (46,XY,t(3;10)(p24;q23)2x), whereas healthy parents were heterozygous. Genome-wide comparative genomic hybridization pattern analysis showed that chromosomal rearrangement had occurred without detectable loss or gain of genetic material at a resolution of 3 Mb (data not shown).

Linkage analysis between the disease trait and polymorphic markers of chromosomes 3p and 10q defined two regions identical by descent of 27 Mb and 11.4 Mb, respectively (**Fig. 1b**). The two-point lod score between the translocation breakpoint used as a marker, and the disease locus peaked at significant values of 3.45. In addition, we excluded linkage to the six known primary microcephaly loci (*MCPH1* to *MCPH6*) (**Supplementary Methods** online). One hypothesis is that a locus involved in neuronal proliferation and/or migration maps to either chromosome 3 or chromosome 10 and that the translocation breakpoint disrupts the disease-causing gene.

We therefore established a physical map of chromosomal regions 3p24 and 10q23 and characterized the BACs that encompassed the breakpoints for each chromosome (BAC RP11-9a14 and RP11-102H24 on chromosomes 3 and 10, respectively; **Supplementary Fig. 2** and **Supplementary Table 1** online). Furthermore, DNA sequencing of long-range PCR products allowed us to characterize the translocation breakpoints and demonstrate that they occurred without any deletion at nucleotide positions 27954024 and 82932753 (NCBI build 36.1) on chromosomes 3p and 10q, respectively (**Supplementary Methods** and **Supplementary Fig. 3** online). Notably, neither of the translocation breakpoints disrupted a known or predicted gene coding sequence on either chromosome, suggesting that the translocation affected surrounding gene(s) by a positional effect.

Among the nine annotated genes located closest to the breakpoints, *EOMES* (MIM 604615) was considered the best candidate gene. *EOMES* encodes a transcription factor, a member of the T-box family, that is critical in vertebrate embryonic development of the central nervous system and mesoderm[2–4]. The *EOMES* locus (NCBI build 36.1, position 27732891–27738789) is located 215 kb 3′ to the translocation breakpoint on chromosome 3p and is transcribed away from it. We sequenced the six annotated coding exons of *EOMES* in affected family members and did not find any mutation in these or in a 5′ predicted noncoding exon that is located 136 bp

[1]Département de Génétique Médicale, Institut National d'Hygiène, Rabat, Maroc. [2]INSERM U781, Hôpital Necker, Département de Génétique, Paris, France. [3]INSERM U619, Faculté de Médecine, Tours, France. [4]Hôpital Necker, Service de Radiologie Pédiatrique and [5]Centre d'étude des déficits immunitaires, Paris, France. [6]Hôpital d'Enfants CHU Avicenne, Rabat, Maroc. [7]Université Réné Descartes - Paris 5, Paris, France. [8]Present address: Laboratoire de génétique, CHR La Source, Orléans, France. Correspondence should be addressed to S.L. (lyonnet@necker.fr).

Received 27 November 2006; accepted 1 February 2007; published online 11 March 2007; doi:10.1038/ng1993

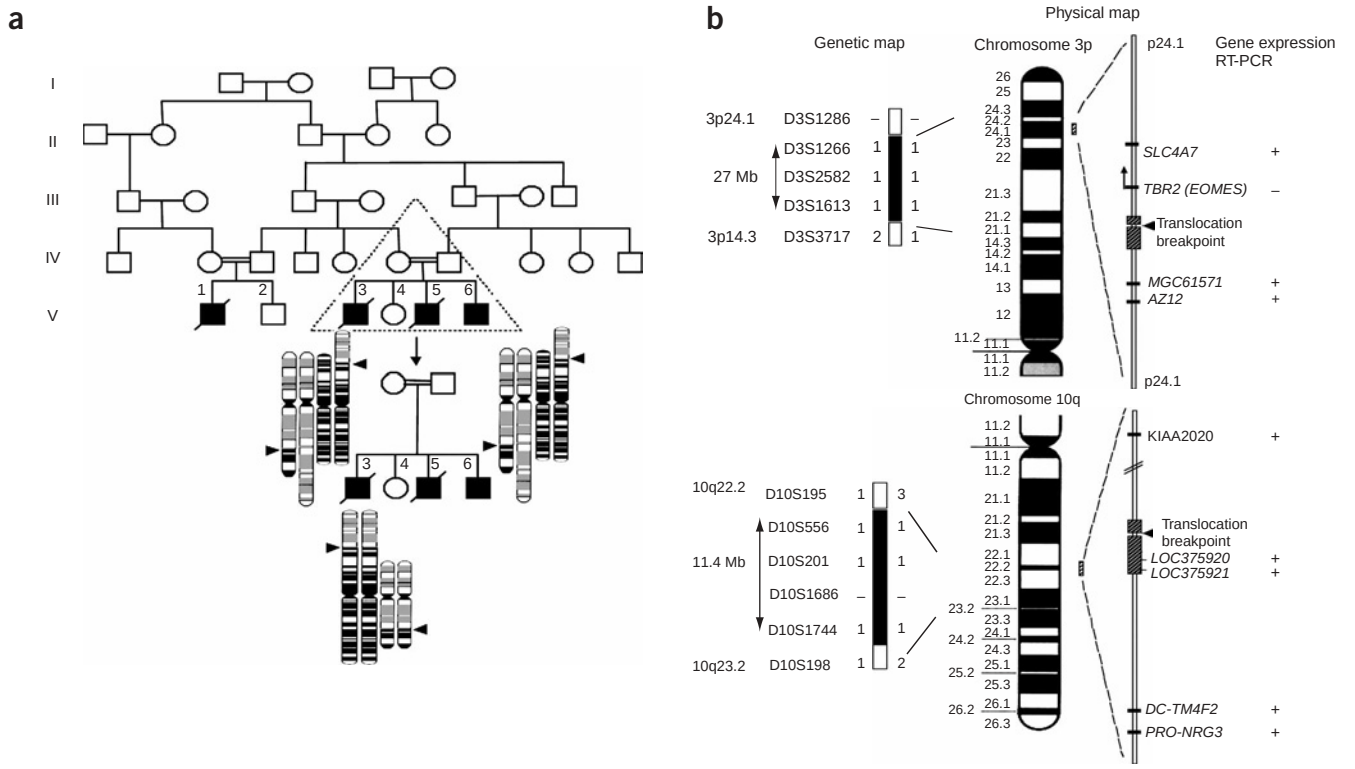

Figure 1 Segregation, genetic and fine physical mapping of the disease locus. (**a**) Simplified family pedigree. Chromosomal and molecular analyses were carried out on the core family (indicated by a triangle) after we obtained their informed, written consent, under supervision by the Necker Hospital ethics committee. Filled black symbols indicate individuals with the microcephaly syndrome. R banding of chromosomes 3 and 10 is schematically presented; arrowheads indicate translocation breakpoints. (**b**) Mapping of the disease locus using homozygosity for a balanced reciprocal translocation, and expression pattern in surrounding candidate genes. The BACs crossing the breakpoints were identified for both chromosomes 3p and 10q (shaded boxes). The genetic map shows the region cosegregating with the disease phenotype (filled black bars). Candidate genes are indicated on the physical map and in **Supplementary Table 2**. Results of qualitative PCR on lymphoblast cDNA from individual V.6 are shown at right (+, expressed; –, not expressed).

5′ to the transcription start site and may be used in several alternative *EOMES* transcripts (**Supplementary Table 2** online).

However, we identified a synonymous SNP in *EOMES* exon 6 (A/G, rs6783101; estimated frequency of the rare allele A in the African American population = 5.9%). The A allele of SNP rs6783101 cosegregated with the derivative 3p–10q translocated chromosome in the family, allowing its use as a *cis* marker to test allele-specific expression at the *EOMES* locus in cell lines. Indeed, quantitative RT-PCR showed no *EOMES* expression in affected individuals (**Fig. 2a**), whereas the only transcribed allele in a heterozygous parent carried the wild-type G nucleotide at SNP rs6783101 (**Fig. 2b**), demonstrating monoallelic expression and specific silencing of the *EOMES* allele on the translocated chromosome. Qualitative RT-PCR showed that, among the nine genes proximate to the breakpoints, the mRNA transcribed from *EOMES* on chromosome 3p24 was the only one absent from lymphoblast cell lines from affected individuals (**Fig. 1b**, **Supplementary Methods** and **Supplementary Table 2**).

Tbr2 has recently been shown to be pivotal in the developing mouse neocortex, along with other transcription factors, including *Pax6*, *NeuroD* and *Tbr1* (refs. 5,6). Therefore, we investigated the expression pattern of *EOMES* in human prenatal tissues at different stages of development (**Fig. 2c–i** and **Supplementary Methods**). The *EOMES* transcript was visibly expressed at 7 weeks of development (Carnegie stage 19) in a pattern apparently restricted to the forebrain floorplate of the central nervous system (**Fig. 2d**). However, we observed distinct *EOMES* expression within the mantle layer (**Fig. 2h**) and migrating neuroblasts (**Fig. 2i**) of the telencephalon at 12.5 weeks. This limited expression pattern differs from that of the mouse, implying evolutionary divergence of noncoding control elements, as shown for brain-specific expression of *WNT7A*[7]. This pattern supports a role for human *EOMES* in late neuronal development and suggests that its silencing contributes to the disease phenotype in individuals with microcephaly syndrome.

Proliferation and neuronal fate specification are key events in the developing ventricular zone and subventricular zone (SVZ) of the central nervous system[5,6]. Mouse *Eomes (Tbr2)* is expressed in these sites and may be involved in precursor proliferation. In humans, neuronal migration occurs largely between the 12th and 24th week of gestation. This period, preceded and accompanied by intense cell division in the ventricular zone, corresponds to the time frame in which we observe *EOMES* expression in the telencephalon. During development, a number of other transcriptional regulators balance cortical cell proliferation and differentiation[8]. In the cortex, radial glia produce both neurons and glia[9], whereas intermediate progenitor cells produce only neurons and divide away from the ventricular surface. The transition from radial glia to intermediate progenitor cell in the mouse is associated with upregulation of *Eomes* and downregulation of *Pax6*, whereas the subsequent transition from intermediate progenitor cell to postmitotic neuron is marked by downregulation of *Eomes* and upregulation of *Tbr1* (ref. 5). Interruption of the efficiency of precursor production, or secondary impairment of neuronal migration, would be predicted to result in a smaller telencephalic

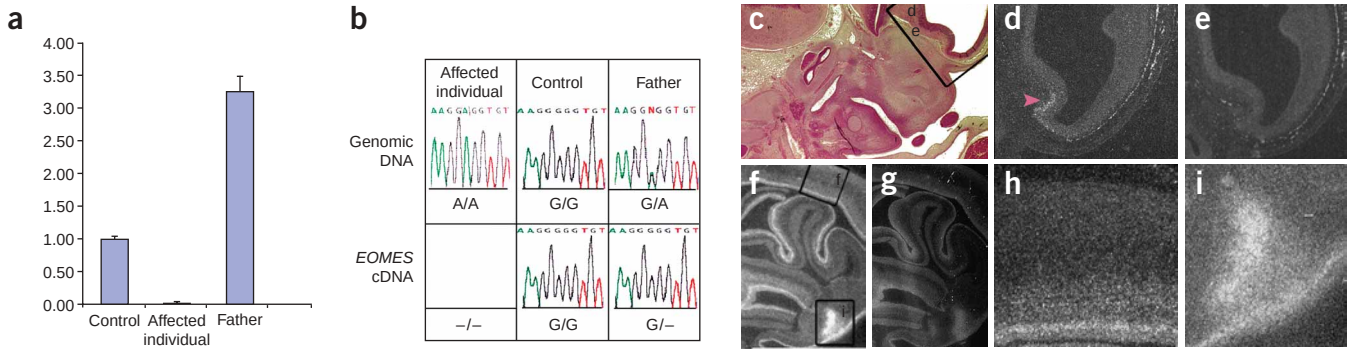

Figure 2 Silencing of the translocated *EOMES* locus and normal *EOMES* expression in the developing human brain. (**a**) Quantitative PCR of *EOMES* exon 6 on cDNA derived from lymphoblast lines of a control individual, the homozygous affected individual V.6 and his heterozygous father, normalized to the expression level of β-actin. Bars represent s.d. from three replicates. (**b**) Monoallelic expression of the wild-type *EOMES* locus. Genomic sequence traces centered on the A/G SNP found in *EOMES* exon 6 are shown for affected individual V.6, his father and a control. RT-PCR sequences of the *EOMES* mRNA in the same individuals are shown below. We did not detect any *EOMES* mRNA in V.6, whereas only the non-translocated *EOMES* allele was expressed in the heterozygous father. (**c**–**i**) Parasagittal sections through the head of a Carnegie stage 19 embryo (7 weeks of development). **c**, hematoxylin-eosin (HE) stain. **d**, enlargement of basal forebrain showing discrete *EOMES* expression in the floorplate (arrowhead) as compared with the adjacent sense control hybridized slide (**e**). **d** and **e** are 75–80 μm medial to **c**. We observed localized *EOMES* expression when we hybridized an antisense probe (**f**) versus a sense probe (**g**) in adjacent frontal sections through the telencephalon of a fetus at 12.5 weeks of development. Magnifications of the cortical mantle layer (**h**), with intense signal in the subventricular zone, and dense neuroblasts (**i**) of the future basal ganglia.

surface. However, the fact that normally sized brains are also associated with corpus callosum agenesis, as well as the complexity of corpus callosum development, does not permit the conclusion that the absence of the corpus callosum in these individuals is readily explained by a neuronal migration or proliferation defect alone. Furthermore, *EOMES* may have a species-specific role in corpus callosum development. We screened six unrelated individuals with absent corpus callosum as a primary feature for coding sequence mutations of the *EOMES* gene and did not find any mutations or rearrangements (data not shown). At least 18 numerical or structural chromosomal aberrations have been reported in individuals with corpus callosum defects, and more heterogeneity is likely[1].

Eomes has been described in mouse as a key transcription factor for memory $CD8^+$ T cells and for full effector differentiation of $CD8^+$ T cells[10]. *Eomes* is induced in effector $CD8^+$ T cells after viral infection and after expression increases in memory T cells; it is induced in memory cells only after bacterial infections leading to high levels of interleukin 12, which favors the acute host response[11]. However, we did not detect any major immune deficiency and/or quantitative abnormalities in the T CD8 subset in affected individual V.6 (**Supplementary Note**). Further T functional studies must be performed to explore the effect of *EOMES* silencing on the immune system.

The genetic and expression evidence that we provide supports the conclusion that homozygous silencing of the human *EOMES* locus results in a microcephaly syndrome with polymicrogyria and agenesis of the corpus callosum. Unusually, silencing of the *EOMES* locus in the individuals studied is ascribed to a position effect resulting from a translocation breakpoint. As no additional *EOMES* exons have been detected (**Supplementary Methods**) and the transcriptional direction of *EOMES* gene is away from the breakpoint on the native chromosome 3p, we hypothesize that a *cis*-regulatory sequence[12] lying 215 kb or more 5′ to the *EOMES* locus may have been separated from the *EOMES* core promoter.

Because the full knockout of *Tbr2* in mice leads to embryonic lethality before implantation[4,13], the essential role of this gene product in brain development has not been hitherto emphasized. The motor delay with hypotonia observed in the individuals with microcephaly syndrome in our study, as well as their reduced cerebellar size, recalls the recently demonstrated co-opting of this developmental gene cascade in the mouse cerebellum, in which precursors of the neurons of the deep cerebellar nuclei both express and require *Eomes* transcripts[14]. We did not observe any *EOMES* expression in the developing human cerebellum at Carnegie stage 19 or 12.5 weeks of development; later stages were not accessible for analysis. Although other T-box family member genes (*TBX3* and *TBX5*) have been reported to be involved in human developmental disorders involving the heart and skeleton (ulnar-mammary (MIM181450) and Holt-Oram (MIM142900) syndromes, respectively), our report is the first to implicate *EOMES* in a severe neurological malformation in humans.

Note: Supplementary information is available on the Nature Genetics website.

ACKNOWLEDGMENTS

The authors thank the microcephaly syndrome family for their participation. We thank Z. Al-Houssaini, N. Bahi-Buisson, C. Chirol, M. Clément-Ziza, N. Moussok, A. Pelet, S. Romana, C. Schatz and M. Vekemans for their assistance. This study was funded by INSERM, Agence Nationale de la Recherche and the Fondation pour le Recherche Médicale.

COMPETING INTERESTS STATEMENT

The authors declare no competing financial interests.

Published online at http://www.nature.com/naturegenetics
Reprints and permissions information is available online at http://npg.nature.com/reprintsandpermissions

1. Barkovich, A.J. *et al. Neurology* **65**, 1873–1887 (2005).
2. Kimura, N. *et al. Brain Res. Dev.* **115**, 183–193 (1999).
3. Bulfone, A. *et al. Mech. Dev.* **84**, 133–138 (1999).
4. Russ, A.P. *et al. Nature* **404**, 95–99 (2000).
5. Englund, C. *et al. J. Neurosci.* **25**, 247–251 (2005).
6. Hevner, R.F. *et al. Neurosci. Res.* **55**, 223–233 (2006).
7. Fougerousse, F. *et al. Hum. Mol. Genet.* **9**, 165–173 (2000).
8. Davis, R.L. & Turner, D.L. *Oncogene* **20**, 8342–8357 (2001).
9. Anthony, T.E. *et al. Neuron* **41**, 881–890 (2004).
10. Pearce, E.L. *et al. Science* **302**, 1041–1043 (2003).
11. Takemoto, N. *et al. J. Immunol.* **177**, 7515–7519 (2006).
12. Fernandez, B.A. *et al. Clin. Genet.* **68**, 349–359 (2005).
13. Strumpf, D. *et al. Development* **132**, 2093–2102 (2005).
14. Fink, A. *et al. J. Neurosci.* **26**, 3066–3076 (2006).

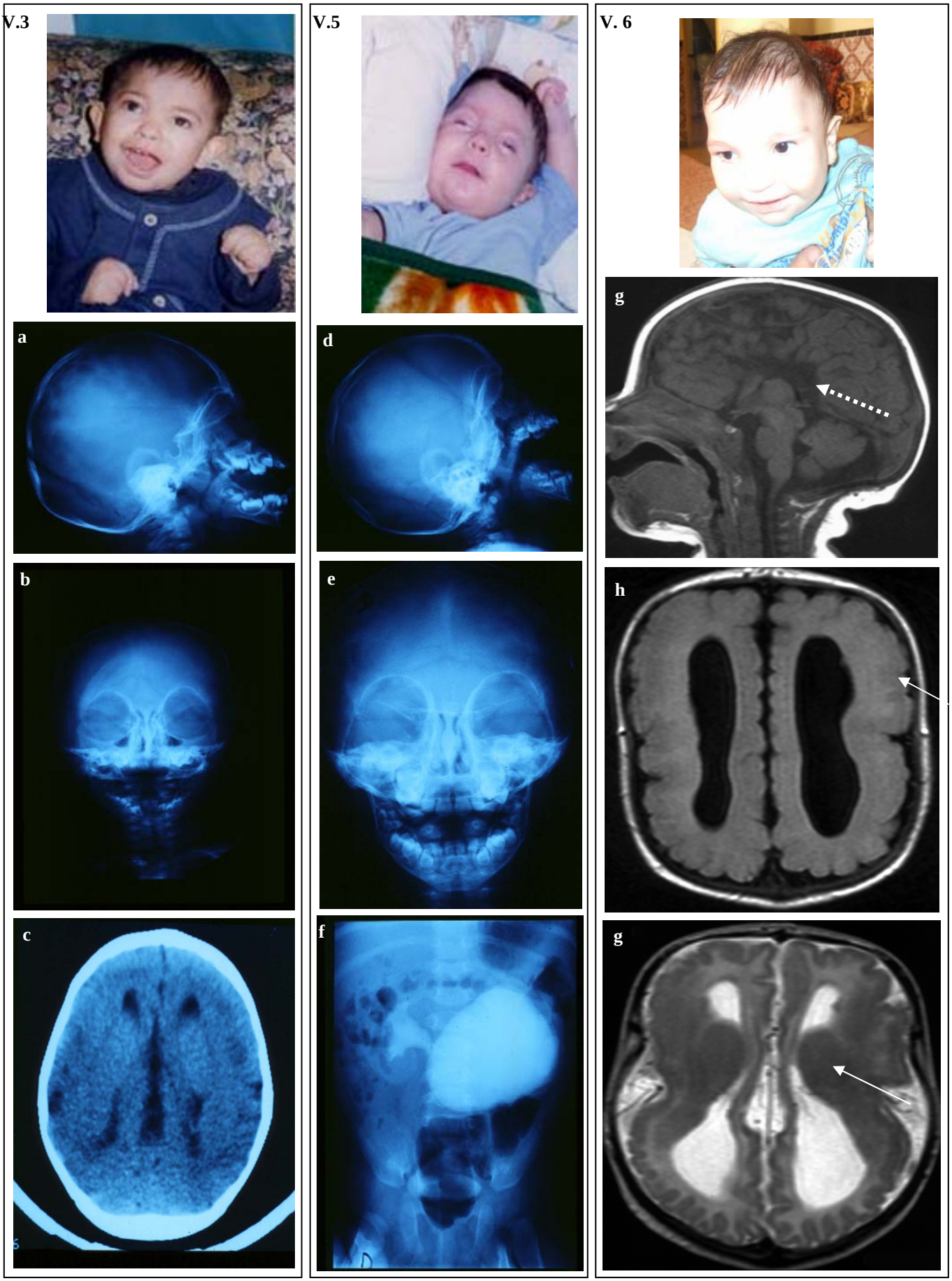

Supplementary figure 1: The following features were observed in all patients : i) extreme microcephaly (V.3, V.5 and V.6), ii) craniosynostosis secondary to microcephaly (**a**, **b**, **d**, **e**), iii) corpus callosum agenesis (CT scan view (**c**) and MRI view (**g**, **h**), iv) other brain malformations, namely: bilateral cortical polymicrogyria (**h** white arrow), myelinization delay on anterior arm of internal capsulae (**i** white arrow), a reduced cerebellum without malformation of posterior fossa (**g**), v) Individual V.5 also presented with a left kidney pyelo-ureteral junction abnormality (**f**). The photographs are published with parental consent.

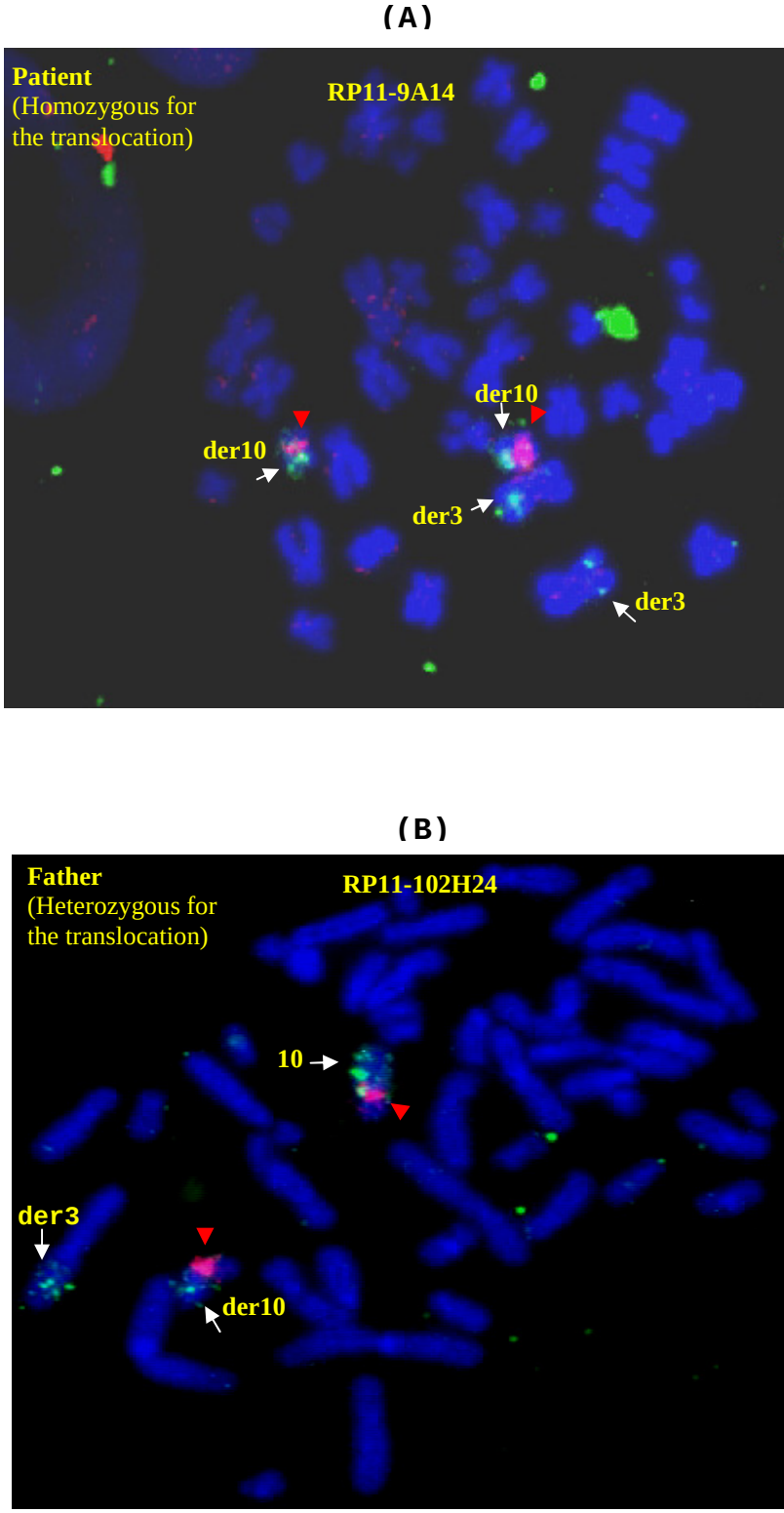

Supplementary Figure 2
FISH analyses of BACs (Bacterial artificial chromosome) RP11-9A14 on chromosome 3p (**A**) and RP11-102H24 on chromosome 10q (**B**), encompassing the breakpoints (green probes indicated by white arrows). The specific chromosome 10 satellite probe is a purple/red colour (red arrows). der3 : derivative chromosome 3; der10 : derivative chromosome 10.

Supplementary figure 3 : Sequencing of the junction fragments on 3p24 (blue arrow) and 10q22 (green arrow) demonstrated that no deletion was involved. A 56 nucleotide sequence originating from a Long Interspersed Nuclear Element (LINE) repeat was intercalated at the translocation breakpoint (red dotted line).

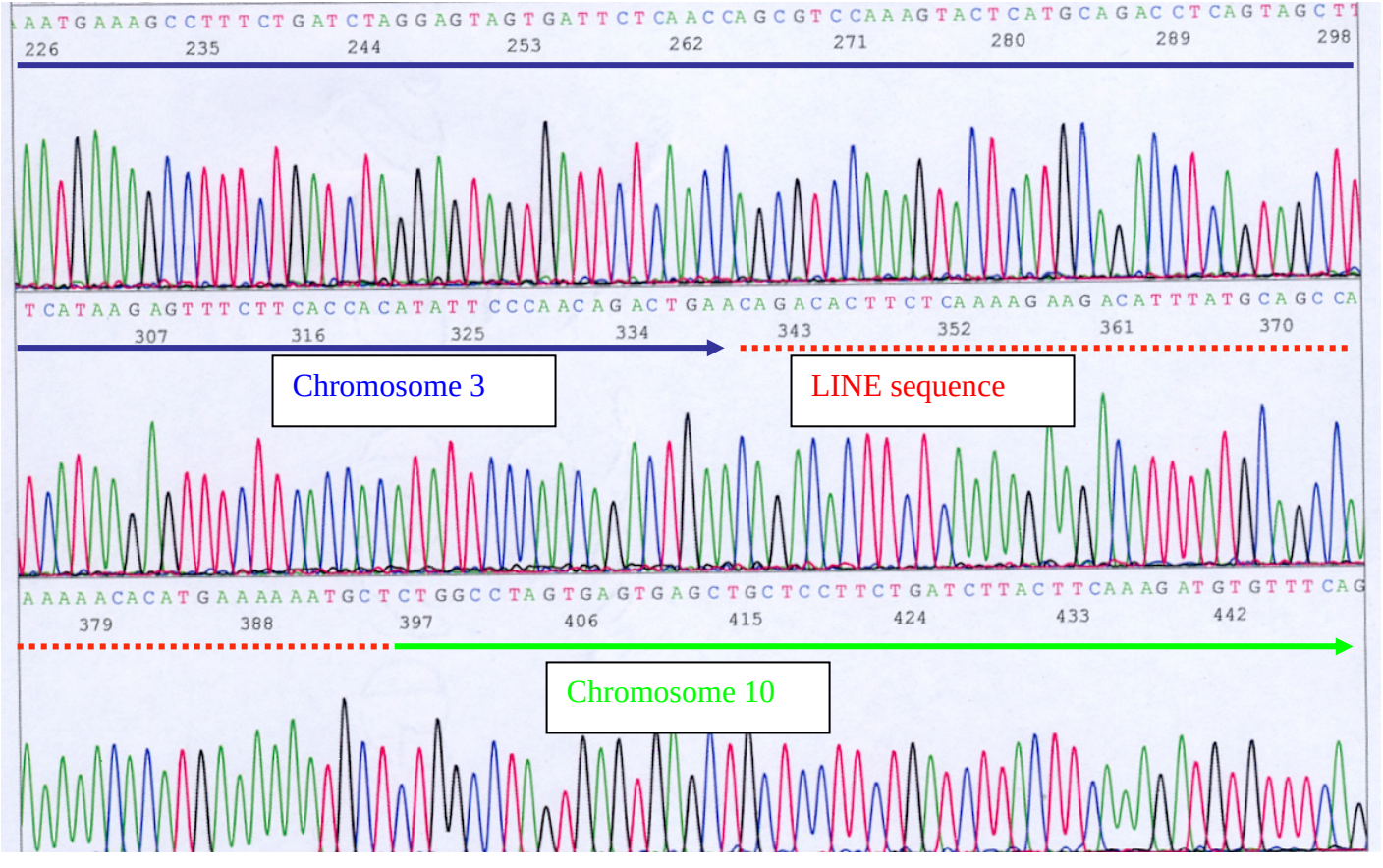

Supplementary Table 1: BAC probes encompassing the 3p and 10q translocation breakpoint. All BAC clones are from the RP11 library. The probes overlapping the breakpoints are in bold case (see **Supplementary Figure 2**)

Chromosome 3				**Chromosome 10**			
Probes	**Accession N°**	**Physical position (UCSC)**	**Probes crossing the breakpoint**	**Probes**	**Accession N°**	**Physical position (UCSC)**	**Probe crossing the breakpoint**
RP11-49D9	AC103585	24.627.517	no	RP11-589B3	BX248123	80.945.468	no
RP11-537O8	AC092422	25.029.895	no	RP11-506M13	AC068139	81.241.465	no
RP11-286D1	AC098973	27.730.346	no	RP11-369J21	AL356095	81.745.793	no
RP11-8L15	**AC117417**	**27.944.512**	**yes**	RP11-36D19	AL513174	81.915.872	no
RP11-9A14	**AC092415**	**27.946.511**	**yes**	RP11-175M21	AC009405	82.411.891	no
RP11-301D8	AC093142	28.336.078	no	**RP11-102H24**	**AL356307**	**82.798.241**	**yes**
				RP11-202D18	AC010157	83.863.806	no
				RP11-156D10	AL354749	84.487.215	no

Supplementary Table 2: Methods for RT-PCR analysis of candidate genes on chromosomes 3p and 10q. In addition, the *PRO-NRG3*, *DC-TM4F2*, and *EOMES* genes were fully sequenced.

Genes & accession N°	Primer sequences and exon location	Physical Position (UCSC)
Chromosome 3		
***SLC4A7* (or *S4A7*_HUMAN)** Solute carrier family 4 member 7	5'-ACGAGGCTTTGGAGAAGCTCTTT, Exon 15 5'-ACACCAAAAGAGCACATCTGGAAT, Exon 17	27,393,200-27,453,960
EOMES T box brain 2 / eomesodermin homolog (*Xenopus laevis*) (NM_005442)	5'-GATCATTACGAAACAGGG- Exon1F 5'-TGAATCATAGTTGTCTCTGA- Exon5R	27,732,891-27,738,789
	5'-AGCATGGAGCCGTAGGGGTAG, Exon1F 5'-TCCGAGCGGTACTACCTCCAGT, Exon1R	
	5'-GGACTACCATGGACCTCCAGAACA, Exon6F 5'-TCTTCAGCATTAATGTCCTCACACTT, Exon6R	
	5'-CCGGTGGCCTTATTATAAAGG, Alt-exon1F 5'-GAATTAGTGTCACCTCCACCAC, Alt-Ex1-2R 5'-CCTGTCTCATCCAGTGGGAACCAG, Exon3R	27,738,925-27,739,206 (Spliced exon)
MGC61571 (hypothetical protein LOC152100) (NM_182523)	5'-TCCTGGCGGTGCTTTGCAAAGGG, Exon1 5'-TTGTTCAGAACACCTCTCTTTCCG, Exon2	28,258,128-28,336,265
AZI2 5-azacytidine induced 2 (NM_022461)	5'-GAACCTGGCTTCGCTAACG, Exon 1F 5'-TTTCTTCTGACTCGGCAGG, Exon1R	28,339,090-28,365,579
	5'-CGGTCCGTTTCCAAACACTAAGG, Exon1F 5'-CAACAGATTCATCTCCTGAATA, Exon2R	
Chromosome 10		
LOC375920 Modified Nov 1, 2006 to ***SH2D4B*** (NM_207372)	5'-GAAGAACAGTTGCGCCGGTCC, Exon 4-5F 5'-GGTGTTCCTCTCGAAGCCAG, Exon 6R	82,287,638-82,396,296
LOC375921 Discontinued from RefSeq 10-May-2005	5'-CAAGCACCAAGATCATGAAGCC, F 5'-GTGGAAACTCTGGAAATTCACAA, R	Amplifies 82,466,224-82,466,794
DC-TM4F2 Tetraspanin-14 (Transmembrane 4 superfamily member 14) (NM_030927)	5'-TGAAGACTGGGACCTCAACG, Exon8F 5'-AGATCAGCGTCCTTGCCAG, Exon11R	82,204,047-82,269,364
PRO-NRG3 Pro-neuregulin-3, membrane-bound isoform precursor (Pro-NRG3) (NM_001010848)	5'-GAGTCTATCCTCTTGCTGCA, Exon8F 5'-CTTGGCAAGGTATCGTATC, Exon8R	83,625,077-84,735,340
KIAA2020	5'-TCCAGGAACCTGTTTACTTT, Exon1F 5'-TGGGTATGCTCCATTTGAAG, Exon1-2R	88,975,237-89,120,432

SUPPLEMENTARY METHODS

Cytogenetic studies

Blood samples were collected from all four patients and their parents. Informed written consent was obtained from the families. Cytogenetic analysis was performed using standard R-band techniques. FISH experiments, using BACs as probes (CHORI Center), were performed on metaphases of patient IV.5 and his father IV.7 (**Fig. 1**). Total DNA from these BACs was labelled with biotin by nick-translation as previously described. The probes were revealed by using avidin-FITC (Sigma). All slides were counter-stained with DAPI (Sigma). The slides were observed under a Zeiss epifluorescence microscope (Axiophot) connected to the Powergene 810 probe system (Perspective Scientific International LTD). After the CGH experiment was performed, the slides were visualized on an epifluorescent microscope (DMRXA, Leica Microsystems). Images were processed and analyzed with the Quips CGH software (Vysis Inc.)

Linkage analysis

- Chromosomes 3p and 10q

Linkage analysis was performed in chromosome 3p and 10q to identify a homozygous region by descent for each of the two chromosomes which prompted us to select BACs for the physical fine mapping of the breakpoint. The following microsatellite markers were used: D3S1304, D3S1263, D3S1259, D3S1286, D3S1293, D3S1266, D3S1582, D3S1613, D3S3717, D3S3721; and D10S556, D10S195, D10S201, D10S1686, D10S1744, D10S198, D10S192, D10S1663, D10S597.

When assuming a fully penetrant autosomal recessive disorder, linkage analysis between the disease phenotype and translocation breakpoints used as polymorphic markers yielded a maximum lodscore of $Z = 3.45$ at 3p24 or 10q23, when including three affected individuals only. If one common ancestor carried the translocation, the likelihood that three affected offspring would be homozygous for the translocation by chance is 1/4,000.

- Exclusion of MCPH loci

We did homozygosity mapping and linkage analysis by using 36 microsatellite markers across the six MCPH loci from the family branch with two affected individuals and one healthy sister. We excluded the following loci: ***MCPH1*** (D8S1798, D8S277); ***MCPH2*** (D19S414, D19S570, D19S220, D19S881, D19S417, D19S223, D19S197, D19S198, D19S423, D19S420, D19S900); ***MCPH3*** (D9S1872, D9S1682); ***MCPH4*** (D15S1007, D15S1042, D15S1012, D15S1044, D15S994, D15S968, D15S1006, D15S978, D15S126, D15S982, D15S1003, D15S117, D15S964, D15S643, D15S155); ***MCPH5*** (D1S238, D1S422, CRB1 [a CA repeat marker designed locally, primers available on request] and D1S413); ***MCPH6*** (D13S742, D13S221).

DNA sequence analysis

DNA was extracted from peripheral blood (or lymphoblastic cell lines) according to standard protocols. We analysed candidate genes by genomic and/or cDNA sequencing. PCR products were purified and directly sequenced in both directions on an ABI PRISM 3130 DNA sequencer (Perkin Elmer-Applied Biosystems) using the dye terminator method according to the manufacturer's instructions (cf. Nature Protocols).

Expression analysis

- Total RNA extraction and RT-PCR analysis

Total RNA was extracted from cultured lymphoblastic cell lines using the RNeasy Mini kit (Qiagen) according to manufacturer's instructions. A sample of extracted RNA was electrophoresed on a 2% agarose gel to verify integrity. First strand cDNA was synthesized using random hexamer primers (GeneAmp RNA PCR kit, Applied Biosystems). Reverse transcription was carried out at 42° for 15 min, at 99° for 5 min, and at 5° for 5 min. RT-PCR was performed using gene-specific primers (**Supplementary Table 2**).

- Quantitative RT-PCR :

Quantitative measurements of changes in gene expression were performed using a LightCycler (Roche Diagnostics, Indianapolis, Ind.) thermocycler. Q-PCR was performed (operating system version 3.0) in 10µl mixtures containing 1 µl of Faststart DNA Sybr Green I (Roche Molecular Biochemicals), 1.5 mM $MgCl_2$, 0.5 mM each primer (*EOMES*-Ex6F2-5'-GGACTACCATGGACCTCCAGAACA-3', and *EOMES*-Ex6R1 5'-TCTTCAGCATTAATGTCCTCACACTT-3'), and 5 µl of extracted DNA (1 to 25 ng). The reaction was performed with preliminary denaturation for 10 min at 95°C (slope, 20°C/s), followed by 40 cycles of denaturation at 94°C for 10 s (slope, 20°C/s), annealing at 60°C for 5 s (slope, 20°C/s), primer extension at 72°C for 8 s (slope 20°C/s), and product detection at 77°C for 5 s (slope, 20°C/s). A final cooling step was performed at 4°C for 1 min (slope, 20°C/s). A 239-bp product resulted from the reaction. Experiments were repeated in triplicate and normalized for input cDNA against beta-actin.

***- RACE** (Rapid Amplification of cDNA Ends)*

We performed 3' RACE analysis using the GeneRacer™ Kit (Invitrogen). The first-strand of cDNA was amplified using a forward gene specific primer within the published first exon (Forward GSP: 5'-TCCGAGCGGTACTACCTCCAGT) and the GeneRacer™ Oligo dT Primer according to manufacturer's instructions. We did not find supplementary exons 3' to the six published exons of *EOMES*.

- In situ *hybridisation*

Normal human embryos and foetal tissues were obtained after elective termination of pregnancy in agreement with current French bioethical legislation (94-654 and 00-800), the Necker Hospital CCPPRB and National Ethics Committee recommendations (N° 1 of May 22, 1984). Embryonic stages were established according to Carnegie staging (CS) classification. Six different embryonic stages (CS8 (d18), CS9 (d20), CS15 (d33), CS19 (d 47–48)) as well as two fetal stages (14.5 and 24 weeks) were studied. Tissues were fixed in 4% phosphate buffered paraformaldehyde, dehydrated, and embedded in paraffin blocks. Five micron thick serial sections were cut. Exon 2 primers were selected for PCR amplification (F: 5'-CCTGTTCTAGGACATCCCAATT-3' R: 5'-GAGGGTTACGATTTCTTC-3'). A T7 promoter sequence extension (TAATACGACTCACTATAGGGAGA) was added at the 5' end of each primer. T7F/R and F/T7R primers allowed the amplification of sense and antisense templates respectively, specific to the *EOMES* gene. Riboprobe labelling with ^{35}S-UTP, tissue fixation, hybridization, and photographic development were carried out according to standard protocols as previously described.

Supplementary note

Patient V.6

During the first week of life, he had a fever (38.6-40.3°C) that was unresponsive to antipyretics, caused by *Escherichia coli* sepsis. Biological explorations showed augmented leucocytes (16 780 /µl) and lymphocytes (61.7 %; Normal: 19 - 48 %), diminished levels of red blood cells, haemoglobin, hematocrit , and polymorphonuclear neutrophils. At the age of 3 months, he presented an urinary infection (pyelonephritis) associated with fever and *Klebsiella pneumoniae* isolated in the urine.

The cytobacterial investigation in the cerebrospinal liquid showed a very high level of red blood cells (120/µl; N: 1 - 2) and leucocytes (4/µl; N: <3). The direct bacteriological exam revealed absence of germs.

The haematological survey was essentially normal except the polymorphonuclear basophils which were two fold higher than normal. At the time of publication, the infant at 9 months of age has had a fever on every measurement and subsequent episodes of infections. The exploration of lymphocyte subtypes of patient V.6 had found normal distribution of T, B and NK cells. For T CD8 subtypes the percentage of memory and naive cells was normal, but the patient presented a slight increase in effector T (CD8) cells with normal expression of CD122.

The results of all other standard immunological explorations were normal, including serum immunoglobulin levels (at the age of 6 and 9 months), antibody responses to proteins and complement (CH50, C3, C4).

Disponible en ligne sur www.sciencedirect.com
ScienceDirect
Archives de pédiatrie ■■ (2007) ■■■
Archives de pédiatrie
http://france.elsevier.com/direct/ARCPED/

Table ronde : Les apports de la génétique dans la compréhension des pathologies pédiatriques (interface Inserm–SFP–SFRP)

Bases génétiques et moléculaires des neurocristopathies

Genetic and molecular bases of neurocristopathies

H.-C. Etchevers, J. Amiel, S. Lyonnet*

Inserm U781, université Paris-V, Assistance publique–hôpitaux de Paris, hôpital Necker–Enfants-malades, 149, rue de Sèvres, 75743 Paris cedex 15, France

Reçu le 6 février 2007 ; accepté le 27 février 2007

Mots clés : Neurocristopathies ; Malformations

Keywords: Neural crest, abnormalities; Malformations, genetics

Les cellules de la crête neurale (CN) sont produites chez l'embryon de la 3e à la 5e semaine de grossesse, au niveau des bourrelets médullaires séparant la plaque neurale de l'ectoderme. Au cours de la fusion des bourrelets médullaires, qui aboutit à la formation d'un tube à l'origine du futur système nerveux central (SNC), les cellules de la CN se détachent et adoptent un type mésenchymateux. Elles migrent alors à travers le corps et envahissent pratiquement tous les organes.

Les cellules dérivées des cellules de la CN comprennent les neurones et les cellules de support de l'ensemble du système nerveux périphérique (sensoriel et autonome), les cellules adrénergiques et autres cellules endocrines, ainsi que toutes les cellules pigmentaires, à l'exception de celles dérivant de la rétine [1,2]. Au niveau de la tête, les cellules de la CN donnent également naissance aux tissus conjonctifs et structuraux du crâne (de type dermique osseux ou cartilagineux), et aux tendons musculaires. Elles infiltrent et sont essentielles au fonctionnement d'éléments glandulaires ou vasculaires tels que le thymus, les glandes thyroïde et parathyroïde, la région conotroncale du cœur et l'ensemble du secteur vasculaire branchial, donnant naissance à des cellules de tissus conjonctifs, adipeux ou encore du muscle lisse.

Le fait que les cellules de la CN n'aient été retrouvées que chez l'embryon exclut de les considérer comme de réelles cellules souches. Cependant, il a été récemment démontré que le système nerveux intestinal du rat adulte contient des cellules de la CN capables de s'autorenouveler et multipotentes. Par ailleurs, les mélanocytes aviaires peuvent, in vitro, se différencier en cellules gliales, en neurones et en cellule de type muscle lisse, ce qui suggère aussi la persistance de progénitors multipotents. Il est probable que les cellules dérivées des cellules de la CN sont le produit d'une restriction progressive du potentiel développemental.

Le choix final du phénotype à mettre en place à tel ou tel endroit de l'organisme résulte de l'action combinée de différents facteurs extrinsèques, appartenant au microenvironnement embryonnaire, et des propriétés qu'ont les cellules elles-mêmes d'adapter leur réponse à ces influences extérieures. On a ainsi observé qu'une déficience en facteurs de croissance neurotrophiques et en gènes codant pour leur récepteur entraîne une pénurie des sous-types cellulaires correspondants dérivés des cellules de la CN. Si la migration et le devenir des cellules de la CN sont imposés par la nature des tissus environnants au moment où elles quittent l'ébauche neurale, ils ne dépendent pas, contrairement à ce qui avait été avancé, des propriétés intrinsèques retrouvées localement le long de l'axe neural.

1. Définition des neurocristopathies

Une anomalie dans la migration, la différenciation, la division ou la durée de vie des cellules de la CN entraîne la formation de dysplasies organiques ou tissulaires, aux caractéristiques cliniques et pathologiques extrêmement diverses. En

* Auteur correspondant.
Adresse e-mail : lyonnet@necker.fr (S. Lyonnet).

0929-693X/$ - see front matter
doi:10.1016/j.arcped.2007.02.072

ARCPED-1681

raison de leur origine embryonnaire commune, Bolande avait suggéré de rassembler ces pathologies sous le terme de « neurocristopathies », pour souligner le fait qu'elles partageaient des mécanismes pathogéniques communs. Des définitions plus nuancées ont été proposées par la suite, permettant de prendre en compte l'importante diversité des cellules dérivées des cellules de la CN et des organes dans lesquelles elles jouent à part entière, et de façon prolongée, un rôle fonctionnel. Cependant, classer telle ou telle maladie dans la catégorie des neurocristopathies s'effectue sur la base des connaissances disponibles à un moment donné, des données scientifiques en perpétuelle évolution avec l'avènement et l'essor de l'embryologie moléculaire.

Certains troubles, notamment ceux entraînés par la défiance fonctionnelle de cellules de la CN déjà différenciées, n'ont pas été inclus dans la liste des neurocristopathies présentée ici (Tableau 1). Ainsi, bien que l'albinisme oculocutané corresponde bien à une affection des mélanocytes dérivés de la CN, il provient moins d'un problème dans leur développement que d'un problème dans leur fonction métabolique finale (la synthèse de mélanine). De fait, l'idée ici est de restreindre la définition d'une neurocristopathie aux pathologies pour lesquelles les perturbations observées dans les cellules de la CN sont causales, et ne constituent pas un phénomène secondaire. Les craniosténoses simples, par exemple, en sont exclues, dans la mesure où elles semblent refléter un défaut de fonction des ostéoblastes associé, dans les formes syndromiques, à des problèmes osseux au niveau des jambes, des côtes ou des vertèbres, aucun de ces éléments n'ayant de composant issu des cellules de la CN (exception faite du syndrome craniofrontonasal, qui implique une perturbation des cascades de gènes intervenant dans la migration des cellules de la CN).

2. Diagnostic clinique des neurocristopathies

Il est important, devant un patient présentant de multiples anomalies congénitales, de considérer la situation d'un point de vue embryologique, afin de déterminer une éventuelle cause commune sous-jacente. Les cellules de la CN colonisent 4 compartiments, de taille différente : la peau, le système nerveux périphérique, une partie du système endocrine et un pôle pharyngocéphalique. Les anomalies touchant l'un ou l'autre de ces compartiments trouvent a priori leur origine dans un même domaine initial, ce qui justifie l'examen soigné des autres compartiments qui en dérivent. Le Tableau 1 compare les neurocristopathies isolées et syndromiques, d'une part, et les distinctions à faire entre symptômes cancéreux et malformatifs d'autre part. Bien entendu, les neurocristopathies syndromiques peuvent à la fois avoir des composantes cancéreuses et malformatives : il est effectivement rare de rencontrer une neurocristopathie syndromique pure. Toutefois, ce concept de neurocristopathie est utile aux cliniciens dans leur approche du patient, puisqu'il permet de regrouper sous un même étendard des symptômes apparemment divergents et non reliés entre eux. Examinons maintenant, à titre d'exemple, quelques cas de figures représentatifs de neurocristopathies de présentation pédiatrique.

Tableau 1
Exemples de neurocristopathies, classées selon leur type et le compartiment concerné

	Peau	Système nerveux périphérique	Système endocrine	Pôle pharyngocéphalique
Cancers				
Isolés	Mélanome Carcinome à cellules de Merkel	Neuroblastome Schwannome Paragangliome	Phéochromocytome Épithéliome médullaire de la thyroïde Paragangliome chromaffine Tumeurs carcinoïdes	Hémangiopéricytome Paragangliome non-chromaffin (oreille)
Syndromique	Neurofibromatose I[b] Mélanose neurocutanée	Hirschsprung + neuroblastome	Néoplasies multiples endocriniennes 2A, B	Hypoventilation congénitale centrale
Malformations				
Isolées	Nævus congénital géant Piébaldisme	Hirschsprung		Malformations artérioveineuses cérébrodurales Fentes palatine et labiale Moya-moya Cardiopathies conotroncales isolées Aplasie des glandes lacrymales et salivaires
Syndromiques	Sturge-Weber	Waardenburg Dysautonomie familiale de type 2	Allgrove Bamforth-Lazarus	CHARGE[a] DiGeorge Pierre Robin Holoprosencéphalie[a,b] Kallmann[a] Rieger[a] Binder[a] Mœbius[a] Johanson-Blizzard[a] Treacher-Collins-Franceschetti Craniofrontonasal[b] Goldenhar[a,b] Orofacial-digital VI[a,b]

[a] Syndromes comportant une composante endocrine imputable aux cellules de la crête neurale non endocrines, essentielles à la formation de l'hypophyse.
[b] Cas combinant une neurocristopathie avec des malformations non neurocristopathiques.

Pour citer cet article : H.-C. Etchevers et al., Bases génétiques et moléculaires des neurocristopathies, Archives de pédiatrie (2007), doi: 10.1016/j.arcped.2007.02.072.

2.1. Anomalies du développement des mélanoblastes

Les mélanoblastes issus des CN migrent essentiellement vers 3 destinations : la jonction derme–épiderme, le bulbe capillaire dans le derme, l'iris et la choroïde au niveau de l'œil (les mélanocytes de la rétine dérivent de la plaque optique). Les anomalies du développement des cellules des CN à destinée mélanocytaire se manifestent par l'existence de zones cutanées dépigmentées dès la naissance du fait de l'absence de mélanocytes. Ces anomalies de la pigmentation se distinguent du vitiligo au cours duquel la dépigmentation est un phénomène acquis après la naissance, et de l'albinisme qui est une anomalie de la fonction et non du développement du mélanocyte. Les anomalies de la pigmentation se retrouvent dans différentes neurocristopathies, soit isolées comme dans le piebaldisme, soit associées à d'autres anomalies du développement comme dans le syndrome de Waardenburg. En matière tumorale, c'est le mélanome, de manifestation pédiatrique exceptionnelle, qui constitue le meilleur exemple (Tableaux 1 et 2).

Tableau 2
Gènes ou loci de neurocristopathies

Maladie ou syndrome	MIM	Hérédité	Gène	Chromosome	Modèle murin spontané ou transgénique (+)
Piebaldisme	172800	AD	*KIT*	4q12	*White-spotting*, +
Mélanome	155600	AD		1p36	
Mélanome	155600	S	*NRAS*	1p13.1	+
Mélanome	155600	S	*BRAF*	7q34	+
Mélanome	155600	AD, S	*CDKN2A*	9p21	+
Mélanome	155600	AR, S	*MC1R*	16q24.3	*Tawny, recessive yellow, tobacco-darkening, sombre*, +
Mélanome	155600	AD, S	*CDK4*	12q14	+
WS1	193500	AD	*PAX3*	2q35	*Splotch*, +
WS3	193500	AR	*PAX3*	2q35	*spLotch*, +
WS2A	193510	AD	*MITF*	3p14	*Microphthalmia, Vitiligo, White, Red eyed white, Brownish*, +
WS2B	600193	AD		1p	
WS2C	606662	?		8p23	
WS2D	608890	AR	*SNAI2*	8q11	+
WS4	277580	AR	*EDNRB*	13q22	*Piebald, piebald lethal*, +
WS4	277580	AR	*EDN3*	20q13	*Lethal spotting*, +
WS4	277580	AD	*SOX10*	22q13	*Dominant megacolon*, +
HSCR	142623	CI*	*RET*	10q11.2	+
HSCR	142623	CI	*GDNF*	5p13.2	+
HSCR	142623	CI	*ARAF*	Xp11.3	+
HSCR	142623	CI	*NTN*	19p13.3	+
HSCR	142623	CI	*EDNRB*	13q22	*Piebald, piebald lethal*, +
HSCR	142623	CI	*EDN3*	20q13	*Lethal spotting*, +
HSCR	142623	AD	*PHOX2B*	4p12	+
HSCR	142623			3p12	
HSCR	142623			19q13	
HSCR	142623	AD	*L1CAM*	Xq28	+
NB	256700	AD, S	*PHOX2B*	4p12	+
Haddad	209880	AD, S	*PHOX2B*	4p12	+
CCHS	209880	AD, S	*PHOX2B*	4p12	+
Phéochromocytome	171300	AD	*RET*	10q12	+
Phéochromocytome	171300	AD	*SDHB*	1p36	
Paragangliome 4	115310	AD	*SDHB*	1p36	
Paragangliome 2	601650	AD		11q13.1	
Paragangliome 3	605373	AD	*SDHC*	1q21	
Paraganglioma 1	168000	AD	*SDHD*	11q23	+
Phéochromocytome	171300	AD	*SDHD*	11q23	+
MC carcinome	602690.0019	S	*SDHD*	11q23	+
NEM2A	171400	AD	*RET*	10q12	+
NEM2B	162300	AD	*RET*	10q12	+
CMT	155240	AD	*RET*	10q12	+
Dysautonomie de type 2	256800	AR	*NTRK1*	1q21	+
NF1	162200	AD	*NF1*	17q11	+
DiGeorge	188400	AD		22q11.2	
CHARGE	214800	AD	*CHD7*	8q12	
Goldenhar	164210	AD		14q32	
Moebius	157900	AD		13q12.2-q13	
Bamforth-Lazarus	241850	AR	*FOXE1*	9q22	+
Rieger 1	180500	AD	*PITX2*	4q25	+
Rieger 2	601499	AD	*FOXC1*	13q14	*Congenital hydrocephalus*, +
Craniofrontonasal	304110	XLD	*EFNB1*	Xq13.1	+
Allgrove	231550	AR	*ALADIN*	12q13	

AD ou AR : autosomique dominant–récessif ; XL : lié aux chromosomes X ; CI : hérédité complexe ; * : locus majeur ; S : somatic.

Pour citer cet article : H.-C. Etchevers et al., Bases génétiques et moléculaires des neurocristopathies, Archives de pédiatrie (2007), doi: 10.1016/j.arcped.2007.02.072.

2.2. Anomalies des dérivés endocrines : néoplasies endocriniennes multiples de type 2

Les néoplasies endocriniennes multiples de type 2 (NEM 2) constituent un groupe de syndromes de prédisposition familiale aux tumeurs des glandes endocrines dérivées des CN (phéochromocytome, carcinome médullaire de la thyroïde). Le cancer médullaire de la thyroïde (CMT) se développe à partir des cellules C sécrétrices de calcitonine et est retrouvé de manière constante, alors qu'un phéochromocytome (tumeur dérivée des cellules chromaffines de la médullosurrénale) est présent dans environ 50 % des cas. Les NEM2 se comportent comme des caractères autosomiques dominants d'expression variable, mais de pénétrance quasi complète au-delà de 30–40 ans. Le gène de susceptibilité a été identifié, il s'agit du proto-oncogène *RET* pour lequel des formes réarrangées avaient été détectées dans des carcinomes papillaires de la thyroïde et dont l'ARN messager avait été retrouvé très fortement exprimé dans des tumeurs d'origine neuroectodermique. Ce gène est localisé sur le bras long du chromosome 10 (10q11-12), et code pour une protéine membranaire appartenant à la superfamille des récepteurs tyrosine-kinase. Contrairement au schéma classique des mutations d'antioncogènes dans les formes familiales de tumeurs, on a affaire ici à des mutations germinales transmises en dominance et conduisant à l'activation constitutionnelle du récepteur tyrosine-kinase RET.

2.3. Système nerveux périphérique : la maladie d'Hirschsprung

La maladie d'Hirschsprung (MH) est la plus fréquente malformation du tube digestif (1 cas sur 4 à 5000 naissances) résultant d'une anomalie du développement du système nerveux entérique (SNE) par défaut de migration, de prolifération, de différentiation ou de survie des cellules dérivées des CN dans la paroi du tube digestif pour former les plexus myentériques et sous-muqueux. Cela définit la MH comme une neurocristopathie pure. Cliniquement, il faut distinguer MH isolée et MH syndromique. Tout les oppose en effet : le pronostic, les bases moléculaires et donc le conseil génétique.

2.3.1. Maladie d'Hirchsprung isolée

Les observations épidémiologiques collectées sur la MH isolée sont en faveur d'une hérédité multifactorielle modifiée par le sexe. En effet :

- le sex-ratio est déséquilibré en faveur des filles (4 garçons pour 1 fille atteinte) ;
- le risque de récidive dans la fratrie du cas index est très augmenté par rapport à celui de la population générale sans pour autant suivre les lois de Mendel et varie de 1 à 33 % ;
- l'incidence varie en fonction de l'ethnie.

Les études de ségrégation plaident pour des modèles différents en fonction de la forme de la maladie :

- un gène majeur autosomique dominant de pénétrance incomplète et avec un taux de mutations de novo d'environ 15 % dans les formes longues ;
- une hérédité multigénique ou autosomique récessive dans les formes courtes (qui n'exclut pas la participation d'un gène majeur).

Le gène majeur a été localisé en 10q11.2 puis identifié par une approche candidate ; il s'agit encore du proto-oncogène RET. Les mutations de *RET* sont hétérozygotes et ici très variées. Fait surprenant, la fréquence des mutations de *RET* détectées n'avoisine que la moitié des cas familiaux alors que toutes les familles multiplexes de MH étudiées sont compatibles avec une liaison au locus *RET*. Le taux de détection est d'à peine 15 % dans les cas sporadiques. Plus récemment, plusieurs équipes ont identifié un haplotype de polymorphismes le long du gène transmis des parents sains aux enfants atteints plus souvent que ne voudrait le hasard. Cet haplotype est centré sur un polymorphisme intronique fréquent (20 % de la population générale), qui pourrait bien être l'allèle hypomorphe recherché, et qui est retrouvé, à l'état homozygote, dans la majorité des cas sporadiques de MH sans mutation de *RET* identifiée. Ainsi, le modèle génétique le plus probable pour la MH est celui d'un gène majeur *RET* impliqué dans tous les cas de MH (soit par une mutation classique, soit plus souvent par un allèle de prédisposition) et de loci modificateurs localisés sur les chromosomes 3p21, 19q12 et 9q31 mais non encore identifiés.

2.3.2. Formes syndromiques de maladie d'Hirchsprung

L'association syndromique ne fait aucun doute lorsqu'elle est forte ; 5–10 % des patients atteints de syndrome *cartilage–hair hypoplasia*, de Bardet-Biedl, ou encore de Smith-Lemli-Opitz ont une MH, par exemple. Il en est de même pour les patients présentant une trisomie 21 ou encore dans le syndrome d'hypoventilation alvéolaire congénitale centrale (syndrome d'Ondine) par mutation hétérozygote du gène *PHOX2B.* L'implication de la voie de signalisation médiée par les endothélines dans le développement des neurones entériques a aussi été démontrée dans le syndrome de Waardenburg de type 4 (MH + Waardenburg).

Dans quelques cas, la MH est le signe clinique qui a permis de rapprocher les malades et de définir un nouveau syndrome. C'est le cas du syndrome de Goldberg-Shprintzen ou du syndrome de Mowat-Wilson par mutation du gène *ZFHX1B*. Lorsque la MH n'est rapportée qu'une fois pour un syndrome, il est difficile de trancher sur le caractère fortuit (lié à la fréquence élevée de la MH) ou réel de cette association.

2.4. Crêtes neurales rhombomériques et malformations de la face

Un certain nombre de malformations de la face et du cou correspondent à une défaillance totale ou partielle du développement d'une unité segmentaire de la région du cerveau postérieur et des structures qui lui sont associées. En allant du

Pour citer cet article : H.-C. Etchevers et al., Bases génétiques et moléculaires des neurocristopathies, Archives de pédiatrie (2007), doi: 10.1016/j.arcped.2007.02.072.

rhombomère 2 au rhombomère 8, on peut distinguer un certain nombre de malformations de la face :

- les syndromes du premier arc correspondent à un défaut du développement de certains dérivés de la CN mésencéphalique et rhombencéphalique antérieure constituant les bourgeons maxillaires et mandibulaires d'une part, et le nerf trijumeau (nerf V) d'autre part, (syndromes de Goldenhar, Franceschetti ou otomandibulaire) ;
- les syndromes du deuxième arc correspondent à un défaut de développement des dérivés de la CN rhombencéphalique constituant le deuxième arc branchial (lobule de l'oreille, derme de la partie moyenne du cou, os hyoïde). Le deuxième arc branchial est innervé par nerf facial (nerf VII), aux anomalies des structures anatomiques sus-citées peut donc s'associer une paralysie faciale (syndrome de Moebius) ;
- les syndromes des troisièmes et quatrièmes arcs branchiaux sont la conséquence d'un défaut du développement des structures dérivées des CN au niveau des rhombomères 6, 7, et 8, c'est-à-dire le thymus, les parathyroïdes, les cellules à calcitonine et le tronc aortopulmonaire ainsi que les dérivés des arcs aortiques. Le syndrome de DiGeorge associe une hypoplasie ou une agénésie du thymus et des parathyroïdes, une anomalie des 3^{e,} 4^{e} et 6^{e} arcs aortiques et des malformations cardiaques conotroncales et du septum interauriculaire. La séquence de Pierre Robin correspond à un défaut de développement du tronc cérébral dérivé des 6^{e}, 7^{e} et 8^{e} rhombomères. Il en résulte une désorganisation anténatale des fonctions orales et céphaliques digestives (succion, déglutition), de la ventilation et de la commande parasympathique du cœur. Ces troubles fonctionnels induisent durant la vie fœtale une division vélopalatine et un rétrognathisme.

3. Conclusion

Les CN participent au développement de cellules aussi différentes que les mélanocytes, les neurones du système nerveux entérique, les tissus de soutien de la face ou encore les structures conotroncales du cœur. Une bonne connaissance du développement des CN et des structures qui en sont dérivées permet de comprendre l'association de malformations d'organes en apparence si différents. De manière très complémentaire, la découverte de gènes impliqués dans les neurocristopathies humaines s'est avérée essentielle pour la connaissance du développement normal des CN.

Références

[1] Le Douarin N, Kalcheim C. The Neural Crest. 2nd ed. Cambridge, UK: Cambridge University Press; 1999.
[2] Etchevers HC, Amiel J, Lyonnet S. Molecular bases of human neurocristopathies. Adv Exp Med Biol 2006;589:213–34.

Pour citer cet article : H.-C. Etchevers et al., Bases génétiques et moléculaires des neurocristopathies, Archives de pédiatrie (2007), doi: 10.1016/j.arcped.2007.02.072.

Matthew-Wood Syndrome Is Caused by Truncating Mutations in the Retinol-Binding Protein Receptor Gene *STRA6*

Christelle Golzio, Jelena Martinovic-Bouriel, Sophie Thomas, Soumaya Mougou-Zrelli, Bettina Grattagliano-Bessières, Maryse Bonnière, Sophie Delahaye, Arnold Munnich, Férechté Encha-Razavi, Stanislas Lyonnet, Michel Vekemans, Tania Attié-Bitach, and Heather C. Etchevers

Retinoic acid (RA) is a potent teratogen in all vertebrates when tight homeostatic controls on its endogenous dose, location, or timing are perturbed during early embryogenesis. *STRA6* encodes an integral cell-membrane protein that favors RA uptake from soluble retinol-binding protein; its transcription is directly regulated by RA levels. Molecular analysis of *STRA6* was undertaken in two human fetuses from consanguineous families we previously described with Matthew-Wood syndrome in a context of severe microphthalmia, pulmonary agenesis, bilateral diaphragmatic eventration, duodenal stenosis, pancreatic malformations, and intrauterine growth retardation. The fetuses had either a homozygous insertion/deletion in exon 2 or a homozygous insertion in exon 7 predicting a premature stop codon in *STRA6* transcripts. Five other fetuses presenting at least one of the two major signs of clinical anophthalmia or pulmonary hypoplasia with at least one of the two associated signs of diaphragmatic closure defect or cardiopathy had no *STRA6* mutations. These findings suggest a molecular basis for the prenatal manifestations of Matthew-Wood syndrome and suggest that phenotypic overlap with other associations may be due to genetic heterogeneity of elements common to the RA- and fibroblast growth factor–signaling cascades.

Microphthalmia refers to a clinical spectrum that is characterized by a congenital reduction in the size of the optic globe(s), which may be reduced to a vestige visible only on histological analysis. This most severe form of microphthalmia is sometimes called "secondary" or "clinical" anophthalmia and occurs later in development than primary anophthalmia because of a lack of optic vesicle formation from the embryonic prosencephalon. Isolated severe microphthalmia/anophthalmia demonstrates both genetic and phenotypic heterogeneity in humans, currently implicating genes coding for transcription factors. *CHX10* mutations lead to microphthalmia, coloboma, and cataracts[1,2]; mutations in the *RAX* gene have been identified in an individual with unilateral anophthalmia and sclerocornea in the other eye.[3] *PAX6* mutations lead to diverse congenital ocular malformations, the most common of which is aniridia, but a few genotypes have been described to date that engender primary anophthalmia[4] or microphthalmia,[5–7] as documented in the PAX Allelic Variant Database.

Syndromic microphthalmias (MIM 164180, 206900, 206920, 248450, 300166, 301590, 309801, 600776, 605856, 607932, 610125, 610126, and 601349) can be associated with craniofacial dysmorphic features, heart and vascular malformations, skeletal and limb anomalies, skin or gut defects, mental retardation, and hydrocephalus, or combinations thereof. Although rare, the association of severe microphthalmia and pulmonary hypoplasia (MIM 601186) is a distinct entity known as "Matthew-Wood syndrome" (MWS [MIM 601186]).[8] Most authors have reported further associations of MWS with cardiac and/or diaphragmatic malformations and intrauterine growth retardation (IUGR).[9–13]

In two familial cases of MWS, we have excluded mutations in the *FGF10* and *FGFR2IIIb* genes encoding fibroblast growth factor 10 and its specific receptor isoform.[14] These proteins are essential for the development of all affected organs in MWS.[15–17] Meanwhile, *STRA6* gene mutations were recently implicated in heterogeneous postnatal associations of clinical anophthalmia, pulmonary hypoplasia, diaphragmatic hernia, and cardiac defects.[18] A molecular analysis of the *STRA6* gene was undertaken in the two families with MWS we had described,[14] as well as in five other fetuses presenting at least one of the two major signs of clinical anophthalmia or pulmonary hypoplasia and at least one of the two associated signs of diaphragmatic closure defect or cardiopathy.

In all seven fetuses examined, the presence of severe malformations was noted on ultrasound examination, and, after genetic counseling, pregnancies were interrupted. Clinical data are summarized in table 1. Chromosome and molecular analyses and pathological exam-

From INSERM U781 (C.G.; S.T.; A.M.; F.E.-R.; S.L.; M.V.; T.A.-B.; H.C.E.), Université René Descartes-Paris 5 (C.G.; S.D.; A.M.; F.E.-R.; S.L.; M.V.; T.A.-B.), Assistance Publique–Hôpitaux de Paris Departments of Genetics (J.M.-B.; S.M.-Z; M.B.; A.M.; F.E.-R.; S.L.; M.V.; T.A.-B.) and Obstetrics (S.D.), Hôpital Necker-Enfants Malades, and Institut de Puériculture Department of Fetal Pathology (B.G.-B.), Paris; and INSERM U563, Hôpital Purpan, Toulouse (H.C.E.), France

Received February 8, 2007; accepted for publication March 16, 2007; electronically published April 11, 2007.

Address for correspondence and reprints: Dr. Heather C. Etchevers, INSERM U781, Hôpital Necker, 149 rue de Sèvres, 75743 Paris Cedex 15, France. E-mail: etchevers@necker.fr

Am. J. Hum. Genet. 2007;80:000–000. 0002-9297/2007/8006-00XX$15.00
DOI: 10.1086/518177

Table 1. Overview of Clinical Features in Cases Undergoing *STRA6* Molecular Analysis from Our Series and Pasutto et al.[18]

Case	*STRA6* Mutation(s)	Clinical Features[a]							Age at Death	Consanguinity
		Eyes	Lungs	Diaphragm	Cardiovascular	Face	Other	Growth		
Fetus 1[b]	p.D17A fsX55	Bi AO	Bi agenesis	Bi eventr	Bi absence of PA branches	Mild dysmorphism	Duodenal stenosis, annular pancreas	IUGR	31 wg	Yes, recurrence
Fetus 2[b]	p.G176G fsX59	Bi AO	Bi agenesis	Bi eventr	Pulmonary trunk and PA absence, VSD	Mild dysmorphism	Duodenal stenosis, absent pancreas, polylobed spleen	IUGR	28 wg	Yes
Fam2-IV:1	p.G50A fsX22	Bi AO	…	CDH	ASD, VSD	Mild dysmorphism	MR	SS	Alive at 14 years	Yes, recurrence
Fam2-IV:3 (sib)	p.G50A fsX22	Bi AO	NA	CDH	NA	Mild dysmorphism	NA	…	23 wg	…
MWS4-BE	p.T644M	Bi AO	Hypo	CDH	…	…	Bi hydronephrosis	…	Alive at 3 mo	No, recurrence
Brother MWS4-BE	NA	NA	Hypo unilobar	…	Fallot, PDA	…	Horseshoe kidney, undescended testes	…	1 d	…
Sister MWS4-BE	NA	Bi AO	Hypo unilobar	…	PDA, CoA	…	Uterine dysplasia	…	1 d	…
MWS1-EE	p.R655C	Bi AO	Hypo	Uni eventr	…	…	Hypotonia uni inguinal hernia	…	3 mo	Yes, recurrence
Brother MWS1-EE	NA	Bi AO	…	…	TA, RAA, PDA, PA atresia	…	…	SS	22 mo	…
MWS6-BK	p.P90L, p.T321P	Bi AO	Hypo	CDH, uni eventr	PDA	…	Hypo kidneys, bicornuate uterus	PTB (36 wg)	1 d	Yes, recurrence?
Fam1-IV:2	p.P293L	Bi AO	ACD	…	PSt, PDA	Mild dysmorphism	Ectopic kidney, DD	PTB (33 wg)	6 mo	Yes, recurrence
Fam1-IV:4 (cousin)	NA	Bi AO	NA	…	Single ventricle PA atresia	NA	…	…	2 d	…
CD50396[b]	…	Bi AO	Hypo	Uni eventr	VSD	CP hypo alae nasi	Hypo bicornuate uterus, hypo spleen	…	1 d	No
Fetus 3[c]	…	Bi AO	Hypo	Bi CDH	Hypo L ventricle and aorta, mitral valve atresia, VSD	CP	CC agenesis, arhinencephaly, Dandy-Walker	…	16 wg	No
Fetus 4	…	Uni AO	…	…	Single ventricle tricuspid valve atresia, ASD	…	Arhinencephaly	…	22 wg	No
MWS3-KH	…	Bi MO/AO	…	CDH	…	…	…	…	NA	No
RHP006.070	…	Bi MO/AO	…	Bi eventr	…	…	MR	…	NA	No
PB-E03_053	…	Bi MO/AO	…	CDH	…	Brachycephaly	MR, sparse hair, bi inguinal hernia	…	Alive at 10 years	No
GM23728	…	Bi MO, abnormal cornea and iris	Hypo unilobar	Hypo, uni eventr	Hypo PA CoA	…	Renal dysplasia	…	Neonatal	No

AS20861-FF264	…	Uni MO	…	CDH	…	…	Ocular cyst, DD	…	Alive at 13 mo	No
MWS2-FA	…	Bi coloboma	…	CDH	…	…	Skin patches, brittle hair	…	NA	Yes
MWS5-LR	…	Coloboma	…	CDH	…	…	…	…	NA	No
Fetus 5	…	…	Hypo	Uni CDH	Dextroposed aorta over VSD	…	SUA	…	32 wg	No
AvdW22260	…	…	Hypo	CDH	…	…	…	PTB (28 wg)	1 d	No
Twin 2 AvdW22260	…	…	Hypo	CDH	…	CP	…	PTB (28 wg)	1 d	…
PM22479[d]	…	…	…	CDH	…	Hypertelorism	Hypo CC omphalocoele	…	Neonatal	Yes, recurrence
Brother[d] PM22479	NA	…	…	CDH	ASD	Bi CLP, hypertelorism	Hypo CC	…	Neonatal	…
Fetus 6	…	…	Bi hypo	L agenesis, R eventr	Hypo L heart	…	Polysplenia renal dysplasia, SUA	IUGR	30 wg	No
Fetus 7	…	…	Bi agenesis	…	L atrial isomerism, R ventricular anomaly	…	Polysplenia renal agenesis	…	24 wg	No

NOTE.—NA = not available. Fetuses 1–7 from our series are highlighted in bold.

[a] ACD = alveolar capillary dysplasia; AO = clinical anophthalmia; ASD = atrial septal defect; bi = bilateral; CC = corpus callosum; CoA = coarctation of aorta; C(L)P = cleft (lip and) palate; DD = developmental delay; eventr = eventration; Fallot = tetralogy of Fallot; hypo = hypoplasia; L = left; MO = microphthalmia; MR = mental retardation; PA = pulmonary artery; PDA = patent ductus arteriosus; PSt = pulmonary valve stenosis; PTB = preterm birth; R = right; RAA = right aortic arch; SS = postnatal short stature; SUA = single umbilical artery; TA = truncus arteriosus; uni = unilateral; VSD = ventricular septal defect; wg = weeks gestation.

[b] Cases given diagnosis of Matthew-Wood syndrome.

[c] Cases given diagnosis of Fryns syndrome.

[d] Cases with suspected Donnai-Barrow syndrome.

inations were performed in all cases with full parental consent. Genomic DNA was extracted from frozen tissue in fetal cases and from peripheral blood samples for parents in accordance with standard protocols.

Polymorphic markers *D15S188, D15S160, D15S991,* and *D15S114,* flanking the *STRA6* gene, were chosen using the UCSC Genome Browser and were examined in fetal cases 1 and 2 (fig. 1). The parents of case 1 are a consanguineous couple of Romanian origin, and the parents of case 2 are a consanguineous couple of Portuguese origin.[14] Homozygous haplotypes were demonstrated in each fetus, although the clinically unaffected parents of case 1 had a heterozygous haplotype with an allele presumably inherited from a common ancestor (DNA was unavailable from the other family members of case 2).

Primers were subsequently designed to cover the 20 exons and exon-intron junctions of the *STRA6* gene (UCSC Genome Browser reference sequence NM_022369), including exons 1A and 1B (the first noncoding exon may be alternatively spliced), with the use of Primer3 software[19] (table 2). PCRs were treated with the ExoSAP enzyme mix as per the manufacturer's instructions (GE-Amersham). Sequencing was performed for all seven fetal DNA samples with the use of Big Dye v3.1 Terminator Cycle Sequencing Reactions on an ABI 3130 (Applied Biosystems). Both the sense and antisense strands of the PCR-amplified fragments were analyzed with Sequence Analysis software (Applied Biosystems).

Cases 1 and 2 both presented homozygous mutations in the coding sequence of *STRA6* (fig. 1). A homozygous insertion/deletion in exon 2 (c.50_52delACTinsCC) for fetus 1 causes a frameshift and the appearance of a premature stop codon (p.Asp17Ala fsX55). An older brother with isolated bilateral coloboma of the retina and iris was heterozygous for this mutation, as were the clinically unaffected parents. Case 2 presented a homozygous single-base insertion in exon 7 (c.527_528insG) that also predicts a premature stop codon (p.Gly176Gly fsX59).

Case 4 had six intronic variations and one conservative amino acid substitution (table 3), all of which were homozygous and documented SNPs in the general population (dbSNP). Parental samples for fetus 4 were not available for analysis. Since the fetus was not known to come

Table 2. ***STRA6*** **Oligonucleotides Used for Sequencing**

Exon(s)	Oligonucleotide Sequences (5′→3′)	
	Forward	Reverse
1a	GGGGTGGGTTCCTCTGAT	CACCCCAGGTCTCCAAACT
1b	GCTGAAGGCAGGTATGTGTG	CCTCTCGTGTCCCCTCCT
2	AAGCCTCTTTTCACATCTGTAGTG	CAGTTGCAACCTCTGCCATC
3	TGGGTAAAGCCTCAGTGTGA	GTTGGACTTGCATCCTGGTT
4	CAAGCCCTCAAACTCAGACC	TGGGGGTCCTGACTAAACCT
5	CCACCTCCTTGATTTATGGAA	GCATCGTTGTAAAGACTGGATG
6 and 7	ACCTTCTCATTTTGCCCTTG	CTCAAAGGAGGCACTGTGGT
8	GCAACGGATTCTGGTTCTTG	GGAGTAGGGCTGTCTTGGG
9 and 10	ACGAATGGGTCGAGGCAG	TCTGTGCAAGGGAGGGTAAC
11	CTTGGGAGGGAGGAGGG	GGTTGAGGGCAGGGCTC
12	CCAGCGTCTCCCCTGTTAG	CATAGACCTTGGGTCTCCCC
13	TGGCAGGGGTTCTGAGG	CACAGGACTCCCACTCCTTC
14	TGGCCCAGAGGAGGATTTAG	CCAACTGAGGCCAGTGTCTG
15 and 16	AAAGCCCTTGGTTCTGGG	ACACCGAAGAAGAGGCGAG
17	AGGTCTGACACTGACCCTGG	GATGCCTTCCTCACTGCTTG
18	TGGATGCCTCCAGTGTGG	AGGGGCACACATCCTTCC
19	GATCAGGTCTGAGGGCCAG	GAGGAGGATGGTAGGCAGG

NOTE.—The annealing temperature for PCR was 60°C for all primers. For QMPSF, fluorescent primers corresponding to *STRA6* exon 13 were used, and *MLH1* was chosen as a reference (GTAGTCTGTGATCTCCGTTT, 5′; ATGTATGAGGTCCTGTCCT, 3′). Coamplification was performed for 21 cycles, and the peaks were integrated and proportional DNA copy numbers were estimated with the use of Genotyper 3.7 software (Applied Biosystems).

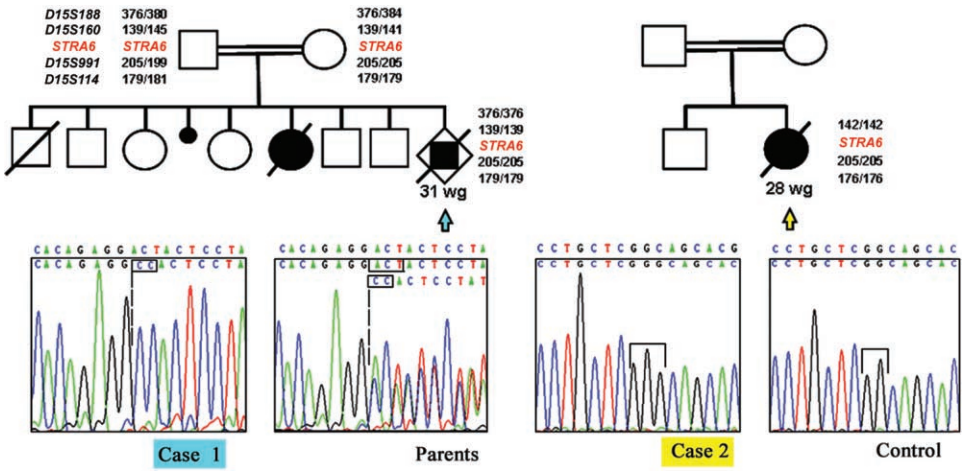

Figure 1. Pedigrees of cases 1 and 2, with markers flanking the *STRA6* gene, and electropherograms. Case 1 (*blue arrow*) had a homozygous insertion/deletion in exon 2 of *STRA6* (c.50_52delACTinsCC p.AspD17Ala fsX55). Case 2 (*yellow arrow*) had a homozygous insertion in exon 7 (c.527_528insG p.Gly176Gly fsX59). Markers *D15S160, D15S991,* and *D15S114* were also homozygous; relatives' DNA was unavailable for further analysis. wg = Weeks gestation.

Table 3. Sequence Variations in *STRA6*

Fetal Case and Nucleotide Change versus NM_022369	Predicted Effect on ORF	dbSNP Reference Number	Status
1:			
c.50_52delACTinsCC	p.Asp17Ala fsX55	…	Homozygous
2:			
c.527_528insG	p.Gly176Gly fsX59	…	Homozygous
4:			
c.331C→T	p.Leu111Leu	*rs11857410*	Homozygous
c.406+97A→G	…	*rs34147822*	Homozygous
c.406+111A→G	…	*rs35255788*	Homozygous
c.430+24T→A	…	*rs971756*	Homozygous
c.431−37C→T	…	*rs971757*	Homozygous
c.1685−24T→C	…	*rs12913041*	Homozygous
c.1840+50T→C	…	*rs12912578*	Homozygous
5:			
c.596+9T→G	…	*rs28541560*	Heterozygous
c.1301−43A→C	p.Ser472Ser	*rs351240*	Heterozygous
c.1416G→A	…	*rs351241*	Heterozygous
6:			
c.1166+32G→A	…	…	Heterozygous
7:			
c.1167−10C→G	…	*rs2277608*	Heterozygous

NOTE.—Case 3 had no sequence variations.

from a consanguineous background and had a normal karyotype, the hypothesis of a small, heterozygous deletion was considered. Quantitative multiplex PCR of small fluorescent fragments (QMPSF)[20] was undertaken to measure the number of genomic *STRA6* copies for case 4. The results indicated that this fetus did not present a deletion of the *STRA6* gene that would explain the observed homozygosity of the SNPs (data not shown).

A single heterozygous variation located in intron 13 (c.1407+32G→A) that was observed in case 5 has not been identified to date in dbSNP (table 3). We screened 260 control chromosomes without observing the c.1407+32G→A variation. The only tissue available from fetus 5 for expression analysis was a frozen lung sample. *STRA6* transcripts were not observed in either total lung RNA extracted from an age-matched fetus affected with an unrelated disorder or from the case 5 tissue sample (data not shown). Therefore, the consequence of this variation on *STRA6* transcription remains to be determined.

We report homozygous mutations in the *STRA6* gene in two fetuses presenting the principal features of MWS, including bilateral severe microphthalmia and pulmonary agenesis. Both also had bilateral diaphragmatic eventration, and one had a cardiac malformation. The observation that both fetuses came from consanguineous families—and, moreover, that one family demonstrated sibling recurrence—had already evoked a recessive model of inheritance for MWS.[14] Since the molecular anomaly has been found, it is now possible to affirm that MWS is indeed an autosomal recessive disorder that can be ascribed to mutations in the *STRA6* gene.

These two fetuses with the *STRA6* mutation would not have survived postnatally. In both cases, the mutations would have led to a truncated protein if translated. Homozygous *STRA6* mutations have also been observed in peri- and postnatal patients from two other families, as well as in three sporadic cases with a similar phenotypic spectrum.[18] However, four missense mutations were found to be associated with a severe clinical phenotype, whereas two cases with a truncating mutation had milder clinical signs with no growth retardation nor apparent pulmonary anomalies. Indeed, one of those patients has survived into his teens. Comparison of all reported patients with *STRA6* mutations (table 1) thus demonstrates that there is no correlation to date between the nature of a coding mutation and the severity of the phenotype.

The recent functional study of 50 random missense mutations introduced into bovine *Stra6* has shown that a few of these are sufficient to prevent cell surface expression and that one, although allowing protein insertion into the membrane, abrogates vitamin A entry into the cell.[21] Similar studies will now need to be conducted with documented human mutations to draw conclusions, but it is probable that phenotypic severity is a result of the reduction in perceived retinoic acid (RA) dose within sensitive target tissues, rather than a simple distinction between missense and nonsense mutations.

We also undertook molecular analysis of *STRA6* in five other fetuses with pulmonary and ocular or cardiac malformations, but no other patent mutations were identified, despite some intriguing variations (table 3). The clinical diversity of patients with *STRA6* mutations, and the large phenotypic overlap with those who do not have the mutations, strongly suggests that MWS and related syndromes are not only clinically but genetically heterogeneous.

The only necessary diagnostic criterion predicting the involvement of *STRA6,* on the basis of the patients currently reported here and in the previous study,[18] is severe microphthalmia (clinical anophthalmia). Microphthalmia with any macroscopically residual presence of the ocular globe does not correlate with *STRA6* mutations in either series (table 1). Obviously, since many genes have previously been identified in both isolated and syndromic microphthalmia, this feature is not sufficient to direct molecular testing. The severe eye malformations subsequent to *STRA6* mutations are always observed in association with one or more of the three following signs: pulmonary defects, congenital diaphragmatic eventration/hernia, or cardiovascular malformation involving the common aorticopulmonary trunk or pulmonary arteries. Furthermore, according to our two MWS cases and descriptions of MWS in the literature, pancreatic malformations and IUGR may also be secondary diagnostic criteria.

Pulmonary defects range from agenesis (this report) to hypoplasia or unilobar lung (among families with MWS mutations) to no obvious lung problems (in either member of family 2 examined by Pasutto et al).[18] Pulmonary and diaphragmatic malformations (eventration/hernia) are not always associated and occur separately or in combination even among members of the same family.[18] This observation leads us to conclude that, in the context of *STRA6* mutations, the pulmonary phenotype of patients with mutations is a primary malformation and is not a consequence of diaphragmatic hernia. However, the joint presence of clinical anophthalmia and pulmonary and/or diaphragmatic anomalies is still not sufficient to guarantee *STRA6* involvement, because other cases with bilateral anophthalmia and hypoplastic lungs (patients with MWS GM23728 and CD50396 from Pasutto et al.[18] and our case 4) do not present coding-sequence mutations (table 1).

Cardiovascular involvement is frequent but inconstant. Case 2 had a ventricular septal defect and pulmonary trunk agenesis, whereas case 1 presented isolated agenesis of the pulmonary arteries. Furthermore, *STRA6* mutations described by Pasutto et al. also give rise to conotruncal or great-artery malformations (i.e., truncus arteriosus, tetralogy of Fallot, pulmonary valve or arterial stenosis, and right aortic arch) in at least some family members.[18] Other affected members with identical mutations had no cardiovascular signs (cf. MWS4-BE). Cases of MWS described elsewhere[9,12] also show a preponderance of pulmonary artery absence, ductus arteriosus, or ventricular septal defects.

Fryns syndrome (MIM 229850) has a clinical spectrum that includes diaphragmatic hernia and, less frequently, microphthalmia, facial dysmorphy, and distal limb anomalies. Fetal case 3, presenting with bilateral microphthalmia, pulmonary hypoplasia, diaphragmatic hernia, cardiac involvement, and cleft palate, was given a diagnosis of Fryns syndrome. Despite the implication of the same organ systems as in MWS and absence of a digital phenotype, no mutations in the *STRA6* coding sequence were found. Patients GM23728 and CD50396 from Pasutto et al.[18] also had a similar phenotype (table 1); the latter was given a diagnosis of MWS, presented true clinical anophthalmia, and had a cleft palate. Palate involvement might therefore be suggestive of Fryns syndrome rather than MWS. Phenotypic overlap between these two disorders indicates that similar cases given a diagnosis of Fryns syndrome or MWS have either a noncoding mutation in *STRA6* or involvement of another gene necessary for the cellular interpretation of RA levels. For some authors, animal models of retinoid deficiency also evoke the PAGOD syndrome (pulmonary tract and pulmonary artery, agonadism, omphalocele, diaphragmatic defect, and dextrocardia [MIM 202660]), which shares features with Fryns syndrome and MWS.[22]

RA, a small lipophilic hormone derived from retinol (vitamin A), is a ligand for nuclear receptors (RARα, -β, and -γ) that act in homodimers or in heterodimers with retinoid X receptor partners to bind DNA and regulate the expression of many genes, including the *Stra* (stimulated by retinoic acid) targets.[23,24] The functionally identified *Stra* genes have different roles and structurally unrelated products. For example, *Stra1* encodes ephrin B1, a bidirectional, membrane-bound signaling molecule highly expressed in the embryonic neural crest[25]; *Stra7,* later identified as the evolutionarily conserved transcription factor Gbx2,[26] partners with the homeobox transcription factor *Otx2* in the specification of the isthmic organizer (midbrain/hindbrain junction).[27]

Otx2 was also subsequently identified as a transcriptional target of RA, which leads to derepression of *Pax6* transcription in the optic cup.[28] Interestingly, both *OTX2*[29] and *PAX6*[4] are responsible for human anophthalmias (MIM 610125 and 607108 [allelic variant .0005], respectively), through heterozygous loss-of-function with incomplete penetrance for the former and compound heterozygous loss-of-function engendering a primary anophthalmia for the latter. Mutations in *EFNB1* (encoding human ephrin B1) induce craniofrontonasal syndrome (MIM 304110), sometimes in association with congenital diaphragmatic hernia (CDH).[30,31] We note that *CRABP1* (cellular retinoic acid–binding protein 1), another transcriptional target and effector of cytoplasmic RA levels,[32] is located close to reported CDH loci in the long arm of chromosome 15. Experimental or teratogenic reductions in RA levels also lead to CDH in both animals and humans.[33,34]

The murine *Stra6* gene encodes an integral transmembrane protein that is expressed in the developing eye, lung, other endodermal gut derivatives, limbs, and somites.[23] In addition to being stimulated by RA, *Stra6* encodes a receptor for soluble retinol-binding protein, efficiently mediating retinol uptake from the circulatory system into target cells.[21]

Signaling by RA within the caudal pharyngeal endoderm of the vertebrate embryo is critical for the organization of the adjacent aortic arch vessels and heart. Sen-

sitivity of only the most posterior aortic arches, which persist in direct continuity with the outflow tract of the heart, may be a result of the localized mesodermal production of retinaldehyde dehydrogenase 2 (Raldh2), a major enzyme for RA synthesis from retinol during development.[35] *Raldh2*$^{-/-}$ mice demonstrate third- and fourth-arch artery malformations, with agenesis of the sixth arch[36] in addition to cardiac septation defects[37] and partial pancreatic agenesis.[38] The variable implication of the cardiac outflow tract and vascular derivatives of the embryonic fourth (definitive aorta) and sixth (ductus arteriosus and proximal pulmonary artery) aortic arches in our patients is consistent with an underlying field defect affecting the perception of RA dose by the endoderm.

Indeed, murine *Stra6* is highly expressed in the pharyngeal endoderm and mesenchyme along the embryonic gut.[23] Our two severely affected patients with mutations had duodenal stenosis and pancreatic malformations in addition to lung agenesis. These organs are among the many derivatives of the embryonic endoderm produced by localized outpocketings into the mesoderm that will consolidate into the definitive structure.

RA is particularly necessary for normal growth and formation of the lung. *Fgf10*$^{-/-}$ mice demonstrate complete lung agenesis,[15,16] whereas, in knockout mice for the appropriate Fgf10-binding isoform of *Fgfr2,* the tracheal bifurcation at the origin of the bronchi is absent.[17] In *Raldh2*$^{-/-}$ mouse embryos, *Fgf10* is no longer expressed in the lung bud, and complete agenesis results.[39] It appears likely that *Stra6* expressed, among other places, in the *Raldh2*$^{+}$ bronchial mesenchyme of the early lung[23] mediates retinol entry into the mesoderm and a subsequent effect on Fgfr2 signaling in the endoderm. Indeed, the supply of exogenous RA for short periods can partially rescue both *Fgf10* expression and lung agenesis, leading to unilobar or unilateral right-sided lung development; longer rescue periods lead to better recovery and more subtle alveolar malformations.[40]

Stra6 is also expressed at all stages of eye development—initially, within the optic vesicle and, later, within the periocular mesenchyme, the choroid, and the optic nerve (and forebrain) meninges. Expression in the retinal pigment epithelium persists throughout adult life in both mice and humans,[18,23] which is indicative of the continued need for RA for ocular function. The consistency of clinical anophthalmia in patients with *STRA6* mutations argues for the need for vitamin A uptake to further all stages of eye development after initial optic specification.

Stra6 transcripts are also detected in several other sites, including the forebrain, the isthmic organizer, and the neurohypophysis. However, no patients with *STRA6* mutations present CNS malformations or pituitary anomalies, although IUGR or short stature may indicate a more subtle effect (table 1). Murine expression patterns do not always suffice to explain clinical outcome.[41] Despite the strong, localized brain expression of the RA target *Gbx2* (*Stra7*), its absence in mice gives rise only to posterior branchial arch anomalies and cardiac malformations, reminiscent of those observed in patients with *STRA6* mutations or in *Raldh2*$^{-/-}$ mice.[42] There may also be species-specific differences in the RA sensitivity of the developing brain; the clinical spectrum of human vitamin A deficiency syndrome does not include the exencephaly observed in mouse models.[43]

In conclusion, *STRA6* mutations are responsible for a large spectrum of congenital malformations with no current evidence of a genotype-phenotype correlation. Different transcriptional targets of RA signaling in humans appear to effect subset phenotypes of those observed in more generalized deficiencies.[43] MWS is thus part of a growing family of human syndromes due to mutations in genes encoding effectors of the powerful developmental morphogen, RA.

Acknowledgments

The authors warmly thank Chantal Esculpavit, Annie Ebrac, Géraldine Goudefroye, and Catherine Ozilou, for their assistance, and Jeanne Amiel and Patrick Calvas, for critical discussion and reflection. Support has been provided by National Institutes of Health grant R01 NS039818-09 (to M.V. and S.T.) and the Association Française contre les Myopathies (to H.E.), in addition to the Assistance Publique and the Institut National de la Santé et de la Recherche Médicale.

Web Resources

Accession numbers and URLs for data presented herein are as follows:

dbSNP, http://www.ncbi.nlm.nih.gov/SNP/

Online Mendelian Inheritance in Man (OMIM), http://www.ncbi.nlm.nih.gov/Omim/ (for syndromic microphthalmias, anophthalmia, anophthalmia and pulmonary hypoplasia, MWS, Fryns syndrome, PAGOD syndrome, and craniofrontonasal syndrome)

PAX6 Allelic Variant Database, http://pax6.hgu.mrc.ac.uk/

Primer3 software, http://frodo.wi.mit.edu/cgi-bin/primer3/primer3_www.cgi

UCSC Genome Browser, http://genome.ucsc.edu/cgi-bin/hgTracks (for reference sequence NM_022369)

References

1. Ferda Percin E, Ploder LA, Yu JJ, Arici K, Horsford DJ, Rutherford A, Bapat B, Cox DW, Duncan AM, Kalnins VI, et al (2000) Human microphthalmia associated with mutations in the retinal homeobox gene *CHX10*. Nat Genet 25:397–401
2. Bar-Yosef U, Abuelaish I, Harel T, Hendler N, Ofir R, Birk OS (2004) *CHX10* mutations cause non-syndromic microphthalmia/anophthalmia in Arab and Jewish kindreds. Hum Genet 115:302–309
3. Voronina VA, Kozhemyakina EA, O'Kernick CM, Kahn ND, Wenger SL, Linberg JV, Schneider AS, Mathers PH (2004) Mutations in the human *RAX* homeobox gene in a patient with anophthalmia and sclerocornea. Hum Mol Genet 13:315–322
4. Glaser T, Jepeal L, Edwards JG, Young SR, Favor J, Maas RL (1994) *PAX6* gene dosage effect in a family with congenital

cataracts, aniridia, anophthalmia and central nervous system defects. Nat Genet 7:463–471
5. Azuma N, Yamaguchi Y, Handa H, Hayakawa M, Kanai A, Yamada M (1999) Missense mutation in the alternative splice region of the *PAX6* gene in eye anomalies. Am J Hum Genet 65:656–663
6. Vincent MC, Pujo AL, Olivier D, Calvas P (2003) Screening for *PAX6* gene mutations is consistent with haploinsufficiency as the main mechanism leading to various ocular defects. Eur J Hum Genet 11:163–169
7. Azuma N, Yamaguchi Y, Handa H, Tadokoro K, Asaka A, Kawase E, Yamada M (2003) Mutations of the *PAX6* gene detected in patients with a variety of optic-nerve malformations. Am J Hum Genet 72:1565–1570
8. Li L, Wei J (2006) A newborn with anophthalmia and pulmonary hypoplasia (the Matthew-Wood syndrome). Am J Med Genet A 140:1564–1566
9. Berkenstadt M, Lev D, Achiron R, Rosner M, Barkai G (1999) Pulmonary agenesis, microphthalmia, and diaphragmatic defect (PMD): new syndrome or association? Am J Med Genet 86:6–8
10. Engellenner W, Kaplan C, Van de Vegte GL (1989) Pulmonary agenesis association with nonimmune hydrops. Pediatr Pathol 9:725–730
11. Seller MJ, Davis TB, Fear CN, Flinter FA, Ellis I, Gibson AG (1996) Two sibs with anophthalmia and pulmonary hypoplasia (the Matthew-Wood syndrome). Am J Med Genet 62: 227–229
12. Spear GS, Yetur P, Beyerlein RA (1987) Bilateral pulmonary agenesis and microphthalmia. Am J Med Genet Suppl 3:379–382
13. Steiner RD, Dignan P St J, Hopkin RJ, Kozielski R, Bove KE (2002) Combination of diaphragmatic eventration and microphthalmia/anophthalmia is probably nonrandom. Am J Med Genet 108:45–50
14. Martinovic-Bouriel J, Bernabe-Dupont C, Golzio C, Grattagliano-Bessieres B, Malan V, Bonniere M, Esculpavit C, Fallet-Bianco C, Mirlesse V, Le Bidois J, et al (2007) Matthew-Wood syndrome: report of two new cases supporting autosomal recessive inheritance and exclusion of *FGF10* and *FGFR2*. Am J Med Genet A 143:219–228
15. Min H, Danilenko DM, Scully SA, Bolon B, Ring BD, Tarpley JE, DeRose M, Simonet WS (1998) Fgf-10 is required for both limb and lung development and exhibits striking functional similarity to Drosophila branchless. Genes Dev 12:3156–3161
16. Sekine K, Ohuchi H, Fujiwara M, Yamasaki M, Yoshizawa T, Sato T, Yagishita N, Matsui D, Koga Y, Itoh N, et al (1999) Fgf10 is essential for limb and lung formation. Nat Genet 21: 138–141
17. De Moerlooze L, Spencer-Dene B, Revest J, Hajihosseini M, Rosewell I, Dickson C (2000) An important role for the IIIb isoform of fibroblast growth factor receptor 2 (FGFR2) in mesenchymal-epithelial signalling during mouse organogenesis. Development 127:483–492
18. Pasutto F, Sticht H, Hammersen G, Gillessen-Kaesbach G, FitzPatrick DR, Nürnberg G, Brasch F, Schirmer-Zimmermann H, Tolmie JL, Chitayat D, et al (2007) Mutations in *STRA6* cause a broad spectrum of malformations including anophthalmia, congenital heart defects, diaphragmatic hernia, alveolar capillary dysplasia, lung hypoplasia, and mental retardation. Am J Hum Genet 80:550–560
19. Rozen S, Skaletsky H (2000) Primer3 on the WWW for general users and for biologist programmers. Methods Mol Biol 132: 365–386
20. Saugier-Veber P, Goldenberg A, Drouin-Garraud V, de La Rochebrochard C, Layet V, Drouot N, Le Meur N, Gilbert-Du-Ssardier B, Joly-Helas G, Moirot H, et al (2006) Simple detection of genomic microdeletions and microduplications using QMPSF in patients with idiopathic mental retardation. Eur J Hum Genet 14:1009–1017
21. Kawaguchi R, Yu J, Honda J, Hu J, Whitelegge J, Ping P, Wiita P, Bok D, Sun H (2007) A membrane receptor for retinol binding protein mediates cellular uptake of vitamin A. Science 315:820–825
22. Macayran JF, Doroshow RW, Phillips J, Sinow RM, Furst BA, Smith LM, Lin HJ (2002) PAGOD syndrome: eighth case and comparison to animal models of congenital vitamin A deficiency. Am J Med Genet 108:229–234
23. Bouillet P, Sapin V, Chazaud C, Messaddeq N, Decimo D, Dolle P, Chambon P (1997) Developmental expression pattern of Stra6, a retinoic acid-responsive gene encoding a new type of membrane protein. Mech Dev 63:173–186
24. Bouillet P, Oulad-Abdelghani M, Vicaire S, Garnier JM, Schuhbaur B, Dolle P, Chambon P (1995) Efficient cloning of cDNAs of retinoic acid-responsive genes in P19 embryonal carcinoma cells and characterization of a novel mouse gene, Stra1 (mouse LERK-2/Eplg2). Dev Biol 170:420–433
25. Davy A, Aubin J, Soriano P (2004) Ephrin-B1 forward and reverse signaling are required during mouse development. Genes Dev 18:572–583
26. Bouillet P, Chazaud C, Oulad-Abdelghani M, Dolle P, Chambon P (1995) Sequence and expression pattern of the Stra7 (Gbx-2) homeobox-containing gene induced by retinoic acid in P19 embryonal carcinoma cells. Dev Dyn 204:372–382
27. Hidalgo-Sanchez M, Millet S, Bloch-Gallego E, Alvarado-Mallart RM (2005) Specification of the meso-isthmo-cerebellar region: the Otx2/Gbx2 boundary. Brain Res Brain Res Rev 49: 134–149
28. Halilagic A, Ribes V, Ghyselinck NB, Zile MH, Dolle P, Studer M (2007) Retinoids control anterior and dorsal properties in the developing forebrain. Dev Biol 303:362–375
29. Ragge NK, Brown AG, Poloschek CM, Lorenz B, Henderson RA, Clarke MP, Russell-Eggitt I, Fielder A, Gerrelli D, Martinez-Barbera JP, et al (2005) Heterozygous mutations of *OTX2* cause severe ocular malformations. Am J Hum Genet 76: 1008–1022
30. McGaughran J, Rees M, Battin M (2002) Craniofrontonasal syndrome and diaphragmatic hernia. Am J Med Genet 110: 391–392
31. Vasudevan PC, Twigg SR, Mulliken JB, Cook JA, Quarrell OW, Wilkie AO (2006) Expanding the phenotype of craniofrontonasal syndrome: two unrelated boys with *EFNB1* mutations and congenital diaphragmatic hernia. Eur J Hum Genet 14: 884–887
32. Means AL, Thompson JR, Gudas LJ (2000) Transcriptional regulation of the cellular retinoic acid binding protein I gene in F9 teratocarcinoma cells. Cell Growth Differ 11:71–82
33. Clugston RD, Klattig J, Englert C, Clagett-Dame M, Martinovic J, Benachi A, Greer JJ (2006) Teratogen-induced, dietary and genetic models of congenital diaphragmatic hernia share a common mechanism of pathogenesis. Am J Pathol 169: 1541–1549
34. Holder AM, Klaassens M, Tibboel D, de Klein A, Lee B, Scott

DA. Genetic factors in congenital diaphragmatic hernia. Am J Hum Genet (in press)
35. Berggren K, McCaffery P, Drager U, Forehand CJ (1999) Differential distribution of retinoic acid synthesis in the chicken embryo as determined by immunolocalization of the retinoic acid synthetic enzyme, RALDH-2. Dev Biol 210:288–304
36. Niederreither K, Vermot J, Le Roux I, Schuhbaur B, Chambon P, Dolle P (2003) The regional pattern of retinoic acid synthesis by RALDH2 is essential for the development of posterior pharyngeal arches and the enteric nervous system. Development 130:2525–2534
37. Niederreither K, Vermot J, Messaddeq N, Schuhbaur B, Chambon P, Dolle P (2001) Embryonic retinoic acid synthesis is essential for heart morphogenesis in the mouse. Development 128:1019–1031
38. Martin M, Gallego-Llamas J, Ribes V, Kedinger M, Niederreither K, Chambon P, Dolle P, Gradwohl G (2005) Dorsal pancreas agenesis in retinoic acid-deficient *Raldh2* mutant mice. Dev Biol 284:399–411
39. Desai TJ, Malpel S, Flentke GR, Smith SM, Cardoso WV (2004) Retinoic acid selectively regulates *Fgf10* expression and maintains cell identity in the prospective lung field of the developing foregut. Dev Biol 273:402–415
40. Vermot J, Messaddeq N, Niederreither K, Dierich A, Dolle P (2006) Rescue of morphogenetic defects and of retinoic acid signaling in retinaldehyde dehydrogenase 2 (Raldh2) mouse mutants by chimerism with wild-type cells. Differentiation 74:661–668
41. Fougerousse F, Bullen P, Herasse M, Lindsay S, Richard I, Wilson D, Suel L, Durand M, Robson S, Abitbol M, et al (2000) Human-mouse differences in the embryonic expression patterns of developmental control genes and disease genes. Hum Mol Genet 9:165–173
42. Byrd NA, Meyers EN (2005) Loss of Gbx2 results in neural crest cell patterning and pharyngeal arch artery defects in the mouse embryo. Dev Biol 284:233–245
43. Kastner P, Mark M, Chambon P (1995) Nonsteroid nuclear receptors: what are genetic studies telling us about their role in real life? Cell 83:859–869

EUROPEAN JOURNAL OF CANCER 43 (2007) 2366–2372

available at www.sciencedirect.com

journal homepage: www.ejconline.com

Methylation-associated *PHOX2B* gene silencing is a rare event in human neuroblastoma

Loïc de Pontual[a], *Delphine Trochet*[a], *Franck Bourdeaut*[b], *Sophie Thomas*[a], *Heather Etchevers*[a], *Agnes Chompret*[c], *Véronique Minard*[c], *Dominique Valteau*[c], *Laurence Brugieres*[c], *Arnold Munnich*[a], *Olivier Delattre*[b], *Stanislas Lyonnet*[a], *Isabelle Janoueix-Lerosey*[b], *Jeanne Amiel*[a,*]

[a]*Unité de Recherches sur les Handicaps Génétiques de l'Enfant INSERM U-781, et Département de Génétique, Université René-Descartes, Faculté de Médecine, Hôpitaux de Paris, Hôpital Necker-Enfants Malades, 149, rue de Sèvres, 75743 Paris Cedex 15, France*
[b]*Laboratoire de Pathologie Moléculaire des Cancers, INSERM U-830, Institut Curie, Paris, France*
[c]*Departement de Pédiatrie, Institut Gustave Roussy, Villejuif Cedex, France*

ARTICLE INFO

Article history:
Received 2 May 2007
Received in revised form 20 June 2007
Accepted 12 July 2007
Available online 31 August 2007

Keywords:
Neuroblastoma
PHOX2B
Methylation
Neural crest

ABSTRACT

Neuroblastoma (NB), an embryonic tumour originating from neural crest cells, is one of the most common solid tumours in childhood. Although NB is characterised by numerous recurrent, large-scale chromosome rearrangements, the genes targeted by these imbalances have remained elusive. We recently identified the paired-like homeobox 2B (*PHOX2B*, MIM 603851) gene as disease-causing in dysautonomic disorders including Congenital Central Hypoventilation Syndrome (CCHS), Hirschsprung disease (HSCR) and NB in various combinations. Most patients with NB due to a germline heterozygous *PHOX2B* gene mutation are familial and/or syndromic. *PHOX2B*, at chromosome 4p12, does not lie in a commonly rearranged locus in NB. To evaluate the role of *PHOX2B* in sporadic, isolated NB, we analysed 13 NB cell lines and 45 tumours for expression, mutations of coding and promoter sequences, loss of heterozygosity (LOH), or aberrant hypermethylation of *PHOX2B* (13 cell lines and 18 tumours). We didn't identify any mutation but LOH in about 10% of the cases and aberrant CpG dinucleotide methylation of the 500 bp *PHOX2B* promoter region in 4/31 tumours and cell lines (12.9%). Altogether, both germinal and somatic anomalies at the *PHOX2B* locus are found in NB.

1. Introduction

Neuroblastoma (NB; MIM 256700) is a tumour of the sympathetic nervous system that accounts for 10% of all cancers in children. Several lines of evidence support the involvement of genetic factors in NB, namely, rare familial cases with vertical transmission and the association of NB with other genetically determined congenital malformations of neural crest origin, such as Hirschsprung disease (HSCR; MIM 142623) and/or Congenital Central Hypoventilation Syndrome (CCHS; MIM 209880). We recently identified the paired-like homeobox 2B (*PHOX2B*; MIM 603851) gene as the major disease-causing gene in CCHS[1] and the first gene for which germline mutations predispose to NB.[2–5] *PHOX2B* is a highly conserved homeotic transcription factor with two alanine tracts of nine and 20 alanines, C terminal to the homeodomain. The vast majority of mutations leading to CCHS result in an expansion of the longer alanine tract. Interestingly, patients harbouring

* *Corresponding author:* Tel.: +33 1 44495648; fax: +33 1 44495150.
E-mail address: amiel@necker.fr (J. Amiel).
0959-8049/$ - see front matter
doi:10.1016/j.ejca.2007.07.016

either a missense mutation in the homeodomain or a frameshift mutation are the ones at risk of developing NB, whether or not they have CCHS.[6] However, both germline and somatic *PHOX2B* coding sequence mutations are rare events in sporadic, isolated NB.[7,4,8]

Epigenetic abnormalities, especially alterations in DNA methylation, are involved in the development of various adult tumours. More recent studies have indicated that epigenetic aberrations may also contribute to paediatric cancer pathogenesis. In neuroblastomas, several potential tumour-suppressor genes have been found to be frequently hypermethylated and consequently down-regulated; in particular, genes of the tumour necrosis factor-related apoptosis-inducing ligand (TRAIL) pathway, CASP8[9] and the DCR receptors (DCR1, DCR2, DCR3 and DCR4.[10,11] DNA methylation has been shown to reduce the binding affinity of sequence-specific transcription factors while methylation-dependent gene silencing may also involve alterations in chromatin structure, mediated by methyl binding proteins. Chromosome distribution of the methyl-targeted genes are clustered and the full pattern of methylation may be generated early in tumourigenesis.[12,13] Finally, in tumours carrying a germline mutation, a second-step methylation of the DNA promoter, if present, occurs exclusively on the wild-type allele.

The possible involvement of non-coding mutations or promoter methylation of the *PHOX2B* locus in sporadic neuroblastoma has not been evaluated. In this study, we examined the level of *PHOX2B* expression and its methylation in NB. *PHOX2B* was silenced in a subset of 3/13 NB cell lines and loss of expression was associated with aberrant 5′CpG dinucleotide methylation of the *PHOX2B* promoter. *PHOX2B* promoter methylation was also detected in 2/18 tumuors analysed. Treatment with the demethyling agent 5-Aza-2′-deoxycytidine (5-Aza-dC) restored *PHOX2B* transcription in *PHOX2B*-negative cell lines, showing that gene silencing was due to aberrant hypermethylation. We conclude that aberrant CpG dinucleotide methylation of *PHOX2B* is an alternative mechanism at least as frequent as coding sequence mutations for inactivation of *PHOX2B* in sporadic NB.

2. Materials and methods

2.1. Patients

13 NB cell lines and 46 sporadic neuroblastic tumours were investigated. Patients were staged according to the International Neuroblastoma Staging System (INSS) and included seven with stage I tumour, ten stage II, seven stage III, 15 stage IV and seven stage IVS. Constitutional and tumour DNA were extracted using standard protocols. We included a patient from a two generation family with predisposition to NB due to a germline *PHOX2B* gene mutation (NBAF5, Table 1).[2]

2.2. Sequence analysis

We screened the coding sequence of the *PHOX2B* gene by direct DNA sequencing, as described elsewhere.[1] We studied a 533 bp sequence of the promotor region that is extremely conserved among species (97% between human and chicken at nucleotide level). The primer sequences for *PHOX2B* promotor region are 5′-GAAGGGGGAAAACACACAC-3′ (forward) and 5′-CGTAGGCAGAGGAATTGAGG-3′ (reverse). PCR Direct DNA sequencing was performed using the fluorometric method (Big Dye Terminator Cycle Sequencing kit [Applied Biosystems]).

2.3. LOH analysis

Matched constitutional and tumour DNA samples were PCR amplified using microsatellitte markers of the Généthon database D4S2974 and D4S1536 flanking the *PHOX2B* locus. D4S1536 is 4.1Mb centromeric to *PHOX2B* and D4S2974 is 95 Kb telomeric to *PHOX2B*. Fluorescent PCR products were electrophoresed and analysed on an automatic sequencer (ABI377, Applied Biosystems, Foster City, USA).

2.4. Cell culture

Cell lines were cultured at 37 °C, 5% CO2, in Dulbecco's modified essential medium (DMEM; Invitrogen/Gibco, NY) containing 10% foetal calf serum, 292 μg/ml L-glutamine, 1% 100X MEM (non-essential amino acids medium, Invitrogen/Gibco), and 0.5% penicillin solution. Primary human neural crest cells were cultured for 3 weeks in FGF2- and EGF-containing embryonic stem cell medium with modifications available upon request.

2.5. PHOX2B expression in NB cell lines and tumours

Total RNA was isolated from cell lines and tumours by use of RNAzolB (Invitrogen). *PHOX2B* expression was first obtained from microarray on Affymetrix HG-U133 Plus 2.0 arrays. Data from 55 neuroblastic tumours were normalised using the GC-RMA method. Detailed methods will be detailed elsewhere (I. Janoueix-Lerosey and O. Delattre, manuscript in preparation). In addition, RT-PCR detection of *PHOX2B* mRNA was performed in order to validate these data in 13 NB cell lines and eight tumours (Fig. 1a). First strand cDNA synthesis was performed on 2 μg of total RNA in a volume of 20 μl by use of [RNA kit, Applied Biosystems] and oligo(dT) primers. The specific primers used for mRNA amplification were designed within exons 2 and 3, as follows: 5′-GAGGCGCGAGTCCA GGTGTGGTTC-3′ (forward) and 5′-CGACAATAGCCTTGGGCC-TACCCG-3′ (reverse). Expression analysis was performed in a 25-μl PCR reaction containing 1 μl of cDNA, 1 μl dNTPs (2.5 mmol/l each), 0.5 μl of each specific primers (150 ng/μl), and 0.2 μl *Taq* polymerase (5 U/μl; Invitrogen). PCR conditions were standard with an annealing temperature of 69 °C. PCR products were loaded on a 2% agarose gel and directly visualised under UV illumination.

2.6. Analysis of PHOX2B gene hypermethylation by bisulfite DNA sequencing

Genomic DNA was isolated from cell lines and primary tissues by standard procedures. Bisulfite treatment and DNA sequencing were performed as described.[14] The primer sequences for *PHOX2B* are 5′-AAATGTAATTTATAAGATGTTT TTTTTTTG-3′ (forward) and 5′-CACACTACTTAAAAATAATAA AAATTAAAT-3′ (reverse). PCR conditions were standard with

Table 1 – Presentation of a series of 13 NB cell lines and 18 tumours for which PHOX2B expression data were analysed on Affymetrix HG U133 Plus 2.0 arrays (Affy Exp) and/or RT-PCR. Mutations, LOH and methylation analyses are presented as well as prognostic factors (stage, loss of 1p36, N-MYC amplification; A, Amplified; NA, Non Amplified)

		PHOX2B							
		Affy Exp	RT-PCR	Mutation	LOH	Methylation	Stage INSS	Loss of 1p36	N-MYC
Cell lines	CLB-BAR	3679	+	–	–	–	4	+	A
	CLB-GA	6956	+	–	–	–	4	+	NA
	CLB-GE	5725	+	–	–	–	4	+	A
	CLB-MA	7820	+	–	–	–	4	+	A
	CLB-PE	387	+	–	–	–	2	–	A
	GIMEN	6	–	–	–	+	4	+	NA
	IMR32	8839	+	–	–	–	2	+	A
	KCNR	5181	+	–	–	–	4	+	A
	SJNB12	11010	+	–	–	–	3A	+	NA
	SKNAS	2169	+	–	–	–	4	+	NA
	SKNSH	23	–	721–740del20nt	–	–	4	–	NA
	SKNBE	6	–	–	–	+	4	+	A
	TR14	2534	+	–	–	–	3	+	A
Tumours	NBAF15	6775	ND	–	–	–	2B	–	NA
	NBAF21	136	–	–	–	+	3	–	NA
	NBAF26	8259	+	–	–	–	4S	–	NA
	NBAF38	23	–	–	+	–	2A	–	NA
	NBAF39	6293	ND	–	–	–	2B	–	NA
	NBAF40	7462	ND	–	+	–	4S	–	NA
	NBAF42	7557	ND	–	–	–	4	–	NA
	NBAF43	3415	+	–	–	–	2B		
	NBAF45	7089	+	–	–	–	1	–	NA
	NBAF46	1394	+	–	–	–	2A	–	NA
	NBAF5	1053	ND	299G > T(R100L)	–	–	1	–	NA
	NBAF50	7811	ND	–	–	–	2B	–	NA
	NBAF54	5166	ND	–	+	–	4S	–	NA
	NBAF56	12059	ND	–	–	–	4S	+	NA
	NBAF59	10706	+	–	+	–	2A	–	NA
	NBAF61	10684	ND	–	+	–	4S	–	NA
	NBAF64	5349	ND	–	–	–	4	+	NA
	NB10	ND	–	–	–	+	2B	–	NA

an annealing temperature of 58 °C. PCR products were loaded on a 2% agarose gel and directly visualised under UV illumination. PCR products were cloned in a TA cloning vector (Promega, Madison, WI) and ten individual clones were sequenced for each sample.

2.7. *Treatment of NB cells with 5-Aza-dC*

Cells were seeded, allowed to attach over a 24 h period, and treated for 72 h with the demethyling reagent 5-Aza-dC (Sigma) at a final concentration of 1 μM. After the treatment period the medium was removed and RNAs were extracted.

3. Results

3.1. *Mutation and LOH at the PHOX2B locus in neuroblastoma*

As previously reported, a heterozygous frameshift mutation was identified in the SK-N-SH cell line (721-740del20nt,[3]). No mutation, either somatic or germinal, of the *PHOX2B* coding sequence and promoter conserved region were identified in the other 12 NB cell lines and the 45 individuals with sporadic NB. A heterozygous missense mutation (R100L) was identified in patient NBAF5 originating from a family predisposed to NB over three generations. No second molecular event could be identified in tumoural DNA (Table 1). We detected three known synonymous base substitutions, 552C > T(S184S), 750G > A (A250A) and 870C > A (P290P). In one patient, the P290P variant was heterozygous in constitutional DNA and homozygous in tumoural DNA. LOH was confirmed in this patient and identified in four other tumours (5/46 tumours, 10.8 %) with fluorescent microsatellite markers.

3.2. *PHOX2B expression in NB cell lines and tumours*

PHOX2B expression levels were obtained from Affymetrix HG U133 Plus 2.0 arrays. High level of *PHOX2B* expression was found in 10/13 cell lines and 15/17 tumours whereas no expression could be detected in three cell lines and two tumours (Table 1). *PHOX2B* expression was examined by RT-PCR in 13 NB cell lines and eight tumours and two neural crest-derived tissues: adrenal gland medulla (MSR) and human trunk-level neural crest cells. These primary, non-transformed cells were derived from a human embryo at 28 days of development with a normal karyotype. Loss of expression was confirmed by the absence of *PHOX2B* mRNA transcripts in 3/13 cell lines (SK-N-SH, SK-N-BE and GIMEN) whereas *PHOX2B* cDNAs were visualised in all other cell lines and non-cancerous adrenal (MSR) and neural crest cells (NC) (Fig. 1a). *PHOX2B* was

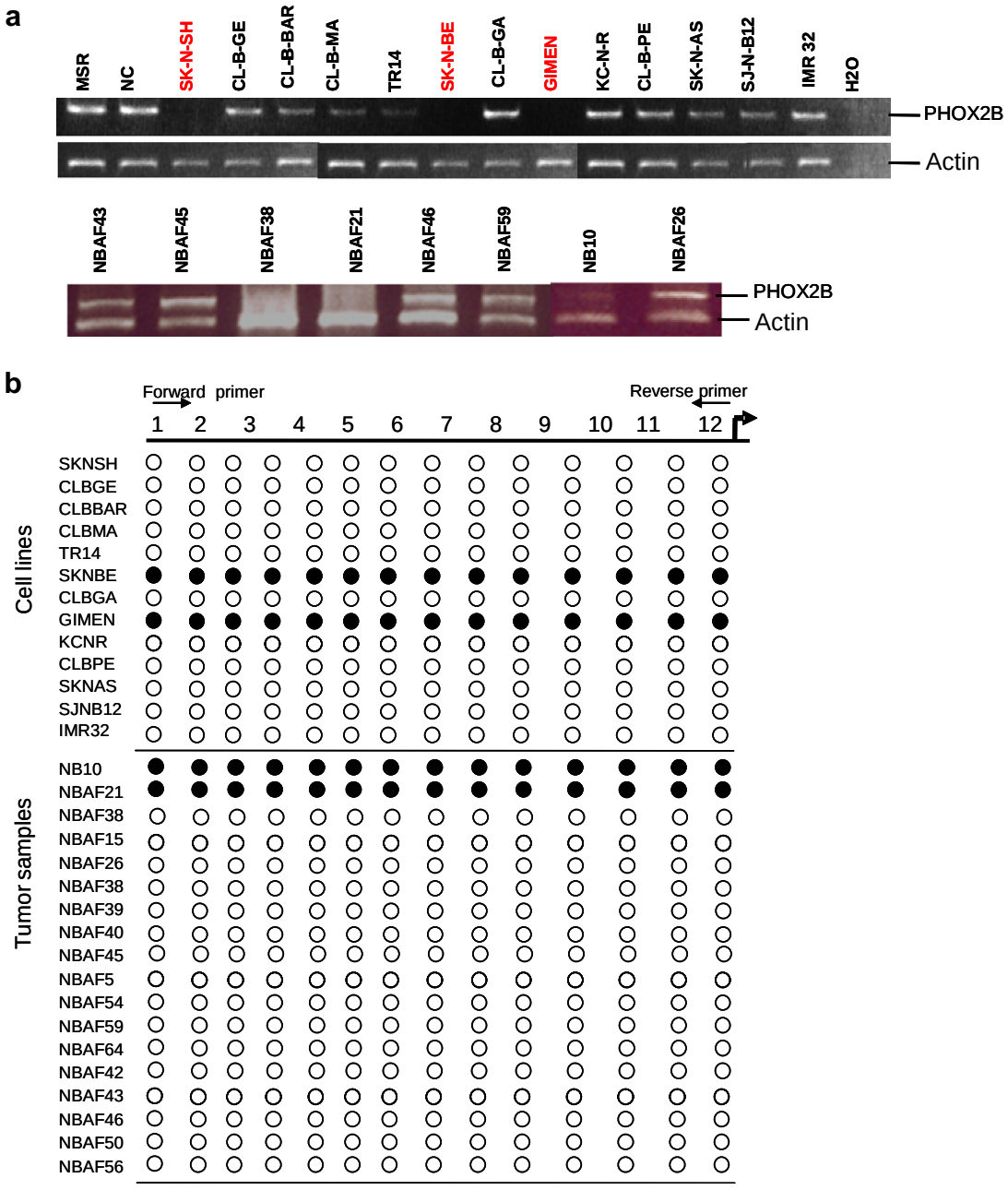

Fig. 1 – (a) *PHOX2B* mRNA in NB cell lines. *PHOX2B* mRNA is detected in 10/13 cell lines as in human adrenal gland medulla (MSR) and non-transformed human neural crest cells (NC). No expression could be observed in three NB cell lines; SKNSH, SKNBE and GIMEN. (b) Bisulfite sequencing analysis of the methylation status of the 12 CpG from the start site. One microgram of tumour DNA was denatured by sodium hydroxide and modified by sodium bisulfite treatment, which converts unmethylated cytosines to uracil. Bisulfite treated DNA was amplified using specific primers (added in methods). *PHOX2B* promotor is 100% methylated in SKNBE and GIMEN but not in other cell lines. All the 12 CpG dinucleotide are methylated in two primary tumours NBAF21 and NB10. All ten clones showed identical methylation in each sample. •methylated cytosine ○ non-methylated cytosine.

silenced in three tumours: one ganglioneuroma (NBAF21), one ganglioneuroblastoma (NBAF38) and one NB (NB10) (Fig. 1a).

3.3. *Methylation and silencing of PHOX2B in NB cell lines and tumours*

Promoter-associated CpG islands of *PHOX2B* were analysed by methyl sequencing in a panel of 13 cell lines, 18 tumours and two neural crest-derived tissues: adrenal gland medulla (MSR) and human trunk-level neural crest cells. All 12 CpG dinucleotides were 100% methylated (10/10 clones) in 2/13 cell lines (SK-N-BE and GIMEN) and in 2/18 tumours (NBAF21 and NB10) (Fig. 1b). As sequencing of the PCR products showed that cytosines outside the CpG sites were converted to thymine, an incomplete bisulfite conversion could be ruled out.

3.4. *Restoration of PHOX2B expression in negative cell lines by 5-Aza-dC*

5-Aza-dC, a methyltransferase inhibitor, was used to investigate whether *PHOX2B* expression could be restored cell lines for which *PHOX2B* was not expressed. *PHOX2B* mRNA expression levels, analysed by RT-PCR, were restored in SK-N-BE and GIMEN cell lines, while no re-expression was observed for SK-N-SH.

4. Discussion

This study of a series of 13 cell lines and 46 neuroblastic tumours aimed to determine the role of *PHOX2B* in sporadic NB. *PHOX2B*, not known so far for being either a tumour-suppressor gene or a proto-oncogene, is the first predisposing gene identified in NB. Most mutations occur in familial and syndromic NB cases. A heterozygous germline mutation was found in about 20% of published pedigrees and reached 50% when HSCR is associated with NB either in the index case or relatives.[2,5,7,4] However, germline *PHOX2B* mutations are rare in sporadic isolated NB (1/215 cases in the series reported by Van Limpt and 2/86 in the series reported by McConville).[3,8] Somatic *PHOX2B* mutations have also been described in NB.[3] In the series of 45 sporadic NB cases we report, no *PHOX2B* gene mutations were identified either in the coding sequence or the promoter region. LOH at the *PHOX2B* locus could be detected in 5/46 cases. This ratio of about 10% has to be balanced with the known high rate of chromosomal rearrangement in NB. It is worth noting that LOH of the short arm of chromosome 4 is found in roughly 20% of NB, but *PHOX2B* is centromeric to the smallest region of overlap (SRO).[15,16]

We subsequently asked the question of epigenetic events at the *PHOX2B* locus and identified clonal aberrant CpG island methylation of the promoter in 2/13 NB cell lines and 2/18 tumours (ganglioneuroma in one case and NB stage II in one case). The demethylating drug 5-Aza-dC re-induced *PHOX2B* expression in NB cell lines, suggesting that *PHOX2B* methylation correlates with gene silencing. Moreover, it is well established that DNA demethylating agents as 5-Aza-dC induce adrenergic differentiation in NB cell lines[17] and have an antiproliferative effect in mouse NB models.[18] Hypermethylation and downregulation of potential tumour-suppressor genes such as genes involved in cell-cycle control or apoptosis is often associated with a poor outcome in NB.[9,19,20]

We first considered *PHOX2B* as a potential tumour-suppressor gene since, i) at least some mutations identified in syndromic or familial NB cases (i.e. missense mutations of the homeodomain) are likely loss-of-function mutations, ii) a 'second hit' model has been proposed in NB[21] and, iii) some constitutional LOH at chromosome 4p encompass the *PHOX2B* locus.[4] However, in patients with germinal *PHOX2B* mutation, neither a second mutation nor LOH or aberrant promoter hypermethylation in the tumours have been identified as reported earlier.[2]

PHOX2B has been shown to promote differentiation by controlling G1-S transition during cell cycle of sympathetic neuroblast precursors[22] and is an essential regulator of normal autonomic nervous system development.[23] Mice with a homozygous inactivation of *Phox2b* fail in proper differentiation of the sympathetic nervous system. A gain-of-function or a dominant negative effect of *PHOX2B* frameshift mutations is not, however, ruled out. When tested, mutant transcripts were present and stable.[2] While mutant proteins localised to the nucleus, we observed some ability to bind DNA for two of the three *PHOX2B* frameshift mutations tested *in vitro*, although transactivation of the dopamine beta-hydroxylase promoter was always severely impaired.[24] Moreover, Bachetti and coworkers reported an increased transactivation of the *PHOX2A* promoter for proteins resulting from frameshift mutations when compared to the wild type protein.[25] *PHOX2B* is expressed not only in neural crest cells but also in mature sympathetic tissue of adrenal gland (Fig. 1a and[1]). Methylation-associated repression of *PHOX2B* could result in a differentiation block of sympathetic neuroblasts. Interestingly, NB10 patient had HSCR. We found aberrant homozygous *PHOX2B* promoter methylation on the tumour sample DNA while neither a mutation nor a deletion could be identified on either germinal or tumour DNA. Interestingly, *PHOX2B* was not methylated on lymphocyte DNA. We could speculate that *PHOX2B* methylation occurred during embryonic development and is responsible for both HSCR and NB development. As malignant transformation of cells could happen at different stages of tissue maturation, aberrant methylation may contribute to the diversity that characterises NB and other genes of the RET-PHOX2B pathway could be implicated. Interestingly, aberrations in the p53/MDM2/p14 (ARF) pathway have recently been described in the two NB cell lines where *PHOX2B* was found methylated[26]; a p53 mutation in SKNBE(2)C and aberrant p14 (ARF) methylation in GIMEN.

Promoter methylation is not only implicated in silencing tumour-suppressor genes but also in regulation of developmental pathways during embryogenesis.[27] Abnormal methylation in NB could result from abnormalities in this process in a self-renewing multipotent stem cell becoming the malignant progenitor of this neural crest cancer. Within a single tumour, cell phenotypes are characteristic of embryonic structures, particulary neuroblasts, Schwann cells and melanocytes. Cellular heterogeneity and maturation stage correlate with clinical stage and prognosis of the disease. However, down-regulation of *PHOX2B* was not always associated with hypermethylation. In SK-N-SH, the mutation is heterozygous and no *PHOX2B* expression could be detected. This result is discordant with the one reported by van Limpt and coworkers who observed the expression of both wild-type and mutant cDNAs in this cell line. However, they observed a *PHOX2B* gene silencing in the SHEP cell line, a stable subclone of SK-N-SH and also carrying the frameshift mutation. One could speculate on aberrant hypermethylation outside of the promoter region studied. However, it is worth noting that no expression of *H-ASH1* could be detected either in the SK-N-SH cell line or in NBAF38 tumour (data not shown). This could also contribute to *PHOX2B* down-regulation. Finally, one can speculate on the effects of other mechanisms such as micro RNAs Fig. 2.

Genetic heterogeneity in predisposition to neuroblastic tumours is likely. The high reocurence of loss of heterozygosity for chromosomes 1p36 and 11q23 supported the existence of putative tumour-suppressor genes within these regions.

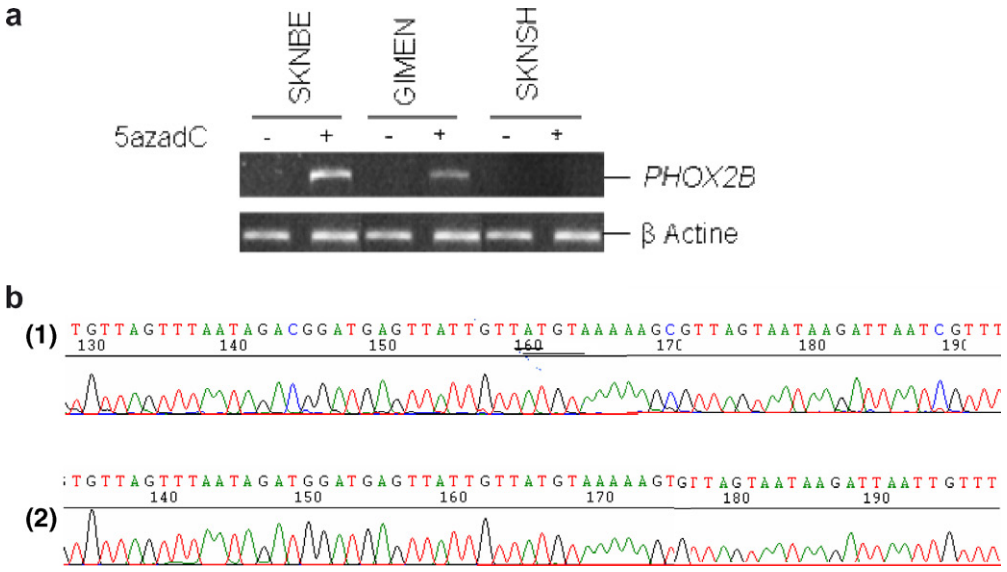

Fig. 2 – (a) RT-PCR: Demethylation of the *PHOX2B* promoter CpG islands restores expression in *PHOX2B*-negative NB cell lines, SKNBE and GIMEN. SKNBE, GIMEN and SKNSH were treated (+) or not treated (–) with 1 μmol/l 5′-aza-2′-deoxycytidine for three days. (b) Methyl sequencing results of *PHOX2B* promotor before (1) and after treatment (2) by 5-azacytidine.

However, these loci do not segregate with NB in most familial cases. On the other hand, linkage analysis has focused attention on 16p12-13 and 4p16.[28,16] Several studies have clearly demonstrated that *PHOX2B* is a major predisposing gene in syndromic NB cases (i.e. associated with other autonomic dysfunction).[6,3,29] Aberrant methylation of the *PHOX2B* promoter seems to be an alternative mechanism as frequent as mutation in sporadic NB cases and argues that loss-of-function by haploinsufficiency is the NB-predisposing mechanism.

Conflict of interest statement

None declared.

Acknowledgement

We thank Férechté Encha Razavi for providing adrenal tissues.

REFERENCES

1. Amiel J, Laudier B, Attie-Bitach T, et al. Polyalanine expansion and frameshift mutations of the paired-like homeobox gene PHOX2B in congenital central hypoventilation syndrome. *Nat Genet* 2003;**33**(4):459–61.
2. Trochet D, Bourdeaut F, Janoueix-Lerosey I, et al. Germline mutations of the paired-like homeobox 2B (PHOX2B) gene in neuroblastoma. *Am J Hum Genet* 2004;**74**(4):761–4.
3. van Limpt V, Schramm A, van Lakeman A, et al. The Phox2B homeobox gene is mutated in sporadic neuroblastomas. *Oncogene* 2004;**23**(57):9280–8.
4. Perri P, Bachetti T, Longo L, et al. PHOX2B mutations and genetic predisposition to neuroblastoma. *Oncogene* 2005;**24**(18):3050–3.
5. Mosse YP, Laudenslager M, Khazi D, et al. Germline PHOX2B mutation in hereditary neuroblastoma. *Am J Hum Genet* 2004;**75**(4):727–30.
6. Trochet D, O'Brien LM, Gozal D, et al. PHOX2B genotype allows for prediction of tumor risk in congenital central hypoventilation syndrome. *Am J Hum Genet* 2005;**76**(3):421–6.
7. van Limpt V, Chan A, Schramm A, et al. Phox2B mutations and the Delta-Notch pathway in neuroblastoma. *Cancer Lett* 2005;**228**(1–2):59–63.
8. McConville C, Reid S, Baskcomb L, et al. PHOX2B analysis in non-syndromic neuroblastoma cases shows novel mutations and genotype-phenotype associations. *Am J Med Genet A* 2006;**140**(12):1297–301.
9. Teitz T, Wei T, Valentine MB, et al. Caspase 8 is deleted or silenced preferentially in childhood neuroblastomas with amplification of MYCN. *Nat Med* 2000;**6**(5):529–35.
10. Abe M, Ohira M, Kaneda A, et al. CpG island methylator phenotype is a strong determinant of poor prognosis in neuroblastomas. *Cancer Res* 2005;**65**(3):828–34.
11. Banelli B, Di Vinci A, Gelvi I, et al. DNA methylation in neuroblastic tumors. *Cancer Lett* 2005;**228**(1–2):37–41.
12. Esteller M, Fraga MF, Guo M, et al. DNA methylation patterns in hereditary human cancers mimic sporadic tumorigenesis. *Hum Mol Genet* 2001;**10**(26):3001–7.
13. Ushijima T, Okochi-Takada E. Aberrant methylations in cancer cells: where do they come from? *Cancer Sci* 2005;**96**(4):206–11.
14. Herman JG, Graff JR, Myohanen S, et al. Methylation-specific PCR: a novel PCR assay for methylation status of CpG islands. *Proc Natl Acad Sci U S A* 1996;**93**(18):9821–6.
15. Caron H, van Sluis P, de Kraker J, et al. Allelic loss of chromosome 1p as a predictor of unfavorable outcome in patients with neuroblastoma. *N Engl J Med* 1996;**334**(4):225–30.
16. Perri P, Longo L, Cusano R, et al. Weak linkage at 4p16 to predisposition for human neuroblastoma. *Oncogene* 2002;**21**(54):8356–60.
17. Okuse K, Mizuno N, Matsuoka I, et al. Induction of cholinergic and adrenergic differentiation in N-18 cells by differentiation

agents and DNA demethylating agents. *Brain Res* 1993;**626**(1-2):225–33.
18. Bartolucci S, Estenoz M, Longo A, et al. 5-Aza-2'-deoxycytidine as inducer of differentiation and growth inhibition in mouse neuroblastoma cells. *Cell Differ Dev* 1989;**27**(1):47–55.
19. van Noesel MM, van Bezouw S, Voute PA, et al. Clustering of hypermethylated genes in neuroblastoma. *Genes Chromosomes Cancer* 2003;**38**(3):226–33.
20. Yang Q, Zage P, Kagan D, et al. Association of epigenetic inactivation of RASSF1A with poor outcome in human neuroblastoma. *Clin Cancer Res* 2004;**10**(24):8493–500.
21. Knudson Jr AG, Meadows AT. Developmental genetics of neuroblastoma. *J Natl Cancer Inst* 1976;**57**(3):675–82.
22. Dubreuil V, Hirsch MR, Pattyn A, et al. The Phox2b transcription factor coordinately regulates neuronal cell cycle exit and identity. *Development* 2000;**127**(23):5191–201.
23. Pattyn A, Morin X, Cremer H, et al. The homeobox gene Phox2b is essential for the development of autonomic neural crest derivatives. *Nature* 1999;**399**(6734):366–70.
24. Trochet D, Hong SJ, Lim JK, et al. Molecular consequences of PHOX2B missense, frameshift and alanine expansion mutations leading to autonomic dysfunction. *Hum Mol Genet* 2005;**14**(23):3697–708.
25. Bachetti T, Borghini S, Ravazzolo R, et al. An in vitro approach to test the possible role of candidate factors in the transcriptional regulation of the RET proto-oncogene. *Gene Expr* 2005;**12**(3):137–49.
26. Carr J, Bell E, Pearson AD, et al. Increased frequency of aberrations in the p53/MDM2/p14(ARF) pathway in neuroblastoma cell lines established at relapse. *Cancer Res* 2006;**66**(4):2138–45.
27. Theise ND, Krause DS. Toward a new paradigm of cell plasticity. *Leukemia* 2002;**16**(4):542–8.
28. Maris JM, Weiss MJ, Mosse Y, et al. Evidence for a hereditary neuroblastoma predisposition locus at chromosome 16p12–13. *Cancer Res* 2002;**62**(22):6651–8.
29. Maris JM. The biologic basis for neuroblastoma heterogeneity and risk stratification. *Curr Opin Pediatr* 2005;**17**(1):7–13.

Disease Models & Mechanisms 1, 241-254 (2008) doi:10.1242/dmm.000711

Analysis of mouse models carrying the I26T and R160C substitutions in the transcriptional repressor HESX1 as models for septo-optic dysplasia and hypopituitarism

Ezat Sajedi[1], Carles Gaston-Massuet[1,*], Massimo Signore[1,*], Cynthia L. Andoniadou[1], Daniel Kelberman[2], Sandra Castro[1], Heather C. Etchevers[3,4], Dianne Gerrelli[1], Mehul T. Dattani[2] and Juan Pedro Martinez-Barbera[1,‡]

SUMMARY

A homozygous substitution of the highly conserved isoleucine at position 26 by threonine (I26T) in the transcriptional repressor HESX1 has been associated with anterior pituitary hypoplasia in a human patient, with no forebrain or eye defects. Two individuals carrying a homozygous substitution of the conserved arginine at position 160 by cysteine (R160C) manifest septo-optic dysplasia (SOD), a condition characterised by pituitary abnormalities associated with midline telencephalic structure defects and optic nerve hypoplasia. We have generated two knock-in mouse models containing either the I26T or R160C substitution in the genomic locus. *Hesx1*$^{I26T/I26T}$ embryos show pituitary defects comparable with *Hesx1*$^{-/-}$ mouse mutants, with frequent occurrence of ocular abnormalities, although the telencephalon develops normally. *Hesx1*$^{R160C/R160C}$ mutants display forebrain and pituitary defects that are identical to those observed in *Hesx1*$^{-/-}$ null mice. We also show that the expression pattern of *HESX1* during early human development is very similar to that described in the mouse, suggesting that the function of HESX1 is conserved between the two species. Together, these results suggest that the I26T mutation yields a hypomorphic allele, whereas R160C produces a null allele and, consequently, a more severe phenotype in both mice and humans.

INTRODUCTION

Developmental defects in pituitary gland formation lead to hypopituitarism, which can range from mild phenotypes involving deficiency of a single hormone, through more severe phenotypes affecting multiple pituitary hormone axes, to panhypopituitarism. Isolated growth hormone deficiency (IGHD) is the most frequent form of human hypopituitarism, affecting 1 in 4000-10,000 live births (Vimpani et al., 1977; Lindsay et al., 1994; Procter et al., 1998). Combined pituitary hormone deficiency (CPHD), in which there is a deficiency of more than one pituitary hormone, is less common, but is associated with considerable morbidity and, if not treated promptly and adequately, occasional mortality. Septo-optic dysplasia (SOD; also referred to as de Morsier syndrome) is a phenotypically and aetiologically heterogeneous disorder in humans, characterised by hypopituitarism occurring in conjunction with midline forebrain defects and optic nerve hypoplasia. This congenital disorder (1 in 10,000 live births) is characterised by a highly variable phenotype with varying degrees of abnormalities in the corpus callosum, septum pellucidum, eyes and pituitary gland (Patel et al., 2006; Kelberman and Dattani, 2007).

Phenotypic analyses of mouse mutants have implicated a number of genes in pituitary development, some of which have also been associated with hypopituitarism in human patients with mutations in orthologous genes (Cushman and Camper, 2001). Several homeobox genes in particular have been shown to play a crucial role in both mouse and human pituitary organogenesis (Kelberman and Dattani, 2007; Cushman and Camper, 2001). One such gene encodes the paired-like homeodomain protein HESX1, a highly conserved transcriptional repressor, which is expressed in the early forebrain primordium and Rathke's pouch during vertebrate development (Thomas and Beddington, 1996; Hermesz et al., 1996). *Hesx1*-deficient embryos show a significant reduction in anterior forebrain structures, such as the telencephalic and optic vesicles, which is caused by a transformation of anterior to posterior forebrain (Andoniadou et al., 2007). *Hesx1*$^{-/-}$ mutants also show severe pituitary gland dysplasia and enhanced cellular proliferation, but terminal differentiation of the hormone-producing cell types is not affected at later stages of development (Dasen et al., 2001). *Hesx1*-deficient mutants also manifest fully penetrant eye defects, ranging from microphthalmia to anophthalmia, disturbances in midline telencephalic commissural tracts (corpus callosum and anterior commissure) and abnormalities in the olfactory bulbs (Dattani et al., 1998; Andoniadou et al., 2007).

In humans, mutations in *HESX1* have been associated with phenotypes affecting the midline forebrain structures, the eyes and, most commonly, the pituitary gland. So far, a total of 13 *HESX1* mutations have been identified in association with SOD and/or hypopituitarism (Dattani et al., 1998; Thomas et al., 2001; Brickman et al., 2001; Carvalho et al., 2003; Cohen et al., 2003; Tajima et al., 2003; Sobrier et al., 2005; Sobrier et al., 2006; Coya et al., 2007). Five of them are recessive and the remaining eight are dominant. They vary from missense to frameshift mutations and result in considerable variability in the penetrance and severity of the phenotype in affected patients. At present, the reasons underlying this variability are not clear.

[1]Neural Development Unit, Institute of Child Health, University College London, London, UK
[2]Developmental Endocrinology Research Group, Clinical and Molecular Genetics Unit, Institute of Child Health, University College London, London, UK
[3]INSERM U563, Toulouse, France
[4]INSERM U781, Paris, France
*These authors contributed equally to this work
‡Author for correspondence (e-mail: j.martinez-barbera@ich.ucl.ac.uk)

Two previously reported, recessive missense mutations involve the substitution of highly conserved residues at position 26 (isoleucine) and 160 (arginine) by threonine and cysteine (I26T and R160C), respectively (Dattani et al., 1998; Carvalho et al., 2003). I26 maps within the engrailed homology (eh-1) domain, an octapeptide sequence shown to be involved in the interaction of HESX1 with the co-repressor TLE1 (transducin-like enhancer of split 1) that is able to recruit histone deacetylases required for transcriptional repression (Dasen et al., 2001; Carvalho et al., 2003). In vitro, the HESX1-I26T mutant protein can bind to DNA, but its ability to repress transcription is reduced in comparison to wild-type HESX1. Carvalho and colleagues reported on a patient with evolving CPHD who was homozygous for the I26T mutation, but who had normal optic nerves and no telencephalic defects (Carvalho et al., 2003). The parents of the affected individual were heterozygous with respect to the mutation and appeared to be clinically unaffected. The reasons for the lack of ocular and telencephalic defects are not fully understood.

R160 is localised within the recognition alpha helix of the homeodomain, which establishes direct contact with target DNA through the major groove (Wilson et al., 1995; Dattani et al., 1998). In vitro, the ability of the HESX1-R160C protein to bind to DNA is abolished by this mutation, but its repressor activity is retained when fused to the Gal4 DNA-binding domain in a mammalian one-hybrid system (Brickman et al., 2001). It has been postulated that HESX1-R160C may have a dominant negative effect, as it is able to inhibit the DNA binding and repressor activities of wild-type HESX1 in vitro (Brickman et al., 2001). However, Dattani and colleagues observed that although two siblings manifesting panhypopituitarism in association with midline telencephalic commissural defects and severe optic nerve hypoplasia were homozygous for the R160C mutation, their heterozygous parents were phenotypically normal (Dattani et al., 1998). This in vivo observation is in direct contrast to the in vitro dominant negative effect of this mutation. The forebrain defects of these two siblings were mild when compared with the severe abnormalities frequently observed in *Hesx1*$^{-/-}$ mice, suggesting that part of the function of HESX1 may be performed independently of its ability to bind to DNA (Dattani et al., 1998; Martinez-Barbera et al., 2000). A more direct analysis of the phenotypic consequences of the R160C mutation in a mouse model can be used to clarify this issue.

Here, we have used an in vivo approach to provide insights into the aetiology, pathogenesis and variable nature of hypopituitarism and SOD associated with the human *HESX1* mutations I26T and R160C.

RESULTS

Morphological analysis of *Hesx1*$^{I26T/I26T}$ and *Hesx1*$^{R160C/R160C}$ mutants

Homozygous loss of *Hesx1* in the mouse has been shown previously to cause perinatal lethality, possibly because of the severe forebrain and craniofacial defects, and/or pituitary dysfunction (Dattani et al., 1998; Andoniadou et al., 2007). However, the phenotypic consequences of replacing the wild-type allele with specific *HESX1* mutations originally identified in human patients with hypopituitarism and SOD have not been reported previously. To gain further insight into the in vivo consequences of the I26T and R160C mutant proteins, we have generated mouse models carrying these two substitutions (Fig. 1).

Hesx1$^{I26T/+}$ mice were phenotypically normal, viable and fertile (n=124). Genotypic analysis of pups and weaners from *Hesx1*$^{I26T/+}$ intercrosses showed a slight deviation from the expected Mendelian ratios. Although this did not reach statistical significance, it may be indicative of sporadic postnatal lethality (Table 1). Of the surviving *Hesx1*$^{I26T/I26T}$ pups, 73.7% exhibited eye defects, usually unilateral or bilateral microphthalmia (n=19). This phenotype was not observed in heterozygous or wild-type littermates. Histological analysis of *Hesx1*$^{I26T/I26T}$ adult brains revealed normal telencephalic commissural tracts with no apparent abnormalities in the corpus callosum or anterior commissure (100%, n=8).

A similar genotypic analysis of embryos from 8.5-17.5 days post coitum (dpc) showed the expected Mendelian proportions (Table 1). The majority of the *Hesx1*$^{I26T/I26T}$ embryos analysed from 12.5-17.5 dpc (n=42) displayed eye abnormalities (76.2%), but telencephalon development appeared normal in most of these embryos (97.6%) when compared with wild-type or heterozygous littermates (Fig. 2C-E; Table 2). The most common forebrain phenotype observed in *Hesx1*$^{I26T/I26T}$ homozygous mutants was the presence of eye defects in the absence of any telencephalic abnormalities (n=42) (Table 2). Eye defects ranged from unilateral or bilateral microphthalmia (59.6%) to anophthalmia (16.7%). The right side was more severely affected, as described previously (Andoniadou et al., 2007). Only one *Hesx1*$^{I26T/I26T}$ embryo showed

Table 1. Genotypes obtained from either *Hesx1*$^{I26T/+}$ or *Hesx1*$^{R160C/+}$ intercrosses

	Genotype					
Stage	*Hesx1*$^{I26T/+}$	*Hesx1*$^{+/+}$	*Hesx1*$^{I26T/I26T}$	*Hesx1*$^{R160C/+}$	*Hesx1*$^{+/+}$	*Hesx1*$^{R160C/R160C}$
Pups	124 (~46%)	97 (~36%)*	50 (~18%)†	94 (~64%)	47 (~32%)	5 (~3%)‡
8.5 dpc	24	17	10	15	8	7
10.5 dpc	9	3	5	13	4	6
12.5 dpc	34	13	16	32	10	15
15.5 dpc	21	11	8	21	8	10
17.5 dpc	24	14	13	42	18	18
Embryos total§	112 (~50%)	58 (26%)	52 (23%)	123 (~54%)	48 (~21%)	56 (~25%)

*Chi-square test showed a significant deviation from the expected 25% ratio (P<0.03).
†Chi-square test showed no significant deviation from the expected 25% ratio.
‡Chi-square test showed a significant deviation from the expected 25% ratio (P<0.001).
§Chi-square test showed no significant deviation from the expected Mendelian ratios.

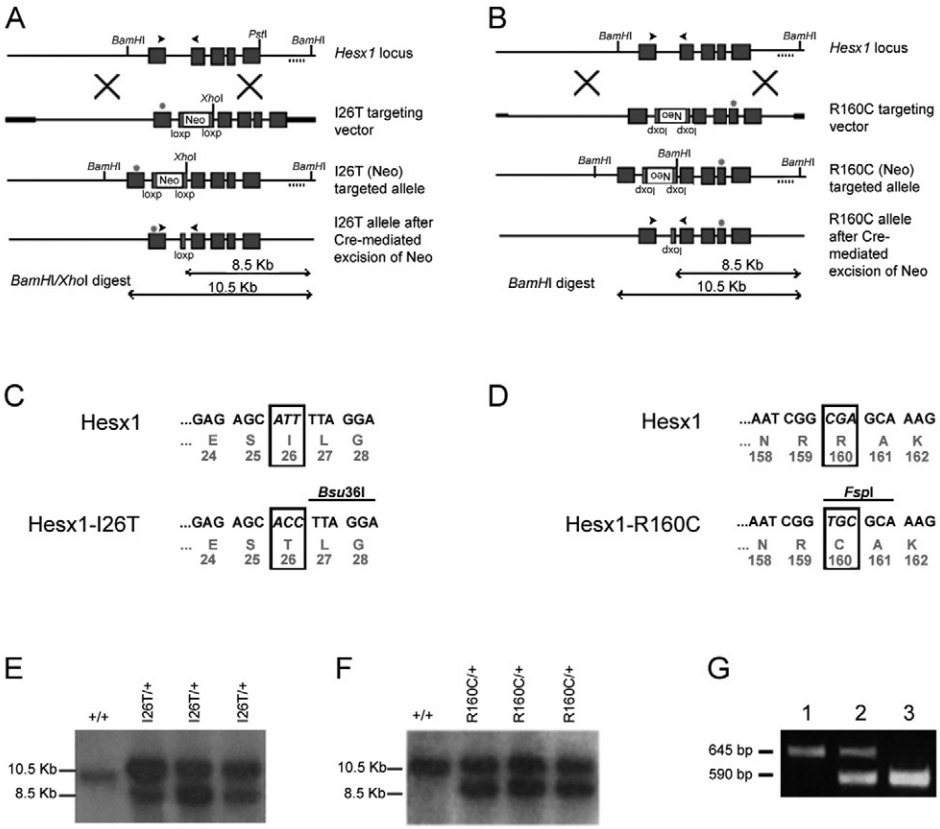

Fig. 1. Generation of the *Hesx1-I26T* and *Hesx1-R160C* targeted alleles. (A,B) Top to bottom: structure of the murine *Hesx1* locus; *Hesx1-I26T* (A) and *Hesx1-R160C* (B) targeting vectors; targeted alleles prior to and after Cre-mediated excision of the *Neo* cassette; expected bands for the targeted and wild-type alleles after Southern blot analysis of DNA samples digested with the indicated restriction enzymes and hybridised with an external probe (dotted line). The position of the mutation is indicated with an asterisk on exons one (I26T) and four (R160C) of the targeting vectors and targeted alleles. Note that the orientation of the *loxP* and *Neo* cassette has been inverted in the *Hesx1-R160C* targeting vector. (C) The triplet ATT encoding isoleucine at position 26 was replaced by ACC, which encodes the amino acid threonine. This mutation introduces a novel *Bsu*36I restriction site on the mutated allele. (D) The triplet encoding arginine at position 160 was replaced by TGC, which encodes the amino acid cysteine. This mutation introduces a novel *Fsp*I restriction site in the mutated allele. (E,F) Southern blot analysis of DNA samples from wild-type (+/+), $Hesx1^{I26T/+}$ (E) and $Hesx1^{R160C/+}$ (F) ES cell clones digested with either *Bam*HI/*Xho*I (E) or *Bam*HI (F) and hybridised with an external probe (dotted line in A,B). (G) Representative example of PCR genotyping of DNA samples from the homozygous $Hesx1^{I26T/I26T}$ or $Hesx1^{R160C/R160C}$ (1), heterozygous $Hesx1^{I26T/+}$ or $Hesx1^{R160C/+}$ (2) and wild-type $Hesx1^{+/+}$ (3) embryos. Note that the primers used for genotyping both targeted alleles are the same [black arrowheads in (A) and (B)].

severe forebrain defects affecting both the eyes and the telencephalon (2.4%). The remaining embryos displayed no evident forebrain abnormalities (21.4%). When *Hesx1* dosage was reduced by 50% in $Hesx1^{I26T/-}$ hemizygous embryos, the severity and penetrance of the ocular and telencephalic defects were increased (Fig. 2F-H; Table 2). All of the embryos analysed from 12.5-14.5 dpc had developed severe bilateral microphthalmia or anophthalmia (100%, *n*=19), some of them in conjunction with reduced telencephalic tissue (26.3%). Although it is likely that the enhanced severity is caused by the reduction of *Hesx1* gene dosage, we cannot exclude a contribution from a genetic background effect.

$Hesx1^{R160C/+}$ mice were normal and fertile. Phenotypic analysis of 146 pups from $Hesx1^{R160C/+}$ heterozygous intercrosses indicated a gross deviation from the expected ratio of genotypes, with a significant loss of $Hesx1^{R160C/R160C}$ animals (Table 1). Only five $Hesx1^{R160C/R160C}$ mice were obtained at weaning, which represents approximately 3% of pups instead of the expected 25% (Table 1). All of the homozygous animals showed dramatic eye defects, typically bilateral microphthalmia or anophthalmia. Furthermore, histological analysis of 17.5 dpc $Hesx1^{R160C/R160C}$ embryos and surviving adults indicated abnormal development of telencephalic commissural tracts with agenesis or hypoplasia of the corpus callosum and anterior commissure (77.8%, *n*=9) (data not shown).

Deviation from the expected Mendelian ratio was not observed in $Hesx1^{R160C/R160C}$ embryos from 8.5-17.5 dpc (Table 1). The most common phenotype in these mutants was anophthalmia, which was associated with a significant reduction of telencephalic tissue (67.4%; *n*=43). This was followed by unilateral or bilateral anophthalmia in the absence of telencephalic defects (32.6%) (Fig. 2I-K; Table 2). Halving the *Hesx1* dosage in $Hesx1^{R160C/-}$ hemizygous embryos did not increase the severity of the phenotype; these embryos displayed the same variable expressivity of telencephalic and eye defects that were observed in $Hesx1^{R160C/R160C}$ mutants (*n*=15) (Fig. 2L-N; Table 2). Severe craniofacial defects, i.e. defective or absent frontonasal mass, were observed in 27.9% of $Hesx1^{R160C/R160C}$ embryos from 12.5-17.5 dpc (supplementary

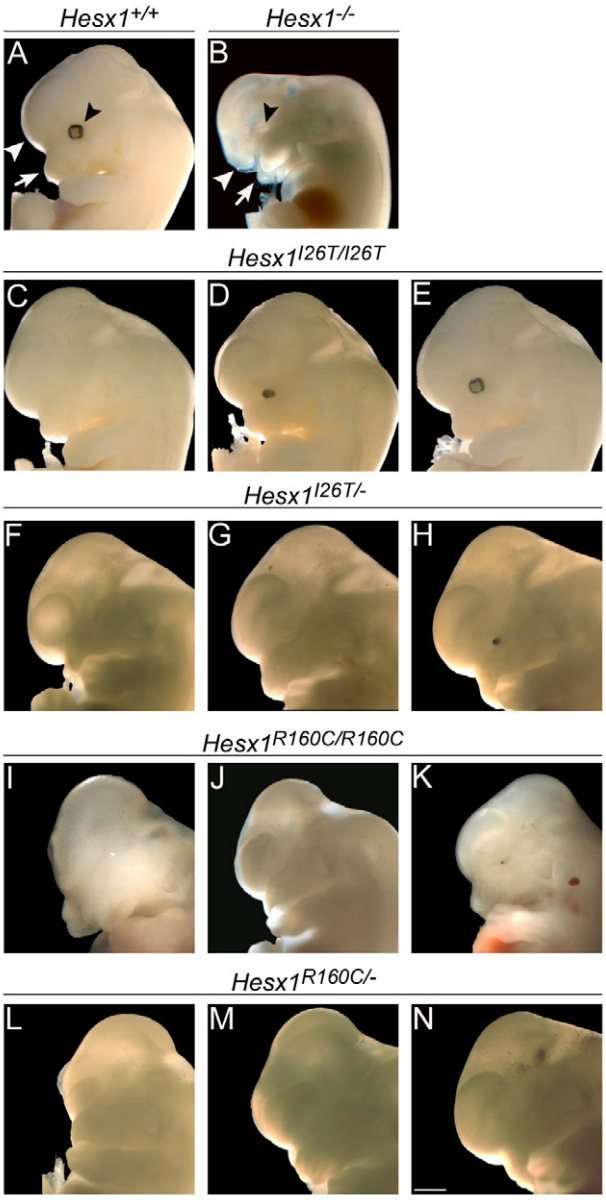

Fig. 2. Forebrain defects in mutant embryos harbouring the *Hesx1-I26T* or *Hesx1-R160C* alleles. Dark-field photographs of 12.5 dpc embryos of specific genotypes (indicated on the top of the pictures). (A,B) Wild-type (A) and *Hesx1*$^{-/-}$ (B) embryos. *Hesx1*$^{-/-}$ embryos carry a null allele, in which a *Neo* cassette replaces the entire *Hesx1* coding region. Note the absence of eyes (black arrowhead), reduced telencephalic vesicles (white arrowhead) and impairment of frontonasal mass development (white arrow) in the *Hesx1*$^{-/-}$ mutant (B) when compared with the wild-type embryo (A). (C-E) Representative examples of *Hesx1*$^{I26T/I26T}$ mutants displaying anophthalmia (C), microphthalmia (D) or normal eyes (E). Telencephalic vesicles are unaffected. (F-H) Representative examples of *Hesx1*$^{I26T/-}$ mutants. Note the increased severity in the eye and telencephalic defects in these embryos when compared with *Hesx1*$^{I26T/I26T}$ embryos (C-E). (I-K) Representative examples of *Hesx1*$^{R160C/R160C}$ mutants showing severe forebrain defects (I) and either anophthalmia (J) or microphthalmia (K) with normal telencephalic vesicles. (L-M) Representative examples of *Hesx1*$^{R160C/-}$ embryos. There is no obvious increase in the severity of eye and telencephalic abnormalities between embryos carrying one (L-M) or two (I-K) copies of the *Hesx1-R160C* allele. Bar, 940 μm.

material Fig. S1D). Similar defects have been observed in *Hesx1*$^{-/-}$ animals (Dattani et al., 1998; Andoniadou et al., 2007) (supplementary material Fig. S1B).

From these analyses, we conclude that the forebrain defects of *Hesx1*$^{I26T/I26T}$ and *Hesx1*$^{R160C/R160C}$ mutants are variable, but that eye tissue has increased sensitivity to impaired HESX1 function compared with the telencephalon. The *Hesx1-I26T* mutation leads to a less severe forebrain phenotype when compared with both the *Hesx1-R160C* and the previously characterised *Hesx1* null alleles (P<0.001, on both severity and penetrance of defects between the *Hesx1*$^{I26T/I26T}$ and *Hesx1*$^{R160C/R160C}$ genotypes). There is a dosage effect for the *Hesx1-I26T* mutation, which is evidenced by the increased frequency and severity of forebrain abnormalities in embryos carrying one copy of the mutated allele in compound heterozygosity with a null allele (*Hesx1*$^{I26T/-}$), compared with those bearing two copies (*Hesx1*$^{I26T/I26T}$) (P<0.01 for severity and P<0.05 for penetrance). However, there are no significant phenotypic differences between *Hesx1*$^{R160C/R160C}$ and *Hesx1*$^{R160C/-}$ embryos, and the forebrain defects are identical to those observed in the *Hesx1*$^{-/-}$ mutants (Dattani et al., 1998; Andoniadou et al., 2007).

Molecular analysis of forebrain defects in *Hesx1*$^{I26T/I26T}$ and *Hesx1*$^{R160C/R160C}$ embryos

Hesx1$^{-/-}$ embryos show a significant reduction of anterior forebrain structures, including the telencephalon, ventral diencephalon, hypothalamus and eyes, which is caused by a posterior transformation of the anterior forebrain (Andoniadou et al., 2007). In these mutants, anterior forebrain descendants ectopically populate posterior forebrain regions and give rise to neural crest cells that colonise the frontonasal mass and first branchial arch. This fate transformation is probably the consequence of the ectopic activation of the Wnt–β-catenin signalling pathway within the anterior forebrain at 8.0 dpc. We analysed whether phenotypic differences in forebrain development between the *Hesx1*$^{I26T/I26T}$ and *Hesx1*$^{R160C/R160C}$ embryos could be traced back to early developmental stages. To determine this, mRNA in situ hybridisation with several diagnostic markers of brain development was performed on mutant and normal littermates between 8.0 and 9.0 dpc.

Hesx1$^{I26T/I26T}$ embryos showed a variety of neural patterning defects, with some showing mild abnormalities in the expression patterns of diagnostic markers, whereas others exhibited no apparent defects. *Hesx1* is normally expressed in the anterior forebrain at 8.0 dpc (Fig. 3A), and by 8.5 dpc transcripts become restricted to the ventral area of the forebrain extending into the proximal regions of the optic stalks (Fig. 3D). At 8.0 dpc, the *Hesx1* expression domain was slightly reduced in the medial part of the anterior neural plate in a proportion of *Hesx1*$^{I26T/I26T}$ homozygotes (three out of five embryos) (Fig. 3B). This was more apparent at 8.5 dpc, when *Hesx1* expression was normal in the prospective ventral forebrain but severely reduced in the developing optic stalks (Fig. 3E) (four out of six embryos). However, four of the analysed *Hesx1*$^{I26T/I26T}$ homozygous embryos (n=11) showed a very similar expression pattern to wild-type littermates (data not shown), possibly reflecting embryos that would subsequently develop normal eyes and a normal telencephalon. The expression of *Wnt1*, a marker of the midbrain and posterior forebrain (Fig. 3G,J) and an important contributor to the fate transformation of anterior

Table 2. Summary of phenotypes associated with specific genotypes in 12.5-17.5 dpc embryos

Phenotype	Genotype			
	§*Hesx1*$^{I26T/I26T}$	§*Hesx1*$^{R160C/R160C}$	¶*Hesx1*$^{I26T/-}$	¶*Hesx1*$^{R160C/-}$
Severe forebrain defects*	1**	29††	5	10
Anophthalmia†	7	8	9	4
Microphthalmia†	25	6	5	1
No defects‡	9	0	0	0
Total	42	43	19	15

*Small or absent telencephalic vesicles and anophthalmia (Fig. 2B,I,J,L,M).
†Normal telencephalic vesicles, but unilateral or bilateral anophthalmia (Fig. 2C,G).
‡Embryos were indistinguishable from wild-type littermates (Fig. 2A,E).
§12.5-17.5 dpc embryos.
¶12.5-14.5 dpc.
**17.5 dpc embryo.
††Twelve embryos showed defects in the formation of the frontonasal mass (Fig. 2I).

forebrain precursors, was clearly expanded in dorsal regions of the anterior forebrain in several *Hesx1*$^{I26T/I26T}$ embryos (three out of five embryos) (Fig. 3H,K) (McMahon and Bradley, 1990; Lagutin et al., 2003; Andoniadou et al., 2007). The reduction of presumptive optic tissue was also evident in some *Hesx1*$^{I26T/I26T}$ embryos hybridised with riboprobes against *Pax6*, a marker of forebrain and eyes at these stages (two out of five embryos) (Fig. 3M,N) (Walther and Gruss, 1991). This reduction was further confirmed by analysing the expression pattern of *Pax2*, whose transcripts are confined to the ventral optic vesicle at early developmental stages (Fig. 3P,Q) (Torres et al., 1996). *Bf1* (*Foxg1b*), a gene essential for proper telencephalic development, was normally expressed in the prospective telencephalon in mutant embryos when compared with wild-type littermates (*n*=2) (supplementary material Fig. S2I,J) (Xuan et al., 1995). From this marker analysis, we conclude that the I26T substitution leads to defective patterning of the anterior neural plate, with the eye region being more sensitive to impaired HESX1 function. This is consistent with previous data showing that the majority of these homozygous embryos have eye abnormalities but develop a normal telencephalon (Fig. 2C-E; Table 2).

Hesx1$^{R160C/R160C}$ embryos showed more dramatic and consistent abnormalities in forebrain patterning at early developmental stages, because anterior forebrain tissue was typically reduced in size. The *Hesx1* expression domain was significantly smaller at 8.0-8.5 dpc in homozygous mutants compared with wild-type and heterozygous littermates (*n*=9) (Fig. 3C,F). The degree of reduction of the *Hesx1* expression domain was variable and correlated with the amount of anterior forebrain tissue present in the homozygous mutant, but all embryos analysed showed an evident decrease of anterior tissue and *Hesx1* expression. This reduction in *Hesx1* expression is likely to reflect the ongoing transformation of the anterior forebrain into a posterior fate in the *Hesx1*$^{R160C/R160C}$ embryos (Andoniadou et al., 2007). In the *Hesx1*$^{R160C/R160C}$ embryos, the expression domain of *Wnt1* was anteriorised (Fig. 3I,L) to a similar extent (*n*=4) to that observed in *Hesx1*$^{I26T/I26T}$ mutants (Fig. 3H,K), despite the fact that the *Hesx1*$^{R160C/R160C}$ embryos show more severe forebrain defects. This supports the hypothesis that *Wnt1* anteriorisation alone cannot account for the anterior defects of *Hesx1*-deficient embryos (Andoniadou et al., 2007). The *Bf1* expression domain was significantly diminished in homozygous mutants when compared with wild-type or *Hesx1*$^{I26T/I26T}$ embryos (*n*=2) (supplementary material Fig. S2I-K). Reduction of telencephalic and optic tissue was further confirmed by an apparent decrease in the *Pax6* expression domain across the entire forebrain of *Hesx1*$^{R160C/R160C}$ embryos (*n*=5) (Fig. 3M,O). Expression of *Pax2* was either reduced (*n*=2) or absent (*n*=3) in optic vesicles, but normal at the mid-hindbrain boundary of these embryos (Fig. 3P,R). As previously suggested (Fig. 2I-K) (Table 2), this mutation leads to a more severe lack of anterior forebrain tissue, including the telencephalon and the eyes, which is a phenotype identical to that observed in *Hesx1*$^{-/-}$ mutants (Dattani et al., 1998; Andoniadou et al., 2007).

Finally, we performed cell fate analysis of *Hesx1*-expressing cells in mutant embryos carrying either the I26T or the R160C alleles. We used two previously characterised mouse models: (1) the *Hesx1-Cre* mouse line, in which the *Cre* recombinase gene replaces the *Hesx1* coding region creating a *Hesx1* null allele. In *Hesx1-Cre* embryos, *Cre* expression recapitulates the endogenous *Hesx1* expression pattern (Andoniadou et al., 2007). (2) *ROSA26-floxstop-lacZ* reporter (*ROSA26-Cond-lacZ*), in which *lacZ* expression is permanently activated upon Cre-mediated excision of a *loxP*-flanked stop sequence (Soriano, 1999).

Compound embryos of specific genotypes were generated by genetic crosses of existing models and were analysed by X-Gal staining at 10.0 dpc. In *Hesx1*$^{Cre/+}$;*ROSA26*$^{Cond\text{-}lacZ/+}$ embryos, which are phenotypically normal, the majority of *lacZ*-positive cells localised within anterior forebrain structures, including the telencephalon, eyes and ventral diencephalon (*n*=4) (Fig. 4A,D). In contrast, *Hesx1*$^{Cre/I26T}$;*ROSA26*$^{Cond\text{-}lacZ/+}$ and *Hesx1*$^{Cre/R160C}$;*ROSA26*$^{Cond\text{-}lacZ/+}$ compound embryos, both of which have impaired HESX1 function owing to the presence of either the I26T or R160C mutations, contained a higher number of *lacZ*-expressing cells in both the posterior forebrain region and the first branchial arch (*n*=9) (Fig. 4B,C,E,F). In *Hesx1*$^{Cre/R160C}$;*ROSA26*$^{Cond\text{-}lacZ/+}$ embryos, we observed a greater contribution of *lacZ*-positive cells to the frontonasal mass and first branchial arch than in *Hesx1*$^{Cre/I26T}$;*ROSA26*$^{Cond\text{-}lacZ/+}$ embryos. This correlates with a higher degree of cell fate transformation, leading to a more severe phenotype in the former, as also observed in the *Hesx1* null mutants (Andoniadou et al., 2007).

Taken together, the marker and cell fate analyses indicate that the anterior forebrain area of the early embryo is abnormally specified in both *Hesx1*$^{I26T/I26T}$ and *Hesx1*$^{R160C/R160C}$ embryos. However, the R160C substitution has a profound effect on anterior

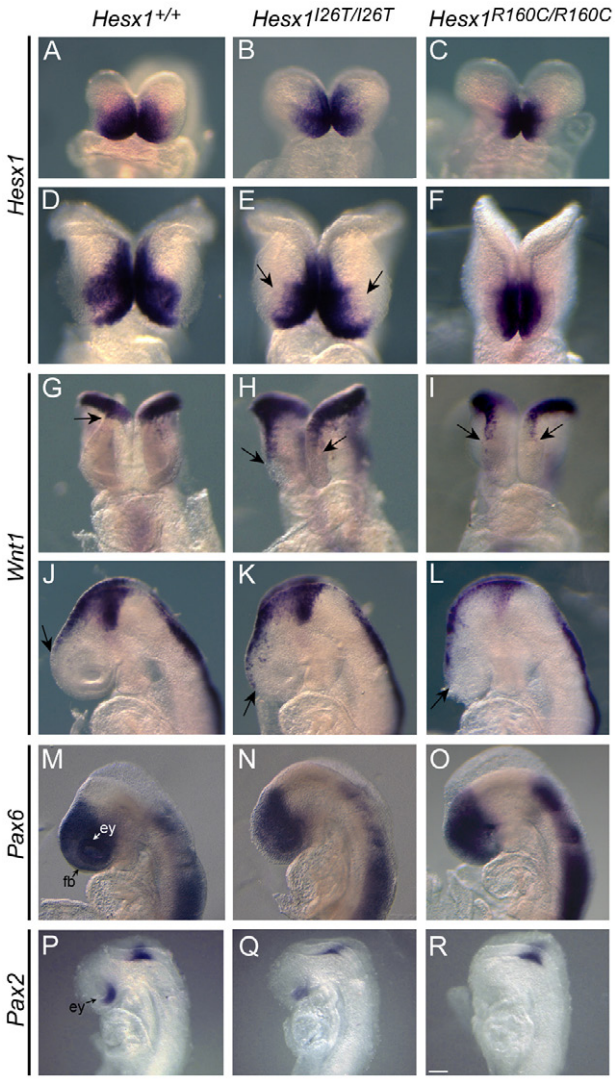

Fig. 3. Early forebrain patterning defects in *Hesx1*$^{I26T/I26T}$ and *Hesx1*$^{R160C/R160C}$ embryos. Photographs of whole-mount in situ hybridisations. Probes used are indicated on the left side. (A-F) Frontal views of 8.0 dpc (A-C) and 8.5 dpc (D-F) embryos hybridised with *Hesx1* antisense riboprobes. The expression domain of *Hesx1* is reduced in *Hesx1*$^{I26T/I26T}$ embryos (B,E) when compared with wild-type embryos (A,D). Note that at 8.5 dpc the reduction is apparent in the proximal region of the developing optic cups (arrows in E). Reduction of the *Hesx1* expression domain is more accentuated in *Hesx1*$^{R160C/R160C}$ embryos (C,F). (G-L) Frontal (G-I) and lateral (J-L) views of embryos hybridised with *Wnt1* antisense riboprobes at 8.5 and 9.0 dpc. Note the anteriorisation of the *Wnt1* expression domain in *Hesx1*$^{I26T/I26T}$ (H,K) and *Hesx1*$^{R160C/R160C}$ (I,L) mutants when compared with wild-type embryos (G,J). The arrows in G-L indicate the rostral limit of the *Wnt1* expression domain in the dorsal forebrain. (M-O) Lateral views of embryos hybridised with *Pax6* antisense riboprobes at 9.0 dpc. The *Pax6* expression domain is reduced in the *Hesx1*$^{I26T/I26T}$ mutants (N) as the eyes (ey) are smaller in size (see text for details). *Hesx1*$^{R160C/R160C}$ mutants (O) show a more severe reduction in forebrain tissue (fb) and no eyes compared with *Hesx1*$^{I26T/I26T}$ mutants (N). (P-R) Lateral views of embryos hybridised with *Pax2* antisense riboprobes at 8.5 dpc. *Pax2* is expressed in the eye (ey) and the mid-hindbrain boundary in a wild-type embryo (P). Note that reduction or absence of eye tissue in the *Hesx1*$^{I26T/I26T}$ (Q) or *Hesx1*$^{R160C/R160C}$ (R) mutants is concomitant with a reduction in *Pax2* expression in the eye. Bar: 130 μm (A-C,J-O), 170 μm (D-F), 215 μm (G-I), 40 μm (P-R).

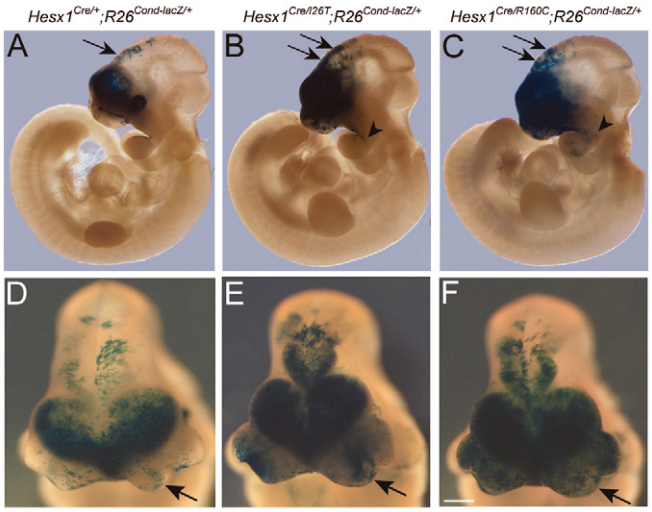

Fig. 4. Posterior transformation of anterior forebrain precursors in *Hesx1*$^{Cre/I26T}$ and *Hesx1*$^{Cre/R160C}$ mutants. (A-F) X-Gal staining on 10.0 dpc embryos of the three genotypes (indicated on the top of the columns) reveals abundant *lacZ*-positive cells in the posterior forebrain (arrowheads) of the *Hesx1*$^{Cre/I26T}$;*R26*$^{Cond\text{-}lacZ/+}$ (B,E) and *Hesx1*$^{Cre/R160C}$;*R26*$^{Cond\text{-}lacZ/+}$ (C,F) mutants in comparison with the *Hesx1*$^{Cre/+}$;*R26*$^{Cond\text{-}lacZ/+}$ control embryo (A,D). Also note that *lacZ*-positive cells are present within the first branchial arch of the mutant embryos (arrows in B,C), whereas, in the control embryo (A), they colonise only the endodermal lining of the first branchial arch. Bar: 550 μm (A-C), 180 μm (D-F).

neural patterning and affects both the telencephalic and eye primordia, whereas the I26T mutation allows for better anterior specification of the neural plate and primarily affects the eye precursors.

Pituitary defects in *Hesx1*$^{I26T/I26T}$ and *Hesx1*$^{R160C/R160C}$ embryos

To assess the development of the pituitary gland in *Hesx1*$^{I26T/I26T}$ and *Hesx1*$^{R160C/R160C}$ embryos, we performed hematoxylin-eosin (H&E) staining and in situ hybridisation analysis with diagnostic markers at different stages of embryogenesis (I26T, n=34; R160C, n=29).

Pituitary defects were clearly evident at 12.5 dpc onwards in all the embryos analysed, but some phenotypic differences were observed between *Hesx1*$^{I26T/I26T}$ and *Hesx1*$^{R160C/R160C}$ genotypes. At 12.5 dpc, *Hesx1*$^{I26T/I26T}$ embryos exhibiting forebrain phenotypes ranging from normal eyes to bilateral anophthalmia (but normal telencephalon) displayed a single pituitary phenotype, which was typically characterised by the presence of an enlarged and bifurcated anterior pituitary, often connected to the oral cavity (type I phenotype) (Fig. 5D) (n=8). This phenotype was also observed in five out of eight *Hesx1*$^{R160C/R160C}$ embryos analysed at this stage (Fig. 5G). In the other three embryos, Rathke's pouch development was clearly delayed, appearing equivalent to that of an 11.5 dpc wild-type littermate, and remained embedded within the oral ectoderm and appeared rostrally expanded (type II phenotype) (Fig. 5J). Invariably, this latter phenotype was observed in embryos with a significant lack of anterior forebrain tissue, affecting the telencephalon and eyes (Fig. 2I). The variable phenotype observed in *Hesx1*$^{R160C/R160C}$ embryos was reminiscent of that previously

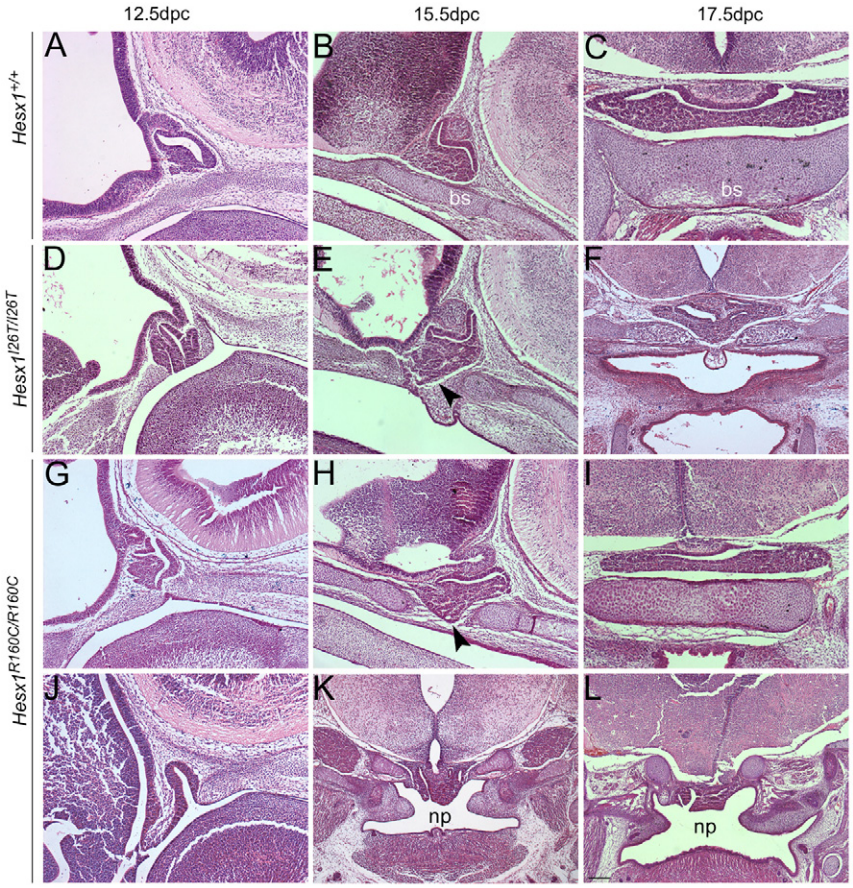

Fig. 5. Histological analysis of the developing pituitary gland in *Hesx1*$^{I26T/I26T}$ and *Hesx1*$^{R160C/R160C}$ mutants. H&E staining of embryos (genotypes are indicated on the left side of the panel) at different stages of development (indicated on top of the panel). (A-C) Wild-type pituitary gland. (D-I) *Hesx1*$^{I26T/I26T}$ (D-F) and *Hesx1*$^{R160C/R160C}$ (G-I) pituitary glands showing the type I phenotype, which typically display anterior pituitary enlargement and bifurcation with or without defective development of the basisphenoid cartilage (bs). (J-L) *Hesx1*$^{R160C/R160C}$ pituitary gland displaying the type II phenotype, which is characterised by a delay of Rathke's pouch development at 12.5 dpc (J), severe impairment of basisphenoid cartilage development and ectopic pituitary in the nasopharynx (np) (K,L). Bar, 110 μm.

described in the *Hesx1*$^{-/-}$ mutants (Dasen et al., 2001), further suggesting that the R160C mutation yields a null allele. At 15.5 and 17.5 dpc, the majority of the *Hesx1*$^{I26T/I26T}$ and *Hesx1*$^{R160C/R160C}$ embryos showed a common phenotype in which the anterior pituitary developed in its normal location but appeared enlarged, often interfering with the normal development of the basisphenoid cartilage, which was fragmented, allowing some pituitary tissue to invade the nasopharynx (Fig. 5E,F,H). In histological sections from one *Hesx1*$^{I26T/I26T}$ (n=15) and three *Hesx1*$^{R160C/R160C}$ (n=13) mutants from 15.5-17.5 dpc, all of which exhibited severe craniofacial defects (supplementary material Fig. S1D), the pituitary gland could not be recognised as a defined structure in its normal location (Fig. 5K,L). It is likely that these abnormalities represent the progression of the type II pituitary phenotype described in a proportion of *Hesx1*$^{R160C/R160C}$ mutants at 12.5 dpc. Absent pituitary has been reported previously in a low proportion of *Hesx1*$^{-/-}$ null mutants (Dasen et al., 2001).

Rathke's pouch induction appeared to occur normally in *Hesx1*$^{I26T/I26T}$ and *Hesx1*$^{R160C/R160C}$ embryos. In both homozygous mutants, the expression domains of both *Fgf8*, a marker of the ventral diencephalon, and *Lhx3*, a marker of the developing Rathke's pouch, were very similar to those observed in wild-type and heterozygous littermates at 10.5 dpc (Crossley and Martin, 1995; Sheng et al., 1996; Treier et al., 1998) (n=11) (supplementary Fig. S2A-H). These data conflict with a previous report suggesting that the *Fgf8* expression domain was rostrally expanded in the ventral diencephalon in 10.5 dpc *Hesx1*-deficient embryos (Dasen et al., 2001). The possibility exists that *Fgf8* deregulation might occur in a very small proportion of these embryos. Alternatively, the use of radioactive (Dasen et al., 2001) versus non-radioactive (this manuscript) in situ hybridisation may have contributed to this discrepancy, as radioactive in situ hybridisation is a more sensitive technique. Taken together, these data suggest that recruitment of additional oral ectoderm into Rathke's pouch at 10.5 dpc is not a major contributor to the enlargement of the anterior pituitary at subsequent developmental stages. In fact, there is a significant increase in cellular proliferation in a proportion of *Hesx1*-deficient embryos from 12.5 dpc, which may account for the pituitary hyperplasia (Gaston-Massuet et al., 2008).

Despite the abnormal morphology, the expression of several diagnostic markers such as *Lhx3* (Fig. 6A-I), *Pit1* (Fig. 6P-R), *Prop1* (Fig. 6S-U) and *Hesx1* (Fig. 6V-X) was normal in the anterior pituitary of both homozygous mutants from 12.5 to 15.5 dpc, although pituitary hyperplasia was evident (Cohen et al., 1996; Treier et al., 1998; Nasonkin et al., 2004). The only significant difference was a reduction in *Pomc1* expression in the developing hypothalamus of both mutant embryos at 12.5 dpc (Fig. 6J-O) and in the developing Rathke's pouch of *Hesx1*$^{R160C/R160C}$ embryos showing the type II phenotype (supplementary material Fig. S3). Likewise, no differences were observed in the expression domains of *Sox2*, *Sox3*, *Wnt4*, *Wnt5a* and *Axin2* between *Hesx1*$^{I26T/I26T}$, *Hesx1*$^{R160C/R160C}$ and wild-type littermates (Treier et al., 1998; Rizzoti et al., 2004; Cha et al., 2004; Kelberman et al., 2006; Olson et al., 2006) (supplementary material

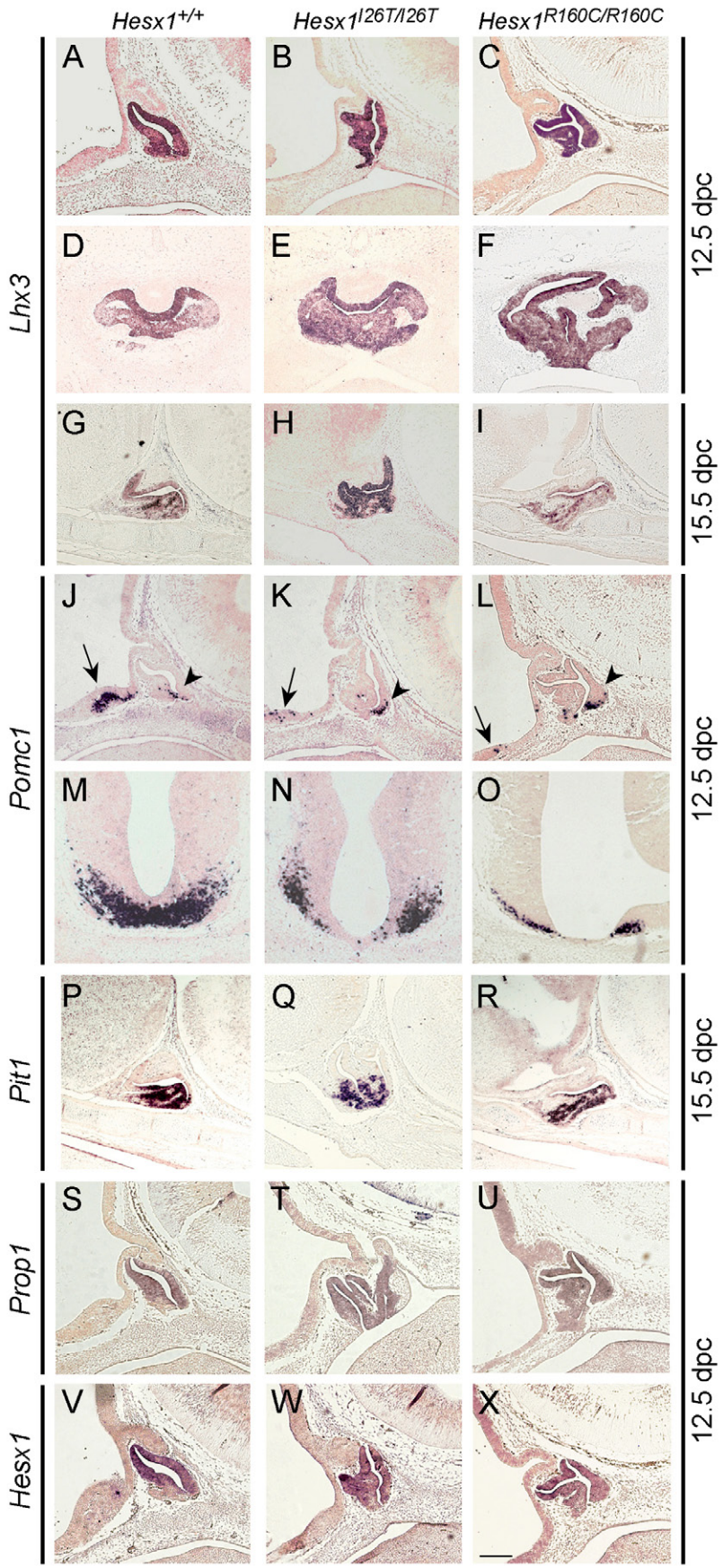

Fig. 6. Rathke's pouch is dysmorphic but properly specified in *Hesx1*$^{I26T/I26T}$ and *Hesx1*$^{R160C/R160C}$ mutants. In situ hybridisation (ISH) on sagittal (A-C, G-L and P-X) and frontal (D-F and M-O) paraffin sections of embryos of different genotypes (indicated on the top of each column). The probes used for ISH and the developmental stages of embryos analysed are indicated on the left and right sides of the panel, respectively. (A-I) *Lhx3* expression is normal, but Rathke's pouch is expanded showing aberrant morphology and contains bifurcated lumens in the *Hesx1*$^{I26T/I26T}$ (B,E,H) and *Hesx1*$^{R160C/R160C}$ (C,F,I) mutants when compared with wild-type embryos (A,D,G). (J-L) *Pomc1* expression in Rathke's pouch is not affected (arrowheads), but there is reduced *Pomc1* expression in the hypothalamic area (arrows) of the *Hesx1*$^{I26T/I26T}$ (K) and *Hesx1*$^{R160C/R160C}$ (L) embryos in comparison with the wild-type embryo (J). (M-O) Reduction of *Pomc1* expression in the hypothalamic area is apparent in frontal sections. (P-R) *Pit1* expression in ventral progenitors is indistinguishable between genotypes. (S-U) *Prop1* expression is unaffected in *Hesx1*$^{I26T/I26T}$ (T) and *Hesx1*$^{R160C/R160C}$ (U) embryos, but Rathke's pouch morphology is aberrant. (V-X) *Hesx1* transcripts are detected in the developing Rathke's pouch in a high-dorsal to low-ventral gradient of expression in the three genotypes. Bar: 155 μm (A-L,P-X), 100 μm (M-O).

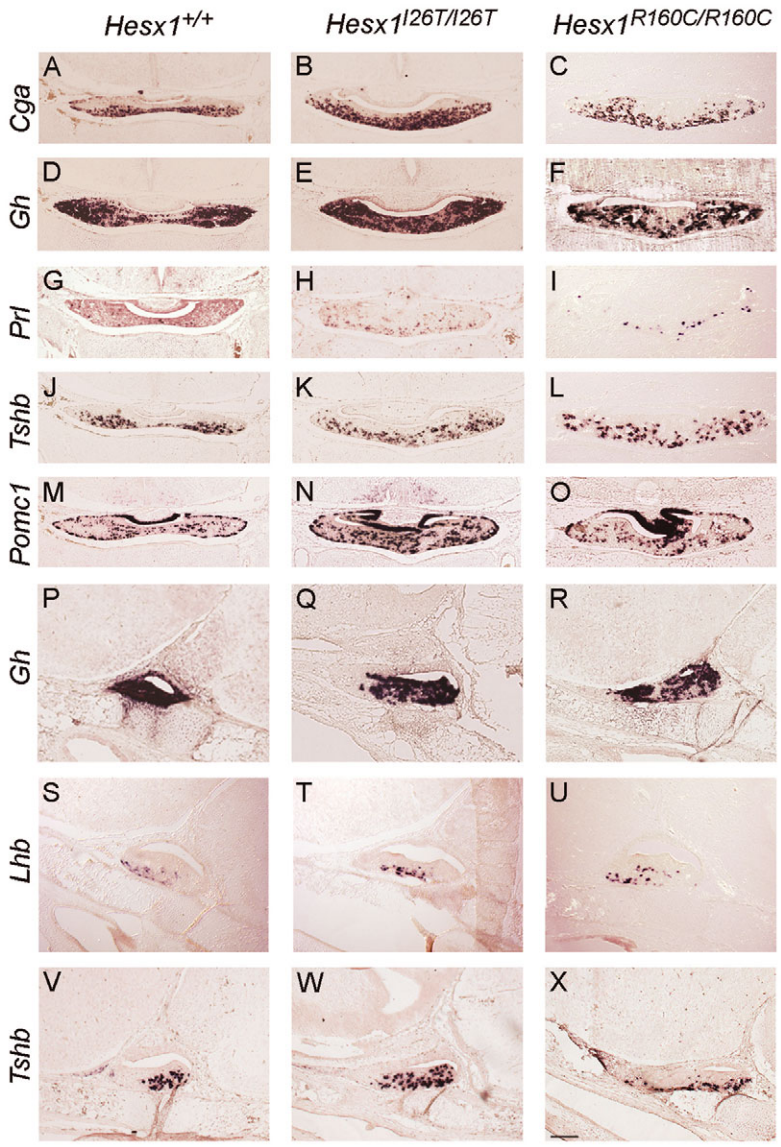

Fig. 7. Terminal differentiation of hormone-producing cells occurs normally in the anterior pituitary of *Hesx1*$^{I26T/I26T}$ and *Hesx1*$^{R160C/R160C}$ embryos. In situ hybridisation (ISH) on frontal (A-O) or sagittal (P-X) paraffin sections of 17.5 dpc embryos. Genotypes and probes used for ISH are indicated on the top and left sides of the panel, respectively. (A-X) The levels of expression for the transcripts *Cga*, *Gh*, *Prl*, *Tshb* and *Pomc1* are normal in all three genotypes; however, numbers of expressing cells appear increased in the mutant pituitaries because of the enlargement of Rathke's pouch at earlier stages. Bar: 170 µm (A-O), 215 µm (P-X).

Fig. S4). Differentiation of hormone-producing cells in the anterior pituitary was unaffected, as shown by the normal temporal and spatial expression of several diagnostic markers for specific cell types, such as *Gh* (somatotrophs) (Fig. 7D-F,P-R), *Prl* (lactotrophs) (Fig. 7G-I), *Tshb* (thyrotrophs) (Fig. 7J-L), *Cga* (encoding glycoprotein hormones, alpha subunit; gonadotrophs and thyrotrophs) (Fig. 7A-C), *Lhb* (gonadotrophs) (Fig. 7S-U) and *Pomc1* (corticotrophs) (Fig. 7M-O). However, in general, the number of hormone-producing cells appeared to be increased in the mutant pituitaries, possibly reflecting the initial enlargement of Rathke's pouch observed in the *Hesx1*$^{I26T/I26T}$ and *Hesx1*$^{R160C/R160C}$ embryos at earlier stages. There appeared to be a decrease in expressing cells in only some embryos (mostly *Hesx1*$^{R160C/R160C}$ mutants), possibly because part of the anterior pituitary tissue is ectopically located in the pharynx and is lost during processing for histological analysis. Remarkably, in those *Hesx1*$^{R160C/R160C}$ mutants where the pituitary was not morphologically recognisable (Fig. 5L), in situ hybridisation analysis with terminal differentiation markers revealed the presence of hormone-producing cells, mostly embedded in the pharyngeal epithelium (Fig. 8). Therefore, rather than being absent, the anterior pituitary tissue was ectopically located in the roof of the nasopharyngeal cavity. A less severe manifestation of this phenotype was found in some *Hesx1*$^{I26T/I26T}$ and *Hesx1*$^{R160C/R160C}$ embryos, where only part of the anterior pituitary invaded the nasopharyngeal mucosa (Fig. 5E,F,H; data not shown).

HESX1 expression in human embryos

Expression of human *HESX1* has not been reported previously. This information is relevant to advance our understanding of the relationship between the phenotypic consequences of particular mutations in mice and humans. At Carnegie stage (CS) 11 (~8.5-9.0 dpc equivalent in mouse), *HESX1* expression was detected by in situ hybridisation in the ventral forebrain and in the invaginating

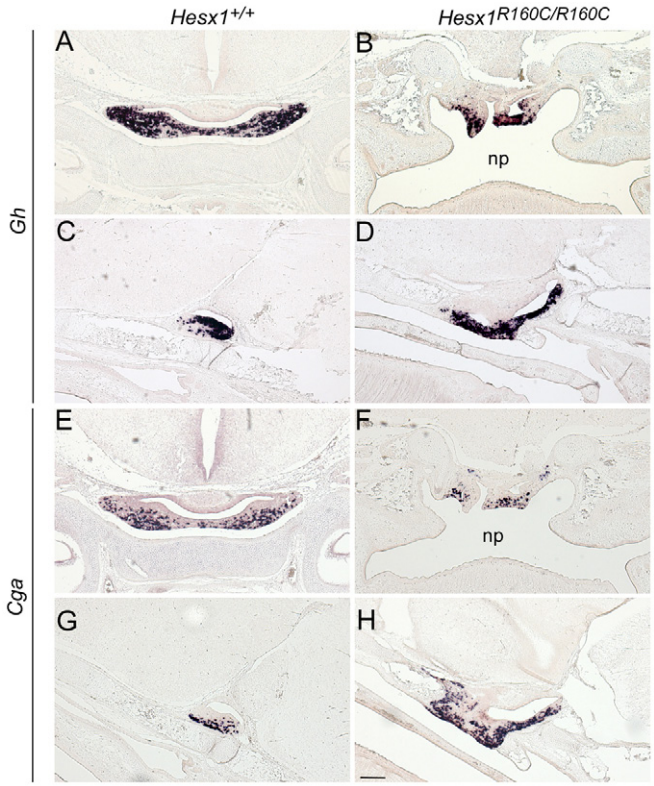

Fig. 8. Ectopic nasopharyngeal pituitary in a proportion of *Hesx1*$^{R160C/R160C}$ mutants. In situ hybridisation (ISH) on frontal (A,B,E,F) or sagittal (C,D,G,H) paraffin sections of 17.5 dpc embryos. Genotypes and probes used for ISH are indicated on the top and left sides of the panel, respectively. Note the presence of *Gh*- (A-D) and *Cga*- (E-H) positive cells in the roof of the nasopharynx (np). Bar, 150 μm.

oral epithelium of the developing Rathke's pouch (Fig. 9A,B). By CS 12 (~9.5-10.25 dpc), neural expression could not be detected but *HESX1* transcripts were abundant in Rathke's pouch, mainly in the dorsal region (Fig. 9C,D). Rathke's pouch expression persisted until CS 15 (~11.0-11.5 dpc) (Fig. 9E-H) but was not detected at CS17 (~12.0-12.5 dpc) (Fig. 9I-J). Two conclusions can be drawn from this analysis: (1) *HESX1* expression is transient in the developing human embryo and is restricted to the anterior region, including ventral forebrain and Rathke's pouch; (2) it establishes the mouse as an ideal model to study the phenotypic consequences of *HESX1* mutations associated with forebrain and pituitary defects in humans.

DISCUSSION

The results presented here have revealed some interesting insights into the function of *Hesx1/HESX1* in the aetiology and pathogenesis of SOD and hypopituitarism. We have shown that the expression domain of human *HESX1* is comparable to that in the mouse, and includes the ventral forebrain and Rathke's pouch. Based on cell fate studies in the mouse and chick, which have shown that *Hesx1*-expressing cells colonise the anterior forebrain (including ventral forebrain) at early somite stages and eyes at later stages (Fernandez-Garre, 2002; Andoniadou et al., 2007), it is likely that *HESX1* is also expressed in the anterior neural plate (presumptive anterior forebrain) at earlier stages of human embryogenesis. Unfortunately, owing to the difficulty of obtaining very early-stage human embryos, we could not confirm this hypothesis. The human expression pattern may also provide an explanation for the eye defects seen in patients carrying *HESX1* mutations (Kelberman and Dattani, 2007).

We have also generated knock-in mouse mutants harbouring the I26T and R160C substitutions to analyse the phenotypic consequences of impaired HESX1 function in mice. Our data indicate that, within the anterior forebrain, eye defects are more common than telencephalic abnormalities, including commissural tract defects, in *Hesx1*$^{I26T/I26T}$ and *Hesx1*$^{R160C/R160C}$ mutant embryos. This suggests that the eye precursors are more sensitive to impaired HESX1 function than the antecedents of the telencephalon. This conclusion is supported by further evidence: (1) *Hesx1*$^{-/-}$ null embryos show fully penetrant eye defects owing to ectopic activation of the Wnt–β-catenin signalling pathway within the anterior forebrain (Dattani et al., 1998; Andoniadou et al., 2007); (2) transgenic overexpression of *Hesx1* within the anterior forebrain of *Hesx1*$^{-/-}$ mouse embryos rescues the telencephalic defects at a lower dosage than for eye abnormalities, which require higher levels of HESX1 (Andoniadou et al., 2007); (3) in Xenopus and zebrafish, activation of the Wnt–β-catenin signalling pathway within the anterior forebrain primarily affects eye development (Fredieu et al., 1997; van de Water et al., 2001). The HESX1-I26T mutant protein shows diminished repressing activity when compared with wild-type HESX1, probably because of reduced binding to the co-repressor TLE1, which requires the highly conserved amino acid I26 within the eh-1 domain for proper binding (Galliot et al., 1999; Dasen et al., 2001; Carvalho et al., 2003). Since TLE1 is expressed across the entire forebrain (Allen and Lobe, 1999; Lopez-Rios et al., 2003), telencephalic precursors are probably less sensitive to the lack of HESX1-repressing activity mediated by TLE1. Studies in zebrafish have shown that TLE1 plays a fundamental role in eye development, as TLE1 overexpression leads to enlargement of the eyes with little or no effect on the telencephalon (Lopez-Rios et al., 2003). Therefore, HESX1-I26T is likely to allow interactions with other co-repressors within telencephalic precursors, which may compensate for the impaired HESX1-I26T–TLE-1 interaction. Among them, nuclear co-repressor (N-CoR) and some of the recently identified HESX1 interactors may contribute to the differences in forebrain phenotype between the I26T and R160C mutations (Dasen et al., 2001; Sajedi et al., 2008) (data not shown).

The pituitary defects of *Hesx1*$^{I26T/I26T}$ and *Hesx1*$^{R160C/R160C}$ are fully penetrant and usually very similar, although the morphogenesis of the pituitary gland is more affected in *Hesx1*$^{R160C/R160C}$ embryos that show severe forebrain defects. Our data suggest that the signals controlling terminal differentiation of anterior pituitary cells are acting at the right place and time, but, because of an initial enlargement of Rathke's pouch at 12.5 dpc, there are more cells that can follow the differentiation pathway. However, a minority of embryos with ectopic pituitary tissue showed fewer numbers of hormone-producing cells compared with wild-type embryos. This is reminiscent of the ectopic pharyngeal pituitary gland that has been reported in humans in association

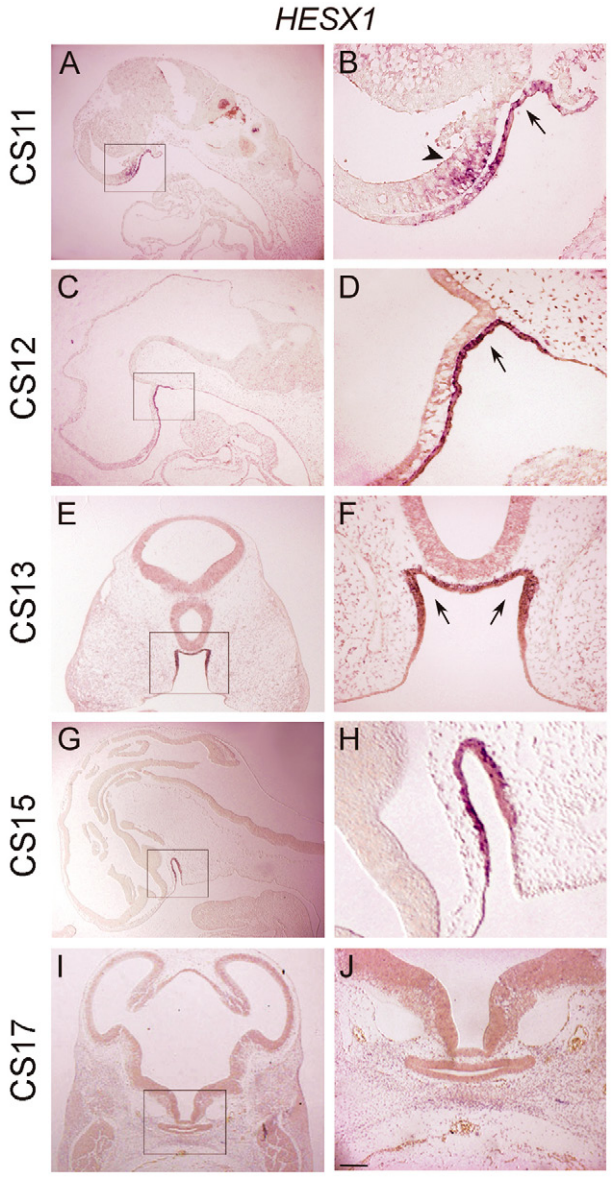

Fig. 9. *HESX1* is expressed in the ventral forebrain and developing Rathke's pouch of human embryos. In situ hybridisation analysis at Carnegie stages (CS) 11-17. Low- (A,C,E,G,I) and high- (B,D,F,H,J) magnification photographs of human embryos hybridised with human *HESX1* anti-sense riboprobes. (A,B) *HESX1* transcripts are observed in the ventral forebrain (arrowhead) and the incipient Rathke's pouch (arrow). The apparent signal in the hindbrain region is likely to be an artefact, as it was not observed in other sections or older embryos. (C,D) At CS12, *HESX1* transcripts are no longer detected in neural tissue but they are abundant in Rathke's pouch (arrow in D). (E-H) At CS13-15, *HESX1* expression is detected in the dorsal region of Rathke's pouch (arrows in F). (I,J) *HESX1* expression is not detected at CS17. A-D,G,H are sagittal and E,F,I,J are coronal sections. Bar: 275 µm (A,C,E,G,I), 125 µm (B,D,F,H,J).

with craniofacial defects (Kjaer and Hansen, 2000; Osman et al., 2006).

The fact that *Hesx1*$^{I26T/I26T}$ embryos display pituitary defects that are comparable to *Hesx1*$^{R160C/R160C}$ and *Hesx1*$^{-/-}$ embryos suggests a fundamental role for the HESX1-TLE1 interaction during normal pituitary development that cannot be compensated for by other HESX1-interacting proteins, as was previously suggested by overexpression experiments in mice (Dasen et al., 2001). Given the complete penetrance of pituitary defects in animals harbouring both the hypomorphic (I26T) and null (R160C) alleles, it is likely that the pituitary gland is highly sensitive to HESX1 dosage, and that the high incidence of hypopituitarism in humans with HESX1 mutations is not a consequence of selection bias. Our studies indicate that the R160C substitution yields a null allele, whereas I26T is a hypomorphic allele. Additionally, they provide in vivo evidence that the R160C substitution does not have a dominant-negative effect as suggested previously by in vitro data (Brickman et al., 2001) as *Hesx1*$^{R160C/+}$ mice are normal, viable and fertile.

We propose that, in the mouse, *Hesx1* function is required primarily in Rathke's pouch, secondarily in eye precursors and finally in the antecedents of the telencephalon. It is possible that this differential sensitivity to HESX1 function is conserved in the human embryo as the *Hesx1*/*HESX1* expression domains are very similar between the two species. Furthermore, phenotypic analysis indicates that anterior pituitary dysfunction, ranging from IGHD to CPHD, is the most common clinical finding in patients with *HESX1* mutations, followed by optic nerve hypoplasia and midline commissural defects (Dattani et al., 1998; Thomas et al., 2001; Brickman et al., 2001; Carvalho et al., 2003; Cohen et al., 2003; Tajima et al., 2003; Sobrier et al., 2005; Sobrier et al., 2006; Coya et al., 2007). It is interesting that the human patient carrying the I26T substitution does not have eye defects (Carvalho et al., 2003), although more than 75% of the *Hesx1*$^{I26T/I26T}$ mutant mice exhibited an eye phenotype. This may be the result of species-specific differences between mice and humans, or, alternatively, the human patient may just have a milder phenotype, as approximately 21% of *Hesx1*$^{I26T/I26T}$ mouse mutants do not have eye defects.

The reasons underlying perinatal lethality in the majority of *Hesx1*$^{R160C/R160C}$ animals and perhaps in a minority of *Hesx1*$^{I26T/I26T}$ mutant pups are not clear. As pituitary defects are fully penetrant and similar in both mutants, it seems unlikely that these morphological abnormalities alone can cause mortality. The severe craniofacial defects in the *Hesx1*$^{R160C/R160C}$ pups are also likely to contribute to some perinatal death; however, pups without gross morphological defects in the brain and craniofacial structures also die soon after birth. Abnormal development of the hypothalamic region and/or its connection to the pituitary gland might underlie the observed perinatal death. Indeed, hypothalamic *Pomc1* expression is reduced in mice carrying the I26T or the R160C substitution, with a more severe loss of signal in *Hesx1*$^{R160C/R160C}$ embryos. As pituitary function is controlled by the neuroendocrine hypothalamus, the *Hesx1*$^{R160C/R160C}$ pups might be expected to show more severe hypopituitarism than the *Hesx1*$^{I26T/I26T}$ mice, as described for human patients carrying these mutations. Unfortunately, the *Hesx1*$^{I26T/I26T}$ mice do not show any sign of hypopituitarism and were viable and fertile, and the *Hesx1*$^{R160C/R160C}$ animals die too early to assess any sign of hypopituitarism in the form of delayed growth. Further investigation will be required to assess, in more detail, the development of the neuroendocrine hypothalamic nuclei and their connections to the pituitary gland. Analysis of a systematic mutational screen has shown that mutations in *HESX1* are a rare cause of SOD and hypopituitarism (McNay et al., 2007). It is possible that those surviving patients

represent the milder end of the phenotypic spectrum. As with the low numbers of surviving mice, it is likely that a significant proportion of *HESX1* mutations in humans are not viable and therefore remain undetected. Although this hypothesis is difficult to test, the mouse data presented here support this idea.

METHODS

Generation of the *Hesx1-I26T* and *Hesx1-R160C* mouse mutants

The *Hesx1-I26T* and *Hesx1-R160C* targeting vectors were generated using homologous regions obtained from plasmids containing the mouse *Hesx1* gene, which have been previously used successfully (Fig. 1A,B). A *PGK-Neo* cassette flanked by *loxP* sequences was inserted in the *Eco*RI site located in the first intron of both targeting constructs. In the *Hesx1-I26T* targeting vector, the *PGK-Neo* cassette was cloned in the same orientation of transcription as the *Hesx1* locus. However, the orientation was inverted in the *Hesx1-R160C* targeting vector in an attempt to reduce the expression of the mutated allele, which may have had a dominant negative effect in embryonic stem (ES) cells since the *Hesx1* locus is transcriptionally active in these cells. The codons for amino acids I26 and R160 of murine wild-type *Hesx1* were mutated by PCR, as indicated in Fig. 1C,D (primer sequences available on request). The mutated codons introduced novel restriction sites that are not present in wild-type *Hesx1*, and which were very useful as a quick method to identify the presence of the mutated alleles during generation of the mouse lines. The linearised targeting vectors were electroporated in CCE ES cells (129/SvEv) (kindly provided by E. Robertson) and 500 colonies were picked, expanded and screened by PCR and Southern blot, as described previously (Andoniadou et al., 2007). For each construct, two correctly targeted clones were isolated and injected into blastocysts from C57BL/6J (Harlan) mice. Male chimeras were backcrossed to C57BL/6J females to establish the F1 generation of heterozygous mice. F1 animals were crossed with *beta-actin-Cre* mice, which were kept on a C57BL/6J background, to excise the *PGK-Neo* cassette (Meyers et al., 1998). After backcrossing with C57BL/6J animals to remove the *beta-actin-Cre* transgene, $Hesx1^{I26T/+}$ and $Hesx1^{R160C/+}$ heterozygotes were kept on a C57BL/6J background. The analysis described here used animals and embryos after three backcrosses to C57BL/6J. The $Hesx1^{+/-}$ mice used in this study had been maintained on a C57BL/6J background for more than 20 generations (Andoniadou et al., 2007). With the exception of the opposite orientation of the remaining *loxP* sequence after Cre-mediated excision of the *PGK-Neo* cassette and the specific point mutation, both *Hesx1-I26T* and *Hesx1-R160C* alleles were identical. This was relevant in order to eliminate any adverse effect of the remaining *loxP* site on transcription and splicing efficiency, which might impact the phenotype.

Genotyping of mice and embryos

Embryos and neonates were genotyped by PCR on DNA samples prepared from tail tips, yolk sacs or whole embryos (Andoniadou et al., 2007). Primer sequences and PCR protocols are available on request.

H&E and X-Gal staining, and whole-mount and section in situ hybridisation

H&E and X-Gal staining, and whole-mount in situ hybridisation were performed as described previously (Andoniadou et al., 2007).

TRANSLATIONAL IMPACT

Clinical issue

The pituitary gland is regulated by the hypothalamus in the brain and is essential for controlling growth, reproduction, and stress responses. Developmental pituitary defects lead to hypopituitarism, which can range from loss of a single pituitary hormone to loss of multiple or all pituitary hormones. Isolated growth hormone deficiency (IGHD) is most common, affecting one in as many as 4000 people. Combined pituitary hormone deficiency (CPHD), characterised by deficiency of multiple pituitary hormones, is less common than IGHD, and is associated with considerable morbidity and mortality. Septo-optic dysplasia (SOD; also referred to as de Morsier syndrome) is associated with anterior brain and eye defects, and may involve the gene for HESX1. HESX1 is a transcription factor required for normal development of the forebrain and pituitary gland in both humans and mice. Mutation of HESX1 is associated with hypopituitarism, although, the wide range of phenotypes manifested in these diseases makes it difficult to determine the influence of these mutations.

Results

Here, HESX1 expression was identified in the anterior brain and pituitary gland of mice and humans, establishing the mouse as a physiologically relevant model for understanding HESX1 mutations associated with human disease. Mouse mutants were created harbouring two common point mutations found in human hypopituitarism, which displayed a hierarchy of defects. Hesx1 function had the greatest influence in the pituitary gland, medium effects on eye precursors and mild effects in the anterior brain (the location of the developing hypothalamus). In addition, the two mutations examined caused distinct phenotypes. An R160C substitution produced a non-functional protein that was lethal, whereas I26T had reduced functionality and a milder phenotype. This study shows very different effects of two knock-in mutations of Hesx1. Although eye defects were noted in both mutants, only the R160C substitution proved lethal, suggesting that the neural control of pituitary function may be impaired in these mutants.

Implications and future directions

This study advances our understanding of the contributions of HESX1 to complex and variable manifestations of human hypopituitarism. Consistent with these findings, pituitary dysfunction is most common in patients with HESX1 mutations, followed by eye defects and then anterior brain abnormalities. This work also demonstrates unique consequences of R160C versus I26T mutations in HESX1, which are commonly associated with human disease.

doi:10.1242/dmm.001669

For in situ hybridisation on paraffin sections, the following protocol was used: mouse embryos at 10.5, 12.5, 15.5 and 17.5 days post coitum (dpc) were dissected and fixed overnight in 4% paraformaldehyde (PFA) (Sigma), followed by dehydration in a graded ethanol series and embedding in paraffin. Sagittal and coronal sections (6-8 mm) were cut using a standard microtome. Sections were de-waxed, hydrated and fixed in 4% PFA (20 minutes). After proteinase K treatment (8 minutes at room temperature) and fixation (4% PFA, 5 minutes), they were treated with 0.1 M triethanolamine plus 0.25% acetic anhydride (10 minutes). Hybridisation was carried out overnight at 55-65°C in 50% formamide, 0.3 M sodium chloride, 20 mM Tris HCl, 5 mM EDTA, 10% dextran sulphate, 1×Denhardt's reagent (Sigma) supplemented with tRNA (Sigma), RNAase inhibitor (Roche) and the relevant digoxigenin-labelled riboprobe. Stringency washes consisting of 2×SSC (twice, 30 minutes), 50% formamide:50% 2×SSC (twice, 30 minutes) and then 2×SSC (twice, 30 minutes)

were carried out the following day at 65°C. Slides were then blocked for 1 hour in 10% foetal calf serum (FCS) and placed in a humid chamber in a buffer containing: 0.1 M Tris pH 7.6, 0.15 M sodium chloride, anti-digoxigenin antibody conjugated with alkaline phosphatase (1:1000 from Roche), and 2% FCS. Staining was carried out the following day using the NBT/BCIP system (Roche). Sections were mounted in Vectamount (Vector Laboratories). Human embryonic/foetal material was obtained from the Human Developmental Biology Resource (HDBR) and from the M. Vekemans Research Group at Necker Hospital, Paris with full ethical approval under both British and French bioethics regulations. In situ hybridisation was performed on histological sections of embryos from Carnegie stages (CS) 11 to 18. Embryos at stages earlier than CS 11 were unavailable.

Statistical analysis on mice and embryos

Deviations from the Mendelian ratios in offspring were analysed for statistical significance using a chi-square test. The severity and penetrance of the forebrain defects between: (1) $Hesx1^{I26T/I26T}$ and $Hesx1^{R160C/R160C}$; (2) $Hesx1^{I26T/I26T}$ and $Hesx1^{I26T/-}$; and (3) $Hesx1^{R160C/R160C}$ and $Hesx1^{R160C/-}$ were analysed using a Fisher's exact test. To detect possible differences in severity, only the proportion of embryos showing the most severe forebrain defects were compared, and for penetrance we used the proportions of embryos with/without forebrain defects (Table 2).

ACKNOWLEDGEMENTS

We are grateful to A. Copp for comments on the manuscript; A. McMahon, G. Martin, P. Gruss, M. Rosenfeld, R. Lovell-Badge, B. Hogan and the MRC Geneservice for probes; the MRC/Wellcome-funded Human Developmental Biology Resource; and M. Vekemans and M. Teboul for access to human tissues and in situ hybridisation. This work was supported by grants 068630 and 078432 from The Wellcome Trust, grant 1ZTG from UCL Central Funds, a grant from the Association Francaise des Myopathies (H.C.E.) and by the Medial Research Council (M.T.D. and D.K.). E.S. is the recipient of a PhD studentship funded by the Child Health Research Appeal Trust. Deposited in PMC for immediate release.

COMPETING INTERESTS

The authors declare no competing financial interests.

AUTHOR CONTRIBUTIONS

J.P.M.-B. and M.T.D. conceived and designed the experiments, and J.P.M.-B. wrote the paper; E.S. and C.G.M. performed the majority of the experiments and analysed the bulk of the data; J.P.M.-B. and M.S. generated the mutant mice; C.L.A. helped experimentally and in the analysis of the data, and prepared several figures and edited the manuscript; D.K., S.C., H.C.E. and D.G. performed the experiments on human material.

SUPPLEMENTARY MATERIAL

Supplementary material for this article is available at
http://dmm.biologists.org/content/1/4-5/241/suppl/DC1

Received 7 May 2008; Accepted 28 August 2008.

REFERENCES

Allen, T. and Lobe, C. G. (1999). A comparison of Notch, Hes and Grg expression during murine embryonic and post-natal development. *Cell Mol. Biol.* **45**, 687-708.

Andoniadou, C. L., Signore, M., Sajedi, E., Gaston-Massuet, C., Kelberman, D., Burns, A. J., Itasaki, N., Dattani, M. and Martinez-Barbera, J. P. (2007). Lack of the murine homeobox gene *Hesx1* leads to a posterior transformation of the anterior forebrain. *Development* **134**, 1499-1508.

Brickman, J. M., Clements, M., Tyrell, R., McNay, D., Woods, K., Warner, J., Stewart, A., Beddington, R. S. P. and Dattani, M. (2001). Molecular effects of novel mutations in *Hesx1/HESX1* associated with human pituitary disorders. *Development* **128**, 5189-5199.

Carvalho, L. R., Woods, K. S., Mendonca, B. B., Marcal, N., Zamparini, A. L., Stifani, S., Brickman, J. M., Arnhold, I. J. and Dattani, M. T. (2003). A homozygous mutation in *HESX1* is associated with evolving hypopituitarism due to impaired repressor-corepressor interaction. *J. Clin. Invest.* **112**, 1192-1201.

Cha, K. B., Douglas, K. R., Potok, M. A., Liang, H., Jones, S. N. and Camper, S. A. (2004). WNT5A signaling affects pituitary gland shape. *Mech. Dev.* **121**, 183-194.

Cohen, L. E., Wondisford, F. E. and Radovick, S. (1996). Role of *Pit-1* in the gene expression of growth hormone, prolactin, and thyrotropin. *Endocrinol. Metab. Clin. North Am.* **25**, 523-540.

Cohen, R. N., Cohen, L. E., Botero, D., Yu, C., Sagar, A., Jurkiewicz, M. and Radovick, S. (2003). Enhanced repression by HESX1 as a cause of hypopituitarism and septo-optic dysplasia. *J. Clin. Endocrinol. Metab.* **88**, 4832-4839.

Coya, R., Vela, A., Perez de Nanclares, G., Rica, I., Castaño, L., Busturia, M. A., Martul, P. and GEDPIT group. (2007). Panhypopituitarism: genetic versus acquired etiological factors. *J. Pediatr. Endocrinol. Metab.* **20**, 27-36.

Crossley, P. H. and Martin, G. R. (1995). The mouse *Fgf8* gene encodes a family of polypeptides and is expressed in regions that direct outgrowth and patterning in the developing embryo. *Development* **121**, 439-451.

Cushman, L. J. and Camper, S. A. (2001). Molecular basis of pituitary dysfunction in mouse and human. *Mamm. Genome* **12**, 485-494.

Dasen, J. S., Barbera, J. P., Herman, T. S., Connell, S. O., Olson, L., Ju, B., Tollkuhn, J., Baek, S. H., Rose, D. W. and Rosenfeld, M. G. (2001). Temporal regulation of a paired-like homeodomain repressor/TLE corepressor complex and a related activator is required for pituitary organogenesis. *Genes Dev.* **15**, 3193-3207.

Dattani, M. T., Martinez-Barbera, J. P., Thomas, P. Q., Brickman, J. M., Gupta, R., Martensson, I. L., Toresson, H., Fox, M., Wales, J. K., Hindmarsh, P. C. et al. (1998). Mutations in the homeobox gene *HESX1/Hesx1* associated with septo-optic dysplasia in human and mouse. *Nat. Genet.* **19**, 125-133.

Fernandez-Garre, P., Rodriguez-Gallardo, L., Gallego-Diaz, V., Alvarez, I. S. and Puelles, L. (2002). Fate map of chicken neural plate at stage 4. *Development* **129**, 2807-2822.

Fredieu, J. R., Cui, Y., Maier, D., Danilchik, M. V. and Christian, J. L. (1997). Xwnt-8 and lithium can act upon either dorsal mesodermal or neurectodermal cells to cause a loss of forebrain in *Xenopus* embryos. *Dev. Biol.* **186**, 100-114.

Galliot, B., de Vargas, C. and Miller, D. (1999). Evolution of homeobox genes: Q50 Paired-like genes founded the Paired class. *Dev. Genes Evol.* **209**, 186-197.

Gaston-Massuet, C., Andoniadou, C. L., Signore, M., Bird, S., Turner, J. M. A. and Martinez-Barbera, J. P. (2008). Genetic interaction between the homeobox transcription factors HESX1 and SIX3 is required for normal pituitary development. *Dev. Biol.* doi:10.1016/j.ydbio.2008.08.008.

Hermesz, E., Mackem, S. and Mahon, K. A. (1996). Rpx: a novel anterior-restricted homeobox gene progressively activated in the prechordal plate, anterior neural plate and Rathke's pouch of the mouse embryo. *Development* **122**, 41-52.

Kelberman, D. and Dattani, M. T. (2007). The role of transcription factors implicated in anterior pituitary development in the aetiology of congenital hypopituitarism. *Ann. Med.* **38**, 560-577.

Kelberman, D., Rizzoti, K., Avilion, A., Bitner-Glindzicz, M., Cianfarani, S., Collins, J., Kling Chong, W., Kirk, J. M. W., Achermann, J. C., Ross, R. et al. (2006). Mutations within *Sox2/SOX2* are associated with abnormalities in the hypothalamo-pituitary-gonadal axis in mice and humans. *J. Clin. Invest.* **116**, 2442-2455.

Kjaer, I. and Hansen, B. F. (2000). The prenatal pituitary gland-hidden and forgotten. *Pediatr. Neurol.* **22**, 155-156.

Lagutin, O. V., Zhu, C. C., Kobayashi, D., Topczewski, J., Shimamura, K., Puelles, L., Russell, H. R., McKinnon, P. J., Solnica-Krezel, L. and Oliver, G. (2003). *Six3* repression of Wnt signaling in the anterior neuroectoderm is essential for vertebrate forebrain development. *Genes Dev.* **17**, 368-379.

Lindsay, R., Feldkamp, M., Harris, D., Robertson, J. and Rallison, M. (1994). Utah growth study: growth standards and the prevalence of growth hormone deficiency. *J. Pediatr.* **125**, 29-35.

Lopez-Rios, J., Tessmar, K., Loosli, F., Wittbrodt, J. and Bovolenta, P. (2003). SIX3 and SIX6 activity is modulated by members of the groucho family. *Development* **130**, 185-195.

Martinez-Barbera, J. P., Rodriguez, T. A. and Beddington, R. S. (2000). The homeobox gene *Hesx1* is required in the anterior neural ectoderm for normal forebrain formation. *Dev. Biol.* **223**, 422-430.

McMahon, A. P. and Bradley, A. (1990). The *Wnt-1* (int-1) proto-oncogene is required for development of a large region of the mouse brain. *Cell* **62**, 1073-1085.

McNay, D. E. G., Turton, J. P., Kelberman, D., Woods, K. S., Brauner, R., Papadimitriou, A., Keller, E., Keller, A., Haufs, N., Krude, H. et al. (2007). *HESX1* mutations are an uncommon cause of septo-optic dysplasia and hypopituitarism. *J. Clin. Endocrinol. Metab.* **92**, 691-697.

Meyers, E. N., Lewandoski, M. and Martin, G. R. (1998). An *Fgf8* mutant allelic series generated by Cre- and Flp-mediated recombination. *Nat. Genet.* **18**, 136-141.

Nasonkin, I. O., Ward, R. D., Raetzman, L. T., Seasholtz, A. F., Saunders, T. L., Gillespie, P. J. and Camper, S. A. (2004). Pituitary hypoplasia and respiratory distress syndrome in *Prop1* knockout mice. *Hum. Mol. Genet.* **13**, 2727-2735.

Olson, L., Tollkuhn, J., Scafoglio, S., Krones, A., Zhang, J., Ohgi, K., Wu, W., Taketo, M., Kemler, R., Grosschedl, R. et al. (2006). Homeodomain-mediated beta-catenin-dependent switching events dictate cell-lineage determination. *Cell* **125**, 593-605.

Osman, M., Allan, J. C. and Kramer, B. (2006). A pharyngeal and ectopic hypophysis in a neonate with craniofacial abnormalities: A case report and review of development and structure. *Cleft Palate Craniofac. J.* **43**, 117-122.

Patel, L., McNally, R. J., Harrison, E., Loyd, I. C. and Clayton, P. E. (2006). Geographical distribution of optic nerve hypoplasia and septo-optic dysplasia in Northwest England. *J. Pediatr*. **148**, 85-88.

Procter, A. M., Phillips, J. A. and Cooper, D. N. (1998). The molecular genetics of growth hormone deficiency. *Hum. Genet*. **103**, 255-272.

Rizzoti, K., Brunelli, S., Carmignac, D., Thomas, P. Q., Robinson, I. C. A. F. and Lovell-Badge, R. (2004). SOX3 is required during the formation of the hypothalamo-pituitary axis. *Nat. Genet.* **36**, 247-255.

Sajedi, E., Gaston-Massuet, C., Andoniadou, C. L., Signore, M., Hurd, P. J., Dattani, M. T. and Martinez-Barbera, J. P. (2008). DNMT1 interacts with the developmental transcriptional repressor HESX1. *Biochem. Biophys. Acta* **1783**, 131-143.

Sheng, H. Z., Zhadanov, A. B., Mosinger, B., Fujii, T., Bertuzzi, S., Grinberg, A., Lee, E. J., Huang, S. P., Mahon, K. A. and Westphal, H. (1996). Specification of pituitary cell lineages by the LIM homeobox gene *Lhx3*. *Science* **272**, 1004-1007.

Sobrier, M. L., Netchine, I., Heinrichs, C., Thibaud, N., Vie-Luton, M. P., Vliet, G. V. and Amselem, S. (2005). Alu-element insertion in the homeodomain of *HESX1* and aplasia of the anterior pituitary. *Hum. Mutat.* **25**, 503.

Sobrier, M. L., Maghnie, M., Vie-Luton, M. P., Secco, A., dilorgi, N., Lorini, R. and Amselem, S. (2006). Novel *HESX1* mutations associated with life-threatening neonatal phenotype, pituitary aplasia, but normally located posterior pituitary and no optic nerve abnormalities. *J. Clin. Endocrinol. Metab*. **91**, 4528-4536.

Soriano, P. (1999). Generalized *lacZ* expression with the ROSA26 Cre reporter strain. *Nat. Genet.* **21**, 70-71.

Tajima, T., Hattori, T., Nakajima, T., Okuhara, K., Sato, K., Abe, S., Nakae, J. and Fujieda, K. (2003). Sporadic heterozygous frameshift mutation of *HESX1* causing pituitary and optic nerve hypoplasia and combined pituitary hormone deficiency in a japanese patient. *J. Clin. Endocrinol. Metab.* **88**, 45-50.

Thomas, P. and Beddington, R. S. P. (1996). Anterior primitive endoderm may be responsible for patterning the anterior neural plate in the mouse embryo. *Curr. Biol.* **6**, 1487-1496.

Thomas, P. Q., Dattani, M. T., Brickman, J. M., McNay, D., Warne, G., Zacharin, M., Cameron, F., Hurst, J., Woods, K., Dunger, D. et al. (2001). Heterozygous *HESX1* mutations associated with isolated congenital pituitary hypoplasia and septo-optic dysplasia. *Hum. Mol. Genet*. **10**, 39-45.

Torres, M., Gomez-Pardo, E. and Gruss, P. (1996). Pax2 contributes to inner ear patterning and optic nerve trajectory. *Development* **122**, 3381-3391.

Treier, M., Gleiberman, A. S., O'Connell, S. M., Szeto, D. P., McMahon, J. A., McMahon, A. P. and Rosenfeld, M. G. (1998). Multistep signaling requirements for pituitary organogenesis *in vivo*. *Genes Dev.* **12**, 1691-1704.

van de Water, S., van de Watering, M., Joore, J., Esseling, J., Bink, R., Clevers, H. and Zivkovic, D. (2001). Ectopic Wnt signal determines the eyeless phenotype of zebrafish masterblind mutant. *Development* **128**, 3877-3888.

Vimpani, G. V., Vimpani, A. F., Lidgard, G. P., Cameron, E. H. and Farquhar, J. W. (1977). Prevalence of severe growth hormone deficiency. *Br. Med. J.* **13**, 427-430.

Walther, C. and Gruss, P. (1991). *Pax-6*, a murine paired box gene, is expressed in the developing CNS. *Development* **113**, 1435-1449.

Wilson, D. S., Guenther, B., Desplan, C. and Kuriyan, J. (1995). High resolution crystal structure of a paired (Pax) class cooperative homeodomain dimer on DNA. *Cell* **82**, 709-719.

Xuan, S., Baptista, C. A., Balas, G., Tao, W., Soares, V. C. and Lai, E. (1995). Winged helix transcription factor BF-1 is essential for the development of the cerebral hemispheres. *Neuron* **14**, 1141-1152.

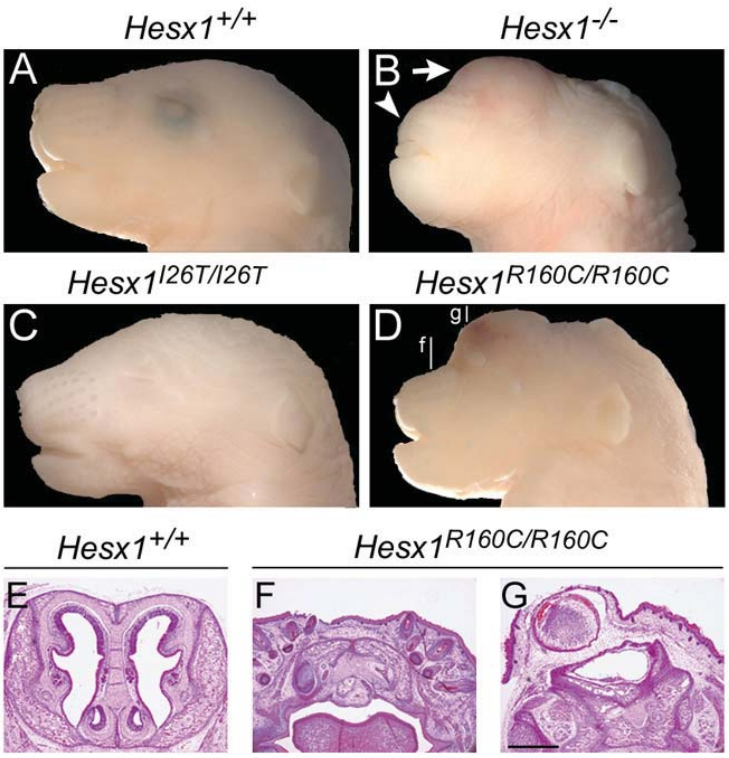
Hesx1+/+
Hesx1-/-
A
B
Hesx1I26T/I26T
Hesx1R160C/R160C
C
D
gl
f
Hesx1+/+
Hesx1R160C/R160C
E
F
G

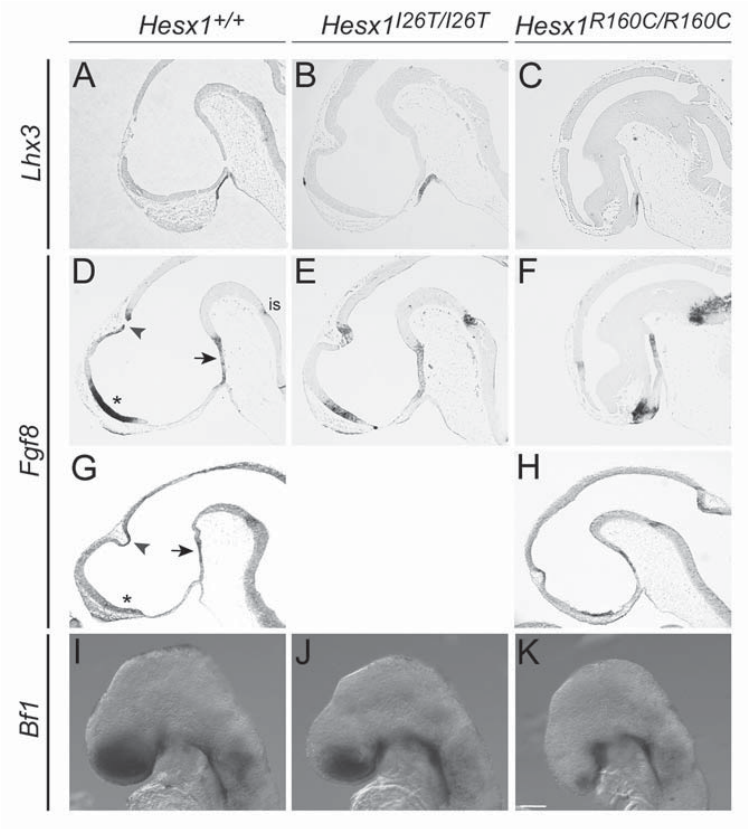
Hesx1+/+
Hesx1I26T/I26T
Hesx1R160C/R160C
Lhx3
Fgf8
Bf1
A
B
C
D
E
F
G
H
I
J
K
is

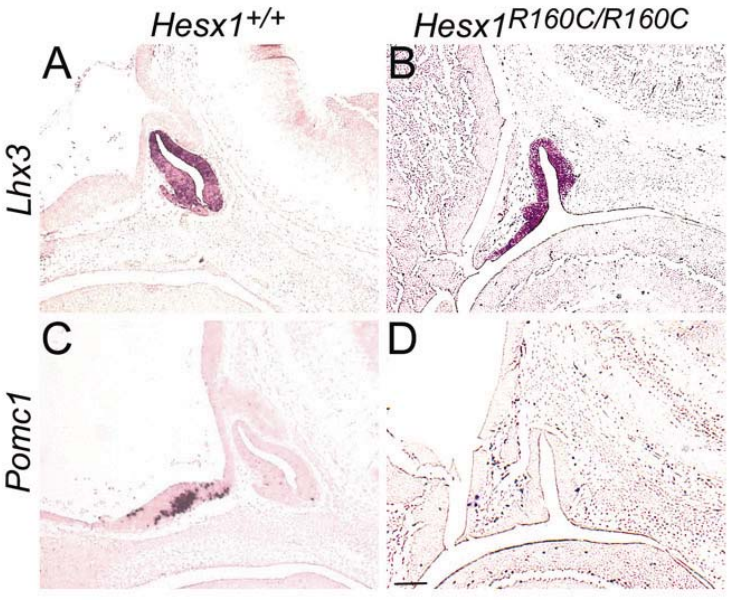
Hesx1+/+
Hesx1R160C/R160C
Lhx3
Pomc1
A
B
C
D

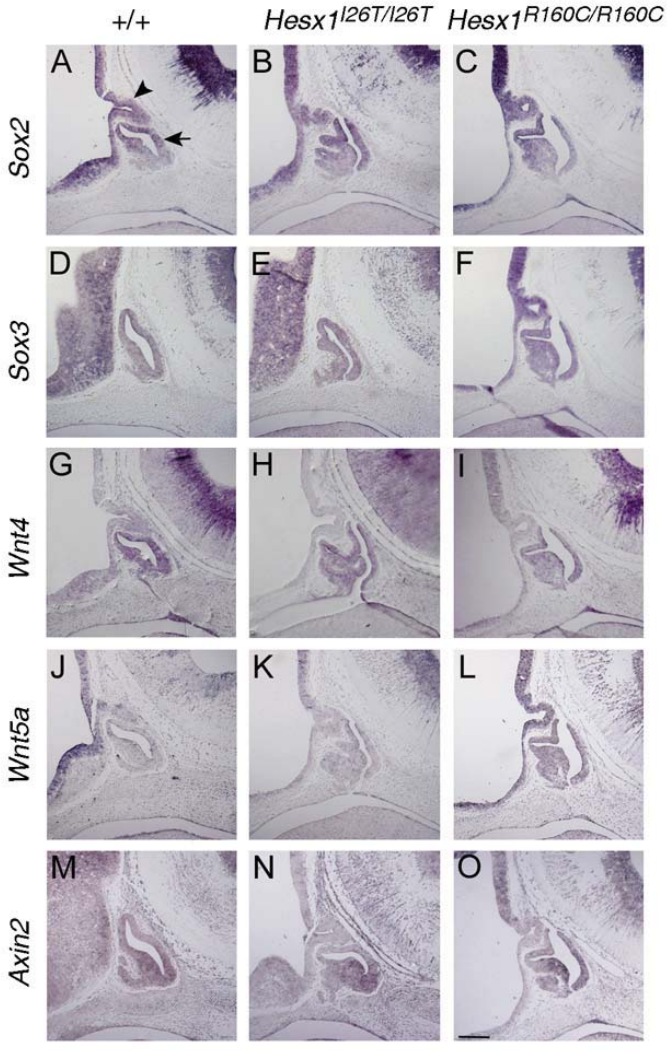
+/+
Hesx1I26T/I26T
Hesx1R160C/R160C
Sox2
Sox3
Wnt4
Wnt5a
Axin2
A
B
C
D
E
F
G
H
I
J
K
L
M
N
O

Human Molecular Genetics, 2008, Vol. 17, No. 21 ***3411–3425***
doi:10.1093/hmg/ddn235
Advance Access published on August 8, 2008

Human neural crest cells display molecular and phenotypic hallmarks of stem cells

Sophie Thomas[1], Marie Thomas[1], Patrick Wincker[2], Candice Babarit[1], Puting Xu[3], Marcy C. Speer[3,†], Arnold Munnich[1,4], Stanislas Lyonnet[1,4], Michel Vekemans[1,4] and Heather C. Etchevers[1,5,*]

[1]INSERM, U781, Hôpital Necker-Enfants Malades, 149 rue de Sèvres, 75015 Paris, France, [2]GENOSCOPE (CEA) and UMR 8030 CNRS-GENOSCOPE-Université d'Evry, 2 rue Gaston Crémieux, 91057 Evry, France, [3]Center for Human Genetics, Department of Medicine, Duke University Medical Center, Durham, North Carolina 27710, USA, [4]Faculté de Médecine, Université Paris Descartes, 15 rue de l'Ecole de Médecine, 75005 Paris, France and [5]INSERM, U563, Centre de Physiopathologie de Toulouse-Purpan, 31300 Toulouse, France

Received June 23, 2008; Revised and Accepted August 6, 2008

The fields of both developmental and stem cell biology explore how functionally distinct cell types arise from a self-renewing founder population. Multipotent, proliferative human neural crest cells (hNCC) develop toward the end of the first month of pregnancy. It is assumed that most differentiate after migrating throughout the organism, although in animal models neural crest stem cells reportedly persist in postnatal tissues. Molecular pathways leading over time from an invasive mesenchyme to differentiated progeny such as the dorsal root ganglion, the maxillary bone or the adrenal medulla are altered in many congenital diseases. To identify additional components of such pathways, we derived and maintained self-renewing hNCC lines from pharyngulas. We show that, unlike their animal counterparts, hNCC are able to self-renew *ex vivo* under feeder-free conditions. While cross species comparisons showed extensive overlap between human, mouse and avian NCC transcriptomes, some molecular cascades are only active in the human cells, correlating with phenotypic differences. Furthermore, we found that the global hNCC molecular profile is highly similar to that of pluripotent embryonic stem cells when compared with other stem cell populations or hNCC derivatives. The pluripotency markers *NANOG*, *POU5F1* and *SOX2* are also expressed by hNCC, and a small subset of transcripts can unambiguously identify hNCC among other cell types. The hNCC molecular profile is thus both unique and globally characteristic of uncommitted stem cells.

INTRODUCTION

Widespread proliferation and progressive fate restriction over time characterize embryonic development. During and after neural tube closure in vertebrate embryos, neural crest cells (NCC) detach from the ectoderm at the boundary between neural and non-neural epithelia, multiply and infiltrate the mesoderm. The site-appropriate differentiation of NCC is the result of a combination of extrinsic factors from the embryonic niche (1,2) and cell-intrinsic properties that modify responsiveness to these influences (3). NCC normally yields neurons and glial cells of the entire peripheral nervous system (PNS), pigment cells and endocrine cells (4). In the head, they also give rise to cephalic tendons, cartilage, bone, dermis, meninges, vascular smooth muscle and adipocytes (5). The original progenitors disappear along with their birthplace as the neural tube closes and matures. However, such locations as the enteric ganglia (6), the dorsal root ganglia (7), the hair follicle (8–10), the tooth (11) and even the bone marrow (12,13) appear to be later niches for the maintenance of persistent, oligopotent avian and rodent neural crest-derived stem cells.

Because of its wide range of derivatives and long-term plasticity, the development of the neural crest has been the topic of

*To whom correspondence should be addressed. Tel: +33 562744587; Fax: +33 562744558; Email: heather.etchevers@inserm.fr
†Died August 4, 2007.

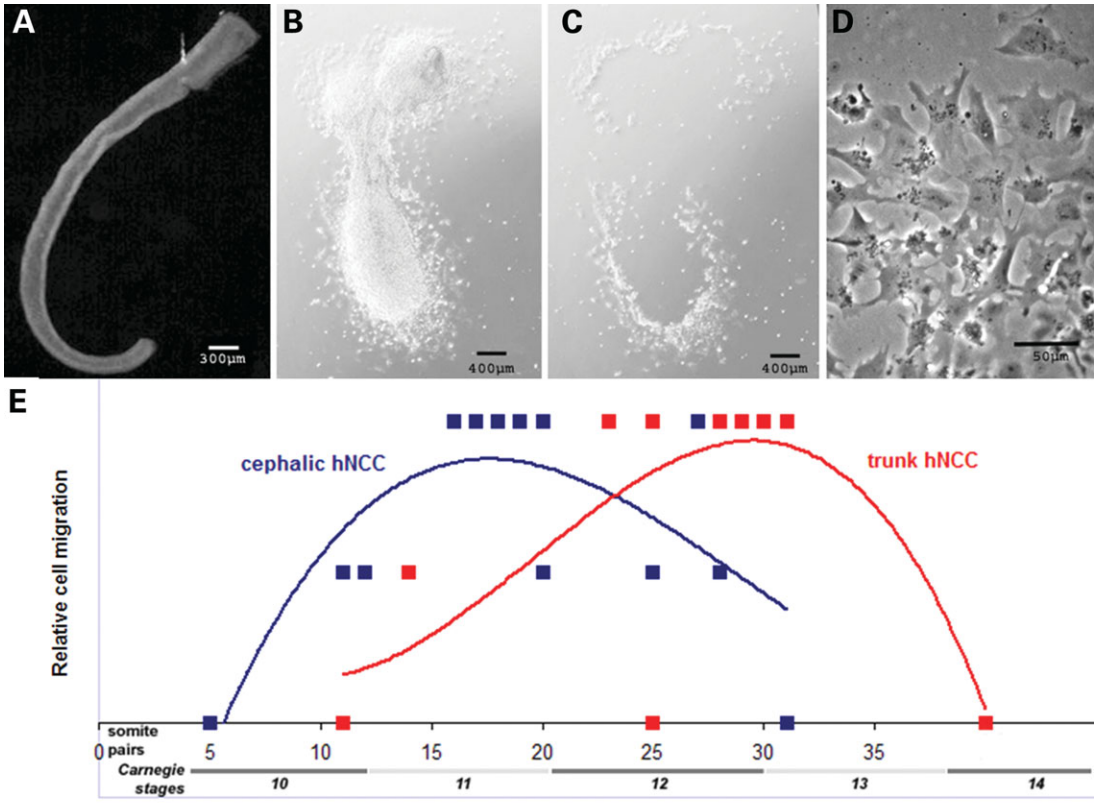

Figure 1. Primary neural crest cells can be isolated from human embryos. (**A**) Human neural tube (NT) from an embryo at Carnegie stage (C)13. (**B**) After 16 h, most hNCC have migrated away from the dorsal NT. (**C**) The intact NT is detached from the culture dish. (**D**) An enriched hNCC population remains, phenotypically similar to murine or avian NCC. (**E**) Empirical evaluation of hNCC migration (none to few, some and many) from 31 explanted neural tubes. Third-order polynomial regressions reflect the rostral-to-caudal temporal maturation gradient of the human NT and maturation of NCC. Peaks occur during C11 at cephalic levels, and during late C12 at rostral trunk levels (segments extending from somites 5 through the last-formed somite pair).

intense study in many vertebrate species. Almost nothing is known about the endogenous characteristics of human (h)NCC, as they mix with other cell types almost immediately. Genetic errors influencing hNCC development seem to be the basis of such common birth defects as congenital heart defects, Hirschsprung disease (HSCR), labiopalatine clefting or cancers such as neuroblastoma and pheochromocytoma, collectively known as neurocristopathies (reviewed in 14). We set out to identify molecular networks that were activated in an early hNCC population before they dispersed to their final sites of differentiation.

To address this issue, we first determined the precise time window during which hNCC separate from the developing neural tube. We then derived primary cell lines that self-renew without a feeder layer and can be propagated and frozen for many cycles. This had not been accomplished to date with NCC from any other species. Rather than focus on known pathways, we examined their entire transcriptome using SAGE to determine an intrinsic molecular profile. A subset of transcripts was validated using RT–PCR, immunohistochemistry and *in situ* hybridization to check representativity. When compared to published data from murine or avian counterparts, hNCC activate novel signaling pathways on top of many evolutionarily conserved modules. Furthermore, the hNCC transcriptional profile was highly evocative of the molecular signature of human embryonic stem (hES) cells, including but not restricted to the expression of the transcription factors *SOX2*, *NANOG* and *POU5F1*. These data indicated that after separation from the neuroepithelium, the plastic hNCC population remains poised to respond to lineage-inductive cues, using much the same transcriptional machinery as hES cells to delay differentiation.

RESULTS

Human neural crest cell isolation

In order to study hNCC before they migrated among unrelated cell types, we first determined the stages during which they emigrate from the dorsal neuroepithelium. To this end, 31 human neural tube fragments from embryos with normal trophoblast karyotype and ranging between Carnegie stages (C) 10 and C14 were isolated and plated on collagen I-coated culture dishes for 16 h (Fig. 1A) in conditions similar to those used in animal model systems (15,16). Cephalic neural tubes (from prospective diencephalon through the rhombencephalon) yielded a halo of hNCC spread onto the dish surface between late C10 to late C12 [23–27 days post-fertilization (dpf); Fig. 1B and C]. A similar halo formed around lengths of trunk-level neural tube caudal to somite 5 between the stages C11 and C13 (24–29 dpf), but not around neural tube fragments taken from outside these spatiotemporal boundaries (Fig. 1E). The neural

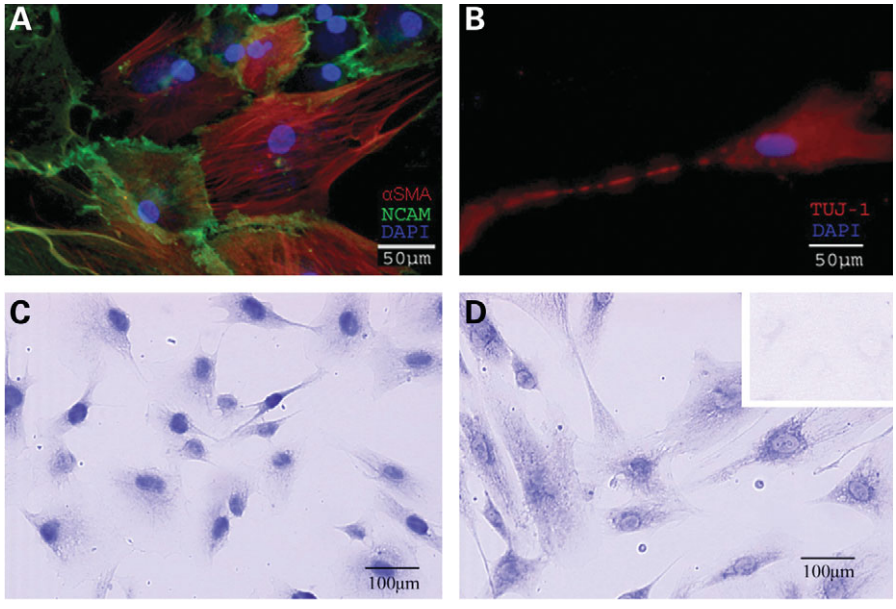

Figure 2. Protein markers of hNCC indicate a heterogeneously uncommitted phenotype. *In vitro*, hNCC synthesized (**A**) α-smooth muscle actin and/or NCAM, separately and sometimes in the same cells; (**B**) neuron-specific beta III tubulin; (**C**) nuclear SOX9; (**D**) nuclear and cytoplasmic SOX2; and unpolymerized GFAP (not shown). Pigment or immunoreactivity to calcitonin or tyrosine hydroxylase was never observed in these culture conditions. Inset: negative control with non-specific primary antibody.

tube was then detached and removed (Fig. 1C), leaving a highly enriched NCC population with a characteristic, fibroblast-like morphology (Fig. 1D). Four cephalic and eight trunk-level cell lines were derived and propagated. Cells remained euploid and morphologically unchanged after more than 20 passages and multiple freeze/thaw cycles. The population doubling time of hNCC cell lines is 40–48 h and does not change substantively after 9 months *in vitro*.

Using immunohistochemistry, we observed that some hNCC expressed proteins typical of partially committed progenitors in avian and murine NCC cultures, such as alpha smooth muscle actin, neural cell adhesion molecule (NCAM) (Fig. 2A) and glial fibrillary acidic protein (not shown). We never observed the hNCC derivative-specific markers tyrosine hydroxylase or calcitonin; however, occasional neurons, revealed by neuron-specific class III beta-tubulin (TuJ-1) staining, were present in cultures (Fig. 2B). The SOX9 protein, which is crucial for differentiation of the full range of NCC derivatives (17), was localized mostly in the nucleus (Fig. 2C). In contrast, the SOX2 protein, a marker of both stem cells and uncommitted neuroepithelium (18), was both nuclear and cytoplasmic (Fig. 2D).

These observations suggest that individual hNCC within a given cell line are poised at various stages of lineage commitment, as observed in animal models immediately after delamination from the neuroepithelium (19,20).

Serial analysis of gene expression and validation

For complete transcriptional characterization of hNCC, we used a modification of the Serial Analysis of Gene Expression (SAGE) technique (21) to generate 'long' 21 basepair tags, representing gene transcripts among the total RNA derived from trunk-level hNCC. These cells have been isolated from a C13 female embryo with a normal trophoblast karyotype and passaged seven times at the time of the analysis. Sequencing of 3546 clones yielded 50 500 tags after exclusion of duplicated ditags (GEO accession GSM207304). Of these, 22 797 were unique tags, representing 8831 transcripts with distinct UniGene identifiers. Of the unique tags, 39% could not be reliably assigned to known mRNAs.

To validate the SAGE data, we examined the expression of 55 genes identified as present in the hNCC library using semi-quantitative RT–PCR (Fig. 3; Supplementary Material, Fig. S1). Among the transcripts tested, 50 were represented by tags with very low (≤ 3) to low ($3 < n < 10$) abundance, or less than 0.02% of total transcripts. Nearly all (96.4%) were confirmed, including all 20 genes with three or fewer tags (Supplementary Material, Table S1).

Eighteen classical signature RNAs of amniote NCC (22,23) were expressed in five different trunk-level hNCC lines, including the one used for SAGE analysis (N5 in Fig. 3). These included transcription factors such as *FOXD3*, *MSX1*, *SNAI2*, *SOX9*, *SOX10* and *TWIST*, as well as signaling molecules or membrane-bound receptors such as *RET*, *GJA1*, *EDN1*, *EDNRB*, *NESTIN*, *NOTCH1, P75*, *PDGFA*, *PDGFB* and *PDGFRB* (Fig. 3A).

All transcripts tested were present in the five hNCC lines as well as in the stage C12–C13 trunk-level neural tubes from which the NCC emigrate, with the exception of *PAX3* and *PAX6*, absent from line N3. The embryonic C13 liver bud also expressed most of these genes. We examined a subset in cDNA from adult human liver, and again, many were detected (Fig. 3A). This expression was not artefactual, as *PAX6* was not expressed by the liver bud, or *MSX1* by the adult liver. Transcripts, such as *PAX3*, *FOXD3*, *NES* and *TWIST*, appeared more abundant in hNCC than in the embryonic liver, unlike *GJA1* or *SMAD2*. We confirmed that the sensitivity of the semi-

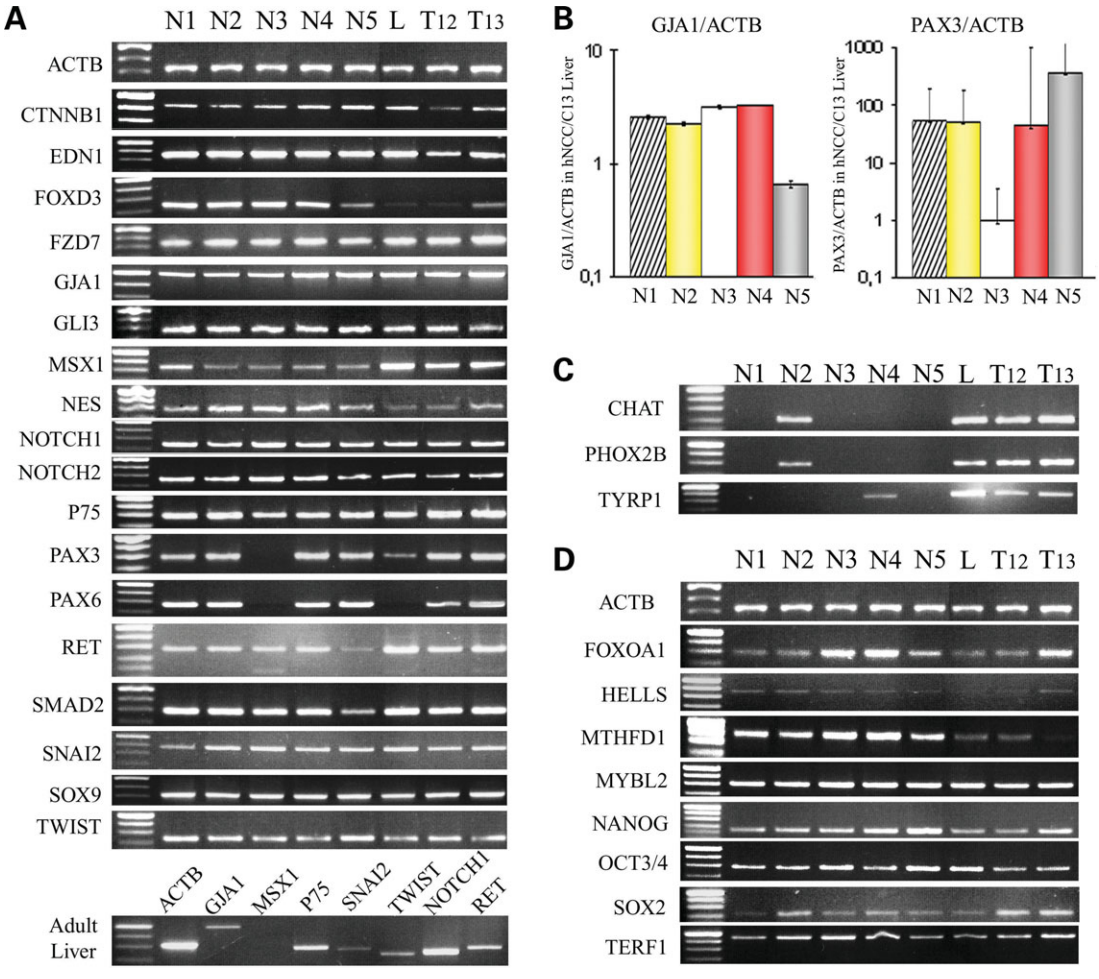

Figure 3. Expression validation of the hNCC SAGE bank. (**A**) Presence in five distinct hNCC lines (N1–N5) of typical animal NCC gene transcripts, as shown by RT–PCR. Most of these genes are also expressed in the C12 and C13 human neural tube (T12 and T13) and in the C13 liver bud (L), as well as in the adult human liver, below. (**B**) *GJA1* (*CX43*) and *PAX3* are expressed more in hNCC than embryonic liver. *ACTB* expression was used to normalize the data before calculating the expression ratio of each gene in the five hNCC lines compared to the C13 liver bud. (**C**) Choline acetyltransferase (*CHAT*) and paired-like homeobox 2b (*PHOX2B*) are expressed by sympathetic neurons and tyrosinase-related protein 1 (*TYRP1*) by melanocytes, both hNCC derivatives: none of the five hNCC lines express all three markers while T12/T13/L samples do. (**D**) Expression in the five distinct hNCC lines of genes reported in the literature as highly characteristic of hES cells.

quantitative approach masked discrete differences in expression levels by quantitative RT–PCR. *PAX3* transcripts were at least 50-fold, and *GJA1* at least 3-fold, more abundant in hNCC compared to the embryonic liver bud, when normalized to *ACTB* abundance (Fig. 3B). In addition, three genes unrepresented in the hNCC SAGE bank and characteristic of differentiated hNCC progeny (Fig. 3C, *CHAT* and *PHOX2B*, sympathetic neurons; *TYRP1*, melanocytes) were not amplified by semi-quantitative RT–PCR in the original hNCC line used (N5). However, the sympathetic markers were detectable in line N2 and *TYRP1* in line N4.

We finally examined the spatial expression of a selection of genes identified by SAGE using *in situ* hybridization on human embryo sections at C13 (Fig. 4). *SOX11* and *MAZ* code for transcription factors and *GJA1* for a critical gap junction protein; other genes we studied (not shown) include the transcription factors *SOX10* (24), *ZEB2* (25) and *CHD7* (26) and *HEYL*; the receptors encoded by *NOTCH2* and *FGFR2*; and the cytoskeleton-associated *CTNNB1* and *MID1* (27). All were expressed in both the neuroepithelium and NCC, with the exception of *SOX10*, which only postmigratory hNCC appeared to express at C13. In addition, *SOX11* (Fig. 4B), *GJA1* (Fig. 4C, F and I) and *MAZ* (Fig. 4D) were transcribed by mesodermal derivatives: *GJA1* by the pronephros, limb bud mesenchyme and, like *SOX11* and *MAZ*, the dermamyotome. Endodermal epithelia expressed *FGFR2*, similar to later stages (28). All genes tested were, therefore, expressed by other tissues, notably by the source neuroepithelium, in addition to hNCC at C13. As in animals, *SOX10* (24) and *FOXD3* (Fig. 3) appeared to be more expressed by early postmigratory hNCC than the neural tube.

Overall, these results show that this hNCC SAGE bank accurately reflects the gene activity of line N5. Its transcriptome is generally representative of hNCC isolated in this manner, although quantitative expression level differences indicate that hNCC lines may be individually heterogeneous, as for other stem cell lines. Moreover, the *in situ* data confirm that gene transcripts that are present in the N5

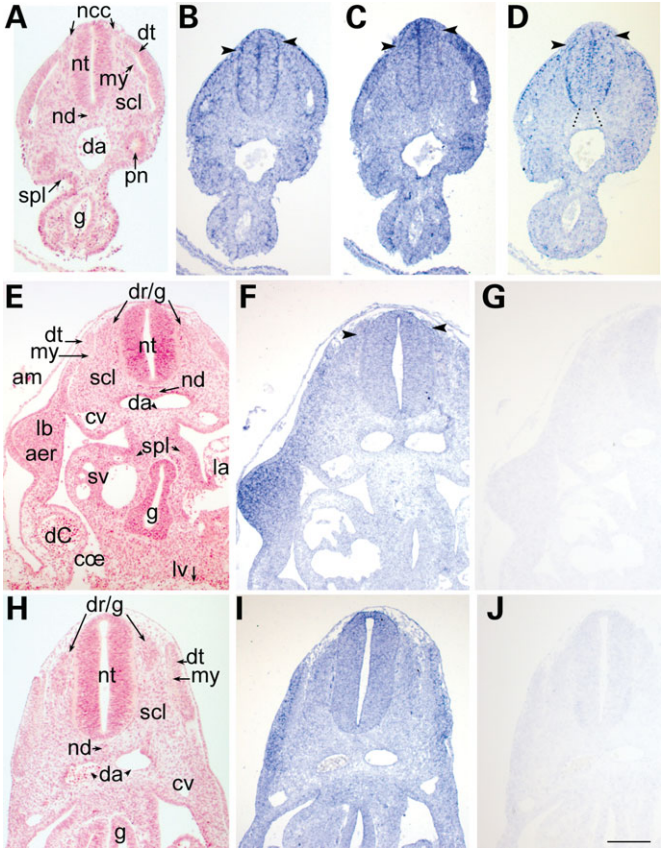

Figure 4. *In situ* expression of *SOX11*, *MAZ* and *GJA1* in the human embryo. (**A**) Hematoxylin-eosin (HE) stain of caudal trunk-level transverse section at stage Carnegie (C)13. (**B**) Adjacent section. Presumptive dermatome, neural tube excluding floorplate, pronephros and splanchnopleural mesoderm and neural crest cells (arrowheads) express *SOX11*. (**C**) The same tissues express *GJA1* in a simultaneously hybridized adjacent section. Expression is higher in the dermatome, dorsal neural tube and migratory neural crest cells (arrowheads). (**D**) *MAZ* is expressed in an adjacent section in most of the neural tube aside from the floorplate (indicated as extension of dotted lines), and lightly in neural crest (arrowheads), dermamyotome and pronephros. (**E**) Forelimb-level HE transverse section in separate C13 embryo. (**F**) *GJA1* antisense probe-hybridized adjacent section. Limb bud, dorsal neural tube and dorsal roots (arrowheads) hybridize more strongly than other tissues, nearly all of which have some basal *GJA1* expression. (**G** and **J**) *GJA1* sense probe-hybridized adjacent section to previous frame, demonstrating specificity of antisense hybridizations. (**H**) Rostral trunk-level HE section of same embryo as in (A–D). (**I**) *GJA1* is highly expressed in the dorsal neural tube, the dorsal roots and ganglia, the dermatome and the splanchnopleural mesoderm, with basal expression in all other tissues of the section as compared with (J). Abbreviations: aer, apical ectodermal ridge; am, amnion; cœ, cœlom; cv, cardinal vein; da, dorsal aorta; dC, duct of Cuvier; dr/g, dorsal root more or less in plane of ganglion; dt, dermatome; g, gut; la, left atrium; lb, limb bud; lv, liver bud; my, myotome; ncc, neural crest cells; nd, notochord; nt, neural tube; pn, pronephros; scl, sclerotome; spl, splanchnopleura; sv, sinus venosus. Bar = 250 μm.

hNCC SAGE bank after cell enrichment *in vitro* are representative of hNCC gene expression *in vivo*.

Interspecies NCC transcriptome comparisons

Most genes that are commonly used to characterize NCC in animal studies are expressed by hNCC as well. Of the 58 transcripts identified in an early survey of avian NCC cDNAs (23), 95% were also observed in the hNCC SAGE bank; some of these have many human paralogues (Supplementary Material, Table S2). A more comprehensive effort using SAGE on mouse NCC after 2 (mNCSC) and 7 (mNCP) days of culture (22) identified approximately 6000 murine gene transcripts. Of these, 67.2% have orthologues in hNCC (Fig. 5A). However, more than 4000 additional Unigene clusters were present only in the human cells. This correlates with such phenotypic differences observed *in vitro* as the adherent human cell independence from a feeder layer and unlimited ability (to date) for propagation without large-scale arrest and differentiation.

The IDEG6 web tool (29) was applied and yielded a list of more than 6000 genes that were differentially regulated in hNCC with statistical significance compared to the combined gene list of mNCSC/NCP. Ontological analysis of the differential group of genes indicated that the most enriched functional categories in hNCC were cell signaling, cell death, gene expression, cellular growth and proliferation and cell-cycle regulation (Fig. 5B). Furthermore, genes annotated as functioning within the insulin, Shh, Wnt and other growth factor signaling pathways were enriched in the human cells (Fig. 5C and D).

Cluster and pathway analyses of whole transcriptomes show similarity between hNCC and embryonic stem cells

In order to assess the global functional significance of the hNCC gene list relative to a variety of other human cell and tissue types, we undertook average linkage hierarchical clustering of the gene lists, using SAGE transcriptome data from 14 other non-transformed samples. This analysis grouped hNCC at a distance from tissues derived from other germ layers, such as the kidney or skeletal muscle, but also from tissues of embryologically closer lineages, such as adult Schwann cells (30) or most of the central nervous system. The closest clustering was observed with hES cell lines hES3 and hES4 (31), in contrast to human mesenchymal stem cells (32) (Fig. 6A). One interpretation of these observations is that transcriptomes cluster cell or tissue types by progenitor commitment rather than embryological origin.

In line with this interpretation, hNCC express many genes considered to play essential roles in the maintenance of multi-/pluripotency. *NANOG*, *POU5F1* (*OCT3/4*) and *SOX2* (33–35), considered emblematic of embryonic stem cells, are all synthesized by hNCC (Fig. 3D). In humans, we observe widespread transcription of *NANOG* and *POU5F1* at pharyngula stages (Fig. 6B–D). Expression remains high in central and PNSs at C15 (Fig. 6E–G) and C17–18 (Supplementary Material, Fig. S2), but decreases dramatically in most other somatic tissues. Many other established stem cell markers such as *CD24*, *FOXH1* and *LIN28* are transcribed by hNCC (Fig. 3D), as are *MYBL2*, *HELLS*, *EPHA1*, *GPR23* and *PHC1* (36).

SOX2, *NANOG* and *POU5F1* co-occupy and appear to positively regulate 180 promoter targets in hES cell line H9 (37). Of these targets, 110 are expressed by hNCC, when compared with the 98 transcribed by hES3 and/or hES4 (Supplementary Material, Table S3). The comparison of quantitative transcriptional levels of common co-occupied targets between hNCC

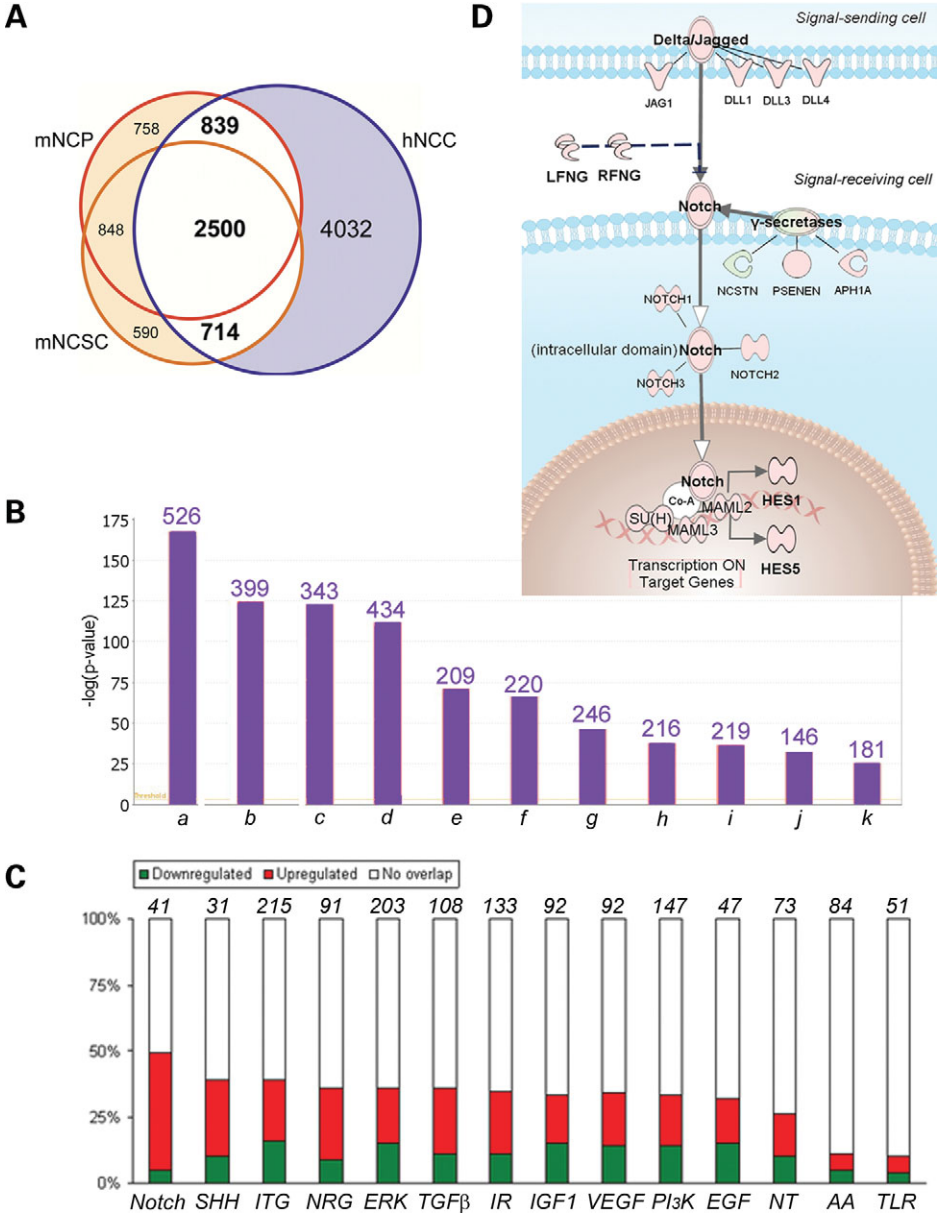

Figure 5. Human and mouse neural crest transcriptomes have much in common but are also species-specific. (**A**) Venn diagram with common and specific genes to hNCC, mouse (m)NCSC (early cultures) and mNCP (later cultures) as described by Hu *et al*. (22). (**B** and **C**) Functional annotation of those hNCC genes differentially expressed ($P < 0.001$; Fisher's exact *t*-test with Benjamini–Hochberg correction for multiple testing) with respect to the combined set of m(NCSC+NCP). (**B**) Statistically over-represented functional groups in hNCC with number of molecules assigned to a given group over each bar. (**C**) Under- and over-expression of genes assigned to individual pathways in hNCC relative to the mouse represented in green and red, respectively. White represents those members of a category absent from one or the other dataset. (**D**) Schematic view of individual components of part of the Notch pathway from (C) with the same color convention, as expressed in hNCC. In contrast to mNCSC/mNCP, hNCC express many Notch ligands, receptors, co-activators, effectors and transcriptional targets. Abbreviations: a, cell signaling; b, cell death; c, gene expression; d, growth and proliferation; e, cell cycle; f; cytokinesis; g, nervous system development and function; h, cell morphology; i, cell–cell interaction; j, embryonic development; k, hematological system development and function; AA, eicosanoids; EGF, epidermal growth factor; ERK, Microtubule-associated protein kinases; hNCC, human neural crest cells; IGF1, insulin-related growth factor 1; IR, insulin receptor; ITG, integrins; mNCP, mouse neural crest progenitors; mNCSC, mouse neural crest stem cells; NRG, neuregulins; NT, neurotrophins; PI3K, Phosphoinositide 3-kinases; SHH, sonic hedgehog; TGFb, transforming growth factor beta family; TLR, Toll-like receptors; VEGF, vascular endothelial growth factors.

and hES3/4 shows that levels of these genes are globally similar among these three cell lines but differ from bone marrow- or umbilical cord-derived mesenchymal stem cells, adult liver or lung (Fig. 6H). Finally, among 280 genes considered to be stem cell-specific after comparison of seven genetically independent hES cell lines (38), 120 are co-expressed by hES3/4 and hNCC (Supplementary Material, Table S4).

Identical broad-category molecular networks were statistically over-represented ($P < 0.001$) in hES and hNCC SAGE libraries (Supplementary Material, Fig. S3), although this

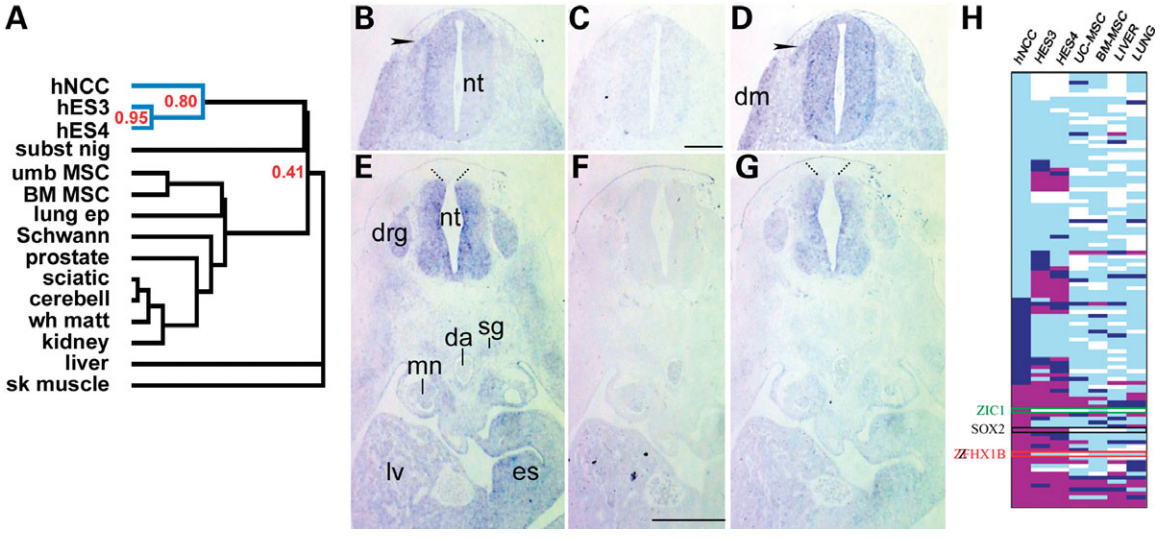

Figure 6. Pluripotent stem cell markers are expressed by uncommitted hNCC. (**A**) Hierarchical cluster dendrogram of hNCC-expressed transcript list compared to 14 publicly available, normal human tissue SAGE banks (uncentered correlation, average linkage). The global transcriptome of hNCC is most similar to two hES cell lines (hES3 and hES4) relative to the transcriptomes of the substantia nigra (subst nig); mesenchymal stem cells from the umbilical cord (umb MSC) or bone marrow (BM-MSC), highly similar to each other by this analysis; pulmonary epithelium (lung ep), Schwann cells *in vitro*, prostate, sciatic nerve, cerebellum, brain white matter (wh matt), kidney, liver or skeletal (sk) muscle. Correlation coefficients are indicated in red. (**B**) Expression of *NANOG* mRNA in transverse section of human Carnegie stage 13 (C13) embryo (cf. Fig. 4H) is discrete but present in neural tube, neural crest cells in the dorsal root (arrowhead) and dermatome, when compared with a sense probe hybridized adjacent section (**C**). (**D**) Expression of *POU5F1* in simultaneously hybridized adjacent section is more visible in equivalent structures, and seems to have a widespread basal expression in all tissues. (**E**) *NANOG* expression at C15 (cf. Fig. 9F and G). After a few days' growth, expression is more distinct in the proliferating neuroepithelium, dorsal root ganglia, the motor horns, stomach, sympathetic ganglia, liver bud and migrating myotome cells. (**F**) Adjacent section hybridized with sense probe. (**G**) *POU5F1* is expressed in a similar pattern. Both *NANOG* and *POU5F1* transcripts appear to be excluded from the roofplate of the neural tube at this stage (extension of dotted lines). (**H**) Heat map of target genes whose promoters can be co-occupied by *SOX2*, *NANOG* and *POU5F1* in hNCC, hES3, hES4, BM-MSC, UC-MSC, adult liver and lung cells, respectively. White stands for a tags-per-million (tpm) value equal to 0, light blue for $1 \leq$ tpm ≤ 49, dark blue for $50 \leq$ tpm ≤ 100 and magenta for tpm value >100. Global modulation is similar in hNCC and hES3/4 compared to the more distantly clustered cell types; for example, *SOX2* itself, although other genes are expressed differentially, such as *ZIC1 or ZFHX1B*. Abbreviations: da, dorsal aorta; dm, dermamyotome; drg, dorsal root ganglion; es, stomach; lv, liver; mn, mesonephros; nt, neural tube; sg, sympathetic ganglion.

observation mostly reflects the gross resolution of such ontologies. More detailed analysis showed that human NCC and ES cells synthesized 840 mRNAs in common that are annotated as involved in 'transcriptional regulation' (Supplementary Material, Table S5). Of these, 114 transcription factors (Supplementary Material, Table S6) included targets of characterized growth factor (*SMAD1/3/4/5*, *CREBBP*, *STAT1/3*, *SRF*, *JUN*, *CUTL1*, *ELK1* and *FOS*) and steroid hormone (*RARA*, *RXRA*, *RXRB*, *RARG*, *NR1D2* and *VDR*) signaling pathways. When transcriptional regulation genes were also expressed by the multipotent BM-MSC or the liver, there was wide fluctuation in expression levels between cell types, which was not the case for the hNCC–hES comparison.

The second most over-represented classification of gene products common to hNCC and hES was that of 'cellular proliferation and growth'. Within the category, hNCC, hES3 and hES4 expressed 1088 genes in common (out of 1350, 1712 and 1601, respectively, in this category) that regulate cell cycle progression and encode growth factors, hormone and cytokine receptors and their effectors (Supplementary Material, Table S7). In all stem cell lines, more members of the hedgehog, fibroblast growth factor, Wnt, transforming growth factor-β, Notch and vascular endothelial growth factor signaling pathways are expressed than in the adult liver transcriptome. In physiological contrast, only the BM-MSC and liver transcribed a statistically significant proportion of genes that are classified as part of the complement system (Supplementary Material, Fig. S3).

Quantitative transcript levels of individual components assigned to statistically over-represented signaling pathways are similar among the hNCC, hES3 and hES4 cells relative to the MSC, liver and lung (Fig. 7), as indicated by the cluster analysis (Fig. 6A). In fact, such pathways are functionally interconnected, as demonstrated by the expression of many intracellular components assigned to both integrin-related and IGF-related cascades (Fig. 8).

In summary, at multiple levels, the type and proportional representation of RNA transcripts in hNCC are most similar to the least committed cell types included in these analyses, the hES cell lines.

Neural crest-specific marker profile

To filter for those transcripts most specific to hNCC that might reside in postnatal tissues, we performed tissue preferential expression (TPE) analysis (39), using SAGE data from 14 other normal postnatal human cells or tissues, initially excluding hES cells. TPE is based both on the number of tissues in which a gene is present (range of expression) and its quantitative expression level in each. A score for each gene was plotted against the number of times that each gene was observed among the list of all tissues (Supplementary Material,

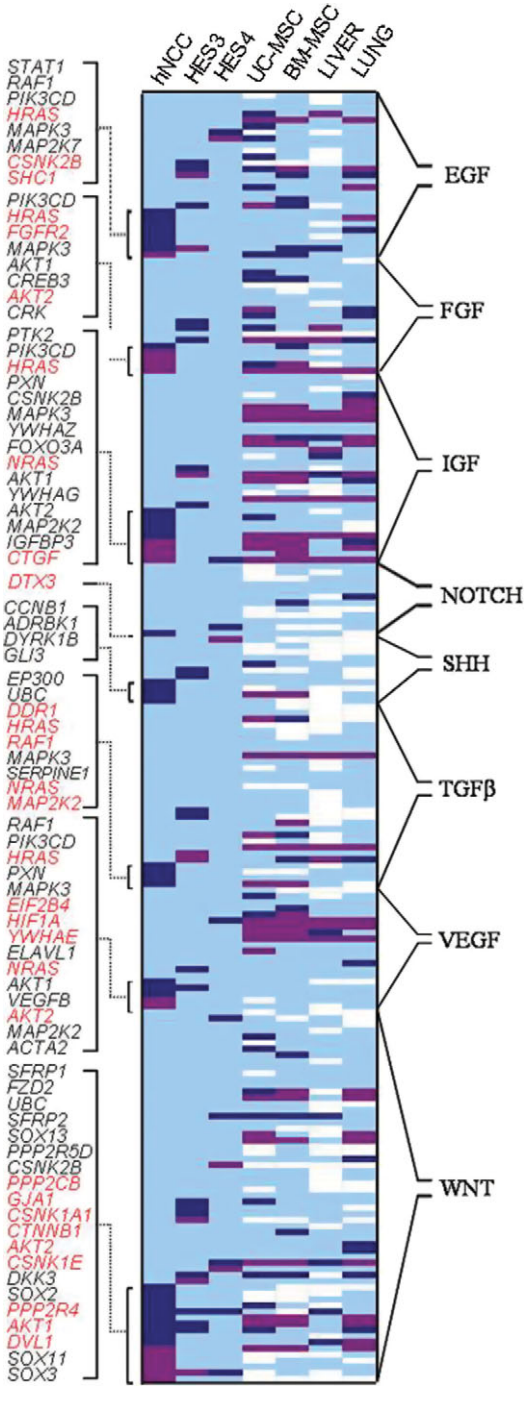

Figure 7. Growth factor pathways are similarly activated in hNCC and hES cells, relative to other cell types. Heat map representing expression levels in hNCC, hES3, hES4, UC-MSC, BM-MSC, adult liver and adult lung cells of lists of genes attributed by IP software to various signaling pathways. These include but are not exclusive to the epidermal growth factor (EGF), fibroblast growth factor (FGF), insulin-like growth factor (IGF), NOTCH, Sonic hedgehog (SHH), transforming growth factor (TGF)-beta, vascular endothelial growth factor (VEGF) and WNT pathways. Gene symbols for the more abundant hNCC tags are listed on the left, with high concomitant hES expression in red text. White, tags-per-million (tpm) value equal to 0; light blue, $1 \leq$ tpm ≤ 49; dark blue, $50 \leq$ tpm ≤ 100; magenta, tpm value >100.

Fig. S4). Functional annotation of the 1248 genes with TPE range = 15 correlated their ubiquitous expression with the finding that ~60% are structural ribosome constituents or proteins involved in primary cellular energy metabolism.

The hNCC most-specific gene list (range = 1) contained 119 transcripts (Supplementary Material, Table S8), many of which are involved in the regulation of transcription and DNA-histone packaging. Parallel analyses of hES3 or hES4, excluding the other hES cell line and hNCC, demonstrated that 48 of these 119 also had a TPE range = 1 in each. Thus, across the 16 distinct human cell and tissue types examined, 43 low-abundance transcripts were most specific to hNCC (Table 1) and 27 of these are also transcribed by C12–13 embryonic neuroepithelium (results not shown), in keeping with other expression data (Figs 3, 4, 6 and 9).

Of the 20 TPE = 1 genes that are currently annotated by Gene Ontology, half encode DNA-binding proteins such as DBX2 (40), ZNF157, HOXC5 and TIGD3. We confirmed hNCC expression of *HOXC5*, *C2ORF63 (FLJ31438)*, *ZNF417* and *AMIGO3* by RT–PCR in five distinct hNCC lines (Fig. 9A). Adult liver also transcribes *ZNF417* and *AMIGO3*, although transcript abundance was below the threshold of SAGE detection in a publicly accessible liver bank with 66861 short (10 bp) tags, accounting for the TPE result. *HOXC5* expression pattern in whole human embryo sections (Fig. 9B–G) correlates well with trunk-level neural tube expression (rhombomere 8 and caudal) noted in mouse embryos (41). Indeed, *HOXC5* is one of only three genes from this list whose orthologue is transcribed by mNCSC/NCP (22), although many of the other human transcripts are novel and do not yet have validated orthologues. *HOXC5* is expressed by hNCC entering the dorsal root, within the neural tube, in hypaxial muscle precursors (Fig. 9D) and in limb mesenchyme (Fig. 9B). Transcripts are more easily detected at C15 in the ventral motor horns, median ventricular zone and floorplate, dorsal root ganglia, as well as in the forming vertebral bodies, muscle precursors and stomach wall (Fig. 9F).

On the whole, these results show that hNCC can naturally be distinguished from hES cells by the expression of a highly specific and small subset of markers. However, like hES cells, hNCC keep many molecular characteristics of their *in vivo* embryonic phenotype, as well as the capacity for self-renewal *in vitro*.

DISCUSSION

The stem cell profile of hNCC

The shared transcriptional signature between hNCC and hES cells was startling. Trunk-level NCC in animals have been historically described as relatively oligopotent compared to the cephalic NCC. However, the extent and onset of trunk-level NCC lineage restriction remains controversial (42). *In vivo*, cartilage and bone, smooth muscle and adipocytes (among other derivatives) come either from the trunk mesoderm or the cephalic neural crest. Avian trunk-level NCC have the

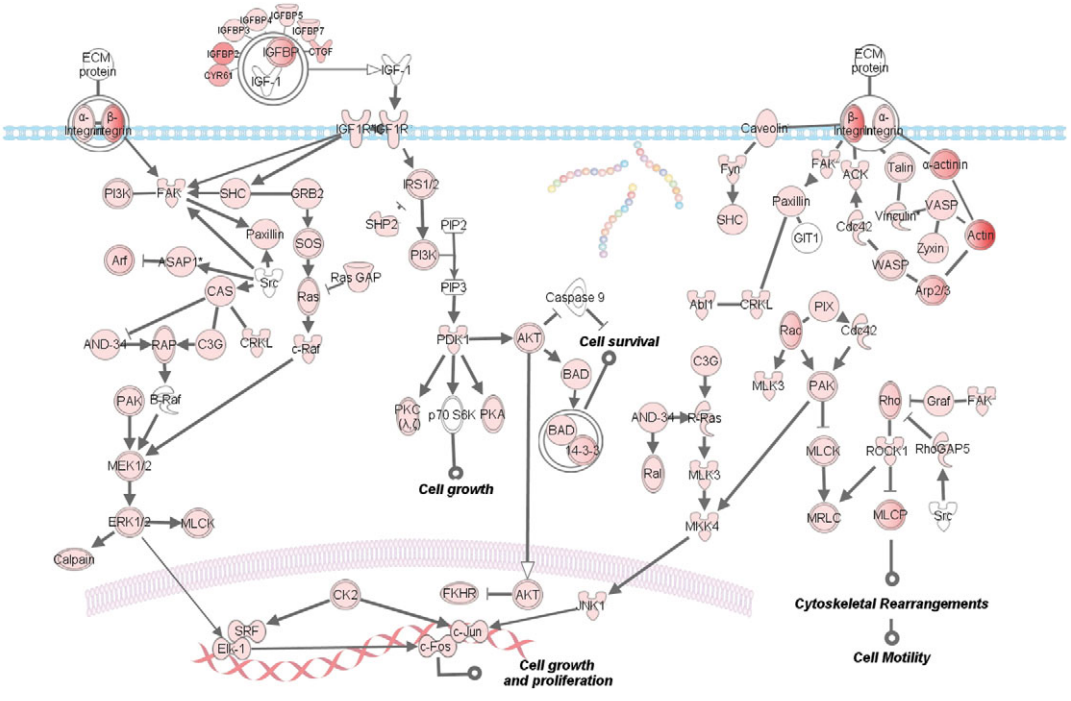

Figure 8. Schematic view of part of the IGF-1 and integrin signaling pathway genes transcribed by hNCC. Pink-tinted symbols are genes expressed by hNCC, and documented physical interactions exist for each edge depicted.

ability *in vitro* to not only give rise to cartilage and bone (3) and smooth muscle cells (43), but to adipocytes as well (44). Cartilage, bone, smooth muscle and adipocytes can of course also differentiate from BM-MSC, as many studies attest. Interestingly, Takashima *et al*. (13) have demonstrated that some murine BM-MSC in fact are seeded by neuroepithelial-derived NCC. We expected to find a closer relationship to BM-MSC or neural crest derivative transcriptomes than to hES lines.

Our data, therefore, have some provocative implications for the use of 'markers' in developmental biology. For example, like in hES lines, some early markers of definitive embryonic endoderm (*FOXA2*, *GPC1*, *TM4SF2* and *CXCR4*) are found in the hNCC bank, but not others (*SOX17* and *HHEX*). This hints that hNCC may have the potential to add new, non-physiological progeny to the already extensive list of *in vivo* derivatives; an overlapping contingent of these genes is expressed by the fully pluripotent hES3 line (31). However, under some initial conditions varying the physical matrix, seeding density and the proportions of exogenous growth factors (available upon request), we have not yet successfully oriented hNCC differentiation *in vitro*. A novel set of conditions that remains to be tested is a medium free specifically of blocks to β-catenin signaling and ERK activation, inhibitors of which are necessary and sufficient for mouse ES cell self-renewal (45).

The simultaneous transcription of *SOX2*, *NANOG* and *POU5F1* is not sufficient to confer ES identity, since we find all three in the hNCC lines. In addition, hNCC express *LIN28*, many members of the *KLF* gene family and *MYCN*, *MYCL1* and a number of MYC-binding proteins. Forced expression of various combinations of members of two of these gene families with *POU5F1* and *SOX2* have all led to pluripotent stem cell induction from human somatic cells (46,47).

Somatic cells from the pharyngula-stage embryo, such as these hNCC, may have a closer ground state to a pluripotent phenotype than do adult somatic cells, with their very low frequency of inducibility. With respect to 'pluripotency' markers, chicken embryonic neuroepithelium and neural folds express *Sox2* from stages preceding NCC formation (48). In contrast with our findings in human embryos, *in situ* hybridization does not demonstrate the presence of *Nanog* transcripts at neurula/pharyngula stages of mouse development (49). However, *Pou5f1* (*Oct3/4*), although best known for its expression by the murine germ-cell lineage and cell lines derived therefrom, is also expressed by both embryonic ectoderm and neuroepithelium (50), and it plays a permissive role in all germ layers in zebrafish (51). We interpret the similar molecular signature of hNCC and hES cells as an unprecedentedly detailed example of a homologous developmental process (52) underlying the state of multipotency. Further studies will be necessary to test the ability of hNCC *in vivo* to differentiate into functional cells representative of any or all tissue types with a teratoma assay; a better test would be their ability to contribute to chimeras, in particular to the germ line of such chimeras, before claims of pluripotency could be supported. However, for ethical and practical reasons, such experiments are impracticable by our laboratories.

Comparative embryology

In humans, as in other vertebrates, there is a lag in time between the peak migration windows for NCC from the cephalic versus

Table 1. Novel hNCC markers

Symbol	hNCC (tpm)	GO annotation Function	Process	Component	EST sources (NCBI) Embryo[a]	Foetus[b]	Adult[c]
AMIGO3	20	Protein binding	Cell adhesion	Membrane	0	1	7
C10ORF85	20	nd	nd	nd	0	3	1
DKFZP761N09121	20	Protein transporter activity	Intracellular vesicle-medicated transport	Golgi-associated vesicle	nd	nd	nd
DNAH1	20	Microtubule motor activity	Ciliary or flagellar motility	Axonemal dynein complex	2	7	84
FAM70B	20	nd	nd	Membrane	0	4	12
FLJ16139=DBX2	20	Transcription factor activity	Regulation of transcription, DNA-dependent		0	0	2
FLJ20345=MKS1	20	nd	nd	nd	5	19	52
FLJ31295=ZNF641	20	DNA binding, metal ion binding	Regulation of transcription, DNA-dependent	Intracellular	4	1	43
FLJ31438	40	nd	nd	nd	1	9	27
FLJ40126=C12orf40	20	nd	nd	nd	nd	nd	nd
GABRR3	20	GABA-A receptor activity	Synaptic transmission	Postsynaptic membrane	nd	nd	nd
HIST1H1D	20	DNA binding, protein binding	Nucleosome assembly, chromosome biogenesis	Nucleosome, chromosome	0	1	1
HIST1H2BE	20	nd	nd	nd	nd	nd	nd
HIST1H2BJ	20	DNA binding	Nucleosome assembly, chromosome organization	Nucleosome, chromosome	0	1	2
HIST1H3B	20	nd	nd	nd	nd	nd	nd
HIST1H4F	20	nd	nd	nd	nd	nd	nd
HMFN0672=C8orf80	40	nd	nd	nd	0	2	0
HOXC5	99	Transcription factor activity	Regulation of transcription from RNA pol II promoter	Nucleus	1	8	10
HOXD9	20	RNA pol ll transcription factor activity	Regulation of transcription, DNA-dependent	Nucleus	0	22	20
KCNG2	20	Potassium channel activity	Ion transport, potassium ion transport	Membrane	nd	nd	Nd
KIAA1822L	20	Catalytic activity	nd	nd	0	1	4
LOC255177	20	nd	nd	nd	0	0	0
LOC352909=C19orf51	20	nd	nd	nd	4	27	56
LOC400340	20	nd	nd	nd	nd	nd	nd
LOC401021	20	nd	nd	nd	nd	nd	nd
LOC401485	20	nd	nd	nd	nd	nd	nd
LOC440502	20	nd	nd	nd	nd	nd	nd
LOC440993	20	nd	nd	nd	nd	nd	nd
LOC441053	20	nd	nd	nd	0	23	177
LOC493860=CCDC73	20	nd	nd	nd	nd	nd	nd
MGC16372=C2orf39	20	nd	nd	nd	0	5	6
MGC48915=C1QTNF9	20	nd	Phosphate transport	Cytoplasm			
PP3856=NAPRT1	20	Nicotinate phosphoribosyltransferase	Pyridine nucleotide biosynthetic process	nd	1	9	64
PRDM12	59	DNA binding, metal ion binding	Regulation of transcription, DNA-dependent	Nucleus	0	2	0
PRH1	20	nd	nd	nd	1	4	353
RHEBL1	20	GTP binding	Small GTPase mediated signal transduction	Intracellular	0	0	6
SH3GLP2	20	nd	nd	nd	nd	nd	nd
STOX2	20	nd	nd	nd	nd	nd	nd
TIGD3	20	DNA binding	Regulation of transcription	Nucleus	0	5	4
UCN	20	Neuropeptide hormone activity	G-protein coupled receptor	Extracellular region	0	0	12
WNT7A	40	Receptor binding, signal transducer activity	Wnt receptor signaling pathway	Extracellular region	0	4	8
ZNF 157	20	DNA binding, metal ion binding	Regulation of transcription, DNA-dependent	Nucleus	0	0	0
ZNF417	40	DNA binding, metal ion binding	Regulation of transcription, DNA-dependent	Nucleus	1	4	13

Genes most specific to hNCC as shown by TPE analysis (range value = 1) and not expressed in hES cells.
[a]Count of human expressed sequence tags, out of 125 776 total from embryonic tissues.
[b]Count of human expressed sequence tags, out of 557 809 total from fetal tissues.
[c]Count of human expressed sequence tags, out of 1 899 694 total from postnatal tissues (UniGene's EST ProfileViewer).

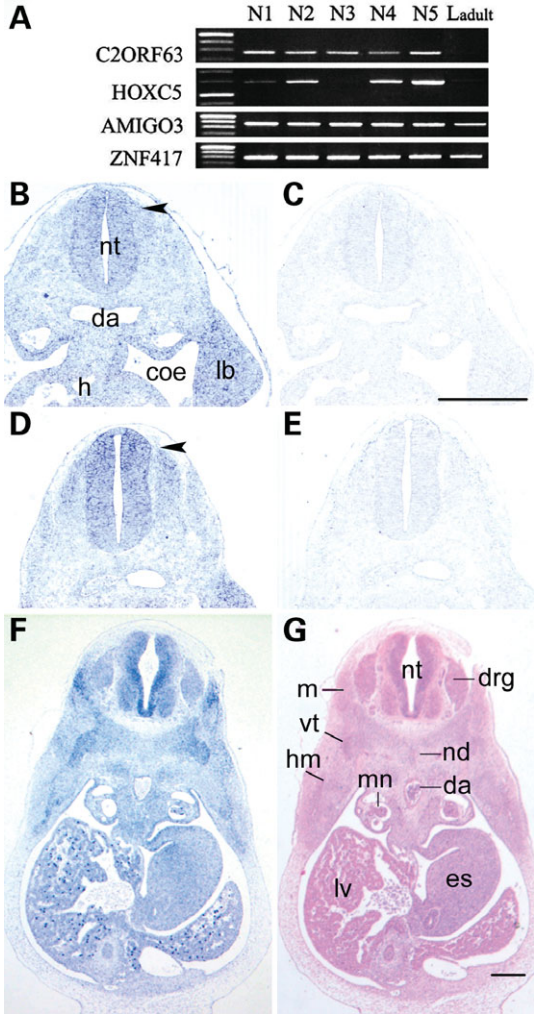

Figure 9. Prediction of mRNA subset specific to hNCC. (**A**) RT–PCR for four genes with TPE score=1 shows that it is possible to amplify *AMIGO3* and *ZNF417* from an adult human liver, although below the level of detection by a publicly available SAGE bank from another sample. *HOXC5* and *C2ORF63* were specific to most or all hNCC lines. (**B**) *In situ* hybridization to *HOXC5* demonstrates expression in the human embryo at Carnegie stage 13 (C13; cf. Fig. 4E) in most cells at the level of the limb bud, with higher levels in the neural tube, the neural crest (arrowhead), the limb mesenchyme and the rest of the somatopleural mesoderm. (**C** and **E**) Sense probe-hybridized adjacent transverse sections to previous frames demonstrate specificity of signal. (**D**) *HOXC5* in a different C13 embryo section taken at a more rostral transverse level than in (B); expression appears reduced in the floorplate relative to the rest of the neural tube. (**F**) At C15 (cf. Fig. 6E–G), *HOXC5* is expressed by the developing vertebra, muscle precursors, ventricular zone of the neural tube and motor horns; it is also transcribed by all other tissues in this section when compared with the sense-hybridized adjacent section (not shown). (**G**) Adjacent HE section. Thus, markers are only specific to a particular cell type within a given spatiotemporal context. Abbreviations: cœ, cœlom; da, dorsal aortae; h, heart; hm, hypaxial muscle precursors; lb, limb bud; lv, liver; m, muscle; nd, notochord; nt, neural tube; vt, vertebra.

the trunk levels. Species differences appear in the uncoupling of migration from that of neural tube closure. We observed that the majority of hNCC migrate after neural fold apposition along the body axis and continue to do so after fusion, similar to other amniotes and amphibia but in contrast to the fish (4). Recent anatomical observations imply that the first cranial hNCC begin migrating well before closure (53), with fusion catching up with hNCC delamination by the hindbrain. These two processes use common molecular mechanisms for the rearrangement of the actin cytoskeleton necessary for both convergent extension (54) and epithelio-mesenchymal transition (EMT)/migration (55), respectively.

Many gene transcripts found in avian or mouse migratory NCC are present in hNCC under their conditions of isolation. However, as many or more appeared to be unique to either mouse or to humans. A larger proportion still was expressed differentially to a statistically significant level. This is perhaps unsurprising considering the phenomenal plasticity of the neural crest lineage and its capacity to engender such diverse and species-specific structures as the turtle shell (56) and the deer antler (57). A greater total tag count in the hNCC bank may also have contributed to the detection of rarer transcripts relative to the mouse SAGE banks.

Among the human-specific expressed genes were a number that fell into characterized signaling pathways from other cellular systems, not necessarily suspected to have a role in the hNCC lineage. One phenotypic difference between human and animal NCC is that mouse cells are described to have a self-renewing potential limited to some weeks (22) while hNCC, cultivated without a feeder layer, can survive many months in our conditions without division arrest or large-scale differentiation. Animal NCC populations appear to be a heterogeneous collection of partially committed progenitors *in vitro*, be they of avian (16,58) or murine (15,59) origin. Henion and Weston (20) concluded that nearly half of the avian NCC from the trunk level was fate-restricted precursors generating a single cell type. Cluster analysis bears out our empirical observations by grouping the cultured hNCC transcriptome most closely with pluripotent embryonic stem cells, rather than with any committed neural crest progeny.

Novel hNCC markers

We have applied TPE to generate two detailed sub-profiles: that of highly specific hNCC markers and another of shared hNCC-hES molecules, which may be applied in the future to cell sorting. Currently, attempts to isolate NCC-like progenitors from human skin have relied on external phenotypic characteristics (10,60). Cell sorting has been used to enrich for rat NCC with tissue-restricted stem cell capacities; however, the marker employed was an elegant but artificial construct only applicable to genetically modified rodents (42). As identified, the rat cells had already become lineage-restricted in their peripheral niche.

Individual transcripts in the most-specific TPE list clearly do not signify NCC identity. The combination of all or a subset of them, and perhaps their quantitative levels, may however be sufficient to uniquely identify hNCC with a similar lack of fate commitment. One advantage of the SAGE approach is illustrated by the fact that 39% of unique tags in the hNCC library could not be reliably assigned to known mRNAs. Some of this ambiguity must be due to sequencing errors or polymorphisms (61), but a large subpopulation probably corresponds to novel transcripts expressed in hNCC. One indication is that 296 (1.3%) of these tags mapped readily to recently predicted natural antisense RNA (naRNA) sequences (62) (Supplementary

Material, Table S9). Others may correspond to primary microRNA transcripts. New membrane proteins will be particularly helpful for fluorescence-activated cell sorting experiments.

The results presented here will help in reliably isolating highly multipotent NCC from pre- or postnatal human tissues. These cells could be used for transplantation therapies in such diseases as peripheral demyelinating neuropathies or HSCR.

Candidate genes for human disease

As a point of comparison between early hNCC and their normal or pathological progeny, this hNCC signature can elucidate the molecular underpinnings of additional diseases. Many genes already known to cause human neurocristopathies are expressed in the hNCC SAGE library, including *PAX3* and *SOX10* (Waardenburg syndrome), *KIT* and *SNAI2* (piebaldism), *MSX1* (tooth agenesis/orofacial cleft), *CHD7* (CHARGE syndrome), and *ECE1*, *EDNRB*, *ITGB1*, *KIAA1279* and *ZEB2* (HSCR). Some neurocristopathies arise from the disruption of hNCC migration and/or the EMT from the neuroepithelium (14). Currently, a limited number of such EMT-associated disease genes include *EFNB1, FOXC1*, *LAMA5*, *SEMA3C* and *SNAI2* and are all known and expressed in this hNCC SAGE bank. The examination of functional modules such as EMT may be a fruitful strategy to identify new neurocristopathy genes. For example, the SNAG corepressor domain of SNAI2, found only in vertebrate homologues of Drosophila *snail*, has recently been implicated in *Xenopus* NCC specification within the neuroepithelium (63). Potential co-repressors *JUB*, *LIMD1*, *TRIP6, WTIP* and *ZYX* are all transcribed by hNCC, demonstrating the utility of such species- and tissue-specific expression banks for integrating dispersed functional data and generating new hypotheses for candidate genes to correlate with known disease loci. The use of our self-renewing hNCC lines for functional analyses of such candidate genes is a particularly appealing application of their potential in all senses of the word.

MATERIALS AND METHODS

Human embryos

Human embryos were collected from pregnancies legally terminated using the mefiprestone protocol, in concordance with French bioethics law 2004-800 and with the approval of the Necker hospital ethics committee.

hNCC isolation

Whole human embryos under 8 weeks' gestation were dissected away from their annexes in ice-cold phosphate-buffered saline (PBS). A piece of chorionic villus was treated immediately for 1 h in colchicine-DMEM before 10 min hypotonic shock in 0.075 M KCl and 1:3 acetic acid:ethanol fixation for three changes of 10 min each. Nuclei were spread, stained for G-bands and chromosomes counted according to standard karyotype procedure. Cephalic neural tube segments were isolated by cutting perpendicular to the long axis behind the optic vesicles and again at somite pair 5, and trunk-level neural tube segments from somite 5 to the last available somite pair. Other tissues were trimmed away and the segment placed in 6 mg/ml pancreatin (Sigma P3292) in PBS for 7 min. Pieces were transferred into clean PBS to tease away all tissues, including the tightly adherent notochord and ectoderm, from neural tubes. The enzymatic reaction was stopped and neural tubes maintained thereafter in complete hNCC medium.

Initial hNCC migration and replating on collagen I-coated plates (Becton Dickinson) used the following medium: Dulbecco's Modified Essential Medium/BGJb (Fitton-Jackson modified)/Ham's F12 [3:1:6 v/v, Sigma] supplemented with 12% complement-inactivated fetal calf serum (PAN Biotech); 1× penicillin/streptomycin (Invitrogen); 2 mM glutamine, 10 mM HEPES, 0.1 μg/ml hydrocortisone, 10 μg/ml transferrin, 0.4 ng/ml T3 (3,3,5-thio-iodo-thyronine), 10 pg/ml glucagon, 100 pg/ml epidermal growth factor, 1 ng/ml insulin and 200 pg/ml fibroblast growth factor 2 (Sigma). Tubes were transferred to the centre of 35 mm collagen-I dishes with 300 μl medium and placed in humidified CO_2 incubators at 37°C for 8 h to facilitate adhesion. One milliliter of medium was then added for a further 16 h, during which cells migrated onto the plastic. Tubes were removed with a fire-polished Pasteur pipette and primary cultures allowed to grow for another day before first replating. Passages were obtained by dissociation from plates using 3 min trypsin-EDTA treatment and complete hNCC medium to stop the reaction. No feeder layer cells or other adjuvants (e.g. leukemia inhibitory factor and embryo extract) were necessary for long-term maintenance for up to 9 months.

Karyotyping

Standard G-band karyotypes were performed on 10 metaphases from fresh trophoblast and thawed embryonic hNCC.

Immunocytochemistry

Cells were prepared for immunostaining by fixation in 4% paraformaldehyde for 20 min and subsequent permeabilization for 25 min with 0.1% Tween-20 in PBS. Primary antibodies: monoclonal anti-α-smooth muscle actin (Cy3-conjugated, Sigma C6198), monoclonal anti-neuron specific class III beta-tubulin (TuJ1) (R&D Systems), polyclonal anti-NCAM (Chemicon), polyclonal anti-tyrosine hydroxylase (Chemicon AB1542), polyclonal anti-calcitonin (Chemicon AB910), monoclonal anti-human glial filament acidic protein (GFAP) (Cymbus Biotechnology), polyclonal anti-SOX9 (Chemicon AB5535) and polyclonal anti-SOX2 (Abcam AB15830). Nuclei were counterstained (Hoechst).

Sage library construction and RT–PCR

Standard protocols (64,65) were used to construct a LongSAGE library from 5 μg total RNA (RNeasy Mini, Qiagen) prepared from trunk-level hNCC of a C13 embryo after 7 passages. In brief, *Nla*III and *MmeI* restriction enzymes (New England Biolabs) were used for tag generation. After 3 h self-ligation, 10′ at 65°C and 2′ on ice, purified concatemers were subsequently cloned into pZERO-1 (Invitrogen). Individual

clones were selected and sequenced. LongSAGE tags (17 bp) were extracted from raw sequence data using SAGE2000 version 4.5 Analysis Software. The LongSAGE tag database was linked to the SAGE Map database (NCBI) and the ACTG web tool (http://retina.med.harvard.edu/ACTG/) (66) for tag-to-gene mapping. The original SAGE data in this paper are available from the NCBI Gene Expression Omnibus (GEO) under accession number GSE8368.

Total RNA from five individual hNCC lines, C12 and C13 isolated neural tubes (four and two pooled, respectively) and four pooled C13 liver buds were prepared using the RNeasy Mini kit (Qiagen); total adult human liver RNA was obtained from Clontech. After reverse transcription (Applied Biosystems), PCR amplifications for gene validations were performed in a final volume of 25 μl using 50 ng of Nanodrop-quantified cDNA and 35 amplification cycles. For quantitative RT–PCR, LightCycler Fast Start DNA Master^{PLUS} SYBR green I (Roche) was used according to the manufacturer's protocol. *ACTB* was used to normalize data for the calculations of ΔCt. Primers are listed in Supplementary Material.

In situ hybridization

Intact, euploid human embryos were processed for *in situ* hybridization as described elsewhere (67). Primers used for DNA matrix synthesis by PCR are listed in Supplementary Material.

Statistical analyses

Hierarchical clustering was performed to create a multi-level binary cluster tree, linking tissue or cell types by similarity. In addition to the hNCC bank, data were obtained from 11 banks of the Gene Expression Omnibus (http://www.ncbi.nlm.nih.gov/geo/): GSM676 (brain white matter), GSM761 (cerebellum), GSM762 (lung), GSM708 (kidney), GSM785 (liver), GSM824 (muscle), GSM31931 (substantia nigra), GSM41359 (hES3), GSM41362 (hES4), GSM48250 (sciatic nerve), GSM48251 (Schwann cells *in vitro*); one from the Cancer Genome Anatomy Project http://cgap.nci.nih.gov/SAGE/SAGELibraryFinder:SAGE_Prostate_normal_B_2 (prostate); and for bone marrow and umbilical cord vein mesenchymal stem cells, data from the website http://bit.fmrp.usp.br/msc_tags/ (32) (current requests for raw data directly to authors). Counts from all SAGE libraries were normalized to a total of one million for input to Cluster 3.0 freeware (http://www.geo.vu.nl/~huik/cluster.htm) (68). Average distances were classed to link samples into clusters. In order to compare and validate the robustness of the results, Euclidean (squared), Pearson (uncentered) and Spearman rank numeric scales were all computed to calculate average distances. The dendogram was made with TreeView freeware (http://jtreeview.sourceforge.net/). Data were functionally annotated using Pathways Analysis 5.0 (Ingenuity Systems) and DAVID software (69).

The TPE analysis (39) was performed with the following additional samples (GEO or CGAP accession numbers): Bone marrow (GSM14784), placenta (GSM14749), muscle (GSM 824), liver (GSM785), stomach (SAGE_Stomach_normal_MD_13), kidney (GSM708), lung (GSM762), breast (SAGE_Breast_normal_myoepithelium_AP_myoepithelial1), prostate (SAGE_Prostate_normal_B_2), ovary (SAGE_Ovary_normal_CS_HOSE_4), endometrium (SAGE_Uterus_endometrium_normal_CS_DI1), brain white matter (GSM676), whole cerebellum (GSM761) and whole spinal cord (SAGE_Spinal_cord_normal_B_1).

For the detection of statistically differentially expressed genes, we used the IDEG6 web tool (http://telethon.bio.unipd.it/bioinfo/IDEG6_form/). The Fisher exact test (significance threshold 0.05) was used with a Bonferroni correction to account for multiple testing (29).

SUPPLEMENTARY MATERIAL

Supplementary Material is available at *HMG* Online.

FUNDING

This work was supported by the Avenir program of the Institut National de la Santé et de la Recherche Médicale, the Consortium National de Recherche en Génomique, the Association Française contre les Myopathies, and Agence National de la Recherche funding (MRAR2007 HIR-GENET). S.T., C.B., P.X. and M.S. are supported by grant NS039818 to M.S. from the US National Institutes of Health. Funding to pay the Open Access Charge was provided by the Fondation pour la Recherche Médicale.

ACKNOWLEDGEMENTS

We thank Dr. M. Téboul and the Service d'Orthogénie at the Hôpital Broussais, Paris, France, for their invaluable help. We are also grateful to Drs. J. Amiel, T. Attié-Bitach, O. Danos, E. Detrait, E. Dupin, E. Jabs and J.-P. Jais for their critical comments and to N. Brahimi, G. Goudefroye, G. Molina and C. Ozilou for their technical assistance.

Conflict of Interest statement. None declared.

REFERENCES

1. Abzhanov, A., Tzahor, E., Lassar, A.B. and Tabin, C.J. (2003) Dissimilar regulation of cell differentiation in mesencephalic (cranial) and sacral (trunk) neural crest cells in vitro. *Development*, **130**, 4567–4579.
2. Couly, G., Creuzet, S., Bennaceur, S., Vincent, C. and Le Douarin, N.M. (2002) Interactions between Hox-negative cephalic neural crest cells and the foregut endoderm in patterning the facial skeleton in the vertebrate head. *Development*, **129**, 1061–1073.
3. McGonnell, I.M. and Graham, A. (2002) Trunk neural crest has skeletogenic potential. *Curr. Biol.*, **12**, 767–771.
4. Le Douarin, N. and Kalcheim, C. (1999) *The Neural Crest.* Cambridge University Press, Cambridge, UK.
5. Le Lievre, C.S. and Le Douarin, N.M. (1975) Mesenchymal derivatives of the neural crest: analysis of chimaeric quail and chick embryos. *J. Embryol. Exp. Morphol.*, **34**, 125–154.
6. Kruger, G.M., Mosher, J.T., Bixby, S., Joseph, N., Iwashita, T. and Morrison, S.J. (2002) Neural crest stem cells persist in the adult gut but undergo changes in self-renewal, neuronal subtype potential, and factor responsiveness. *Neuron*, **35**, 657–669.
7. Li, H.Y., Say, E.H. and Zhou, X.F. (2007) Isolation and characterization of neural crest progenitors from adult dorsal root Ganglia. *Stem Cells*, **25**, 2053–2065.

8. Fernandes, K.J., McKenzie, I.A., Mill, P., Smith, K.M., Akhavan, M., Barnabe-Heider, F., Biernaskie, J., Junek, A., Kobayashi, N.R., Toma, J.G. *et al.* (2004) A dermal niche for multipotent adult skin-derived precursor cells. *Nat. Cell Biol.*, **6**, 1082–1093.
9. Sieber-Blum, M., Grim, M., Hu, Y.F. and Szeder, V. (2004) Pluripotent neural crest stem cells in the adult hair follicle. *Dev. Dyn.*, **231**, 258–269.
10. Wong, C.E., Paratore, C., Dours-Zimmermann, M.T., Rochat, A., Pietri, T., Suter, U., Zimmermann, D.R., Dufour, S., Thiery, J.P., Meijer, D. *et al.* (2006) Neural crest-derived cells with stem cell features can be traced back to multiple lineages in the adult skin. *J. Cell Biol.*, **175**, 1005–1015.
11. Miura, M., Gronthos, S., Zhao, M., Lu, B., Fisher, L.W., Robey, P.G. and Shi, S. (2003) SHED: stem cells from human exfoliated deciduous teeth. *Proc. Natl. Acad. Sci. USA*, **100**, 5807–5812.
12. Motohashi, T., Aoki, H., Chiba, K., Yoshimura, N. and Kunisada, T. (2007) Multipotent cell fate of neural crest-like cells derived from embryonic stem cells. *Stem Cells*, **25**, 402–410.
13. Takashima, Y., Era, T., Nakao, K., Kondo, S., Kasuga, M., Smith, A.G. and Nishikawa, S. (2007) Neuroepithelial cells supply an initial transient wave of MSC differentiation. *Cell*, **129**, 1377–1388.
14. Etchevers, H.C., Amiel, J. and Lyonnet, S. (2006) Molecular bases of human neurocristopathies. *Adv. Exp. Med. Biol.*, **589**, 213–234.
15. Smith-Thomas, L.C. and Fawcett, J.W. (1989) Expression of Schwann cell markers by mammalian neural crest cells in vitro. *Development*, **105**, 251–262.
16. Baroffio, A., Dupin, E. and Le Douarin, N.M. (1988) Clone-forming ability and differentiation potential of migratory neural crest cells. *Proc. Natl. Acad. Sci. USA*, **85**, 5325–5329.
17. Spokony, R.F., Aoki, Y., Saint-Germain, N., Magner-Fink, E. and Saint-Jeannet, J.P. (2002) The transcription factor Sox9 is required for cranial neural crest development in Xenopus. *Development*, **129**, 421–432.
18. Uwanogho, D., Rex, M., Cartwright, E.J., Pearl, G., Healy, C., Scotting, P.J. and Sharpe, P.T. (1995) Embryonic expression of the chicken Sox2, Sox3 and Sox11 genes suggests an interactive role in neuronal development. *Mech. Dev.*, **49**, 23–36.
19. Baroffio, A. and Blot, M. (1992) Statistical evidence for a random commitment of pluripotent cephalic neural crest cells. *J. Cell Sci.*, **103**, 581–587.
20. Henion, P.D. and Weston, J.A. (1997) Timing and pattern of cell fate restrictions in the neural crest lineage. *Development*, **124**, 4351–4359.
21. Saha, S., Sparks, A.B., Rago, C., Akmaev, V., Wang, C.J., Vogelstein, B., Kinzler, K.W. and Velculescu, V.E. (2002) Using the transcriptome to annotate the genome. *Nat. Biotechnol.*, **20**, 508–512.
22. Hu, Y.F., Zhang, Z.J. and Sieber-Blum, M. (2006) An epidermal neural crest stem cell (EPI-NCSC) molecular signature. *Stem Cells*, **24**, 2692–2702.
23. Gammill, L.S. and Bronner-Fraser, M. (2002) Genomic analysis of neural crest induction. *Development*, **129**, 5731–5741.
24. Touraine, R.L., Attie-Bitach, T., Manceau, E., Korsch, E., Sarda, P., Pingault, V., Encha-Razavi, F., Pelet, A., Auge, J., Nivelon-Chevallier, A. *et al.* (2000) Neurological phenotype in Waardenburg syndrome type 4 correlates with novel SOX10 truncating mutations and expression in developing brain. *Am. J. Hum. Genet.*, **66**, 1496–1503.
25. Espinosa-Parrilla, Y., Amiel, J., Auge, J., Encha-Razavi, F., Munnich, A., Lyonnet, S., Vekemans, M. and Attie-Bitach, T. (2002) Expression of the SMADIP1 gene during early human development. *Mech. Dev.*, **114**, 187–191.
26. Sanlaville, D., Etchevers, H.C., Gonzales, M., Martinovic, J., Clement-Ziza, M., Delezoide, A.L., Aubry, M.C., Pelet, A., Chemouny, S., Cruaud, C. *et al.* (2006) Phenotypic spectrum of CHARGE syndrome in fetuses with CHD7 truncating mutations correlates with expression during human development. *J. Med. Genet.*, **43**, 211–217.
27. Pinson, L., Auge, J., Audollent, S., Mattei, G., Etchevers, H., Gigarel, N., Razavi, F., Lacombe, D., Odent, S., Le Merrer, M. *et al.* (2004) Embryonic expression of the human MID1 gene and its mutations in Opitz syndrome. *J. Med. Genet.*, **41**, 381–386.
28. Martinovic-Bouriel, J., Bernabe-Dupont, C., Golzio, C., Grattagliano-Bessieres, B., Malan, V., Bonniere, M., Esculpavit, C., Fallet-Bianco, C., Mirlesse, V., Le Bidois, J. *et al.* (2007) Matthew-Wood syndrome: report of two new cases supporting autosomal recessive inheritance and exclusion of FGF10 and FGFR2. *Am. J. Med. Genet. A*, **143**, 219–228.
29. Romualdi, C., Bortoluzzi, S., D'Alessi, F. and Danieli, G.A. (2003) IDEG6: a web tool for detection of differentially expressed genes in multiple tag sampling experiments. *Physiol. Genomics*, **12**, 159–162.
30. de Jonge, R.R., Vreijling, J.P., Meintjes, A., Kwa, M.S., van Kampen, A.H., van Schaik, I.N. and Baas, F. (2003) Transcriptional profile of the human peripheral nervous system by serial analysis of gene expression. *Genomics*, **82**, 97–108.
31. Richards, M., Tan, S.P., Tan, J.H., Chan, W.K. and Bongso, A. (2004) The transcriptome profile of human embryonic stem cells as defined by SAGE. *Stem Cells*, **22**, 51–64.
32. Panepucci, R.A., Siufi, J.L., Silva, W.A., Jr, Proto-Siquiera, R., Neder, L., Orellana, M., Rocha, V., Covas, D.T. and Zago, M.A. (2004) Comparison of gene expression of umbilical cord vein and bone marrow-derived mesenchymal stem cells. *Stem Cells*, **22**, 1263–1278.
33. Loh, Y.H., Wu, Q., Chew, J.L., Vega, V.B., Zhang, W., Chen, X., Bourque, G., George, J., Leong, B., Liu, J. *et al.* (2006) The Oct4 and Nanog transcription network regulates pluripotency in mouse embryonic stem cells. *Nat. Genet.*, **38**, 431–440.
34. Masui, S., Nakatake, Y., Toyooka, Y., Shimosato, D., Yagi, R., Takahashi, K., Okochi, H., Okuda, A., Matoba, R., Sharov, A.A. *et al.* (2007) Pluripotency governed by Sox2 via regulation of Oct3/4 expression in mouse embryonic stem cells. *Nat. Cell Biol.*, **9**, 625–635.
35. Zaehres, H., Lensch, M.W., Daheron, L., Stewart, S.A., Itskovitz-Eldor, J. and Daley, G.Q. (2005) High-efficiency RNA interference in human embryonic stem cells. *Stem Cells*, **23**, 299–305.
36. Walker, E., Ohishi, M., Davey, R.E., Zhang, W., Cassar, P.A., Tanaka, T.S., Der, S.D., Morris, Q., Hughes, T.R., Zandstra, P.W. and Stanford, W.L. (2007) Prediction and testing of novel transcriptional networks regulating embryonic stem cell self-renewal and commitment. *Cell Stem Cell*, **1**, 71–86.
37. Boyer, L.A., Lee, T.I., Cole, M.F., Johnstone, S.E., Levine, S.S., Zucker, J.P., Guenther, M.G., Kumar, R.M., Murray, H.L., Jenner, R.G. *et al.* (2005) Core transcriptional regulatory circuitry in human embryonic stem cells. *Cell*, **122**, 947–956.
38. Skottman, H., Mikkola, M., Lundin, K., Olsson, C., Stromberg, A.M., Tuuri, T., Otonkoski, T., Hovatta, O. and Lahesmaa, R. (2005) Gene expression signatures of seven individual human embryonic stem cell lines. *Stem Cells*, **23**, 1343–1356.
39. Moreno, J.C., Pauws, E., van Kampen, A.H., Jedlickova, M., de Vijlder, J.J. and Ris-Stalpers, C. (2001) Cloning of tissue-specific genes using serial analysis of gene expression and a novel computational substraction approach. *Genomics*, **75**, 70–76.
40. Shoji, H., Ito, T., Wakamatsu, Y., Hayasaka, N., Ohsaki, K., Oyanagi, M., Kominami, R., Kondoh, H. and Takahashi, N. (1996) Regionalized expression of the Dbx family homeobox genes in the embryonic CNS of the mouse. *Mech. Dev.*, **56**, 25–39.
41. Geada, A.M., Gaunt, S.J., Azzawi, M., Shimeld, S.M., Pearce, J. and Sharpe, P.T. (1992) Sequence and embryonic expression of the murine *Hox-3.5* gene. *Development*, **116**, 497–506.
42. Mosher, J.T., Yeager, K.J., Kruger, G.M., Joseph, N.M., Hutchin, M.E., Dlugosz, A.A. and Morrison, S.J. (2007) Intrinsic differences among spatially distinct neural crest stem cells in terms of migratory properties, fate determination, and ability to colonize the enteric nervous system. *Dev. Biol.*, **303**, 1–15.
43. Real, C., Glavieux-Pardanaud, C., Vaigot, P., Le Douarin, N. and Dupin, E. (2005) The instability of the neural crest phenotypes: Schwann cells can differentiate into myofibroblasts. *Int. J. Dev. Biol.*, **49**, 151–159.
44. Billon, N., Iannarelli, P., Monteiro, M.C., Glavieux-Pardanaud, C., Richardson, W.D., Kessaris, N., Dani, C. and Dupin, E. (2007) The generation of adipocytes by the neural crest. *Development*, **134**, 2283–2292.
45. Ying, Q.L., Wray, J., Nichols, J., Batlle-Morera, L., Doble, B., Woodgett, J., Cohen, P. and Smith, A. (2008) The ground state of embryonic stem cell self-renewal. *Nature*, **453**, 519–523.
46. Takahashi, K., Tanabe, K., Ohnuki, M., Narita, M., Ichisaka, T., Tomoda, K. and Yamanaka, S. (2007) Induction of pluripotent stem cells from adult human fibroblasts by defined factors. *Cell*, **131**, 861–872.
47. Yu, J., Vodyanik, M.A., Smuga-Otto, K., Antosiewicz-Bourget, J., Frane, J.L., Tian, S., Nie, J., Jonsdottir, G.A., Ruotti, V., Stewart, R. *et al.* (2007) Induced pluripotent stem cell lines derived from human somatic cells. *Science*, **318**, 1917–1920.
48. Rex, M., Orme, A., Uwanogho, D., Tointon, K., Wigmore, P.M., Sharpe, P.T. and Scotting, P.J. (1997) Dynamic expression of chicken *Sox2* and

Sox3 genes in ectoderm induced to form neural tissue. *Dev. Dyn.*, **209**, 323–332.
49. Hart, A.H., Hartley, L., Ibrahim, M. and Robb, L. (2004) Identification, cloning and expression analysis of the pluripotency promoting *Nanog* genes in mouse and human. *Dev. Dyn.*, **230**, 187–198.
50. Scholer, H.R., Dressler, G.R., Balling, R., Rohdewohld, H. and Gruss, P. (1990) Oct-4: a germline-specific transcription factor mapping to the mouse t-complex. *EMBO J.*, **9**, 2185–2195.
51. Reim, G., Mizoguchi, T., Stainier, D.Y., Kikuchi, Y. and Brand, M. (2004) The POU domain protein spg (pou2/Oct4) is essential for endoderm formation in cooperation with the HMG domain protein casanova. *Dev.Cell*, **6**, 91–101.
52. Gilbert, S.F. and Bolker, J.A. (2001) Homologies of process and modular elements of embryonic construction. *J. Exp. Zool.*, **291**, 1–12.
53. O'Rahilly, R. and Muller, F. (2007) The development of the neural crest in the human. *J. Anat.*, **211**, 335–351.
54. Copp, A.J., Greene, N.D. and Murdoch, J.N. (2003) The genetic basis of mammalian neurulation. *Nat. Rev. Genet.*, **4**, 784–793.
55. De Calisto, J., Araya, C., Marchant, L., Riaz, C.F. and Mayor, R. (2005) Essential role of non-canonical Wnt signalling in neural crest migration. *Development*, **132**, 2587–2597.
56. Cebra-Thomas, J.A., Betters, E., Yin, M., Plafkin, C., McDow, K. and Gilbert, S.F. (2007) Evidence that a late-emerging population of trunk neural crest cells forms the plastron bones in the turtle Trachemys scripta. *Evol. Dev.*, **9**, 267–277.
57. Allen, S.P., Maden, M. and Price, J.S. (2002) A role for retinoic acid in regulating the regeneration of deer antlers. *Dev. Biol.*, **251**, 409–423.
58. Sieber-Blum, M. and Cohen, A.M. (1980) Clonal analysis of quail neural crest cells: they are pluripotent and differentiate in vitro in the absence of noncrest cells. *Dev. Biol.*, **80**, 96–106.
59. Stainier, D.Y., Bilder, D.H. and Gilbert, W. (1991) The B30 ganglioside is a cell surface marker for neural crest-derived neurons in the developing mouse. *Dev. Biol.*, **144**, 177–188.
60. Fernandes, K.J., Kobayashi, N.R., Gallagher, C.J., Barnabe-Heider, F., Aumont, A., Kaplan, D.R. and Miller, F.D. (2006) Analysis of the neurogenic potential of multipotent skin-derived precursors. *Exp. Neurol.*, **201**, 32–48.
61. Keime, C., Semon, M., Mouchiroud, D., Duret, L. and Gandrillon, O. (2007) Unexpected observations after mapping LongSAGE tags to the human genome. *BMC Bioinformatics*, **8**, 154.
62. Ge, X., Wu, Q., Jung, Y.C., Chen, J. and Wang, S.M. (2006) A large quantity of novel human antisense transcripts detected by LongSAGE. *Bioinformatics*, **22**, 2475–2479.
63. Langer, E.M., Feng, Y., Zhaoyuan, H., Rauscher, F.J., III, Kroll, K.L. and Longmore, G.D. (2008) Ajuba LIM proteins are snail/slug corepressors required for neural crest development in xenopus. *Dev. Cell*, **14**, 424–436.
64. Basrai, M.A. and Hieter, P. (2002) Transcriptome analysis of Saccharomyces cerevisiae using serial analysis of gene expression. *Methods Enzymol.*, **350**, 414–444.
65. Velculescu, V.E., Zhang, L., Vogelstein, B. and Kinzler, K.W. (1995) Serial analysis of gene expression. *Science*, **270**, 484–487.
66. Galante, P.A., Trimarchi, J., Cepko, C.L., de Souza, S.J., Ohno-Machado, L. and Kuo, W.P. (2007) Automatic correspondence of tags and genes (ACTG): a tool for the analysis of SAGE, MPSS and SBS data. *Bioinformatics*, **23**, 903–905.
67. Delous, M., Baala, L., Salomon, R., Laclef, C., Vierkotten, J., Tory, K., Golzio, C., Lacoste, T., Besse, L., Ozilou, C. *et al.* (2007) The ciliary gene RPGRIP1L is mutated in cerebello-oculo-renal syndrome (Joubert syndrome type B) and Meckel syndrome. *Nat. Genet.*, **39**, 875–881.
68. de Hoon, M.J., Imoto, S., Nolan, J. and Miyano, S. (2004) Open source clustering software. *Bioinformatics.*, **20**, 1453–1454.
69. Dennis, G., Jr, Sherman, B.T., Hosack, D.A., Yang, J., Gao, W., Lane, H.C. and Lempicki, R.A. (2003) DAVID: Database for Annotation, Visualization, and Integrated Discovery. *Genome Biol.*, **4**, 3.


size marker
β-Actin
EDNB
SMAD3
TGFβ1
WNT4
SEMA6A
SCF
STAT3
LIN-28
HELLS
SALL1
GAL
BMPR1

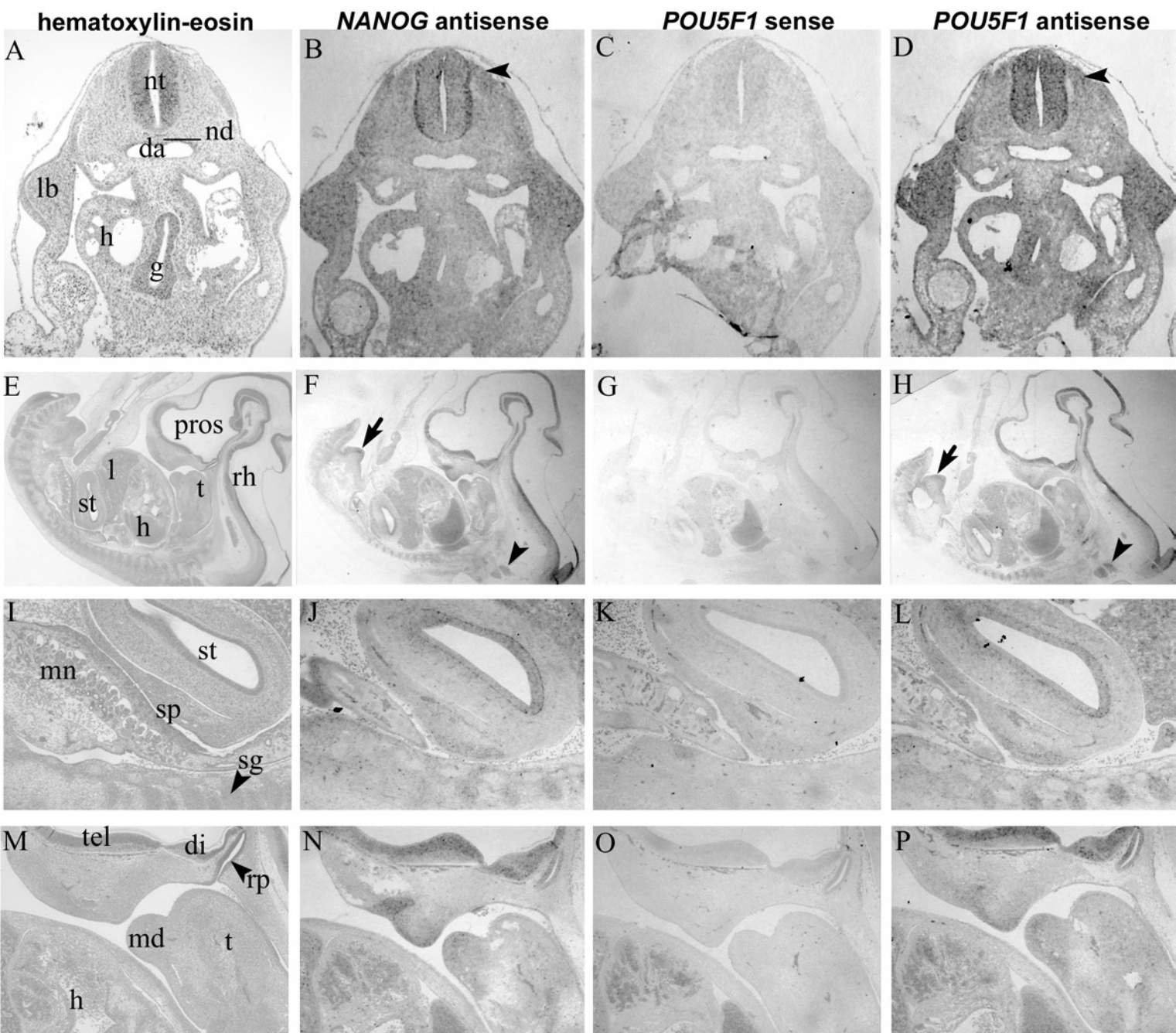
hematoxylin-eosin
NANOG antisense
POU5F1 sense
POU5F1 antisense
A
nt
nd
da
lb
h
g
B
C
D
E
pros
l
st
h
t
rh
F
G
H
I
st
mn
sp
sg
J
K
L
M
tel
di
rp
md
t
h
N
O
P

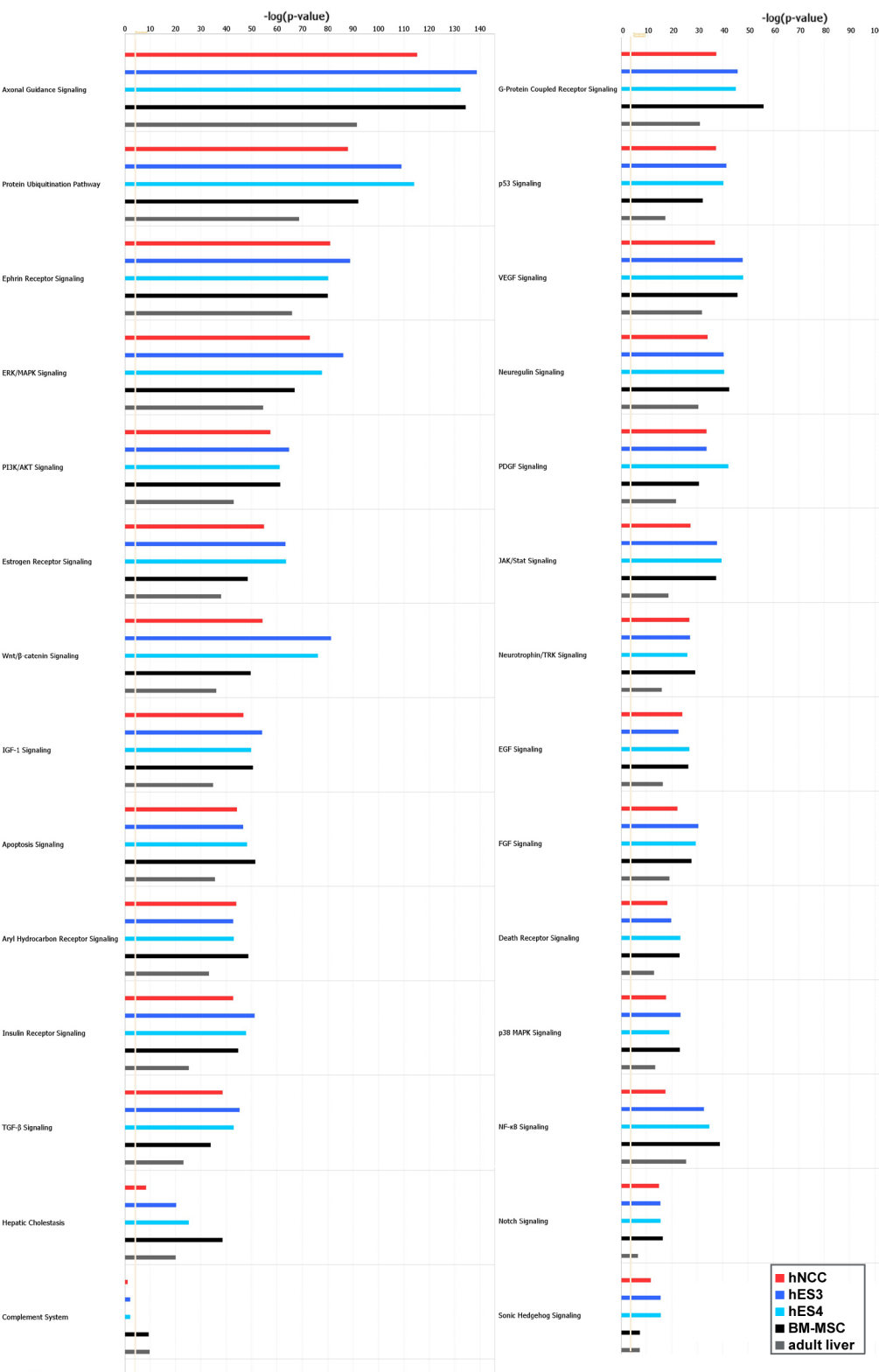
-log(p-value)
0
10
20
30
40
50
60
70
80
90
100
110
120
130
140
Axonal Guidance Signaling
Protein Ubiquitination Pathway
Ephrin Receptor Signaling
ERK/MAPK Signaling
PI3K/AKT Signaling
Estrogen Receptor Signaling
Wnt/β-catenin Signaling
IGF-1 Signaling
Apoptosis Signaling
Aryl Hydrocarbon Receptor Signaling
Insulin Receptor Signaling
TGF-β Signaling
Hepatic Cholestasis
Complement System
-log(p-value)
0
10
20
30
40
50
60
70
80
90
10
G-Protein Coupled Receptor Signaling
p53 Signaling
VEGF Signaling
Neuregulin Signaling
PDGF Signaling
JAK/Stat Signaling
Neurotrophin/TRK Signaling
EGF Signaling
FGF Signaling
Death Receptor Signaling
p38 MAPK Signaling
NF-κB Signaling
Notch Signaling
Sonic Hedgehog Signaling
hNCC
hES3
hES4
BM-MSC
adult liver

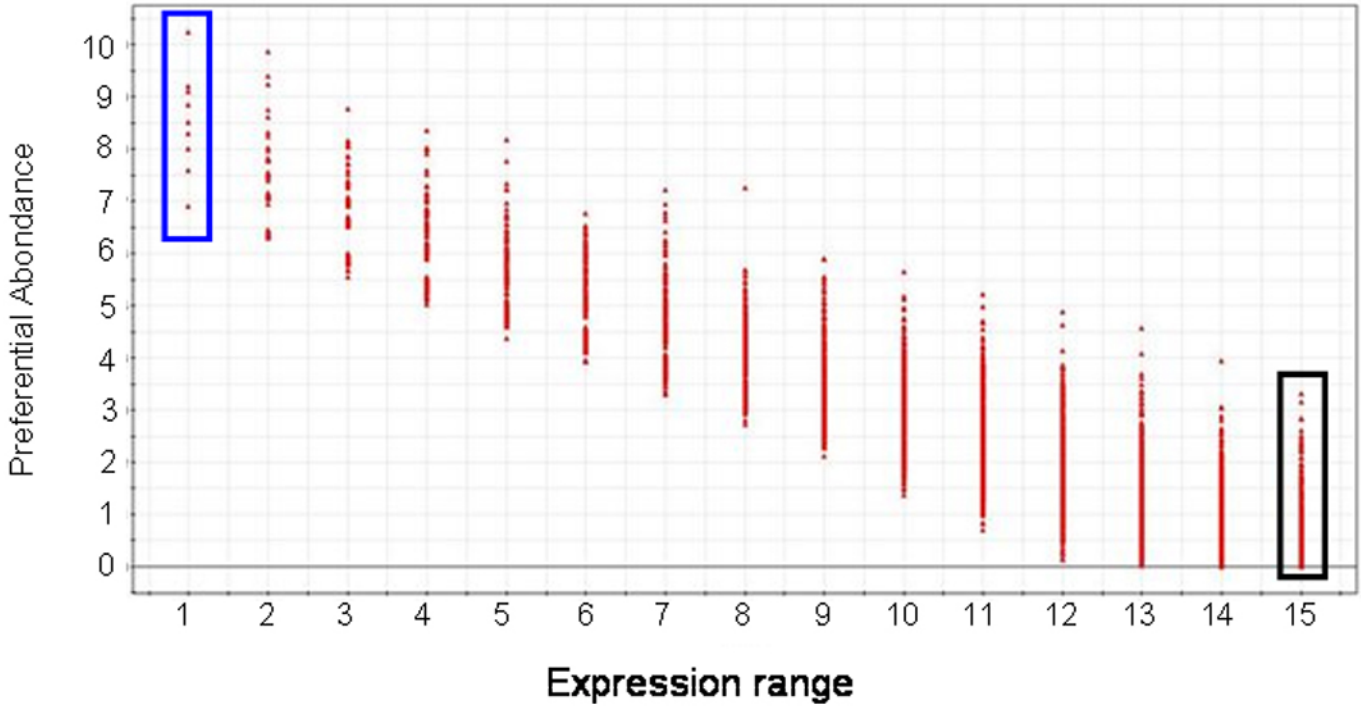
Preferential Abondance
10
9
8
7
6
5
4
3
2
1
0
1
2
3
4
5
6
7
8
9
10
11
12
13
14
15
Expression range

SUPPLEMENTARY METHODS

Primers (human-specific)

FORWARD PRIMER		REVERSE PRIMER		Tm
ACTB-RT-F	ATTGGCAATGAGCGGTTCCGC	*ACTB-RT-R*	CTCCTGCTTGCTGATCCACATC	60
BMPR1A RT F	GCAATTGCTCATCGAGACCT	*BMPR1A RT R*	ATTCTTCCACGATCCCTCCT	60
CD24 RT F	ATCCAAGCATCCTGAGCAAC	*CD24 RT R*	GCCTGTAATCCCAGCACTTT	60
CHAT RT F	CCACTCCATTCCCACTGACT	*CHAT RT R*	GAGTGAACAGATCCCCCTCA	60
CTNNB1 RT F	TAGAGGCTCTTGTGCGTACT	*CTNNB1 RT R*	ATCCCGAGCTAGGATGTGAA	55
EDN1 RT F	TTCCCACAAAGGCAACAGACCG	*EDN1 RT R*	GACAGGCCCCGAAGTCTGTCA	60
EDNRB RT F	TACAAGACAGCAAAAGATTGGTGG	*EDNRB RT R*	GGACTGTTTTTCTTCAAATGACTG	65
EPHA1 RT F	GTGGAGTGAACAGCAACAGA	*EPHA1 RT R*	ATCCTGGTCACTCTCCATGT	55
FGFR1 RT F	CGTCAATGTTTCAGATGCTCTCCC	*FGFR1 RT R*	CAGAGTCCATTATGATGCTCCAGG	65
FGFR2 RT F	GTCTCCGAGTATGAACTTCCAGAG	*FGFR2 RT R*	CATCATCTCCATCTCTGACACCAG	60
FGFR3 RT F	AGATGCTGAAAGACGATGCC	*FGFR3 RT R*	TTGCAGGTGTCGAAGGAGTA	60
FGFR4 RT F	AGTCAAGCTCATCCCTGGTA	*FGFR4 RT R*	TGTCAGAGGCGTTGTCTTTG	55
FOXD3-RT-F	AGTGAAGCCGCCTTACTCGTACAT	*FOXD3-RT-R*	AGGAAGCTGCCGTTGTCGAACAT	65
FOXOA1 RTbis F	CCCAACCAAAGCTTCCCACA	*FOXOA1 RTbis R*	CCTGCACACATTGGGCAAAC	65
FZD7 RT F	TGCTGTCACACACCGTTAAG	*FZD7 RT R*	AGACAGGGTCAGCATATGGA	55
GAL RT F	ACAAGAATGGCCTCACCAGCAA	*GAL RT R*	AGCACACAGACAAACATGCCCA	65
GJA1 HIS F	CGCCTTAGGCAAACTCCTT	*GJA1 HIS R*	ATGATGTAGGTTCGCAGCAA	55
GJA1 RT F	GGAGTTCAATCACTTGGCGTG	*GJA1 RT R*	CTTACCATGCTCTTCAATACCG	60
GLI3-RT-F	AACGCAATCACTATGCAGCCACAG	*GLI3-RT-R*	TGCAATGGAGGAATCGGAGATGGA	65
GP130 RT F	CTGGAGTGAAGAAGCAAGTG	*GP130 RT R*	GCGATGCACGGTACCATCT	55
GPR23 RT F	ACAATGCAACCACCACCTGCTT	*GPR23 RT R*	AGTTGCAAGGCACAAGGTGA	62
HELLS RT F	ACCGAGAAAGAGCTGTTGTGGA	*HELLS RT R*	TCCGTGTTGAAGCTGTGCATGT	55
HOXC5 F	CCTTTTCGCCTTTCCTCTCT	*HOXC5 R*	GCCTCTAGGACCACTTGCTG	60
LIFR RT F	GGCCGTGGTACTGATTATGA	*LIFR RT R*	GCTCCAGTCACTCCACTCT	55
LIN-28 RT F	AGTAAGCTGCACATGGAAGG	*LIN-28 RT R*	ATTGTGGCTCAATTCTGTGC	55
MAZ HIS F	AGAAGACAAAGAGCAAGGGGC	*MAZ HIS R*	TGCGACAGCTTGTGTCGGTT	60
MSX1-RT-F	ACTCCTCAAGCTGCCAGAAGAT	*MSX1-RT-R*	TTCTCCAGCTCTGCCTCTTGTAGT	60
MTHFD1 RT F	TTGTTGGCCCAGAAGGGTTTGT	*MTHFD1 RT R*	AGTGCACTTCACGGCATCAA	65
MYBL2 RT F	TGCACCAGAAACATGCTGCGTT	*MYBL2 RT R*	TTGGGCAGTGTGGACATCATCA	65
NANOG HIS F	ACCCCAGCCTTTACTCTTCCT	*NANOG HIS R*	TTCAGGTTGCATGTTCATGGA	60
NANOG RT F	AGTAAGCTGCACATGGAAGG	*NANOG RT R*	TGTTCCAGGCCTGATTGTTC	55
NES-RT-F	AGGTAGAGGAGCTGGCAAGG	*NES-RT-R*	GAGCGATCTGGCTCTGTAGG	60
NOTCH1-RT-F	AGGTCAATGAGTGCAACAGCAACC	*NOTCH1-RT-R*	TCAATACACGTGCCCTGGTTCAGA	65
NOTCH2-RT-F	TCCAGGAGAGGTGTGCTTGTTGAA	*NOTCH2-RT-R*	ACAAGGTCAATACAGGTGCCTCCA	65
OCT3/4 HIS F	TGAACAGGGAATGGGTGAATG	*OCT3/4 HIS R*	CAAATAGAACCCCCAGGGTGA	60
OCT3/4 RT F	GAGCAAAACCCGGAGGAGT	*OCT3/4 RT R*	TTCTCTTTCGGGCCTGCAC	62
P75 RT F	CTGCAAGCAGAACAAGCAAG	*P75 RT R*	GGCCTCATGGGTAAAGGAGT	60
PAX3-RT-F	TGTTCAGCTGGGAAATCCGAGACA	*PAX3-RT-F*	AGCTGTTCTGCTGTGAAGGTGGTT	65
PAX6-RT-F	ATCAGAGAAGACAGGCCAGCAACA	*PAX6-RT-F*	ATCATAACTCCGCCCATTCACCGA	65
PDGFA-RT-F	CCCCTGCCCATTCGGAGGAAGAG	*PDGFA-RT-R*	TTGGCCACCTTGACGCTGCGGTG	60
PDGFB-RT-F	GATCCGCTCCTTTGATGATC	*PDGFB-RT-R*	GTCTCACACTTGCATGCCAG	60
PDGFRB-RT-F	AATGTCTCCAGCACCTTCGT	*PDGFRB-RT-R*	AGCGGATGTGGTAAGGCATA	60
PHOX2B RT F	CTCAACGAGAAGCGCAAGCA	*PHOX2B RT R*	TGTCCGGGTCAGTGCTCTTG	65
PTPN11 RT F	CATGCGTGTTAGGAACGTCA	*PTPN11 RT R*	ATTCGTGCCCTTTCCTCTTG	60
RET RT F	CTACGGCACGTACCGCACAC	*RET RT R*	GGCCTTGTCTCTGGGAAGCA	65
SCF-RT-F	GATGTTTTGCCAAGTCATTGTTGG	*SCF-RT-R*	ACTGACTCTGGAATCTTTCTCAGG	60
SEMA6A RT F	ACCTCATCAATGCCTGCACA	*SEMA6A RT R*	TGCATTTCCAGCCGCTTGCTTA	65
SMAD2-RT-F	AATCAGAGATATGGCTGGCACCCT	*SMAD2-RT-F*	GACATGCTTGAGCAACGCACTGAA	65
SMAD3-RT-F	AAGAAGGACGAGGTCTGCGTGAAT	*SMAD3-RT-F*	TAGGTTTGGAGAACCTGCGTCCAT	65
SNAI2 RTbis F	TTTCTGGGCTGGCCAAACAT	*SNAI2 RTbis R*	TGCTACACAGCAGCCAGATTCC	65
SOS1 RT F	AAATGTATGTCGGCACTGGG	*SOS1 RT R*	ACAGAGTGAGGTTGGTGGTA	55
SOX10 RTter F	TGAACGCCTTCATGGTGTGG	*SOX10 RTter R*	TCTTGTAGTGGGCCTGGATGG	65
SOX11 HIS F	TCCCCACCATTTTTCCTG	*SOX11 HIS F*	CATTCGGTCTCGCCAAATCT	55
SOX2 RTbis F	ACGGTGCCTTGGATGAAGGA	*SOX2 RTbis R*	ATGGCTGTTGCCTGGCTTCT	65
SOX9-RT-F	AAGGAGAGCGAGGAGGACAAGTT	*SOX9-RT-F*	TGTAATCCGGGTGGTCCTTCTTGT	65
STAT3 RT F	AAACTTAAGCAGCCGGGCAT	*STAT3 RT R*	AAAGCACCAAGGAGGCTGTT	62
TERF1 RT F	ACAGCTTGCCAGTTGAGAACGA	*TERF1 RT R*	TTGCCGCTGCCTTCATTAGA	62
TGFB1-RT-F	ACAATTCCTGGCGATACCTCAGCA	*TGFB1-RT-R*	TCTTCTCCGTGGAGCTGAAGCAAT	65
TYRP1 RT F	CTCCTGCACACCTTCACAGA	*TYRP1 RT R*	TCAGTGAGGAGAGGCTGGTT	60
TWIST RT F	TGCAGCTATGTGGCTCACGA	*TWIST RT R*	CCCACGCCCTGTTTCTTTGA	65
WNT4-RT-F	CATTGAGGAGTGCCAGTACCAGTT	*WNT4-RT-R*	ACAAACGACTGTGAGAAGGCCACA	65

RNA quality upon extraction from hNCC

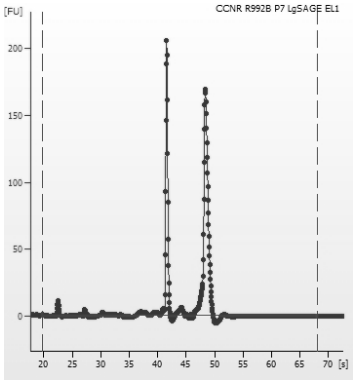

Bioanalyzer (Agilent) analysis yielded a 28S/18S ratio of 1.8 from hNCC line N5, sufficient to ensure representativity in the SAGE bank presented in this paper. Subsequent extractions of hNCC subjected to RNA Integrity Number assessment [Schroeder *et al.*, The RIN: an RNA integrity number for assigning integrity values to RNA measurements. *BMC Molecular Biology* **7**:3 (2006)], gave values between RIN 9.5-10.0.

Supplementary Table 1.

Validation of SAGE data by RT-PCR on 55 genes represented by tags with very low (count ≤3), low (3<count<10) and high (>10) abundance

Tag Count	Tested RT	Positive RT
1	13	13
2	7	6
3	5	5
4	8	8
5	2	2
6	5	5
7	6	5
8	4	4
>10	3	3
>100	2	2
TOTAL	55	53

Supplementary Table 2.

Human orthologues of genes expressed in avian migratory NCC (Gammill and Bronner-Fraser, 2002).
Bold = common to human, mouse and chick

AARS
ABCF1
ABCF2
ABCF3
ADD1
AHCY
ALDH9A1
ARHGAP1
ATPAF1
CAPG
CDKN1C
CNAP1
COL1A1
COL18A1
DKC1
DNMT3B
EIF3S1
EIF3S2
EIF3S3
EIF3S4
EIF3S5
EIF3S6
EIF3S7
EIF3S8
EIF3S9
EIF3S10
EIF3S12
EIF3S6IP
EIF4G1
EIF4G2
EIF4G3
FTSJ2
FTSJ3
FUSIP1
GOT2
GSN
HK1
KIAA0174
KIF4A
LAMA5
NOTCH1
NOTCH2
NOTCH3
NRP1
NRP2
PALLD
PCNA

PES1
PRPF3
PRPF19
PUM2
RAP1A
RAP1B
SLC7A1
SLC7A5
SLC7A6
SLC7A11
SNAI2
TAX1BP1
TAX1BP3
TCF3
THOP1
TPD52
UQCR

Supplementary Table 3.

Ninety hNCC and hES cell expressed targets whose promoters are co-occupied by POU5F1 (*OCT3/4)*, *NANOG* and *SOX2* transcription factors (cf. Boyer, L. A. et al. 2005. *Cell* 122, 947-956).

SYMBOL	HNCC_TPM	HES3_TPM	HES4_TPM	LIVER_TPM
ANKRD1	277	5	10	0
ARID1B	140	73	30	75
ATAD2	20	29	5	15
ATP6V1G1	20	0	0	0
BAMBI	20	103	53	15
BMP7	60	34	24	30
BUB1B	20	35	24	0
BUB3	59	151	96	30
C13orf7	60	15	39	15
C15orf29	20	0	0	0
C6orf111	278	0	0	0
C9orf74	40	34	38	15
CABLES1	20	10	34	0
CACNA2D1	40	0	0	0
CAPZA2	40	117	96	90
CDC14B	20	59	24	30
CDW92	20	20	10	0
CDYL	60	30	39	15
COL12A1	159	5	19	15
CTGF	494	88	421	120
DHDDS	20	0	15	30
DHRS3	60	20	34	60
DPPA4	40	190	402	15
DPYSL2	456	137	164	45
DPYSL3	198	659	551	0
DTNA	40	5	10	15
DUSP12	20	10	34	15
DUSP6	59	30	120	45
EDD	20	34	39	30
EXOSC9	40	138	116	45
FAM33A	60	98	63	30
FBXW11	80	44	73	0
FGFR1	138	259	265	60
FGFR2	119	122	72	30
FLJ10769	20	0	0	0
FLJ11029	20	0	0	0
FLJ14936	20	0	0	0
FOXO1A	20	77	34	0
FRAT2	20	171	182	30
FUS	436	507	235	60
GJA1	119	2134	1430	30
H2AFJ	40	54	19	75
HN1	138	317	307	90
ICMT	79	102	134	30
IER5L	238	20	5	15
IRX2	40	87	140	0
JARID2	40	287	327	30
JUP	99	195	120	120
KIAA1143	20	0	0	0

KIAA1623	40	0	0	0
KIF15	20	10	0	0
KLF5	40	5	5	0
KLHL5	60	10	20	30
LARGE	40	15	29	30
LRRN1	100	133	201	0
LRRN6A	40	73	34	15
MAN2C1	20	29	25	60
MED12	40	10	14	0
MGEA5	139	219	136	45
MLLT10	60	39	29	0
MSC	40	0	0	0
MTM1	40	10	14	15
MYST3	40	15	44	30
NEBL	20	15	38	45
NUCKS	772	387	390	75
ORC1L	20	44	33	0
PARG	20	93	111	0
PFTK1	20	5	10	15
PHF17	20	108	178	30
PIPOX	20	385	464	0
PPAP2A	20	122	153	15
PPP2R1B	40	40	15	15
PPP2R3A	40	15	10	45
PRKCDBP	60	5	19	30
PTPN2	60	35	20	30
RAD54B	20	5	20	0
RIF1	60	40	30	45
RNF24	40	15	10	30
ROR1	20	29	29	0
RPS18	2475	3698	3018	299
RPS3A	1981	3393	3458	314
SALL1	79	44	53	15
SET	912	1749	1415	120
SFRP1	337	401	263	165
SFRP2	59	244	239	0
SFRS4	198	68	100	30
SKIL	60	93	117	0
SNRPN	258	708	1070	120
SOX2	159	337	340	0
SPAG9	60	15	30	0
SPRED1	20	20	24	0
STAT3	20	24	39	344
TAF12	40	15	58	0
TALDO1	59	74	82	75
TBL1XR1	160	59	58	15
TCF20	40	49	44	45
TCF7L1	40	113	72	15
THBS2	40	1651	483	15
TIF1	40	60	48	0
TLE3	40	69	20	45
TNC	60	20	15	15
TNRC6A	60	107	96	0
TOP2A	257	166	187	0
TSC22D1	119	180	129	45
UBE2D3	179	274	265	90

USP7	179	117	72	30
ZFHX1B	159	15	5	75
ZFP36L1	1227	122	181	135
ZIC1	139	0	0	0
ZIC2	40	254	124	15

****Liver count in tag per million (SAGE library total count=66861)
***hES4 count in tag per million (SAGE library total count=209232)
**hES3 count in tag per million (SAGE library total count=205353)
*hNCC count in tag per million (SAGE library total count=50500)

Bold symbols: HNCC specifically expressed *NANOG*, *OCT3/4* and *SOX2* target genes

Supplementary Table 4.

hES cells "stemness" genes (Skottman et al. 2005) expressed in hNCC

symbol	hNCC tpm*	HES3 tpm**	HES4 tpm***
AFF1	20	15	49
ARNT2	40	5	10
ATF3	20	5	10
ATF4	257	19	273
ATF7	20	5	10
ATRX	40	5	5
BRD8	40	24	5
BTAF1	20	5	5
BTG2	20	15	5
CEBPB	40	19	19
CNOT7	59	78	5
CREB1	20	5	5
CREM	20	15	5
CUTL1	20	5	5
DRAP1	257	112	73
E2F1	40	10	5
E2F3	40	29	5
E2F4	20	5	5
E2F5	20	5	5
EGR1	158	49	5
ELF2	20	24	5
ELK1	20	39	39
ELK3	20	5	15
EP300	20	19	19
ERF	139	83	5
ETS1	337	5	15
ETS2	20	29	15
ETV1	20	5	10
ETV6	40	5	5
FOXD3	40	5	10
FOXK2	40	5	15
FOXM1	20	58	5
FOXP1	20	5	5
FOXP4	59	5	487
FUBP1	20	5	5
GABPA	20	29	29
GLI2	20	19	15
GLI3	99	5	5
GTF2I	178	5	5
HCFC1	40	19	34
HDAC1	20	5	39
HDAC2	40	29	5
HES6	416	44	29
HIRA	99	10	24
HSF1	20	34	5
JUNB	20	5	5
JUND	99	68	24
KLF7	40	5	15

LMO4	20	5	10
MBD1	20	19	5
MDS1	20	10	10
MEF2A	20	5	5
MEF2B	20	15	5
MEF2D	20	10	5
MEIS2	20	5	15
MNT	20	5	19
MSX1	139	44	15
MSX2	20	5	5
MTA1	20	170	5
MTF1	20	5	5
MYCN	20	5	5
NFAT5	20	5	5
NFKB2	20	5	10
NFX1	20	5	5
NFYA	20	10	5
NFYC	20	10	15
NR1D2	20	5	5
NR1H2	20	34	19
NR6A1	20	5	5
PA2G4	20	5	15
PAX3	20	5	10
PAX6	40	10	10
PBX1	20	5	5
PCGF2	20	5	15
PHF5A	40	10	5
PITX2	20	10	5
PML	20	15	5
PRDM2	20	5	10
PTTG1	99	5	5
RARA	20	5	5
RXRA	20	5	5
RXRB	40	24	5
SALL1	79	34	54
SALL2	20	5	58
SATB1	40	15	15
SIX5	20	44	58
SMAD1	20	5	10
SMAD3	99	5	5
SMAD4	20	5	19
SMAD5	20	19	5
SOX2	119	175	19
SOX21	20	24	136
SRF	40	10	10
STAT1	59	24	5
STAT2	257	122	93
STAT3	20	5	5
STAT6	20	5	10
TAF11	20	5	102
TAF6L	20	15	19
TAF7	40	10	73

TBX3	20	5	5
TCEA1	158	5	5
TCEA2	40	15	24
TCF19	20	5	5
TCFL5	40	5	10
TEAD1	20	5	5
TEAD2	40	44	5
TEAD3	40	721	195
TEAD4	20	73	10
TGIF2	40	54	49
VDR	40	15	39
XBP1	20	5	5
ZNF24	20	10	5

***hES4 count in tag per million (SAGE library total count=209232)
**hES3 count in tag per million (SAGE library total count=205353)
*hNCC count in tag per million (SAGE library total count=50500)

Supplementary Table 5.

Genes annotated as involved in transcription regulation common to both hNCC and hES3/4

symbol	CCN tpm*	HES3 tpm**	HES4 tpm***
ABL1	59	10	34
ACTB	436	5	15
ACTR1B	20	5	10
ACVR1B	20	15	5
ACVR2A	0	0	0
ADM	20	29	15
ADORA2A	20	10	5
ADRA2A	20	5	15
ADRBK1	59	19	15
AEBP2	20	44	5
AES	20	10	5
AFF1	20	15	49
AGRIN	0	0	0
AKAP13	20	5	5
AKT1	139	5	5
ANP32A	40	15	10
AP2A2	20	15	5
APBA2	40	10	5
APBB1	40	29	54
APBB2	20	5	5
APC	20	5	5
APEX1	20	443	5
APLP1	139	19	5
APLP2	40	5	15
APP	158	5	15
APPBP1	79	5	5
ARID1A	119	5	78
ARID3A	59	5	19
ARID4B	20	19	10
ARNT2	40	5	10
ASXL1	20	5	5
ATF2	20	19	19
ATF3	20	5	10
ATF4	257	19	273
ATF5	99	15	10
ATF7	20	5	10
ATF7IP	20	5	5
ATM	20	10	29
ATN1	20	34	24
ATP2B4	20	5	5
ATP2C1	40	10	5
ATRX	40	5	5
ATXN3	40	5	5
BASP1	20	44	63
BAZ2A	40	83	5
BCKDHA	20	58	73
BCL10	20	10	34
BCL9L	20	19	5
BCLAF1	20	44	5
BCOR	79	10	24
BCR	79	5	5

BHLHB2	59	19	5
BIRC2	99	44	34
BIRC4	40	5	19
BMP7	40	5	24
BMPR1A	20	19	34
BMPR2	20	10	5
BPTF	0	0	0
BRD7	20	44	39
BRD8	40	24	5
BRF2	20	15	10
BTAF1	20	5	5
BTBD14B	40	5	5
BTF3	376	15	10
BTG1	20	15	5
BTG2	20	15	5
BTRC	20	10	15
CALR	455	273	122
CAMK2D	40	5	5
CAMKK2	40	5	5
CARM1	20	24	5
CASK	20	5	5
CASP3	20	49	102
CAV1	20	5	15
CBFB	20	5	5
CBX1	139	5	5
CBX3	20	219	5
CBX5	79	15	5
CCNA2	20	44	58
CCNB1	40	5	5
CCND1	139	10	19
CCND2	297	5	15
CCNDBP1	40	29	34
CCNH	20	5	24
CCNK	59	5	5
CCNT2	20	15	19
CD44	20	5	5
CDC2	158	5	5
CDC25B	40	15	5
CDC42	20	39	5
CDC5L	20	19	19
CDCA4	59	10	5
CDK2	40	29	29
CDK3	59	5	5
CDK7	20	44	5
CDK8	40	15	5
CDK9	20	44	24
CDKN1A	139	5	15
CDKN1B	40	15	5
CDKN1C	20	15	5
CDR2	59	24	24
CEBPB	40	19	19
CEBPZ	20	15	10
CENPF	40	5	10
CHAF1A	20	10	5
CHD1	20	19	5
CHD2	20	24	29

CHD3	20	5	5
CHD4	396	239	54
CHES1	40	5	5
CIAO1	0	0	0
CITED2	59	161	102
CNBP	0	0	0
CNN1	99	19	34
CNOT7	59	78	5
COPS5	20	93	5
CRABP2	20	317	5
CREB1	20	5	5
CREB3L4	40	19	15
CREBBP	20	5	19
CREBL2	20	5	24
CREM	20	15	5
CRK	455	34	88
CRKL	20	5	10
CRSP2	20	15	5
CRSP6	20	5	19
CRSP8	20	54	34
CRTC1	40	5	0
CSDA	40	10	10
CSNK1E	139	5	24
CTBP1	40	39	19
CTBP2	99	5	5
CTDSP1	40	63	10
CTDSP2	20	5	5
CTDSPL	40	10	24
CTNNB1	20	156	58
CTNNBIP1	59	24	10
CUL1	59	112	58
CUL4A	20	10	5
CUTL1	20	5	5
CXCL12	20	404	5
CXORF15	20	5	5
DAP3	99	54	5
DAXX	59	10	39
DCAMKL1	20	5	10
DDB1	119	10	5
DDB2	20	5	10
DDX5	79	29	5
DDX54	40	146	10
DEAF1	40	49	78
DEDD	20	10	5
DEK	356	29	58
DHX9	20	190	15
DIXDC1	20	15	15
DKK3	119	5	34
DLL1	40	15	19
DMTF1	20	5	5
DNAJA3	59	5	5
DNAJB6	59	151	151
DNMT1	79	5	73
DNTTIP1	40	34	15
DR1	20	5	5
DRAP1	257	112	73

DSCR1	20	15	5
DUSP1	79	10	5
DUSP22	20	19	5
DUSP3	20	5	5
DUSP4	20	5	5
DVL1	158	88	73
DYRK1B	59	19	5
E2F1	40	10	5
E2F3	40	29	5
E2F4	20	5	5
E2F5	20	5	5
E2F7	20	10	5
ECT2	79	88	15
EDF1	40	15	5
EEF1D	20	10	5
EGR1	158	49	5
EID1	0	0	0
EIF2S1	20	5	5
EIF4G2	40	5	190
ELF2	20	24	5
ELK1	20	39	39
ELK3	20	5	15
ELL	40	5	5
ELL2	20	5	10
ELP3	20	24	5
ENO1	20	10	122
EP300	20	19	19
EPC1	20	5	5
EPN2	20	5	5
ERBB2	79	88	5
ERBB2IP	20	5	19
ERCC2	59	19	10
ERCC3	79	24	5
ERF	139	83	5
ESRRA	40	44	10
ETF1	20	5	5
ETS1	337	5	15
ETS2	20	29	15
ETV1	20	5	10
ETV6	40	5	5
EWSR1	139	5	19
EZH2	119	63	49
F2R	79	5	10
FADD	79	19	54
FGFR1	20	5	5
FHIT	20	5	19
FKBP1A	20	19	15
FLII	59	5	29
FN1	20	112	5
FOS	59	5	487
FOSB	40	5	0
FOXA2	79	39	10
FOXD3	40	5	10
FOXK2	40	5	15
FOXM1	20	58	5
FOXO1A	20	19	5

FOXO3A	20	10	15
FOXP1	20	5	5
FOXP4	59	5	487
FRAT1	20	5	5
FUBP1	20	5	5
FUBP3	40	5	5
FZD2	59	39	5
FZD3	20	19	15
FZD6	20	5	5
FZD7	20	19	10
GABPA	20	29	29
GABPB2	20	10	10
GAS6	40	19	5
GCN5L2	40	24	10
GJA1	79	15	19
GLI2	20	19	15
GLI3	99	5	5
GLMN	20	5	5
GNA12	59	39	5
GNA13	40	10	15
GNAQ	20	5	15
GRB10	40	19	5
GRB2	40	5	5
GRIP1	20	5	5
GRLF1	20	10	5
GRN	79	5	5
GSK3B	20	5	10
GSTP1	20	5	15
GTF2A1	20	34	10
GTF2A2	20	54	93
GTF2B	119	19	39
GTF2F1	20	29	545
GTF2F2	139	5	5
GTF2H4	20	10	19
GTF2I	178	5	5
GTF3C1	40	5	5
GTF3C2	20	5	5
GTF3C3	99	10	5
GTF3C4	20	10	10
GTF3C5	59	5	5
HCFC1	40	19	34
HDAC1	20	5	39
HDAC10	20	19	10
HDAC2	40	29	5
HDAC3	20	5	5
HDAC5	59	5	5
HDAC7A	59	44	29
HDAC9	40	15	5
HES1	40	10	44
HES6	416	44	29
HGS	20	83	5
HIF1A	20	10	5
HIP1	20	5	10
HIPK2	20	5	10
HIRA	99	10	24
HLTF	0	0	0

HMGA1	40	58	107
HMGA2	20	34	34
HMGB1	119	10	925
HMGB2	950	375	419
HMGN2	79	5	360
HNRPA1	59	5	29
HNRPAB	20	10	39
HNRPK	20	34	175
HOXA2	20	5	5
HRAS	59	54	34
HSBP1	257	24	44
HSF1	20	34	5
HSP90B1	20	467	273
HTATIP2	59	63	5
ID1	337	5	10
ID2	40	78	10
ID3	20	156	5
ID4	40	5	19
IFNAR1	20	5	44
IFRD1	20	29	5
IGF2	20	5	5
IGFBP2	20	394	10
IGFBP3	20	29	5
IGFBP4	20	97	88
IGFBP5	178	10	5
IKBKAP	40	10	10
IKBKB	20	5	10
IL2RA	20	10	5
IL6ST	20	5	3394
ILF2	198	24	5
ILF3	20	5	5
ILK	59	141	63
ING1	20	10	5
INHBE	20	5	5
INPPL1	79	117	58
IQGAP1	20	29	10
IRAK1	337	88	68
ITGA5	158	10	10
ITGA6	20	15	15
ITGAV	59	15	39
ITGB1	59	5	5
ITSN1	20	5	5
IVNS1ABP	20	19	10
JARID2	20	5	112
JAZF1	20	5	10
JMJD1C	20	5	5
JUN	20	10	93
JUNB	20	5	5
JUND	99	68	24
JUP	20	180	112
KHDRBS1	20	5	10
KHDRBS3	40	5	49
KLF16	20	54	5
KLF5	20	5	5
KLF6	40	19	15
KLF7	40	5	15

KPNA2	99	166	19
KRAS	0	44	5
LBH	59	5	15
LEP	1168	297	765
LEPR	20	10	5
LGALS1	20	29	10
LHCGR	59	5	5
LIMD1	40	5	5
LITAF	59	10	146
LMCD1	40	15	10
LMNA	79	15	39
LMO4	20	5	10
LRCH4	20	5	5
LRRFIP2	59	5	5
LYN	20	10	5
MACF1	59	5	5
MAFF	20	156	200
MAGED1	158	5	5
MAML1	20	5	49
MAP2K1	40	39	5
MAP2K1IP1	20	29	78
MAP2K5	20	10	5
MAP2K7	79	10	10
MAP3K1	40	15	10
MAP3K11	119	49	10
MAP3K2	20	5	5
MAP3K7IP1	20	19	5
MAP3K7IP2	20	19	34
MAP4K4	20	29	5
MAPK1	20	5	5
MAPK14	20	29	5
MAPK3	79	5	10
MAPK7	20	5	39
MAPK8	20	10	5
MAPK8IP1	20	39	19
MAPKAPK2	20	68	5
MAPKAPK3	20	5	54
MAX	20	5	10
MAZ	40	44	10
MBD1	20	19	5
MBD2	20	29	10
MBD3	20	5	5
MCM5	99	5	5
MCM7	257	589	10
MCRS1	20	44	5
MDM2	20	24	24
MDM4	59	5	5
MDS1	20	10	10
MECP2	40	10	10
MED12	40	10	15
MED28	20	15	15
MED4	20	10	68
MEF2A	20	5	5
MEF2B	20	15	5
MEF2D	20	10	5
MEIS2	20	5	15

MEN1	20	15	5
MIF	515	5	5
MIZF	40	19	34
MKL2	20	5	5
MLL	20	10	10
MNAT1	20	5	5
MNT	20	5	19
MPG	20	73	34
MSX1	139	44	15
MSX2	20	5	5
MTA1	20	170	5
MTF1	20	5	5
MTPN	79	5	19
MXD3	40	10	5
MXD4	20	5	15
MXI1	20	5	5
MYBBP1A	20	54	5
MYBL2	158	5	5
MYCBP2	40	29	10
MYCN	20	5	5
MYD88	20	10	5
MYEF2	20	10	15
MYH9	20	15	10
MYO6	20	5	5
MYST3	20	10	19
MYST4	20	5	10
MZF1	0	0	0
NAB1	20	5	5
NAB2	79	34	63
NAP1L1	20	39	10
NARG1	59	24	5
NCAM1	20	5	49
NCOA1	20	15	5
NCOA2	20	5	5
NCOA3	20	15	15
NCOA4	20	5	34
NCOA5	40	19	5
NCOA6	40	10	5
NCOR1	79	5	5
NCOR2	20	24	5
NDN	158	5	5
NDNL2	20	5	5
NEK6	20	5	5
NFAT5	20	5	5
NFATC2IP	40	10	54
NFE2L1	59	15	10
NFE2L2	99	10	24
NFKB2	20	5	10
NFKBIA	20	10	5
NFKBIB	40	5	5
NFX1	20	5	5
NFYA	20	10	5
NFYC	20	10	15
NKRF	20	19	15
NME1	20	5	5
NME2	20	321	584

NOLC1	20	5	5
NOTCH1	59	15	10
NOTCH2	59	29	5
NOTCH3	20	73	49
NR1D2	20	5	5
NR1H2	20	34	19
NR2F1	20	5	10
NR2F2	59	5	10
NR2F6	20	117	141
NR6A1	20	5	5
NRAS	99	63	5
NRG1	59	5	10
NRIP1	59	5	5
NRIP2	2020	243	190
NSBP1	20	5	10
NSD1	20	5	5
NUP62	20	10	5
OGT	20	15	15
ORC1L	20	39	34
ORC2L	20	19	5
PA2G4	20	5	15
PABPN1	59	54	200
PAK2	99	15	10
PARD3	20	5	5
PARP1	99	209	34
PATZ1	0	0	0
PAWR	20	15	5
PAX3	20	5	10
PAX6	40	10	10
PBX1	20	5	5
PCGF2	20	5	15
PCOLN3	40	5	5
PCQAP	40	5	5
PDCD11	20	5	5
PDCD4	40	5	10
PDGFA	20	5	10
PDLIM1	20	88	10
PDPK1	20	5	5
PEA15	20	10	19
PEBP1	317	5	200
PEG10	20	10	5
PELP1	20	102	54
PER1	20	44	19
PFDN5	20	336	5
PFN1	238	29	10
PHB	99	24	10
PHF12	40	10	24
PHF5A	40	10	5
PIAS3	40	15	34
PIAS4	20	15	5
PIN1	40	73	49
PITX2	20	10	5
PKN1	20	5	5
PKN2	20	5	5
PKNOX1	20	5	5
PLK2	59	5	5

PMF1	40	5	68
PML	20	15	5
PODXL	59	10	29
POLR1C	20	5	34
POLR2A	20	83	29
POLR2B	20	5	34
POLR2C	20	19	5
POLR2E	59	219	5
POLR2F	139	5	5
POLR2G	59	122	5
POLR2I	40	78	5
POLR2J	20	5	78
POLR2L	20	19	15
POLR3H	40	5	10
POLRMT	59	34	5
POMC	20	5	10
POU2F1	20	10	15
PPARBP	79	5	15
PPARD	40	5	5
PPIE	20	15	5
PPM1D	40	5	10
PPP1CC	475	15	10
PPP1R8	20	39	44
PPP2R5C	20	5	5
PPP3CA	20	5	5
PPP4C	20	131	136
PPP5C	119	5	10
PQBP1	20	54	63
PRDM2	20	5	10
PRDM4	20	10	15
PRDX1	178	24	19
PREB	20	5	44
PRIM1	20	29	15
PRIM2A	40	5	44
PRKAR1A	20	54	78
PRKAR2A	20	5	5
PRKAR2B	20	15	29
PRKCA	20	5	19
PRKCI	40	10	5
PRKDC	79	5	19
PRMT2	40	15	5
PRPF6	0	0	0
PSEN1	20	5	5
PSMC3	139	200	127
PSMC5	40	5	5
PSMD14	40	136	5
PSMD9	40	39	19
PTBP1	475	5	10
PTEN	20	5	5
PTGES2	20	10	5
PTK2	20	5	5
PTMA	376	5	5
PTMS	40	229	219
PTPN1	20	5	39
PTPN11	40	34	5
PTRF	297	10	49

PTTG1	99	5	5
PURB	20	10	5
PXN	79	5	5
PYCARD	79	34	29
PYGO2	59	5	19
RAC1	158	351	331
RAC3	79	5	5
RAF1	59	5	10
RALBP1	20	5	5
RAP1A	20	10	5
RAPGEF1	20	5	49
RARA	20	5	5
RARG	20	29	10
RASA1	20	5	5
RBBP7	20	19	5
RBBP8	40	5	5
RBM14	139	49	24
RBM39	0	0	0
RBM9	79	5	15
RBPSUH	20	10	5
RBX1	178	5	156
RDBP	218	5	141
RELA	20	5	5
RFWD2	59	19	15
RFXANK	99	49	24
RGS12	20	10	5
RHOA	20	19	97
RHOB	356	5	5
RHOC	20	5	44
RING1	20	15	15
RIPK2	20	5	29
RNF11	40	10	5
RNF14	20	5	5
RNF2	20	10	15
RNF6	20	15	15
RNPS1	40	10	5
RPL6	1228	10	5
RPL7A	40	19	5
RRN3	20	15	10
RSF1	0	0	0
RUVBL1	59	5	131
RXRA	20	5	5
RXRB	40	24	5
SAFB	356	102	5
SALL1	79	34	54
SALL2	20	5	58
SALL4	139	5	34
SAP18	20	10	229
SAR1A	99	39	34
SART3	20	34	19
SATB1	40	15	15
SCAP	139	5	29
SEC61A1	20	5	10
SERPINE1	99	10	5
SERTAD1	20	5	5
SET	20	141	19

SF1	79	10	44
SFPQ	20	5	5
SFRP1	20	10	5
SGK	20	19	5
SH3BP2	40	10	5
SHC1	139	19	10
SIN3A	20	5	10
SIN3B	40	5	29
SIRT1	59	63	54
SIRT2	20	19	19
SIX5	20	44	58
SKI	40	10	10
SKIL	79	63	5
SLC19A2	20	5	5
SLC20A1	20	10	5
SLC2A4RG	20	78	5
SLC3A1	20	10	5
SMAD1	20	5	10
SMAD2	40	10	10
SMAD3	99	5	5
SMAD4	20	5	19
SMAD5	20	19	5
SMARCA4	297	10	5
SMARCA5	20	146	5
SMARCC1	20	15	39
SMARCC2	20	5	15
SMARCD1	20	5	5
SMARCD3	40	5	5
SMARCE1	40	29	5
SMURF1	20	10	10
SMURF2	40	5	5
SNAPC3	20	24	10
SNAPC4	20	34	15
SNAPC5	20	15	15
SND1	297	5	5
SNF1LK	20	10	5
SNF1LK2	20	5	5
SNRPC	119	10	141
SNW1	40	34	5
SNX6	20	5	24
SOCS3	79	5	15
SOX10	20	5	15
SOX11	257	5	24
SOX12	139	15	5
SOX2	119	175	19
SOX21	20	24	136
SOX9	40	10	5
SP1	20	5	19
SP2	20	10	5
SP3	59	10	5
SPEN	20	5	10
SPHK2	40	49	5
SQSTM1	20	5	39
SRA1	20	10	10
SREBF1	79	39	39
SREBF2	20	15	5

SRF	40	10	10
SSB	119	5	97
SSRP1	20	200	131
STAG2	20	24	39
STAMBP	20	5	10
STAT1	59	24	5
STAT2	257	122	93
STAT3	20	5	5
STAT5B	40	5	10
STAT6	20	5	10
STATIP1	20	5	19
STK4	20	5	5
STRAP	178	24	409
STUB1	40	44	54
SUFU	40	5	5
SUMO1	20	5	5
SUMO3	59	29	49
SUPT16H	99	5	5
SUPT3H	20	10	15
SUPT4H1	20	10	19
SUPT5H	79	15	10
SURF5	20	54	24
SUV39H1	20	10	24
SUZ12	40	5	10
SYNJ2BP	40	5	5
TADA2L	20	10	0
TADA3L	40	10	19
TAF1	20	19	5
TAF11	20	5	102
TAF15	20	5	73
TAF1B	20	5	5
TAF3	20	5	10
TAF6L	20	15	19
TAF7	40	10	73
TAF9	40	5	5
TAGLN	20	5	15
TARBP2	40	5	34
TARDBP	119	10	5
TAT	40	15	15
TBL1X	20	5	5
TBL1XR1	40	24	24
TBPL1	119	29	34
TBX3	20	5	5
TCEA1	158	5	5
TCEA2	40	15	24
TCEB1	20	127	5
TCEB2	238	263	15
TCEB3	20	24	5
TCERG1	20	10	5
TCF12	79	5	58
TCF19	20	5	5
TCF20	40	5	5
TCF3	40	24	24
TCF4	20	15	5
TCF7	40	10	5
TCF7L1	20	10	68

TCF7L2	20	10	15
TCFL5	40	5	10
TCOF1	178	39	5
TDG	40	24	49
TEAD1	20	5	5
TEAD2	40	44	5
TEAD3	40	721	195
TEAD4	20	73	10
TFAP4	20	10	5
TFCP2	40	15	24
TFDP1	20	15	10
TFDP2	20	19	10
TFG	178	5	5
TGFB1	20	19	24
TGFBR1	20	10	34
TGFBR3	40	10	10
TGIF2	40	54	49
THOC1	40	29	10
THOC4	20	5	5
THRAP1	20	5	15
THRAP3	59	5	5
THRAP4	40	78	24
THRAP5	20	49	5
THRAP6	20	15	29
TIAL1	20	5	44
TIAM1	20	5	15
TIMELESS	20	5	29
TIMP1	59	5	5
TLE1	20	10	10
TLE3	20	34	5
TMF1	40	10	5
TMPO	20	10	5
TNFRSF1A	20	34	19
TNFSF10	79	19	29
TOP1	40	5	5
TOP2A	20	5	10
TOPBP1	20	34	5
TOPORS	40	10	5
TP53	40	5	10
TP53BP1	20	5	19
TP53BP2	79	5	10
TRAF2	20	29	24
TRAF3	20	5	5
TRAPPC2	20	15	24
TRIM13	0	0	0
TRIM16	40	10	10
TRIM24	0	10	5
TRIM27	0	0	0
TRIM28	20	925	5
TRIM38	20	5	0
TRIP11	20	5	5
TRIP13	20	44	5
TRIP4	20	15	5
TROVE2	0	5	5
TRRAP	59	5	10
TSC2	20	15	5

TSC22D1	119	180	131
TSC22D3	59	5	19
TSG101	20	24	44
TTF1	40	5	5
TTF2	20	10	24
TXN	40	10	175
TXNIP	20	10	5
TXNRD1	59	5	5
UBA52	20	730	677
UBE1C	20	73	5
UBE2I	20	5	19
UBP1	20	19	5
UBTF	20	19	24
UCP2	59	73	10
UPF1	79	5	19
VAPA	20	58	5
VDR	40	15	39
VEGFA	0	0	0
VEZF1	0	0	0
VHL	40	34	34
VPS39	59	5	5
VPS4B	20	5	34
VPS72	20	54	44
VRK1	20	5	44
WIPF1	0	0	0
WWP1	20	19	15
WWTR1	20	5	5
XAB2	40	19	24
XBP1	20	5	5
XIST	119	5	19
XRCC6	297	5	628
YAP1	218	5	5
YBX1	59	1188	1281
YWHAH	20	39	63
YWHAQ	20	5	10
YWHAZ	20	5	5
YY1	59	54	5
ZBTB10	20	5	10
ZBTB4	59	5	5
ZBTB7A	20	0	5
ZFP161	40	5	10
ZMYND11	20	10	19
ZNF143	20	19	5
ZNF146	99	10	58
ZNF148	20	5	5
ZNF224	20	5	5
ZNF238	20	10	5
ZNF24	20	10	5
ZNF254	0	0	0
ZNF263	20	39	19
ZNF274	20	19	5
ZNF281	20	5	39
ZNF367	20	5	10
ZNF384	20	5	5
ZNF423	40	19	5
ZNF496	59	10	10

ZNF589	59	10	5
ZNF593	40	19	58
ZNF76	20	5	10
ZNHIT3	20	68	122

*hNCC count in tag per million (SAGE library total count=50500)
**hES3 count in tag per million (SAGE library total count=205353)
***hES4 count in tag per million (SAGE library total count=209232)

Supplementary Table 6.

Common transcription factors to hNCC and hES3/4

symbol	hNCC tpm*	HES3 tpm**	HES4 tpm***
AFF1	20	15	49
ARNT2	40	5	10
ATF3	20	5	10
ATF4	257	19	273
ATF7	20	5	10
ATRX	40	5	5
BRD8	40	24	5
BTAF1	20	5	5
BTG2	20	15	5
CEBPB	40	19	19
CNOT7	59	78	5
CREB1	20	5	5
CREM	20	15	5
CUTL1	20	5	5
DRAP1	257	112	73
E2F1	40	10	5
E2F3	40	29	5
E2F4	20	5	5
E2F5	20	5	5
EGR1	158	49	5
ELF2	20	24	5
ELK1	20	39	39
ELK3	20	5	15
EP300	20	19	19
ERF	139	83	5
ETS1	337	5	15
ETS2	20	29	15
ETV1	20	5	10
ETV6	40	5	5
FOXD3	40	5	10
FOXK2	40	5	15
FOXM1	20	58	5
FOXP1	20	5	5
FOXP4	59	5	487
FUBP1	20	5	5
GABPA	20	29	29
GLI2	20	19	15
GLI3	99	5	5
GTF2I	178	5	5
HCFC1	40	19	34
HDAC1	20	5	39
HDAC2	40	29	5
HES6	416	44	29
HIRA	99	10	24
HSF1	20	34	5
JUNB	20	5	5
JUND	99	68	24
KLF7	40	5	15

LMO4	20	5	10
MBD1	20	19	5
MDS1	20	10	10
MEF2A	20	5	5
MEF2B	20	15	5
MEF2D	20	10	5
MEIS2	20	5	15
MNT	20	5	19
MSX1	139	44	15
MSX2	20	5	5
MTA1	20	170	5
MTF1	20	5	5
MYCN	20	5	5
NFAT5	20	5	5
NFKB2	20	5	10
NFX1	20	5	5
NFYA	20	10	5
NFYC	20	10	15
NR1D2	20	5	5
NR1H2	20	34	19
NR6A1	20	5	5
PA2G4	20	5	15
PAX3	20	5	10
PAX6	40	10	10
PBX1	20	5	5
PCGF2	20	5	15
PHF5A	40	10	5
PITX2	20	10	5
PML	20	15	5
PRDM2	20	5	10
PTTG1	99	5	5
RARA	20	5	5
RXRA	20	5	5
RXRB	40	24	5
SALL1	79	34	54
SALL2	20	5	58
SATB1	40	15	15
SIX5	20	44	58
SMAD1	20	5	10
SMAD3	99	5	5
SMAD4	20	5	19
SMAD5	20	19	5
SOX2	119	175	19
SOX21	20	24	136
SRF	40	10	10
STAT1	59	24	5
STAT2	257	122	93
STAT3	20	5	5
STAT6	20	5	10
TAF11	20	5	102
TAF6L	20	15	19
TAF7	40	10	73

TBX3	20	5	5
TCEA1	158	5	5
TCEA2	40	15	24
TCF19	20	5	5
TCFL5	40	5	10
TEAD1	20	5	5
TEAD2	40	44	5
TEAD3	40	721	195
TEAD4	20	73	10
TGIF2	40	54	49
VDR	40	15	39
XBP1	20	5	5
ZNF24	20	10	5

*hNCC count in tags per million (SAGE library total count=50500)
**hES3 count in tags per million (SAGE library total count=205353)
***hES4 count in tags per million (SAGE library total count=209232)

Supplementary Table 7.

hNCC and hES commonly expressed genes involved in cell proliferation

Symbol	hNCC tpm*	HES3 tpm**	HES4 tpm***
AATF	20	5	5
ABL1	59	10	33
ABL2	20	10	10
ACACA	20	5	5
ACIN1	59	102	5
ACP1	20	5	5
ACTB	436	5	5
ACTG1	20	15	19
ACTN1	20	5	10
ACTN4	20	5	14
ACVR1B	20	15	5
ADAM10	59	5	5
ADAM15	119	10	19
ADAMTS1	40	15	29
ADAR	59	5	5
ADFP	40	19	91
ADM	20	5	14
ADRA2A	20	5	14
ADRBK1	59	5	14
AFF1	20	15	48
AHCY	59	205	153
AK2	20	5	5
AK3L1	20	34	10
AKAP12	20	5	5
AKAP13	198	10	14
AKT1	139	5	5
AKT2	20	68	5
AKT3	20	5	10
ALDH1A1	20	15	5
AMACR	20	10	5
ANAPC5	20	93	43
ANP32A	40	5	5
ANXA1	59	19	76
ANXA11	20	24	10
ANXA2	20	5	19
ANXA7	20	15	19
APBB1	40	29	53
APBB2	20	10	5
APC	20	5	5
APOE	20	24	10
APP	20	5	5
APRIN	20	19	24
ARAF	59	34	5
ARD1A	99	58	43
ARF1	20	15	5
ARHGAP5	20	5	5
ARHGEF1	20	19	24

ARHGEF2	20	5	14
ARID3A	59	10	19
ARL1	59	19	24
ARL3	20	24	10
ARRB2	20	5	478
ATF2	20	10	19
ATF3	20	5	10
ATF4	40	5	5
ATF5	99	263	201
ATM	20	10	29
ATP5B	733	10	10
ATP5F1	20	243	5
ATP5G1	40	166	100
ATP5G2	20	15	5
ATP6AP1	20	29	24
ATPIF1	20	5	5
AXL	40	5	5
B4GALT2	40	44	57
B4GALT7	40	10	19
BAMBI	20	10	5
BAP1	40	63	5
BARD1	40	10	5
BAX	20	5	10
BCAR1	158	54	38
BCAR3	20	5	5
BCAT1	79	5	5
BCL10	20	10	33
BCL2L1	20	5	14
BCL2L11	20	15	5
BCR	79	5	10
BID	20	78	29
BIN1	99	5	19
BIRC4	20	5	19
BIRC5	20	5	5
BIRC6	20	5	5
BLM	40	5	14
BMP7	40	10	24
BMPR1A	20	5	33
BMPR2	59	10	5
BRD4	20	10	5
BRF2	20	15	10
BSG	515	5	167
BTG1	59	34	53
BTG2	40	15	10
BTG3	20	1641	478
BTRC	20	5	5
BUB1B	20	5	19
BUB3	59	5	5
C19ORF10	20	58	5
C1QBP	20	15	5
C5ORF13	20	5	5
C6ORF108	40	34	24

C6ORF66	20	88	5
C9ORF78	20	5	5
CABLES1	20	5	10
CACNA2D2	40	19	19
CALM1	20	112	5
CALM3	40	58	5
CALR	455	273	119
CAMKK2	40	5	5
CAPN1	59	200	53
CAPNS1	139	10	10
CAPZA1	59	5	24
CASC3	20	68	5
CASP2	40	29	5
CASP3	20	10	100
CAST	20	5	5
CAV1	20	5	5
CBFB	20	5	10
CBLB	59	5	5
CBX1	139	127	5
CCDC6	20	15	5
CCNA2	20	44	5
CCNB1	59	19	10
CCND1	20	19	10
CCND2	20	24	5
CCNF	20	5	38
CCNG1	40	19	5
CCNI	20	151	5
CCNL2	20	5	5
CCT2	257	5	5
CCT3	20	278	292
CCT5	297	195	311
CCT7	158	443	454
CD24	20	5	14
CD44	20	5	5
CD46	59	24	67
CD47	20	5	29
CD63	218	253	5
CD81	20	10	5
CD99	416	5	162
CDC16	20	29	19
CDC2	158	68	62
CDC25B	40	15	5
CDC27	20	15	5
CDC2L1	20	5	5
CDC2L5	20	15	5
CDC2L6	20	5	5
CDC37	178	117	43
CDC42	20	5	24
CDC42BPB	20	29	29
CDCA4	20	5	5
CDCA7	20	15	29
CDH2	40	5	5

CDH4	40	5	5
CDK10	40	5	53
CDK2	40	29	29
CDK2AP1	178	5	14
CDK3	59	5	5
CDK4	158	5	153
CDK5	20	5	5
CDK6	40	5	10
CDK7	20	44	5
CDK9	40	44	24
CDKN1A	139	5	14
CDKN1B	40	15	5
CDKN1C	178	5	5
CDKN3	20	73	14
CDT1	59	15	10
CEBPB	40	19	19
CENPF	59	5	10
CFDP1	178	24	33
CFL1	40	5	5
CHEK1	20	5	5
CHERP	40	10	5
CHKA	20	5	19
CIRBP	20	5	5
CITED2	20	5	10
CKLF	40	10	29
CKS1B	59	5	5
CKS2	218	234	5
CLCN7	20	49	5
CLK1	99	24	10
CLN3	20	341	5
CLTC	79	5	5
CLU	40	5	139
CNN1	99	19	33
CNOT7	20	5	5
CNOT8	20	5	10
CNP	20	15	5
CNTFR	20	1641	5
COL18A1	79	68	62
COL1A1	20	5	14
COL2A1	119	19	14
COL4A1	20	10	5
COL4A2	20	63	48
COL6A1	40	78	29
COL6A2	59	10	10
COL6A3	59	5	48
COPE	20	15	5
COPS5	20	93	53
CORT	20	10	5
COX17	40	5	81
CPSF4	59	5	5
CRABP2	317	317	124
CREB1	20	5	5

CREBBP	20	5	19
CREM	20	15	5
CRIP2	20	10	5
CRK	238	44	86
CSDA	40	10	43
CSE1L	119	112	5
CSF1R	20	10	5
CSNK1D	40	19	5
CSNK1E	20	5	5
CSNK2A1	20	5	10
CSNK2A2	20	29	38
CSNK2B	79	185	5
CSPG2	20	5	5
CST3	218	5	53
CTBP1	40	15	10
CTBP2	20	10	24
CTDSPL	40	5	5
CTGF	59	88	48
CTNNA1	40	19	5
CTNNB1	99	156	57
CTNNBIP1	20	10	14
CTSB	59	5	10
CTSC	20	297	10
CTSD	594	355	201
CTSL	20	63	48
CTSL2	20	141	119
CUL1	59	112	5
CUL3	20	5	10
CUL4A	20	34	5
CUL5	20	10	14
CUL7	40	29	10
CUTL1	20	5	5
CXCL12	20	15	5
CYP20A1	40	10	5
CYR61	20	97	14
DAP	20	5	5
DAP3	99	5	5
DAXX	59	10	38
DBN1	20	5	24
DCBLD2	158	5	14
DCHS1	20	5	10
DCTN2	59	127	5
DDB1	119	5	5
DDR1	59	15	5
DDX11	40	5	14
DDX21	59	10	5
DDX3X	178	5	10
DDX5	20	5	5
DDX56	59	5	5
DERL2	20	93	57
DGKZ	40	29	29
DHCR7	40	54	5

DHFR	20	15	5
DHPS	40	44	53
DIABLO	20	19	10
DICER1	40	5	5
DIRAS1	20	15	5
DKC1	20	5	72
DKK3	119	5	33
DLG1	20	5	5
DLG5	59	49	29
DLG7	20	5	14
DLL1	40	15	19
DMTF1	20	15	29
DNAJA1	317	161	124
DNAJA2	40	5	5
DNAJA3	59	5	5
DNAJB1	178	5	57
DNAJB2	99	19	5
DNAJB6	20	127	105
DNM2	178	5	5
DOK1	20	5	14
DPH1	20	29	24
DSCR1	20	15	5
DSP	59	10	5
DTYMK	40	107	119
DUSP1	79	10	5
DUSP22	20	10	5
DUSP6	59	10	10
DVL1	158	88	72
DYNC1H1	20	1641	478
DYRK1B	59	19	5
E2F1	40	10	5
E2F3	40	5	5
E2F4	20	5	19
E2F7	20	10	5
EBNA1BP2	20	127	105
EDF1	40	15	10
EDG4	20	39	33
EDNRB	59	5	14
EEF1D	238	93	53
EEF1E1	59	5	10
EEF2K	40	5	14
EFEMP2	79	15	5
EFNB1	40	10	5
EFNB3	20	15	5
EGLN3	20	5	10
EGR1	20	29	72
EI24	79	141	72
EIF1AY	20	5	10
EIF2AK1	40	68	86
EIF2C2	20	15	10
EIF3S2	59	15	10
EIF4A1	337	716	10

EIF4B	20	15	5
EIF4E	20	58	62
EIF4EBP1	79	93	110
EIF4G2	139	5	5
EIF5A	99	5	10
ELAVL1	99	5	5
ELK1	20	5	38
ELL	40	5	5
EMP3	40	5	19
ENO1	20	10	10
EP300	20	5	19
EPB41L3	40	10	19
EPHA2	20	5	5
EPHB2	20	5	10
EPHB3	20	10	14
EPHB4	20	24	10
EPS15	20	5	5
ERBB2	79	5	5
ERBB3	99	5	10
ERCC3	79	5	5
ERF	139	83	5
ESPL1	20	15	5
ESRRA	40	44	24
ETFB	40	19	33
ETS1	337	5	14
ETS2	20	5	19
ETV6	20	5	5
EWSR1	139	5	72
EXTL3	40	29	33
EZH2	119	63	48
F11R	257	5	158
F2R	79	5	10
FADD	79	19	53
FADS1	257	5	24
FADS2	317	15	5
FANCA	20	15	5
FANCL	20	10	5
FASN	59	5	33
FBLN1	59	10	5
FBN2	119	5	10
FBXW11	20	29	5
FDXR	20	39	62
FGFR1	20	146	5
FGFR1OP	20	5	5
FGFR2	20	5	5
FGFR3	20	5	67
FGFRL1	40	5	5
FHIT	20	5	19
FKBP1A	20	5	14
FKBP1B	40	107	100
FKBP4	40	15	10
FLOT1	79	5	10

FN1	20	5	5
FOS	59	15	5
FOXA2	79	39	10
FOXM1	20	5	5
FOXO1A	20	19	5
FOXO3A	20	10	5
FRS2	20	5	5
FSCN1	40	34	14
FTH1	20	15	5
FTL	40	44	5
FURIN	40	58	43
FXN	40	5	10
FYN	20	5	5
FZD3	20	19	14
G6PD	20	54	10
GABARAP	20	10	220
GADD45GIP1	99	5	5
GAK	20	19	5
GAP43	40	5	5
GAS1	59	34	14
GAS6	40	19	24
GBF1	139	34	24
GCNT1	20	5	19
GDF11	20	19	10
GDF15	20	15	14
GFM1	59	5	19
GFRA1	20	10	5
GGA1	20	5	5
GGA2	40	5	10
GIPC1	20	29	24
GJA1	40	5	153
GLI2	20	5	14
GLI3	99	5	5
GLMN	20	5	5
GMEB1	20	5	10
GNA11	79	5	24
GNA12	59	39	5
GNAI2	59	219	5
GNAQ	20	5	10
GNB2L1	40	127	57
GNG2	99	5	14
GNG4	20	19	19
GNL3	20	102	148
GPC1	20	5	10
GPC3	20	5	5
GPC4	20	15	76
GPI	40	5	5
GPIAP1	20	10	5
GPX1	218	24	225
GPX3	20	24	10
GPX4	238	769	5
GRB10	40	19	5

GRB2	40	10	5
GRN	79	5	5
GSK3B	20	5	10
GSN	40	34	5
GSTM1	20	29	10
GSTP1	1030	5	5
GTF2B	119	19	38
GTPBP1	20	5	5
HADHA	356	58	5
HADHB	20	24	19
HDAC1	20	15	38
HDAC10	20	5	10
HDAC2	40	19	29
HDAC3	20	5	5
HDAC5	59	63	5
HDAC6	40	44	14
HDGF	20	10	14
HES1	40	5	29
HGS	20	83	29
HIF1A	79	117	91
HIP1	20	49	5
HIPK1	20	5	5
HIPK2	20	5	19
HK1	40	5	5
HLA-DRB1	20	5	10
HMGA1	20	44	19
HMGA2	20	5	5
HMGB1	119	15	5
HMGCR	40	5	14
HMGN1	20	5	5
HMMR	59	10	5
HMOX1	40	5	24
HNRPA0	59	10	14
HNRPA1	40	49	48
HNRPA2B1	20	5	5
HNRPAB	20	29	38
HNRPC	139	497	5
HNRPD	416	677	540
HNRPF	59	10	210
HNRPK	317	15	110
HNRPM	277	10	253
HNRPR	40	19	14
HNRPU	20	73	5
HRAS	59	54	33
HRASLS3	20	29	105
HSD11B2	20	10	29
HSF1	20	5	5
HSH2D	20	5	464
HSP90B1	99	5	10
HSPA1A	356	24	14
HSPA5	277	472	249
HSPB8	79	5	14

HSPD1	59	19	5
HSPG2	178	19	10
ICAM3	20	5	14
ICMT	59	68	5
ID1	337	497	358
ID2	40	5	33
ID3	40	10	5
ID4	40	19	5
IFIT3	40	15	10
IFITM3	59	15	10
IFNAR1	20	10	43
IGBP1	40	10	43
IGF1R	20	5	5
IGF2	20	68	10
IGF2R	20	5	24
IGFBP2	20	394	10
IGFBP3	20	5	5
IGFBP4	20	5	86
IGFBP5	20	10	5
IGFBP7	218	24	14
IGSF4	59	5	5
IHPK2	20	5	5
IK	40	24	5
IKBKB	20	5	10
IL13RA1	40	10	14
IL27RA	40	10	5
IL2RA	20	10	5
IL6ST	20	5	14
ILF2	198	10	5
ILF3	20	29	10
ILK	59	10	62
IMPDH1	20	5	14
IMPDH2	119	5	5
ING1	20	5	5
ING5	20	5	38
INPP4A	20	5	5
INSIG1	40	10	24
INSR	20	5	5
IRS1	20	15	10
IRS2	20	5	5
ITCH	20	5	5
ITGA3	20	5	24
ITGA5	158	10	10
ITGA6	59	73	76
ITGAV	59	15	5
ITGB1	970	5	177
ITGB5	40	10	5
IVNS1ABP	20	19	10
JARID2	20	5	5
JMJD1B	20	39	24
JUB	59	5	14
JUN	20	5	10

JUNB	20	5	5
JUND	99	5	24
JUP	79	180	110
KHDRBS1	139	5	48
KIF11	20	5	48
KIF13A	20	5	5
KIF2C	79	10	48
KLC2	20	24	5
KLF5	20	5	5
KLF6	40	24	5
KRT8	20	15	5
LAMA1	40	29	29
LAMA2	20	5	14
LAMA5	40	68	5
LAMB1	40	63	62
LAMC1	20	5	33
LAPTM4B	59	15	24
LASS1	20	5	5
LATS1	20	10	14
LDHA	20	5	196
LEP	1168	297	750
LEPR	20	10	5
LGALS1	693	29	81
LGALS3	20	5	10
LGR4	20	5	72
LIFR	79	5	10
LIG1	79	34	19
LIMK1	59	58	33
LITAF	20	5	10
LMNA	79	15	14
LOX	139	5	5
LPIN1	20	5	5
LRDD	40	15	19
LRIG1	99	5	5
LRP1	20	5	10
LRP2	40	5	5
LRPAP1	20	5	5
LTBP1	40	24	10
LTBP3	198	5	14
LUM	79	10	29
LY6E	59	170	57
LYN	20	10	5
LZTS1	20	5	14
LZTS2	99	5	5
MAD1L1	40	15	14
MAD2L1	59	5	10
MAFF	20	156	196
MAGED1	158	5	5
MAGED2	119	5	10
MAGED4	20	10	5
MAP2K1	40	5	5
MAP2K2	158	5	5

MAP2K4	20	34	14
MAP2K5	20	10	5
MAP2K7	79	63	10
MAP3K1	40	15	10
MAP3K11	119	5	10
MAP3K2	20	5	5
MAPK1	20	5	5
MAPK12	20	34	19
MAPK14	20	29	24
MAPK3	79	5	5
MAPK6	40	107	53
MAPK7	20	88	38
MAPK8	20	10	24
MAPKAPK2	20	68	38
MAPRE1	119	5	86
MAPRE2	20	10	5
MAX	20	5	5
MAZ	40	78	57
MBD1	20	19	5
MBD2	20	29	10
MBD3	40	88	5
MCAM	119	5	19
MCL1	198	10	5
MCM2	20	10	53
MCM3	20	5	119
MCM5	99	5	5
MCM7	257	5	282
MCTS1	40	97	139
MDK	713	5	5
MDM2	20	24	24
MDM4	20	5	5
MDS1	20	10	10
MECP2	40	10	5
MED28	20	5	5
MEN1	20	15	5
MEST	20	10	5
METAP2	79	44	14
METTL3	40	88	158
MFN2	20	10	24
MGAT4B	337	10	53
MICA	40	10	5
MIF	515	10	10
MKI67	40	5	5
MLL	20	5	5
MMP14	119	10	5
MMP15	20	54	38
MMP2	20	10	14
MMP24	20	10	5
MNAT1	20	5	5
MNT	20	5	5
MOG	990	287	531
MORF4L1	79	131	253

MSI1	59	5	14
MSI2	20	10	5
MST1R	40	10	5
MSX1	139	5	14
MSX2	20	15	5
MT2A	218	34	38
MTA1	198	170	5
MTAP	20	5	10
MTCH1	20	5	5
MTHFD1	20	68	10
MVP	178	15	10
MXD4	20	10	14
MXI1	59	5	10
MYBBP1A	20	54	14
MYBL2	158	5	10
MYCL1	20	5	10
MYCN	40	5	5
MYD88	20	10	5
MYH10	59	5	5
MYL9	238	127	5
MYST4	20	15	10
NAB2	79	5	62
NAP1L1	99	19	268
NASP	99	10	10
NBN	40	10	5
NCAM1	20	229	48
NCK2	59	58	29
NCOA1	20	5	5
NCOA2	713	5	91
NCOA3	20	15	14
NCOA4	20	5	33
NCOA6	40	10	5
NDE1	20	5	10
NDN	158	10	5
NDNL2	20	5	24
NDUFV1	20	5	5
NEU1	20	10	10
NF2	40	5	5
NFAT5	20	5	5
NFKB2	20	29	10
NFKBIA	20	5	5
NFKBIB	40	5	5
NKIRAS2	158	15	24
NME1	20	321	5
NME2	20	5	5
NOL8	40	5	10
NOTCH1	20	15	5
NOTCH2	20	29	14
NP	20	5	48
NPDC1	79	49	33
NPM1	99	15	19
NR1H2	20	34	19

NR6A1	20	19	5
NRAS	99	63	5
NRD1	79	5	5
NRG1	59	5	10
NRG4	20	49	5
NRIP1	20	5	10
NUDC	119	5	5
NUP62	20	10	5
NUP98	59	10	5
OAZ1	40	19	5
ODC1	455	161	5
OGFR	20	15	5
OPTN	40	19	5
PA2G4	40	5	86
PAFAH1B1	20	15	5
PAK4	40	10	38
PALM	337	39	5
PAPPA	40	5	5
PARK7	139	5	119
PARP1	99	5	10
PAWR	20	24	38
PAX3	20	5	10
PAX6	20	10	10
PBEF1	20	5	10
PBX1	119	5	76
PCBP4	158	5	19
PCGF2	20	5	14
PCNA	119	268	105
PCOLN3	40	5	5
PCYT1A	20	5	5
PDAP1	119	151	100
PDGFA	20	34	10
PDGFC	40	5	14
PDIA3	238	5	14
PDLIM2	20	19	19
PDPK1	20	5	14
PEA15	20	5	19
PEBP1	317	307	196
PEG10	20	49	19
PELP1	20	102	53
PEMT	79	73	5
PER1	20	44	19
PFDN5	297	336	5
PFN1	574	15	5
PFN2	79	10	19
PGK1	20	5	24
PHB	99	278	5
PHC1	20	78	158
PHLDA2	99	5	5
PIK3CB	20	29	10
PIK3CD	59	5	19
PIK3R2	20	34	33

PIN1	40	73	48
PITPNA	139	5	14
PITX2	20	10	5
PKM2	119	10	19
PKN1	20	10	5
PLA2G6	20	10	5
PLAUR	20	5	5
PLCD1	20	5	5
PLEC1	139	5	29
PLK1	40	5	5
PLK2	59	5	5
PLP1	40	5	5
PLSCR1	20	5	10
PMAIP1	40	10	5
PML	20	15	5
PNN	20	5	5
PNPT1	20	5	10
POLD4	40	44	5
POLL	20	15	5
POLR2J	20	5	5
POMC	20	5	10
POR	20	29	57
PPARBP	79	5	5
PPARD	40	5	5
PPAT	20	10	5
PPIA	1881	5	2232
PPM1D	40	5	10
PPM1G	40	5	91
PPP1CA	20	5	10
PPP1CC	475	282	14
PPP1R12C	40	10	5
PPP1R15A	20	5	19
PPP1R8	20	5	5
PPP2CA	20	5	33
PPP2R1A	119	5	172
PPP2R5C	20	19	29
PPP3CA	20	5	5
PPP5C	119	5	5
PPT1	40	5	33
PRCC	20	15	5
PRDM4	20	10	14
PRDX1	59	24	5
PRDX3	40	5	24
PRDX4	99	5	72
PREB	20	5	43
PRKAR1A	20	15	33
PRKAR2B	20	5	29
PRKCA	20	5	19
PRKCI	40	10	10
PRKCSH	20	10	5
PRKRA	20	5	19
PRMT5	20	146	119

PRNP	20	5	5
PRPF19	158	122	76
PRPF8	20	5	5
PRRX2	20	10	5
PRUNE	20	10	24
PSAP	20	5	5
PSEN1	20	5	5
PSMB2	59	10	5
PSMC1	40	73	38
PSMC3	139	15	124
PSMC4	40	10	10
PSMC5	40	5	5
PSMD2	317	5	10
PSME2	317	5	143
PSMF1	20	29	5
PTEN	20	5	5
PTK2	59	68	76
PTMA	20	5	5
PTN	40	10	5
PTP4A3	40	5	10
PTPN1	20	34	38
PTPN11	40	34	5
PTPN14	20	136	722
PTPN2	20	15	5
PTPRA	20	34	33
PTPRF	158	146	86
PTPRG	594	15	5
PTPRS	20	5	10
PTTG1	99	5	5
PVR	178	10	10
QSCN6	119	10	29
RAB1A	20	5	10
RABGEF1	40	5	5
RAC1	158	5	5
RAF1	59	5	48
RALA	40	34	29
RALBP1	119	15	5
RALGDS	59	39	5
RAP1B	20	5	5
RAPGEF1	20	5	5
RAPGEF2	40	19	5
RARA	20	5	5
RARG	20	29	10
RASA1	40	5	5
RASSF4	20	10	5
RB1CC1	20	5	5
RBBP4	20	102	33
RBBP7	20	19	5
RBBP9	20	24	14
RBM3	20	5	5
RBM5	20	15	62
RBM6	40	102	38

RBM9	40	5	14
RBP1	198	34	67
RBPSUH	20	5	5
RCE1	20	15	5
RDBP	218	122	139
RELA	20	5	5
RFC1	20	34	10
RGL2	99	5	29
RGS2	20	15	5
RGS4	20	5	10
RHOA	20	5	5
RHOB	356	19	38
RHOC	59	112	43
RING1	20	15	14
RIPK2	20	5	29
RPL23A	40	29	43
RPS19	20	5	29
RPS27	99	5	24
RPS3A	20	19	10
RPS4X	20	10	5
RPSA	1703	8985	19
RRM1	20	5	10
RRM2	20	15	43
RSN	20	5	5
RUVBL1	59	5	129
RUVBL2	20	5	19
RXRA	20	5	5
RXRB	40	24	5
RYK	20	29	24
S100A11	158	5	5
SAE1	20	19	14
SALL2	20	5	57
SART1	40	34	19
SART3	40	34	5
SBF1	20	24	24
SCAMP2	20	10	5
SCAMP3	20	5	48
SCAMP4	20	5	5
SCYE1	20	5	5
SDC2	20	5	14
SEC61A1	198	5	10
SEMA3F	59	49	5
SEMA6A	40	5	5
SENP1	20	15	5
SERPINE1	297	10	5
SERPINF1	40	34	29
SERPINH1	20	15	5
SERTAD1	20	5	5
SESN1	20	5	5
SET	198	687	578
SF1	20	5	43
SF3A2	99	5	76

SF3A3	20	5	19
SF3B2	59	5	5
SF3B3	20	5	29
SFN	20	5	10
SFRP1	20	10	5
SFRP2	59	93	38
SFRS1	20	15	10
SFRS2	20	5	5
SFRS2IP	40	5	10
SFRS3	20	278	210
SFRS5	178	10	5
SGK	20	19	5
SH3BP2	40	15	5
SHB	20	5	10
SHC1	20	19	5
SHFM1	158	224	5
SIN3A	20	5	10
SIRT1	59	63	5
SKI	40	10	5
SKIL	20	5	5
SKP1A	297	5	5
SLC12A4	59	19	19
SLC1A3	20	5	10
SLC29A1	59	5	5
SLC29A2	20	10	14
SLC3A2	20	49	48
SLC7A5	20	63	5
SMAD1	20	5	10
SMAD2	1505	1549	4459
SMAD3	40	5	5
SMAD4	20	44	43
SMAD5	20	19	24
SMARCA4	158	156	48
SMARCA5	198	146	158
SMARCE1	59	5	5
SMO	20	5	5
SMOX	40	5	5
SMYD3	20	5	5
SOCS3	79	15	14
SOD1	99	10	10
SOX9	40	10	10
SP1	20	5	19
SPARC	20	273	206
SPHK2	40	49	5
SPINT2	20	15	19
SPRED1	20	15	14
SPRY4	20	10	5
SPTBN1	79	5	10
SRA1	20	10	14
SREBF1	79	5	38
SRF	40	5	10
SS18	40	44	10

SSR1	20	24	19
STAMBP	20	5	10
STARD10	20	10	14
STARD13	20	5	5
STAT1	59	24	33
STAT3	20	19	5
STAT5B	40	5	10
STAT6	20	5	10
STAU1	59	44	53
STK11	20	5	5
STK17B	99	5	5
STMN1	20	351	411
STRAP	20	24	14
STUB1	40	44	53
SUFU	40	5	5
SUMO1	158	5	5
SUMO2	20	5	10
SUMO3	59	29	10
SURF1	20	88	19
SURF4	40	5	10
SURF6	20	29	14
SUV39H1	20	10	24
SUZ12	40	15	10
SYMPK	20	39	5
TACC1	59	5	5
TAF7	40	10	5
TAX1BP3	337	44	19
TBC1D8	20	10	5
TBPL1	119	29	33
TBRG4	20	5	43
TCEB3	20	24	10
TCF12	79	5	5
TCF19	20	5	5
TCF3	20	24	14
TCF4	20	15	5
TCF7	40	10	5
TCOF1	20	5	14
TCP1	554	5	5
TEAD4	20	73	10
TERF1	20	5	5
TFDP1	20	5	14
TFG	178	161	5
TFRC	20	5	5
TGFB1	20	19	24
TGFBR1	40	10	33
TGFBR3	40	10	10
THBS1	20	5	14
THBS2	20	1641	478
THOC1	40	29	10
THY1	139	97	5
TIAL1	20	24	10
TIAM1	20	5	14

TIMELESS	20	5	5
TIMP1	59	5	5
TIMP2	79	5	10
TIMP3	158	10	5
TJP1	119	5	10
TMSB10	1129	1305	808
TMSB4X	20	19	5
TNC	40	15	10
TNFAIP8	20	49	14
TNFRSF12A	218	102	91
TNFRSF19	20	15	10
TNFRSF1A	20	5	19
TNFRSF21	20	19	5
TNFRSF6B	20	5	10
TNFSF10	79	19	29
TNK2	20	15	5
TNKS	20	5	14
TOB1	20	10	5
TOP1	40	5	5
TOPORS	40	10	29
TP53	20	49	33
TP53BP1	20	5	19
TP53I11	40	5	33
TP53INP1	20	5	5
TPM1	772	5	717
TPM2	1010	44	53
TPM3	1683	2844	2748
TPT1	20	5	5
TPX2	20	24	5
TRAF2	20	29	24
TRAF4	20	58	14
TRAP1	99	5	5
TRIB1	20	39	38
TRIM25	20	5	5
TRIM28	356	5	5
TRIM35	20	15	5
TRIT1	20	15	5
TRO	40	39	29
TRRAP	59	5	10
TSC2	20	15	10
TSC22D1	119	180	129
TSG101	20	24	43
TSN	20	5	5
TSPAN3	178	78	105
TSPAN31	40	29	19
TTK	59	5	19
TUSC2	40	29	5
TXN	40	5	24
TXNIP	20	10	10
TXNL1	20	5	5
TXNRD1	20	10	5
TYMS	20	112	19

TYRO3	20	63	5
UBC	59	5	5
UBE1	20	5	14
UBE2B	20	5	5
UBE2C	99	156	5
UBE2E3	20	10	5
UBE2V2	40	15	5
UBTF	20	5	5
UCHL1	257	5	722
UCP2	59	5	10
UGCG	20	5	10
UNC119	79	73	43
UPP1	20	273	86
USP21	20	19	5
USP3	20	5	10
USP7	119	5	48
USP9X	20	5	10
VDAC1	218	10	5
VDR	40	15	38
VEGFB	139	44	5
VEGFC	20	5	5
VHL	40	5	24
VIL2	20	10	10
VIM	20	5	5
VPS28	59	34	10
VRK3	59	10	5
VTI1B	40	5	5
WARS	79	10	5
WASF2	20	5	10
WEE1	40	5	62
WNT5A	20	5	5
XBP1	20	5	5
XPC	59	24	5
XRCC1	139	15	19
XRCC2	495	5	167
XRCC3	20	49	19
XRCC6	297	5	617
XRN2	79	5	5
YAP1	218	102	33
YBX1	59	5	5
YME1L1	20	5	5
YPEL3	59	39	38
YTHDF2	40	83	129
YY1	59	5	10
ZDHHC17	20	5	14
ZFP36L1	198	5	38
ZFP36L2	99	10	5
ZMYND11	20	10	19
ZNF148	20	5	5
ZNF259	20	5	10
ZNF639	20	5	5
ZRF1	20	5	5

ZYX	59	5	76

*hNCC count in tags per million (SAGE library total count=50500)
**hES3 count in tags per million (SAGE library total count=205353)
***hES4 count in tags per million (SAGE library total count=209232)

Supplementary Table 8.

Genes expressed in hNCC with a Tissue Preferential Expression analysis range value = 1

symbol	hNCC PA score	hNCC tpm*	HES3 tpm**	HES4 tpm***
AMIGO3	6.91	20	0	0
C10ORF85	6.91	20	0	0
DKFZP761N09121	6.91	20	0	0
DNAH1	6.91	20	0	0
FAM70B	6.91	20	0	0
FLJ16139	6.91	20	0	0
FLJ20345	6.91	20	0	0
FLJ31295	6.91	20	0	0
FLJ31438	7.6	40	0	0
FLJ40126	6.91	20	0	0
GABRR3	6.91	20	0	0
HIST1H1D	6.91	20	0	0
HIST1H2BE	6.91	20	0	0
HIST1H2BJ	6.91	20	0	0
HIST1H3B	6.91	20	0	0
HIST1H4F	6.91	20	0	0
HMFN0672	7.6	40	0	0
HOXC5	8.52	99	0	0
HOXD9	6.91	20	0	0
KCNG2	6.91	20	0	0
KIAA1822L	6.91	20	0	0
LOC255177	6.91	20	0	0
LOC352909	6.91	20	0	0
LOC400340	6.91	20	0	0
LOC401021	6.91	20	0	0
LOC401485	6.91	20	0	0
LOC440502	6.91	20	0	0
LOC440993	6.91	20	0	0
LOC441053	6.91	20	0	0
LOC493860	6.91	20	0	0
MGC16372	6.91	20	0	0
MGC48915	6.91	20	0	0
PP3856	6.91	20	0	0
PRDM12	8.01	59	0	0
PRH1	6.91	20	0	0
RHEBL1	6.91	20	0	0
SH3GLP2	6.91	20	0	0
STOX2	6.91	20	0	0
TIGD3	6.91	20	0	0
UCN	6.91	20	0	0
WNT7A	7.6	40	0	0
ZNF157	6.91	20	0	0
ZNF417	7.6	40	0	0
ACBD7	6.91	20	0	5
ADAMTS16	6.91	20	0	5
D21S2088E	6.91	20	0	5
FLJ45079	6.91	20	0	5
HIST1H1E	6.91	20	0	5

INSM1	6.91	20	0	5
KIAA0889	7.6	40	0	5
LOC283731	7.6	40	0	5
OR2A9P	6.91	20	0	5
RPRM	6.91	20	0	5
TRIM61	6.91	20	0	5
ZNF426	7.6	40	0	5
LOC390980	7.6	40	0	10
MTMR11	6.91	20	0	10
TMTC4	8.29	79	0	10
C1ORF83	6.91	20	0	14
C20ORF160	6.91	20	5	0
FLJ45850	6.91	20	5	0
FLJ90166	7.6	40	5	0
GDF6	6.91	20	5	0
HOXB9	9.11	178	5	0
KIAA1817	6.91	20	5	0
LOC220074	6.91	20	5	0
MGC4767	6.91	20	5	0
FLJ10560	7.6	40	5	5
FLJ20291	6.91	20	5	5
FLJ45950	7.6	40	5	5
GTF2IP1	6.91	20	5	5
INHBE	6.91	20	5	5
LOC113655	6.91	20	5	5
MGC33867	6.91	20	5	5
PHF21B	6.91	20	5	5
SHRM	6.91	20	5	5
TMEM116	7.6	40	5	5
ZNF454	7.6	40	5	5
CEP68	6.91	20	5	10
FLJ10945	8.01	59	5	10
LOC161527	6.91	20	5	10
RP13-297E16.1	6.91	20	5	10
SPSB4	8.29	79	5	10
ST6GALNAC3	6.91	20	5	10
FGD1	7.6	40	5	14
SETD1B	8.29	79	5	14
ZNF667	9.21	198	5	19
ARL10	8.01	59	5	29
KIF15	6.91	20	10	0
SRG	6.91	20	10	0
UPK2	6.91	20	10	0
C2ORF15	7.6	40	10	5
FAM57B	7.6	40	10	5
IGF2BP1	6.91	20	10	5
SOX3	9.21	198	10	5
TM4SF6	7.6	40	10	5
LOC254848	8.01	59	10	14
MGC35402	8.29	79	10	14
SYT6	6.91	20	10	19
ZNF669	8.01	59	10	38

TCF15	6.91	20	15	0
ARL4D	6.91	20	15	5
C20ORF127	6.91	20	15	10
MPRA	6.91	20	15	10
ZNF660	7.6	40	15	10
PROCR	8.01	59	15	14
MTERFD1	6.91	20	15	24
FOXD3	7.6	40	19	5
RAB42	7.6	40	19	5
C17ORF62	6.91	20	19	10
ADAMTS7	6.91	20	24	5
LOC440395	8.01	59	34	43
FZD2	8.29	79	39	5
C16ORF59	6.91	20	49	33
PAP2D	8.85	139	49	33
SLCO5A1	10.24	554	83	5
LOC339231	8.29	79	88	67
INT1	6.91	20	161	57
LOC400948	8.52	99	234	139

*hNCC count in tag per million (SAGE library total count=50500)

**hES3 count in tag per million (SAGE library total count=205353)

***hES4 count in tag per million (SAGE library total count=209232)

Bold symbols: hNCC most specific genes (not expressed in HES3 nor HES4)

Red symbols: hNCC preferentially expressed genes also found preferentially in hES

Supplementary Table 9.

Orphan hNCC-expressed tags mapping to potential naRNA as predicted by Ge et al., 2006.

CCNRLongTag	hNCC coun	RefSeq	Position From 3'	UniGeneID*	Symbol
TGGCGGGCAGGGGGTCC	1	NM_006640	1467	Hs.440932	-
AATCTTTAATCATAAGG	1	XM_371175	12	-	-
ACCGAAGGACTGCTTGC	2	XM_496146	617	Hs.531536	-
AGTTCTGTAAGTCAGGT	1	XM_371141	471	Hs.512823	-
CAACAAGACACTGGCGT	1	XM_027307	460	-	-
CAGTACACACGGAACCA	1	XM_374260	190	Hs.440258	-
CCCCACTGGCAGTGGGA	1	NM_106552	228	-	-
CCCCGCGGCCGCATCCG	1	XM_496504	570	Hs.533020	-
CCTGGCGCGGAACAGGC	1	XM_371215	499	-	-
GCGGCGGCCAGCGGGGC	1	XM_496848	1385	-	-
GCGGCGGCCAGCGGGGC	1	XM_499254	1385	-	-
GTAGCCAGGGCACCCGC	1	NM_033346	9612	-	-
TACTAAAATAATAGACA	1	XM_495832	326	-	-
TCTCTTCACAGTGAAGG	1	XM_371151	1633	Hs.55304	-
TACAAACTCAGGTGGGT	1	NM_153332	1624	Hs.20000	*3'HEXO*
TGGTCAGTGTGACCAAT	1	NM_005845	1839	Hs.508423	*ABCC4*
GTGTCCGCACTCCTGGC	1	NM_000033	146	Hs.159546	*ABCD1*
TCCTGGGGCCGAATAAG	1	NM_001124	1075	Hs.441047	*ADM*
CAGCGTAGGAAGCAGTA	1	NM_017825	808	Hs.18021	*ADPRHL2*
GCAACGCCTGCCCCCAA	1	NM_001132	2419	Hs.558297	*AFG3L1*
ACACAGTCGTTTTCGTA	1	NM_198576	6160	Hs.273330	*AGRN*
GGGTTGGCACCATTGAG	1	NM_000697	1586	Hs.422967	*ALOX12*
GCGGCCCGAGACTAAGT	1	NM_016237	2429	Hs.7101	*ANAPC5*
GGGGTCGCAGACCCAGG	1	NM_015013	2609	Hs.549117	*AOF2*
TCCCGGCCCTTGCGCCC	1	NM_005166	2313	Hs.74565	*APLP1*
ATGGCGGCCGGGAGCGA	1	NM_018184	2785	Hs.250009	*ARL10C*
CAGCTGCAGTGCCTGCC	1	NM_152285	988	Hs.12999	*ARRDC1*
CTTTTCCCACTCCCATC	1	NM_024095	296	Hs.432699	*ASB8*
AAAGGCTCGCCTATGAC	1	NM_00100148 7	3130	Hs.567267	*ATP2C1*
AAAGGCTCGCCTATGAC	1	NM_014382	4399	Hs.567267	*ATP2C1*
AAAGGCTCGCCTATGAC	1	NM_00100148 6	3160	Hs.567267	*ATP2C1*
AAAGGCTCGCCTATGAC	1	NM_00100148 5	3035	Hs.567267	*ATP2C1*
ATACTGGGTTTGTAAAC	1	NM_020452	302	Hs.435700	*ATP8B2*
ATGTGAGCCAACTTACC	1	NM_030660	360	Hs.526425	*ATXN3*
ATGTGAGCCAACTTACC	1	NM_004993	360	Hs.526425	*ATXN3*
ACAGTCCCACAGAGGGG	1	XM_375456	1247	Hs.512651	*ATXN7L3*
ATGTGCCCAGCCTTGCC	1	NM_013449	3093	Hs.314263	*BAZ2A*
AAATAAGGGATTTCTCT	1	NM_005504	2900	Hs.438993	*BCAT1*
TTCCTAATGCTAGACCA	1	NM_005504	4082	Hs.438993	*BCAT1*
GTAGCCAGGGCACCCGC	1	NM_001204	10892	Hs.471119	*BMPR2*
GAGGTGAGGGGTGGGGC	1	NM_058243	2199	Hs.187763	*BRD4*
TACACGATGTATGGGCC	1	NM_015399	717	Hs.100426	*BRMS1*
TTAACTACTTCTCTGAC	1	NM_00100872 6	2112	Hs.497301	*C14orf150*
TTAACTACTTCTCTGAC	1	NM_080666	2112	Hs.497301	*C14orf150*
CCAGAAGTGTATGGTTC	1	NM_016039	147	Hs.534457	*C14orf166*

AAGGATGCTCGGCTGGA	1	NM_019107	127	Hs.465645	*C19orf10*
CTGTTGCTTCTTGGGGA	1	NM_201569	1253	Hs.270775	*C1orf16*
CTGTTGCTTCTTGGGGA	1	NM_201568	1253	Hs.270775	*C1orf16*
CTGTTGCTTCTTGGGGA	1	NM_014837	1253	Hs.270775	*C1orf16*
CTGTTGCTTCTTGGGGA	1	NM_173156	1253	Hs.270775	*C1orf16*
GTTTAATTAAAGGCAAA	1	NM_173156	64	Hs.270775	*C1orf16*
GTTTAATTAAAGGCAAA	1	NM_014837	64	Hs.270775	*C1orf16*
GTTTAATTAAAGGCAAA	1	NM_201568	64	Hs.270775	*C1orf16*
GTTTAATTAAAGGCAAA	1	NM_201569	64	Hs.270775	*C1orf16*
GGTAGCTGTGGGTCAAC	1	NM_080821	674	Hs.143736	*C20orf108*
AGTGTCTTGACCAGGAC	2	NM_018462	468	Hs.517792	*C3orf10*
CTCTTCATCTGTGATGA	1	NM_018132	903	Hs.88663	*C6orf139*
ATGAGCAGGAACAGGGC	1	NM_015921	100	Hs.520070	*C6orf82*
GACCTTGTAAAGTTGCT	1	NM_022343	256	Hs.493819	*C9orf19*
GCCTCCACGGGCGGGGG	1	NM_173691	643	Hs.323445	*C9orf75*
ACCGCGTGCCAGAAGTC	1	NM_015447	1061	Hs.522493	*CAMSAP1*
GCACTGCTGTCCCTCTG	1	NM_005188	2144	Hs.504096	*CBL*
AAGTTATACCAAAGCTA	1	NM_194454	1110	Hs.531987	*CCM1*
AAGTTATACCAAAGCTA	1	NM_194456	1110	Hs.531987	*CCM1*
AAGTTATACCAAAGCTA	1	NM_004912	1110	Hs.531987	*CCM1*
AAGTTATACCAAAGCTA	1	NM_194455	1110	Hs.531987	*CCM1*
GATATTCCCAAACCATT	1	NM_053056	2102	Hs.523852	*CCND1*
AGATGCTGGTTAAACTG	1	NM_138477	2877	Hs.437819	*CDAN1*
CTGATGGCACCGTCGAG	1	NM_004932	4193	Hs.171054	*CDH6*
GTTACTGCCTCTGGTGC	1	NM_058195	525	Hs.512599	*CDKN2A*
GTTACTGCCTCTGGTGC	1	NM_058197	525	Hs.512599	*CDKN2A*
GTTACTGCCTCTGGTGC	1	NM_000077	525	Hs.512599	*CDKN2A*
TGCTATCATCAAAGGGC	1	NM_014914	817	Hs.435039	*CENTG2*
TTGATGTAATGCTGGGC	1	NM_032142	402	Hs.100914	*Cep192*
TTGATGTAATGCTGGGC	1	NM_018069	402	Hs.100914	*Cep192*
GGCTGGAAGCAGCAGGT	1	NM_018223	1722	Hs.507336	*CHFR*
CGGGAGACATCTTTGGC	2	NM_007096	330	Hs.522114	*CLTA*
CGGGAGACATCTTTGGC	2	NM_001833	330	Hs.522114	*CLTA*
TGGCACAAAATGGGTTG	2	NM_080629	509	Hs.523446	*COL11A1*
TGGCACAAAATGGGTTG	2	NM_080630	509	Hs.523446	*COL11A1*
TGGCACAAAATGGGTTG	2	NM_001854	509	Hs.523446	*COL11A1*
CAATTCCCTCTCTGCAG	1	NM_004370	216	Hs.101302	*COL12A1*
CAATTCCCTCTCTGCAG	1	NM_080645	216	Hs.101302	*COL12A1*
ACCTGGCAAACCAGGGG	1	NM_001850	2011	Hs.134830	*COL8A1*
ACCTGGCAAACCAGGGG	1	NM_020351	2011	Hs.134830	*COL8A1*
CTGATTTATTACAGGGA	6	NM_016128	52	Hs.518250	*COPG*
GGCGCCGTGGCCAGGGG	1	NM_016128	1257	Hs.518250	*COPG*
CTTTGTCGTTCAGTTGG	1	NM_004379	1054	Hs.516646	*CREB1*
CTTTGTCGTTCAGTTGG	1	NM_134442	1054	Hs.516646	*CREB1*
AGTCACCAGCAATGACG	1	NM_004380	855	Hs.459759	*CREBBP*
CACACAAATACTTTTGT	1	NM_016441	1323	Hs.332847	*CRIM1*
CATCAACTATCCTAGAA	1	NM_001313	619	Hs.135270	*CRMP1*
TCAAAAGCACTTTAATG	1	NM_001324	4	Hs.172865	*CSTF1*
CTGGCCCCTGGCTGATC	1	NM_001330	1642	Hs.483811	*CTF1*
GAAAGTGGCAGTGGTTG	1	NM_017949	141	Hs.46679	*CUEDC1*
TGGGTCCACTCAGACTT	1	NM_003592	175	Hs.146806	*CUL1*
GAAGAGACAAGTTAGAA	1	NM_000397	2525	Hs.292356	*CYBB*
TATCATCTATGGTCCTG	1	NM_015247	975	Hs.432993	*CYLD*

TTTACTGCTGATGCTTT	1	NM_004938	4696	Hs.380277	*DAPK1*
AGAGAGGCAGGAATATT	1	NM_022487	835	Hs.524156	*DCLRE1C*
CTAATGGCTATCCTTTC	1	NM_178153	4981	Hs.34780	*DCX*
CTAATGGCTATCCTTTC	1	NM_178152	4981	Hs.34780	*DCX*
CTAATGGCTATCCTTTC	1	NM_000555	4981	Hs.34780	*DCX*
CTAATGGCTATCCTTTC	1	NM_178151	4981	Hs.34780	*DCX*
CAGAATATAATGATAGC	1	NM_003887	1759	Hs.555902	*DDEF2*
GCATAGACTCCCTGGAG	1	NM_018332	2521	Hs.461196	*DDX19L*
TCAAACATTCTGTCTGC	1	NM_014829	3917	Hs.533245	*DDX46*
CTGTTTTAATTGCAAAG	1	NM_004397	3845	Hs.408461	*DDX6*
TTTAAAGTATGTGCTTT	1	NM_019030	103	Hs.444208	*DHX29*
TGGGATTGCTCTAAATA	1	NM_006729	3565	Hs.226483	*DIAPH2*
TTATGTGAAATACTTCC	1	NM_018710	596	Hs.202517	*DKFZp762O07 6*
TGGCTTTCAGGAATGCC	2	NM_182643	1348	Hs.134296	*DLC1*
TGGCTTTCAGGAATGCC	2	NM_006094	1348	Hs.134296	*DLC1*
AGTCTGGATGAATCCCA	2	NM_175629	208	Hs.515840	*DNMT3A*
AGTCTGGATGAATCCCA	2	NM_022552	208	Hs.515840	*DNMT3A*
AGTCTGGATGAATCCCA	2	NM_153759	208	Hs.515840	*DNMT3A*
GAGGCTGCAGCGGCGGC	1	NM_001949	4580	Hs.269408	*E2F3*
TGGGTTGAAAAAAAAGA	1	NM_033083	1166	Hs.474479	*EAF1*
ACTGCTGGCATCGCTGT	1	NM_024757	4888	Hs.495511	*EHMT1*
ATGTATAATTTTGACAT	1	NM_001415	937	Hs.539684	*EIF2S3*
CACTCACAACACTGATC	1	NM_013333	390	Hs.279953	*EPN1*
GATGACTGCAGTGAATT	1	NM_000127	1148	Hs.492618	*EXT1*
TGAAGCCGCCAATGGTG	1	NM_000138	2091	Hs.146447	*FBN1*
GTGGCTGAATGAAACAC	1	NM_133337	4987	Hs.500572	*FER1L3*
GTGGCTGAATGAAACAC	1	NM_013451	4987	Hs.500572	*FER1L3*
TATTTGGGAGAGAGACC	1	NM_133337	4539	Hs.500572	*FER1L3*
TATTTGGGAGAGAGACC	1	NM_013451	4539	Hs.500572	*FER1L3*
AACCTCTTGGAAAACTT	1	NM_018250	194	Hs.162397	*FLJ10871*
GCCTATCGAGGACAGCT	1	NM_018357	142	Hs.416755	*FLJ11196*
CCTTAGACCTCGCGGGC	1	NM_024809	2803	Hs.167165	*FLJ12975*
CTTCAAGGAGAGAGGGT	1	NM_024598	524	Hs.408702	*FLJ13154*
CCCCACTGGCAGTGGGA	1	NM_022460	228	Hs.531785	*FLJ14249*
AAATGGGTGCAGGTTTT	1	NM_022837	1561	Hs.118183	*FLJ22833*
CGGACAAAAAGCTACAA	1	NM_152493	391	Hs.524248	*FLJ25476*
TTCCATTGTACTGATCT	1	NM_144643	662	Hs.404000	*FLJ30655*
CCCCCACTTGCCAGAGC	1	NM_016206	3946	Hs.435013	*FLJ38507*
GAAACAGAGCCCAGGGC	1	NM_198582	102	Hs.24951	*FLJ43374*
ACTCCGGCGTCAGTGCC	1	NM_00100530 3	2983	Hs.516603	*FLJ46347*
GCTGGGCCACTTTGTGG	1	NM_013231	6380	Hs.533710	*FLRT2*
GCTGTACAGACCCAATT	1	NM_007085	2829	Hs.269512	*FSTL1*
GTAACAGTCACAAAATT	1	NM_001483	154	Hs.437367	*GBAS*
ACAAAGTGGAAAAAAGT	1	NM_006496	902	Hs.73799	*GNAI3*
CTTTCAATACCAAATTA	1	NM_018178	652	Hs.203699	*GOLPH3L*
GGGACCTGACCAGCAAC	1	NM_002081	349	Hs.328232	*GPC1*
GCGGCAGGGTGGGCAGC	1	NM_005332	532	Hs.449632	*HBZ*
GGTCTCCTCCCCCCAGG	1	NM_015094	2619	Hs.517434	*HIC2*
GAGGAGCTCTTGTGGAA	1	NM_013332	242	Hs.521171	*HIG2*
ACAGGTAGTTCTGCCCT	1	NM_018200	1099	Hs.69594	*HMG20A*
GCAAATAGGAAGAAGCT	1	NM_031243	530	Hs.487774	*HNRPA2B1*

GCAAATAGGAAGAAGCT	1	NM_002137	500	Hs.487774	*HNRPA2B1*
GGGGGAATTTTTTAAAC	1	NM_031262	904	Hs.522257	*HNRPK*
GGGGGAATTTTTTAAAC	1	NM_031263	904	Hs.522257	*HNRPK*
GGGGGAATTTTTTAAAC	1	NM_002140	904	Hs.522257	*HNRPK*
CCATTCATCATCCGGCA	1	NM_005968	329	Hs.465808	*HNRPM*
CCATTCATCATCCGGCA	1	NM_031203	329	Hs.465808	*HNRPM*
CGGCCGGCGAGGCAGGG	1	NM_014620	1189	Hs.820	*HOXC6*
TCTTTCTCCTGGTAAAA	1	NM_153693	1312	Hs.820	*HOXC6*
TCTTTCTCCTGGTAAAA	1	NM_004503	1312	Hs.820	*HOXC6*
TACGAGCAGCCAAGTTC	1	NM_007216	3473	Hs.437599	*HPS5*
TACGAGCAGCCAAGTTC	1	NM_181507	3473	Hs.437599	*HPS5*
TACGAGCAGCCAAGTTC	1	NM_181508	3473	Hs.437599	*HPS5*
CTCTTTGTTCAGCCACT	1	NM_012262	225	Hs.48823	*HS2ST1*
CCGGTTCCCTGCTCTCT	1	NM_005345	2184	Hs.520028	*HSPA1A*
CCAAACACTCAAAAGCC	1	NM_000867	1844	Hs.421649	*HTR2B*
CGCCGCGCGCCACCCGC	1	NM_203434	1238	Hs.529857	*IER5L*
TTACTCAGGAACAGCTT	1	NM_014214	717	Hs.367992	*IMPA2*
AACTGCACTCTATCTGG	1	NM_198266	155	Hs.489811	*ING3*
AACTGCACTCTATCTGG	1	NM_019071	155	Hs.489811	*ING3*
AGGTAGCGAGGGTACGG	1	NM_001567	3889	Hs.523875	*INPPL1*
TATGTGGACAGCACCTG	1	NM_152713	1135	Hs.504237	*ITM1*
AATCAGTGACGGATCAA	1	NM_018433	3843	Hs.531819	*JMJD1A*
CTGGCGCGCGGGACCAG	1	NM_004982	2190	Hs.102308	*KCNJ8*
CCTGTAATCCGAGTCAC	1	NM_176816	799	Hs.482372	*KENAE*
GCCAGCAAGGGATAAAG	1	NM_015330	598	Hs.474384	*KIAA0376*
TACCCTGAGCAGCTGCC	1	NM_015104	5467	Hs.370671	*KIAA0404*
GGTGCAAACCCTAGCGG	1	NM_014867	1463	Hs.5333	*KIAA0711*
ACATCCTTGCAAATCTG	1	NM_020710	1178	Hs.268488	*KIAA1185*
AATTACAAAGCTAAGAT	1	NM_020782	3903	Hs.505104	*KIAA1340*
TGTCCAAATGATAAAAG	1	XM_371590	2234	Hs.110489	*KIAA1571*
TCTCCAGCACTCTCCCC	1	XM_035497	2569	Hs.143067	*KIAA1602*
TCAACTCCCCCTCCTGA	1	NM_194286	510	Hs.112577	*KIAA1853*
AAGCCCACTGCCTCCTG	1	NM_004798	194	Hs.369670	*KIF3B*
GCCCGCTCGGCCGGGCG	1	NM_007246	3088	Hs.388668	*KLHL2*
GGTGATCAGTTATGTGG	1	NM_012316	743	Hs.470588	*KPNA6*
GGACCCGGGTTACAGCC	1	NM_016027	1394	Hs.118554	*LACTB2*
GATACTGTGCCATCTGT	1	NM_005559	2821	Hs.270364	*LAMA1*
AGGGCTGACTGCTCCAC	1	NM_002291	1441	Hs.489646	*LAMB1*
GCCGTTAGCACCTAAGG	1	NM_018192	447	Hs.374191	*LEPREL1*
AGGAGGGGCAGGGAGCC	1	NM_002314	345	Hs.36566	*LIMK1*
AGGAGGGGCAGGGAGCC	1	NM_016735	345	Hs.36566	*LIMK1*
GGGCAGAAGCAGGACAG	1	NM_145239	1341	Hs.556007	*LOC112476*
GGGTCGGCTTAGCCCAG	1	NM_139016	2188	Hs.16936	*LOC128439*
TACCACTGAGTAGCCAG	1	NM_207325	3688	Hs.194392	*LOC147991*
TCAGACTTGCAGGCAGG	1	NM_145284	3337	Hs.404706	*LOC159090*
CTTTCTATAAACTCATT	1	NM_212554	210	Hs.468488	*LOC399818*
TGAAACCTGGGAACACA	1	XM_378793	136	Hs.438766	*LOC400684*
TCTTCAATTTCCTTTGC	1	NM_021179	493	Hs.130746	*LOC57821*
CAGACCAAAGGAGTGTT	1	NM_032603	2317	Hs.469045	*LOXL3*
ACCCGGGAACACAGGAG	2	NM_018032	57	Hs.16803	*LUC7L*
ACCCGGGAACACAGGAG	2	NM_201412	55	Hs.16803	*LUC7L*
CTGAATAAATAATCCCC	1	NM_000081	146	Hs.532411	*LYST*
GTAAAAGGAAAATGGCA	1	XM_042066	1414	Hs.508461	*MAP3K1*

AATATATTCATAAAGTA	1	NM_145686	1952	Hs.431550	*MAP4K4*
AATATATTCATAAAGTA	1	NM_004834	1952	Hs.431550	*MAP4K4*
AATATATTCATAAAGTA	1	NM_145687	1952	Hs.431550	*MAP4K4*
ACCGATGCTTTGCTCAG	1	NM_002398	403	Hs.526754	*MEIS1*
TATTCTATATTGCCCAA	1	NM_006838	857	Hs.444986	*METAP2*
CTCCTTCCGCAGCGCCT	1	NM_014275	894	Hs.437277	*MGAT4B*
CTCCTTCCGCAGCGCCT	1	NM_054013	894	Hs.437277	*MGAT4B*
CCCCAGGTGGAGGACGG	1	NM_024107	1342	Hs.181391	*MGC3123*
CCCCAGGTGGAGGACGG	1	NM_177441	1605	Hs.181391	*MGC3123*
GGGGTAAGGCCTGAATG	1	NM_020948	1465	Hs.21757	*MI-ER1*
GAGGGTGGGGGGACTGA	1	NM_199054	1021	Hs.515032	*MKNK2*
TTCTGGCAAGCGGTGGA	1	NM_002430	4110	Hs.268515	*MN1*
CCATAGTCCTGGCTACT	1	NM_024761	2758	Hs.369022	*MOBKL2B*
GGCGTGAAAATATTGCA	1	NM_024761	2590	Hs.369022	*MOBKL2B*
GTAGCGGATGCGTTTCA	1	NM_014180	251	Hs.483924	*MRPL22*
ACAATGTCATTGTTGCC	1	NM_145212	146	Hs.346736	*MRPL30*
ACAATGTCATTGTTGCC	1	NM_145213	146	Hs.346736	*MRPL30*
CATTAATGAATAGTATG	1	NM_182640	916	Hs.469537	*MRPS9*
AGGTCTTCTATGGCATC	1	NM_000179	1781	Hs.445052	*MSH6*
AAGCCCCAACCTAGGTA	7	NM_002442	810	Hs.158311	*MSI1*
AAAGGGATAAGGTGGCC	1	NM_000254	4584	Hs.498187	*MTR*
TGGAAGAACTGGAGGCC	1	NM_152832	331	Hs.25723	*MTVR1*
GTGACTTATAGCCAGGA	1	NM_002473	7288	Hs.474751	*MYH9*
TTTAAGAAAACAGAAGC	1	NM_013262	401	Hs.484738	*MYLIP*
GTGGGGGCAACTCAAAC	1	NM_004539	152	Hs.465224	*NARS*
GGTAGCCGCCGGGGTCC	1	NM_020170	3675	Hs.501420	*NCLN*
TCACCCTCCCTTTGGAG	1	NM_006617	241	Hs.527971	*NES*
ATGGAACTACTCATCCC	1	NM_015384	1437	Hs.481927	*NIPBL*
ATGGAACTACTCATCCC	1	NM_133433	2506	Hs.481927	*NIPBL*
GTTCCAAGAATGGTAGG	1	NM_181689	1128	Hs.504703	*NNAT*
GTTCCAAGAATGGTAGG	1	NM_005386	1209	Hs.504703	*NNAT*
GGCTCCACAGTCACAGG	4	NM_007363	1854	Hs.533282	*NONO*
AGTTCCCCCTGGGAGTC	1	NM_024408	6414	Hs.487360	*NOTCH2*
CTGTTACAAAACTCCTG	1	NM_003297	680	Hs.108301	*NR2C1*
AGCATCTCTCTCTGTTT	1	NM_022731	716	Hs.213061	*NUCKS*
AACATTTATTTTTGTTA	1	NM_00100574 5	16	Hs.509909	*NUMB*
AACATTTATTTTTGTTA	1	NM_00100574 3	16	Hs.509909	*NUMB*
AACATTTATTTTTGTTA	1	NM_003744	16	Hs.509909	*NUMB*
AACATTTATTTTTGTTA	1	NM_00100574 4	16	Hs.509909	*NUMB*
CTGAGAAATGGGCTGAG	1	NM_018230	1312	Hs.12457	*NUP133*
CCTATGCGTTATTACCT	1	NM_00100856 4	798	Hs.507537	*NUPL1*
CCTATGCGTTATTACCT	1	NM_014089	798	Hs.507537	*NUPL1*
ATCCACGTTCCCATCAC	1	NM_016118	1817	Hs.173024	*NYREN18*
AAGGCCTGGTTATGTCT	1	XM_047995	2058	Hs.155915	*ODZ2*
CGTTTTATCTGCTTGGA	1	NM_000436	2910	Hs.278277	*OXCT1*
CAGTAAAATACAAAGTC	1	NM_005109	37	Hs.475970	*OXSR1*
TCGGACACGGATCAGGC	1	NM_000918	2392	Hs.464336	*P4HB*
GTGGACGGTGGCAGGGG	1	NM_002584	672	Hs.113253	*PAX7*
GTGGACGGTGGCAGGGG	1	NM_013945	661	Hs.113253	*PAX7*

TTATCATCTCTGCTGCT	1	NM_006713	1092	Hs.229641	*PC4*
GCTCGGCGTCAGCGCTG	1	NM_004708	533	Hs.443831	*PDCD5*
CTGGGTTTTTCACCAGC	1	NM_003681	4225	Hs.284491	*PDXK*
CGCAGCCCCCGTCCCGC	1	NM_015946	2263	Hs.519304	*PELO*
TGAATTTGCTTTGGAGA	1	NM_002857	1258	Hs.517232	*PEX19*
TACTTGCCCTTGCGCTC	1	NM_007350	1256	Hs.558462	*PHLDA1*
TAGTGGGAGACTGGACA	1	NM_006099	1402	Hs.435761	*PIAS3*
TCTCTTGATATAGTCCT	1	NM_002647	2865	Hs.464971	*PIK3C3*
CGCTTCTCCCAGCCGGG	1	NM_006221	931	Hs.465849	*PIN1*
CCGCCGCCGCCACCTCC	1	NM_032812	1955	Hs.498939	*PLXDC2*
ACAGCCTGCAAGTTCAC	1	NM_015425	4327	Hs.26962	*POLR1A*
CTTCTTGCCACAAATCC	1	NM_000938	3629	Hs.479814	*POLR2B*
GGCGGCCCCCAGCAGCG	1	NM_052932	3041	Hs.503709	*PORIMIN*
CACACATTGGAGGATAT	1	NM_002716	1262	Hs.269128	*PPP2R1B*
GGATACTCAGCAACGCT	1	NM_178013	458	Hs.432401	*PRIMA1*
GGATACTCAGCAACGCT	1	NM_178004	458	Hs.432401	*PRIMA1*
CTGGGCTCTGGAGCCGC	1	NM_004697	2704	Hs.374973	*PRPF4*
TTCTGAATTGTTTCCAG	1	NM_002815	338	Hs.443379	*PSMD11*
GTGGTACGGGGACAACC	1	NM_080840	152	Hs.269577	*PTPRA*
GTGGTACGGGGACAACC	1	NM_080841	152	Hs.269577	*PTPRA*
GTGGTACGGGGACAACC	1	NM_002836	152	Hs.269577	*PTPRA*
TGTGGCCTCTGTAGCCG	1	NM_080841	636	Hs.269577	*PTPRA*
TGTGGCCTCTGTAGCCG	1	NM_002836	636	Hs.269577	*PTPRA*
TGTGGCCTCTGTAGCCG	1	NM_080840	636	Hs.269577	*PTPRA*
CCTGCTCAGCAGCGCGG	1	NM_004884	3042	Hs.128292	*PUNC*
TGGGTACCAGGCAGAGG	1	NM_004884	194	Hs.128292	*PUNC*
ACTGCATACAAGATGGA	1	NM_012414	1550	Hs.558471	*RAB3-GAP150*
CACTGTATTTATCCCTG	1	NM_002874	2362	Hs.521640	*RAD23B*
TGTAAAGCTGATAGAGT	1	NM_020850	2013	Hs.368569	*RANBP10*
GCATTCTCTGCTCTTCA	1	NM_002883	452	Hs.183800	*RANGAP1*
GAGTGCTGGTTTCTGGC	1	NM_133452	244	Hs.337228	*RAVER1*
TAGCATTACATTCAACA	1	NM_002893	338	Hs.495755	*RBBP7*
CAATACTGACAAATTTG	1	NM_016316	139	Hs.443077	*REV1L*
CGGACGGCAAAGGTCAG	1	NM_020211	2057	Hs.271277	*RGMA*
ATGATTTAATTCAGTAG	1	NM_018307	2272	Hs.462742	*RHOT1*
GACCGAAGCAGAGGTCG	1	NM_004292	1500	Hs.1030	*RIN1*
GCATTTGGTAATTCGTC	1	NM_025065	94	Hs.481202	*RPF1*
GTGCAAACAGAAATGCA	1	NM_002948	338	Hs.558382	*RPL15*
CATCCTCCACCCCTGCC	1	NM_003161	673	Hs.463642	*RPS6KB1*
CCTGAGGTGACTGGCGG	1	NM_004348	343	Hs.535845	*RUNX2*
ATTTCACATCCAGAAGC	1	NM_014363	81	Hs.159492	*SACS*
CTGCCTCTCAATGTCGG	1	NM_173551	3249	Hs.558684	*SAMD6*
ATGAGGCGCTGTGCCAG	1	NM_012235	2416	Hs.531789	*SCAP*
CTGATGCGACTGAAGCG	1	NM_182895	1898	Hs.474251	*SCARF2*
CTGATGCGACTGAAGCG	1	NM_153334	1898	Hs.474251	*SCARF2*
GAGGGAAGGAGGAGCAG	1	NM_019064	402	Hs.435719	*SDK2*
TCTATGCCACAGCACAG	1	NM_004186	566	Hs.32981	*SEMA3F*
ATAGAGTAAACAAAAGT	1	NM_020796	1045	Hs.156967	*SEMA6A*
CACACTGTTTCTGGGGA	1	NM_000602	956	Hs.414795	*SERPINE1*
TCTGTGGTCAAGGGGCG	1	NM_005066	2984	Hs.355934	*SFPQ*
TCATTGTACAAGGATAG	3	NM_007373	889	Hs.104315	*SHOC2*
TAGTGCTCAGCCACACG	1	NM_006749	412	Hs.549066	*SLC20A2*
GCGGGCGGGAGGCGGGG	1	NM_005984	1518	Hs.111024	*SLC25A1*

GGGAGTTAGCAAACTGA	1	NM_133496	1310	Hs.533903	*SLC30A7*
TGTCTGGGCAGCTGTCC	1	NM_003486	2487	Hs.513797	*SLC7A5*
ATTATGGCAACAATAGG	1	NM_024624	3362	Hs.526728	*SMC6L1*
GTAGCCATTCATACCAC	1	NM_023071	2209	Hs.146679	*SPATS2*
CGTGTGAAATATGAAGA	1	XM_031553	302	Hs.529577	*SR140*
TGCCTGGCAAGACACTT	1	NM_020762	2336	Hs.450763	*SRGAP1*
ATTGCAGACATTTACAA	1	NM_012446	119	Hs.102735	*SSBP2*
TTAACTTTTCGGGATAA	1	NM_003957	1120	Hs.170819	*STK29*
CTATGGGCTGGCCTCAG	1	NM_015690	724	Hs.471404	*STK36*
GCGCCGCGCGGCACGGC	1	NM_005861	1233	Hs.533771	*STUB1*
GCACAGACATATGTGGC	1	NM_181491	138	Hs.78354	*SURF5*
GCACAGACATATGTGGC	1	NM_006752	134	Hs.78354	*SURF5*
GCACAGACATATGTGGC	1	NM_133640	134	Hs.78354	*SURF5*
CCGGCCTGGGAGGCCCC	5	NM_003186	487	Hs.503998	*TAGLN*
CCGGCCTGGGAGGCCCC	5	NM_00100152 2	487	Hs.503998	*TAGLN*
CTTTCCCTCCTGCAGCT	1	NM_003186	537	Hs.503998	*TAGLN*
CTTTCCCTCCTGCAGCT	1	NM_00100152 2	537	Hs.503998	*TAGLN*
CTGTTTAAGAACTCTCA	1	XM_051081	1962	Hs.500598	*TBC1D12*
TTCTTTGCAGTATCCTG	1	NM_020755	1299	Hs.146668	*TDE2*
GAGTTGGCCTTGCAGGC	1	NM_014466	258	Hs.127111	*TEKT2*
CTCCAGCACAGAAGTTG	1	NM_003238	466	Hs.133379	*TGFB2*
AGTAAGCCACCGATATC	2	NM_012338	1761	Hs.16529	*TM4SF12*
CTGGCTCTGAGAAATCC	2	NM_015008	899	Hs.477547	*TMCC1*
CACTTGTCCAGGTCCGC	1	NM_016639	810	Hs.355899	*TNFRSF12A*
AGATGGTCACTATTTAG	2	NM_001067	784	Hs.156346	*TOP2A*
CCCTCGAAGCTCCGGTT	1	NM_006670	1360	Hs.82128	*TPBG*
CACGGGGAGAGAAGTTG	1	NM_177452	1825	Hs.13303	*TRAPPC6B*
GCTAGTTTCACTTGCAA	1	NM_013381	2249	Hs.199814	*TRHDE*
CCAGCCAGGGGTGGGGC	1	NM_005762	1051	Hs.467408	*TRIM28*
ATCATAACTAAGCCTTG	1	NM_021648	924	Hs.284141	*TSPYL4*
AAACCCAAGCTGAATAG	3	NM_025250	42	Hs.440899	*TTYH3*
CTTATCTGATGTGGTGC	1	NM_003324	426	Hs.524187	*TULP3*
TTTCCATCAAAGTAGAG	1	NM_130466	523	Hs.374067	*UBE3B*
TTTCCATCAAAGTAGAG	1	NM_183414	523	Hs.374067	*UBE3B*
TTTCCATCAAAGTAGAG	1	NM_183415	519	Hs.374067	*UBE3B*
GCGCAGGCGGGCCGGGG	1	NM_003565	4958	Hs.47061	*ULK1*
AAAAATACACATTAGGC	1	NM_014683	1103	Hs.168762	*ULK2*
GCCCGGCCTGCCGCCGG	1	NM_014683	5530	Hs.168762	*ULK2*
GGCCTGGCTTTTACGAC	1	NM_023011	1367	Hs.533855	*UPF3A*
GGCCTGGCTTTTACGAC	1	NM_080687	1367	Hs.533855	*UPF3A*
GTGCTGTTGTTGACAGG	1	NM_199512	1751	Hs.477128	*URB*
GTGCTGTTGTTGACAGG	1	NM_199511	1751	Hs.477128	*URB*
GCTGCCCGTTTCATTGG	1	NM_005153	2894	Hs.136778	*USP10*
CAAGATATCTTACAAGA	1	XM_042698	2234	Hs.462492	*USP22*
TCTCTCAGTTCAACCCT	1	NM_032582	5865	Hs.132868	*USP32*
CAATGTGCTGAGCCAGT	1	NM_021645	2445	Hs.512963	*UTP14C*
CAACATCAGGGTAGAGA	1	NM_003371	1044	Hs.369921	*VAV2*
AGCCCGGCTTCCGAGCG	1	NM_003376	870	Hs.73793	*VEGF*
GCATTTCACATCAATTT	1	NM_022459	1017	Hs.507452	*XPO4*
GCTTCTGCCTCCCCCGA	1	NM_006106	4877	Hs.503692	*YAP1*
ACTTGGGCAGTGAGTGG	1	NM_006555	836	Hs.520794	*YKT6*

ACAAACACCAGACATTA	1	NM_012479	266	Hs.520974	*YWHAG*
TTAGTAATACAGTGCTG	1	NM_007146	71	Hs.463569	*ZNF161*
ATTGGCTTGGCAGTGAA	1	NM_005095	1725	Hs.269211	*ZNF262*
GCAGAGTACTTCTAGGT	1	XM_372267	650	Hs.348963	*ZNF275*
CAACAAGATAATGGATT	1	NM_020657	156	Hs.287374	*ZNF304*
TGATAGAAGTCTGGAAG	1	NM_020933	57	Hs.465829	*ZNF317*
CCCTGCTCTGGCCAAAG	1	NM_203282	3603	Hs.434406	*ZNF539*
CCCTGCTCTGGCCAAAG	1	NM_004876	1186	Hs.434406	*ZNF539*
TCCTGCATTAGCTGCTG	1	NM_003461	1058	Hs.490415	*ZYX*
TGGAAGTTCTTGTCCAG	1	NM_003461	572	Hs.490415	*ZYX*

*Database Annotating antisense tags UniGeneID

Clin Genet 2008: 74: 392–395
Printed in Singapore. All rights reserved

CLINICAL GENETICS
doi: 10.1111/j.1399-0004.2008.01078.x

Short Report

Confirmation of *RAX* gene involvement in human anophthalmia

Lequeux L, Rio M, Vigouroux A, Titeux M, Etchevers H, Malecaze F, Chassaing N, Calvas P. Confirmation of *RAX* gene involvement in human anophthalmia.
Clin Genet 2008: 74: 392–395. © Blackwell Munksgaard, 2008

Microphthalmia and anophthalmia are at the severe end of the spectrum of abnormalities in ocular development. Mutations in several genes have been involved in syndromic and non-syndromic anophthalmia. Previously, *RAX* recessive mutations were implicated in a single patient with right anophthalmia, left microphthalmia and sclerocornea. In this study, we report the findings of novel compound heterozygous *RAX* mutations in a child with bilateral anophthalmia. Both mutations are located in exon 3. c.664delT is a frameshifting deletion predicted to introduce a premature stop codon (p.Ser222ArgfsX62), and c.909C>G is a nonsense mutation with similar consequences (p.Tyr303X). This is the second report of a patient with anophthalmia caused by *RAX* mutations. These findings confirm that *RAX* plays a major role in the early stages of eye development and is involved in human anophthalmia.

L Lequeux[a,b], M Rio[c], A Vigouroux[a,b], M Titeux[a], H Etchevers[a], F Malecaze[a,d,e], N Chassaing[a,b,d] and P Calvas[a,b,d]

[a]INSERM, U563, Centre de Physiopathologie de Toulouse Purpan, Toulouse, France, [b]CHU Toulouse, Hôpital Purpan, Service de Génétique Médicale, Toulouse, France, [c]Département de Génétique Médicale, Hôpital Necker-Enfants Malades, Paris, France, [d]Université Toulouse III Paul-Sabatier, Toulouse, France and [e]CHU Toulouse, Hôpital Purpan, Service d'Ophtalmologie, Toulouse, France

Key words: anophthalmia – microphthalmia – OAR transactivation domain – *RAX*

Corresponding author: Professor Patrick Calvas, Service de Génétique Médicale, Pavillon Lefebvre, CHU Purpan, Place du Dr Baylac, 31059 Toulouse Cedex 9, France.
Tel.: +33 5 61 77 90 79;
fax: +33 5 61 77 90 73;
e-mail: calvas.p@chu-toulouse.fr

Received 27 March 2008, revised and accepted for publication 3 July 2008

Microphthalmia and anophthalmia are at the severe end of the spectrum of abnormalities in ocular development. The combined occurrence rate for these two malformations is 1/10,000 births (1, 2). Mutations in several genes have been isolated in syndromic and non-syndromic anophthalmia. Heterozygous mutations in *SOX2* account for approximately 10% of anophthalmia (3, 4). Other genes have been identified as causing anophthalmia or extreme microphthalmia in humans (*PAX6*, *OTX2*, *CHX10*, *STRA6*, and *BMP4*) (5, 6). These latter genes are implicated in a very small proportion of affected individuals, implying wide genetic heterogeneity to match the phenotypic variability.

The *RAX* homeobox gene is essential for vertebrate eye development. *RAX* transcription begins in the anterior neural plate and then simultaneously in the eye field and in the ventral forebrain (7). Even before *PAX6*, its expression is critical to defining the eye field during early development in animal models (8). The lack of *RAX* expression hampers optic vesicle formation and leads to brain size reduction in mouse, while ectopic expression induces the appearance and proliferation of retinal pigment epithelium cells in *Xenopus* (9). The function of the *RAX* gene in eye development is yet not fully understood, but there is additional evidence from animal studies that it is involved in the proliferation of neural and retinal cells (10). In humans, the role of *RAX* in eye formation is clearly supported by the association of anophthalmia and sclerocornea in a patient bearing

a truncating mutation and a missense mutation, both located in the DNA-binding helix of the homeodomain and reducing the DNA-binding ability of the resulting protein (11). We report in this study the case of a new patient with bilateral anophthalmia associated with two distinct and novel truncating mutations of the *RAX* gene.

Patient, materials and methods

Patient

The proband, a 2-year-old girl, is the third child born to non-consanguineous, healthy Algerian parents. There was no relevant familial history of ocular malformation or remarkable disease. The pregnancy was uneventful, and the prenatal ultrasonography was not suggestive of anomaly. Delivery occurred at 41 weeks of amenorrhea without neonatal difficulties. Birth weight was 3200 g. At birth, bilateral small palpebral fissures were noted without other malformation or dysmorphic features. Anophthalmia was subsequently confirmed. Psychomotor development was within the normal range with head held up at 3 months, sitting at 10 months, and walking at 1 year. Speech developed normally. A slight growth defect was recorded at 14 months, with weight at −0.5 standard deviation (DS) (9020 g), height at −1 DS (72 cm) and head circumference at −2 DS (44 cm). Abdominal and pelvic ultrasonography detected no visceral anomalies. Orbital and cranial magnetic resonance imaging scan showed bilateral absence of eyes with only fibrous tissue in the orbits (Fig. 1). Optic nerves and chiasma were hypoplastic. Extraocular muscles appeared to be relatively preserved. The hypothalamus and pituitary gland were normal. No cerebral malformation was observed.

Molecular analysis

Parents gave their informed consent, according to French law, to participate in this study. DNA was isolated by standard procedures from peripheral white blood cells of the proband. Routine examination ruled out rearrangements or point mutations of *SOX2* and *PAX6* genes. The three *RAX* exons, with exon–intron borders, were amplified by polymerase chain reaction (PCR) using previously published primers (11). PCR fragments were subsequently purified with QIAquick Gel Extraction Kit (QIAGEN SA, Courtaboeuf, France), and both strands were sequenced using Big Dye DNA sequencing kit (Applied Biosystems, Warrington, UK). Reactions were analyzed in an ABI 3100 sequencer (Applied Biosystems).

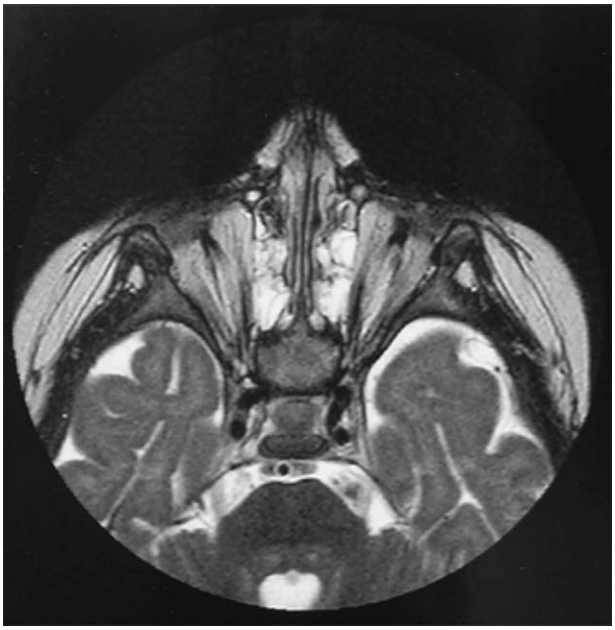

Fig. 1. Magnetic resonance imaging scan of the proband. Note absence of ocular structures replaced by fibrous tissue.

Sequence variations were numbered considering adenine of the ATG initiation codon as the first nucleotide (GenBank accession no. NM_013435.2). The changes were verified by performing independent PCR and sequencing reactions on the proband's DNA.

Exon 3 of the *RAX* gene was PCR amplified from the patient's DNA as above (11). The resulting 602-bp fragments were cloned into the pGEM-T vector (Promega, Charbonnières, France). JM109 competent cells were transformed and grown on Luria-Bertani agar plates. DNAs from 10 expanded LacZ-deficient clones were extracted using Promega Wizard miniprep purification system. Further sequencing was performed using the ABI-Big Dye terminator 3.1 on an ABI 3100 sequencer (Applied Biosystems).

Results

Sequence analysis of the proband's DNA revealed two novel mutations, both located in exon 3 of the *RAX* gene. c.664delT frameshifting deletion generates a premature stop codon (p.Ser222-ArgfsX62). c.909C>G is a nonsense mutation changing a tyrosine at position 303 to a stop codon (p.Tyr303X). These mutations were not found in a panel of 96 control chromosomes. Both are predicted to lead to a truncated protein so that, if not submitted to nonsense-mediated mRNA decay, the predicted RAX proteins lack the putative otp, aristaless, rax (OAR) transactivation domain and are non-functional (7).

As this family left the country, DNA from the proband's parents was unavailable, and thus, segregation analysis of these two mutations was impossible. Nevertheless, the c.664delT and the c.909C>G mutations were shown to lie in *trans* after sequencing of the cloned products of the patient's *RAX* exon 3 (Fig. 2).

Discussion

This is the second report of human anophthalmia-associated mutations of the *RAX* homeobox gene (11). While the parents were not carefully examined, they did not complain of any visual impairment at the time their child was evaluated. The proband was demonstrated to bear composite heterozygous mutations on both alleles of the *RAX* gene. The parents are thus likely to each be healthy carriers of a heterozygous mutation, unless one of these mutations appeared *de novo*. This would confirm the recessive inheritance of *RAX* mutations in ocular dysgenesis.

The phenotype, reported in this study, consisting in bilateral and symmetric anophthalmia is more severe than the one previously described. This first patient had right anophthalmia and left microphthalmia and sclerocornea (11). One of the causative mutations (p.Gln147X) induced, as predicted for the two mutations reported in this study, a truncation of the protein. The other was a missense p.Arg192Gln, with a milder effect on the protein, which conserved a low activity. This could suggest that the observed phenotypic variability be correlated with the mutation severity. However, definite conclusions cannot be drawn in view of the limited number of observations.

In animal models, all truncating mutations have been reported to have severe effects and lead to the absence of eye development (9, 12, 13). In contrast, antisense or morpholino inhibition in *Xenopus* acts in a dose-dependant manner, leading to graduated phenotypes ranging from eye reduction to anophthalmia (14). In this report, the location of the mutations in the last exon makes nonsense-mediated mRNA decay unlikely (15). This is in accordance with the observation that, in the cellular model used by Voronina et al (11), the more proximal p.Gln147X mutation allowed translation of a large amount of protein. These facts suggest that the two mutations we report in this study lead to truncated proteins, both lacking the C-terminal part containing the critical OAR functional domain (7). Absence of RAX C-terminus is known to abolish its proliferative effect in *Xenopus* (14). Furthermore, regulation of transcriptional activity of several other homeobox genes by the OAR domain has been suggested in other studies (7, 16, 17). Thus, p.Ser222ArgfsX62 and p.Tyr303X are thought to drastically impair RAX target genes expression. The precise delineation of the mechanistic effects of these mutations must therefore await binding studies, and an important goal for future research will be the identification of the putative genes that can modulate *RAX* activity through direct interaction.

To date, no cerebral malformation has been associated with *RAX* mutations in man. This is

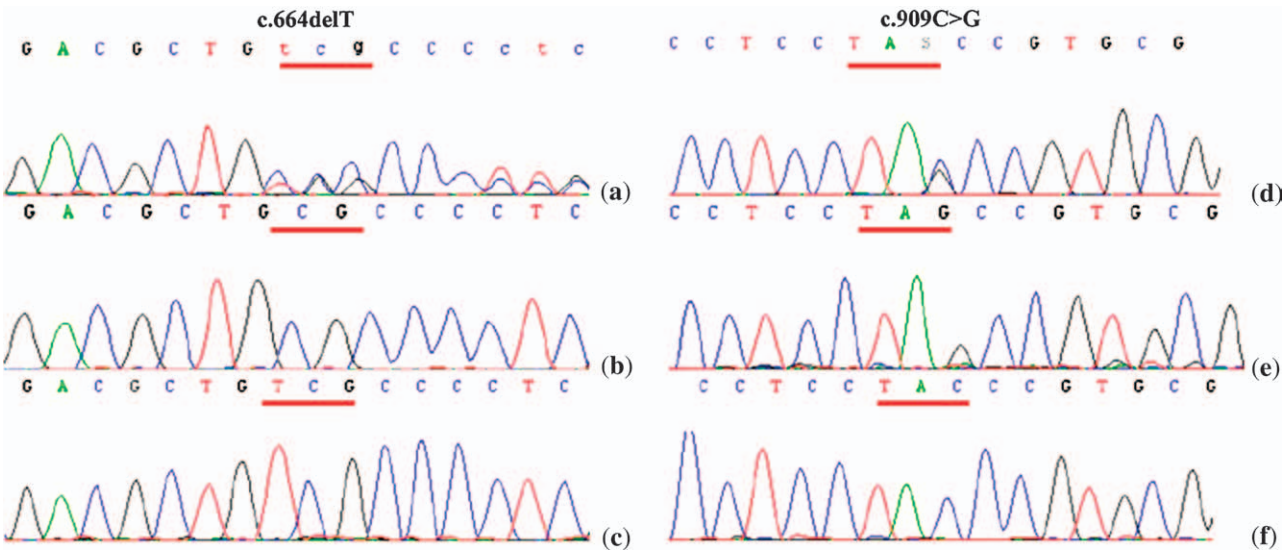

Fig. 2. Electropherograms showing the two mutations on *RAX* exon 3 (a and d) in comparison with wild-type sequence (c and f). Sequencing of cloned patient's exon 3 amplimers in a pGEM-T vector (b and e) demonstrated that mutations were not located on the same alleles. Mutated codons are underlined.

surprising in the light of the observations in insect, batracian, fish and rodent models, where *RAX* consistently participates in brain development and homozygous null alleles cause severe cerebral malformations (9, 14, 18, 19). A similar situation is seen, however, with respect to the Hesx1 homeobox-containing transcription factor, which in mice has a similar early role and an overlapping domain to that of *Rax* but is downstream of *Pax6* and *Otx2* (20) and *Rax* itself (21). While *Hesx1* mouse mutants can demonstrate anophthalmia in addition to cerebral anomalies, human patients have either isolated pituitary malformations or septo-ocular dysplasia, with no further retinal involvement (22). In a complementary fashion and unlike *SOX2* or *OTX2* mutations, no extra-ocular malformations have been observed in *RAX* ocular dysgenesis patients. The patient reported previously by Voronina et al. (11) was diagnosed as autistic. The patient reported in this study seems to have normal psychomotor development, although she is too young to exclude the possibility of developmental delay and/or autistic features. Thus, *RAX* phenotypic spectrum is still unclear, and due to the limited number of cases reported so far, the existence of *RAX* involvement in syndromic forms of anophthalmia cannot be excluded.

Acknowledgements

The authors are grateful to Dr Iba Zizen for providing magnetic resonance imaging scan pictures.

References

1. Morrison D, FitzPatrick D, Hanson I et al. National study of microphthalmia, anophthalmia, and coloboma (MAC) in Scotland: investigation of genetic aetiology. J Med Genet 2002: 39: 16–22.
2. Lowry RB, Kohut R, Sibbald B et al. Anophthalmia and microphthalmia in the Alberta Congenital Anomalies Surveillance System. Can J Ophthalmol 2005: 40: 38–44.
3. Fantes J, Ragge NK, Lynch SA et al. Mutations in SOX2 cause anophthalmia. Nat Genet 2003: 33: 461–463.
4. Ragge NK, Lorenz B, Schneider A et al. SOX2 anophthalmia syndrome. Am J Med Genet A 2005: 135: 1–7; discussion 8.
5. Bakrania P, Efthymiou M, Klein JC et al. Mutations in BMP4 cause eye, brain, and digit developmental anomalies: overlap between the BMP4 and hedgehog signaling pathways. Am J Hum Genet 2008: 82: 304–319.
6. Verma AS, Fitzpatrick DR. Anophthalmia and microphthalmia. Orphanet J Rare Dis 2007: 2: 47.
7. Furukawa T, Kozak CA, Cepko CL. rax, a novel paired-type homeobox gene, shows expression in the anterior neural fold and developing retina. Proc Natl Acad Sci U S A 1997: 94: 3088–3093.
8. Zhang L, Mathers PH, Jamrich M. Function of Rx, but not Pax6, is essential for the formation of retinal progenitor cells in mice. Genesis 2000: 28: 135–142.
9. Mathers PH, Grinberg A, Mahon KA et al. The Rx homeobox gene is essential for vertebrate eye development. Nature 1997: 387: 603–607.
10. Bailey TJ, El-Hodiri H, Zhang L et al. Regulation of vertebrate eye development by Rx genes. Int J Dev Biol 2004: 48: 761–770.
11. Voronina VA, Kozhemyakina EA, O'Kernick CM et al. Mutations in the human RAX homeobox gene in a patient with anophthalmia and sclerocornea. Hum Mol Genet 2004: 13: 315–322.
12. Tucker P, Laemle L, Munson A et al. The eyeless mouse mutation (ey1) removes an alternative start codon from the Rx/rax homeobox gene. Genesis 2001: 31: 43–53.
13. Loosli F, Staub W, Finger-Baier KC et al. Loss of eyes in zebrafish caused by mutation of chokh/rx3. EMBO Rep 2003: 4: 894–899.
14. Andreazzoli M, Gestri G, Angeloni D et al. Role of Xrx1 in Xenopus eye and anterior brain development. Development 1999: 126: 2451–2460.
15. Harries LW, Bingham C, Bellanne-Chantelot C et al. The position of premature termination codons in the hepatocyte nuclear factor-1 beta gene determines susceptibility to nonsense-mediated decay. Hum Genet 2005: 118: 214–224.
16. Amendt BA, Sutherland LB, Russo AF. Multifunctional role of the Pitx2 homeodomain protein C-terminal tail. Mol Cell Biol 1999: 19: 7001–7010.
17. Norris RA, Kern MJ. Identification of domains mediating transcription activation, repression, and inhibition in the paired-related homeobox protein, Prx2 (S8). DNA Cell Biol 2001: 20: 89–99.
18. Eggert T, Hauck B, Hildebrandt N et al. Isolation of a Drosophila homolog of the vertebrate homeobox gene Rx and its possible role in brain and eye development. Proc Natl Acad Sci U S A 1998: 95: 2343–2348.
19. Andreazzoli M, Gestri G, Cremisi F et al. Xrx1 controls proliferation and neurogenesis in Xenopus anterior neural plate. Development 2003: 130: 5143–5154.
20. Spieler D, Baumer N, Stebler J et al. Involvement of Pax6 and Otx2 in the forebrain-specific regulation of the vertebrate homeobox gene ANF/Hesx1. Dev Biol 2004: 269: 567–579.
21. Martinez-Barbera JP, Rodriguez TA, Beddington RS. The homeobox gene Hesx1 is required in the anterior neural ectoderm for normal forebrain formation. Dev Biol 2000: 223: 422–430.
22. Dattani MT, Martinez-Barbera JP, Thomas PQ et al. Mutations in the homeobox gene HESX1/Hesx1 associated with septo-optic dysplasia in human and mouse. Nat Genet 1998: 19: 125–133.

Index case	Heredity	Mutation	G-banding karyotype	Skeletal X-rays (1)	Eye examination (2)	Cardiac echography (3)	Holter-ECG (4)	Brain CT scan or MRI (5)	Kidney echography (6)	Tracheostomy (7)	Gastrostomy (8)	Polysomnography (9)	Hearing (10)	Psychomotor development (11)
JMP	F1	del5'	N	N	N	N	VOA	N	N	+	-	Severe UAO	N	N
GD	Sp		N	N	N (+ VEP, ERG)	N	VOA	N	N	+	-	Severe UAO	-40db (Seromucous otitis)	N
TD	Sp	del3'	N	N	N (+ VEP, ERG)	N	N	N	N	+	-	Severe UAO	N	N
NG	Sp		N	N	N (+ VEP)	N	N	nd	N	+ NIMV	-	Severe UAO	-30db (Seromucous otitis)	N
SA	Sp	del5'	nd	N	N	Atrial SD	N	N	nd	-	-	Normal oxymetry	nd	N
NL	F3		N	N	N (+ VEP, ERG)	N	VOA	N	N	+	-	Severe UAO	-30db (Seromucous otitis)	N
LM	Sp		N	N	N	N	N	Mild cortical atrophy	N	+	-	Severe UAO	N	Transient hyperlaxity
ER	F4		N	N	Astygmatism	N	N	nd	nd	-	-	Mild and transitory UAO	-30db (Seromucous otitis)	N
MF	Sp		N	N	N	N	N	nd	nd	-	-	Normal oxymetry	N	N
TF	F2	mutHCNE	N	N	Mild myopia	Mild septal hypertrophy	N	N	N	+	+	Severe UAO	N	N
AD	Sp		N	N	N	N	nd	N	N	-	+	Mild and transitory UAO	nd	N
MB	F5		N	Delayed bone age	N	Retroesophageal artery	VOA	nd	N	+	+	Severe UAO	-30db (Seromucous otitis)	N

Legend:

(1) In order to eliminate a collagen anomaly, all children get a vertebral and limb X-Ray in the neonatal period

(2) In order to eliminate a congenital myopia or an ocular malformation, all children have an ophtalmologic assessment before 6 months of age. VEP = Visual evoked potential ; ERG = electroretinogram

(3) Cardiac echography is performed in the neonatal period

(4) Holter- ECG is performed between 1 and 2 months of age. VOA = Vagal over-activity is frequently observed at this age and resolves after the age of 1 year.

(5) Brain imaging is not systematically performed because it is almost always normal if clinical examination is normal.

Nature Genetics: doi:10.1038/ng.329

(6) Kidney and urinary track echography is not systematically performed because it is almost always normal if clinical examination is normal.

(7) Tracheostomy and non-invasive mask ventilation (NIMV) are the 2 treatments of severe upper airway obstruction (UAO) in our center.

(8) All the children of this series had transient gastric tube feeding but 3 of them needed gastrostomy because their gastro-oesophageal reflux was severe or the duration of their tube feeding was long (over 1 year).

(9) Oxymetry (transcutaneous O2 and CO2 pressure) is systematically and regularely recorded for all children in the first weeks of life, continued monitoring is then dependant on clinical data. A full polysomnography is performed if the oxymetry and clinical observations are not sufficient then the UAO gravity has to be quantified.

(10) Audition is systematically tested between 9 and 12 months of age

(11) Psychomotor and cognitive development is regularely evaluated during infancy

N = normal

nd = not done

Nature Genetics: doi:10.1038/ng.329

Supplementary Methods

Metaphase FISH and Breakpoint Cloning

Metaphase chromosome analysis using two-color fluorescent *in situ* hybridization (FISH) was performed as previously described[1]. For each hybridization, ≥10 metaphases were analyzed using a Zeiss Axioskop 2 microscope with the appropriate filters, (#83000 for DAPI, FITC and rhodamine; Chroma Technology). Images were collected and merged using a Coolsnap HQ CCD camera (Photometrics) and SmartCapture 2 (Digital Scientific) software or IPlab Software (Scanalytics).

For Southern blots, PCR-amplified probes were sequenced and verified probes radiolabeled with α^{32}P-dCTP using Rediprime II Random Prime labeling System (Amersham Biosciences). Expand Long Template PCR System (Roche) was used to amplify genomic DNA with primers: 2.7F, 2.7R, 2.7B and17.3R (**Supplementary Table**).

Production and analysis of reporter transgenic mice

The **9CE4-Z** reporter construct was made as follows: A 2.8 kb fragment was PCR amplified from human BAC RP11-1003J3 (EMBL accession number AC005181.1) using a high fidelity Pfu polymerase mix with PCR primers containing *NotI* and *EagI* restriction sites. This fragment was subcloned into the *NotI* site of the p610+ reporter construct containing an Hsp68 minimal promotor-LacZ cassette. Microinjection fragments were isolated following restriction digestion with appropriate enzymes, and microinjected according to standard procedures. Transgenic mice and embryos were identified by PCR using LacZ specific primers (**Supplementary Table**).

To analyze the potential tissue-specific enhancer activity of the HCNE-F2 element in transgenic mice we generated a reporter construct bearing three copies of the wildtype HCNE-F2 element in front of a beta-globin minimal promotor – LacZ reporter cassette. This was achieved by insertion of a 3-way Gateway (Invitrogen, Carlsbad USA) cassette (attR4-R3) into a beta-globin minimal promotor – LacZ reporter vector. The HCNE-F2 element was PCR amplified with three sets of att site containing primers (**Supplementary Table**), cloned and sequence verified into the three Gateway entry vectors. The three HCNE-F2 element containing entry vectors and LacZ reporter vector were recombined to generate the **HCNE-F2(3xwt)bZ** reporter construct. The **HCNE-F2(3xwt)bZ** microinjection fragment was generated from this construct by restriction digestion and gel purification and microinjected into mouse oocytes via standard procedures. Transgenic embryos were identified by PCR using LacZ specific primers (**Supplementary Table**).

Embryos were collected at relevant stages, washed in PBS and fixed for 1 hour in a solution of 1% formaldehyde; 0.2% glutaraldehyde; 2mM $MgCl_2$; 5mM EDTA and 0.02% NP-40 in PBS. After fixation the embryos were washed in PBS containing 0.02% NP-40, before being stained for several hours at 37^{o}C in the dark in a solution containing 5mM $K_3Fe(CN)_6$; 5mM $K_4Fe(CN)_6.3H_2O$; 2mM $MgCl_2$; 0.01% sodium deoxycholate; 0.02% NP-40 and 0.1% 5-bromo-4-chloro-3-indolyl-b-D-galactopyranoside (X-gal). Embryos were photographed on a Leica MZ FLIII Microscope fitted with a Hamamatsu Orca-ER digital camera with a CRI micro-color filter.

Optical Projection Tomography (OPT)

Whole mouse embryos were mounted in 1% agarose, dehydrated in methanol and then cleared overnight in BABB (1 part Benzyl Alcohol: 2 parts Benzyl Benzoate). The sample was then imaged using a Bioptonics OPT Scanner 3001 (Bioptonics, UK) using brightfield to detect the LacZ staining and for tissue autofluorescence (excitation 425nm/emmision 475nm) to capture the anatomy[2]. The resulting images were reconstructed using Bioptonics propriatory software, automatically thresholded and merged to a single 3D image output using Bioptonics Viewer software. The downstream digital dissection and sectioning was performed using Amira (Visage Imaging, USA) software.

Fine-tiling CGH-array analysis of chromosome 17q

Fine-tiling array-based comparative genomic hybridization (CGH; NimbleGen) was performed with a Promega reference sample, on 12 isolated PRS patients with normal karyotype (5 familial and 7 sporadic cases; see table in the **Supplementary note**). The custom tiling array was designed containing 385,000 probes of 50-75-mer length with a median probe spacing of 5 base pairs covering the region chr17:65,689,756-69,390,437. Identified microrearrangements were tested by semi-quantitative PCR on a LightCyclerR2.0 machine (Roche) using LightCyclerR FastStart DNA MasterPLUS SYBR Green I protocol and *MAP2K6* as a reference gene (sequences of used primers are listed in **Supplementary Table**).

Nature Genetics: doi:10.1038/ng.329

Electrophoretic mobility shift assays (EMSA)

MSX1 and POU2F1 expression vectors were constructed by insertion of the human *MSX1* or *POU2F1* cDNA (Geneservice) into **pcDNA3.0/zeo+** (Invitrogen) and used to synthesize MSX1 and POU2F1 protein following the TNT Coupled Reticulocyte Lysate Systems protocol (Promega). Gelshift assays were performed using in vitro transcribed MSX1 and POU2F1 protein. Double-stranded probes were obtained by hybridizing biotin 3' end-labeled oligonucleotides and non-labeled oligonucleotides for the competition reaction. Oligonucleotides were 3' end-labeled using the Biotin 3′ End DNA Labeling Kit (Pierce) protocol. The sequences of the wild type and the mutant probes are described in **Figure 2a**. EMSA was performed following the LightShift Chemiluminescent EMSA Kit (Pierce) protocol. For identification of the DNA-bound proteins resolved protein:DNA complexes were transferred to PVDF membrane and probed with primary rabbit anti-MSX1 or POU2F1 polyclonal antibody respectively (Santa Cruz Biotechnology) and donkey ECL™ anti-rabbit IgG, horseradish peroxidase-linked whole antibody (GE Healthcare) as a secondary antibody.

Cell culture

Mandibular and maxillary processes were excised from E11.5 embryos from CD1 females crossed with a male "Immortomouse", which carries a constitutively-expressed, temperature-sensitive SV40 T (tumor) antigen (TAg) transgene[3,4]. DNA extracted from hindlimbs of each embryo was used to verify the presence of the TAg by PCR analysis (**Supplementary Table**). The mandibular and maxillary tissue was homogenised and plated on non-coated culture plastic dishes in medium (1xDMEM/ 10% fetal calf serum (FCS)/ 1% penicillin/streptomycin) containing 100U/ml murine γ-interferon (Peprotech, Inc). Cells were cultured at 33°C, under a humidified atmosphere containing 5% CO2. The cell lines were designated MEPA (mouse embryonic pharyngeal arch) with the prefix of mx (maxillary) and md (mandibular).

Chromatin immunoprecipitation (ChIP)

The ChIP protocol was carried out as previously described[5]. Cells used in the ChIP experiment were mxMEPA and mdMEPA cells cultured at 33° in atmosphere containing 5%CO2. For the immunprecipitation of chromatin-bound proteins the following antibodies were used: PolII, H3K4me3, H3K4me and p300 from Abcam; CTCF and H3ac from Upstate; MSX1 from Santa Cruz Biotechnology. As positive controls, predicted CTCF-binding sites, conserved between mouse and human, were located within the centromeric (mmu chr11:111,475,754-111,475,979) and telomeric (mmu chr11:113,933,183-113,933,416) deleted regions[6,7]. Standard PCR reactions were then performed on the purified DNA (**Supplementary Table**). The primers used for real-time quantitative fluorescent PCR (QPCR) were designed using the Universal ProbeLibrary Assay Design Center (Roche Applied Science) and the Universal ProbeLibrary for mouse was purchased from Roche Applied Science (**Supplementary Table**). Reactions were performed in triplicate in 10μl volumes. Each reaction contained 5μl of 1x TaqMan® Universal PCR Master Mix (Applied Biosystems), 1μl of 10μM primer mix and 0.1μl Universal probe. PCR amplification was carried out on the ABI PRISM® 7900 HT sequence detection system (Applied Biosystems). C_T , DD C_T and fold-change errors were calculated using DART-PCR[8]. Confidence intervals (CI) were calculated on each of the mean C_T values allowing a maximum and minimum DD C_T to be calculated over IgG background which are given as the error bars in **Figure 3b**.

Sox9 immunohistochemistry and interphase FISH

Embryos were harvested at E13.5, fixed in 4% PFA and dehydrated in 70% EtOH. Following decapitation the heads were embedded in wax, 4μm coronal sections were cut and stained with Haematoxylin and Eosin using standard protocols. Primary rabbit anti-Sox9 polyclonal antibody (Chemicon) and as secondary antibody Alexa Flour 488 $F(Ab)_2$ goat anti-rabbit fragments (Invitrogen) were used. "Antigen retrieval" was performed by boiling slides in 10mM citrate pH6.0 and allowing slides to cool followed by washes in PBS. Blocking was performed with 2%inactivated sheep serum, 1%BSA, 0.1%Triton, 0.05% Tween-20 in PBS. The slides were mounted in Vectashield with DAPI stain.

Interphase FISH used mouse BAC probes obtained from BACPAC resources Children's Hospital Oakland Research Institute. BAC clones were DIG labeled or labeled with direct fluorescent label Spectrum Orange-dUTP (Vysis). Anti Dig antibody labeled with fluorescein (Roche) was used to light up the DIG probes[9].

The imaging system comprises a Coolsnap HQ CCD camera (Photometrics Ltd) Zeiss Axioskop II fluorescence microscope with Plan-neofluar objectives, a 100W Hg source (Carl Zeiss) and Chroma #83000 triple band pass filter set (Chroma Technology Corp). Image capture and analysis were performed using in-house scripts written for IPLab Spectrum (Scanalytics Corp). 3D stacks were taken on universal imaging system x100 objective, bin

Nature Genetics: doi:10.1038/ng.329

1,+/-3μm with 0.2μm z plane slices. Inter-spot distances were calculated using the custom software IP lab script (available form Paul Perry, MRC Human Genetics Unit) the xyz coordinates of the centroid for each probe's fluorescent signal was determined. The distance (d) between the two probes (space diagonal) was the distance between two spots at opposite corners of a cuboid. $d_{ABC} = (a^2 + b^2 + c^2)$ a, b and c are length of the side of the cuboid. 3D distance means, standard deviations and confidence intervals were calculated.

***In situ* expression pattern study**

Embryonic stages were established according to the Carnegie staging (CS) classification. Three embryonic stages: CS13 (day 30), CS15 (day 34) and CS18 (day 45) were studied. Primers were selected for PCR amplification of a fragment of SOX9 cDNA (**Supplementary Table**). A T7 promotor sequence extension (TAATACGACTCACTATAGGGAGA) was added at the 5' end of each primer and riboprobes synthesized using digoxygenin-labelled UTP. Tissue fixation, sectioning and in situ hybridization were carried out according to standard protocols[10].

SAGE corroboration

Human embryonic primordia had been used to construct SAGE (Serial Analysis of Gene Expression) banks from CS12-13 (BA1_4wk) and CS15 (BA1_5wk) first pharyngeal arches. Publicly available COGENE SAGE data was mined to examine expression of *SOX9*, *EN1*, *ZNF628*, *MSX1* and *POU2F1*; ACTG web tool was used for tag to gene mapping of the 2 SAGE libraries; tag counts, representing transcripts, were normalized to 1 million per bank and, when multiple tags existed for one transcript, these were summed.

Supplementary Methods References

1. Morey, C., Da Silva, N. R., Perry, P., & Bickmore, W. A. Nuclear reorganisation and chromatin decondensation are conserved, but distinct, mechanisms linked to Hox gene activation. *Development* **134**, 909-919 (2007).

2. Sharpe, J. *et al.* Optical projection tomography as a tool for 3D microscopy and gene expression studies. *Science* **296**, 541-545 (2002).

3. Ali, S. H. & DeCaprio, J. A. Cellular transformation by SV40 large T antigen: interaction with host proteins. *Semin.Cancer Biol* **11**, 15-23 (2001).

4. Barald, K. F. *et al.* Immortalized cell lines from embryonic avian and murine otocysts: tools for molecular studies of the developing inner ear. *Int.J.Dev.Neurosci.* **15**, 523-540 (1997).

5. Essafi, A. *et al.* Direct transcriptional regulation of Bim by FoxO3a mediates STI571-induced apoptosis in Bcr-Abl-expressing cells. *Oncogene* **24**, 2317-2329 (2005).

6. Bao, L., Zhou, M., & Cui, Y. CTCFBSDB: a CTCF-binding site database for characterization of vertebrate genomic insulators. *Nucleic Acids Res.* **36**, D83-D87 (2008).

7. Barski, A. *et al.* High-resolution profiling of histone methylations in the human genome. *Cell* **129**, 823-837 (2007).

8. Peirson, S. N., Butler, J. N., & Foster, R. G. Experimental validation of novel and conventional approaches to quantitative real-time PCR data analysis. *Nucleic Acids Res.* **31**, e73 (2003).

9. Chambeyron, S., Da Silva, N. R., Lawson, K. A., & Bickmore, W. A. Nuclear re-organisation of the Hoxb complex during mouse embryonic development. *Development* **132**, 2215-2223 (2005).

10. Delous, M. *et al.* The ciliary gene RPGRIP1L is mutated in cerebello-oculo-renal syndrome (Joubert syndrome type B) and Meckel syndrome. *Nat.Genet.* **39**, 875-881 (2007).

Nature Genetics: doi:10.1038/ng.329

Supplementary Table

Primer (F, forward ; R, reverse)	Sequence 5' -> 3'
Sequencing primers used for verification of *POU2F1* cDNA sequence	
POU2F1-cDNA-1-F	GAGGAGCAGCGAGTCAAGATG
POU2F1-cDNA-1-R	AGGCGTCAAAGTAAGCCCAGT
POU2F1-cDNA-2-F	TTCCCCAGACCCAGCTTATG
POU2F1-cDNA-2-R	GGCAAACTGCTCAAGCTCCT
POU2F1-cDNA-3-F	AGCCCAGTGACCTTGAGGAG
POU2F1-cDNA-3-R	TCACAAGGCTTGGTGTGGTC
POU2F1-cDNA-4-F	AAAGAATCAACCCACCAAGCA
POU2F1-cDNA-4-R	TTAGAGCTGGGCTGAGAGCAC
POU2F1-cDNA-5-F	TGATGGCACCCTCACAGTTT
POU2F1-cDNA-5-R	CCTTCTCTCCTTTGCCCTCA
Sequencing primers used for verification of *MSX1* cDNA sequence	
MSX1-cDNA-1-F	CCACTCGGTGTCAAAGTGGA
MSX1-cDNA-1-R	GGTACTGCTTCTGGCGGAAC
MSX1-cDNA-2-F	GCAAACACAAGACGAACCGTAA
MSX1-cDNA-2-R	AGGGAGCAAAGAGGTGAAACTG
MSX1-cDNA-3-F	GAGCTGGAGAAGCTGAAGATGG
MSX1-cDNA-3-R	TCGTCAGACACCGATTTCTCTG
Primers used for amplification and subcloning of the mouse *Sox9* minimal promotor with BglII and HindIII restriction sites	
Sox9 Mus musculus minimal promotor-BglII-F	GGAAGATCTCCCTCCAAGTCCCCTCAC
Sox9 Mus musculus minimal promotor-HindIII-R	CCCAAGCTTCCGGGAAAGGCGAGAAG
Primers used for amplification and subcloning of the HCNE-F2 element with MluI and XhoI restriction sites	
HCNE-F2-MluI-F	CGACGCGTCCCACTACCTATTCTAAACAGTAACG
HCNE-F2-XhoI-R	CCGCACGAGCCTATTTCACATGTGGCAACC
***SOX9 in situ* hybridization primers - a T7 promoter sequence extension (bold) was added to the 5' end of each primer used for the amplification of a fragment of *SOX9* cDNA**	
HIS.SOX9-F	TACGACTACACCGACCACCA
HIS.SOX9-R	GCGCTTGGATAGGTCATGTT
SOX9 HIS + T7extension-F	**TAATACGACTCACTATAGGGAGA**TACGACTACACCGACCACCA
SOX9 HIS + T7extension-R	**TAATACGACTCACTATAGGGAGA**GCGCTTGGATAGGTCATGTT
LacZ specific primers used for PCR identification of transgenic embryos	
LacZ-F	GTTGCGCAGCCTGAATGGCG
LacZ-R	GCCGTCACTCCAACGCAGCA
Primers used for PCR amplification and insertion into the 9CE4-Z reporter construct	
9CE4-Z-F	AGGAAAGTTCCAGAGAGGTTGA
9CE4-Z-R	TTGCCCTCCAAGTGCCTTCA
Primers used for PCR amplification and insertion into the HCNE-F2(3xwt)bZ reporter construct	
HCNE-F2(3xwt)bZ-1-F	attB4-CACTTGATGAATTTCGGCA
HCNE-F2(3xwt)bZ-1-R	attB1r-CAATTACATTTCATACTGGAG
HCNE-F2(3xwt)bZ-2-F	B1-CACTTGATGAATTTCGGCA
HCNE-F2(3xwt)bZ-2-R	B2-CAATTACATTTCATACTGGAG
HCNE-F2(3xwt)bZ-3-F	B2r-CACTTGATGAATTTCGGCA
HCNE-F2(3xwt)bZ-3-R	B3-CAATTACATTTCATACTGGAG
***KCNJ2* sequencing primers**	
KCNJ2-exon1-F	GGCTCCAGACGGAGTAGGAA
KCNJ2-exon1-R	TCTGGTGCGCACACAAACTA
KCNJ2-exon2/1-F	GGATATCAATGCTGCGTCCA
KCNJ2-exon2/1-R	GGGACTCCAGTGCTTCTGCT
KCNJ2-exon2/2-F	AGAACCACAAGGCTCCCAGA
KCNJ2-exon2/2-R	CCCCATGGAGCAGAGCTATC
KCNJ2-exon2/3-F	AGGAGCCGCTTTGTGAAGAA
KCNJ2-exon2/3-R	CGAACATGAGCTTCCACCAA
KCNJ2-exon2/4-F	CTTTCATCATTGGCGCAGTC
KCNJ2-exon2/4-R	AAGGGGAGTGTTGGGGACTT
KCNJ2-exon2/5-F	ACTGGAAGGCATGGTGGAAG
KCNJ2-exon2/5-R	AAGGCTTGCCTGCAAGTTCA
KCNJ2-exon2/6-F	GGCAAGCACAATGGTTTCAA
KCNJ2-exon2/6-R	CCATGGGGCTTTGTTTTCTT
KCNJ2-exon2/7-F	CTGCCAAAACAAGAGCCTGA
KCNJ2-exon2/7-R	TCATGCTGGATGGCTCAGTT
KCNJ2-exon2/8-F	CTGGCCAGGCTCATGTGTAG
KCNJ2-exon2/8-R	AGGGGAGGCTTCTGGAAAAC
KCNJ2-exon2/9-F	GCCAGTTTGATGCAGCACTT
KCNJ2-exon2/9-R	CCTTCCCAAACCTGCCTTTA
***KCNJ16* sequencing primers**	
KCNJ16-exon1-V1,V2-F	CTGCCACAGCTGACTGGCTA
KCNJ16-exon1-V1,V2-R	AGTGTTGCTGCTCCCCAAAC
KCNJ16-exon2-V1,V2-F	TTGCCTGGTACTGTTTTAAGTGC
KCNJ16-exon2-V1,V2-R	GCTGGACTTCTGGAAAAATGC
KCNJ16-exon1-F	AATGCAGCCTTCCAGGACAA
KCNJ16-exon1-R	GCATGACTGCTGAGCCAAAA
KCNJ16-exon2-F	CCGCCCTTTGTAGCACCATA
KCNJ16-exon2-R	GAAGAAGCCACTGGGACACG
KCNJ16-exon3-F	TTTTGCAGCAGAGAAGGTGCT
KCNJ16-exon3-R	GGCAGCTCTTCTCTTTCCCTCT
KCNJ16-exon4.1-F	TGAGGCATCATTTGGGATAATCA
KCNJ16-exon4.1-R	TGGTGTCCACAAGAGTGGTGA
KCNJ16-exon4.2-F	CAATGCGGACGCAAAATACC
KCNJ16-exon4.2-R	TTGGGCTCTCTTTCGAGCAG
KCNJ16-exon4.3-F	CAGGGGCCTTTTTGTTCTCC
KCNJ16-exon4.3-R	GGAGCTGCTGGTCTTTCCAG
KCNJ16-exon4.4-F	AAGCTCCTATGTTCCCCGAGA
KCNJ16-exon4.4-R	GCCTCCTTCCTGCCTTCATT
***MAP2K6* sequencing primers**	
MAP2K6-exon1-F	GACCACGTTTCCTTAAATCAGAGC
MAP2K6-exon1-R	AACCTCAAACTTAAAAATGCACTCG
MAP2K6-exon2-F	GCCTGTGCAGGTCAGCTCTT
MAP2K6-exon2-R	GGATGTGGGTCCTCACCAAA
MAP2K6-exon3-F	GAAAGGGAGCCCCAAAGAGA
MAP2K6-exon3-R	GCCATGACCCTTCATTGTGTC
MAP2K6-exon4-F	TCTTGTAGCTTCTTGCTTTCAGAGG
MAP2K6-exon4-R	CACCAAGGAAGACTTTTCCATACCT
MAP2K6-exon5-F	TTCACAATGTCATCGCCAGAA
MAP2K6-exon5-R	GCTCCTAAAGCAGTCAAAAGACCA
MAP2K6-exon6-F	GGGTAGGAGAGCACATGCAG
MAP2K6-exon6-R	TCTGCCAAACCAAAGCAGTG
MAP2K6-exon7-F	CAGTCCTCTCTGGTGGATGGA
MAP2K6-exon7-R	CCAACAAGCTCTCATGTGATGG
MAP2K6-exon8-F	TGGGTCAGGGATGGCAGTTA
MAP2K6-exon8-R	GTGAGCCCTCATTGGACACC
MAP2K6-exon9-F	CCCACGGAGGCATTGATATT
MAP2K6-exon9-R	GGAATCTGGTCAGATCCTCTCG
MAP2K6-exon10-F	TGAAGTGCCACAGTGGGTTT
MAP2K6-exon10-R	AGTGAGGGCAGGGAGTGTGA
MAP2K6-exon11-F	AAGGCACAACCAGGGTGATTT
MAP2K6-exon11-R	TCCTGGAGTTCAATTCCTGTCA
MAP2K6-exon12-F	GGAAAAGCCCAGCCTAGCTC

Nature Genetics: doi:10.1038/ng.329

MAP2K6-exon12-R	TGGAATCTTTTCAACCAAGCAC
***SOX9* sequencing primers**	
SOX9-EXON1/1-F	CCAAAATCGGGTCCAATCAG
SOX9-EXON1/1-R	TGTCCTCCTCGCTCTCCTTC
SOX9-EXON1/2-F	TGAATCTCCTGGACCCCTTC
SOX9-EXON1/2-R	TTACACCCCATTCCCACTCC
SOX9-EXON2-F	GAGTGACCGCTCAGGTCAGA
SOX9-EXON2-R	GGGATTGAGTTGGGGTGTGT
SOX9-EXON3/1-F	AGGGGGCTGTCCAGTGTGTA
SOX9-EXON3/1-R	TCAGCTGCTCCGTCTTGATG
SOX9-EXON3/2-F	ACGTGTGGATGTCCAAGCAG
SOX9-EXON3/2-R	AGGCCTCCTCAAGGTCGAGT
SOX9-EXON3/3-F	CGACTACACCGACCACCAGA
SOX9-EXON3/3-R	TCCCCTCAAAATGGTAATGAA
SOX9-EXON3/4-F	AAGCGTGGAGGATGATGGAG
SOX9-EXON3/4-R	GTGTGCTCGGGCACTTATTG
SOX9-EXON3/5-F	CATTTCCTCCTGCCTTTGCT
SOX9-EXON3/5-R	TGTGGCAGAAAACACTGCAA
SOX9-EXON3/6-F	GCCTTTTTGTCCATCCCTTTT
SOX9-EXON3/6-R	TCCACAGGGCCACTTTCTTT
Primers used to clone the family T3 translocation breakpoints	
2.7	GATGAAAGGCAAGGGAATC
2.7B	CCACCTGCTTTAACTGTTG
17.3	GTTGTTGGTGCTGTTGTAAATC
Chromosome 2 Southern blot probes used for identification of the family T3 translocation breakpoints	
Chr 2.7 F	GATGAAAGGCAAGGGAATC
Chr 2.7 R	CAACAGTTAAAGCAGGTGG
Primers used for amplification and sequencing of highly conserved non-coding elements (HCNE) located in the family F1 deletion	
delF1-HCNE1/1-F	TACTAACGGGTTGGGCTCAGA
delF1-HCNE1/1-R	TCTGGGTGGGCTCAATGTATC
delF1-HCNE1/2-F	GCCATCCCGATCCTATTCTTC
delF1-HCNE1/2-R	AGGGAGCAGGATGCATTGTTA
delF1-HCNE2/1-F	AGCCTGATGGGAAGTTGTGAG
delF1-HCNE2/1-R	GTTTTGCCTCCTGAACTGGTG
delF1-HCNE2/2-F	GGCTACTGACCTGGGAGCTTT
delF1-HCNE2/2-R	GCTGGAGGATCTGATGTCACC
delF1-HCNE3/1-F	CATATGCGAACTCCTGCTCCT
delF1-HCNE3/1-F	TGGGCTGAAATGTACCTCCA
delF1-HCNE3/2-F	TGGGGAGTTGTTCACCAATG
delF1-HCNE3/2-R	ATCACCGTGCTGGAGGATCT
delF1-HCNE4-F	TTCCTGCCATCTCTGACTTCC
delF1-HCNE4-R	TTCAGACCTGGGCACATAGTGTA
delF1-HCNE5-F	GACTTGTCCGTGCGAATACTTT
delF1-HCNE5-R	CAATTGGAAAGACCGAAACAAG
delF1-HCNE6-F	AGGGCTTTAGAGCAGCAAAAA
delF1-HCNE6-R	TCGAAGATCTGGCAAAGGAA
delF1-HCNE7/1-F	CAGTGCCCTCAGTCAGGTCTT
delF1-HCNE7/1-R	GCAGCCAGGAATGCTAAGAGA
delF1-HCNE7/2-F	TCTTCTACCAGTGGCCCTGAA
delF1-HCNE7/2-R	TAAGCTCTCGGCTCCCTTTTT
delF1-HCNE8/1-F	GGCAAAATCATCTAGGGCAAAG
delF1-HCNE8/1-R	TCAGTCTGGCTCATTCGGAGT
delF1-HCNE8/2-F	GGCACATTGAGGTGATTTGC
delF1-HCNE8/2-R	CACGGTCGGAATTTGGATCT
delF1-HCNE9-F	CAAGGACAGGACCTTTCAAAAC
delF1-HCNE9-R	AGATCGAGGGGTTCTTTGCT
delF1-HCNE10-F	AAGGAAACAACACTGGCATGA
delF1-HCNE10-R	GGAAATCCTGAACCTTTTCCA
Primers used for semi-quantitative PCR confirmation of deletions identified by CGH	
*MAP2K6*reference-F	CTCACTTGGCAGCTGGTGCT
*MAP2K6*reference-R	CATCGTGATGCCCAGACTCC
delF1-qPCR-F	CCTGGCCCCGAATATCAGTA
delF1-qPCR-R	TGGGCAGTCTGAGGAAGTCA
delSp4-qPCR-F	TGCACTGAATGCCTGTGTGTTC
delSp4-qPCR-R	CAGGACCCTCCAAGGAATGTGT
delSp2-qPCR-F	GATTCTGGGGACGGAGGAGAC
delSp2-qPCR-R	TTGGAAATCTGCCCAAAGCTG
QF-PCR primers used for qPCR in ChIP experiments	
ChIP.mm.mut.UP.F	CAAGTGCTGAGACTGTAATGAAGTTA
ChIP.mm.mut.UP.R	ACGGTAGCTGGGAACTTGC
ChIP.mm.ctrl.UP.F	CAATGGCAAGGCTAAATTGC
ChIP.mm.ctrl.UP.R	TAGAGGAAATTACGAAGTGTGCTG
ChIP.mm.5'del.UP.F	CCCAGGCACTACCCCTCT
ChIP.mm.5'del.UP.R	CGACCCAGCTTACTTGGTG
ChIP.mm.3'del.UP.F	TGAAAAGATTCTCCAAGCACAG
ChIP.mm.3'del.UP.R	GCTCCCAACCAACATAGCTG
ChIP.mm.Sox9P.UP.F	TGATTGGCCCGAGGTATCTA
ChIP.mm.Sox9P.UP.R	GACTTCCAGCTCAGGGTCTCT
Primers used for PCR amplification following the MSX1 ChIP experiment	
ChIP.mm.mut.F	TTGCAAGTTCCCAGCTACCG
ChIP.mm.mut.R	TCAAAACACCCTCTGGCAACA
ChIP.mm.ctrl.F	CCAAATCTCAGGCATCCACA
ChIP.mm.ctrl.R	CCAGGGAAAAAGGGGAAGTC

Nature Genetics: doi:10.1038/ng.329

nature genetics

Highly conserved non-coding elements on either side of *SOX9* associated with Pierre Robin sequence

Sabina Benko[1,14], Judy A Fantes[2,14], Jeanne Amiel[1,3], Dirk-Jan Kleinjan[2], Sophie Thomas[1], Jacqueline Ramsay[2], Negar Jamshidi[4], Abdelkader Essafi[2], Simon Heaney[2], Christopher T Gordon[4], David McBride[2], Christelle Golzio[1], Malcolm Fisher[2], Paul Perry[2], Véronique Abadie[5,6], Carmen Ayuso[7], Muriel Holder-Espinasse[8], Nicky Kilpatrick[4], Melissa M Lees[9], Arnaud Picard[10,11], I Karen Temple[12], Paul Thomas[4], Marie-Paule Vazquez[10,11], Michel Vekemans[1,3,5], Hugues Roest Crollius[13], Nicholas D Hastie[2], Arnold Munnich[1,3,5], Heather C Etchevers[1], Anna Pelet[1], Peter G Farlie[4], David R FitzPatrick[2,14] & Stanislas Lyonnet[1,3,5,14]

Pierre Robin sequence (PRS) is an important subgroup of cleft palate. We report several lines of evidence for the existence of a 17q24 locus underlying PRS, including linkage analysis results, a clustering of translocation breakpoints 1.06–1.23 Mb upstream of *SOX9*, and microdeletions both ~1.5 Mb centromeric and ~1.5 Mb telomeric of *SOX9*. We have also identified a heterozygous point mutation in an evolutionarily conserved region of DNA with *in vitro* and *in vivo* features of a developmental enhancer. This enhancer is centromeric to the breakpoint cluster and maps within one of the microdeletion regions. The mutation abrogates the *in vitro* enhancer function and alters binding of the transcription factor MSX1 as compared to the wild-type sequence. In the developing mouse mandible, the 3-Mb region bounded by the microdeletions shows a regionally specific chromatin decompaction in cells expressing *Sox9*. Some cases of PRS may thus result from developmental misexpression of *SOX9* due to disruption of very-long-range *cis*-regulatory elements.

Pierre Robin sequence (PRS, OMIM 261800)[1], defined by micrognathia, glossoptosis and a posterior U-shaped cleft palate, is a complex anomaly resulting in life-threatening feeding and breathing difficulties in 1/2,000–1/10,000 of neonates. PRS represents an embryological sequence in which the primary abnormality is in mandibular growth, with a retropositioned tongue resulting in a physical obstruction of palatal shelf elevation and/or fusion. The core triad of features suggests that PRS may be considered a cranial neurocristopathy[2].

We mapped an autosomal dominant and highly penetrant PRS locus to chromosome 17q24.3–25.1 (the *PRS1* locus) by genetic linkage analysis in 12 affected individuals from a four-generation PRS-affected family (F1) (**Fig. 1a**). The maximum lod score of 3.32 (recombination fraction $\theta = 0$) for the *PRS1* locus was obtained in between polymorphic DNA markers D17S795 and D17S929. This genetic interval of 5.4 Mb encompasses a gene desert of 2.46 Mb (**Fig. 1b**). *SOX9, KCNJ2, KCNJ16* and *MAP2K6* were selected as candidate genes on the basis of expression pattern, their involvement in molecular pathways relevant to mandibular development, or the phenotypes of available knockout mice. No gross genomic alterations or coding-sequence mutations could be detected by direct sequencing of those genes in six individuals with PRS from family F1.

Concomitantly, we identified three independent families with autosomal dominant, isolated PRS segregating with different reciprocal translocations, each of them sharing one breakpoint at 17q24 (**Fig. 1a**). Family T1 is a father and daughter with PRS who carry the translocation t(2;17)(q32;q24), which occurred *de novo* in the father. The 2q and 17q breakpoints lie within the BAC clones CTD-2053I13 and RP11-1003J3, respectively. The 17q breakpoint was narrowed to 113–149 kb from the centromeric end of RP11-1003J3 (**Supplementary Fig. 1a** online). In family T2, the breakpoint-spanning clones were RP11-420O5 on 17q and RP11-496M2 on 5q (ref. 3; **Supplementary Fig. 1b**). In family T3, PRS segregates with t(2;17)(q24.1;q24.3)[4]. RP11-510H11 on 2q and RP11-1003J3 (as above) on 17q spanned the breakpoints. Southern blotting and inverse PCR localized the breakpoint to Chr17:66,400,448 (NCBI Build 36.1; **Supplementary Fig. 2** online). The 2q32, 5q15 and 2q24.1 breakpoints

[1]INSERM U-781, Hôpital Necker–Enfants Malades, Paris, France. [2]Medical Research Council Human Genetics Unit (MRC HGU), Institute of Genetic and Molecular Medicine, Edinburgh EH4 2XU, UK. [3]Assistance Publique–Hôpitaux de Paris (AP-HP), Département de Génétique, Hôpital Necker–Enfants Malades, Paris, France. [4]Murdoch Children's Research Institute, Royal Children's Hospital, Parkville, Australia. [5]Université Paris Descartes, Faculté de Médecine, Paris, France. [6]AP-HP, Service de Pédiatrie, Hôpital Necker–Enfants Malades, Paris, France. [7]Fundación Jiménez Díaz, Genética, Ciberer Madrid, Spain. [8]CHRU de Lille, Hôpital Jeanne de Flandre, Lille, France. [9]North Thames Regional Genetics Service, Great Ormond Street Hospital, London, UK. [10]AP-HP, Service de Chirurgie Maxillo-Faciale et Chirurgie Plastique, Hôpital d'Enfants Armand Trousseau, Paris, France. [11]Université Pierre et Marie Curie–Paris 6, UFR de Médecine Pierre et Marie Curie, Paris. [12]Wessex Clinical Genetics Academic Group, Division of Human Genetics, University of Southampton, Southampton, UK. [13]Department of Biology, École Normale Supérieure, CNRS UMR-8541, Paris, France. [14]These authors contributed equally to this work. Correspondence should be addressed to S.L. (stanislas.lyonnet@inserm.fr) or D.R.F. (david.fitzpatrick@hgu.mrc.ac.uk).

Received 19 May 2008; accepted 12 January 2009; published online 22 February 2009; doi:10.1038/ng.329

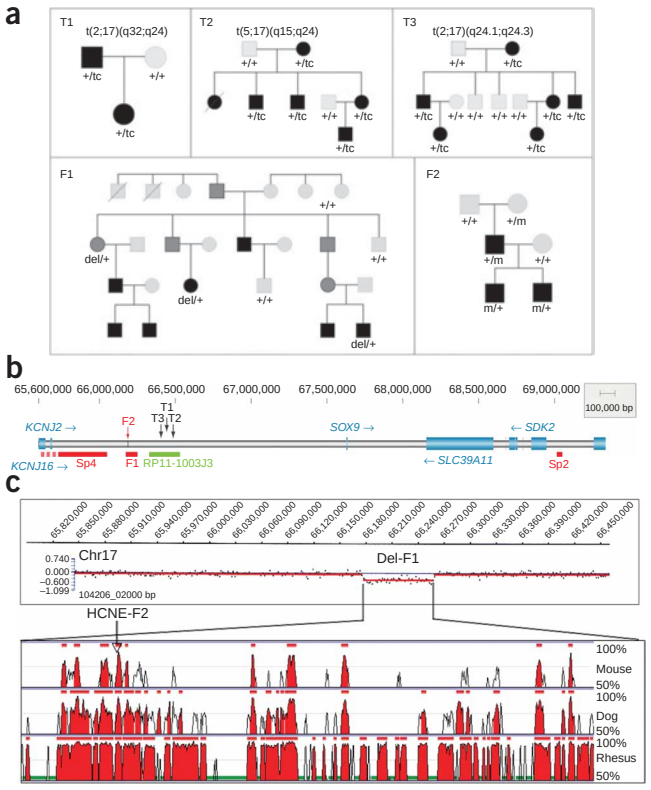

Figure 1 Family trees and highly conserved noncoding element (HCNE) rearrangements. (**a**) Segregation of full (black symbols; posterior cleft palate, micrognathia, glossoptosis) and partial (gray symbols; micrognathia, glossoptosis) PRS phenotypes with the mutant chromosomes in families T1–T3 (tc: translocation t(N;17)(N;q24)), family F1 (del: deleted chromosome 17q24.3) and family F2 (m: mutated HCNE). All affected individuals are heterozygous for the mutant allele. (**b**) Genomic organization of the *SOX9* locus and its 5′ and 3′ flanking regions. Black arrows, T1, T2 and T3 translocation breakpoints; green box, human BAC clone RP11-1003J3 (within which translocation breakpoints T1 and T3 were located); red boxes, deletions found in family F1 and individuals Sp2 and Sp4 (as detected by CGH and confirmed by semiquantitative PCR; **Supplementary Figs. 4–6** online); red arrow, point mutation detected by sequence analysis (not shown) in family F2. (**c**) CGH profile of the F1 deletion, presented with a conservation plot (ECR browser; conservation throughout human, rhesus monkey, dog and mouse of fragments >350 bp at 75% identity indicated in red). Arrow indicates the HCNE harboring the point mutation in family F2 (HCNE-F2).

in families T1, T2 and T3 did not disrupt any known genes. The 17q24 breakpoints cluster within 160 kb in the gene desert between the genes *KCNJ2* (Chr17:65,677,271–65,687,778) and *SOX9* (Chr17:67,628,756–67,634,155; **Fig. 1b**). Another PRS-associated translocation in the same region has been reported[5]. Comparative genomics analysis indicated that this region contains over 200 highly conserved noncoding elements (HCNEs; **Fig. 1c**) with >75% identity over 350 bp across humans, rhesus, dog and mouse[6–8]. The notable clustering of these breakpoints led us to hypothesize that one or more HCNEs centromeric to the T3 breakpoint had a critical regulatory function in mandibular development. We constructed multiple stable reporter transgenic lines of mice to test the potential enhancer function of an HCNE immediately centromeric to the T3 breakpoint (9CE4Z, Chr17:66373309–66376106; **Fig. 2a–c**). Embryos from these lines showed reporter expression in the proximal mandibular mesenchyme, which is compatible with the pathogenesis of PRS (**Fig. 2a**,**b**).

As a first step to determine whether specific regulatory mutations at this chromosomal locus cause PRS, we designed a high-density-tiling-path comparative genomic hybridization (CGH) array extending 1.94 Mb centromeric (5′) and 1.76 Mb telomeric (3′) to *SOX9* (Chr17:65,689,756–69,390,437; **Fig. 1b**), as breakpoints downstream of *SOX9* have been associated with campomelic dysplasia featuring PRS[9]. We observed heterozygous deletions in 3 of 12 unrelated cases of PRS (**Table 1**, **Fig. 1b**): a centromeric 75-kb deletion (Chr17:66,175,000–66,250,000; **Fig. 1c**, **Supplementary Fig. 3a** online) segregating with PRS in family F1, and *de novo* deletions in two individuals with sporadic PRS, respectively a centromeric deletion of >319 kb (Chr17:65,730,750–66,049,600; **Supplementary Fig. 3b**) in individual Sp4 and a *de novo* telomeric 36-kb deletion (Chr17:69,153,000–69,189,000; **Supplementary Fig. 3c**) in individual Sp2. Each of the three alterations comprised at least 1 and up to >27 HCNEs (**Table 1**).

Subsequent DNA sequencing analysis, in the remaining nine individuals with PRS who did not carry deletions, of the ten HCNEs located in the F1 deletion identified a heterozygous T-to-C transition in PRS-affected family F2 (**Fig. 1a**)—absent in 440 control chromosomes—within an HCNE that shows 94% identity between human and mouse over a distance of 220 bp (HCNE-F2; Chr17:66,187,898; **Table 1**, **Fig. 1c**). To determine whether HCNE-F2 has tissue-specific enhancer properties, we performed *in vivo* reporter assays. A transient transgenic assay using the wild-type HCNE-F2 showed strong activity in the craniofacial region in mouse embryos at 11.5 days post coitum (d.p.c.) (**Fig. 2c**,**d**). In addition, transcription-factor binding-site predictions identified MSX1, EN1 and ZNF628 (ZEC) as potential transcription factors for which binding to the HCNE-F2 would be altered by the F2 mutation. Although ZNF628 and EN1 were excluded on the basis of lack of expression within the human first branchial arch, MSX1 (OMIM 142983) is a transcriptional regulator expressed in the human first pharyngeal arch[10] (**Supplementary Fig. 4q** online) that is required for the development of craniofacial skeletal elements, including the palate and mandible, in mice[11] and has been found to be mutated in some families with orofacial clefting. Electrophoretic mobility shift assay (EMSA) analysis, using *in vitro*–transcribed and –translated MSX1, showed significantly greater MSX1 binding (by 33%, $P = 0.031$) to the mutant target sequence than to the wild-type consensus sequence (**Fig. 3a**). A control EMSA experiment was performed with the nearby POU2F1 (**Supplementary Fig. 4q**) binding site, in which we observed no affinity difference in POU2F1 binding to either the wild-type or the mutant probes (data not shown). Chromatin immunoprecipitation (ChIP) from mouse cell lines derived from 11.5-d.p.c. embryonic mandibular and maxillary mesenchyme (mdMEPA and mxMEPA) confirmed that endogenous Msx1 binds wild-type HCNE-F2 (**Fig. 3b**). In addition, we performed *in vitro* assays using three cell types (HEK293, SKNBE(2c) and mdMEPA) with wild-type or mutant HCNE-F2 or minimal promoter reporter constructs[12]. As compared to the minimal promoter, the wild-type HCNE-F2 had an enhancer activity only in mdMEPA that was abolished when the element was mutated ($P = 0.017$, **Fig. 3c**). These findings suggest that the family F2 mutation would abolish enhancer activity of the HCNE-F2 in a tissue-specific manner.

Finally, further ChIP analysis of the HCNE-F2 using the mdMEPA cell line showed strong binding of p300, CTCF and K4-methylated histone H3 (K4Me) to this region (**Fig. 4a**), a pattern that suggests a role in both chromatin remodeling and transcriptional activation and is consistent with the hypothesized active mandibular mesenchymal

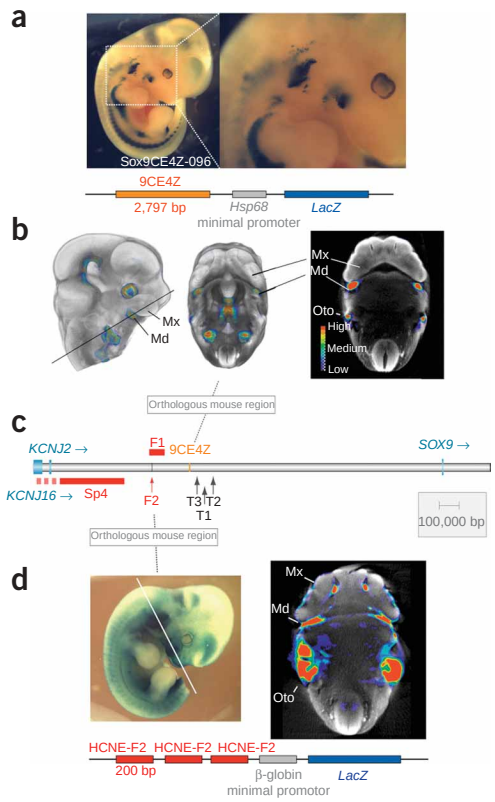

Figure 2 HCNEs at the *PRS1* locus have tissue-specific enhancer activity. (**a**) The 9CE4Z element, located just upstream of the translocation breakpoint cluster, was cloned 5′ to an *Hsp68* minimal promoter–*LacZ* reporter gene cassette and used to make transgenic lines of mice. At 9.5 d.p.c., these lines showed consistent LacZ expression in a subset of cells in the mandibular mesenchyme and some extracraniofacial expression. (**b**) Left, 3D digital reconstructions from an OPT scan of the embryo shown in **a**. Middle, digital dissection of the craniofacial region viewed from below. Right, digital section through the plane indicated in the whole-embryo image in **a** with expression in the proximal mandible (Md) and otocyst (Oto). (**c**) Cartoon of the genomic region, showing the location of 9CE4Z and HNCE-F2 (F2). (**d**) Left, LacZ expression at 11.5 d.p.c. in a whole embryo containing three copies of HCNE-F2 cloned 5′ into a minimal promoter–*LacZ* reporter gene cassette, showing a pattern consistent with a subset of the normal mouse *Sox9* and human *SOX9* expression pattern (compare with **Supplementary Fig. 3**). Right, digital section from an optical projection tomography (OPT) scan of the same embryo using the section plane illustrated. This shows expression in the proximal mandible (Md), the maxilla (Mx) and the otocyst (Oto).

enhancer function. The SP2 region also showed strong binding of p300, CTCF and K4Me in mdMEPA cells but also showed weaker binding to acetylated histone H3 (H3Ac) and K4-trimethylated histone H3 that was not seen in HNCE-F2 (data not shown).

Such enhancer activity is often associated with changes in the degree of chromatin condensation of the locus[13]. We reasoned that an *in vivo* assay of chromatin alterations during development of the mandible would help determine which gene(s) is being transcriptionally regulated by the HCNEs in question. The closest flanking genes are *KCNJ2* and *SOX9*. We measured the three-dimensional (3D) distance between pairs of BAC probes from the orthologous genomic region in mouse embryos using interphase fluorescence *in situ* hybridization (FISH; **Table 2** and **Supplementary Fig. 5** online). These BACs contained *Kcnj2* (RP23-408D5 Chr11:110,809,076–111,002,979), the breakpoint–HCNE-F2 region (BP-F2; RP23-76P19 Chr11:111,402,479–111,629,783) and the telomeric *de novo* deletion detected in individual Sp2 (delSp2; RP23-418P13 Chr11:113,809,869–114,025,688) (**Fig. 4b**). Mouse embryos were examined at 13.5 d.p.c., just before palate fusion, a stage critical for PRS. The interphase distance between *Kcnj2* and the BP-F2 probe remained unchanged in all tissues tested (**Table 2**). However, the distance between the BP-F2 probe and the delSp2 probe was significantly greater in *Sox9*-expressing mandibular arch cells than in the periocular mesenchyme, which does not express *Sox9* (**Table 2**); a similar tissue distinction was seen for the distance between BP-F2 and *Sox9*, although this was not statistically significant. This chromatin decompaction implicates *Sox9* as the best candidate target of the enhancer activity associated with the *PRS1* locus. Indeed, the pattern of enhancer activity in the transgenic reporter mice is consistent with the pattern of endogenous *SOX9* expression in human embryos (**Supplementary Fig. 4a–p**), which, among other locations, is found in the nervous system and skeletal structures, including Meckel's and Reichert's cartilages.

Collectively these data support the deregulation of tissue-specific *SOX9* expression following mutation or disruption of regulatory HCNEs as a highly plausible pathogenic mechanism at the *PRS1* locus. HCNEs located in the gene desert surrounding *SOX9*, such as the Sox9Cre1 or E1–E7 regulatory elements[14–16], have already been reported as putative regulators of *Sox9* tissue-specific expression. Heterozygous loss-of-function coding-sequence mutations of the *SOX9* gene cause campomelic dysplasia (CD, MIM114290) a severe, often lethal skeletal dysplasia associated with sex reversal. PRS is a feature both of CD and of a milder variant of the condition (acampomelic campomelic dysplasia, ACD) caused by hypomorphic intragenic mutations or 'position effect' translocation breakpoints[9]. Moreover, *Sox9* is an early, direct activator of *Col2a1*, *Col11a1* and *Col11a2* in avian cranial neural crest (CNC) cells[17] and mouse chondrocytes[18,19].

Table 1 ***SOX9*** **locus alterations in isolated Pierre Robin sequence (PRS)**

			Position relative to *SOX9*		Conserved element		
	Molecular event	Genomic position	5′	3′	HCNEs	Human/mouse, >200 bp, >90%	Heredity
F1	75-kb deletion	Chr17:66,175,000–66,250,000	−1.38 Mb		**10**	**5**	+
F2	T>C mutation	Chr17:66,187,898	−1.44 Mb				+
Sp4	>319-kb deletion	Chr17:65,730,750–66,049,600	−1.58 Mb		**≥27**	**≥5**	*De novo*
T1	Translocation	Chr17:66,431,112–66,467,874	−1.16 Mb		*75*	*29*	+
T2	Translocation	Chr17:66,518,875–66,602,885	−1.03 Mb		*98*	*39*	+
T3	Translocation	Chr17:66,400,448	−1.23 Mb		*66*	*25*	+
Sp2	36-kb deletion	Chr17:69,153,000–69,189,000		+1.56 Mb	**1**	**1**	*De novo*

Nucleotide positions at the *SOX9* locus are numbered according to Human NCBI Build 36.1. Position of the genomic alteration reported is given relative to *SOX9* start codon. The number of highly conserved noncoding elements (HCNEs) involved in *SOX9* genomic alterations in PRS are indicated, including the elements showing a higher conservation (>200 bp in length, with a 90% identity between *Homo sapiens* and *Mus musculus*). Bold, regions included in deletions or mutated; italics, regions located in between 17q translocation breakpoints and the 3′ end of the copy number–polymorphic BAC RP11-300G13 (Chr17:65,725,854).

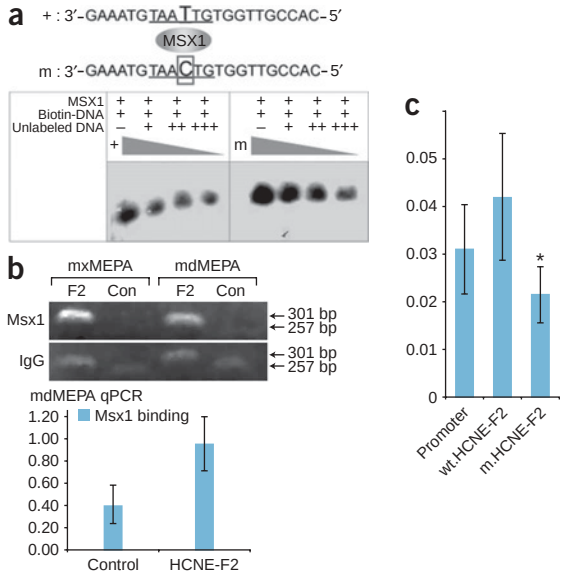

Figure 3 HCNE-F2 has enhancer activity. (**a**) Nucleotide sequences of normal and mutant transcription-factor binding probes derived from HCNE-F2 and used in EMSA, with the MSX1 binding site underlined. The mutant base is enlarged and boxed in red. MSX1 was incubated with biotin-labeled probes (normal (+) and mutated (m), respectively) with or without an unlabeled probe for the competition reactions (normal unlabeled probe for + and mutated unlabeled probe for m). (**b**) Above, ChIP results showing that endogenous Msx1 binds HCNE-F2 (301-bp amplicon; F2) but not a 257-bp control amplicon (Chr11:111450487–111450743; Con), in mandibular (md) and maxillary (mx) mouse embryonic pharyngeal arch (MEPA) cells. Anti-rabbit IgG antibody was used as a negative control. Below, quantitative real-time PCR analysis of the same ChIP experiment revealed a ~2.5-fold greater binding of Msx1 to HCNE-F2 compared to the control region. Errors bars represent the calculated fold change error (see **Supplementary Methods).** (**c**) Enhancer function of HCNE-F2 in mdMEPA cells. The cells were transfected with reporter constructs containing only the *Sox9* minimal promoter (Promoter) or with either the wild-type HCNE-F2 (wt.HCNE-F2) or the HCNE-F2 harboring the F2 mutation (m.HCNE-F2) inserted 5′ to the promoter. The wild-type HCNE-F2 showed enhancer function, which was abolished when the element harbored the mutation found in the PRS-affected F2 family ($P = 0.001$).

Dominant negative mutations in these collagen genes cause Stickler syndrome, the most common syndromic diagnosis associated with PRS[20]. It is possible that a tissue-specific loss of *SOX9* enhancer activity could lead to a coordinated reduction in the transcription of all three targets during development, cumulatively phenocopying mutations in the individual genes. Furthermore, conditional inactivation of mouse *Sox9* in CNC cells results in a phenotype of reduced jaw and cleft palate strongly reminiscent of PRS[21].

Still, the expression of other genes in the vicinity may well be affected by deletions or mutations at the *PRS1* locus. The most obvious alternative candidate is *KCNJ2*, dominant negative mutations in which cause Andersen cardiodysrhythmic periodic paralysis syndrome[22] (OMIM 170390). This condition is occasionally associated with micrognathia and cleft palate, although not in the context of PRS. The absence of any detectable alteration in chromatin compaction within the *Kcnj2*–BP-F2 interval in the developing mouse mandible would argue against *KCNJ2* being a target of the enhancers reported here. Conversely, we demonstrated chromatin decompaction in areas normally expressing *Sox9*, and campomelic and acampomelic dysplasias are due to *SOX9* haploinsufficiency that frequently culminates in PRS features[23]. Collectively, these data support *SOX9* as a more likely enhancer target than *KCNJ2*.

The finding of very distant mutations on both sides of a gene promoter suggests that *cis*-regulatory domains of developmental genes may extend over megabases of DNA flanking its coding sequences. Long-range regulatory mutations have been identified in several diseases in humans and animals[24]. These can be broadly classed into two groups: those that phenocopy intragenic null mutations and those that result in a phenotype distinct from that associated with loss or gain of function. In the first category, the best-studied disease/gene combinations are aniridia/*PAX6* (ref. 24) and campomelic dysplasia/*SOX9* (refs. 9,16). These mutations cause failure of normal transcriptional activation of the affected allele. The most clearly defined example of the second category is preaxial mirror polydactyly/*SHH*[25], in which the disease is due to ectopic transcriptional activation. We propose that PRS/*SOX9* mutations represent a site- and stage-specific loss of transcription most closely analogous to a mouse conditional knockout—in this case, of *SOX9* in human CNC cells[21,26,27].

In conclusion, disruption of noncoding DNA sequences with site- and stage-specific enhancer function surrounding master developmental genes[14,28] may be regarded as a general mutational mechanism for some human congenital malformations. It is likely that

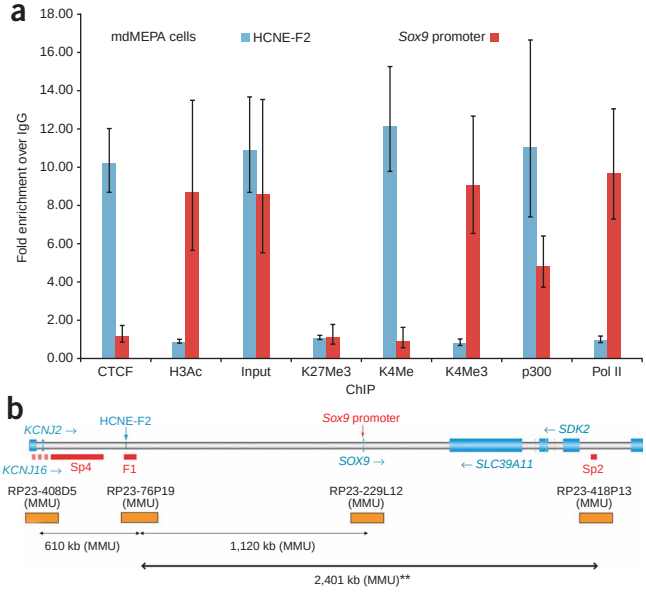

Figure 4 Chromatin characteristics of the region around *SOX9*. (**a**) ChIP using mdMEPA cell line combined with quantitative real-time PCR analysis shows that HCNE-F2 strongly binds K4 methylated histone H3 (K4Me), CTCF and p300, suggesting that this region has a role in transcriptional activation and chromatin remodeling consistent with its functioning as a mandibular mesenchymal enhancer. The *Sox9* promoter region shows a different pattern consistent with a regulated promoter region, with strong binding RNA polymerase II (Pol II), acetylated histone H3 (H3Ac) and trimethylated K4 histone H3 (K4Me3) and weaker binding to p300. K27Me3, trimethyllysine 27 form of histone H3. Error bars are equivalent to 95% confidence intervals (see **Supplementary Methods**). (**b**) Genomic organization of the *SOX9* locus. Family F1 and individuals Sp2 and Sp4 (all carrying deletions) are indicated as red boxes. Blue arrow, HCNE-F2; red arrow, *SOX9* promoter region. Orange boxes below represent orthologous positions of mouse BAC probes around *Sox9* relative to the human *SOX9* locus. MMU, *M. musculus*. Distances between BAC probes in the mouse genome are indicated in kbp.

Table 2 Localized tissue-specific chromatin decompaction at the *Sox9* locus

BAC			408D5-76P19			76P19-229L12			76P19-418P13		
Region			*Kcnj2*–BP-F2			BP-F2–*Sox9*			BP-F2–delSP2		
Genomic distance (kb)			610			1,120			2,401		
Stage	Tissue	*Sox9* expression	Nuclei	Mean 3D separation (nm)	95% CI, ±	Nuclei	Mean 3D separation (nm)	95% CI, ±	Nuclei	Mean 3D separation (nm)	95% CI, ±
9.5 d.p.c.	Pharyngeal arch	++	107	419	31	130	344	22	–	–	–
13.5 d.p.c.	Meckel's cartilage	++	106	418	29	93	332	23	123	705**	59
13.5 d.p.c.	Palatal shelf/maxillary mesenchyme	+	51	425	43	70	322	31	118	590	42
13.5 d.p.c.	Periocular mesenchyme	–	91	417	30	99	289	24	133	585	49

Measurements of the 3D distance between interphase FISH signals in sections of embryonic mouse tissues. The mouse BAC probes positions spanning the orthologous regions around mouse *Sox9* relative to human *SOX9* locus are shown in **Figure 1b**. Optical sectioning of individual nuclei in sections of craniofacial tissue was used to determine the distance between probe signals from interphase 3D FISH. '**' indicates a significant transcription-dependent chromatin decondensation; the lower 95% CI for the BP-F2–delSP2 distance in the high-expressing region does not overlap with the upper 95% CI of either the medium- or low-expressing regions.

high-resolution genome-wide analyses will identify mutations with *cis*-regulatory effects for increasing numbers of diseases. Our study suggests that these may have a much wider range of action than that traditionally understood.

METHODS

Sample selection. Only individuals with isolated PRS were selected for study (see **Supplementary Note** online for details of inclusion and exclusion criteria). Controls were healthy, unrelated middle-aged individuals of European ancestry with no known craniofacial defects. Informed consent was obtained from all study participants. Studies were approved by the ethical institutional committees of the Comité Consultatif de Protection des Personnes dans la Recherche Biomédicale, the Hôpital Necker–Enfants Malades and the Royal Children's Hospital and by the UK national Multicentre Research Ethics Committee.

Genetic linkage. Genome-wide microsatellite genotyping was performed in the PRS-affected family F1 by deCODE Genetics at an average marker density of 4 cM (1,000 markers). We computed two-point LOD score values using the linkage package (MLINK program). PRS was assumed to behave as an autosomal dominant trait with incomplete penetrance (90%) and no gender bias.

Nucleotide variation screening. PCR products were directly sequenced on both strands on an ABI PRISM 3130XL DNA sequencer (Perkin Elmer–Applied Biosystems) using the Big Dye Terminator method according to the manufacturer's instructions. All primer sequences are listed in **Supplementary Table 1** online.

Metaphase FISH and breakpoint cloning. Metaphase chromosome analysis using two-color FISH was performed as previously described[13] (**Supplementary Methods** online). For Southern blots, PCR-amplified probes were sequenced and verified probes radiolabeled with [α^{32}P]dCTP using Rediprime II Random Prime Labeling System (Amersham Biosciences) (**Supplementary Methods** and **Supplementary Table 1**).

Production and analysis of reporter transgenic mice. To make the 9CE4Z reporter construct, a 2.8-kb fragment was PCR amplified from human BAC RP11-1003J3 using primers containing *Not*I and *Eag*I restriction sites (**Supplementary Table 1**). This fragment was subcloned into the *Not*I site of the p610+ reporter construct containing an Hsp68 minimal promoter–*LacZ* cassette. To generate the HCNE-F2(3xwt)bZ reporter construct, the wild-type HCNE-F2 element was PCR amplified with three sets of *attB* site–containing primers (**Supplementary Table 1**) and cloned into the three-way Gateway (Invitrogen) entry vector, which was then recombined with a vector bearing a *LacZ* reporter cassette containing the human β-globin minimal promoter. To create transgenic animals, linearized 9CE4Z and HCNE-F2(3xwt)bZ constructs were microinjected using standard procedures (**Supplementary Methods**). Embryos were collected at relevant stages, fixed and analyzed for reporter activity by Xgal staining (**Supplementary Methods**).

Optical projection tomography. Optical projection tomography (OPT) was performed as previously described[29] (**Supplementary Methods**).

Fine-tiling CGH-array analysis. For the fine-tiling CGH (NimbleGen), a tiling array was designed containing 385,000 probes of 50–75-mer length with a median probe spacing of 5 bp covering the region Chr17:65,689,756–69,390,437. Identified microrearrangements were tested by semiquantitative PCR (**Supplementary Table 1** and **Supplementary Methods**).

SAGE corroboration. Publicly available COGENE SAGE data[10] were mined to examine expression of *SOX9*, *EN1*, *ZNF628*, *MSX1* and *POU2F1*; the ACTG web tool was used for tag to gene mapping of the two SAGE libraries (**Supplementary Methods**).

Electrophoretic mobility shift assays (EMSA). MSX1 and POU2F1 expression vectors were constructed by insertion of the human *MSX1* or *POU2F1* cDNA (Geneservice) into pcDNA3.0/zeo+ (Invitrogen) and used to synthesize MSX1 and POU2F1 protein following the TNT Coupled Reticulocyte Lysate Systems protocol (Promega). EMSA was performed following the LightShift Chemiluminescent EMSA Kit (Pierce) protocol. The results were quantified using ImageJ software. The applied statistical test was the nonparametric Wilcoxon test ($n = 15$, $\alpha = 0.05$) (**Supplementary Methods**).

Cell culture. Mandibular and maxillary processes were excised from 11.5 d.p.c. embryos from CD1 females crossed with a male 'Immortomouse'. The mandibular and maxillary tissue was dissociated and plated in medium (1× DMEM/10% FCS/1% penicillin/streptomycin) containing 100 U ml^{-1} murine γ-interferon (Peprotech). Cells were cultured at 33 °C in an atmosphere containing 5% CO_2 (**Supplementary Methods**). The cell lines were designated MEPA (mouse embryonic pharyngeal arch) with the prefix of mx (maxillary) and md (mandibular). Adherent HEK293 and SKNBE(2c) cells were cultured in 1× DMEM/10% FCS (FCS)/1% penicillin/streptomycin at 37 °C in an atmosphere containing 5% CO_2.

Chromatin immunoprecipitation (ChIP). The ChIP protocol was carried out as previously described[30]. For the immunoprecipitation of chromatin-bound proteins, the following antibodies were used: PolII, H3K4me3, H3K4me and p300 from Abcam; CTCF and H3ac from Upstate. The MSX1 ChIP antibody was from Santa Cruz Biotechnology (**Supplementary Methods**).

***In vitro* enhancer activity assays.** To generate the pr.*Sox9* reporter construct, the *Sox9* minimal promoter[15] was amplified with PCR primers containing *Bgl*II and *Hin*dIII restriction sites. This fragment was subcloned into the *Bgl*II/*Hin*dIII restriction site upstream of *luc*+ of the pGL3-basic vector (Promega). The HCNE-F2 wild-type and mutated elements were amplified using PCR primers containing *Mlu*I and *Xho*I restriction sites, and were subcloned into the *Mlu*I/*Xho*I restriction site of the pr.*Sox9* reporter construct. This generated the wtHCNE-F2-pr.*Sox9* and m.HCNE-F2-pr.*Sox9* reporter constructs, respectively.

Transfection experiments were performed on adherent HEK293 and SKNBE(2c) cells cultured in the conditions described above, and in mdMEPA cells cultures at 33 °C in an atmosphere containing 7% CO_2. For the transfection experiment, cells were grown to 80% confluency in 12-well plates. Cells were transfected with 600 ng of plasmid DNA, 30 ng of pRL-CMV (Promega) and 3 μl of FuGeneHD (Roche) according to the FuGeneHD

transfection protocol. Cells were harvested and lysed 24–48 h after transfection. Firefly and *Renilla* luciferase activities were measured (Dual-Luciferase Reporter Assay System, Promega). The firefly luciferase activity of each construct was normalized to the *Renilla* luciferase internal control, pRL-CMV. The applied statistical test was the nonparametric Mann-Whitney test ($n = 18$, $\alpha = 0.05$). 95% confidence intervals (CI 95%) given as the error bars in **Figure 3c** were calculated using the following formula: CI 95% = mean ± $t_{0,25}$ × s.e.m., where t = Student t-test value.

Sox9 immunohistochemistry and interphase FISH. Rabbit polyclonal anti-Sox9 (Chemicon) was used as primary antibody and Alexa Fluor 488–conjugated goat anti-rabbit $F(Ab)_2$ fragments (Invitrogen) as secondary antibody. The slides were counterstained with 4′,6-diamidino-2-phenylindole (DAPI) upon mounting (**Supplementary Methods**).

Interphase FISH used mouse BAC probes obtained from BACPAC resources of the Children's Hospital Oakland Research Institute. BAC clones were labeled with digoxygenin or with the direct fluorescent label Spectrum Orange-dUTP (Vysis) (**Supplementary Methods**).

Image capture and analysis were performed using in-house scripts written for IPLab Spectrum (Scanalytics). Inter-spot distances were calculated using the custom software IP lab script (available from P. Perry, MRC HGU). 3D distance means, s.d. and confidence intervals were calculated (**Supplementary Methods**).

***In situ* expression pattern study.** *SOX9 in situ* expression was examined in normal human embryos (CS13, CS15 and CS18) obtained from electively terminated pregnancies in concordance with French legislation (94-654 and 08-400) and with oversight by a local ethics committee. Tissue fixation, sectioning and *in situ* hybridization were carried out according to standard protocols (**Supplementary Methods** and **Supplementary Table 1**).

Accession codes. RefSeq: *SOX9*, NM_000346; *Sox9*, NM_011448; KCNJ2, NM_000891; *KCNJ16*, NM_170741, NM_018658, NM_170742; *MAP2K6*, NM_002758; human chromosome 2, NC_000002.10; human chromosome 5, NC_000005.8, human chromosome 17, NC_000017.9; rhesus chromosome 16, NC_007873; mouse chromosome 11, NC_000077; dog chromosome 9, NC_006591. GenBank: RP11-1003J3, AC005181.1; CTD-2053I13, AC098485.6; RP11-420O5, AC007642.5; RP11-496M2, AC009126.2; RP11-510H11, AC092662.2; *MSX1* cDNA clone, BC021285; *POU2F1* cDNA clone, BC052274. OMIM: *SOX9*, *608160; campomelic dysplasia, #114290; Pierre Robin sequence, 261800; *KCNJ2*, *600681; Andersen syndrome, #170390; *MSX1*, *142983.

URLs. rVista 2.0, http://rvista.dcode.org/; ECR browser, http://ecrbrowser.dcode.org/; eShadow, http://eshadow.dcode.org/; SNP, http://www.ncbi.nlm.nih.gov/projects/SNP/; Database of Genomic Variants, http://projects.tcag.ca/variation/; DECIPHER, http://decipher.sanger.ac.uk/; Human Genome Structural Variation Project, http://humanparalogy.gs.washington.edu/structuralvariation/; COGENE, http://hg.wustl.edu/COGENE/SAGE/index.html; ACTG, http://retina.med.harvard.edu/ACTG.

Note: Supplementary information is available on the Nature Genetics website.

ACKNOWLEDGMENTS

We are grateful to the affected individuals and their families who participated in this study, to the Associations Françaises du Syndrome de Robin, to the Centres de Références Anomalies Cranio-Faciales Rares (AP-HP, Necker and Trousseau hospitals), and to C. Ozilou, G. Staub and G. Guédu-Molina for assistance. We thank T. Attié-Bitach, G. Couly and L. Legeai-Mallet (Necker) and V. van Heyningen and R. Hill (MRC HGU) for useful discussion. This study was underwritten by grants from the Agence Nationale de la Recherche (ERARE grant CraniRare), EUROCRAN FP5, the Fondation pour la Recherche Médicale (FRM), the MRC (UK) and the National Health and Medical Research Council (Australia). S.T. was supported in part by grant NS039818 from the US National Institutes of Health and S.B. by the FRM.

AUTHOR CONTRIBUTIONS

S.B., J.A.F. and A.P. performed molecular genetics studies. J.A.F., C.T.G. and N.J. performed chromosomal studies. S.B. and J.R. performed the *in vitro* enhancer activity experiments. S.B., S.T., C.G., M.V. and H.C.E. performed human expression studies. J.R., S.B. and A.E. performed immunoprecipitation experiments. D.-J.K. performed transgenic assays. J.A.F., S.H., P.P. and D.B. performed the *in vivo* chromatin compaction studies. M.F. did the OPT image analysis. S.B. and H.R.C. performed the comparative genomic analysis. J.A., V.A., C.A., M.H.-E., N.K., M.M.L., A.P., I.K.T., M.V., P.T., M.-P.V., D.R.F. and S.L. recruited individuals and families affected with PRS. S.L., D.R.F., P.G.F. and J.A. contributed to the concept, strategy, study design and project management. S.B., H.C.E., S.T., P.G.F., D.R.F. and S.L. contributed to the writing of the manuscript. All authors discussed the results.

Published online at http://www.nature.com/naturegenetics/
Reprints and permissions information is available online at http://npg.nature.com/reprintsandpermissions/

1. Robin, P. A fall of the base of the tongue considered as a new cause of nasopharyngeal respiratory impairment: Pierre Robin sequence, a translation. 1923. *Plast. Reconstr. Surg.* **93**, 1301–1303 (1994).
2. Etchevers, H.C., Amiel, J. & Lyonnet, S. Molecular bases of human neurocristopathies. *Adv. Exp. Med. Biol.* **589**, 213–234 (2006).
3. Vintiner, G.M., Temple, I.K., Middleton-Price, H.R., Baraitser, M. & Malcolm, S. Genetic and clinical heterogeneity of Stickler syndrome. *Am. J. Med. Genet.* **41**, 44–48 (1991).
4. Jamshidi, N. *et al.* Isolated Robin sequence associated with a balanced t(2;17) chromosomal translocation. *J. Med. Genet.* **41**, e1 (2004).
5. Jakobsen, L.P. *et al.* Pierre Robin sequence may be caused by dysregulation of *SOX9* and *KCNJ2*. *J. Med. Genet.* **44**, 381–386 (2007).
6. Ahituv, N., Prabhakar, S., Poulin, F., Rubin, E.M. & Couronne, O. Mapping cis-regulatory domains in the human genome using multi-species conservation of synteny. *Hum. Mol. Genet.* **14**, 3057–3063 (2005).
7. Dermitzakis, E.T., Reymond, A. & Antonarakis, S.E. Conserved non-genic sequences—an unexpected feature of mammalian genomes. *Nat. Rev. Genet.* **6**, 151–157 (2005).
8. Woolfe, A. *et al.* Highly conserved non-coding sequences are associated with vertebrate development. *PLoS Biol.* **3**, e7 (2005).
9. Velagaleti, G.V. *et al.* Position effects due to chromosome breakpoints that map approximately 900 Kb upstream and approximately 1.3 Mb downstream of *SOX9* in two patients with campomelic dysplasia. *Am. J. Hum. Genet.* **76**, 652–662 (2005).
10. Cai, J. *et al.* Gene expression in pharyngeal arch 1 during human embryonic development. *Hum. Mol. Genet.* **14**, 903–912 (2005).
11. Satokata, I. & Maas, R. *Msx1* deficient mice exhibit cleft palate and abnormalities of craniofacial and tooth development. *Nat. Genet.* **6**, 348–356 (1994).
12. Cirulli, E.T. & Goldstein, D.B. In vitro assays fail to predict in vivo effects of regulatory polymorphisms. *Hum. Mol. Genet.* **16**, 1931–1939 (2007).
13. Morey, C., Da Silva, N.R., Perry, P. & Bickmore, W.A. Nuclear reorganisation and chromatin decondensation are conserved, but distinct, mechanisms linked to *Hox* gene activation. *Development* **134**, 909–919 (2007).
14. Bagheri-Fam, S., Ferraz, C., Demaille, J., Scherer, G. & Pfeifer, D. Comparative genomics of the *SOX9* region in human and *Fugu rubripes*: conservation of short regulatory sequence elements within large intergenic regions. *Genomics* **78**, 73–82 (2001).
15. Bagheri-Fam, S. *et al.* Long-range upstream and downstream enhancers control distinct subsets of the complex spatiotemporal *Sox9* expression pattern. *Dev. Biol.* **291**, 382–397 (2006).
16. Bien-Willner, G.A., Stankiewicz, P. & Lupski, J.R. SOX9cre1, a cis-acting regulatory element located 1.1 Mb upstream of *SOX9*, mediates its enhancement through the SHH pathway. *Hum. Mol. Genet.* **16**, 1143–1156 (2007).
17. Suzuki, T., Sakai, D., Osumi, N., Wada, H. & Wakamatsu, Y. Sox genes regulate type 2 collagen expression in avian neural crest cells. *Dev. Growth Differ.* **48**, 477–486 (2006).
18. Akiyama, H. *et al.* Interactions between Sox9 and beta-catenin control chondrocyte differentiation. *Genes Dev.* **18**, 1072–1087 (2004).
19. Bi, W., Deng, J.M., Zhang, Z., Behringer, R.R. & de Crombrugghe, B. Sox9 is required for cartilage formation. *Nat. Genet.* **22**, 85–89 (1999).
20. Holder-Espinasse, M. *et al.* Pierre Robin sequence: a series of 117 consecutive cases. *J. Pediatr.* **139**, 588–590 (2001).
21. Mori-Akiyama, Y., Akiyama, H., Rowitch, D.H. & de Crombrugghe, B. Sox9 is required for determination of the chondrogenic cell lineage in the cranial neural crest. *Proc. Natl. Acad. Sci. USA* **100**, 9360–9365 (2003).
22. Andelfinger, G. *et al. KCNJ2* mutation results in Andersen syndrome with sex-specific cardiac and skeletal muscle phenotypes. *Am. J. Hum. Genet.* **71**, 663–668 (2002).
23. Wagner, T. *et al.* Autosomal sex reversal and campomelic dysplasia are caused by mutations in and around the SRY-related gene *SOX9*. *Cell* **79**, 1111–1120 (1994).
24. Kleinjan, D.A. & van Heyningen, V. Long-range control of gene expression: emerging mechanisms and disruption in disease. *Am. J. Hum. Genet.* **76**, 8–32 (2005).
25. Lettice, L.A. *et al.* A long-range Shh enhancer regulates expression in the developing limb and fin and is associated with preaxial polydactyly. *Hum. Mol. Genet.* **12**, 1725–1735 (2003).
26. Hong, C.S. & Saint-Jeannet, J.P. Sox proteins and neural crest development. *Semin. Cell Dev. Biol.* **16**, 694–703 (2005).
27. McCauley, D.W. & Bronner-Fraser, M. Importance of SoxE in neural crest development and the evolution of the pharynx. *Nature* **441**, 750–752 (2006).
28. Pheasant, M. & Mattick, J.S. Raising the estimate of functional human sequences. *Genome Res.* **17**, 1245–1253 (2007).
29. Sharpe, J. *et al.* Optical projection tomography as a tool for 3D microscopy and gene expression studies. *Science* **296**, 541–545 (2002).
30. Essafi, A. *et al.* Direct transcriptional regulation of Bim by FoxO3a mediates STI571-induced apoptosis in Bcr-Abl-expressing cells. *Oncogene* **24**, 2317–2329 (2005).

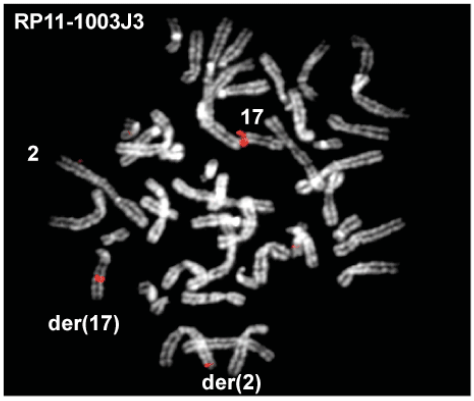

1a

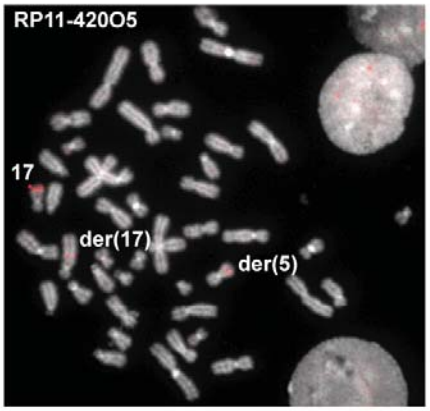

1b

Supplementary Figure 1. Family T1 and T2 translocation mapping. a. Karyotype of family T1 with an image of the metaphase FISH of the 17q breakpoint spanning BAC clone RP11-1003J3. **b** Family T2 karyotype with the FISH image of the breakpoint-spanning clone RP11-420O5.

Nature Genetics: doi:10.1038/ng.329

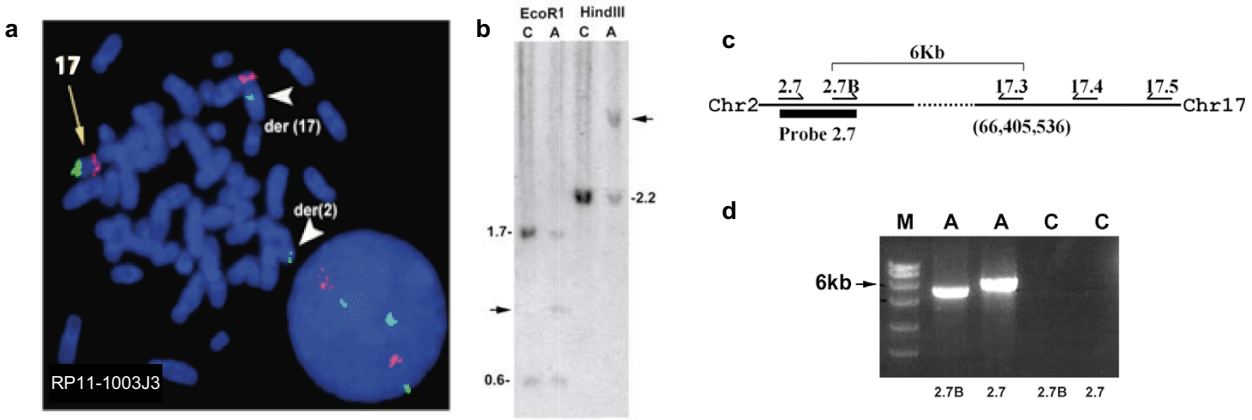

Supplementary Figure 2 Family T3 Translocation mapping, breakpoint cloning and sequencing. a. Family T3 karyotype with a FISH image of the breakpoint clone on 17q 1003J3. **b.** Image of a genomic Southern blot of control (C) and affected (A) lymphoblast DNA digested with EcoRI and HindIII and probed with a 622bp chromosome 2-specific probe (probe 2.7) corresponding to nucleotides 155,859,897- 155,860,518 (NCBI Build 36.1) used for identification of the translocation breakpoints. Sizes of predicted bands are indicated and novel, translocation specific bands are denoted by arrows. **c.** Diagram illustrating PCR strategy used to determine location of the breakpoint on chromosome 17. Forward primers 2.7 and 2.7B, designed against sequences in probe 2.7, were each paired with a series of reverse primers specific to sequences on Chromosome 17. **d.** Genomic PCR using primer 17.3 in conjunction with primers 2.7 or 2.7B yielded products from affected (A) but not control (C). DNA. **e.** Sequences at the 2,17 and 17,2 breakpoints. Numbers refer to the base position of the last nucleotide before the translocation (NCBI Build 36.1). The translocation was balanced except for the loss of 8 nucleotides from Chromosome 17 (indicated by dashed line).

Nature Genetics: doi:10.1038/ng.329

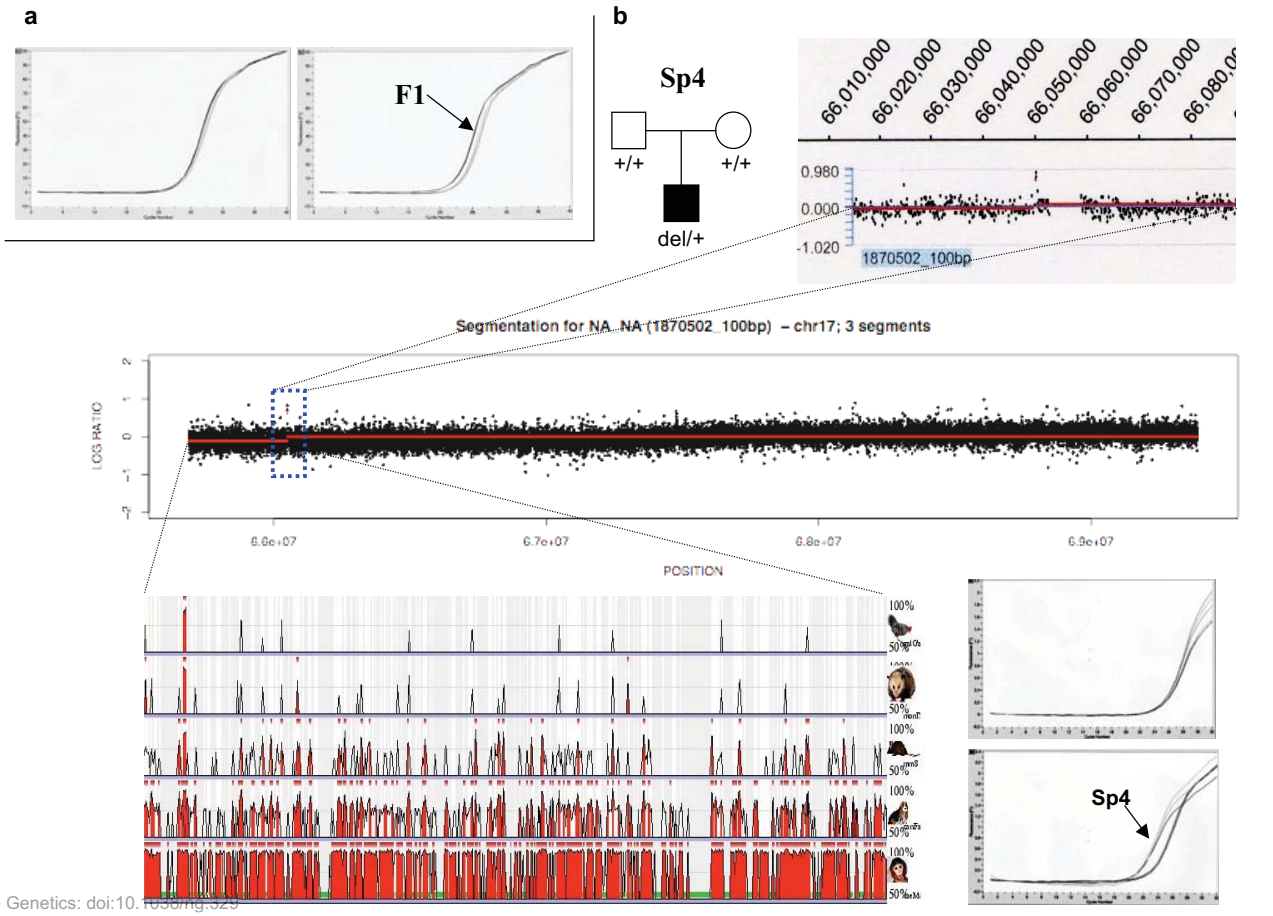

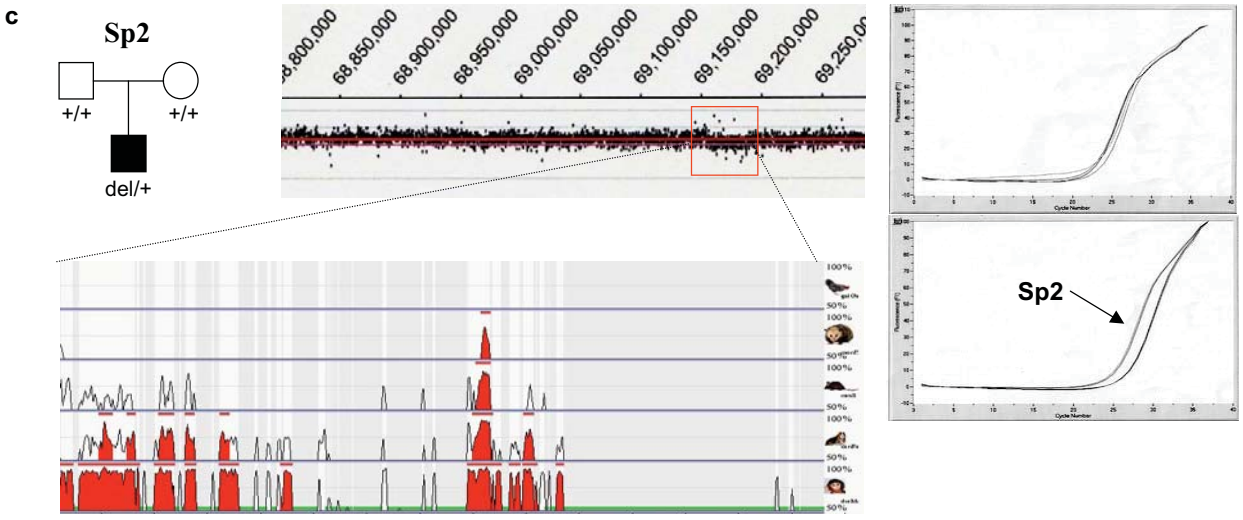

Supplementary Figure 3. Deletion of highly conserved non-coding elements in PRS family F1 and PRS sporadic cases Sp4 and Sp2. a. Quantitative PCR profile of a patient from the PRS family F1 compared to an unaffected control, using the reference gene *MAP2K6* and the genomic region deleted in family F1. **b.** The CGH profile of the *PRS1* locus with an enlarged view of the region containing the 3' end of the *de novo* occurring genomic deletion observed in the sporadic patient Sp4 (indicated del/+; the centromeric position of this deletion is not yet known since it is located outside the region covered by the CGH array used in this study). Multiple species conservation plot of the deleted region according to ECR browser (conservation of fragments >350 bp at 75% identity) and the quantitative PCR profile of PRS patient Sp4 compared to an unaffected control, using the reference gene *MAP2K6* and the genomic region deleted, are shown. **c.** CGH profile view of the 36kb deletion that occurs *de novo* in the sporadic PRS patient Sp2 (indicated del/+). Multiple species conservation plot of the Sp2 deleted region according to ECR browser (conservation of fragments >350 pb at 75% identity) and the quantitative PCR profile of the PRS patient Sp2 compared to an unaffected control, using the reference gene *MAP2K6* and the genomic region deleted in family Sp2, are shown.

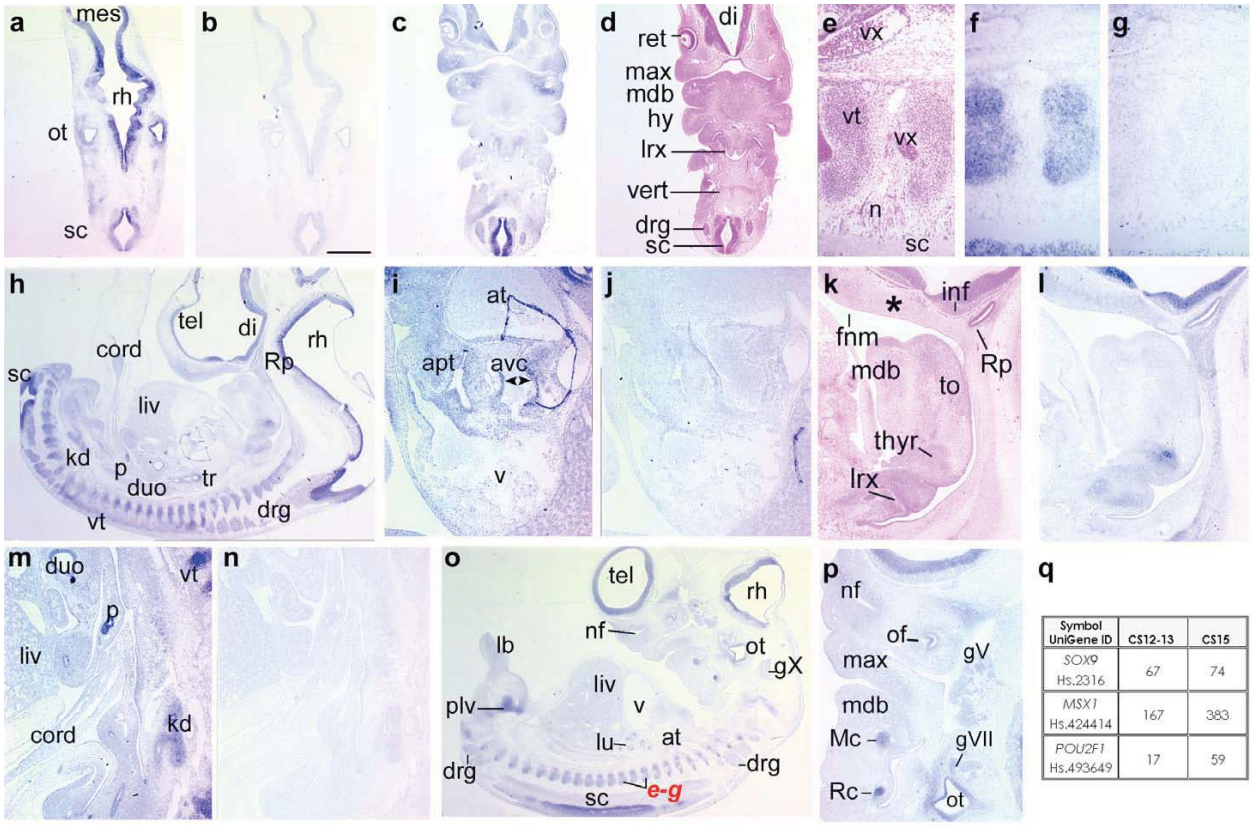

Symbol UniGene ID	CS12-13	CS15
SOX9 Hs.2316	67	74
MSX1 Hs.424414	167	383
POU2F1 Hs.493649	17	59

Nature Genetics: doi:10.1038/ng.329

Supplementary Figure 4. Expression of SOX9 during human embryonic development. At Carnegie stage (CS) 13 (not shown; 28 days), SOX9 expression is observed throughout the central nervous system (CNS), diffuse within early craniofacial mesenchyme. a. Strong expression is observed in coronal section at CS15 (34 days) within the ventricular zone of the central nervous system (CNS), as well as in cranial ganglia and the otic vesicles. b. No signal was observed on an adjacent section hybridized with sense probe. c: A more caudal section shows distinct SOX9 transcription in the maxillary and mandibular primordia, as well as around the larynx. d: Adjacent section with hematoxylin-eosin stain. e-g: Magnification of two vertebrae from panel o in hematoxylin-eosin stain (e), showing SOX9 transcripts in cartilage condensations and developing spinal cord gray matter (f) as compared with a negative control probe (g). h. A sagittal section at C18 (44 days) demonstrates continued SOX9 expression in the CNS with highly intense signal in the ventricular zone, in Rathke's pouch and the infundibulum; in the cranial and dorsal root ganglia and otic vesicles; in the epithelial endoderm of the trachea, duodenum and pancreas; in both tubules and mesenchyme of the early kidney, in developing palate (asterisk) and in the prospective thyroid and cricoid cartilages of the larynx (enlarged in k – hematoxylin - and l – antisense probe). i. The myocardium expresses SOX9 faintly with localized stronger signal in the atrioventricular canal (arrowheads). The J-shaped object is a paper fiber. No signal was observed in the sense probe-hybridized adjacent section (j, n). m. Enlargement of internal organs. o. A parasagittal section from the same embryo in which SOX9 is expressed weakly in craniofacial mesenchyme as compared to the vertebral, pelvic and the Meckel's and Reichert's cartilages (enlarged in p), and in pulmonary bronchi. Vertebrae in panels e-g indicated in red. q. Serial Analysis of Gene Expression (SAGE) tag counts from publicly available COGENE SAGE data for SOX9 and potential partner transcription factors. Number of tags (representing transcripts) normalized to one million transcripts from the human first pharyngeal arch at four (CS12-13) and five (CS15) weeks' development. Scale bar: 100 mm for a-d; 50 mm for k, l, p. Abbreviations: at, atrium; apt, aorticopulmonary trunk; avc, atrioventricular canal; cord, umbilicus; di, diencephalon; drg, dorsal root ganglia; duo, duodenum; gX, vagal ganglion; gV, trigeminal ganglion; gVII, facial ganglion kd, kidney; lb, (hind)limb; liv, liver; lrx, larynx; lu, lung; mes, mesencephalon; n, intersegmental nerve; nf, nasal fossa; ot, otic vesicle; p, pancreas; plv, pelvis; ret, retina; rh, rhombencephalon; Rp, Rathke's pouch; sc, spinal cord; tel, telencephalon; tr, trachea; v, ventricle; vt, vertebra; vx, blood vessel.

Nature Genetics: doi:10.1038/ng.329

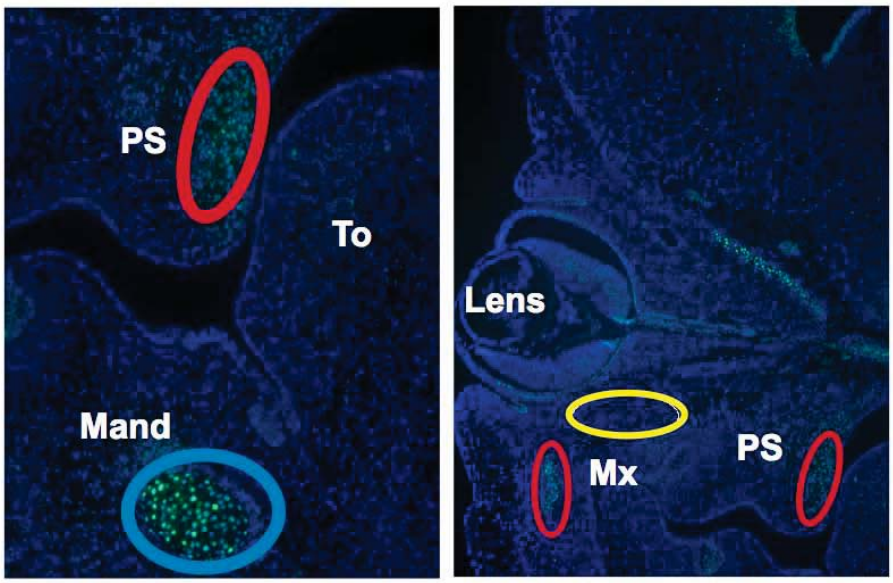

Supplementary Figure 5. Mouse embryo craniofacial regions at 13.5 dpc used for the analysis in the interphase FISH experiments. The embryos are shown as fluorescent DAPI-stained images stained with Sox9 antibody, shown as green signal. The mandibular region circled in blue with high Sox9 expression is Meckel's cartilage. The regions circled in red are the medium expression level areas of the palatal shelf and lateral maxillary mesenchyme. The infraorbital region circled in yellow had no obvious Sox9 protein expression. PS, palatal shelf; To, tongue; Mand, mandible; Mx, maxilla.

Nature Genetics: doi:10.1038/ng.329

Supplementary Note

Clinical data

Clinical criteria for PRS were at least 3 among the following features: i) micrognathia and/or retrognathia, ii) glossoptosis, iii) posterior U-shaped cleft palate, and iv) functional signs related to involvement of IX, X and XII cranial nerves (suction, swallowing, feeding, breathing and cardiac rhythm anomalies). In addition, patients were selected for isolated PRS (Supplementary clinical table), excluding, in particular, cleft lip, cardiac defects, bone dysplasia, eye findings, brain or hindbrain malformations, and mental retardation. In sporadic cases, posterior cleft palate was an obligatory criterion; only familial cases with at least 2 individuals with posterior cleft palate were included. For linkage studies, PRS was assumed to behave as an autosomal dominant trait with incomplete penetrance (90%), and no gender-bias. Family T2 was originally reported as a Stickler-like syndrome but clinical reassessment concluded that this family has autosomal dominant isolated PRS (Vintiner et al., *Am.J.Med.Genet* 1991). The control population used in our study is a middle-aged population of European ancestry, unaffected with any craniofacial defects and composed of healthy unrelated individuals.

RESEARCH ARTICLE

Human Mutation

OFFICIAL JOURNAL HGVS HUMAN GENOME VARIATION SOCIETY www.hgvs.org

Mutational, Functional, and Expression Studies of the *TCF4* Gene in Pitt-Hopkins Syndrome

Loïc de Pontual,[1] Yves Mathieu,[1] Christelle Golzio,[1] Marlène Rio,[2] Valérie Malan,[1] Nathalie Boddaert,[3] Christine Soufflet,[4] Capucine Picard,[5,6] Anne Durandy,[5] Angus Dobbie,[7] Delphine Heron,[8] Bertrand Isidor,[9] Jacques Motte,[10] Ruth Newburry-Ecob,[11] Laurent Pasquier,[12] Marc Tardieu,[13] Géraldine Viot,[14] Francis Jaubert,[15] Arnold Munnich,[1,2] Laurence Colleaux,[1] Michel Vekemans,[1,2] Heather Etchevers,[1] Stanislas Lyonnet,[1,2] and Jeanne Amiel[1,2]*

[1]*Unité INSERM U-781, Université Paris Descartes, Faculté de Médecine, INSERM*

[2]*Service de Génétique et de Cytogénétique, Hôpital Necker-Enfants Malades, AP-HP, Paris, France*

[3]*Radiologie Pédiatrique, INSERM U-797, Hôpital Necker-Enfants Malades, Paris, France*

[4]*Service de Neurophysiologie, INSERM U-663, Hôpital Necker-Enfants Malades, Paris, France*

[5]*Unité INSERM U-768, Hôpital Necker-Enfants Malades, Paris, France*

[6]*Study Center of Immunodeficiencies, Université Paris-Descartes, Faculté de Médecine; AP-HP, Hôpital Necker-Enfants Malades, Paris, France*

[7]*Genetics Service, St. James's University Hospital, Leeds, United Kingdom*

[8]*Département de Génétique, Hôpital de la Pitié-Salpétrière, Paris, France*

[9]*Service de Génétique, Hôpital de l'Hôtel Dieu, Nantes, France*

[10]*Service de Neurologie Pédiatrique, American Memorial Hospital, CHU de Reims, France*

[11]*Department of Clinical Genetics, Level B, St. Michael's Hill, Southwell Street, Bristol BS2 8EG, United Kingdom*

[12]*Service de Génétique Clinique, Hôpital Sud, Rennes, France*

[13]*Service de Neurologie Pédiatrique, Hôpital Bicètre, Le Kremlin Bicètre, France*

[14]*Service de Génétique, Hôpital Cochin, Paris, France*

[15]*Service d'anatomie pathologique, Hôpital Necker-Enfants Malades, Paris, France*

Communicated by Ian McIntosh

Received 15 July 2008; accepted revised manuscript 7 October 2008.
Published online 20 February 2009 in Wiley InterScience (www.interscience.wiley.com). DOI 10.1002/humu.20935

ABSTRACT: Pitt-Hopkins syndrome is a severe congenital encephalopathy recently ascribed to de novo heterozygous *TCF4* gene mutations. We report a series of 13 novel PHS cases with a *TCF4* mutation and show that EEG, brain magnetic resonance imagain (MRI), and immunological investigations provide valuable additional clues to the diagnosis. We confirm a mutational hot spot in the basic domain of the E-protein. Functional studies illustrate that heterodimerisation of mutant TCF4 proteins with a tissue-specific transcription factor is less effective than that homodimerisation in a luciferase reporter assay. We also show that the *TCF4* expression pattern in human embryonic development is widespread but not ubiquitous. In summary, we further delineate an underdiagnosed mental retardation syndrome, highlighting TCF4 function during development and facilitating diagnosis within the first year of life.
Hum Mutat 30, 669–676, 2009. © 2009 Wiley-Liss, Inc.

KEY WORDS: Pitt-Hopkins; TCF4; bHLH; E-protein; mental retardation

Introduction

Pitt-Hopkins syndrome (PHS; MIM# 610954) was originally described in 1978 in two unrelated patients with mental retardation, recurrent episodes of hyperventilation, and a wide mouth [Pitt and Hopkins, 1978]. Only a few additional cases were reported during the following quarter century [Orrico et al., 2001; Peippo et al., 2006; Singh, 1993; Van Balkom et al., 1998]. Using a systematic 1-Mb resolution genome-wide BAC-array screening, we and others recently identified de novo microdeletions on chromosome 18q21.1 in PHS cases [Amiel et al., 2007; Brockschmidt et al., 2007; Gustavsson et al., 1999; Zweier, et al., 2007]. Fine mapping of the deleted region led to the identification of heterozygous *TCF4* gene mutation in nondeleted cases. TCF-4 (MIM# 602272), also known as ITF-2 (for immunoglobulin transcription factor), E2-2, or SEF2 (for SL3-3 enhancer factor 2), belongs to the class I basic helix-loop-helix (bHLH) or E-protein family. Ubiquitously expressed class I bHLH factors consist of TCF4, HEB, and the differentially spliced products of the E2A gene: E12 and E47 (Murre, 2005). E-proteins contain a common bHLH structural motif that mediates homo- and heterodimerization between bHLH proteins via their HLH domain, while the adjacent basic region mediates the binding of the dimers to a common DNA sequence (CANNTG), known as an E- BOX [Ross et al., 2003].

Here we report 13 molecularly confirmed novel cases with PHS and further delineate the syndrome. Although severe mental retardation and a facial gestalt are the only consistently observed features, diagnosis can be made in the first year of life. Electroencephalograms (EEG), magnetic resonance imaging

*Correspondence to: Jeanne Amiel, Département de Génétique, Hôpital Necker-Enfants Malades, 149, rue de Sèvres, 75743 Paris Cedex 15, France.
E-mail: Jeanne.amiel@inserm.fr

Grant sponsors: Agence Nationale pour la Recherche (ANR); the Fondation pour la Recherche Médicale (FRM)

(MRI) of the brain, and immunological investigations provide further evidence to support the diagnosis.

We confirm a mutational hot spot within the basic domain of *TCF4*. Although *TCF4* is widely expressed in early human embryo, its spatiotemporal pattern is quite specific. Finally, because certain features of PHS depend on dimeric interactions with tissue-specific bHLH proteins, we studied the transactivation induced by ASCL1/TCF4 wild-type and mutant dimmers in a neuronal cell line, by using a *Delta 1* promoter reporter construct. Overall, we demonstrate that E-proteins are not fully redundant during human development, and that *TCF4* is required for normal development of central and enteric nervous systems.

Materials and Methods

Patients

A total of 36 patients were included in the study. Inclusion criteria were: (1) severe psychomotor delay and (2) facial features compatible with those previously described in PHS patients. Ten patients were selected from photographs of a series of about 80 patients previously suspected of having Rett and/or Angelman syndromes but were negative for *UBE3A* and *MECP2* mutations. One patient was selected from the photographs of 30 patients referred for possible Mowat-Wilson syndrome, negative for *ZFHX1B* mutation. Twenty-five patients were directly referred for possible PHS.

TCF4 screening for mutations

Blood samples were obtained with informed consent and DNA was extracted according to standard protocols. The PCR reaction mixture (25 µl) contained 100 ng of leukocyte DNA, 20 pmol of each primer (sequences of primers available on request), 0.1 µM dNTP, and 1 U *Taq* DNA polymerase (Invitrogen, San Diego, CA). DNA sequencing of the 21 coding exons and intronic flanking regions was performed by the fluorometric method on both strands (ABI BigDye Terminator Sequencing Kit V.2.1, Applied Biosystems, Foster City, CA). At least five isoforms of *TCF4* are known; we chose the longer one (GenBank accession number NM_003199.2) for mutation classification. Nucleotide numbering reflects cDNA numbering with +1 corresponding to the A of the ATG translation initiation codon. The initiation codon is codon 1. In all cases, chromosome analyses showed a normal karyotype. When no mutations were identified, patients were genotyped with two intragenic microsatellite DNA markers *D18S1119* and *D18S1127*, and FISH analyses was performed for homo/hemizygous patients on metaphase nuclei from blood lymphocytes with the probe RP11-397A16.

Construction of Plasmids and Luciferase Assay

Human cDNA of *TCF4* and ASCL1 insert in a pBluescriptR vector were obtained from the MRC Laboratory and inserted into pcDNA 3.1/zeo (−). Known *TCF4* mutations (c.1727G>A p.R576Q, c.1726C>T p.R576W, c.1714G>A p.R572G, c.1521_1522insC p.Ser508LeufsX5, c.1498G>T p.G500X) were generated using the quikChange® XL Site-Directed Mutagenesis Kit (Stratagene, LaJolla, CA) according to the manufacturer's protocol. All constructs were validated by DNA sequencing and subcloned into a pcDNA3.1 vector (Invitrogen) containing a T7 promoter. The luciferase reporter construct (F. Guillemot, National Institute for Medical Research, Mill Hill, Londres) contains the firefly luciferase gene under the control of a *Delta 1* promoter and 6 E-boxes [Castro et al., 2006]. HeLa cells were grown to 95% confluency in Dulbecco's minimum essential medium supplemented with 10% fetal bovine serum in 12-well plates. Cells were transfected with 300 ng of expression vector, 600 ng of the firefly luciferase reporter promoter, 30 ng of pRL-CMV Renilla luciferase internal control (Promega, Madison, WI), and 4 µl of Fugene HD (Roche, Indianapolis, IN) in 100 µl of OPTI-MEM (Invitrogen). Cells were harvested and lysed 24–48 hr after transfection. Firefly and Renilla luciferase activities were assayed according to the manufacturer's protocol. Luciferase activity of each construct was normalized by the internal control pRL-CMV. Experiments were repeated three times in duplicate.

Immunological Investigations

Serum immunoglobulin levels were determined by immunoenzymatic assays using monoclonal antibodies. B and T lymphocytes counts were enumerated using specific antibodies to surface markers on a Fluorescent Analysis Cell Sorter as previously described [Revy et al., 2000].

In Situ Hybridization and Immunohistochemistry on Human Tissues

Human embryos were collected from terminated pregnancies using the mefiprestone protocol in agreement with French bioethics laws (94–654 and 04–800) and the Necker Hospital ethics committee. Intact embryos were fixed in either 4% paraformaldehyde, pH 7.4, or 11% formaldehyde, 60% ethanol, and 10% acetic acid, embedded in paraffin blocks and sectioned at 5 µm. Primers were selected for PCR amplification between exons 7 and 8 (F: ccagactggagatgctgtgg, R: ggagactctgccctgta). A T7 promoter sequence extension (taatacgactcactatagggaga) was added at the 5′ end of each primer; probe synthesis and hybridization were carried out as described previously [Delous et al., 2007]. Immunohistochemistry was carried out on paraffin sections using an anti-CD56 (antineural cell adhesion molecule) or antisynaptotagmin primary antibody and a standard protocol for signal staining by diaminobenzidine precipitation with a hematoxylin counterstain. The gut sample is from a five year old boy who underwent surgery for Meckel diverticulum.

Results

Clinical Presentation of Patients Harbouring a *TCF4* Gene Mutation

All patients had severe mental retardation with speech limited to a few single words or no speech. Motor delay was also constant only some patients could walk unaided after 4 years of age. Facial features consistently included enophthalmia, strabismus, thin eyebrows with flaring in their midline portion, a large nose with high bridge and flared nostril, a protruding philtrum, M-shaped Cupid's bow, fleshy lips and wide mouth with shallow and broad palate, widely spaced teeth, dysplastic and thick ear helices (Table 1 and Fig. 1). With age, traits coarsen and the lower face protrudes more. Acquired microcephaly was observed in nine cases, among which growth retardation was present in three patients only. Stereotypic and restless movements of hands, head, and trunk was found in eight patients that retained purposeful hand skills. Relatives described bouts of shouting and aggressive behavior, being difficult to handle. The "happy, easy-going" temper is not as frequent as initially mentioned. Sleep disorders were only reported in a minority of patients.

Only six patients suffered from epilepsy, usually of late onset (after 5 years of age in this series) and of variable severity.

Table 1. Clinical Features in the Series of 13 Newly Described PHS Patients, the 4 Patients Previously Reported by Us and the 9 Reported by Others.

	This report (N = 13)	Amiel *et al.* (N = 4)	Zweier *et al.* (N = 6)	Gustavsson *et al.*	Brockschmidt *et al.*	Andrieux *et al.*
Age at diagnosis (years)	0.8 to 29	4.5 to 10	8 to 29	5	6	12
Sex	10M/3F	2M/2F	4M/2F	F	F	M
Birth parameters	50th c.	50th c.	25 to 50th c.	50th c.		50th c.
Growth retardation ($\leq$-2 SD)	3/12	0/4	4/6	−		+
Neurologic findings						
Severe mental retardation	13/13	4/4	6/6	+	+	+
Postnatal microcephaly	9/12	4/4	4/6	−	−	+
Epilepsy (age at onset)	6/11 (0.2–18y)	3/4	2/6	+	−	−
Hyperventilation (age at onset)	4/13 (3–7y)	3/4	5/6	+	+	−
Stereotypic movements	8/11	4/4 (4,2)	?	+		−
Strabismus	11/13	4/4	2/4	+		?
Facial gestalt	13/13	4/4	6/6	+	+	+
Abormal genitalia[a]	7/9M	2/2M	?			−
Intestinal manifestations	9/12	4/4	3/6	+	−	−
Scoliosis	2/12	1/4	2/6	+	−	−
Hands (small, SPC)	5/13	4/4	?	−	SPC	SPC
Flexion of thumbs	2	1	−			
Supernumerary nipple	1	2/4	1	−	−	+
EEG abnormalities	8/9	4/4	2			
MRI	6/7	3/3	2	CCA	−	CCH
Results of TCF4 gene screening	3del, 2S, 3T, 4Ms	1del, 3Ms	1del, 1S, 2T, 1Ms, 1Fs	del18q21.1q2.3	del 0.5 Mb	del 6.2 Mb

[a]Cryptorchidism and/or small penis. GenBank accession number NM_003199.2.
M, male; F, female; SPC, single palmer crease; CCA, corpus callosum agenesia; CCH, corpus callosum hypoplasia; del, deletion; S, slice site mutation; T, trucating mutation; Ms, missense mutation.

However, two patients presented with infantile spasms at 4 and 6 months of age, respectively. In one case, this followed enterovirus meningitis at 4 months of age; del18q21 was diagnosed at 4 years of age. An EEG performed at 16 months of age showed left rolandic focal spikes subcontinuous during sleep with several focal seizures recorded. Episodes of hyperventilation also were not constant; they tended to be more frequent in epileptic patients and of earlier occurrence than the epilepsy itself. Frontal Pseudoperiodic Delta Waves (FPDW) during wakefulness and sleep were observed in five of eight cases and preceded the onset of epilepsy in three cases. MRI of the brain was available for 11 patients. All but one shown a thin corpus callosum, marked white-matter hyperintensity in the temporal poles, and small hippocampi.

Minor anomalies of the extremities were frequent and included small and slender palms with single palmar crease, and slender feet with pes planus and valgus. Of note, limited flexion of the P1–P2 thumb joint with absent flexion crease was noted in three of four patients harbouring a deletion encompassing the *TCF4* locus and none of the patients harbouring a *TCF4* coding sequence mutation. This was seen also in the patient reported by Andrieux et al. [2008]. Cryptorchidism and/or small penis was frequently noted (six to eight males). Severe chronic constipation of early onset (within the first year of life) was frequently recorded as well as gastrooesophageal reflux and eructation. However, no patient had Hirschsprung disease or other organ malformations in our series.

Among the patients with no coding sequence mutations and no deletions detected by FISH analyses none have the PHS facial gestalt identified among patients with a *TCF4* mutation.

TCF4 Mutations

We screened the coding sequence of the 21 exons of the *TCF4* gene for nucleotide variations in a series of 36 PHS patients and identified 13 mutations (Fig. 2). No mutations observed were detected in a panel of 120 control chromosomes. We identified five putative null alleles mutations: two splice site mutations (c.923-2A>G and c.1146 +1G>A), two frameshift mutations (c.1472_1473insA p.Asp492GlyfsX21 and c.1521_1522insC p.Ser508LeufsX5), and one nonsense mutation (c.1498G>T p.G500X). Any polypeptide translated from transcripts bearing one of these mutations would be predicted to lack the bHLH domain.

We also identified four missense mutations (c.1471A>G, p.D535G, c.1714G>A, p. R572G, c.1727C>G, p.R576Q, and c.1823C>T, p.A610V). All missense mutations modify amino acids highly conserved in mammalian *TCF4* genes (ClustalW analysis, data not shown). All mutations were de novo except for the p. R572G, c.1725C>G mutation. It was also identified in the patient's mother for DNA extracted from leucocytes and urethral cells but not for buccal swabs. A mosaic state for the mutation was confirmed by direct sequencing from buccal swabs that showed a normal sequence (data not shown). We concluded that the mother, who was treated for chronic depression and epilepsy from 20 years of age, is somatic mosaic for the mutation. Finally, a deletion encompassing the *TCF4* gene was detected in three cases by FISH analysis.

Functional Analysis of TCF4 Mutant Alleles

Mutant cDNAs were stable and therefore could be amplified by RT-PCR extracted from lymphocytes. Cotransfection of *TCF4* and *ASCL1* cDNAs with a luciferase reporter construct containing a *Delta1* promoter with six E-boxes in HeLa (data not shown) and SKNBE(2)C cells (Fig. 5) showed that wild-type *TCF4* activates the reporter construct only when cotransfected with *ASCL1*. The activation was significantly and similarly impaired for nonsense, frameshift, and missense *TCF4* mutants, c.1498G>T p.G500X, c.1727G>A p.R576Q, and c.1726C>T p.R576W (Fig. 3). We therefore showed a loss of function effect of all mutants. Finally, a dominant negative effect cannot be ruled out as luciferase activity of ASCL1+/TCF4 mutants is lower than the one of ASCL1+/TCF4−.

Immunologic Investigations

As *Tcf4* is involved in fetal B lymphocyte development in mice [Zhuang et al. 1996], we investigated cellular and humoral

(a)

(b)

Figure 1. Consistent facial features include enophthalmia, strabismus, thin eyebrows in their midline portion, a large nose with high bridge and flared nostrils, a protruding philtrum, fleshy lips, wide upper mouth, and dysplastic ear helices in 10 patients with *TCF4* mutations (**A**) and two patients with *TCF4* deletions (**B**).

immunity in eight PHS patients. No susceptibility to infections was reported, except for one case who experienced one episode of urinary tract infection and severe chickenpox. Immunologic investigations revealed normal B (including switched memory) and T CD4+and CD8+lymphocyte count, and appropriate postvaccination or postinfection serology. However, serum

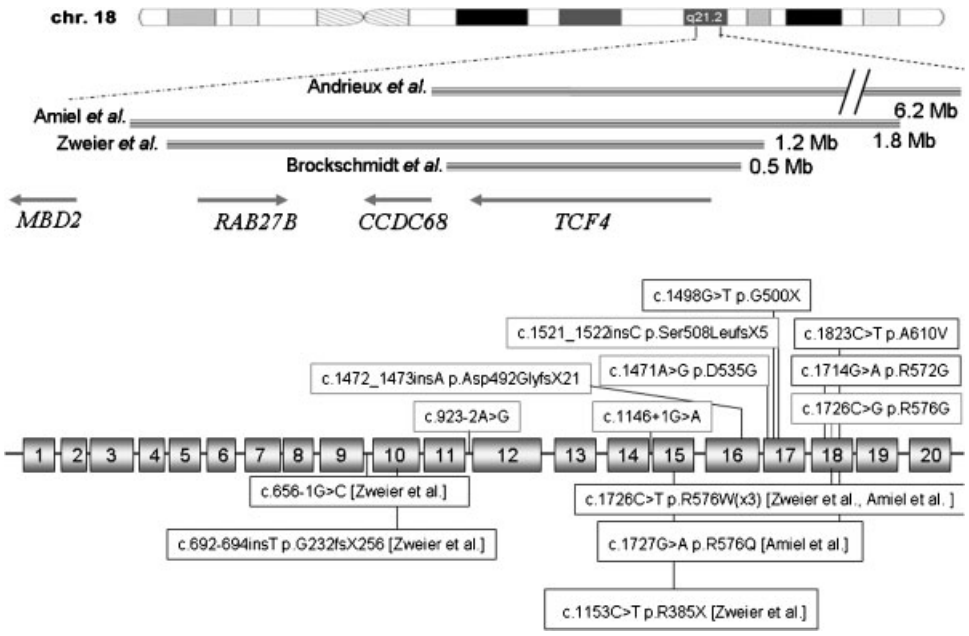

Figure 2. Schematic representation of deletion and *TCF4* gene mutations in our series (top) and in the literature (bottom).

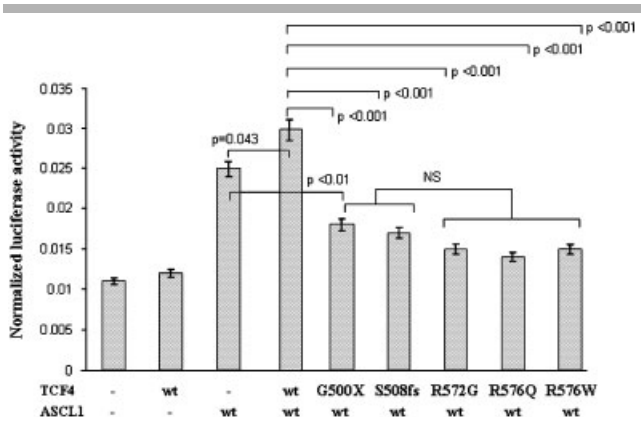

Figure 3. Transcriptional reporter assay with TCF4 wild type (WT) and mutants. SKNBE(2)C cells were transiently transfected with a luciferase reporter construct with a *Delta1* promoter containing two E-boxes. TCF4 alone does not increase the activation of the reporter construct, whereas cotransfection with ASCL1 yields the highest values of luciferase activity. ASCL1/TCF4 mutant (G500X, R576Q, or R576W) activity is significantly lower than with ASCL1/TCF4 wild-type heterodimers (significant p values <0.05 obtained by the Student t-test are indicated by a star).

immunoglobulin M levels were in the low normal range according to age in one case and bellow this range in the seven other cases. Interestingly, the mother carrying the c.1714G>A p.R572G mutation had normal immunoglobulin M levels.

TCF4 Expression in Early Human Development

We studied the pattern of expression of *TCF4* in early human development (Fig. 4). *TCF4* is highly expressed throughout the central nervous system (CNS) and sclerotomal component of the somites (Fig. 4A) from Carnegie stage (C)13 (28–32 days postfertilization [dpf]). At C15 (35–38 dpf), *TCF4* is highly expressed in the condensing vertebral body (Fig. 4C), as well as throughout the limb bud and splanchopleural mesenchyme. The gonadal ridge also expresses *TCF4* at this point.

By C18 (44–48 dpf), many but not all additional sites transcribe *TCF4* (Fig. 4F). These include mesenchyme of the developing digits (Fig. 4G); the primordium of the pituitary gland (Fig. 4I); NCAM-expressing sympathetic, parasympathetic, and enteric ganglia (Fig. 3K–P); peribronchial mesenchyme (Fig. 4N), the gonad, mesonephros and definitive kidney (Fig. 4Q), and the thyroid and thymus primordial (Fig. 4S). Vertebrae and the ventricular zone of the CNS continue to strongly express *TCF4*.

TCF4 expression continues through postnatal life, as we detect its transcripts by RT-PCR in adult lymphocytes, fibroblasts, gut, muscle, but not the heart (data not shown). In the small intestine at 5 years of age, *TCF4* mRNA is found in enteric ganglia of the myenteric plexus (Fig. 5A), which also produce NCAM (Fig. 5B). However, *TCF4* is also transcribed in Paneth cells of the epithelial crypts (Fig. 5D) as shown by immunoreactivity to synaptotagmin on an adjacent section (Fig. 5E).

Discussion

PHS is a syndromic encephalopathy with an autosomal dominant mode of inheritance, due to de novo mutations at the *TCF4* locus. However, genetic counselling should take into account the possibility of somatic/germinal mosaicism as this was observed in one case from our series. We confirm in a larger series than reported previously, a mutational hot spot lying in the basic domain, with six mutations among 14 coding sequence mutation PHS cases and four at the same codon ([Amiel et al., 2007], and this report). The association of severe mental retardation and facial gestalt allows diagnosis in early life, youngest being diagnosed at 9 months old in our series. The recognition of a series of 13 cases over a 12-month period confirms that PHS is more frequent than implied by the scattered reports made over the past 30 years. Differential diagnoses include Rett (MIM# 312750), Angelman (MIM# 105830), and Mowat-Wilson (MIM# 235730) syndromes. PHS should therefore be systematically considered for patients with negative molecular screening for *MECP2*, *UBE3A*, and/

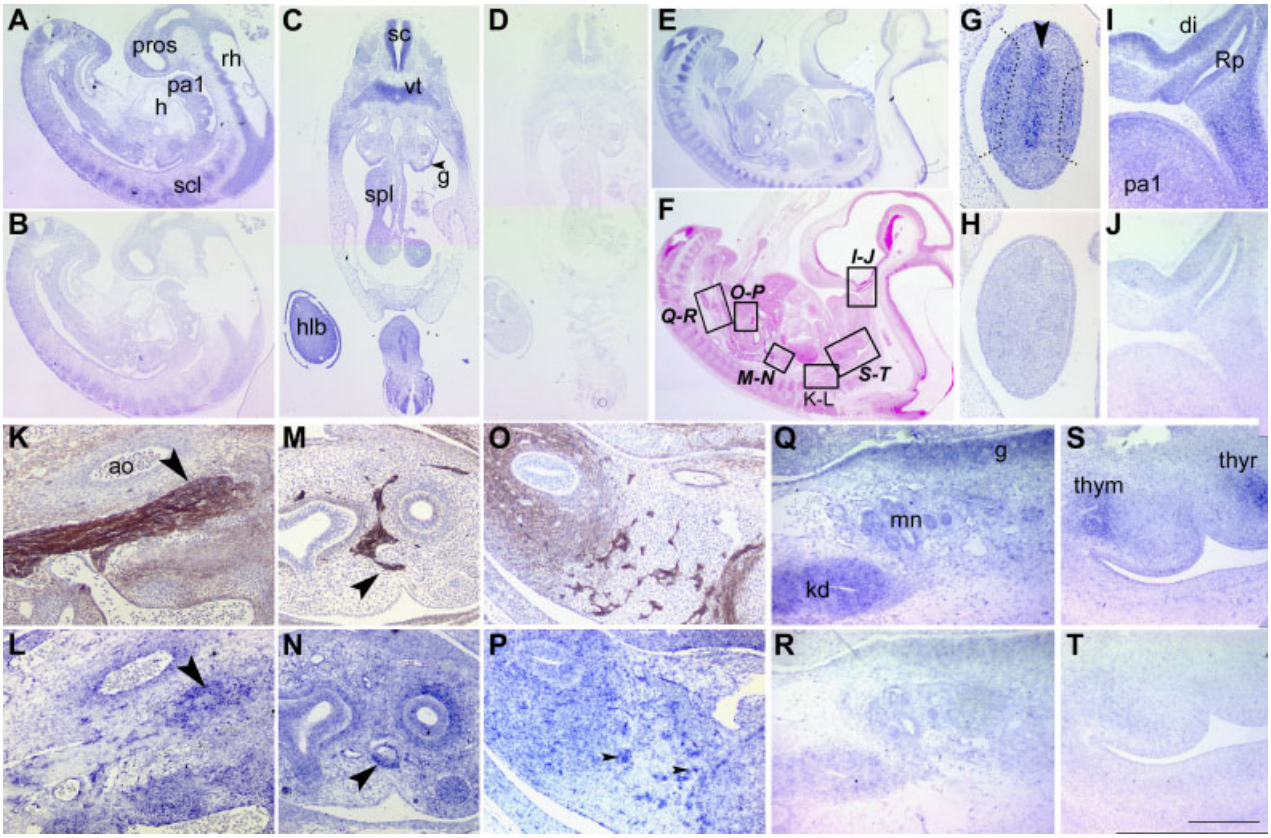

Figure 4. Pattern of expression of *TCF4* in early human development. **A**: *TCF4* is observed throughout the central nervous system (CNS), sclerotome, and lateral plate mesoderm, and all pharyngeal arch mesenchyme at Carnegie stage (C)13 (28–32 days postfertilization [dpf]). **B**: Sense (control) probe hybridization. **C**: At C15 (35–38 dpf), *TCF4* is seen in the condensing vertebral body, throughout the limb bud and splanchopleural mesenchyme and gonadal ridge. **D**: Sense probe. **E**: By C18 (44–48 dpf), many but not all additional sites transcribe *TCF4*. **F**: Hematoxylin-eosin stain of adjacent section indicating magnifications of zones featured in **I**–**T**. **G**: At C19 (49 dpf), precartilaginous (arrow) and lateral mesenchyme of the developing digits show higher expression of *TCF4* than surrounding cells. **H**: Sense probe. **I**: At C18 (section in **F**), Rathke's pouch, the diencephalon, pharyngeal arch subectodermal mesenchyme, and the cartilaginous primordia of the *sella turcica* all show strong expression. **J**: Sense probe. **K**: CD56 (NCAM) immunostain in brown of adjacent section to *TCF4* antisense hybridization in blue in **L** demonstrates *TCF4* transcription in the soma of the sympathetic ganglia. **M**: CD56 in a parasympathetic ganglion of the lung (arrowhead) and nerve fibers shows overlap with *TCF4* expression (**N**) only within the ganglion itself. Mesenchymal *TCF4* expression surrounds the bronchi. **O**: CD56 in mesenchyme (diffuse) and developing enteric plexi of the duodenum. **P**: The enteric ganglia (arrowheads) coexpress *TCF4*. **Q**: The gonad continues to strongly transcribe *TCF4*, as do the mesonephrotic tubules and glomeruli and metanephric mesenchyme (kd). **R**: Sense probe. **S**: Mesenchyme of the thyroid and thymic primordial express *TCF4* at C18. **H**: Sense probe. Scale bar: **A**–**B**, 1 mm; **C**–**D**, 1.3 mm; **E**–**F**, 2 mm; **G**–**T**, 250 μm.

or *ZFHX1B*. We suggest first screening for *TCF4* gene deletion (by FISH, MLPA, or quantitative PCR) when thumb anomalies are noted, and to start with direct sequencing when thumbs are normal (exons 17 and 18 being first). Whether limited flexion of the thumbs is directly due to *TCF4* gene dysfunction or due to adjacent genes in a contiguous gene syndrome is uncertain. However, we detected a high level of *TCF4* expression in limb buds during foetal development, whereas no obvious candidate gene is included in the minimal region of overlap (Fig. 2).

TCF-4 is a downstream target of the WNT/β-catenin/TCF pathway and, like cMYC and cyclin D1, has been shown to function as an oncogene when deregulated. Of note, one patient reported with a *TCF4* mutation developed lymphoma [Zweier et al., 2007]. Recently, Kuiper et al. [2007] identified deletions of the *TCF4* gene in paediatric lymphoblastic leukaemias. The question of whether PHS patients are predisposed to lymphomas remains a possibility. *Tcf4–/–* knockout mice have a reduced numbers of pro-B cells [Zhuang et al., 1996]. We confirmed *TCF4* expression in the thymus and presplenic mesenchyme, and observed low levels of immunoglobulin M in all patients tested. These findings help clinical diagnoses of PHS. However, normal B cell counts (including the more mature, memory-switched B) in the eight patients tested strongly suggests that either *TCF4* is not involved in B cell differentiation in humans or that *TCF4* loss of function is compensated by other transcription factors. A subtle humoral defect was nevertheless observed, because all patients present with a rather low serum IgM level. Of note, μE5/κE2 enhancer sites of immunoglobulin genes are direct targets of TCF4 homodimers as well a TCF3/TCF4 heterodimer [Bain et al., 1993; Henthorn et al., 1990]. Long-term follow-up should resolve the question of whether PHS patients are prone to infections, autoimmune disorders or tumors.

Molecular interaction between TCF4 and ASCL1 has been demonstrated in humans and mice [Castro et al., 2006; Persson et al., 2000], and *ASCL1* may play a role in the control of breathing [de Pontual et al., 2003]. We hypothesized that the breathing anomalies observed in some PHS cases may result from impaired noradrenergic neuronal development after defective TCF4 interaction with the ASCL1–PHOX–RET pathway. Zweier et al. [2007] studied three different TCF4 mutants with a

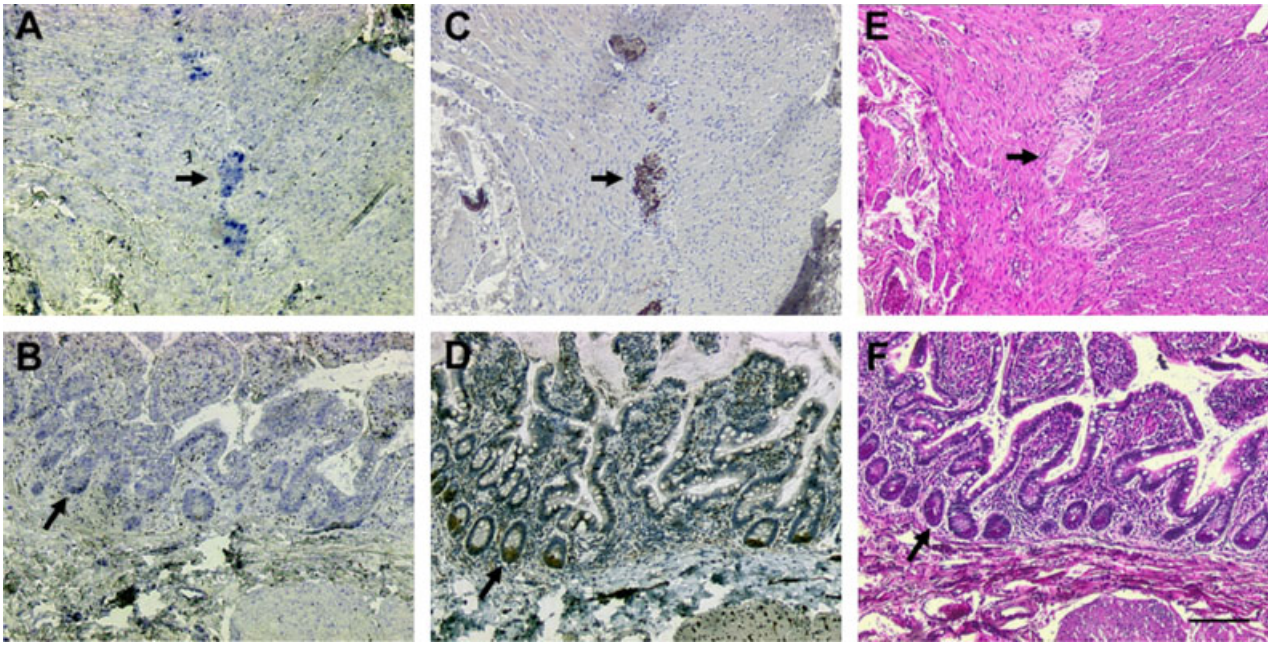

Figure 5. Expression of *TCF4* in the small intestine at age 5. **A**: Myenteric ganglia (arrow) are colabeled (**B**) by CD56. **C**: Hematoxylin-eosin stain of adjacent section. **D**: Paneth crypt cells (arrow) of the intestinal epithelium also express *TCF4*. **E**: These are colabeled by synaptotagmin. **F**: Hematoxylin-eosin stain of adjacent section. Bar 40 μm.

transcriptional reporter assay with a herpes simplex thymidine kinase promoter in JEG-3 cells and showed that the activation of TCF4/ASCL1 dimer was significantly impaired for all TCF4 mutants tested. We confirmed these results in a more relevant neural cell line using a *Delta 1* promoter reporter construct (Fig. 3).

Unexpectedly, the *TCF4* spatiotemporal expression pattern is broad but not ubiquitous. For example, *TCF4* expression could not be detected in the myocardium by either in situ hybridization or RT-PCR. Moreover, *TCF4* expression is highest in the central nervous system, the sclerotome, peribronchial and kidney mesenchyme, and the genital bud. E proteins have recently been considered redundant during brain development [Ravanpay and Olson, 2008]. However, *Tcf4* has recently been shown to play an exclusive role in pontine neuron differentiation via heterodimerization with *Math1* (also known as *Atoh1* and encoding a proneuronal class II bHLH) [Flora et al., 2007]. These data demonstrate that *TCF4* is specifically required during brain development and sheds light on the ventilatory and movement disorders observed in PHS patients. Indeed, the pontine nucleus is involved in the central autonomic pathway and in storing the memory of intention during motor activity. Furthermore, *Math1* is essential for intestinal secretory cell differentiation and intestinal secretory cell production in adult mice [Shroyer et al., 2007]. Although, Tcf4 has not currently been shown to heterodimerize with Math1 in these cells also, this could explain the intestinal dysfunction observed in the vast majority of PHS patients. We show that *TCF4* is expressed in both enteric ganglia and epithelial crypt cells of the intestine. Therefore, whether HSCR occurred by chance in one patient with PHS or is a feature to be ascribed to TCF4 dysfunction [Peippo et al., 2006] is not fully answered; PHS should still be considered for patients presenting an unexplained combination of HSCR or severe constipation and mental retardation.

Altogether, clinical, imaging, and immunological data identified in PHS highlight the dose-sensitive and nonredundant functions of E-proteins for normal development in humans.

Acknowledgments

We are grateful to François Guillemot (National Institute for Medical Research, Mill Hill, Londres) for providing luciferase reporter plasmids, Candice Babarit for in situ hybridization, and Tania Attié-Bitach for helpful discussion. We thank the PHS families and their referring clinicians for their participation. While the paper was under review, two series of PHS cases have been published. This raises the number of PHS cases up to 50 [Giurgea et al., 2008; Zweier et al., 2008).

References

Amiel J, Rio M, de Pontual L, Redon R, Malan V, Boddaert N, Plouin P, Carter NP, Lyonnet S, Munnich A, Colleaux L. 2007. Mutations in TCF4, encoding a class I basic helix-loop-helix transcription factor, are responsible for Pitt-Hopkins syndrome, a severe epileptic encephalopathy associated with autonomic dysfunction. Am J Hum Genet 80:988–993.

Andrieux J, Lepretre F, Cuisset JM, Goldenberg A, Delobel B, Manouvrier-Hanu S, Holder-Espinasse M. 2008. Deletion 18q21.2q21.32 involving TCF4 in a boy diagnosed by CGH-array. Eur J Med Genet 51:172–177.

Bain G, Gruenwald S, Murre C. 1993. E2A and E2-2 are subunits of B-cell-specific E2-box DNA-binding proteins. Mol Cell Biol 13:3522–3529.

Brockschmidt A, Todt U, Ryu S, Hoischen A, Landwehr C, Birnbaum S, Frenck W, Radlwimmer B, Lichter P, Engels H, Driever W, Kubisch C, Weber RG. 2007. Severe mental retardation with breathing abnormalities (Pitt-Hopkins syndrome) is caused by haploinsufficiency of the neuronal bHLH transcription factor TCF4. Hum Mol Genet 16:1488–1494.

Castro DS, Skowronska-Krawczyk D, Armant O, Donaldson IJ, Parras C, Hunt C, Critchley JA, Nguyen L, Gossler A, Gottgens B, Matter JM, Guillemet F. 2006. Proneural bHLH and Brn proteins coregulate a neurogenic program through cooperative binding to a conserved DNA motif. Dev Cell 11:831–844.

de Pontual L, Nepote V, Attie-Bitach T, Al Halabiah H, Trang H, Elghouzzi V, Levacher B, Benihoud K, Auge J, Faure C, Laudier B, Vekemans, M, Munnich A, Perricaudet M, Guillemot F, Galtier C, Lyonnet S, Simonneau M, Amiel J. 2003. Noradrenergic neuronal development is impaired by mutation of the proneural HASH-1 gene in congenital central hypoventilation syndrome (Ondine's curse). Hum Mol Genet 12:3173–3180.

Delous M, Baala L, Salomon R, Laclef C, Vierkotten J, Tory K, Golzio C, Lacoste T, Besse L, Ozilou C, Moutkine I, Hellman NE, Anselme I, Sibermann F, Vesque C, Gerhardt C, Rattenberry E, Wolf MT, Gubier MC, Martinovic J, Encha-Razavi F, Boddaert N, Gonzales M, Macher MA, Nivet H, Champion G, Berthélémé JP, Niaudet P, Mcdonald F, Hildebrandt F, Johnson CA, Vekemans M, Antignac C, Rüther U, Schneider-Mauoury S, Attié-Bitach T, Seunier S. 2007. The ciliary

gene RPGRIP1L is mutated in cerebello-oculo-renal syndrome (Joubert syndrome type B) and Meckel syndrome. Nat Genet 39:875–881.

Flora A, Garcia JJ, Thaller C, Zoghbi HY. 2007. The E-protein Tcf4 interacts with Math1 to regulate differentiation of a specific subset of neuronal progenitors. Proc Natl Acad Sci USA 104:15382–15387.

Gustavsson P, Kimber E, Wahlstrom J, Anneren G. 1999. Monosomy 18q syndrome and atypical Rett syndrome in a girl with an interstitial deletion (18)(q21.1q22.3). Am J Med Genet 82:348–351.

Giurgea I, Missirian C, Cacciagli P, Whalen S, Fredriksen T, Gaillon T, Rankin J, Mathieu-Dramard M, Morin G, Martin-Coignard D, Dubourg C, Chabrol B, Arfi J, Giuliano F, Claude Lambert J, Philip N, Sarda P, Villard L, Goossens M, Moncla A. 2008. TCF4 deletions in Pitt-Hopkins ayndrome. Hum Mutat Epub ahead of print.

Henthorn P, Kiledjian M, Kadesch T. 1990. Two distinct transcription factors that bind the immunoglobulin enhancer microE5/kappa 2 motif. Science 247:467–470.

Kuiper RP, Schoenmakers EF, van Reijmersdal SV, Hehir-Kwa JY, van Kessel AG, van Leeuwen FN, Hoogerbrugge PM. 2007. High-resolution genomic profiling of childhood ALL reveals novel recurrent genetic lesions affecting pathways involved in lymphocyte differentiation and cell cycle progression. Leukemia 21:1258–1266.

Murre C. 2005. Helix-loop-helix proteins and lymphocyte development. Nat Immunol 6:1079–1086.

Orrico A, Galli L, Zappella M, Lam CW, Bonifacio S, Torricelli F, Hayek G. 2001. Possible case of Pitt-Hopkins syndrome in sibs. Am J Med Genet 103:157–159.

Peippo MM, Simola KO, Valanne LK, Larsen AT, Kahkonen M, Auranen MP, Ignatius J. 2006. Pitt-Hopkins syndrome in two patients and further definition of the phenotype. Clin Dysmorphol 15:47–54.

Persson P, Jogi A, Grynfeld A, Pahlman S, Axelson H. 2000. HASH-1 and E2-2 are expressed in human neuroblastoma cells and form a functional complex. Biochem Biophys Res Commun 274:22–31.

Pitt D, Hopkins I. 1978. A syndrome of mental retardation, wide mouth and intermittent overbreathing. Aust Paediatr J 14:182–184.

Ravanpay AC, Olson JM. 2008. E protein dosage influences brain development more than family member identity. J Neurosci Res 86:1472–1481.

Revy P, Busslinger M, Tashiro K, Arenzana F, Pillet P, Fischer A, Durandy A. 2000. A syndrome involving intrauterine growth retardation, microcephaly, cerebellar hypoplasia, B lymphocyte deficiency, and progressive pancytopenia. Pediatrics 105:E39.

Ross SE, Greenberg ME, Stiles CD. 2003. Basic helix-loop-helix factors in cortical development. Neuron 39:13–25.

Shroyer NF, Helmrath MA, Wang VY, Antalffy B, Henning SJ, Zoghbi HY. 2007. Intestine-specific ablation of mouse atonal homolog 1 (Math1) reveals a role in cellular homeostasis. Gastroenterology 132:2478–2488.

Singh HA. 1993. Mental retardation, macrostomia and hyperpnoea syndrome. J Paediatr Child Health 29:156–157.

Van Balkom ID, Quartel S, Hennekam RC. 1998. Mental retardation, "coarse" face, and hyperbreathing: confirmation of the Pitt-Hopkins syndrome. Am J Med Genet 75:273–276.

Zhuang Y, Cheng P, Weintraub H. 1996. B-lymphocyte development is regulated by the combined dosage of three basic helix-loop-helix genes, E2A, E2-2, and HEB. Mol Cell Biol 16:2898–2905.

Zweier C, Peippo MM, Hoyer J, Sousa S, Bottani A, Clayton-Smith J, Reardon W, Saraiva J, Cabral A, Gohring I and others. 2007. Haploinsufficiency of TCF4 causes syndromal mental retardation with intermittent hyperventilation (Pitt-Hopkins syndrome). Am J Hum Genet 80:994–1001.

Zweier C, Sticht H, Bijlsma E, Clayton-Smith J, Boonen SE, Fryer A, Greally MT, Hoffmann L, den Hollander NS, Jongmans M, Kant SG, King MD, Lynch SA, McKee S, Midro AT, Park SM, Ricotti V, Tarantino E, Wessels M, Peippo M, Rauch A. 2008. Further delineation of Pitt-Hopkins syndrome: phenotypic and genotypic description of sixteen novel patients. J Med Genet Aug 2008; doi:10.1136/jmg.2008.060129.

MUTATION IN BRIEF

Phenotypic Spectrum of *STRA6* Mutations: from Matthew-Wood Syndrome to Non-lethal Anophthalmia

Nicolas Chassaing[1,2,3], Christelle Golzio[4,5], Sylvie Odent[6], Léopoldine Lequeux[3], Adeline Vigouroux[3], Jelena Martinovic-Bouriel[7], Francesco Danilo Tiziano[8], Lucia Masini[9], Francesca Piro[10], Giovanna Maragliano[11], Anne-Lise Delezoide[12], Tania Attié-Bitach[4,5,7], Sylvie Manouvrier-Hanu[13], Heather C. Etchevers[1,4], and Patrick Calvas[1,2,3*]

[1] INSERM, U563, Centre de Physiopathologie de Toulouse Purpan, Toulouse, 31300 France; [2] Université Toulouse III Paul-Sabatier, Toulouse, 31400 France; [3] CHU Toulouse, Hôpital Purpan, Service de Génétique Médicale, Toulouse, 31300 France; [4] INSERM, U781, Hôpital Necker-Enfants Malades, Paris Cedex 15, 75743 France; [5] Université Paris Descartes, Hôpital Necker-Enfants Malades, Paris, 75743 France; [6] CHU Rennes, Hôpital Sud, Service de Génétique Médicale, Rennes, 35203 France; [7] Département de Génétique, Hôpital Necker-Enfants Malades, Paris Cedex 15, 75743 France [8] Institute of Medical Genetics, Catholic University, Rome, Italy; [9] Institute of Obstetrics and Gynecology, Catholic University, Rome, Italy; [10] Operative Unit of Pathology, S. Giovanni Hospital, Rome, Italy; [11] Complex Unit of Neonatology, S. Giovanni Hospital, Rome, Italy; [12] GHU Nord, Hôpital Robert Debré, Service de Biologie du Développement, Paris Cedex 19, 75935 France; [13] CHRU Lille, Hôpital Jeanne de Flandre, Service de Génétique Clinique, Lille Cedex, 59037 France

*Correspondence to Pr Patrick Calvas, Service de Génétique Médicale, Pavillon Lefebvre, CHU Purpan, Place du Dr Baylac, 31059 Toulouse Cedex 9, France.
Tel.: +33 5 61 77 90 79; fax: +33 5 62 74 45 58.
E-mail : calvas.p@chu-toulouse.fr

Received 11 December 2008; accepted revised manuscript 08 March 2009.

Communicated by Mark H. Paalman

Matthew-Wood, Spear, PDAC or MCOPS9 syndrome are alternative names used to refer to combinations of microphthalmia/anophthalmia, malformative cardiac defects, pulmonary dysgenesis, and diaphragmatic hernia. Recently, mutations in *STRA6*, encoding a membrane receptor for vitamin A-bearing plasma retinol binding protein, have been identified in such patients. We performed *STRA6* molecular analysis in three fetuses and one child diagnosed with Matthew-Wood syndrome and in three siblings where two adult living brothers are affected with combinations of clinical anophthalmia, tetralogy of Fallot, and mental retardation. Among these patients, six novel mutations were identified, bringing the current total of known *STRA6* mutations to seventeen. We extensively reviewed clinical data pertaining to all twenty-one reported patients with *STRA6* mutations (the seven of this report and fourteen described elsewhere) and discuss additional features that may be part of the syndrome. The clinical spectrum associated with STRA6 deficiency is even more variable than initially described. © 2009 Wiley-Liss, Inc.

KEY WORDS: *STRA6*, anophthalmia, Matthew-Wood syndrome, PDAC syndrome, MCOPS9

DOI: 10.1002/humu.21023

INTRODUCTION

Variable combinations of microphthalmia/anophthalmia, pulmonary agenesis/dysplasia, diaphragmatic hernia and malformative cardiac defects have been infrequently reported over the last three decades (Ostor et al., 1978; Spear et al., 1987; Smith et al., 1994; Seller et al., 1996; Berkenstadt et al., 1999; Priolo et al., 2004; Lee et al., 2006; Li and Wei, 2006; Chitayat et al., 2007; Golzio et al., 2007; Pasutto et al., 2007). Such associations have been called Matthew-Wood or Spear syndrome, while Chitayat et al. (2007) devised the acronym PDAC (Pulmonary hypoplasia/agenesis, Diaphragmatic hernia/eventration, Anophthalmia/microphthalmia and Cardiac Defect), and the Mendelian Inheritance in Man database has adopted the term MCOPS9 for "syndromic microphthalmia 9" (MIM# 601186). Recently, mutations in *STRA6* (MIM# 610745), encoding a membrane receptor for the vitamin A-bearing plasma retinol binding protein, have been found in patients with malformations in the PDAC spectrum (Golzio et al., 2007; Pasutto et al., 2007; White et al., 2008; West et al., 2009).

We report herein novel *STRA6* mutations in three fetuses and one child diagnosed with Matthew-Wood syndrome, and in three siblings where two adult living brothers are affected with combinations of clinical anophthalmia, tetralogy of Fallot, and mental retardation. This is the first description of adult patients bearing *STRA6* mutations. These additional cases emphasize that the clinical spectrum associated with *STRA6* mutations is extremely variable.

PATIENTS AND METHODS

Patients

Case 1

This male fetus from healthy and unrelated parents was delivered at 23 weeks of gestation after an ultrasound scan documented bilateral diaphragmatic hernia, anophthalmia and cardiopathy. Autopsy confirmed the presence of bilateral severe microphthalmia (Fig 1A), bilateral diaphragmatic hernia, and a complex heart malformation (hypoplastic left heart syndrome with common atrium and dextroposition of the aorta). The lungs were hypoplastic and dysplastic. The karyotype was 46, XY.

Case 2

This patient has previously been described (Chitayat et al., 2007; patient 7). Briefly, she was the fifth child of consanguineous parents, born at term after a normal pregnancy, with normal growth parameters. She displayed an association of bilateral anophthalmia (Fig 1B), heart malformation, subglottic laryngeal stenosis, bilateral unilobar lungs, hypoplastic left kidney and right vesico-ureteral reflux, supernumerary spleen and hypoplastic uterus. Her karyotype was 46, XX. She died at 19 months post-operatively for an unknown reason, after surgery was performed to expand ocular orbits.

Family 3 (Cases 3-1, 3-2, 3-3)

Case 3-1:

A 40 year old patient was referred after his healthy sister came in for genetic counseling. He is the first child of healthy and unrelated parents. He has moderate mental retardation associated with bilateral anophthalmia and tetralogy of Fallot. Facial dysmorphy includes very short palpebral fissures and closed eyelids, a thin nasal bridge and broad nasal tip (Fig 1C). The hands are small and broad. His height is 160 cm (-2.25 SD) and his karyotype is 46, XY.

Case 3-2:

A sister of case 3-1 died in the first days of life from a tetralogy of Fallot. She reportedly had bilateral clinical anophthalmia but did not undergo autopsy.

Case 3-3:

The adult brother of cases 3-1 and 3-2 is more severely mentally retarded than case 3-1, associated with autistic features. Cerebral CT scan demonstrates small residual ocular structures and presence of optic nerves, thus indicating an extreme bilateral microphthalmia. Cardiac examination shows no malformations. Radiological findings show decreased bone mineral density and a spina bifida occulta at L5-S1.

Family 4 (cases 4-1 and 4-2)

Case 4-1:

This was the third child of consanguineous parents. At 26 weeks of pregnancy, micro/anophthalmia, congenital heart disease and diaphragmatic hernia were diagnosed by ultrasound. Karyotype analysis was performed fetal blood sample (46,XY). At 38 weeks, an elective cesarean section was performed. The child died soon after birth due to respiratory insufficiency. At autopsy, the following observations were made: anophthalmia (absent globes but presence of optic nerves), left diaphragmatic hernia with partial herniation of stomach into thorax, a complex congenital heart malformation characterized by truncus arteriosus (absence of truncal septum, single valvular orifice and short common tract). Liver, pancreas, and gut were normal both macroscopically and histologically.

Case 4-2:

Brother of case 4-1. At 26 weeks of gestation, ultrasound revealed suspicion of anophthalmia, hypoplastic left lung and complex congenital heart disease (left rotation of cardiac axis, and thickened wall of the right heart), suggesting the recurrence of a clinical phenotype strikingly similar to the previous pregnancy. The child died soon after birth, again due to respiratory insufficiency. Clinical anophthalmia (Fig 1D) and hypoplastic left lung was confirmed. Echocardiography showed left rotation of the cardiac axis secondary to lung hypoplasia, but without heart malformation.

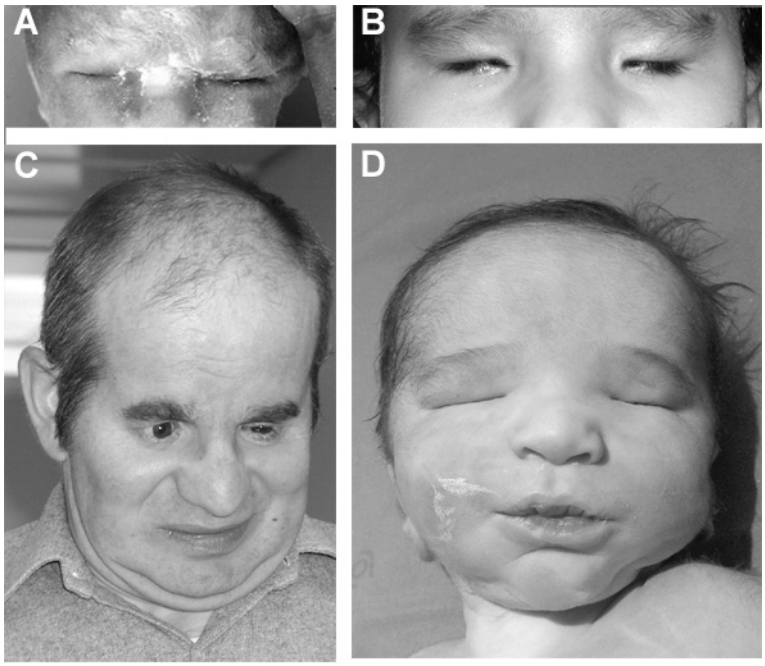

Figure 1. Representative oculofacial phenotypes. A: Case 1 had short palpebral fissures reflecting bilateral severe microphthalmia. **B**: Case 2 presented deep-set orbits, narrow palpebral fissures associated with anophthalmia and wide, diffuse implantation of eyebrows. **C:** Case 3-1 has mild facial dysmorphy with a broad nasal tip. This patient has orbital implants. **D**: Case 4-2 also had a broad nasal bridge and the deep-set orbits associated with clinical anophthalmia.

STRA6 molecular analysis

After informed consent for inclusion in the study was obtained from the parents, DNA was isolated by standard procedures from paraffin-embedded blocks of case 1, from frozen tissue samples of case 2, and from peripheral blood of cases 3-1, 3-3, 4-2 and their unaffected parents and siblings. *STRA6* noncoding and coding exons and exon-intron junctions were amplified by PCR using previously published primers (Golzio et al., 2007).

PCR fragments were subsequently purified with QIAquick Gel Extraction kits (QIAGEN SA France), and sequenced using the Big Dye DNA sequencing kit (Applied Biosystems, UK). Reactions were analyzed in an ABI3100 sequencer (Applied Biosystems, UK).

A sequence variant was considered as disease-causing when: (1) the variant cosegregated with the disease phenotype; *and* (2a) the sequence variant resulted in the prediction of a stop codon, or was predicted to lead to splice-site alteration (BDGP splice site prediction software); or (2b) the substitution involved an amino acid conserved between three vertebrate subclasses (ClustalW software) or (2c) the substitution was predicted to be functionally damaging (PolyPhen software); *and* (3) the sequence variant was absent from a panel of 200 chromosomes from unaffected, unrelated individuals.

Sequence variations were numbered based on GenBank accession NM_022369.3. Nucleotide numbering reflects cDNA numbering with +1 corresponding to the A of the ATG translation initiation codon in the reference sequence, according to journal guidelines (www.hgvs.org/mutnomen). The initiation codon is codon 1.

Table 1. PDAC/MCOPS9 features in *STRA6* mutated patients

		Nucleotide variation	**Protein alteration**	**Lung**	**Diaphragm**	**Eyes**	**Heart**	**Other**
This report	1	c.1090+1G>A c.859C>T	abnormal splicing p.Gln287X	+ +		+	+	-
	2	c.1662delG c.1662delG	p.Arg555GlufsX16 p.Arg555GlufsX16	+ - +			+	Subglottic laryngeal stenosis Hypoplastic left kidney Right vesico-ureteral reflux Supernumerary spleen Hypoplastic uterus
	3-1	c.1313A>G c.1913G>C	p.Gln438Arg p.Arg638Pro	- -		+	+	Mental retardation
	3-2	c.1313A>G c.1913G>C	p.Gln438Arg* p.Arg638Pro*	- -		+	+	-
	3-3	c.1313A>G c.1913G>C	p.Gln438Arg p.Arg638Pro	- -		+	-	Mental retardation Short stature Spina bifida occulta
	4-1	c.1329delC c.1329delC	p.Leu444TrpfsX34* p.Leu444TrpfsX34*	- +		+	+	-
	4-2	c.1329delC c.1329delC	p.Leu444TrpfsX34 p.Leu444TrpfsX34	+ - +			-	-

		Nucleotide variation	Protein alteration	Lung	Diaphragm	Eyes	Heart	Other
Pasutto *et al.* 2007	5	c.878C>T c.878C>T	p.Pro293Leu p.Pro293Leu	+ - +			+	Ectopic pelvic kidney
	6	c.878C>T c.878C>T	p.Pro293Leu* p.Pro293Leu*	- -		+	+	-
	7	c.145-147delC c.145-147delC	p.Gly50AlafsX22 p.Gly50AlafsX22	- +		+	+	Mental retardation Short stature
	8	c.145-147delC c.145-147delC	p.Gly50AlafsX22 p.Gly50AlafsX22	- +		+	-	-
	9	c.1963C>T c.1963C>T	p.Arg655Cys p.Arg655Cys	+ +		+	-	Hypotonia Failure to thrive
	10	c.1963C>T c.1963C>T	p.Arg655Cys* p.Arg655Cys*	- -		+	+	-
	11	c.1931C>T c.1931C>T	p.Thr644Met p.Thr644Met	+ +		+	-	Hydronephrosis
	12	c.1931C>T c.1931C>T	p.Thr644Met* p.Thr644Met*	+ -		?	+	Horseshoe kidney
	13	c.1931C>T c.1931C>T	p.Thr644Met* p.Thr644Met*	+ - +			+	
	14	c.269C>T c.961A>C	p.Pro90Leu p.Thr321Pro	+ +		+	+	Hypoplasic kidneys Bicornuate uterus
Golzio *et al.* 2007	15	c.50_52delACT insCC c.50_52delACT insCC	p.Asp17AlafsX55 p.Asp17AlafsX55	+ +		+	-	Annular pancreas Duodenal stenosis Intra-uterine growth retardation
	16	c.527_528insG c.527_528insG	p.Gly176GlyfsX59 p.Gly176GlyfsX59	+ +		+	+	Multilobed spleen Duodenal stenosis Pancreatic agenesis Intra-uterine growth retardation
White *et al.* 2008	17	c.650G>A c.1774C>T	p.Gly217Glu p.Gln592X	- -		+	-	Duplicated kidney collecting system
West *et al.* 2009	18	c.31_32dupCC c.69G>A	p.Gly13ProfsX72 p.Trp23X	+ +		+	+	Intra-uterine growth retardation Cryptorchidism Bilateral inguinal hernias Thin corpus callosum
Total (%)				12/21 (57)	10/21 (48)	20/20 (100)	14/21 (67)	

+ : presence ; - : absence ; ?: unknown ;

* These patients had no molecular analysis but their genotype was deduced from that of an affected sib.

Sequence variations were numbered based on GenBank accession NM_022369.3, with +1 corresponding to the A of ATG translation initiation codon.

RESULTS AND DISCUSSION

STRA6 molecular analysis was performed in cases 1, 2, 3-1, 3-3, and 4-2. Case 1 was compound heterozygous for a splicing mutation (c.1090+1G>A) and a stop codon (c.859C>T; p.Gln287X), both leading to the prediction of premature termination of transcription. Case 2 was homozygous for the mutation c.1662delG (p.Arg555GlufsX16), with a predicted premature stop codon. Case 3-1, like case 3-3, was compound heterozygous for two missense mutations, c.1313A>G (p.Gln438Arg) and c.1913G>C (p.Arg638Pro). Mutation p.Arg638Pro was inherited from the mother and p.Gln438Arg was inherited from the father. Both mutations involved a conserved amino acid (Figure 2), and were predicted *in silico* to be damaging (Polyphen software). Case 4-2, was homozygous for the mutation c.1329delC (p.Leu444TrpfsX34) leading to a premature termination of the translation. The positions of *STRA6* mutations described to date are represented on Figure 3.

Figure 2: Alignment of part of human, murine, and avian STRA6 proteins, showing conservation of glutamine 438 and arginine 638 (shaded) in these species.

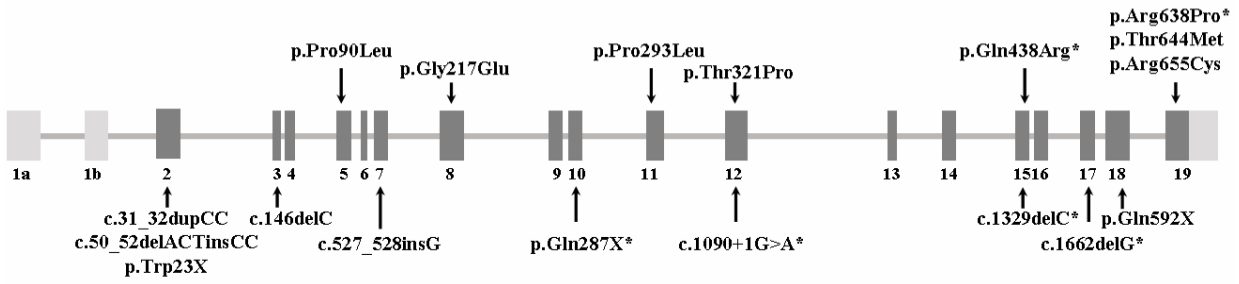

Figure 3: Locations of the different mutations identified to date. Missense mutations are positioned above the representation of *STRA6* gene, while nonsense and frameshift mutations are positioned underneath. Novel mutations identified in this study are indicated with an asterisk (*).

To date, no correlations between the nature of a *STRA6* mutation and phenotypic severity have been found. Patients with missense mutations have had severe phenotypes, whereas some patients with truncating mutations have had milder clinical involvement (Golzio et al., 2007; Pasutto et al., 2007). In previously reported families, there was little intrafamilial variation in severity (Chitayat et al., 2007; Pasutto et al., 2007). Likewise, in the first family reported here, all three affected siblings had bilateral severe microphthalmia, while none was described having diaphragmatic or lung involvement. However, case 3-2 died in the first days of life in the 1970s without further investigation, and a lung defect or diaphragmatic hernia cannot be ruled out. In addition, patients 3-1 and 3-2 had a tetralogy of Fallot while patient 3-3 had no cardiac malformation but rather a neural tube closure defect, not previously observed in association with PDAC syndrome.

Patients 3-1 and 3-3 are the first adult patients described with *STRA6* mutations, although other mutated children have already been reported (Pasutto et al., 2007; White et al., 2008). It is interesting to note that apart from clinical anophthalmia, none of the other principal features of PDAC syndrome (diaphragmatic, pulmonary or

cardiac involvement) is systematically present in those patients with *STRA6* mutations currently reported. Including these seven cases, mutations in *STRA6* have been observed in 21 phenotypically diverse patients sharing features of the MCOPS9 syndrome (Golzio et al., 2007; Pasutto et al., 2007; White et al., 2008; West et al., 2009). Their clinical presentation is summarized in Table 1. Phenotypic variability could be related to vitamin A metabolic variability (from absorption to degradation) in either fetuses or their pregnant mothers.

Bilateral microphthalmia/anophthalmia was constant and cardiopathy frequent (14/21; 67 %); pulmonary and/or diaphragmatic involvement were present in about half of the patients. Moreover, additional features appear to be associated with *STRA6* mutations, such as renal abnormalities (6/21), intra-uterine growth retardation (3/21), uterine malformations (2/21), and spleen and/or pancreatic malformations with attendant duodenal atresia (2/21) (Martinovic-Bouriel et al., 2007; White et al., 2008; West et al., 2009). Interestingly, mental retardation appears to be a constant finding in living patients.

Considering this phenotypic variability, it remains difficult to conclude whether Matthew-Wood/Spear/PDAC is a genetically homogeneous syndrome or an association of distinct syndromes overlapping in their clinical presentation. Negative molecular analysis for *STRA6* mutations in some PDAC patients suggests that this spectrum of anomalies is probably genetically heterogeneous, even though *STRA6* screening may ignore some mutations (such as exonic rearrangements, splicing mutations distant from the coding sequence, or mutations in regulatory sequences) (Chitayat et al., 2007; Golzio et al., 2007; Pasutto et al., 2007). STRA6 was recently identified as the cell membrane receptor for plasma retinol binding protein, which transfers circulating vitamin A from the blood into target cells (Kawaguchi et al., 2007). All *STRA6* mutations associated with human disease to date have been shown to largely abolish vitamin A uptake activity (Kawaguchi et al., 2008). It therefore remains likely that other genes implicated in the control of vitamin A intracellular levels during embryonic development are causative in those MCOPS9 associations not linked to *STRA6* mutations. The vitamin A signalling pathway directly regulates the levels of over 500 target proteins (Blomhoff and Blomhoff, 2006) and its own metabolism, while imperfectly understood, involves dozens of intracellular enzymes.

Extensive data from teratogenic and genetic animal models, as well as from Donnai-Barrow syndrome (MIM# 222448) patients with *LRP2* mutations, confirm the important role of vitamin A in human diaphragm and lung development (Kluth et al., 1990; Kantarci et al., 2007). Case 3.3, with a minor form of spina bifida, has the first reported association of *STRA6* mutations with a neural tube closure defect, which is a result of vitamin A metabolite deficiency in mouse models (Kastner et al., 1995). Splenic, pancreatic, intestinal and urogenital malformations sometimes observed in Matthew-Wood patients, as well as the conotruncal nature of the cardiac defects, are also effects of lower perceived retinoid levels in the primordia of these organs in embryonic mice (Kastner et al., 1995).

In conclusion, we report herein five new patients with MCOPS9 syndrome caused by *STRA6* mutations. These data contribute to an expanding database of *STRA6* mutations and to the delineation of the phenotypic variability in patients with such mutations. Further molecular studies on Matthew-Wood/Spear/PDAC/MCOPS9 patients may identify mutations in other genes implicated in the retinoic acid signaling pathway.

ACKNOWLEDGMENTS

The authors thank Drs. Férechté Encha-Razavi, Louise Devisme and Michel Vekemans for their advice and Chantal Esculpavit and Sophie Audollent for their technical assistance. Patient recognizable photos were reproduced with permission from the families, to whom the authors express their gratitude for their participation.

REFERENCES

Berkenstadt M, Lev D, Achiron R, Rosner M, Barkai G. 1999. Pulmonary agenesis, microphthalmia, and diaphragmatic defect (PMD): new syndrome or association? Am J Med Genet 86(1):6-8.

Blomhoff R, Blomhoff HK. 2006. Overview of retinoid metabolism and function. J Neurobiol 66(7):606-30.

Chitayat D, Sroka H, Keating S , Colby RS, Ryan G, To i A, Blaser S, Viero S, Devisme L, Bou te-Benejean O, Manouvrier-Hanu S, Mortier G, Loey s B , Rauch A , Bitoun P. 2007. The PDAC sy ndrome (pulmo nary h ypoplasia/agenesis, diaphragmatic h ernia/eventration, a nophthalmia/microphthalmia, and cardiac d efect) (Spear s yndrome, Matth ew-Wood syndrome): repo rt of eight case s including a living child and fur ther evid ence fo r au tosomal re cessive inh eritance. Am J Med Genet A 143(12):1268-81.

Golzio C, Martinovic-Bouriel J, Thomas S, Mougou-Zrelli S, Grattagliano-Bessieres B, Bonniere M, Delahay e S, Munnich A , Encha-Razavi F , L yonnet S, Ve kemans M, Att ie-Bitach T etchevers HC. 2007. Matth ew-Wood s yndrome is c aused b y truncating mutations in the retinol-binding protein receptor gene STRA6. Am J Hum Genet 80(6):1179-87.

Kantarci S, Al-Gazali L, Hill RS, Donnai D, Black GC, Bieth E, Chassaing N, Lacombe D, Devriendt K, Teebi A, Loscertales M, Robson C, Liu T, Macla ughlin DT, Noonan KM, Russell MK, Walsh CA, Donahoe PK, Pob er BR. 2007. Mutations in LRP2, which encodes the multiligand r eceptor megalin , cause Donnai-Barrow and facio-oculo-acoustico-renal syndromes. Nat Genet 39(8):957-9.

Kastner P, Mark M, Chambon P . 1995. Nonsteroid nuclear receptors: what are genetic studies telling us about their role in real life? Cell 83(6):859-69.

Kawaguchi R, Yu J, Honda J, Hu J, White legge J, Ping P, Wiita P, Bok D , Sun H. 2007. A membrane receptor for retinol binding protein mediates cellular uptake of vitamin A. Science 315(5813):820-5.

Kawaguchi R , Yu J, W iita P, Honda J, Sun H. 2008. An Essential Ligand-binding Dom ain in the Mem brane Receptor for Retinol-binding Protein Revealed by Large-scale Mutagenesis and a Human Polymorphism. J Biol Chem 283(22):15160-8.

Kluth D, Kangah R, Reich P, Tenbrinck R, Tibboel D, Lambrecht W. 1990. Nitro fen-induced diaphragmatic hernias in rats: an animal model. J Pediatr Surg 25(8):850-4.

Lee SYR, Shiu YK, Ng WF, Chow CB. 2006. Another patient with pulmonary hypoplasia, microphthalmia and diaphragmatic hernia. Clin Dysmorphol 15(1):43-4.

Li L, Wei J. 2006. A newborn with anophthalmia and pulmonary hypoplasia (the Matthew-Wood syndrome). Am J Med Genet A 140(14):1564-6.

Martinovic-Bouriel J, Bernab e-Dupont C, Go lzio C, Grattagliano -Bessieres B , M alan V, Bonnier e M, Escu lpavit C, Fallet-Bianco C , Mirle sse V, Le Bidoi s J, A ubry MC, Vekemans M, Morichon N etc hevers H, Atti e-Bitach T, Encha-Razavi F, Benachi A . 200 7. Ma tthew-Wood s yndrome: r eport of two n ew cases support ing autosomal r ecessive inh eritance and exclusion of FGF10 and FGFR2. Am J Med Genet A 143(3):219-28.

Ostor AG, Stillwell R, Fortune DW. 1978. Bilateral pulmonary agenesis. Pathology 10(3):243-8.

Pasutto F, Sticht H, Hammersen G, Gillessen-Kaesbach G, Fitzpatrick DR, Nurnberg G, Brasch F, Schirmer-Zimmermann H, Tolmie JL , Chi tayat D, Houg e G, Fern andez-Martinez L , Keating S , Mortier G, Henn ekam RC, von der Wense A, Slavotinek A , M einecke P, Bitou n P, Becker C , Nurnberg P, R eis A, Rau ch A. 2 007. Mutations in STRA6 cause a bro ad spectrum of malformations including anophth almia, cong enital heart defects, diaphragmatic h ernia, al veolar capillar y dysplasia, lung hypoplasia, and mental retardation. Am J Hum Genet 80(3):550-60.

Priolo M, C asile G, Lagana C. 2004. Pulmonary agenesis/hypoplasia, microphthalmia, and diaphragmatic defects: report of an additional case. Clin Dysmorphol 13(1):45-6.

Seller MJ, Davis TB, Fear CN, Flinter FA, E llis I, Gibson AG. 1996. Two sibs with anophthalmia and pulmonary hypoplasia (the Matthew-Wood syndrome). Am J Med Genet 62(3):227-29.

Smith SA, Mar tin KE, Dodd KL, Young ID . 1994. Severe microphthalmia, diaphr agmatic hernia and Fallot' s tetralogy associated with a chromosome 1;15 translocation. Clin Dysmorphol 3(4):287-91.

Spear GS, Yetur P, Beyerlein RA. 1987. Bilateral pulmonary agenesis and microphthalmia. Am J Med Genet Suppl 3:379-82.

West B, Bove KE, Slavotinek AM. 2009. Two novel STRA6 mutations in a patient with anophthalmia and diaphragmatic eventration. Am J Med Genet A.

White T, Lu T, Metlapally R, Katowitz J, Kherani F, Wang TY, Tran-Viet KN, Young TL. 2008. Identification of STRA6 and SKI sequence variants in patients with anophthalmia/microphthalmia. Mol Vis 14:2458-65.

Loss-of-Function Mutation in the Dioxygenase-Encoding *FTO* Gene Causes Severe Growth Retardation and Multiple Malformations

Sarah Boissel,[1,7] Orit Reish,[2,7] Karine Proulx,[3,7] Hiroko Kawagoe-Takaki,[4] Barbara Sedgwick,[4] Giles S.H. Yeo,[3] David Meyre,[5] Christelle Golzio,[1] Florence Molinari,[1] Noman Kadhom,[1] Heather C. Etchevers,[1] Vladimir Saudek,[3] I. Sadaf Farooqi,[3] Philippe Froguel,[5,6] Tomas Lindahl,[4] Stephen O'Rahilly,[3] Arnold Munnich,[1] and Laurence Colleaux[1,*]

FTO is a nuclear protein belonging to the AlkB-related non-haem iron- and 2-oxoglutarate-dependent dioxygenase family. Although polymorphisms within the first intron of the FTO gene have been associated with obesity, the physiological role of FTO remains unknown. Here we show that a R316Q mutation, inactivating FTO enzymatic activity, is responsible for an autosomal-recessive lethal syndrome. Cultured skin fibroblasts from affected subjects showed impaired proliferation and accelerated senescence. These findings indicate that FTO is essential for normal development of the central nervous and cardiovascular systems in human and establish that a mutation in a human member of the AlkB-related dioxygenase family results in a severe polymalformation syndrome.

Fto was originally identified in mice as one of the genes encoded by the 1.6 Mb deletion causing the fused toes (Ft) mutant, an autosomal-dominant mouse mutation generated by a transgene integration into region D of mouse Chr 8.[1] In addition to *Fto*, the deleted segment also contains three members of the Iroquois gene family (*Irx3*, *Irx5*, and *Irx6*, also known as the IrxB complex) as well as the *Fts/Aktip* and *Ftm/Rpgrip1l* genes. Mice heterozygous for the Ft mutation are characterized by partial syndactyly of forelimbs and thymic hyperplasia.[1] Ft/Ft embryos die in midgestation and present many abnormalities including limb polydactyly and distal truncations, major brain and heart defects, delay or absence of neural tube closure, and facial structure hypoplasia.[2,3]

Interestingly, a human genome-wide search for type 2 diabetes susceptibility genes identified the strong association of a series of single nucleotide polymorphisms (SNPs), in tight linkage disequilibrium with rs9939609 and located in the first intron of the *FTO* gene (MIM 610966), with higher body mass index (BMI) and obesity risk in European cohorts.[4,5] This association was replicated in various European cohorts and several studies have been performed trying to identify association between the obesity risk allele and energy intake/expenditure or eating behavior trait.[6–8] However, how *FTO* variants modulate components of the energy balance remains elusive so far. FTO has been recognized as a member of the AlkB-related family of non-haem iron- and 2-oxoglutarate-dependent dioxygenases.[9] These non-heme iron enzymes, which require Fe^{2+} as a cofactor and 2-oxoglutarate and dioxygen as cosubstrates, reverse alkylated DNA and RNA damages by oxidative demethylation.[10–14] *Fto*-deficient mice have been recently described.[15] Homozygous mutant mice are viable but postnatal death occurs frequently and loss of Fto leads to postnatal growth retardation, significant reduction in adipose tissue, and lean body mass.

We ascertained a large Palestinian Arab consanguineous multiplex family in which nine affected individuals presented with a previously unreported polymalformation syndrome (Figure 1A). The study was approved by the supreme Israeli Helsinki Review Board (33/07-08) and informed consent was obtained from all family members. All affected individuals had postnatal growth retardation, microcephaly, severe psychomotor delay, functional brain deficits, and characteristic facial dysmorphism. In some patients, structural brain malformations, cardiac defects, genital anomalies, and cleft palate were also observed (Table 1). Early lethality resulting from intercurrent infection or unidentified cause occurred at 1–30 months of age. Extensive biochemical, metabolic, and genetic analyses failed to diagnose any previously known inherited disorders. Because the pedigree suggested an autosomal-recessive mode of inheritance, we performed a genome-wide autozygosity screen with the Perkin Elmer Biosystems linkage mapping set (version 1) and identified a unique region of shared homozygosity on chromosome 16q12 (Figure S1 available online). Further genotype and haplotype analyses reduced the critical region to a 6.5 Mb interval between loci D16S411 and D16S3140 (maximum LOD score Zmax = 4.16 at $\theta = 0$ at the D16S3136 locus). No other genomic region showed consistent linkage. This genetic interval encompasses 28 genes that were all systematically

[1]INSERM U781 and Département de Génétique, Université Paris Descartes, Hôpital Necker-Enfants Malades, 75015 Paris, France; [2]Department of Medical Genetics, Assaf Harofeh, Medical Center, Zerifin, The Sackler School of Medicine, Tel Aviv University, Tel Aviv 70300, Israel; [3]Institute of Metabolic Science, University of Cambridge, Addenbrooke's Hospital, Cambridge CB2 0QQ, UK; [4]Cancer Research UK London Research Institute, Clare Hall Laboratories, South Mimms, Hertfordshire EN6 3LD, UK; [5]CNRS 8090-Institute of Biology, Pasteur Institute, 59019 Lille, France; [6]Section of Genomic Medicine, Hammersmith Hospital, Imperial College London, London W12 0NN, UK
[7]These authors contributed equally to this work
*Correspondence: laurence.colleaux@inserm.fr
DOI 10.1016/j.ajhg.2009.06.002.

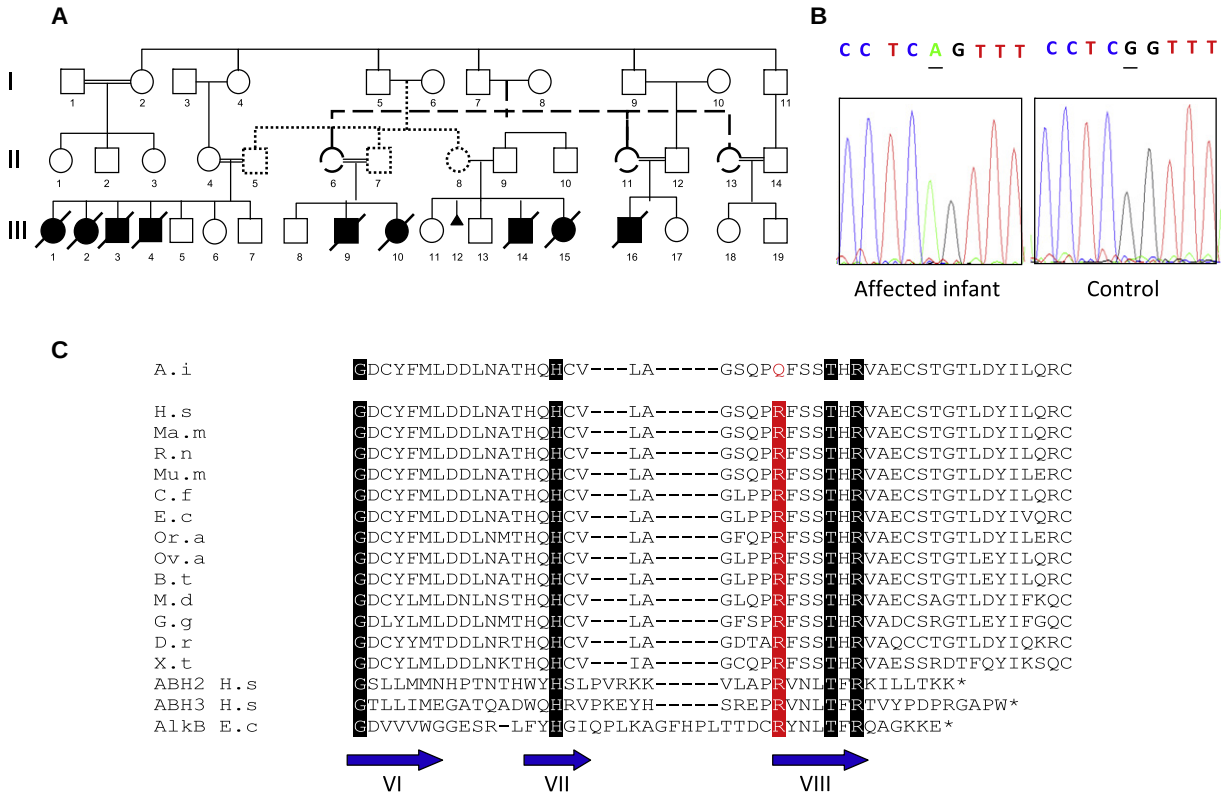

Figure 1. Genetic Analysis of a Family with Ante- and Postnatal Growth Retardation and a Severe Polymalformative Syndrome
(A) Pedigree of the family. Filled symbols and slashes indicate affected and deceased infants.
(B) Electrophoregrams showing the variation of *FTO* gene sequence in an affected infant and a healthy control.
(C) Part of the multiple sequence alignment of FTO representative orthologs (H.s, *Homo sapiens*; Ma.m, *Macaca mulatta*; R.n, *Rattus norvegicus*; Mu.m, *Mus musculus*; C.f, *Canis familiaris*; E.c, *Equus caballus*; Or.a, *Ornithorhynchus anatinus*; Ov.a, *Ovis aries*; B.t, *Bos taurus*; M.d, *Monodelphis domestica*; G.g, *Gallus gallus*; D.r, *Danio rerio*; X.t, *Xenopus tropicalis*; ABH2 H.s, human ABH2; ABH3 H.s, Human ABH3; AlkB E.c, *E. coli* AlkB). The conserved residues are highlighted and the amino acid highlighted in red is the absolutely conserved arginine involved in the R316Q mutation in patients (Ai, affected infant). Blue strands labeled with roman numerals identify three of the eight β strands that form the conserved double-stranded β-helix of the 2OG-oxygenases.

analyzed at both DNA and/or RNA levels (Table S1). We identified a homozygous single-nucleotide variation at cDNA position 947 (c.947G→A) within the *FTO* gene (Figure 1B). The c.947G→A transition predicts a p.R316Q substitution. Notably, this amino acid residue is absolutely conserved across all known FTO paralogs and AlkB orthologs (Figure 1C) and is involved in 2-oxoglutarate coordination by forming stabilizing salt bridges with the carboxylates of this cosubstrate.[9] This variant cosegregated with the disease and was not found in 730 control chromosomes, including 378 chromosomes from individuals of Palestinian Arab origin. We subsequently undertook to estimate the frequency of *FTO* sequence variants within the general population. *FTO* coding exons and intron-exon boundaries sequence was determined in 1492 controls of European descent without overt disease or syndromic features. No nonsense variant was identified and the prevalence of missense variants was 0.87%. In addition, neither homozygous missense mutation nor composite heterozygous mutations were detected in this large series of control subjects (data not shown), further supporting the hypothesis that the R316Q mutation is the disease-causing defect. To estimate the prevalence of *FTO* mutations, 27 unrelated children with partially overlapping clinical features were tested but no mutation in the *FTO* gene was identified, strengthening the idea that the new syndrome described here is a very rare condition.

FTO belongs to the AlkB-related protein family and was shown to localize in the nucleus.[9] Immunofluorescence experiments performed on patient and control fibroblasts demonstrated that the mutation did not affect its nuclear localization (data not shown). Murine and human Fto have been shown to demethylate 3-methylthymine and 3-methyluracil residues in single-stranded DNA and RNA in vitro, albeit with a relatively low efficiency. Fto was less active on the more common forms of methylated DNA base damage, 1-methyladenine and 3-methylcytosine.[9–14,16] Moreover, the recombinant murine Fto protein mutated in the residue corresponding to human R316 amino acid displays a much reduced or absent DNA demethylation activity. To investigate the functional consequences of the R316Q mutation, we tested the catalytic activity of the wild-type and mutant R316Q FTO proteins in vitro. Two different assays were used: the first followed the conversion of the cosubstrate 2-oxoglutarate to succinate and the second monitored the ability of FTO to demethylate

Table 1. Major Clinical Features in Affected Individuals with c.947G→A Mutation in *FTO*

Clinical Features	Number of Patients Presenting the Symptom/Number of Patients Examined
Survival	
Death before 3 years of age	8/8
Build	
Intrauterine growth retardation	3/7
Failure to thrive (severe)	8/8
CNS	
Developmental delay (severe)	8/8
Postnatal microcephaly (severe)	8/8
Hypertonicity	6/6
Hydrocephalus	4/8
Lissencephaly	3/8
Seizures	3/8
Dandy walker malformation	2/8
Brain atrophy	1/8
Heart	
Ventricular septal defect, atrio ventricular defect, atent ductus arteriosus	6/8
Hypertrophic cardiomopathy	4/8
Dysmorphism	
Ante verted nostrils	7/7
Thin vermilion	7/7
Prominent alveolar ridge	6/6
Retrognathia	7/7
Coarse face	7/7
Protruding tongue	3/7
Other	
Short neck	7/7
Cutis marmorata	7/7
Drumstick fingers	6/6
Brachydactyly	6/6
Toenail hypoplasia	6/6
Skull asymmetry	6/6
Neuro sensory deafness	5/5
Weak cry	4/6
Umbilical hernia	4/6
Hypertrophy of labia/genital ambiguity/undescending testis	4/7
Cleft palate/Bifid uvula	3/6
Optic disk abnormality	3/7

Medical information was available from 8/9 patients.

3-methylthymine in DNA. Most 2-oxoglutarate- and Fe^{2+}-dependent dioxygenases slowly catalyze the conversion of 2-oxoglutarate to succinate even in the absence of their prime substrate,[16] and this uncoupled reaction may be stimulated by substrates or their analogs. We optimized conditions to assay the ability of human recombinant FTO protein to convert ^{14}C-2-oxoglutarate to ^{14}C-succinate and found that this activity was stimulated 6- to 8- fold by free 3-methylthymidine (Figure 2A). Other nucleosides such as 1-methyldeoxyadenosine and thymidine or the base 3-methylthymine did not stimulate the activity (data not shown). Interestingly, the R316Q FTO mutant protein had no detectable ability to catalyze the uncoupled reaction and also was not stimulated by 3-methylthymidine (Figure 2A). The ability of FTO to demethylate ^{14}C-labeled 3-methylthymine in single-stranded poly(dT) substrate was assayed by measuring the release of ^{14}C-formaldehyde. The optimum pH for the demethylation of 3-methylthymine in DNA by AlkB, ABH2 (MIM 610602), and ABH3 (MIM 610603) is 6 to 6.5 and this is also the case for human FTO. Wild-type FTO[11,16,17] actively but slowly demethylated this substrate whereas the mutant R316Q protein was inactive in the assay (Figure 2B). The defective activity of FTO, as observed in both assays, is most likely due to the inability of the mutant protein to interact with the cosubstrate 2-oxoglutarate.

To gain insight into the function of the *FTO* gene product and the pathophysiology of the disease, we investigated the expression of *FTO* in human embryos and adult tissues. RT-PCR showed an ubiquitous expression in all fetal and adult tissues tested, as has been observed in mice (data not shown).[18] Human embryo sections were hybridized in situ at stages Carnegie (C)15, 33–36 days postfertilization (dpf) and C18 (44–46 dpf) with antisense probes against *FTO* and sense probes as negative controls. We observed a nearly ubiquitous expression of *FTO*, with higher expression in the central nervous system and the liver. In the heart, the mitral and semilunar valves and the wall of the pulmonary trunk stained as did the ventricular myocardium, and a strong and uniform expression was observed in the developing pituitary and the frontonasal and mandibular mesenchyme (Figure S2). It is worth noting that this wide spatiotemporal pattern of expression is consistent with the broad spectrum of clinical manifestations of the disease (Table 1).

Interestingly, the cultured skin fibroblasts of patient III.15 displayed an altered morphology (including hypertrophy), an increased number of vacuoles and cellular debris (Figure 3A), a reduced life span, and decreased proliferative abilities when compared to controls (Figure 3B). Cellular expression of the senescence-associated β-galactosidase (SA-β-Gal) is thought to be a reliable indicator of the switch mechanism that occurs when cells enter the senescent phenotype.[19] Notably, a significantly elevated number of SA-β-Gal-positive cells, increasing with passage numbers, was found in patient cultured cells compared to passage-matched control fibroblasts (Figure 3C). Although further analyses on skin fibroblasts of additional patients

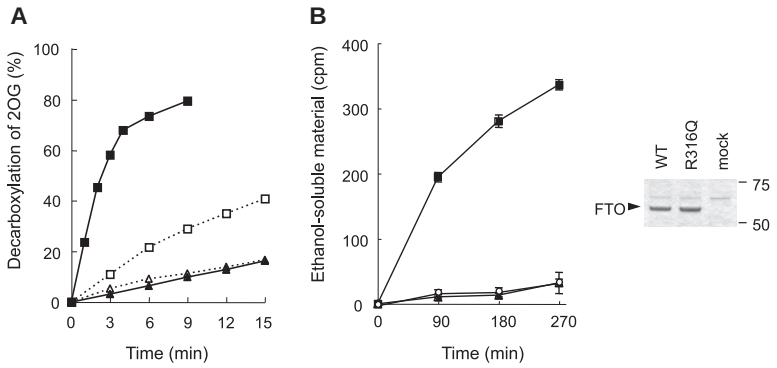

Figure 2. Biochemical Analyses of the Wild-Type and Mutant FTO Proteins

(A) Purified FTO was added to 10 μl reaction mixture containing 50 mM HEPES.KOH (pH 7), 50 μg/ml BSA, 4 mM ascorbate, 75 μM $Fe(NH_4)_2(SO_4)_2$, and 20 μM [5-^{14}C]-2-oxoglutarate (30 mCi/mmol from Moravek Biochemicals) and incubated at 37°C for various times. To measure stimulation of this activity by 3-methylthymidine, 1 mM 3-methylthymidine (Moravek Biochemicals) was included in the assay mix. The reaction was stopped by adding 5 μl stop solution containing 20 mM succinate, 20 mM 2-oxoglutarate followed by 5 μl 160 mM dinitrophenylhydrazine, which precipitates 2-oxoglutarate. This mix was incubated at room temperature for 30 min. An additional 10 μl 1M 2-oxoglutarate was added and incubated for a further 30 min. The precipitate was removed by centrifugation. Clear supernatant (10 μl) was scintillation counted to monitor the ^{14}C-succinate generated. Time course of activity of 1.5 μM FTO: open and closed squares, wild-type FTO protein; open and closed triangles, mutant R316Q FTO protein. Open symbols and dotted line: without 3-methylthymidine; closed symbols and solid line: with 3-methylthymidine (1 mM).

(B) A DNA substrate containing ^{14}C-3-methylthymine was prepared by treating poly(dT) with [^{14}C]-methyl iodide (54 Ci/mmole, Amersham Biosciences) as previously described[11] and had a specific activity of 1580 cpm/μg poly(dT). FTO was added to the ^{14}C-methylated poly(dT) substrate (1000 cpm) in a 100 μl reaction mix containing 50 mM MES-HCl (pH 6), 75 μM $Fe(NH_4)_2(SO_4)_2$, 100 μM 2-oxoglutarate, 2 mM ascorbate, 10 μg/ml bovine serum albumin and incubated at 20°C for various times. All assays were performed in triplicate. To stop the reaction, EDTA was added to a final concentration of 10 mM. The polynucleotide substrate was then ethanol precipitated in the presence of carrier calf thymus DNA. Two-thirds of the ethanol-soluble radioactive material was monitored by scintillation counting. Equal volumes of the protein preparations were assayed. Standard error of the mean is shown for each time point. Closed square, 2 μM wild-type FTO protein; closed triangle, 2 μM mutant R316Q FTO protein; open circle, "mock prep" prepared in the absence of recombinant FTO expression. Equal volumes of the protein preparations were also examined by SDS-10% PAGE.

are necessary to validate these findings, taken together these data could yet suggest that the defective FTO activity may cause premature senescence-like phenotype.

Although repair of alkylated nucleic acid by oxidative demethylation is crucial to maintain genome integrity, no AlkB-related protein mutations have been hitherto identified in human. The results reported here provide therefore the first example of a human disorder related to the defect of an AlkB-related protein. The *Escherichia coli* AlkB protein catalyzes the oxidative demethylation of 1-methyladenine, 3-methylcytosine, and 3-methylthymine in DNA and RNA. Eight mammalian orthologs of AlkB have been previously identified (ABH1 to 8),[20] and FTO is the ninth member of this family. Of this family, only ABH2 and ABH3 have been demonstrated to be highly active in repairing methylation damage to DNA.[13,14] In comparison, ABH1 (MIM 605345) has a modest activity on 3-methylcytosine in single-stranded DNA or RNA[21] whereas FTO has a similar low activity on 3-methylthymine in these substrates.[9,16] Mice lacking either Abh2 or Abh3 have no overt phenotype but the *Abh2*$^{-/-}$ mice accumulate significant levels of 1-methyladenine in their genomes.[22] Notably, *Abh1*$^{-/-}$ mice are viable but have intrauterine growth retardation and defects in placental differentiation.[23]

Surprisingly, although homozygous *Fto*$^{-/-}$ mice have postnatal growth retardation, significant reduction in adipose tissue, and lean body mass, they are not, however, reported to have any developmental abnormalities in the central nervous or cardiovascular systems.[15] Thus, humans homozygous for a catalytically inactive FTO and *Fto* null mice share the growth retardation phenotype but both mutations differ in the impact on development of central nervous and cardiovascular systems. There are several possible reasons for the different findings in our patients versus the *Fto*$^{-/-}$ mouse. First, major phenotypic differences between rodent models and humans harboring identical mutations are well described. For example, maturity-onset diabetes of the young subtype 3 (MODY3 [MIM 600496]) is caused by heterozygous mutations in the transcription factor hepatocyte nuclear factor (*HNF*)-*1α* (MIM 142410).[24] By contrast, mice with heterozygous mutations in *Hnf-1α* gene are phenotypically normal.[25] Second, it is possible that the presence, in the nucleus, of a mutant catalytically inactive FTO might have biochemical consequences over and above that seen with complete deficiency of Fto. These could include toxic "gain-of-function" effects or dominant-negative interference with other related family members. Finally, it is formally possible that the phenotype seen in the human subjects is due to a combination of the mutant FTO and a second, as yet undetected, mutation in the 6 Mb critical region. The fact that no mutations were detected on sequencing of the coding regions and splice junctions of all 28 known and putative genes in that linked region makes the chances of such a second mutation very small.

A cluster of variants located within the first intron of *FTO* has recently been strongly and reproducibly associated with human adiposity.[4,5] Yet, whether these variants influence the risk of obesity directly, via the altered expression of FTO or through other mechanisms, remains questionable. In this regard, it is worth noting that homozygosity for the R316Q FTO mutation caused severe growth retardation. Detailed anthropometric measurements are not available on unaffected family members but, noticeably, none of

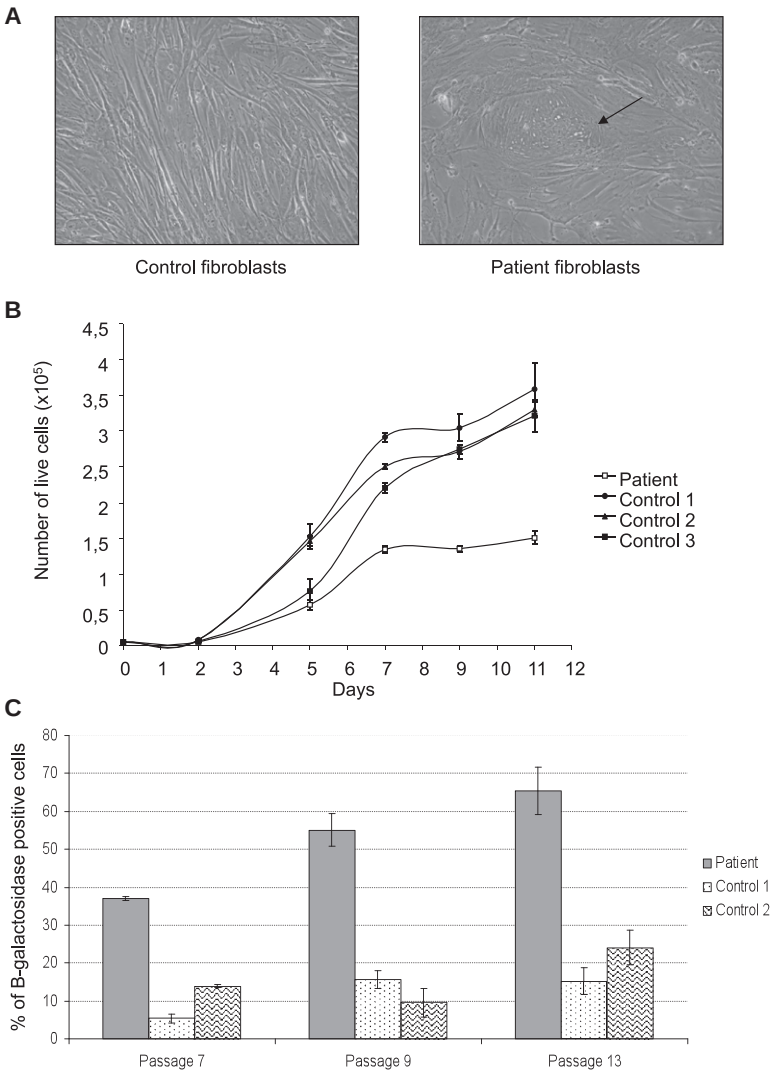

Figure 3. Cell Morphology and Proliferative Abilities of Cultured Skin Fibroblasts Harboring the R316Q *FTO* Mutation

(A) Fibroblast morphology. The arrow shows altered cell morphology and enlarged cell size of a patient fibroblast.

(B) Fibroblast growth curves. Fibroblasts were seeded at a density of 5000 cells/well in 12-well dishes. The number of cells per dish was determined with a CASY cell counter on days 2, 5, 7, 9, and 11 after seeding. Filled and open symbols correspond to patient and control fibroblasts, respectively. Data correspond to the mean of three replicates. Standard error of the mean is shown for each point.

(C) Senescence-associated β-galactosidase assay. Fibroblasts were seeded on 6-well dishes at a density of 130,000 cells/well. Senescent fibroblasts were stained with the Senescence β-Galactosidase Staining Kit (Cell Signaling Technology). Percentages of β-galactosidase-positive cells for passages 7, 9, and 13 were calculated on the basis of approximately 100 cells. Data correspond to the mean of three replicates. Standard error of the mean is shown for each point.

the parents were clinically obese. Given the results from the Fto-deficient mice, it might be hypothesized that humans heterozygous for a loss-of-function mutation in FTO might actually be relatively resistant to becoming obese. Future studies of the body composition of carrier and noncarrier relatives will be required to clarify the relationship between FTO variant heterozygosity and adiposity.

The molecular mechanisms whereby the mutant FTO leads to the severe phenotype observed in our patients remain unknown. The fact that (1) FTO is a member of the Alk-B-related family of dioxygenases, (2) at least two of the mammalian members of this family have established roles in DNA repair, and (3) FTO can demethylate 3-methylthymine in the context of DNA might suggest that FTO plays a role in the maintenance of genome integrity. If that were the case, one could easily understand how FTO defect relates to developmental malformations and the accelerated senescence observed in cultured fibroblasts derived from the patients. However, it should also be pointed out that (1) several members of the mammalian Alk-B-related family have no established role in DNA repair, (2) FTO demethylates 3-methylthymine slowly and inefficiently, suggesting that this is not its true physiological substrate, (3) 3-methylthymine is a very rare lesion in vivo, and (4) defective repair of rare methylated bases in DNA can hardly be related to the striking increase in energy expenditure observed in Fto-deficient mice. Taken together, this suggests that FTO roles in the nucleus are presumably not restricted to DNA repair.

Because of its association with obesity, FTO is currently the subject of intense interest. The finding of obesity resistance in Fto-deficient mice has led to the suggestion that interference with Fto enzymatic function might be a novel and interesting antiobesity therapeutic strategy. The discovery that humans homozygous for an enzymatically inactive mutant form of FTO have multiple congenital abnormalities suggests that any program of research exploring the therapeutic utility of FTO inhibitors should incorporate a particularly careful assessment of teratogenicity and other toxic effects.

Supplemental Data

Supplemental data include two figures and one table and can be found with this article online at http://www.ajhg.org/.

Acknowledgments

We are grateful to the patients for their participation in the study. We acknowledge Jean Philippe Jais for LOD score calculation, Carron Sher for participation to clinical evaluation, Uli Rüther for kindly providing FTO antibodies, Céline Cluzeau for help with western blotting, Peter Robins for purification of FTO protein, and Marcella Ma and Debbie Lyon for additional technical assistance. This study was supported by the Centre National de la Recherche Scientifique, the Agence Nationale de la Recherche, the Région Ile-de-France, EU

FP6 EUGENE2 (LSHM-CT-2004-512013), EC FP6 Marie Curie, the Medical Research Council UK, Cancer Research UK, the Wellcome Trust, and NIHR Cambridge Biomedical Research Centre.

Received: April 27, 2009
Revised: May 29, 2009
Accepted: June 2, 2009
Published online: June 25, 2009

Web Resources

The URLs for data presented herein are as follows:

Ensembl Genome Browser, http://www.ensembl.org/
GenBank, http://www.ncbi.nlm.nih.gov/Genbank/
National Center for Biotechnology Information, http://www.ncbi.nlm.nih.gov/
Online Mendelian Inheritance in Man (OMIM), http://www.ncbi.nlm.nih.gov/Omim/

References

1. Peters, T., Ausmeier, K., and Ruther, U. (1999). Cloning of Fatso (Fto), a novel gene deleted by the Fused toes (Ft) mouse mutation. Mamm. Genome *10*, 983–986.
2. Gotz, K., Briscoe, J., and Ruther, U. (2005). Homozygous Ft embryos are affected in floor plate maintenance and ventral neural tube patterning. Dev. Dyn. *233*, 623–630.
3. Anselme, I., Laclef, C., Lanaud, M., Ruther, U., and Schneider-Maunoury, S. (2007). Defects in brain patterning and head morphogenesis in the mouse mutant Fused toes. Dev. Biol. *304*, 208–220.
4. Frayling, T.M., Timpson, N.J., Weedon, M.N., Zeggini, E., Freathy, R.M., Lindgren, C.M., Perry, J.R., Elliott, K.S., Lango, H., Rayner, N.W., et al. (2007). A common variant in the FTO gene is associated with body mass index and predisposes to childhood and adult obesity. Science *316*, 889–894.
5. Dina, C., Meyre, D., Gallina, S., Durand, E., Korner, A., Jacobson, P., Carlsson, L.M., Kiess, W., Vatin, V., Lecoeur, C., et al. (2007). Variation in FTO contributes to childhood obesity and severe adult obesity. Nat. Genet. *39*, 724–726.
6. Speakman, J.R., Rance, K.A., and Johnstone, A.M. (2008). Polymorphisms of the FTO gene are associated with variation in energy intake, but not energy expenditure. Obesity (Silver Spring) *16*, 1961–1965.
7. Haupt, A., Thamer, C., Staiger, H., Tschritter, O., Kirchhoff, K., Machicao, F., Haring, H.U., Stefan, N., and Fritsche, A. (2009). Variation in the FTO gene influences food intake but not energy expenditure. Exp. Clin. Endocrinol. Diabetes *117*, 194–197.
8. Cecil, J.E., Tavendale, R., Watt, P., Hetherington, M.M., and Palmer, C.N. (2008). An obesity-associated FTO gene variant and increased energy intake in children. N. Engl. J. Med. *359*, 2558–2566.
9. Gerken, T., Girard, C.A., Tung, Y.C., Webby, C.J., Saudek, V., Hewitson, K.S., Yeo, G.S., McDonough, M.A., Cunliffe, S., McNeill, L.A., et al. (2007). The obesity-associated FTO gene encodes a 2-oxoglutarate-dependent nucleic acid demethylase. Science *318*, 1469–1472.
10. Trewick, S.C., Henshaw, T.F., Hausinger, R.P., Lindahl, T., and Sedgwick, B. (2002). Oxidative demethylation by *Escherichia coli* AlkB directly reverts DNA base damage. Nature *419*, 174–178.
11. Koivisto, P., Robins, P., Lindahl, T., and Sedgwick, B. (2004). Demethylation of 3-methylthymine in DNA by bacterial and human DNA dioxygenases. J. Biol. Chem. *279*, 40470–40474.
12. Falnes, P.O., Johansen, R.F., and Seeberg, E. (2002). AlkB-mediated oxidative demethylation reverses DNA damage in *Escherichia coli*. Nature *419*, 178–182.
13. Duncan, T., Trewick, S.C., Koivisto, P., Bates, P.A., Lindahl, T., and Sedgwick, B. (2002). Reversal of DNA alkylation damage by two human dioxygenases. Proc. Natl. Acad. Sci. USA *99*, 16660–16665.
14. Aas, P.A., Otterlei, M., Falnes, P.O., Vagbo, C.B., Skorpen, F., Akbari, M., Sundheim, O., Bjoras, M., Slupphaug, G., Seeberg, E., et al. (2003). Human and bacterial oxidative demethylases repair alkylation damage in both RNA and DNA. Nature *421*, 859–863.
15. Fischer, J., Koch, L., Emmerling, C., Vierkotten, J., Peters, T., Bruning, J.C., and Ruther, U. (2009). Inactivation of the Fto gene protects from obesity. Nature *458*, 894–898.
16. Jia, G., Yang, C.G., Yang, S., Jian, X., Yi, C., Zhou, Z., and He, C. (2008). Oxidative demethylation of 3-methylthymine and 3-methyluracil in single-stranded DNA and RNA by mouse and human FTO. FEBS Lett. *582*, 3313–3319.
17. Kaule, G., and Gunzler, V. (1990). Assay for 2-oxoglutarate decarboxylating enzymes based on the determination of [1–14C]succinate: Application to prolyl 4-hydroxylase. Anal. Biochem. *184*, 291–297.
18. Stratigopoulos, G., Padilla, S.L., LeDuc, C.A., Watson, E., Hattersley, A.T., McCarthy, M.I., Zeltser, L.M., Chung, W.K., and Leibel, R.L. (2008). Regulation of Fto/Ftm gene expression in mice and humans. Am. J. Physiol. Regul. Integr. Comp. Physiol. *294*, R1185–R1196.
19. Dimri, G.P., Lee, X., Basile, G., Acosta, M., Scott, G., Roskelley, C., Medrano, E.E., Linskens, M., Rubelj, I., Pereira-Smith, O., et al. (1995). A biomarker that identifies senescent human cells in culture and in aging skin in vivo. Proc. Natl. Acad. Sci. USA *92*, 9363–9367.
20. Kurowski, M.A., Bhagwat, A.S., Papaj, G., and Bujnicki, J.M. (2003). Phylogenomic identification of five new human homologs of the DNA repair enzyme AlkB. BMC Genomics *4*, 48.
21. Westbye, M.P., Feyzi, E., Aas, P.A., Vagbo, C.B., Talstad, V.A., Kavli, B., Hagen, L., Sundheim, O., Akbari, M., Liabakk, N.B., et al. (2008). Human AlkB homolog 1 is a mitochondrial protein that demethylates 3-methylcytosine in DNA and RNA. J. Biol. Chem. *283*, 25046–25056.
22. Ringvoll, J., Nordstrand, L.M., Vagbo, C.B., Talstad, V., Reite, K., Aas, P.A., Lauritzen, K.H., Liabakk, N.B., Bjork, A., Doughty, R.W., et al. (2006). Repair deficient mice reveal mABH2 as the primary oxidative demethylase for repairing 1meA and 3meC lesions in DNA. EMBO J. *25*, 2189–2198.
23. Pan, Z., Sikandar, S., Witherspoon, M., Dizon, D., Nguyen, T., Benirschke, K., Wiley, C., Vrana, P., and Lipkin, S.M. (2008). Impaired placental trophoblast lineage differentiation in Alkbh1(−/−) mice. Dev. Dyn. *237*, 316–327.
24. Yamagata, K., Oda, N., Kaisaki, P.J., Menzel, S., Furuta, H., Vaxillaire, M., Southam, L., Cox, R.D., Lathrop, G.M., Boriraj, V.V., et al. (1996). Mutations in the hepatocyte nuclear factor-1alpha gene in maturity-onset diabetes of the young (MODY3). Nature *384*, 455–458.
25. Pontoglio, M., Barra, J., Hadchouel, M., Doyen, A., Kress, C., Bach, J.P., Babinet, C., and Yaniv, M. (1996). Hepatocyte nuclear factor 1 inactivation results in hepatic dysfunction, phenylketonuria, and renal Fanconi syndrome. Cell *84*, 575–585.

American Journal of Human Genetics, Volume *85*

Supplemental Data

Loss-of-Function Mutation in the Dioxygenase-Encoding *FTO* Gene Causes Severe Growth Retardation and Multiple Malformations

Sarah Boissel, Orit Reish, Karine Proulx, Hiroko Kawagoe-Takaki, Barbara Sedgwick, Giles S.H. Yeo, David Meyre, Christelle Golzio, Florence Molinari, Noman Kadhom, Heather C. Etchevers, Vladimir Saudek, I. Sadaf Farooqi, Philippe Froguel, Tomas Lindahl, Stephen O'Rahilly, Arnold Munnich, and Laurence Colleaux

Table S1: Positional candidate genes analyzed

				Genomic position		
Gene Name	**Accession number**	**OMIM Number**	**Strand**	**Start**	**End**	**Number of exons**
ZNF423	NM_015069	MIM 604557	-	48082021	48418419	9
TMEM188	NM_153261	-	+	48616689	48628500	7
HEATR3	NM_182922	-	+	48657381	48696876	15
PAPD5	NM_001040284	MIM 605540	+	48745568	48826720	12
ADCY7	NM_001114	MIM 600385	+	48879323	48909544	25
BRD7	NM_013263	-	-	48910441	48960330	18
NKD1	NM_033119	MIM 607851	+	49139741	49226142	10
SNX20	NM_153337	-	-	49257711	49272765	4
NOD2	NM_022162	MIM 605956	+	49288550	49324488	12
CYLD	NM_015247	MIM 605018	+	49333461	49393347	20
TOX3	NM_001146188	MIM 611416	-	51029418	51139215	8
CHD9	NM_025134	-	+	51646445	51918915	39
RBL2	NM_005611	MIM 180203	+	52025851	52083061	22
AKTIP	NM_001012398	MIM 608483	-	52082692	52094671	10
RPGRIP1L	NM_015272	MIM 610937	-	52191318	52295272	27
FTO	NM_001080432	MIM 610966	+	52295375	52705879	9
IRX3	NM_024336	-	-	52874712	52877879	4
IRX5	NM_005853	-	+	53522611	53525896	3
IRX6	NM_024335	MIM 606196	+	53915971	53922173	6
MMP2	NM_004530	MIM 120360	+	54070581	54098087	13
LPCAT2	NM_017839	MIM 612040	+	54100413	54178082	14
CAPNS2	NM_032330	-	+	54158084	54159093	1
SLC6A2	NM_001043	MIM 163970	+	54248056	54295201	14
CES4	NR_003276	-	+	54352011	54366325	6
CES1	NM_001266	MIM 114835	-	54394264	54424576	14
CES7	NM_001143685	-	-	54437566	54466783	13
GNAO1	NM_020988	MIM 139311	+	54782751	54948857	9

Figure S1: Pedigree and haplotype analysis of the family.

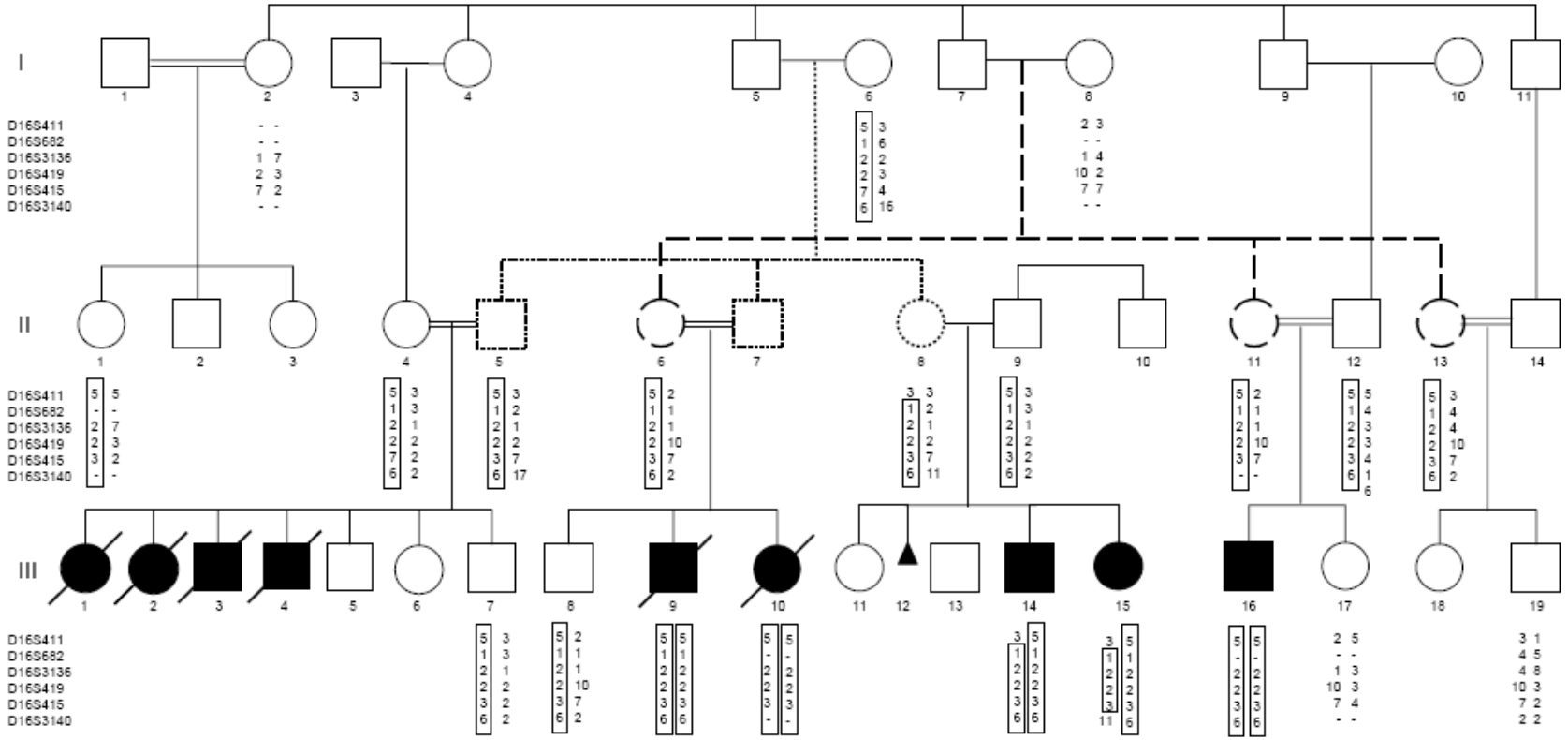

Filled symbols and slashes indicate affected and deceased infants. Haplotypes, based on the CEPH human diversity panel are represented as column numbers. The ancestral disease-associated haplotype is boxed.

Figure S2: Pattern of *FTO* expression in early human development.

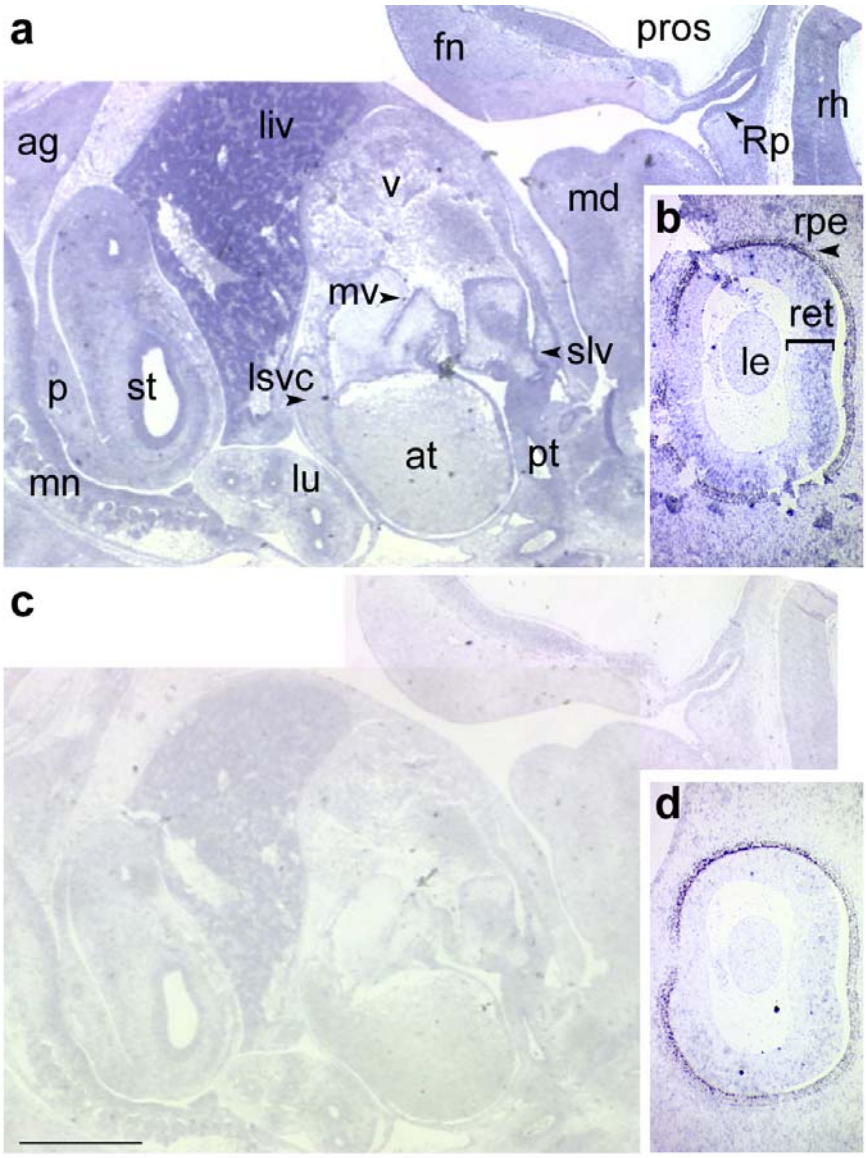

Adjacent sections of human embryos hybridized *in situ* against *FTO* antisense (A,B) and sense (C, D) probes at Carnegie stage 18 (44-46 days post fertilization). *FTO* expression is nearly ubiquitous, with higher signal throughout the central nervous system and the liver than in other tissues. Sections through the eye in A, C are from a distinct embryo from those in B, D. Abbreviations: ag, adrenal gland; at, atrium; fn, frontonasal eminence; le, lens; liv, liver; lsvc, left superior vena cava; lu, lung; md, mandible; mn, mesonephros; mv, mitral valve; p, pancreas; pros, prosencephalon; pt, pulmonary trunk; ret, neurosensorial retina; rh, rhombencephalon; Rp, Rathke's pouch (prospective anterior pituitary); rpe, retinal pigmented epithelium; slv, semilunar valve; st, stomach; v, ventricle. Scale bar: 0.5 mm for A, C and 240 μm for B, D.

European Journal of Medical Genetics xxx (2009) 1–7

Contents lists available at ScienceDirect

European Journal of Medical Genetics

journal homepage: http://www.elsevier.com/locate/ejmg

Refining the clinicopathological pattern of cerebral proliferative glomeruloid vasculopathy (Fowler syndrome): Report of 16 fetal cases

B Bessières-Grattagliano [a], B Foliguet [b], L Devisme [c], L Loeuillet [d], P Marcorelles [e], M Bonnière [f], A Laquerrière [g], C Fallet-Bianco [h], J Martinovic [f], S Zrelli [f,j], N Leticee [i], V Cayrol [i], HC Etchevers [j], M Vekemans [f,j,k], T Attie-Bitach [f,j,k], F Encha-Razavi [f,j,k,*]

Q1

[a] Laboratoire d'Anatomo-Foeto-Pathologie, Institut de Puériculture et de Périnatalogie, Paris, France
[b] Laboratoire de Placentologie et de Fœtopathologie, Maternité Régionale Universitaire, Nancy, France
[c] Pôle de Pathologie, Centre de Biologie Pathologie, Lille, France
[d] Laboratoire d'Anatomie Pathologique CHI de Poissy St-germain-en-Laye, France
[e] Service d'anatomie pathologique, Pole de biologie-pathologie, CHU Brest, France
[f] Service Histologie-Embryologie-Cytogénétique, Hôpital Necker Enfants Malades, Paris, France
[g] Laboratoire d'Anatomie Pathologique, Hôpital de Rouen, Rouen, France
[h] Laboratoire de Neuropathologie, Centre Hospitalier Sainte-Anne, Paris, France
[i] Service de Gynécologie Obstétrique, Hôpital Necker Enfants Malades, Paris, France
[j] INSERM U 781, Hôpital Necker Enfants Malades, Paris, France
[k] Université Paris Descartes, Paris, France

ARTICLE INFO

Article history:
Received 26 June 2009
Accepted 20 July 2009
Available online xxx

Keywords:
Fowler syndrome
Fowler-like syndrome
Hydrocephalus
Fetal akinesia deformation sequence
Hydranencephaly
Vascular malformation
Cerebral proliferative glomeruloid vasculopathy
Congenital malformation

ABSTRACT

Cerebral proliferative glomeruloid vasculopathy (PGV) is a severe disorder of brain angiogenesis, resulting in abnormally thickened and aberrant perforating vessels, forming glomeruloids with inclusion-bearing endothelial cells. This peculiar vascular malformation was delineated by Fowler in 1972 as a stereotyped lethal fetal phenotype associating hydranencephaly–hydrocephaly with limb deformities, called Fowler syndrome (FS) or "proliferative vasculopathy and hydranencephaly-hydrocephaly" or "encephaloclastic proliferative vasculopathy" (OMIM # 2255790). In PGV, the disruptive impact of vascular malformation on the developing central nervous system (CNS) is now well admitted. However, molecular mechanisms of abnormal angiogenesis involving the CNS vasculature exclusively remain unknown, as no genes have been localized nor identified to date.

We observed the pathognomonic FS vascular malformation in 16 fetuses, born to eight families, four consanguineous and four non-consanguineous. A diffuse form of PGV affecting the entire CNS and resulting in classical FS in 14 cases, can be contrasted to two cases with focal forms, confined to restricted territories of the CNS. Interestingly, immunohistological response to a marker of pericytes (SMA, Smooth Muscle Actin), was drastically reduced as compared to a match control.

Our studies has expanded the description of FS to additional phenotypes, that could be called Fowler-like syndromes and suggest that the pathogenesis of PGV may be related to abnormal pericyte-dependent remodelling of the CNS vasculature, during CNS angiogenesis. Gene identification will determine the molecular basis of PGV and will help to know whether the Fowler-like phenotypes are due to the same underlying molecular mechanisms.

1. Introduction

Cerebral proliferative glomeruloid vasculopathy (PGV) is a severe disorder of brain angiogenesis, resulting in abnormally thickened and aberrant perforating vessels, forming glomeruloids with inclusion-bearing endothelial cells. This peculiar vascular malformation was delineated by Fowler in 1972 in relation with a stereotyped lethal fetal phenotype, associating hydranencephaly-hydrocephaly with limb deformities [1]. This association was termed proliferative vasculopathy and hydranencephaly-hydrocephaly (PVHH) or encephaloclastic proliferative vasculopathy (EPV), also called Fowler syndrome (FS) (OMIM#225 790). The disruptive impact of PGV on the developing central nervous system

* Corresponding author. Service Histologie-Embryologie-Cytogénétique, Hôpital Necker Enfants Malades, Paris, France. Tel.: +33 1 44494984; fax: +33 1 71196420.
E-mail address: ferechte.razavi@nck.aphp.fr (F. Encha-Razavi).

1769-7212/$ – see front matter © 2009 Elsevier Ltd. All rights reserved.
doi:10.1016/j.ejmg.2009.07.006

(CNS) is now well acknowledged. However, the mechanism of abnormal angiogenesis that restricts lesions to the CNS vasculature exclusively remains unknown. Moreover, despite recurrence and consanguinity in some cases, no genes have been identified nor localized to date.

FS is considered as rare. Since the first description, only 14 cases have been reported on the basis of histological criteria of PGV [2–10]. In 16 fetuses, born to eight unrelated families, our neuropathological analysis allowed to define the FS pathognomonic vascular malformation. In this series, a diffuse form of EPV, affecting the entire CNS and resulting in classical FS was observed in 14 cases. By contrast in two cases a focal form of EPV was observed. In both forms, response to immunohistological marker of pericytes (SMA, smooth muscle actin) was drastically reduced. Based on our findings, we postulate that EPV may be linked to abnormal remodelling of CNS vasculature due to a possible deficit of pericytes.

2. Material & methods

After routine neuropathological analysis, we identified 16 fetuses with characteristic EPV in eight unrelated families (four consanguineous and four non-consanguineous). Recurrences occurred in five families, in three consanguineous and in two non-consanguineous.

2.1. Clinicopathological study

After parental consent and in conformity with French laws and rules a complete autopsy was performed in each case. It included an external examination, X-rays, photographs, macroscopical and histological examination of viscera. Brain, spinal cord and eyes were studied after fixation in zinc formalin. Paraffin embedded sections were processed for routine histology. Slices of 7 microns thick were stained with hematoxylin and eosin (H&E). In index cases, Periodic acid Schiff (PAS) stain was performed as well as immunostainings using classical methods. Monoclonal antibodies from DakoCytomation against CD34, Smooth Muscle Actin (SMA), and VEGF (Santa Cruz Biotechnology) were used.

3. Results

Our major clinical and neuropathological findings are summarized in Table 1. They are illustrated in composite Fig. 1.

Family I (Ask…): In this family, parents of Turkish origin are first cousins with double consanguinity. They already had a healthy daughter. Malformations occurred in the two following pregnancies.

Fetus 1: Routine ultrasound (US) performed at 16 weeks gestation (WG) disclosed severe hydrocephalus, decreased fetal movements and arthrogryposis, confirmed at 17 WG. Pregnancy termination was performed at 18 WG. The female fetus had a 46,XX karyotype. On the external examination, a mild generalized edema, multiple arthrogryposis with pterygia and muscular hypoplasia were observed. X-rays revealed scoliosis, numerous intracranial calcifications, aberrant and ectopic mineralization of basis cranii. Internal organ examination was unremarkable. Neuropathological examination disclosed massive EPV in the thin walled, fluctuant cerebral hemispheres and hypoplastic brainstem, cerebellum and spinal cord. Optic tracts were thin and contained also vascular proliferation, but no glomeruloid lesions, nor PAS-positive inclusions. Immunostainings using CD34, VEGF antibodies, showed strong positivity in PGV, while SMA compare to an age matched, was weakly and focally positive.

Fetus 2: In this pregnancy, US at 12.5 WG disclosed voluminous hygroma coli and cerebral abnormality. Spontaneous intrauterine fetal death occurred rapidly and led to pregnancy termination at 13.2 WG. The fetus had a normal 46.XX karyotype. On the external examination, the fetus displayed severe arthrogryposis with webs. Despite advanced autolysis, histological screening of the cerebrospinal tissues found characteristic EPV.

Table 1
Major clinical and neuropathological distribution of the PGV. Keys & abreviations: PGV: Proliferative glomeruloid vasculopathy, Cons: Consanguinity, H: Hydrocephalus, FADS: Fetal akinesia deformation sequence.

Cases	Sexe	Cons	H	FADS	Extension of PGV	Severity of PGV
Fam I		+				
Case1	M		+	+	Cerebral & Spinal	+++
Case 2	F		+	+	Cerebral & spinal	
Fam II		+				
Case 3	F		+	+	Cerebral & Spinal	
Case 4	F		+	+	Cerebral & Spinal	+++
Case 5	M		+	+	Cerebral & spinal	
Fam III		–				
Case 6	M		+	+	Cerebral & Spinal	
Case 7	M		+	+	Cerebral & Spinal	+++
Case 8	F		+	+	Cerebral & Spinal	
Fam IV		–				
Case 9	F		+	–	Cerebral	++
Case 10	M		+	–	Cerebral	++
Fam V		+				
Case 11	M		+	+	Cerebral & Spinal	+++
Case 12	F		+	+	Cerebral & Spinal	+++
Fam VI		–				
Case 13	F		+	+	Cerebral & Spinal	+++
Case 14	F		+	+	Cerebral & Spinal	+++
Fam VII		–				
Case 15	F		+	+	Cerebral & Spinal	+++
Fam VIII		–				
Case 16	M		+	+	Cerebral & Spinal	+++

Family II (Bos…): In this Turkish family parents were distantly related. They had two healthy children (boy and girl), and three affected fetuses.

Fetus 3: The pregnancy was terminated at 22 WG for limb malformations and cystic hygroma. The female fetus had in addition to cystic hygroma, severe arthrogryposis of four limbs with pterygia. Karyotype was not performed. Postmortem study was restricted to neuropathological analysis. It disclosed fluctuant cerebral hemispheres and massive EPV involving also the brainstem, the cerebellum and the spinal cord.

Fetus 4: Pregnancy was terminated at 14 WG for recurrence of fetal malformations. The female fetus had macrocrania, cervical hygroma, arthrogryposis of four limbs with pterygia and cleft palate. Neuropathological study disclosed fluctuant cerebral hemispheres reduced to 2 mm. Histology of the cerebral and cerebellar specimen and of the spinal cord disclosed diffuse EPV.

Fetus 5: Recurrence of fetal akinesia with hydrocephalus led to pregnancy termination at 21 WG. The male fetus had generalized oedema with macrocrania and arthrogryposis of four limbs with large cleft palate. X-rays showed diffuse intracranial calcifications. Neuropathological analysis linked the hydrocephalus to severe EPV involving the entire CNS.

Family III (Lec…): This consanguineous family (consanguinity1/32) underwent three terminations of pregnancy for fetal hydrocephalus and limb deformations, one early miscarriage and one spontaneous unexplained fetal at 20 WG and a pregnancy with delivery of a normal girl.

Fetus 6: This first pregnancy was terminated at 20 WG for major hydrocephalus disclosed on US. The male fetus had normal 46,XY karyotype and presented with macrocrania, severe arthrogryposis of the four limbs and microretrognathism. Neuropathological study

Please cite this article in press as: B Bessières-Grattagliano et al., Refining the clinicopathological pattern of cerebral proliferative glomeruloid..., European Journal of Medical Genetics (2009), doi:10.1016/j.ejmg.2009.07.006

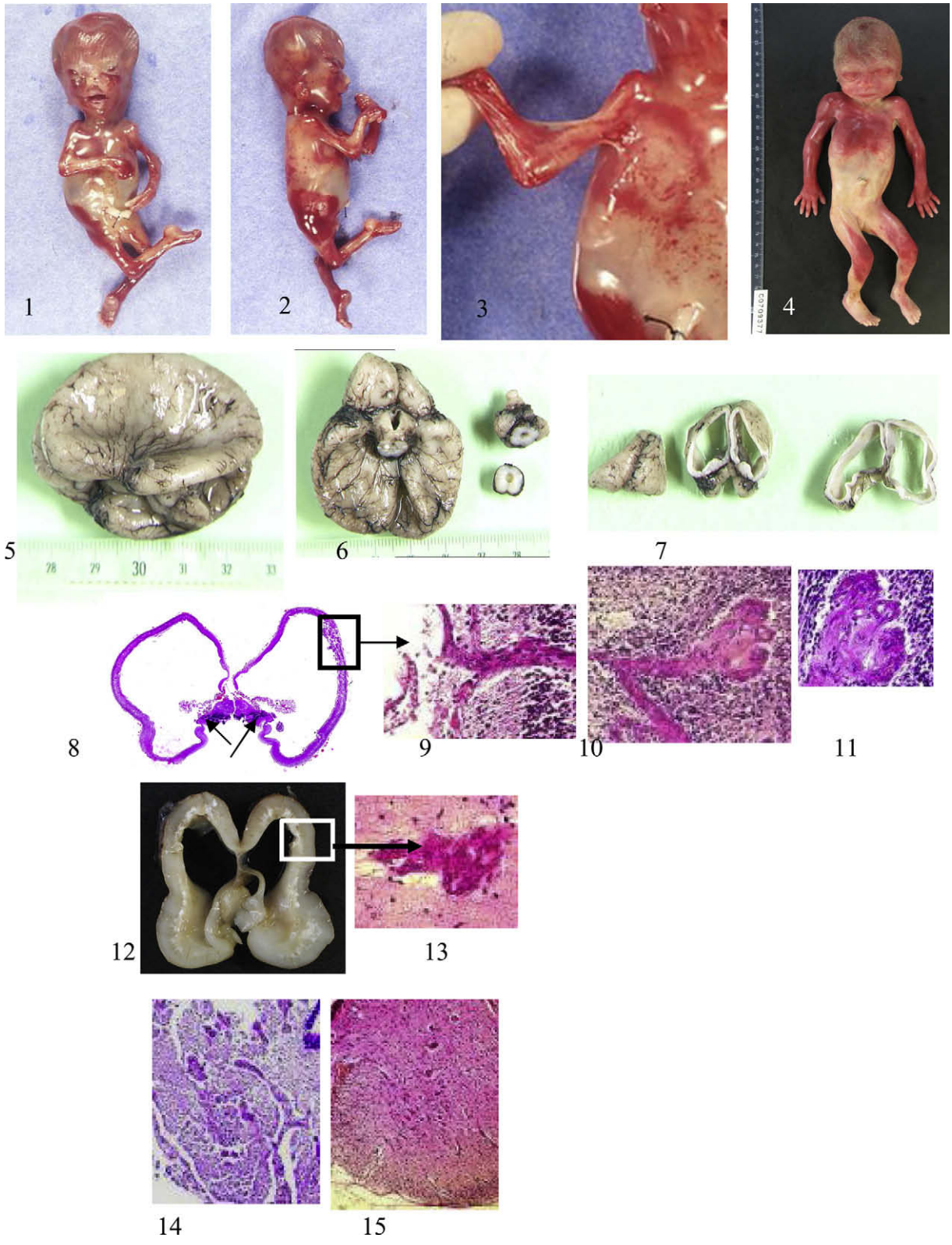

Fig. 1. 1, **2**, **3**. External features of fetus 1: note macrocrania and severe akinesia deformation sequence and palmure. **4**. External features of fetus 9: note isolated macrocrania without arthrogryposis. **5**, **6**, **7**, **8**. Neuropathological findings in case 15: Lateral and basal view and coronal sections of the dilated cerebral hemispheres, showing on the transversal section of the brainstem a dilated acqueduct of Sylvius, surrounded by whitish calcification. Note the lamination of cerebral wall and calcifications of the basal ganglia (arrows).**9**, **10**, **11**. Histological appearance of PGV in case 15 (H&E) at low and higher magnifications : Note the thickened perforating cerebral vessels, ending in glomeruloid formations, devoid of recognizable lumina. **12**, **13**. Neuropathological findings in fetus 9: Coronal section of cerebral hemispheres, showing ventricular enlargement and periventricular calcifications, with characteristic PGV (H&E). **14**, **15**. Transversal section of the spinal cords (H&E) showing compare to fetus 9 with a well preserved spinal cord, the chaotic organisation with PGV found in fetus 15.

Please cite this article in press as: B Bessières-Grattagliano et al., Refining the clinicopathological pattern of cerebral proliferative glomeruloid..., European Journal of Medical Genetics (2009), doi:10.1016/j.ejmg.2009.07.006

confirmed hydrocephalus and disclosed severe EGV, involving the supra and infratentorial levels. The spinal cord was not examined. Immunostainings against CD34 showed strong positivity, while anti-SMA was negative.

Fetus 7: Diagnosis by US of recurrence of hydrocephalus led to pregnancy termination at 15 WG and 6 days. The male fetus had normal 46,XY karyotype, macrocrania and deformations of the four limbs. Neuropathological examination found a cerebral mantle reduced to 2 mm. Characteristic EPG was identified throughout the cerebral hemispheres, the brainstem and the cerebellum. The spinal cord was not examined.

Fetus 8: This 7th pregnancy was terminated at 18 WG and 6 days for hydrocephalus and limb deformations. The female fetus had macrocrania, microretrognathism and four limbs arthrogryposis, without cleft palate. Neuropathological examination confirmed severe hydrocephalus and found diffuse EPV at the supra- and infratentorial levels and in the spinal cord. Eyes were normal.

Family IV (Thu…): This non-consanguineous family had a spontaneous miscarriage between two pregnancy terminations for fetal abnormalities.

Fetuse 9: US performed at 17 WG and 4 days, for toxoplasmosis seroconversion, disclosed a large 4th cerebral ventricle and a small cerebellar vermis. At 22 WG, US found moderate tetraventricular dilatation, short corpus callosum, basal ganglia calcifications and a small cerebellum. It led to pregnancy termination at 23 WG. The female fetus had normal 46,XX karyotype, microretrognathism and a small nose with asymmetric ears, abnormal pulmonary lobulation and unique ombilical artery. He had no limb deformations. Neuropathological examination founds characteristic EPV affecting the supra and infratentorial levels. Surprisingly, the spinal cord examined at the cervical level was well organised, and devoid of vascular malformation. Immunostainings using anti-CD34 confirmed the endothelial nature of proliferating cells. The SMA was weakly and focally positive. Infectious assessment (toxoplasmosis) was negative.

Fetus 10: US found the recurrence of hydrocephalus at 18 WG. A termination of pregnancy was performed at 22 WG. The male fetus had mild facial dymorphism and no limb contractures. Neuropathological study disclosed characteristic EPV involving the cerebral hemispheres, the brainstem and the cerebellum. The spinal cord was spared.

Family V (Gas…): In this family, the parents of Moroccan extraction are first cousins with double consanguinity. They have three healthy children and underwent two pregnancy terminations for fetal malformations.

Fetus 11: This first pregnancy was terminated at 15WG for generalized edema, cervical hygroma and hydrocephalus. X-rays showed advanced bone maturation with intracranial calcifications. The male fetus had a normal 46,XY karyotype. A severe sequence of fetal akinesia with enlarged neck, retrognathism, cleft palate, arthrogryposis of the four limbs, pterygia and muscle hypoplasia were found. Except for mild ascitis, autopsy was unremarkable. Neuropathological examination founds in the cerebral hemispheres diffuse EPV affecting also in the brainstem, the cerebellum and the spinal cord.

Fetus 12: This fifth pregnancy was terminated at 12WG for generalized edema, cervical hygroma and hydrocephalus. X-rays showed advanced bone maturation with intracranial calcifications. The female fetus had normal 46,XX karyotype. On external examination, a severe sequence of fetal akinesia with enlarged neck, retrognathism and cleft palate, arthrogryposis of the four limbs, pterygia and muscular hypoplasia were found. Autopsy was otherwise unremarkable. Neuropathological examination showed dilated cerebral hemispheres and diffuses EPV.

Family VI (Mar…). This non-consanguineous family underwent two pregnancy terminations for fetal abnormalities.

Fetus 13: Pregnancy termination was obtained for severe hydrocephalus disclosed by US at 16WG. The female fetus had macrocrania with a severe fetal akinesia deformation sequence. It was characterized by arthrogryposis with pterygia of four limbs, a small jaw and cleft palate. X-rays were unremarkable. Except for gut malrotation, autopsy was unremarkable. Neuropatholgical evaluation found severe hydocephalus and major cerebral mantle lamination reduced to 1 mm. Histology disclosed characteristic EPV affecting the supra- and infratentorial structures and the spinal cord. Immunostaining using antisera against CD34 confirmed the endothelial nature of proliferating cells and showed punctuate expression of VEGF, SMA was negative.

Fetus 14. Recurrence of brain malformation found on US led to pregnancy termination at 14 WG. The female fetus had macrocrania and limb contracture with pterygia. Autopsy was unremarkable. Neuropathological examination disclosed a thin cerebral wall containing characteristic EPV, also found at the infratentorial levels and in the spinal cord.

Family VII (Hou…): In this non-consanguineous family, pregnancy was terminated at 18WG for severe hydrocephalus and cerebellar hypoplasia disclosed on routine US.

Fetus 15: The female fetus had cervical edema, macrocrania and arthrogryposis of four limbs, with pterygia and muscular hypoplasia. No cleft palate was found. X-rays showed diffuse intracranial calcifications. At autopsy, internal organs were unremarkable. Neuropathological study disclosed major tetraventicular dilatation, and characteristic EPV at all examined levels, including the spinal cord. The optic tracts contained thickened vessels without glomeruloids. Muscles showed neurogenic atrophy. The superficial layer of leptomeningeal vessels was unremarkable. Immunostaining using CD34 confirmed the endothelial nature of proliferating cells in PGV, but anti-VEGF was negative. Immunostaining against SMA was drastically reduced in PGV, while it was positive in the arachnoidal vessels (internal control).

Family VIII (Laq…): In this non-consanguineous family, US examination performed at 22 WG revealed hydrocephalus and ascites. Fetal death occurred and led to pregnancy termination at 23 WG. Karyotype was not carried out.

Fetus 16: The macerated male fetus presented with massive skin edema, macrocrania, deformations of the upper and lower extremities. Autopsy found bilateral pleural effusion, ascites and bilateral adrenal hypoplasia (0.2 g, $N = 0.90$ at 23 WG). No visceral abnormalities were observed. Neuropathological examination disclosed a thin cerebral mantle, of less than 1 mm, fulfilled with characteristic EPV. PGV was also found on the infratentorial samples. The spinal cord was not evaluated. Intracytoplasmic PAS-positive inclusions were observed in some endothelial cells. Immunmarkers were positive for CD34 but negative with VEGF SMA.

4. Discussion

Cerebral proliferative glomeruloid vasculopathy (PGV) is a severe vascular malformation affecting perforating vessels of the developing central nervous system (CNS) exclusively. Classically, visceral vasculature is not involved. This peculiar vascular malformation also called encephaloclastic prolifrative vasculopathy (EPV) is pathognomonic for the syndrome of proliferative vasculopathy and hydranencephaly-hydrocephalus (PVH) or Fowler syndrome (FS) (OMIM#225 790). The etiopathogenesis of PGV is unknown. No gene have been mapped nor identified to date. The present neuropathological and molecular analysis of a series of 16 fetuses expands the spectrum of FS to new phenotypes and mapped the disease locus. It also links this peculiar malformation to a possible deficit of pericytes, an important actor of vascular remodelling during brain angiogenesis.

Please cite this article in press as: B Bessières-Grattagliano et al., Refining the clinicopathological pattern of cerebral proliferative glomeruloid..., European Journal of Medical Genetics (2009), doi:10.1016/j.ejmg.2009.07.006

The diagnosis of cerebral PGV is histological. It relies on the identification of bundles of thick vessels of variable shape with abnormal orientation, running horizontally or vertically between glomeruloid formations, containing enlarged inclusion-bearing (usually PAS-positive) endothelial cells [1–4]. Immunocytological studies support the endothelial nature of proliferating cells [4]. Using electron microscopy, these inclusions have been described as highly variable in size, enclosed within a single membrane, coated externally by ribosomes, and interpreted as dilated rough endoplasmic reticulum [4]. Inclusions are localised within cells just external to the endothelium, possibly in pericytes [1].

Our analysis of cerebral vasculature in PGV shows that the normal thin walled leptomeningeal superficial vascular channels are followed by a deeper sheet of thickened vessels, some containing PAS-positive bodies. In the brain parenchyma, the wall of abnormal vessels contained enlarged, spumous, CD34-positive endothelial cells. VEGF was variously positive. In PGV, the most striking abnormality, best seen in the glomeruloids, is the lack of a single vascular lumina, replaced by multiple small microcavities, containing few red blood cells. Interestingly, immunostaining against smooth muscle actin (SMA), a marker of pericytes (and vascular smooth muscle in larger vessels), was drastically reduced in PGV, while it was normally expressed in the normal superficial leptomeningeal vasculature (used as an internal control) and in age matched controls.

PAS stain showed intracytoplasmic PAS-positive endothelial cells in PGV and in the emerging perforating vessels of deep leptomeningeal vessels. In addition in PGV, PAS showed a thickened vascular basement membrane.

PGV is considered to be pathognomonic for the familial, lethal syndrome of hydranencephaly-hydrocephaly and limb contractures, identified by Fowler in 1972, in two of five female affected siblings (Fowler et al., 1972) [1]. Fowler syndrome (FS) is considered to be rare, but its frequency is probably underestimated because of early fetal lethality, retention and autolysis, making postmortem identification of PGV a challenge. On the basis of histological criteria, since Fowler's first description, 14 other cases have been documented to date in the literature [2–10]. We report clinicopathological data and molecular findings in a series of 16 fetal FS, collected on the basis of neuropathological criteria.

4.1. Pathogenesis of PGV

Primitive embryonic vessels including those of the head and hematopoietic cells differentiate during vasculogenesis [11]. Endothelial precursors first migrate from the splanchnopleuric mesoderm into the head to form through vasculogenesis a capillary-like, perineural vascular plexus, which surrounds the forming brain as it grows. Definitive blood vessels, including those of the CNS, are formed by angiogenesis [12]. Angiogenesis is a distinct mechanism which permits the extension and formation of a mature vasculature, by sprouting from pre-existing vessels. Robust endothelial proliferation accompanies vascular sprouting. Naked capillaries first sprout from the pial face and penetrate the thickening neurectoderm. Vascular branching is followed by maturation and remodelling, which consist in lumen formation, contact with astrocytic processes and, sometimes, regression. The network then matures in part thanks to the accrual of leptomeningeal pericytes derived from the neural crest in the forebrain, but from the mesoderm in the rest of the CNS [11,13,14].

Angiogenesis requires interactions of endothelial cells with the extracellular matrix as well as cross-talk with intimately associated support cells, known as pericytes [12]. Pericytes are essential for capillary stabilisation and remodelling during brain angiogenesis. [15]. In the brain parenchyma pericytes in addition become important partners in establishing the blood–brain barrier. These multipotent cells can inhibit endothelial proliferation *in vitro* and are thought to be the major mediators of blood vessel growth *in vivo*, in part through the activity of the VEGF-related platelet-derived growth factor (PDGF) family [16]. Exogenous VEGF can disrupt pericytic coverage of blood vessels by inactivating the principal pericytic PDGF receptor. This experimental imbalance between the VEGF-A and PDGF signals perceived by endothelial cells and pericytes can lead to reduced angiogenesis [17]. Surgical removal of the neural crest source of forebrain pericytes and leptomeninges also leads to regression of the perineural vascular plexus and severe embryonic neurodegeneration [14,18]. Targeting only the pericyte population has not yet been performed in animal models. The closest equivalent has been the careful examination of PDGF-B^{-} and PDGFR-β^{-} null mouse embryos [19]. These endothelial cells undergo uncontrolled hyperplasia, leading to increased capillary diameters and microaneurysms. However, vessel branching and length were unaffected by the knockout of the cognate ligand or receptor. In PGV, the low endothelial expression of VEGF is concordant with the slowdown of endothelial cell proliferation. Some zones of endothelial cells can be seen to express actively VEGF. This is consistent with a known autocrine signalling role [20].

A striking lack of SMA immunostaining in our patients, relative to internal controls and age-matched cases, suggests a deficit in pericytes, but it is unclear whether this absence is causative or secondary. It is evocative that all pericytes of the telencephalon have a distinct neural crest cell origin [13]. The focal cases of PGV we observed had a regionally restricted distribution that may be linked to this particular pericyte lineage [21]. Either all or subpopulations of pericytes may be susceptible to a molecular defect that solely affects their coverage of intraparenchymal CNS vessels. We have observed that PGV concerns only the perforating vessels of the CNS, while the superficial arachnoid and other blood vessels appear unaffected. Concordantly, SMA was found in the external vascular walls within leptomeninges, while it was drastically reduced in the PGV within the CNS. A total or partial absence of pericytes on vessels in territories of the primitive neural tube appears to correlate with diffuse or focal forms of PGV, respectively. Further studies or identification of a responsible gene should elucidate whether the pericytic defect we observe is the primary cause or an effect in this disease.

4.2. Clinicopathological phenotypes

A diffuse and severe form of PGV, affecting the entire CNS and resulting in classical FS is found in 14 fetuses of our series. In contrast two cases with focal forms had authentic PGV, confined to restricted territories of the CNS.

In the diffuse forms of PGV, fetuses displayed hydranencephaly-hydrocephalus with a severe phenotype of fetal akinesia deformation sequence (FADS), also known under the umbrella terms "Lethal Multiple Pterygium syndromes" (LMPS) or "Lethal Congenital Contracture syndromes" (LCCS). These are not syndromes, but various degrees of a sequence of fetal akinesia, regardless of its mechanism, which can be myogenic or neurogenic. In neurogenic-FADS (N-FADS), the common denominator is a deficit of spinal motor neurons due to primary neurodegeneration or secondary to perfusion failure. Depending on the extension of motor neuron deficit, lack of movement affects large and/or small joints and leads to a diffuse or partial arthrogryposis. The early onset of akinesia results in joint webbing. The motor neurons of the brainstem may be also affected. Depending on the timing, lesions of the hypoglossal nuclei (XII^{th} cranial nerve) may mechanically impair palatal shelf fusion before 10 weeks' gestation and later on, fetal swallowing, resulting in cleft palate and polyhydramnios. Lack of movement explains also skin edema, serosal effusion ascites and bone hypoplasia.

In our diffuse forms of PGV, fetuses presented with hydranencephaly-hydrocephalus and severe FADS. This association found

Please cite this article in press as: B Bessières-Grattagliano et al., Refining the clinicopathological pattern of cerebral proliferative glomeruloid..., European Journal of Medical Genetics (2009), doi:10.1016/j.ejmg.2009.07.006

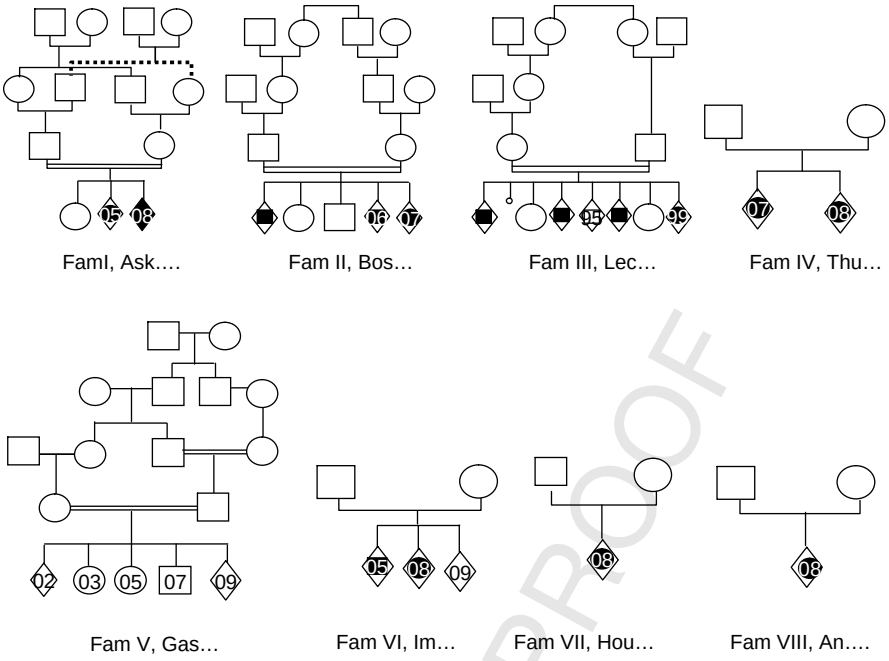

Fig. 2. Pedigrees of families.

in 14 of the 16 cases, remains the most frequent autopsy findings in histologically confirmed PGV. In all cases examined, the cerebral mantle was reduced to a thin band, containing nests of immature cells, intermingled with large calcifications between bundles of vertically and horizontally oriented channels of thickened vessels and glomeruloid bodies. Ganglionic eminences and basal ganglia were also involved. No fibres or tracts were identifiable, suggesting the precocity of lesions. The brainstem contained PGV with numerous calcifications. In the cerebellum, PGV makes foliation and lamination chaotic. The ependymal sheet was destroyed all over the ventricular system. PGV was also found in the chaotic spinal cord. In family I, the recurrence of PGV in the brain and the spinal cord could be confirmed on histological examination, despite fetal death and autolysis. Cerebellar lesions may mimic a Dandy-Walker malformation phenotype, as in our first case [2,10].

Interestingly, in both fetuses of family IV we found a focal form of PGV confined to restricted territories of CNS. In this family, both affected fetuses had hydrocephalus without limb deformities. Authentic PGV was found exclusively in the cerebral mantle, in the brainstem and the cerebellum, while the spinal cord well preserved. Most studies on FS focus on the association of hydranencephaly/hydrocephaly with polyhydramnios and FADS. Focal forms of PGV have been mentioned in the literature but received little attention. In particular, polyhydramnios and hydrocephalus without FADS is reported in association with characteristic PGV [2,6,10]. Because of the lack of limb deformity, one might assume that the spinal cord although not examined has been spared by the vascular malformation. These cases that could be called Fowler-like phenotypes raise the question of the lesional spectrum of PGV and its genetic heterogeneity.

Despite recurrence and consanguinity in FS, no gene has been mapped nor identified to date. An excess of female was noticed in the first reported cases. However, consanguinity and reports on affected males (7 males over 16 cases in our series) are concordant with recessive autosomal inheritance.

In order to conduct a genetic study it is necessary to identify PGV through a histological study. Our neuropathological examination allowed to establish a series of 16 affected fetuses, born to eight families. Among them, four families were consanguineous. Each had at least two fetuses affected with a diffuse form of PGV. A genome wide linkage scan was performed in consanguineous families I–IV (see Fig. 2 pedigrees), using an Affymetrix 250K SNP chip. This points to two an unique homozygous region of 13 MB was. Gene identification will determine the molecular basis of PGV and will help to know whether the Fowler-like phenotypes are due to the same underlying molecular mechanism.

Acknowledgement

Authors whish to thank Dr V. Hennequin and Dr Alain Miton from Maternité Régionale de Nancy for prenatal screenings in family II and Chantal Esculpavit for technical assistance.

References

[1] M. Fowler, R. Dow, T.A. White, C.H. Greer, Congenital hydrocephalus-hydranencephaly in five siblings with autopsy studies: a new disease, Dev. Med. Child. Neurol. 14 (1972) 173–188.
[2] C. Harper, A. Hockey, Proliferative vasculopathy and an hydranencephalic hydrocephalic syndrome: a neuropathological study of two siblings, Dev. Med. Child. Neurol. 25 (1983) 23–244.
[3] M.G. Norman, B. McGillivray, Fetal neuropathology of proliferative vasculopathy and hydranencephaly-hydrocephaly with multiple limb pterygia, Ped Neurosc 14 (1988) 301–306.
[4] J.B. Moeschler, M. Martin-Padilla, Autosomal recessive encephaloclastic proliferative vasculopathy (hydrocephaly/hydranencepahly) (Abstr), Am. J. Hum. Genet. 45 (Suppl) (1989) A55.
[5] B.N. Harding, P. Ramani, P. Thurley, The familial syndrome of proliferative vasculopathy and hydranencephaly-hydrocephaly: immunohistochemical and ultrastructural evidence for endothelial proliferation, Neuropathol. Appl. Neurobiol. 236 (25) (1995) 61–67.
[6] M. Castro-Gago, E. Pintos-Martinez, J. Forteza-Vila, Congenital hydranencephalic hydrocephalic syndrome with proliferative vasculopathy: a possible relation with mitochondrial dysfunction, J. Child. Neurol. 16 (2001) 858–862.
[7] I. Witters, P. Moerman, K. Devriendt, P. Braet, D. Van Schoubroeck, F.A. Van Assche, J.P. Fryns, Two siblings with early onset fetal autosomal recessive inheritance of hydranencephaly, Fowler type, Am. J. Med. Genet. 108 (2002) 41–44.
[8] H. Laurichesse-Delmas, A.M. Beaufrere, A. Martin, et al., First-trimester features of Fowler syndrome (hydrocephaly-hydranencephaly proliferative vasculopathy) 244, Ultrasound Obstet. Gynecol. 20 (2002) 612–615.

[9] A. Ibrahim, P. Murthy, A.S. Arunkalaivanan, A case of recurrent first-trimester Fowler syndrome, J. Obstet. Gynaecol. 27 (2007) 201–202.
[10] M. Al-Adnani, L. Kiho, I. Scheimberg, Fowler syndrome presenting as a dandy-walker malformation: a second case report, Pediatr. Dev. Pathol. 12 (1) (2009 Jan–Feb) 68–72.
[11] G. Couly, P. Coltey, A. Eichmann, N.M. Le Douarin, The angiogenic potentials of the cephalic mesoderm and the origin of brain and head blood vessels, Mech. Dev. 53 (1995) 97–112.
[12] K.H. Plate, Mechanisms of angiogenesis in the brain, Jl Neuropathol. Exp. Neurol. 58 (1999) 313–320.
[13] C.S. Le Lièvre, N.M. Le Douarin, Mesenchymal derivatives of the neural crest: analysis of chimaeric quail and chick embryos, J. Embryol. Exp. Morphol. 34 (1) (1975 Aug) 125–154.
[14] H.C. Etchevers, G. Couly, C. Vincent, N.M. Le Douarin, Anterior cephalic neural crest is required for forebrain viability, Development 126 (16) (1999 Aug) 3533–3543.
[15] J. Folkman, P.A. D'Amore, Blood vessel formation: what is its molecular basis? Cell 87 (7) (1996 Dec 27) 1153–1155 (Review. No abstract available).
[16] M. Crisan, J. Huard, B. Zheng, B. Sun, S. Yap, A. Logar, J.P. Giacobino, L. Casteilla, B. Péault, Purification and culture of human blood vessel-associated progenitor cells, Curr. Protoc. Stem Cell Biol. (2008 Mar) [chapter 2]:Unit 2B.2.1–2B.2.13.
[17] J.I. Greenberg, A. Suliman, S. Barillas, N. Angle, Mouse models of ischemic angiogenesis and ischemia-reperfusion injury, Methods Enzymol 444 (2008) 159–174 [chapter 7].
[18] S. Creuzet, B. Schuler, G. Couly, N.M. Le Douarin, Reciprocsal relationships between Fgf8 and neural crest cells in facial and forebrain development, Proc. Natl. Acad. Sci. U.S.A. 101 (14) (2004 Apr 6) 4843–4847 Epub 2004 Mar 23.
[19] M. Hellström, H. Gerhardt, M. Kalén, X. Li, U. Eriksson, H. Wolburg, C. Betsholtz, Lack of pericytes leads to endothelial hyperplasia and abnormal vascular morphogenesis, J. Cell Biol. 153 (3) (2001 Apr 30) 543–553.
[20] J.C. Tille, J. Wood, S.J. Mandriota, C. Schnell, S. Ferrari, J. Mestan, Z. Zhu, L. Witte, M.S. Pepper, Vascular endothelial growth factor (VEGF) receptor-2 antagonists inhibit VEGF-and basic fibroblast growth factor-induced angiogenesis in vivo and in vitro, J. Pharmacol. Exp. Ther. 299 (3) (2001 Dec) 1073–1085.
[21] H.C. Etchevers, C. Vincent, N.M. Le Douarin, G.F. Couly, The cephalic neural crest provides pericytes and smooth muscle cells to all blood vessels of the face and forebrain, Development 128 (7) (2001 Apr) 1059–1068.

Please cite this article in press as: B Bessières-Grattagliano et al., Refining the clinicopathological pattern of cerebral proliferative glomeruloid..., European Journal of Medical Genetics (2009), doi:10.1016/j.ejmg.2009.07.006

Supporting Information

de Pontual et al. 10.1073/pnas.0901219106

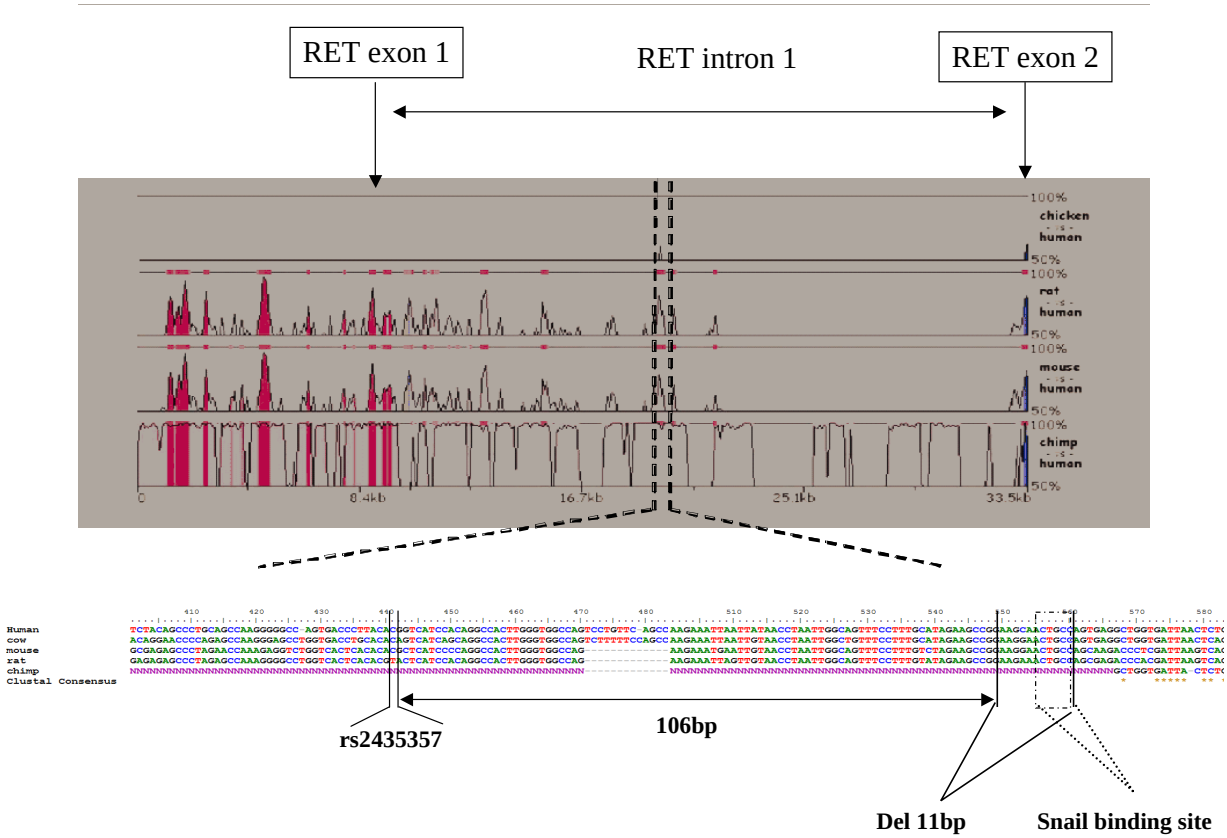

Fig. S1. Considering the rs2435357 SNP lying in intron one of the *RET* gene, the T allele is the hypomorphic Hirschsprung disease (HSCR) predisposing *RET* allele, and the C is the WT type allele. del, the (AAGCAACTGCC) 11-bp deletion identified in intron 1 of *RET* gene.

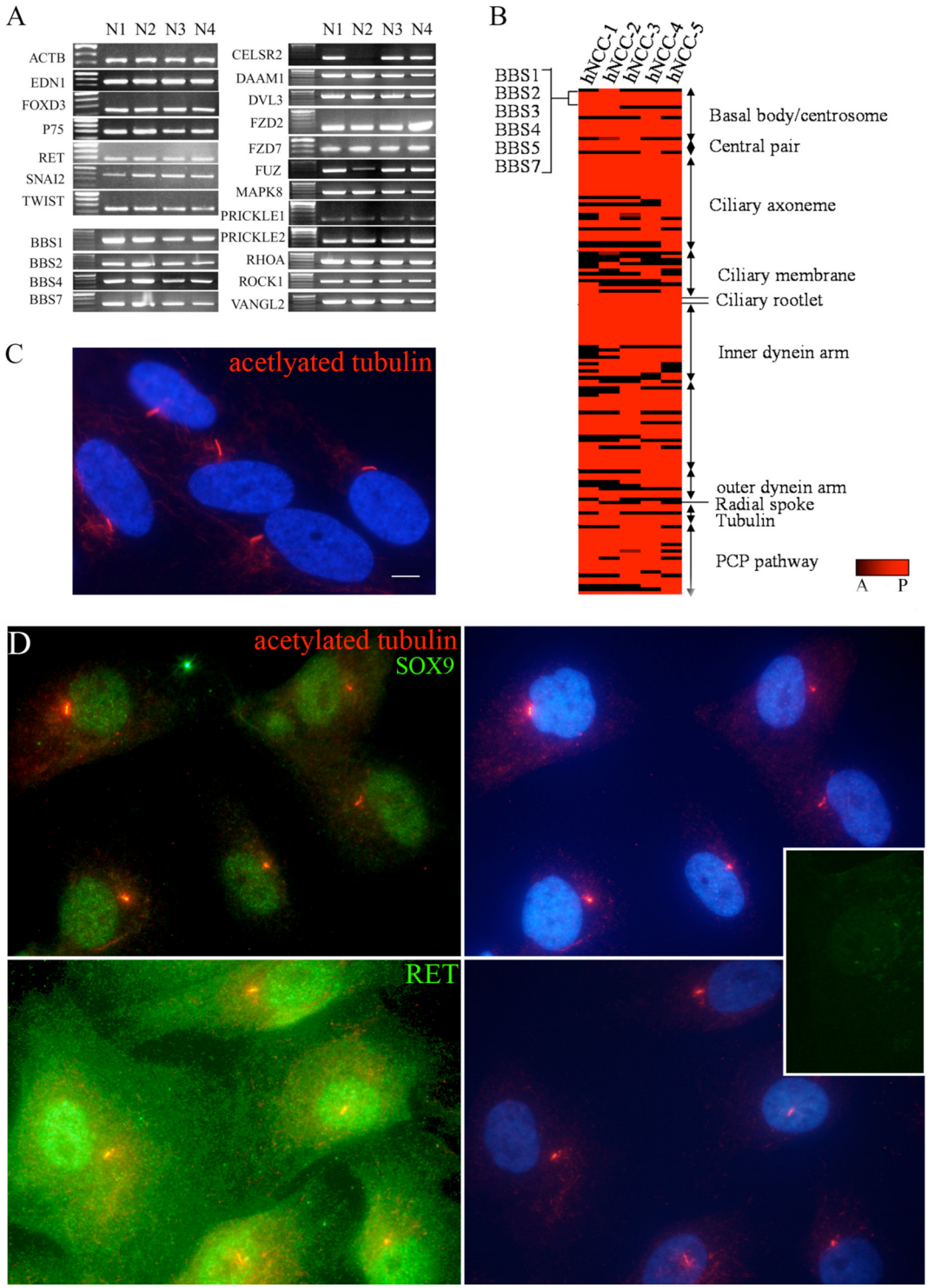

Fig. S2. Human neural crest cells (hNCCs) possess a primary cilium and express BBS genes. (*A*) RT-PCR showing the expression of BBS genes in NCC lines isolated from individual human fetuses. (*B*) Heat map showing the expression (red) or not (black) of confirmed ciliary and basal body/centrosomal proteins in 5 individual hNCC lines (A, absent; P, present). (*C*) Immunocytochemistry on hNCC using antiacetylated α-tubulin antibody and showing that hNCC possess primary cilia. (Scale bar, 5 μm.) (*D*) Human NCCs labeled with acetylated α-tubulin (red) express RET and SOX9 (green). (*Inset*) No appreciable staining could be detected in cells not treated with primary antibody.

Table S1. Ciliary proteins expressed in cultured human NCC

Protein	Cellular localization
BBS1	Basal body/centrosome
BBS10	Basal body/centrosome
BBS2	Basal body/centrosome
BBS3	Basal body/centrosome
BBS4	Basal body/centrosome
BBS5	Basal body/centrosome
BBS6	Basal body/centrosome
BBS7	Basal body/centrosome
BBS8	Basal body/centrosome
BBS9	Basal body/centrosome
CCDC28B	Basal body/centrosome
CETN3	Basal body/centrosome
LRRC1	Basal body/centrosome
MKS1	Basal body/centrosome
MKS3	Basal body/centrosome
OFD1	Basal body/centrosome
TUBE1	Basal body/centrosome
TUBG1	Basal body/centrosome
TUBG2	Basal body/centrosome
PPP1CC	Central pair
SPAG6	Central pair
CALM3	Ciliary axoneme
CCDC146	Ciliary axoneme
Cys1	Ciliary axoneme
EFHC1	Ciliary axoneme
GLI2	Ciliary axoneme
HSPA1A	Ciliary axoneme
HYDIN	Ciliary axoneme
PPP2R1A	Ciliary axoneme
RIBC1	Ciliary axoneme
SSNA1	Ciliary axoneme
TEKT2	Ciliary axoneme
TEKT3	Ciliary axoneme
HTR1B	Ciliary membrane
HTR2C	Ciliary membrane
PDGFRA	Ciliary membrane
PKD1	Ciliary membrane
PKD2	Ciliary membrane
PKHD1	Ciliary membrane
SMO	Ciliary membrane
CROCC	Ciliary rootlet
GAS8	Dynein regulatory complex
ACTG1	Inner dynein arm
DNAH7	Inner dynein arm
DNALI1	Inner dynein arm
DYNLT1	Inner dynein arm
WDR63	Inner dynein arm
WDR78	Inner dynein arm
DNCH2	Intraflagellar transport
IFT122	Intraflagellar transport
IFT140	Intraflagellar transport
IFT172	Intraflagellar transport
IFT20	Intraflagellar transport
IFT52	Intraflagellar transport
IFT57	Intraflagellar transport
IFT72	Intraflagellar transport
IFT74	Intraflagellar transport
IFT80	Intraflagellar transport
IFT81	Intraflagellar transport
IFT88	Intraflagellar transport
KIF3A	Intraflagellar transport
KIF3B	Intraflagellar transport
KIFAP3	Intraflagellar transport
AK5	Outer dynein arm

Protein	Cellular localization
CCDC63	Outer dynein arm
DNAH5	Outer dynein arm
DNAH9	Outer dynein arm
DNAI1	Outer dynein arm
DNAI2	Outer dynein arm
DNAL1	Outer dynein arm
DYNLL2	Outer dynein arm
DYNLRB2	Outer dynein arm
TCTEX1D2	Outer dynein arm
DAAM1	PCP pathway
DVL1	PCP pathway
DVL2	PCP pathway
DVL3	PCP pathway
MAPK8	PCP pathway
ROCK1	PCP pathway
VANGL2	PCP pathway
RSHL3	Radial spoke
RSPH3	Radial spoke
TUBA1A	Tubulin
TUBB2C	Tubulin

Epistasis between *RET* and *BBS* mutations modulates enteric innervation and causes syndromic Hirschsprung disease

Loïc de Pontual[a,1], Norann A. Zaghloul[b,1], Sophie Thomas[a,1], Erica E. Davis[b], David M. Mcgaughey[b], Hélène Dollfus[c], Clarisse Baumann[d], Seneca L. Bessling[b], Candice Babarit[a], Anna Pelet[a], Cecilia Gascue[e], Philip Beales[f], Arnold Munnich[a,f,g], Stanislas Lyonnet[a,f,g], Heather Etchevers[a], Tania Attie-Bitach[a,g], Jose L. Badano[e], Andrew S. McCallion[b,h], Nicholas Katsanis[b,i,j,k,2], and Jeanne Amiel[a,f,2]

[a]Institut National de la Santé et de la Recherche Médicale U781, 6 Service de Génétique, Hôpital Necker-Enfants-Malades, AP-HP, 75743 Paris, France; [g]Faculté de Médecine, Université Paris Descartes, 75270 Paris, France; [b]McKusick–Nathans Institute of Genetic Medicine, [h]Department of Molecular and Comparative Pathology, [i]Department of Molecular Biology and Genetics, and [j]Wilmer Eye Institute, Johns Hopkins University School of Medicine, Baltimore, MD 21205; [c]Service de Génétique Médicale, Hôpital de Haute-Pierre, F-67098 Strasbourg, France; [d]Service de Génétique Médicale, Hôpital Robert Debré, 75935 Paris, France; [e]Institut Pasteur de Montevideo, CP11400 Montevideo, Uruguay; [f]Molecular Medicine Unit, Institute of Child Health, University College London, London WC1N 1EH, United Kingdom; and [k]Center for Human Disease Modeling, Department of Cell Biology, Duke University Medical Center, Durham, NC 27708

Edited by Jeremy Nathans, Johns Hopkins University School of Medicine, Baltimore, MD, and approved June 19, 2009 (received for review February 3, 2009)

Hirschsprung disease (HSCR) is a common, multigenic neurocristopathy characterized by incomplete innervation along a variable length of the gut. The pivotal gene in isolated HSCR cases, either sporadic or familial, is *RET*. HSCR also presents in various syndromes, including Shah–Waardenburg syndrome (WS), Down (DS), and Bardet–Biedl (BBS). Here, we report 3 families with BBS and HSCR with concomitant mutations in BBS genes and regulatory *RET* elements, whose functionality is tested in physiologically relevant assays. Our data suggest that BBS mutations can potentiate HSCR predisposing *RET* alleles, which by themselves are insufficient to cause disease. We also demonstrate that these genes interact genetically in vivo to modulate gut innervation, and that this interaction likely occurs through complementary, yet independent, pathways that converge on the same biological process.

Bardet-Biedl | neural crest cells | genetic interaction | zebrafish

Hirschsprung disease (HSCR, MIM 164761) is the most common (1/5,000 live births) form of structural intestinal obstruction. It is defined by the absence of neural crest (NC)-derived enteric ganglia along a variable length of the bowel, invariably involving the recto-anal junction. This phenotype has been attributed to defects in migration, proliferation, and/or survival of the NC cells (NCC) that normally give rise to all neurons and supporting cells of the enteric nervous system (ENS), defining HSCR as a neurocristopathy. HSCR is also a useful model oligogenic disorder; it displays non-Mendelian modes of inheritance with low, sex-dependant penetrance in isolated HSCR cases. Although oligogenic multiplicative models have been proposed, mutations in the *RET* proto-oncogene have emerged as pivotal (1–4). Almost all HSCR patients harbor either a heterozygous mutation in the *RET* coding sequence or, more frequently, a hypomorphic allele in a conserved noncoding element in intron 1 that acts as a spatially restricted transcriptional enhancer (4–6).

In addition to HCSR, some 30% of patients also exhibit other congenital anomalies as the result of chromosomal rearrangements [mostly Down syndrome (DS)], monogenic Mendelian disorders regardless of the mode of inheritance, or undiagnosed associations (6). In such cases, penetrance for the HSCR trait is 5 to 70%, suggesting additional predisposing genetic factor(s). Interestingly, alleles at the *RET* locus can have a role in modifying the risk of HSCR to be associated with several HSCR predisposing syndromes [congenital central hypoventilation, DS, Waardenburg (WS) type IV due to *EDNRB* mutations, and Bardet-Biedl (BBS)], but not all (Mowat-Wilson and Waardenburg type IV due to *SOX10* mutations) (6–8). These observations are suggestive of *RET*-dependent and *RET*-independent HSCR cases (9); consistent with *RET* acting as a modifier gene in some HSCR predisposing syndromes, no correlation between the genotype for the syndrome disease causing gene and the HSCR trait could be drawn in monogenic HSCR syndromes (9, 10).

Surprisingly, the greatest *RET* dependence has been observed in the group of patients with both BBS and HSCR. No interactions between RET and BBS proteins are known; also, whereas *RET* is a cell-surface tyrosine kinase receptor essential for enteric neuron population of the gut (11), BBS is a ciliopathy caused by mutations in at least 14 genes (ref. 12 and references therein), with all BBS proteins examined to date localizing in the basal body and the ciliary axoneme where they likely affect various signaling processes (13). Nonetheless, despite any obvious biochemical or subcellular links between RET and the BBS proteins, a zebrafish model of BBS was shown recently to manifest a Shh-dependent defect in the migration of neural crest cells with concomitant defects in the innervation of the ENS (14), suggesting that the observed enrichment of *RET* hypomorphic alleles in BBS-HSCR patients might underlie a synthetic interaction at a higher level of systems organization.

Here, we report 2 families and 1 sporadic case with BBS and HSCR, each with variations at both a *BBS* locus and *RET*. Using both in vitro and in vivo models, we show that each individual variation has deleterious effects. Importantly, the interaction of these genetic lesions is tissue dependent, modulating the extent of intestinal aganglionosis during the development of the zebrafish ENS.

Results

BBS Mutations in BBS+HSCR Patients. To investigate a possible genetic interaction between BBS and HSCR, we searched for BBS patients also diagnosed with HSCR. We found 2 informative BBS families, one of Caucasian origin (F1), and one of

Author contributions: L.d.P., N.A.Z., S.T., H.D., C. Baumann, P.B., A.M., S.L., H.E., T.A.-B., A.S.M., N.K., and J.A. designed research; L.d.P., N.A.Z., S.T., E.E.D., D.M.M., H.D., C. Baumann, S.L.B., C. Babarit, A.P., C.G., and J.L.B. performed research; C.G. and J.L.B. contributed new reagents/analytic tools; L.d.P., N.A.Z., S.T., E.E.D., D.M.M., H.D., C. Baumann, C.G., A.M., S.L., H.E., T.A.-B., J.L.B., A.S.M., N.K., and J.A. analyzed data; and N.A.Z., A.S.M., N.K., and J.A. wrote the paper.

The authors declare no conflict of interest.

This article is a PNAS Direct Submission.

[1]L.d.P., N.A.Z., and S.T. contributed equally to this work.

[2]To whom correspondence may be addressed. E-mail: katsanis@jhmi.edu or jeanne.amiel@inserm.fr.

This article contains supporting information online at www.pnas.org/cgi/content/full/0901219106/DCSupplemental.

GENETICS

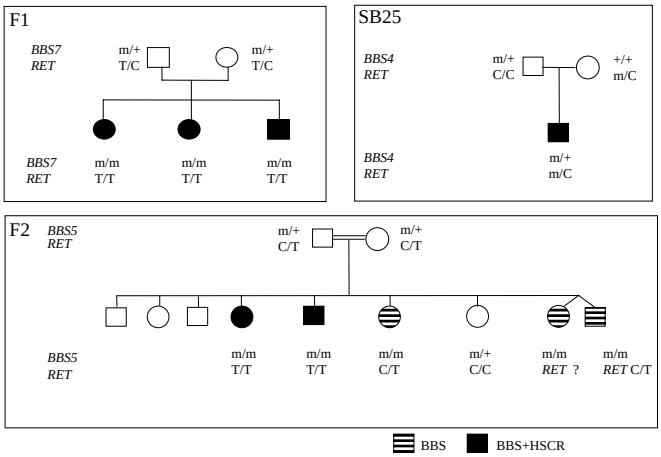

Fig. 1. *RET* and *BBS* mutations found in BBS+HSCR cases. Segregation of *BBS* and *RET* mutations in 2 BBS families with BBS±HSCR and 1 BBS+HSCR sporadic case (SB25).

Moroccan origin (F2) (Fig. 1). F1 had 3 sibs, all affected with short segment HSCR as confirmed by histological criteria that included absence of enteric plexuses and increased acetylcholinesterase histochemical staining in nerve fibers. F2 consisted of consanguineous parents (f = 1/16) of 5 BBS sibs, 2 of which also had confirmed HSCR. We also identified a third sporadic case (SB25) born to healthy unrelated parents of Caucasian origin and presenting both BBS and HSCR (Fig. 1).

To determine the genetic lesion contributing to these cases, we first investigated all known BBS loci. We found all affected sibs in F1 to harbor 2 heterozygous missense mutations in *BBS7*; a paternal c.691T>C, p.W230R, and a maternal c.1512 G>A, p.R504K. Both mutations altered a conserved amino acid and were not found in 250 control chromosomes. In F2, all 5 sibs had a homozygous 1-bp deletion in exon 15 (c.1909-1910delT) of *BBS5*, causing a frameshift (p.K41fsX52). Both parents were heterozygous for the mutation, which was also not detected in controls. Last, the sporadic case SB25 bore a heterozygous missense *BBS4* mutation (1372 C>T; S457I), which was inherited from the father and not found in 195 controls.

Genotyping of RET in Patients. Previous reports have shown that BBS patients with HSCR are more frequent carriers of a *RET* hypomorphic allele than expected from population frequency (9). Therefore, we hypothesized that the BBS+HSCR patients in our families might also have a RET variant. To test this possibility, we sequenced the patients for mutations in *RET*. The 3 F1 sibs were homozygous for the common intronic hypomorphic T allele; both parents were heterozygous. In F2, only the 2 BBS+HSCR, but not the other 3 BBS-only patients were homozygous for the same *RET* allele. Last, the sporadic SB25 case was WT for the intron 1 allele, but had a novel, maternally inherited heterozygous 11-bp deletion (del AAGCAACTGCC). This deletion lies 106-bp downstream of the known intron 1 hypomorphic allele, maps within the highly conserved enhancer region, and was not found in over 800 control chromosomes (Fig. 1; Fig. S1).

Functional Assessment of BBS and RET Mutations. Our genetic data provide strong evidence that the *BBS5* and *BBS7* alleles in families F1 and F2 are sufficient to cause BBS. By contrast, the pathogenic potential of the *BBS4* S457I allele cannot be established unequivocally, despite its absence from ethnically matched controls. Therefore, we investigated the (non)neutrality of this allele using an established zebrafish BBS model. We have reported previously that suppression of Bbs proteins results in Wnt-dependent gastrulation movement defects in zebrafish (15, 16), which can be rescued by coinjection of WT human mRNA. This system has enabled us establish the pathogenic potential of several novel BBS-causing alleles (12).

Therefore, we suppressed endogenous *bbs4* and evaluated the ability of a 457I-encoding *BBS4* message to rescue the phenotype. Approximately 63% of embryos injected with *bbs4* morpholino (MO) had broadened somites, kinked notochords, and shortened body axes (Fig. 2 *A* and *B*). The observed phenotypes not only fully recapitulated our previous observations (15), but were also shown to be specific to the MO, because coinjection of mRNA encoding WT human *BBS4* efficiently rescued the morphant phenotypes (Fig. 2*B*). By contrast, embryos injected with 457I were indistinguishable from embryos injected with *bbs4* MO alone (n = 96 embryos, scored blind to injection mixture), suggesting that the introduction of the 457I residue results in functionally null protein (Fig. 2 *A* and *B*); expression of 457I-encoding mRNA alone yielded modest phenotypes, indicating that this allele does not act in a dominant-negative fashion (Fig. 2*B*). To validate the pathogenic nature of this mutation further, we investigated the cellular localization of the 457I protein in ciliated mammalian cells. Previous studies have established the reproducible localization of BBS4 near the 2 centrioles by overexpression of tagged protein in transformed cell lines (17, 18). Upon transient transfection of a BBS4-MYC construct, we observed a similar localization pattern (Fig. 2*C*). However, expression of a BBS4 S457I mutant protein resulted in complete mislocalization of the protein (Fig. 2*C*), with the mutant protein forming apparent intracellular aggregates away from the pericentriolar region (visualized by γ-tubulin staining), providing further evidence that the mutation is a likely null.

Next, we turned our attention to the *RET* alleles in our patients. Although the functional significance of the intronic HSCR predisposing allele in *RET* is known, the pathogenic potential of the 11-bp deletion within intron 1 is highly suggestive, but not conclusive. We have shown previously that the multispecies conserved sequence (MCS) within intron 1 (MCS + 9.7) acts as an enhancer element, and contains the previously described hypomorphic allele (5); the 11-bp deletion is 106 bp downstream of this SNP. To investigate the function of the deletion, we constructed pD*Sma-RET* vectors with luciferase under the control of an SV40 promoter and the MCS + 9.7 enhancer plus a 1215-bp encompassing region either with (WT) or without (Δ11bp) the 11-bp sequence, and assayed relative luciferase activity in SK-N-SH neuroblastoma cells or HeLa cells. The WT *RET* enhancer sequence significantly decreased reporter gene expression (P = 0.001) compared with the promoter alone, and also as compared with MCS + 9.7, suggesting that it contains a putative transcription repressor-binding site. However, the vector harboring the 11-bp deletion significantly derepresses reporter gene expression compared with WT (P = 0.05) to a level statistically indistinguishable from the promoter alone (NS), suggesting specific disruption of the repressor element binding motif (Fig. 3). Reporter assays conducted in HeLa cells produced similar results. These findings suggest that deletion of 11 bp within the intronic enhancer results in defects in transcriptional regulation in vitro, although they do not abolish the effect of this genomic segment, raising the possibility that Δ11bp represents a mild allele. Together, these results suggest that the individual *BBS* and *RET* mutations identified in the sporadic case of BBS and HSCR are likely detrimental to gene function. Among putative consensus binding sites encompassing the 11-bp deletion, only the zinc finger transcription factor *SNAIL* is expressed in hNCC. However, ChIP experiments in SK-N-SH cells did not detect an interaction with this protein, suggesting that potentially novel components are associated with the observed suppression regulatory element.

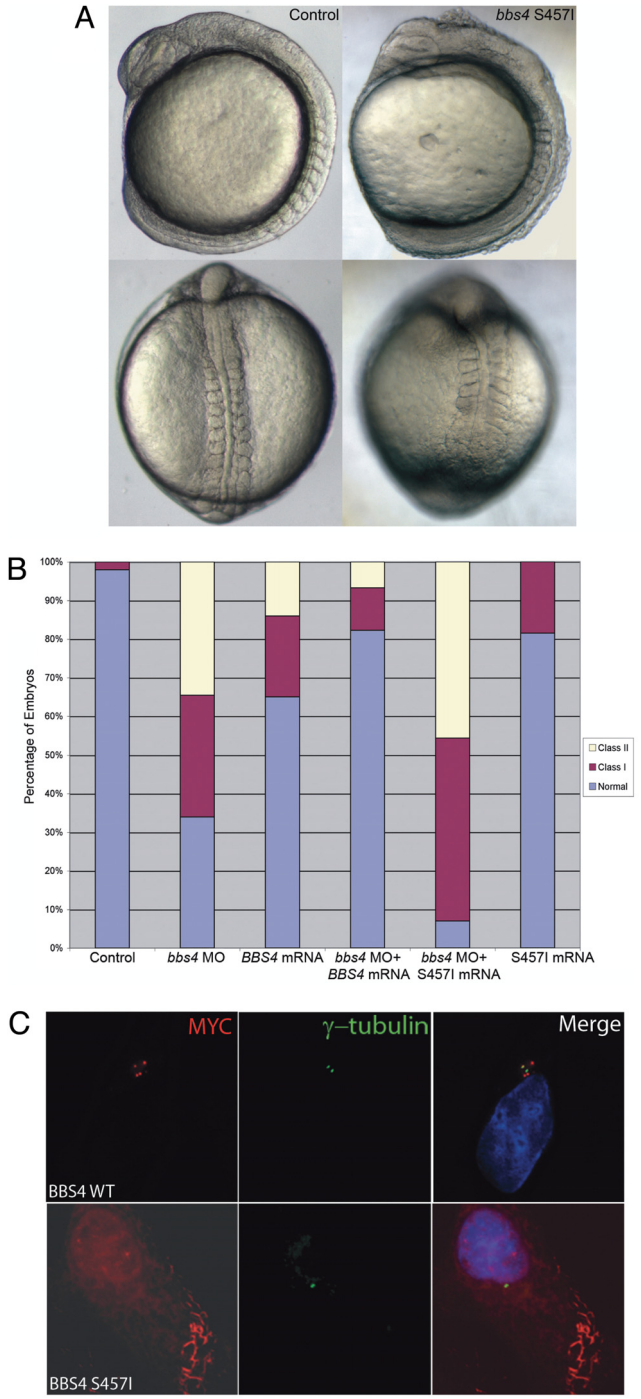

Fig. 2. In vivo assessment of the pathogenic potential of BBS4 S457I variant. (*A*) Zebrafish embryos coinjected with a MO against *bbs4* and mRNA expressing the S457I variant exhibited defects, including short body axes, broad somites, wider and kinked notochords, and detachment of cells along the dorsal axis. (*B*) Compared to rescue with WT BBS4 mRNA, rescue with the mutated mRNA produced an increase in the proportion of both moderately (Class I) and severely (Class II) affected embryos, but injection of S457I mRNA alone does not produce severe defects, suggesting that the variant is functionally null. (*C*) HeLa cells transfected with either WT or S457I mutant BBS4 protein (red). WT protein localizes to the basal body (γ-tubulin, green), but mutant protein completely mislocalizes to form cytoplasmic aggregates.

Genetic Interaction of BBS and RET in Vivo. Our data are consistent with previous studies, in which a higher-than-expected frequency of *RET* hypomorphic alleles were found in BBS-HSCR patients, and suggest that this property is not restricted to a specific BBS gene (9), not least because *BBS4*, *BBS5*, and *BBS7* are 3 of the least commonly mutated BBS genes (13). To test this possibility in vivo, we assayed the effects of suppression of each of Ret and Bbs proteins on enteric neuron migration in the developing zebrafish gut. As shown previously, suppression of *ret* by MO injection results in a reduction of enteric neurons populating the proximal and distal hindgut, as labeled by in situ hybridization with a *phox2b* riboprobe (Fig. 4 *B* and *I*) (19). Likewise, and consistent with recent data for *bbs8*, suppression of either *bbs4*, *bbs5*, or *bbs7* also results in a reduction of enteric neuron migration, although not as severe (Fig. 4 *C*, *E*, *G*, and *I*). However, coinjection of *ret* MO with any of the 3 *bbs* genes tested resulted in a significantly greater decrease in the enteric neurons in the hindgut, with phenotypic synthesis particularly prominent in the distal hindgut (Fig. 4 *D*, *F*, *H*, and *I*). The increased severity is greater than a mere additive effect, suggesting an epistatic interaction between *ret* and *bbs* function. These findings indicate that suppression of *ret* in addition to loss of *bbs* function results in more severe defects in ENS development than with loss of these genes independently.

NCCs as Likely Sites of Epistasis. The finding that *ret* and *bbs* genes interact genetically to produce enteric neuron defects suggests the possibility that these genes function in overlapping pathways to regulate ENS development. Several lines of evidence support this conjecture: the role of RET signaling in NCC migration is well established (20, 21), whereas suppression of *bbs8* has been shown to result in similar defects, potentially in a Shh-dependent fashion (14). Also, transcriptional profiling of NCC cells demonstrated the presence of mRNA message for several BBS proteins, as well as mRNA for genes encoding numerous ciliary and basal body proteins (Table S1; Fig. S2 *A* and *B*). Last, immunocytochemistry using antiacetylated α-tubulin revealed a clear presence of monocilia and basal bodies, respectively, in these cells (Fig. S2 *C* and *D*). To confirm that the ciliated NCCs are, in fact, those that will contribute to enteric innervation, we performed immunofluorescence using either anti-RET or anti-SOX9 and observed expression of both proteins in NCCs positive for antiacetylated tubulin staining (Fig. S2*D*).

Given these findings, one possibility is that RET signaling functions through the cilium, because several other paracrine receptors are known to localize there or to indirectly require the primary cilium for signal transduction (22). However, RET immunofluorescence has never detected the protein in the ciliary axoneme, suggesting that the observed genetic interaction between RET and the BBS proteins might occur at a higher level of systems organization. To test this possibility we attempted to rescue the enteric neuron phenotype of RET knock-down by coinjecting *BBS4* mRNA in embryos injected with *ret* MO; we did not observe any amelioration of the gut innervation defect (Fig. 4*I*), suggesting that BBS4 is not downstream of RET and supporting the notion that the 2 pathways likely converge at the same endpoint.

Discussion

Here, we have described 3 families segregating BBS in concert with HSCR. Mutation detection in affected individuals revealed mutations in *BBS4*, *BBS5*, and *BBS7*, consistent with their phenotypic presentation. Also, each affected was also homozygous for the common *RET* intronic hypomorphic allele or, in one instance, harbored a novel heterozygous 11-bp deletion that was absent from control chromosomes. We verified the functional potential of all novel alleles identified, integrating in vitro and in vivo approaches to determine their impact. These data led us to posit that interactions between RET and either BBS4, 5, or 7 in each instance would explain the coexpression of BBS and HSCR phenotypes. We have

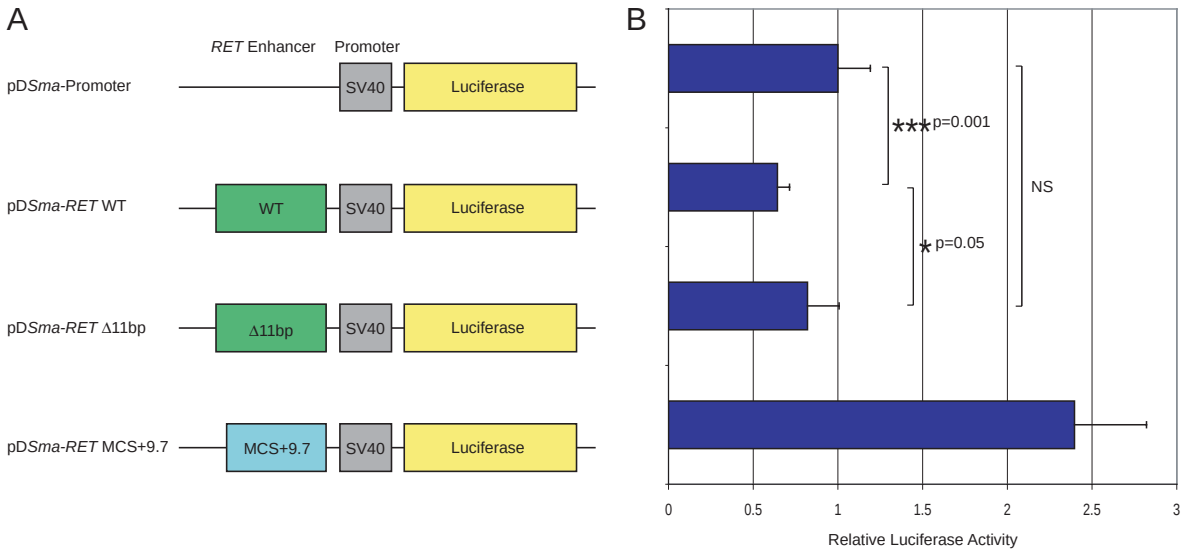

Fig. 3. Deletion in the *RET* regulatory sequence perturbs reporter gene expression in vitro. (*A*) Schematic representation of vectors used to assay the effect of the 11-bp deletion on reporter gene expression in vitro. WT or mutated (Δ11bp) *RET* enhancer sequence (green) was placed upstream of an SV40 promoter (gray) driving firefly luciferase expression (yellow). The pD*Sma-RET* MCS + 9.7, described previously (5), was used as a positive control. (*B*) Relative luciferase activity of pD*Sma-RET* vectors (depicted in *A*) in SK-N-SH neuroblastoma cells. Cells were lysed 48 h posttransfection, and relative luciferase activity was normalized to values obtained from the promoter alone (pD*Sma*-Promoter). The WT *RET* enhancer sequence significantly decreases reporter gene expression ($P = 0.001$) compared with promoter alone, suggesting that it contains a putative transcription repressor-binding site. However, the vector harboring the 11-bp deletion significantly derepresses reporter gene expression compared with WT ($P = 0.05$) to a level statistically indistinguishable (NS) from the promoter alone, suggesting specific disruption of the repressor element binding motif. Assays were performed in triplicate wells and repeated thrice.

used nonallelic, noncomplementation through MO-based approaches in zebrafish to test these observations.

We have demonstrated that pairwise compound reduction in RET and each independent BBS protein product (BBS4, 5, or 7), which independently yield mild intestinal aganglionosis, severely exacerbates the observed enteric defects, with particular prominence in the distal hindgut. Interestingly this synergy in mutational effect appears to be tissue dependent, not resulting in an overt worsening of other associated phenotypes (e.g., convergence extension) suggesting that the pleiotropic activities of these genes may only be amenable to interaction with each other in a cell type dependent manner. As with other systems in the vertebrate organism, nervous system development relies on a delicate balance of interactions. Importantly, our data also illuminate interrelated roles for these BBS loci and *RET* in buffering the effects of genetic variation during ENS development, and between their mutant alleles in the copresentation of BBS and HSCR phenotypes. Interestingly, HSCR has been recurrently reported in association with other ciliopathies, namely Jeune and Joubert syndromes (23, 24).

Complex inheritance is underlined by a requirement for the combined influence of alleles at >1 locus in the transmission and expression of a phenotype; homeostatic genetic networks minimize the consequence of variation. Both BBS and HSCR are models of such traits, requiring the interaction of multiple genes for disease expression.

Just as interactions between different *BBS* loci explain the risk of BBS in subsets of families, interactions between *RET* and other loci can also explain disease risk in subsets of isolated and syndromic HSCR cases/families (1–3, 7, 12, 25, 26). Many of the genes implicated in these disorders display markedly pleiotropic effects when evaluated independently and occasionally these effects can coincide.

The interaction of genes involved in the same biochemical system and the observation of their failure to complement each other (intrinsic noncomplementation) is well established (3, 27, 28). However, there is no evidence to suggest that RET-mediated receptor tyrosine kinase signaling, and its role in neuronal precursor proliferation (21), directly intersects the role of BBS proteins in the development and function of ciliated cells and their proposed role in cell migration (13). Thus, their observed synergy is unlikely to arise from biochemical interaction, but rather from extrinsic noncomplementation raising predisposition to a common phenotype. Importantly, intrinsic noncomplementation is the commonly recognized basis of both HSCR and BBS. Although it cannot at this stage be distinguished definitively, we speculate that the syndromic copresentation of BBS and HSCR observed here, as well as similar interactions between HSCR and WS, support a model of extrinsic noncomplementation, where perturbations in unrelated biochemical signaling cascades converge at the same biological process (namely, neuronal migration and specification).

Materials and Methods

Patient Genotyping and Sequencing. Blood samples were obtained with informed consent, and DNA was extracted according to standard protocols. Genotyping the *BBS1-12* loci was performed by using fluorescent microsatellite markers (available on request). Mutation screening of *RET* and *BBS* genes have been described elsewhere (29), and intronic primers designed for *BBS* genes are available on request. Direct sequencing on both strands was performed using the Big Dye Terminator Cycle Sequencing kit (Applied Biosystems) and was analyzed on an ABI 3100 automated sequencer (Applied Biosystems). Also, patients were genotyped for SNP rs2435357 lying in the intron 1 of the *RET* gene. Of note, variable allelic frequencies are observed according to ethnicity and range from <5% in South Africa to ≈50% in Asia. The European Caucasian population has been thoroughly investigated in France, Italy, Spain, the Netherlands, and Germany, allowing approximation of the frequency of the T HSCR predisposing allele to ≈25% in the Caucasian population (30).

Luciferase Reporter Assay. SK-N-SH or HeLa cells were plated in 24-well plates at a density of 10^5 cells/well, and were transfected at ≈60% confluence with FuGENE6 transfection reagent (Roche) according to manufacturer's instructions, using a 2:1 ratio of pD*Sma* vector and pRLSV40 *Renilla* luciferase control vector (Promega), respectively. At 48 h posttransfection, cells were lysed and assayed using the Dual-Luciferase Reporter Assay System (Promega), and a

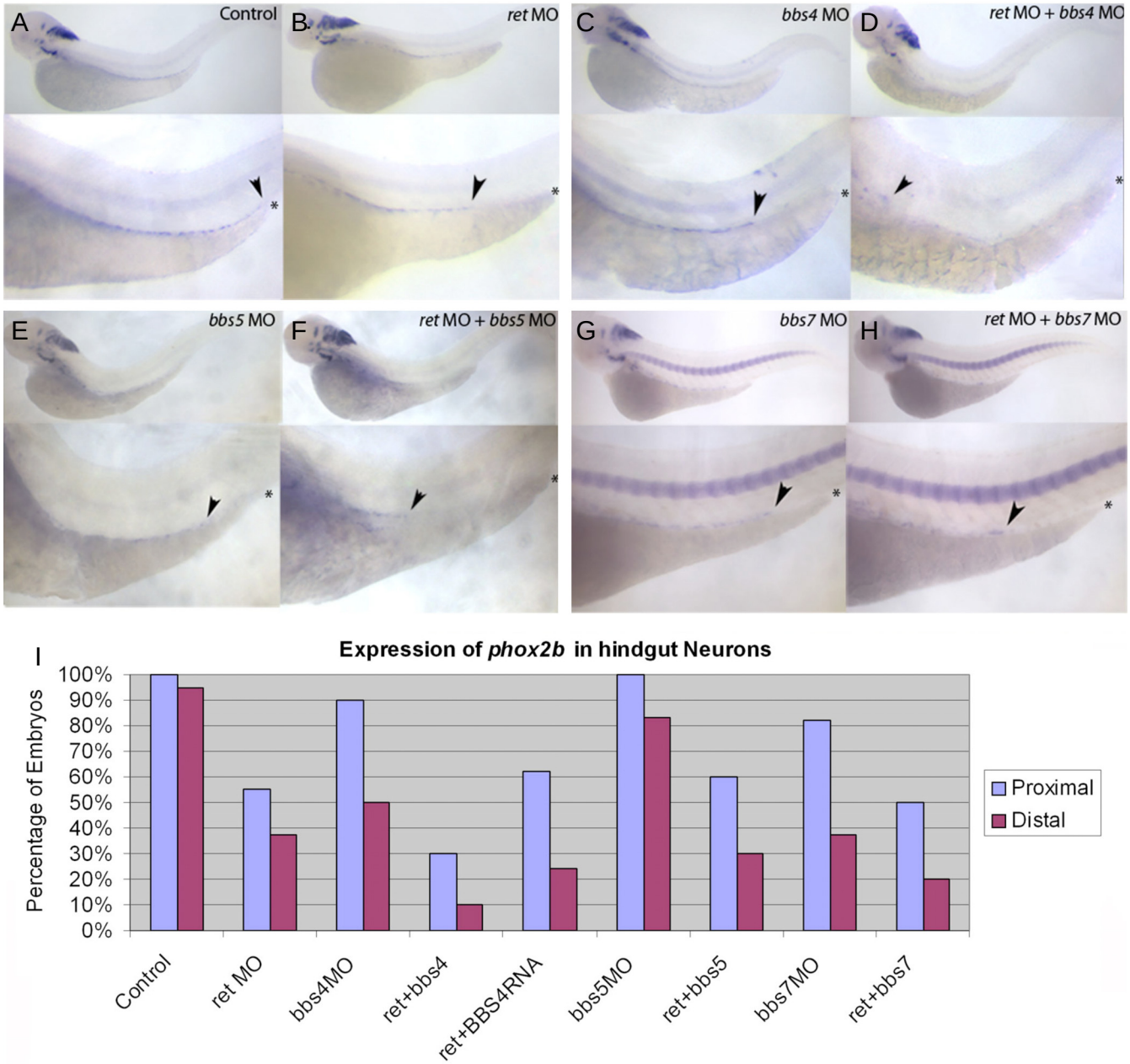

Fig. 4. Genetic interaction of *Ret* and *Bbs* in zebrafish. (*A*) Migration of enteric neurons in 4-day-old embryos normally proceeds along the developing hindgut to reach the anus (asterisks). Embryos injected with MO against either (*B*) *ret* or (*C*) *bbs4*, (*E*) *bbs5*, or (*G*) *bbs7* exhibit premature termination of enteric neuron migration (arrowhead). This defect is exacerbated in embryos injected with a combination of *ret* MO and either (*D*) *bbs4*, (*F*) *bbs5*, or (*H*) *bbs7* MO. (*I*) The extent of the defect was quantified by assessment of the presence of *phox2b* expression in the proximal hindgut (somites 4–9) or the distal hindgut (somites 10 and beyond) as previously described (31).

Tecan microplate reader equipped with the XFluor4GENiosPro macro. Assays were performed on triplicate wells, and were repeated at least twice. Relative luciferase activity was normalized to values obtained from the promoter alone (pD*Sma*-Promoter).

Zebrafish Embryo Manipulation and MO Injection. Embryos were injected with a previously described and validated oligonucleotide MO against *bbs4* to suppress translation of the endogenous protein, resulting in phenotypes consistent with PCP defects including shortened body axes, broad notochords, and widened somites (15, 16). They were subsequently coinjected with mRNA encoding WT human *BBS4* or the S457I variant of *BBS4*. Embryos were classified as normal, moderately (Class I), and severely (Class II) affected according to phenotype.

In Situ Hybridization. Embryos were cultured for 4 days in embryo media at 28 °C, fixed in 4% Paraformaldehyde overnight at 4 °C, and stored at −20 °C in 100% MeOH until in situ hybridization, which was carried out according to previously described protocols (15). Enteric neurons were labeled using a *phox2b* digoxigenin ripoprobe (31).

Human NC Isolation and Culture. Human embryos were collected from pregnancies legally terminated using the mefiprestone protocol, in concordance with French bioethics law 2004-800 and with the approval of the Necker hospital ethics committee. Human NCCs were isolated from posterior hindbrain and thoracic-level neural tube and cultured as previously described (32) to 80% confluency on 8-well collagen I-coated slides (BD BioCoat).

Immunocytochemistry. Twenty-four hours after seeding, hNCC were starved in DMEM/F12 with 0.4 ng/mL FGF2 for a further 72 h. Cells were fixed for 20 min in 4% paraformaldehyde, then treated in 50 mM NH_4Cl 10 min, 0.3% Triton X-100 in PBS 15 min, followed by 1 h in a solution of 1% BSA, 0.1% Tween-20,

10% goat serum in PBS. Cells were then incubated with antiacetylated α-tubulin (TUBA4A; Sigma T6793), anti-RET (SC13104, 1:50; Santa Cruz), or anti-SOX9 (ab5535, 1:200; Chemicon) for 2 h at room temperature, and rinsed. SOX9 and RET were revealed using an Alexa Fluor 488 goat anti-rabbit IgG and TUBA4A with an Alexa Fluor 555 donkey anti-mouse IgG (1:200 each; Invitrogen). The slides were mounted with Prolong Gold antifade reagent with DAPI (Invitrogen).

HeLa cells were grown on glass coverslips in DMEM supplemented with 10% FBS at 37 °C in 5% CO_2. Transient transfections of WT or mutant BBS4 constructs were carried out using calcium phosphate (Invitrogen), and cells processed 24 h later with anti-MYC mouse monoclonal and anti-γ-tubulin rabbit polyclonal antibodies (T3559; Sigma).

Microarray and RT-PCR. Total RNA from 5 human trunk NCCs were extracted using Rneasy Mini kit (Qiagen). Gene profiling was done using the Affymetrix Human Genome U133 Plus 2.0 GeneChip array. Hybridization data were analyzed with dChip software. Heat map was constructed using a list of 75 experimentally confirmed ciliary and basal body/centrosomal proteins defined in ref. 33. Reverse transcription was performed using GeneAmp RNA PCR core kit (Applied Biosystems), and PCR amplifications were performed using 50 ng of cDNA and 35 amplification cycles. Primers are available on request. Affymetrix data are available from the National Center for Biotechnology Information Gene Expression Omnibus under accession number GSE 14340.

ACKNOWLEDGMENTS. We thank the families and their referring clinical teams for participation, the Association Françcaise de la Maladie de Hirschsprung for its support, Sophie Audollent for technical assistance, and the Johns Hopkins University Finz Center for husbandry and technical support with the zebrafish experiments. This work was supported by grants from the Association Nationale pour la Recherche, the Fondation pour la Recherche Médicale, and the National Institute of General Medical Sciences (A.S.M.), by National Institute of Child Health and Development Grant R01HD04260, by National Institute of Diabetes, Digestive, and Kidney Disorders Grants R01DK072301 and R01DK075972, by the Macular Vision Research Foundation (N.K.), by a Visual Neuroscience Training Program fellowship (N.A.Z.), by and National Institute of Diabetes, Digestive, and Kidney Disorders National Research Service Award Fellowship F32 DK079541 (to E.E.D.). A.S.M. and D.M. were supported by award GM071648 (to A.S.M.).

1. Bolk S, et al. (2000) A human model for multigenic inheritance: Phenotypic expression in hirschsprung disease requires both the RET gene and a new 9q31 locus. *Proc Natl Acad Sci USA* 97:268–273.
2. Gabriel SB, et al. (2002) Segregation at three loci explains familial and population risk in Hirschsprung disease. *Nat Genet* 31:89–93.
3. McCallion AS, et al. (2003) Genomic variation in multigenic traits: Hirschsprung disease. *Cold Spring Harb Symp Quant Biol* 68:373–381.
4. Emison ES, et al. (2005) A common sex-dependent mutation in a RET enhancer underlies Hirschsprung disease risk. *Nature* 434:857–863.
5. Grice EA, Rochelle ES, Green ED, Chakravarti A, McCallion AS (2005) Evaluation of the RET regulatory landscape reveals the biological relevance of a HSCR-implicated enhancer. *Hum Mol Genet* 14:3837–3845.
6. Amiel J, et al. (2008) Hirschsprung disease, associated syndromes and genetics: A review. *J Med Genet* 45:1–14.
7. Carrasquillo MM, et al. (2002) Genome-wide association study and mouse model identify interaction between RET and EDNRB pathways in Hirschsprung disease. *Nat Genet* 32:237–244.
8. McCallion AS, Stames E, Conlon RA, Chakravarti A (2003) Phenotype variation in two-locus mouse models of Hirschsprung disease: Tissue-specific interaction between Ret and Ednrb. *Proc Natl Acad Sci USA* 100:1826–1831.
9. de Pontual L, et al. (2007) Epistatic interactions with a common hypomorphic Ret allele in syndromic Hirschsprung disease. *Hum Mutat* 28:790–796.
10. de Pontual L, et al. (2006) Mutations of the RET gene in isolated and syndromic Hirschsprung's disease in human disclose major and modifier alleles at a single locus. *J Med Genet* 43:419–423.
11. Schuchardt A, D'Agati V, Larsson-Blomberg L, Costantini F, Pachnis V (1994) Defects in the kidney and enteric nervous system of mice lacking the tyrosine kinase receptor Ret. *Nature* 367:380–383.
12. Leitch CC, et al. (2008) Hypomorphic mutations in syndromic encephalocele genes are associated with Bardet-Biedl syndrome. *Nat Genet* 40:443–448.
13. Zaghloul NA, Katsanis N (2009) Mechanistic insights into Bardet-Biedl Syndrome: A model ciliopathy. *J Clin Invest* 119:428–437.
14. Tobin JL, et al. (2008) Inhibition of neural crest migration underlies craniofacial dysmorphology and Hirschsprung's disease in Bardet-Biedl syndrome. *Proc Natl Acad Sci USA* 105:6714–6719.
15. Gerdes JM, et al. (2007) Disruption of the basal body compromises proteasomal function and perturbs intracellular Wnt response. *Nat Genet* 39:1350–1360.
16. Ross AJ, et al. (2005) Disruption of Bardet-Biedl syndrome ciliary proteins perturbs planar cell polarity in vertebrates. *Nat Genet* 37:1135–1140.
17. Nachury MV, et al. (2007) A core complex of BBS proteins cooperates with the GTPase Rab8 to promote ciliary membrane biogenesis. *Cell* 129:1201–1213.
18. Kim JC, et al. (2004) The Bardet-Biedl protein BBS4 targets cargo to the pericentriolar region and is required for microtubule anchoring and cell cycle progression. *Nat Genet* 36:462–470.
19. Heanue TA, Pachnis V (2008) Ret isoform function and marker gene expression in the enteric nervous system is conserved across diverse vertebrate species. *Mech Dev* 125:687–699.
20. Chakravarti A, McCallion AS, Lyonnet S (2007) Hirschsprung Disease. *The Metabolic and Molecular Bases of Inherited Disease*, eds Scriver CR, Beaudet AR, Valle D, Sly W (McGraw-Hill, New York), Chap 251, 8th Ed.
21. McCallion AS (2008) RET, Hirschsprung disease and multiple endocrine neoplasia type 2. *Inborn Errors of Development*, eds Epstein C, Erickson R, Wynshaw-Boris A (Oxford Univ Press, San Francisco), 2nd Ed.
22. Davis EE, Brueckner M, Katsanis N (2006) The emerging complexity fo the vertebrate cilium: New functional roles for an ancient organelle. *Dev Cell* 11:9–19.
23. Aurora P, Wallis CE (1999) Jeune syndrome (asphyxiating thoracic dystrophy) associated with Hirschsprung disease. *Clin Dysmorphol* 8:259–263.
24. Ozyurek H, Kayacik OE, Gungor O, Karagoz F (2008) Rare association of Hirschsprung's disease and Joubert syndrome. *Eur J Pediatr* 167:475–477.
25. Auricchio A, et al. (1999) Double Heterozygosity for a RET Substitution Interfering with Splicing and an EDNRB Missense Mutation in Hirschsprung Disease. *Am J Hum Genet* 64:1216–1221.
26. Puffenberger EG, et al. (1994) A missense mutation of the endothelin-B receptor gene in multigenic Hirschsprung's disease. *Cell* 79:1257–1266.
27. Hartman JL, Garvik B, Hartwell L (2001) Principles for the buffering of genetic variation. *Science* 291:1001–1004.
28. Kacser H, Burns JA (1981) The molecular basis of dominance. *Genetics* 97:639–666.
29. Pelet A, et al. (2005) Homozygosity for a frequent and weakly penetrant predisposing allele at the RET locus in sporadic Hirschsprung disease. *J Med Genet* 42:e18.
30. Chattopadhyay P, et al. (2003) Global survey of haplotype frequencies and linkage disequilibrium at the RET locus. *Eur J Hum Genet* 11:760–769.
31. Elworthy S, Pinto JP, Pettifer A, Cancela ML, Kelsh RN (2005) Phox2b function in the enteric nervous system is conserved in zebrafish and is sox10-dependent. *Mech Dev* 122:659–669.
32. Thomas S, et al. (2008) Human neural crest cells display molecular and phenotypic hallmarks of stem cells. *Hum Mol Genet* 17:3411–3425.
33. Gherman A, Davis EE, Katsanis N (2006) The ciliary proteome database: An integrated community resource for the genetic and functional dissection of cilia. *Nat Genet* 38:961–962.

Identification of the *IRXB* Gene Cluster as Candidate Genes in Severe Dysgenesis of the Ocular Anterior Segment

Myriam Chaabouni,[*,1,2] *Heather Etchevers,*[3,4] *Marie Christine De Blois,*[1] *Patrick Calvas,*[3] *Marie Christine Waill-Perrier,*[1] *Michel Vekemans,*[1] *and Serge Pierrick Romana*[*,1]

Purpose. Anterior segment ocular dysgenesis (ASOD) is a broad heterogeneous group of diseases detectable at the clinical and molecular level. In a patient with bilateral congenital ASOD including aniridia and aphakia, a complex chromosomal rearrangement, inv(2)(p22.3q12.1)t(2;16)(q12.1;q12.2), was characterized at the molecular level, to identify candidate genes implicated in ASOD.

Methods. After negative sequencing of the *PAX6*, *FOXC1*, and *PITX2* genes, we used fluorescence in situ hybridization (FISH) and Southern blot analysis to characterize the chromosomal breakpoints. Candidate genes were selected, and in situ tissue expression analysis was performed on human fetuses and embryos.

Results. Molecular analyses showed that the 16q12.2 breakpoint in this rearrangement occurs in a 625-bp region centromeric to the *IRX3* gene, which belongs to the IRXB cluster. In situ hybridization expression studies showed that during early human embryonic development, the *IRX3* gene is expressed in the anterior segment of the eye. Of interest, it has been shown previously that a highly conserved noncoding region (HCNCR) is located 300 kb centromeric to the *IRX3* gene and induces, in a murine transgenic assay, an expression pattern fitting that of the *IRX3* gene.

Conclusions. The authors propose that the 16q12.2 breakpoint of this complex translocation is causally related to the ocular anterior segment dysgenesis observed in this patient. This translocation is assumed to separate the HCNCR from the IRXB cluster genes, thus deregulating the IRXB cluster and leading to the ASOD observed by a positional effect. (*Invest Ophthalmol Vis Sci.* 2010;51:4380–4386) DOI: 10.1167/iovs.09-4111

From the [1]Service de Cytogénétique and [4]INSERM U781, Hôpital Necker Enfants Malades, Paris, France; [2]Service des Maladies Héréditaires et Congénitales, Hôpital Charles Nicolle, Tunis, Tunisia; and [3]INSERM (Institut National de le Santé et de la Recherche Médicale) U563, CPTP (Centre de Physiopathologie de Toulouse Purpan), Hôpital Purpan, Toulouse, France.

Submitted for publication June 8, 2009; revised November 6, 2009; accepted December 10, 2009.

Disclosure: **M. Chaabouni**, None; **H. Etchevers**, None; **M.C. De Blois**, None; **P. Calvas**, None; **M.C. Waill-Perrier**, None; **M. Vekemans**, None; **S.P. Romana**, None

*Each of the following is a corresponding author: Myriam Chaabouni, Service des Maladies Héréditaires et Congénitales, Hôpital Charles Nicolle, Boulevard du 9 Avril, 1006 Tunis, Tunisia; chaabouni_myriam@yahoo.fr.

Serge Pierrick Romana, Service de Cytogénétique, Hôpital Necker Enfants Malades, 149 rue de Sèvres 75015 Paris, France; serge.romana@nck.aphp.fr.

Broad genetic variability underlies disorders of the anterior segment of the eye, collectively termed anterior segment ocular dysgenesis (ASOD). *PAX6*, a major gene for all stages of eye development, has been found to be mutated in phenotypically variable cases of ASOD.[1–5] In addition, other transcription factors are crucial for the coordinated development of the cornea, iris, lens, and ciliary bodies, including members of the forkhead (FOX), PITX, and MAF families.

Several studies have shown that patients with Rieger anomaly, Peters' anomaly or iris hypoplasia, which are dominant disorders, have mutations in *FOXC1* and *PITX2*,[6–10] whereas mutations in *PITX3* can cause anterior segment mesenchymal dysgenesis.[11–13] *FOXE3*, with an evolutionarily conserved role in induction of the lens placode, is mutated in patients with aphakia and in patients presenting with ASOD clinical features.[14–17] *MAF* has been implicated in congenital cataract.[18–20] The number of identified genes implicated in anterior segment development is increasing, reflecting wide phenotypic as well as genetic heterogeneity. It is likely that these transcription factors regulate each other's bioavailability in both space and time.

The Iroquois family genes (*IRX*) encode homeoproteins, conserved throughout the animal kingdom, that are involved in tissue patterning and regional differentiation. Various knockdown experiments and the endogenous expression patterns in vertebrate embryo models have demonstrated the implication, particularly of *IRX3* and *IRX5*, in ocular morphogenesis.[21–23] The six mammalian IRX genes are organized in two clusters (IRXA and IRXB) located on different chromosomes. IRXA and IRXB undoubtedly underwent duplication over the course of evolution.[21,24–27] In humans, *IRX1*, *IRX2*, and *IRX4* of the IRXA complex are located on 5p15.3, whereas *IRX3*, *IRX5*, and *IRX6* of the IRXB cluster are localized on 16q12.2. Thus far and despite their involvement in the development of several organ systems,[21,28–39] none of these IRX genes has been implicated in human disease.

We describe herein a child with bilateral congenital dysgenesis of the anterior segment of the eye, including aphakia and aniridia, associated with a complex chromosomal abnormality: inv(2)(p22.3q12.1)t(2;16)(q12.1;q12.2). The translocation breakpoint lies near the *IRX3* gene. Moreover, we show that *IRX3* is expressed in the eye anterior segment during early human embryonic development. We propose that this translocation deregulates by a positional effect the expression of an IRXB cluster gene(s), leading to the anterior segment dysgenesis observed in this patient.

Material and Methods

Case Report

The propositus was born of nonconsanguineous parents after a normal pregnancy with no history of intrauterine infection or exposure to teratogenic agents, and delivery at term was uncomplicated. At birth,

Investigative Ophthalmology & Visual Science, September 2010, Vol. 51, No. 9

bilateral megalocornea, photophobia, and tearing were noticed. A detailed ophthalmic examination performed with the subject under anesthesia at the age of 3 months showed bilateral corneal opacification with epithelial edema, corneal central thinning, retrodescemetic pigmentation, aniridia, secondary glaucoma, and vascularization of the cornea. IOP was 18 mm Hg in the right eye and 10 mm Hg in the left one. No lens was found. The posterior segment of the eyes were normal. On ultrasound examination (20 MHz), neither the lenses nor the irises were observable. No other malformation was detected. The clinical features in our patient did not seem to fit a particular category. We conclude that these anomalies are compatible with a dysgenesis of the anterior segment of the eye with secondary glaucoma. Only the proband's mother was examined. She had normal vision and no abnormality was found. No ocular abnormalities of the father were reported.

All analyses performed in this study were made after the parents' informed consent was obtained. The protocol of the study was in compliance with the guidelines in the Declaration of Helsinki.

Classic and Molecular Cytogenetic Techniques

Metaphase chromosome spreads of the patient and his parents were prepared from peripheral blood lymphocytes and analyzed by using classic banding techniques. An EBV-transformed lymphoblast cell line of the patient was established for chromosome, DNA, and RNA preparations.

BAC and PAC clones were selected from the UCSC Human Genome Browser (http://genome.ucsc.edu/ provided in the public domain by UCSC Genome Bioinformatics, University of California at Santa Cruz). They were obtained from the French national sequencing center. BAC DNAs were extracted by using a classic phenol-chloroform method and labeled using standard nick translation incorporating FITC, cyanine (Cy)3.5, Cy3, biotin-16-dUTP, and digoxigenin-11-dUTP (Roche Diagnostics, Mannheim, Germany). Biotin- and digoxigenin-labeled probes were subsequently revealed with streptavidin or an anti-digoxigenin antibody coupled to Cy5 and Cy5.5. Fluorescence in situ hybridization was performed as described previously.[40]

To look for a deletion at the translocation breakpoints, we used BAC array slides (PerkinElmer, Courtaboeuf, France), which offer a resolution of 0.65 Mb, in CGH array experiments. Hybridization was performed as described previously.[41]

Southern Blot Analysis

For molecular cloning, Southern blot analysis was performed us usual, with the use of different probes located around the *IRX3* locus. In particular, probe H, which allowed us to localize the rearrangement, was built by PCR with the following primer set: forward (5′ TTG TGA GGC GTG AGC TGT T 3′) and reverse (5′ TCT TTT TCC TCT CGC AGT CA 3′). Probe H hybridizes to nucleotides 79118-79880 of clone RP11-1146I14 (GenBank accession number AQ776753; http://www.ncbi.nlm.nih.gov/Genbank; provided in the public domain by the National Center for Biotechnology Information, Bethesda, MD) localized at 16q12.2.

Expression Analysis

Cytoplasmic RNAs of lymphoblast cell lines from the patient and 15 control individuals were isolated (RNeasy Mini Kit; Qiagen, Courtaboeuf, France) and reverse transcribed (Superscript II reverse transcriptase; Invitrogen, Cergy Pontoise, France) and random primers from 200 ng of each RNA. Real-time quantitative RT-PCR analyses of *IRX3* and *IRX5* transcripts were performed with predesigned and optimized gene expression assays (TaqMan; Applied Biosystems, Inc. [ABI], Foster City, CA) on a real-time PCR system (model 7500; ABI) according to the manufacturer's instructions. Relative quantification was performed by the $^{\Delta\Delta}$CT method, with the Abelson transcript used as an endogenous control.

Sequencing

Direct sequencing of the coding regions of genes *PITX2a*, *PITX2b*, *PAX6*, and *FOXC1* in both forward and reverse directions was performed.

In Situ Tissue Expression Pattern

IRX3 expression was examined in situ in human embryos and fetuses with normal karyotypes between 29 days' and 14.5 weeks' development, obtained from terminated pregnancies in concordance with French legislation (Acts 94-654 and 08-400) and with oversight by the Necker hospital ethics committee. Primers were selected for PCR amplification of a fragment of *IRX3* cDNA. A T7 promoter sequence extension (TAATACGACTCACTATAGGGAGA) was added to the 5′ end of each primer (forward [F]: agcgatggctggggctcactcg; reverse [R]: TGGCCGCGCCGTCTAAGTTCTC), and RNA was synthesized in vitro with F and T7R for antisense and T7F and R for sense probes, using ^{35}S- or digoxigenin-labeled UTP. Tissue fixation and sectioning and in situ hybridization were performed according to standard protocols.[42]

Results

Classic banding techniques of the patient's chromosomes showed an apparently balanced rearrangement between chromosomes 2 and 16 (Figs. 1A, 1B). Parental karyotypes were normal. Thus, the chromosomal rearrangement occurred de novo. FISH experiments, with the WCP2 and WCP16 centromeric probes of chromosomes 2 and 16 and the 16p/16q and 2p/2q subtelomeric probes, showed two normal chromosomes 2 and 16 and two derivatives of chromosomes 2 and 16, confirming a translocation between the long arm of chromosome 16 and the long arm of chromosome 2 (Fig. 1C). However, the long arm of the der(2) chromosome was shorter than expected. We hypothesized that in addition to the translocation, a chromosome 2 inversion may be present. We interpreted the karyotype as: 46, XY, inv(2)(p22.3q12.1)t(2;16)(q12.1;q12.2). CGH array experiments with a resolution of 1 Mb demonstrated that no microscopic rearrangements greater than 1 Mb were present at the chromosomal breakpoint.

Direct sequencing of currently known genes involved in human diseases of the anterior segment of the eye showed that *PITX2* (isoforms *a* and *b*), *PAX6*, and *FOXC1* were not mutated. Considering these results, we decided to clone the chromosomal breakpoints by FISH. For this purpose, we selected a panel of 2p22.3, 2q12.1, and 16q12.2 BAC clones as probes for FISH experiments. RP11-68N21 generated three signals, one at 2p22.3 on the nonrearranged chromosome 2 and two on the inverted chromosome 2, respectively, at 2p22.3 and 2q12.1, attesting that this BAC spanned the locus involved in the chromosome 2 inversion. RP11-315P20 also generated three signals, one at 2q12.1 on the nonrearranged chromosome 2, one at 2p22.3 on the rearranged chromosome 2, and one at 16q12.2 on the derivative chromosome (der)16. This finding suggested that the 2q inversion locus and the translocation locus were identical and localized within the BAC 315P20 at 2q12.1. Finally, we found that RP11-1061C23, localized at 16q12.2, also gave three signals: one clearly localized on the nonrearranged chromosome 16, one on the der(16) chromosome, and one on the long arm of the der(2) chromosome, attesting that this BAC was hybridizing at the chromosome 16 breakpoint. Cohybridization of these three BACS showed colocalization of the BACs RP11-68N21 and RP11-315P20 at 2p22.3, BACs RP11-68N21 and RP11-1061C23 at 2q12.1, and BACs RP11-315P20 and RP11-1061C23 at 16q12.2 (Fig. 1D). These findings confirmed the complex chromosomal rearrangement. According to the UCSC database (http://genome.ucsc.edu; NCBI human genome build 36.1), the clones

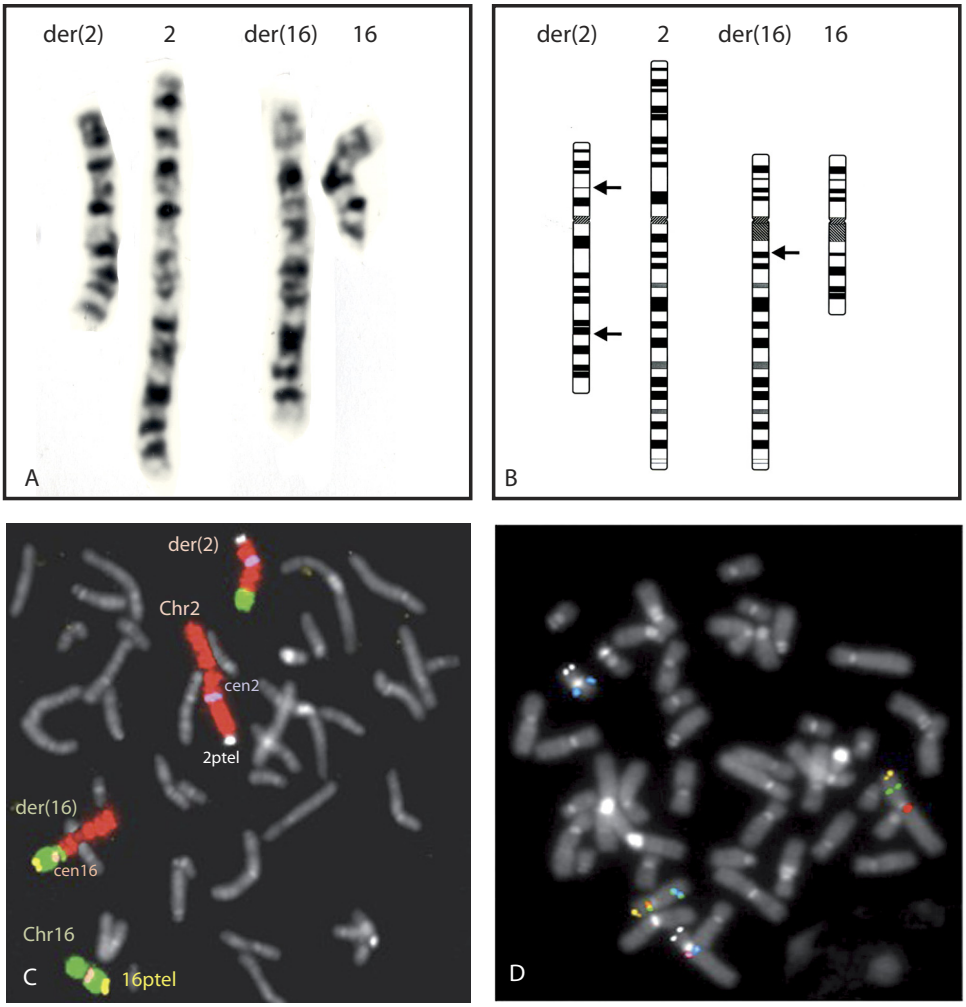

FIGURE 1. Cytogenetic and molecular characterization of the inv(2)(p22.3q12.1)t(2;16)(q12.1;q12.2) complex translocation. (**A**, **B**) Partial karyotype (**A**) and ideogram (**B**) with G-banding technique showing respectively the normal and derivative chromosomes 2 and 16. *Arrow*: the chromosomal breakpoint localization. (**C**) FISH results using the 2p subtelomeric probe RP5-892G20, the 16p subtelomeric probe CTB-191K2, chromosome 2 and 16 centromeric probes pBS4D and pZ16.A, respectively, labeled with biotin/Cy5 (*white*), digoxigenin/Cy5.5 (*yellow*), FITC (*purple*), and rhodamine (*pink*). Whole chromosome painting of chromosomes 2 (*red*) and 16 (*green*) showing the translocation between chromosome 2 and 16 and an unexpected aspect of der(2) leading to a supplementary investigation as shown in (**D**). (**D**) FISH results using clones spanning the three breakpoints: RP11-68N21 (labeled with FITC; *green*) at 2p22.3, RP11-315P20 (labeled with rhodamine; *red*) at 2q12.1, and RP11-1061C23 (labeled with Cy3.5; *blue*) at 16q12.2. 2p (RP5-892G20) and 16p (CTB-191K2) subtelomeric probes respectively labeled with biotin (*yellow*) and digoxigenin (*white*) were used for chromosome identification. Cohybridization of *red* and *blue* signals on der(16) confirms the t(2;16); cohybridization of *red* and *green* signals on der(2) demonstrate the pericentric inversion of chromosome 2.

spanning the inversion breakpoints 2p22.3 and 2q12.1 are free of known genes or ESTs. However, RP11-1061C23, which overlaps the 16q12.2 breakpoint, contains the *IRX3* gene, which belongs to the IRXB cluster.

To better localize the chromosome 16 breakpoint, we performed Southern blot analysis with probes surrounding the *IRX3* locus. As shown in Figure 2, one of these probes, probe H, allowed us to map the breakpoint located approximately 2 kb from the *IRX3* 3′UTR within a 625-bp region. Unfortunately, we were not able to clone the breakpoint at a better resolution by using inverse PCR. UCSC database analysis of this region showed a 331-bp Alu sequence and no conserved noncoding element.

Because the evolutionarily conserved Irx genes are involved in eye development in many animals, from fruit flies to mice, we performed in situ hybridization with probes against *IRX3* in

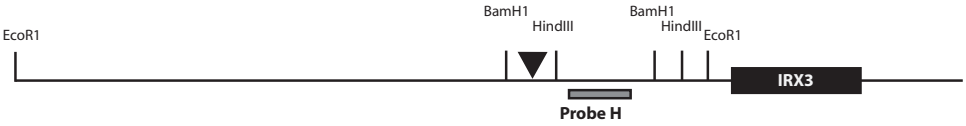

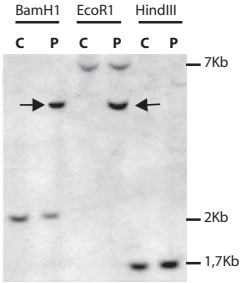

FIGURE 2. Mapping of the translocation breakpoint by Southern blot. Genomic DNA of our patient (P) compared with control DNA (C), after digestion with restriction enzymes. Additional bands (*arrows*) were detected in the P sample for both *Bam*HI and *Eco*RI but not for *Hin*dIII. *Arrowhead*: the breakpoint localization approximately 2 kb from the *IRX3* 3′UTR between the *Bam*HI and *Hin*dIII sites in a 625-bp region.

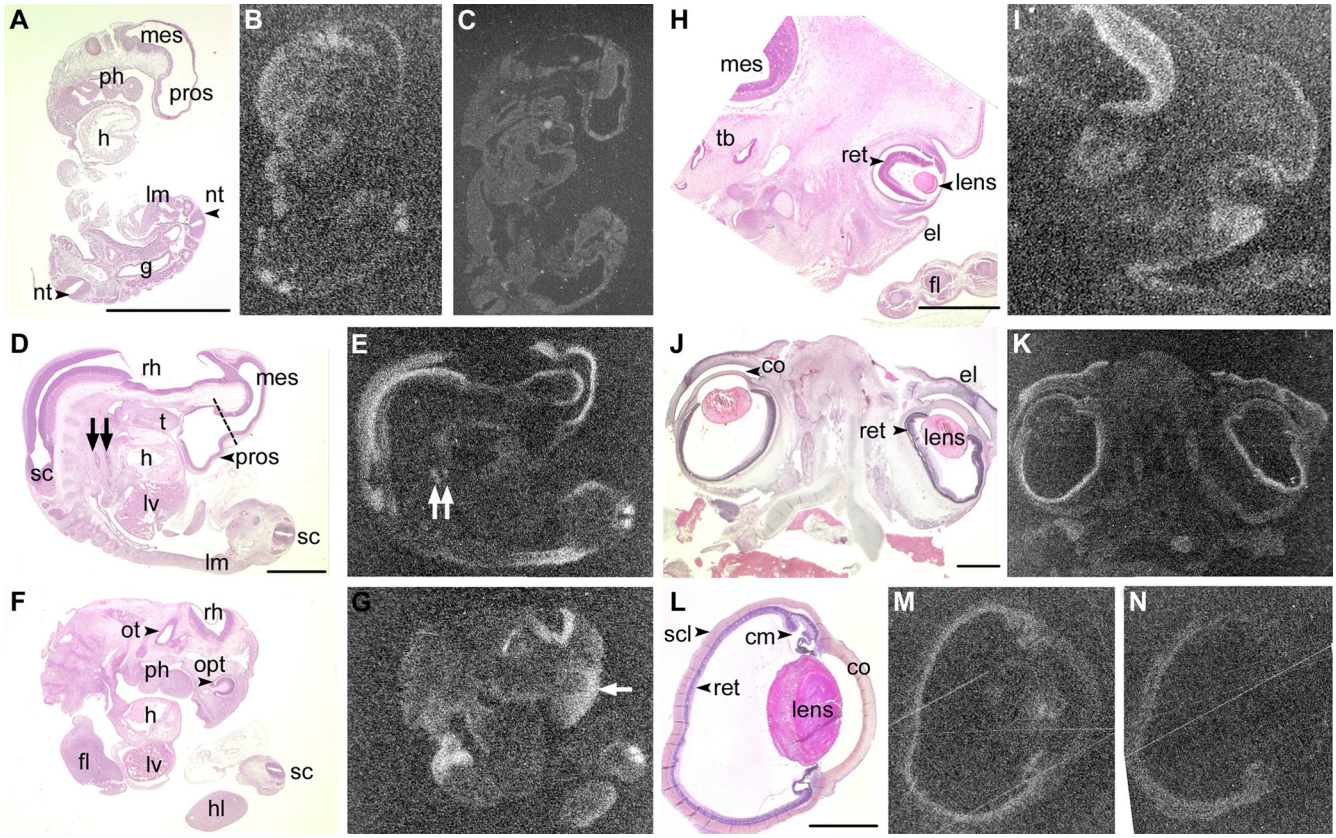

Figure 3. In situ hybridization to probes against *IRX3* in human embryonic and fetal sections. (**A**) Embryo at C13 (29–31 dpf), hematoxylin-eosin (HE) stain. Sagittal section in the head, transverse in the body. (**B**) Adjacent section shows signal with antisense probe to *IRX3* transcripts (*white*), in dorsal cephalic mesenchyme, brain, lateral mesoderm, and the neural tube. (**C**) Negative control using sense *IRX3* probe. (**D**) Sagittal section (transverse caudally) of embryo at C15 (35–38 dpf), HE stain. *Arrows*: esophagus (*left*); and trachea (*right*). (**E**) Adjacent section with antisense probe signal in the central nervous system except the prosencephalon, lateral mesoderm, tongue, and (*arrows*) esophageal and tracheal mesenchyme. (**F**) Lateral parasagittal section from the same embryo with limbs and developing inner ear structures. (**G**) *IRX3* is expressed in the midbrain, proximal forelimb and outer hindlimb mesenchyme, and strongly in the facial mesenchyme surrounding the nonexpressing optic evagination from the forebrain. (**H**) Sagittal section through the face and distal forelimb of a C19 (48–51 dpf) embryo, HE stain. (**I**) Adjacent section showing intense *IRX3* expression in the midbrain and facial ectoderm—in particular, of the eyelids and lower ocular mesenchyme—and more discrete expression in the retina, the temporal bone surrounding the inner ear, and the perichondria of the digits. (**J**) Coronal section through eyes of fetus at 9.5 wpf, HE stain. (**K**) Adjacent section with *IRX3* transcripts in retina, cornea, eyelid epidermis, and ciliary margin. (**L**) Sagittal section through eye of fetus at 14.5 wpf, HE stain. (**M**) *IRX3* antisense probe shows signal in ciliary margin, lens, neural retina, and diffusely in the cornea. (**N**) Compared with sense probe negative control hybridization to this adjacent section, the sclera does not express *IRX3* at this stage. cm, ciliary margin; co, cornea; el, eyelid; fl, forelimb; g, gut; h, heart; hl, hindlimb; lm, lateral mesoderm; lv, liver; mes, mesencephalon; nt, neural tube; opt, optic evagination; ot, otic vesicle; ph, pharynx; pros, prosencephalon; ret, retina; rh, rhombencephalon; sc, spinal cord; scl, sclera; t, tongue; tb, temporal bone. Scale bar, 1 mm.

human embryonic sections at Carnegie stage (C)13 (29–31 days after fertilization, dpf), C15 (35-38 dpf), and C19 (48-51 dpf) and on fetal sections at 9.5 and 14.5 weeks after fertilization (wpf). *IRX3* is expressed (Fig. 3) in the central nervous system, particularly the midbrain, limb mesenchyme, and the esophageal and tracheal mesenchyme. From C15 on, *IRX3* was expressed in facial mesenchyme involved in eye formation, in particular anterior segment development. At C19, *IRX3* was expressed in the facial ectoderm of the eyelid. In addition, *IRX3* transcripts could be observed in the mesenchyme of the gut as well as in the developing limb bud, in particular in the perichondrium. At 9.5 wpf, *IRX3* was clearly expressed again in the eyelid epidermis, in the cornea, in the ciliary margin and weakly in the retina. Finally, at 14.5 wpf, we found *IRX3* expression in the ciliary margin, lens, cornea, and the neural retina itself. *IRX3* is therefore clearly expressed in regions involved in the embryologic development of the anterior segment of the eye.

These results prompted us to use quantitative RT-PCR to evaluate *IRX3* and *IRX5* expression in peripheral blood lymphocytes of our patient versus that in 15 unaffected control blood samples. We did not find any difference in *IRX3* or *IRX5* expression between our patient and the 15 control samples. *IRX3* does not appear to be expressed in postnatal lymphocytes. Unfortunately fibroblasts, where the IRX genes may be expressed, were not available from the patient.

Discussion

We describe the molecular characterization of an inv(2)(p22.3q12.1)t(2;16)(q12.1;q12.2) complex chromosomal rearrangement associated with a congenital, bilateral malformation of the anterior segment of the eye designated as severe ASOD with glaucoma. We propose that this rearrangement may be responsible for disruption of the expression of *IRX3* or other IRXB genes, leading to the severe malformation of the anterior segment of the eye.

During the third to fifth weeks of gestation, development of the anterior segment is in great part due to reciprocal induc-

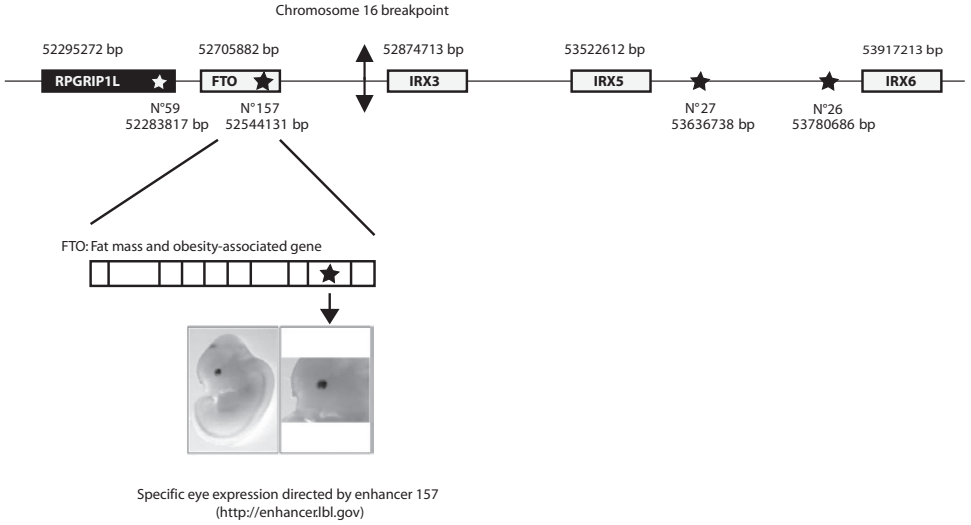

FIGURE 4. HCNCRs having an enhancer activity and driving expression in the eye during mouse development. *Double-pointed vertical arrow*: the translocation breakpoint; *star*: sequence with enhancer activity.

tions between the neural optic evagination, the overlying ectoderm, and intervening neural-crest–derived mesenchyme. On the basis of clinical data, animal models and temporal pattern of expression, some genes are particularly important in coordinating these processes. This is the case for the *PAX6*, *FOXC1*, and *PITX2* transcription factor genes. *PAX6* is considered by some to be a "master" gene in eye development that encodes multiple protein isoforms involved in both cornea and lens formation.[43] Many reports show that in humans, this gene is implicated in aniridia, isolated cataracts, macular hypoplasia, keratitis, and Peters' anomaly.[3–5,44] These clinical permutations are registered in the *PAX6* mutation database (http://pax6.hgu.mrc.ac.uk/ provided in the public domain by the Human Genetics Unit, Medical Research Council, Edinburgh, Scotland, UK).[45] Similarly, both human disease and murine models have demonstrated the importance of *FOXC1* and *PITX2* in the development of the anterior segment of the eye. For example, mutations in *FOXC1* are associated with Axenfeld-Rieger anomaly or iris hypoplasia and *FOXC1*-knockout mice have anterior segment abnormalities similar to those reported in humans.[46] Rieger syndrome is linked with certain *PITX2* mutations.[47–51]

In our patient, no mutation of these genes was found. However, in this complex chromosomal translocation, the der(16) breakpoint is located close (~2 kb) to the *IRX3* 3′UTR. *IRX3* belongs to the Iroquois gene family (named after the *Drosophila* bristle phenotype), which has been conserved during animal evolution from at least the time of a common ancestor with *Caenorhabditis elegans* (in which there is only one such gene) to vertebrates, in which there are between 6 and 11 IRX genes subsequent to multiple duplication events.[21,22,24–26,29,52,53] These genes encode for proteins with a highly conserved homeodomain of the TALE (three amino acid loop extension) superclass, as well as a 13-amino-acid domain called the Iroquois domain.[54] In all species, Irx proteins are involved in early embryonic organ specification and patterning—in particular, the head, limbs, and eyes.[28,31–39] In the mouse eye, *Irx1*, *Irx3*, *Irx5*, and *Irx6* display very similar patterns of expression during organogenesis. At E9.5, *Irx3* and *Irx5* expression is first observed in the cephalic mesenchyme of neural crest origin, surrounding the optic vesicle. *Irx1* and *Irx6* are only subsequently coexpressed in this region at E10.5. By E12.5, the Irx genes are still expressed in the mesenchyme but also begin to be expressed in the neural retina, while decreasing in intensity in the mesenchyme. Irx genes are finally expressed exclusively in the neural cell layer of the retina at E16.5.[22] These data are concordant with our results of *IRX3* expression in human embryonic and fetal sections. In particular, we observed *IRX3* expression in midfacial mesenchyme surrounding the nonexpressing optic evagination, in preocular ectoderm, and later in the ciliary margin and in the lens. Altogether, these data indicate that the *IRX3* gene is functionally involved in the development of the anterior segment of the human eye.

Like other genes implicated in several developmental processes, regulation of IRX gene expression is coordinated in a spatial and temporal manner. Such coordination can be accomplished by tissue-specific transcription factors binding of enhancers, sometimes at distances ranging over 1 Mb 5′ or 3′ to the coding sequences that control either the expression of individual homeobox genes or the entire cluster. Examples are the *SOX9* gene or the HOXD gene cluster, respectively.[55,56] The human IRXA cluster spans 1.8 Mb, and the IRXB cluster spans 1.3 Mb. No other genes are interspaced between the IRX genes in the clusters. In the IRXB cluster, *IRX3* is located at the centromeric end and has a 5′ telomere to 3′ centromere transcriptional orientation, which is opposite that of *IRX5* and *IRX6*. In 2005, de la Calle-Mustienes et al.,[23] using transgenic *Xenopus* and zebrafish embryos, demonstrated that 22 highly conserved noncoding regions (HCNCRs) that lie within the IrxB cluster (and one located just telomeric to the *Irx6* locus) direct the spatiotemporally specific expression of IrxB genes. In 2006, Pennacchio et al.[57] tested 167 HCNCRs, conserved between humans and the pufferfish *Takifugu rubripes* or ultraconserved between humans and rodents, in a transgenic mouse assay. A meticulous analysis of these data showed that 21 HCNCRs lay within the IRXB cluster, 17 between *IRX3* and *IRX5* and 4 between *IRX5* and *IRX6* (Fig. 4). Functional tests showed that only 4 HCNCRs among the 21 have an enhancer activity in the eye during the mouse's embryonic development. Enhancers 26 and 27 are located between *IRX5* and *IRX6* and are probably involved in *IRX5* and *IRX6* expression. Enhancer 157, located 330 kb centromeric to *IRX3* in intron 11of the *FTO* gene induces in a murine transgenic assay an eye-specific expression resembling that of *IRX3*. This gene is involved in controlling body fat. Its expression during embryonic development and its invalidation in mice did not show any activity in ocular embryogenesis.[58,59] Enhancer 59 is located in the first intron of the *RPGRIP1L* gene (retinitis pigmentosa GTPase regulator interacting protein 1–like gene). This gene is expressed in several types of fetal and adult tissues but mainly in the brain, kidneys, ovaries, and testes and at the level of the retinal photoreceptors.[60,61] Knockout mice *Rpgrip1l*$^{-/-}$ which are not viable, show exencephaly, polydactyly, abnor-

malities of lateralization, and microphthalmia.[60] In humans, mutations of *RPGRIP1L* are found in patients presenting with the recessive syndromes oculo-cerebro-renal or type B Joubert and Meckel syndromes.[60,61] This gene is involved in eye embryogenesis. It is reasonable to assume that enhancer 59 is associated with the control of the expression of *RPGRIP1L* in the eye. We therefore hypothesize that enhancer 157 plausibly plays a role in IRXB gene expression in the developing human eye. In addition, the chromosomal rearrangement delocalizes the IRXB cluster at the 2p22.3 region covered by the RP11-68N21. No known genes or HCNCRs were found. Accordingly, the translocation separates the IRXB cluster from enhancer 157, which has a specific eye expression thus deregulating the complex spatiotemporal expression and generating the ASOD observed in our patient.

In our patient, the translocation separates the IRXB complex from this enhancer, among others, and may deregulate the spatiotemporal expression of the IRXB cluster gene(s).

Although the evolutionarily conserved IRX genes have been implicated in various developmental processes in animal models, so far no human disease linked to an IRX gene has been reported, perhaps due in part to the existence of functional compensation between these genes, as has been reported.[62] We describe a child with a severe ASOD associated with a complex chromosomal rearrangement inv(2)(p22.3q12.1)t(2:16)(q12.1;q12.2) because of the potential deregulation of IRXB genes by a positional effect.

Acknowledgments

The authors thank the patient and his family for participating in the study, Tania Attié-Bitach for constructive discussion, and Geraldine Goudefroye and Genevieve Molina for technical assistance.

References

1. Hill RE, Favor J, Hogan BL, et al. Mouse small eye results from mutations in a paired-like homeobox-containing gene. *Nature.* 1991;354:522–525.
2. Favor J, Peters H, Hermann T, et al. Molecular characterization of Pax6(2Neu) through Pax6(10Neu): an extension of the Pax6 allelic series and the identification of two possible hypomorph alleles in the mouse Mus musculus. *Genetics.* 2001;159:1689–1700.
3. Glaser T, Jepeal L, Edwards JG, Young SR, Favor J, Maas RL. PAX6 gene dosage effect in a family with congenital cataracts, aniridia, anophthalmia and central nervous system defects. *Nat Genet.* 1994;7:463–471.
4. Hanson I, Churchill A, Love J, et al. Missense mutations in the most ancient residues of the PAX6 paired domain underlie a spectrum of human congenital eye malformations. *Hum Mol Genet.* 1999;8:165–172.
5. van Heyningen V, Williamson KA. PAX6 in sensory development. *Hum Mol Genet.* 2002;11:1161–1167.
6. Saleem RA, Banerjee-Basu S, Berry FB, Baxevanis AD, Walter MA. Analyses of the effects that disease-causing missense mutations have on the structure and function of the winged-helix protein FOXC1. *Am J Hum Genet.* 2001;68:627–641.
7. Nishimura DY, Searby CC, Alward WL, et al. A spectrum of FOXC1 mutations suggests gene dosage as a mechanism for developmental defects of the anterior chamber of the eye. *Am J Hum Genet.* 2001;68:364–372.
8. Panicker SG, Sampath S, Mandal AK, Reddy AB, Ahmed N, Hasnain SE. Novel mutation in FOXC1 wing region causing Axenfeld-Rieger anomaly. *Invest Ophthalmol Vis Sci.* 2002;43:3613–3616.
9. Komatireddy S, Chakrabarti S, Mandal AK, et al. Mutation spectrum of FOXC1 and clinical genetic heterogeneity of Axenfeld-Rieger anomaly in India. *Mol Vis.* 2003;9:43–48.
10. Priston M, Kozlowski K, Gill D, et al. Functional analyses of two newly identified PITX2 mutants reveal a novel molecular mechanism for Axenfeld-Rieger syndrome. *Hum Mol Genet.* 2001;10:1631–1638.
11. Semina EV, Ferrell RE, Mintz-Hittner HA, et al. A novel homeobox gene PITX3 is mutated in families with autosomal-dominant cataracts and ASMD. *Nat Genet.* 1998;19:167–170.
12. Semina EV, Murray JC, Reiter R, Hrstka RF, Graw J. Deletion in the promoter region and altered expression of Pitx3 homeobox gene in aphakia mice. *Hum Mol Genet.* 2000;9:1575–1585.
13. Rieger DK, Reichenberger E, McLean W, Sidow A, Olsen BR. A double-deletion mutation in the Pitx3 gene causes arrested lens development in aphakia mice. *Genomics.* 2001;72:61–72.
14. Semina EV, Brownell I, Mintz-Hittner HA, Murray JC, Jamrich M. Mutations in the human forkhead transcription factor FOXE3 associated with anterior segment ocular dysgenesis and cataracts. *Hum Mol Genet.* 2001;10:231–236.
15. Ormestad M, Blixt A, Churchill A, Martinsson T, Enerback S, Carlsson P. Foxe3 haploinsufficiency in mice: a model for Peters' anomaly. *Invest Ophthalmol Vis Sci.* 2002;43:1350–1357.
16. Blixt A, Mahlapuu M, Aitola M, Pelto-Huikko M, Enerback S, Carlsson P. A forkhead gene, FoxE3, is essential for lens epithelial proliferation and closure of the lens vesicle. *Genes Dev.* 2000;14:245–254.
17. Valleix S, Niel F, Nedelec B, et al. Homozygous nonsense mutation in the FOXE3 gene as a cause of congenital primary aphakia in humans. *Am J Hum Genet.* 2006;79:358–364.
18. Jamieson RV, Perveen R, Kerr B, et al. Domain disruption and mutation of the bZIP transcription factor, MAF, associated with cataract, ocular anterior segment dysgenesis and coloboma. *Hum Mol Genet.* 2002;11:33–42.
19. Lyon MF, Jamieson RV, Perveen R, et al. A dominant mutation within the DNA-binding domain of the bZIP transcription factor Maf causes murine cataract and results in selective alteration in DNA binding. *Hum Mol Genet.* 2003;12:585–594.
20. Vincent A, Billingsley G, Priston M, et al. Phenotypic heterogeneity of CYP1B1: mutations in a patient with Peters' anomaly. *J Med Genet.* 2001;38:324–326.
21. Christoffels VM, Keijser AG, Houweling AC, Clout DE, Moorman AF. Patterning the embryonic heart: identification of five mouse Iroquois homeobox genes in the developing heart. *Dev Biol.* 2000;224:263–274.
22. Cohen DR, Cheng CW, Cheng SH, Hui CC. Expression of two novel mouse Iroquois homeobox genes during neurogenesis. *Mech Dev.* 2000;91:317–321.
23. de la Calle-Mustienes E, Feijóo CG, Manzanares M, et al. A functional survey of the enhancer activity of conserved non-coding sequences from vertebrate Iroquois cluster gene deserts. *Genome Res.* 2005;15:1061–1072.
24. Bosse A, Stoykova A, Nieselt-Struwe K, et al. Identification of a novel mouse Iroquois homeobox gene, Irx5, and chromosomal localisation of all members of the mouse Iroquois gene family. *Dev Dyn.* 2000;218:160–174.
25. Ogura K, Matsumoto K, Kuroiwa A, et al. Cloning and chromosome mapping of human and chicken Iroquois (IRX) genes. *Cytogenet Cell Genet.* 2001;92:320–325.
26. Peters T, Dildrop R, Ausmeier K, Ruther U. Organization of mouse Iroquois homeobox genes in two clusters suggests a conserved regulation and function in vertebrate development. *Genome Res.* 2000;10:1453–1462.
27. Wang X, Emelyanov A, Sleptsova-Friedrich I, Korzh V, Gong Z. Expression of two novel zebrafish iroquois homologues (ziro1 and ziro5) during early development of axial structures and central nervous system. *Mech Dev.* 2001;105:191–195.
28. Bellefroid EJ, Kobbe A, Gruss P, Pieler T, Gurdon JB, Papalopulu N. Xiro3 encodes a Xenopus homolog of the Drosophila Iroquois genes and functions in neural specification. *EMBO J.* 1998;17:191–203.
29. Bosse A, Zulch A, Becker MB, et al. Identification of the vertebrate Iroquois homeobox gene family with overlapping expression during early development of the nervous system. *Mech Dev.* 1997;69:169–181.
30. Mummenhoff J, Houweling AC, Peters T, Christoffels VM, Ruther U. Expression of Irx6 during mouse morphogenesis. *Mech Dev.* 2001;103:193–195.

31. Bao ZZ, Bruneau BG, Seidman JG, Seidman CE, Cepko CL. Regulation of chamber-specific gene expression in the developing heart by Irx4. *Science.* 1999;283:1161–1164.
32. Briscoe J, Pierani A, Jessell TM, Ericson J. A homeodomain protein code specifies progenitor cell identity and neuronal fate in the ventral neural tube. *Cell.* 2000;101:435–445.
33. Glavic A, Gomez-Skarmeta JL, Mayor R. The homeoprotein Xiro1 is required for midbrain-hindbrain boundary formation. *Development.* 2002;129:1609–1621.
34. Glavic A, Gomez-Skarmeta JL, Mayor R. Xiro-1 controls mesoderm patterning by repressing bmp-4 expression in the Spemann organizer. *Dev Dyn.* 2001;222:368–376.
35. Gomez-Skarmeta JL, Glavic A, de la Calle-Mustienes E, Modolell J, Mayor R. Xiro, a Xenopus homolog of the Drosophila Iroquois complex genes, controls development at the neural plate. *EMBO J.* 1998;17:181–190.
36. Itoh M, Kudoh T, Dedekian M, Kim CH, Chitnis AB. A role for iro1 and iro7 in the establishment of an anteroposterior compartment of the ectoderm adjacent to the midbrain-hindbrain boundary. *Development.* 2002;129:2317–2327.
37. Jin Z, Zhang J, Klar A, et al. Irx4-mediated regulation of Slit1 expression contributes to the definition of early axonal paths inside the retina. *Development.* 2003;130:1037–1048.
38. Kobayashi D, Kobayashi M, Matsumoto K, Ogura T, Nakafuku M, Shimamura K. Early subdivisions in the neural plate define distinct competence for inductive signals. *Development.* 2002;129:83–93.
39. Kudoh T, Dawid IB. Role of the iroquois3 homeobox gene in organizer formation. *Proc Natl Acad Sci U S A.* 2001;98:7852–7857.
40. Romana SP, Le Coniat M, Berger R. t(12;21): a new recurrent translocation in acute lymphoblastic leukemia. *Genes Chromosomes Cancer.* 1994;9:186–191.
41. Idbaih A, Coindre JM, Derre J, et al. Myxoid malignant fibrous histiocytoma and pleomorphic liposarcoma share very similar genomic imbalances. *Lab Invest.* 2005;85:176–181.
42. Sanlaville D, Etchevers HC, Gonzales M, et al. Phenotypic spectrum of CHARGE syndrome in fetuses with CHD7 truncating mutations correlates with expression during human development. *J Med Genet.* 2006;43:211–217.
43. Graw J. The genetic and molecular basis of congenital eye defects. *Nat Rev Genet.* 2003;4:876–888.
44. Morrison D, FitzPatrick D, Hanson I, et al. National study of microphthalmia, anophthalmia, and coloboma (MAC) in Scotland: investigation of genetic aetiology. *J Med Genet.* 2002;39:16–22.
45. Brown A, McKie M, van Heyningen V, Prosser J. The Human PAX6 Mutation Database. *Nucleic Acids Res.* 1998;26:259–264.
46. Smith RS, Zabaleta A, Kume T, et al. Haploinsufficiency of the transcription factors FOXC1 and FOXC2 results in aberrant ocular development. *Hum Mol Genet.* 2000;9:1021–1032.
47. Semina EV, Reiter R, Leysens NJ, et al. Cloning and characterization of a novel bicoid-related homeobox transcription factor gene, RIEG, involved in Rieger syndrome. *Nat Genet.* 1996;14:392–399.
48. Kulak SC, Kozlowski K, Semina EV, Pearce WG, Walter MA. Mutation in the RIEG1 gene in patients with iridogoniodysgenesis syndrome. *Hum Mol Genet.* 1998;7:1113–1117.
49. Doward W, Perveen R, Lloyd IC, Ridgway AE, Wilson L, Black GC. A mutation in the RIEG1 gene associated with Peters' anomaly. *J Med Genet.* 1999;36:152–155.
50. Lin CR, Kioussi C, O'Connell S, et al. Pitx2 regulates lung asymmetry, cardiac positioning and pituitary and tooth morphogenesis. *Nature.* 1999;401:279–282.
51. Lu MF, Pressman C, Dyer R, Johnson RL, Martin JF. Function of Rieger syndrome gene in left-right asymmetry and craniofacial development. *Nature.* 1999;401:276–278.
52. Gomez-Skarmeta JL, Diez del Corral R, de la Calle-Mustienes E, Ferre-Marco D, Modolell J. Araucan and caupolican, two members of the novel iroquois complex, encode homeoproteins that control proneural and vein-forming genes. *Cell.* 1996;85:95–105.
53. Netter S, Fauvarque MO, Diez del Corral R, Dura JM, Coen D. White+ transgene insertions presenting a dorsal/ventral pattern define a single cluster of homeobox genes that is silenced by the polycomb-group proteins in Drosophila melanogaster. *Genetics.* 1998;149:257–275.
54. Burglin TR. Analysis of TALE superclass homeobox genes (MEIS, PBC, KNOX, Iroquois, TGIF) reveals a novel domain conserved between plants and animals. *Nucleic Acids Res.* 1997;25:4173–4180.
55. Duboule D. The rise and fall of Hox gene clusters. *Development.* 2007;134:2549–2560.
56. Benko S, Fantes JA, Amiel J, et al. Highly conserved non-coding elements on either side of SOX9 associated with Pierre Robin sequence. *Nat Genet.* 2009;41:359–364.
57. Pennacchio LA, Ahituv N, Moses AM, et al. In vivo enhancer analysis of human conserved non-coding sequences. *Nature.* 2006;444:499–502.
58. Peters T, Ausmeier K, Ruther U. Cloning of Fatso (Fto), a novel gene deleted by the Fused toes (Ft) mouse mutation. *Mamm Genome.* 1999;10:983–986.
59. Frayling TM, Timpson NJ, Weedon MN, et al. A common variant in the FTO gene is associated with body mass index and predisposes to childhood and adult obesity. *Science.* 2007;316:889–894.
60. Delous M, Baala L, Salomon R, et al. The ciliary gene RPGRIP1L is mutated in cerebello-oculo-renal syndrome (Joubert syndrome type B) and Meckel syndrome. *Nat Genet.* 2007;39:875–881.
61. Arts HH, Doherty D, van Beersum SE, et al. Mutations in the gene encoding the basal body protein RPGRIP1L, a nephrocystin-4 interactor, cause Joubert syndrome. *Nat Genet.* 2007;39:882–888.
62. Lebel M, Agarwal P, Cheng CW, et al. The Iroquois homeobox gene Irx2 is not essential for normal development of the heart and midbrain-hindbrain boundary in mice. *Mol Cell Biol.* 2003;23:8216–8225.

RESEARCH ARTICLE

Human Mutation

OFFICIAL JOURNAL HGVS HUMAN GENOME VARIATION SOCIETY www.hgvs.org

High-Throughput Sequencing of a 4.1 Mb Linkage Interval Reveals *FLVCR2* Deletions and Mutations in Lethal Cerebral Vasculopathy

Sophie Thomas,[1,2] Ferechté Encha-Razavi,[1–3] Louise Devisme,[4] Heather Etchevers,[1,2] Bettina Bessieres-Grattagliano,[5] Géraldine Goudefroye,[3] Nadia Elkhartoufi,[3] Emilie Pateau,[6] Amale Ichkou,[3] Maryse Bonnière,[3,7] Pascale Marcorelle,[8] Philippe Parent,[9] Sylvie Manouvrier,[10] Muriel Holder,[10] Annie Laquerrière,[11] Laurence Loeuillet,[12] Joelle Roume,[13] Jelena Martinovic,[3] Soumaya Mougou-Zerelli,[1,2,14] Marie Gonzales,[15] Vincent Meyer,[6] Marc Wessner,[6] Christine Bole Feysot,[16] Patrick Nitschke,[17] Nadia Leticee,[18] Arnold Munnich,[1–3] Stanislas Lyonnet,[1–3] Peter Wookey,[19] Gabor Gyapay,[6] Bernard Foliguet,[20] Michel Vekemans,[1–3] and Tania Attié-Bitach[1–3]*

[1]INSERM U-781, Hôpital Necker-Enfants Malades, Paris, France; [2]Université Paris Descartes, Paris, France; [3]Département de Génétique, Hôpital Necker-Enfants Malades, AP-HP, Paris, France; [4]Pôle de Pathologie, Centre de Biologie Pathologie, CHRU Lille, France; [5]Laboratoire d'Anatomo-Foeto-Pathologie, Institut de Puériculture et de Périnatalogie, Paris, France; [6]CEA, DSV, Institut de Génomique, Genoscope, Evry, France; [7]Laboratoire Nord Pathologie, Lille, France; [8]Laboratoire d'anatomopathologie, CHRU Hôpital Morvan, Brest, France; [9]Département de pédiatrie et génétique médicale, CHRU Hôpital Morvan, Brest, France; [10]Service de Génétique Clinique et Université Lille 2, CHRU de Lille, Hôpital Jeanne de Flandre, Lille, France; [11]Laboratoire d'Anatomie Pathologique, Hôpital de Rouen, Rouen, France; [12]Service d'Anatomie et de Cytologie Pathologiques, CHI Poissy, Saint Germain en Laye, France; [13]Génétique Médicale, CHI Poissy, Saint Germain en Laye, France; [14]Service de Cytogénétique, Génétique moléculaire et Biologie de la reproduction, Hôpital Farhat Hached, Sousse, Tunisie; [15]Service de Génétique et d'Embryologie Médicales, Hôpital Armand Trousseau, AP-HP, et Université Pierre et Marie Curie, Paris 6, France; [16]Plateforme de génomique, Fondation IMAGINE, Hôpital Necker-Enfants Malades, Paris, France; [17]Service de Bioinformatique, Université Paris Descartes, Paris, France; [18]Service de Gynécologie Obstétrique, Hôpital Necker-Enfants Malades, Paris, France; [19]Department of Medicine, University of Melbourne, Australia; [20]Laboratoire de Biologie de la Reproduction et du Développement, Maternité de Nancy, France

Communicated by Claude Fèrec

Received 11 May 2010; accepted revised manuscript 12 July 2010.
Published online 5 August 2010 in Wiley Online Library (wileyonlinelibrary.com). DOI 10.1002/humu.21329

ABSTRACT: Rare lethal disease gene identification remains a challenging issue, but it is amenable to new techniques in high-throughput sequencing (HTS). Cerebral proliferative glomeruloid vasculopathy (PGV), or Fowler syndrome, is a severe autosomal recessive disorder of brain angiogenesis, resulting in abnormally thickened and aberrant perforating vessels leading to hydranencephaly. In three multiplex consanguineous families, genome-wide SNP analysis identified a locus of 14 Mb on chromosome 14. In addition, 280 consecutive SNPs were identical in two Turkish families unknown to be related, suggesting a founder mutation reducing the interval to 4.1 Mb. To identify the causative gene, we then specifically enriched for this region with sequence capture and performed HTS in a proband of seven families. Due to technical constraints related to the disease, the average coverage was only 7×. Nonetheless, iterative bioinformatic analyses of the sequence data identified mutations and a large deletion in the *FLVCR2* gene, encoding a 12 transmembrane domain-containing putative transporter. A striking absence of alpha-smooth muscle actin immunostaining in abnormal vessels in fetal PGV brains, suggests a deficit in pericytes, cells essential for capillary stabilization and remodeling during brain angiogenesis. This is the first lethal disease-causing gene to be identified by comprehensive HTS of an entire linkage interval.
Hum Mutat 31:1134–1141, 2010. © 2010 Wiley-Liss, Inc.

KEY WORDS: Fowler syndrome; cerebral proliferative vasculopathy; *FLVCR2*; hydranencephaly; fetal lethality; arthrogryposis

Introduction

Cerebral proliferative glomeruloid vasculopathy (PGV) is a severe autosomal recessive disorder of brain angiogenesis, resulting in abnormally thickened and aberrant perforating vessels, forming glomeruloids with inclusion-bearing endothelial cells. This peculiar vascular malformation was delineated by Fowler in 1972 in relation to a stereotyped, lethal fetal phenotype (MIM# 225790), associating hydranencephaly and hydrocephaly with limb deformities [Fowler et al., 1972]. PGV disrupts the developing central nervous system (CNS) but the reason for which abnormal angiogenesis is restricted to the CNS parenchyme remains unknown. Arthryogryposis, when present, appears to be a secondary result of CNS motoneuron degeneration, itself one potential outcome of perfusion failure. Since its earliest description, 42 PGV cases from 26 families have been reported on the basis of histological criteria [Bessieres-Grattagliano et al., 2009; Williams et al., 2010].

Additional Supporting Information may be found in the online version of this article.

*Correspondence to: Tania Attie-Bitach, Département de Génétique et Unité INSERM U-781, Hôpital Necker-Enfants Malades, Paris, France. E-mail: tania.attie@inserm.fr

Identification of a causative gene for a very rare lethal syndrome is a challenge at many levels. The first issue is to find a family that allows the identification of a linkage interval. Such an interval may contain too many genes to make the classical subsequent strategy practical, consisting in designing primers that will permit sequencing of each exon of all the genes of the region. The second difficulty is that sequencing of all the exons is sometimes vain in light of the growing number of noncoding regions identified as pathogenic alleles [Benko et al., 2009; Kleinjan and van Heyningen, 2005; Lettice et al., 2003]. Finally, for prenatally lethal syndromes such as PGV, technical constraints such as poor-quality genomic DNA samples are added. Recent advances in biotechnology permit the sequencing of all the DNA, including the noncoding regions, in most genomic intervals. After homozygosity mapping of a 4.1-Mb region, we applied targeted genome capture by using a NimbleGen array and high-throughput Roche 454 GS FLX sequencing to the genomic DNA of the proband of six families. Bioinformatic analysis of the data allowed us to identify *FLVCR2* (MIM♯ 610865) as the gene responsible for Fowler syndrome (FS). High-throughput sequencing (HTS) generated false positive and false negative results, in part due to insufficient sequencing coverage, and unless care is taken, these can engender the risk of missing mutations during the analysis.

Materials and Methods

Patients

The seven families analysed have been previously reported (Families I to VII) [Bessieres-Grattagliano et al., 2009]. Genomic DNA was extracted from frozen tissue or cultured amniocyte cells in fetal cases and from peripheral blood samples for parents and unaffected siblings.

Genome Linkage Screening and Linkage Analysis

Genome-wide homozygosity mapping was performed using 250 K Affymetrix single nucleotide polymorphism (SNP) arrays in five affected and three unaffected individuals of two Turkish and one French multiplex, consanguineous families. Data were evaluated by calculating multipoint lod scores across the whole genome using MERLIN software, assuming recessive inheritance with complete penetrance.

NimbleGen Sequence Capture and High-Throughput Sequencing

A custom sequence capture array was designed and manufactured by Roche NimbleGen (Madison, WI). Twenty-one micrograms of genomic DNA was used for sequence capture in accordance with the manufacturer's instructions (Roche NimbleGen) and a final amount of 3 µg of amplified enriched DNA was used as input for generating a ssDNA library for HTS; 25% lane of a Roche 454 GS FLX sequencer with Titanium reagents) yielding 135 Mb of sequence data per sample.

Capillary Sequencing of *FLVCR2*

Primers were designed in introns flanking the 10 exons using the "Primer 3" program (http://fokker.wi.mit.edu/primer3/input.htm) and are listed in Supp. Table S1. PCR were all performed in the same conditions, with a touchdown protocol consisting of denaturation for 30 sec at 96°C, annealing for 30 sec at a temperature ranging from 64 to 50°C (decreasing 1° during 14 cycles, then 20 cycles at 50°) and extension at 72°C for 30 sec. PCR products were treated with Exo-SAP IT (AP Biotech, Buckinghamshire, UK), and both strands were sequenced with the appropriate primer and the "BigDye" terminator cycle sequencing kit (Applied Biosystems Inc., Bedford, MA) and analyzed on ABI3130 automated sequencers. Mutation numbering is based on cDNA reference sequence NM_017791.2.

Immunohistochemistry

Immunohistochemistry was carried out on 6-µm selected sections using antisera directed against smooth muscle actin (diluted 1:800). Immunohistochemical procedures included a classical microwave pretreatment protocol in citrate buffer to aid antigen retrieval. Incubations were performed for 1 hr at room temperature, using the TECHMATE system (DAKOPATTS, Trappes, France). After incubation, histological slides were processed using the LSAB detection kit (DAKOPPATTS). Peroxidase was visualized by means of either 3-3′ diaminobenzidine or amino-ethyl carbazole.

Results

We have collected DNA from fetuses of seven families reported earlier (Families I to VII) [Bessieres-Grattagliano et al., 2009]. All 14 fetal cases bore the brain-specific angiogenic anomalies characteristic of PGV, resulting in thickened and aberrant perforating vessels and glomeruloids, as exemplified in Figure 1A. Endothelial cells (ECs) were positive for CD34 in both control fetal brains (Fig. 1B) and in the tortuous glomerular capillaries (Fig. 1C). VEGF-A, although not normally expressed by small brain capillaries (Fig. 1D), was strikingly found in the glomerular ECs of PGV fetuses (Fig. 1E, arrowhead). Like normal ECs though, PGV ECs expressed VEGFR2 and, weakly, Glut-1 (not shown). CD68, characteristic of macrophages, was completely absent (data not shown). Numerous GFAP-positive astrocytes were observed throughout the cerebral mantle, with immunoreactive endfeet justaposed to glomeruloids (Fig. 1F). An antibody to alpha-smooth muscle actin (αSMA) stained vessels within the outer leptomeninges and the walls of perforating vessels in normal fetal brains (Fig. 1G). In contrast, although PGV meningeal vessels had similar aSMA expression, the dysplastic intraparenchymous vessels were irregularly stained, if at all (Fig. 1H), while most glomeruloid vessels were negative for aSMA (Fig. 1I).

To find the molecular basis for this phenotype, we first undertook a genome-wide SNP analysis using an Affymetrix 250 K SNP chip with five affected and three unaffected members of two Turkish and one French multiplex, consanguineous families. Informed consent was obtained from all patients and their relatives; clinical data of all families have previously been reported [Bessieres-Grattagliano et al., 2009]. Genome-wide linkage analysis conducted with the MERLIN program revealed a 13-Mb genomic region on chromosome 14 from rs10151019 to rs12897284, with a lodscore of 5.4. Moreover, four affected sibs from the two Turkish families shared the same alleles for 280 consecutive SNPs, suggesting a founder effect and reducing the interval to 4.1 MB, from rs2803958 to rs11159220. These two families originated from villages 12 km apart in Khramanmaraps (central Turkey). Microsatellite marker analysis further confirmed the same disease allele in both families, and showed linkage in three additional families (Fig. 2).

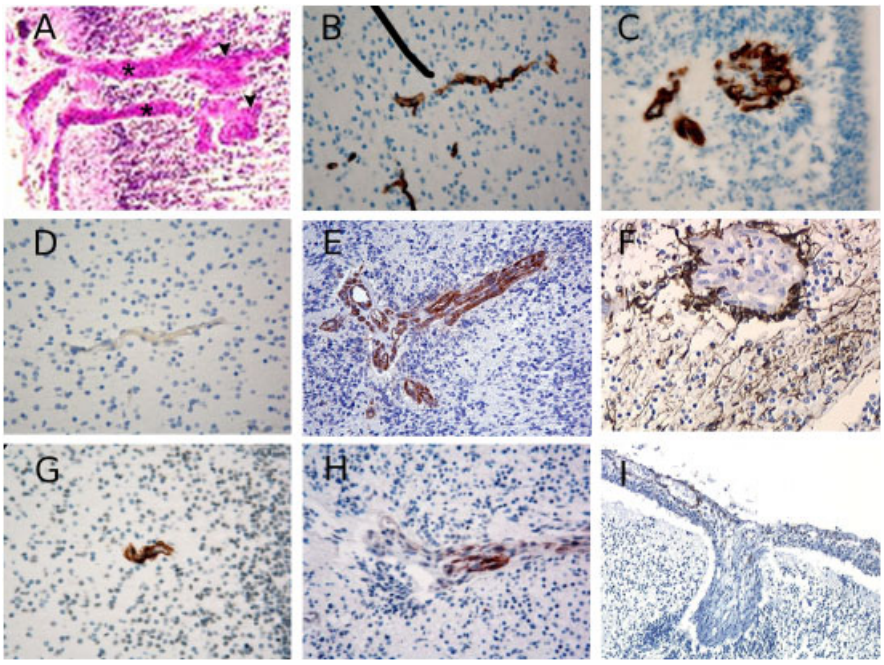

Figure 1. Marker analysis in Fowler syndrome fetal brain. **A**: Cortical plate of Fowler syndrome (FS) fetal brain (family IV) showing abnormal perforating vessels. Note the characteristic thickened vessels (asterisks), ending in glomeruloid formations (arrowheads), often devoid of recognizable lumina. CD34 capillary staining in (**B**) on a brain from a control, stage matched fetus and (**C**) from a FS fetus (family I). VEGF immunostaining arround (**D**) a brain parenchymal capillary from a control fetus in which it is essentially absent, and (**E**) from a FS fetus in which it appears markedly increased. **F**: GFAP astroglial immunostaining on a FS fetal brain. Alpha SMA immunostaining of pericytes on (**G**) a brain section from a control fetus versus (**H** and **I**) from two FS fetuses.

To identify the causative gene, we applied array-based sequence capture of the complete 4.1-MB region followed by high-throughput sequencing. DNA from one proband of six families, the heterozygous mother from family I, and a healthy brother not carrying the at-risk allele were selected (Fig. 2). Coverage varied from 2× to 12× in individuals depending on the integrity of their DNA (Table 1), with an average coverage depth of 7×; 60% (851,147) of the enriched reads were located on the targeted regions. Only 25% of the targeted regions reached 10× coverage depth.

The number of the detected variations was too large to handle them manually. To facilitate the analysis of these variations a specific genome browser was set up to visualize the locations of variations on the genome, and at the same time an analysis tool has been developed. This analysis tool applied a series of filters to the identified variations. These filters were based on the following criteria: (1) the quality of the sequence variant measured as the number of reads that detected the variant, (2) the presence or absence of variants in public databases such as dbSNP and HapMap, (3) the presence or absence of the variants among the studied samples, (4) annotation of the sequence variants based on their location (intron, exon, etc.), and the characteristics of the resulting change such as synonymous, nonsynonymous or stop mutation. Filtered results were visualized in an interactive table permitting us to sort and analyze the results. Thus, initial analysis of the sequence data that met an arbitrary threshold of at least three reads, of which at least one was required to be in the opposing orientation, detected a total of 23,262 variations, 17,031 of which were on chromosome 14 (73%, Supp. Table S2). Of these, 3,457 variants were found to not correspond to known SNPs, and were absent from the normal control individual (E). After initial exclusion of nonexonic and synonymous variants, 42 variants in 29 candidate genes remained. In 20 of these genes, a single variation was found in one individual, whereas two and three variations were found in six and two genes, respectively (Fig. 3).

FLVCR2 was the only gene with variations identified in four out of seven individuals. In addition, careful examination of the *FLVCR2* locus in the proband of family II revealed a homozygous deletion of exons 2 to 10, as the absence of both nucleotide variations and reads over a 46.8-kb genomic region (Fig. 4A). The deletion was confirmed to segregate in families I and II, and cloning of the breakpoints revealed the inclusion of the last two exons of the neighboring *C14orf1* gene, with no repeated DNA sequences at the boundaries. It is noteworthy that this deletion was not detected by Affymetrix 250 K SNP chip. Indeed, only one SNP was located in the nondeleted portion of intron 1. Direct sequencing of the 10 exons of *FLVCR2* (Supp. Table S2), identified mutations in two additional families (Table 1), such that mutant *FLVCR2* alleles were identified in each of the seven families studied (five homozygotes and two compound heterozygotes; Table 1 and Fig. 4B).

Reasons for false-negative results using HTS approaches are summarized in Table 1, and emphasize the need for complementary confirmation. In particular, in family IV, a second heterozygous mutation was found by direct resequencing, although it had an apparently homozygous mutation as indicated by the HTS analysis. In family III, the homozygous mutation found with Sanger sequencing had only been read two times in the HTS and had thus been excluded by the stringency of the filter. As a third example, the second heterozygous mutation in family VII had been read four times but was excluded for unidirectionality. Interestingly, in family VI, not known to be consanguineous, the identical nonsense mutation was found in the three affected sibs (homozygous in fetuses and heterozygous in parents), suggesting more distant consanguinity or a founder effect.

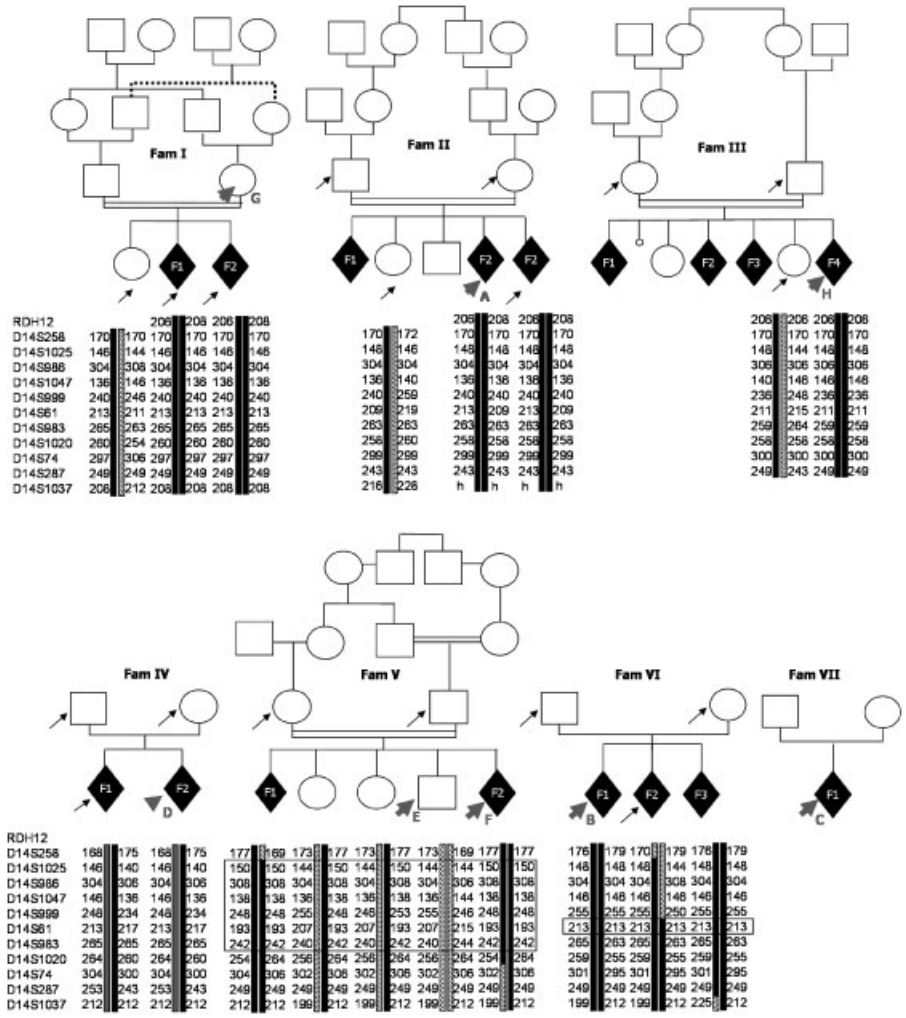

Figure 2. Pedigree and linkage analysis results. Pedigrees of families included in this study. Arrows indicate individuals for whom DNA was available, and arrowheads indicate the samples sequenced by HTS. Homozygosity or linkage was analyzed by microsatellite markers analysis and confirmed a founder effect by haplotype identity in two Turkish families (I and II) that were later discovered to carry the same *FLVCR2* exon 2 to 10 deletion.

FLVCR2 is a member of the major facilitator superfamily (MFS) of transporter proteins, that shuttle small molecules in response to ion gradients [Pao et al., 1991]. Like other MFS members, FLVCR2 is predicted to contain 12 membrane-spanning segments and six extracellular loops. As shown in Figure 5A, the three homozygous mutations are predicted to alter an amino acid localized to one transmembrane domain (TM): TM2 in family VI, TM8 in family III, and TM10 in family V. In family IV, one of the two mutations alters an amino acid predicted to be localized in TM8 and the other in the intracellular loop 5.

Amino acid sequence alignment for FLVCR2 from 10 different species showed that T430 and G412 have been conserved because our common ancestor with *Caenorhabditis elegans*, whereas R84 has been conserved in common with *Drosophila melanogaster* (Fig. 5B). T352R and L398V alter residues less evolutionary conserved, especially L398V. However, those mutations are absent from both the dbSNP and the 1000 Genome database not yet integrated in dbSNP. Although the L398V mutation was predicted to be benign by the Polyphen algorithm (http://genetics.bwh.harvard.edu/pph/), the T352R mutation as well as the other missense mutations identified in this study were predicted to be damaging to protein function. Thus, the pathogenicity of these two last mutations is likely but not totally proven. In total, eight different mutations including one nonsense mutation (homozygous in family VI), six missense mutations, and one homozygous deletion in two families (I and II) have been found in *FLVCR2*.

Discussion

PGV is a very rare and lethal genetic condition. Since its first description, 42 cases from 26 families have been reported on the basis of histological criteria of PGV [Bessieres-Grattagliano et al., 2009; Williams et al., 2010]. In the 16 fetuses of our series born to eight unrelated families, neuropathological analysis defined a diffuse form of encephaloclastic prolifrative vasculopathy (EPV), affecting the entire CNS and resulting in classical PGV with pterygia and a severe fetal akinesia deformation sequence in 14 cases. In contrast, two cases from the single family IV presented a more focal form of EPV, without spinal cord involvement and subsequent arthrogryposis/pterygia. Identification of *FLVCR2* mutations in this family suggests that the anteroposterior extent of CNS degeneration can be variable, and that PGV may be an extreme phenotype of a broader spectrum of proliferative vasculopathies. Stabilization of newly formed capillary sprouts during angiogenesis requires interactions of endothelial cells with

Table 1. Analysis of Variations by Individual and *FLVCR2* Variations Identified by High-throughput or Capillary Sequencing

	Individual	A (Fam II)	B (Fam VI)	C (Fam VII)	D (Fam IV)	F (Fam V)	G (Fam I)	H (Fam III)	Total
	Origin	Turkish	French	French	French	Maroccan	Turkish	French	
	Coverage	8,8X	4X	8,6X	2,3X	11,8X	11,6X	6,6X	7X
	All	2852	1804	2639	823	3067	3841	2005	17 031
Number of Variations (total)	Variations in E removed	1379	790	1154	282	1527	2075	1182	
	SNP removed	565	380	608	112	695	872	821	
	Variations in E and SNPs removed	546	300	465	80	569	750	747	
Number of variations on mRNA	Total	100	74	105	41	87	139	58	
	Variations in E and SNP removed	23	14	17	6	20	26	29	
	Total	41	22	44	13	42	60	25	
Number of variations on CDS	Variations in E and SNP removed	8	2	4	2	11	12	15	
	Non synonymous	22	8	23	9	23	28	13	
	Non synonymous and SNP removed	8	2	4	2	9	8	9	*42*
	Next generation sequencing	Del exons 2–10 hmz	c.402C>G, p.Tyr134Stop hmz	c.251G>A, p.Arg84His htz	c.1056C>G, p.Thr352Arg hmz	c.1234G>C, p.Gly412Arg hmz	(mother)	–	
FLVCR2 variations	Capillary sequencing	Del exons 2–10 hmz	c.402C>G, p.Tyr134Stop hmz	c.251G>A, p.Arg84His htz c.1192C>G, p.Leu398Val htz	c.1056C>G, p.Thr352Arg htz c.1289C>T, p.Thr430Met htz	c.1234G>C, p.Gly412Arg hmz	Del Ex 2–10 htz in mother	c.1076T>C, p.Leu359 Pro hmz	
	Comparison and reason for discrepancy	confirmation	confirmation	Arg84His: confirmation Leu398Val: 7 reads, 4 with the mutation, but excluded for unidirectionality	T352R: 4 reads of only the mutated allele, T430M: no reads	confirmation	Deletion confirmed in foetuses (hmz), htz in parents	2 reads of only the mutated allele	

E is a healthy brother in family V not carrying the disease allele by haplotyping, and taken as healthy control. Mutation numbering is based on cDNA sequence with a "c." symbol before the number, where +1 corresponds to the A of ATG translation codon (codon 1) of the cDNA reference sequences (NM_017791.2). Mutation names were checked by the Mutalyzer program [Wildeman et al., 2008]. SNP, single nucleotide polymorphisms; hmz, homozygous; htz, heterozygous.

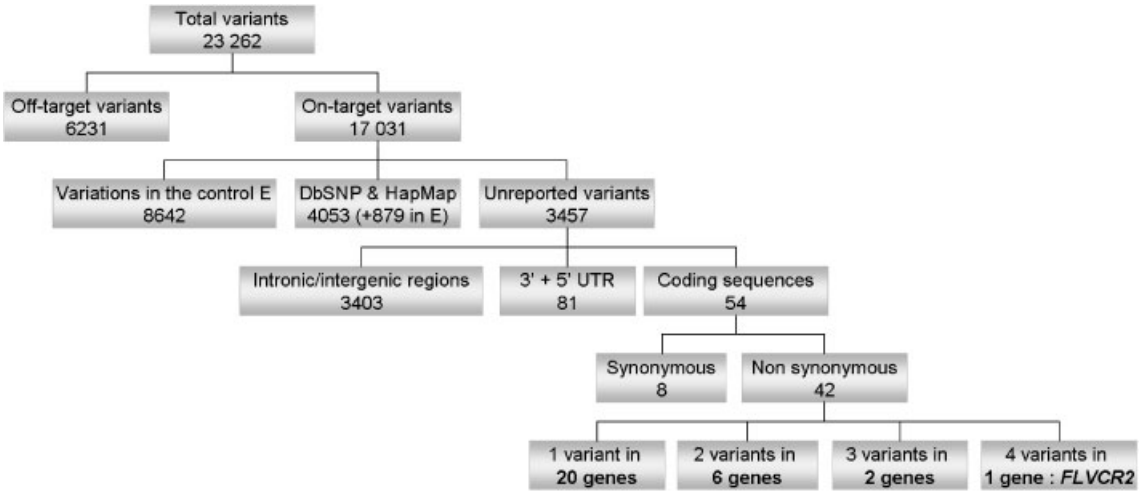

Figure 3. Summary of HTS data analysis. This diagram illustrates the flow chart of HTS data analysis. After elimination of variants found outside of the mapping region (27% of total variants) and those corresponding to known SNPs (29% of on-target variants) or shared with the control individual E (50% of on-target variants), HTS identified 54 variants in coding sequences, eight of which were synonymous. The remaining 46 variants were located in 29 candidate genes, 20 of which were excluded because only one variant was identified. Finally, only one gene, *FLVCR2,* presented four variants.

mural support cells, known as pericytes. The regionally restricted distribution of PGV in family IV might be linked to the embryonic lineage of the telencephalic pericytes, of a distinct neural crest cell origin from those of the spinal cord [Etchevers et al., 2001]. Interestingly, immunostaining for αSMA (a marker for mature pericytes) in fetal PGV brains was drastically reduced in the PGV within the CNS while normal aSMA expression was found in the leptomeninges (Fig. 1I). Further studies should elucidate whether this observed effect on pericytes is the primary cause or an effect of this disease.

Recently, *FLVCR2* mutations were also reported in five families with Fowler syndrome [Meyer et al., 2010], with the same homozygous Thr430Arg mutation in three families, and two compound heterozygous cases. Interestingely, Thr430Arg is associated with both forms of the disease, namely, with or without spinal cord involvement, suggesting no genotype phenotype correlations. It is noteworthy that the mutation concerned the same codon (Thr430) as in our family IV, the only one of our series without spinal cord involvement. More recently, Lalonde et al. [2010] also reported four *FLVCR2* compound mutations in two FS families with spinal cord involvement. Interestingly, the only missense mutation predicted to be "benign" in our study (L398V) was identified by two distinct approaches in a common case reported by both Lalonde et al. [2010] and Meyer et al. [2010], adding to the likely pathogenicity of this variation. To sum up, 15 different *FLVCR2* mutations (including those described in our study) have now been reported in 13 cases: one large deletion, two nonsense mutations, one splice site mutation, one insertion/deletion change, and 10 missense variations.

The *FLVCR2* gene encodes a transmembrane protein that belongs to the MFS of secondary carriers that transport small solutes such as calcium [Pao et al., 1991]. It is closely related in both sequence and topology to the better-known FLVCR1, sharing 60% amino acid identity [Lipovich et al., 2002]. FLVCR1 has been identified as the receptor for a feline leukemia virus (FeLV-C), and like FLVCR2 and other MFS members, is predicted to contain 12 membrane-spanning segments and six extracellular loops. A single mutation in the sixth extracellular loop is sufficient to confer FeLV-C receptor activity on FLVCR2, which does not otherwise bind the native virus [Brown et al., 2006]. However, FLVCR2 functions as a receptor for the FeLV-C variant FY981 [Shalev et al., 2009]. FLVCR1 is found only in hematopoietic tissues, the pancreas, and kidney [Tailor et al., 1999], but rodent Flvcr2 is widely expressed during embryonic development, in particular within the CNS and in the vessels of the maturing retina, and human FLVCR2, within the fetal pituitary [Brasier et al., 2004]. FLVCR1 has been shown to function as a heme exporter, essential for erythropoiesis [Quigley et al., 2004]. Interestingly, the five glutamate residues in the C-terminal putative coiled-coil domain of FLVCR2, not present in FLVCR1, may serve an analogous function to the same ferric ion-binding glutamate sequence in glycine-extended gastrin, by stimulating cell proliferation [He et al., 2004]. Based on the cell types in which it is expressed and MFS transport of chelated complexes of divalent metal ions, the FLVCR2 transporter was postulated to be a gatekeeper for the controlled entry of calcium into target cell types [Brasier et al., 2004]. Calcium signaling is involved in virtually all cellular processes and its homeostasis is tightly regulated. Angiogenic factors such as VEGF-A and FGF2 induce a transient increase of endothelial cell intracellular calcium concentrations, which acts as a second messenger to induce proliferation, among other effects [Tomatis et al., 2007]. Blood vessels are susceptible to responding to angiogenic signals and undergoing calcification when their pericytic coverage has been disrupted [Collett and Canfield, 2005], both of which signs we have observed in PGV patient brain sections.

HTS of the entire exome has been used so far to identify disease-causing genes in the rare Miller and Bartter syndromes, respectively [Choi et al., 2009; Ng et al., 2010]. Recently, targeted exon-specific sequencing within a restricted 40 MB linkage interval allowed the identification of an additional gene for Familial Exudative Vitreoretinopathy [Nikopoulos et al., 2010]. Our study underlines the use of HTS for the coverage of an entire linkage interval with no compelling candidate genes and no justification for the exclusion of noncoding regions. Our nested analysis approach led rapidly to the identification of a disease-causing gene. Although it further demonstrates the power of this new technology, it also highlights other potential risks of missing

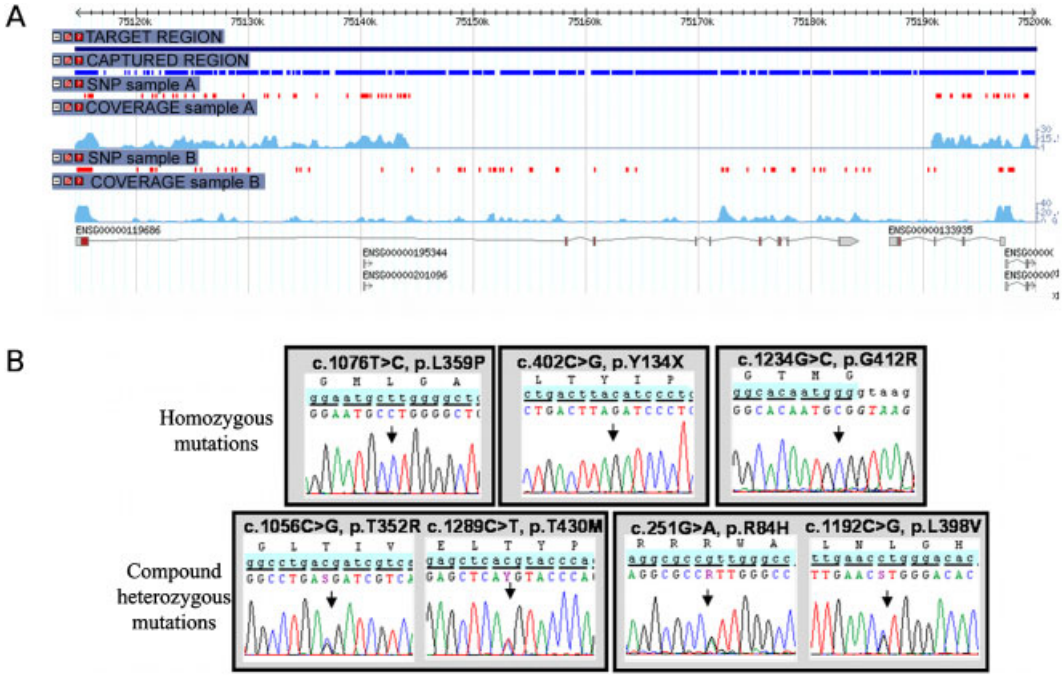

Figure 4. *FLVCR2* deletion and mutations. **A:** Genome browser view centered on the *FLVCR2* locus (ENSG00000119686) showing all variations (red dots) and reads coverage (light blue) in individuals A (fetus, family II) and B (fetus, family V). Note the absence of variations and reads in individual A, suggesting a homozygous deletion of exons 2 to 10, as well as the two final exons of the adjacent c14orf1 transcript (ENSG00000133935). **B:** Chromatograms of *FLVCR2* homozygous (upper panel) and compound heterozygous mutations (lower panel).

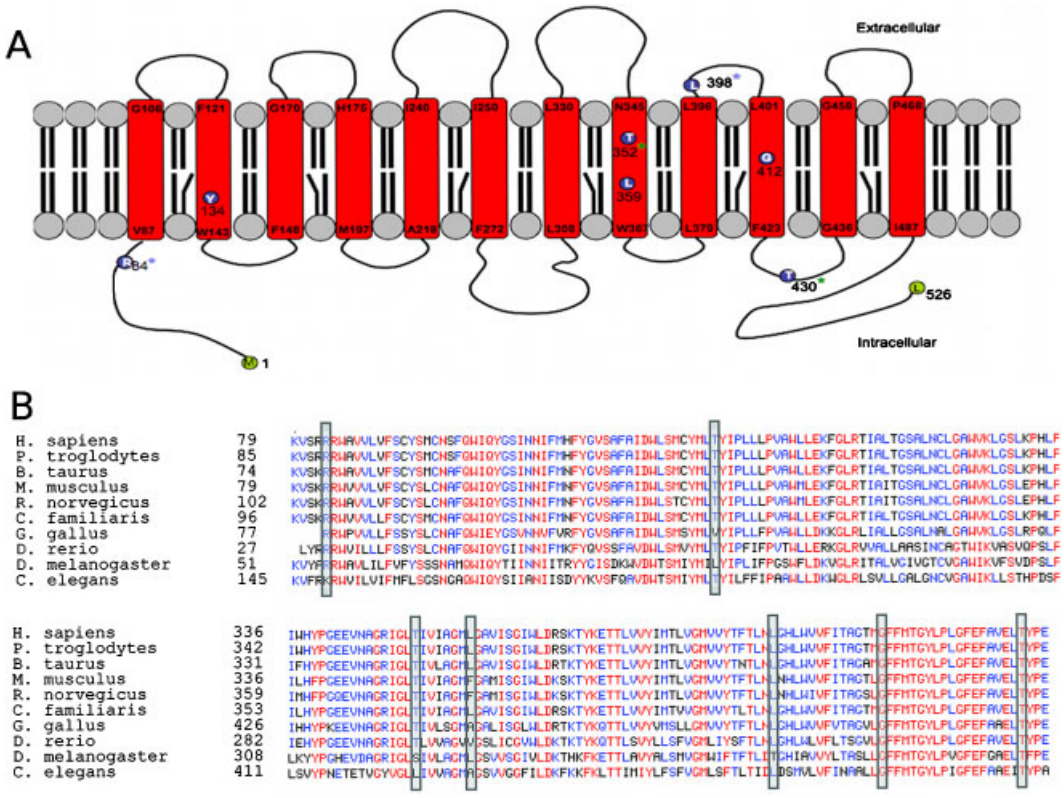

Figure 5. Localization of mutations in *FLVCR2* and conservation of mutated FLVCR2 amino acids. **A:** Localization of mutations on a secondary structure prediction of the FLVCR2 transporter. The three homozygous mutations are predicted to alter an amino acid localized in one of the 12 transmenbrane (TM) domains: p.Y134X is located in TM2, p.L359P in TM8, and p.G412R in TM10. Compound heterozygous mutations in family VI alter amino acids at the N-terminal cytoplasmic end and in the extracellular loop 5 (blue asterisk). Compound heterozygous mutations in family IV alter an amino acid predicted to be localized in TM8 and in the intracellular loop 5 (green asterisk). **B:** Alignment and conservation of mutated FLVCR2 amino acids. Sequences for FLVCR2 from 10 different species have been aligned using the Multialin tool ("mnultiple sequence alignment with hierarchical clustering") [Corpet, 1988]. Highly conserved amino acids are represented in red, moderately conserved amino acids are in blue and nonconserved ones are in black. Mutated amino acids are boxed.

mutations during data analyses. The number of patients, diagnostic accuracy and genetic homogeneity allowed us to compensate for low capture efficiency due to suboptimal DNA quality, and in the future, as the technology develops, furthering the depth of coverage should ensure a better distinction of background from true mutations. Finally, identification of the gene for Fowler syndrome will permit accurate genetic counseling for PGV and prenatal diagnosis, in particular, for the late-onset forms of the disease without spinal cord involvement.

Acknowledgments

We are grateful to families and to the French Society of Fetal Pathology (SOFFOET) for participating in the study. We thank Chantal Esculpavit for technical help. Grant sponsor: GIS-Maladies Rares. Grant sponsor: U.S. National Institute of Health (NIH) (grant NS039818 to S.T.).

References

Benko S, Fantes JA, Amiel J, Kleinjan DJ, Thomas S, Ramsay J, Jamshidi N, Essafi A, Heaney S, Gordon CT, McBride D, Golzio C, Fisher M, Perry P, Abadie V, Ayuso C, Holder-Espinasse M, Kilpatrick N, Lees MM, Picard A, Temple IK, Thomas P, Vazquez MP, Vekemans M, Roest Crollius H, Hastie ND, Munnich A, Etchevers HC, Pelet A, Farlie PG, Fitzpatrick DR, Lyonnet S. 2009. Highly conserved non-coding elements on either side of SOX9 associated with Pierre Robin sequence. Nat Genet 41:359–364.

Bessieres-Grattagliano B, Foliguet B, Devisme L, Loeuillet L, Marcorelles P, Bonniere M, Laquerriere A, Fallet-Bianco C, Martinovic J, Zrelli S, Leticee N, Cayol V, Etchevers HC, Vekemans M, Attie-Bitach T, Encha-Razavi F. 2009. Refining the clinicopathological pattern of cerebral proliferative glomeruloid vasculopathy (Fowler syndrome): report of 16 fetal cases. Eur J Med Genet 52:386–392.

Brasier G, Tikellis C, Xuereb L, Craigie J, Casley D, Kovacs CS, Fudge NJ, Kalnins R, Cooper ME, Wookey PJ. 2004. Novel hexad repeats conserved in a putative transporter with restricted expression in cell types associated with growth, calcium exchange and homeostasis. Exp Cell Res 293:31–42.

Brown JK, Fung C, Tailor CS. 2006. Comprehensive mapping of receptor-functioning domains in feline leukemia virus subgroup C receptor FLVCR1. J Virol 80: 1742–1751.

Choi M, Scholl UI, Ji W, Liu T, Tikhonova IR, Zumbo P, Nayir A, Bakkaloglu A, Ozen S, Sanjad S, Nelson-Williams C, Farhi A, Mane S, Lifton RP. 2009. Genetic diagnosis by whole exome capture and massively parallel DNA sequencing. Proc Natl Acad Sci USA 106:19096–19101.

Collett GD, Canfield AE. 2005. Angiogenesis and pericytes in the initiation of ectopic calcification. Circ Res 96:930–938.

Corpet F. 1988. Multiple sequence alignment with hierarchical clustering. Nucleic Acids Res 16:10881–10890.

Etchevers HC, Vincent C, Le Douarin NM, Couly GF. 2001. The cephalic neural crest provides pericytes and smooth muscle cells to all blood vessels of the face and forebrain. Development 128:1059–1068.

Fowler M, Dow R, White TA, Greer CH. 1972. Congenital hydrocephalus–hydrencephaly in five siblings, with autopsy studies: a new disease. Dev Med Child Neurol 14:173–188.

He H, Shehan BP, Barnham KJ, Norton RS, Shulkes A, Baldwin GS. 2004. Biological activity and ferric ion binding of fragments of glycine-extended gastrin. Biochemistry 43:11853–11861.

Kleinjan DA, van Heyningen V. 2005. Long-range control of gene expression: emerging mechanisms and disruption in disease. Am J Hum Genet 76:8–32.

Lalonde E, Albrecht S, Ha KC, Jacob K, Bolduc N, Polychronakos C, Dechelotte P, Majewski J, Jabado N. 2010. Unexpected allelic heterogeneity and spectrum of mutations in Fowler syndrome revealed by next-generation exome sequencing. Hum Mutat 31:918–923.

Lettice LA, Heaney SJ, Purdie LA, Li L, de Beer P, Oostra BA, Goode D, Elgar G, Hill RE, de Graaff E. 2003. A long-range Shh enhancer regulates expression in the developing limb and fin and is associated with preaxial polydactyly. Hum Mol Genet 12:1725–1735.

Lipovich L, Hughes AL, King MC, Abkowitz JL, Quigley JG. 2002. Genomic structure and evolutionary context of the human feline leukemia virus subgroup C receptor (hFLVCR) gene: evidence for block duplications and de novo gene formation within duplicons of the hFLVCR locus. Gene 286:203–213.

Meyer E, Ricketts C, Morgan NV, Morris MR, Pasha S, Tee LJ, Rahman F, Bazin A, Bessieres B, Dechelotte P, Yacoubi MT, Al-Adnani M, Marton T, Tannahill D, Trembath RC, Fallet-Bianco C, Cox P, Williams D, Maher ER. 2010. Mutations in FLVCR2 are associated with proliferative vasculopathy and hydranencephaly–hydrocephaly syndrome (Fowler syndrome). Am J Hum Genet 86:471–478.

Ng SB, Buckingham KJ, Lee C, Bigham AW, Tabor HK, Dent KM, Huff CD, Shannon PT, Jabs EW, Nickerson DA, Shendure J, Bamshad MJ. 2010. Exome sequencing identifies the cause of a mendelian disorder. Nat Genet 42:30–35.

Nikopoulos K, Gilissen C, Hoischen A, van Nouhuys CE, Boonstra FN, Blokland EA, Arts P, Wieskamp N, Strom TM, Ayuso C, Tilanus MA, Bouwhuis S, Mukhopadhyay A, Scheffer H, Hoefsloot LH, Veltman JA, Cremers FP, Collin RW. 2010. Next-generation sequencing of a 40 Mb linkage interval reveals TSPAN12 mutations in patients with familial exudative vitreoretinopathy. Am J Hum Genet 86:240–247.

Pao GM, Wu LF, Johnson KD, Hofte H, Chrispeels MJ, Sweet G, Sandal NN, Saier Jr MH. 1991. Evolution of the MIP family of integral membrane transport proteins. Mol Microbiol 5:33–37.

Quigley JG, Yang Z, Worthington MT, Phillips JD, Sabo KM, Sabath DE, Berg CL, Sassa S, Wood BL, Abkowitz JL. 2004. Identification of a human heme exporter that is essential for erythropoiesis. Cell 118:757–766.

Shalev Z, Duffy SP, Adema KW, Prasad R, Hussain N, Willett BJ, Tailor CS. 2009. Identification of a feline leukemia virus variant that can use THTR1, FLVCR1, and FLVCR2 for infection. J Virol 83:6706–6716.

Tailor CS, Willett BJ, Kabat D. 1999. A putative cell surface receptor for anemia-inducing feline leukemia virus subgroup C is a member of a transporter superfamily. J Virol 73:6500–6505.

Tomatis C, Fiorio Pla A, Munaron L. 2007. Cytosolic calcium microdomains by arachidonic acid and nitric oxide in endothelial cells. Cell Calcium 41: 261–269.

Wildeman M, van Ophuizen E, den Dunnen JT, Taschner PE. 2008. Improving sequence variant descriptions in mutation databases and literature using the Mutalyzer sequence variation nomenclature checker. Hum Mutat 29:6–13.

Williams D, Patel C, Fallet-Bianco C, Kalyanasundaram K, Yacoubi M, Dechelotte P, Scott R, Bazin A, Bessieres B, Marton T, Cox P. 2010. Fowler syndrome—a clinical, radiological, and pathological study of 14 cases. Am J Med Genet A 152A:153–160.

European Journal of Human Genetics (2011), 1–5

www.nature.com/ejhg

SHORT REPORT

Dissection of the *MYCN* locus in Feingold syndrome and isolated oesophageal atresia

Marie Cognet[1], Agnés Nougayrede[1], Valérie Malan[1,9], Patrick Callier[2], Celia Cretole[3], Laurence Faivre[2], David Genevieve[4], Alice Goldenberg[5], Delphine Heron[6], Sandra Mercier[7], Nicole Philip[8], Sabine Sigaudy[8], Alain Verloes[9], Sabine Sarnaki[3], Arnold Munnich[1,10], Michel Vekemans[1,10], Stanislas Lyonnet[1,10], Heather Etchevers[1], Jeanne Amiel[1,10] and Loïc de Pontual*[,1,11]

Feingold syndrome (FS) is a syndromic microcephaly entity for which *MYCN* is the major disease-causing gene. We studied the expression pattern of *MYCN* at different stages of human embryonic development and collected a series of 17 FS and 12 isolated oesophageal atresia (IOA) cases. An *MYCN* gene deletion/mutation was identified in 47% of FS cases exclusively. We hypothesized that mutations or deletions of highly conserved non-coding elements (HCNEs) at the *MYCN* locus could lead to its misregulation and thereby to FS and/or IOA. We subsequently sequenced five HCNEs at the *MYCN* locus and designed a high-density tiling path comparative genomic hybridization array of 3.3 Mb at the *MYCN* locus. We found no mutations or deletions in this region, supporting the hypothesis of genetic heterogeneity in FS.
European Journal of Human Genetics advance online publication, 12 January 2011; doi:10.1038/ejhg.2010.225

Keywords: Feingold syndrome; *MYCN*; genetic heterogeneity

INTRODUCTION

Feingold syndrome (FS, MIM164280) combines characteristic digital anomalies (ie, brachymesophalangy of the second and fifth fingers and brachysyndactyly of the toes), microcephaly, oesophageal/duodenal atresia, and variable learning disabilities.[1] FS has been mapped to 2p23–24[2] and is the consequence of *MYCN* gene (MIM 164840) loss-of-function either by germline deletions or by coding-sequence mutations.[3,4] Conversely, *MYCN* amplification is a prognostic factor for a bad outcome and is found in about 10% of neuroblastomas.[5]

In this study, we studied the expression pattern of *MYCN* at different stages of human embryonic development, and screened a cohort of 17 patients suspected of FS and 12 patients with isolated oesophageal atresia (IOA). We identified a heterozygous mutation/deletion in seven FS cases (47%) and no mutation or deletion in IOA. Some highly conserved non-coding elements (HCNEs), able to direct *N-myc* expression, have been identified in transgenic mice[6–8] We hypothesized that deregulation of tissue- or stage-specific *MYCN* expression following mutation or disruption of regulatory HCNEs at the *MYCN* locus could lead to FS and/or IOA. We subsequently sequenced five HCNEs at the *MYCN* locus and searched for small deletions in the 3.3-Mb vicinity of *MYCN*.

PATIENTS AND METHODS

A total of 29 patients were included in the study: 17 patients with possible FS (Table 1) and 12 patients with IOA. Diagnostic criteria for FS were the presence of three or more of the core features: (i) microcephaly, (ii) brachymesophalangy of the second and fifth finger, (iii) 2/3 or 4/5 toe syndactylies, and (iv) oesophageal or duodenal atresia. Whereas postnatal microcephaly was constant after 3 years of age, head circumference was normal at birth in three cases. All patients showed mild-to-moderate mental retardation and eight developed postnatal growth retardation. Brachymesophalangy of the second and fifth finger was noted in 15 cases, syndactylies in 12 cases, and oesophageal atresia in 14 of the 17 cases (Figure 1, Table 1). Additional features are listed in Table 1. All IOA cases were sporadic (10 type III and 2 type I), with no additional malformations.

Blood samples were obtained with informed consent and DNA was extracted according to standard protocols. DNA sequencing of the three coding exons and intronic flanking regions was performed by the fluorometric method on both strands (ABI BigDye Terminator Sequencing Kit V.2.1, Applied Biosystems). Comparative genomics analysis of the *MYCN* locus indicated five HCNEs with >75% identity over 350 bp across humans, rhesus, dog, and mouse (Figure 1). These HCNEs were studied by direct sequencing in all patients with no coding-sequence mutation (primers available on request).

A 3.3-Mb region extending 1.94 Mb centromeric (5′) and 1.36 Mb telomeric (3′) to *MYCN* (chr2: 12 800 000–16 590 000; NCBI Build 36.1) was studied by fine-tiling array-based comparative genomic hybridization (CGH; NimbleGen Systems, http://www.nimblegen.com/products/cgh/human.html#cnv) on 6 FS and 10 IOA patients with no *MYCN* coding-sequence mutation, as well as 550 normal-banded chromosomes on blood karyotype. The average spacing of probes in Nimblegen fine-tiling array is 52 bp. A deletion was considered when at least 10 probes were abnormal, giving a deletion detection resolution of about 500 bp at the *MYCN* locus. Genome-wide array-CGH with a resolution of 50 kb was performed in the five FS patients with no *MYCN* mutation and normal Nimblegen fine-tiling array, using the Agilent Human Genome CGH Microarray Kit 244 K (Agilent Technologies, Santa Clara, CA, USA).

To study *MYCN* expression during human development, embryos were collected from terminated pregnancies in agreement with French bioethics laws

[1]Unité INSERM U-781, Université Paris Descartes, Paris, France; [2]Service de Génétique, Hôpital d'enfants, Dijon, France; [3]Services de Chirurgie pédiatrique, Hôpital Necker-Enfant Malades, AP-HP, Paris, France; [4]Département de Génétique Médicale, Centre de référence anomalies du développement, Hôpital Arnaud de Villeneuve, Montpellier, France; [5]Service de Génétique, Hôpital Charles Nicolle, Rouen, France; [6]Service de Génétique, Hôpital de la Pitié Salpêtriére, Paris, France; [7]Service de Génétique, Hôpital Sud, Rennes, France; [8]Service de Génétique, Hôpital de la Timone, Marseille, France; [9]Service de Génétique, Hôpital Robert Debré, Paris, France; [10]Services de Génétique et cytogénétique, Hôpital Necker-Enfant Malades, AP-HP, Paris, France; [11]Services de Pédiatrie, Hôpital Jean Verdier, AP-HP, Bondy, France
*Correspondence: Professor L de Pontual, Département de Génétique, Hôpital Necker-Enfants Malades, 149, rue de Sévres, 75743 Paris Cedex 15, France. Tel: +33 14 449 5648; Fax: +33 14 449 5150; E-mail: loic.de-pontual@inserm.fr
Received 7 April 2010; revised 19 October 2010; accepted 19 October 2010

Table 1 Clinical features in the series of 17 FS patients with and without *MYCN* mutation

Mutated patients	*AO2*	*AO28*	*AO37*	*A056*	*A060*	*A065*	*A067*	*A068*	*Total*
Sex	F	F	M	M	F	M	F	M	4M/4F
Familial history	–	+	–	–	+	–	+	–	3/8
Head circumference at birth	−2	−3	−4	−3	−2	−4	−3	−2	8/8
Postnatal microcephaly (SD)	−3	−3	−4	−3	−2	−4	−3	−2	8/8
Weight and size at birth	50th c.	25th c.	25–50th c.	2550th c.	25–50th c.	25–50th c.	25–50th c.	25–50th c.	
Postnatal growth retardation (SD)	−2	−2.5	−2	−2	−1	−2	0	0	5/8
Mental retardation	Mild	Moderate	Mild	Mild	Mild	Moderate	Mild	Mild	8/8
Micrognatia	–	–	–	–	–	+	+	–	2/8
Brachymesophalangy II et V	+	+	+	+	+	+	+	+	8/8
Toe syndactyly 2/3	–	+	–	+	+	+	+	–	5/8
Toe syndactyly 4/5	+	+	+	–	–	+	+	–	5/8
Oesophageal atresia	+	+	+	+	+	+	+	–	7/8
Duodenal atresia	–	–	–	–	–	–	–	–	0/8
Renal hypoplasia	+	–	+	–	–	–	–	–	2/8
Congenital cardiac defect	ASD	VSD	–	–	–	–	–	–	2/8
Deafness	–	–	–	–	–	–	–	–	0/8
Asplenia	–	+	–	–	–	–	–	–	1/8
Result of *MYCN* gene screening	c.1180G>A	c.1293delC	c.1110insG	c.928-930insGT	c.474-514del	c.1177C>T	c.134dupC	del 2p24.3	8/8

Non-mutated patients	*AO3*	*AO4*	*AO22*	*AO35*	*AO36*	*AO39*	*AO41*	*AO42*	*AO43*	*Total*
Sex	M	F	F	M	M	F	M	F	F	4M/5F
Familial history	–	–	–	–	–	+[a]	+[b]	–	–	2/9
Head circumference at birth	–2.5	0	−2	0	−2.5	0	–3	−4	−1	5/9
Postnatal microcephaly (SD)	–2.5	−2	−2.5	−2	−2.5	–3	–3	−4	−2	9/9
Weight and size at birth	25–50th c.	50th c.	50th c.	50th c.	50th c.	50th c.	25–50th c.	50th c.	50th c.	
Postnatal growth retardation (SD)	−1	−1	–	−2	−1.5	0	−2.5	−3	0	3/9
Mental retardation	Mild	Moderate	Mild	Mild	Mild	Mild	Moderate	Mild	Mild	9/9
Micrognatia	–	+	–	+	–	–	–	–	–	2/9
Brachymesophalangy II et V	+	–	+	+	+	+	+	+	–	7/9
Toe syndactyly 2/3	–	+	+	–	–	+	–	+	–	4/9
Toe syndactyly 4/5	–	–	–	+	–	+	–	–	–	2/9
Oesophageal atresia	+	+	–	+	+	+	–	+	+	7/9
Duodenal atresia	–	–	–	+	–	–	–	–	–	1/9
Renal hypoplasia	–	–	–	–	–	–	–	–	–	0/9
Congenital cardiac defect	–	–	–	–	VSD, MA, AC	–	–	–	VSD	1/9
Deafness	–	–	–	+	–	–	–	–	–	0/9
Asplenia	–	–	–	–	–	–	–	–	–	0/9
Result of *MYCN* gene screening	–	–	–	–	–	–	–	–	–	0/9
Result of Nimblegen fine-tiling array	Normal	Normal	Normal	Normal	Normal	Normal	NP	NP	NP	0/6
Result of 244K genome wide array	Normal	Normal	Normal	Normal	Normal	NP	NP	NP	NP	0/5

Abbreviations: AC, aortic coarctation; ASD, atrial septal defect; del, deletion; F, female; M, male; MA, mitral atresia; VSD, ventricular septal defect.
[a]The father and a sister of AO39 are microcephalic and have digital anomalies (brachymesophalangy of the second and fifth fingers and brachysyndactyly of the toes). The sister has also learning disabilities.
[b]The mother of AO41 is microcephalic and has anomalies in the hand (brachymesophalangy of the second and fifth fingers).

(94-654 and 04-800) and the Necker Hospital ethics committee. Probe synthesis and hybridization were carried out as described previously.[9]

RESULTS

Direct sequencing and searching for deletion in *MYCN* locus

We identified a heterozygous coding-sequence mutation in seven patients (five novel, Table 1). All mutations resulted in a premature stop codon that removed the basic helix-loop-helix (b-HLH) and the leucine-zipper (LeuZ) domains or modified a conserved amino acid essential for DNA binding (Figure 2). One patient had a deletion of 425 kb encompassing the *MYCN* gene alone. Six mutations occurred *de novo* and one was inherited from the affected father (AO28, Table 1), who showed brachymesophalangy of the second and fifth fingers, syndactyly between the fourth and fifth toes, microcephaly, and mild mental retardation. Additional features observed in patients harbouring a *MYCN* coding-sequence mutation or deletion were congenital heart malformations (two cases), kidney hypoplasia (two cases), asplenia (one case), and diaphragmatic hernia (one case). This last malformation had never been reported previously and CGH analysis showed no additional rearrangements in this patient. The *MYCN* locus was further investigated in patients with no coding-sequence mutations; we sequenced five HCNEs identified in the *MYCN* locus (Figure 2) and identified no nucleotide variations in either FS or IOA patients. Fine-tiling array-based CGH identified no micro-rearrangements in the 3.3-Mb region encompassing *MYCN*. Genome-wide array-CGH 244 K was normal in the five patients with no *MYCN* coding-sequence mutation and normal Nimblegen fine-tiling array (Table 1).

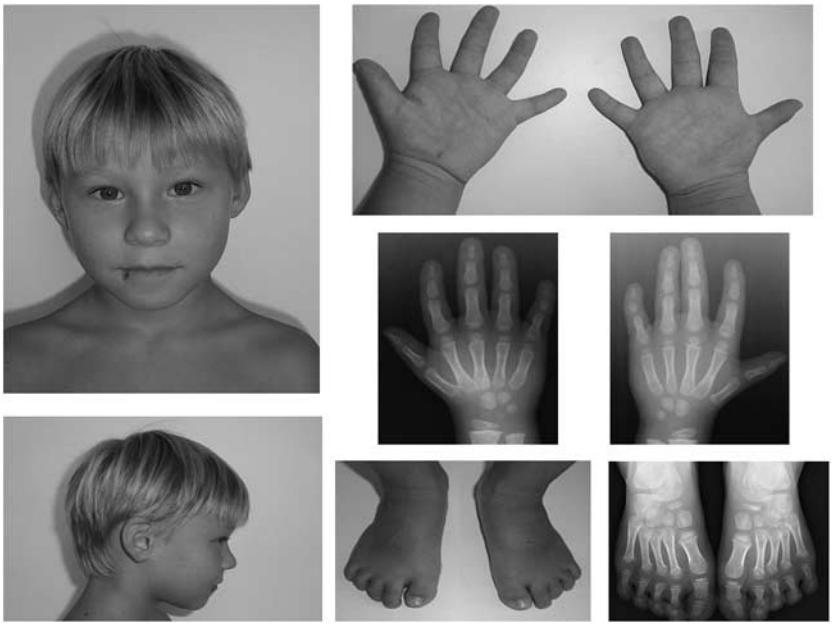

Figure 1 Patient AO68 with FS and *MYCN* deletion. Note the round face, brachymesophalangy of the second and fifth fingers, and short feet with brachydactyly.

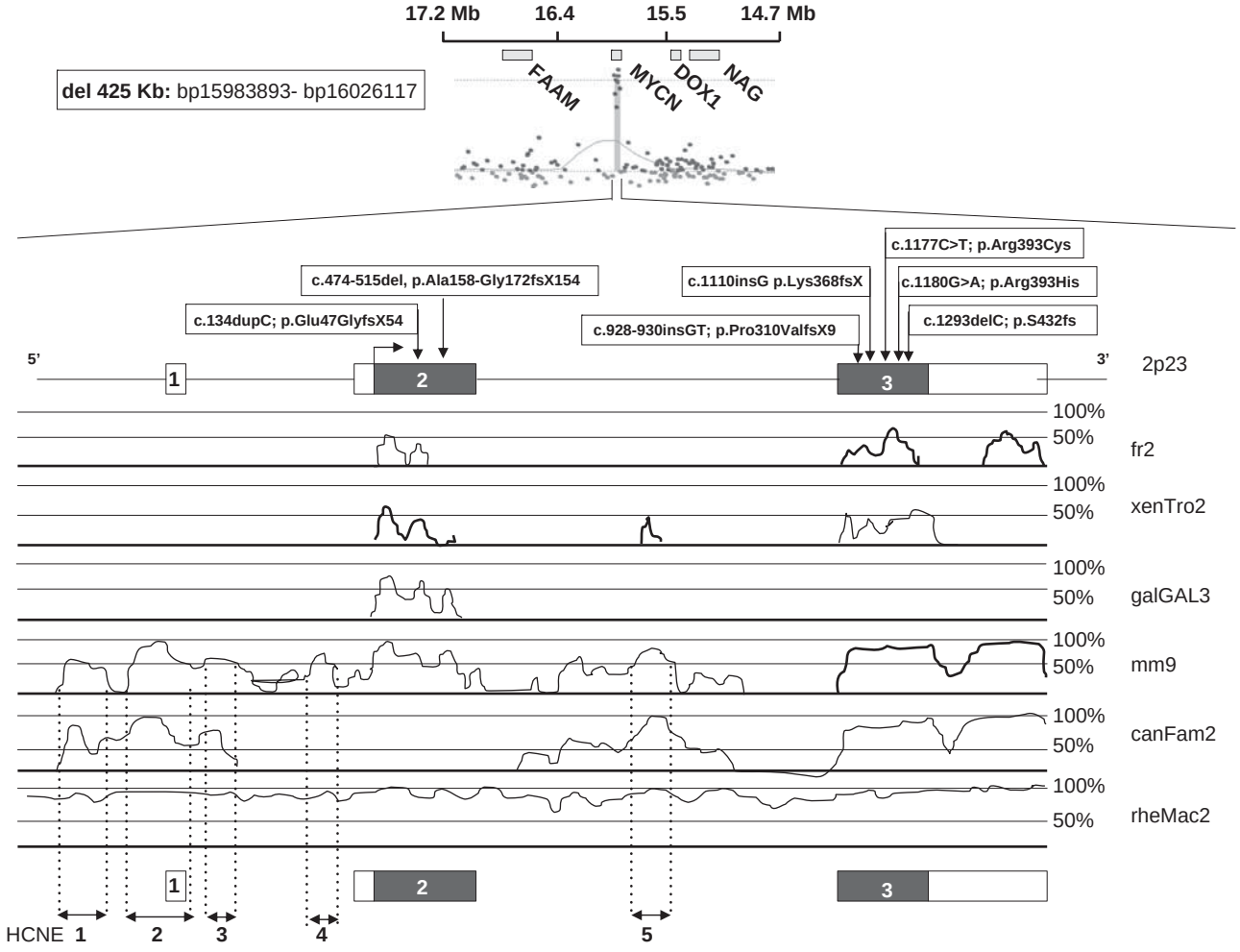

Figure 2 Schematic representation of the *MYCN* locus (6647 bp). The deletion and mutations identified in five FS patients and HCNEs with >75% identity over 350 bp across humans, rhesus, dog, and mouse (ECR browser software) are shown.

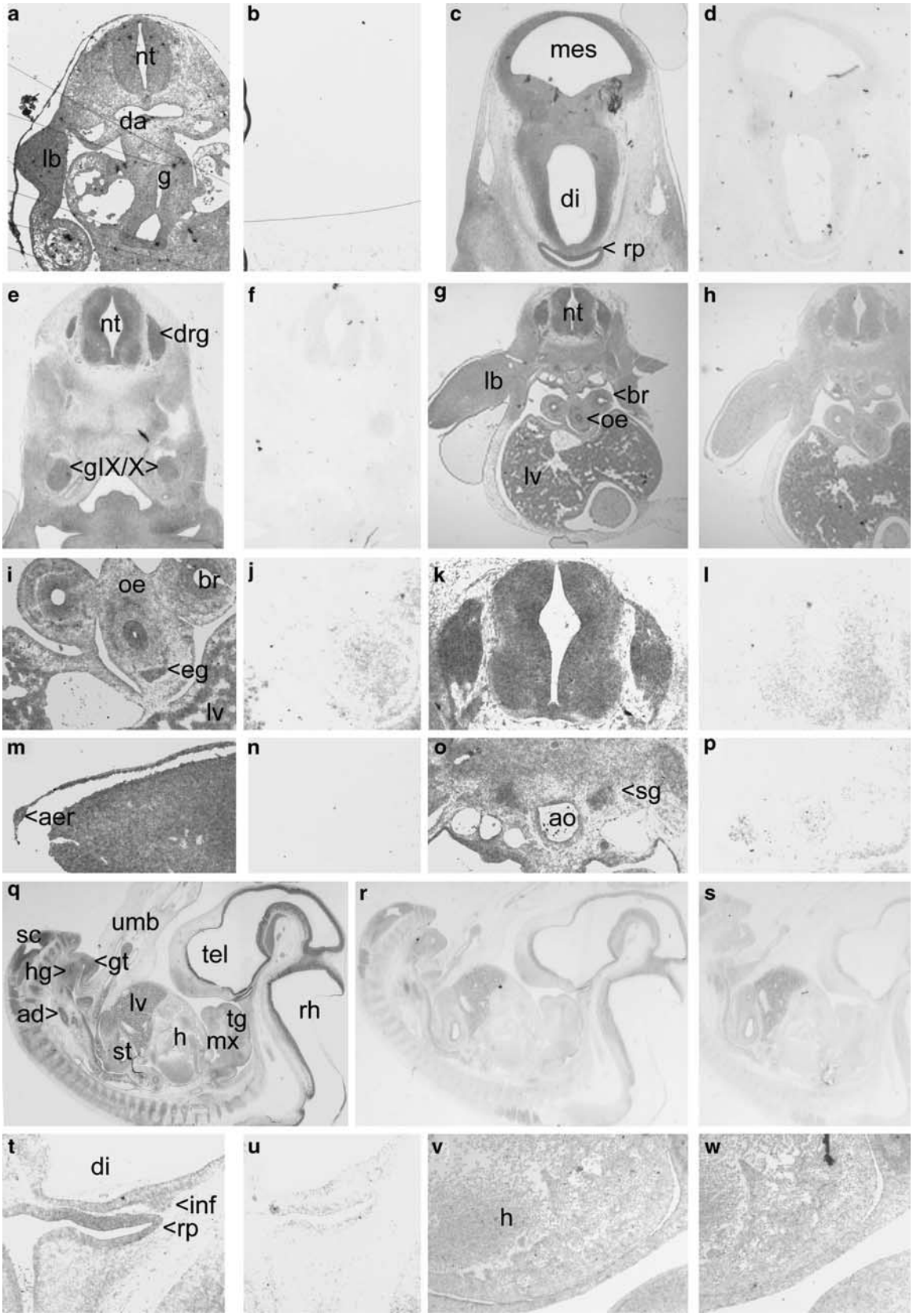
a
nt
da
lb
g
b
c
mes
di
< rp
d
e
nt
<drg
<glX/X>
f
g
nt
lb
<br
<oe
lv
h
i
oe
br
<eg
lv
j
k
l
m
<aer
n
o
<sg
ao
p
q
umb
sc
hg>
<gt
tel
ad>
lv
tg
rh
h
mx
st
r
s
t
di
<inf
<rp
u
v
h
w

Figure 3 *MYCN* expression in early human development. Antisense and sense (negative control, **b**, **d**, **f**) riboprobes are presented side by side in panels **a** to **p**. (**a**) At CS 13 (37 days' gestation) *MYCN* is ubiquitously expressed. (**c**) CS 15 (36 days' gestation), transverse section in head, showing *MYCN* expression is still widespread but is particularly strong in the brain and craniofacial mesenchyme, as well as in the precursors to the pituitary gland. (**e**) CS 15, transverse section through the cervical neural tube. (**g**) CS 15, section at the level of the forelimb. As compared with the control (**h**), no expression is observed in the liver, but is specific to both epithelia and mesenchyme of bronchi, oesophagus (**i**, **j**), and forelimb bud (**m, n**), as well as at levels of the central and peripheral nervous system (CNS/PNS; **i–l**, **o**, **p**). (**q**) Hematoxylin–eosin stain of sagittal section at CS 17 and 18 (42–45 days' gestation). *MYCN* expression in an adjacent section (**r**) shows continued but diminished expression in the CNS/PNS and craniofacial mesenchyme, and presence of transcripts in the adrenal gland, hindgut, and genital tubercule. (**t**) *MYCN* continues to be expressed in the developing pituitary, unlike in the ventricular myocardium (**v** *vs* **w**). Abbreviations: ad, adrenal gland; aer, apical ectodermal ridge; ao, aorta; br, bronchi; da, dorsal aorta; di, diencephalon; drg, dorsal root ganglia; eg, enteric ganglia; g, gut; g/IX/X, cranial ganglia IX/X; gt, genital tubercule; h, heart; hg, hindgut; inf, infundibulum; lb, limb bud; lv, liver; mes, mesencephalon; mx, maxilla; nt, neural tube; oe, oesophagus; rp, rathke's pouch; rh, rhombencephalon; sc, spinal cord; sg, sympathetic ganglion; st, stomach; tel, telencephalon; tg, tongue; umb, umbilical cord. Scale bars: 0.5 mm, except for **q–s**, 1 mm.

MYCN expression in early human development

Additional features observed in patients with an *MYCN* mutation motivated the study of *MYCN* expression at different stages of human embryonic development (Figure 3). At Carnegie stage (CS) 13, *MYCN* appears ubiquitously expressed, with higher expression in the limb-bud mesenchyme (Figures 2a and b). At CS 15, *MYCN* is differentially and highly expressed in the CNS/PNS, the oesophageal and bronchic epithelia, Rathke's pouch, sympathetic ganglia, and both ectodermal and mesenchymal components of the forelimb. At CS 17 and 18, *MYCN* is highly expressed throughout the CNS/PNS and in both Rathke's pouch and the corresponding precursor of the neurohypophysis, the infundibulum (Figures 3t and u), the smooth muscle of the umbilical arteries, the adrenal gland, and the hindgut as well as other sites (Figures 3q–u). However, despite low levels of cardiac expression seen *in situ* at CS 13, we no longer observed any cardiac expression at CS 18 (Figures 3v and w).

DISCUSSION

We identified an *MYCN* mutation in 50% of our cases (8/17). No major phenotypic differences could be found among the core features of FS retrospectively, between patients with and without a *MYCN* mutation (Table 1). Only syndactyly of toes 4 and 5 was more frequent in the group with *MYCN* mutations. The high frequency of oesophageal atresia in our series is due to a recruitment bias through paediatric surgeons. Importantly, no additional malformations were present in the group of patients without mutations. Although head circumference can be normal at birth, postnatal microcephaly is constant in our series. Most patients were sporadic cases, contrasting with a previous report.[4] This discrepancy could be ascribed to both a recruitment bias for familial cases before the gene was identified, and the fact that, clinically, the entity is better recognized since then. Several additional congenital malformations have been reported in FS; ie, vertebral malformations, congenital cardiac defects, and renal hypoplasia.[4] Renal hypoplasia needs to be detected early on in order to prevent renal failure.[2] One of our patients presented asplenia. This has not hitherto been reported in FS but is present in the *N-myc* hypomorphic mouse model.[10] A diaphragmatic hernia was detected in the same patient at birth. Facial features reported in FS are tenuous and combine short palpebral fissures, broad nasal bridge, and micrognathia.

We studied the pattern of expression of *MYCN* at different stages of normal human embryonic development. *MYCN* is widely expressed in forelimb mesenchyme at the stages we studied, consistent with the constant distal bone malformations observed in FS. Expression in Rathke's pouch raises the question of involvement of the pituitary gland in the growth deficit. We observed *MYCN* expression in both bronchial tubes and the oesophagus at CS 15, but not in the diaphragm at CS 17 and 18. *N-myc* knockout mice had been generated concomitantly by three independent groups.[11–13] Embryonic lethality was consistently observed between embryonic days E10.5 and E12.5 of gestation, with developmental delay and small size of mesonephros, lung, heart, and gut. Interestingly, mutant mice with 25% of wild-type levels of N-myc protein die at birth and are unable to breathe because of a severe deficiency in lung-branching morphogenesis.[10]

The molecular mechanisms underlying the regulation of *MYCN* expression have not been totally elucidated. It has been shown, by replacing endogenous *N-myc* coding sequences by the *c-myc* ones, that *c-myc* can complement *N-myc* functions.[14] Therefore, the specificity of both genes resides in their controlled expression patterns. No mutation/deletion of *MYCN* regulatory elements could be identified in humans. Altogether, these results are suggestive of genetic heterogeneity in FS.

CONFLICT OF INTEREST

The authors declare no conflict of interest.

1 Feingold M: Case report 30. *Synd Ident* 1975; **3**: 16–17.
2 Celli J, van Beusekom E, Hennekam RC *et al*: Familial syndromic esophageal atresia maps to 2p23-p24. *Am J Hum Genet* 2000; **66**: 436–444.
3 van Bokhoven H, Celli J, van Reeuwijk J *et al*: MYCN haploinsufficiency is associated with reduced brain size and intestinal atresias in Feingold syndrome. *Nat Genet* 2005; **37**: 465–467.
4 Marcelis CL, Hol FA, Graham GE *et al*: Genotype-phenotype correlations in MYCN-related Feingold syndrome. *Hum Mutat* 2008; **29**: 1125–1132.
5 Brodeur GM, Seeger RC, Schwab M, Varmus HE, Bishop JM: Amplification of N-myc in untreated human neuroblastomas correlates with advanced disease stage. *Science* 1984; **224**: 1121–1124.
6 Hiller S, Breit S, Wang ZQ, Wagner EF, Schwab M: Localization of regulatory elements controlling human MYCN expression. *Oncogene* 1991; **6**: 969–977.
7 Sivak LE, Pont-Kingdon G, Le K *et al*: A novel intron element operates posttranscriptionally to regulate human N-myc expression. *Mol Cell Biol* 1999; **19**: 155–163.
8 Tai KF, Rogers SW, Pont-Kingdon G, Carroll WL: Definition of the human N-myc promoter region during development in a transgenic mouse model. *Pediatr Res* 1999; **46**: 255–262.
9 Delous M, Baala L, Salomon R *et al*: The ciliary gene RPGRIP1L is mutated in cerebello-oculo-renal syndrome (Joubert syndrome type B) and Meckel syndrome. *Nat Genet* 2007; **39**: 875–881.
10 Moens CB, Auerbach AB, Conlon RA, Joyner AL, Rossant J: A targeted mutation reveals a role for N-myc in branching morphogenesis in the embryonic mouse lung. *Genes Dev* 1992; **6**: 691–704.
11 Stanton BR, Reid SW, Parada LF: Germ line transmission of an inactive N-myc allele generated by homologous recombination in mouse embryonic stem cells. *Mol Cell Biol* 1990; **10**: 6755–6758.
12 Sawai S, Shimono A, Hanaoka K, Kondoh H: Embryonic lethality resulting from disruption of both N-myc alleles in mouse zygotes. *New Biol* 1991; **3**: 861–869.
13 Charron J, Malynn BA, Fisher P *et al*: Embryonic lethality in mice homozygous for a targeted disruption of the N-myc gene. *Genes Dev* 1992; **6**: 2248–2257.
14 Malynn BA, de Alboran IM, O'Hagan RC *et al*: N-myc can functionally replace c-myc in murine development, cellular growth, and differentiation. *Genes Dev* 2000; **14**: 1390–1399.

RAPID COMMUNICATION

Human Mutation

OFFICIAL JOURNAL
HGVS
HUMAN GENOME VARIATION SOCIETY
www.hgvs.org

Germline Gain-of-Function Mutations of *ALK* Disrupt Central Nervous System Development

Loïc de Pontual,[1,2] Dania Kettaneh,[1] Christopher T. Gordon,[1] Myriam Oufadem,[1] Nathalie Boddaert,[3] Melissa Lees,[4] Laurent Balu,[5] Eric Lachassinne,[2] Andy Petros,[6] Julie Mollet,[9] Louise C. Wilson,[4] Arnold Munnich,[1,7] Laurence Brugière,[8] Olivier Delattre,[9] Michel Vekemans,[1,7] Heather Etchevers,[1] Stanislas Lyonnet,[1,7] Isabelle Janoueix-Lerosey,[9] and Jeanne Amiel[1,7]*

[1]*Université Paris Descartes, INSERM U-781, Paris, France;* [2]*Service de Pédiatrie, Hôpital Jean Verdier, AP-HP, Bondy, France;* [3]*Service de Radiologie Pédiatrique, INSERM U-1000, Hôpital Necker-Enfants Malades, AP-HP, Paris, France;* [4]*Department of Clinical Genetics, Great-Ormond Street Hospital for Children, London, United Kingdom;* [5]*Service de Réanimation Pédiatrique, Hôpital Bicêtre, AP-HP, Kremlin-Bicêtre, France;* [6]*Paediatric and Neonatal Intensive Care Unit, Great Ormond Street Hospital for Children, London, United, Kingdom;* [7]*Département de Génétique, Faculté de Médecine; AP-HP, Hôpital Necker-Enfants Malades, Paris, France;* [8]*Service d'Oncologie Pédiatrique, Institut Gustave Roussy, Villejuif, France;* [9]*INSERM U-830, Institut Curie, Paris, France*

Communicated by Andrew O.M. Wilkie

Received 6 November 2010; accepted revised manuscript 21 December 2010.
Published online 18 January 2011 in Wiley Online Library (www.wiley.com/humanmutation). DOI 10.1002/humu.21442

ABSTRACT: Neuroblastoma (NB) is a frequent embryonal tumor of sympathetic ganglia and adrenals with extremely variable outcome. Recently, somatic amplification and gain-of-function mutations of the anaplastic lymphoma receptor tyrosine kinase (*ALK*) gene, either somatic or germline, were identified in a significant proportion of NB cases. Here we report a novel syndromic presentation associating congenital NB with severe encephalopathy and abnormal shape of the brainstem on brain MRI in two unrelated sporadic cases harboring de novo, germline, heterozygous *ALK* gene mutations. Both mutations are gain-of-function mutations that have been reported in NB and NB cell lines. These observations further illustrate the role of oncogenes in both tumour predisposition and normal development, and shed light on the pleiotropic and activity-dependent role of ALK in humans. More generally, missing germline mutations relative to the spectrum of somatic mutations reported for a given oncogene may be a reflection of severe effects during embryonic development, and may prompt mutation screening in patients with extreme phenotypes. Hum Mutat 32:272–276, 2011. © 2011 Wiley-Liss, Inc.

KEY WORDS: ALK; neuroblastoma; NB; neurodevelopment; syndrome with cancer

Introduction

Neuroblastoma (NB; MIM♯ 256700) is the most frequent extracranial solid tumour in children. Both familial cases with vertical transmission, and predisposition in chromosomal and monogenic syndromes, have long supported the involvement of genetic factors. Several NB predisposing genes were recently identified, such as *PHOX2B*, *CREBBP*, *NSD1*, *HRAS*, *NF1*, and *ALK*. The last three genes encode proteins involved in the RAS/MAPK pathway [Chiarle et al., 2008; Palmer et al., 2009] and *ALK* is a downstream target of *PHOX2B* [Bachetti et al., 2010].

ALK (MIM♯ 105590), a tyrosine kinase receptor gene of the insulin receptor family, is activated by fusion with various partners in anaplastic large cell lymphomas, inflammatory myofibroblastic tumors, and in some lung cancers [Chiarle et al., 2008]. Recently, somatic amplification and gain-of-function mutations of *ALK* were identified in about 2–4 and 7–10% of NB cases, respectively [Chen et al., 2008; De Brouwer et al., 2010; Janoueix-Lerosey et al., 2008; Mosse et al., 2008]. Germline gain-of-function mutations have also been reported in half of the familial cases of NB tested thus far [Janoueix-Lerosey et al., 2008; Mosse et al., 2008]. *ALK* is preferentially expressed in the central and peripheral nervous systems during development, but its role in the normal development of the nervous system remains speculative [Hurley et al., 2006; Iwahara et al., 1997; Vernersson et al., 2006]. Indeed, familial *ALK* gain-of-function mutations predispose to isolated NB, but are not associated with developmental anomalies, and $Alk^{-/-}$ mice have no obvious embryonic phenotype. However, behavioral impairment has been described in the $Alk^{-/-}$ mice, a phenotype attributed to neurochemical alterations in the hippocampi and basal cortex [Bilsland et al., 2008].

Here we report two unrelated cases with an association of congenital NB and severe encephalopathy characterized by a specific abnormal shape of the brainstem on brain magnetic resonance imaging (MRI). In both cases we identified a heterozygous, germline de novo missense mutation located in the tyrosine kinase domain (TKD) of ALK at positions previously identified as somatic mutational hot spots in NB and NB cell lines.

Patients and Methods

Case 1, a female, was the second child born to unrelated healthy parents, aged 29 and 31 years at the time of birth, with no relevant family medical history. She was born at term by Caesarean section

*Correspondence to: Jeanne Amiel, Département de Génétique, Hôpital Necker-Enfants Malades, 149 rue de Sévres, 75743 Paris Cedex 15, France. E-mail: jeanne.amiel@inserm.fr

Contract grant sponsors: The Agence Nationale de la Recherche (ANR); The Foundation pour la Recherche Médicale (FRM); The INCa-DHOS; The Institut National du Cancer; The Ligue Nationale contre le Cancer (Equipe labellisée); The Association Hubert Gouin; Les Bagouz à Manon; les amis de Claire; Enfance et Santé.

with normal birth parameters following an uneventful pregnancy (birth weight [BW]: 3100 g, body length [BL]: 46 cm, occipito frontal circumference (OFC): 34 cm). She was hypotonic, hypomotile, and presented with major feeding difficulties, no sucking and swallowing reflexes, episodes of abdominal distension and apneas. Mechanical ventilation and tube feeding were required. An adrenal NB with pelvic extension was diagnosed at 3 days of life. Levels of urinary catecholamine and its metabolites were raised. Rapid tumor progression led to chemotherapy by vincristine and cyclophosphamide with no improvement of the tumor mass or catecholamine excretion. Boli of corticosteroids were delivered and plasmapheresis performed with the hypothesis of a paraneoplasic syndrome, but no neurological improvement was seen.

There was no congenital malformation or morphologic abnormality at clinical examination except for a high arched palate. Neurologic development was poor. She could fix and follow with normal eye movements and remained hypotonic with little spontaneous movements, sucking and swallowing were absent, she experienced severe episodes of desaturation and sweating, and she displayed hyperextension of the limbs. A tracheostomy tube was inserted at 6 weeks of age. Osteotendinous reflexes were present. A deceleration of the head circumference's growth was noticeable with an OFC of 39 cm (fifth centile) at 4 months. She died at age 4.5 months from a severe apnea with no attempt at resuscitation. Necropsy was not performed.

The tumor was classified as stage 3 by histology [Brodeur et al., 1993]. Neither *MYCN* amplification nor 1p36 deletion were detected by FISH. No antineuronal antibodies were secreted in the cerebral spinal fluid (CSF). A computerized tomography (CT) scan showed no spinal cord compression. Meta-iodo-benzylguanidine (MIBG) scintiscan showed no bone fixation. Electromyography and muscle histology were within the normal limits. Electroencephalography (EEG) showed slow activity without epilepsy. Auditory evoked potential was normal. Histological examination of a rectal biopsy showed normal enteric plexuses eliminating Hirschsprung disease as the cause of abdominal distension. Blood karyotype and a comparative genomic hybridization (CGH)-array with a 650-kb resolution showed normal chromosomes 46, XX. Brain magnetic resonance imaging (MRI) was performed at 3 days and again at 15 weeks of age. At the latter time point, an abnormal shape of the brainstem was noted with an enlarged medulla oblongata eclipsing the ovoid form of the pons. In retrospect, the same image was present from birth (Fig. 1A).

Case 2, a female, was the first child born to unrelated healthy parents with no relevant family medical history. Intrauterine growth retardation and sinusoidal cardiotocograph led to emergency Cesarean section at 31 weeks gestation (BW 1300 g, and a head circumference of 28.5 cm; both at approximately the 25th centile). Paternal and maternal ages at time of birth were 42 and 37 years, respectively. Hypotonia with little spontaneous movements, poor sucking, gastrooesophageal reflux, and distended abdomen were noted at birth. She presented daily episodes of desaturation and tracheobronchomalacia necessitating respiratory support and a tracheostomy tube was inserted at age 3 months. A thoracoabdominal CT scan at age 3 weeks showed bilateral large heterogeneous and calcified adrenal masses. She underwent four courses of chemotherapy leading to a reduction in the size of the tumors, but a MIBG scintiscan showed uptake of dye in the right hemithorax that was later confirmed by CT scan. She had a patent foramen ovale with prolonged QT segments on electrocardiography. Bilateral hernias were surgically repaired at age 2 months. She was kept on nasogastric feeds for persistent difficulties in swallowing. Intermittent abdominal distension remained unexplained; a contrast enema showed no obstruction and endoscopic intestinal biopsies were normal. Temperature instability was also observed. At age 5 months, she developed

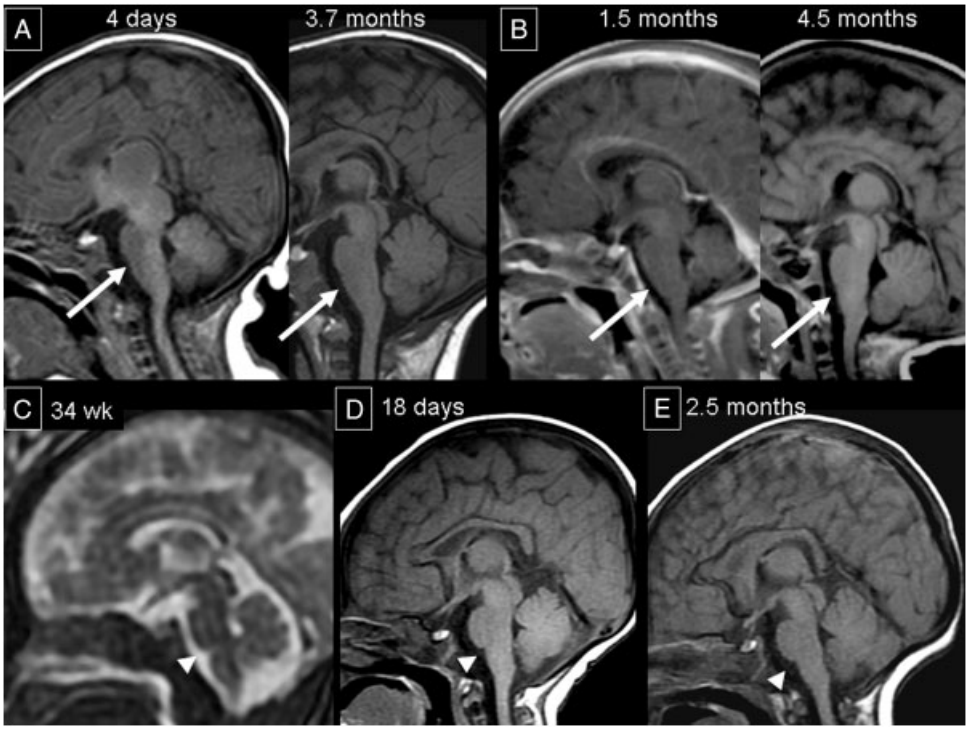

Figure 1. Brain MRI of the two patients and three controls. Note the abnormal shape of the brainstem with enlarged medulla oblongata eclipsing the ovoid form of the pons (arrows) on brain MRI (T1-weighted sagittal images) in both cases (top) compared to controls (bottom, arrowheads). **A:** Patient 1; **B:** patient 2; **C:** antenatal MRI of a control fetus at 34 weeks gestation; **D**–**E:** controls.

abnormal movements of the right arm and leg. Repeated EEGs failed to show focal epileptiform activity and seizures arising from the brainstem were hypothesized. Although initially normal, cranial ultrasound showed an ischaemic cortical lesion on the right inferior parietal lobe. Growth parameters had all fallen below the 0.4th centile by age 5 months. At 9 months, she could fix, had a left convergent squint with normal fundi, and responded to sound. Sensory motor deficit was suspected. She died at age 9 months following a decision to withdraw intensive care. Necropsy was not performed.

In retrospect, the brain MRIs performed at age 6 and 15 weeks showed a brainstem shape very similar to that observed in case 1 (Fig. 1B). At histology, both adrenal biopsies showed infiltrating islands of undifferentiated neuroblasts. FISH analysis identified four copies of the *MYCN* gene, trisomy of chromosomes 1 and 9, and tetrasomy of chromosome 17.

Blood samples for both cases were obtained with informed consent and DNA was extracted according to standard protocols. Direct sequencing of the *ALK* and *PHOX2B* genes was performed on both strands as previously described using the Big Dye Terminator Cycle Sequencing kit (Applied Biosystems, Bedford, MA) and was analyzed on an ABI 3100 automated sequencer.

Results

No nucleotidic variation of the *PHOX2B* gene was found. A heterozygous variation of the *ALK* gene was identified in each case (c.3733T>G, p.F1245V in case 1 and c.3520T>G, p.F1174V in case 2; numbering is based on the cDNA sequence from NM_004304.3 (ALK_v001); Fig. 2). Each missense mutation altered a conserved amino acid within the intracellular TKD of the protein at a position already found mutated in several NB cell lines and tumours (reviewed in [Palmer et al., 2009] and [Janoueix-Lerosey et al., 2010]). Both mutations occurred de novo. A paternal contribution to the child genotype was confirmed for nine unlinked and polymorphic CA repeat microsatellite markers in case 1 and 2 (data available on request).

Discussion

In both cases described in this report, we identified a de novo heterozygous germline *ALK* gene mutation. Importantly, mutations

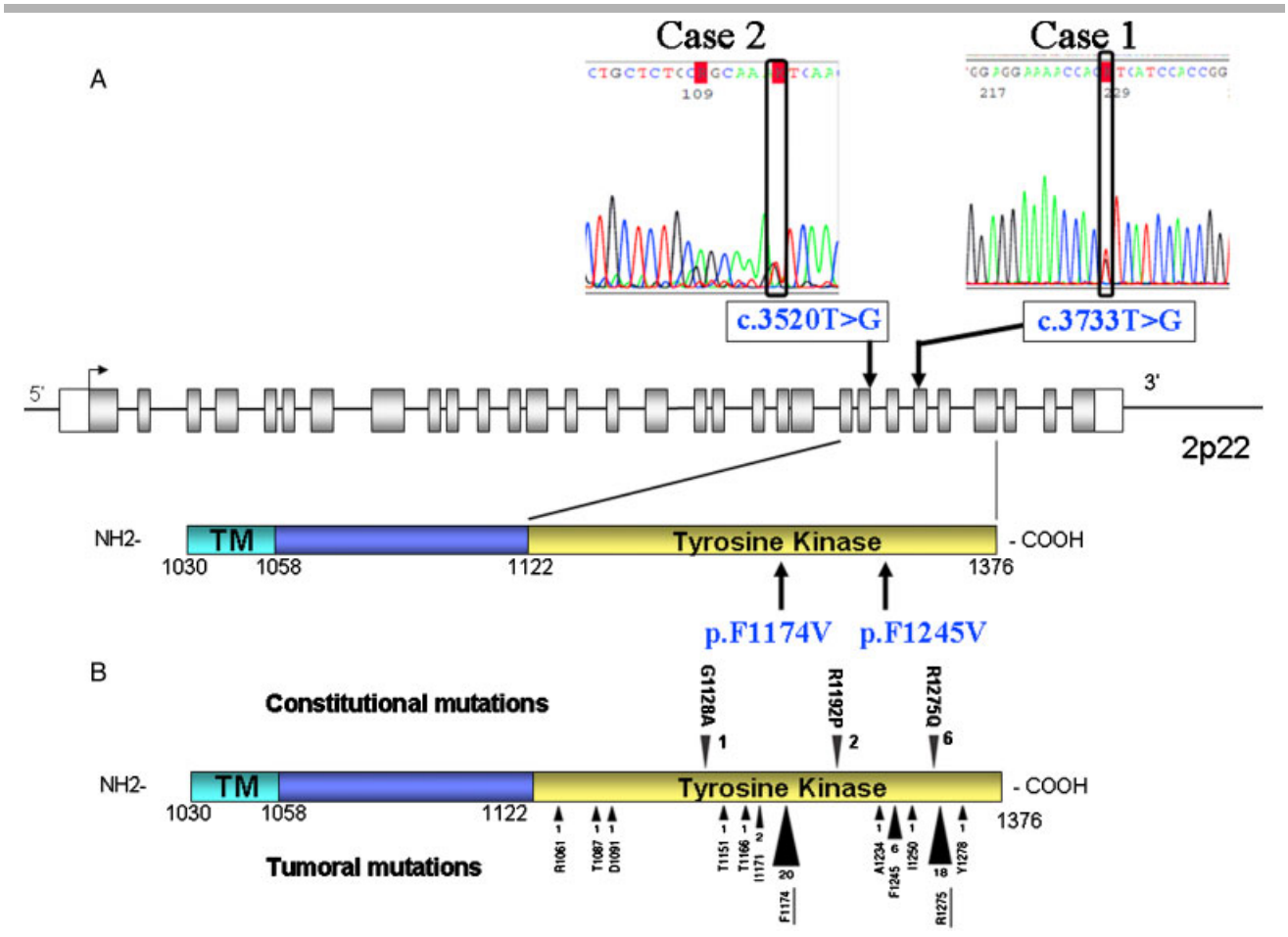

Figure 2. *ALK* gene mutations. **A:** A constitutional heterozygous missense variation of the *ALK* gene having occurred de novo was identified in each case (c.3733T>G, p.F1245V in case 1 and c.3520T>G, p.F1174V in case 2, with numbering based on the cDNA sequence from NM_004304.3 (ALK_v001). There is no evidence that the *ALK* mutations are present in mosaic state. Indeed, mutant allele is not underrepresented compared to wild-type allele. Residue F1245 is located in the catalytic loop and residue F1174 in the C helix of the TKD [Bossi et al., 2010; Lee et al., 2010]. **B:** Published *ALK* mutations in NB (adapted from [Janoueix-Lerosey et al., 2010] with permission). Mutations are indicated by arrows, with the number of mutations identified at each position to date indicated underneath. The mutations are mainly located in the TK domain, with two hotspots at positions 1174 and 1275. [Color figure can be viewed in the online issue, which is available at www.wiley.com/humanmutation.]

at position p.F1174 and p.F1245 have been reported already (with substitution for I, C, V, and L amino acids in both cases), but were invariably somatic [De Brouwer et al., 2010; Janoueix-Lerosey et al., 2010; Palmer et al., 2009]. However, the missense mutations p.G1128A, p.R1192P, and p.R1275Q, lying in the TKD of ALK, have been reported in familial cases segregating NB predisposition with incomplete penetrance and without presenting any neurological symptoms, and have not been reported as somatic mutations [Janoueix-Lerosey et al., 2008; Mosse et al., 2008]. Conversely, both children reported here presented with multifocal NB of neonatal onset and, severe, nonepileptic encephalopathy with a fatal outcome. They were initially referred for possible central congenital hypoventilation syndrome (CCHS, Ondine's curse; MIM# 209880) due to episodes of apnoeas and desaturation, abdominal distension, and NB. However, these episodes were independent of the sleep–wake state and direct sequencing of the *PHOX2B* gene failed to identify a coding sequence mutation. Opsomyoclonic syndrome had also been considered but electroencephalographic recordings showed no epilepsy and eye movements were normal. Moreover, plasmapheresis and corticosteroids did not lead to neurological improvement. Compression by the abdominal mass and Hirschsprung disease were also considered as explanations for the episodes of abdominal distension. An alternative hypothesis is enteric nervous system dysfunction given that *Alk* is expressed in the developing gut in mice [Vernersson et al., 2006]. The brainstem anomaly in the two patients reported here does not seem progressive, although this could not be assessed fully, given that both patients died at an early age. Nonetheless, the medulla oblongata was enlarged from birth in both cases. The presence of this feature upon brain MRI may be a good indication of an *ALK* germline mutation in a newborn with severe encephalopathy and brainstem dysfunction of unknown cause with or without NB. Indeed, whether neonatal NB is a consistent feature of the syndrome remains to be defined. The differential diagnosis would be a tumor of the medulla (more often a pylocytic astrocytoma), but enlargement would be asymmetric and presenting hypointensity on T1-weighted images.

There is a sharp contrast between the brain phenotype of the patients described in this report, and that of patients with Cardio-Facio-Cutaneous syndromes, in which germline gain-of-function mutations in several genes involved in the RAS signaling pathway have been described, and for whom absolute or relative macrocephaly is the rule (see [Tidyman and Rauen, 2009] for review). This is particularly true for Costello syndrome, which is ascribed to *HRAS* gain-of-function mutations, with amino acid substitution hotspots at codons p.G12 and p.G13 [Aoki et al., 2005]. Interestingly, a progressive enlargement of the cerebellum leading to posterior fossa crowding and cerebellar tonsilar herniation has been described in a majority of patients with Costello syndrome, while the shape of the brainstem remains normal [Gripp et al., 2010].

ALK is an extremely conserved tyrosine kinase receptor of the insulin receptor family with Midkine and Pleiotrophin as putative ligands in mammals. Ligand binding leads to ALK heterodimerisation, autophosphorylation, and activation of the RAS/MAPK, phosphoinositide-3 kinase (PI3K)/AKT, JAK/STAT3, or PLCγ pathways, promoting proliferation, differentiation or survival [Chiarle et al., 2008; Palmer et al., 2009; Wasik et al., 2009]. Fusion proteins arising from somatic rearrangements have been reported in anaplastic large cell lymphomas and other tumours (reviewed in [Palmer et al., 2009]). In NB and NB cell lines, both *ALK* amplification and gain-of-function missense mutations of conserved codons of the TKD have been reported [Chen et al., 2008; George et al., 2008; Janoueix-Lerosey et al., 2008; Passoni et al., 2009]. Some experimental data indicate variable oncogenic potential of ALK mutants with p.F1174L having an increased transforming capacity compared to p.R1275Q and p.K1062M [Chen et al., 2008; De Brouwer et al., 2010]. Altogether, these observations suggest different effects on ALK signalling for different mutations, with variable biological consequences. An interesting possibility is that there is an ALK activity threshold, above which CNS development would be impaired, but which is not reached by all ALK gain-of-function mutations reported thus far. Animal models are not yet available but knock-in mice bearing mutations at codon p.F1174 and p.R1245 are being generated in several groups. In the CNS of mice, *Alk* is expressed in several thalamic and hypothalamic nuclei, the pons, the medulla oblongata, and the ventral horn of the spinal cord [Vernersson et al., 2006]. It will be of high interest to explore the consequences of endogenous expression of mutant ALK on both neurological function and anatomic development of the pons, medulla, and motor neurons.

There is a growing list of genes for which somatic and germline gain-of-function mutations have been reported in tumours (of various types) and syndromes, respectively (Table 1). Interestingly, tumor predisposition burdens a minority of these syndromes. The repertoire of mutations and the relative proportion of each nucleotidic variation (and amino acid substitution) are different between somatic and germline cases. As a general rule, mutations exhibiting the highest activating effect in vitro are prevalent in the somatic repertoire and absent from its germline counterpart. The *HRAS* gene stands as a paradigm. Somatic gain-of-function mutations at codons p.G12, p.G13, and p.Q61 are found in various tumors, whereas germline mutations at codon p.Q61 have not been reported in patients with Costello syndrome. Moreover, when considering amino acid changes at codon 12, p.G12V is far more frequent somatically than p.G12S (and leading to a greater

Table 1. List of Genes for Which Somatic and Germline Gain-of-Function Mutations Have Been Reported in Tumors and Syndromes, Respectively

Gene	OMIM	Somatic mutation/tumour predisposition	Germline mutation/Syndromes	Reference
RET	164761	Thyroid	MEN2A/MEN2B*	[Hofstra et al., 1994; Mulligan et al., 1993]
FGFR3	134934	Bladder/Skin/Haematopoietic	Achondroplasia/TD	[Rousseau et al., 1994]
FGFR2	176943	Uterus/Skin/Testicle	Crouzon/Apert/Pfeiffer	[Reardon et al., 1994; Wilkie et al., 1995]
HRAS	190020	Bladder/Thyroid/Skin	Costello*	[Aoki et al., 2005]
KRAS	190070	Colon/Pancreas/Lung	Noonan/CFC	[Niihori et al., 2006]
BRAF	164757	Colon/Thyroid/Skin	CFC	[Niihori et al., 2006]
PTPN11	176876	Haematopoietic	Noonan	[Tartaglia et al., 2001]
IDH2	147650	CNS/Haematopoietic	D2 Hydroxyglutaric Aciduria	[Kranendijk et al., 2010]
ALK	105590	PNS	Congenital encephalopathy	This report

Syndromes predisposing to tumors are indicated with an asterisk. Several cases of leukemia have been reported in CFC. A paternal age effect is observed for germline mutations of *RET, FGFR2, FGFR3, HRAS,* and *PTPN11*.

activation [Fasano et al., 1984]), while in Costello syndrome p.G12S is the most common substitution, with p.G12V having been reported only twice; both of these patients had a severe phenotype [van der Burgt et al., 2007]. Most interestingly, two "missing germline mutations" at codon 61 (Q61R and Q61K) of *HRAS* have been identified in 5/30 spermatocytic seminomas (a rare testicular germ cell tumor of late-age onset) [Goriely et al., 2009]. We thus speculate that such mutations are to be found in patients with a de novo germline mutation but probably lead to an extreme, possibly foetal lethal phenotype, distinct from Costello syndrome.

Here we report a novel syndrome with predisposition to NB due to constitutive *ALK* gain-of-function mutations. In doing so, we provide evidence that normal CNS development requires regulation of ALK activity, with a threshold being exceeded for some mutations only, and therefore we add *ALK* to the list of oncogenes with important roles in normal development.

References

Aoki Y, Niihori T, Kawame H, Kurosawa K, Ohashi H, Tanaka Y, Filocamo M, Kato K, Suzuki Y, Kure S, Matsubara Y. 2005. Germline mutations in HRAS proto-oncogene cause Costello syndrome. Nat Genet 37:1038–1040.

Bachetti T, Di Paolo D, Di Lascio S, Mirisola V, Brignole C, Bellotti M, Caffa I, Ferraris C, Fiore M, Fornasari D, Chiarle R, Borghini S, Pfeffer U, Ponzoni M, Ceccherini I, Perri P. 2010. PHOX2B-mediated regulation of ALK expression: in vitro identification of a functional relationship between two genes involved in neuroblastoma. PLoS One 5:e13108.

Bilsland JG, Wheeldon A, Mead A, Znamenskiy P, Almond S, Waters KA, Thakur M, Beaumont V, Bonnert TP, Heavens R, Whiting P, McAllister G, Munoz-Sanjuan I. 2008. Behavioral and neurochemical alterations in mice deficient in anaplastic lymphoma kinase suggest therapeutic potential for psychiatric indications. Neuropsychopharmacology 33:685–700.

Bossi RT, Saccardo MB, Ardini E, Menichincheri M, Rusconi L, Magnaghi P, Orsini P, Avanzi N, Borgia AL, Nesi M, Bandiera T, Fogliatto G, Bertrand JA. 2010. Crystal structures of anaplastic lymphoma kinase in complex with ATP competitive inhibitors. Biochemistry 49:6813–6825.

Brodeur GM, Pritchard J, Berthold F, Carlsen NL, Castel V, Castelberry RP, De Bernardi B, Evans AE, Favrot M, Hedborg F. 1993. Revisions of the international criteria for neuroblastoma diagnosis, staging, and response to treatment. J Clin Oncol 11:1466–1477.

Chen Y, Takita J, Choi YL, Kato M, Ohira M, Sanada M, Wang L, Soda M, Kikuchi A, Igarashi T, Nakagawara A, Hayashi Y, Mano H, Ogawa S. 2008. Oncogenic mutations of ALK kinase in neuroblastoma. Nature 455:971–974.

Chiarle R, Voena C, Ambrogio C, Piva R, Inghirami G. 2008. The anaplastic lymphoma kinase in the pathogenesis of cancer. Nat Rev Cancer 8:11–23.

De Brouwer S, De Preter K, Kumps C, Zabrocki P, Porcu M, Westerhout EM, Lakeman A, Vandesompele J, Hoebeeck J, Van Maerken T, De Paepe A, Laureys G, Schulte JH, Schramm A, Van Den Broecke C, Vermeulen J, Van Roy N, Beiske K, Renard M, Noguera R, Delattre O, Janoueix-Lerosey I, Kogner P, Martinsson T, Nakagawara A, Ohira M, Caron H, Eggert A, Cools J, Versteeg R, Speleman F. 2010. Meta-analysis of neuroblastomas reveals a skewed ALK mutation spectrum in tumors with *MYCN* amplification. Clin Cancer Res 16:4353–4362.

Fasano O, Aldrich T, Tamanoi F, Taparowsky E, Furth M, Wigler M. 1984. Analysis of the transforming potential of the human H-ras gene by random mutagenesis. Proc Natl Acad Sci USA 81:4008–4012.

George RE, Sanda T, Hanna M, Frohling S, Luther 2nd W, Zhang J, Ahn Y, Zhou W, London WB, McGrady P, Xue L, Zozulya S, Gregor V, Webb TR, Gray NS, Gilliland DG, Diller L, Greulich H, Morris SW, Meyerson M, Look AT. 2008. Activating mutations in ALK provide a therapeutic target in neuroblastoma. Nature 455:975–978.

Goriely A, Hansen RM, Taylor IB, Olesen IA, Jacobsen GK, McGowan SJ, Pfeifer SP, McVean GA, Meyts ER, Wilkie AO. 2009. Activating mutations in FGFR3 and HRAS reveal a shared genetic origin for congenital disorders and testicular tumors. Nat Genet 41:1247–1252.

Gripp KW, Hopkins E, Doyle D, Dobyns WB. 2010. High incidence of progressive postnatal cerebellar enlargement in Costello syndrome: brain overgrowth associated with HRAS mutations as the likely cause of structural brain and spinal cord abnormalities. Am J Med Genet A 152A:1161–1168.

Hofstra RM, Landsvater RM, Ceccherini I, Stulp RP, Stelwagen T, Luo Y, Pasini B, Hoppener JW, van Amstel HK, Romeo G, Lips CJM, Buys CHCM. 1994. A mutation in the RET proto-oncogene associated with multiple endocrine neoplasia type 2B and sporadic medullary thyroid carcinoma. Nature 367: 375–376.

Hurley SP, Clary DO, Copie V, Lefcort F. 2006. Anaplastic lymphoma kinase is dynamically expressed on subsets of motor neurons and in the peripheral nervous system. J Comp Neurol 495:202–212.

Iwahara T, Fujimoto J, Wen D, Cupples R, Bucay N, Arakawa T, Mori S, Ratzkin B, Yamamoto T. 1997. Molecular characterization of ALK, a receptor tyrosine kinase expressed specifically in the nervous system. Oncogene 14:439–449.

Janoueix-Lerosey I, Lequin D, Brugieres L, Ribeiro A, de Pontual L, Combaret V, Raynal V, Puisieux A, Schleiermacher G, Pierron G, Valteau-Couanet D, Frebourg T, Michon J, Lyonnet S, Amiel J, Delattre O. 2008. Somatic and germline activating mutations of the ALK kinase receptor in neuroblastoma. Nature 455:967–970.

Janoueix-Lerosey I, Schleiermacher G, Delattre O. 2010. Molecular pathogenesis of peripheral neuroblastic tumors. Oncogene 29:1566–1579.

Kranendijk M, Struys EA, van Schaftingen E, Gibson KM, Kanhai WA, van der Knaap MS, Amiel J, Buist NR, Das AM, de Klerk JB, Feigenbaum AS, Grange DK, Hofstede FC, Holme E, Kirk EP, Korman SH, Morava E, Morris A, Smeitink J, Sukhai RN, Vallance H, Jakobs C, Salomons GS. 2010. IDH2 mutations in patients with D-2-hydroxyglutaric aciduria. Science 330:336.

Lee CC, Jia Y, Li N, Sun X, Ng K, Ambing E, Gao MY, Hua S, Chen C, Kim S Michellys PY, Lesley SA, Harris JL, Spraggon G. 2010. Crystal structure of the ALK (anaplastic lymphoma kinase) catalytic domain. Biochem J 430: 425–437.

Mosse YP, Laudenslager M, Longo L, Cole KA, Wood A, Attiyeh EF, Laquaglia MJ, Sennett R, Lynch JE, Perri P, Laureys G, Speleman F, Kim C, Hou C, Hakonarson H, Torkamani A, Schork NJ, Brodeur GM, Tonini GP, Rappaport E, Devoto M, Maris JM. 2008. Identification of ALK as a major familial neuroblastoma predisposition gene. Nature 455:930–935.

Mulligan LM, Kwok JB, Healey CS, Elsdon MJ, Eng C, Gardner E, Love DR, Mole SE, Moore JK, Papi L, Ponder MA, Telenius H, Tunnacliffe A, Ponder BAJ. 1993. Germ-line mutations of the RET proto-oncogene in multiple endocrine neoplasia type 2A. Nature 363:458–460.

Niihori T, Aoki Y, Narumi Y, Neri G, Cave H, Verloes A, Okamoto N, Hennekam RC, Gillessen-Kaesbach G, Wieczorek D, Kavamura MI, Kurosawa K, Ohashi H, Wilson L, Heron D, Bonneau D, Corona G, Kaname T, Naritomi K, Baumann C, Matsumoto N, Kato K, Kure S, Matsubara Y. 2006. Germline KRAS and BRAF mutations in cardio-facio-cutaneous syndrome. Nat Genet 38:294–296.

Palmer RH, Vernersson E, Grabbe C, Hallberg B. 2009. Anaplastic lymphoma kinase: signalling in development and disease. Biochem J 420:345–361.

Passoni L, Longo L, Collini P, Coluccia AM, Bozzi F, Podda M, Gregorio A, Gambini C, Garaventa A, Pistoia V, Del Grosso F, Tonini GP, Cheng M, Gambacorti-Passerini C, Anichini A, Fossati-Bellani F, Di Nicola M, Luksch R. 2009. Mutation-independent anaplastic lymphoma kinase overexpression in poor prognosis neuroblastoma patients. Cancer Res 69:7338–7346.

Reardon W, Winter RM, Rutland P, Pulleyn LJ, Jones BM, Malcolm S. 1994. Mutations in the fibroblast growth factor receptor 2 gene cause Crouzon syndrome. Nat Genet 8:98–103.

Rousseau F, Bonaventure J, Legeai-Mallet L, Pelet A, Rozet JM, Maroteaux P, Le Merrer M, Munnich A. 1994. Mutations in the gene encoding fibroblast growth factor receptor-3 in achondroplasia. Nature 371:252–254.

Tartaglia M, Mehler EL, Goldberg R, Zampino G, Brunner HG, Kremer H, van der Burgt I, Crosby AH, Ion A, Jeffery S, Kalidas K, Patton MA, Kucherlapati RS, Gelb BD. 2001. Mutations in PTPN11, encoding the protein tyrosine phosphatase SHP-2, cause Noonan syndrome. Nat Genet 29:465–468.

Tidyman WE, Rauen KA. 2009. The RASopathies: developmental syndromes of Ras/MAPK pathway dysregulation. Curr Opin Genet Dev 19:230–236.

van der Burgt I, Kupsky W, Stassou S, Nadroo A, Barroso C, Diem A, Kratz CP, Dvorsky R, Ahmadian MR, Zenker M. 2007. Myopathy caused by HRAS germline mutations: implications for disturbed myogenic differentiation in the presence of constitutive HRas activation. J Med Genet 44:459–462.

Vernersson E, Khoo NK, Henriksson ML, Roos G, Palmer RH, Hallberg B. 2006. Characterization of the expression of the ALK receptor tyrosine kinase in mice. Gene Expr Patterns 6:448–461.

Wasik MA, Zhang Q, Marzec M, Kasprzycka M, Wang HY, Liu X. 2009. Anaplastic lymphoma kinase (ALK)-induced malignancies: novel mechanisms of cell transformation and potential therapeutic approaches. Semin Oncol 36: S27–S35.

Wilkie AO, Slaney SF, Oldridge M, Poole MD, Ashworth GJ, Hockley AD, Hayward RD, David DJ, Pulleyn LJ, Rutland P, Malcolm S, Winter RM, Reardon W. 1995. Apert syndrome results from localized mutations of FGFR2 and is allelic with Crouzon syndrome. Nat Genet 9:165–172.

IOVS Papers in Press. Published on June 15, 2011 as Manuscript iovs.10-70981

Comparative transcriptome and network biology analyses demonstrate antiproliferative and hyperapoptotic phenotypes in human keratoconus corneas

Matthias Macé[1,2,§], Stéphane D. Galiacy[1], Angélique Erraud[2], José Enrique Mejía[1,2], Heather Etchevers[3], Michèle Allouche[1,2], Laurence Desjardins[6], Patrick Calvas[1,2,4], and François Malecaze[1,2,3]

[1] INSERM, U563, Toulouse, F-31300 France

[2] Université de Toulouse, UPS, Centre de Physiopathologie de Toulouse Purpan and Institut Biomédical de Toulouse, Toulouse, F-31300, France

[3] INSERM UMR910, Faculté de Médecine La Timone, F-13005 Marseille, France

[4] CHU de Toulouse, Hôpital Purpan, Service d'Ophtalmologie, F-31300 Toulouse, France

[5] CHU de Toulouse, Hôpital Purpan, Service de Génétique Médicale, F-31300 Toulouse, France

[6] Institut Curie, Paris, France

[§] Corresponding author.
Telephone: +33 562 744 509.
E-mail: matthias.mace@inserm.fr

Running Title: Keratoconus transcriptomics

Keywords: Keratoconus, cornea, microarrays, transcriptome, network biology, apoptosis, proliferation.

Word count: 5 350

Abstract

Purpose. To decipher the biological pathways involved in keratoconus pathophysiology by determining the patterns of differential gene expression between keratoconus and control corneas.

Methods. RNA was extracted from surgically removed corneas of 10 keratoconus patients, and from normal corneas of 10 control patients who had been enucleated for ocular melanoma. Several hundred thousand RNA transcripts were assessed using Affymetrix exon microarrays. Statistical comparison and identification of differentially regulated and differentially spliced RNA transcripts was carried out by comparing keratoconus cases and controls. In addition, relevant biological pathways were identified by information extraction using network biology.

Results. Eighty-seven genes showed significant differences in expression levels. Among these, 69 were downregulated in keratoconus patients, particularly partners of the transcription factor AP-1. The 18 over-expressed genes include mucins, keratins, and genes involved in fibroblast proliferation. In addition, 36 genes were shown to be differentially spliced, including nine among those that were differentially expressed. Network biology and analysis using Gene Ontology descriptors suggest that many members of both groups belong to pathways of apoptosis and the regulation of the balance between cellular differentiation and proliferation.

Conclusion. This work constitutes the first genome-wide transcriptome analysis of keratoconus patient corneas that include all currently known genes and exons. Differential expression suggests that mechanisms of cell loss resulting from antiproliferative and hyperapoptotic phenotypes may be responsible for the pathogenesis of keratoconus.

Array information, experimental design, raw intensities and processed $\log_2$ ratio values were deposited at the European Bioinformatic Institute's ArrayExpress database (http://www.ebi.ac.uk/arrayexpress/). Accession number is pending until the embargo date (2010-12-23).

Introduction

Keratoconus (KC) is a vision-threatening condition characterized by thinning and deformation of the cornea. It is one of the most common indications for corneal grafting in industrialized countries. The disease prevalence is around 1 in 2000, and familial aggregation, together with increased familial risk, suggests important genetic influences on its pathogenesis, but the etiology of keratoconus is still poorly understood. Aside from genetic determinants, environmental stresses such as eye rubbing or atopy have been suggested as possible causes or aggravating factors in keratoconus [1]. To date, several loci for familial keratoconus have been described [2-8]. These have been mapped by genome-wide scans of varying resolutions to the chromosomal regions 2p24, 3p14-q13, 5q14.3-q21.1, and 16q22.3-q23.1 in familial studies, and to the chromosomal regions 4q31, 5q31, 9q34, 12p12, 14p11, 17q24, and 20q12 using an affected-only linkage analysis. However, no genes have yet been identified as responsible for the development of the vast majority of keratoconus cases. Within these chromosomal regions, several candidate genes (*COL6A1, SOD1, MMP9, MMP2, COL8A1*) have been excluded [2, 3, 9, 10] while mutations in *VSX1* have been reported in a few keratoconus patients [11]. In addition, one differential expression study pointed to *AQP5* encoding aquaporin 5 [12]. Taken together, these data suggest that keratoconus is a complex disease involving multiple susceptibility *loci* [6].

Holistic approaches integrating various "-omics" techniques are promising for discovering the molecular bases of genetic disorders with complex patterns of inheritance, such as keratoconus [13]. Variation in gene expression is an important mechanism underlying the susceptibility to complex diseases, and it has been established that the steady-state abundance of mRNA transcripts for many human genes is a highly heritable, quantitative phenotypic trait [14]. Recent technical advances for the profiling of virtually all human or mouse exons on genome-wide transcriptome microarrays [15, 16] have made the comprehension of molecular disease mechanisms possible [17]. Thus far, most published analyses have only assessed variations in levels of gene expression, without taking into account exon content. However, about 50% of all human genes are predicted to be alternatively spliced [18], and disruptions in the balance of multiple transcript isoforms have been shown to be at play in conditions ranging from Alzheimer

disease to a number of cancers [19, 20]. In this study, we therefore aimed to analyze the keratoconus corneal transcriptome in a comparison with normal corneas, to identify differentially expressed or spliced genes that would highlight the pathophysiological pathways involved in keratoconus. Network biology allowed us to assign a number of these gene products to a small number of molecular cascades pertaining to proliferation, differentiation, and programmed cell death.

Methods

Ethics statement

This study was carried out in accordance with French regulations following the tenets of the Declaration of Helsinki. The samples were assigned a laboratory number and have remained anonymous throughout. The experimental protocol was approved by the relevant the inter-regional ethics committee, CPP Sud-Ouest Outre-Mer N° 2. Written consent was obtained from all participants involved in this study.

Patients and control tissue collection and storage

Ten corneas were collected from non-related patients during a penetrating keratoplasty procedure for advanced keratoconus in the Centre National de Référence du Kératocône (Toulouse, France). All keratoconus eyes included in the study were stage III (Amsler-krumeich classification) with high refractive errors, severe loss of visual acuity, and absence of scarring. In addition all patients had contact lens intolerance and none of them weared contact lens since at least 6 months. Patients were 34 ± 10.3 years old, 6 were males and 4 females. Ten control corneas were obtained in the Institut Curie (Paris, France) from unrelated patients enucleated for choroidal melanomas strictly localized to the posterior pole of the eye. These patients did not receive antineoplastic treatment before surgery. None were wearing contact lenses. Patients were 59 ± 10.1 years old, 5 were males and 5 females. In addition, for each control cornea, anatomical or topographical abnormality was ruled out by careful examination. Excised corneal buttons were 8 mm in diameter. They were processed according to identical standard

procedures in the two centres, and were immediately stored in 1.5 ml microtubes in liquid nitrogen until RNA extraction.

RNA isolation from whole corneas

Corneas were transferred from liquid nitrogen to a 500 µl RLT (RNeasy Mini kit, Qiagen, Hilden, Germany)/ß-mercaptoethanol (GE Healthcare Biosciences, Pittsburg, PA) solution, in a Lysing Matrix D 2-ml microtube (MP Biomedicals, Irvine, CA), and kept on ice. This mix was then subjected to 8 cycles of 20 s. shaking followed by 5 minutes of cooling at 4°C on a FastPrep®-24 System (MP Biomedicals). The supernatant was then retrieved, and total RNA was extracted and further purified using an RNeasy Mini kit (Qiagen) and RNase-Free DNase Set (Qiagen), according to the manufacturer's protocols. RNA quality was assessed using Agilent RNA 6000 Nano Chips (Agilent Technologies, Santa Clara, CA) on the Agilent 2100 Bioanalyzer. RNA samples were immediately stored frozen at −80°C. RNAs with an Agilent RNA integrity number (RIN ^{21}) > 9 were selected for further analysis i.e. above the 8.5 threshold recommended by Agilent. RNA concentration and purity was determined immediately before reverse transcription through measurement of A_{260}/A_{280} ratios with a NanoDrop ND-1000 spectrophotometer (NanoDrop Technologies, Wilmington, DE).

Microarray transcriptome hybridization

We used the Affymetrix GeneChip® Exon Array platform designed to interrogate expression levels at both exon and gene level, querying 1.4 million probesets. To minimize background and increase the sensitivity of the assay, ribosomal RNA was removed from 0.7-1 µg of total RNA from each preparation (RiboMinus Human/Mouse Transcriptome Isolation Kit, Invitrogen, Carlsbad, CA). The resulting RNA was then subjected to reverse transcription using random hexamers tagged with a T7 promoter sequence followed by second strand cDNA synthesis using a DNA polymerase (GeneChip WT cDNA Synthesis Kit, Affymetrix, Santa Clara, CA). The resulting double stranded cDNA was then used for amplification of antisense cRNA and cleaned using the Gene Chip Sample Cleanup Module (Affymetrix). A second cycle of cDNA synthesis was then performed using random primers to reverse transcribe the cRNA into sense single stranded DNA. This DNA was then fragmented, labeled, and hybridized to

Affymetrix Human Gene Chip Exon 1.0 ST Arrays. Target labeling, array hybridization, washing and staining were performed as described in the Affymetrix GeneChip Whole Transcript (WT) Sense Target Labeling manual. Arrays were then hybridized, washed and stained using the GeneChip® Hybridization, Wash and Stain Kit in a GeneChip® Hybridization Oven 645 and a GeneChip® Fluidics Station 450. Arrays were then scanned on a GeneChip Scanner 3000 7G.

Array information, experimental design, raw intensities and processed $\log_2$ ratio values are all available through ArrayExpress (http://www.ebi.ac.uk/arrayexpress/) (embargo until 2010-12-23).

In silico *data filtering for probes, signal normalization, and summarization*

Standard methods for outlier removal were used, including principal component analysis on the sample covariance matrix ($V = \sum_{j=1}^{n} (y_i - \bar{y})(y_i - \bar{y})^T / n$ where $\bar{y} = \sum_{j=1}^{n} y_i / n$) and hierarchical clustering by defining a dissimilarity between the expression signatures between two samples as $1 - |\rho|$, ρ being the sample correlation [22] as implemented in the OneChannelGUI package [23] of the R programming language. A hierarchical clustering tree is thus a dendrogram representing the pairwise similarity structure between arrays. A cut-off value is given as a proportion of the tree depth in order to remove too divergent arrays as potential artifacts.

After quantile normalization [24], data from the 20 probes were fitted to a global model of expression and probe affinities (model=chip effecti+probe affinityj+_ for the jth probe on the ith array). Expression levels were summarized using the Robust Multichip Average (RMA [25]) model, which is based on the dependence of the measured intensity upon the amount of material (chip effect), the probe affinity and a reading error (measurement error). Model fitting was performed using the fast median polish algorithm [26]. This expression summary provides an estimated value for the abundance of the transcript in the sample but does not provide a measurement of the reliability of this estimation. Exon arrays lack paired mismatch probes but instead comprise a separate pool of ca. 25 000 background probes that allows the computation of a Detection Above Background (DABG) score by matching those probes to members of the

background with the same GC content. It is used to discard poorly performing probesets. In addition to this probe-level summary, gene-level summaries (expression levels averaged across probes) are calculated as median expression of probes that (i) are not multiply-targeted and (ii) hit an exon with all probes in the probeset.

Mapping to annotation

Probesets were mapped to the genome and to gene annotations using various X.to.Y functions included in the Exonmap R package [27] and a local MySQL instance of the X:MAP database [28]. This allowed to discriminate between probesets hitting introns, transcripts or genes as well as to interrogate known alternative splicings.

Identification of differentially expressed genes

Linear modeling and tests for differential expression, adjusted for multiple testing, were performed by using Limma R package [29]. The use of linear modeling allows the borrowing of information from all the transcripts in order to assist inference about each transcript individually. Briefly, Limma first adjusts a linear model over the systematic part of the data, intending to estimate its variability (function lmfit). Then, a contrast step allows the fitted coefficients to be compared regardless of their number. For single-channel microarrays such as Affymetrix Exon, linear modeling is equivalent to ANOVA but with the fitting of a model for every gene. The fitted matrix and a contrast matrix are used to compute fold-changes (FC) and t-statistics (function makeContrasts). Change in expression (fold change, FC) was considered biologically relevant when the variation was 2-fold or greater (i.e. $\log_2(FC)>1$). Differential expression is then assessed by empirical Bayes statistics: the eBayes function is used to compute moderated t-statistics, moderated F-statistic, and log-odds of differential expression by empirical Bayes shrinkage of the standard errors towards a common value. « Moderated » means that the residual mean squares and degrees of freedom are moderated between probes. An adjustment for multiple testing was applied using the decideTests function. The Benjamini-Hochberg method for controlling the false discovery rate (FDR) [30] was used.

The end result is a list of significant probes within genes of interest. Lastly, we assessed whether for each of these genes all their probesets showed the same fold-change, thus reflecting gene-level differential expression. For this purpose, we computed for each gene the variance of the fold-change for its exonic probeset. This allowed us to filter differentially expressed genes, characterized by a low variance (i.e. < 1).

Identification of differentially spliced variants

Detection of alternative splicing events was performed using two parallel approaches, the Splicing Index and MiDAS. For both tests, given the much lower number of tests involved (equaling the number of probes per gene) as compared to gene-level differential expression, a p-value of 0.05 was applied.

In the Splicing Index (SI) [15, 31] method, the expression values of the probesets are first converted to $\log_2$ space. For each probeset examined, the expression value is substracted from the mean expression value of all constitutive aligning probesets to create a constitutive corrected $\log_2$ expression difference. This difference is calculated for each individual in the study, using microarray data from that subject only, and is then used to calculate the mean expression difference in each of the patient and control groups. The probeset SI value is then derived by substracting the keratoconus group mean from the control sample group mean. This value represents the change in exon-inclusion (dI). A t-test (two tailed, assuming unequal variance) of the means is performed for statistical significance. A dI of -1 indicates a two-fold change in the expression of a probeset relative to the mean constitutive expression, with expression being higher in the keratoconus patient group than in the control group.

The MiDAS (Microarray Detection of Alternative Splicing) approach is a 2-way ANOVA-based method measuring differences between the exon level and aggregating gene level signals, including an error term and possible interactions [31]. First, probe logarithmic intensity error (PLIER) normalization is performed. This generates both exon-level signals and gene-level estimates which are robust against exon-level anomalous signals across samples. Under the null-hypothesis of no alternative splicing at an exon level, the expectation is to observe a constant difference between the exon and the corresponding gene across all the samples.

Functional association and network biology analyses

The Cytoscape platform [32] was used as a network visualisation and analysis tool for differentially expressed and spliced transcripts. We specifically used several plug-ins for interaction retrieval, network statistics and Gene Ontology enrichment (below).

Annotation and interactome characterization

To harvest protein–protein physical and functional interactions, we used the STRING (Search Tool for the Retrieval of Interacting Genes/Proteins) database which aggregates most of the available information on protein–protein interactions, organizing them by scoring and weighting [33]. The database is queried for interaction matrices derived from data and text mining, including experimental data and predicted interactions. STRING querying is characterized by a unique scoring-framework based on benchmarks of the different types of associations against a common reference set. This results into a single confidence score per prediction. For each type of interaction, a different algorithm is used to provide a score (listed in [34]). In order to recover the proteins belonging to given metabolic maps and so presumed to interact in the same metabolic pathways, we also interrogated the KEGG (Kyoto Encyclopaedia of Genes and Genomes) database [35]. Networks were then represented by a cloud of nodes connected by edges. Node connectivity (number of edges of the node) was assessed using the Hubba plug-in for Cytoscape [36].

Identification of molecular pathways

We used the BINGO plug-in from Cytoscape [37] to identify enriched Gene Ontology (GO) terms [38] among the differentially expressed genes, as follows: when sampling K genes (set) out of R genes (an annotation reference set), we aimed to infer the probability that k or more of these genes belonged to a functional category shared by r of the R genes in the reference set. By performing a binomial test, sampling with replacement, we were able to provide an approximate p-value. Only well-characterized genes (excluding hypothetical proteins) were included in the analysis. GO terms that were overrepresented in the analysis set were selected (five or more hits, binomial test $Pc < 0.05$ after Benjamini-Hochberg [BH] correction [39]). The enrichment score of each term cluster is computed as the geometric mean of each member's -Log(p-value).

Reverse transcription and real-time polymerase chain reaction amplification

In addition to the microarray experiment, quantitation of selected gene transcripts was carried out by reverse transcription and real-time quantitative PCR amplification (RT-qPCR). Eight keratoconus and 10 control corneas (of which 5 keratoconus and 5 control corneas were shared with the microarray hybridizations) were used in this experiment. One microgram of each of the total RNA preparations was reverse-transcribed into single stranded cDNA using the SuperScript III reverse transcriptase from the SuperScript VILO kit (Invitrogen, Carlsbad, CA USA). The following genes were selected to cover a range of fold-changes and gene locations within the interaction network considered: *JUN*, *FOS*, *FOSB*, *BTG2*, *EGR1*, *MCL1*, *HSP90AA1*, *S100A6*, *MAT2A*, *ANO1*, and *KRT78*. Three further genes, *TBP*, *FBRS*, and *PIH1D1*, were selected as standard baseline genes because they displayed some of the lowest differences between cases and controls in the microarray experiment. Relevant gene-specific PCR primers are listed in Supplementary Material S8. qPCR was performed using DNA Master SYBR Green I reagents in a LightCycler 480 system (F. Hoffmann-La Roche, Basel, Switzerland). Thermal cycling conditions were as follows: 95°C for 5 min (denaturation); 40 cycles at 95°C for 15 s, 60°C for 10 s (amplification), and 72°C for 20 s.; then melting curve: 95°C for 10 s, 70°C for 20 s, and 97°C for 0.1 s. qPCR data were analyzed using the comparative CT method using geometric averaging of the three internal control genes [40, 41].

To assess the correlation between the fold-change levels from qPCR and from the microarrays (at both gene and probe levels), we computed Spearman's rank correlation coefficient (Rho) statistics that estimate a rank-based measure of association.

Results

RNA extraction and data quality control

On average, 2.3 µg of total RNA was recovered from each of twenty individual whole corneas – ten keratoconus corneas, and ten from control donors. The quality control (QC) of microarray hybridization data, using exon and gene level signal densities (Supplementary Online Material S3), exon-level principal component analysis, and average-linkage hierarchical

clustering (with 20% from the tree height as the cut-off) detected one obvious outlier among the controls, namely Ctlr7, which was excluded from the subsequent analysis of the data.

About one hundred transcripts show moderate differential expression between keratoconus and non-affected corneas

One hundred and sixteen transcripts, represented by 794 probes, displayed significant differential expression levels at one or more probesets, with absolute $\log_2$(fold-change) > 1, and FDR-adjusted p-value < 0.05. Among these transcripts, 87 displayed probeset fold-change variance low enough (< 1) to be considered as differentially expressed at the gene level. The most significant differential annotations are listed in Table 1, together with their fold changes and levels of significance. Of note, the majority of differently expressed transcripts meeting these statistical criteria were downregulated in keratoconus (69 downregulated for 18 upregulated genes). Interestingly, although considered to be a housekeeping gene, *ACTB* belongs to this list. A subset of downregulated genes, namely *FOS*, *JUN*, *FOSB*, *MYC*, and *CDKN1A*, are involved in cell cycle regulation and varied most significantly in expression between keratoconus and control corneas. Figure 1 presents the relative distribution of transcript expression levels in keratoconus and control corneas for overexpressed (1a) and underexpressed (1b) genes.

Only 18 genes displayed upregulation by this analysis. Among these are several genes involved in the extracellular matrix and the epithelial cell cytoskeleton (*PTCH2*, *KRT5*, *KRT78*, *LYPD3*), in the stress response (*HSP90AA1*, *ALDH1A3*), or encoding mucins (*MUC4*, *MUC16*).

Markers considered to be melanoma-specific [42-44] were absent from the differentially expressed transcripts, consistent with our screening of the control corneas.

In parallel, a weighted correlation network analysis using the WGCNA R package [45] identified a module of 134 transcripts (Supplementary Online Material S4) that are co-expressed in correlation with the disease status across the microarray samples ($p = 9.10^{-4}$) and globally decreased in keratoconus (average $\log_2$(fold-change) = -0.68). The correlation network and individual gene analyses are convergent in that 33 transcripts in the above set of 69 individually underexpressed transcripts belong also to the WGCNA module.

Keratoconus patients express different splice isoforms of certain transcripts

We next set out to identify genes that are differentially spliced in the comparison between the keratoconus and control groups. Thirty-six candidates were identified with a threshold of p = 0.05 with either the Splicing Index or MiDAS methods (Table 2, and see Methods for details on significance levels). *MUC4*, encoding a membrane-tethered sialomucin of the ocular surface epithelium [46] is remarkable among these since it displays profound changes in transcript regulation at both the gene (over-expression in keratoconus) and splice regulation levels.

Network biology and Gene Ontology annotations

An interaction network was inferred to test whether under-expressed genes were involved in one or more biological signaling pathways. This network was obtained after retrieving a protein-protein interaction matrix from a high confidence STRING database query (score ≥ 0.7). The representation of weighted protein interactions from STRING provides a high-level view of functional linkage, enhancing the analysis of modularity in biological processes. Without the addition of further molecular partners, we were able to cluster the majority of both differentially expressed and differentially spliced proteins into a single, highly connected network (Fig. 2). A core of those genes seems central to this network, as they are the most connected nodes. In decreasing order of connectivity, they are: *JUN, MYC, FOS, PTGS2, CDKN1A, ODC1, HSP90AA1, ALDH3A1, ANXA1, and NQO1*.

After loading this network into Cytoscape, BINGO plug-in was used to further investigate whether specific gene ontologies (GO) or pathways were over-represented in the whole network. Within the first cluster of GO terms relative to biological function (enrichment score = 3.080), we filtered out several redundant terms (Supplementary Online Material S5), mainly within categories related to apoptosis regulation. On the other hand, within clusters 3 to 5 (scores 2.43, 2.22 and 2.09 respectively), there were many cell-cycle/proliferation-oriented categories. More than half of the genes had GO terms within these categories and corresponding GO term p-values, after correction, were below 10-6, meaning these categories were significantly over-represented relative to their frequency in a randomized sample of expressed transcripts. Further examination showed that keratoconus patients had significantly

lower expression of genes that fell into a limited number of KEGG signalling pathways: ErbB (*CDKN1A, JUN, MYC*), MAP kinases (*FOS, DUSP1, JUN, HSPB1, MYC*) and focal adhesion (*ACTG1, ACTB, CDKN1A, JUN, THBS1*) molecular cascades.

In addition, we mapped the fold-changes (FC) in expression between cases and controls (Supplementary Online Material S6) over the loci identified in previously published linkage analyses [2-8]. In agreement with the genetic heterogeneity of these studies and their difficulty in reproducing each others' results, no obvious candidate genes for keratoconus were distinguishable, as their FC ranged from -0.45 to +0.58. We also scrutinized the previously hypothesized candidate genes for KC (*COL6A1, SOD1, MMP9, MMP2* and *AQP5*). None of them showed significance at the bonferroni-corrected threshold of 10^{-6}.

Validation of gene microarray data

Relative quantitative real time polymerase chain reaction (qPCR) was conducted as an independent technique to validate the expression level changes in the microarray experiment. Results in Figure 3 show a good level of correlation between the three empirical assessment of expression as shown by Rho values around 0.9. Even considering as a replicate the samples used only for the qPCR experiment, the same levels of correlation are observed (data not shown).

Discussion

Using full human trancriptomic microarray, our study is the first comparison of expression of all know genes between control and keratoconus whole corneas. The use of Affymetrix Exon microarray was motivated because it is a multitarget array including several probesets per exon and four neighbor replicates per probeset, allowing a better confidence in gene-level expression estimates, and as such also provide the possibility to explore alternative RNA splicing. As a matter of fact, quantitative RT-PCR validated the microarray data even though this last method reflects the expression of only one portion of the whole transcript (i.e. the amplicon). Moreover, the interest of the use of network biology in transcriptome analysis is to make use of available limited sampling and to combine it with extant knowledge (interactome)

for enhancing meaningful extraction, the global pathway being more meaningful in a first step than individual gene expression. Previous comparative transcriptomic studies were performed on human keratoconus tissue such as corneal epithelium [47], *in vivo* [48] and *in vitro* [49] keratocytes. Two studies used restricted microarray chips targeting 5600 genes with a limited number of probeset [47, 48] and one study directly targeted the expression of 164 apoptotic genes [49]. However, none of these studies replicate with each other. This could be due to a limited number of corneal sample, as well as the limited probeset distribution and redundancy on micrroarray chips used in these studies as compared to currently used microarrays (e.g. the Affymetrix Exon array).

Our own study on human keratoconus tissue was conducted on whole corneas. As controls, we used corneas from patients enucleated for posterior pole (i.e. choroidal) melanoma. They were considered as a proper control since: i) collection was achieved in similar conditions as keratoconus corneas discarding previously treated subjects; ii) anterior segment of the eye was free of neoplastic extensions; iii) melanoma extensions is blood-borne [50], cornea is avascular and melanoma transmission was not observed after grafting cornea from a melanoma donor [51]. Consistently, we did not observe overexpression of any melanoma-specific transcript.

In this context, our aim was to reassess the genetic component of the keratoconus taking into account the following hypotheses: a condition characterized by genetic heterogeneity, with various loci linked in different populations, and a complex phenotypic trait whose transmission appears to deviate from a Mendelian model. Because transcriptomics have helped identify molecular pathways and alternatively spliced variants involved in other complex diseases, e.g. in oncology [15, 20, 52] and autoimmunity [53], we have transposed this approach to keratoconus. The interplay of both experimental and predicted interactions of the annotation database we used (STRING), is supposed to offer a more accurate approximation of the interactome than Gene Ontology alone. Nevertheless, this analysis infers statistical links between keratoconus phenotype and gene expression, and requires experimental validation, perhaps in animal models. We identified mice mutants for 29 of the differentially expressed genes, and 27 of the differentially spliced ones (Supplementary Online Material S7) in the Mouse Genome

Informatics database (http://www.informatics.jax.org/). Some of them display corneal clinical phenotypes: the Jun mutant shows eye opacity and increased incidence of corneal inflammation, significant in the light of a recent study also implicating a downstream *JUN* effector, *JNK2*, in abnormal corneal barrier response to dry eyes [54]. The *THBS1* (thrombospondin 1) mutant displays abnormal corneal epithelial morphology and Ldlr (low density lipoprotein receptor) mutant also has dry eyes. However, their relevance remains to be tested, especially in human pathology. *JUN* is a human proto-oncogene implicated in carcinogenesis, while *LDLR* mutations lead to autosomal dominant hypercholesterolemia.

The majority (69 over 87) of the genes highlighted were downregulated in keratoconus patient corneas. They include a number of genes globally involved in cellular proliferation and the prevention of differentiation (e.g. the AP-1 transcription factor partners *FOS, JUN, FOSB*) [55] or *MYC*, required for proliferation or stem cell mobilization [56]. Confirming previous studies, we did not find any significant change regarding putative candidate genes previously proposed (*MMP2, MMP9, COL6A1, SOD1,* and *AQ5*). Another original finding is that the beta-actin *ACTB* is down-regulated thus confirming that, at least in pathological conditions, it cannot be considered a good reference gene for expression in cornea. Gene Ontology terms enrichment analysis demonstrated, independently of the algorithms used, that these down-regulated genes are more widely involved in so-called (cellular) developmental processes or cell differentiation. First, we observed a redundancy of GO terms in the first three annotation clusters (GO:0032502 developmental process, GO:0048869 cellular developmental process , GO:0030154 cell differentiation). Their congruence strengthens the conclusion that some keratoconus corneal cells are maintained in a less differentiated, proliferative state [57, 58]. Simultaneously, decreased protection from apoptosis may be implied by the terms GO: 0043066 (negative regulation of apoptosis) or GO: 0048468 (cell development). The “gene population background”-based enrichment analysis from DAVID's web-based annotation tool [59], which uses both GO terms and the Kyoto Encyclopedia of Genes and Genomes (KEGG [60]), as well as GO pruning and filtering of WikiPathways using GO-Elite [61] gave similar results. The weighted correlation network analysis showed significant co-expression of modules containing intermediaries consistent with the highlighted pathways. Finally, GO enrichment analysis gave roughly the same results when

applied to the $p<0.01$ and $p<0.05$ differentially expressed gene lists. Moreover, the qPCR results show that for all genes selected for validation, the direction and magnitude of changes were consistent with the results obtained from the microarray analysis.

Finally, we failed to replicate previous differential expression experiments on KC *versus* normal corneas [47-49]: none of the differentially expressed genes found in these studies did overlap between each other and with ou results. Nevertheless, we performed a network biology analysis combining the highlighted genes from these and our studies as well as three genes involved in communication between the epithelium and the stroma, namely *HGF, KGF* and *EGF* [62, 63] (Supplementary Online Material S9). We found that while we did not highlight the same genes, the same biological pathways seem to be involved. The dataset from Stachs et al. [48] comes from freshly isolated keratocytes, while the one of Nielsen et al. [47] comes from fresh epithelial cells. Our own dataset composed of both epithelial and stromal components is linked with both datasets, showing that these different studies are congruent. In addition, the links observed between the majority of our highlighted genes and Nielsen's ones by means of *EGF*, *KGF* and *EGF*, considered to be involved in epithelium/strom signalisation [63], are a further argument that there is probably an interplay between both cellular layers in keratoconus.

Our results implicate both known and novel pathways that may play a key role in the pathophysiology of keratoconus. It is noteworthy to mention here that many of the selected genes have elsewhere been associated with cancer. Nevertheless, they are also primarily involved in developmental processes and cell proliferation. Thus, is is not surprising that a change in mRNA expression could be associated with a disease suspected to derive from cell loss. In fact, apoptosis has been observed in keratoconus corneas by direct confocal microscopy and histology showing decreased lower cell densities in the three corneal layers [58, 64], as well as biochemical or expression studies [9, 65-68]. This is in full agreement with the over-representation of GO terms annotation in our dataset. The primary cause for apoptosis in keratoconus remains unknown, but it may be a secondary consequence of another molecular defect. Several reports have suggested a decreased resistance to environmental aggressions by hypersensitivity to oxidative stress in cultivated keratocytes from keratoconus corneas [69] as

well as *in vivo* [57]. Cultured keratoconus fibroblasts also may have an inherent, hypersensitive response to oxidative stressors that involves mitochondrial damage and the expression of intermediate filaments such as vimentin or tenascin or the pro-inflammatory TGF-• and IL-1 [70]. Apoptosis in keratoconus may also result from mechanical trauma or be secondary to the production of cytokines after atopy.

At this point, the cellular population suffering these network alterations remains uncertain. This lack of hypothesis led us to perform, in a first approach, a full thickness corneal study. The recovered amounts of mRNAs are largely in favor of epithelial cells and this could have biased the results and consequently their interpretation. Nevertheless, one can imagine that both epithelial cells and keratocytes may represent key players. Keratocytes are specialized fibroblasts, derived from neural crest mesenchyme in common with the cartilaginous stromal layer behind the eyeball [71] produce collagen fibres and proteoglycans constituting the corneal stroma. Throughout life, most keratocytes are in a quiescent state [72]. By the end of eye development a keratocyte network, interconnected through dendritic processes, is established. Keratocyte apoptosis, either of quiescent or actively dividing cells, is a process of great interest for corneal growth and remodeling. Previous reports have speculated that keratocytes may be involved in keratoconus development through increased catabolism, either misregulation of metalloprotease activity [67] or a modification of collagen subtype composition [73]. We bring here a novel hypothesis that keratocytes implication would be mediated by a tissue-specific misregulation of apoptosis that may be due to possibly less redundant anti-apoptotic pathways in the cornea. In a healthy cornea, programmed cell death is a rare occasion, but immediately after an injury, keratocytes directly below the injury site undergo apoptosis when the basal membrane is broken. In the following steps of the healing and scarring process, this cell loss is counteracted by mitoses among the remaining adjacent keratocytes [62]. In keratoconus corneas, impairment of apoptotic signalling pathways upon minor corneal injuries sustained through life may impact upon appropriate keratocyte proliferation, itself necessary for the recovery of the initial normal cell density. Keratocyte-restricted deficiencies in the regulation of apoptosis may lead to the gene expression differences we have observed in this study. This could provide an explanation to the loss of cell density and corneal thinning observed in KC. Interestingly, a

recent study underlined the role of *TWIST2*, a bHLH transcription factor, in keratocyte proliferation in mouse leading to a corneal thinning [74]. Epithelium whose cells are continuously renewed may also be affected by the antiproliferative and hyperapoptotic phenotypes. The eighteen overexpressed genes we observed to be significantly differentially expressed included *KRT78, ROR2, S100A6 and MUC4. KRT78* is a structural protein of epithelial cells whose cross-linking helps withstand mechanical and chemical stresses [75]. *ROR2* encodes a nuclear orphan receptor in the non-canonical Wnt pathway that appears to trigger, among other effects, the maintenance and proliferation of stem cells [76]. *S100A6* (calcyclin) is involved in the fibroblast cell cycle [77] and over-expressed during wound healing after corneal injury. In addition, sialomucin (*MUC4*) is expressed by the corneal epithelium. This raises the question of how epithelial cells may also be involved in the pathogenesis of keratoconus. We found increased expression of the whole transcript population of *MUC4* in keratoconus corneas. The apical location of mucins could suggest their general involvement in mechanisms of response to epithelial damage [78]. In addition, among mucins, *MUC4* displays tissue-specific expression patterns - notably, a conjunctival-type expression pattern is observed on the corneal surface in limbal stem cell deficiency [79]. Both mucin-4 (the product of the *MUC4* gene) and calcyclin are implicated in corneal protection and wound healing by the constitution of the lacrymal film [80, 81]. In addition, mutations in other mucin genes are already implicated in human pathology, notably the dry eye syndromes [82] (Supplementary Online Material S6). Alternatively sialomucin is also an activator partner of the epidermal growth factor ErbB2 receptor, potentially implicating its overexpression in growth factor signalling pathways leading to either differentiation or increased cell proliferation [78]. Each of these over-expressed transcripts therefore could conceivably be either pathogenic or simply deregulated as a consequence of other causal molecular mechanisms. Over-expression of *MUC4* might be a protective response, or could be causative in keratoconus, and a corneal-specific mouse over-expression model would be welcome to resolve this question.

Another differentially spliced molecule is annexin A1 (*ANXA1*). This calcium-dependent phospholipid-binding protein has no allelic variants described, regulates phospholipase A2 activity and promotes membrane fusion. It was previously shown to be upregulated (x1.5) in

keratoconus corneal epithelial cells relative to normal epithelial cells [47]. *ANXA1* is located within the chromosomal interval 9q21, which has been suggestively linked to keratoconus using non-parametric linkage [83]. However, it is the only differentially expressed gene that showed consensus with the chromosomal regions linked to keratoconus so far. This observation confirms that expression analysis is an interesting complementary approach to linkage analyses, and that our having included the keratocyte population from whole keratoconus versus normal corneas not only found this difference but has implicated broad functional pathways in addition to individual molecules.

Altogether these results cannot exclude that, whatever the pathways involved, keratoconus could result from a distorsion of the cross talk between epithelial and stromal cells of the cornea. In the future, more precise, layer specific, expression studies should be conducted. Such expression results may be combined with the latest possibilities for genome-wide association studies in order to identify genomic variants that correlate with both expression and keratoconus phenotype.

Acknowledgments

Many thanks go to Nathalie Marsaud (Genotoul Biopuces, Toulouse Biochip Facility) for help and advice about the experimental protocol as well as to Didier Laborie and the Bioinfo-Genotoul team at the Toulouse Bioinformatics Facility. This study was supported by Rétina France Foundation and French Ministère de la Santé**.**

Tables

Table 1. Transcripts with differentially levels of expression between keratoconus and control corneas.

Gene names (HUGO Gene Nomenclature Committee at the European Bioinformatics Institute) are provided alongside their respective fold-change (FC) and the p-value from a Student t test. A more complete table (including annotation) is provided as supplementary material S1.

HUGO Gene Symbol	log2 (fold-change)	P-value	Gene Name	Fold-change
KRT78	1.21	$1.62.10^{-05}$	Keratin 78 – Keratin 5B	2.31
MUC4	0.49	$7.46.10^{-06}$	Mucin 4	1.40
S100A6	0.27	$7.92.10^{-06}$	S100 Calcium Binding Protein A6 (Calcicyclin)	1.21
ROR2	0.12	$9.57.10^{-05}$	Receptor Tyrosine Kinas.10-like Orphan Receptor 2	1.09
SQSTM1	-0.1	$4.90.10^{-05}$	Sequestosome 1	0.93
INSIG1	-0.15	$4.59.10^{-05}$	Insulin induced Gene 1	0.90
HSPB1	-0.16	$4.87.10^{-05}$	Heat Shock 27kDa Protein 1	0.90
NQO1	-0.2	$1.51.10^{-05}$	NAD(P)H Dehydrogenase, Quinone 1	0.87
DDX3X	-0.2	$9.23.10^{-06}$	DEAD (ASP-GLU-ALA-ASP) Box Polypeptide 3, X-linked	0.87
KRT5	-0.24	$6.86.10^{-07}$	Keratin 5A	0.85
HSP90AA1	-0.27	$4.64.10^{-05}$	Heat Shock Protein 90kDa alpha (cytosolic), class A member 1	0.83
FTH1	-0.32	$3.45.10^{-07}$	Ferritin, heavy polypeptide 1	0.80
RNF39	-0.35	$1.10.10^{-05}$	Ring Finger Protein 39	0.78
DDX5	-0.39	$1.33.10^{-05}$	Dead (Asp-Glu-Ala-Asp) Box Polypeptide 5	0.76
ACTB	-0.45	$3.12.10^{-06}$	Actin, Beta	0.73
SAT1	-0.59	$1.56.10^{-06}$	Spermidine/Spermine N1-Acetyltransferase	0.66
DNAJB1	-0.59	$1.65.10^{-05}$	Dnaj (Hsp40) Homolog, Subfamily B, Member 1	0.66
ZNF750	-0.61	$1.54.10^{-05}$	Hypothetical Protein Loc79755	0.66
THBS1	-0.63	$6.60.10^{-06}$	Thrombospondin 1	0.65
MYC	-0.64	$9.27.10^{-06}$	V-Myc Myelocytomatosis Viral Oncogene Homolog (Avian)	0.64
HES1	-0.71	$1.13.10^{-05}$	Hairy And Enhancer Of Split 1, (Drosophila)	0.61
CDKN1A	-0.76	$2.79.10^{-06}$	Cyclin-Dependent Kinase Inhibitor 1a (P21, Cip1)	0.59
MAT2A	-0.83	$3.16.10^{-06}$	Methionine Adenosyltransferase Ii, Alpha	0.56
ZFP36L1	-0.87	$6.85.10^{-06}$	Zinc Finger Protein 36, C3h Typ.10-Like 1	0.55
MCL1	-1.01	$9.20.10^{-06}$	Myeloid Cell Leukemia Sequence 1 (Bcl2-Related)	0.50
ID1	-1.08	$3.59.10^{-05}$	Inhibitor Of Dna Binding 1, Dominant Negative Helix-Loop-Helix Protein	0.47
ODC1	-1.08	$3.37.10^{-06}$	Ornithine Decarboxylase 1	0.47
SLC20A1	-1.08	$3.56.10^{-06}$	Solute Carrier Family 20 (Phosphate Transporter), Member 1	0.47
NUAK2	-1.16	$9.61.10^{-05}$	Nuak Family, Snf1-Like Kinase, 2	0.45
BTG2	-1.52	$1.24.10^{-05}$	Btg Family, Member 2	0.35
UBC (RPS27A)	-1.84	$1.83.10^{-05}$	Ubiquitin C	0.28

ZFP36	-1.92	$1.02.10^{-05}$	Zinc Finger Protein 36, C3h Type, Homolog (Mouse)	0.26
DUSP1	-2.19	$2.02.10^{-05}$	Dual Specificity Phosphatase 1	0.22
JUN	-3.13	$9.98.10^{-05}$	V-Jun Sarcoma Virus 17 Oncogene Homolog (Avian)	0.11
FOSB	-3.69	$1.87.10^{-05}$	Fbj Murine Osteosarcoma Viral Oncogene Homolog B	0.08
FOS	-4.2	$2.93.10^{-05}$	V-Fos Fbj Murine Osteosarcoma Viral Oncogene Homolog	0.05

Table 2. Genes differentially spliced between keratoconus and control corneas.

Gene names (HGNC - HUGO Gene Nomenclature Committee at the European Bioinformatics Institute) are provided alongside their respective Splicing Index (SI) or MiDAS (Microarray Detection of Alternative Splicing) readouts. A more complete table (including annotation) is provided as supplementary material S2.

HUGO Gene Symbol	SI	SI p-value	MiDAS p-value	Description
PTGS2	1.58	$2.50.10^{-05}$	$3.93.10^{-02}$	Prostaglandin-endoperoxide synthase 2 (prostaglandin G/H synthase and cyclooxygenase)
FOSL2	1.24	$8.35.10^{-05}$	$3.71.10^{-02}$	FOS-like antigen 2
MYL6	1.35	$1.86.10^{-04}$	$3.80.10^{-02}$	Myosin, light chain 6, alkali, smooth muscle and non-muscle
HSPB1	2.72	$2.32.10^{-06}$	$1.54.10^{-02}$	Heat shock 27kDa protein 1
BAG1	1.18	$5.88.10^{-04}$	$4.82.10^{-02}$	BCL2-associated athanogene
ALDH3A1	1.16	$8.26.10^{-05}$	$3.46.10^{-02}$	Aldehyde dehydrogenase 3 family, memberA1
DDX5	1.40	$6.13.10^{-05}$	$3.30.10^{-02}$	DEAD (Asp-Glu-Ala-Asp) box polypeptide 5
ODC1	3.00	$8.16.10^{-05}$	$3.26.10^{-02}$	Ornithine decarboxylase 1
SDC1	1.74	$2.65.10^{-04}$	$3.60.10^{-02}$	Syndecan 1
SLC2A1	1.19	$2.25.10^{-04}$	$4.06.10^{-02}$	Solute carrier family 2 (facilitated glucose transporter), member 1
CDKN1A	1.04	$2.99.10^{-05}$	$2.77.10^{-02}$	Cyclin-dependent kinase inhibitor 1A (p21, Cip1)
ID1	1.31	$2.26.10^{-05}$	$2.34.10^{-02}$	Inhibitor of DNA binding 1, dominant negative helix-loop-helix protein
SAT1	1.30	$3.23.10^{-06}$	$2.21.10^{-02}$	Spermidine/spermine N1-acetyltransferase 1
LDLR	1.72	$1.14.10^{-06}$	$1.86.10^{-02}$	Low density lipoprotein receptor (familial hypercholesterolemia)
H3F3B	1.23	$8.80.10^{-05}$	$3.64.10^{-02}$	H3 histone, family 3B (H3.3B)
TPT1	1.82	$1.88.10^{-04}$	$3.37.10^{-02}$	Tumor protein, translationally-controlled 1
	1.77	$2.82.10^{-04}$	$4.21.10^{-02}$	--
RRAS2	1.54	$6.83.10^{-04}$	$4.04.10^{-02}$	Related RAS viral (r-ras) oncogene homolog 2
BHLHB2/BHLHE40	1.15	$4.97.10^{-07}$	$1.70.10^{-02}$	Basic helix-loop-helix domain containing, class B, 2//Class E basic helix-loop-helix protein 40
ANXA1	2.80	$2.80.10^{-04}$	$3.39.10^{-02}$	Annexin A1
GLUL	1.10	$1.97.10^{-04}$	$4.36.10^{-02}$	Glutamat.10-ammonia ligase (glutamine synthetase)
CTSL2	1.09	$4.41.10^{-04}$	$4.34.10^{-02}$	Cathepsin L2
JDP2	1.53	$4.19.10^{-04}$	$4.61.10^{-02}$	Jun dimerization protein 2
MUC4	-2.38	$2.31.10^{-04}$	$3.56.10^{-02}$	Mucin 4, cell surface associated
KIAA1754/ITPRIP	1.38	$5.19.10^{-04}$	$4.78.10^{-02}$	Inositol 1,4,5-triphosphate receptor-interacting protein
RPS27A/UBC	2.52	$9.01.10^{-07}$	$1.41.10^{-02}$	Ubiquitin C
	2.38	$1.90.10^{-07}$	$1.20.10^{-02}$	Ubiquitin C
NUAK2	1.48	$4.37.10^{-05}$	$3.10.10^{-02}$	NUAK family, SNF1-like kinase, 2
WEE1	1.23	$2.18.10^{-04}$	$4.51.10^{-02}$	WEE1 homolog (S. pombe)
SERTAD3	1.46	$3.36.10^{-05}$	$3.06.10^{-02}$	SERTA domain containing 3
MAT2A	1.31	$9.77.10^{-07}$	$1.44.10^{-02}$	Methionine adenosyltransferase II, alpha
EFNA1	1.30	$4.66.10^{-06}$	$2.36.10^{-02}$	Ephrin-A1
OVOL1	1.18	$3.77.10^{-05}$	$3.38.10^{-02}$	Ovo-like 1(Drosophila)
ACTG1	1.80	$2.19.10^{-04}$	$4.04.10^{-02}$	Actin, gamma 1
TACSTD2	1.49	$7.17.10^{-05}$	$3.35.10^{-02}$	Tumor-associated calcium signal transducer 2

INSIG1	1.39	$7.39.10^{-05}$	$3.26.10^{-02}$	Insulin induced gene 1
PTMA	1.41	$4.21.10^{-05}$	$3.20.10^{-02}$	Prothymosin, alpha
CD55	2.56	$2.02.10^{-05}$	$1.89.10^{-02}$	CD55 molecule, decay accelerating factor for complement (Cromer blood group)

Figure legends

Figure 1. Levels of expression of the differentially expressed genes.

The boxplots represent dispersion among samples. Keratoconus samples are indicated by KC while controls are indicated by ctrl. **A.** Transcripts under-expressed in KC, ordered by decreasing absolute fold-change. **B.** Transcripts over-expressed in KC, ordered by increasing absolute fold-change.

A

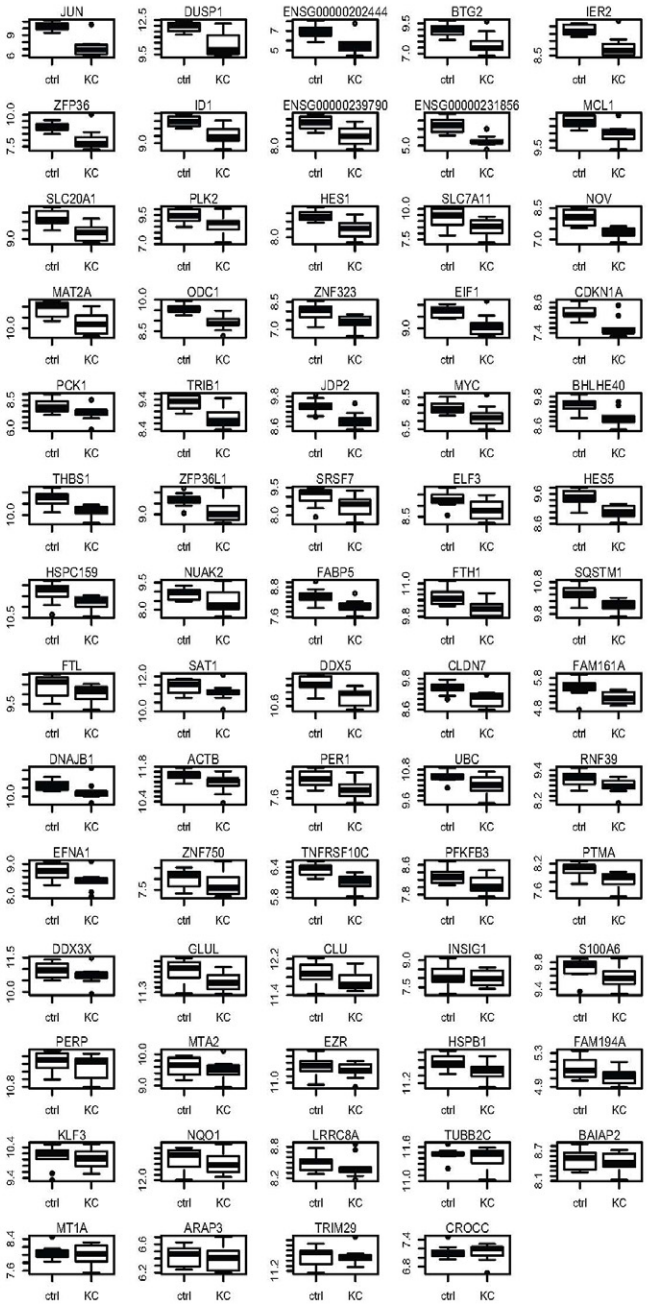
JUN
DUSP1
ENSG00000202444
BTG2
IER2
ZFP36
ID1
ENSG00000239790
ENSG00000231856
MCL1
SLC20A1
PLK2
HES1
SLC7A11
NOV
MAT2A
ODC1
ZNF323
EIF1
CDKN1A
PCK1
TRIB1
JDP2
MYC
BHLHE40
THBS1
ZFP36L1
SRSF7
ELF3
HES5
HSPC159
NUAK2
FABP5
FTH1
SQSTM1
FTL
SAT1
DDX5
CLDN7
FAM161A
DNAJB1
ACTB
PER1
UBC
RNF39
EFNA1
ZNF750
TNFRSF10C
PFKFB3
PTMA
DDX3X
CLUL
CLU
INSIG1
S100A6
PERP
MTA2
EZR
HSPB1
FAM194A
KLF3
NQO1
LRRC8A
TUBB2C
BAIAP2
MT1A
ARAP3
TRIM29
CROCC
ctrl
KC

B

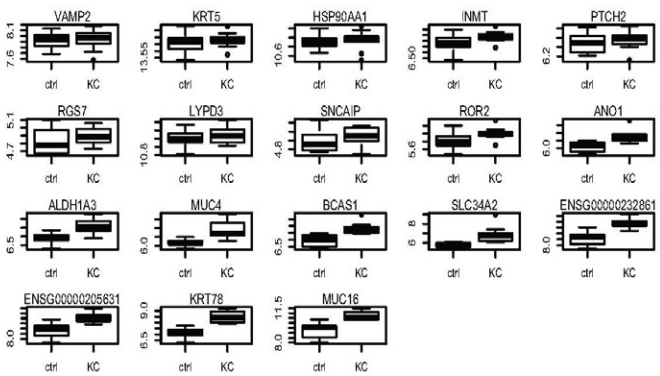
VAMP2
KRT5
HSP90AA1
INMT
PTCH2
RGS7
LYPD3
SNCAIP
ROR2
ANO1
ALDH1A3
MUC4
BCAS1
SLC34A2
ENSG00000232861
ENSG00000205631
KRT78
MUC16
ctrl
KC

Figure 2. Interaction network showing links between differentially expressed and differentially spliced genes.

The network includes interactions retrieved from the STRING interactome database. HGNC official names are given. The colors of interaction partners describe the modifications we observed between cases and controls in the dataset. Downregulated genes are shown in red, upregulated in blue, differentially spliced in yellow, upregulated and differentially spliced in green, and downregulated and differentially spliced in orange. Colors of edges between partner nodes show the type of interaction. Blue lines represent binding, activation is represented by a green line, modification of expression by a yellow line and post-translational modification by a pink line. For interactions inferred from text-mining (shown in grey), the level of confidence is proportional to line thickness. Unlinked genes are represented by three rows at the top of the figure. The first row includes the genes that would be linked by addind one intermediary connecting node, the second row, by adding two intermediary connecting nodes and the third, other genes.

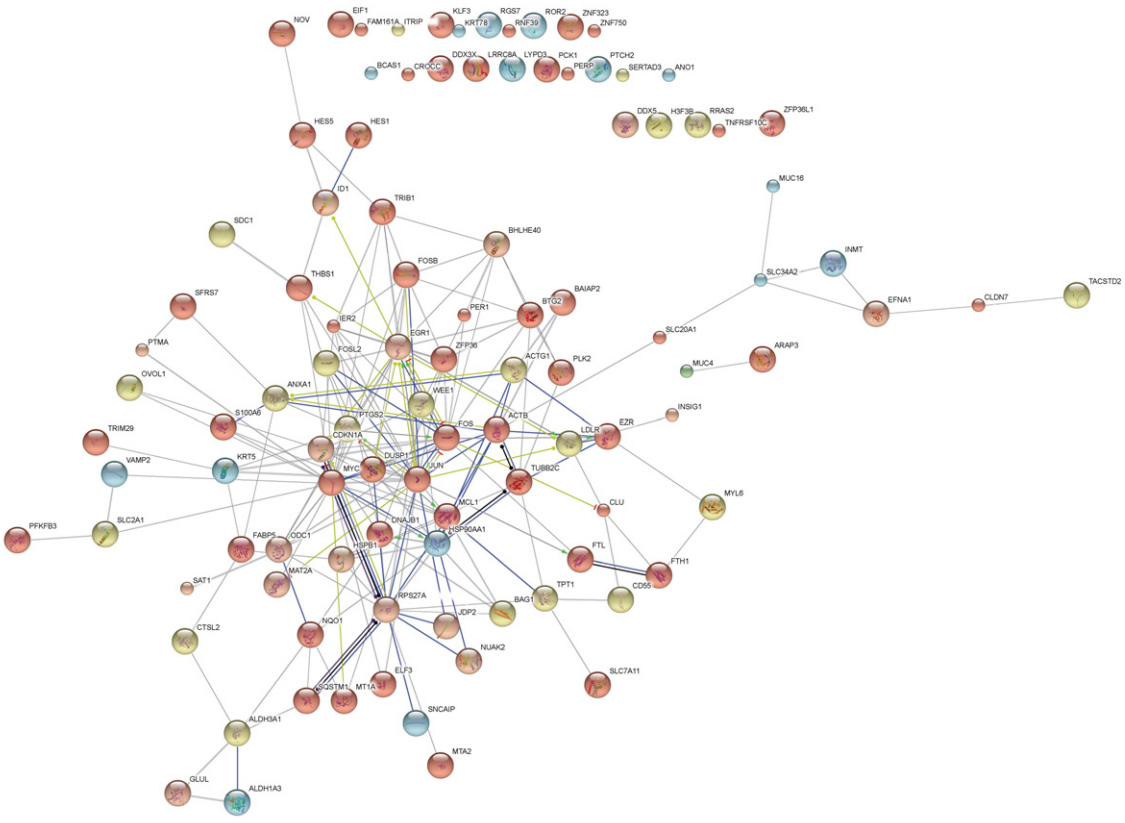

Figure 3. Quantitative Real-Time PCR (qPCR) experiment.

Results are represented as an histogram, grouped by gene. For each gene, three results are presented: in white, the gene level expression estimated by averaging microarray probesets; in grey, the level of expression at the microarray probeset corresponding to the region amplified in the qPCR experiment; in black, the level of expression as estimated in the qPCR (primer pair sequences and location provided in Supplementary Material S8). The pairwise levels of correlation between the three estimated is also given as Spearman's rho statistics.

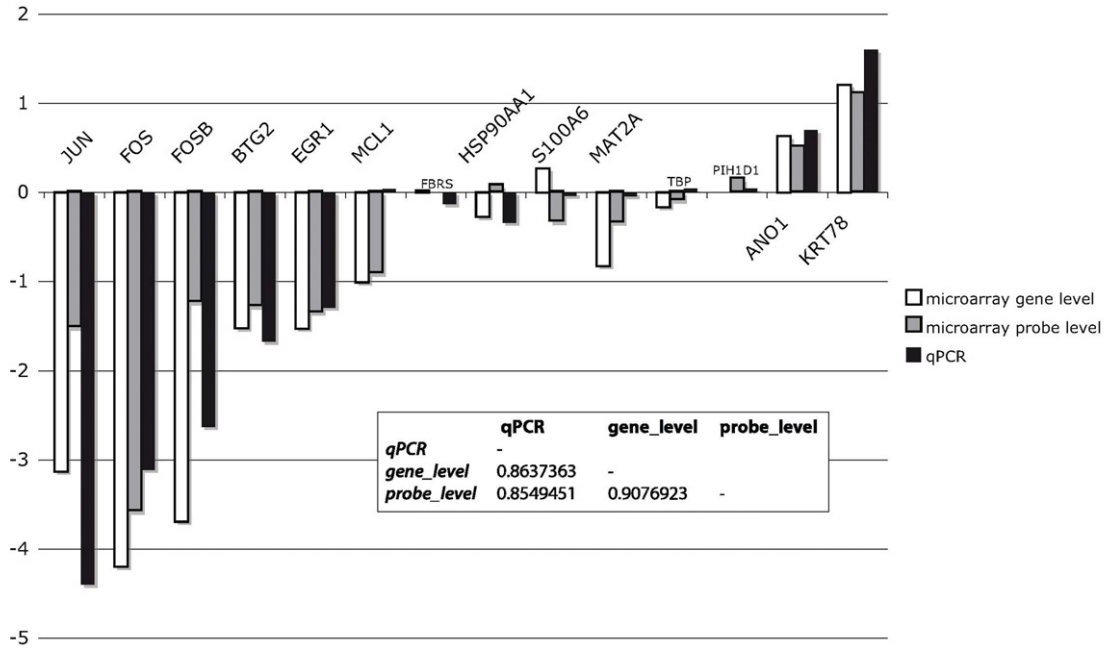

References

1. Karseras AG, Ruben M. Aetiology of keratoconus. *British Journal of Ophthalmology* 1976;60:522-525.
2. Brancati F, Valente E, Sarkozy A, Feher J. A locus for autosomal dominant keratoconus maps to human chromosome 3p14-q13. *Journal of Medical Genetics* 2004;41:188-192.
3. Fullerton J, Paprocki P, Foote S, Mackey DA, Williamson R, Forrest S. Identity-by-descent approach to gene localisation in eight individuals affected by keratoconus from north-west Tasmania, Australia. *Human genetics* 2002;110:462-470.
4. Hughes AE, Dash DP, Jackson AJ, Frazer DG, Silvestri G. Familial keratoconus with cataract: linkage to the long arm of chromosome 15 and exclusion of candidate genes. *Investigative ophthalmology & visual science* 2003;44:5063-5066.
5. Hutchings H, Ginisty H, Le Gallo M, et al. Identification of a new locus for isolated familial keratoconus at 2p24. *British Medical Journal* 2005;42:88.
6. Li X, Rabinowitz YS, Tang YG, et al. Two-stage genome-wide linkage scan in keratoconus sib pair families. *Investigative ophthalmology & visual science* 2006;47:3791-3795.
7. Tang YG, Rabinowitz YS, Taylor KD, et al. Genomewide linkage scan in a multigeneration Caucasian pedigree identifies a novel locus for keratoconus on chromosome 5q14.3-q21.1. *Genetics in medicine : official journal of the American College of Medical Genetics* 2005;7:397-405.
8. Tyynismaa H, Sistonen P, Tuupanen S, et al. A locus for autosomal dominant keratoconus: linkage to 16q22. 3-q23. 1 in Finnish families. *Investigative ophthalmology & visual science* 2002;43:3160.
9. Rabinowitz YS, Maumenee I, Lundergan M, et al. Molecular genetic analysis in autosomal dominant keratoconus. *Cornea* 1992;11:302-308.
10. Udar N, Atilano S, Brown D, Holguin B. SOD1: a candidate gene for keratoconus. *Investigative ophthalmology & visual science* 2006;47:3345-3351.
11. Bisceglia L, Ciaschetti M, De Bonis P, et al. VSX1 mutational analysis in a series of Italian patients affected by keratoconus: detection of a novel mutation. *Investigative ophthalmology & visual science* 2005;46:39.
12. Rabinowitz YS, Dong L, Wistow G. Gene expression profile studies of human keratoconus cornea for NEIBank: a novel cornea-expressed gene and the absence of transcripts for aquaporin 5. *Investigative ophthalmology & visual science* 2005;46:1239-1246.
13. Ostrowski J, Wyrwicz LS. Integrating genomics, proteomics and bioinformatics in translational studies of molecular medicine. *Expert review of molecular diagnostics* 2009;9:623-630.
14. Monks SA, Leonardson A, Zhu H, et al. Genetic inheritance of gene expression in human cell lines. *American journal of human genetics* 2004;75:1094-1105.
15. Gardina PJ, Clark TA, Shimada B, et al. Alternative splicing and differential gene expression in colon cancer detected by a whole genome exon array. *BMC genomics* 2006;7:325.
16. Licatalosi DD, Darnell RB. RNA processing and its regulation: global insights into biological networks. *Nature reviews Genetics* 2010;11:75-87.

17. Clark TA, Schweitzer AC, Chen TX, et al. Discovery of tissue-specific exons using comprehensive human exon microarrays. *Genome biology* 2007;8:R64.
18. Johnson JM, Castle J, Garrett-Engele P, et al. Genome-wide survey of human alternative pre-mRNA splicing with exon junction microarrays. *Science (New York, NY)* 2003;302:2141-2144.
19. Faustino NA, Cooper TA. Pre-mRNA splicing and human disease. *Genes & development* 2003;17:419-437.
20. Venables JP. Unbalanced alternative splicing and its significance in cancer. *BioEssays : news and reviews in molecular, cellular and developmental biology* 2006;28:378-386.
21. Schroeder A, Mueller O, Stocker S, et al. The RIN: an RNA integrity number for assigning integrity values to RNA measurements. *BMC molecular biology* 2006;7:3.
22. McLachlan GJ, Do K-A, Ambroise C. *Analyzing microarray gene expression data, Vol. 422 from Wiley Series in Probability and Statistics - Applied Probability and Statistics Section Series*. Hoboken, NJ: Wiley-IEEE; 2004:320.
23. Sanges R, Cordero F, Calogero RA. oneChannelGUI: a graphical interface to Bioconductor tools, designed for life scientists who are not familiar with R language. *Bioinformatics (Oxford, England)* 2007;23:3406-3408.
24. Bolstad BM, Irizarry Ra, Astrand M, Speed TP. A comparison of normalization methods for high density oligonucleotide array data based on variance and bias. *Bioinformatics (Oxford, England)* 2003;19:185-193.
25. Irizarry RA, Bolstad BM, Collin F, Cope LM, Hobbs B, Speed TP. Summaries of Affymetrix GeneChip probe level data. *Nucleic acids research* 2003;31:e15.
26. Mosteller F, Tukey J. *Data Analysis and Regression*. Reading, MA: Addison-Wesley; 1977.
27. Okoniewski MJ, Miller CJ. Comprehensive analysis of affymetrix exon arrays using BioConductor. *PLoS computational biology* 2008;4:e6.
28. Tai TYT, Damani MR, Vo R, et al. Keratoconus associated with corneal stromal amyloid deposition containing TGFBIp. *Cornea* 2009;28:589-593.
29. Smyth GK. Limma: linear models for microarray data. In: Gentleman R, Carey V, Huber W, Irizarry R, Dudoit S (eds), *Bioinformatics and Computational Biology Solutions using R and Bioconductor*. New York: Springer; 2005:397-420.
30. Benjamini Y, Hochberg Y. Controlling the false discovery rate: a practical and powerful approach to multiple testing. *Journal of the Royal Statistical Society Series B (Methodological)* 1995;57:289-300.
31. Srinivasan K, Shiue L, Hayes JD, et al. Detection and measurement of alternative splicing using splicing-sensitive microarrays. *Methods (San Diego, Calif)* 2005;37:345-359.
32. Cline MS, Smoot M, Cerami E, et al. Integration of biological networks and gene expression data using Cytoscape. *Nature protocols* 2007;2:2366-2382.
33. Jensen LJ, Kuhn M, Stark M, et al. STRING 8--a global view on proteins and their functional interactions in 630 organisms. *Nucleic acids research* 2009;37:D412-416.
34. von Mering C, Huynen M, Jaeggi D, Schmidt S, Bork P, Snel B. STRING: a database of predicted functional associations between proteins. *Nucleic acids research* 2003;31:258-261.
35. Kanehisa M, Goto S, Kawashima S, Okuno Y, Hattori M. The KEGG resource for deciphering the genome. *Nucleic acids research* 2004;32:D277-280.

36. Lin C-Y, Chin C-H, Wu H-H, Chen S-H, Ho C-W, Ko M-T. Hubba: hub objects analyzer--a framework of interactome hubs identification for network biology. *Nucleic acids research* 2008;36:W438-443.
37. Maere S, Heymans K, Kuiper M. BiNGO: a Cytoscape plugin to assess overrepresentation of gene ontology categories in biological networks. *Bioinformatics (Oxford, England)* 2005;21:3448-3449.
38. Ashburner M, Ball CA, Blake JA, et al. Gene ontology: tool for the unification of biology. The Gene Ontology Consortium. *Nature genetics* 2000;25:25-29.
39. Gilbert PB. A modified false discovery rate multiple-comparisons procedure for discrete data, applied to human immunodeficiency virus genetics. *Journal of the Royal Statistical Society: Series C (Applied Statistics)* 2005;54:143-158.
40. Livak KJ, Flood SJ, Marmaro J, Giusti W, Deetz K. Oligonucleotides with fluorescent dyes at opposite ends provide a quenched probe system useful for detecting PCR product and nucleic acid hybridization. *PCR methods and applications* 1995;4:357-362.
41. Vandesompele J, De Preter K, Pattyn F, et al. Accurate normalization of real-time quantitative RT-PCR data by geometric averaging of multiple internal control genes. *Genome Biol* 2002;3:research0034.0031–0034.0011.
42. Böni R, Heizmann CW, Doguoglu A, et al. Ca(2+)-binding proteins S100A6 and S100B in primary cutaneous melanoma. *J Cutan Pathol* 1997;24:76-80.
43. Indrei A, Cianga P, Florea ID, Haba D, Foia L, Cianga CM. A rare case of double recurrent choroidal melanoma, with distinctive immunohistochemical features. *Romanian journal of morphology and embryology = Revue roumaine de morphologie et embryologie* 51:187-193.
44. Kan-Mitchell J, Liggett PE, Taylor CR, et al. Differential S100 beta expression in choroidal and skin melanomas: quantitation by the polymerase chain reaction. *Investigative ophthalmology & visual science* 1993;34:3366-3375.
45. Langfelder P, Horvath S. WGCNA: an R package for weighted correlation network analysis. *BMC bioinformatics* 2008;9:559.
46. Govindarajan B, Gipson IK. Membrane-tethered mucins have multiple functions on the ocular surface. *Exp Eye Res* 90:655-663.
47. Nielsen K, Birkenkamp-Demtröder K, Ehlers N, Orntoft TF. Identification of differentially expressed genes in keratoconus epithelium analyzed on microarrays. *Investigative ophthalmology & visual science* 2003;44:2466-2476.
48. Stachs O, Bochert A, Gerber T, Koczan D, Thiessen HJ, Guthoff RF. [The extracellular matrix structure in keratoconus]. *Ophthalmologe* 2004;101:384-389.
49. Ha NT, Nakayasu K, Murakami A, Ishidoh K, Kanai A. Microarray analysis identified differentially expressed genes in keratocytes from keratoconus patients. *Current eye research* 2004;28:373-379.
50. Zakka KA, Foos RY, Omphroy CA, Straatsma BR. Malignant melanoma. Analysis of an autopsy population. *Ophthalmology* 1980;87:549-556.
51. Harrison DA, Hodge DO, Bourne WM. Outcome of corneal grafting with donor tissue from eyes with primary choroidal melanomas. A retrospective cohort comparison. *Archives of ophthalmology* 1995;113:753-756.
52. Dong L, Jensen R, De Rienzo A, et al. Differentially expressed alternatively spliced genes in Malignant Pleural Mesothelioma identified using massively parallel transcriptome sequencing. *BMC medical genetics* 2009;10:149.

53. Gillett A, Maratou K. Alternative splicing and transcriptome profiling of experimental autoimmune encephalomyelitis using genome-wide exon arrays. *PloS one* 2009;4:e7773.
54. De Paiva CS, Pangelinan SB, Chang E, et al. Essential role for c-Jun N-terminal kinase 2 in corneal epithelial response to desiccating stress. *Archives of ophthalmology* 2009;127:1625-1631.
55. Eferl R, Wagner EF. AP-1: a double-edged sword in tumorigenesis. *Nature reviews Cancer* 2003;3:859-868.
56. Arnold I, Watt FM. c-Myc activation in transgenic mouse epidermis results in mobilization of stem cells and differentiation of their progeny. *Current biology : CB* 2001;11:558-568.
57. Kenney MC, Chwa M, Atilano SR, et al. Increased levels of catalase and cathepsin V/L2 but decreased TIMP-1 in keratoconus corneas: evidence that oxidative stress plays a role in this disorder. *Investigative ophthalmology & visual science* 2005;46:823-832.
58. Uçakhan OO, Kanpolat A, Ylmaz N, Ozkan M. In vivo confocal microscopy findings in keratoconus. *Eye & contact lens* 2006;32:183-191.
59. Huang DW, Sherman BT, Lempicki Ra. Systematic and integrative analysis of large gene lists using DAVID bioinformatics resources. *Nature protocols* 2009;4:44-57.
60. Kanehisa M, Goto S. KEGG: kyoto encyclopedia of genes and genomes. *Nucleic acids research* 2000;28:27-30.
61. Pico AR, Kelder T, van Iersel MP, Hanspers K, Conklin BR, Evelo C. WikiPathways: pathway editing for the people. *PLoS biology* 2008;6:e184.
62. Wilson SE, He YG, Weng J, et al. Epithelial injury induces keratocyte apoptosis: hypothesized role for the interleukin-1 system in the modulation of corneal tissue organization and wound healing. *Experimental eye research* 1996;62:325-327.
63. Wilson SE, Liu JJ, Mohan RR. Stromal-epithelial interactions in the cornea. *Progress in retinal and eye research* 1999;18:293-309.
64. Ali Javadi M, Kanavi MR, Mahdavi M, et al. Comparison of keratocyte density between keratoconus, post-laser in situ keratomileusis keratectasia, and uncomplicated post-laser in situ keratomileusis cases. A confocal scan study. *Cornea* 2009;28:774-779.
65. Kaldawy RM, Wagner J, Ching S, Seigel GM. Evidence of apoptotic cell death in keratoconus. *Cornea* 2002;21:206-209.
66. Kim WJ, Rabinowitz YS, Meisler DM, Wilson SE. Keratocyte apoptosis associated with keratoconus. *Experimental eye research* 1999;69:475-481.
67. Matthews FJ, Cook SD, Majid MA, Dick AD, Smith VA. Changes in the balance of the tissue inhibitor of matrix metalloproteinases (TIMPs)-1 and -3 may promote keratocyte apoptosis in keratoconus. *Experimental eye research* 2007;84:1125-1134.
68. Nielsen K, Vorum H, Fagerholm P, et al. Proteome profiling of corneal epithelium and identification of marker proteins for keratoconus, a pilot study. *Experimental eye research* 2006;82:201-209.
69. Chwa M, Atilano S, Hertzog D, et al. Hypersensitive response to oxidative stress in keratoconus corneal fibroblasts. *Investigative ophthalmology & visual science* 2008;49:4361-4369.
70. Zhou L, Yue BY, Twining SS, Sugar J, Feder RS. Expression of wound healing and stress-related proteins in keratoconus corneas. *Current eye research* 1996;15:1124-1131.

71. Le Lièvre CS, Le Douarin NM. Mesenchymal derivatives of the neural crest: analysis of chimaeric quail and chick embryos. *Journal of embryology and experimental morphology* 1975;34:125-154.
72. West-Mays JA, Dwivedi DJ. The keratocyte: corneal stromal cell with variable repair phenotypes. *The international journal of biochemistry & cell biology* 2006;38:1625-1631.
73. Newsome DA, Foidart JM, Hassell JR, Krachmer JH, Rodrigues MM, Katz SI. Detection of specific collagen types in normal and keratoconus corneas. *Investigative ophthalmology & visual science* 1981;20:738-750.
74. Weaving L, Mihelec M, Storen R, et al. Twist2: role in corneal stromal keratocyte proliferation and corneal thickness. *Investigative ophthalmology & visual science* 51:5561-5570.
75. Coulombe PA, Omary MB. 'Hard' and 'soft' principles defining the structure, function and regulation of keratin intermediate filaments. *Current opinion in cell biology* 2002;14:110-122.
76. Willert K, Brown JD, Danenberg E, et al. Wnt proteins are lipid-modified and can act as stem cell growth factors. *Nature* 2003;423:448-452.
77. Breen EC, Tang K. Calcyclin (S100A6) regulates pulmonary fibroblast proliferation, morphology, and cytoskeletal organization in vitro. *Journal of cellular biochemistry* 2003;88:848-854.
78. Carraway K, Ramsauer V, Haq B. Cell signaling through membrane mucins. *Bioessays* 2002;25:66-71.
79. Pauklin M, Kakkassery V, Steuhl K-P, Meller D. Expression of membrane-associated mucins in limbal stem cell deficiency and after transplantation of cultivated limbal epithelium. *Current eye research* 2009;34:221-230.
80. Bazan HE, Allan G, Bazan NG. Enhanced expression of the growth-regulated calcyclin gene during corneal wound healing. *Experimental eye research* 1992;55:173-177.
81. Pflugfelder SC, Liu Z, Monroy D, et al. Detection of sialomucin complex (MUC4) in human ocular surface epithelium and tear fluid. *Investigative ophthalmology & visual science* 2000;41:1316-1326.
82. Paulsen F, Langer G, Hoffmann W, Berry M. Human lacrimal gland mucins. *Cell and tissue research* 2004;316:167-177.
83. Bisceglia L, De Bonis P, Pizzicoli C, et al. Linkage analysis in keratoconus: replication of locus 5q21.2 and identification of other suggestive Loci. *Investigative ophthalmology & visual science* 2009;50:1081-1086.

Down-regulation of Wnt/β-catenin signalling by Edar involves Hipk2, a new NF-κB target gene

Céline Cluzeau[1,§], Chunyan Mou[2], Elodie Bal[1], Sabina Benko[1], Candice Babarit[1], Paul A Overbeek[3], Christine Perret[4], Sylvie Mémet[5,6], Gilles Courtois[1], Stanislas Lyonnet[1], Heather Etchevers[1], Marja L. Mikkola[7], Arnold Munnich[1], Denis J. Headon[2] and Asma Smahi[1,*]

1. Université Paris Descartes, and INSERM U781, Hôpital Necker-Enfants Malades, Paris 75015, France.
2. The Roslin Institute and Royal (Dick) School of Veterinary Studies, University of Edinburgh, Easter Bush, Midlothian, EH25 9RG, United Kingdom.
3. Department of Molecular and Cellular Biology, Baylor College of Medicine, Houston, TX 77030, USA.
4. Unité INSERM U567, Hôpital Cochin, Paris 75014, France.
5. Institut Pasteur, Unité de Mycologie Moléculaire, Paris 75015, France
6. URA CNRS 3012, Paris 75015, France
7. Developmental Biology Program, Institute of Biotechnology, University of Helsinki, Helsinki, Finland

§Current address: Program in Developmental Endocrinology and Genetics, Eunice Kennedy Shriver National Institute of Child Health and Human Development, National Institutes of Health, Department of Health and Human Services, Bethesda, MD 20892, USA.

*Correspondence: asma.smahi@inserm.fr, denis.headon@roslin.ed.ac.uk
INSERM U781 – Tour Lavoisier 2e étage
Hôpital Necker-Enfants Malades
149 rue de Sèvres 75015 PARIS
Phone number: (+33) 1 44 49 40 00 exp 97816
Fax number: (+33) 1 44 49 51 50

Abstract

The ectodysplasin/NF-κB and Wnt/β-catenin signalling pathways are central to the development of skin appendages. Reduced function of either of these pathways results in anhidrotic/hypohidrotic ectodermal dysplasia (HED). The interaction between these two pathways, and which factors mediate their crosstalk are poorly understood. We report that the ectodysplasin receptor (Edar) inhibits the Wnt/β-catenin pathway in an NF-κB dependent manner. The Edar-mediated negative regulation of the Wnt/β-catenin pathway did not occur *via* canonical mechanisms of β-catenin regulation, but instead involved the homeodomain-interacting protein kinase 2 (HIPK2). We show here that Edar regulates HIPK2 at two distinct levels: i) through post-translational stimulation of complex formation, between existing HIPK2 and β-catenin and ii) via transcription of *HIPK2*, an NF-κB target gene. The pattern of *HIPK2* expression overlaps that of EDAR pathway components, supporting the idea that Edar/NF-κB and HIPK2 function in concert to modulate β–catenin action in developing skin appendages.

Introduction

Ectodermal appendages (EA), including hair follicles, teeth and sweat glands, form during early skin development from ectodermal placodes, through complex reciprocal and sequential signalling interactions between the ectoderm and the underlying mesoderm (1, 2). A wide range of intercellular signalling pathways are involved in their formation including members of the Wnt, fibroblast growth factor family, transforming growth factor β (TGFβ), hedgehog, Tumor Necrosis Factor (TNF) families and their downstream target genes (3). A conserved set of signals normally control early stages of hair follicle, tooth and glandular development and also account for a common pattern of phenotypic anomalies when these signals are abrogated by germ-line mutations in human and mouse.

Anhidrotic/hypohidrotic ectodermal dysplasia (HED) is characterized by developmental defects at the level of placode initiation (4, 5). HED results from mutations in any of the three genes controlling the EDA signalling pathway, namely ectodysplasin (EDA), its receptor (EDAR) and an EDAR-associated death domain adapter protein (EDARADD) (6-8). EDAR, a TNF receptor family member, is activated by ectodysplasin and employs EDARADD as an adapter to activate the NF-κB signalling pathway (9). Mouse phenotypes arising from abrogation of this pathway (*tabby*, *downless*, *crinkled*) are indistinguishable, and share common features, namely misshapen or absent teeth and hair, and absence of sweat glands (10-12).

Ectodysplasin, the ligand of EDAR, controls several steps of EA formation, principally through activation of the transcription factor NF-κB (5). In the absence of ectodysplasin/NF-κB signalling, only unstable pre-placodes form, while overexpression of ectodysplasin increases the size of placodes and gives rise to supernumerary tooth and mammary placodes (13-15). Edar signalling is also involved in maintaining the growth phase of the hair cycle and in the hair shaft structure (16, 17). The genetic variant V370A in the *EDAR* gene is associated with increased hair thickness in East Asian human populations, which apparently results from enhanced EDAR/NF-κB signalling (18, 19).

In contrast to the tissue-restricted role of EDAR signalling, the canonical Wnt/β-catenin signalling pathway, which activates transcription factors of the Lymphoid enhancer factor/T-Cell Factor family (Lef-TCF), plays an essential role in the development of many organ systems and is indispensable for EA formation (20-22). In hair follicles, Wnt ligands are required during all phases of development, from initiation, placode formation and mesenchyme condensation, to hair shaft differentiation and hair cycling (21, 23-25). β-catenin is also essential for lineage determination by adult skin stem cells, promoting a follicular, rather than epidermal keratinocyte fate (26). Wnt/β–catenin signalling is both necessary and sufficient for assumption of a hair

follicle fate in developing epidermis, with widespread forced activation of β–catenin causing ubiquitous adoption of a hair placode fate in embryonic ectoderm (21, 22, 27, 28). However, this widespread adoption of hair follicle fate is accompanied by a complete failure of placode morphogenesis, such that no hair follicle is actually constructed under conditions of ubiquitous epidermal β-catenin activity (27, 28). These findings emphasise that appropriate spatially and temporally controlled Wnt/β–catenin activity is a prerequisite for appropriate hair follicle formation, involving positive and negative control over this central regulator. It appears likely that fine tuning of Wnt/β–catenin activity is achieved, at least in part, through crosstalk with the other key pathways involved in EA development, such as the EDAR pathway. It has been demonstrated that the canonical Wnt pathway inhibitor Dkk4, and the Wnt ligand Wnt10b, are direct transcriptional targets of Edar signalling, and both of these transcripts display prominent expression in embryonic hair placodes, consistent with a functional role in hair follicle development (22, 29).

Despite the elucidation of these connections between Edar activity and upstream components of the Wnt/β-catenin pathway, full knowledge of the relationships between these pathways, and the probable multiple points of contact between them, remains incomplete.

In this work, we have explored the crosstalk between Edar/NF-κB and Wnt/β-catenin signalling both *in vitro* and *in vivo* during skin appendage development. We show that the homeodomain-interacting protein kinase type 2 (HIPK2) acts as an intermediate between the Edar and Wnt/β-catenin signalling pathways at both the transcriptional and post-translational level. These findings shed light on the interplay between the widely employed β-catenin pathway and the tissue-specific Edar signalling pathway, which together direct the development of skin appendages.

Results

Edar inhibits Wnt/β-catenin signalling

To study the effects of Edar signalling on β–catenin activity, we used transient transfection assays in immortalized cell lines. Edar and EDARADD are known to promote signalling in a ligand-independent manner upon overexpression, probably via a multimerisation that allows the recruitment of downstream proteins required for signal propagation. To investigate whether Edar influences Wnt/β-catenin transcriptional activity, we studied the transcriptional regulatory activity of an activated form of β-catenin (carrying the S45Y mutation which impairs β-catenin phosphorylation and degradation) in HEK293 cells (30, 31). As expected, β-catenin S45Y led to a high activation of Lef-TCF reporter activity in transfected cells, but this effect was strongly

inhibited by co-transfection of Edar or EDARADD (Figure 1A). When a reporter plasmid with mutated Lef-TCF binding sites was used, no activation or inhibition was observed, demonstrating the specific inhibition of Lef-TCF transcriptional activity by Edar (data not shown).

β-catenin signalling is initiated by the binding of Wnt ligands to their cognate receptors of the frizzled (Fz) family, using Lipoprotein Receptor-related Protein (LRP) membrane-bound co-receptors. In order to exclude potential artifacts arising from the constitutive activation of β-catenin, we established conditions in which the β-catenin pathway was activated by signal transduction initiated by a Wnt ligand-receptor complex at the plasma membrane. For this, we used a plasmid encoding a previously characterized Wnt-Frizzled fusion protein (Wnt8-Fz5), known to activate the Wnt/β-catenin pathway (32). In agreement with our previous results, expression of Wnt8-Fz5 resulted in the transactivation of the Lef-TCF luciferase reporter in HEK293T cells and this activation was strongly inhibited upon co-transfection of Edar (Figure 1A).

In order to confirm the inhibition of the Wnt/β-catenin pathway by Edar stimulation, we used SW480 and HepG2 cells, two cancer-derived cell lines in which Wnt signalling is constitutively active due to mutations affecting proteins acting at distinct levels in the Wnt/β–catenin pathway. SW480 cells are human colorectal cancer-derived cells carrying a mutation in the APC protein. HepG2 is a human liver cancer-derived strain carrying an activating mutation in β-catenin itself (33, 34). Consistently, transfection of Edar and EDARADD strongly inhibited the endogenous Lef-TCF activity in both cell lines (Figure 1A). These results show that Edar signalling significantly inhibits the Wnt/β-catenin pathway and suggest, based on the suppression of β-catenin activity in the HepG2 line, that this inhibition operates far downstream in the Wnt/β-catenin pathway.

Edar inhibits Wnt/β-catenin signalling *via* NF-κB activation

Edar is known to induce NF-κB activity, *via* activation of Edaradd, Traf6, Tab2, Tak1 and Nemo, thereby altering gene expression in receiving cells (5, 35, 36). Yet, activation of other pathways, such as c-Jun-N-terminal kinase (JNK) signalling, may also occur (9). To determine at which level of Edar signalling the interaction with the Wnt/β–catenin pathway occurs, we used a dominant negative form of the NF-κB inhibitor Iκ-Bα (Iκ-Bα SS-AA) mutated on two critical serine residues (S32 and S36), the phosphorylation of which is required for Iκ-Bα degradation and subsequent NF-κB activation. We performed the transactivation experiments described above in the presence of Iκ-Bα SS-AA. Depending on the pathway analyzed, either an Igκ-luc (luciferase under control of NF-κB response elements) or a Topflash reporter plasmid were used (luciferase under the control of a Lef-TCF responsive promoter). In both HEK293T and SW480

cells, transfection of Iκ-Bα SS-AA inhibited Edar-mediated NF-κB activation (Figure 1B). SW480 cells display a basal NF-κB activity, and this activity was also abolished by expression of Iκ-Bα SS-AA. The effect of the dominant negative form of Iκ-Bα on the Wnt/β-catenin pathway was then assessed. Under these conditions, Edar was no longer able to inhibit the Wnt/β-catenin pathway in the presence of Iκ-Bα SS-AA in either cell type (Figure 1C). Hence, the ability of Edar to inhibit Wnt/β-catenin signalling is dependent on the nuclear localization of NF-κB. The same results were obtained in experiments performed using HepG2 cells (data not shown).

Pathological *EDAR* mutations co-ordinately impair NF-κB activation and Wnt/β-catenin inhibition

We studied the effects of four dominant (p.R358X, p.I418T, p.L377F and p.T413P) and three recessive *EDAR* mutations (p.T403M, p.R375H and p.W434C) identified in HED families on activation of the NF-κB pathway in HEK293T cells (37). We found that the effects on NF-κB activation depended on the nature of the specific *EDAR* mutation. Dominant mutations severely affected NF-κB activation while recessive ones produced a milder effect (Figure 1D). These *EDAR* mutants were then used to quantify Wnt/β-catenin inhibition with respect to NF-κB activity. A marked inverse trend between EDAR driven NF-κB activation and Wnt/β-catenin inhibition was observed (Figure 1D and 1E), with dominant *EDAR* mutations displaying a weaker effect on suppression of Wnt/β-catenin activity than recessive mutations.

Edar-mediated Wnt/β-catenin/Lef-TCF pathway inhibition does not alter β-catenin level or subcellular distribution

The canonical Wnt/β–catenin pathway relies on precise regulation of the degradation and subcellular localization of β–catenin (20). In order to investigate the mechanism of Edar-driven repression of β-catenin activity, we assessed Edar effects on β–catenin protein levels and subcellular localization. We found that the level of total β-catenin S45Y protein was not altered following Edar transfection (Figure 2A). In addition, β-catenin S45Y was found in nuclear extracts from cells transfected with Edar (Figure 2B). Finally, β-catenin S45Y was immunocytochemically detected in the nucleus both in the absence and in the presence of active Edar signalling (Figure 2C). Taken together, these results demonstrate that Edar inhibits the Wnt/β-catenin/Lef-TCF pathway without altering the total amount or the subcellular location of β-catenin.

Edar signalling does not disrupt the interaction between β-catenin and TCF4

TCF4 and β-catenin are known to interact physically and the integrity of this complex is required for its action as a transcriptional regulator (38). Since Edar-mediated Wnt/β-catenin inhibition

does not alter the bulk amount or subcellular location of β-catenin, we hypothesized that Edar signalling could disrupt the interaction between β-catenin and the transcription factor TCF4. We transfected TCF4 into HEK293T cells, as no endogenous TCF4 was detected in this cell line, and found that the β-catenin/TCF4 interaction was not diminished upon overexpression of Edar (Figure 2D). We also tested the possibility of an interaction between NF-κB subunits (p50 and p65) and the β-catenin/TCF4 complex, but did not detect an interaction between these proteins (data not shown).

HIPK2 is involved in Edar-mediated inhibition of the Wnt/β-catenin pathway

We next hypothesized that the inhibition of Wnt/β-catenin signalling by Edar could be mediated by a co-repressor protein *via* a direct interaction with β-catenin/Lef-TCF complexes in the nucleus. We considered HIPK2 as a candidate molecule for mediating this crosstalk. HIPK2 is a member of a conserved family of serine/threonine kinases with a wide range of functions including apoptosis, cell growth and proliferation (39). It can interact with several proteins containing the high-mobility group I (HMG1) domain, which is highly conserved in Lef-TCF transcription factors. HIPK2 has been previously shown to be highly expressed in adult hair follicles and to inhibit the Wnt/β-catenin pathway by interacting with the β-catenin/Lef-TCF complex (40). We assessed the ability of HIPK2 to form a complex with β-catenin either in the presence or in the absence of Edar signalling. A weak interaction between endogenous HIPK2 and β-catenin was observed when both TCF4 and β-catenin S45Y were cotransfected in HEK293T cells (Figure 3A). Interestingly, recruitment of HIPK2 to the β-catenin complex was strongly enhanced upon Edar transfection, the condition in which Wnt/β-catenin activity is down-regulated. These results were confirmed in SW480 cells on endogenous HIPK2-β-catenin complexes when Edar and EDARADD were cotransfected (Figure 3B). Thus, β-catenin and HIPK2 proteins are present in the same protein complex and their association is increased by Edar signalling.

HIPK2 is necessary for Edar-mediated inhibition of Wnt/β-catenin signalling

In order to determine whether HIPK2 is functionally required for Edar-driven inhibition of Wnt/β-catenin signalling, we knocked down *HIPK2* transcript levels by expression of a short hairpin RNA (shRNA) targeted against *HIPK2*. Three stable SW480 cells clones were generated with different levels of *HIPK2* repression quantified by qRT-PCR (Figure 4A). We then demonstrated that Edar-mediated Wnt/β-catenin inhibition was lost, albeit incompletely, upon *HIPK2* down-regulation (Figure 4B). We confirmed that, under these conditions, the expression of Edar itself was unaltered (data not shown). These findings demonstrate a functional contribution of *HIPK2* to Edar-mediated inhibition of Wnt/β-catenin signalling.

HIPK2 is expressed during placode formation and is regulated by EDAR signalling

Having determined that Edar stimulates HIPK2-β–catenin association, and that HIPK2 contributes to EDAR-β–catenin cross talk, we compared the expression pattern of these factors to question their possible interaction in developing skin *in vivo*.

We performed whole mount *in situ* hybridization on developing mouse skin, and found that *Hipk2* is widely expressed in the skin and is upregulated in the primary hair follicle placodes at embryonic days 14 and 15 (E14-E15) (Figure 5A, C, E). This expression pattern matches that of *Edaradd* (Figure 5I, K, M). Sectioning of these embryos revealed prominent expression of *Hipk2* in the epidermis (Figure 5G, H), the tissue layer in which Edar/Edaradd signalling is active (8, 41).

Interestingly, and in contrast to wild-type mice, *Hipk2* was not focally expressed in Eda^{Ta} *(tabby)* mutant embryos, which carry a loss-of-function mutation in the ectodysplasin gene (Figure 5B, D, F, H), while widespread expression throughout the epidermis was evident. This absence of focal *Hipk2* expression in the *Eda* mutant mirrors the absence of focal expression of Eda pathway components in this line (Figure 5J, L, N).

Hipk2 expression and β-catenin transcriptional activity occur in non-overlapping follicular domains

To determine whether Hipk2 could inhibit β-catenin activity in developing skin and EA placodes, we compared the spatio-temporal pattern of Hipk2 and β–catenin expression in developing mouse skin. We used various transgenic mouse strains expressing the β-galactosidase gene under the control of Lef-TCF responsive elements, namely the TOPgal, BATgal and Axin2-lacZ mouse models (25) (42) (43). All three lines displayed β–catenin activity at the hair placodes, though the BATgal and Axin2-lacZ lines had a broader spectrum of expression (Figure 6A-C). The TOPgal line displayed β-catenin activity in hair placodes, but in a much more restricted domain that the other two strains (Figure 6D). Sectioning showed β– galactosidase expression in the dermal compartment of the placode of BATgal and Axin2-lacZ strains, while it was exclusively epidermal in TOPgal strains. Hipk2 was expressed in the epidermis, particularly in the epithelial component of incipient hair follicles. Thus Hipk2 expression was detected in the tissue compartment which displays restricted β–catenin activity. These results are consistent with a role of Hipk2 in restraining and shaping epidermal β-catenin activity in the skin.

NF-κB regulates *HIPK2* expression

As Edar and Hipk2 are co-expressed in embryonic/foetal skin, we hypothesized that Edar signalling could transcriptionally regulate the expression of *HIPK2*. We screened the entire

HIPK2 gene for the presence of putative NF-κB responsive elements and evolutionary conserved sites by computational analysis using mouse and human sequences (PreMod, ConSite, and rVISTA programs). The canonical NF-κB DNA binding sequence is a 10-bp consensus DNA element that has been identified as the following : 5'-GGGRNNYYCC-3' (44). We found five distinct putative NF-κB binding sites in *HIPK2* introns and decided to analyze three of them based on their conservation scores (named sites 1, 2 and 3; Figure 7A).

Electrophoretic Mobility Shift Assay (EMSA) was used to validate these predicted NF-κB binding sites. To obtain maximal activation of NF-κB, we co-transfected plasmids encoding the NF-κB subunits p65 and p50 into HEK293T cells. We detected a DNA-protein complex between nuclear extracts and each of the three probes (Figure 7B), the specificity of which was confirmed by a competition assay. Binding specificity was further confirmed when the NF-κB binding sequences of *HIPK2* were mutated to alter the NF-κB consensus sequence. Super shift experiments indicated that the two complexes containing p65/p50 heterodimers and p50/p50 homodimers (the most intense shift) are most likely involved in these interactions.

To further test the hypothesis that NF-κB factors bind the putative NF-κB recognition sequences identified in the *HIPK2* gene, we used a chromatin immunoprecipitation assay (ChIP) to precipitate the NF-κB-DNA complexes from Edar transfected-HEK293T cells with anti-p65 and anti-p50 antibodies. The *NFKBIA* (encoding IκBα) promoter, a well-known NF-κB target gene was used as a positive control (Figure 7C). Interestingly, the fragments containing sites 1 and 3 were amplified following p65 or p50 immunoprecipitation, while no interaction with fragment 2 was detected, suggesting that sites 1 and 3 are recognition sites for Edar-stimulated NF-κB.

To test the regulatory function of the NF-κB binding sequences in the *HIPK2* gene, we constructed a luciferase reporter gene driven by tandem copies of sites 1, 2 or 3 upstream of the *Firefly* luciferase gene. Constructs containing site 1 induced a significant transcriptional response after Edar transfection in HEK293T cells (Figure 7D). The specificity of activation was confirmed by mutating the NF-κB consensus sequences, or by transfecting cells with the Iκ-Bα SS-AA encoding vector. No activation was detected for sites 2 and 3. Based on ChIP results (Figure 7C), site 3 could also be functional *in vivo*, in its native chromatin configuration.

To confirm the *in vivo* relevance of this regulation, we determined whether stimulation of Edar signalling in explant cultured skin would lead to upregulated *Hipk2* expression. We stimulated Edar signalling in embryonic Eda^{Ta} skin using recombinant ectodysplasin A1 and analysed *Hipk2* expression by quantitative RT-PCR. We found that *Hipk2* expression was activated within 10 hours of ectodysplasin treatment (Figure 7E). Ectodysplasin caused a mild yet reproducible change in total *Hipk2* levels in the developing skin. This modest increase in bulk transcript level

is likely due to the widespread expression of *Hipk2* observed in the absence of Edar signalling (Figure 5 J, L). The formation of hair follicle placodes primarily involves the focalization of gene expression in the skin with little change in total transcript levels across the entire skin, limiting the fold-changes in gene expression that can be achieved with ectodysplasin supplementation (13). Thus *Hipk2* expression is stimulated by the Edar pathway, consistent with its regulation by the Edar/NF-κB axis *in vivo*.

Discussion

We show here that Edar/NF-κB signalling inhibited the Wnt/β-catenin pathway through a non-classical mechanism. Our results demonstrate the involvement of Hipk2 in Edar-mediated Wnt/β-catenin inhibition, *via i*) up-regulation of *Hipk2* expression, and *ii*) enhanced interaction of Hipk2 with nuclear β-catenin. This crosstalk between Edar/NF-κB and Wnt/β-catenin signalling pathways is likely to influence skin appendage development *in vivo.*

Both Edar/NF-κB and Wnt/β-catenin signalling are known to be positive regulators of skin appendage formation and play central roles during several stages of hair morphogenesis (3). Thus it is paradoxical to find negative crosstalk between these two pathways. However, controlled down-regulation of Wnt/β-catenin signalling in the epidermis has recently been suggested to be required for normal placode patterning, hair follicle down-growth and adoption of the full range of follicular fates (27, 28). Accordingly, loss-of-function mutations in the *APCDD1* gene, encoding an inhibitor of Wnt/β-catenin signalling, has been recently associated with hereditary hypotrichosis simplex disease, characterised by abrogation of hair follicle formation (45).

We have demonstrated that down-regulation of Wnt/β-catenin signalling is mediated in part by the activation of Edar/NF-κB signalling pathway using *HIPK2*, which we identified as a new NF-κB target gene. Our findings are consistent with Schmidt-Ullrich et al who demonstrated that epidermal NF-κB activation is essential for placode down-growth (14). The complexity of β-catenin function *in vivo* is illustrated by the X-gal staining pattern obtained for the three different reporter lines TOPgal, BATgal, Axin2-lacZ. These reporter lines show that β-catenin transcriptional activity is widespread in the dermis. However, the TOPgal line shows a highly restricted activity of β-catenin in the epidermis, the tissue compartment in which the Edar pathway operates and in which we showed that *Hipk2* is expressed. The TOPgal line is most similar to our *in vitro* cellular model as the Topflash-luciferase reporter used in cell transfection and the TOPgal transgene in mice are driven by the same promoter.

Several points of crosstalk between the Eda and Wnt/β-catenin pathways have been previously described, but all involve mechanisms clearly distinct from those that we report here. Edar-mediated inhibition of Wnt/β-catenin signalling was reported by Shindo and Chaudhary to occur independently of NF-κB (46). More recently, a series of links between Edar and β-catenin have been inferred based on the identification of new Edar target genes. *Dickkopf4* (Dkk4), an inhibitor of Wnt ligand reception, as well as the Wnt family member *Wnt10b* were shown to be Edar-inducible NF-κB target genes (22, 29). Thus, Edar is able to induce expression of both activatory and inhibitory components of Wnt/β-catenin signalling, but the actual impact of these opposing signals on β-catenin activity was hitherto unknown. As both Wnt10b and Dkk4 are secreted factors, they likely impact on β-catenin activity at a distance from their site of synthesis. However, Hipk2 is a non-secreted protein that acts far downstream in the signalling pathway, by interacting with β-catenin itself, and probably functions in a cell-autonomous manner. Thus we predict that Hipk2-mediated suppression of β-catenin transcriptional activity occurs in cells which actively undergo Edar/NF-κB signalling, while secretion of Dkk4 and Wnt10b factors from these cells modulates β-catenin activity in nearby cells.

The incomplete loss of Edar-β-catenin crosstalk we observed in *HIPK2* knockdown cells could arise from the incomplete inhibition of *HIPK2* expression by the shRNA we used, or alternatively could be a result of the action of HIPK2-independent points (or components) of pathway crosstalk.

HIPK2 is emerging as a regulator of cell growth and apoptosis in various cell types. Growth-suppressor and growth-promoting functions of HIPK2 probably depend on the cell and tissue context. For example, HIPK2 was found to be down-regulated in thyroid and breast carcinoma and to be over expressed in certain brain tumors (pilocytic astrocytomas; (47). Wei et al demonstrated that Hipk2 represses β-catenin-mediated transcription in mouse skin while Lee et al demonstrated an opposite function of Hipk2 in Drosophila as a promoter of Wnt/β-catenin signalling (40, 48). Wei et al have demonstrated that loss of Hipk2 leads to susceptibility to squamous cell carcinoma development (40). Considering on the one hand, the tumor suppressor functions of HIPK2, and on the other hand Wnt/β-catenin upregulation in many skin tumors (49), we believe that HIPK2 should be regarded as an important pathogenic interactor in basal and squamous cell carcinomas, as well as in skin appendage-derived tumors.

Materials and methods

Antibodies

Antibodies used in our experiments were: anti-HA (Santa Cruz, F-7), anti-myc (Neomarkers, 9E10.3), anti-β-catenin (BD Pharmingen, clone 14), anti-TCF4 (Cell Signalling, C9B9), anti-Hipk2 (Abnova, M03), anti-Edar (Abnova, M01), anti-p50, (Upstate, 06-886), anti-p65 (Santa Cruz, A), anti-β-galactosidase (eBiosciences); anti-mouse and anti-rabbit HRP-conjugated antibodies (GE Healthcare); Alexa Fluor 488 labelled secondary antibody (Molecular Probes).

Cell lines and plasmids

HEK293T, SW480 and HepG2 cell lines were grown in DMEM supplemented with 10% foetal bovine serum (Invitrogen). Constructs encoding HA-Edar, Myc-EDARADD were described in Bal et al., 2007 (50). Dominant negative form of Iκ-Bα (Iκ-Bα SS-AA) has two alanines instead of the two serines 32 and 36, and cannot be phosphorylated and degraded by the proteasome machinery. Mutations were introduced into a HA-Edar plasmid by site-directed mutagenesis using the Quick change XL kit (Stratagene). Topflash and Fopflash reporter plasmids, as well as Myc-β-catenin S45Y and Myc-TCF4 were obtained from Dr Christine Perret. Wnt8-Fz5 fusion plasmid was obtained from Dr Bart Williams. Reporter plasmids (pIgk-luc, pRenilla, Topflash, Fopflash) were described elsewhere (50, 51).

Transfection

Transient transfections of HEK293T cells were performed with standard calcium phosphate procedure. Transient transfection of SW480 and HepG2 cells were performed using Fugene HD reagent (Roche).

Luciferase reporter assays

HEK293T, SW480 and HepG2 cells were transfected in triplicate in a 24-well plate with 200 ng of *Firefly* luciferase reporter vectors (pIgk-luc, Topflash or Fopflash), 50 ng of pRenilla plasmid and 250 ng of other plasmids as indicated. The total amount of transfected DNA was kept constant by adding pcDNA3.1 empty vector. Twenty-four hours later, cells were lysed and measurement of luciferase activities was conducted with Dual Luciferase Reporter System (Promega).

Luciferase reporter plasmids containing *HIPK2* sequences (wild-type and mutated) were constructed using complementary short oligonucleotides encompassing the NF-κB binding sequences, cloned in tandem repeats upstream to the *Firefly* luciferase encoding gene into pGL2 vector (Promega) by XhoI digestion.

Immunoblotting analysis

Cells were lysed with total lysis buffer EBC (50 mM Tris–HCl pH 8, 170 mM NaCl, 0.5% NP-40, 50 mM NaF) containing the Complete protease inhibitor cocktail (Roche), or with buffers A and C, to obtain cytoplasmic and nuclear extracts (buffer A: 10mM Hepes pH7.8, 10mM KCl,

2mM $MgCl_2$, 0,1 mM EDTA, 1mM DTT; buffer C: 50mM Hepes pH7.8, 50mM KCl, 350mM NaCl, 0,1mM EDTA, 1mM DTT, 10% glycerol). Immunoblotting was performed classically.

Immunoprecipitation

After preclearing for 1 h with 30 µl of a slurry of protein A– or protein G–Sepharose (Sigma), 200 µg of total lysates were incubated overnight at 4°C with antibodies and then incubated for 1 h with 30 µl of a slurry of protein A– or protein G–Sepharose. Beads were washed three times in EBC and resuspended in 30 µl of Laemmli buffer (Sigma) for immunoblotting analysis.

Immunohistochemistry

Following X-gal staining and fixation, mouse embryos were processed, embedded in wax, and 8 µm sections were cut. Slides were dewaxed, rehydrated, H_2O_2 treated and antigen retrieval was performed by boiling in 10 mM citrate buffer (pH6) for 10 minutes. Sections were blocked using the M.O.M. kit (Vector laboratories), then stained with 1 µg/ml mouse anti-Hipk2 monoclonal antibody (Abnova, clone 1F10) overnight at 4°C. Primary antibody was detected using M.O.M. biotinylated anti-mouse IgG (Vector laboratories) followed by the ABC peroxidase kit (Pierce) and then diamino-benzidine (DAB, Sigma).

Immunocytochemistry was performed on HEK293T cells seeded in labtek (Nalge Nunc International). Cells were fixed with PFA 4% and permeabilized with PBS/Triton 0,1%. After hybridization, nuclei were stained using propidium iodure and sections were mounted in Vectashield (AbCys). Acquisition was performed with a motorized confocal microscope system (Zeiss LSM5 Pascal) equipped with lasers Argon (488nm) and Helium Neon (543nm), and the LSM Pascal software (Zeiss).

Electromobility Shift Assay

For EMSA, probes were labeled with biotin using Biotin 3' End DNA Labelling Kit (Pierce). Samples were prepared using Light Shift Chemiluminescent EMSA Kit (Pierce): 20 µg of nuclear extracts from HEK293T cells transfected with p50 and p65-encoding plasmids were used for each reaction. 1µL of glycerol 50% and 1 µL of NP-40 1% were added to the binding reaction recommended by the manufacturer. Competition and supershift experiments were performed with pre-incubation with either 4 pmol of unlabeled probe, or 1 µg of antibody for 15 minutes. Sequences of the probes are available upon request.

Chromatin immunoprecipitation(ChIP)

ChIP was performed using EZ Chip kit (Millipore), according to the manufacturer's recommendations. DNA from HEK293T cells transfected with HA-Edar-encoding plasmid was

sonicated for 20 cycles and 10 µg was used for each immunoprecipitation. Primers used to amplify purified DNA are available upon request.

In situ hybridization

Embryos were fixed overnight in 4% paraformaldehyde in PBS at 4°C. Samples were dehydrated in methanol, bleached using H_2O_2, rehydrated, treated with 10 µg/mL protease K, post-fixed and hybridized overnight at 65°C. After washing, embryos were blocked, incubated in 1/2000 alkaline-phosphatase conjugated anti-digoxigenin (Roche) overnight, washed and hybridization signal detected using BCIP/NBT.

Explant culture

Dorsolateral skins from E14 embryos from an $Eda^{Ta/Y}$ X $Eda^{Ta/Ta}$ cross were dissected and cultured on an MF-millipore filter on a metal grid submerged in DMEM plus 2% FBS in a centre well dish (Falcon) at 37°C and 5% CO_2. Experimental samples were treated with 1 µg/mL recombinant Fc-EDA-A1 (52) for 10 hours and then experimental and control samples were homogenised in TRI reagent (Sigma) to isolate total RNA. RNA was reverse transcribed using random primers and AMV reverse transcriptase (Roche) in a 20 µl reaction. Reactions were diluted 10-fold and 5 µl were used as template for quantitative PCR. TaqMan probes were supplied by Applied Biosystems (*β-actin* probe: 4352341E; *Hipk2* probe: Mm00439329_m1). Twenty-microlitre reactions were performed in triplicate on an Opticon II thermal cycler. Relative amounts of *β-actin* and *Hipk2* transcripts were calculated from a cDNA standard curve.

shRNA experiments

To generate SW480 cell clones expressing a shRNA against HIPK2, we constructed a pCEP4 vector encoding the shRNA (pCEP4-shHIPK2) by inserting the shRNA-encoding element of the pSUPER-Hipk2 vector kindly provided by Dr CY Choi (53), after digestion of both plasmids with SalI and SacI enzymes. We then isolated clones from SW480 cells transfected with pCEP4-shHIPK2, after selection with 200 µg/mL hygromycin. The levels of *HIPK2* expression were assessed for each clone by qRT-PCR, using the SybrGreen System (Applied Biosystems), and *TBP* as control gene (primers sequences available upon request).

Acknowledgements

The authors declare no conflict of interest. We wish to thank Christelle Golzio and Sophie Thomas for technical advice. We thank Williams Bart for the gift of Wnt8-Fz5 plasmid, and CY Choi for the gift of the pSUPER plasmid encoding the shRNA against HIPK2. This work was supported by the Agence Nationale de la Recherche (ANR); Biotechnology and Biological

Sciences Research Council (BBSRC); and by a Fondation pour la Recherche Médicale PhD student grant to C.C.

References

1. Schneider, M.R., R. Schmidt-Ullrich, and R. Paus, ***The hair follicle as a dynamic miniorgan.*** Curr Biol, 2009. **19**(3): p. R132-42.
2. Millar, S.E., ***An ideal society? Neighbors of diverse origins interact to create and maintain complex mini-organs in the skin.*** PLoS Biol, 2005. **3**(11): p. e372.
3. Mikkola, M.L., ***Genetic basis of skin appendage development.*** Semin Cell Dev Biol, 2007. **18**(2): p. 225-36.
4. Lamartine, J., ***Towards a new classification of ectodermal dysplasias.*** Clin Exp Dermatol, 2003. **28**(4): p. 351-5.
5. Mikkola, M.L., ***TNF superfamily in skin appendage development.*** Cytokine Growth Factor Rev, 2008. **19**(3-4): p. 219-30.
6. Kere, J., et al., ***X-linked anhidrotic (hypohidrotic) ectodermal dysplasia is caused by mutation in a novel transmembrane protein.*** Nat Genet, 1996. **13**(4): p. 409-16.
7. Monreal, A.W., et al., ***Mutations in the human homologue of mouse dl cause autosomal recessive and dominant hypohidrotic ectodermal dysplasia.*** Nat Genet, 1999. **22**(4): p. 366-9.
8. Headon, D.J., et al., ***Gene defect in ectodermal dysplasia implicates a death domain adapter in development.*** Nature, 2001. **414**(6866): p. 913-6.
9. Kumar, A., et al., ***The ectodermal dysplasia receptor activates the nuclear factor-kappaB, JNK, and cell death pathways and binds to ectodysplasin A.*** J Biol Chem, 2001. **276**(4): p. 2668-77.
10. Gruneberg, H., ***Genes and genotypes affecting the teeth of the mouse.*** J Embryol Exp Morphol, 1965. **14**(2): p. 137-59.
11. Gruneberg, H., ***The tabby syndrome in the mouse.*** Proc R Soc Lond B Biol Sci, 1971. **179**(55): p. 139-56.
12. Gruneberg, H., ***The glandular aspects of the tabby syndrome in the mouse.*** J Embryol Exp Morphol, 1971. **25**(1): p. 1-19.
13. Mou, C., et al., ***Generation of the primary hair follicle pattern.*** Proc Natl Acad Sci U S A, 2006. **103**(24): p. 9075-80.
14. Schmidt-Ullrich, R., et al., ***NF-kappaB transmits Eda A1/EdaR signalling to activate Shh and cyclin D1 expression, and controls post-initiation hair placode down growth.*** Development, 2006. **133**(6): p. 1045-57.
15. Mustonen, T., et al., ***Stimulation of ectodermal organ development by Ectodysplasin-A1.*** Dev Biol, 2003. **259**(1): p. 123-36.
16. Fessing, M.Y., et al., ***Involvement of the Edar signaling in the control of hair follicle involution (catagen).*** Am J Pathol, 2006. **169**(6): p. 2075-84.
17. Hammerschmidt, B. and T. Schlake, ***Localization of Shh expression by Wnt and Eda affects axial polarity and shape of hairs.*** Dev Biol, 2007. **305**(1): p. 246-61.
18. Fujimoto, A., et al., ***A scan for genetic determinants of human hair morphology: EDAR is associated with Asian hair thickness.*** Hum Mol Genet, 2008. **17**(6): p. 835-43.
19. Mou, C., et al., ***Enhanced ectodysplasin-A receptor (EDAR) signaling alters multiple fiber characteristics to produce the East Asian hair form.*** Hum Mutat, 2008. **29**(12): p. 1405-11.
20. Clevers, H., ***Wnt/beta-catenin signaling in development and disease.*** Cell, 2006. **127**(3): p. 469-80.
21. Andl, T., et al., ***WNT signals are required for the initiation of hair follicle development.*** Dev Cell, 2002. **2**(5): p. 643-53.
22. Zhang, Y., et al., ***Reciprocal requirements for EDA/EDAR/NF-kappaB and Wnt/beta-catenin signaling pathways in hair follicle induction.*** Dev Cell, 2009. **17**(1): p. 49-61.

23. Gat, U., et al., ***De Novo hair follicle morphogenesis and hair tumors in mice expressing a truncated beta-catenin in skin.*** Cell, 1998. **95**(5): p. 605-14.
24. Millar, S.E., et al., ***WNT signaling in the control of hair growth and structure.*** Dev Biol, 1999. **207**(1): p. 133-49.
25. DasGupta, R. and E. Fuchs, ***Multiple roles for activated LEF/TCF transcription complexes during hair follicle development and differentiation.*** Development, 1999. **126**(20): p. 4557-68.
26. Huelsken, J., et al., ***beta-Catenin controls hair follicle morphogenesis and stem cell differentiation in the skin.*** Cell, 2001. **105**(4): p. 533-45.
27. Zhang, Y., et al., ***Activation of beta-catenin signaling programs embryonic epidermis to hair follicle fate.*** Development, 2008. **135**(12): p. 2161-72.
28. Narhi, K., et al., ***Sustained epithelial beta-catenin activity induces precocious hair development but disrupts hair follicle down-growth and hair shaft formation.*** Development, 2008. **135**(6): p. 1019-28.
29. Fliniaux, I., et al., ***Identification of dkk4 as a target of Eda-A1/Edar pathway reveals an unexpected role of ectodysplasin as inhibitor of Wnt signalling in ectodermal placodes.*** Dev Biol, 2008. **320**(1): p. 60-71.
30. Hagen, T., et al., ***Expression and characterization of GSK-3 mutants and their effect on beta-catenin phosphorylation in intact cells.*** J Biol Chem, 2002. **277**(26): p. 23330-5.
31. Hagen, T. and A. Vidal-Puig, ***Characterisation of the phosphorylation of beta-catenin at the GSK-3 priming site Ser45.*** Biochem Biophys Res Commun, 2002. **294**(2): p. 324-8.
32. Holmen, S.L., et al., ***A novel set of Wnt-Frizzled fusion proteins identifies receptor components that activate beta -catenin-dependent signaling.*** J Biol Chem, 2002. **277**(38): p. 34727-35.
33. Bhattacharya, G. and B.M. Boman, ***Phosphorylation of the adenomatous polyposis coli protein and its possible regulatory effects in cells.*** Biochem Biophys Res Commun, 1995. **208**(1): p. 103-10.
34. de La Coste, A., et al., ***Somatic mutations of the beta-catenin gene are frequent in mouse and human hepatocellular carcinomas.*** Proc Natl Acad Sci U S A, 1998. **95**(15): p. 8847-51.
35. Morlon, A., A. Munnich, and A. Smahi, ***TAB2, TRAF6 and TAK1 are involved in NF-kappaB activation induced by the TNF-receptor, Edar and its adaptator Edaradd.*** Hum Mol Genet, 2005. **14**(23): p. 3751-7.
36. Doffinger, R., et al., ***X-linked anhidrotic ectodermal dysplasia with immunodeficiency is caused by impaired NF-kappaB signaling.*** Nat Genet, 2001. **27**(3): p. 277-85.
37. Chassaing, N., et al., ***Mutations in EDAR account for one-quarter of non-ED1-related hypohidrotic ectodermal dysplasia.*** Hum Mutat, 2006. **27**(3): p. 255-9.
38. van de Wetering, M., et al., ***Armadillo coactivates transcription driven by the product of the Drosophila segment polarity gene dTCF.*** Cell, 1997. **88**(6): p. 789-99.
39. Calzado, M.A., et al., ***HIPK2: a versatile switchboard regulating the transcription machinery and cell death.*** Cell Cycle, 2007. **6**(2): p. 139-43.
40. Wei, G., et al., ***HIPK2 represses beta-catenin-mediated transcription, epidermal stem cell expansion, and skin tumorigenesis.*** Proc Natl Acad Sci U S A, 2007. **104**(32): p. 13040-5.
41. Headon, D.J. and P.A. Overbeek, ***Involvement of a novel Tnf receptor homologue in hair follicle induction.*** Nat Genet, 1999. **22**(4): p. 370-4.
42. Maretto, S., et al., ***Mapping Wnt/beta-catenin signaling during mouse development and in colorectal tumors.*** Proc Natl Acad Sci U S A, 2003. **100**(6): p. 3299-304.
43. Lustig, B., et al., ***Negative feedback loop of Wnt signaling through upregulation of conductin/axin2 in colorectal and liver tumors.*** Mol Cell Biol, 2002. **22**(4): p. 1184-93.
44. Hayden, M.S. and S. Ghosh, ***Signaling to NF-kappaB.*** Genes Dev, 2004. **18**(18): p. 2195-224.

45. Shimomura, Y., et al., ***APCDD1 is a novel Wnt inhibitor mutated in hereditary hypotrichosis simplex.*** Nature, 2010. **464**(7291): p. 1043-7.
46. Shindo, M. and P.M. Chaudhary, ***The ectodermal dysplasia receptor represses the Lef-1/beta-catenin-dependent transcription independent of NF-kappaB activation.*** Biochem Biophys Res Commun, 2004. **315**(1): p. 73-8.
47. Deshmukh, H., et al., ***High-resolution, dual-platform aCGH analysis reveals frequent HIPK2 amplification and increased expression in pilocytic astrocytomas.*** Oncogene, 2008. **27**(34): p. 4745-51.
48. Lee, W., et al., ***Homeodomain-interacting protein kinases (Hipks) promote Wnt/Wg signaling through stabilization of beta-catenin/Arm and stimulation of target gene expression.*** Development, 2009. **136**(2): p. 241-51.
49. Polakis, P., ***The many ways of Wnt in cancer.*** Curr Opin Genet Dev, 2007. **17**(1): p. 45-51.
50. Bal, E., et al., ***Autosomal dominant anhidrotic ectodermal dysplasias at the EDARADD locus.*** Hum Mutat, 2007. **28**(7): p. 703-9.
51. Desbois-Mouthon, C., et al., ***Insulin and IGF-1 stimulate the beta-catenin pathway through two signalling cascades involving GSK-3beta inhibition and Ras activation.*** Oncogene, 2001. **20**(2): p. 252-9.
52. Gaide, O. and P. Schneider, ***Permanent correction of an inherited ectodermal dysplasia with recombinant EDA.*** Nat Med, 2003. **9**(5): p. 614-8.
53. Kim, E.A., et al., ***Phosphorylation and transactivation of Pax6 by homeodomain-interacting protein kinase 2.*** J Biol Chem, 2006. **281**(11): p. 7489-97.

Legends to figures

Figure 1

Edar and EDARADD inhibit Wnt/β-catenin signalling pathway *via* activation of NF-κB. Two different reporter plasmids were used depending on whether NF-κB (pIgκ-luc) or Wnt/β-catenin activity (Topflash) was measured. Transcriptional activity was measured as *Firefly* luciferase activity and normalized to *Renilla* luciferase activity. Iκ-Bα SS-AA plasmid encodes a strong repressor of NF-κB activity. The results represent the mean value from three experiments.

A: HEK293T cells were transfected with either myc-β-catenin S45Y plasmid encoding a constitutively active form of β-catenin, or Wnt8-Fz5 fusion plasmid. Transfection of HA-Edar plasmid alone or together with Myc-EDARADD inhibited Wnt/β-catenin mediated transcription in HEK293T, SW480 and HepG2 cells.

B: Iκ-Bα SS-AA strongly inhibited Edar-dependent NF-κB activity in HEK293T and SW480 cells.

C: Iκ-Bα SS-AA transfection prevented Edar-dependent Wnt/β-catenin inhibition in HEK293T and SW480 cells.

D and **E**: Effects of *EDAR* mutations on NF-κB activation and Wnt/β-catenin inhibition. The dominant mutations (p.R358X, p.I418T, p.L377F and p.T413P) severely impaired NF-κB activity and had little effect on Wnt/β-catenin mediated transcription, whereas the recessive mutations (p.T403M, p.R375H and p.W434C) retained a residual ability to stimulate NF-κB and then to down-regulate Wnt/β-catenin activity. At high doses (500 ng and 1 µg), the recessive mutations gave similar Wnt/β-catenin activity values as wild-type showing that small activities of NF-κB were able to inhibit Wnt/β-catenin activity.

Figure 2

Edar-mediated Wnt/β-catenin downregulation is not achieved through classical mechanisms of Wnt/β-catenin inhibition.

HEK293T cells were transfected with plasmids as indicated.

A: Total cell lysates used for transactivation experiments were analyzed by immunoblotting using anti-β-catenin antibody. A faint band was observed corresponding to endogenous β-catenin when no myc-β-catenin S45Y is transfected. Immunoblotting with anti-actin antibody serves as loading control. Transfection of Edar in conditions where Wnt/β-catenin activity was completely abolished is not associated with β-catenin degradation.

B: Cytoplasmic and nuclear extracts were analyzed separately by immunoblotting. The anti-c-myc antibody only revealed the transfected β-catenin form. The presence of Edar did not affect the subcellular localization of β-catenin.

C: The cellular distribution of β-catenin was not affected by the presence of Edar, as determined by confocal microscopy using anti-β-catenin antibody (green) on HEK293T cells transfected either with myc-β-catenin S45Y alone or together with HA-Edar. Nuclei were stained using propidium iodide (red). Both nuclear and cytoplasmic β-catenin staining was apparent in both experimental conditions.

D: Edar transfection did not affect β-catenin/TCF4 interaction. β-catenin was immunoprecipitated using anti-β-catenin antibody and TCF4 was detected by immunoblotting. Cell lysates were immunoblotted with anti-β-catenin, anti-HA and anti-TCF4 antibodies.

Figure 3

Edar transfection enhances association of HIPK2 to β-catenin

A: HEK293T cells were transfected for 24 h as indicated. Lysates were immunoprecipitated using anti-Hipk2 antibody and analyzed by immunoblotting using anti-β-catenin antibody. The amount of immunoprecipitated HIPK2 was determined by immunoblotting with anti-Hipk2 antibody. To control for Edar, β-catenin, and TCF4 transfection, total cell lysates were subjected to immnuoblotting using corresponding antibodies. Lysates correspond to experiments shown in figure 2D.

B: SW480 cells were cotransfected with HA-Edar and myc-EDARADD and the interaction between the endogenous HIPK2 and β-catenin proteins was analyzed as in panel A.

Figure 4

HIPK2 contributes to Edar-mediated inhibition of Wnt/β-catenin signaling

A: Quantification of *HIPK2* expression in 3 distinct stably transfected SW480 clones expressing short hairpin RNA against *HIPK2* transcript. Approximately 35-60% knockdown of *HIPK2* expression was achieved in the different lines.

B: The effect of Edar signaling on β−catenin transcriptional activity under conditions of *HIPK2* knockdown. In control SW480 cells, Edar transfection strongly suppressed β−catenin function. Knockdown of HIPK2 reduced this effect, allowing greater β−catenin activity in the presence of Edar signalling.

Figure 5

***Hipk2* is co-expressed with *Edaradd* during hair follicle formation**

A-F and I-N: Whole mount *in situ* hybridizations detecting *Hipk2* (A-F) and *Edaradd* (I-N) expression during the first wave of hair follicle formation from embryonic day 14 (E14; A-D and I-L) to E15 (E-F and M-N), in wild-type and Eda^{Ta} mice. C-D and K-L panels show higher magnification of the dorsal region of E14 embryos. G and H are sections of E14 embryos; arrow indicates a hair placode in wild type skin. Both genes displayed elevated expression in primary hair placodes and developing vibrissae in wild-type embryos, and were moderately expressed throughout the whole epidermis in the *Eda* mutant strain. The scale bar is 1 mm for A-F, I-N, and 100 μm for G,H.

Figure 6

***Hipk2* is expressed in a domain distinct from that of β-catenin transcriptional activity**.

A-D: Whole mount staining of E14 mouse embryos detecting: A: β-catenin (or *CTNNB1*) expression by *in situ* hybridization and B-D: X-gal staining in β-catenin reporter lines BATgal Axin2-lacZ and TOPgal. E-K: Immunohistochemistry of E14 embryos from β-catenin reporter lines TOPgal, BATgal and Axin2-lacZ mouse model. β-galactosidase activity (blue color) was first stained. The embryos were subsequently processed for Hipk2 immunohistochemistry (brown color). The BATgal and Axin2-lacZ lines showed that β-catenin transcriptional activity was mostly present in dermal papilla, from which Hipk2 is absent. The TOPgal line showed restricted epidermal β-catenin activity within nascent placodes. The scale bar is 100 μm.

Figure 7

***HIPK2* is transcriptionally regulated by NF-κB**

A: Schematic organization of the human *HIPK2* gene. Positions of the three putative NF-κB binding sites used in experiments below (sites 1, 2 and 3) are shown with respect to the exon/intron structure of *HIPK2*.

B: *in vitr*o NF-κB p65 and p50 binding to the *HIPK2* gene. DNA binding to fragments 1, 2 and 3 corresponding to the three putative NF-κB binding sites of *HIPK2* was performed with nuclear extracts from cells co-transfected with plasmids encoding p65 and p50 NF-κB subunits.

25-pb fragments were used as biotin labeled probes. The same experiments were performed with labeled probes mutated on conserved nucleotides in the putative binding sequence. A 200 fold molar excess of unlabelled wild-type or mutated oligonucleotides was added as competitor. Supershift experiments were performed in the presence of the indicated antibody.

C: *in vivo* NF-κB p50 and p65 binding on the three putative NF-κB binding sites in human *HIPK2* gene. Chromatin immunoprecipitation (ChIP) assays were performed on HEK293T cells transfected with HA-Edar encoding plasmid, and using anti-p50 and anti-p65-antibodies. Mouse IgG were used as a negative control. The Input corresponds to PCR on DNA extracted and sonicated without immunoprecipitation (IP). ChIP was prepared and subjected to PCR analysis using primers flanking putative NF-κB binding sequences of *HIPK2* gene. *NFKBIA* primers flanking an NF-κB-response binding site were used as a positive control. Amplification was obtained for both fragments 1 and 3 in unstimulated cells. This amplification was enhanced after Edar transfection. No amplification was observed for fragment 2.

D: NF-κB binding sequence (site 1) in intron 1 regulates the transcriptional activity of the *HIPK2* gene. HEK293T cells were transiently transfected with either empty pGL2 vector or with the luciferase reporter constructs downstream of multimers of the three NF-κB binding sites of the *HIPK2* gene, together with or without a Ha-Edar encoding plasmid for 24 h, and IκBα SS-AA super-repressor, as indicated. As a negative control, a construct with mutated site 1 multimers was also tested for NF-κB transcriptional activity. Transcriptional activity was measured as *Firefly* luciferase activity and normalized to *Renilla* luciferase activity.

E: Quantitative RT-PCR of *Hipk2* expression levels in E14.5 Eda^{Ta} skin. Administration of 1000 ng/ml recombinant EDA-A1 for 10 hours significantly increased *Hipk2* levels above the basal values (p-value < 0.001).

Abbreviations

EA: ectodermal appendages; EDA: Ectodysplasin; HED: hypohidrotic ectodermal dysplasia; HIPK2: homeodomain interacting protein 2; shRNA: short hairpin RNA.

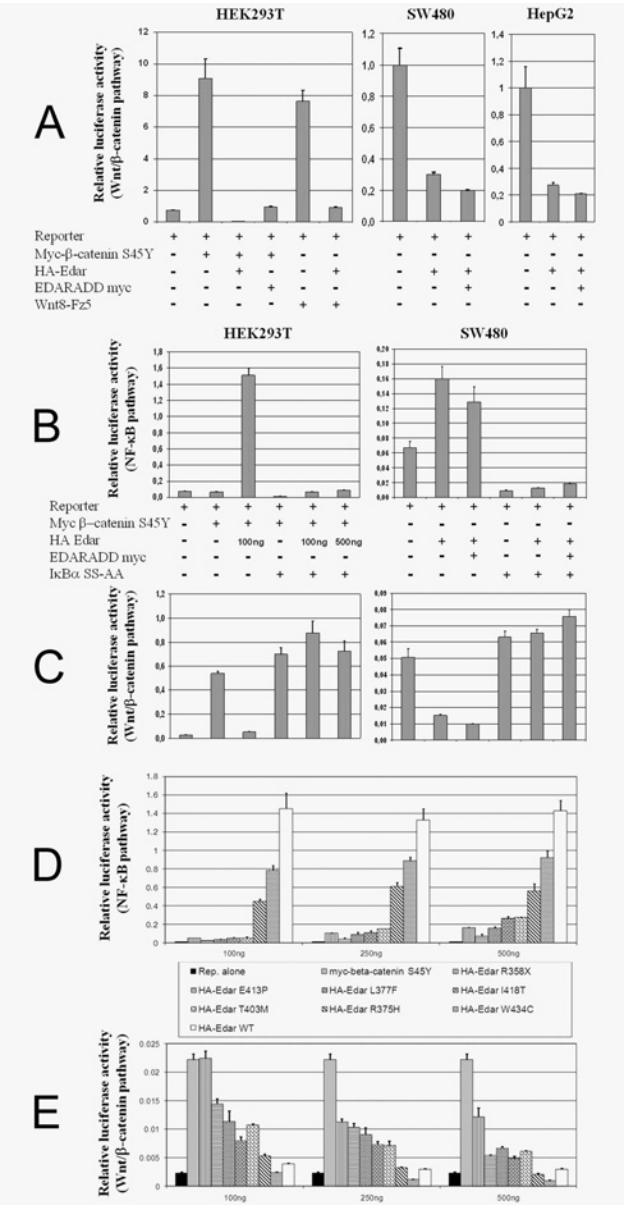

Figure 1 : Edar and EDARADD inhibit Wnt/β-catenin signalling pathway via activation of NF-κB. Two different reporter plasmids were used depending on whether NF-κB (pIgκ-luc) or Wnt/β-catenin activity (Topflash) was measured. Transcriptional activity was measured as Firefly luciferase activity and normalized to Renilla luciferase activity. Iκ-Bα SS-AA plasmid encodes a strong repressor of NF-κB activity. The results represent the mean value from three experiments.

A: HEK293T cells were transfected with either myc-β-catenin S45Y plasmid encoding a constitutively active form of β-catenin, or Wnt8-Fz5 fusion plasmid. Transfection of HA-Edar plasmid alone or together with Myc-EDARADD inhibited Wnt/β-catenin mediated transcription in HEK293T, SW480 and HepG2 cells.

B: Iκ-Bα SS-AA strongly inhibited Edar-dependent NF-κB activity in HEK293T and SW480 cells.

C: Iκ-Bα SS-AA transfection prevented Edar-dependent Wnt/β-catenin inhibition in HEK293T and SW480 cells.

D and E: Effects of EDAR mutations on NF-κB activation and Wnt/β-catenin inhibition. The dominant

mutations (p.R358X, p.I418T, p.L377F and p.T413P) severely impaired NF-κB activity and had little effect on Wnt/β-catenin mediated transcription, whereas the recessive mutations (p.T403M, p.R375H and p.W434C) retained a residual ability to stimulate NF-κB and then to down-regulate Wnt/β-catenin activity. At high doses (500 ng and 1 µg), the recessive mutations gave similar Wnt/β-catenin activity values as wild-type showing that small activities of NF-κB were able to inhibit Wnt/β-catenin activity.

80x153mm (500 x 500 DPI)

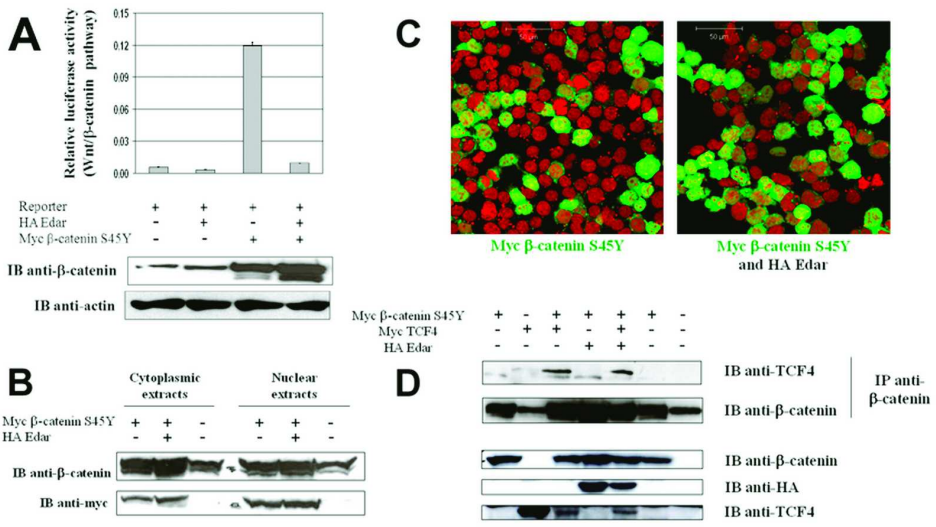

Figure 2: Edar-mediated Wnt/β-catenin downregulation is not achieved through classical mechanisms of Wnt/-β-catenin inhibition.

HEK293T cells were transfected with plasmids as indicated.

A: Total cell lysates used for transactivation experiments were analyzed by immunoblotting using anti-β-catenin antibody. A faint band was observed corresponding to endogenous β-catenin when no myc-β-catenin S45Y is transfected. Immunoblotting with anti-actin antibody serves as loading control. Transfection of Edar in conditions where Wnt/β-catenin activity was completely abolished is not associated with β-catenin degradation.

B: Cytoplasmic and nuclear extracts were analyzed separately by immunoblotting. The anti-c-myc antibody only revealed the transfected β-catenin form. The presence of Edar did not affect the subcellular localization of β-catenin.

C: The cellular distribution of β-catenin was not affected by the presence of Edar, as determined by confocal microscopy using anti-β-catenin antibody (green) on HEK293T cells transfected either with myc-β-catenin S45Y alone or together with HA-Edar. Nuclei were stained using propidium iodide (red). Both nuclear and cytoplasmic β-catenin staining was apparent in both experimental conditions.

D: Edar transfection did not affect β-catenin/TCF4 interaction. β-catenin was immunoprecipitated using anti-β-catenin antibody and TCF4 was detected by immunoblotting. Cell lysates were immunoblotted with anti-β-catenin, anti-HA and anti-TCF4 antibodies.

86x47mm (500 x 500 DPI)

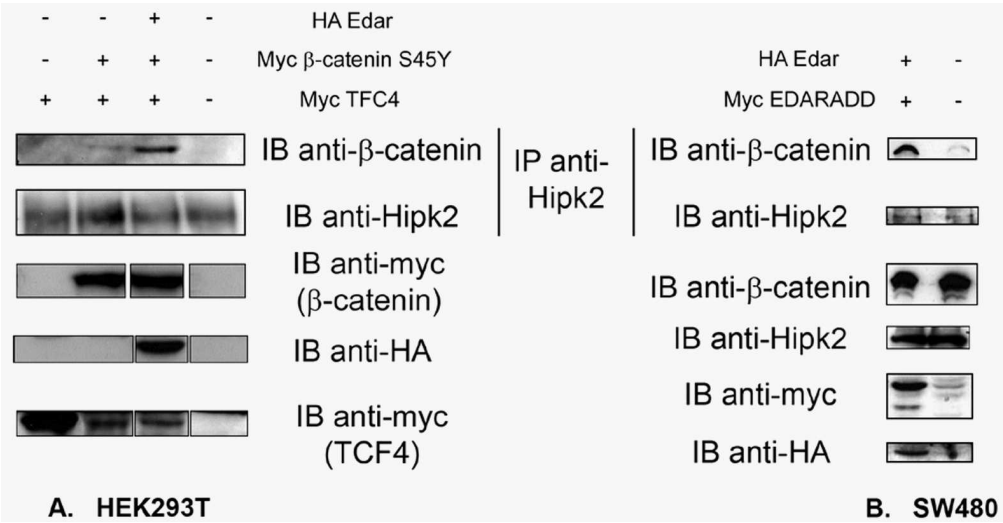

Figure 3: Edar transfection enhances association of HIPK2 to β-catenin
A: HEK293T cells were transfected for 24 h as indicated. Lysates were immunoprecipitated using anti-Hipk2 antibody and analyzed by immunoblotting using anti-β-catenin antibody. The amount of immunoprecipitated HIPK2 was determined by immunoblotting with anti-Hipk2 antibody. To control for Edar, β-catenin, and TCF4 transfection, total cell lysates were subjected to immnuoblotting using corresponding antibodies. Lysates correspond to experiments shown in figure 2D.
B: SW480 cells were cotransfected with HA-Edar and myc-EDARADD and the interaction between the endogenous HIPK2 and β-catenin proteins was analyzed as in panel A.

80x41mm (500 x 500 DPI)

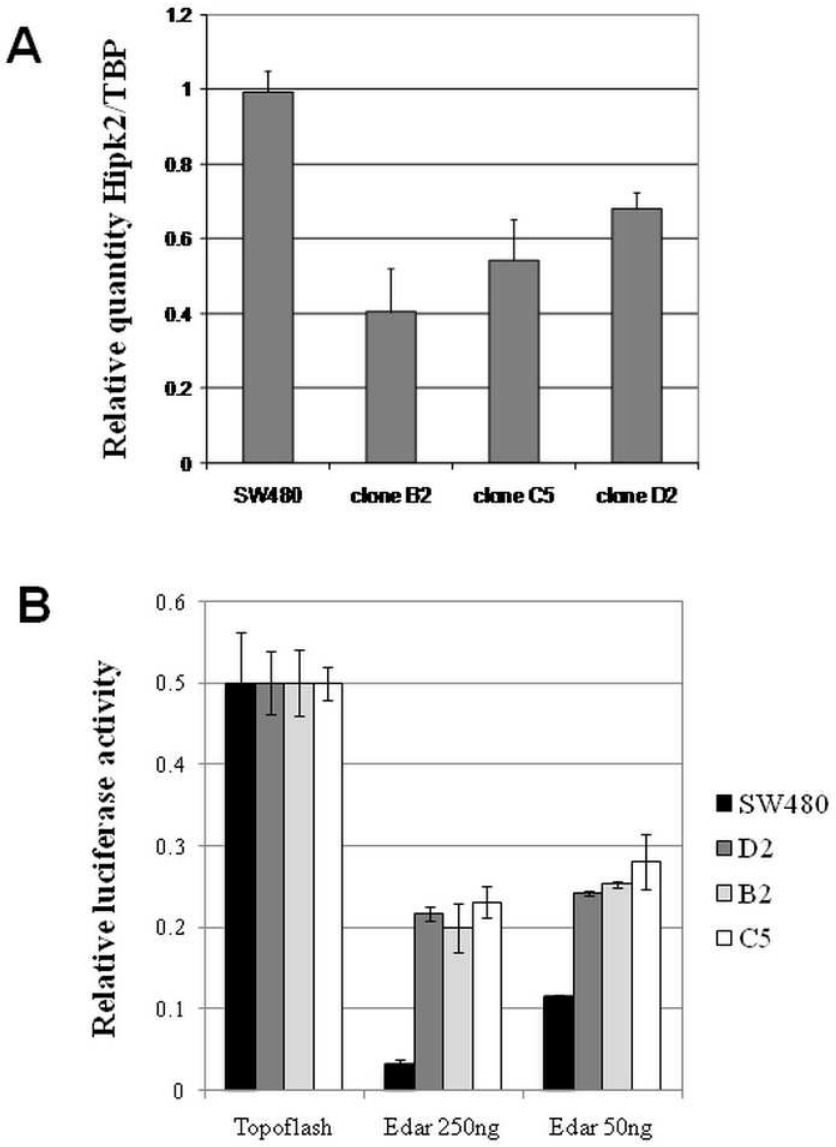

Figure 4: HIPK2 contributes to Edar-mediated inhibition of Wnt/β-catenin signaling
A: Quantification of HIPK2 expression in 3 distinct stably transfected SW480 clones expressing short hairpin RNA against HIPK2 transcript. Approximately 35-60% knockdown of HIPK2 expression was achieved in the different lines.
B: The effect of Edar signaling on β-catenin transcriptional activity under conditions of HIPK2 knockdown. In control SW480 cells, Edar transfection strongly suppressed β-catenin function. Knockdown of HIPK2 reduced this effect, allowing greater β-catenin activity in the presence of Edar signalling.

67x84mm (300 x 300 DPI)

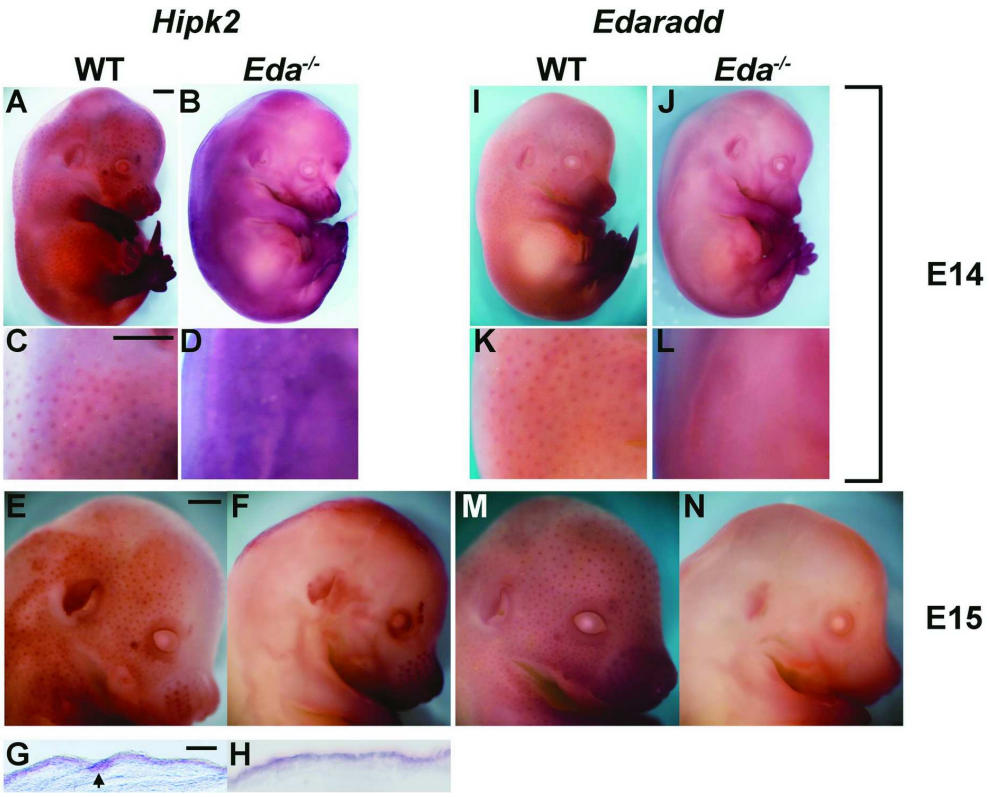

Figure 5: Hipk2 is co-expressed with Edaradd during hair follicle formation
A-F and I-N: Whole mount in situ hybridizations detecting Hipk2 (A-F) and Edaradd (I-N) expression during the first wave of hair follicle formation from embryonic day 14 (E14; A-D and I-L) to E15 (E-F and M-N), in wild-type and Eda mice. C-D and K-L panels show higher magnification of the dorsal region of E14 embryos. G and H are sections of E14 embryos; arrow indicates a hair placode in wild type skin. Both genes displayed elevated expression in primary hair placodes and developing vibrissae in wild-type embryos, and were moderately expressed throughout the whole epidermis in the Eda mutant strain. The scale bar is 1 mm for A-F, I-N, and 100 μm for G,H.

160x125mm (300 x 300 DPI)

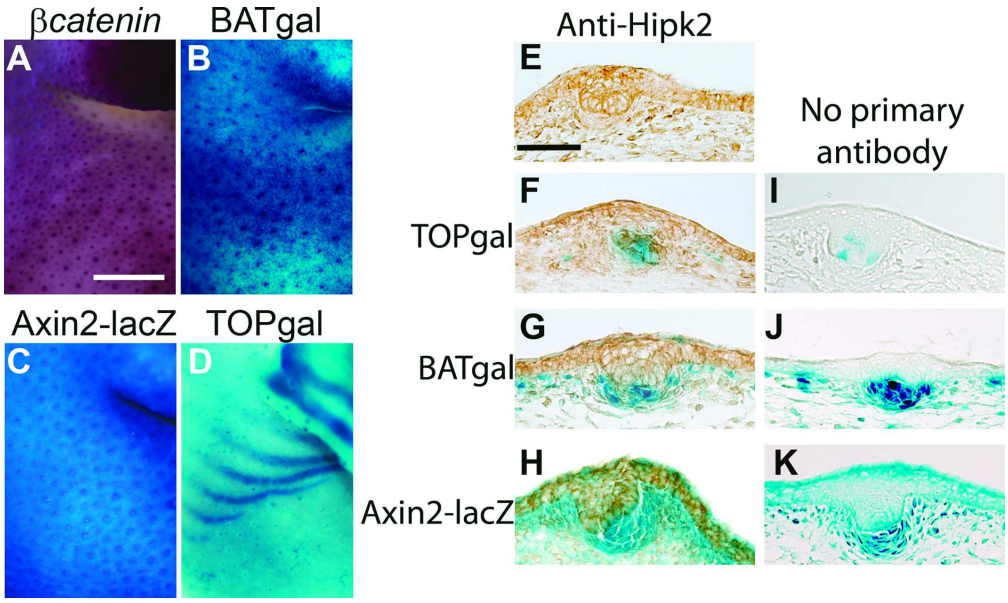

Figure 6: Hipk2 is expressed in a domain distinct from that of β-catenin transcriptional activity. A-D: Whole mount staining of E14 mouse embryos detecting: A: β-catenin (or CTNNB1) expression by in situ hybridization and B-D: X-gal staining in β-catenin reporter lines BATgal Axin2-lacZ and TOPgal. E-K: Immunohistochemistry of E14 embryos from β-catenin reporter lines TOPgal, BATgal and Axin2-lacZ mouse model. β-galactosidase activity (blue color) was first stained. The embryos were subsequently processed for Hipk2 immunohistochemistry (brown color). The BATgal and Axin2-lacZ lines showed that β-catenin transcriptional activity was mostly present in dermal papilla, from which Hipk2 is absent. The TOPgal line showed restricted epidermal β-catenin activity within nascent placodes. The scale bar is 100 μm.

180x106mm (300 x 300 DPI)

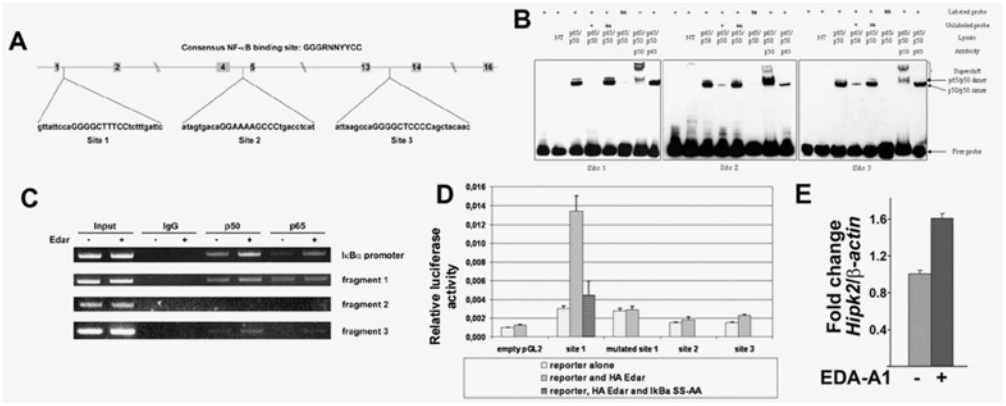

Figure 7: HIPK2 is transcriptionally regulated by NF-κB

A: Schematic organization of the human HIPK2 gene. Positions of the three putative NF-κB binding sites used in experiments below (sites 1, 2 and 3) are shown with respect to the exon/intron structure of HIPK2.

B: in vitro NF-κB p65 and p50 binding to the HIPK2 gene. DNA binding to fragments 1, 2 and 3 corresponding to the three putative NF-κB binding sites of HIPK2 was performed with nuclear extracts from cells co-transfected with plasmids encoding p65 and p50 NF-κB subunits. 25-pb fragments were used as biotin labeled probes. The same experiments were performed with labeled probes mutated on conserved nucleotides in the putative binding sequence. A 200 fold molar excess of unlabelled wild-type or mutated oligonucleotides was added as competitor. Supershift experiments were performed in the presence of the indicated antibody.

C: in vivo NF-κB p50 and p65 binding on the three putative NF-κB binding sites in human HIPK2 gene. Chromatin immunoprecipitation (ChIP) assays were performed on HEK293T cells transfected with HA-Edar encoding plasmid, and using anti-p50 and anti-p65-antibodies. Mouse IgG were used as a negative control. The Input corresponds to PCR on DNA extracted and sonicated without immunoprecipitation (IP). ChIP was prepared and subjected to PCR analysis using primers flanking putative NF-κB binding sequences of HIPK2 gene. NFKBIA primers flanking an NF-κB-response binding site were used as a positive control. Amplification was obtained for both fragments 1 and 3 in unstimulated cells. This amplification was enhanced after Edar transfection. No amplification was observed for fragment 2.

D: NF-κB binding sequence (site 1) in intron 1 regulates the transcriptional activity of the HIPK2 gene. HEK293T cells were transiently transfected with either empty pGL2 vector or with the luciferase reporter constructs downstream of multimers of the three NF-κB binding sites of the HIPK2 gene, together with or without a Ha-Edar encoding plasmid for 24 h, and IκBα SS-AA super-repressor, as indicated. As a negative control, a construct with mutated site 1 multimers was also tested for NF-κB transcriptional activity. Transcriptional activity was measured as Firefly luciferase activity and normalized to Renilla luciferase activity.

E: Quantitative RT-PCR of Hipk2 expression levels in E14.5 EdaTa skin. Administration of 1000 ng/ml recombinant EDA-A1 for 10 hours significantly increased Hipk2 levels above the basal values (p-value < 0.001).

180x71mm (300 x 300 DPI)

Editorial Manager(tm) for Gastroenterology
Manuscript Draft

Manuscript Number: GASTRO-D-11-00563

Title: Mutations in CLMP cause Congenital Short Bowel Syndrome, pointing to the major role of CLMP in intestinal development

Article Type: Basic - Alimentary Tract

Corresponding Author: robert m.w. Hofstra, PhD

Corresponding Author's Institution: University of Groningen

First Author: Christine van der Werf

Order of Authors: Christine van der Werf;Tara Wabbersen;Nai-Hua Hsiao;Joana Parades;Heather Etchevers;Peter Kroisel;Dick Tibboel;Candice Babarit;Richard Schreiber;Edward Hoffenberg;Michel Vekemans;Sirkka Zeder;Isabella Ceccherini;Stanislas Lyonnet;Ana Ribeiro;Raquel Seruca;Gerard te Meerman;Sven Ijzendoorn;Iain Shepherd;Joke Verheij;robert m.w. Hofstra, PhD

Mutations in *CLMP* cause Congenital Short Bowel Syndrome, pointing to the major role of *CLMP* in intestinal development

Christine S. van der Werf[1], Tara D. Wabbersen[2], Nai-Hua Hsiao[3], Joana Paredes[4], Heather C. Etchevers[5], Peter M. Kroisel[6], Dick Tibboel[7], Candice Babarit[5], Richard A. Schreiber[8], Edward J. Hoffenberg[9], Michel Vekemans[5], Sirkka L. Zeder[10], Isabella Ceccherini[11], Stanislas Lyonnet[5], Ana S. Ribeiro[4], Raquel Seruca[4], Gerard J. te Meerman[1], Sven C. D. van IJzendoorn[3], Iain T. Shepherd[2], Joke B. G. M. Verheij[1], Robert M. W. Hofstra[1].

[1]Department of Genetics, University Medical Center Groningen, University of Groningen, Groningen, P.O. Box 30.001, 9700 RB, Groningen, The Netherlands. [2]Department of Biology, Emory University, Atlanta, USA. [5]Département de Génétique, INSERM, U781, Hôpital Necker-Enfants Malades, Université Paris Descartes, Paris, France. [3]The Membrane Cell Biology section, Department of Cell Biology, University Medical Center Groningen, University of Groningen, Groningen, The Netherlands. [4] The Cancer Genetics Group, the Institute of Molecular Pathology and Immunology of the University of Porto, Porto, Portugal. [5]Département de Génétique, INSERM, U781, Hôpital Necker-Enfants Malades, Université Paris Descartes, Paris, France. [6]Institute of Human Genetics, Medical University of Graz, Graz, Austria. [7]Department of Pediatric Surgery, Medical University of Graz, Graz, Austria. [8]Department of Pediatric Surgery, Erasmus MC-Sophia Children's Hospital, PO Box 2060, 3000 CB, Rotterdam, The Netherlands. [9]The Division of Gastroenterology, BC Children's Hospital, Rm K4-200, 4480 Oak Street, Vancouver, Canada. [10]Department of Pediatrics, Section of Pediatric Gastroenterology, Hepatology, and Nutrition, University of Colorado, Denver, CO, USA. [11]Laboratorio di Genetica Molecolare, Istituto Giannina Gaslini - 16148 Genoa, Italy.

Grant support

The work was funded by the Junior Scientific Masterclass (University of Groningen), the Ter Meulen Fund and the van Walree Fund, Royal Netherlands Academy of Arts and Sciences, The Netherlands, the Maag Lever Darm Stichting, the J.K. de Cock Stichting, and the Stichting Simonsfonds.

Abbreviations

CSBS-Congenital Short Bowel Syndrome, SBS-Short Bowel Syndrome, CLMP-Coxackie and adenovirus receptor-Like Membrane Protein, ASAM-Adipocyte Specific Adhesion Molecule.

Correspondence

Robert Hofstra.

phone +31-50-361 7100, e-mail r.m.w.hofstra@medgen.umcg.nl

Short title: Mutations in CLMP cause Congenital Short Bowel Syndrome.

Disclosures

The authors declare that there is no conflict of interest

Author contributions

Conception and design of the study; van der Werf, Verheij, Hofstra.

Generation, collection, assembly, analysis and/or interpretation of data; van der Werf, Wabbersen, Hsiao, Paredes, Etchevers, Kroisel, Tibboel, Babarit, Schreiber, Hoffenberg, Ceccherini, Ribeiro, Vekemans, Lyonnet, Zeder, Seruca, te Meerman, Verheij, Hofstra.

Drafting or revision of the manuscript; van der Werf, Hofstra.

Approval of the final version of the manuscript; Hofstra.

Short title

Mutations in CLMP cause CSBS

Abstract

Background & Aims: Short Bowel Syndrome usually results from surgical resection of the small intestine for diseases such as Crohn's disease, intestinal atresias, volvulus and necrotizing enterocolitis. Patients with Congenital Short Bowel Syndrome (CSBS) are born with a substantial shortening of the small intestine with a mean length of 50 cm compared to a normal length at birth of 190-280 cm. They are also born with intestinal malrotation. Because of the many consanguineous families reported CSBS is considered as an autosomal recessive disorder. In this study we aimed at identifying and characterizing the gene underlying CSBS.

Methods: We applied homozygosity mapping using 610 K SNP arrays on five CSBS patients. After the identification of the underlying gene we determined the expression pattern of the encoded protein in human embryos. Moreover, we overexpressed both wild type and mutant proteins in CHO and T84 cells and we generated a zebrafish model.

Results: We identified loss-of-function mutations in *Coxsackie- and adenovirus receptor like membrane protein (CLMP)* underlying CSBS. CLMP, a tight-junction protein, is expressed in the intestine of human embryos throughout development. Mutation of CLMP abrogated its normal localization at the cell membrane. Knock-down experiments in zebrafish resulted in general developmental defects, including shortening of the intestine and absence of goblet cells, which are characteristic for the mid-intestine in zebrafish, which resembles the small intestine in humans.

Conclusions: Loss-of-function of *CLMP* leads to Congenital Short Bowel Syndrome, likely by interfering with tight-junction formation, with intestinal development and with gut length determination.

Keywords:

Congenital Short Bowel Syndrome, autosomal recessive, CLMP, ASAM, intestinal development.

INTRODUCTION

Patients with Congenital Short Bowel Syndrome (CSBS) are born with a shortened small intestine. The mean length of the small intestine in CSBS patients is approximately 50 cm, compared to a normal length at birth of 190-280 cm.[1-3] Patients with CSBS may develop severe malnutrition as a result of the hugely reduced absorptive surface of the small intestine. This is similar to acquired Short Bowel Syndrome (SBS) from surgical resection of the small intestine for diseases such as Crohn's disease, intestinal atresias, volvulus and necrotizing enterocolitis. CSBS is usually diagnosed by barium contrast X-rays and confirmed by exploratory laparotomy. Infants with SBS, whether congenital or acquired, need parenteral nutrition to survive, although parenteral nutrition itself causes life-threatening complications like sepsis and liver failure, and a high rate of mortality early in life. However, some long-term survivors of CSBS have been reported.[4-7] As consanguinity is frequently seen in families in which CSBS occurs, an autosomal recessive pattern of inheritance is suspected. Untill now, nothing was known about the genetic cause of this disease.

Here, we report, for the first time, the identification and characterization of *CLMP* as the gene underlying CSBS.

METHODS

Research subjects

The CSBS patients included in this study, aged 0-26 years, were either previously described in the literature or were known to physicians in the field[4-7]. Patients were born with a shortened small intestine with a length of 30 to 54 cm (see Table 1). Patients, of which some were seen by an experienced clinical geneticist, did not show any other clinical features besides CSBS. All parents were reported as normal. Patients 2-1, 3-1 and 3-2 were from consanguineous families. All patients were Caucasians, except for patients 3-1 and 3-2 who were of Turkish ancestry. The study protocol was approved by the institutional and national ethics review committees at the University Medical Centre Groningen (NL31708.042.10), and written informed consent was obtained.

Homozygosity mapping.

Genomic DNA of all participants was extracted from peripheral lymphocytes by standard methods. A genome-wide scan was performed on five patients of families 1 to 4 using the 610K SNP array of Illumina according to the manufacturer's instructions. Homozygosity mapping was performed by an automatic search for a minimum of 400 markers in a row (~2-3 MB) which were homozygous in at least 3 of the 4 families, and identical for patient 3-1 and 3-2 (as they were from the same consanguineous family).

Mutation screening

Analysis of the seven exons of *CLMP* (NM_024769.2) and the flanking intronic regions was performed in all patients and their parents as well as in 77 Caucasian control individuals (154 control chromosomes). For primer sequences see Supplementary Table 1. Sequencing was performed (forward and reverse) with dye labelled primers (Big Dye Terminator v3.1 Sequencing Kit, Applied Biosystems, Foster City, USA) on an ABI 3730 automated sequencer.

In Silico Analysis of the missense mutation

CLMP homologous proteins were obtained by blasting the CLMP protein (NP_079045.1). For the alignment of these homologues proteins the program Mcoffee was used (http://www.tcoffee.org) (Moretti et al., 2007). The effect of the missense mutation was evaluated by the 'Russell method' at

EMBL (http://www.russell.embl-heidelberg.de/aas/; Betts and Russell, 2003), the polymorphism phenotyping (PolyPhen) algorithm (http://genetics.bwh.harvard.edu/pph/) and the 'Sort Intolerant From Tolerant' (SIFT) algorithm (http://sift.jcvi.org/).

Functional analysis of the splice site mutation

To determine the effect of the splice site mutation found in patient 1-1, we performed an exon trapping assay. We first generated PCR 2.1-TOPO plasmids (invitrogen), containing the sequences of the exon of interest (wild type or mutant) and the flanking intronic sequences. The sequence of interest was PCR amplified using either a control or the patient's genomic DNA as the DNA template. We used the primers GGCG-Ecor1, 5'-AAACCTGCAAATACTCATTC-3', and GACG-BamH1, 5'-AAGTGTTTGTTGAGGATAAG-3'. The amplification was performed using Pushion High-fidelity DNA polymerase (Finnzymes, Helsinki Finland). The PCR products were inserted into The PCR 2.1 Topo constructs and thereafter digested with BamH1 and EcoR. The inserts from control and mutant were subsequently cloned into the exon trapping vector pSPL3 (invitrogen). The inserts were checked by direct sequencing.

Human embryonic kidney (HEK) 293 cells were grown in DMEM supplemented with 10% fetal calf serum and 1% antibiotic solution (penicillin/streptomycin, Invitrogen) at 37 °C in 5% CO_2. HEK 293 cells were plated in 6-wells plates containing 6 x 10^5 cells/well. After 24 hours the cells were transfected with 1 μgram of the corresponding plasmid using polyethylenimine (polyscience INC) according to manufacter's instruction. Transfection of both the vector containing the wild-type sequences and the empty pSPL3 vector were used as controls. After 48 hours cells were lysed and RNA was isolated according to manufacter's instruction (Qiagen). 5 μgram of total RNA was used as a template to synthesise cDNA using the cDNA primer pd(N)6 (GE Healthcare). PCR was performed using the primers (SD6) 5'-CTGAGTCACCTGGACAACC- 3' and (SA2) 5'-ATCTCAGTGGTATTTGTGAGC-3' and the following amplification program: 5 minutes 94 °C, 35 cycles 1 minute 94 °C, 1 minute 60°C and 5 minutes 72 °C, and a final elongation time of 10 minutes at 72 °C. 5 microL of cDNA was used for the PCR in a total volume of 50 microL. PCR products were checked by gel electrophoresis and the exon trapping results were confirmed by direct sequencing.

Expression of wild-type and mutant CLMP in Chinese Hamster Ovary cells and T84 cells

A pCMV6-CLMP-GFP vector was obtained from Origene. The missense mutation was introduced in this vector by site-directed mutagenesis (stratagene, for primer sequences see Supplementary Table 2). The WT- and mutant cDNA were amplified using the primers CCGCC-NheI, 5'-ATGTCCCTCCTCCTTCTCC-3', and GGGCGC-XhoI, 5'-TCAGACCGTTTGGAAGGCTCTG-3'. The amplification was performed using Pushion High-fidelity DNA polymerase (Finnzymes, Helsinki Finland). The PCR products were inserted into PCR 2.1-TOPO plasmid (invitrogen). The PCR 2.1 Topo constructs were digested by NheI and XhoI restriction enzymes and the fragments were cloned into the vector pCMV-IRES-EGFP. The clones were checked by direct sequencing.

Chinese hamster ovary (CHO-K1) and human intestinal epithelial T84 cells were grown in commercially available *α*-MEM medium (Invitrogen, Carlsbad, CA) and DMEM/F-12 (Invitrogen) respectively, supplemented with 4.5 mg/L L-glutamine, 10% heat-inactivated Fetal Bovine serum (FBS, Invitrogen) and 1% antibiotic solution (penicillin–streptomycin, Invitrogen). The cells were maintained at 37 °C in a humidified atmosphere with 5% CO_2.

WT or mutant pCMV-CLMP-IRES-EGFP was transfected in CHO-K1 cells and T84 cells (1.5 x 10^5) with Lipofectamine 2000 Transfection Reagent (Invitrogen) in a 1:3 dilution, and transfection efficiencies were evaluated by measuring EGFP expression by flow cytometry.

In order to observe the cell localization of CLMP, transfected CHO-K1 cells were stained by immunofluorescence. Cells were cultured on glass coverslips (Becton Dickinson Labware, Franklin Lakes, NJ, USA), and fixed with 4% paraformaldehyde (20 minutes). After fixation, cells were treated with 50mM NH4Cl for 10 minutes, washed with PBS, and permeablilized with 0.1% Triton X-100 in PBS for 5 minutes at room temperature. Non-specific binding was blocked by cell treatment with PBS containing 5% BSA, for 30 minutes at room temperature. Cells were then stained with the rabbit primary antibody anti-human CLMP (anti-AP000926.6, Sigma HPA002385), during 1 hour and at a 1:100 dilution. Then anti-rabbit antibody conjugated with Alexa 594 (Invitrogen) was used as secondary antibody. After a wash with PBS, each sample was mounted with vectashield with DAPI. The cell staining was observed with a Zeiss microscope (Imager Z1) with apotome and images were taken using the Axiovision software.

Transfected T84 cells were fixed with 4% paraformaldehyde at 37 °C for 30 min. Cells were then treated with 0.1 M glycin for 10 minutes, washed with PBS, and permeabilized with 0.1% Triton X-100 in PBS at room temperature for 2 min. Non-specific binding sites were blocked by incubating the cells with PBS containing 1% BSA and 0.05% tween 20 at room temperature for 1 min. Cells were immunolabeled with the rabbit polyclonal antibody for CLMP (anti-AP000926.6, Sigma HPA002385), in 1:100 dilution at 37 °C for 1 h. Cells were subsequently washed 5 times with PBS and incubated with mouse monoclonal anti-ZO-1 antibodies (Zymed) at 1:100 dilution. Goat anti-rabbit antibody conjugated with Alexa-546 (Invitrogen) and goat anti-mouse antibody conjugated with Cy5 were used as secondary antibodies (1:500). DAPI (1:1000) and/or DRAQ5 (1:500) were used for nuclear staining. After a wash with PBS, samples were mounted and analysed with a Leica SP2 AOBS confocal laser scanning microscope.

CLMP expression during human development

CLMP expression was examined by immunohistochemistry in human embryos and fetal tissue, obtained from terminated pregnancies using the mefiprestone protocol in concordance with French legislation (94-654 and 08-400) and approved by the Necker Hospital ethics committee. Embryonic and fetal tissues were fixed in 4% paraformaldehyde, pH 7.4 or in 11% formaldehyde, 60% ethanol, and 10% acetic acid, embedded in paraffin blocks and sectioned at 5 μm. Sections were deparaffinated, rinsed in PBS and incubated 30 minutes in 0.5 M ammonium chloride, rinsed again, and non-specific binding blocked by 10% fetal calf serum (FCS) in PBS for 30 minutes. Classical antigen unmasking in citrate buffer was performed for 20 minutes. Slides were incubated overnight at 4°C in a humid chamber with the rabbit primary antibody anti-human CLMP (anti-AP000926.6, Sigma HPA002385) 1:50 in PBS with 2% FCS and then rinsed. A secondary goat anti-rabbit-alkaline phosphatase (AP) antibody was applied at 1:200 in PBS/2% FCS and AP activity, and thereby immunolocalization of CLMP, was revealed by the standard NBT-BCIP chromogenic reaction. Adjacent sections stained without the primary antibody anti-human CLMP were used as negative controls.

Expression pattern of orthologs in zebrafish and knock down experiments

Zebrafish are kept and bred under standard conditions at 28.5°C (Westerfield, 1993). Embryos were staged and fixed at specific hours post fertilization (hpf). To better visualize the phenotype and the *in situ* hybridization results, embryos were grown in 0.2 mM 1-phenyl-2-thiourea (Sigma) to inhibit pigment formation (Westerfield, 1993).

A search for the predicted orthologs was performed in the ensemble database (www.ensemble.org). To clone the complete open reading frames of the zebrafish orthologs, multiple RT-PCR primers were designed to amplify up 5' and 3' overlapping segments of the open reading frame based on the predicted sequences. The cDNA segments were subcloned and sequenced. Sequencher DNA sequence analysis software was used to assemble the resulting sequences. RACE (rapid amplification of cDNA ends) was used to amplify the 5' and 3' ends of the open reading frame. RACE cDNA was isolated from 72hpf embryos using a Smart RACE cDNA Amplification Kit (Clonetech). The resulting PCR products were subcloned and sequenced to complete the open reading frame sequence for the orthologs. The continuity of the full length sequence assembled from the sequences was confirmed by RT-PCR on single-stranded cDNA isolated from 48-hpf embryos. The orthologs were cloned and the sequences were determined by direct sequencing.

Homology studies were completed using publicly accessible programs from SDSC Biology Workbench. ClustalW was used to align the amino acid sequences of both orthologs in zebrafish (called *CLMPa* and *CLMPb*), rat, and human CLMP (called h.CLMP) (supplementary Figure 2).

To determine the temporal expression of *CLMPa* and *CLMPb*, RT-PCR was performed at various time points with primers used to amplify up a segment of the open reading frame spanning nucleotides 38-881 of *CLMPa* and nucleotides -3-851 of *CLMPb*. The following primers were used: *CLMPa* forward, 5'-GTGATGTCTGCCAGCGCTCG-3', *CLMPa* reverse, 5'-GGGACGACGACAGAGAGTTC-3', *CLMPb* forward, 5'- CTGCAGCTGACTGACTCTGG-3' and *CLMPb* reverse, 5'- GTCTGAAAGGCCTTGCTTTG-3' The predicted fragment sizes were as follows: for *CLMPa*, 843 base pairs and for *CLMPb*, 854 base pairs. To determine the spatial expression patterns of *CLMPa* and *CLMPb*, antisense Digoxigenin-labeled probes for both genes were generated and whole mount in situ hybridization was performed as described by Thisse et al. (1993).

Two different, non-overlapping translation-blocking morpholinos as well as a splice-blocking morpholino and a 5-mispair morpholino were designed and generated by gene tools (www.gene-tools.com, for morpholino sequences see Supplementary Table 3) and injected to determine the effects of knocking down CLMPa protein levels (Nasevicius and Ekker, 2000). Morpholino antisense oligonucleotides were designed to correspond to the translational start site and splice-blocking morpholino antisense oligonucleotides (Gene Tools) were designed to the splice donor site at the predicted exon2/ exon3 junction for *CLMPa* (see for morpholino sequences Supplementary Table 3). The morpholinos were diluted in sterile filtered water over a range of concentrations from 1 μg/μl to 10 μg/μl. Approximately 1 nL of diluted morpholino was injected at the one- to two-cell stage using a gas-driven microinjection apparatus to determine the effects of knocking down *CLMPa*. We determined the dilution of the morpholinos in which we saw a consistent knockdown of *CLMPa* as follows: *CLMPa* TBMO1 and TBMO2: 2μg/μl, SBMO: 1 μg/μl. A p53 translation-blocking morpholino was co-injected in a concentration of 1,5 x the morpholino concentration to rule out cytotoxic site effects of the morpholinos. A 5–base pair mismatch morpholinos was injected in a concentration of 2μg/μl as a negative control for the experiments with the first translation-blocking morpholino (see Supplementary Table 3). The following primers were designed for RT-PCR to verify the effectiveness of the splice-blocking morpholino: CLMPaRTPCR forward, 5'- CGCCCTGCTCTTAGTATTGC –3' and CLMP-aRTPCR reverse, 5'- GGGGTTTTGATGGCTTCAAG - 3'.

Both 96 hpf control and SBMO injected embryos were fixed and embedded in paraffin wax, and cut in sections of 3 μm. Haematoxylin and Eosin staining was performed using standard procedures. The sections were heated for 20 minutes at 60°C, deparaffinised and hydrated to water. The sections were stained in Haematoxylin 7211 (Richard Allan) for 4 minutes, rinsed in water and after placing them for 1 minute in Clarifier (Richard Allan) rinsed again in water. Then they were placed in Bluing (Richard Allan) for 1 minute, dipped in 95% ethanol, placed in Eosin-Y 7111 (Richard Allan) for 45 sec and dehydrated in 95% Ethanol, absolute ethanol, and cleared in xylene and coversliped.

For the rescue experiment CLMP mRNA was made using a pCS2+ expression vector containing the complete Open Reading Frame sequence of *CLMPa* ortholog. MRNA was synthesized from this using the mMessage mMachine kit (Ambion).

RESULTS

Loss-of-function mutations in CLMP cause Congenital Short Bowel Syndrome

In order to map the disease gene we performed 610K-SNP arrays of Illumina on five patients (1-1, 2-1, 3-1, 3-2 and 4-1: Figure 1a). We identified a homozygous region shared by four (patients 2-1, 3-1, 3-2 and 4-1) of them on 11q24.1 comprising approximately 2 MB and containing 20 genes. Furthermore, a homozygous deletion in patient 4-1 was identified which involved five SNPs (rs7113273, rs7109445, rs4936775, rs7121089 and rs11218981), leading to loss of exonic and flanking intronic sequences of exon 2 of *CLMP* (*Coxackie and adenovirus receptor-Like Membrane Protein*, also called *ASAM*, *Adipocyte Specific Adhesion Molecule*). The deletion results in a frameshift and a premature stopcodon. Through PCR and direct sequencing we confirmed that 12483 base pairs were deleted. Direct sequencing of *CLMP* in the other patients revealed more mutations. Patient 1-1 was compound heterozygous, carrying a paternally derived heterozygous frameshift mutation (c.589delA) in exon 3 leading to a premature stopcodon, and a maternally derived heterozygous potential splice donor site mutation (c.1180G>A). In an *in vitro* exon trapping assay, we confirmed that c.1180G>A gives rise to incorrect splicing resulting in a loss of exon 6 (Supplementary Figure 1a). For the WT sequences the exon was trapped, while for the mutant it was not. Patient 2-1 carried a homozygous missense mutation (c.730T>A, p.V124D) in exon 3. This highly conserved missense mutation is predicted to be pathogenic by the programs Russell, Polyphen and SIFT (Supplementary Figure 1b). In patients 3-1 and 3-2 we identified a homozygous deletion (on the array) in the first intron of *CLMP* concerning SNP rs7115102. PCR using primer sets flanking the deletion yielded results in the controls, but no PCR product was detected in the patients (Supplementary Figure 1C). Finally, in patient 5-1, we found a homozygous nonsense mutation (c.1025C>T, p.R222X) in exon 5. The mutations identified are not reported in any of the known SNP databases and are all presumably loss-of-function mutations (Table 1 and Figure 1B), and all were inherited from non-affected heterozygous parents (data not shown). None of the mutations were found in 154 control chromosomes of Caucasian origin.

CLMP expression during human development

As CSBS is a developmental anomaly of the intestine we wondered whether, when and where *CLMP* was expressed in the intestine during human development. Immunostainings on human embryos at 7 and 8 weeks of development (Figure 2A and B) showed that CLMP was highly abundant in the rapidly

dividing cells of the central and peripheral nervous systems, the mesenchyme of the frontonasal and mandibular processes and the dermamyotome, and critically it was expressed in the endodermal derivatives of the fore-, mid- and hindgut and also in the liver, lung, esophagus and trachea. It was less strongly expressed in the prevertebral condensations and extra-embryonic tissues, and the dorsal head mesenchyme. During mid-term fetal stages, 18 and 23 weeks of development (Figure 2C and D), increased immuno-reactivity for CLMP was observed in the intestinal crypts while expression continued to be present in all tissues, with the lowest expression in the muscular and interstitial layers. Mid-term liver and kidney tissues strongly express CLMP in the parenchyma of the lobes and cortex respectively (Figure 2E and F). CLMP was also observed in the collecting ducts and to a lesser extent in the bile ducts and urethra.

CLMP expression was thus seen in the intestine during different stages of human development. As *CLMP* was also expressed in many other tissues, this argues for functional redundancy resulting in a specific function of *CLMP* during intestinal development.

Mutation of *CLMP* abrogated its normal localization at the cell membrane

CLMP encodes for a transmembrane protein belonging to the CTX (cortical thymocyte marker) subfamily of the Immunoglobulin superfamily. It acts as an adhesion molecule and co-localizes with tight junction proteins.[8] In order to determine whether the missense mutation (c.730T>A, p.V124D) affected the normal cell membrane localization, we transfected CHO and T84 cells with pCMV-CLMP-IRES-EGFP constructs. We expressed both the wild-type protein (CLMP-WT) and the mutant protein (c.730T>A, p.V124D, CLMP-mutant). CLMP was localized at the cell membrane when two neighbouring CHO cells expressed the WT protein (Figure 3A). In contrast, the mutant protein was localized in the cytoplasm (Figure 3B). Similar results were obtained in a human intestinal epithelial cell model (T84 cells) (Figure 3C and D). However, expression of the WT protein in a cell that did not have a transfected neighbouring cell resulted in the retention of the protein in intracellular punctate structures (Figure 3E). As CLMP has been shown to co-localize with tight junction markers, we determined co-localization of CLMP with the tight junction marker ZO-1 (zonula occludens 1). Importantly, WT protein showed co-localization with ZO-1, while the mutant protein did not (Figure 3H, I, L and K, see arrows). Overexpression of the WT protein did not alter the localization of ZO-1

(compare Figure 2J with K). Instead, expression of the mutant protein resulted in an increased cytoplasmatic pool of ZO-1 (Figure 2L).

Together these results indicate that CLMP plays a role in tight junctions and that the mislocalization of the mutant protein influences the localization of the tight junction protein ZO-1.

A zebrafish model for Congenital Short Bowel Syndrome

To understand the role of CLMP in intestinal development and gut length determination we decided to generate a zebrafish model. Analysis of the zebrafish genome (Sanger Zv8) revealed two potential zebrafish orthologs of *CLMP* (ENSDARG00000003145 and ENSDARG00000073678) (Supplementary Figure 2). The temporal and spatial expression pattern of both orthologs were determined by *in situ* hybridizaton (Figure 4A). One ortholog (*CLMPa*) was expressed in the intestine specifically at 48 and 72 hours post fertilization (hpf), while the expression of the other ortholog in the intestine was not so pronounced (see Figure 4A, arrowheads). In order to determine whether loss-of-function of *CLMPa* leads to a similar CSBS phenotype in zebrafish as is observed for loss-of-function mutations of *CLMP* in humans, we performed a knock-down experiment of *CLMPa*. We injected a splice-blocking morpholino (SBMO, Supplementary Table 3). A severe, developmental delayed morphant phenotype was seen in more than 60% of the surviving embryos, they were smaller and the length of the intestine was shorter (mean length 2.5 mm and 1.9 mm for WT versus morphant respectively, p=7,0637E-06, n=10 versus n=9). To confirm the specificity of the morpholino we injected two different translation-blocking morpholinos for *CLMPa* (Supplementary Table 3), which induced a similar phenotype (data not shown). A 5-mispair morpholino did not show any phenotype (data not shown), supporting specificity of the translation-blocking morpholino and cytotoxicity was excluded by co-injection of a translation-blocking morpholino for p53 (Supplementary Table 3). Critically, the phenotype was rescued by co-injection of CLMP mRNA with the SBMO (Figure 4B).

Hematoxylin and eosin staining of sections of both 96 hpf control embryos and SBMO-injected embryos showed a gross difference in gut morphology (Figure 4C). Goblet cells, characteristic of the mid-intestine in zebrafish, which resembles the small intestine in humans,[9] were seen in the control embryos but these cells were absent in the SBMO-injected embryos (Figure 4C, see arrowheads). This suggests that loss-of-function of *CLMPa* in zebrafish results in a very maldeveloped and potentially absent small intestine, that resembles the CSBS phenotype in humans.

Discussion

Congenital Short Bowel Syndrome is a gastrointestinal disorder of which the cause and incidence is unknown. Here we report different loss-of-function mutations in *CLMP* in patients with CSBS. The mutations we found presumably result in a loss-of-function due to nonsense mutations (family 5), frameshift/splicing mutations (family 1 and 4) and in mislocalization of the protein due to a missense mutation (family 2). In addition, the missense mutation has an influence on the localization of the tight junction protein ZO-1.

In family 3 we did not find any mutations in the coding sequences of CLMP. We did identify a homozygous deletion concerning SNP rs7115102 in the first intron. We confirmed the presence of this deletion with PCR and we showed that the deletion co-segregates with the disease phenotype in this family (Supplementary Figure 1C). However, we were not able to fine-map the deletion using primers in the flanking region, of which we knew they were present as we were able to amplify these sequences. This made us hypothesize that an inversion might be present explaining the fact that we were not able to amplify the flanking regions. However, using FISH we were not able to identify a large inversion (data not shown), a small inversion cannot be excluded.

To understand how loss-of function of CLMP leads to CSBS, we performed zebrafish experiments. We showed that a zebrafish ortholog *(CLMPa)* was expressed in the intestine at 48 hpf and 72 hpf. Knock-down of *CLMPa* in zebrafish resulted in a very severe phenotype including an affected intestine. A significant reduction of intestinal length was measured in the *CLMPa* morphants. Critically, the absence of goblets cells in the gut of the SBMO-injected embryos indicated that the mid-intestine was not well developed, suggesting that the function of CLMP in the development of the small intestine is conserved. These zebrafish data confirm the phenotype in humans.

Given the wide expression of CLMP during both human and zebrafish development (as shown in Figures 2 and 4A) and the severe phenotype of the zebrafish knock-down, it is intriguing that the phenotype in the human families we studied is so discrete (as the patients we included in our study do not have additional clinical features besides malrotation and intestinal neuronal dysplasia only reported in patients 3-1 and 3-2). This all argues for functional redundancy of CLMP.

As we have shown that loss-of-function mutations of *CLMP* underlies CSBS, we can further speculate on the pathogenesis of this disease. We and others showed that CLMP co-localizes with tight junction proteins. It is known that overexpression of CLMP in CHO cells induces cell aggregation and

overexpression of CLMP in MDCK cells enhances trans-epithelial resistance.[8] Thus CLMP might play a crucial role in tight junctions. As tight junction markers like ZO-1 and its interacting protein ZONAB play an important role in cell proliferation,[10,11] loss-of-function of CLMP may also play a crucial role in downregulation of proliferation of the small intestinal epithelial cells during human development resulting in the CSBS phenotype. As CLMP is also expressed in the small intestine in adults,[8] CLMP might have an important function in adult life too, for example, by playing a role in the elongation process which occurs during life (the length of the intestine in adults is 600 cm on average, ranging from 260 to 800 cm[12]) and in the intestinal adaptation process after surgical resection. The effect on intestinal adaptation of growth factors like growth hormone, keratinocyte growth factor, epidermal growth factor, and glucagon-like peptide-2 on intestinal adaptation has been studied.[13-16] Similar studies will elucidate the role of CLMP in intestinal adaptation in adults and its therapeutic potential.

Table 1 Clinical and molecular data from all Congenital Short Bowel Syndrome patients.

Figure 1 Identification of loss-of-function mutations in CLMP in Congenital Short Bowel Syndrome patients. (a) An overlapping homozygous region (yellow bars) was found in 4 of the 5 patients on the array. A homozygous deletion (pointed out in red bars) concerning exon 2 of *CLMP* was detected in patient 4-1. (b) An overview of *CLMP* with its seven exons and all the identified mutations.

Figure 2 Immunohistochemistry of CLMP on human embryo and fetal tissues shows expression of CLMP in the intestine and in many other tissues.

(**a**) Carnegie stage 15 (*circa* 33-36 dpf), cross-section, dorsal to left (and right, for tail bud). CLMP protein was expressed strongly by all embryonic tissues and the umbilical cord. Panel A'-F': Adjacent sections to Panel A-B and D-F, non-specific immunoglobulin negative controls. (**b**) Carnegie stage 18 (*circa* 44 dpf), parasagittal section, dorsal to right. CLMP protein was abundant throughout the central and peripheral nervous systems, through the endodermal layer derivatives of the fore-, mid- and hindgut including the liver, lung, esophagus and trachea, and in the mesenchyme of the frontonasal and mandibular processes. (**c**, **d**) Cross- and tangential sections respectively of the small intestine and a portion of the large intestine at 18 wd, with increased immunoreactivity in the crypts. (**e**) Liver parenchyme at 21 wd strongly expressed CLMP, which was also present but to a lesser degree in the bile ducts. (**f**) Cross-section of kidney at 23 wd, showing medullocortical expression gradient with more CLMP in the glomerules than the collecting ducts, and only light expression in the urethral smooth muscle.

ao, aorta; bd, bile duct; dpf, days post fertilization; drg, dorsal root ganglion; fn, frontonasal process; h, heart; int, midgut intestinal herniation (arrowheads in B); lu, lung; lv, liver; md, mandible; nt, neural tube; oe, esophagus; rh, rhombencephalon; sc, spinal cord; st, stomach; tb, tailbud; tel, telencephalon; tr, trachea; ua, umbilical arteries; ur, ureter; wd, weeks development. Scale bar: 1 mm.

Figure 3 CLMP-mutant (c.730T>A, p.V124D) abrogated the normal cell membrane localization of CLMP when transiently expressed in CHO and human intestinal epithelial T84 cells. (**a**) CLMP-WT localized to the cell-cell contact area of CHO cells. (**b**) In contrast, CLMP-mutant did not localize at the cell membrane but in the cytoplasm. (**c**) CLMP-WT localized at the cell membrane of human intestinal

epithelial T84 cells. (**d**) While CLMP-mutant did not. (**e**) Expression of CLMP-WT in a cell that did not have a CLMP-expressing neighbor cell caused an intracellular retention of CLMP in punctate structures. (**f**) CLMP-mutant did not show these structures. (**g**) T84 cells do not express CLMP endogenously. (**h)** CLMP-WT co-localized with the tight junction associated protein ZO-1 (compare with **k**, see arrows). (**i**) CLMP-mutant failed to co-localize with the tight junction associated protein ZO-1 (compare with **l**, see arrows) (**j**) Endogenous expression of ZO-1 in T84 cells. (**k**) Expression of CLMP-WT did not visibly alter the localization of ZO-1 (compare with **j**) (**l**) The intracellular expression of CLMP-mutant (shown in **i**) resulted in an increased cytoplasmic pool of ZO-1 that overlapped with CLMP-mutant, but did not inhibit the localization of ZO-1 at the cell membrane (see arrows).

Figure 4 *CLMPa* ortholog is expressed in the intestine of zebrafish embryos and knock-down of this ortholog results in a shortened and maldeveloped intestine. (**a**) 24hpf (I,II), 48hpf (III, IV), and 72hpf (V, VI) whole mount in situ hybridized zebrafish embryos hybridized with either *CLMPa* (I, III, V) or *CLMPb* (II,IV,VI) antisense riboprobes. Arrowheads (I, III, IV, V, VI) indicate intestinal expression of *CLMP* orthologs. (**b**) Effect of *CLMPa* splice blocking morpholino (SBMO) on morphological development. Lateral views of control (I, IV, VII) *CLMPa* SBMO alone (II, V, VIII) and *CLMPa* SBMO plus *CLMPa* mRNA (III, VI, IX) injected embryos at 48hpf (I, II, III), 72hpf (IV, V, VI) and 96hpf (VII, VIII, IX). (**c**) Hematoxylin and Eosin stained parasagittal cross-sections of 96hpf control (I, III and V) and *CLMPa* morphant (II, IV, VI) embryos. Arrowheads (V) indicate goblet cells. Intestinal muscle layer (m) and intestinal epithelia (e) are indicated (V, VI). (**d**) Knock-down of *CLMPa* verified by RT-PCR. Splice-blocking morpholino injected embryos (S) show alternative RT-PCR products compared to the WT embryos (C), meaning that the splice-blocking morpholino targets the exon2/ exon3 junction and thereby induces knock-down of CLMPa. (e) The length of the intestine of the SBMO injected embryos was significantly shorter. All scale bars are 50μm.

Acknowledgements:

We would like to thank the patients and their families for participating in this study. We are grateful to Dr. Arrigo Barabino (Paediatric Gastroenterology Unit, G. Gaslini Institute) for providing details about Italian patients, whose samples were obtained from the "Cell Line and DNA Biobank from Patients affected by Genetic Diseases" (G. Gaslini Institute) - Telethon Genetic Biobank Network (Project No. GTB07001).

References

1. Fitzsimmons J, Chin A, Shepard TH. Normal length of the human fetal gastrointestinal tract. Pediatr 1998;132:80-84.
2. Reiguam CW, Allen RP, Akers DR. Normal and abnormal small bowel lengths: an analysis of 389 autopsy cases in infants and children. Am J Dis Child 1965;109:447-51.
3. Siebert JR. Small-intestine length in infants and children. Am J Dis Child 1980;134:593-595.
4. Huysman WA, Tibboel D, Bergmeijer JH, et al. Long-term survival of a patient with congenital short bowel and malrotation. J Pediatr Surg 1991;26:103-105.
5. Ordonez P, Sondheimer JM, Fidanza S, et al. Long-Term Outcome of a Patient with Congenital Short Bowel Syndrome. J Pediatr Gastroenterol Nutr 2006;42:576-580.
6. Hasosah M, Lemberg DA, Skarsgard E, et al. Congenital short bowel syndrome: a case report and review of the literature. Can J Gastroenterol 2008;22:71-74.
7. Schalamon J, Schober PH, Gallippi P, et al. Congenital short-bowel; a case study and review of the literature. Eur J Pediatr Surg 1999;9:248-250.
8. Raschperger E, Engstrom U, Pettersson RF, et al. CLMP, a novel member of the CTX family and a new component of epithelial tight junctions. J Biol Chem 2004;279:796-804.
9. Ng AN, de Jong-Curtain TA, Mawdsley DJ, et al. Formation of the digestive system in zebrafish: III. Intestinal epithelium morphogenesis. Dev Biol 2005;286:114-135.
10. Balda MS, Matter K. The tight junction protein ZO-1 and an interacting transcription factor regulate ErbB-2 expression. EMBO J 2000;19:2024-2033.
11. Matter K, Balda MS. Signalling to and from tight junctions. Nat Rev Mol Cell Biol 2003;4:225-366.
12. Requam CW, Allen RP, Akers DR. Normal and abnormal small bowel lengths: An analysis of 389 autopsy cases in infants and children. Am J Dis Child 1965;109:447-51.
13. Wales PW, Nasr A, de Silva N, et al. Human growth hormone and glutamine for patients with short bowel syndrome. Cochrane Database Syst Rev 2010;6:CD006321
14. Yang H, Wildhaber BE, Teitelbaum DH. Keratinocyte growth factor improves epithelial function after massive small bowel resection. JPEN J Parenter Enteral Nutr 2003;27:198-206.
15. Kato Y, Yu D, Schwartz MZ. Enhancement of intestinal adaptation by hepatocyte growth factor. J Pedriatr Surg 1998;33:235-239.

16. Martin GR, Beck PL, Sigalet DL. Gut hormones, and short bowel syndrome: the enigmatic role of glucagons-like peptide-2 in regulation of intestinal adaptation. World J Gastroenterol 2006;12:4117-4129.

Table 1 Clinical and molecular data from all Congenital Short Bowel Syndrome patients.

Family	Patient	Ethnicity	Consanguinity	Sex	length small bowel at birth (cm)	Additional features	Mutations
1	1-1	German -American	unknown	Female	30		c.230delA, (p.E77Gfsx24), exon 3 Heterozygous frameshift c.821G>A, exon 6 Heterozygous splice site mutation
2	2-1	Italian	+	Male	Unkonwn		c.371T>A, (pV124D), exon 3 Homozygous missense mutation
3	3-1	Turkish	+	Male	47	Intestinal neuronal dysplasia	Homozygous deletion/inversion in intron 1
	3-2	Turkish	+	Female	unknown	Intestinal neuronal dysplasia	Homozygous deletion/inversion in intron 1
4	4-1	Dutch	unknown	Female	54		Homozygous deletion of 12483 bp (inclusing exon2)
5	5-1	Canadian	unknown	Male	50		c.666C>T (p.R222X), exon 5 Homozygous nonsense mutation
	5-2	Canadian	unknown	Female	unknown		c.666C>T (p.R222X), exon 5 Homozygous nonsense mutation

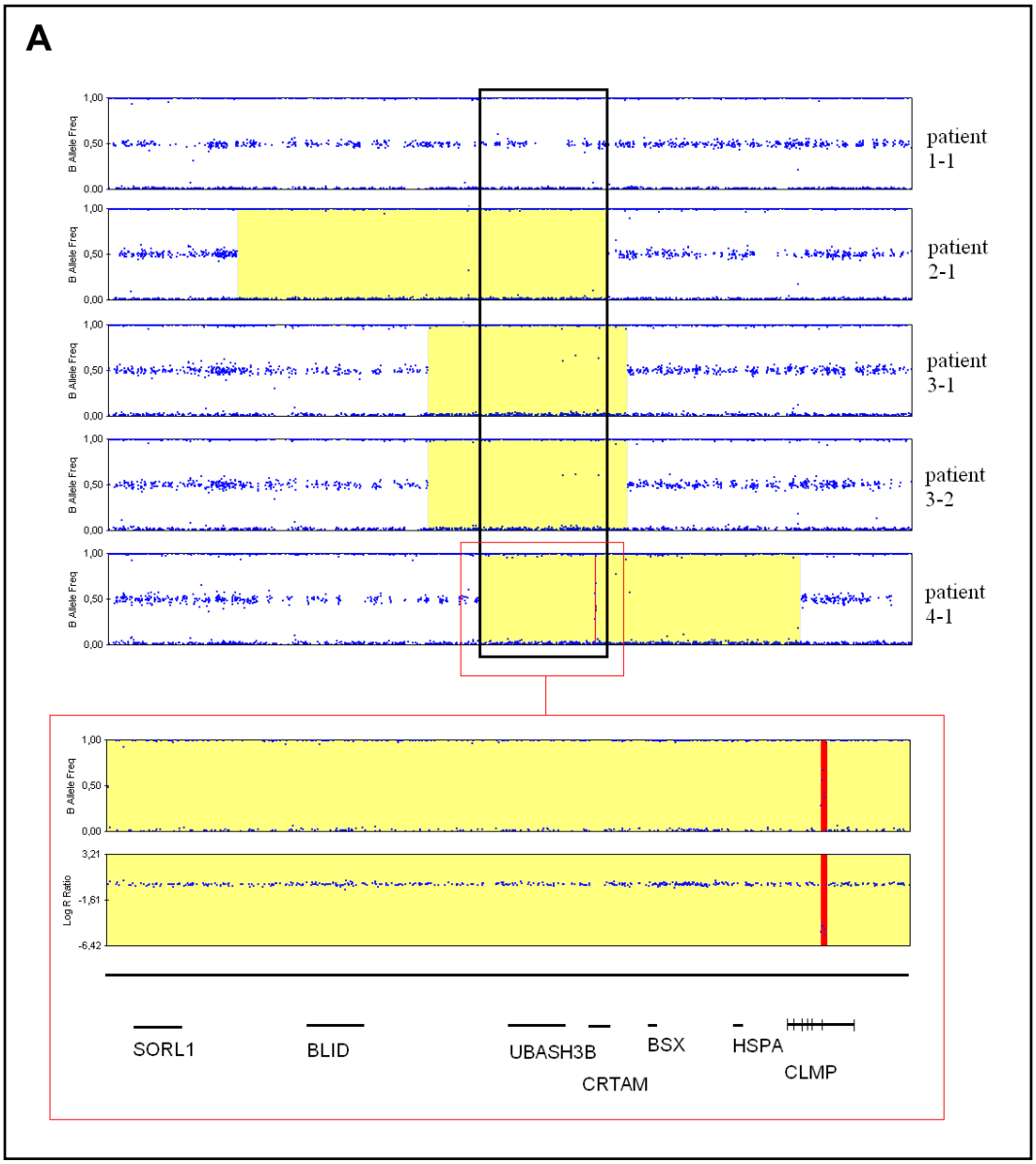
A
B Allele Freq
1,00
0,50
0,00
patient 1-1
patient 2-1
patient 3-1
patient 3-2
patient 4-1
Log R Ratio
3,21
-1,61
-6,42
SORL1
BLID
UBASH3B
CRTAM
BSX
HSPA
CLMP
B
Homozygous p.V124D
Homozygous p.R222X
Homozygous deletion /inversion
Homozygous 12483 bp del.
Heterozygous c.589delA
Heterozygous c.1180G>A
1
2
3
4
5
6
7

Figure 2

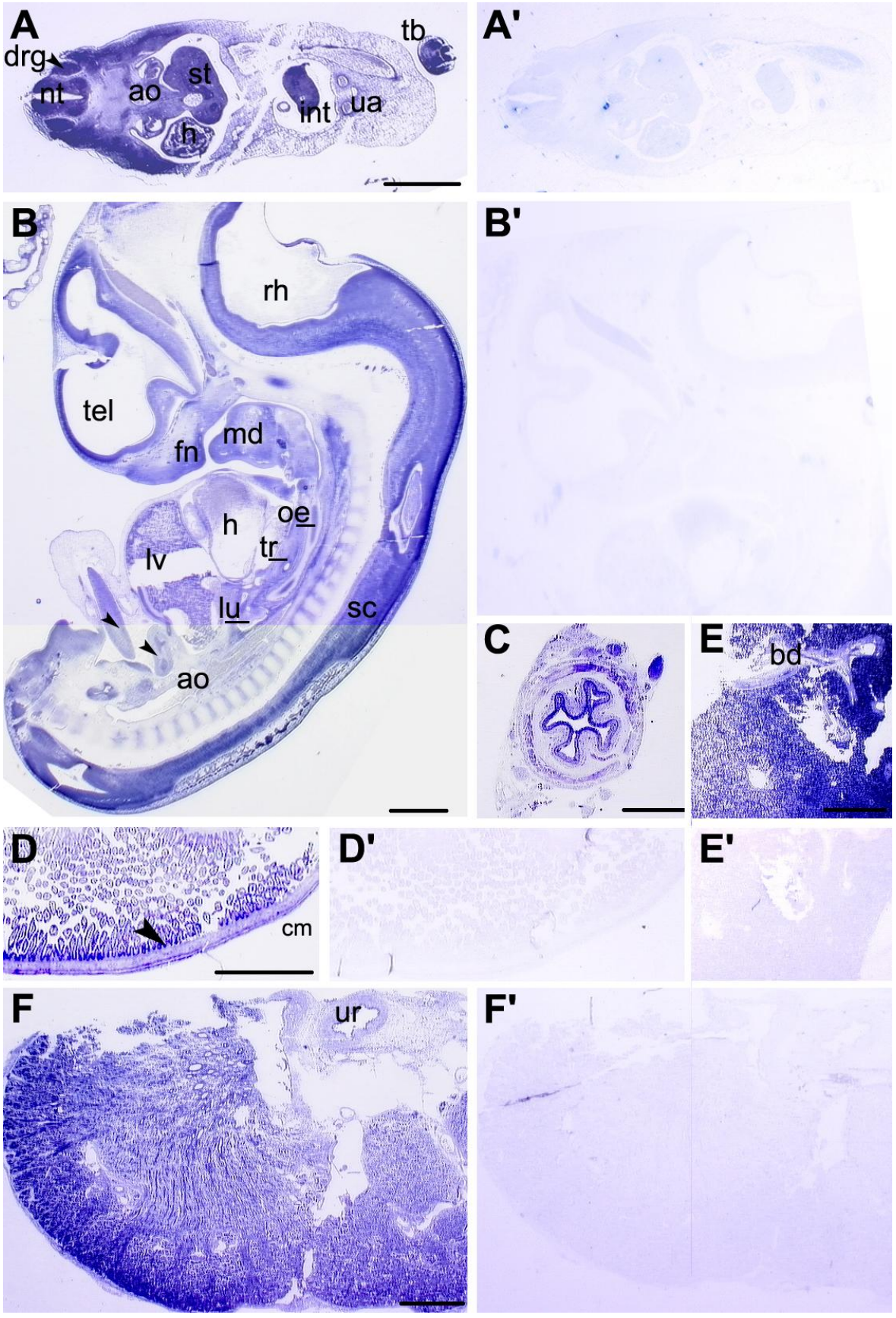

Figure 2

Figure 3

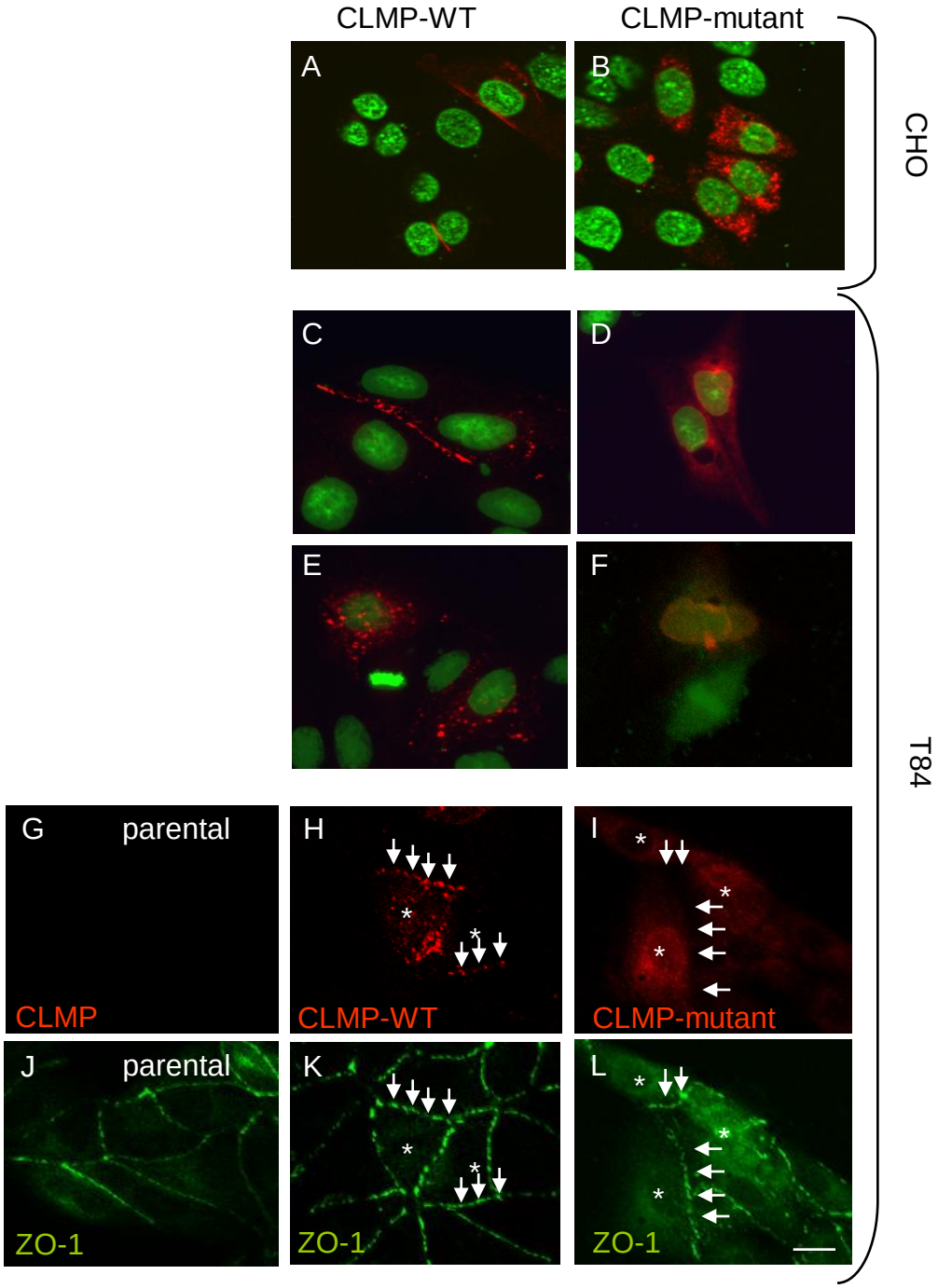
CLMP-WT
CLMP-mutant
A
B
CHO
C
D
E
F
T84
G
parental
CLMP
H
CLMP-WT
I
CLMP-mutant
J
parental
ZO-1
K
ZO-1
L
ZO-1

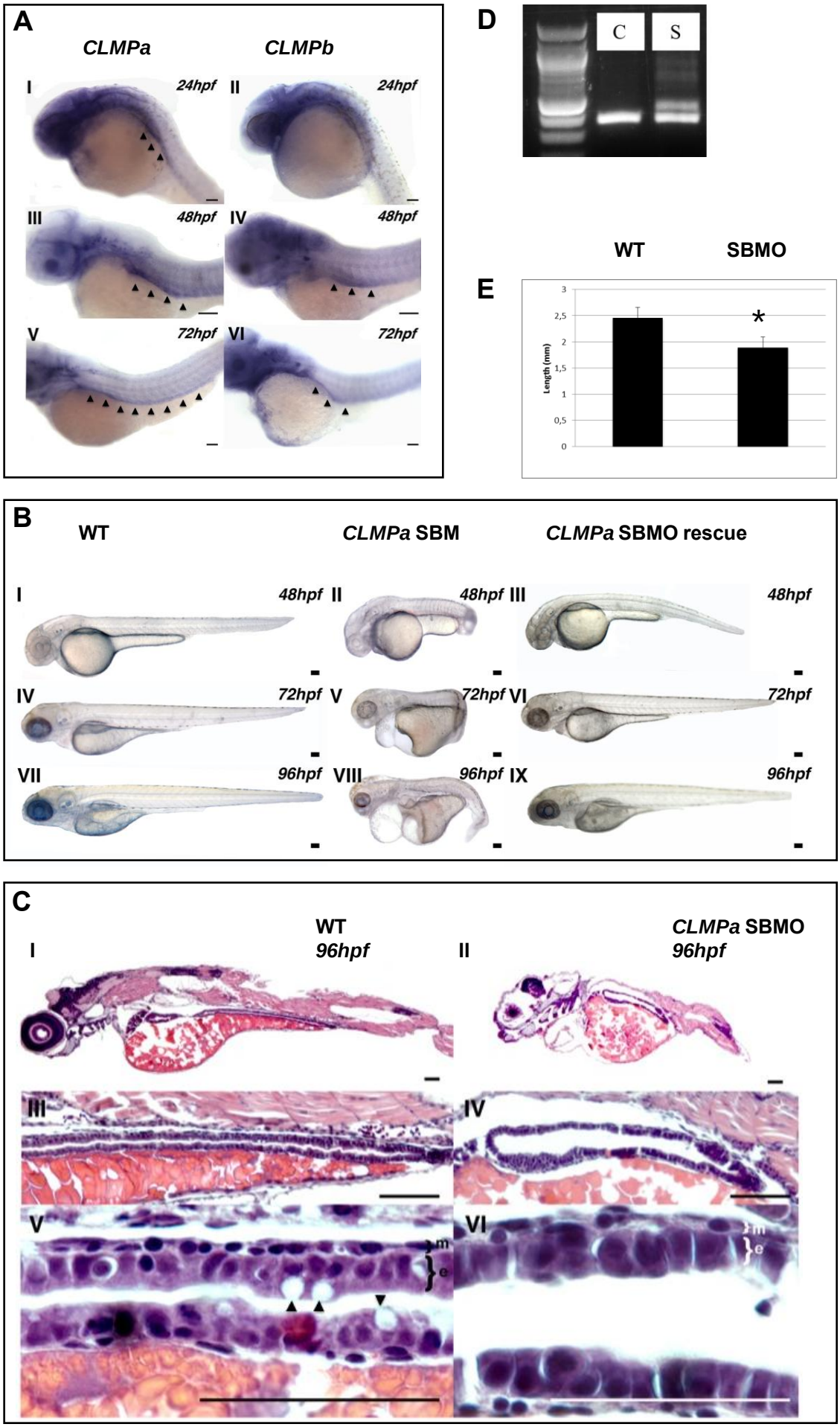
A
CLMPa
CLMPb
I 24hpf
II 24hpf
III 48hpf
IV 48hpf
V 72hpf
VI 72hpf
D
C
S
WT
SBMO
E
Length (mm)
3
2,5
2
1,5
1
0,5
0
*
B
WT
CLMPa SBM
CLMPa SBMO rescue
I 48hpf
II 48hpf
III 48hpf
IV 72hpf
V 72hpf
VI 72hpf
VII 96hpf
VIII 96hpf
IX 96hpf
C
I
WT
96hpf
II
CLMPa SBMO
96hpf
III
IV
V
VI
m
e

Figure 4

Supplementary Online Content

Van der Werf C, Wabbersen T, Hsiao N, et al. Mutations in CLMP cause Congenital Short Bowel Syndrome, pointing to the major role of CLMP in intestinal development.

eFigure 1. Conservation and intronic deletion in family 3.

(a**)** Hek293 cells were transfected with the pSPL3 vector only (V), the pSPL3 vector with the wild type sequence of exon 6 and its flanking sequences (W) and the pSPL3 vector containing the sequences of exon 6 and the presumed splice site mutation (M). The results of the amplification of the cDNA made of the mRNA of these transfected cells using the SA and SD primers are shown. The exon has been trapped in the wild type situation (W), but has not been trapped in the mutated situation (M). This means that the splice site mutation affects the splice donor site so that it is not recognized by the splicing machinery.

(**b**) The missense mutation found in patient 2-1 affects a codon which is evolutionary highly conserved. In the figure it can be observed hat this amino acid and all the surrounding amino acids are coloured red (labelled as good). Good indicates that highly conserved, bad (blue) means not conserved.

(**c**) A homozygous deletion in intron 1 was detected in patients 3-1 and 3-2. Using primers flanking the deletion (forward, 5'-ATTGGAGGATGTGACCTCTGAGTCTTATGG-3' and reverse, 5'-GGCAGAGAAAGTGGGAAACCTATAGTAAGC-3') a PCR product of approximately 5 kb was expected for the normal situation, while for the patients at least 4 kb should be present. PCR yielded results for the parents (f: father, m: mother) as well as for the unaffected sibling (s) and for the control (c), but no PCR product was detected in the patients (p). Lane b is a PCR without adding DNA.

eFigure 2. CLMP alignment for human, rat and zebrafish.

eTable 1. Primer sequences for CLMP mutation analysis

Primer sequences (5'→ 3')			
Exon	Forward	Reverse	PCR product size (bp)
1	AGGAGGCAACCATGTGGTTC	ACAATCTCGATGGCCGACTG	580
2	CACTTGCCCACGGGAACATC	GCCACCACACCCAGCAATAC	443
3	AAGGCAGGCTGAGAGTTACG	CGAGGTGACCTCTGAATGTG	383
4	AAACAGCACCACTGGAGTTG	AATGGCAGTTCAGGAGGTTC	512
5	GCATTACGGAATCTCAGCTCAG	GGCCAGTCAATTGTTGAGTG	402
6	AAACCTGCAAATACTCATTC	AAGTGTTTGTTGAGGATAAG	455
7	TACGAGGAAGCACCTATGAC	GTGACTTGAGCTCCAATGAC	525

PCR conditions: 35 cycles of denaturation at 95°C for 1 minute, annealing at 60°C for 1 minute and polymerization at 72°C for 1 minute.

eTable 2. Primer sequences for side-directed mutagenesis of pCMV6-CLMP-GFP vector

Target	Primer sequence (5'→ 3')	Base pair change	Amino acid change
Forward primer	CGCTACGTGTGGAGCCATGACATCTTAAAAGTCTTAG	T → A	Val125Asp
Reverse primer	CTAAGACTTTTAAGATGTCATGGCTCCACACGTAGCG	A → T	Val125Asp

eTable 3 Morpholino sequences

Morpholino sequences (5'→ 3')	
1st translation blocking morpholino	CGGACTGGGAATCCAACACAAATGT
2nd translation blocking morpholino	CTGCTTTGCTCCTCAAACCGAACAC
5 mispair morpholino	CTcCTTTcCTgCTCAAAgCcAACAC
splice blocking morpholino	GGCACACACCAGCACTCACCACTTT
p53 translation blocking morpholino	GCGCCATTGCTTTGCAAGAATTG

Supplementary Figure 1

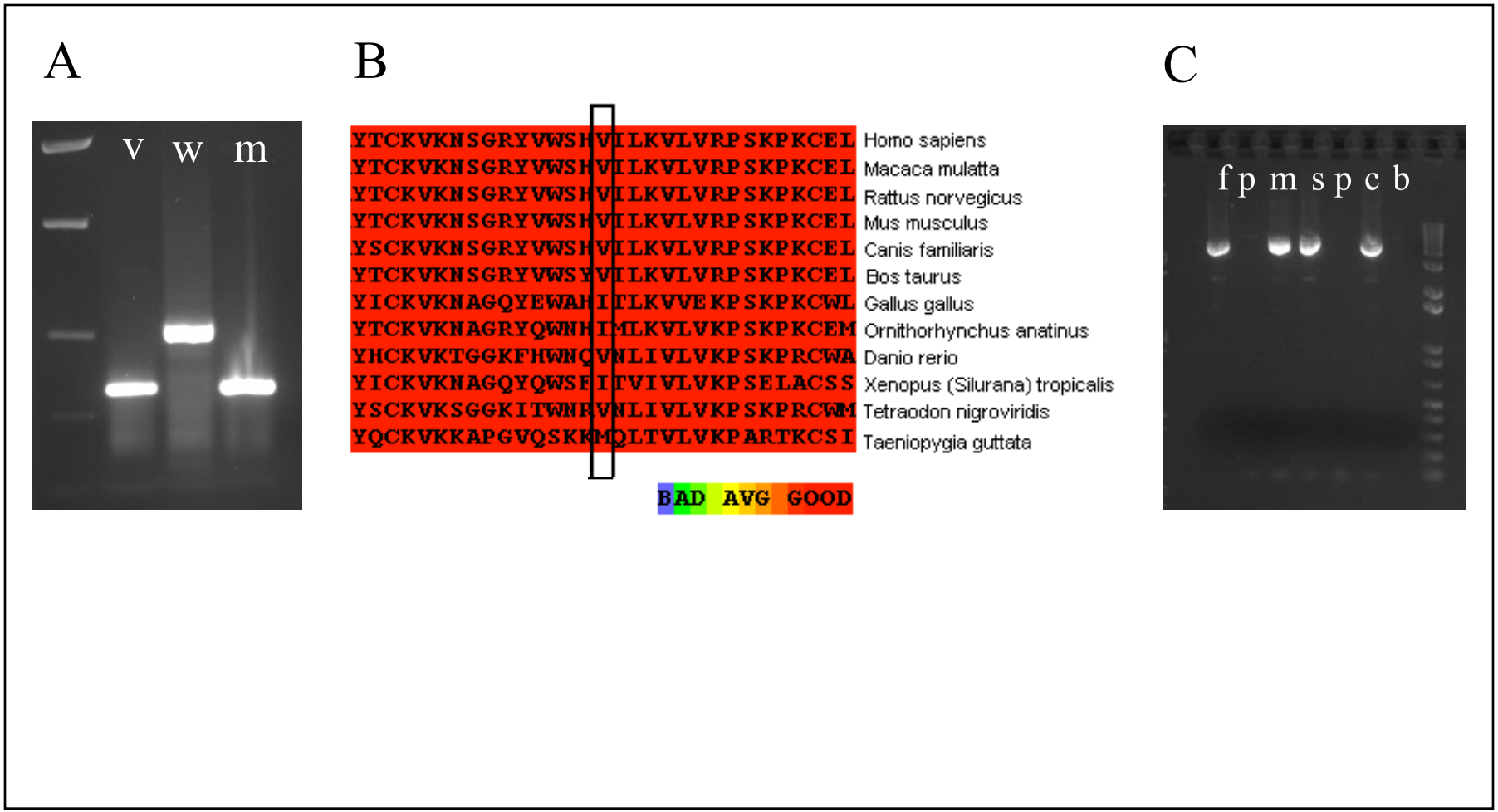

eFigure 1

Supplementary Figure 2

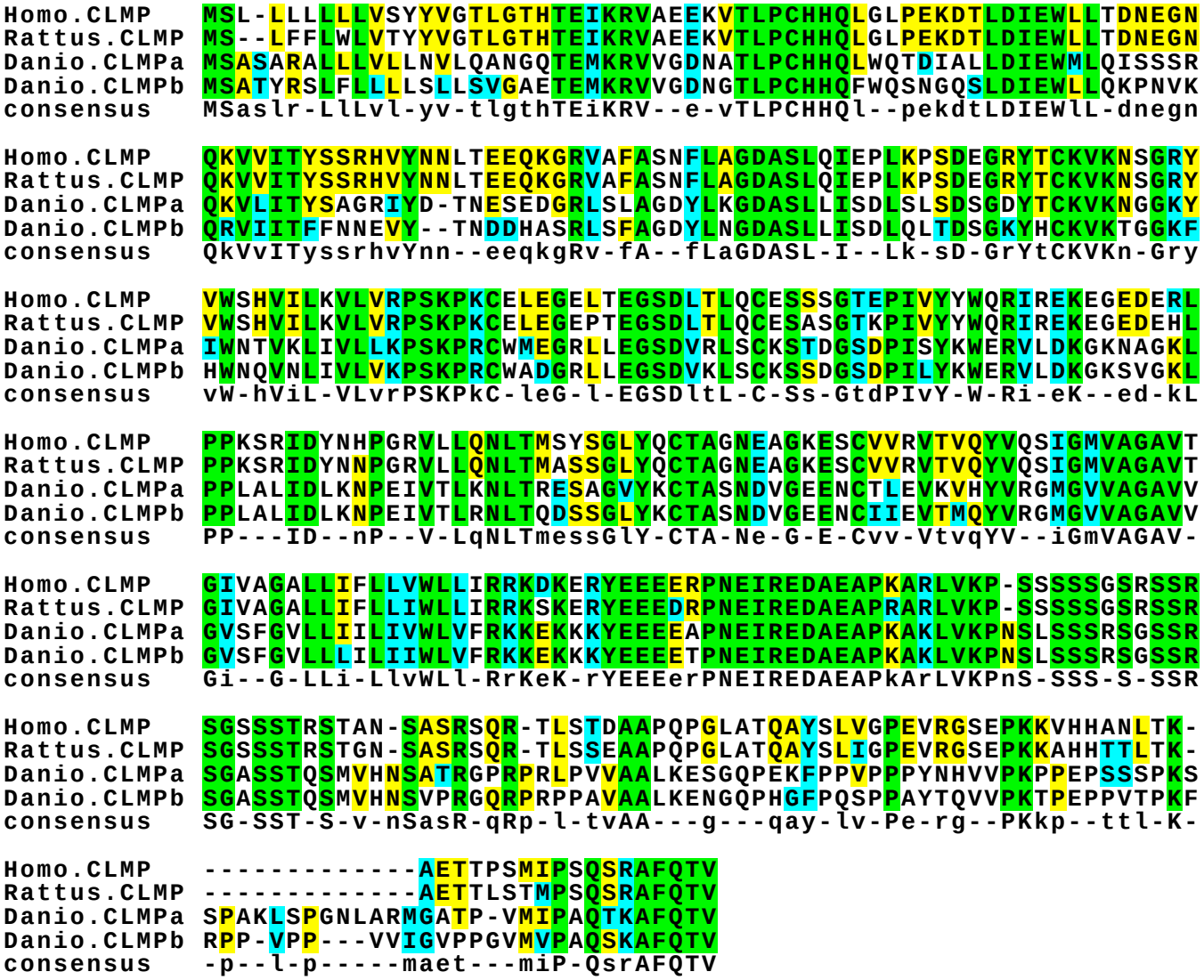

(in Production at Nature Protocols as of 14 June 2011)

Primary culture of chick, mouse or human neural crest cells

Heather Etchevers, INSERM U910, Université de la Méditerranée Faculté de Médecine, Marseille, France

Telephone : +33 491 324 937

Fax : +33 491 804 319

Lab webpage : http://www.zaffranlab.com/

Keywords : neural crest, cell culture, human, mouse, chick, fgf2, egf, stem cell, passage, collagen

Summary

A highly enriched population of neural crest cells from amniote embryos such as chick, mouse and humans is desirable for experiments in fate determination. They are also useful for testing the functional effects of molecular changes underlying numerous human diseases of neural crest derivatives and for investigating their potential for therapeutic compensation. This protocol details embryonic microdissection followed by neural tube explantation. Conditions favoring neural crest cell expansion and the maintenance of their stem cell-like properties are described. While neural crest-like cells can be derived from a number of sites in the mature organism, full potential is best ensured by their purification from their source tissue at the outset of migration. From embryo to established cell line takes four days, with the first day being the most labor-intensive and minimal intervention required thereafter.

Introduction

The neural crest cell (NCC) population is one of the most intriguing in the vertebrate body, because of the wide range of tissue derivatives to which it gives rise, and because of the persistence of some descendants of these embryonic cells in adult tissues that retain at least some of the multipotency of the original population [1]. Many fundamental questions in developmental biology can be addressed by the study of this group of cells: how do intrinsic and extrinsic influences integrate over time to direct their spatially appropriate differentiation? What favors the maintenance of multipotent but partially committed progenitors? Can they be exploited as cell replacement therapies in the many diseases affecting the proliferation and development of NCC-derived tissues or be used for tissue engineering?

Development of NCC culture methods

The lineage of tissue and cell culture techniques can be traced back to the turn of the 19th century, with the seminal contributions of embryologists Wilhelm Roux and Ross G. Harrison to keeping tissues and cells alive *ex vivo* [2,3]. More than a century later, dozens if not hundreds of biologists have made their contributions to the study of NCC in culture, both through testing reagents that have been co-opted from their original use in other cell types [4], and through direct improvement of

methods that augment migration, survival or the determination of conditions in which a reproducible response to exogenous factors could be studied. Early culture of quail NCC established the basic principles of explanting a neural tube enzymatically dissociated from its surrounding tissues to tissue culture ware coated with favorable extracellular matrix components[5]. These dissociation enzymes have varied from trypsin to collagenase[6] to pancreatin[7] and the matrices have included collagen I, collagen IV, fibronectin, and laminin among others[8-11].

It is possible to alter certain cell types from other sources so that they differentiate into a number of standard NCC derivatives, insofar as the markers used and physical location for *in vivo* assays indicate cellular identity. These sources have included tooth pulp[12-14] and periodontal ligaments[15], peripheral nerve sheaths and ganglia[16-18], mouse or human embryonic stem cells[19,20], and even the bone marrow[21].

In particular, a number of groups have concentrated on the possibility of deriving neural crest-like precursors from neonatal[22] and later postnatal [23,24] mammalian skin, more specifically from hair follicles[25] and the dermis thereof[26]. Cells from these sources vary in their differentiation potential, or the palette of derivatives demonstrated was by necessity limited so that their potential is not necessarily comparable. It has yet to be shown that a whisker follicle can yield mesectodermal cells that will integrate into a tooth bud and secrete enamel, but a human trunk-level, terminal hair follicle can yield cells with osteoblast properties[27]. Consistently, trunk NCC in culture, initially distinct, can acquire certain differentiation and molecular properties of cephalic NCC[28,29].

Uses of cultured NCC

Standard uses for NCC include experimental embryology such as mouse-chick chimeras for fate-mapping and phenotypic characterization[30]; clonal analysis in numerous differentiation protocols[7]; examination of the transcriptome and comparison with that of disease states in cancers derived from NCC, such as neuroblastoma, or with other stem cell types [31,32]. Such investigations can easily be extended to include other profiling such as that of genomic or histone covalent modifications, lipids, microRNAs or proteins. Cell behaviors such as migration can be followed using immunocytochemistry and live imaging, and a wide variety of markers have already been tested in these species to differentiate subpopulations within the NCC lines [9,22,33].

Overview of the Procedure

Our group developed the protocol described here in order to study the transcriptome of human primary pluripotent NCC cultures[32], with the idea of favoring a simple, inexpensive matrix if possible and defining the medium so that it would not contain chick embryo extract or leukemia inhibitory factor (a common adjuvant for murine stem cells but unnecessary for pluripotency in human ES cells[34]) and, initially, deriving transcripts before passages. Small adjustments to the culture medium and the absence of irradiated fibroblast feeder cells are the major differences with similar protocols [7,9,35]. The self-renewing potential was unexpected (we kept line N5 cycling for nine months, and have frozen and thawed it and other lines many times). Empirically, we have found this protocol to be equally applicable to the derivation and maintenance of avian, rodent and human NCC, permitting a laboratory that acquires expertise in isolating cell lines from one species to apply the technique for interspecies comparisons or the analysis of experimental chimeras.

In brief, the technique involves microdissection and isolation of a length of embryonic neural tube at stages at or preceding the period of NCC emigration from the desired level. The neural tube is placed on a collagen I-coated tissue culture dish under a meniscus of medium to ensure adhesion and maximal contact, and then fully submerged in a medium that favors proliferation of undifferentiated cells to enable NCC to migrate away from the neural tube. The tube is removed with a customized glass tool, the cells detached and re-seeded at low density into a new collagen I-coated plate. These cells multiply vigorously and are available for further experimentation.

Key features of NCC cultured using this protocol

Under the culture conditions described here, human NCC co-express naturally a number of transcription factors (NANOG, POU5F1, SOX2, MYC)[32] identified as effective for inducing pluripotent stem cells from somatic cell types. Although we have since tried a number of serum substitutes for the maintenance of pluripotency, all have led to morphological or molecular changes in the makeup of the cultured population. However, such substitutes, and the use of human-derived growth factors in the defined medium, may be excellent adjuvants to direct differentiation under controlled circumstances and develop animal-free assays for therapeutic testing.

Although earlier reports have grown avian NCC for short-term cultures, on the order of two-four weeks[29], we have found it possible to maintain avian cells, like their human equivalents, without a fibroblast feeder layer or exogenous immortalization for three months. While we do not have experience with mouse cultures beyond a couple of weeks, reportedly these cannot be maintained beyond 6-10 passages[11] or 3-4 weeks[36], although virally administered Myc-immortalized murine NCC can be maintained for at least six months[37]. Perhaps our conditions favor the continued expression of *Myc* in animal as well as in human primary NCC; this remains to be examined.

Chick NCC, if derived from a pigmented race, sometimes differentiate spontaneously and visibly into melanocytes and alpha smooth muscle actin-containing cells; we believe this has to do with stochastic signals exchanged among densely maintained cells. On occasion, vacuolated cells also can appear in high density cultures of the three species. Otherwise, individual cells in an “immortal” culture of human, chick (and quail) undifferentiated NCC express the sulfated glycolipid recognized by the HNK1 antibody[38,39], the cell adhesion molecule NCAM, and the transcription factors SOX2 and SOX9, and usually some cells begin to grow large and express alpha smooth muscle actin in the population of cultures beyond 10 passages, without full differentiation of the entire population. Full differentiation does happen with greater ease at higher passage numbers or if one of the passages becomes too dense, though. If, after replating, all the cells become large and show actin fibers, visible under phase contrast, or very thin and bipolar, cultures in our conditions go senescent, though they remain viable for weeks without passage. We consider these as “differentiated” (although into what is not clear) and no longer useful as lines. Self-renewing human[32] and mouse[11] cultures express the p75-NTR protein, a less reliable marker for early avian NCC in our hands.

Generally, only a handful of descendant cell types have typically been examined among the wide range of potential tissues to which NCC give rise[1], in part because of the paucity of admissible defining markers and distinct morphologies. It is therefore possible that NCC derived from embryos have more developmental plasticity relative to their descendants or stem cell cousins that have been

conditioned *ex vivo* to give rise to some of the same cell types, and that the former are more representative of an endogenous, baseline phenotype.

Advantages and limitations of this protocol

Key advantages of the protocol described here include:

- Successful cultures are easy to establish and passage
- Inexpensive reagents relative to other derivation techniques
- No cell sorting required
- Relatively defined medium
- No requirement for feeder cells

Key disadvantages of this protocol compared to other culture methods include:

- Isolates a population with clonally varying degrees of potential for proliferation, differentiation and migration
- Clonal analyses do not work well on a collagen I substrate
- Self-renewing primary human NCC lines can be refractory to some differentiation protocols
- Potential variability in primary cultures from individual to individual
- Tendency to senescence increases over passaging, depending on the line

The selection for certain properties by the current culture conditions may prevent the acquisition of others in cells that may otherwise have that potential. For example, immortalized mouse NCC, selected by their expression of p75 and infected with a retrovirus for the stable expression of the *myc* oncogene, do not differentiate into pigmented melanocytes[37] using similar reagents to those in protocols generating these NCC derivatives easily from primary cultures[40,41] or embryonic stem cells[42]. Like these immortal mouse NCC, both human NCC resident in adult niches[14] and embryonic human NCC[32] acquire some molecular markers and morphology of melanoblasts under similar conditions, without completing pigmentation. An additional inconvenience of deriving primary human NCC as opposed to differentiating NC-like cells from hES cells is the necessity to karyotype the anonymously donated embryonic tissue so as to exclude rare but occasional aneuploidies, which are over-represented relative to live births, although high passage numbers may also contribute to their occurrence in the latter[43].

In summary, this is the first detailed protocol describing a successful consensus method to derive primary neural crest cell lines from avian or rodent or human embryos. Cell lines can be maintained for long periods in a self-renewing state, which renders them amenable to a wide variety of studies into molecular function or cellular behavior in response to changes in experimental parameters.

Experimental Design

Pancreatin preparation and optimization: Because powdered pancreatin is not entirely soluble, there may be some variability in lot activity after filtration. A sufficient volume of stock solution

should be prepared and aliquotted by 1 mL at least the day before, and frozen so as to minimize variability from one tube to the next. Digestion that loosens epithelia before dissociating different tissue layers from one another is too harsh and more PBS should be used to dilute the stock; optimal digestion occurs in more than three but fewer than ten minutes. Pancreatin lots should be tested in advance: when the somites fall out intact from between ectoderm and endoderm upon gentle agitation by the forceps, the pancreatin concentration is optimal.

Materials

Reagents

Gestating mice from commercial sources such as Jackson Laboratories [Bar Harbor, ME, USA], Charles River [http://www.criver.com] or Janvier [Genest-Saint-Isle, France]) or fertilized, incubated chicken eggs (EARL Morizeau, Dangers, France). (see Reagent Setup)

> **!CAUTION** Animal embryos must be obtained under controlled conditions in accordance with relevant national and institutional authorities' guidelines and legal regulations for ethical use of animals.

or

Human embryos (see Reagent Setup).

> **!CAUTION** Embryos must be obtained under rigourous conditions of ethical information and consent for participants in biomedical research, and for the control of temperature and cleanliness, in accordance with relevant national and institutional authorities' guidelines and legal regulations. Gloves should be worn at all times and similar precautions to handling and disposing of blood samples should be taken.

Ethanol (70% (vol/vol) and 100%)
Phosphate-buffered saline, without Ca^{2+} or Mg^{2+}
Pancreatin 6 mg/ml in PBS (Sigma-Aldrich, P3292) (see Reagent Setup) **!CRITICAL** Should be prepared in advance; will be slightly turbid.
Fetal Calf Serum (EU Quality) primary human cell culture tested (Promocell, C-37355)
ESC-qualified Fetal Calf Serum (Promocell, C37388) or ESC-qualified FCS 100 mL from PAN Biotech (Dutscher, 500101ES)
DMEM supplemented with Glutamax-HEPES and 4.5 g/L glucose (Invitrogen, 32430027)
F12 supplemented with Glutamax (Invitrogen, 31765027)
Penicillin/Streptomycin (Invitrogen, 15140148)
HEPES buffer 1M (Invitrogen, 15630049)
Hydrocortisone 1 mg (Sigma-Aldrich, H0135) (see Reagent Setup)
Transferrin 10 mg (Sigma-Aldrich, T5391) (see Reagent Setup)
T3 (3,3,5-thio-iodo-thyronine) 1 mg (Sigma-Aldrich, T5516) (see Reagent Setup)
Glucagon 2 mg (Sigma-Aldrich, G3157) (see Reagent Setup)
Epidermal growth factor (EGF) 10 µg (Invitrogen, PHG0314) (see Reagent Setup)
Fibroblast growth factor 2 (FGF) 10 µg (Invitrogen - PHG0024) (see Reagent Setup)
Insulin 50 mg (Sigma-Aldrich, I6634) (see Reagent Setup)
BSA 1 g (Sigma-Aldrich, A8806) (see Reagent Setup)
Trypsin 0.25% (w/v) with EDTA 1 mM in HBSS (eg. Invitrogen, 25200-056)

10x Dulbecco's Phosphate buffered saline (see Reagent Setup)

Complete culture medium (see Reagent Setup)

Enzymatic stop medium (see Reagent Setup) Optionally used to dilute and saturate trypsin-EDTA during cell collection for passages, or to stop pancreatin digestion. Expired lots of complete culture medium can also be used for this purpose.

Freezing medium (see Reagent Setup)

Sterile, tissue culture-grade water
Glacial acetic acid
Colcemid (10 µg/mL N-methyl-N-deacetyl-colchicine) (Roche, 10295892)Optionally used for karyotype analysis of the euploidy of human tissues.

Equipment

Stereomicroscope e.g. Leica MZ 7.5
Swan-neck fiber optic illumination
Stericup GV 0,22 µm de Millipore (Dutscher, 51249)
35 mm dish Collagen I Biocoat (Becton Dickinson, 356456)
100 mm dish Collagen I Biocoat (Becton Dickinson, 354450)
100 mm sterile tissue culture dishes
35 mm sterile tissue culture dishes
Dissecting forceps: 2 pairs Dumont no 5 (Fine Science Tools, 11252-20 or Euronexia SAS)
Perforated spoon (Fine Science Tools, 10370-17)
Microsurgery tools: (**Figure 1a**) CRITICAL: Bake microdissection tools in a dry oven for two hours at 150°C to sterilize. Let cool before use.

- Vannas or Pascheff-Wolff spring scissors (Fine Science Tools 15000-00 or 15371-92)
- Cotton-plugged glass Pasteur pipettes (VWR, 14672-410) (see Equipment Setup)
- Bunsen burner or other butane flame

Steel sterilization box for Pasteur pipettes (VWR, 82027-606)
Rubber bulbs for Pasteur pipettes
Sterile tissue culture hoods – possible use of a horizontal laminar flow for initial set-up (animals only) and vertical flux for human tissues and subsequent passages
Tissue culture CO_2 incubator
Inverted microscope with phase contrast (eg. Olympus CK2)

Reagent set-up

Mouse embryo preparation: To attain the stages listed in Table 1, gestating mice (NMRI or other Swiss-type strains yield numerous embryos per female eg. Janvier, ref. SN-NM-GE-NG) should be plugged 8-10 days earlier.

Chicken embryo preparation: To attain the stages listed in Table 1, freshly laid eggs, stored at 15°C, should then be incubated at 38°C, 60% humidity for 26-55 hours.

Human embryo preparation: Obtaining human embryos is highly dependent on national bioethics laws. Obtaining the necessary approvals and establishing an appropriate protocol for tissue donations can take months if not years of advance work. Once in place, intact human embryos donated after voluntary interruption of pregnancy with the mefiprestone protocol from the fourth-fifth weeks of gestation are best from a cell derivation standpoint, but the aspiration technique sometimes also spares the neural tube and may be more appropriate for studies specifically focusing on the estrogen signaling pathway. Staging is naturally dependent on known days of gestation but on morphological criteria [46]. Transport in sterile RPMI medium at 4°C if possible.

10x Dulbecco's Phosphate-Buffered Saline solution Dissolve into 900ml distilled H_2O: 80 g of NaCl, 14.4 g of $Na_2HPO_4 \bullet 2H_2O$ (or 11.5 g Na_2HPO_4), 2 g of KCl, 2 g of KH_2PO_4. Adjust pH to 7.4 with NaOH or HCl, then the volume to 1 L with additional distilled H_2O. Sterilize by autoclaving. Dilute one part of this solution with nine parts sterile distilled H_2O, to extemporaneously prepare ready-for-use PBS. 10x PBS may be stored for a year at 4-23°C; 1x PBS should be made fresh or stored at 4°C and discarded at the first sign of turbidity.

Pancreatin 4X Make up at 25 mg/mL in 50 mL PBS, dissolve at room temperature (20-23°C) overnight with agitation, centrifuge the remaining deposit, filter-sterilize and aliquot by 1 mL. Store at -20°C. Upon thawing, recentrifuge in a microcentrifuge at maximum speed, then dilute the supernatant with three parts warmed PBS (37°C) for use. Do not keep dilute pancreatin.

Stock solutions of medium additives: It is best to prepare the stock solutions for the medium the day before the embryo dissections, if not earlier, and to make up the working medium the morning of the dissection.

!CRITICAL All solutions and plastic must be sterile and manipulated under sterile conditions when open. Thawed working aliquots should not be refrozen. Concentrations indicated are of the aliquots.

- *Hydrocortisone* (50 µg/mL): Resuspend 1 mg with 1 mL 100% ethanol. Add 19 mL sterile water . Store as 0.2 mL aliquots at -20°C.
- *Transferrin* (10 mg/mL): Resuspend 100 mg with 10 mL sterile water. Store as 0.1 and 1 mL aliquots; keeps up to 12 months at -80°C, up to a month at -20°C, and a week at 4°C.T
- *T3*(2 µg/mL): Resuspend 1 mg with 1 mL NaOH 1M. Add 49 mL sterile water for stock at 20 µg/mL. Aliquot by 1 mL and store at -80°C. To 1 mL T3 stock solution, add 9 mL sterile water.. Aliquot by 20 µL and store at -20°C.
- *Glucagon* (50 ng/mL): add 4 mL 1M acetic acid to 2 mg to dissolve, then 36 mL water . Dilute 10 µL of this stock in 10 mL water; aliquot stock by 1 mL and store at -80°C and 20 µL working solution aliquots at -20°C.
- *Insulin* (10 µg/mL): Add to 5 g powder, 4.95 mL water and 50 µL glacial acetic acid at 10 mg/mL. Dilute 10 µL of this stock into 10 mL water . Stock is stable for 1 year at 4°C, but tolerates freezing.
- *10% (w/v) BSA*: Dissolve 1 g BSA in 9 mL PBS with gentle agitation at 4-25°C overnight, complete to 10 mL and filter-sterilize.
- *FGF* (2.5 µg/mL): Use 4 mL 10% (w/v) BSA solution to dissolve 25 µg FGF. Store aliquots at -80°C.
- *EGF* (10 µg/mL): Use 100 µL BSA solution and 900 µL PBS to reconstitute 10 µg EGF. Store aliquots at -20°C or for up to 2 weeks at 2-8°C.

Complete culture medium In a filter cup combine the following reagents: 12 mL ESC-qualified serum, 34 mL DMEM, 51 mL F12, 1 mL penicillin/streptomycin, 1 mL HEPES, 0.2 mL hydrocortisone, 100 µL transferrin, 20 µL T3, 20 µL glucagon, 10 µL insulin as prepared above. Sterilize under vacuum in vertical laminar-flow hood. Add 1 µL EGF and 8 µL FGF. Store at 4°C. May be kept for up to 2 weeks at 4°C.

Enzymatic stop medium (optional): DMEM or RPMI with 12% fetal calf serum. Kept as long as it is sterile.

Freezing medium: 8 parts complete culture medium, 1 part fetal calf serum and 1 part DMSO (10% (v/v) final concentration); extemporaneous preparation is best.

Equipment Setup

Collagen I-coated polystyrene tissue culture ware: manually coat tissue culture plastic with bovine or rat tail collagen I by diluting cold solubilized collagen with sterile 17 µM acetic acid in water (111 µL glacial acetic acid in 100 mL, filter-sterilized) to 60 mg/mL, and soaking plastic in this solution for two hours at room temperature in a laminar flow hood before rinsing twice in PBS and drying. TROUBLESHOOTING

Fire-polished Pasteur pipettes Place the tip of a glass pipette just above the flame. When the tip begins to close, withdraw from the flame. (**Figure 1b**) This will polish the sharp end of the glass so that tissue will not rasp over the edge when being drawn into the fine part of the pipette. Prepare many ahead of time, place into a metal box or glass jar with gauze cotton pads at the bottom, to prevent breakage, and sterilize in the autoclave. **!CAUTION** Take necessary precautions for operating an open flame on a surface away from inflammable objects and air currents. Wear safety goggles.

Pulled Pasteur pipettes: These should be prepared just before use (step 12 of the Procedure). When it is necessary to remove the neural tube from the culture dish, grasp the cotton end of a pipette in one hand, and the tip in the other, and hold the pipette over the flame at about 4 cm proximal to the tip, rotating to heat all sides. As the glass reddens, remove from flame, quickly pull about 40 cm apart to make a thin thread, let cool an instant, and then break by bringing hands closer in a sharp movement. Bring tip from the larger part back into flame for one second, to round and seal (**Figure 1b**). Place immediately into the laminar flow hood and let cool without touching the tip to a surface. **!CAUTION** Take necessary precautions for operating an open flame on a surface away from inflammable objects and air currents. Wear safety goggles.

Procedure

CRITICAL: Wear gloves and maintain hygienic conditions throughout for the protection of both scientist and cultures, using fresh plasticware when possible, oven-baked instruments and sterile solutions at the outset of each explant series.

> **DAY 1 – Embryo isolation, dissection and culture initiation Timing: approximately 3-4 hours.**

1. Isolate the embryos from extraembryonic tissues and other contaminants. Option A describes isolation of mouse tissue, option B describes isolation of chick embryos and option C describes isolation of human embryos.

Option A: Isolation of mouse embryos:

i. Transfer uterus in ice-cold PBS from animal facility to culture facility.

ii. With the uterus in a 10 cm dish, remove embryos with blunt forceps and scissors from uterus and using a perforated spoon, transfer into a clean 10 cm dish with PBS.

iii. Remove deciduas (**Figure 2a**), amniotic and yolk sac membranes (**Figure 2b**), and transfer embryos into PBS or RPMI in a new dish for initial dissections.

Option B: Isolation of chicken embryos

i. Wipe blunt end of egg with 70% ethanol, and cut a 3 cm diameter hole with dissecting scissors.

ii. Deflect chorion (**Figure 2a**), and use eggshell-free dissecting scissors to cut around embryo, maintaining a corner above the yolk with blunt forceps.

iii. Wet the perforated spoon in PBS, slide between embryo and yolk, and remove to plastic dish with PBS to rinse off any remaining yolk.

iv. Trim close to embryo, cut and remove amnion if present, and change to a new dish with clean PBS or RPMI with spoon or a plastic transfer pipette (**Figure 2b**).

Option C: Isolation of human embryos

i. If karyotyping is to be carried out, remove a few chorionic villi and treat these as described in Box 1 before proceeding with step 1C(ii).

CRITICAL STEP: Keep tissues and solutions cold until dissection.

For karyotyping: Remove a few chorionic villi, rinse in PBS, and treat these immediately for one hour at 37°C in a mix of 2 mL RPMI containing 12% fetal calf serum with 1 mL colchicine stock solution, added extemporaneously. After that time, subject the tissue to a hypotonic shock for 10 minutes in 0.075 M KCl followed by a 1:3 glacial acetic acid:ethanol fixation for 3 changes of 10 minutes each. Spread nuclei, stain for G-bands and count chromosomes as per standard procedures[23].

ii. Remove amniotic and yolk sac membranes with forceps and spring scissors, and transfer embryo into clean RPMI for initial dissections.

!CAUTION Wear gloves at all times for handling human tissues (preferred for animal tissues as well), and incinerate contaminated liquids and plasticware.

PAUSE POINT Multiple embryos can be freed of their annexes and kept in PBS or RPMI on ice for up to two hours with no adverse effects.

2. Isolate neural tube portions from surrounding tissues under the dissecting binocular microscope:

    a. Option A: For cephalic neural crest up to 2-3 pharyngeal arches maximum, insert the Vannas scissors through the lateral part of the oral cavity, pointing caudally through the pharynx, and make one cut on the right and another on the left, down to the level of the heart. Remove the heart tube and the pharyngeal arches with dissection forceps. Place the embryo dorsal face up and make a transverse cut with the Vannas scissors just posterior to the optic vesicles, through the diencephalon, and again at the level of the fifth somite pair. Trim ventrolateral tissues closely to the neural tube.

    b. Option B: For vagal/cardiac NCC, cut a rhombencephalic segment between just caudal to the otic vesicle, down to the third-to-fifth somite.

    c. Option C: For trunk-level NCC, make transverse cuts at the 6th and last somites, or the prospective hindlimb level in older embryos (**Figure 2c**). Trim lateral tissues to the somites (**Figure 2d**).

3. Using a Pasteur pipette, transfer segments into 22-37°C prepared pancreatin in a 35 mm dish.

4. Allow segments to incubate at room temperature for 6-7 minutes. The ectoderm may appear as a thin veil that is detaching from the somites. When the neural tube becomes slightly wavy, it is time to slow the reaction by removing the tubes to clean PBS with minimal transfer of the enzyme solution, using the same Pasteur pipette.

    Critical step Monitor digestion carefully. With experience, the timing is very reproducible at a given stage, species and level of neural tube.

5. Quickly tease away the sticky lateral tissues with fine forceps, without directly touching the neural tube so as not to damage the epithelial integrity of the desired tissue. Peel away the veil of endoderm, then the ectoderm. Lateral movements along the tube (holding to the mesoderm, or to an excess length of neural tube) will detach somites or pharyngeal and head mesoderm easily, to yield a clean neural tube (**Figure 3a**). Lastly, it is possible to grasp an end of the notochord and separate it from the neural tube, which may be maintained against a forcep tip but not pinched between them, thereby carrying some paraxial mesoderm. Transfer cleaned neural tubes to 1 mL complete NCC medium in a 35 mm dish to arrest digestion. TROUBLESHOOTING

Critical step Work quickly during tissue dissociation as digestion continues until transfer to complete medium.

PAUSE POINT Cleaned neural tubes can be kept for up to an hour in enzymatic stop medium at room temperature before transfer to culture dishes.

6. In the tissue culture hood, place 315 µL sterile, complete medium into 35 mm collagen dishes or 6-well plates, one dish/well per explant. Wet the entire surface, but do not scrape collagen with pipette tip so as to maintain optimal adhesion and outgrowth conditions.

7. Bring neural tubes from step 9 into hood. Using a fire-polished Pasteur pipette, carefully draw one neural tube into the opening with some medium. Let the tube fall to the bottom of the liquid within the pipette by gently moving up and down within the thin portion, until it abuts the lower meniscus. Gently appose the tip at a 45° angle to the center of a moistened dish, apply pressure to the bulb, and draw the tip across a few millimeters with a slight lifting movement, to allow tube to be wicked out onto the dish with minimum addition of complete medium. The neural tube will flatten and be pinned under the meniscus at the air-liquid interface.

   Critical step Accompany the neural tube with a few microlitres of liquid or it will stretch and break.

8. Replace cover of dish and place in incubator at 37°C, 5% CO_2 overnight. TROUBLESHOOTING

DAY 2 – Cell migration Timing: 30 minutes.

9. The following morning, warm a 10 mL aliquot of complete medium.

10. Slowly add 1 mL of medium to each explant by moistening first, gently, around the adherent neural tube, and avoiding a strong jet.

11. **Critical step** It is essential that explants remain attached to the substrate, and submerged, otherwise no NCC will migrate onto the culture dishReplace dishes in incubator and allow cells to migrate on undisturbed plates for 24 hours (**Figure 3b**).

DAY 3 – Removal of explant Timing: 30 minutes.

12. Remove the lid from the culture dish and, using a freshly-prepared pulled glass pipette with rounded tip (Equipment Setup and **Figure 1b**), push at one end of the adherent neural tube as if gathering the tissue into the center. It should detach readily, along with any adjacent ectoderm, from the surface, without fragmentation. Push inwards from the other end as well until detached. Tease these epithelia and stray floating debris away from the mesenchymal cells and aspirate the medium, replacing with fresh, complete medium pre-warmed to 37°C. Verify under the inverted microscope that no pieces remain either in the center of the explants or float in the medium, as they will re-attach and spread.

13. Return the dish to the incubator. Cells may be dissociated and re-seeded at this stage, although we see better survival rates if we allow them to continue proliferating for an additional day before first passage. TROUBLESHOOTING

DAY 4 AND BEYOND – Passaging and maintenance Timing: 1 hour

14. To pass cells, remove the medium by aspiration, rinse the culture with sterile PBS pre-warmed to 37°C, and add 0.5 mL (for 35 mm dishes) or 1 mL (for 10 cm dishes) trypsin-EDTA to the dishes. Return dishes to the incubator for 3 minutes. A gentle, lateral shake should show most cells to have detached when examined under the inverted microscope. Do not incubate more than 5 minutes so as to conserve cell viability. TROUBLESHOOTING

CRITICAL STEP: Cells will need to be passed every 2-3 days. They must not be more than 70% confluent unless spontaneous differentiation and arrest of proliferation is desired. Nonetheless, even in highly confluent cultures, some highly proliferative cells often persist and can be amplified at a lower density.

15. Use pipette to add 0.5 or 1 mL respectively, PBS pre-warmed to 37°C, so that the jet of liquid completes cell detachment. Avoid vigorous up-and-down shearing movements of liquid or bubbles that can damage cells.

16. Transfer liquid to a 15 mL conical centrifuge tube, add 10 mL of enzymatic stop medium or PBS, and spin at room temperature at 1,100 *g* for 5 minutes.

17. Aspirate supernatant, and gently resuspend pellet in complete medium with an appropriate volume for the new matrix-coated vessel, using a fire-polished Pasteur pipette.

18. Transfer to new dish and replace in 37°C incubator.

19. Cells may be stored at 5.10^5 cells per mL of cold freezing medium: freeze cryotubes progressively in an isopropanol-filled container at -20°C for two hours, followed by overnight at -80°C and long-term banking over liquid nitrogen vapours.

20. Thaw cells according to standard procedures with a rapid warm-up in a 37°C waterbath, immediate transfer to 10 mL warmed complete medium, centrifugation as per step 21, and resuspension of the pellet in fresh medium. Seeding density for regrowth can be anywhere from 2,000-6,000 cells per cm^2. TROUBLESHOOTING

Troubleshooting

It is not necessary, if working in a clean laboratory environment, to dissect embryos and prepare the neural tube explants in a horizontal flow hood, but it reduces the chances of contamination of the subsequent cultures. One set of polished Pasteur pipettes can be maintained out of the cell culture facility for embryo work. Transfer the neural tubes into freshly-poured medium before bringing into the cell culture facility; we keep expired lots of complete medium for this purpose. Further Troubleshooting advice can be found in Table 2.

Table 2: Troubleshooting

Step	Problem	Possible reason	Possible solution
5	Contamination with non-neural ectoderm	Insufficiently close lateral dissection	Trim tissues closely and cleanly with the spring scissors for successful explantation. Contaminating non-neural ectoderm is easily removed with the neural tube, as it remains epithelial and keeps its integrity *in vitro* (**Figure 2b**); however, as NCC must migrate over it to reach the collagen, many NCC may be removed along with the tube and ectoderm, thereby depleting cultures.
5	Contamination with mesoderm	Insufficient separation of pancreatin-dissociated tissues	Visually inspect neural tubes to be explanted for any adherent mesenchyme and remove with forceps. If endoderm remains, there will surely be mesodermal contamination as well. Mesoderm is more white and opaque than the epithelial neural tube, or the notochord; the endoderm is a sticky veil. For mouse NCC culture, tissues are stickier than human or chick after pancreatin treatment. If the application is for cell tracing after recombination with other cell types, in organotypic culture, in experimental chimeras[30], or simply to determine if there is any contamination by non-NCC, it may be useful to use the B6CBA-Tg(Wnt1-lacZ)206Amc/J mouse developed by the McMahon group[47] and available from Jackson Laboratories. The Wnt1 promoter activates lacZ expression in all premigratory NCC of the posterior cephalic, vagal and trunk lineages.
8	Neural tube wicks to side of 35 mm dish upon transfer	Liquid sloshing pushed the tube from under the meniscus to the edge	It is possible to replace the tube in the middle of the dish using the same gesture without damage. Maintain horizontal during transfer to incubator.
13	Few or no NCC migrate	1. The explants may be too dry. 2. The staging may not be appropriate for the neural tube level explanted. 3. The collagen substrate is uneven on the culture plastic. 4. The neural tube was not in close apposition to the plastic the first night and did not adhere	1. If the air circulation does not bring enough humidity to the early explants, one must place each 35 mm dish in a 10 cm dish (or perhaps many into a larger, clean recipient) with sterile, wet gauze in the larger plate, before incubating. 2. Dissect a more caudal piece of neural tube or the same level but from a younger embryo. 3. Neural crest cells migrate happily on collagen I-coated plates. Reduce variability in coating by using commercially produced coated 35 mm plates for explantation; for precious cell cultures, we continue to use commercial ware for subsequent passages as well. 4. Ensure that the neural tube does not detach upon addition of medium on Day 2. Empirically, hundreds of neural crest cells

			migrate away from avian neural tubes (chick or quail) while human and mouse neural tubes yield 60-150 cells for equivalent length fragments.
14	Trypsinization damages cells	1. Adherent chicken, mouse and human NCC all secrete other extracellular matrix factors. If the cells are approaching confluence, they can sometimes be refractory to detachment after trypsin treatment. 2. The trypsin may have been warmed then refrigerated more than a couple of times.	1. Pass cells at a lower density 2. Aliquot trypsin-EDTA by 10 mL, freeze at -20°C and use within a week of thawing, or use the trypsin-like enzyme in the TrypLE-Express formulation by Invitrogen (12604-013) which remains active after repeated heat-cool cycles.
20	Cells do not proliferate	1. Loss of growth factor activity. 2. Contamination. 3. Unknown additives. 4. Differentiation.	1. Supplement the basic medium (DMEM and F12) and use it within two weeks, otherwise necessary factors may no longer be bioactive. Other brands of culture media work well, if the catalogue references used here are unavailable. 2. Cell cultures should be checked for bacterial or yeast contamination, and if the problem persists, then mycoplasma may also be an issue. A standard PCR-based test (Sigma-Aldrich, MP0035) should yield results quickly. In our hands, this has never been a problem, but we check cultures for mycoplasma at each freeze and thaw, and periodically in the facility. 3. Serum lots vary and should be tested. We have successfully tested multiple lots for chicken NCC proliferation and survival for later use with human cells. Serum substitutes have not given as satisfactory results to date but do often promote survival, and on occasion differentiation. 4. Some cells change morphology over time, with the majority favoring an elongated, thin spindle shape or a large, stellate form with visible polymerized actin fibers under phase-contrast illumination. These cells will continue to proliferate for some time but will stop after a certain number of passages. However, if all the stem cells have been depleted, the entire culture will survive for months, even at low cell density, but no longer divide.

Anticipated results

The neural tube should be adherent to the bottom of the 35 mm plate by 4-16 hours after explantation, but no cells will have migrated away from the tube. After 8-10 additional hours fully

submerged, the first cells begin to emerge, and a partial or full halo of cells should be visible by 24 hours, as illustrated in **Figure 3** and elsewhere[32].

Once regular passaging is established, it is possible to move cultures into collagen-coated flasks, which reduces the possibility of contamination. We have successfully cultured chick and human cells on flasks as large as 150 cm^2.

Cells can be prepared for immunostaining by fixation in 4% paraformaldehyde for 20 min and, if appropriate, subsequent permeabilization for 25 min with 0.1% Tween-20 in PBS. **Figure 2b** shows immunocytochemistry with the HNK1 antibody (which does not require permeabilization). At the stages of NCC derivation, among the three potential cell types in the initial explants, HNK1 specifically labels a sulfated glycolipid on adhesion molecules present on avian and human NCC, but does not work on murine NCC. p75 is a preferred marker for mouse and rat NCC (and also works for human NCC, though signal can be low).

Best results for RNA isolation are obtained by adding 350 μL lysis buffer directly to a 35 mm dish, or 1 mL to a 10 cm dish, directly after removal of medium, and spreading and lysing with a cell scraper. We have used this approach to isolate total RNA and examine the transcriptome of multiple human NCC lines, both cephalic and trunk-level, which are remarkably similar to each other in their profiles[31,32] and distinct from multipotent precursors isolated from human embryonic dorsal root ganglia and cultured in the same medium (unpublished).

Like other primary cell cultures, it is possible to inefficiently transfect the cells using transitory transfection techniques (calcium phosphate or lipid-based [35] or electroporation [unpublished]). Precise conditions remain to be optimized. We have not attempted selection for stable transfectants, although this will be one of the more interesting uses of human cells: to compare molecular and phenotypic changes between normal hNCC and their equivalents carrying various mutations identified in human neurocristopathies or neural crest-related cancers such as neuroblastoma and melanoma[48].

References

1. Le Douarin, N. & Kalcheim, C. *The Neural Crest*. (Cambridge University Press: Cambridge, U.K., 1999).

2. Roux, W. Beiträge zur entzicklungsmechanik des embryo. *Zeitschrift fuer Biologie* **21**, 411 (1885).

3. Harrison, R.G. The outgrowth of the nerve fiber as a mode of protoplasmic movement. *Journal of Experimental Zoology* **9**, 787-846 (1910).

4. Pannett, C.A. & Compton, A. The cultivation of tissues in saline embryonic juice. *The Lancet* **203**, 381–384 (1924).

5. Sieber-Blum, M. & Cohen, A. Clonal analysis of quail neural crest cells: they are pluripotent and differentiate in vitro in the absence of noncrest cells. *Dev Biol* **80**, 96-106 (1980).

6. Smith-Thomas, L.C. & Fawcett, J.W. Expression of Schwann cell markers by mammalian neural crest cells in vitro. *Development* **105**, 251-62 (1989).

7. Baroffio, A., Dupin, E. & Le Douarin, N.M. Common precursors for neural and mesectodermal derivatives in the cephalic neural crest. *Development* **112**, 301-5 (1991).

8. Boot, M.J. et al. Spatiotemporally separated cardiac neural crest subpopulations that target the outflow tract septum and pharyngeal arch arteries. *Anat Rec* **275**, 1009-18 (2003).

9. Morrison, S.J. et al. Prospective identification, isolation by flow cytometry, and in vivo self-renewal of multipotent mammalian neural crest stem cells. *Cell* **96**, 737-49 (1999).

10. Perris, R. et al. Molecular mechanisms of neural crest cell attachment and migration on types I and IV collagen. *J Cell Sci* **106**, 1357-1368 (1993).

11. Stemple, D.L. & Anderson, D.J. Isolation of a stem cell for neurons and glia from the mammalian neural crest. *Cell* **71**, 973-85 (1992).

12. Karbanová, J. et al. Characterization of Dental Pulp Stem Cells from Impacted Third Molars Cultured in Low Serum-Containing Medium. *Cells Tissues Organs* **193**, 1-22 (2010).

13. Miura, M. et al. SHED: stem cells from human exfoliated deciduous teeth. *PNAS* **100**, 5807-12 (2003).

14. Stevens, A. et al. Human dental pulp stem cells differentiate into neural crest-derived melanocytes and have label-retaining and sphere-forming abilities. *Stem Cells Dev* **17**, 1175-84 (2008).

15. Coura, G.S. et al. Human periodontal ligament: a niche of neural crest stem cells. *J Periodontal Res* **43**, 531-6 (2008).

16. Kruger, G.M. et al. Neural crest stem cells persist in the adult gut but undergo changes in self-renewal, neuronal subtype potential, and factor responsiveness. *Neuron* **35**, 657-69 (2002).

17. Li, H.-Y., Say, E.H.M. & Zhou, X.-F. Isolation and characterization of neural crest progenitors from adult dorsal root ganglia. *Stem Cells* **25**, 2053-65 (2007).

18. Coulpier, F. et al. Novel features of boundary cap cells revealed by the analysis of newly identified molecular markers. *Glia* **57**, 1450-7 (2009).

19. Lee, G. et al. Isolation and directed differentiation of neural crest stem cells derived from human embryonic stem cells. *Nat Biotech* **25**, 1468-75 (2007).

20. Kawaguchi, J. et al. Isolation and propagation of enteric neural crest progenitor cells from mouse embryonic stem cells and embryos. *Development* **137**, 693-704 (2010).

21. Nagoshi, N. et al. Ontogeny and Multipotency of Neural Crest-Derived Stem Cells in Mouse Bone Marrow, Dorsal Root Ganglia, and Whisker Pad. *Cell Stem Cell* **2**, 392-403 (2008).

22. Sviderskaya, E.V. et al. Functional neurons and melanocytes induced from immortal lines of postnatal neural crest-like stem cells. *FASEB J* **23**, 3179-92(2009).

23. Biernaskie, J.A. et al. Isolation of skin-derived precursors (SKPs) and differentiation and enrichment of their Schwann cell progeny. *Nat Protoc* **1**, 2803-12(2006).

24. Wong, C.E. et al. Neural crest-derived cells with stem cell features can be traced back to multiple lineages in the adult skin. *J Cell Biol* **175**, 1005-15(2006).

25. Sieber-Blum, M. et al. Pluripotent neural crest stem cells in the adult hair follicle. *Dev Dyn* **231**, 258-269(2004).

26. Fernandes, K.J.L. et al. A dermal niche for multipotent adult skin-derived precursor cells. *Nat Cell Biology* **6**, 1082-93 (2004).

27. Clewes, O. et al. Human Epidermal Neural Crest Stem Cells (hEPI-NCSC)-Characterization and Directed Differentiation into Osteocytes and Melanocytes. *Stem Cell Rev* (2011). doi: 10.1007/s12015-011-9255-5

28. Abzhanov, A. et al. Dissimilar regulation of cell differentiation in mesencephalic (cranial) and sacral (trunk) neural crest cells in vitro. *Development* **130**, 4567-79 (2003).

29. McGonnell, I.M. & Graham, A. Trunk neural crest has skeletogenic potential. *Curr Biol* **12**, 767-71 (2002).

30. Fontaine-Pérus, J. & Chéraud, Y. Mouse-chick neural chimeras. *Int J Dev Biol* **49**, 349-53 (2005).

31. de Pontual, L. et al. Epistasis between RET and BBS mutations modulates enteric innervation and causes syndromic Hirschsprung disease. *PNAS* **106**, 13921-6 (2009).

32. Thomas, S. et al. Human neural crest cells display molecular and phenotypic hallmarks of stem cells. *Hum Mol Genet* **17**, 3411-25 (2008).

33. Lahav, R. et al. Endothelin 3 selectively promotes survival and proliferation of neural crest-derived glial and melanocytic precursors in vitro. *PNAS* **95**, 14214-9 (1998).

34. Dahéron, L. et al. LIF/STAT3 signaling fails to maintain self-renewal of human embryonic stem cells. *Stem Cells* **22**, 770-8 (2004).

35. Wakamatsu, Y. et al. Regulation of the neural crest cell fate by N-myc: promotion of ventral migration and neuronal differentiation. *Development* **124**, 1953-62 (1997).

36. Hu, Y.F., Zhang, Z.-J. & Sieber-Blum, M. An epidermal neural crest stem cell (EPI-NCSC) molecular signature. *Stem Cells* **24**, 2692-2702 (2006).

37. Rao, M.S. & Anderson, D.J. Immortalization and controlled in vitro differentiation of murine multipotent neural crest stem cells. *J Neurobiol* **32**, 722-46 (1997).

38. Terayama, K. et al. Cloning and functional expression of a novel glucuronyltransferase involved in the biosynthesis of the carbohydrate epitope HNK-1. *PNAS* **94**, 6093-8 (1997).

39. Bakker, H. et al. Expression cloning of a cDNA encoding a sulfotransferase involved in the biosynthesis of the HNK-1 carbohydrate epitope. *J Biol Chem* **272**, 29942-6 (1997).

40. Ito, K., Morita, T. & Sieber-Blum, M. In vitro clonal analysis of mouse neural crest development. *Dev Biol* **157**, 517-25 (1993).

41. Garcez, R.C. et al. Epidermal growth factor (EGF) promotes the in vitro differentiation of neural crest cells to neurons and melanocytes. *Cell Mol Neurobiol* **29**, 1087-91 (2009).

42. Pla, P. et al. Ednrb2 orients cell migration towards the dorsolateral neural crest pathway and promotes melanocyte differentiation. *Pigment Cell Res* **18**, 181-187 (2005).

43. Campos, P.B. et al. Chromosomal spread preparation of human embryonic stem cells for karyotyping. *JoVE* (2009). doi:10.3791/1512

44. Theiler, K. *The House Mouse: Atlas of Embryonic Development*. (Springer-Verlag: New York, 1989).

45. Hamburger, V. & Hamilton, H.L. A series of normal stages in the development of the chick embryo. 1951. *Dev Dyn* **195**, 231-72 (1992).

46. O'Rahilly, R. & Müller, F. *Developmental Stages in Humans: including a revision of Streeter's "Horizons" and a survey of the Carnegie collection*. (Carnegie Institution of Washington: Washington, D.C., 1987).

47. Echelard, Y., Vassileva, G. & McMahon, A.P. Cis-acting regulatory sequences governing Wnt-1 expression in the developing mouse CNS. *Development* **120**, 2213-24 (1994).

48. White, R.M. et al. DHODH modulates transcriptional elongation in the neural crest and melanoma. *Nature* **471**, 518-22 (2011).

Acknowledgements

In addition to all the authors who have developed neural crest culture protocols referenced herein and to the directors of INSERM U781 and U910 who have made it possible for me to obtain embryonic tissues over the years, I extend my particular gratitude to Elisabeth Dupin, Corinne Glavieux-Pardanaud, Andréa Gonçalves-Trentin, Sophie Thomas, and Catherine Ziller for aiding me in optimizing conditions.

The author declares that she has no competing financial interests.

Table 1. A comparison of the developmental stages which are optimal for preparing neural crest cultures from chicken, mouse or human embryos. Stages are taken respectively from the Hamburger-Hamilton (HH), Theiler and Carnegie series, respectively. h, d = hours or days of gestation.

Species	**Stages for cephalic NCC**	**Stages for cardiac/vagal NCC**	**Stages for trunk-level NCC**
Chick	HH8-10 (26-38h)	HH9-11 (30-45h)	HH11-16 (40-55h)
Mouse	Theiler 12-13 (8.0-8.5d)	Theiler 13-14 (8.5-9.0d)	Theiler 14-16 (9.0-10.0d)
Human	Carnegie 11-12 (23-28d)	Carnegie 12-13 (25-28d)	Carnegie 12-14 (25-32d)

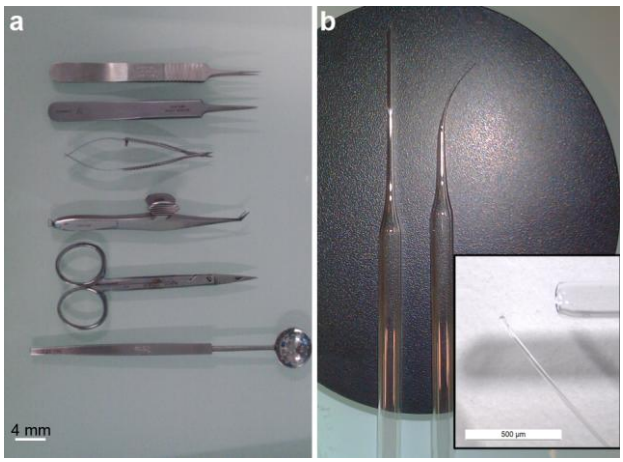

Figure 1

Some of the equipment required for this protocol. (**a**) Recommended microsurgery tools and (**b**) custom-made glass tools for neural tube and cell transfer, straight, or for detaching the explants after neural crest migration without scratching the dish, curved. Inset: magnification of the tips.

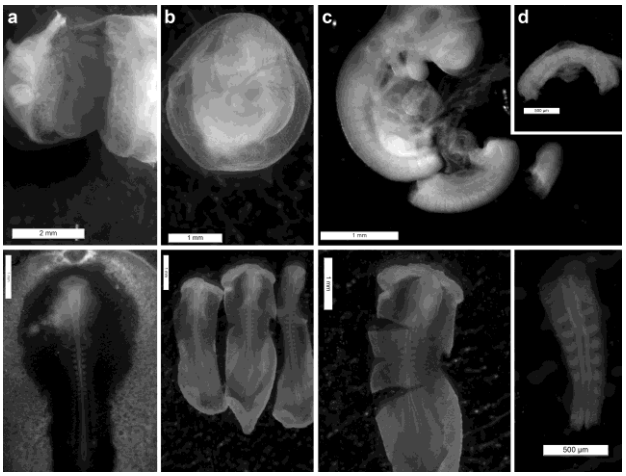

Figure 2

Dissection of neural tube fragments from mouse and chick for explantation. Top = mouse (human is very similar[32]); bottom = chick. (**a**) Remove embryo from large decidua or egg yolk. (**b**) Cut away from yolk sac and amnion. (**c**) Select segment to dissociate in pancreatin (trunk above, cardiac/trunk below). (**d**) Cut away lateral tissues before beginning dissociation.

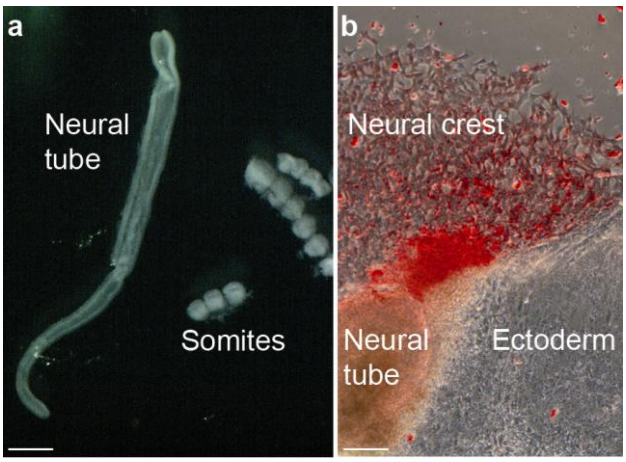

Figure 3

Examples of explanted neural tubes. (**a**) Pancreatin-cleaned human neural tube and detached somites before placement of tube in culture for NCC derivation. Bar = 0.4 mm. (**b**) Quail trunk-level neural tube and ectoderm explant after step 11. Superposition of phase-contrast photo and HNK1 immunohistochemistry in red fluorescence, to distinguish neural crest cells from other tissues. The HNK1-negative neural tube and epithelial ectoderm have not yet been removed, on the lower left and right, respectively, while the neural crest cells fan away from the explant. Better initial yields can be obtained from explants free of attached ectoderm. Bar = 120 µm.

Submission date: 01 June 2011

Accepted date: 10 June-2011

Topic header: Prevention & Epidemiology (PRE)

Meeting report from the 2011 International Expert Meeting on Large Congenital Melanocytic Nevi and Neurocutaneous Melanocytosis, Tübingen

Sven Krengel[1,*], Helmut Breuninger[2], Mark Beckwith[3] and Heather C. Etchevers[4]

[1] Dermatological Group Practice, Moislinger Allee 95, 23558 Lübeck, Germany
[2] Surgical Dermatology, Universitätsklinikum Tübingen, Liebermeisterstraße 25, 72076 Tübingen, Germany
[3] Nevus Outreach, Inc., 600 S. Delaware Ave., Suite 200, Bartlesville, OK 74003, USA
[4] INSERM U910, Université de la Méditerranée, Faculté de Médecine d'Aix-Marseille II, 27 boulevard Jean Moulin, 13005 Marseille, France

* Corresponding author

Abstract

An unconventional symposium on the subject of pathogenetic, clinical, and therapeutic aspects of large and giant congenital melanocytic nevi and neurocutaneous melanocytosis, was held at the University of Tübingen, Germany, on May 6-7, 2011. Exchanges were made between physicians from a wide range of clinical disciplines, including pathology, dermatology, plastic and pediatric surgery, neurosurgery, pediatric neurology and genetics; basic scientists in cell and developmental biology; psychologists; and an unprecedented gathering of international patient advocacy group representatives. This diversity of outlooks brought fresh perspectives to the discussions about current scientific and therapeutic advances in the field of these rare congenital diseases and their oncogenic associations. A roadmap for future actions sketched out promising therapeutic developments to follow and fostering of interdisciplinary collaboration among all the involved parties.

Running title: Report from 2011 International GCMN/NCM Meeting
This is an Accepted Article that has been peer-reviewed and approved for publication in the *Pigment Cell & Melanoma Research*, but has yet to undergo copy-editing and proof correction. Please cite this article as an "Accepted Article"; doi: 10.1111/j.1755-148X.2011.00875.x

Introduction

Nearly 150 participants from 14 countries participated in the multidisciplinary 2011 Expert Meeting for large and giant congenital melanocytic nevi (GCMN) and neurocutaneous melanocytosis (NCM). Congenital cutaneous nevi with a projected adult diameter of over 10 or 20 cm are considered “large” or “giant”, respectively (Ruiz-Maldonado 2004). Neurocutaneous melanocytosis is a neurological disorder characterized by abnormal aggregations of nevomelanocytes within the central nervous system, in conjunction with a GCMN. It can be asymptomatic or present as variably severe and progressive neurological impairment, sometimes resulting in death (Kadonaga & I J Frieden 1991; Burstein et al. 2005). Affected GCMN or NCM patients and their families are faced with psychosocial difficulties, complex therapeutic management decisions, and the risk of neurological problems and malignant degeneration (Krengel, Hauschild & Schafer 2006; Slutsky et al. 2010). The goal of this conference was to enrich a traditional academic exchange by actively encouraging the participation not only of the speakers but of the audience, in order to inform each about relevant advances in fields they may not otherwise follow and to accomplish tangible group measures. To attain this goal, we held moderated but informal discussions after each talk, extended restorative periods during which speakers and physician trainees mingled with an often unwittingly excluded type of expert – representatives of patient advocacy groups from around the world, and final summary and brainstorming sessions. The conference was conducted in English but there were enough multilingual participants to facilitate comprehension and exchange.

Twenty-one speakers from Germany, Switzerland, France, the United States, Great Britain, and Israel contributed to the scientific programme (Table 1). A parallel and

coincident programme was attended by patient association delegates from these same countries as well as Portugal, Spain, the Netherlands, Macedonia and Australia, for most of whom this was the first opportunity to network in person with analogous groups. As an important result of this meeting, the patient associations committed to supporting and encouraging their members to participate in a single worldwide GCMN/NCM registry, and to spearhead an Internet-based, multilingual and curated GCMN/NCM patient information portal through which patients and researchers can access the registry.

Molecular, cell and developmental biology

In his keynote lecture, *Miguel Reyes-Múgica* (Pittsburgh) reviewed a few of the wide range of diseases that are grouped under the term “neurocristopathies”. These pathologies include neuroblastoma, the most common malignant solid extra-cranial tumor of children; Hirschsprung disease, a deficiency in the development of the enteric nervous system; and different forms of cutaneous and neurocutaneous melanocytic disorders (Etchevers et al. 2006). Because of the endogenous migratory aspect of neural crest cell (NCC) behaviour during embryonic development, the still images seen by pathologists of melanocytic proliferations must be placed in a dynamic context. For example, the concept of “Abtropfung” that has enjoyed a certain vogue for over a century, where (G)CMN would mature from the predominant localization of melanocytes in the epidermis down into the deeper layers of the skin, has been fully discredited by both histological observations and recent findings that melanocytic precursors normally reside in the dermis, the meninges and along peripheral nerves. From these locations, they can not only give rise to pigmented nevi but also to sometimes extremely bulky proliferations that may resemble

neurofibromas, rhabdomyosarcomas or malignant melanoma without necessarily presenting all the canonical features (Cajaiba et al. 2008). Defining new cytogenetic and histological markers for these GCMN-associated tumors will help determine their prognosis and optimal treatment.

Because invasive and proliferative behaviour is a normal characteristic of NCC, understanding the effects of timing and embryonic context is crucial to discovering the molecular bases of isolated and syndromic forms of GCMN. *Heather Etchevers* (Marseille) in her talk about signaling pathways in neural crest and early melanocyte development, addressed the dynamic expression of some of the molecules involved in pigment cell fate specification. The temporal progression of melanocyte differentiation mobilizes signaling cascades well known for their later implication in carcinogenesis. These include tyrosine kinase receptors such as KIT and MET and their intracellular effectors of the RAS and RAF families and alternative second messenger pathways; influences from the melanocortin 1 receptor MC1R; and transcriptional control exerted in particular by SOX10 on the master pigment cell transcription factor, MITF (Sommer 2011). Preliminary data demonstrated the persistence of unpigmented, Sox10+ Kit+ precursors in both follicular and dermal locations throughout avian skin development, long after the onset of epidermal pigmentation.

Bernhard Wehrle-Haller (Geneva) presented both contextual and novel results about the role of the membrane-bound isoform of Kit ligand (mb-KitL) in the control of the biological properties of melanocytes (Paulhe et al. 2009). Essential, soluble KitL is secreted during development by the embryonic dermamyotome, past which melanoblasts migrate during their maturation. In addition to maintenance signaling, a

dimerized, membrane-bound isoform appears to serve as a mechanical anchor for hematopoietic stem cells in their bone marrow niche (Heissig et al. 2002). Results presented in this talk demonstrated that melanocyte stem cells and potentially within GCMN as well adhere to their niche through mb-KitL/Kit complexes, and that certain protein domains of this complex can be susceptible to enzymatic cleavage, leading to shedding. Disrupting the interaction of Mb-KitL and Kit is therefore being examined as a potential therapeutic strategy for pigmentary proliferative disorders.

In his comprehensive lecture on cytogenetic alterations and *BRAF*/*NRAS* mutations in GCMN, *Pierre Heimann* (Brussels) emphasized that, in contrast to malignant melanoma, chromosomal abnormalities are rather rare and single in GCMN. He described his group's findings that many more *NRAS* mutations are observed in GCMN, than in medium-small and acquired nevi, where *BRAF* mutations are predominant. Among the few GCMN with involvement of *BRAF*, gain-of-function was shown to arise through chromosomal translocation that removed the auto-inhibitory N-terminal regulatory domain of *BRAF* from its protein kinase domain (Dessars et al. 2007). Other mutations involving *BRAF* regulatory domains represent an alternative mechanism of RAS-MAPK pathway activation in GCMN that harbor neither a *BRAF* nor an *NRAS* coding mutation. Comparison of the transcriptomes of nevocytes to normal melanocytes demonstrated GCMN upregulation of many genes involved in the DNA damage response, and in particular stronger expression of the *CDNK2A* $p16^{INK4A}$ transcript, likely leading to the cellular senescence most often observed in GCMN (Dessars et al. 2009).

In his opening address on the genetics of GCMN, *Rudolf Happle* (Freiburg) presented arguments supporting the hypothesis that GCMN represent a superimposed mosaic

manifestation of a polygenic trait. Cases of GCMN are very often associated with multiple smaller melanocytic nevi involving the entire body, some congenital and some acquired during early childhood. These small nevi should no longer be termed “satellite nevi”, but Dr. Happle would rather call them “disseminated background lesions”. At an early developmental stage, loss of a wild-type allele or a postzygotic mutation at a predisposing gene locus may give rise to a segmental distribution of descendant cells, on an inherited background of the same or an additional predisposing gene locus. The proposed concept would predict that family members of patients with GCMN should show increased numbers of small melanocytic nevi, but this question has so far not been investigated systematically, although some epidemiological work hints at this result (Danarti et al. 2003). In addition, the distinction between small and GCMN, and congenital and acquired, may not be so much at the level of the type of mutation but rather a question of its timing in the melanocyte lineage.

Veronica Kinsler (London) discussed phenotypic and genetic characteristics of patients with GCMN. More than a third of affected individuals present with positive family history of any sized CMN, and 10% with a family history of adult-onset melanoma. The comparison of a cohort of 222 patients with two independent control cohorts showed that children with GCMN and their parents exhibit certain phototypic characteristics (red hair and freckling in patients and first-degree relatives) significantly more often than the control groups. Accordingly, children with GCMN of over 60 cm diameter projected adult size, which largest size category covaries with the presence of more than 50 additional disseminated nevi, demonstrated highly increased frequencies of common variant alleles in *MC1R*. These alleles were not confined in a mosaic pattern to nevus skin, implying a predisposing rather than a

cumulative somatic event in this cohort. At the phenotypic level, the examination of facial features in children with GCMN by experienced dysmorphologists showed interobserver confirmation of typical facial characteristics. Moreover, Dr. Kinsler presented as yet unpublished results that indicate changed hormone levels in some children with GCMN, correlated with effects on longitudinal growth, body mass index and premature thelarque (onset of breast bud growth in girls) in certain individuals. Taken together, the results presented show a tendency to other measurable phenotypic traits in the GCMN patient population, all potentially caused by the same underlying genetic variations, and leading to the proposal of the term “CMN syndrome”.

Clinical management of GCMN and melanoma risk

In a comprehensive kickoff lecture, *Ashfaq Marghoob* (New York) asserted that there is insufficient evidence in the literature to recommend strongly for or against surgery on the basis of risk for developing melanoma. While the main impetus for the prophylactic excision of GCMN stems from the knowledge that the relative risk for developing melanoma in GCMN is high, the absolute risk for developing melanoma in association with GCMN is low (range, 0-10%, thought to be somewhere in the middle). Each GCMN patient requires a tailored management plan based on the size, thickness, nodularity and location of the nevus, as well as on its potential psychosocial impact and the age of the person seeking treatment (J. Slutsky et al. 2010). Aspects of all these recommendations were taken up and discussed by many of the following speakers and audience members throughout the meeting. Dr. Marghoob recommended palpation for the detection of tumors in the deep layers of the skin that are not detectable through dermoscopy, and brought up the provocative observation that as yet, there have been no reports of malignant melanoma in

“satellite” (disseminated) CMN. As far as other intralesional tumors, he reports cases with diagnosed rhabdomyosarcoma, melanosarcoma/-blastoma, spindle cell or nevoid carcinoma, and one associated with neuroblastoma. Absolute risk for neurocutaneous melanocytosis as well as oncogenic associations increases with CMN size and the numbers of disseminated nevi in a linear, rather than a dichotomous, fashion.

For those patients opting for surgical intervention, the treatment should attempt to reduce the risk of developing cutaneous melanoma while simultaneously optimizing aesthetic and functional outcomes. Dr. Marghoob discussed work in preparation for publication in which three-quarters of respondents preferred their surgical scar over their original nevus because the scar was felt to be more socially acceptable, but urged the audience to also assist the other quarter of their patients who regretted surgery by associating psychological accompaniment with the management plan.

Alon Scope (Sheba) focussed on the use of non-invasive, *in vivo* imaging techniques in the evaluation of pigmented skin lesions for the early detection of melanoma. Dermoscopic structures that can be observed within CMN include milia-like cysts, terminal hair, perifollicular pigmentary changes, globules and network-like areas. Reflectance confocal microscopy (RCM) allows the examination of skin lesions at a cellular-level resolution. With dermoscopy and RCM, effective imaging depth is limited to the papillary and upper reticular dermis and thus these methods are recommended for the evaluation and monitoring of small to medium CMN that are relatively flat and superficial (Brooks et al. 2011). In larger CMN, particularly ones that are elevated, thick or nodular, dermoscopic and RCM evaluations are less likely to be informative. Nonetheless, these techniques allow the dermatologist to undertake a

kind of gross pathology at the bedside and avert unnecessary surgical interventions for many cases.

One precondition for a proper assessment of GCMN-associated melanoma risk and characteristics is to compare with the full range of melanomas from a similar age group. *Sven Krengel* (Lübeck) summarized current knowledge about childhood cutaneous melanoma (ChM). The incidence of ChM is 3 per million per year for children under the age of 14, and 2 per 100,000 per year for adolescents between 15 and 19 years of age (SEER database). For comparison, adults in northern latitudes have incidences of 12-15 per 100,000 per year. Clinically, ChM - unlike the prevailing adult superficial spreading type - often present as nodular, pedunculated, or amelanotic lesions, sometimes simulating pyogenic granuloma. Diagnostic uncertainty is worsened by the fact that the histological demarcation from Spitz nevi is notoriously tricky. Lymph node metastasis is more frequent in children and may occur in cases of atypical, but often benign pediatric melanocytic tumors. Regarding overall survival, children with melanoma starting before puberty generally have a better prognosis than older children. Only 20% of ChM develop in contiguity to a congenital nevus, and only 3% are intralesional to a GCMN. Melanoma in GCMN tends to arise from deeper tissue layers and often presents with a dedifferentiated, small-cell type histomorphology (“melanoblastoma”) (Krengel, Hauschild & Schäfer 2006). Dr. Krengel presented preliminary results from a systematic literature review indicating that *fatal* melanomas in GCMN predominantly arise in early infancy (median, 2 years), and mostly affect children with multiple disseminated nevi.

Proliferative nodules in GCMN are rapidly growing masses that clinically and histopathologically simulate melanoma. *Jürgen Bauer* (Tübingen) reviewed the

patterns of chromosomal aberrations occurring in proliferative nodules associated with melanocytic lesions. As demonstrable by comparative genomic hybridization arrays using DNA from paraffin-embedded tissue (a technical advantage over karyotyping of biopsies), proliferative nodules mostly show only numerical aberrations in atypical cellular foci. Melanoma, on the other hand exhibits complex profiles with both numerical and structural abnormalities. In comparison, Spitz nevi display typical numerical aberrations only in particular chromosomes. The combination of histopathologic and cytogenetic criteria represents a highly specific means to distinguish proliferative nodules in GCMN from nevus-associated melanoma (Bastian et al. 2002).

Alain Taïeb (Bordeaux) presented his perspective on future therapeutic modalities for the treatment of GCMN and neurocutaneous melanocytosis (NCM). Spontaneous disappearance of pigment cells is observable in certain cases of melanocytic nevi, melanoma, and vitiligo. The study of these phenomena may therefore enable the development of non-surgical approaches to treating pigmented proliferations. Recent evidence suggests that a specific autoimmune/inflammatory response is triggered in vitiligo by CD8+ T-cell responses to certain tyrosinase variants (Jin et al. 2010). These variants, much like the haptenation of tyrosinase effected by the depigmenting agent monobenzone (van den Boorn et al. 2011), enhance immune surveillance, in contrast to melanoma-associated variants. This presentation stimulated speculation about the role of excess nevomelanocytes in the hair cycle, as follicles can be crowded, the cycle accelerated and the terminal hair in CMN of any size, coarser and darker. Discussion then turned to the chemotherapeutic use of RAS, RAF or mTOR inhibitors in the treatment of neurocutaneous melanocytosis.

Neurocutaneous melanocytosis

Neurocutaneous melanocytosis (NCM) is a rare neurocutaneous syndrome defined by the presence of three or more CMN in conjunction with pigmented deposits in the central nervous system (CNS), either meningeal melanocytosis or CNS melanoma. *Yasmin Khakoo* (New York) gave us an advance look at her group's study of central nervous system abnormalities in children with NCM. In a retrospective review of NCM referrals to the pediatric neurology service at the Memorial Sloan Kettering Cancer Center between 2003 and 2010, fourteen NCM patients were identified, of whom eight are still alive. Diffuse leptomeningeal deposits or confirmed meningeal melanoma were associated with most of the deceased cases. While more than a third of the living patients remained asymptomatic at last evaluation, the mean age of presentation of neurological symptoms such as epilepsy and hydrocephalus was before two years of age. Other observations in these NCM patients include a Dandy Walker malformation, a benign spindle cell tumor, dorsal arachnoid cysts (three patients who have been asymptomatic and stable over time, but are under three years old), and three patients with profound developmental delay. NCM can be associated with hamartomous-like disruption of the underlying neuronal architecture.

Marcos Tatagiba (Tübingen), in his presentation of neurosurgical approaches to melanocytic neoplasms of the central nervous system, highlighted difficulties in determining the malignant potential of any given melanocytic tumor of the leptomeninges of the brain or the spine (Rades et al. 2001). The neutral denomination "meningeal melanocytoma" reflects the spectrum of these tumors of intermediate to low malignant potential, somewhere between melanoma and nevus; transformation from a named melanocytoma to a malignant CNS melanoma has been described. Spontaneous, circumscribed tumors most frequently occur in the

posterior fossa, Meckel's cave, and the thoracic spinal cord, where normal extracutaneous melanocytes congregate, and are usually identifiable by magnetic resonance imaging due to their melanin content. Neurological deficits are mainly caused by compression of neural structures. Whenever possible, complete tumor resection should be performed; a video of one such intervention was projected. Postsurgical radiation therapy is strongly recommended based on a retrospective review of all published cases.

Surgical options for GCMN treatment

Newly developed surgical techniques used for large skin defects after severe burn wounds, as well as reconstructive procedures after burns, can partially also be applied to children with giant congenital nevi. *Clemens Schiestl* and *Thomas Biedermann* (Zürich) in their joint talk, presented recent developments from their multidisciplinary team in skin tissue engineering. The application of a sophisticated two-layered autologous skin substitute to children with burn wounds is at an advanced stage of clinical testing. It presents the advantages of a non-cross-linked collagen hydrogel dermal equivalent, which is rapidly revascularized, and growth in a custom silicon transplant chamber to obtain particularly large surfaces (Braziulis et al. 2011). With the help of illustrative cases, advantages and limitations of this method for the treatment of children with GCMN were presented.

On a case-by-case basis, complete excision of a GCMN may be impossible. *Rainer Rompel* (Kassel) presented his experience with hundreds of patients for whom dermabrasion and/or curettage were safe and effective means to reduce the nevomelanocytic load of the epidermis and upper dermis, in order to improve surveillance (Rompel et al. 1997). Due to optimal wound healing and incomplete

maturation of the skin structure at this age, the procedures are best performed from the 6th week of life and completed, if iterative, in the first year. An experienced interdisciplinary team of dermatological surgeons, pediatricians, and anesthesiologists, is crucial for the success of this method. The ablative Erbium YAG laser can be a therapeutic alternative for difficult locations such as eyelids, ears, and the genital area. Recurrent pigmentation after dermabrasion is often observed, especially in smaller or facial nevi, and in older patients, but is preferable to the potential hypertrophic scarring that can accompany deeper ablations. Dermabrasion may be combined with full-thickness excisional strategies. Some discussion was held about a compensatory effect dermabrasion might induce in remaining nevus cells; however, among the handful of reports of melanoma arising in hundreds of dermabraded GCMN, they were found between two and twenty years following intervention.

Helmut Breuninger (Tübingen) presented results from 60 children with GCMN treated by early serial excisions and natural enforced skin expansion. A high tension technique (“power stretching”) with intracutaneous double butterfly sutures, after extensive loosening of the adjacent nevus-free skin, was developed to close long wounds. This surgical procedure takes advantage of the small absolute size and the high skin elasticity of the first years of life. For a total of 204 excisions (mean, 3.5 per child), a good aesthetic and functional outcome was achieved in most of the cases by this sutural reinforcement (Rothfuss et al. 2009).

In his keynote lecture, *Bruce Bauer* (Chicago) USA, demonstrated his results with the use of more than 2,300 tissue expanders in over one thousand patients with GCMN, with a follow-up as long as 30 years. This vast experience has led to clear regional

considerations in the choice of expander size, flap design, and sequence of procedures. Expanded transposition and rotation flaps are preferable over advancement flaps for many reconstructions (Bauer & Corcoran 2005). Weekly expansion over 11-12 weeks is typical. Using an internal remote port allows outpatient filling of the expander(s) in most of the cases, and a case was made for parental education and involvement in this procedure. Tissue expansion is the “workhorse” treatment modality for scalp and forehead nevi and for GCMN of the trunk. Nevi that cross multiple facial units may require combination with full-thickness skin grafts or serial expansions. Expansion of the extremities is limited by the geometry and the difficulty of moving flaps in an axial direction. In GCMN of the upper extremity, large expanded flaps from abdomen/flank/back can provide optimal aesthetic and functional treatment. Free tissue transfer, and expanded pedicle flaps offer unconventional but effective means of dealing with GCMN of the lower extremity. Regulatory restrictions on the availability of certain preferred expanders across continents were lamented during the discussion, and osmotic expanders not recommended until speed of filling can be better regulated.

Better clinical indicators and diagnostic markers in the future will enable more doctors and their patients to be comfortable with the proactive choice of no further surgical intervention when the decision is based on risk of transformation. However, interventions may still play an important role in the psychological growth of affected children. For this reason, an interdisciplinary surgical plan should be broached in the first months of life, taking in account all established therapeutical methods.

Patient and family initiatives in medical research and psychosocial management

In her keynote address about the psychosocial situation of children with GCMN and their families, *Ornella Masnari* (Zürich) presented preliminary results from the "Stigmatization in children and adolescents with facial burns or birthmarks" project (http://bit.ly/Stigma-study). Data were obtained from a cohort of 91 children between 9 months and 16 years with facial burns, port-wine stains, hemangiomas or GCMN, through standardized interviews with 31 affected children and adolescents over the age of seven, and from 83 parental reports, using standardized questionnaires. A large majority of the interviewed children had received expressions of pity, been stared at or drawn unwanted attention, and more than one-quarter reported outright hostile behaviour from other children. Parental descriptions of stigmatizing experiences encountered by their children underestimated numbers of occurrences, but significant associations were found in both child and parent groups between social rejection and increasing age or size of the facial lesion, and not with gender. Of children who did not report feeling stigmatized, these were better adjusted than the norm for age-matched children without facial marks, while fully half of the stigmatized children demonstrated behavioural problems. Both physicians and patient representatives confirmed these findings after the presentation. They discussed how much to adjust the child physically, as opposed to adjusting the psychological support provided to parents and indirectly or directly to the children, or to adjusting negative attitudes in society at large with media campaigns. In particular, there is currently little followup from parents to whom psychological counselling is recommended. Perceived control over a birthmark may be less than over a scar due to a medical intervention, a

hypothesis concordant with earlier studies. General consensus was that much work remains to do in this area.

Mark Beckwith (Bartlesville) briefly recapitulated the history of Nevus Outreach, Inc., of which he is executive director, and introduced the other patient association attendees present. Nevus Outreach was founded in 1997 by three families affected by GCMN. Over time it has become arguably the largest and most active patient association in the world. Because of the federative actions undertaken by Nevus Outreach, more than 60 people with a GCMN themselves or with an affected family member attended this conference from 11 different countries and as many currently constituted advocacy groups (some countries with more than one, some with none).

The study of rare diseases requires the collaboration of physicians, scientists and patients. Disease-specific registries are an important means to better study and understand these conditions. Pinch hitting, Dr. Marghoob summarized past cohort studies and GCMN registry data published in the literature (Price & Schaffer 2010). The progress in GCMN research that has already been made by the evaluation of existing registries, and the constraints imposed by the lack of statistical power, are strong arguments for the unification of the currently existing databases into a collaborative and prospective international GCMN registry.

During the final recapitulation, the patient associations put forth two initiatives: the first committing to support and participate in the above-mentioned GCMN/NCM registry, and a second agreeing on an Internet-based, multilingual and globally accessible GCMN/NCM patient information clearinghouse. This platform will serve both as a portal to the registry and provide links to each of the worldwide patient

associations, serving researchers, physicians and patients alike; more information will be made available meanwhile on the progress of this undertaking on http://www.nevus.org. Translations will be initially provided by volunteer scientists and doctors in these languages: English, German, French, Spanish, Portuguese, Italian and Dutch. A working group was constituted to standardize the data categories and resource links to be included in the new registry, with the goal of inaugurating it by the next Expert Meeting, projected to take place in 2013. A first brainstorming session will take place on the sidelines of the International Pigment Cell Conference in Bordeaux, France, on September 24, 2011.

Acknowledgements

Financial support was generously and exclusively provided by the National Institute of Arthritis and Musculoskeletal and Skin Diseases and National Institutes of Health Office of Rare Disease Research (USA), the Morgan Family Foundation (USA), Nevus Outreach, Inc. (USA), and the Center for Rare Skin Diseases, University of Tübingen (Germany).

References

Bastian, B.C. et al. (2002). Genetic changes in neoplasms arising in congenital melanocytic nevi: differences between nodular proliferations and melanomas. The American Journal of Pathology, 161(4), pp.1163-9.

Bauer, B.S. & Corcoran, J. (2005). Treatment of large and giant nevi. Clinics in Plastic Surgery, 32(1), pp.11-8, vii.

Braziulis, E. et al. (2011). Skingineering I: engineering porcine dermo-epidermal skin analogues for autologous transplantation in a large animal model. Pediatric Surgery International, 27(3), pp.241-7.

Brooks, C. et al. (2011). Dermoscopy of nevi and melanoma in childhood. Expert Review of Dermatology, 6(1), p.19–34.

Burstein, F. et al. (2005). Neurocutaneous melanosis. The Journal of Craniofacial Surgery, 16(5), pp.874-6.

Cajaiba, M.M. et al. (2008). Metastatic peritoneal neurocutaneous melanocytosis. The American Journal of Surgical Pathology, 32(1), pp.156-61.

Danarti, R., Konig, A. & Happle, R. (2003). Large congenital melanocytic nevi may reflect paradominant inheritance implying allelic loss. European Journal of Dermatology, 13(5), pp.430-432.

Dessars, B. et al. (2007). Chromosomal translocations as a mechanism of BRAF activation in two cases of large congenital melanocytic nevi. The Journal of Investigative Dermatology, 127(6), pp.1468-70.

Dessars, B. et al. (2009). Genotypic and gene expression studies in congenital melanocytic nevi: insight into initial steps of melanotumorigenesis. The Journal of Investigative Dermatology, 129(1), pp.139-47.

Etchevers, H.C., Amiel, J. & Lyonnet, S. (2006). Molecular bases of human neurocristopathies. In J.-P. Saint-Jeannet, ed. Neural Crest Induction and Differentiation. Texas: Landes Bioscience, pp. 213-34.

Heissig, B. et al. (2002). Recruitment of stem and progenitor cells from the bone marrow niche requires MMP-9 mediated release of kit-ligand. Cell, 109(5), pp.625-37.

Jin, Y. et al. (2010). Variant of *TYR* and autoimmunity susceptibility loci in generalized vitiligo. The New England Journal of Medicine, 362(18), pp.1686-97.

Kadonaga, J.N. & Frieden, I.J. (1991). Neurocutaneous melanosis: definition and review of the literature. Journal of the American Academy of Dermatology, 24(5 Pt 1), pp.747-55.

Krengel, S., Hauschild, A. & Schafer, T. (2006). Melanoma risk in congenital melanocytic naevi: a systematic review. British Journal of Dermatology, 155(1), pp.1-8.

Paulhe, F. et al. (2009). Dimerization of Kit-ligand and efficient cell-surface presentation requires a conserved Ser-Gly-Gly-Tyr motif in its transmembrane domain. The FASEB Journal, 23(9), pp.1-12.

Price, H.N. & Schaffer, J.V. (2010). Congenital melanocytic nevi-when to worry and how to treat: Facts and controversies. Clinics in Dermatology, 28(3), pp.293-302.

Rades, D. et al. (2001). Therapeutic options for meningeal melanocytoma. Case report. Journal of Neurosurgery, 95(2 Suppl), pp.225-31.

Rompel, R., Möser, M. & Petres, J. (1997). Dermabrasion of congenital nevocellular nevi: experience in 215 patients. Dermatology, 194(3), pp.261-7.

Rothfuss, M., Schilling, M. & Breuninger, H. (2009). Early excision of congenital melanocytic nevi under tumescent anesthesia and skin expansion by intracutaneous double butterfly sutures. Journal der Deutschen Dermatologischen Gesellschaft, 7(5), pp.427-33.

Ruiz-Maldonado, R. (2004). Measuring congenital melanocytic nevi. Pediatric Dermatology, 21(2), pp.178-9.

Slutsky, J.B. et al. (2010). Large congenital melanocytic nevi: associated risks and management considerations. Seminars in cutaneous medicine and surgery, 29(2), pp.79-84.

Sommer, L. (2011). Generation of melanocytes from neural crest cells. Pigment Cell & Melanoma Research, 24(3), pp.411-21.

van den Boorn, J.G. et al. (2011). Skin-depigmenting agent monobenzone induces potent T-Cell autoimmunity toward pigmented cells by tyrosinase haptenation and melanosome autophagy. The Journal of Investigative Dermatology, 131(6), pp.1240-1251.

Table 1: Scientific talks held at the 2011 Expert Meeting on large and giant congenital melanocytic nevi and neurocutaneous melanocytosis

Friday, May 6th, 2011

Session 1: Overview and neurological aspects of CMN

Rudolf Happle: A fresh look at congenital melanocytic nevi

Ashfaq Marghoob: Epidemiology, classification and clinical management of congenital melanocytic nevi

Alon Scope: Dermoscopy and confocal reflectance microscopy in the surveillance of congenital melanocytic nevi

Yasmin Khakoo: Spectrum of neurological dysfunction in neurocutaneous melanocytosis

Marcos Tatagiba: Neurosurgical management of neurocutaneous melanocytosis

Session 2: Integrating the CMN patient experience

Mark Beckwith: Patient groups: International initiatives

Ornella Masnari: Stigma experiences in children and adolescents with a facial difference

Ashfaq Marghoob/ Harper Price: A cooperative international registry of CMN and NCM

Saturday, May 7th, 2011

Session 3: Biological bases of CMN

Miguel Reyes-Múgica: The neurocristopathies: a pathologist's viewpoint

Heather Etchevers: Signalling pathways in neural crest and early melanocyte development

Bernhard Wehrle-Haller: The kit-ligand/c-kit receptor interaction: potential therapies for pigmented lesions

Veronica Kinsler: The genetics of congenital melanocytic naevi

Session 4: Surgical options for CMN treatment

Clemens Schiestl / Thomas Biedermann: Tissue engineering of skin: best wishes from the petri dishes

Rainer Rompel: Indications and long-term results of dermabrasion

Helmut Breuninger: Early treatment of large congenital melanocytic nevi by serial power stretching of the skin with intracutaneous butterfly sutures under high tension.

Bruce Bauer: The role of tissue expansion in the treatment of large and giant congenital melanocytic nevi

Session 5: Syndromic aspects of inappropriate proliferation

Sven Krengel: Childhood melanoma: a distinct entity?

Pierre Heimann: Cytogenetic alterations and BRAF/NRAS mutations in congenital melanocytic nevi

Jürgen Bauer / Gisela Metzler: Proliferative nodules - clinical, histologic and molecular diagnosis

Veronica Kinsler: Endocrinological aspects of CMN syndrome

Alain Taïeb: Future therapies: lessons from vitiligo and melanoma

To appear as a chapter in Nevogenesis (Practical Clinical Medicine series) eds. A. Marghoob, J. Grinchik, A. Scope and S. Dusza, Springer, New York), 2011.

Etiology of congenital melanocytic nevi and related conditions

Miguel Reyes-Múgica[1], Mark Beckwith[2] and Heather C. Etchevers[3]

[1] Department of Pathology, Children's Hospital of Pittsburgh, One Children's Hospital Drive, 4401 Penn Avenue, Pittsburgh PA 15224, USA

[2] Nevus Outreach, Inc., 600 SE Delaware Avenue, Suite 200, Bartlesville, OK 74003, USA

[3] INSERM UMR_S910, Université de la Méditerranée Aix-Marseille II, Faculté de Médecine, 27 boulevard Jean Moulin, 13005 Marseille, France

Abstract

Large and giant congenital melanocytic nevi (CMN) are the rarest types of a proliferative malformation affecting the pigment cells of the skin. The phenotypic presentation is highly variable and few reports of familial transmission exist. Current models favor a somatic mutational event occurring during at or after the end of the first trimester of gestation, within the melanocyte precursor lineage, in a predisposing genetic background. The effect of potentially implicated signaling molecules on progenitor neural crest and derivative melanocyte development are discussed. Candidates include effectors such as NRAS and BRAF of the MAP kinase pathway, but also other pathways that converge on transcription factors critical for either multipotent precursor maintenance or melanocyte differentiation, and which may predispose cells to inappropriate proliferation in the central nervous system or at other sites. These associated proliferations can lead in a patient-dependent manner to a clinically favorable or fatal outcome. Continued exploration of the molecular bases of large and giant CMN development will lead to new tools for more accurate prognoses in both isolated and syndromic forms.

Introduction

Congenital melanocytic nevi (CMN) are visible melanocytic proliferations in the skin that are present at birth. CMN can be light brown to black patches or plaques, potentially very heterogeneous, and cover any size surface area and any part of the body. The incidence of CMN seems to be independent of skin color or other ethnic factors. Common, small CMN are found in 1-6% of the general population and can be distinguished by non-invasive dermoscopy (Brooks et al. 2011) from nevi acquired after childhood. Large and especially giant CMN, of which the size classification is defined in other chapters (L/GCMN, OMIM 137550) form a far rarer subset, with prevalence estimated at around 0.002% of births (Price and Schaffer 2010).

Unpigmented tardive congenital lesions can also be present; the emergence of so-called "satellite" naevi throughout the first few years of life in conjunction with larger CMN probably reflects the postnatal maturation of such precursors, and on occasion a primary CMN can appear in a tardive manner. (“Satellite” is a commonly used description of discrete small or medium CMN or tardive nevi in the presence of a large/giant CMN, though semantically it is subject to some criticism [Kinsler 2011].) Based on size or even histology, the congenital nature of such lesions remains somewhat controversial (Barnhill et al. 2010; Tokuda et al. 2010), despite a certain embryological justification.

The epidemiology and nosology of the giant forms of CMN, at anatomical, histological and molecular levels, allow us to evoke testable hypotheses as to the underlying developmental and genetic causes of this malformation and of its potential attendant complications. Such complications include neurocutaneous melanocytosis (NCM; an excess of pigmented melanocytes within the central nervous system), malignant melanoma, and other hamartoma-like tumors of various classes. When considering non-random associations with certain other congenital malformations, it may be more appropriate to discuss apparently isolated versus syndromic forms of large CMN (Krengel et al., 2011).

Histology of normal and CMN skin

Human skin is made up of two distinct compartments, the epidermis and dermis, which are normally separated by a basement membrane. The epidermis, derived from the ectoderm, ensures a semi-permeable barrier function with the extracorporeal environment. It contains adnexa that develop from specialized areas of epithelial thickenings called placodes into hair follicles, sebaceous and sudoriferous glands. These become embedded into the dermis and the underlying adipose hypodermis as the skin develops prenatally and matures postnatally, in such a way that the continuous epidermis, made of a highly stratified succession of keratinocyte lipids and extracellular proteins, folds and buckles. The dermis is an innervated and vascularized connective tissue, made up of fibroblasts, which secrete the collagen and elastin fibers, as well as other proteoglycan elements of the amorphous matrix in which all these elements are embedded. These extracellular elements confer local mechanical properties to the organ as a whole. This layer also plays an important role in the homeostasis of the overlying epidermis.

Normally, melanocytes are distributed around the base of epidermal annexes, most numerous at the base of the hair follicles, and in humans, in the basal layer of the interfollicular epidermis, where the keratinocytes self-renew (Fig. 1a). Within the epidermis, melanocytes assume a dendritic morphology with their cell membranes in contact with an average of thirty keratinocytes, independent of skin phototype. The normal melanocyte will produce membrane-bound vesicles containing eumelanin (black) or pheomelanin (red) in varying proportions depending on genetic background. These vesicles, known as melanosomes, are conferred on specific recipient keratinocytes (Weiner et al. 2007) whereby they are protected from UV and oxidative damage (Im et al. 1998). Most of the pigment in mature skin as seen in a histological section is in the recipient cells, rather than in the melanocytes themselves.

In contrast, small CMN show nests or large aggregates of self-pigmented *nevo*melanocytes (the abnormally proliferating counterpart of melanocytes), mostly in the upper third or *papillary* portion of the dermis. These aggregates are often grouped around hair follicles and sweat gland ducts, adopting a “single file” pattern when seen in section. Small CMN can histologically appear similar to (postnatally) acquired compound or intradermal melanocytic nevi. In contrast, larger CMN show nests not only at the epidermal-dermal junction, but often within deeper tissues, including the reticular dermis, subcutaneous fat, muscle fascia, and around vessels and nerves (Krengel et al. 2006; Miller 2004) (Fig. 1b, c).

A pachydermatous, rugous clinical appearance is imparted by the massive growth of nevus cells (the deeper ones of which are generally not self-pigmented), pilosebaceous adnexa and partly disorganized dermal elements in a “hamartomatous” distribution. These areas are frequently associated with bundled, fibrous neuroid structures that have been referred to as Wagner-Meissner-like bodies or *lames foliacées*, and are more often observed in larger CMN specimens (Fig. 1d). Some authors have historically referred to this aspect as “neurotized”. Growth of coarse, highly pigmented terminal hair in CMN areas and their distributed nevi is frequently encountered, with follicular crowding. Other epidermal adnexa may but do not systematically develop or function normally (Slutsky et al. 2010), which can be associated with clinically refractory eczema and pruritis (Lovett et al. 2009).

Neural crest migration and differentiation

Both isolated and syndromic forms of CMN involve anomalies in the development, growth or differentiation of derivatives of the neural crest cell (NCC) population (Etchevers et al. 2006). NCC constitute a transitory stem cell population that arises in the human embryo between the third and fourth weeks of pregnancy. During the fusion of the neural folds, a process that gives rise to a tube that will itself later become the central nervous system (CNS), NCC detach by undergoing an initial epithelial-mesenchymal transition (EMT). They migrate throughout the body, integrating into nearly every tissue. Over successive divisions, neural crest stem cells give rise to a mix of progenitors with varying degrees of potential to become any or some or a single NCC derivative, depending on both intrinsic and extrinsic variables (Dupin 2011; Thomas et al. 2008; Trentin et al. 2004).

Like all cellular components of the peripheral nervous system, the adrenal medulla, skeletal elements, dermis and vascular smooth muscle of the face, forebrain meninges and many other cell types, melanocytes are derived from NCC (Le Douarin and Kalcheim 1999). Their unpigmented precursor melanoblasts disperse evenly within the mesenchymal dermis and then home to the developing basal keratinocyte layer in human epidermis, whereupon they continue to proliferate, self-renew, and differentiate (Wilkie et al. 2002). Both melanoblasts and melanocytes also persist and differentiate into self-pigmented cells in a number of other sites including the meninges and heart valves, without seeming to interfere with organ function (Yajima and Larue 2008). This phenomenon may explain associations between nevi and other complex malformations involving these organs.

The precise developmental timing of the transitions from highly multipotent precursors to restricted progenitors to unpigmented melanoblasts has not been determined. (Much more work has been done on the production of melanosomes, because of the many forms of albinism that interfere with these last steps of melanocyte differentiation, but such work is beyond the scope of this review.) Different cell types co-exist or persist as a function of the moment and the environment examined (dermis, nerve sheath or small blood vessels, epidermal adnexa, glabrous epidermis, interfollicular epidermis) (Lu et al. 2010; Steel et al. 1992).

What appear to be fairly constant are the sequence of transitional events and the remarkable evolutionary conservation of molecules involved in melanocyte differentiation throughout the vertebrates. Therefore, fish, amphibian, avian and multiple mammalian models have all made their useful contributions to understanding the signals involved in expansion of the melanocyte progenitor pool during development, its maintenance during postnatal life, and terminal differentiation in distinct epidermal compartments. In the mouse embryo, which has long been a favored animal model for pigmentation studies, it has been demonstrated that only a few ancestral neural crest cells along the body axis are sufficient to give rise to the many thousands of precursors that eventually seed the entire surface of the skin (Mort et al. 2010; Thomas and Erickson 2008).

NCC contribute most visibly to the structure of the skin in their melanocytic progeny, but other cutaneous cell types are also derived from NCC. The dermis of the face, scalp and neck, as well as the underlying hypodermic adipose tissue, and the cells supporting the arrector pili muscles and accompanying the outer walls of blood vessels in these locations differentiate from cephalic NCC (Etchevers et al. 2001; Le Douarin and Kalcheim 1999). Merkel cells, a widely distributed mechanosensory receptor type, have been proven after years of controversy and indirect evidence of ectodermal origin to in fact derive from NCC, taking a similar route to maturation as melanocytes through the maturing dermis (Szeder et al. 2003). Multiple cell types have been shown to be able to differentiate from a highly multipotent NCC pool that was initially identified and characterized from the root (bulge) of whisker follicles in the rodent model (Sieber-Blum et al. 2004), and recently has been found to also persist in adult human epidermis at the base of hair follicles from the ventral abdomen (Clewes et al. 2011). In culture, such cells can be induced to express markers typical of glia, melanocytes, cartilage, osteocytes, myofibroblasts, neurons or adrenal cells.

Painstaking work with single-cell clonal cultures of early neural crest established that as soon as NCC can be morphologically distinguished from the neural tube, they are equally heterogeneous in their differentiation potential. Initially, most but not all are highly multipotent. Rapidly, though, certain lineages were distinguished – among them, a common progenitor of peripheral neurons, neural support cells such as myelinating Schwann cells (glia), and melanocytes, were identified in both chick and rat embryos (Baroffio et al. 1991; Rao and Anderson 1997). It is possible over time to isolate cells that have acquired what appears to be a differentiated phenotype among these and to "dedifferentiate" them in culture, such that they divide and some of their progeny will become other derivatives among the potential cells coming from the same initial precursor. Glial-melanocyte precursors can self-renew and the successive generations of cells continue to give rise to either glia or melanocytes without commitment (Trentin et al. 2004).

Even more strikingly, adult Schwann cells or melanocytes can be induced by the application of a growth factor, endothelin-3 (EDN3, discussed below), to revert to such a bipotent precursor. Thereby, after cell divisions, the apparently differentiated cell type can continue to engender new melanocytes or Schwann cells after exposure to this environmental stimulus (Dupin et al. 2000; Dupin et al. 2003). More recently, peripheral nerves of both chick and mouse were shown to represent a pool of naturally maintained precursors for both Schwann cells and melanocytes, and those Schwann cells on peripheral nerves that have already begun myelination can be diverted to a melanocyte fate by severing the nerve's provision of a glial growth factor (Adameyko et al. 2009). Even adult human melanocytes in culture can readily be induced to acquire characteristics of their embryonic precursors and to express markers of multipotent cells (Kormos et al. 2011).

Human NCC in the embryo share a surprising 95% of their transcripts with embryonic stem cells, which are pluripotent and can give rise to all cell types of the body (including the NCC derivative subset)(Thomas et al. 2008). Maintenance of partial stem cell-like potential, or developmental plasticity, appears to be a more general property of many of the postnatal progeny of NCC (Real et al. 2005) and may explain the particular sensitivity of NCC derivatives to misdirected differentiation or pediatric tumor development (Etchevers et al. 2006). NCC-derived progenitors, expressing such developmental plasticity and capable of becoming melanocytes among other cells, have only in the last few years been demonstrated to persist throughout life in amniotes. They can be found, among other sites, along peripheral nerve sheaths traversing the dermis to innervate the skin (Adameyko et al. 2009), within

glabrous dermis (Li et al. 2010), and at the base of regularly spaced hair follicles in both facial and body locations (Clewes et al. 2011).

Molecular signaling pathways in melanocyte differentiation and pathology

Remarkably, the signaling cascades that are involved in melanocyte differentiation, maintenance and proliferation are widely used in nearly all organ systems during development. They are once again co-opted in the onset and growth of an equally wide variety of tumors and cancers. Because the literature is extensive on the implications of these molecules in other systems, hypotheses are straightforward to formulate but less commonly tested as to their precise roles in how nevi and melanoma may form, and hardly examined at all for melanocytosis of the central nervous system or the growth of hamartoma-like tumors within congenital nevi.

The RAS/MAPK pathway: a unified field theory of development and tumorigenesis?

The Noonan, cardio-facio-cutaneous, and Costello syndromes are complex congenital syndromes with significant phenotypic overlap (Aoki et al. 2005; Aoki et al. 2008). As a class of diseases, each demonstrating genetic heterogeneity, they have nonetheless all been found to be caused by autosomal dominant germline mutations of molecules necessary for signal transduction from the membrane to the nucleus of the developing and surviving melanocyte. Such mutations, by altering the conformation of the resultant enzyme, lead in different ways to excess phosphorylation of the ubiquitous ERK1 and ERK2 kinases, in cellular *in vitro* assays (Niihori et al. 2006; Rodriguez-Viciana et al. 2006). At this point, nuclear-translocated ERK1/2 can permanently phosphorylate and activate many other protein targets, which though context-dependent can include such transcription factors as MYC, involved in the maintenance of the undifferentiated state, or indirectly, CREB, mentioned below.

This remarkable convergence of nosologically related diseases on one complex, functional signalling pathway has led to the proposal of the term “RAS/MAPK syndromes”, to refer to them as a group and to take into account their genetic and phenotypic overlap (Aoki et al. 2008). In addition to malformations of craniofacial and cardiac neural crest derivatives, the RAS/MAPK syndromes present all pigment anomalies, including dark skin, woolly or curly hair, multiple lentigines or café-au-lait spots. Neurofibromatosis 1, also distinguished by multiple café-au-lait spots, can occur in conjunction with Noonan syndrome. The causative gene of neurofibromatosis-1, *NF1*, normally also represses RAS enzymatic activity and likewise impacts this pathway (Fig. 2). Inactivation of *Nf1* specifically in murine Schwann cell progenitors not only favors the development of dermal neurofibromas along peripheral nerves but in a significant proportion of cases, either the tumors or the dorsal spinal cord are heavily pigmented – an underappreciated potential model for neurocutaneous melanocytosis (Wu et al. 2008).

“RAS/MAPK” is a catch-all group term to refer simultaneously to a number of proteins known by the acronyms of PTPN11, KRAS, HRAS, NRAS, BRAF, RAF1, SOS1 and MEK1, for those that have been already demonstrated to cause human pathology through germline mutations to date. There are many others that are integral components of the cascade; for instance, the RAFs come in ARAF, BRAF and CRAF. Many of these enzymes are tyrosine kinases, adding covalent modifications to the tyrosine residues of other proteins. They belong to larger families of kinases that are highly similar in sequence and structure to one another both across species during evolution and within a given organism. Each of these families of related proteins constitute additional candidate genes for disease in an appropriate context.

Reproducible somatic mutations (hotspots) in the *BRAF* gene, leading to demonstratedly increased kinase activity of the resultant protein, are involved in diverse cancers, malignant melanoma in particular (Davies et al. 2002). Surprisingly, the same mutations can be found in a number of non-congenital ("acquired") nevi (Pollock et al. 2003). In this pioneering study, some 9% of benign nevi demonstrated heterogeneity at the single cell level in the same tumor, with coincidence of *NRAS* and *BRAF* mutations (Pollock et al. 2003). However, among melanomas, such mutations are mutually exclusive and give rise to different phenotypes, with *NRAS*-mutated cells proliferating more and *BRAF*-mutated cells presenting more invasive capacity (Sensi et al. 2006). This heterogeneity at the cellular level has been confirmed for CSPG4-expressing melanoma cells by another group, who stated recently that “precancerous melanocytes already harbouring an unknown first hit may subsequently acquire multiple driver mutations; thus, the acquisition of *BRAF* mutation might be one of these secondary events” (Lin et al. 2011). The single-cell analysis bore out former observations that *BRAF* mutations are less present in early-stage melanoma and the conclusions that such mutations would therefore not be the predisposing cause (Dong et al. 2003).

Indeed, a specific examination of the prevalence of *BRAF* and *NRAS* mutations in confirmed congenital nevi of any size, found no *BRAF* mutations at all in 32 samples, but hotspot, activating *NRAS* mutations (codon 61) in 26 of them (Bauer et al. 2007). This finding was borne out by another study concentrating on large/giant CMN, again demonstrating frequent activating mutations in *NRAS* (70%), but also finding less frequent *BRAF* mutations at the same hotspots as in melanoma (15%) and a few chromosomal rearrangements at the *BRAF* locus (7.5%, of a cohort of 27) (Dessars et al. 2009). One case had a deletion of most of the long arm of chromosome 6 in addition to an activating *NRAS* mutation. While the *BRAF* mutations may have been acquired postnatally, as postulated by Bauer et al. (Bauer et al. 2007), it is striking that they occur only within large/giant CMN that do not already have an *NRAS* mutation, implying some functional redundancy in their effects on melanoblast proliferation and CMN growth that is distinct from their roles in carcinogenesis.

RAS and RAF molecules are positioned at a cytoplasmic signal transduction bottleneck where multiple extracellular stimuli effect changes in levels of gene transcription, or directly promote migration or proliferation (Fig. 2). Context-dependent effects of their inappropriate activation may be what lead either to congenital nevus formation or to tumor development.

One hint that this may be the case is that deeper melanocytic proliferations in the dermis (so-called "blue" nevi), internal organs, uvea or central nervous system tend to have activating mutations in a gene known as *GNAQ* (Küsters-Vandevelde et al. 2009; Van Raamsdonk et al. 2009). *GNAQ*, discussed more below, codes for a signal transduction protein subunit that has been found to activate the MAPK pathway in melanocytes, in addition to its more canonical role in cyclic AMP production and activation of the CREB transcription factor (Fitch et al. 2003; Van Raamsdonk et al. 2004). In addition, certain cases of NF1 present large cutaneous lesions that resemble large/giant CMN (Schaffer et al. 2007; Wu et al. 2008). Conversely, some large/giant CMN patients demonstrate cafe-au-lait macules or neurofibromas highly typical of neurofibromatosis, arguing for infrequent impingement on nevus development through the loss of *NF1* repression of RAS/MAPK signaling (Fig. 2) (Bett 2006; Kinsler et al. 2008; Reyes-Mugica et al. 1993) Large/giant CMN can feature extensive neuroid morphology (Fig. 1d).

Although it is unclear how RAS/MAPK signal transduction might participate in human nevogenesis, some animal models of CMN development are genetic mutants in this pathway. Overexpression of *Hras* specifically in mouse melanocytes led to their massive proliferation in both epidermis and dermis, with blue nevus-like accumulations, as well as in the meninges, ocular tissues including the uvea, and within the inner ear – where hamartoma-like development of the naturally occurring melanocytes led to malformation of the cochlea (Powell et al. 1995). In murine melanocytes, activating mutations of *Nras* induces proliferation but does not induce immortalization without the intervention of mutations in other gene products, notably transcription factors (Delmas et al. 2007).

The activating mutation of *Braf* found most frequently in human pigmented lesions (V600E) has been forcibly expressed in zebrafish melanophores, under the control of the promoter for the highly conserved microphthalmia-associated transcription factor, MITF (also responsible for Waardenburg syndrome; see below). While wild-type *Braf* did not change the fish coloration, the activated form led to the appearance of nevus-like clusters of pigment covering large areas of up to 40% of the body surface (Patton et al. 2005).

Genetic crosses of these fish with those deficient in the tumor suppressor transcription factor p53, also discussed briefly below, led to the development of aggressively invasive melanoma in half of the double mutants (Patton et al. 2005). Primary human melanocytes, transformed with the SV40 virus to induce a similarly malignant melanoma phenotype, re-activate a latent molecular program that reflects the capacity of their progenitors to migrate and disseminate. These findings dovetailed with the fact that a similar set of genes, associated with the epithelio-mesenchymal transition of NCC, can be found expressed in benign melanocytic nevi. Such expression may explain the ability of histologically normal melanocytes to home to the axillary, cervical and inguinal lymph nodes, outside of any metastatic behavior (Gupta et al. 2005). Unsurprisingly, sentinel lymph nodes positive for melanoma dissemination are notoriously unreliable as an indicator of tumor aggressiveness and potential for distant metastases of early pediatric, as opposed to adolescent or adult, melanoma (Barnhill et al. 2010; Moore-Olufemi et al. 2011).

At the cell surface – signal transduction through protein receptors and their ligands

Tyrosine kinase receptor ligands: KITL, HGF, FGF, EGF

Environmental growth factor sensors, among which tyrosine kinase receptors (TKRs), lie upstream of the RAS/RAF proteins and their partners. TKRs all share the following physical characteristics: they weave in and out

of the lipid membrane seven times and at their cytoplasmic tail, they display enzymatic activity which phosphorylates tyrosine residues on target intracellular effectors, launching a cascade of modifications that finishes in an effect on the availability or processing of mRNA or other proteins. The constitutive activation of many of these receptors, even in the absence of ligand, has been implicated in the onset of melanoma, recapitulating in an inappropriate context an embryonic program for proliferation, migration and fate restriction (Easty et al. 2011).

The survival and migration of embryonic melanocytes is dependent on their expression and the engagement of the TKR Kit, as well as on the keratinocyte-specific expression of Kit-ligand (KitL), also known as stem cell factor or SCF (Wehrle-Haller 2003). In addition to a critical role in melanocyte maintenance throughout life, Kit is also essential for the survival and expansion of hematopoietic and gamete stem cells. Mouse mutants for Kit are deaf from the loss of melanocytes from the stria vascularis of the inner ear, can be anemic, sterile, and their coats, on a black background, display large white patches known as spots, which gave rise to the original "W" denomination, for white-spotting (Dunn 1937). Transgenic over-expression of KitL in the basal layer of the mouse epidermis results in a hyperpigmented phenotype, with increased densities of melanocytes localized at the basal keratinocyte layer (Kunisada et al. 1998; Kunisada et al. 2000). Moreover, injection of soluble KITL into human skin xenografts increases the number of melanocytes, while the inhibition of the KIT/KITL pathway by blocking antibodies results in the loss of melanocytes (Grichnik et al. 1998). These data demonstrate that the KIT signaling pathway is active even in adult human skin and critical for the survival of melanocytes in the epidermis, or perhaps their production from resident, quiescent melanoblasts, for example during the hair cycle.

In skin of café-au-lait macules of NF1 patients, more soluble KITL is secreted by dermal fibroblasts than for control skin, and KIT-expressing, unpigmented melanocyte precursors are also more numerous in this compartment (De Schepper et al. 2006). Because the balance between secreted and membrane-bound isoforms of KITL seems to play an important role in the migration, adhesion and continued survival of melanoblasts and melanocytes (Paulhe et al. 2009; Wehrle-Haller 2003), altering that balance pharmacologically may be a promising therapeutic avenue for many types of melanocytosis, including those associated with large/giant CMN.

Exploration of the roles that hepatocyte growth factor (Hgf) and its receptor, Met, play in development led to the first animal model of neurocutaneous melanocytosis. In the earliest transgenic mice, in which HGF was overexpressed in all cells of the body (Takayama et al. 1996), pigmented melanocytes accumulated ectopically at the interfollicular epidermal-dermal junction and throughout the dermis, at stereotyped locations on the limbs, muzzle, belly and tail, and all over the back. Simultaneous melanocytosis developed in the meninges, visible at the dorsal spinal cord at postnatal day (P)4, subsequently engaging the cerebellum at P8, and by adulthood massively engaging the meninges of the forebrain. Melanocytes were also observed, unusually, in the lymph nodes, and even more unusually, skeletal muscle differentiated within the central nervous system.

A subsequently refined murine model demonstrated that the cutaneous phenotype could be induced by secretion of Hgf by the epidermis alone, though normally it is also produced by murine dermal fibroblasts. Targeting Hgf overexpression to epidermal keratinocytes with a keratin-14 promoter drove dermal melanocytosis – again, after birth, and comprising essentially all of the skin (Kunisada et al. 2000). This demonstrated the paracrine action of Hgf on Met-expressing melanocyte precursors. Interestingly, most of the ectopic cells did not co-express Kit at a time when normal melanoblasts and melanocytes usually have this receptor as well. Unlike those mice in which Hgf was overexpressed in all cells including melanocytes, the many hyperpigmented mice due to epidermal overexpression never developed spontaneous melanomas. Cell-autonomous activation of a downstream effector common to these pathways could be responsible for localized melanocytosis during development.

The pleiotropic roles of KITL/KIT and HGF/MET in human cancers affecting the liver, breast or lung translate the complexity of characterizing their stimulation of cellular proliferation and fate decisions both during development and out of context in the adult. Interestingly, the melanocyte, unlike the epidermal keratinocyte, is naturally possessed of a tendency, after neoplastic transformation, to home to the liver and lymph node, among other sites (Gupta et al. 2005). This migratory tendency is a vestige of its embryonic origin and the homing sites may reflect the normal importance of MET and KIT signaling in the development and growth of these organs.

Summarizing the many roles of over two dozen members of the fibroblast growth factor (FGF) family and its four alternatively spliced receptors in neural crest and skin development and homeostasis is far beyond the scope of this chapter. However, these are canonical RAS/MAPK cascade-activating receptors that also result in ERK1 and

ERK2 phosphorylation at the level of the nucleus, with subsequent changes in target gene transcription (Easty et al. 2011).

For example, the dermal papilla of hair roots expresses FGF7 protein (Rendl et al. 2005), just below the site of terminally differentiated melanocytes that color the hair shaft during the anagen phase. Melanin-receiving keratinocytes secrete more FGF2 than their immediate neighbors, which presumably either exerts an effect on melanocyte dendritic pathfinding to effect specific epidermal pigment patterns, or potentially on the transfer of melanosomes (Weiner et al. 2007). Low concentrations of FGF2 are also a common adjuvant in melanoblast, embryonic stem cell and NCC media for the maintenance of multipotency and cell divisions (Motohashi et al. 2009; Sviderskaya et al. 2009; Thomas et al. 2008)

Interestingly, it has been shown recently that Fgf2 promotes uncommitted primary NCC to differentiate into Schwann cells *in vitro*, while epidermal growth factor (Egf) favors the differentiation of neurons and melanocytes (Garcez et al. 2009). Both are often added for propagating a number of progenitor cell types, and were shown by Garcez et al. to prevent the differentiation effect of the other to maintain bipotent glial-melanocyte cells, a situation possibly encountered by dermal melanoblasts or nerve sheath cells – or the nerve sheath cells that subsequently become dermal melanoblasts (Adameyko et al. 2009).

Egfr, like many of the other TKRs mentioned above (Kit, Met), acts through more than one signaling pathway on transcriptional events. Egfr responds to more than one ligand, Egf only being the most important of them, and Egf can engage any of three other Egfr-like receptors, known respectively as ErbB2, -3 and -4, stimulating them to form homo- or heterodimers. Indeed, glial growth factor, or neuregulin, is normally produced by peripheral nerves to maintain ErbB3-expressing Schwann cells, ErbB3 being the preferred receptor for this ligand (Adameyko et al. 2009). ErbB3 is expressed by both keratinocytes and melanocytes in the differentiated epidermis, while a number of potential ligands are secreted by proliferating progenitors in the basal portion of the epithelium (Poumay and Mitev 2009). It would be interesting to test whether stimulation of ErbB3 prevents the engagement of Egfr homodimers and vice-versa in bipotent glial/melanocyte progenitors.

A better-known role for Egfr signaling is its requirement in mature keratinocytes in the basal layer of the epidermis. One of numerous mouse models with unusually dark skin, known as *Dsk5*, carries a mutation that causes excess phosphorylation of the Egfr upon ligand binding, leading first to hyperkeratosis and then to excess pigmentation during adult life (Fitch et al. 2003). Large acquired melanocytic nevi can develop in conjunction with recessive forms of the human genetic disease known as epidermiolysis bullosa (Bauer et al. 2001), where dysfunctional collagens fail to keep the epidermis in contact with the dermis. In both situations, melanocytosis was induced by postnatal stimuli.

EGFR binding can lead to cleavage and shedding of the part of the MET receptor that projects from the extracellular side of an adenocarcinoma cell model, through tyrosine kinase activity and activation of secreted proteases (Nath et al. 2001). It remains to be demonstrated, but appears likely, that integration of such cell signaling events is relevant to the maturation of pigment cells in the basal layer of the epidermis.

G-protein-coupled receptors: KIT, EDNRB, EDNRA

Kit, as well as a number of receptors that convey lipid- or hormone signals, can associate with G proteins anchored to the underside of cell membranes. The conformation of these multi-unit complexes changes upon receptor binding and the release of energy associated with the catalytic transfer of a phosphate group away from the nucleotide derivative guanosine triphosphate (GTP), yielding guanosine diphosphate (GDP). In this way, G proteins act as molecular switch gate-keepers, converting binding of a ligand into a binary on/off signal within the cytoplasm and raising intracellular cyclic adenosine monophosphate (cAMP) levels by stimulation of adenylate cyclase.

Oncogenic activating mutations in the KRAS, HRAS, NRAS molecules lead to the suppression of their GTP cleavage activity, locking them "on" and stimulating targets downstream of both G-protein-coupled receptor and TKR signaling pathways. The "**P**hosphatase and **Ten**sin homolog deleted on chromosome 10" gene (*PTEN*) encodes another tumor suppressor enzyme at an intracellular signaling crossroads, which interacts indirectly with the RAS/MAPK pathway, and directly with an alternative signaling pathway for Kit not mediated by its intracellular kinase activity (Lev et al. 1992). Mutations in *PTEN* are associated with a broad variety of human cancers. Interestingly, mice in which *Pten* is specifically inactivated within tripotent (neural/glial/melanocytic) NCC precursors die of intestinal pseudoobstruction and are hyperpigmented like HGF-overexpressing mice, including with olfactory bulb melanocytosis (Puig et al. 2009).

Perhaps the most important signaling through G proteins for melanocyte development is that of the endothelin (EDN) family. Endothelins are a family of three similar, small peptides that were first identified for their

vasoconstrictive activity and are produced by endothelial cells. EDNs are post-translationally cleaved from large precursor proteins. By signaling through either of two receptors in amniotes, they play important roles in the homeostasis of many mature organ systems, including the heart and lung, but also in discrete systems during development of the nervous system and NCC.

Edn3 acts through the G-protein coupled receptor, Ednrb. Mutations in either *EDN3* or *EDNRB* that reduce the latter's signaling activity lead to the development of Waardenburg syndrome (WS) type 4. WS4 is the quintessential neurocristopathy: a syndromic form of Hirschsprung disease (a form of congenital megacolon due to defects in migration, differentiation and survival of enteric ganglionic precursors during their colonization of the colon) with pigmentation and hearing defects due to the non-maintenance of melanoblasts in the skin and inner ear (Bondurand et al. 2000). The mutations of genes for essential transcription factors for melanocyte identity and function, that are directly activated as a result of Ednrb signaling in NCC, are responsible for other forms of WS and will be discussed briefly below.

The effect of GNAQ activation appears to mimic constitutive Ednrb signaling in melanocytic precursors (Van Raamsdonk et al. 2009; Van Raamsdonk et al. 2004). Mutations causing constitutive activation of the G protein subunit encoded by *GNAQ* have been found in the dermal nevi of the "blue nevus" type, but also in uveal melanomas – that is, in proliferations of non-cutaneous melanocytes (Van Raamsdonk et al. 2009). This distinction is borne out by a similar finding of activating *GNAQ* mutations in CNS melanocytomas (Küsters-Vandevelde et al. 2009). An alternative subunit to the one encoded by *GNAQ*, GNA11, is found to be constitutively activated in many metastatic uveal melanomas, but only a few blue nevi (Van Raamsdonk et al. 2010), reminiscent of the BRAF/NRAS dichotomy for cutaneous large/giant CMN.

EDN3 is not the only endothelin with important effects on neural crest development. Edn1, by signaling through the Ednra receptor on NCC, has been shown in animal models to be critical for the specification of NCC from the neuroepithelium that will later give rise to the CNS (Bonano et al. 2008), and then subsequently for craniofacial morphogenesis and particularly the specification of the lower jaw (Brand et al. 1998; Clouthier et al. 2010). Mutations in the EDNR signaling pathway could conceivably lead to association of pigmentary with dysmorphic features.

Melanocytes will not only produce more pigment and divide extensively in the presence of exogenous Edn3 *in vitro* or *in vivo*, but they appear to do so by reverting to a bipotent phenotype and thereafter can also produce glial-like progeny (Dupin 2000). Ednrb is required for the specification and the dissemination of melanoblasts during what is usually a restricted window of development (Shin, Levorse, Ingram, & Tilghman, 1999). However, since forced expression of Ednrb is by itself sufficient to direct melanocytic differentiation in non-committed embryonic stem cells (Pla et al. 2005), it seems likely that ectopic Ednrb pathway stimulation could lead to new proliferation of resident precursors and perhaps to nevogenesis.

Melanocyte-stimulating hormone

Alpha-melanocyte-stimulating hormone, αMSH, is one of many encoded by the pro-opiomelanocortin (*POMC*) gene (Bicknell 2008). Subtilisin-like proprotein convertases process such neurohormones from a large precursor peptide. In this respect αMSH is similar to the endothelins. While largely produced by a subsection of the pituitary gland, αMSH is also made in a tissue-specific manner, particularly by the mature human skin. Part of the spatial specificity may be conferred by the localized and dynamic expression of the different processing enzymes.

Canonical signaling by αMSH occurs through the first of the four melanocortin receptors, MC1R. Intracellular signal transduction is effected by cAMP (Fig. 2) and results in the activation of the "cAMP response element-binding" transcription factor (CREB). The release of cAMP by exogenous chemical agents can also provoke hyperpigmentation. Other hormone receptors, such as those for estrogen or epinephrine, are not only themselves transcriptional targets of CREB in melanocytes, but are also capable of promoting pigmentation through positive feedback loops involving G proteins and activating CREB itself (Schallreuter et al. 2008).

MC1R signaling is what enables the melanocyte to produce additional melanin in response to ultraviolet-B-induced sublethal DNA damage and to load keratinocytes, which confers some radiation protection by promoting tanning. Stereotyped amino acid substitutions within the intracellular domain disable fully effective cAMP activation and stimulation of transcription factor availability; these are associated with red hair, freckling and fair skin, as well as a higher population risk of developing adult-onset melanoma (Valverde et al. 1996). Intriguingly, binding of MC1R can lead to activation of both ERK1 and ERK2 by the transactivation of the KIT receptor, whether

or not those cAMP-inhibiting variations are present, implying that MC1R may also play a hitherto unsuspected role during melanocyte development and differentiation (Herraiz et al. 2011).

Transcription factors: MITF, SOX10, PAX3, CREB, MYB, ETS1/2

MITF, as mentioned above, is the master transcription factor essential for the assumption of pigmented cell fate - both for the melanocyte lineage but also for the pigmented epithelium of the retina, a direct derivative of the central nervous system. As such, outside of the eye, its expression is considered to be the gold standard for melanoblast identity, even when the cells are not yet pigmented. MITF is part of a cascade of transcription factors that regulate one another in positive and negative feedback lops. While it affects the melanocyte lineage-specific production of both signaling receptors and numerous enzymes involved in melanogenesis, the gene itself is subject to highly complex regulation of functionally non-equivalent isoforms from no fewer than nine distinct promoter regions (Hou and Pavan 2008).

Sox10 is a transcription factor with certain DNA-binding modules of the protein that highly resemble the other twenty-odd members of the Sox gene family, all involved in cell fate specification and organogenesis . It is critical for early NCC development and is again important for survival and differentiation of the glial (Britsch et al. 2001), melanocytic (Aoki et al. 2003) and enteric nervous system (Paratore et al. 2001) lineages.

Pax3, a member of the paired-homeobox transcription factor family, is both a target of CREB and an activator of both *Sox10* and *MITF* (Watanabe et al. 1998) transcription, the latter in cooperation with Sox10 (Bondurand et al. 2000). Similarly, CREB, after MC1R signaling through cAMP, appears to require Sox10 as a co-factor to drive the transcription of the melanocyte-specific *MITF* isoform (Huber et al. 2003).

Mutations in *SOX10*, *PAX3* or *MITF* lead to WS types 1-3, in variants with specific features but always comprising the pigmentary and secondary auditory phenotype (melanocytes of the inner ear being critical for hearing). Because all are transcriptional targets of EDNR signaling, it is not surprising that WS type 4A, with additional Hirschsprung disease, can be caused by *EDNRB* mutations, while WS4B is caused by mutations in its ligand, *EDN3*. Mutations in *EDN3*/*EDNRB* can also cause isolated Hirschsprung disease (reviewed in Etchevers et al. 2006).

Remarkably, the same transcription factor genes that with germline mutations lead to WS can be mutated somatically in malignant melanoma. Both *MITF* and *SOX10* are mutated in a significant fraction of both metastatic melanoma cell lines and primary tumors. While *MITF* is often amplified in copy number, the mutations in *SOX10* are likely to interfere with its function as a transcriptional activator of *MITF* (Potterf et al. 2000).

Among other transcription factors important for melanoblast development, both the Myb and Ets-1 transcription factors were found to bind to a promoter element that controls the earliest *Sox10* expression in chicken NCC (Betancur et al. 2010). Since Myb overexpression increases the presence of Kit in neural crest cells and thereby converts them to the melanocyte lineage (Karafiat et al. 2007), coincident signaling through Ras/MAPK receptors to Ets1 may be a necessary condition for this fate conversion. Indeed, Myb and Ets2 have already been demonstrated to cooperatively bind the promoter and upregulate *Kit* receptor transcription *in vitro* (Ratajczak et al. 1998), while in the presence of excess Myb, exogenous Fgf2 massively promotes melanocyte proliferation and differentiation, probably through Ets1/2 (Karafiat et al. 2007).

In combination with signaling through the endothelin receptors, which display the appropriate spatiotemporal activity, or EGFR/ErbB-type signaling (Bell and Frampton, 1999), Myb and Ets factors may also regulate *Sox10* expression more specifically in the context of melanocyte specification and population expansion. A number of other factors, such as Wnt-activated beta-catenin (Aoki et al. 2003), also appear to control Sox10 availability. Like other members of the large Sox transcription factor family, *Sox10* is regulated at great genomic distances from the coding region itself by multiple, highly conserved elements that confer spatial and temporal specificity (Antonellis et al. 2008; Benko et al. 2009).

Genetic models

A female preponderance has been noted in large/giant CMN (male/female ratio of 1 to 1.4 (Bett 2005; Kinsler et al. 2009).While reporting bias is a theoretical possibility, the absence of a statistically significant size difference in naevi between genders, and large sample sizes, argue in favor of a true if slight skew. In addition, the segmental blue nevi known as nevus of Ito (upper back, chest, neck, shoulder and upper arm) and nevus of Ota (along

ophthalmic and maxillary branches of the trigeminal nerve, within the domain of anterior rhombencephalic NCC) present a true gender bias in Pacific Asian populations. Although a separate entity, the dermal melanocytosis characteristic of blue nevi may be caused by other molecular players in the same pathways important for melanocyte development, incident to G proteins. For example, on rare occasion, melanotic schwannoma can occur in patients with nevus of Ota or Ito (Trufant et al. 2009), as it can in large/giant CMN (Bae et al. 2007); the developmental relationship between melanoblasts and Schwann cell precursors is clear.

The most likely etiology for CMN, or blue nevi for that matter, is that of a somatic mutation anywhere from the second month of pregnancy to the perinatal period in either the self-renewing, immediate precursor of the pigment cell lineage, the melanoblast, or potentially in the surrounding cell lineages that constitute their "niche". Earlier events hypothetically lead to more of the cutaneous surface being implicated than later events. The end result is differently sized, clonal contribution(s) to a given area of the body (Hui et al. 2001).

One group has made use of the high-molecular-weight melanoma-associated antigen (CSPG4) to sort cells from small congenital or acquired nevi (Lin et al. 2009) or melanoma (Lin et al. 2011), in order to demonstrate non-clonality of the lesions with respect to single-cell analyses of *BRAF* mutations. A significant drawback of the technique is that this proteoglycan is not present on normal melanocytes or restricted to melanoma cells but is also expressed on keratinocytes (Lin et al. 2009) and in particular, microvascular pericytes (Schlingemann et al. 1990). Cell type contamination might therefore contribute to the apparent heterogeneity. These findings were in contrast with the conclusions of work in which the distinct cytogenetic profile of congenital nevi analyzed was imputed to their clonal homogeneity (Bastian et al. 2002).

From what is known about the dispersal of melanocytes in animal models and conjectured to be the case in humans, it should be possible for later progeny of a single melanoblast precursor carrying a pathogenic second hit to be progressively dispersed among non-mutated cells over embryogenesis. These would give rise to small clonal proliferations at some distance from one another and from the original and larger concentration of cells that arise from the earlier progenitor.

This hypothesis cannot be tested until the molecular bases of large/giant CMN formation have been identified, but it is supported by a few observations. First, smaller CMN associated with a principal large/giant CMN are widely distributed around the body, but can also be observed in clusters, while the timing of appearance can be either at birth or pigmenting during the first few years of life. Second, some individuals with large/giant CMN have what are known as “multiple medium-sized” nevi, where one large lesion does not obviously predominate in size over the others, but the total body surface affected approximates that of a large or giant CMN (Krengel et al., submitted).

Finally, there are now more and more examples of scattered but clonal benign cutaneous tumors that appear to arise in this staged manner. A precedent exists, as reported by Maertens et al (2007) in the identical biallelic inactivation of the *NF1* gene that occurs in widely scattered plexiform neurofibromas and café-au-lait macules (CALM) of NF1 patients, with identical mutations that point to a common affected cell whose progeny became distributed in a segmental manner. The patient described as SNF1-2, appears to have a very pale GCMN over the entire right leg, hip and lower back, in which CALMs can be distinguished; the hyperpigmented area has a single allelic microdeletion of NF1 exclusively in the melanocytes and not its fibroblasts, while again, only the melanocytes derived from the CALMs carried a second hit in the form of a frameshift mutation (Maertens et al. 2007). A second precedent is that of seborrhagic keratoses, which can also be distributed in a segmental manner, and which display identical mutations in any given individual examined despite being multicentric (Hafner et al. 2010).

The “paradominance” concept was developed to express the idea that a heterozygous individual mutated in a particular developmental gene may, within a somatic cell lineage during embryogenesis, acquire a mosaic status in which only the affected tissues and their progeny are homozygous or compound heterozygous for the mutation (Happle 1999). If the gene product is only usually required during a prenatal window, this may lead to apparently sporadic malformations, when in fact the predisposition is inherited, while only an environmental or stochastic “second hit” to the other allele reveals pathogenic potential (Danarti et al. 2003).

This attractive model has now been demonstrated in two syndromic malformation classes that are relevant to large/giant CMN. The first is the demonstration that a somatic mutation in the *PTEN* phosphatase repressor of the RAS/MAPK signaling pathway on one allele can accumulate in affected tissues with a germline *PTEN* mutation on the other allele, to give rise to a Proteus-like syndrome. In a seminal paper, the patient was affected with typical Proteus-like hemihypertrophy, arteriovenous malformations in the hypertrophic tissue, lipomas, epidermal (not melanocytic) nevi and macrocephaly. This presentation is quite distinct from the frequent, numerous hamartomatous tumors that develop in patients affected with germline mutations of both alleles of *PTEN*, or from the wide variety

of cancers that develop with late biallelic somatic mutations of *PTEN*, including malignant melanoma (Wu et al. 2003).

Congenital vascular malformations can affect all components of the vascular system individually or in combination: capillary, arterial, venous and lymphatic. As summarized in the comprehensive review by Limaye et al. (Limaye et al. 2009), capillary cavernous malformations (CCM) are an excellent illustration of a paradominant-type inheritance in sporadic cases. The inherited types of CCM, in which vascular malformations can affect both cutaneous and central nervous systems, had been found to be genetically heterogenous, with three genes identified. The products of these genes, like for WS, physically interact at a cytoplasmic signaling checkpoint with small GTPases.

Future efforts in identifying the molecular bases of large/giant CMN development will need to focus on the comparison of lesional tissues – preferentially, isolated pigment cells from the lesions, although alterations in support cell types perhaps should not be excluded – with the genome represented by a germline-representative tissue, as well as with parental genomes. For a methodical approach, no less will tease apart the etiology of a large/giant CMN as well as its relationship with any associated conditions such as neurocutaneous melanocytosis or proliferative nodules within the lesions.

Neurocutaneous melanocytosis

Neurocutaneous melanocytosis, cited in earlier literature as neurocutaneous *melanosis* (NCM), is a neurological and cutaneous disorder characterized by abnormal aggregations of nevomelanocytes within the central nervous system (Fig. 3) and the skin. NCM is a complication of large/giant CMN, or multiple smaller CMN, in a fraction of patients. Recent studies using patient registries with many hundreds of registrants find the incidence of NCM to range between 5-15% of all persons with large and giant CMN (Agero et al. 2005; Bett 2006; Kinsler et al. 2009).

A major associated predisposing factor to NCM is more than twenty "satellite" nevi (DeDavid et al. 1996; Lovett et al. 2009; Marghoob et al. 2004), which may in fact be a form of multiple CMN (Kinsler 2011). When the predisposing and somatic molecular events leading to CMN have been identified, the interlesional clonality of distant congenital and/or tardive nevi can be assessed.

A second predisposing factor identified in univariate analysis and retrospective studies is when the large/giant CMN covers the posterior midline axis (Agero et al. 2005; Hale et al. 2005). In other analyses, however, this latter risk factor is not so clearly associated (Marghoob et al. 2004; Lovett et al. 2009). Indeed, Lovett et al. concluded that either of these two factors "do not predict underlying NCM very well. On the other hand, in [their absence], NCM is very unlikely."

Unlike for large/giant CMN themselves or nevus of Ota, there appears to be little to no sex bias in NCM, either according to earlier reports (DeDavid et al. 1996) or recent examination of the Nevus Outreach patient registry (48% male, 52% female, for 67 individuals). Approximately half are neurologically asymptomatic (36/67 for the registry, also as reported [Foster et al. 2001]).

Melanocytes are normally found in the leptomeninges (*pia mater*) of parts of the hindbrain and cervical spinal cord, the basal frontal and temporal lobes of the cerebral hemispheres, the optic chiasm, anterior perforated substance and within the Sylvian fissure (Miller 2004). The telencephalic regions are covered by leptomeninges of entirely NCC origin, perhaps offering a pool of precursors susceptible to growth factor signaling (Etchevers et al. 2001). However, the ventral areas are also in close proximity to the hypophysis, and melanogenesis may be favored by the hormone α-MSH in the local environment. It is rare for true NCM to occur in the absence of medium-sized or larger cutaneous CMN, although a case with no pigmented lesions and another with only café-au-lait spots have been reported with symptomatic, eventually lethal NCM (Reyes-Mugica et al. 1993).

Asymptomatic NCM

In some cases there appear to be no ill-effects from the presence of melanocytosis in the brain (DeDavid et al. 1996; Foster et al. 2001; Frieden et al. 1994; Kadonaga and Frieden 1991; Miller 2004) There also exist a number of animals with heavily melanocyte-infiltrated muscles, internal organs and/or meninges. These include the epidermally over-expressing *Hgf* mouse (Kunisada et al. 2000), the melanocyte-specific activated *Braf* zebrafish (Patton et al. 2005), and naturally occurring Silky Fowl (Dorshorst et al. 2010; Lecoin et al. 1995; Li et al. 2011) and Kadaknath strains of chicken (Thakur et al. 2006), all of which are able to reach an asymptomatic adulthood. Spontaneous GCMN with associated massive, but asymptomatic, NCM has even been identified in a macaque (Chen et al. 2009).

There may be subtle neurological problems, more stereotyped in the pediatric population, that are also caused by NCM and that could be a clue for the vigilant clinician (V. A. Kinsler et al., 2008), but these are not yet widely included in the "symptomatic NCM" subset. It is not straightforward to attribute such non-specific findings as speech difficulties, depression or psychoses to the same physical cause as visible neurocutaneous manifestations (Azzoni et al., 2001; Koot, de Waard-van der Spek, Peer, Mulder, & Oranje, 2000; Makin et al., 1999; Thompson & Kent, 2001; Ye et al., 2008).

In either asymptomatic or symptomatic NCM, ectopic nevomelanocytes are found in discrete masses within the parenchyma and/or within the leptomeninges (Fig. 3b-d). Proliferating nevomelanocytes present variable degrees of differentiation, ranging from benign-looking cells, similar to those seen in small CMN, to atypical, melanoma-like cells associated with abnormal mitoses, necrosis and other classic histologic signs of malignancy. However, the most frequent appearance is that of a well differentiated small cell population, growing within the leptomeninges and focally invading the brain from either the interface with the surface meninges, or from the ingressions of the *pia mater* into the parenchyme, as melanocytes can follow the blood vessels along the Virchow-Robin spaces well into the gray matter (Burstein et al. 2005; Chen et al. 2009; Makin et al. 1999; Pavlidou et al. 2008b; Ye et al. 2008, and Fig. 3b-d). Their common origin with the pericytes that line those spaces in the forebrain, at least, may favor their differentiation and dissemination *in situ* during meningeal development (Etchevers et al. 2001). It is still unclear to date whether it is the total proliferative mass or the location of ectopic melanocytes that interfere with neurological function and can lead to fatal NCM.

NCM can occur in conjunction with Chiari malformation of the brainstem, a non-specific sign. Reported patients have been entirely asymptomatic (Bett 2006; Foster et al. 2001)

Symptomatic NCM

Symptoms, when they do occur, can include headaches, seizures, vomiting, visual disorders, movement and learning disorders, paralysis, mental retardation, papilledema, and hydrocephalus (Miller 2004; Pavlidou et al. 2008b; Shah 2010). No patients develop all of these potential neurological signs. Many of them are secondary to raised intracranial pressure; anywhere from one-sixth (Kinsler et al. 2008) to two-thirds (Pavlidou et al. 2008a) of symptomatic NCM cases develop hydrocephalus.

At least three possible hypotheses address this association, the first of which being the most popular: the nevomelanocytes are passively obstructive to cerebrospinal fluid (CSF) flow (Miller 2004); melanocytes are simply found in conjunction with, but are not responsible, for choroid plexus malfunction; pigment metabolites may be damaging to the tissues responsible for CSF secretion or reuptake.

NCM-associated hydrocephalus, like other forms of hydrocephalus, is treated initially with a ventriculo-peritoneal shunt. However, this approach can be prone to difficulties, such as clogging of the shunting catheter by the proliferating nevomelanocytes (Fig. 3e) or by melanoma developing within the NCM (Shinno et al. 2003). Furthermore, several instances of peritoneal dissemination of proliferating cells, facilitated by this shunting, leading to massive peritoneal "metastatic" disease, have been observed (Cajaiba et al. 2008; Fig. 3f).

Syndromic forms of LCMN-NCM-HC

HC is often reported in conjunction with other brain malformations in symptomatic NCM cases, such as Dandy-Walker complex (Frieden et al. 1994). More so than NCM itself, this represents a form of syndromic large/giant CMN (Cajaiba et al. 2008; Gönül et al. 2009; Livingstone et al. 2009; Makin et al. 1999; Marnet et al. 2009; Walbert et al. 2009). Other syndromic forms include a report of ring chromosome 7 in which over 100 small CMN were associated with clinodactyly and adducted thumbs, hydrocephalus, microcephaly, mental retardation, and facial dysmorphy, but no NCM (Mehraein et al. 2004).

Another report mentions the association of NCM with transposition of the great arteries and unilateral renal agenesis (Köksal et al. 2003). NCM associations with renal anomalies have been described elsewhere (Kadonaga and Frieden 1991), including with additional skeletal anomalies (Huang and Lee 2000). The phenotypically and genetically heterogeneous association of multiple congenital malformations known by the acronym of VACTERL (OMIM 192350) occurs sometimes in conjunction with hydrocephalus (VACTERL-H), suggesting common molecular regulation of the development of brain size and the choroid plexus of the fourth ventricle, and the morphogenesis of the skeletal, digestive, cardiac outflow tract and renal systems. A missense amino acid substitution in the tumor suppressor gene *PTEN* has been identified in a VACTERL-H patient (bilateral hand malformations, 13 pairs of ribs, tracheo-oesophageal fistula, macrocephaly, progressive ventriculomegaly), probably abolishing its phosphatase activity and thereby its repressive action on the RAS/MAPK signaling pathway (Reardon

et al. 2001). Interestingly, cases of GCMN with NCM and features of the PTEN syndrome spectrum (lipomatosis, hemihypertrophy) have also been described (Gönül et al. 2009; Wieselthaler et al. 2002; Won et al. 1993) evoking a possible role for PTEN misregulation in syndromic large/giant CMN-NCM-HC patients, in particular those for whom the NCM develops into melanoma (Wu et al. 2003).

Prognosis for symptomatic NCM

NCM is either diagnosed after a pre-emptive MRI or because a patient presents neurological symptoms. Since NCM occurs among a restricted subset of patients affected with an already rare disease, it is not often encountered by most physicians.

The literature offers a grim outlook for those with symptomatic NCM, top-heavy with reports of fatal outcomes. Syndromic NCM with hydrocephaly does appear to have a very poor prognosis, although occasional cases have been reported with what appears to be stable recovery on long-term follow-up (Lovett et al. 2009; Peters et al. 2000). Nevomelanocytes may gain access to the CSF and circulate through the brain ventricles and their foramina. CSF collected from such patients at either VPS ports or spinal taps can show cells with dendritic prolongations and occasional intracytoplasmic melanin granules (Fig. 3c). In cases with a very atypical morphology showing active mitotic proliferation, necrosis and nuclear pleomorphism, the appearance of cells is indistinguishable from melanoma arising in any other location. Patients either die from complications of their hydrocephalus (Pavlidou et al. 2008a) or from the development of melanocytoma or CNS melanoma (DeDavid et al. 1996; Kadonaga and Frieden 1991; Livingstone et al. 2009; Shah 2010)

Symptomatic NCM can be lethal, but it is not systematically so. This makes it imperative to find better biomarkers for distinct clinical entities, and to establish improved clinical or imaging criteria, to offer a more accurate prognosis to patients with neurological symptoms. In certain patients, the parenchymal melanocytosis gives rise to discrete tumors that appear focal, hyperintense on axial T1-weighted and hypointense on axial T2-weighted MRI, without signs of edema or mass effect. Chronic epilepsy may be the primary, and indeed, the only symptom. Two distinct reports of epileptogenic, melanocytic hamartomas in the amygdala, where treatment consisted in a rather standard temporal lobotomy, have led to absence of subsequent seizures or other symptoms for 15 (Ye et al. 2008) and 30 post-operative months (Fu et al. 2010), respectively.

The large prospective registry of currently over a thousand patients with large and giant CMN maintained by Nevus Outreach, Inc. in the United States, has ten individuals with symptomatic NCM presenting seizures but no other neurological signs. As of this writing, eight of these cases are confirmed to be living and healthy. Their average age is 12 years (range: 1-15 years with one 28-year-old adult). Their epilepsy was first reported to the registry an average of 8 years ago (range: 1-14 years ago; the adult, four years ago). The remaining two cases have not been reported as deceased. Contrary to the impression left by the majority of reports to which practitioners have access, this cohort demonstrates that a significant group of those with symptomatic NCM are doing well, in agreement with other observations (Khakoo and Marghoob 2009; Kinsler et al. 2008; Peters et al. 2000).

Tumors arising in LCMN

A number of heterologous tumors arising in large CMN appear on record in the literature. Of these, the series published by Hendrickson and Ross (Hendrickson and Ross 1981) describes the widest spectrum of lesions and clinical behaviors, although it is likely that this collection of tumors combines benign and malignant lesions, including some currently defined as proliferative nodules (*vide infra*). However, in more recent series, tumors arising within CMN have become better defined (Herron et al. 2004; Phadke et al. 2011). The malignancy most frequently seen in this context is malignant melanoma, although its incidence has been difficult to define, ranging from 2 to 42% due to the disparate definitions and wide variations in methodologies used to study them. Modern analyses have established that its real incidence hovers around 4% for giant CMN. Other malignant tumors, rarely arising within CMN, are dominated by rhabdomyosarcoma (Hoang et al. 2002; Ilyas et al. 2004; Schmitt et al. 1992), although the features of these lesions are somewhat different from classic rhabdomyosarcoma arising outside the context of nevomelanocytic proliferations. Unfortunately, no studies on the biological and genetic features of these nevus-related rhabdomyosarcomatous lesions have been published even as single case reports.

The group of lesions more frequently seen arising within CMN is represented by the so-called proliferative nodules, which usually appear during the first years of life if they are not already noted at or before birth (Hösli et al. 2001). These nodules appear as well defined elevations within the area of the nevus, can vary in size and tend to be darker in color than the surrounding nevomelanocytic lesion. Their macroscopic and histological appearance varies,

but they are striking lesions (Fig. 3f), frequently leading to biopsy and surgical attempts at removal with “wide excision”. However, most are benign, despite their alarming appearance, both macroscopically and under the microscope. In a large series (Leech et al. 2004) these nodules are described as benign, although an *atypical* variant, with sharp demarcation from the surrounding nevus, no transition between surrounding nevus cells and nodular cells (lack of so-called “maturation”) and increased mitotic activity. Recent studies on these proliferations support the notion that at least some of these atypical nodules are nevomelanocytic neoplasias that share morphological and genetic features with melanoma, and probably represent an intermediate stage in the progression from a CMN toward a malignant melanoma (Phadke et al. 2011).

It is important to notice that many clinical and histological characteristics accepted as evidence of melanoma in adults may occur in benign lesions in infancy (e.g., rapid growth, ulceration, mitotic activity, pagetoid melanocytic proliferation) (Zúñiga et al. 1987). Deep dermal or subcutaneous nodules may exhibit cellular features of neural or mesenchymal differentiation. Comparative genomic hybridization has shown a high percentage of numerical aberrations of one or few whole chromosomes (Bastian et al. 2002). In contrast, in most melanomas, numerical aberrations affect only portions of often many individual chromosomes. Recent chromosomal analyses of 27 well-characterized large and giant CMN demonstrated three rearrangements – two transpositions involving *BRAF* and presumed to remove inhibitory regulation of the gene product because of increased ERK1/2 phosphorylation, and one with a deletion of the long arm distal to 6q21 (Dessars et al. 2009). This is a clinically relevant issue, since cases in which these proliferative nodules are biopsied, occasionally are subjected to additional, extended and unnecessary surgery based on "alarming" histology. However, it is important to stress that even atypical proliferative nodules tend to behave in a benign fashion and probably do not warrant aggressive surgical removal (Phadke et al. 2011).

It is important to note that cutaneous melanomas arising in CMN may differ significantly in clinical and histological behaviour. Although in part overlapping, two main categories are recognized (Magaña and Magaña 2007). First, melanoma arising in CMN may originate from the dermo-epidermal junction or the upper dermis. Histologically, these melanomas tend to develop in adolescence and adulthood and exhibit similar changes to the conventional superficial spreading or nodular melanomas of adulthood. Second, melanoma may seem to arise from deeper tissue structures, *i.e.*, mostly from deeper, dermally located melanocytic (precursor) cells. This type of CMN-related melanoma is a small-cell neoplasm and has been termed in the past a “dermal congenital tumorous dysplasia-blastoma” (Reed 1993). In contrast to conventional melanoma, it often develops during infancy or childhood and mainly accounts for the fact that the mean age of melanoma in CMN is 15.5 years (median, 7 years; (Krengel et al. 2006)). It will be worth examining these childhood melanomas for mutations not only in *BRAF* and *NRAS*, but in *GNAQ* and *GNA11*, among even more novel candidates that are likely to emerge in the near future, impinging on these intersecting signaling pathways (Broekaert et al. 2010). When costs permit, whole exome (or whole genome) sequencing of germline DNA and tumor DNA from patients will finally allow the research community to develop more dichotomous classifications and prognoses by simultaneously examining all coding regions (and their regulation), and carefully classifying tumors by their clinical and histopathological characteristics.

Besides melanoma, other malignancies have been reported in CMN, probably reflecting the undifferentiated, pluripotent state of neural crest-derived melanocytic precursor cells. A number of entities have been mentioned, including rhabdomyosarcoma, liposarcoma, malignant spindle cell neoplasm, neuroblastoma, and malignant peripheral nerve sheath tumor (DeDavid et al. 1996; Hendrickson and Ross 1981; Schaffer et al. 2007). Many of these are likely to represent heterologous elements sometimes associated with proliferative nodules. Given what we are now learning about the embryological maturation of normal melanocytes and the effects of modifying genes needed for their development, it will be unsurprising to learn that these difficult neoplasms arise as a result of the same mechanisms, candidates for similar chemotherapies both within or distinct from the context of a large or giant CMN.

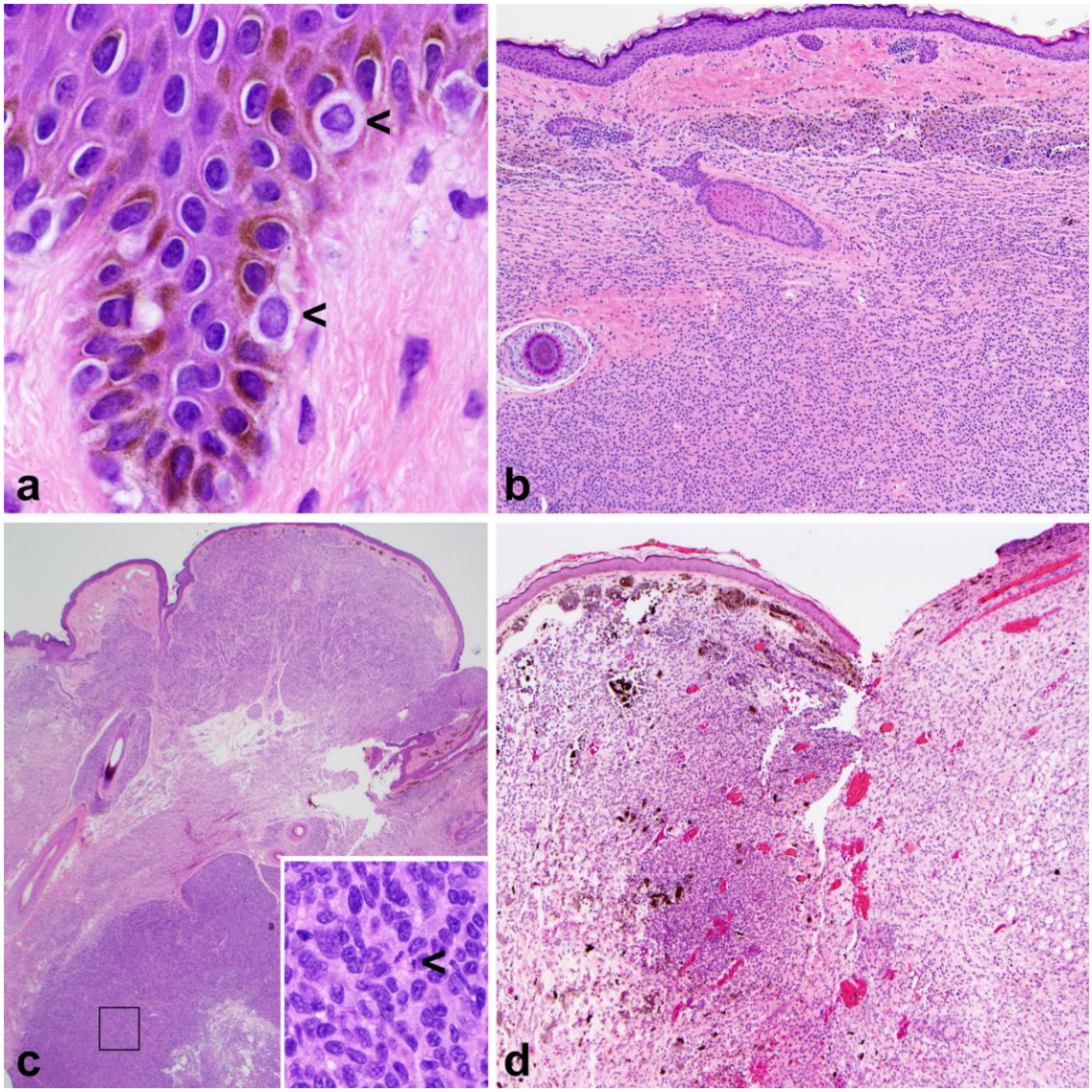

Figure 1. (a) Normal skin with melanocytes (clear cells, arrowheads) and melanin pigment transferred to keratinocytes. Hematoxylin-eosin (H&E) 60X. (b) Giant congenital melanocytic nevus, with nevus cells both pigmented and not pigmented throughout the dermis. H&E 4X. (c) CMN with proliferative nodule in the deeper portion which appears hypercellular. Boxed area represents inset, which shows a typical mitotic figure (arrowhead) within the nodule. (d) Giant CMN with an area of small, round nevomelanocytes on the left, and heterologous adipocyte elements on the right. Note the marked neuroid (wavy) appearance of the architectural pattern.

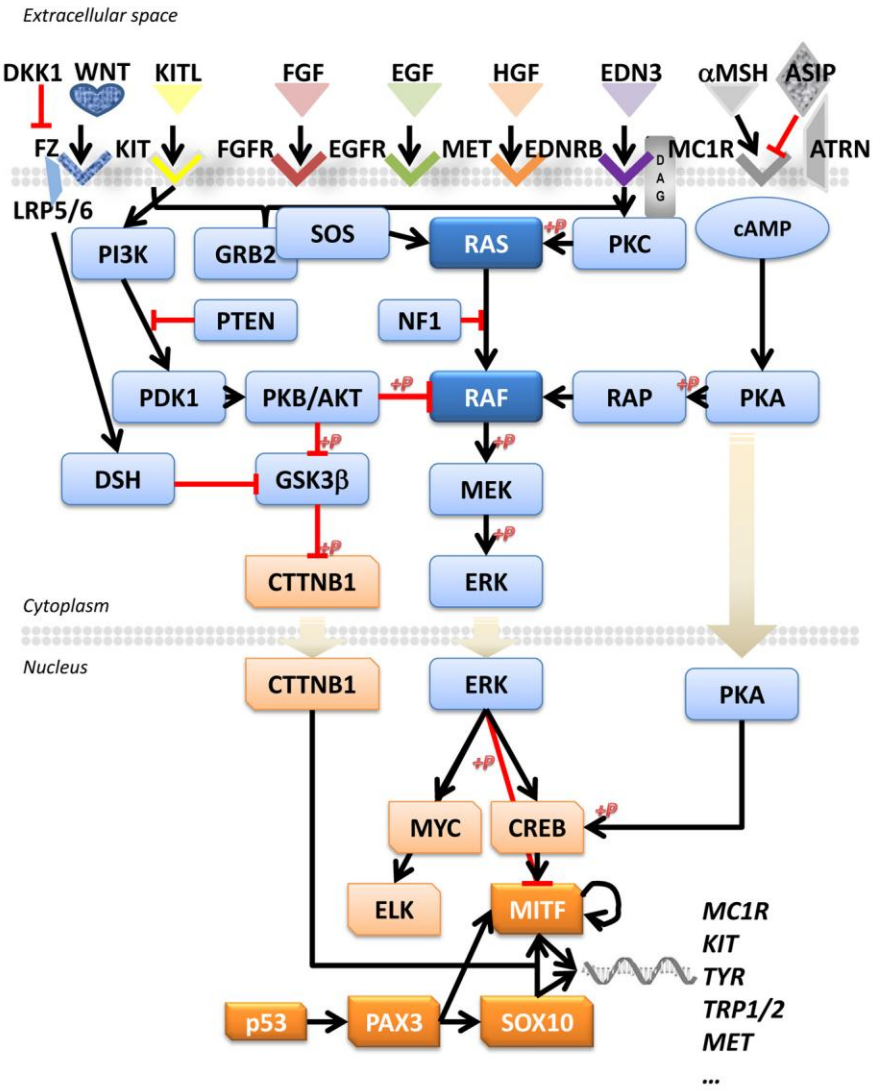

Figure 2. Major signaling pathways from extracellular ligands to transcriptional targets, important for neural crest and more specifically melanocyte specification, proliferation, maintenance, response to environmental stimuli and senescence.

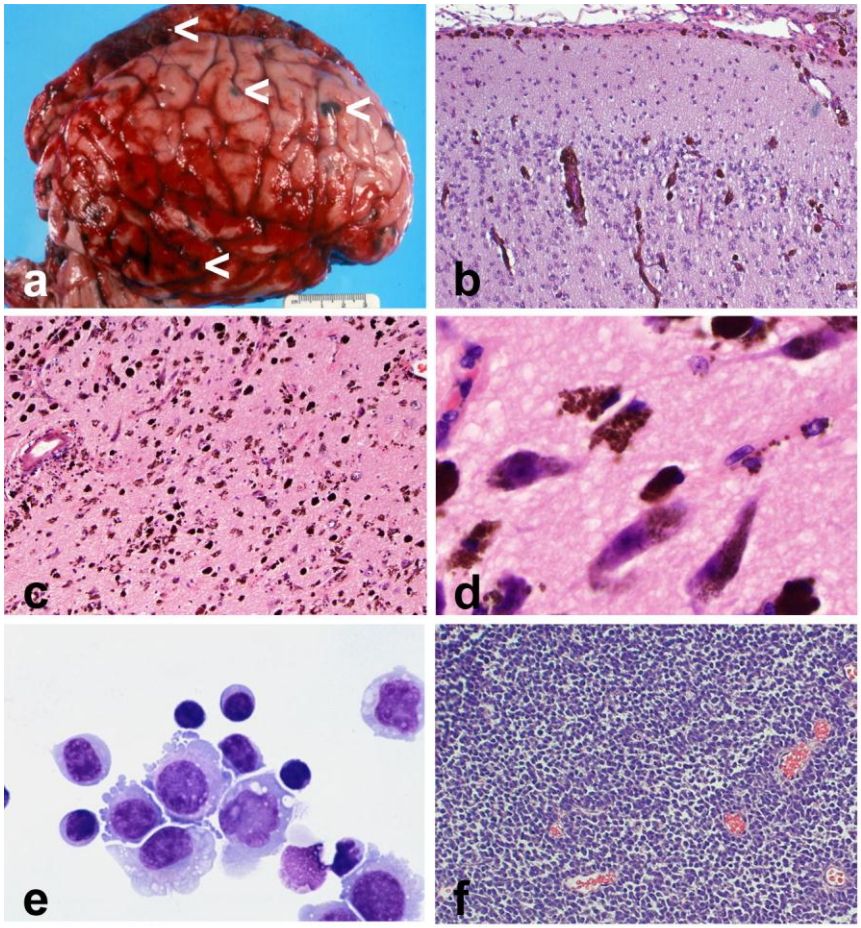

Figure 3. (a) Macroscopic appearance of a brain from a patient with neurocutaneous melanocytosis (NCM; anterior to right). Dark lesions correspond to foci of parenchymal invasion of frontal and temporal lobes by NCM cells, some of which are indicated by arrowheads. (b) NCM at surface leptomeninges (top) and along Virschow-Robin spaces. H&E 20X. (c, d) Brain parenchyma from a previously unreported case of NCM, demonstrating ectopic nevomelanocytes and apparent uptake of melanin granules by adjacent neurons. H&E 10X and 40X, respectively. This patient is alive at the time of writing. (e) Cerebrospinal fluid specimen from a patient with lethal NCM. Atypical nevomelanocytes with short dendrites recapitulate the morphology of melanocytes. (f) "Metastasis" of NCM from same patient to nodules in the peritoneal cavity after ventriculoperitoneal shunting (Cajaiba et al. 2008).

Acknowledgements

MB and HCE were supported in part by funding from Nevus Outreach, Inc. The authors thank Dr. Valérie Matagne for constructive criticism of the manuscript.

References

Adameyko I, Lallemend F, Aquino JB, et al. (2009) Schwann cell precursors from nerve innervation are a cellular origin of melanocytes in skin. Cell 139:366-79. doi: 10.1016/j.cell.2009.07.049

Agero ALC, Benvenuto-Andrade C, Dusza SW, et al. (2005) Asymptomatic neurocutaneous melanocytosis in patients with large congenital melanocytic nevi: a study of cases from an Internet-based registry. Journal of the American Academy of Dermatology 53:959-65. doi: 10.1016/j.jaad.2005.07.046

Antonellis A, Huynh JL, Lee-Lin S-Q, et al. (2008) Identification of neural crest and glial enhancers at the mouse Sox10 locus through transgenesis in zebrafish. PLoS Genetics 4:e1000174. doi: 10.1371/journal.pgen.1000174

Aoki Y, Niihori T, Kawame H, et al. (2005) Germline mutations in HRAS proto-oncogene cause Costello syndrome. Nature Genetics 37:1038-1040.

Aoki Y, Niihori T, Narumi Y, et al. (2008) The RAS/MAPK syndromes: novel roles of the RAS pathway in human genetic disorders. Human Mutation 29:992-1006. doi: 10.1002/humu.20748

Aoki Y, Saint-Germain N, Gyda M, et al. (2003) Sox10 regulates the development of neural crest-derived melanocytes in Xenopus. Developmental Biology 259:19-33.

Azzoni A, Argentieri R, Raja M (2001) Neurocutaneous melanosis and psychosis: a case report. Psychiatry and Clinical Neurosciences 55:93-5. doi: 10.1046/j.1440-1819.2001.00794.x

Bae JM, Kim MY, Kim HO, Park YM (2007) Schwannoma coexisting with congenital melanocytic nevus: is it coincidence? Journal of the American Academy of Dermatology 56:S111-2. doi:10.1016/j.jaad.2006.07.033

Barnhill RL, Cerroni L, Cook M, et al. (2010) State of the art, nomenclature, and points of consensus and controversy concerning benign melanocytic lesions: outcome of an international workshop. Advances in Anatomic Pathology 17:73-90.

Baroffio A, Dupin E, Le Douarin NM (1991) Common precursors for neural and mesectodermal derivatives in the cephalic neural crest. Development 112:301-5.

Bastian BC, Xiong J, Frieden IJ, et al. (2002) Genetic changes in neoplasms arising in congenital melanocytic nevi: differences between nodular proliferations and melanomas. The American Journal of Pathology 161:1163-9.

Bauer JW, Schaeppi H, Kaserer C, et al. (2001) Large melanocytic nevi in hereditary epidermolysis bullosa. Journal of the American Academy of Dermatology 44:577-84.

Bauer J, Curtin JA, Pinkel D, Bastian BC (2007) Congenital melanocytic nevi frequently harbor NRAS mutations but no BRAF mutations. The Journal of Investigative Dermatology 127:179-82. doi: 10.1038/sj.jid.5700490

Benko S, Fantes JA, Amiel J, et al. (2009) Highly conserved non-coding elements on either side of SOX9 associated with Pierre Robin sequence. Nature Genetics 41:359-64. doi: 10.1038/ng.329

Betancur P, Bronner-Fraser M, Sauka-Spengler T (2010) Genomic code for Sox10 activation reveals a key regulatory enhancer for cranial neural crest. Proceedings of the National Academy of Sciences of the United States of America 107:3570-5. doi: 10.1073/pnas.0906596107

Bett BJ (2006) Large or multiple congenital melanocytic nevi: occurrence of neurocutaneous melanocytosis in 1008 persons. Journal of the American Academy of Dermatology 54:767-77. doi: 10.1016/j.jaad.2005.10.040

Bett BJ (2005) Large or multiple congenital melanocytic nevi: occurrence of cutaneous melanoma in 1008 persons. Journal of the American Academy of Dermatology 52:793-7. doi: 10.1016/j.jaad.2005.02.024

Bicknell AB (2008) The tissue-specific processing of pro-opiomelanocortin. Journal of Neuroendocrinology 20:692-9. doi: 10.1111/j.1365-2826.2008.01709.x

Bonano M, Tribulo C, De Calisto J, et al. (2008) A new role for the Endothelin-1/Endothelin-A receptor signaling during early neural crest specification. 323:114-129.

Bondurand N, Pingault V, Goerich DE, et al. (2000) Interaction among SOX10, PAX3 and MITF, three genes altered in Waardenburg syndrome. Hum Mol Genet 9:1907-1917.

Brand M, Le Moullec JM, Corvol P, Gasc JM (1998) Ontogeny of endothelins-1 and -3, their receptors, and endothelin converting enzyme-1 in the early human embryo. 101:549-559.

Britsch S, Goerich DE, Riethmacher D, et al. (2001) The transcription factor Sox10 is a key regulator of peripheral glial development. Genes Dev 15:66-78.

Broekaert SMC, Roy R, Okamoto I, et al. (2010) Genetic and morphologic features for melanoma classification. Pigment Cell & Melanoma Research 23:763-70.

Brooks C, Scope A, Braun RP, Marghoob AA (2011) Dermoscopy of nevi and melanoma in childhood. Expert Review of Dermatology 6:19–34.

Burstein F, Seier H, Hudgins PA, Zapiach L (2005) Neurocutaneous melanosis. The Journal of Craniofacial Surgery 16:874-6.

Cajaiba MM, Benjamin D, Halaban R, Reyes-Múgica M (2008) Metastatic peritoneal neurocutaneous melanocytosis. The American Journal of Surgical Pathology 32:156-61.

Chen Y, Deng W, Zhu H, et al. (2009) The pathologic features of neurocutaneous melanosis in a cynomolgus macaque. Veterinary Pathology 46:773-5. doi: 10.1354/vp.08-VP-0243-Q-BC

Clewes O, Narytnyk A, Gillinder KR, et al. (2011) Human Epidermal Neural Crest Stem Cells (hEPI-NCSC)-Characterization and Directed Differentiation into Osteocytes and Melanocytes. Stem Cell Reviews (online version). doi: 10.1007/s12015-011-9255-5

Clouthier DE, Garcia E, Schilling TF (2010) Regulation of facial morphogenesis by endothelin signaling: insights from mice and fish. American Journal of Medical Genetics. Part A 152A:2962-73. doi: 10.1002/ajmg.a.33568

Danarti R, Konig A, Happle R (2003) Large congenital melanocytic nevi may reflect paradominant inheritance implying allelic loss. Eur J Dermatol 13:430-432.

Davies H, Bignell GR, Cox C, et al. (2002) Mutations of the BRAF gene in human cancer. Nature 417:949-54. doi: 10.1038/nature00766

De Schepper S, Boucneau J, Vander Haeghen Y, et al. (2006) Café-au-lait spots in neurofibromatosis type 1 and in healthy control individuals: hyperpigmentation of a different kind? Archives of Dermatological Research 297:439-49. doi: 10.1007/s00403-006-0644-6

DeDavid M, Orlow SJ, Provost N, et al. (1996) Neurocutaneous melanosis: clinical features of large congenital melanocytic nevi in patients with manifest central nervous system melanosis. Journal of the American Academy of Dermatology 35:529-38.

Delmas V, Beermann F, Martinozzi S, et al. (2007) Beta-catenin induces immortalization of melanocytes by suppressing p16INK4a expression and cooperates with N-Ras in melanoma development. Genes & development 21:2923-35. doi: 10.1101/gad.450107

Dessars B, De Raeve LE, Morandini R, et al. (2009) Genotypic and gene expression studies in congenital melanocytic nevi: insight into initial steps of melanotumorigenesis. The Journal of Investigative Dermatology 129:139-47. doi: 10.1038/jid.2008.203

Dong J, Phelps RG, Qiao R, et al. (2003) BRAF oncogenic mutations correlate with progression rather than initiation of human melanoma. Cancer Research 63:3883-5.

Dorshorst B, Okimoto R, Ashwell C (2010) Genomic regions associated with dermal hyperpigmentation, polydactyly and other morphological traits in the Silkie chicken. The Journal of Heredity 101:339-50. doi: 10.1093/jhered/esp120

Dunn LC (1937) Studies on Spotting Patterns II. Genetic Analysis of Variegated Spotting in the House Mouse. Genetics 22:43-64.

Dupin E, Glavieux C, Vaigot P, Le Douarin NM (2000) Endothelin 3 induces the reversion of melanocytes to glia through a neural crest-derived glial-melanocytic progenitor. Proceedings of the National Academy of Sciences of the United States of America 97:7882-7.

Dupin E (2011) [Phenotypic plasticity of neural crest-derived melanocytes and Schwann cells.]. Biologie Aujourd'hui 205:53-61. doi: 10.1051/jbio/2011008

Dupin E, Real C, Glavieux-Pardanaud C, et al. (2003) Reversal of developmental restrictions in neural crest lineages: transition from Schwann cells to glial-melanocytic precursors in vitro. Proceedings of the National Academy of Sciences of the United States of America 100:5229-33.

Easty DJ, Gray SG, O'Byrne KJ, et al. (2011) Receptor tyrosine kinases and their activation in melanoma. Pigment Cell & Melanoma Research. doi: 10.1111/j.1755-148X.2011.00836.x

Etchevers HC, Amiel J, Lyonnet S (2006) Molecular bases of human neurocristopathies. In: Saint-Jeannet J-P(ed) Neural Crest Induction and Differentiation ed. Landes Bioscience, Texas, pp213-34

Etchevers HC, Vincent C, Le Douarin NM, Couly GF (2001) The cephalic neural crest provides pericytes and smooth muscle cells to all blood vessels of the face and forebrain. Development 128:1059-68.

Fitch KR, McGowan K a, van Raamsdonk CD, et al. (2003) Genetics of dark skin in mice. Genes & development 17:214-28. doi: 10.1101/gad.1023703

Foster RD, Williams ML, Barkovich AJ, et al. (2001) Giant congenital melanocytic nevi: the significance of neurocutaneous melanosis in neurologically asymptomatic children. Plastic and Reconstructive Surgery 107:933-41.

Frieden IJ, Williams ML, Barkovich AJ (1994) Giant congenital melanocytic nevi: brain magnetic resonance findings in neurologically asymptomatic children. Journal of the American Academy of Dermatology 31:423-9.

Fu Y-J, Morota N, Nakagawa A, et al. (2010) Neurocutaneous melanosis: surgical pathological features of an apparently hamartomatous lesion in the amygdala. Journal of Neurosurgery: Pediatrics 6:82-6.

Garcez RC, Teixeira BL, Schmitt SDS, et al. (2009) Epidermal growth factor (EGF) promotes the in vitro differentiation of neural crest cells to neurons and melanocytes. Cellular and Molecular Neurobiology 29:1087-91.

Grichnik JM, Burch JA, Burchette J, Shea CR (1998) The SCF/KIT pathway plays a critical role in the control of normal human melanocyte homeostasis. The Journal of Investigative Dermatology 111:233-8.

Gupta PB, Kuperwasser C, Brunet J-P, et al. (2005) The melanocyte differentiation program predisposes to metastasis after neoplastic transformation. Nature Genetics 37:1047-54.

Gönül M, Soylu S, Gül U, et al. (2009) Giant congenital melanocytic naevus associated with Dandy-Walker malformation, lipomatosis and hemihypertrophy of the leg. Clinical and Experimental Dermatology 34:e106-9. doi: 10.1111/j.1365-2230.2008.03191.x

Hafner C, Toll A, Fernández-Casado A, et al. (2010) Multiple oncogenic mutations and clonal relationship in spatially distinct benign human epidermal tumors. Proceedings of the National Academy of Sciences of the United States of America 107:20780-20785. doi: 10.1073/pnas.1008365107

Hale EK, Stein J, Ben-Porat L, et al. (2005) Association of melanoma and neurocutaneous melanocytosis with large congenital melanocytic naevi--results from the NYU-LCMN registry. The British Journal of Dermatology 152:512-7. doi: 10.1111/j.1365-2133.2005.06316.x

Happle R (1999) Loss of heterozygosity in human skin. Journal of the American Academy of Dermatology 41:143-64.

Hendrickson MR, Ross JC (1981) Neoplasms arising in congenital giant nevi: morphologic study of seven cases and a review of the literature. The American Journal of Surgical Pathology 5:109-35.

Herraiz C, Journé F, Abdel-Malek Z, et al. (2011) Signaling from the human melanocortin 1 receptor to ERK1 and ERK2 mitogen-activated protein kinases involves transactivation of cKIT. Molecular Endocrinology 25:138-56. doi: 10.1210/me.2010-0217

Herron MD, Vanderhooft SL, Smock K, et al. (2004) Proliferative nodules in congenital melanocytic nevi: a clinicopathologic and immunohistochemical analysis. The American Journal of Surgical Pathology 28:1017-25.

Hoang MP, Sinkre P, Albores-Saavedra J (2002) Rhabdomyosarcoma arising in a congenital melanocytic nevus. The American Journal of Dermatopathology 24:26-9.

Hou L, Pavan WJ (2008) Transcriptional and signaling regulation in neural crest stem cell-derived melanocyte development: do all roads lead to Mitf? Cell Research 18:1163-76.

Huang C, Lee P (2000) Phakomatosis pigmentovascularis IIb with renal anomaly. Clinical and Experimental Dermatology 25:51-4.

Huber WE, Price ER, Widlund HR, et al. (2003) A tissue-restricted cAMP transcriptional response: SOX10 modulates alpha-melanocyte-stimulating hormone-triggered expression of microphthalmia-associated transcription factor in melanocytes. The Journal of Biological Chemistry 278:45224-30.

Hui P, Perkins A, Glusac E (2001) Assessment of clonality in melanocytic nevi. Journal of Cutaneous Pathology 28:140-4.

Hösli I, Holzgreve W, Danzer E, Tercanli S (2001) Two case reports of rare fetal tumors: an indication for surface rendering? Ultrasound in Obstetrics & Gynecology 17:522-6. doi: 10.1046/j.1469-0705.2001.00407.x

Ilyas EN, Goldsmith K, Lintner R, Manders SM (2004) Rhabdomyosarcoma arising in a giant congenital melanocytic nevus. Cutis; cutaneous medicine for the practitioner 73:39-43.

Im S, Moro O, Peng F, Nordlund J (1998) Activation of the Cyclic AMP Pathway by α -Melanotropin Mediates the Response of Human Melanocytes to Ultraviolet B Radiation of Human Melanocytes to Ultraviolet B Radiation ’. Cancer Research 47-54.

Kadonaga JN, Frieden IJ (1991) Neurocutaneous melanosis: definition and review of the literature. Journal of the American Academy of Dermatology 24:747-55.

Karafiat V, Dvorakova M, Pajer P, et al. (2007) Melanocyte fate in neural crest is triggered by Myb proteins through activation of c-kit. Cellular and Molecular Life Sciences 64:2975-84.

Khakoo Y, Marghoob A (2009) Neurocutaneous melanocytosis: outcome not uniformly fatal. Journal of Clinical Oncology 27:e136; author reply e137. doi: 10.1200/JCO.2009.24.0309

Kinsler VA, Birley J, Atherton DJ (2009) Great Ormond Street Hospital for Children Registry for congenital melanocytic naevi: prospective study 1988-2007. Part 1-epidemiology, phenotype and outcomes. The British Journal of Dermatology 160:143-50. doi: 10.1111/j.1365-2133.2008.08849.x

Kinsler VA, Chong WK, Aylett SE, Atherton DJ (2008) Complications of congenital melanocytic naevi in children: analysis of 16 years’ experience and clinical practice. The British Journal of Dermatology 159:907-14. doi: 10.1111/j.1365-2133.2008.08775.x

Kinsler V (2011) Satellite lesions in congenital melanocytic nevi-time for a change of name. Pediatric Dermatology 1-2. doi: 10.1111/j.1525-1470.2010.01199.x

Koot HM, de Waard-van der Spek F, Peer CD, et al. (2000) Psychosocial sequelae in 29 children with giant congenital melanocytic naevi. Clinical and Experimental Dermatology 25:589-93.

Kormos B, Belső N, Bebes A, et al. (2011) In vitro dedifferentiation of melanocytes from adult epidermis. PLoS ONE 6:e17197. doi: 10.1371/journal.pone.0017197

Krengel S, Hauschild A, Schäfer T (2006) Melanoma risk in congenital melanocytic naevi: a systematic review. The British Journal of Dermatology 155:1-8. doi: 10.1111/j.1365-2133.2006.07218.x

Krengel S, Breuninger H, Beckwith M, Etchevers HC (2011) Meeting report from the 2011 International Expert Meeting on Large Congenital Melanocytic Nevi and Neurocutaneous Melanocytosis, Tübingen. Pigment Cell and Melanoma Research, in press.

Kunisada T, Lu SZ, Yoshida H, et al. (1998) Murine cutaneous mastocytosis and epidermal melanocytosis induced by keratinocyte expression of transgenic stem cell factor. The Journal of Experimental Medicine 187:1565-73.

Kunisada T, Yamazaki H, Hirobe T, et al. (2000) Keratinocyte expression of transgenic hepatocyte growth factor affects melanocyte development, leading to dermal melanocytosis. Mechanisms of Development 94:67-78.

Köksal N, Bayram Y, Murat I, et al. (2003) Neurocutaneous melanosis with transposition of the great arteries and renal agenesis. Pediatric Dermatology 20:332-4.

Küsters-Vandevelde HVN, Klaasen A, Küsters B, et al. (2009) Activating mutations of the GNAQ gene: a frequent event in primary melanocytic neoplasms of the central nervous system. Acta neuropathologica 317-323. doi: 10.1007/s00401-009-0611-3

Le Douarin NM, Kalcheim C (1999) The Neural Crest. 2nd ed. Cambridge University Press, Cambridge, U.K., pp 1-445

Lecoin L, Lahav R, Martin FH, et al. (1995) Steel and c-kit in the development of avian melanocytes: a study of normally pigmented birds and of the hyperpigmented mutant silky fowl. Developmental Dynamics 203:106-18. doi: 10.1002/aja.1002030111

Leech SN, Bell H, Leonard N, et al. (2004) Neonatal giant congenital nevi with proliferative nodules: a clinicopathologic study and literature review of neonatal melanoma. Archives of Dermatology 140:83-8. doi: 10.1001/archderm.140.1.83

Lev S, Givol D, Yarden Y (1992) Interkinase domain of kit contains the binding site for phosphatidylinositol 3' kinase. Proceedings of the National Academy of Sciences of the United States of America 89:678-82.

Li L, Fukunaga-Kalabis M, Yu H, et al. (2010) Human dermal stem cells differentiate into functional epidermal melanocytes. Journal of Cell Science 123:853-60. doi: 10.1242/jcs.061598

Li Y, Zhu X, Yang L, et al. (2011) Expression and network analysis of genes related to melanocyte development in the Silky Fowl and White Leghorn embryos. Molecular Biology Reports 38:1433-41.

Limaye N, Boon LM, Vikkula M (2009) From germline towards somatic mutations in the pathophysiology of vascular anomalies. Human Molecular Genetics 18:R65-74. doi: 10.1093/hmg/ddp002

Lin J, Goto Y, Murata H, et al. (2011) Polyclonality of BRAF mutations in primary melanoma and the selection of mutant alleles during progression. British Journal of Cancer 104:464-8. doi: 10.1038/sj.bjc.6606072

Lin J, Takata M, Murata H, et al. (2009) Polyclonality of BRAF mutations in acquired melanocytic nevi. Journal of the National Cancer Institute 101:1423-7. doi: 10.1093/jnci/djp309

Livingstone E, Claviez A, Spengler D, et al. (2009) Neurocutaneous melanosis: a fatal disease in early childhood. Journal of Clinical Oncology 27:2290-1. doi: 10.1200/JCO.2008.20.4388

Lovett A, Maari C, Decarie J-C, et al. (2009) Large congenital melanocytic nevi and neurocutaneous melanocytosis: one pediatric center's experience. Journal of the American Academy of Dermatology 61:766-74. doi: 10.1016/j.jaad.2008.11.022

Lu S, Slominski A, Yang S-E, et al. (2010) The correlation of TRPM1 (Melastatin) mRNA expression with microphthalmia-associated transcription factor (MITF) and other melanogenesis-related proteins in normal and pathological skin, hair follicles and melanocytic nevi. Journal of Cutaneous Pathology 37 (Suppl :26-40. doi: 10.1111/j.1600-0560.2010.01504.x

Maertens O, De Schepper S, Vandesompele J, et al. (2007) Molecular dissection of isolated disease features in mosaic neurofibromatosis type 1. American Journal of Human Genetics 81:243-51. doi: 10.1086/519562

Magaña M, Magaña ML (2007) Congenital melanocytic nevus is a disease with two clinicopathologic forms of presentation. Journal of the American Academy of Dermatology 56:521-2. doi: 10.1016/j.jaad.2006.09.022

Makin GW, Eden OB, Lashford LS, et al. (1999) Leptomeningeal melanoma in childhood. Cancer 86:878-86.

Marghoob AA, Dusza S, Oliveria S, Halpern A (2004) Number of satellite nevi as a correlate for neurocutaneous melanocytosis in patients with large congenital melanocytic nevi. Archives of Dermatology 140:171-5. doi: 10.1001/archderm.140.2.171

Marnet D, Vinchon M, Mostofi K, et al. (2009) Neurocutaneous melanosis and the Dandy-Walker complex: an uncommon but not so insignificant association. Child's Nervous System 25:1533-9. doi: 10.1007/s00381-009-0976-6

Mehraein Y, Ehlhardt S, Wagner A, et al. (2004) Somatic mosaicism of chromosome 7 in a highly proliferating melanocytic congenital naevus in a ring chromosome 7 patient. American Journal of Medical Genetics. Part A 131:179-85.

Miller VS (2004) Neurocutaneous Melanosis. In:Roach ES, Miller VS(ed) Neurocutaneous Disorders ed. Cambridge University Press, Cambridge, U.K., pp71-76

Moore-Olufemi S, Herzog C, Warneke C, et al. (2011) Outcomes in Pediatric Melanoma: Comparing Prepubertal to Adolescent Pediatric Patients. Annals of Surgery (in press). doi: 10.1097/SLA.0b013e318217e852

Mort RL, Hay L, Jackson IJ (2010) Ex vivo live imaging of melanoblast migration in embryonic mouse skin. Pigment Cell & Melanoma Research 23:299-301.

Motohashi T, Yamanaka K, Chiba K, et al. (2009) Unexpected multipotency of melanoblasts isolated from murine skin. Stem Cells 27:888-97. doi: 10.1634/stemcells.2008-0678

Nath D, Williamson NJ, Jarvis R, Murphy G (2001) Shedding of c-Met is regulated by crosstalk between a G-protein coupled receptor and the EGF receptor and is mediated by a TIMP-3 sensitive metalloproteinase. Journal of Cell Science 114:1213-20.

Niihori T, Aoki Y, Narumi Y, et al. (2006) Germline KRAS and BRAF mutations in cardio-facio-cutaneous syndrome. Nature Genetics 38:294-6. doi: 10.1038/ng1749

Paratore C, Goerich DE, Suter U, et al. (2001) Survival and glial fate acquisition of neural crest cells are regulated by an interplay between the transcription factor Sox10 and extrinsic combinatorial signaling. Development 128:3949-3961.

Patton EE, Widlund HR, Kutok JL, et al. (2005) BRAF mutations are sufficient to promote nevi formation and cooperate with p53 in the genesis of melanoma. Current Biology 15:249-54. doi: 10.1016/j.cub.2005.01.031

Paulhe F, Wehrle-Haller M, Jacquier M-C, et al. (2009) Dimerization of Kit-ligand and efficient cell-surface presentation requires a conserved Ser-Gly-Gly-Tyr motif in its transmembrane domain. The FASEB Journal 1-12.

Pavlidou E, Hagel C, Papavasilliou A, et al. (2008a) Neurocutaneous melanosis: report of three cases and up-to-date review. Journal of Child Neurology 23:1382-91. doi: 10.1177/0883073808319069

Pavlidou E, Hagel C, Papavasilliou A, et al. (2008b) Neurocutaneous melanosis: report of three cases and up-to-date review. Journal of Child Neurology 23:1382-91. doi: 10.1177/0883073808319069

Peters R, Jansen G, Engelbrecht V (2000) Neurocutaneous melanosis with hydrocephalus, intraspinal arachnoid collections and syringomyelia: case report and literature review. Pediatric Radiology 30:284-8.

Phadke PA, Rakheja D, Le LP, et al. (2011) Proliferative nodules arising within congenital melanocytic nevi: a histologic, immunohistochemical, and molecular analyses of 43 cases. The American Journal of Surgical Pathology 35:656-69.

Pla P, Alberti C, Solov'eva O, et al. (2005) Ednrb2 orients cell migration towards the dorsolateral neural crest pathway and promotes melanocyte differentiation. Pigment Cell Research 18:181-187.

Pollock PM, Harper UL, Hansen KS, et al. (2003) High frequency of BRAF mutations in nevi. Nat Genet 33:19-20.

Potterf SB, Furumura M, Dunn KJ, et al. (2000) Transcription factor hierarchy in Waardenburg syndrome: regulation of MITF expression by SOX10 and PAX3. Human Genetics 107:1-6.

Poumay Y, Mitev V (2009) Members of the EGF receptor family in normal and pathological epidermis. Folia Medica 51:5-17.

Powell MB, Hyman P, Bell OD, et al. (1995) Hyperpigmentation and melanocytic hyperplasia in transgenic mice expressing the human T24 Ha-ras gene regulated by a mouse tyrosinase promoter. Molecular Carcinogenesis 12:82-90.

Price HN, Schaffer JV (2010) Congenital melanocytic nevi-when to worry and how to treat: Facts and controversies. Clinics in Dermatology 28:293-302. doi: 10.1016/j.clindermatol.2010.04.004

Puig I, Champeval D, De Santa Barbara P, et al. (2009) Deletion of Pten in the mouse enteric nervous system induces ganglioneuromatosis and mimics intestinal pseudoobstruction. The Journal of Clinical Investigation 119:3586-96. doi: 10.1172/JCI39929

Rao MS, Anderson DJ (1997) Immortalization and controlled in vitro differentiation of murine multipotent neural crest stem cells. Journal of Neurobiology 32:722-46.

Ratajczak MZ, Perrotti D, Melotti P, et al. (1998) Myb and ets proteins are candidate regulators of c-kit expression in human hematopoietic cells. Blood 91:1934-46.

Real C, Glavieux-Pardanaud C, Vaigot P, et al. (2005) The instability of the neural crest phenotypes: Schwann cells can differentiate into myofibroblasts. International Journal of Developmental Biology 49:151-159.

Reardon W, Zhou X-P, Eng C (2001) A novel germline mutation of the PTEN gene in a patient with macrocephaly, ventricular dilatation, and features of VATER association. Journal of Medical Genetics 38:820-823. doi: 10.1136/jmg.38.12.820

Reed RJ (1993) Giant congenital nevi: a conceptualization of patterns. The Journal of Investigative Dermatology 100:300S-312S.

Rendl M, Lewis L, Fuchs E (2005) Molecular dissection of mesenchymal-epithelial interactions in the hair follicle. PLoS Biology 3:e331.

Reyes-Mugica M, Chou P, Byrd S, et al. (1993) Nevomelanocytic proliferations in the central nervous system of children. Cancer 72:2277-85.

Rodriguez-Viciana P, Tetsu O, Tidyman WE, et al. (2006) Germline mutations in genes within the MAPK pathway cause cardio-facio-cutaneous syndrome. Science 311:1287-90. doi: 10.1126/science.1124642

Schaffer JV, Chang MW, Kovich OI, et al. (2007) Pigmented plexiform neurofibroma: Distinction from a large congenital melanocytic nevus. Journal of the American Academy of Dermatology 56:862-8. doi: 10.1016/j.jaad.2006.11.022

Schallreuter KU, Kothari S, Chavan B, Spencer JD (2008) Regulation of melanogenesis--controversies and new concepts. Experimental Dermatology 17:395-404. doi: 10.1111/j.1600-0625.2007.00675.x

Schlingemann RO, Rietveld FJ, de Waal RM, et al. (1990) Expression of the high molecular weight melanoma-associated antigen by pericytes during angiogenesis in tumors and in healing wounds. The American Journal of Pathology 136:1393-405.

Schmitt FC, Bittencourt A, Mendonca N, Dorea M (1992) Rhabdomyosarcoma in a congenital pigmented nevus. Pediatric Pathology 12:93-8.

Sensi M, Nicolini G, Petti C, et al. (2006) Mutually exclusive NRASQ61R and BRAFV600E mutations at the single-cell level in the same human melanoma. Oncogene 25:3357-64. doi: 10.1038/sj.onc.1209379

Shah KN (2010) The risk of melanoma and neurocutaneous melanosis associated with congenital melanocytic nevi. Seminars in Cutaneous Medicine and Surgery 29:159-64. doi: 10.1016/j.sder.2010.06.007

Shin MK, Levorse JM, Ingram RS, Tilghman SM (1999) The temporal requirement for endothelin receptor-B signalling during neural crest development. Nature 402:496-501.

Shinno K, Nagahiro S, Uno M, et al. (2003) Neurocutaneous melanosis associated with malignant leptomeningeal melanoma in an adult: clinical significance of 5-S-cysteinyldopa in the cerebrospinal fluid---case report. Neurologia Medico-Chirurgica 43:619-25.

Sieber-Blum M, Grim M, Hu YF, Szeder V (2004) Pluripotent neural crest stem cells in the adult hair follicle. Dev Dyn 231:258-269.

Slutsky JB, Barr JM, Femia AN, Marghoob AA (2010) Large congenital melanocytic nevi: associated risks and management considerations. Seminars in Cutaneous Medicine and Surgery 29:79-84. doi: 10.1016/j.sder.2010.04.007

Steel KP, Davidson DR, Jackson IJ (1992) TRP-2/DT, a new early melanoblast marker, shows that steel growth factor (c-kit ligand) is a survival factor. Development 115:1111-9.

Sviderskaya EV, Easty DJ, Lawrence M a, et al. (2009) Functional neurons and melanocytes induced from immortal lines of postnatal neural crest-like stem cells. The FASEB Journal 23:3179-92. doi: 10.1096/fj.08-123596

Szeder V, Grim M, Halata Z, Sieber-Blum M (2003) Neural crest origin of mammalian Merkel cells. Developmental Biology 253:258-63.

Takayama H, La Rochelle WJ, Anver M, et al. (1996) Scatter factor/hepatocyte growth factor as a regulator of skeletal muscle and neural crest development. Proceedings of the National Academy of Sciences of the United States of America 93:5866-71.

Thakur MS, Parmar SNS, Pillai PVA (2006) Studies on growth performance in Kadaknath breed of poultry. Livestock Research for Rural Development 18:article #116.

Thomas AJ, Erickson C a (2008) The making of a melanocyte: the specification of melanoblasts from the neural crest. Pigment Cell & Melanoma Research 21:598-610. doi: 10.1111/j.1755-148X.2008.00506.x

Thomas S, Thomas M, Wincker P, et al. (2008) Human neural crest cells display molecular and phenotypic hallmarks of stem cells. Human Molecular Genetics 17:3411-25. doi: 10.1093/hmg/ddn235

Thompson A, Kent G (2001) Adjusting to disfigurement: processes involved in dealing with being visibly different. Clinical Psychology Review 21:663-682.

Tokuda Y, Saida T, Murata H, et al. (2010) Histogenesis of congenital and acquired melanocytic nevi based on histological study of lesion size and thickness. The Journal of Dermatology 37:1011-8.

Trentin A, Glavieux-Pardanaud C, Le Douarin NM, Dupin E (2004) Self-renewal capacity is a widespread property of various types of neural crest precursor cells. Proceedings of the National Academy of Sciences of the United States of America 101:4495-500. doi: 10.1073/pnas.0400629101

Trufant JW, Brenn T, Fletcher CDM, et al. (2009) Melanotic schwannoma arising in association with nevus of Ota: 2 cases suggesting a shared mechanism. The American Journal of Dermatopathology 31:808-13.

Valverde P, Healy E, Sikkink S, et al. (1996) The Asp84Glu variant of the melanocortin 1 receptor (MC1R) is associated with melanoma. Human molecular genetics 5:1663-6.

Van Raamsdonk CD, Bezrookove V, Green G, et al. (2009) Frequent somatic mutations of GNAQ in uveal melanoma and blue naevi. Nature 457:599-602.

Van Raamsdonk CD, Fitch KR, Fuchs H, et al. (2004) Effects of G-protein mutations on skin color. Nature Genetics 36:961-8.

Van Raamsdonk CD, Griewank KG, Crosby MB, et al. (2010) Mutations in GNA11 in uveal melanoma. The New England Journal of Medicine 363:2191-2199. doi: 10.1056/NEJMoa1000584

Walbert T, Sloan AE, Cohen ML, Koubeissi MZ (2009) Symptomatic neurocutaneous melanosis and Dandy-Walker malformation in an adult. Journal of Clinical Oncology 27:2886-7. doi: 10.1200/JCO.2008.21.5830

Watanabe A, Takeda K, Ploplis B, Tachibana M (1998) Epistatic relationship between Waardenburg syndrome genes MITF and PAX3. Nature Genetics 18:283-286.

Wehrle-Haller B (2003) The role of Kit-ligand in melanocyte development and epidermal homeostasis. Pigment Cell Research 16:287-96.

Weiner L, Han R, Scicchitano BM, et al. (2007) Dedicated epithelial recipient cells determine pigmentation patterns. Cell 130:932-42.

Wieselthaler NA, van Toorn R, Wilmshurst JM (2002) Giant congenital melanocytic nevi in a patient with brain structural malformations and multiple lipomatosis. Journal of Child Neurology 17:289-91.

Wilkie AL, Jordan SA, Jackson IJ (2002) Neural crest progenitors of the melanocyte lineage: coat colour patterns revisited. Development 129:3349.

Won JH, Ahn SK, Lee SH, et al. (1993) Congenital giant pigmented nevus associated with angiolipoma. The Journal of Dermatology 20:381-3.

Wu H, Goel V, Haluska FG (2003) PTEN signaling pathways in melanoma. Oncogene 22:3113-22. doi: 10.1038/sj.onc.1206451

Wu J, Williams JP, Rizvi T a, et al. (2008) Plexiform and dermal neurofibromas and pigmentation are caused by Nf1 loss in desert hedgehog-expressing cells. Cancer Cell 13:105-16.

Yajima I, Larue L (2008) The location of heart melanocytes is specified and the level of pigmentation in the heart may correlate with coat color. Pigment Cell & Melanoma Research 21:471-6. doi: 10.1111/j.1755-148X.2008.00483.x

Ye BS, Cho Y-J, Jang SH, et al. (2008) Neurocutaneous melanosis presenting as chronic partial epilepsy. Journal of Clinical Neurology (Seoul, Korea) 4:134-7. doi: 10.3988/jcn.2008.4.3.134

Zúñiga S, Las Heras J, Benveniste S (1987) Rhabdomyosarcoma arising in a congenital giant nevus associated with neurocutaneous melanosis in a neonate. Journal of Pediatric Surgery 22:1036-8.